TN
1
A5
Vol. 213
NIC

TRANSACTIONS

of the

American Institute of Mining, Metallurgical, and Petroleum Engineers

(Incorporated)

VOLUME 213

PETROLEUM DEVELOPMENT AND TECHNOLOGY 1958

SOCIETY OF PETROLEUM ENGINEERS of AIME

PAPERS AND DISCUSSIONS INCLUDED HAVE BEEN APPROVED FOR PUBLICATION BY THE SOCIETY OF PETROLEUM ENGINEERS TRANSACTIONS EDITORIAL COMMITTEE. THEY WERE SELECTED FROM PAPERS PRESENTED BEFORE THE SOCIETY AT MEETINGS HELD IN LOS ANGELES, OCT. 14-15, 1956; AUSTIN, TEX., FEB. 14-15, 1957; NORMAN, OKLA., SEPT. 24, 1957; DALLAS, OCT. 6-9, 1957; LOS ANGELES, OCT. 17-18, 1957; CARACAS, NOV. 6-9, 1957; DENVER, MARCH 3-4, 1958; TULSA, MARCH 20-21, 1958; SHREVEPORT, LA., APRIL 17-18, 1958; WICHITA FALLS, TEX., MAY 5-6, 1958; HOUSTON, OCT. 5-8, 1958; LOS ANGELES, OCT. 16-17, 1958; AND PAPERS NOT PRESENTED AT THESE MEETINGS BUT OFFERED TO THE SOCIETY OF PETROLEUM ENGINEERS OF AIME FOR PUBLICATION.

PUBLISHED BY THE INSTITUTE

AT THE OFFICE OF THE SOCIETY OF PETROLEUM ENGINEERS

800 FIDELITY UNION BUILDING

DALLAS, TEXAS

Headquarters of the Institute are at 29 West 39th Street, New York, N. Y.

Copyright, 1959, by the
American Institute of Mining, Metallurgical,
& Petroleum Engineers
(Incorporated)

Printed in the United States of America

Storm Printing Company, Dallas, Texas

ERRATA

Technical Paper 8023, "Streaming Potential and the SP Log," by M. Gondouin and C. Scala.

P. 172—Col. 1, second complete paragraph in column, fifth sentence should read: "Knowing the length, L, of the fluid column comprised between the two rubber diaphragms of the pressure bomb and the density, ρ, of the fluid, the alternating pressure was given by $P = L\ \rho\gamma$.

Table 3 of T.P. 8023 was omitted and is shown below:

TABLE 3—STREAMING POTENTIAL COEFFICIENT AND "SHALINESS" OF VARIOUS SAMPLES

Shale No.	(dE_0/dP) (.01 N NaCl)	B.E.C. meq./100 gr	b Factor	K_{sh}/59 NaCl .1N	K_{sh}/59 NaCl 1N	Permeability* md	Porosity per cent
	.18						
A	(.2 N NaCl)	12.1	.26	—	—	2×10^{-6}	14.2
B	.204	10.1	.44	.88	.70	—	7.0
C	.24	13.4	.62	1.0	.80	4×10^{-4}	7.4
D	.21	20.1	.67	1.0	.72	(6×10^{-4})	9.5
E	.17	7.18	.54	1.0	.72	(7×10^{-6})	4.6
F	.76	9.48	.21	—	—	8×10^{-4}	13.6
G	.34	8.53	.76	1.0	.94	2×10^{-6}	3.8
LK	.53	12.7	—	.96	.77	7×10^{-6}	—
1	.47	4.06	.14	—	—	—	
1-B	1.6	—	—	.84	.50	9×10^{-6}	—
7	.43	5.29	.27	.98	.67	—	6.2
11-1	.44	5.8	.19	.92	.71	—	10.1
14	.30	7.18	—	1.0	.61	4×10^{-4}	—
29	.32	26.7	.65	—	—	(4×10^{-3})	12.7

*Permeability in 0.2-N NaCl solution

FOREWORD

PETROLEUM TRANSACTIONS Volume 213 is the largest ever published by the Society of Petroleum Engineers. We are especially proud to have accomplished publication of this large number of excellent technical papers for it was done during a period of economic recession which forced drastic changes in our publications policy.

The 1958 Society officers and Board of Directors were faced early in the year with the prospect of a severe decline in advertising income originally anticipated for the year and an unusually large quantity of outstanding technical contributions awaiting publication space. The solution, as recommended by the Transactions Editorial Committee, was to publish some papers in a manner which permitted a limited, less expensive form of distribution.

The Board approved a recommendation that some papers be published in their entirety only in this TRANSACTIONS volume, with summaries appearing in JOURNAL OF PETROLEUM TECHNOLOGY. Free reprints of all papers were sent to members on request as soon as summaries of the papers had appeared in JOURNAL OF PETROLEUM TECHNOLOGY.

Realizing our economic situation, the membership accepted this streamlining of our publications procedure. This new policy enabled us to accomplish publication of this larger TRANSACTIONS volume.

In spite of the economic problems of the industry and nation, membership growth of the Society continued at a rapid rate. During the year 1,338 new members were added to the rolls. New petroleum sections were established in Williston, N. D.; the Austin-San Antonio area of Texas; and in Edmonton, Canada (a joint AIME-Canadian Institute of Mining and Metallurgy section). New petroleum sub-sections were recognized in San Francisco and in the Central Appalachian area, and a new student chapter was formed at Marietta College, Ohio.

Five very successful regional meetings were held by petroleum sections—in Denver, Tulsa, Shreveport, Wichita Falls and Los Angeles. The 33rd Annual Fall Meeting of the Society in Houston attracted the second largest attendance in our history.

Sets of the slide presentation on "Careers in the Petroleum Sciences," prepared by our staff and designed to interest young people in the petroleum industry, were placed in the hands of all petroleum sections. Many of them immediately began active programs showing the presentation to junior high and high school groups. Literature recording highlights of the slide presentation was also prepared and distributed under the sponsorship of the Henry L. Doherty Fund of AIME.

Recipients were selected during the year for our top petroleum engineering awards for 1958. Honored in the introductory pages of this volume, they are: Carl E. Reistle, Jr., recipient of the Anthony F. Lucas Gold Medal; Lt. Gen. E. O. Thompson, recipient of the John Franklin Carll Award; and Jim Douglas, Jr., Philip M. Blair and R. J. Wagner, joint recipients of the Cedric K. Ferguson Medal. Our congratulations to these outstanding men.

We are very pleased with the progress of the Society of Petroleum Engineers during 1958. By tightening our belts, we have kept our finances in good condition. We have continued to move ahead in every facet of our program, much to the credit of our individual members who have remained faithful during a trying economic period.

BASIL P. KANTZER, President
Society of Petroleum Engineers of AIME, 1958

January 1, 1959
Houston, Texas

OFFICERS AND STAFF OF THE AIME

(For the Year Ending February, 1959)

PRESIDENT and DIRECTOR

AUGUSTUS B. KINZEL

VICE-PRESIDENTS and DIRECTORS

E. C. BABSON
L. E. ELKINS
JOSEPH L. GILLSON
J. C. KINNEAR, JR.
R. V. PIERCE
A. W. THORNTON

DIRECTORS

L. CAMPBELL
R. B. CAPLES
CHARLES R. DODSON
ANDREW FLETCHER
T. C. FRICK
JOHN P. HAMMOND
W. R. HIBBARD, JR.
ELMER A. JONES
BASIL P. KANTZER
CHARLES R. KUZELL
FRED J. MEEK
S. D. MICHAELSON
GAIL F. MOULTON
F. W. STRANDBERG
J. S. VANICK
LAMAR WEAVER

DIRECTORS EX OFFICIIS

J. W. WOOMER (Coal Division)
ROBERT M. GROGAN (Industrial Minerals Division)
NATHANIEL ARBITER (Minerals Beneficiation Division)
H. CARROLL WEED (Mining and Exploration Division)
W. J. HARRIS, JR. (Institute of Metals Division)
K. L. FETTERS (Iron and Steel Division)
H. H. KELLOGG (Extractive Metallurgy Division)
FRANZ R. DYKSTRA (Council of Economics of AIME)
O. CUTLER SHEPARD (Council of Education of AIME)

DIRECTOR, TREASURER, and CONTROLLER

C. R. DODSON

STAFF OF INSTITUTE IN NEW YORK

SECRETARY

E. O. KIRKENDALL

ASSISTANT SECRETARIES

ROY O'BRIEN
JOHN C. FOX
JOE B. ALFORD
ROBERT W. SHEARMAN
H. NEWELL APPLETON

ASSISTANT TREASURER

JOHN F. LYNCH

STAFF OF SOCIETY OF PETROLEUM ENGINEERS OF AIME IN DALLAS

JOE B. ALFORD
EXECUTIVE SECRETARY

R. W. TAYLOR
EDITOR, *JOURNAL OF PETROLEUM TECHNOLOGY*

MAURICE D. BRATT
ADVERTISING, *JOURNAL OF PETROLEUM TECHNOLOGY*

DON A. WILLIAMS
ACTIVITIES MANAGER

HATTIE HIGHT
ASSISTANT SECRETARY

SOCIETY OF PETROLEUM ENGINEERS OFFICERS AND COMMITTEE CHAIRMEN

(For the Year Ending February, 1959)

PRESIDENT

BASIL P. KANTZER
Union Oil Co. of California
Houston, Tex.

VICE-PRESIDENTS

B. L. FRANCIS
The Texas Co.
Houston, Tex.

E. N. VAN DUZEE
Shell Oil Co.
Midland, Tex.

BOARD OF DIRECTORS

B. L. FRANCIS

BASIL P. KANTZER

E. N. VAN DUZEE

R. J. BETHANCOURT
Sun Oil Co.
Dallas, Tex.

ROY A. BOBO
Phillips Petroleum Co.
Houston, Tex.

H. D. CAMPBELL
Franco Western Oil Co.
Bakersfield, Calif.

GORDON H. FISHER
Plymouth Oil Co.
Sinton, Tex.

WAYNE E. GLENN
Continental Oil Co.
Houston, Tex.

R. E. HOWARD
The Atlantic Refining Co.
Midland, Tex.

H. N. LYLE
Renwar Oil Corp.
Corpus Christi, Tex.

JACK M. MOORE
Dowell Incorporated
Midland, Tex.

R. A. MORSE
Gulf Research & Development Co.
Pittsburgh, Pa.

GLENN M. STEARNS, Treasurer
British-American Oil Producing Co.
Dallas, Tex.

COMMITTEE CHAIRMEN

ADMISSIONS

JOSEPH C. GORDON
Three States Natural Gas Co.
Dallas, Tex.

ADVERTISING

JOHN D. WISENBAKER
Core Laboratories, Inc.
Dallas, Tex.

CEDRIC K. FERGUSON MEDAL

M. J. RZASA
Cities Service Research & Development Co.
Cranbury, N. J.

EDUCATION

R. L. WHITING
A&M College of Texas
College Station, Tex.

GENERAL EDITORIAL

NORMAN J. CLARK
Norman J. Clark Engineering
Dallas, Tex.

JOHN FRANKLIN CARLL AWARD

H. D. WILDE
Humble Oil & Refining Co.
Houston, Tex.

MEMBERSHIP

CHARLES F. HUNKINS
Northern Pacific Railway Co.
Billings, Mont.

NOMINATING

JOHN P. HAMMOND
Amerada Petroleum Corp.
Tulsa, Okla.

PRODUCTION REVIEW

MILTON WILLIAMS, *Chairman*
Humble Oil & Refining Co.
Houston, Tex.

RICHARD W. HILLYER, *Vice-Chairman (Domestic)*
Ralph C. Cummins Co.
Houston, Tex.

H. J. WHARTON, *Vice-Chairman (Foreign)*
Gulf Oil Corp.
Pittsburgh, Pa.

SYMBOLS

FRANCIS A. COLLINS
The Atlantic Refining Co.
Dallas, Tex.

TECHNOLOGY

F. E. SCHOONOVER
Monterey Oil Co.
Los Angeles, Calif.

TRANSACTIONS EDITORIAL

LEWIS FINCH, JR.
Pan American Petroleum Corp.
Tulsa, Okla.

CONTENTS

FOREWORD, *by* BASIL P. KANTZER iii
OFFICERS AND STAFF OF AIME iv
SOCIETY OF PETROLEUM ENGINEERS OFFICERS AND COMMITTEE CHAIRMEN v
1958 SOCIETY OF PETROLEUM ENGINEERS TRANSACTIONS EDITORIAL COMMITTEE ix
THE JOHN FRANKLIN CARLL AWARD x
THE ANTHONY F. LUCAS MEDAL AND FUND xi
THE CEDRIC K. FERGUSON MEDAL xii
SOCIETY OF PETROLEUM ENGINEERS PAST CHAIRMEN xiii
LOCAL SECTION OFFICERS FOR 1958 xiv

PAPERS

DRILLING — EQUIPMENT, METHODS AND MATERIALS

Effect of Pressure on Rock Drillability, by John R. Eckel 1
Properties of Cementing Compositions at Elevated Temperatures and Pressure, by Greg Carter and Dwight K. Smith 20
Use of Chemicals to Maintain Clear Water for Drilling, by J. P. Gallus, J. L. Lummus and J. E. Fox, Jr. 70
The Cutting Carrying Capacity of Air at Pressures Above Atmospheric, by Kenneth E. Gray 180
Mechanics of Differential Pressure Sticking of Drill Collars, by H. D. Outmans 265
A Correlation of the Electrical Properties of Drilling Fluids with Solids Content, by Harold L. Overton and Leonard B. Lipson 333
Development and Field Testing of a Core Barrel for Recovering Unconsolidated Oil Sands, by A. B. Hildebrandt, H. C. Bridwell and J. M. Kellner 347
Effect of Low Frequency Percussion in Drilling Hard Rock, by E. Topanelian, Jr. 393
The Effect of Temperature on the Flow Properties of Clay-Water Drilling Muds, by S. Srini-Vasan and Carl Gatlin 438

PRODUCING — EQUIPMENT, METHODS AND MATERIALS

Factors Affecting the Rate of Deposition of Cement in Unfractured Perforations During Squeeze-Cementing Operations, by G. W. Binkley, G. K. Dumbauld and R. E. Collins 51
Pressure Measurements During Formation Fracturing Operations, by J. K. Godbey and H. D. Hodges . 65
Effect of Flow Rate on Paraffin Accumulation in Plastic, Steel, and Coated Pipe, by F. W. Jessen and James N. Howell 80
Hydraulic Fracturing—Fracture Flow Capacity vs Well Productivity, by H. K. van Poollen, John M. Tinsley, and Calvin D. Saunders 91
Producing Wells on Casing Flow — An Analysis of Flowing Pressure Gradients, by P. B. Baxendell . . 345
A Copper Ion Displacement Test for Screening Corrosion Inhibitors, by William B. Hughes 350
Note on Buckling of Tubing in Pumping Wells, by T. Seldenrath and A. W. Wright 396
Identification of Mixtures of Waters from Chemical Water Analyses, by J. C. McKinnell 402

LOGGING AND LOG INTERPRETATION

Departure Curves for the Self-Potential Log, by A. E. Worthington and R. F. Meldau 11
Porosity Balance Verifies Water Saturation Determined from Logs, by M. P. Tixier 161
Streaming Potential and the SP Log, by M. Gondouin and C. Scala 170
Velocity Log Characteristics, by A. A. Stripling 207
Reverse-Wetting Logging, by J. W. Graham 304
A Report on the Displacement Log, by R. H. Winn 353
Evaluation of Porosity Derivation from Neutron Logs, by R. H. Widmyer and G. M. Wood 371
On the Streaming Potential Problem in Well Logging, by M. R. J. Wyllie, A. J. deWitte and J. E. Warren 409

NATURAL GAS TECHNOLOGY

Spacing of Natural Gas Wells, by R. C. Craze 213
The Importance of Reliable Data in Gas-Condensate Calculations, by R. F. Hinds 433

RESERVOIR ENGINEERING EQUIPMENT

Application of a Resistance Network for Studying Mobility Ratio Effects, by M. A. Nobles and Harold B. Janzen 356

A Linear Programming Model for Scheduling Crude Oil Production, by A. S. Lee and J. S. Aronofsky . 389

RESERVOIR ENGINEERING — GENERAL

A Model for the Mechanism of Oil Recovery from the Porous Matrix Due to Water Invasion in Fractured Reservoirs, by J. S. Aronofsky, L. Massé and S. G. Natanson 17

A Study of Anomalous Pressure Build-Up Behavior, by G. L. Stegemeier and C. S. Matthews . . . 44

A Method for Predicting Pressure Maintenance Performance for Reservoirs Producing Volatile Crude Oil, by R. H. Jacoby and V. J. Berry, Jr. 59

The Effect of Partial Penetration on Pressure Build-Up in Oil Wells, by Robert G. Nisle 85

Calculation of Linear Waterflood Behavior Including the Effects of Capillary Pressure, by Jim Douglas, Jr., P. M. Blair and R. J. Wagner 96

Comparison Between the Predicted and Actual Production History of a Condensate Reservoir, by J. K. Rodgers, N. H. Harrison and S. Regier 127

Estimation of Ultimate Recovery from Solution Gas-Drive Reservoirs, by W. L. Wahl, L. D. Mullins and E. B. Elfrink 132

The Use of High-Speed Computers for Predicting Flood-Out Patterns, by D. G. McCarty and E. C. Barfield 139

Application of Numerical Methods to Predict Recovery from Thin Oil Columns, by H. H. Rachford, Jr., R. D. Taylor, Jim Douglas, Jr., and P. M. Dyke 193

Spacing of Natural Gas Wells, by R. C. Craze 213

Reservoir Analysis for Pressure Maintenance Operations Based on Complete Segregation of Mobile Fluids, by John C. Martin 220

Field Results of South Belridge Thermal Recovery Experiment, by C. F. Gates and H. J. Ramey, Jr. . 236

Pressure Fall-Off in Water Injection Wells, by P. Hazebroek, H. Rainbow and C. S. Matthews . . . 250

Application of Decline Curves to Gravity-Drainage Reservoirs in the Stripper Stage, by H. C. Lefkovits and C. S. Matthews 275

Improving Miscible Displacement by Gas-Water Injection, by B. H. Caudle and A. B. Dyes 281

Extensions of the Muskat Depletion Performance Equation, by R. D. West 285

The Simplification of the Material Balance Formulas by the Laplace Transformation, by William Hurst . 292

Profitability of Capital Expenditures for Development Drilling and Producing Property Appraisal, by J. J. Arps 337

The Application of the Buckley-Leverett Frontal Advance Theory to Petroleum Recovery, by Stephen G. Dardaganian 365

A Method for Determining Optimum Second Stage Pressure in Three Stage Separation, by Kenneth F. Whinery and John M. Campbell 369

Bubble Point Pressure Correlation, by J. S. Lasater 379

Laboratory Evaluation of Prospective Enriched Gas-Drive Projects, by D. M. Kehn, G. T. Pyndus and M. H. Gaskell 382

Application of Statistics to the Analysis of Production Decline Data, by A. T. Chatas and W. W. Yankie, Jr. 399

Pressure Interference Correction to the Material Balance Equation for Water-Drive Reservoirs Using a Digital Computer, by Michael P. Robinson 418

Limitations on Pressure Predictions for Water-Drive Reservoirs, by L. H. Simons and H. H. Spain . . 427

A Comparison of Calculated k_{rg}/k_{ro} Ratios with a Correlation of Field Data, by Michael A. Torcaso and M. R. J. Wyllie 436

RESERVOIR ENGINEERING — LABORATORY RESEARCH

Miscible Displacements of Reservoir Oil Using Flue Gas, by H. A. Koch, Jr. and C. A. Hutchinson, Jr. . 7

Process Variables of In Situ Combustion, by William L. Martin, John D. Alexander and John N. Dew . 28

The Effect of Fluid-Flow Rate and Viscosity on Laboratory Determinations of Oil-Water Relative Permeabilities, by C. R. Sandberg, L. S. Gournay and R. F. Sippel 36

Miscible Fluid Displacement in Porous Media, by James W. Lacey, Arthur L. Draper and George G. Binder, Jr. 76

The Thermal Recovery Process — An Analysis of Laboratory Combustion Data, by A. L. Benham and Fred H. Poettmann 83

A Theoretical Description of Water-Drive Processes Involving Viscous Fingering, by P. van Meurs and C. van der Poel 103

Laboratory Studies of Five-Spot Waterflood Performance, by L. A. Rapoport, C. W. Carpenter, Jr. and W. J. Leas 113

A Laboratory Study of Laminar and Turbulent Flow in Heterogeneous Porosity Limestones, by Charles R. Stewart and William W. Owens 121

Fluid Dynamics During an Underground Combustion Process, by L. A. Wilson, R. J. Wygal, D. W. Reed, R. L. Gergins and J. H. Henderson 146

Reservoir Rock Wettability — Its Significance and Evaluation, by J. E. Bobek, C. C. Mattax and M. O. Denekas 155

The Injection of Detergent Slugs in Water Floods, by J. J. Taber 186

The Deterioration of Miscible Zones in Porous Media, by John A. Sievert, John N. Dew and Francis R. Conley 228

Effect of Fractures on Sweep-Out Pattern, by A. B. Dyes, C. E. Kemp and B. H. Caudle 245

Determination of Wettability by Dye Adsorption, by O. C. Holbrook and George G. Bernard . . . 261

A Laboratory Study of Oil Recovery by Solution Gas Drive, by L. L. Handy 310

A Practical Utilization of the Theory of Bingham Plastic Flow in Stationary Pipes and Annuli, by J. C. Melrose, J. G. Savins, W. R. Foster and E. R. Parish 316

Generalized Newtonian (Pseudoplastic) Flow in Stationary Pipes and Annuli, by J. G. Savins . . . 325

Evidence of Chromatographic Effect During Flow of Gases Through Oilfield Cores, by W A. Roper, Todd Doscher and Riki Kobayashi 359

Pore Volume Compressibilities of Sandstone Reservoir Rocks, by I. Fatt 362

Laboratory Evaluation of Prospective Enriched Gas-Drive Projects, by D. M. Kehn, G. T. Pyndus and M. H. Gaskell 382

The Effective Compressibility of Reservoir Rock and Its Effects on Permeability, by A. S. McLatchie, R. A. Hemstock and J. W. Young 386

Linear Waterflood Behavior and End Effects in Water-Wet Porous Media, by J. R. Kyte and L. A. Rapoport 423

Effect of Applied Pressure on the Conductivity, Porosity and Permeability of Sandstones, by D. O. Wyble 430

SECONDARY RECOVERY

Miscible Displacements of Reservoir Oil Using Flue Gas, by H. A. Koch, Jr. and C. A. Hutchinson, Jr. 7

Process Variables of In Situ Combustion, by William L. Martin, John D. Alexander and John N. Dew . 28

A Method for Predicting Pressure Maintenance Performance for Reservoirs Producing Volatile Crude Oil, by R. H. Jacoby and V. J. Berry, Jr. 59

Miscible Fluid Displacement in Porous Media, by James W. Lacey, Arthur L. Draper and George G. Binder, Jr. 76

Calculation of Linear Waterflood Behavior Including the Effects of Capillary Pressure, by Jim Douglas, Jr., P. M. Blair and R. J. Wagner 96

A Theoretical Description of Water-Drive Processes Involving Viscous Fingering, by P. van Meurs and C. van der Poel 103

Laboratory Studies of Five-Spot Waterflood Performance, by L. A. Rapaport, C. W. Carpenter, Jr. and W. J. Leas 113

The Use of High-Speed Computers for Predicting Flood-Out Patterns, by D. G. McCarty and E. C. Barfield 139

Fluid Dynamics During an Underground Combustion Process, by L. A. Wilson, R. J. Wygal, D. W. Reed, R. L. Gergins and J. H. Henderson 146

The Injection of Detergent Slugs in Water Floods, by J. J. Taber 186

Reservoir Analysis for Pressure Maintenance Operations Based on Complete Segregation of Mobile Fluids, by John C. Martin 220

The Deterioration of Miscible Zones in Porous Media, by John A. Sievert, John N. Dew and Francis R. Conley 228

Field Results of South Belridge Thermal Recovery Experiment, by C. F. Gates and H. J. Ramey, Jr. . 236

Effect of Fractures on Sweep-Out Pattern, by A. B. Dyes, C. E. Kemp and B. H. Caudle 245

Pressure Fall-Off in Water Injection Wells, by P. Hazebroek, H. Rainbow and C. S. Matthews . . . 250

Improving Miscible Displacement by Gas-Water Injection, by B. H. Caudle and A. B. Dyes 281

Some Thermal Characteristics of Porous Rocks, by Wilbur H. Somerton 375

Laboratory Evaluation of Prospective Enriched Gas-Drive Projects, by D. M. Kehn, G. T. Pyndus and M. H. Gaskell 382

The Thermal Recovery Process — An Analysis of Laboratory Combustion Data, by A. L. Benham and Fred H. Poettmann 406

1958 SOCIETY OF PETROLEUM ENGINEERS OF AIME
TRANSACTIONS EDITORIAL COMMITTEE

LEWIS FINCH, JR., *Chairman*
Pan American Petroleum Co.
Tulsa, Okla.

FREDERICK E. MERLISS
Cities Service Research & Development Co.
Tulsa, Okla.

LEO A. RAPOPORT
The Carter Oil Co.
Tulsa, Okla.

RAYMOND E. OUSTERHOUT
Dowell Incorporated
Tulsa, Okla.

SHOFNER SMITH
Phillips Petroleum Co.
Bartlesville, Okla.

DUNCAN V. PATTY
Anderson Prichard Oil Corp.
Oklahoma City, Okla.

FRANK O. REUDELHUBER
Core Laboratories, Inc.
Dallas, Texas

W. E. STILES
W. E. Stiles Engineering
Tulsa, Okla.

The primary function of the Transactions Editorial Committee is to receive the papers tendered for publication by the Society of Petroleum Engineers, and to select from them those papers that shall be published in the TRANSACTIONS Section of JOURNAL OF PETROLEUM TECHNOLOGY. This selection shall be based on the merit of such papers in the light of existing standards. The committee shall be the final authority on the selection of papers for publication in TRANSACTIONS.

THE TECHNICAL PAPER

Manuscripts should present completed original work embodying the results of extensive field, plant, laboratory, or theoretical investigations, or new views on old but important problems. Originality does not necessarily justify publication. The work must be sufficiently significant to warrant inclusion in the permanent literature of the Society. Previous publication in media normally available to petroleum engineers is usually a bar to acceptance. In addition to technical acceptability, the material should be presented clearly and concisely. In reviewing a paper, it is important to distinguish between technological error, erroneous conclusions, and valid conclusions which may be in conflict with those previously held on subjects of a controversial nature. When the data presented appear to be accurate and complete and the conclusions drawn in accord with the data, then the author is entitled to the right of publication even though his conclusion may be open to valid argument as a result of alternative, but equally valid, interpretations or because of unpublished data in the possession of the reviewer. There will be ample opportunity for objections when the paper is published. On the other hand, important experimental, analytical, or mathematical errors or erroneous conclusions drawn from the data presented constitute a reasonable basis for rejection of the manuscript pending appropriate corrections.

THE TECHNICAL NOTE

The Technical Note shall constitute a contribution to the technical literature and shall be:

1. Material submitted by an author as a short manuscript.
2. Material condensed from a longer manuscript at the request of the Transactions Editorial Committee.

Technical Notes which are designated as such when submitted by authors will be considered promptly by the Transactions Editorial Committee and, if approved, will be published promptly. Such Notes should consist of the following:

1. Results of short investigations which do not warrant a Technical Paper. (Investigations of wide scope and interest, even though short, constitute material for Technical Papers.)
2. Results of limited scope from extensive investigations that do not warrant a Technical Paper.
3. Results or conclusions arising in the course of an investigation which the author wishes to present prior to completion of the investigation.

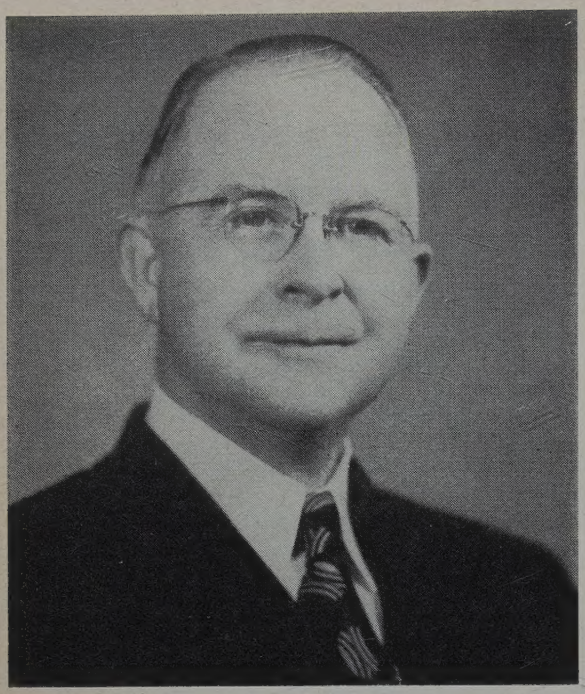

ERNEST O. THOMPSON
John Franklin Carll Award, 1958

"For his significant contribution to petroleum engineering in the public acceptance of reservoir engineering principles in petroleum conservation regulation and practice."

THE JOHN FRANKLIN CARLL AWARD

Established in 1956 and first presented in 1957, the John Franklin Carll Award is awarded "to recognize distinguished achievement in or contributions to petroleum engineering." The medal memorializes John Franklin Carll (1828-1904) whose ideas and writings first expressed principles of petroleum engineering which are now considered commonplace. Herbert C. Otis, Sr., was the first recipient of the award. Members of the 1958 John Franklin Carll Award Committee are: H. D. Wilde, Chairman; H. F. Beardmore, B. C. Craft, R. W. French, Harry P. Stolz and Harold Vance.

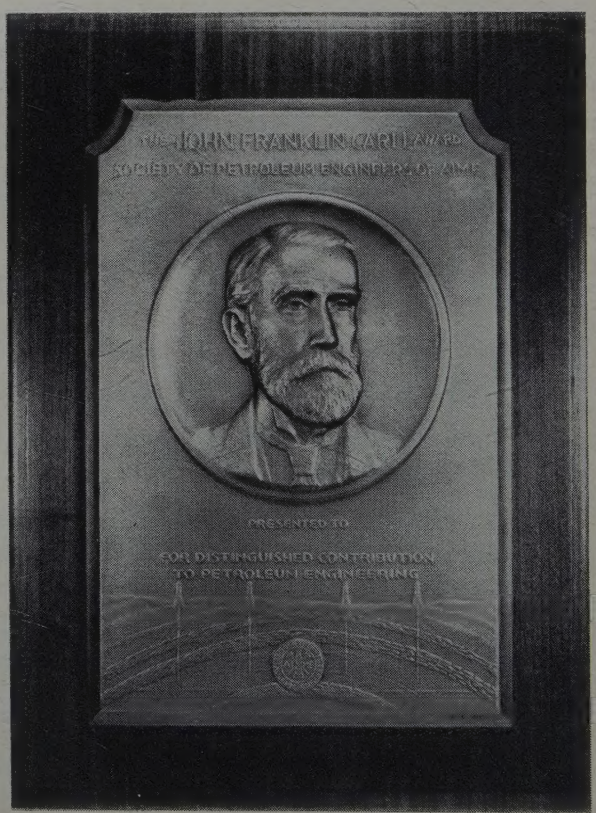

CARL E. REISTLE, JR.
Lucas Medalist, 1958

"For his distinguished achievements in advancing the science of Petroleum Engineering through his own technical contributions and his ability to inspire others; for his forward concepts and his untiring energy in advancing the profession of Petroleum Engineering as a practitioner, administrator, and executive."

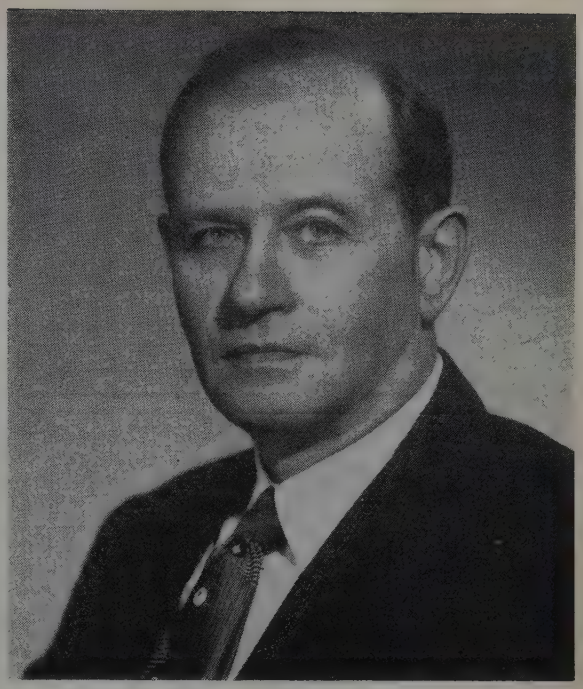

THE ANTHONY F. LUCAS FUND AND MEDAL

In 1936 the Institute established the Anthony F. Lucas Gold Medal, to be awarded from time to time "for distinguished achievement in improving the technique and practice of finding and producing petroleum." These awards are sponsored by the Society of Petroleum Engineers of AIME. Members of the Committee of Award of the Lucas Medal are: H. H. Kaveler, Chairman; H. F. Beardmore, Lyon F. Terry, Harold Decker, Claude R. Hocott, John R. McMillan, L. E. Elkins, Howard C. Pyle, T. C. Frick, Earl M. Kipp, Charles H. Pishny and Everett G. Trostel. Members ex officiis are: M. J. Ankey, Director, USBM; Frank M. Porter, President, API; G. S. Buchanan, President, AAPG; and Grover J. Holt, President, AIME.

MEDALS AWARDED

J. Edgar Pew, 1937
Henry L. Doherty, 1938
E. DeGolyer, 1940
Conrad (Posthumously) and Marcel Schlumberger, 1941
John Robert Suman, 1943
Charles Van Ormer Millikan, 1944
James Ogier Lewis, 1946
William Noble Lacey, 1947
Wallace Everette Pratt, 1948
William Embry Wrather, 1950
Morris Muskat, 1953
Bruce H. Sage, 1954
Stuart E. Buckley, 1956
John Edward Brantly, 1957
Carl E. Reistle, Jr., 1958

JIM DOUGLAS, JR.

PHILIP M. BLAIR

R. J. WAGNER

THE CEDRIC K. FERGUSON MEDAL

Jim Douglas, Jr., Philip M. Blair and R. J. Wagner are the joint recipients of the 1958 Cedric K. Ferguson Medal. They were selected to receive this award for AIME T.P. 8013 entitled, "Calculation of Linear Waterflood Behavior Including the Effects of Capillary Pressure," published on page 96 of PETROLEUM TRANSACTIONS Volume 213. This was the fourth presentation of the Feguson Medal, first awarded posthumously to Cedric K. Ferguson in 1954. Co-recipients in 1956 were the late John L. Martin and William M. Campbell. W. O. Brown received the medal in 1957.

The purpose of the medal is to recognize the writing of an outstanding technical paper by a young member or members (under 33 years of age) of the profession.

The medal is presented annually unless waived for lack of a worthy candidate. Members of the 1958 Cedric K. Ferguson Medal Committee are: M. J. Rzasa, Chairman; Preston E. Chaney and M. R. J. Wyllie.

SOCIETY OF PETROLEUM ENGINEERS of AIME

Established as a Division March 24, 1922
Established as a Branch in 1948
Established as a Society in 1957

PAST CHAIRMEN AND PRESIDENTS

Ralph Arnold, 1922
E. DeGolyer, 1923, 1924
F. Julius Fohs, 1925, 1926
John M. Lovejoy, 1927
A. W. Ambrose, 1928
Joseph B. Umpleby, 1929
C. V. Millikan, 1930
C. E. Beecher, 1931
Earl Oliver, 1932
W. E. Wrather, 1933
H. D. Wilde, Jr., 1934
Harry H. Power, 1935
Hallan N. Marsh, 1936
M. Albertson, 1937
George B. Corless, 1938
W. H. Geis, 1939
T. V. Moore, 1940
Eugene A. Stephenson, 1941
Harry P. Stolz, 1942
C. A. Warner, 1943
W. S. Morris, 1944
M. L. Haider, 1945
H. F. Beardmore, 1946
Howard C. Pyle, 1947
Irwin W. Alcorn, 1948
Lloyd E. Elkins, 1949
John E. Sherborne, 1950
R. W. French, 1951
Paul R. Turnbull, 1952
Claude R. Hocott, 1953
John R. McMillan, 1954
Robert B. Gilmore, 1955
T. C. Frick, 1956
John P. Hammond, 1957

LOCAL SECTION OFFICERS FOR 1958

BALCONES LOCAL SECTION

NORMAN LAMONT, *Chairman*, U. of Texas, Austin, Tex.; JAMES R. BUCKLEY, *Secretary-Treasurer*, R. K. Guthrie & Assoc., San Antonio, Tex.

BILLINGS PETROLEUM SECTION

FRASER M. BURBACK, *Chairman*, Mobil Producing Co., Billings, Mont.; N. J. MATTHEWS, *First Vice-Chairman*, Shell Oil Co., Billings, Mont.; CHARLES B. EVANS, *Second Vice-Chairman*, Billings, Mont.; DON M. MADDEN, *Secretary-Treasurer*, Mobil Producing Co., Billings, Mont.

CALIFORNIA COASTAL SECTION

JACK R. SEVERNS, *Chairman*, Schlumberger Well Surveying Corp., Ventura, Calif.; GILBERT L. JEMMOTT, *Vice-Chairman*, Shell Oil Co., Ventura, Calif.; JACK A. BIREN, *Secretary*, Continental Oil Co., Ventura, Calif.; ROBERT L. RICHARDSON, *Treasurer*, Consultant, Ventura, Calif.

CARACAS PETROLEUM SECTION

W. F. SHELTON, *Chairman*, Creole Petroleum Corp., Caracas, Venezuela; HOMER N. MEAD, *Vice-Chairman*, Martin, Sykes & Assoc., C.A., Caracas, Venezuela; JOSE G. PAEZ, *Vice-Chairman*, Minsterio de Minas e Hidrocarburos, Caracas, Venezuela; E. A. MOORE, *Secretary*, Cia. Shell de Venezuela, Caracas, Venezuela; T. A. MOORE, *Treasurer*, Texas Petroleum Co., Caracas, Venezuela.

DALLAS LOCAL SECTION

FRED L. OLIVER, *Chairman*, Fred L. Oliver & Assoc., Dallas, Tex.; WELDON L. PORTER, *First Vice-Chairman*, Welex, Inc., Dallas, Tex.; J. H. SULLIVAN, *Second Vice-Chairman*, The Atlantic Refining Co., Dallas, Tex.; R. E. VICKREY, *Treasurer*, Sun Oil Co., Dallas, Tex.; W. F. WEST, *Secretary*, Fred L. Oliver & Assoc., Dallas, Tex.

DELTA LOCAL SECTION

E. H. LEEMANN, *Chairman*, Shell Oil Co., New Orleans, La.; J. M. C. GAFFRON, *First Vice-Chairman*, Freeport Oil Co., New Orleans, La.; DALE H. AUNSPAUGH, *Second Vice-Chairman*, Gulf Refining Co., New Orleans, La.; F. J. OLIVIER, *Secretary*, Humble Oil & Refining Co., New Orleans, La.; E. O. PRICE, JR., *Treasurer*, The California Co., New Orleans, La.

DENVER PETROLEUM SECTION

J. D. HARRIS, *Chairman*, Core Laboratories, Inc., Denver, Colo.; C. D. GAINES, JR., *First Vice-Chairman*, Sinclair Oil & Gas Co., Denver, Colo.; J. A. BANISTER, *Second Vice-Chairman*, Halliburton Oil Well Cementing Co., Denver, Colo.; W. E. BAUMAN, *Secretary-Treasurer*, Gulf Oil Corp., Denver, Colo.

EAST TEXAS LOCAL SECTION

M. O. LANGHAM, *Chairman*, Humble Oil & Refining Co., Tyler, Tex.; M. L. REED, *Vice-Chairman*, Shell Oil Corp., Kilgore, Tex.; HUGH B. BARTON, *Secretary-Treasurer*, Humble Oil & Refining Co., Tyler, Tex.

EASTERN VENEZUELA PETROLEUM SECTION

THOMAS G. WALL, *Chairman*, Socony Mobil Oil Co. de Venezuela, Caracas, Venezuela; G. J. CLARKE, *First Vice-Chairman*, Mene Grande Oil Co., Caracas, Venezuela; D. SWANSON, *Second Vice-Chairman*, Sinclair Oil Co., El Roble, Venezuela; ROBERT E. HUTCHINSON, *Treasurer*, Creole Petroleum Corp., Barcelona, Venezuela; ROGER D. WEST, *Secretary*, Mene Grande Oil Co., Caracas, Venezuela.

EVANGELINE LOCAL SECTION

JOHN O. HENDRICK, *Chairman*, Dowell Incorporated, Lafayette, La.; LESTER E. BEIHL, *First Vice-Chairman*, Cherokee Laboratories, Lafayette, La.; J. FRANK CREWS, *Second Vice-Chairman*, The Atlantic Refining Co., Lafayette, La.; CHESTER A. NENNEY, JR., *Third Vice-Chairman*, Columbian Carbon Co., Lafayette, La.; JACK MAHAN, JR., *Secretary-Treasurer*, Pan American Petroleum Corp., Lafayette, La.

FORT WORTH LOCAL SECTION

K. L. DOMINY, *Chairman*, Midwest Oil Corp., Fort Worth, Tex.; T. E. MCGAUGH, *First Vice-Chairman*, Texas Pacific Coal & Oil Co., Fort Worth, Tex.; BRYAN O. BISHOP, *Second Vice-Chairman*, Perforating Guns Atlas Corp., Fort Worth, Tex.; ALEX CLARKE, JR., *Third Vice-Chairman*, Pan American Petroleum Corp., Fort Worth, Tex.; CLARKE B. GILLESPIE, *Fourth Vice-Chairman*, Gulf Oil Corp., Fort Worth, Tex.; WALTER L. HAHN, *Secretary-Treasurer*, The Texas Co., Fort Worth, Tex.

FOUR CORNERS PETROLEUM SECTION

OLIVER W. FOWLER, *Chairman*, El Paso Natural Gas Co., Farmington, N. M.; WILBUR E. RENEAU, JR., *Vice-Chairman*, Core Laboratories, Inc., Farmington, N. M.; ROY M. BAUER, JR., *Vice-Chairman*, Pan American Petroleum Corp., Farmington, N. M.; THOMAS A. DUGAN, *Secretary-Treasurer*, Pacific Northwest Pipeline Corp., Farmington, N. M.

GREAT BEND LOCAL SECTION

CHARLES R. MOORE, *Chairman*, National Cooperative Refinery Assn., Great Bend, Kans.; WILLIAM A. DOW, *First Vice-Chairman*, Cities Service Oil Co. Great Bend, Kans.; ROBERT L. STOVER, *Second Vice-Chairman*, Anderson-Prichard Oil Corp., Great Bend, Kans.; STEPHEN F. HOSS, *Secretary-Treasurer*, Perforating Guns Atlas Corp., Great Bend, Kans.

GULF COAST LOCAL SECTION

RUPERT C. CRAZE, *Chairman*, Humble Oil & Refining Co., Houston, Tex.; M. SCOTT KRAEMER, *Vice-Chairman*, Pan American Petroleum Corp., Houston, Tex.; BOB DIGGS BROWN, *Secretary-Treasurer*, Halliburton Oil Well Cementing Co., Houston, Tex.

HOBBS PETROLEUM SECTION

E. F. MOTTER, *Chairman*, Cities Service Oil Co., Hobbs, N. M.; R. M. WILLIAMS, *First Vice-Chairman*, Monterey Oil Co., Hobbs, N. M.; REX L. RADCLIFFE, *Second Vice-Chairman*, Halliburton Oil Well Cementing Co., Hobbs, N. M.; ROBERT N. MILLER, *Secretary-Treasurer*, Tidewater Oil Co., Hobbs, N. M.

HUGOTON LOCAL SECTION	R. C. RITCHIE, *Chairman*, Columbian Fuel Corp., Liberal, Kans.; D. W. JACKSON, *First Vice-Chairman*, Panhandle Eastern Pipe Line Co., Liberal, Kans.; JOHN D. FORD, *Second Vice-Chairman*, Panhandle Eastern Pipe Line Co., Liberal, Kans.; GALE T. BRADSHAW, *Secretary-Treasurer*, Schlumberger Well Surveying Corp., Liberal, Kans.
ILLINOIS BASIN PETROLEUM SECTION	FLETCHER F. FARRAR, *Chairman*, Farrar Drilling Co., Mt. Vernon, Ill.; BILL G. HARMON, *First Vice-Chairman*, B. G. Harmon Service & Eqpt., Carmi, Ill.; JAMES A. MCCARTY, *Second Vice-Chairman*, Shakespeare Oil Co., Inc., Salem, Ill.; RAY DOST, *Secretary-Treasurer*, Kingwood Oil Co., Mt. Vernon, Ill.
KANSAS LOCAL SECTION	DALE E. BOYLE, *Chairman*, Core Laboratories, Inc., Wichita, Kans.; DERYL W. JOHNSTON, *Vice-Chairman*, Sinclair Oil & Gas Co., Thrall, Kans.; JAMES J. JAMIESON, *Secretary*, Gulf Oil Corp., Wichita, Kans.; WILLIAM J. CRAWFORD, *Treasurer*, The Ohio Oil Co., Eureka, Kans.
LOS ANGELES BASIN SECTION	MAX J. TAVES, *Chairman*, Richfield Oil Corp., Los Angeles, Calif.; W. F. CERINI, *Vice-Chairman and Secretary*, Union Oil Co. of California, Whittier, Calif.; ROBERT J. FERNANDEZ, *Treasurer*, Western Gulf Oil Corp., Los Angeles, Calif.
LOU-ARK LOCAL SECTION	WAYNE L. MCCANN, *Chairman*, McCann & Rogers, Shreveport, La.; DON R. BOLING, *First Vice-Chairman*, National Tank Co., Shreveport, La.; M. T. FARRELL, *Second Vice-Chairman*, Gulf Refining Co., Shreveport, La.; PAUL S. CLINKENBEARD, *Secretary-Treasurer*, Dowell Incorporated, Shreveport, La.
MID-CONTINENT LOCAL SECTION	JOHN E. ECKEL, *Chairman*, Jersey Production Research Co., Tulsa, Okla.; WILLIAM E. STILES, *First Vice-Chairman*, W. E. Stiles Engineering Co., Tulsa, Okla.; VIRGIL J. BERRY, JR., *Second Vice-Chairman*, Pan American Petroleum Corp., Tulsa, Okla.; H. ARTHUR NEDOM, *Secretary*, Amerada Petroleum Corp., Tulsa, Okla.; ERNEST E. FINKLEA, *Treasurer*, Schlumberger Well Surveying Corp., Tulsa, Okla.
MISSISSIPPI LOCAL SECTION	S. R. COLEMAN, *Chairman*, Union Producing Co., Jackson, Miss.; BRYON O. SIMS, JR., *First Vice-Chairman*, Magnolia Petroleum Co., Natchez, Miss.; JAMES M. OTTS, JR., *Second Vice-Chairman*, Gulf Oil Corp., Jackson, Miss.; WILBUR R. LILLY, *Secretary-Treasurer*, Gulf Oil Corp., Jackson, Miss.
NEW YORK PETROLEUM SECTION	WILLIAM R. WAGG, *Chairman*, Empire Trust Co., New York, N. Y.; W. BOYD MCCOY, *Vice-Chairman*, Halliburton Oil Well Cementing Co., New York, N. Y.; TODD L. TAPP, *Secretary*, American Overseas Petroleum, Ltd., New York, N. Y.; ROBERT M. BRACKBILL, *Treasurer*, Shell Oil Co., New York, N. Y.
NORTH TEXAS LOCAL SECTION	RICHARD R. DARNER, *Chairman*, W. R. Hammon, Wichita Falls, Tex.; JAMES F. ZAPP, *Vice-Chairman*, Phillips Petroleum Co., Wichita Falls, Tex.; DON V. HESTER, *Secretary*, The Texas Co., Wichita Falls, Tex.; ERNEST SLAUGHTER, JR., *Treasurer*, Lufkin Foundry & Machine Co., Wichita Falls, Tex.
OKLAHOMA CITY LOCAL SECTION	ALBERT E. SWEENEY, JR., *Chairman*, Interstate Oil Compact Commission, Oklahoma City, Okla.; BURRELL G. TAYLOR, *First Vice-Chairman*, Kerr-McGee Oil Industries, Oklahoma City, Okla.; LOUIS T. MOFFATT, *Second Vice-Chairman*, Sunray Mid-Continent Oil Co., Oklahoma City, Okla.; EUGENE N. BENNETT, *Secretary*, Pan American Petroleum Corp., Oklahoma City, Okla.; EDWARD B. HARRY, JR., *Treasurer*, Sohio Petroleum Co., Oklahoma City, Okla.
PANHANDLE LOCAL SECTION	EDWARD S. MORRIS, *Chairman*, Amarillo Oil Co., Amarillo, Tex.; JOE D. KENWORTHY, *First Vice-Chairman*, Kewanee Oil Co., Pampa, Tex.; RAY W. MILLER, *Second Vice-Chairman*, U. S. Bureau of Mines, Amarillo, Tex.; ALBERT S. KNOX, *Secretary-Treasurer*, Gulf Oil Corp., Borger, Tex.
PERMIAN BASIN LOCAL SECTION	MARION K. MAIN, *Chairman*, Shell Oil Co., Midland, Tex.; GEORGE N. WILSON, SR., *First Vice-Chairman*, Seaboard Oil Co., Midland, Tex.; HARRY L. HORTON, *Second Vice-Chairman*, Dowell Incorporated, Odessa, Tex.; NEAL MCCASKILL, *Second Vice-Chairman*, The Atlantic Refining Co., Midland, Tex.; DONALD C. BROWN, *Secretary-Treasurer*, Sun Oil Co., Midland, Tex.
ROSWELL PETROLEUM SECTION	RALPH L. GRAY, *Chairman*, Buffalo Oil Co., Artesia, N. M.; GEORGE W. EATON, JR., *First Vice-Chairman*, Pan American Petroleum Corp., Roswell, N. M.; OMA K. GILBRETH, JR., *Second Vice-Chairman*, Gulf Oil Corp., Roswell, N. M.; REX C. CABANISS, *Secretary-Treasurer*, Sperry-Sun Well Surveying Co., Roswell, N. M.
SAN JOAQUIN VALLEY LOCAL SECTION	K. R. EVANS, *Chairman*, Consultant, Bakersfield, Calif.; N. B. CLARK, JR., *Vice-Chairman*, Union Oil Co. of California, Bakersfield, Calif.; A. J. HORN, *Secretary*, Standard Oil Co. of California, Taft, Calif.; WILLIAM PLASCH, *Treasurer*, Schlumberger Well Surveying Corp., Taft, Calif.
SOUTH PLAINS LOCAL SECTION	J. B. LIVINGSTON, *Chairman*, Halliburton Oil Well Cementing Co., Lubbock, Tex.; W. H. WADLINGTON, *First Vice-Chairman*, Pan American Petroleum Corp., Levelland, Tex.; BARNEY M. VACHAL, *Second Vice-Chairman*, Cities Service Co., Brownfield, Tex.; R. J. BOREN, *Secretary-Treasurer*, Honolulu Oil Corp., Brownfield, Tex.

SOUTHWEST TEXAS LOCAL SECTION	TODD C. STORER, *Chairman*, Pan American Petroleum Corp., Corpus Christi, Tex.; R. B. SALE, *First Vice-Chairman*, The Texas Co., Corpus Christi, Tex.; W. W. WILSON, *Second Vice-Chairman*, Lane-Wells Co., Alice, Tex.; W. J. BIELSTEIN, *Secretary-Treasurer*, Humble Oil & Refining Co., Corpus Christi, Tex.
SNYDER LOCAL SECTION	WILLIAM A. VESTAL, *Chairman*, SACROC, Snyder, Tex.; D. A. NORTH, *First Vice-Chairman*, Humble Oil & Refining Co., Snyder, Tex.; E. C. HUTCHINSON, *Second Vice-Chairman*, Humble Oil & Refining Co., Snyder, Tex.; J. M. EUBANKS, *Secretary, Sun Oil Co., Snyder, Tex.;* BILL H. FRY, *Treasurer*, Schlumberger Well Surveying Corp., Snyder, Tex.
SPINDLETOP LOCAL SECTION	GEORGE B. DOWELL, *Chairman*, Sun Oil Co., Stowell, Tex.; G. P. COKINOS, *Vice-Chairman*, Railroad Commission of Texas, Beaumont, Tex.; CARL B. RUSH, *Secretary*, Pan American Petroleum Corp., Beaumont, Tex.; E. J. NOONE, *Treasurer*, Gulf Oil Corp., Beaumont, Tex.
WEST CENTRAL TEXAS LOCAL SECTION	A. J. EVANS, *Chairman*, Warren Petroleum Corp., Abilene, Tex.; E. L. ANDERS, JR., *First Vice-Chairman*, Consultant, Abilene, Tex.; P. M. BRIDGES, *Second Vice-Chairman*, Russell Engineering, Abilene, Tex.; L. D. WEBSTER, *Secretary-Treasurer*, Katz Oil Co., Abilene, Tex.
WESTERN VENEZUELA PETROLEUM SECTION	R. W. BALDWIN, *Chairman*, Mene Grande Oil Co., Maracaibo, Venezuela; CHRISTOPHER R. MORGAN, *First Vice-Chairman*, Mene Grande Oil Co., Maracaibo, Venezuela; ERNEST ALLEN, JR., *Second Vice-Chairman*, Core Laboratories, de Venezuela, Maracaibo, Venezuela; PETER A. MORENO, *Third Vice-Chairman*, Creole Petroleum Corp., Quirquire, Venezuela; R. L. SEAY, JR., *Secretary*, Richmond Exploration Co., Maracaibo, Venezuela; LOREN A. SCHMIDT, *Treasurer*, Compania Shell de Venezuela, Maracaibo, Venezuela.
WYOMING LOCAL SECTION	L. B. CURTIS, *Chairman*, Continental Oil Co., Casper, Wyo.; J. S. WINN, *Vice-Chairman*, Trigood Oil Co., Casper, Wyo.; D. L. GARTHWAITE, *Secretary-Treasurer*, Pan American Petroleum Corp., Casper, Wyo.
CIM-AIME PETROLEUM ENGINEERING SECTION, CALGARY	S. B. RICHARDS, *Chairman*, Pan American Petroleum Corp., Calgary, Alta., Canada; L. C. STEVENS, *First Vice-Chairman*, Mobil Oil of Canada Ltd., Calgary, Alta., Canada; R. V. [illegible] LAIDLAW, *Second Vice-Chairman*, Husky Oil & Refining Ltd., Calgary, Alta., Canada; J. R. LYON, *Secretary-Treasurer*, Shell Oil Co., Calgary, Alta., Canada.
CIM-AIME PETROLEUM ENGINEERING SECTION, EDMONTON	W. T. WILSON, *Chairman*, Schlumberger Well Surveying Corp., Edmonton, Alta, Canada; D. J. MCEACHERN, *First Vice-Chairman*, Imperial Oil, Ltd., Edmonton, Alta, Canada; H. W. HINKLE, *Second Vice-Chairman*, Pan American Petroleum Corp., Edmonton, Alta, Canada; V. E. BOHME, *Secretary-Treasurer*, Oil & Gas Conservation Board, Edmonton, Alta., Canada.

Effect of Pressure on Rock Drillability

JOHN R. ECKEL
JUNIOR MEMBER AIME

HUMBLE OIL & REFINING CO.
HOUSTON, TEX.

ABSTRACT

A laboratory drilling rig has been devised and placed in operation which permits the application of hydrostatic, terrastatic, and formation pore pressures to a rock sample for drilling under controlled conditions. Calibrated tests of this equipment indicate qualitative agreement with field results on the effect of weight on bit, rotary speed, and rate of circulation on drilling rate. Tests under pressure, using water and air as the drilling fluids, indicate that when drilling saturated limestone samples, a pressure differential between hydrostatic and formation pressure is the only pressure which affects drilling rate. A differential in either direction causes a reduction in rate, but the same differential from the wellbore into the formation causes the greater reduction. Also, in limestone, air favorably affected drilling rate only when compared to water at high hydrostatic pressure, all other conditions remaining constant. Large increases in drilling rate with air could be obtained in the laboratory only while drilling a shale, which offered a limited permeability to nitrogen and which could be drilled with a differential from the formation into the wellbore. In general, the magnitude of the changes due to the pressure effect were small compared to changes in drilling rate obtainable by changing either bit weight or rotary speed.

INTRODUCTION

In the course of Humble's drilling research program, the desirability of investigating several factors which lend themselves to laboratory rather than field study became obvious. Principal reasons for this are the expense involved in field studies and the difficulty of exercising the required degree of control. Of primary importance are investigations of the effect of fluid properties on drilling rate, the effect of pressure on rock drillability, and a study of the fundamental mechanics of rock failure and chip generation.

Several years ago some work in the laboratory on the effect of mud properties on drilling rate was reported to the API[1], but the completion of this work and the investigation of the other variables affecting drilling rate required equipment somewhat more elaborate than that used on these earlier tests. This equipment has been assembled to form Humble's Drilling Engineering laboratory.

To date only the effect of pressure on rock drillability while using water and air has been investigated, and this work is not yet complete. Facilities are available to investigate the effect of fluid properties on rate of penetration, and information is being assembled on a current basis on the mechanics of drilling.

The sequence of presentation in this progress report is somewhat different from that in which the data were obtained since the order of ex-

[1]References given at end of paper.

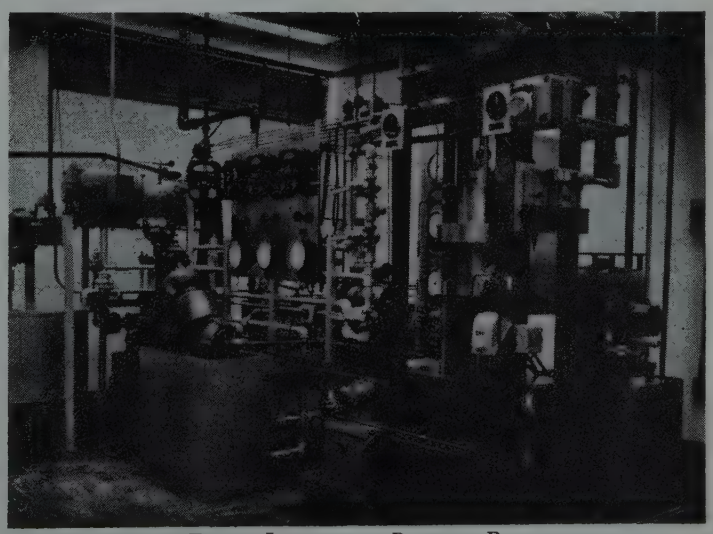

FIG. 1—LABORATORY DRILLING RIG.

Manuscript received in Society of Petroleum Engineers office on July 22, 1957. Paper presented at 32nd Annual Fall Meeting of Society of Petroleum Engineers in Dallas, Tex., Oct. 6-9, 1957.

Discussion of this and all following technical papers is invited. Discussion in writing (three copies) may be sent to the offices of the *Journal of Petroleum Technology*. Any discussion offered after Dec. 31, 1958, should be in the form of a new paper.

periment was controlled to some extent by changes in technique dictated by increased knowledge of the phenomena being investigated. This was done to provide as much continuity as possible and to justify the limited conclusions which are indicated at the present state of the research program.

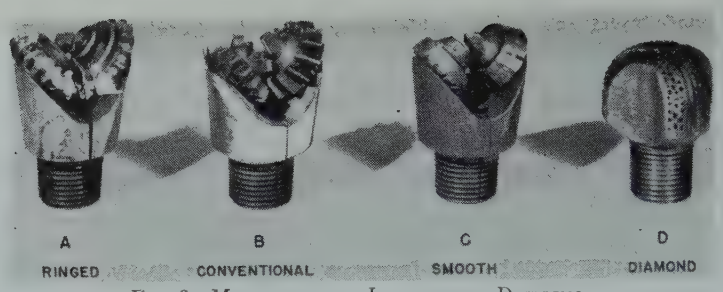

FIG. 3—MICROBITS FOR LABORATORY DRILLING.

DISCUSSION

EQUIPMENT

The equipment comprising this present laboratory drilling rig is shown in Fig. 1. Provision in this equipment is made for circulating mud or water at any pressure up to 5,000 psi for the application of hydrostatic, terrastatic and formation pore pressure to duplicate the pressure environment of rock in a drilling well. The equipment will also circulate air as the drilling fluid. The bit is driven by a variable speed hydraulic motor and bit weight is applied by a hydraulic cylinder, the rate of movement of which is timed for drilling rate indication. Hydrostatic, terrastatic, and formation fluid pressures are applied by three separate but similar systems, each consisting of a remotely controlled plunger pump for pressure generation and a remote pressure controller and diaphragm-operated valve for control purposes. These three pressures are denoted by the symbols, P_h, P_t, and P_f, respectively, on the drilling rate graphs in this report. For the high pressure tests the circulation pump takes suction at the elevated pressure through a strainer to minimize the horsepower requirements for circulation. For the air drilling experiments, the circulation rate can be remotely controlled from the driller's position and is recorded on an orifice meter.

In Fig. 2 the drilling chamber is shown in cross section. An artificial annulus is utilized so that packing on moving parts is required for only one type of motion at each seal. It will be noted that the bit rotates and that loading is accomplished by forcing the rock into the bit rather than requiring vertical motion of the drill stem.

This system was designed to use 1¼-in. two-cone microbits. In addition to these bits, diamond bits of various types in this size have also been utilized. Some of the different bits used in the laboratory study are pictured in Fig. 3. The results presented in this report were obtained using the 1¼-in. two-cone microbits. Only preliminary testing has been done using the miniature diamond bits and all designs in this type of bit obtained so far have been such that it has been impossible to maintain a constant rate of circulation while drilling. To solve this particular problem the rate of circulation control equipment has been made more flexible and bits with more adequate circulating ports have been ordered.

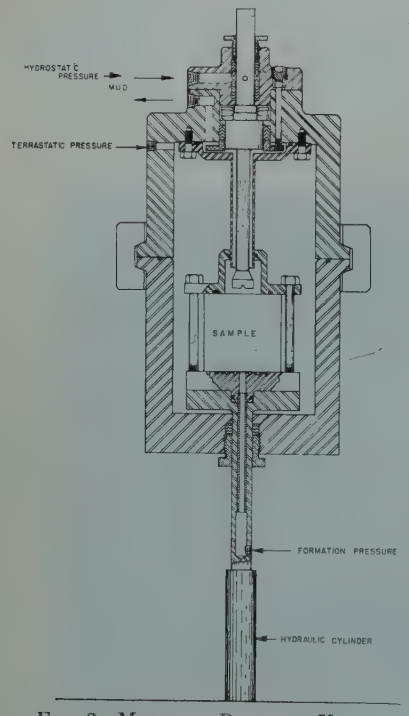

FIG. 2—MICROBIT DRILLING UNIT.

SAMPLE PREPARATION

The bulk of the material drilled in the laboratory studies has been quarry stone, although some work has been done with core samples. The quarry rock was selected to improve formation uniformity and due to its ready availability in quantity. Sample preparation is similar for both types of rock. This consists of jacketing the samples by coating with an epoxy resin. This jacketing procedure is necessary to separate the applied pressures when drilling a permeable sample.

The epoxy jacketing seals the entire rock except for uncoated circular areas on the top and bottom of the sample which allow the hydrostatic and formation pressures to be introduced into the pores. O-ring seals are maintained around these uncoated circular areas to insure separation between the pressures introduced into the rock and the terrastatic pressure which is applied to the jacketed surfaces of the sample. Plastic plates are placed against the top and bottom of the samples, before the epoxy jacket has hardened, to provide a surface which will be sufficiently flat and smooth to allow an O-ring seal between the jacket surface and the metal plates above and below the sample.

In addition to jacketing, all permeable samples are vacuum saturated with water. This is done because most geologists consider that all sedimentary rock which occurs in nature below the water table is fluid saturated, since original deposition occurred in water, and that pore space will therefore still contain water only, or water plus some other fluids such as hydrocarbons. Typical data showing drilling rate as a function of hydrostatic pressure for a permeable lime, shale, and marble,

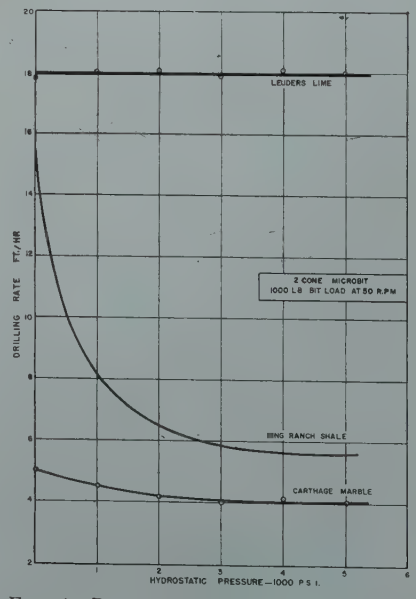

FIG. 4—DRILLING RATE VS HYDROSTATIC PRESSURE.

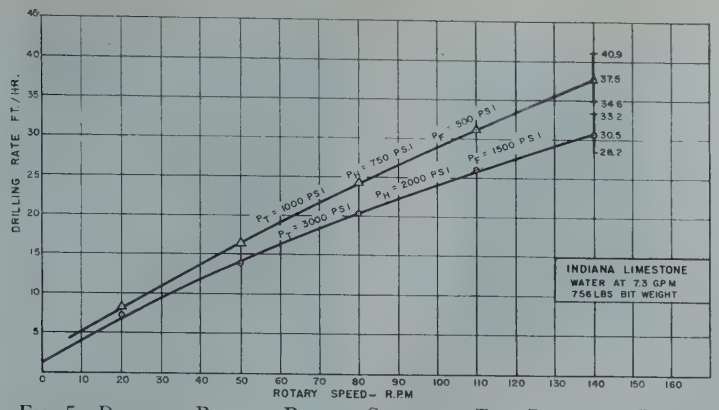

FIG. 5—DRILLING RATE VS ROTARY SPEED FOR TWO DIFFERENT PRESSURE COMBINATIONS.

all unjacketed, are shown in Fig. 4. In this case "hydrostatic pressure" means applied fluid pressure since there is no pressure segregation with unjacketed samples. The limestone and the marble were vacuum saturated while the shale was not, due to its lack of permeability. The marble typically shows an intermediate pressure effect, due, it is believed, to incomplete saturation because of its limited permeability. The limestone shows no pressure effect when the sample is saturated as it occurs in nature, but exhibits a reduction in drilling rate with increasing pressure, similar to that shown for the shale sample, when drilled either in an unsaturated condition (as reported by Murray and Cunningham[2]) or with a pressure differential across the saturated rock (see Fig. 5). It is important then, if field drilling characteristics are to be approached, that the rock be saturated as it is in place in order that realistic results may be obtained.

CALIBRATION OF EQUIPMENT

The first operational requirement in conducting the laboratory drilling investigation was to determine the effect of the recognized variables on drilling rate under laboratory conditions in order that tests might be conducted under conditions that were at least qualitatively similar to those encountered in the field.

The first test was conducted to determine the effect, if any, of depth of penetration into the sample on drilling rate and to determine the variation in drillability of the Indiana limestone which had been selected for the tests. Fig. 6, which shows drilling rate as a function of drilling increment number or depth of penetration, showed that, under the conditions imposed, depth did not affect the rate of penetration. It was further determined from this initial

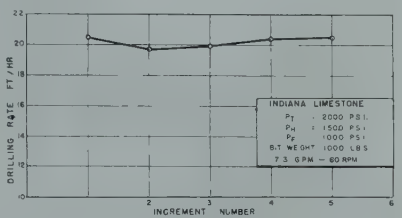

FIG. 6—DRILLING RATE VS DEPTH IN SAMPLE.

series of tests that the drillability variation in this rock from sample to sample and from increment to increment was such that the average of increments in each of six samples was required to obtain data which on the average would vary from the true mean by no more than 10 per cent. This system of statistical data handling has been used on all succeeding experiments.

The effects of the following on drilling rate were then investigated: (1) bit weight at constant rotary speed and rate of circulation, (2) rotary speed at constant bit weight and rate of circulation, and (3) rate of circulation at constant bit weight and rotary speed. Results of these tests are shown graphically in Figs. 7, 8, and 9. Results obtained were generally in qualitative agreement with field experience. That is, at constant rotary speed and rate of circulation, drilling rate is a linear function of bit weight until cleaning limitations are reached. Also, drilling rate, at constant bit weight and rate of circulation, is linear with rotary speed under similar limitations. The effect of this limitation can be seen in Fig. 9. With water as the circulating medium, and at a bit load of 2,500 lb and a rotary speed of 60 rpm, the drilling rate increased linearly with rate of circulation, indicating that the maximum rate of a little more than 7 gal/min was not adequate to insure full cleaning of the hole. At a bit load of 1,000 lb a saturation effect at this

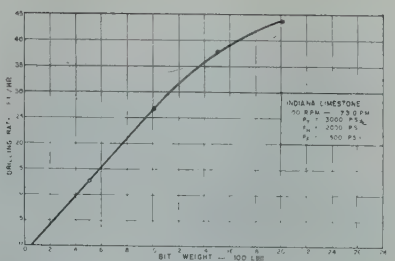

FIG. 7 — DRILLING RATE VS BIT WEIGHT.

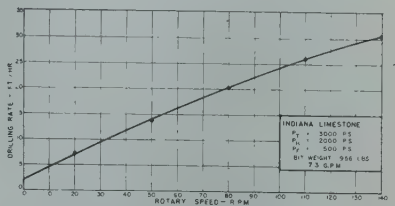

FIG. 8 — DRILLING RATE VS ROTARY SPEED

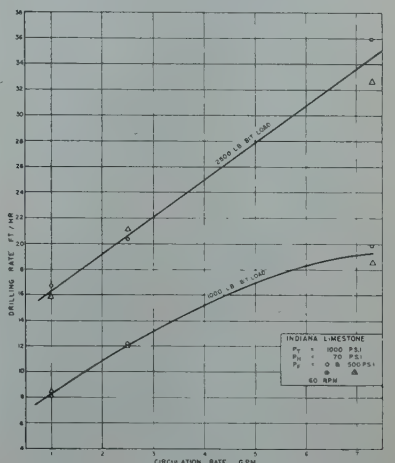

FIG. 9 — DRILLING RATE VS CIRCULATION RATE.

maximum rate of circulation is noted, indicating that the rate under these conditions was adequate for full cleaning.

EFFECT OF PRESSURE ON ROCK DRILLABILITY

Following the calibration tests, a series of experiments were conducted under conditions of constant bit load and constant rate of circulation to determine the effects of the three pressures at variable rotary speeds. For this experiment terrastatic pressures of 1,000 and 3,000 psi were compared. The formation pressure was made equal to one-half the terrastatic pressure and the hydrostatic pressure was made equal to the formation pressure, plus over balance, or in this case, 750 and 2,000 psi. The results shown in Fig. 5 indicate an average reduction in drilling rate of 18 per cent when the terrastatic, hydrostatic and formation pressures were changed from 1,000, 750, 500 to 3,000, 2,000, and 1,500 psi, respectively. These particular pressures were selected since they correspond

with normal conditions in field drilling. The curves shown in Fig. 5 are plotted through the root mean square values of the experimental data and the scatter in these data points are indicated at the extreme values to give an index to the reproducibility of the experiment.

The results of a test conducted to determine the effect of formation pressure on drilling rate for various bit weights and under conditions of constant rotary speed, rate of circulation, terrastatic pressure and hydrostatic pressure are shown in Fig. 10. This test indicates that increasing the formation pressure above the hydrostatic pressure may cause reduced drilling rate. A similar test comparing the effects of hydrostatic pressure on drilling rate at various rotary speeds, under otherwise constant conditions, is shown in Fig. 11. In this case the pressure differentials from the wellbore into the formation

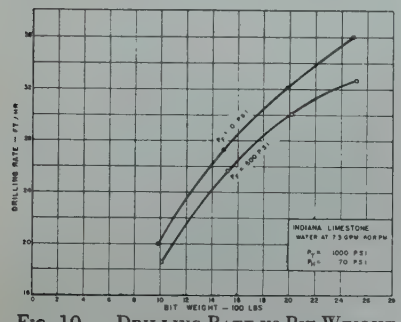

FIG. 10 — DRILLING RATE VS BIT WEIGHT FOR TWO DIFFERENT FORMATION PRESSURES.

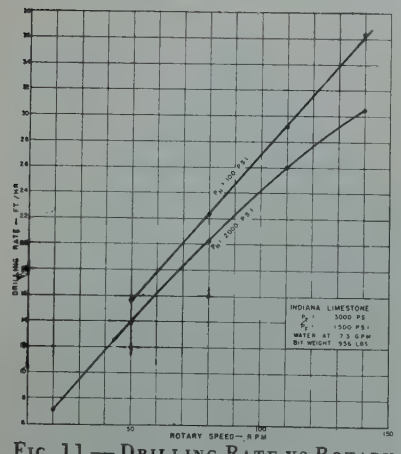

FIG. 11 — DRILLING RATE VS ROTARY SPEED FOR TWO DIFFERENT HYDROSTATIC PRESSURES.

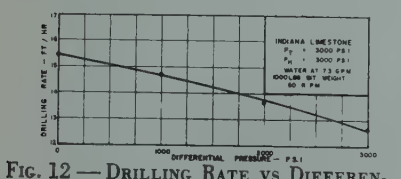

FIG. 12 — DRILLING RATE VS DIFFERENTIAL PRESSURE FROM WELL-BORE INTO FORMATION.

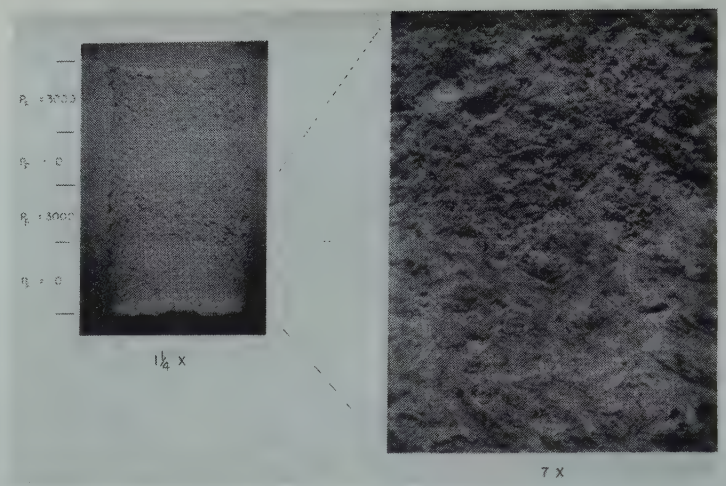

FIG. 13—SECTION OF DRILLED SAMPLE. TERRASTATIC AND HYDROSTATIC PRESSURE = 3,000 PSI.

also caused a reduction in the drilling rate.

Additional tests were then performed in which the differential of hydrostatic pressure over formation pressure was varied from 0 to 3,000 psi. It was found that an increase in this differential was accompanied by a reduction in drilling rate of as much as 27 per cent at the maximum differential of 3,000 psi (see Fig. 12). In all cases maximum drilling rate has been obtained when the formation fluid pressure and the hydrostatic pressure were equal. A significant differential in these pressures in either direction caused a reduction in drilling rate, although an increase in hydrostatic over formation pressure caused the greater reduction.

This laboratory investigation of the effect of pressure on drilling rate divides itself into two phases. The first phase is to determine which pressures or differential pressures cause this effect. This part of the work, at least for the lime samples tested, appears to be complete. The more difficult, or second phase, that is, the mechanics through which pressure or pressure differential accomplishes this reduction, and what, if anything, may be done to control this reduction, is the problem still to be investigated.

A visual indication of the change that takes place in the rock with a change in pressure of this magnitude is shown in Fig. 13. Under conditions of differential pressure the rock apparently becomes more plastic. The wall "plasticizing" effect takes place simultaneously with the drilling operation as shown by the alternate bands in the figure. That is, the observed effect is a plasticizing effect and not just a layer of cuttings plastered against the wall of the hole by the outward flow of fluid from the hole. If cuttings were being plastered against the hole by an outward flow, the upper "open pore bands" in Fig. 13 would have been coated when the final increment was drilled with a high differential pressure into the rock pores.

AIR DRILLING

Concurrent with the investigation of the effects of pressure on drilling rate when using water as the circulating medium, tests were conducted to determine the effect of air on drilling rate. The amount of air required for adequate cleaning was determined first. The results of this test are shown in Fig. 14 which corresponds to Fig. 9 for water. It will be noted that drilling rate increased almost linearly with rate of air circulation up to about 28 scf/min. For further air rate increases the saturation effect indicated that cleaning was adequate. This limit for adequate circulation having been determined, all succeeding tests were conducted at a circulating rate of 40 scf/min. Air drilling rates, with different bit types, were determined as a function of bit weight and were compared to

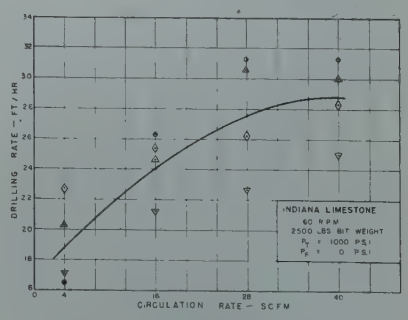

FIG. 14—DRILLING RATE VS AIR CIRCULATION RATE.

water drilling rates under similar and also under higher pressures. These results for Indiana lime are shown in Figs. 15, 16, and 17, and for marble are shown in Figs. 18, 19, and 20. It may be seen in these figures that neither air nor water drilled consistently faster under reduced pressures. However, the drilling rate with water was significantly reduced when the water was under a hydrostatic pressure equal to that which would be exerted by a column of fluid in a drilling well. This would indicate that, when circulating sufficient air or sufficient water to provide adequate cleaning (as was possibly not the case in the 750 psi water curve in Fig. 15), there is no essential difference in the drilling rates obtainable with air and water under similar conditions of pressure. Although the greatest improvements in field penetration rates with air or gas are obtained in shale, some improvement is also reported in lime. These laboratory results suggest then that either the comparable field water circulation rates were not adequate for full cleaning or that some additional difference occurs in the field that is not present in the laboratory.

The reduced pressure curves in Figs. 15, 16, and 17 have been rearranged in Figs. 21 and 22 to facilitate comparison of the drilling characteristics of the three different bits in water and air. The three bits are shown as A, B, and C in Fig. 3. Bit A, with ringed cutter cones, drilled almost as fast as Bit B equipped with conventional cones. Bit C, the smooth cone bit, drilled approximately half as fast as Bits A and B.

One other observation in connection with the smooth cones which is not reflected in the drilling rate curves, except in that this bit was able to drill at all, is that the cuttings generated were generally larger than those obtained with the conventional bit. This was discovered when the larger cuttings bridged in the circulating passages in the test chamber (this difficulty with the conventional bit cuttings had not been experienced) and required that clearances be increased in order that tests of this bit could be continued. A more quantitative measure of this effect is not possible due to the distance the cuttings must be transported from the bottom of the hole to the strainer where they are collected.

In addition to the air drilling experiments using the quarry samples, a series of tests were conducted on a silty shale which exhibited a limited permeability to nitrogen. The results and conditions of this test are shown in the form of bar graphs in Fig. 23. Under conditions of equal pressure, as was the case in the quarry samples, drilling rates for air and water were approximately equal (Bars 2 and 3). Increased hydrostatic pressure with water caused a marked reduction in drilling rate (Bar 1). Increased terrastatic pressure caused a reduction in drilling rate (Bars 3 and 4). However, increased formation pressure, contrary

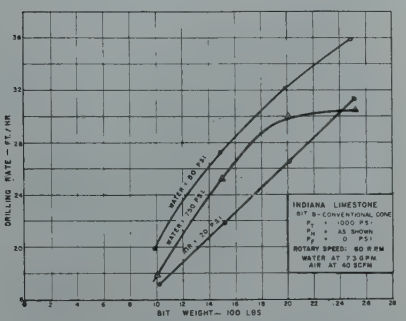

FIG. 15 — DRILLING RATE VS BIT WEIGHT FOR WATER AND AIR AT REDUCED PRESSURE AND FOR WATER AT A HIGHER PRESSURE.

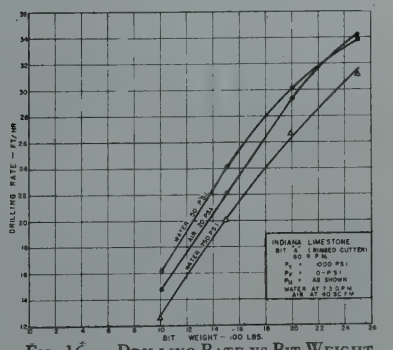

FIG. 16 — DRILLING RATE VS BIT WEIGHT FOR WATER AND AIR AT LOW PRESSURE AND FOR WATER AT A HIGHER PRESSURE.

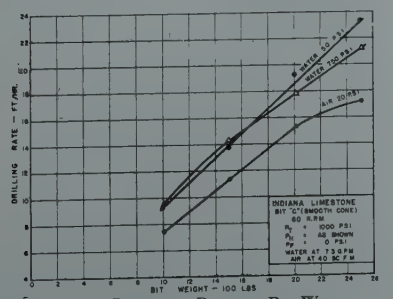

FIG. 17 — DRILLING RATE VS BIT WEIGHT FOR WATER AND AIR AT LOW PRESSURE AND FOR WATER AT A HIGHER PRESSURE.

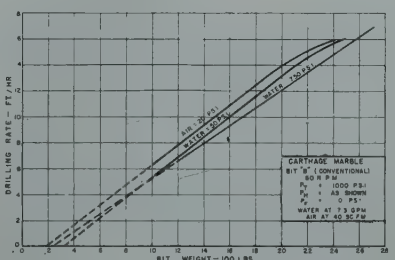

FIG. 18 — DRILLING RATE VS BIT WEIGHT FOR WATER AND AIR AT LOW PRESSURE AND FOR WATER AT A HIGHER PRESSURE.

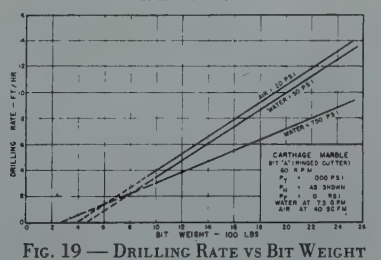

FIG. 19 — DRILLING RATE VS BIT WEIGHT FOR WATER AND AIR AT LOW PRESSURE AND FOR WATER AT A HIGHER PRESSURE.

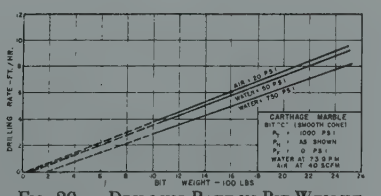

FIG. 20 — DRILLING RATE VS BIT WEIGHT FOR WATER AND AIR AT LOW PRESSURE AND FOR WATER AT A HIGHER PRESSURE.

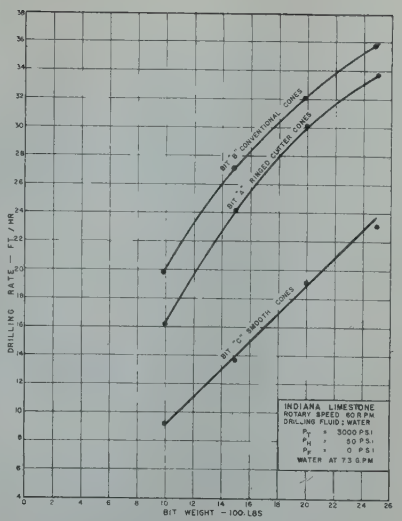

FIG. 21—DRILLING RATE VS BIT WEIGHT FOR THREE BIT TYPES IN WATER.

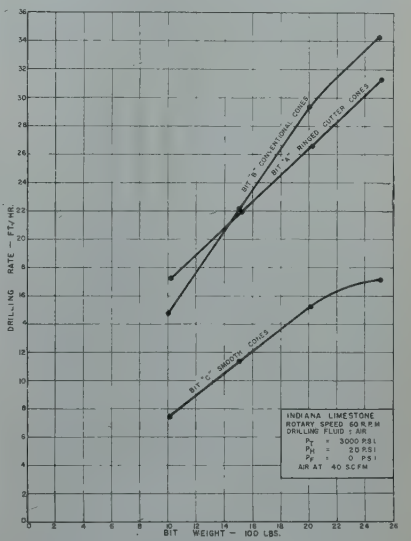

FIG. 22—DRILLING RATE VS BIT WEIGHT FOR THREE BIT TYPES IN AIR.

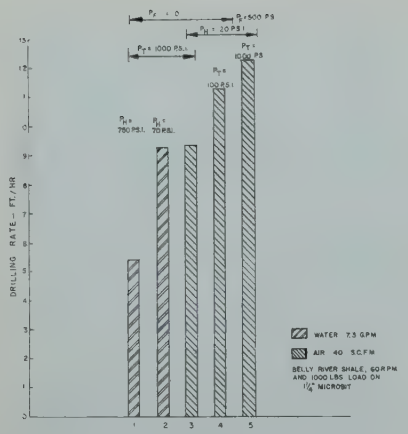

FIG. 23—EFFECT OF PRESSURE ON DRILLING RATE.

to previous experience with the quarry samples, caused an increase in drilling rate (Bars 3 and 5). This reduced differential effect is believed to be an indication of the reason that best results from the use of air or gas in the field have been obtained while drilling shales.

CONCLUSIONS

1. Tests with the variables, weight on bit, rotary speed, and rate of circulation, the effects of which have been established in the field, have shown a good correlation between field and laboratory results. It appears reasonable to assume, then, that laboratory tests with variables possessing heretofore unknown effects will yield results which will substantially conform to corresponding drilling characteristics in the earth. It is not presumed that the stresses induced in the rock sample by the three pressures applied in the laboratory precisely duplicate those induced in a block of rock below the earth's surface. However, the application of these pressures approaches the natural stress configuration with a great deal more reality than the application of only one pressure to the entire rock, as has been done in the laboratory prior to the construction of this apparatus.

2. Tests with air drilling have indicated that increased drilling rates achieved in the laboratory have resulted through no characteristic of the air other than its relatively low static pressure at the bottom of he hole. Air and water exhibited similar drilling characteristics when used at near equal static pressures and when circulated with sufficient volume to provide ample hole cleaning. Air favorably affected drilling rate only when compared to water at high static pressure, all other conditions remaining constant.

3. Pressure tests with limestone have shown that drilling rate in that rock is substantially affected only by the differential between the hydrostatic pressure and the formation pressure. A differential in either direction causes a reduction in drilling rate, but an increase of hydrostatic pressure over formation pressure has a much greater effect than a differential in the opposite direction.

Shale samples exhibited a pressure effect; but, in this case, the effect was primarily due to the magnitude of the hydrostatic pressure. A possible explanation for the difference between the pressure reactions in the shale and in the limestone might lie in the fact that the limestone samples were satisfactorily saturated while the shale samples were not.

It should also be noted that the magnitude of the pressure effects observed in the course of these experiments has been relatively small and generally much less than can be caused by a moderate change in either bit load or rotary speed.

4. While the phenomena to be investigated in the laboratory have been separated into three categories: (a) the effect of pressure, (b) the effect of fluid properties on rock drillability, and (c) a study of the fundamental mechanics of rock failure, it appears that considerable work must be done in each field in order to understand any single one of them; this is due to their very close relationship. For that reason, work has begun on investigating the effect of fluid properties on drilling rate, and data are currently being accumulated on rock failure.

ACKNOWLEDGMENT

The author wishes to thank the management of Humble Oil & Refining Co. for permission to publish this paper and to acknowledge the assistance of his associates, particularly W. E. Holland and P. L. Moore, who worked with him on this problem.

REFERENCES

1. Eckel, John R.: "Effect of Mud Properties on Drilling Rate," API Division of Production, Southwest District Meeting (March, 1954).
2. Murray, A. S., and Cunningham, R. A.: "Effect of Mud Column Pressure on Drilling Rates," *Trans.* AIME (1955) **204**, 196. ★★★

Miscible Displacements of Reservoir Oil Using Flue Gas

H. A. KOCH, JR.
C. A. HUTCHINSON, JR.
MEMBERS AIME

THE ATLANTIC REFINING CO.
DALLAS, TEX.

SUMMARY

Miscible phase displacement of oil from reservoirs has been emphasized in the past few years.[1,2,3,4,5,6,7,8,9] The reason for this emphasis lies in the high oil recovery attainable by this process. Removal of capillary effects in the reservoir leads to recoveries approaching 100 per cent in the area contacted by the miscible phase.

The miscible slug process[7,8,9] is one means of obtaining a miscible displacement. Here a band or slug of LPG is injected into the reservoir prior to gas injection. The idea is to maintain the band of LPG "wedged" between the gas and oil phases and thus achieve a miscible phase displacement. A second method for achieving miscibility is through the injection of a gas which is not miscible with the reservoir fluid but which develops a zone of miscibility in the reservoir through mass transfer with the reservoir oil.[2] This mass transfer results in either an enrichment of the lean injected gas by intermediates from the oil or an enrichment of the oil by intermediates from a rich injection gas or one that has been enriched on the surface by LPG addition. We are interested here in discussing the process in which miscibility is developed at the displacement front by the evaporation of intermediates from the oil phase into the gas phase. This process "builds up" its own slug of miscible material at the displacement front and therefore does not require the injection of LPG to obtain miscibility. Each process has its own area of applicability. Generally, the high pressure gas process is applicable only with reservoir fluids which contain a high concentration of intermediates. If the high pressure gas process is technically feasible at pressures less than 4,500 psi, it is probably more desirable economically than the slug process. The slug process has broad applicability in the shallower reservoirs and with reservoir fluids which contain a relatively low concentration of LPG and natural gasoline constituents.

This paper deals with some new concepts of the high pressure gas injection process where it is proposed that flue gas can be substituted for hydrocarbon gas without sacrificing our goal of miscibility.

MECHANISM

Introduction

Considerable effort has been devoted to study of the mechanics of the high pressure gas injection process.[1,2,3,4,5,6] One generalization resulting from some of these studies[1,2,3,4] was that the composition of the injected gas is relatively unimportant in establishing the miscibility pressure* for a given reservoir fluid. This generalization is correct for the composition range of gases typically encountered in the field. Two such gases are a gasoline plant tail gas containing 85 per cent methane and 15 per cent ethane, and a field separator gas containing 70 per cent methane and 30 per cent heavier components. The most important factor which sets the miscibility pressure in the operation is the reservoir fluid composition, particularly the concentration of LPG-natural gasoline constituents. The injected gas is the agent by which the LPG-natural gasoline constituents are concentrated at the displacing front to create a miscible displacement. Based on these results, it appeared feasible that some inexpensive gas, such as flue gas, might be substituted for hydrocarbon gas for use in the high pressure gas process. A re-examination of the phase relations of the high pressure gas injection process should clarify the principle behind using flue gas (essentially nitrogen) as an injection gas.

Three Component Diagram

The phase relations of the high pressure gas injection process have been illustrated by the use of the three component diagrams.[2,6] In Fig. 1 we have arbitrarily represented the multi-component reservoir system by three components; methane, ethane through hexane, and heptanes plus. The solid curve ABC is the phase boundary curve. It represents the locus of compositions which have a fixed saturation pressure at a fixed temperature; the lower branch AB shows bubble point compositions, the upper branch BC, the dew point compositions. Point B is the composition of the critical mixture at this temperature and pressure. The dashed lines (tie lines) connect vapor and liquid compositions which are in equilibrium.

Let us consider Reservoir Fluid D which we wish to displace in a miscible manner by gas injection. Let us further restrict the discussion to the case where miscibility between an injection gas and the reservoir fluid at the displacement front is developed by gas enrichment in the reservoir. For this case, any gas whose composition lies between Points C and E on the right side of the three component diagram can be used to give a miscible displacement of Reservoir Fluid D. This is true because the more mobile injected gas moves faster than the displaced oil and is in continuous contact with virgin oil at the displacement front. This leads to a continuing enrichment of the gas at the displacement front by evaporation of the $C_2 - C_6$

Original manuscript received in Society of Petroleum Engineers office on July 22, 1957. Paper presented at 32nd Annual Fall Meeting of Society of Petroleum Engineers in Dallas, Tex., Oct. 6-9, 1957.
[1]References given at end of paper.

*Miscibility pressure means the minimum reservoir pressure required for developing a miscible phase displacement.

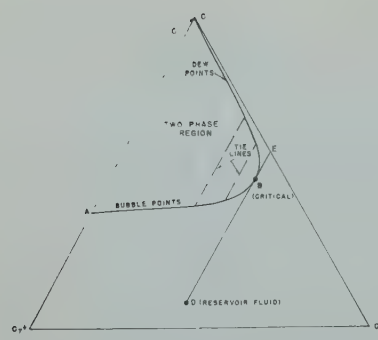

FIG. 1—PHASE RELATIONS FOR MISCIBLE-TYPE HIGH PRESSURE GAS INJECTION PROCESS.

fraction until Composition B is reached by the gas phase. Since Composition B is miscible in all proportions with the reservoir fluid Composition D, the displacement of the reservoir fluid from this point forward is miscible and approaches 100 per cent.

In practice some oil is by-passed at the front due to small scale pore system inhomogeneities, and this material is either added to the volume of oil flowing in the transition zone between Compositions D and B, or is by-passed permanently as a nonflowing phase in the region of flowing gas phase. In the latter case the intermediates will be evaporated into the gas phase, broadening the region of enriched gas. This material will be recovered late in the life of the project. In reservoir applications the length of the transition zone between Compositions B and D is large compared to small scale inhomogeneities, and thus, the amount of oil permanently by-passed is small.

We have reviewed briefly the phase relations of the high pressure gas injection process where a miscible displacement is developed by enriching in the reservoir the lean injected gas to the point that it is miscible with the oil at the displacement front. Since in this process the composition of injected gas appears relatively unimportant, we designed an experimental program to test the substitution of flue gas for the previously employed lean natural gas.

A second use of flue gas is in miscible slug process applications. Here flue gas is considered for use in following a slug of hydrocarbon gas in a high pressure gas injection operation, or in following a propane slug in a miscible slug process application. We will cover the basic idea first.

In our laboratory work we have used nitrogen instead of flue gas which is about 12 per cent CO_2 and 88 per cent N_2. In the reservoir the flue gas front will be essentially 100 per cent N_2 in that the CO_2 will be stripped from the gas stream by solution in the interstitial water.

EFFECT OF INJECTED GAS COMPOSITION

Reservoir Fluid A, whose properties are shown in Table 1, was used in this study. Table 2 summarizes the results of displacing this fluid from a 123 ft unconsolidated sand packed column at various pressures by four gases of different compositions. The gases used were 100 per cent nitrogen, 100 per cent lean gas (85 per cent C_1, 15 per cent C_2), and two mixtures of the foregoing gases (one 15 per cent nitrogen, the other 66 per cent nitrogen).

Fig. 2 presents the results of these displacements as oil produced at gas breakthrough vs reservoir pressure. For a specific injected gas composition the recovery at breakthrough is a function of pressure up to miscibility pressure. Breakthrough recovery increases with pressure increase.

At and above the miscibility pressure, the breakthrough recovery is a constant. The effluent high pressure stream from the core is a single phase when operating at or above the miscibility pressure. As observed in a windowed cell, this high pressure effluent changes gradually from the single phase virgin oil before breakthrough to a single phase gas at abandonment. (Abandonment gas-oil ratio was chosen as 30,000 scf/STB).

At sufficiently high pressure two simultaneously flowing phases will not appear. The minimum reservoir pressure at which this occurs is the miscibility pressure. The miscibility pressure for 100 per cent nitrogen was found to be 3,870 psi. This is only 370 psi greater than the 3,500 psi miscibility pressure determined for 100 per cent lean gas. The miscibility pressures for the other gases were 3,730 psi for 66 per cent nitrogen and 3,700 for 15 per cent nitrogen. It is noteworthy that there is a relatively small spread in miscibility pressures over a fairly wide range of injected gas compositions. That is, the miscibility pressure only increased from 3,700 psi to 3,730 psi when the nitrogen content of the injected gas was increased from 15 per cent to 66 per cent. The addition of the first 15 per cent nitrogen to the injection gas increased the miscibility pressure by 200 psi (from 3,500 psi to 3,700 psi). Increasing the nitrogen content of the injected gas from 66 per cent to 100 per cent increased the miscibility pressure from 3,730 psi to 3,870 psi. These data suggest that dilution of nitrogen with relatively small amounts of hydrocarbon gas can be helpful in reducing the miscibility pressure.

TABLE 1

Component	Reservoir Fluid Designation A	B	C	D
N_2	...	0.8	0.3	.
C_1	42.7	13.0	21.2	51.4
C_2	12.5	13.2	10.0	11.2
C_3	10.2	13.3	11.3	8.8
C_4's	6.2	8.4	8.5	5.4
C_5's	3.8	6.1	6.2	2.6
C_6	3.3	4.5	5.2	1.8
C_{7+}	21.3	40.7	37.3	18.8
	100.0	100.0	100.0	100.0
MWC_{7+}	191	197	194	142
Bubble pt. psig	2,760	905	1,240	3,780
Temp. ° F	140	176	176	237

GAS COMPOSITIONS

Component	Flue Gas	Lean Gas
N_2	88.0	1.0
C_1		88.0
C_2		8.6
C_3		0.3
CO_2	12.0	2.1
	100.0	100.0

TABLE 2

Run No.	Injection Gas Composition % N_2	Injection Pressure psig	Stock Tank Oil Recovery % of OIP Initially At Breakthrough	Ultimate**
L-2	0	2900	53.2	66.0
L-20	0	3250	66.4	76.6
L-19	0	3500	82.0	95.4
L-1	0	4000	82.0	95.0
L-44	15	3500	68.0	77.5
L-45	15	3600	74.0	82.9
L-46	15	3700	80.4	86.0
L-42	66	3500	67.3	76.5
L-41	66	3700	77.9	87.3
L-40	100	2900	49.2	59.6
L-38	100	3500	67.2	69.4
L-37	100	3800	77.6	83.6
L-39	100	4000	80.6	83.2
L-32	100	4300	80.6	84.7

*Lean gas composition is shown in Table 1.

Additional experiments were carried out above the miscibility pressure using 100 per cent nitrogen as the injection gas to check the value of the ultimate displacement efficiency. Table 3 lists the results of displacing Reservoir Fluid A from a 143 ft unconsolidated sand column at 4,000 psi by nitrogen and compares them with miscible lean gas sweeps. The 143-ft core was formed by joining in series the 123-ft sand column with a 20-ft sand column of the same diameter. This scheme pro-

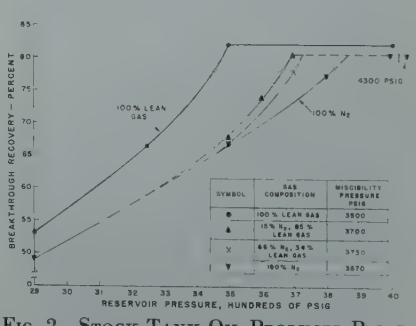

FIG. 2—STOCK TANK OIL PRODUCED PRIOR TO GAS BREAKTHROUGH AS A FUNCTION OF RESERVOIR PRESSURE AND INJECTION GAS COMPOSITION. 123 FT UNCONSOLIDATED SAND COLUMN—RESERVOIR FLUID A.

vided for analysis of the residual oil value in each core separately.

The ultimate displacement efficiency in the first 123 ft of this column was 83.2 per cent for the nitrogen sweep as compared to 95.0 per cent for lean gas sweep. In the final 20 ft of the 143-ft sand column the ultimate displacement efficiency had increased to 94 per cent with nitrogen injection, which compares favorably to the 95.3 per cent obtained by use of lean gas in this length core. This result is interpreted to mean that with nitrogen it takes longer (more contacts) to develop miscibility. As a result, more of the oil is by-passed in the first 123 ft when nitrogen is the injection gas. However, for longer reservoir path lengths (approaching field dimensions), the quantity of intermediates is sufficient in both cases to lead to an ultimate recovery in the order of 97 to 98 per cent. The small difference observed in laboratory core oil recovery at gas breakthrough between the miscible nitrogen and miscible lean gas sweep (82 per cent for lean gas, 80.6 per cent for nitrogen) is probably due to the longer path length required to reach miscibility in nitrogen injection.

In summary, it was found that nitrogen could be substituted for hydrocarbon gas for use with the favorable Reservoir Fluid A, without seriously increasing the miscibility pressure. Furthermore, there was a broad range of gas compositions over which there was an inappreciable change in miscibility pressure. This helped substantiate the concept that injected gas composition was relatively unimportant. To check this further it was decided to do some additional work on the effect of reservoir fluid composition on the miscibility pressure using nitrogen as the injection gas.

Effect of Reservoir Fluid Composition

When a natural gas, which is substantially methane, is used to displace an oil, the miscibility pressure was found to be determined by the fraction of LPG-natural gasoline constituents in the oil (the $C_2 - C_6$ fraction). As a result of the present study dealing with the use of nitrogen as the injection gas, a new concept evolved. That is, when an inert injection gas is used the concentration of methane as well as of the LPG-natural gasoline constituents in the reservoir fluid is important in fixing the miscibility pressure.

The presence of sizable quantities of methane in the reservoir fluid is helpful in volatilizing the $C_2 - C_6$ fraction into the gas stream. The presence of methane in the nitrogen-lean gas mixtures used as injection gases (described earlier) probably causes a similar result. Displacements by nitrogen of reservoir fluids containing various amounts of methane illustrate this effect. For this study the reservoir pressure was fixed at 4,300 psi, and displacements were made from the 123 ft unconsolidated sand column. The $C_1 - C_6$ fraction was varied in this study by varying the proportion of separator gas and liquid in the reservoir fluid mixture. The $(C_2 - C_6)/C_{7+}$ ratio remained essentially constant. The highest saturation pressure fluids contained the highest methane concentration.

TABLE 3

Core Length ft	Injection Gas	Displacement Efficiency Per Cent*
0-20	Nitrogen	77.3
0-20	Lean Gas	91.1
0-123	Nitrogen	83.2
0-123	Lean Gas	95.0
123-143	Nitrogen	94.0
123-143	Lean Gas	95.3

*Displacement efficiency determined by analysis of residual oil left in column after abandonment conditions (gas-oil ratio = 30,000 scf/STB) have been reached.
Displacement efficiency equals 100 minus the residual oil saturation (expressed as per cent of oil originally in place).

Table 4 summarizes the results obtained in these displacements. Fig. 3 is a plot of oil recovery at breakthrough vs saturation pressure and shows that 4,300 psi is the miscibility pressure for a reservoir fluid having a saturation pressure of 2,600 psi at 176° F. For saturation pressures above 2,600 psi, the minimum miscibility pressure is less than 4,300 psi. Thus, the minimum miscibility pressure and the saturation pressure approach each other. In the limit, the minimum miscibility pressure must be somewhat above the saturation pressure to satisfy the requirement that the reservoir be undersaturated in a miscible-type high pressure gas operation.

Analyses of the gas and liquid phases flowing from the core were made in many of these displacements and the results are plotted on the triangular diagram shown in Fig. 4. (Several reservoir fluids are included in this figure for comparison). In this diagram, methane (C_1) is included as an intermediate, and the "three" components are then N_2, $C_1 - C_6$, and C_{7+}. Such a plot is not thermodynamically rigorous, but it has value in that generalizations resulting from such a representation have been confirmed experimentally.

It can be seen in Fig. 4 that as the concentration of the $C_1 - C_6$ fraction in the reservoir fluid is increased, the compositions of the phases in equilibrium at the front approach each other. Finally, when the reservoir fluid composition reaches Point A (or a saturation pressure of 2,600 psig as shown in Fig. 3), a miscible phase displacement is achieved at 4,300 psi. Thus, it can be seen that methane in the reservoir fluid is acting as an intermediate when nitrogen is used as an injection gas.

A further observation from these data is that the spread in miscibility pressures between nitrogen and lean gas injection decreases with increasing methane in the reservoir fluid (this assumes the $C_2 - C_6$ concentration is fixed). An example of this is Reservoir Fluid B which requires reservoir pressures in excess of 4,300 psi to reach miscibility with nitrogen while only 3,400 psi is needed for lean gas. (Table 5 presents the results of the lean gas displacements of Reservoir Fluid B). This is a spread of over 900 psi compared to only a 370 psi spread between lean gas and nitrogen for Fluid A. This means that the injected gas composition is more important with the lower saturation pressure crudes.

The qualitative phase relations for systems containing nitrogen are illustrated in the tetrahedron shown in Fig. 5. Here the front face contains the familiar three component system C_1, $C_2 - C_6$, and C_{7+}. The far corner of the tetrahedron is the 100 per cent nitrogen apex. The phase boundary is the surface of a solid whose important areas are shaded in Fig. 5. If Reservoir Fluid D is displaced by methane, C_1, the critical Composition C is developed at the front and miscibility results. If Reservoir Fluid D is displaced by N_2 at the miscibility pressure a critical composition such as E is developed at the front and miscibility results because Composition E is completely miscible with Reservoir Fluid D. As methane is removed from the Reser-

TABLE 4

Run No.	Reservoir Fluid (Table 1)	Saturation Pressure* psig at 176° F	Stock-Tank Oil Recovery Per Cent of OIP Initially: At Breakthrough	Ultimate
L-30	B	905	65.8	66.5
L-34	C	1,240	64.3	69.5
L-35	--	2,340	77.4	84.4
L-32	A	2,760**	80.6	84.7
L-33	--	3,000	80.6	82.6

*Various saturation pressures were obtained by mixing separator liquid and separator gas† to the desired saturation pressures.
**This run was made at 140° F. The small difference in temperature (140° F compared to 176° F) has a negligible effect on the displacement results.
†The products were obtained by flash separation of Reservoir Fluid A at 300 psig.

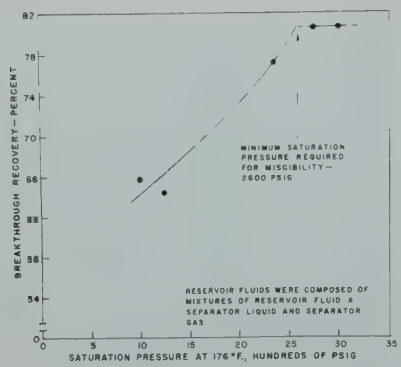
BREAKTHROUGH RECOVERY—PERCENT
SATURATION PRESSURE AT 176°F., HUNDREDS OF PSIG
MINIMUM SATURATION PRESSURE REQUIRED FOR MISCIBILITY—2600 PSIG
RESERVOIR FLUIDS WERE COMPOSED OF MIXTURES OF RESERVOIR FLUID A SEPARATOR LIQUID AND SEPARATOR GAS

FIG. 3—EFFECT OF SATURATION PRESSURE ON MISCIBILITY PRESSURE. NITROGEN DISPLACEMENTS FROM 123 FT UNCONSOLIDATED SAND COLUMN AT 123 PSIG—176° F.

voir Fluid D, the phase relations become less favorable for obtaining a miscible phase displacement with nitrogen. In the extreme, if all the methane were removed from Composition D, Composition G would result, and very high pressures would be required for the obtention of a miscible phase displacement with N_2. For this extreme case, the composition of the reservoir fluid would have to be at Point F to obtain a miscible phase displacement.

VOLUME ADVANTAGE

An added advantage of flue gas over hydrocarbon gas arises from its pressure-compressibility relationships. In the range of 1,000 to 4,000 psig usually encountered in reservoir operations the number of standard cubic feet of flue gas required to produce a reservoir volume of gas is significantly lower than the requirement for natural gas. Fig. 6 shows the ratio of standard volumes of flue gas to standard volumes of natural gas to form one reservoir volume of high pressure gas. (Flue gas was 88 mol per cent N_2, 12 mol per cent CO_2. Natural gas was 88 mol per cent C_1, 12 mol per cent C_2). The data points shown in Fig. 6 are based on literature correlations[10,11] of compressibility factors with reduced temperatures and pressures. In addition to the calculation of the compressibility factors for the gases, allowance was made for the volume decrease of the flue gas by solution of carbon dioxide into the connate water existing in the reservoir.

This calculation was based on experimental data obtained in the laboratory in which flue gas at 4,000 psi and 150° F was brought in contact with salt water containing 180,000 ppm total solids. These data showed that 0.035 volumes of the high pressure flue gas dissolved in one volume of the salt water. If the

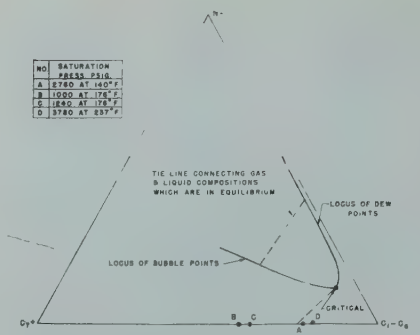
NO. SATURATION PRESS. PSIG
A 2780 AT 140° F
B 1000 AT 176° F
C 1640 AT 176° F
D 3780 AT 237° F
TIE LINE CONNECTING GAS & LIQUID COMPOSITIONS WHICH ARE IN EQUILIBRIUM
LOCUS OF DEW POINTS
LOCUS OF BUBBLE POINTS
CRITICAL
C_7^+
C_1-C_6

FIG. 4—PHASE BOUNDARY CURVE FOR THE SYSTEM NITROGEN, RESERVOIR FLUID AT 4,300 PSIG—176° F.

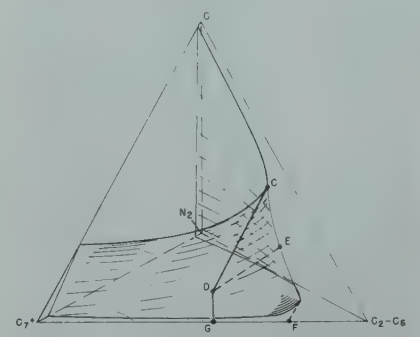

FIG. 5—ILLUSTRATION OF PHASE RELATIONS OF HIGH PRESSURE GAS PROCESS USING NITROGEN AS INJECTION GAS.

TABLE 5

Run No.	Injection Pressure psig	Stock-Tank Oil Recovery Per Cent of OIP Initially: At Breakthrough	Ultimate
L-27	3,000	69.2	79.8
L-28	3,250	76.9	86.5
L-26	3,500	82.8	90.7

Reservoir Fluid B saturation pressure in these experiments was 905 psig at 176° F.
Miscibility pressure was estimated to be 3,400 psig.

reservoir has a 25 per cent connate water saturation, the injected gas volume would shrink by only 1.2 per cent due to solution effects. Based on these results, we feel that the volume shrinkage of the flue gas by solution effects is minor. As we can see above, substantial savings in injected gas quantities can be achieved by substituting flue gas for natural gas. This savings amounts to about 18 per cent of the injected gas volume at 3,000 psig and 150° F.

MISCELLANEOUS USE OF FLUE GAS IN GAS INJECTION OPERATIONS

USE OF FLUE GAS TO FOLLOW LEAN GAS IN HIGH PRESSURE GAS INJECTION PROCESS

Because flue gas is miscible with hydrocarbon gas at reservoir conditions of temperature and pressure, it appeared feasible to use the inert gas as a fill-up material in certain reservoir applications. This idea would be applicable in those cases where

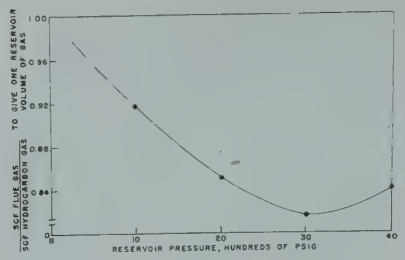

FIG. 6—VOLUME ADVANTAGE IN USING FLUE GAS AS A SUBSTITUTE FOR NATURAL GAS. BASIS: 1 RESERVOIR VOLUME OF GAS AT PRESSURE AND TEMP. 150° F.

an unacceptably large pressure increase over a hydrocarbon gas operation would obtain if flue gas were used alone to achieve miscibility.

Based on previous work on the miscible slug process[7] it was determined that the size of hydrocarbon gas slug to inject prior to inert gas injection would be small. Hydrocarbon gas slugs less than 5 per cent of the hydrocarbon pore space contacted should be sufficient.

USE OF FLUE GAS TO FOLLOW SLUG IN THE MISCIBLE SLUG PROCESS

In cases where miscibility can be achieved between the flue gas and the miscible slug, use of flue gas should be considered. However, the phase relationships for the flue gas-miscible slug-reservoir fluid system are less favorable than for the system containing the hydrocarbon gas. A larger slug is thus required. It is a problem of economic evaluation whether flue gas should be substituted directly for hydrocarbon gas, effecting an increase in slug size requirements or whether a slug of hydrocarbon gas should be used as a buffer between flue gas and slug.

REFERENCES

1. Whorton, L. P., and Kieschnick, W. F., Jr.: *Drill. and Prod. Prac.*, API, (1950) 247.
2. Slobod, R. L., and Koch, H. A., Jr.: *Drill. and Prod. Prac.*, API (1953) 82.
3. Koch, H. A., Jr.: *World Oil* (Oct. 1956) **143**, 260.
4. Griffith, B. L., and Hollrah, V. M.: *Oil and Gas Jour.*, (June 30, 1952) 86.
5. Stone, H. L., and Crump, J. S.: *Trans.* AIME, (1956) **207**, 105.
6. Clark, Norman J.: *Petr. Engr.*, (Oct. 1956) B-43.
7. Koch, H. A. Jr., and Slobod, R. L.: *Trans.* AIME (1957) **210**, 40.
8. Hall, H. N., and Geffen, T. M.: *Trans.* AIME (1957) **210**, 48.
9. Jenks, L. H., Campbell, John B., and Bender, G. G., Jr.: *Trans.* AIME (1957) **210**, 34.
10. *Chemical Engineering Thermodynamics*—Dodge, McGraw-Hill Book Co., Inc., N.Y. (1944) 161.
11. Natural Gasoline Supply Men's Association *Engineering Data Book*, 6th Ed. (1953) 81. ★★★

Departure Curves for the Self-Potential Log

A. E. WORTHINGTON
R. F. MELDAU
JUNIOR MEMBER AIME

CALIFORNIA RESEARCH CORP.
LA HABRA, CALIF.

ABSTRACT

An analog computer study was made of the reduction of the magnitude of the SP by formation geometry and resistivity effects. Practical field situations were studied. The analog data were converted to the form of departure charts. These charts may be used to determine the reduction in the SP due to the above effects with good precision.

INTRODUCTION

Quantitative interpretation of the SP log in terms of formation water resistivity is presently based on the premise that the observed SP is equal to the electrochemical potential developed across a shale between the mud filtrate and the formation water. This procedure inherently assumes that, first, no electrokinetic (streaming) potential is present, and, second, that the SP is not reduced by resistivity or geometry effects in the formation. When, however, such a reduction of the observed SP does occur, one may write,

$$SP = b_c E_c + b_k E_k \quad , \quad . \quad . \quad . \quad . \quad . \quad . \quad . \quad . \quad . \quad (1)$$

where SP is the observed self-potential opposite the center of the bed under consideration. In this case, E_c is the electrochemical potential, E_k is the electrokinetic potential, b_c is the electrochemical reduction factor, and b_k is the electrokinetic reduction factor. The first assumption above is equivalent to assuming $E_k = 0$ in Eq. 1 and the second assumption is equivalent to $b_c = b_k = 1$.

Examination of electric logs shows that for many formations of interest the observed SP is reduced below its maximum value. The object of this work is to aid quantitative SP interpretation in at least some of these situations by obtaining values for b_c and b_k in Eq. 1 as functions of realistic combinations of bed thickness, depth of invasion, and formation resistivity.

The only previously published work in this field known to the authors is by H. G. Doll[1] in 1948. He evaluated b_c under conditions permitting exact analytical solution. His work clearly established the importance and qualitative nature of formation geometry and resistivity effects upon the SP, but the necessity of obtaining analytical solutions restricted his study to situations of limited practical interest.

In order to extend such studies to practical combinations of formation parameters which do not lend themselves to feasible analytical solutions, the results reported in this paper were obtained by use of a special analog computer.

Original manuscript received in Society of Petroleum Engineers office on July 15, 1957. Revised manuscript received Dec. 9, 1957. Paper presented at 32nd Annual Fall Meeting of Society of Petroleum Engineers in Dallas, Tex., Oct. 6-9, 1957.
[1]References given at end of paper.

THE ANALOG MODEL

The analog model used for this study was the Guyod Analog Computer which originally was designed and built for resistivity log departure curve studies. It consists of a two-dimensional mesh of resistors, with the vertical mesh corresponding linearly to vertical distance along the borehole, and the horizontal mesh corresponding to radial distance from the borehole axis. By proper choice of horizontal resistor values, a three-dimensional, axially symmetric, borehole-formation problem can be modeled with this two-dimensional array. These and other details of the model are contained in a paper by H. Guyod[2].

The geometry used for the SP studies with the analog is depicted in Fig. 1. This configuration has a horizontal plane of symmetry, and, hence, the model, and the following discussion, need only to be concerned with one quadrant such as shown in Fig. 2. A further simplification arises by considering that both the natural potential sources and those used in the model have fixed internal impedance. Therefore, the current flows produced by these sources can be separated and studied independently (i.e., the superposition theorem can be applied).

$$SP = SP_c + SP_k = b_c E_c + b_k E_k \quad , \quad . \quad . \quad . \quad (2)$$

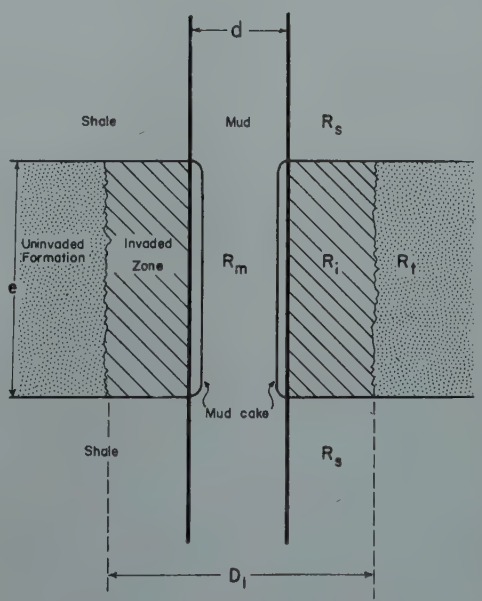

FIG. 1—CROSS SECTION OF FORMATION CONFIGURATION MODELED.

e = bed thickness
d = borehole diameter
D_i = equivalent electrical diameter of invasion
R_m = mud resistivity
R_t = resistivity of uninvaded formation
R_i = resistivity of invaded zone
R_s = resistivity of flanking shale beds

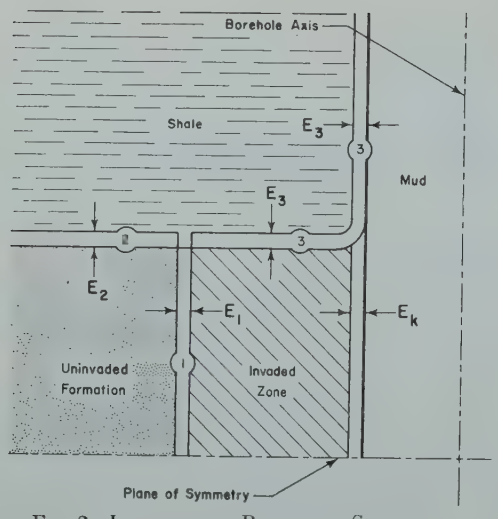

FIG. 2—LOCATION OF POTENTIAL SOURCES IN THE ANALOG MODEL.

where

$$b_c = \frac{SP_c}{E_c} \text{ and } b_k = \frac{SP_k}{E_k}, \quad . \quad . \quad . \quad . \quad . \quad . \quad . \quad . \quad (3)$$

where SP_c and SP_k refer to SP's observed in the model independently, i.e., with only one kind of potential source present. In the actual modeling, both the E_c and E_k sources were built into the network. Measurement of SP_c was made with $E_c = 100$ mv and $E_k = 0$ mv. A second measurement of SP_k was then taken with $E_c = 0$ mv and $E_k = 100$ mv. b_c and b_k were calculated from Eq. 3.

The natural location of the electrochemical potential is somewhat obscure; however, it is usual to divide it into three parts and distribute it between the three boundaries[3] shown in Fig. 2, (here $E_c = E_1 + E_2 + E_3$). Furthermore, as shown by Doll in a mathematical appendix to the preprint of his paper[1] mentioned earlier, the three potentials (E_1, E_2, and E_3) can be lumped together on any one boundary without changing the current flow or potential distribution in the borehole. It is particularly convenient to place the entire E_c potential on Boundary 1, as this boundary is finite and requires a minimum number of potential sources in the model.

The electrokinetic potential occurs either in the borehole across the mudcake at the borehole-invaded zone interface or, in addition, into the shale at the shale-borehole interface. In either case, applying Doll's concept as before, the entire electrokinetic potential may be placed on the borehole-invaded zone boundary.

The potential sources in the analog were small, 60 cycle alternating current transformers, each connected with its low impendance side in series with a normal resistor element between two mesh points in the model. The transformers were separately powered and controlled, and thus could be used to insert a potential along a line in the model without introducing any change in the resistance components of the model. As the transformers were not directly coupled together, such a line of potential sources was not necessarily an equipotential line in the model. Reactive effects do not distort the apparent resistivity of the model, as the frequency used is low and the actual resistance in the current paths is also low.

In the resistivity studies, the logging sonde was built into a mud network, and the mud network including the sonde was moved past the formation by means of a 1,000 pole, 1,000 position switch. For the SP study, the mud network with a sonde was wired directly to the formation. The single SP electrode was then moved along the proper mesh points in the mud network by means of a single pole stepping relay.

TESTING OF THE ANALOG MODEL

The reproducibility of the analog was studied by means of five pairs of tests. Each pair comprised tests of identical situations set up into analog form at different times. The average variation over the five pairs was ± 2 per cent in the reduction factor obtained by one test compared to that from the other. This reproducibility is believed to be typical.

The model was tested once without use of the plane of symmetry. That is, with shales on both sides of a sand bed and potential sources in the E_k position. As the SP sonde was stepped past the bed, a typical symmetrical SP curve was recorded. The model was then cut in half along the plane of symmetry and the first half of the run repeated. The half curve obtained was identical within the reproducibility of the model to the upper half of the full SP curve.

Next, using the quadrant model and a configuration with invasion, potential sources were placed in turn along each of the boundaries in Fig. 2. The results were identical in each case, indicating that the model conformed to Doll's theorem.

Several special setups were then run to specifically check some of the analytical solutions of Doll. The results agreed with his values within 2 per cent.

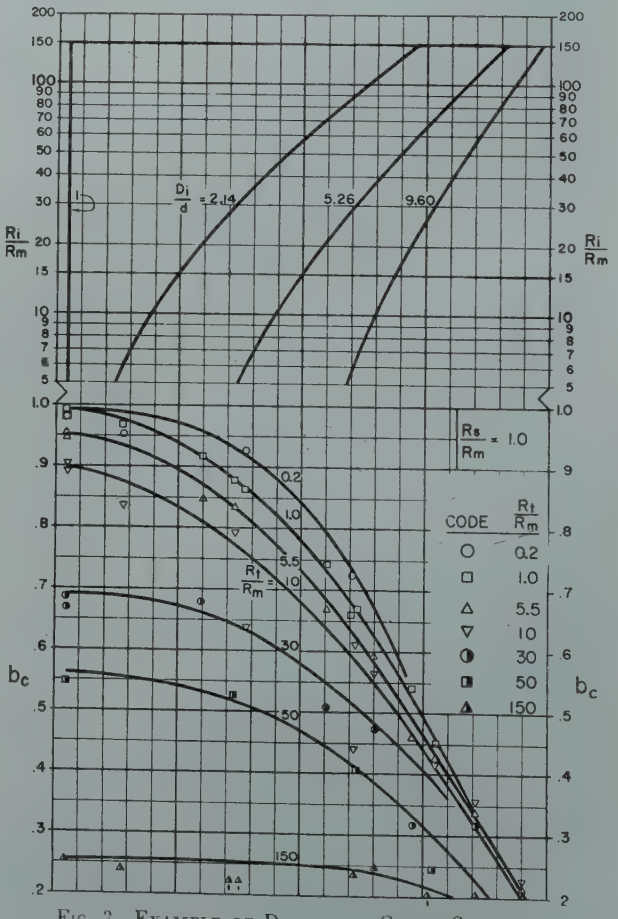

FIG. 3—EXAMPLE OF DEPARTURE CHART SHOWING ORIGINAL ANALOG DATA.

The effect of sonde diameter was studied by making several runs with representative formation conditions but with the SP electrode first at a radial position of $0.2d$ and then at $0.0625d$; corresponding to SP electrodes on the sonde and on the cable, respectively. No difference could be detected between these observed SP's for either of the significantly different choices of formation parameters used. Hence it is concluded that there is no significant effect upon the observed SP when some of the drilling fluid in the borehole is displaced by a logging sonde. Therefore, the check reported in the previous paragraph between Doll's analytical solutions obtained for a point electrode and the analog studies with an electrode on a logging sonde of finite diameter truly reflects the absolute accuracy of the analog model.

CASES STUDIED

As an aid in limiting the size of the program, the following guiding decisions were made.

1. The configuration studied was to be that of a single uniform bed lying between two shales of equal resistivity extending to infinity in the direction away from the bed of interest.

2. Formation factors corresponding to a range of porosities from 10 to 35 per cent were chosen. This defined a range of R_i/R_m's according to the relationship, $R_i = FR_m$.

3. Formation water resistivities corresponding to fresh, saline and hypersaline waters were then combined with the selected formation factors to obtain values of $R_t = FR_w$. R_t/R_m was obtained by using the realistic range of R_m's available in the model.

TABLE 1

Parameter	Range Studied
e/d	2 to 30
D_i/d	1.0 to 9.6
R_t/R_m	0.2 to 150
R_i/R_m	6 to 105
R_s/R_m	0.2 to 25
R_i/R_t	0.6 to 30

4. e/d, D_i/d, and R_s/R_m were varied over the values in Table 1 independently of the formation resistivities.

REDUCTION OF THE DATA

Examination of the b_k data suggested that an average, or effective resistivity, as seen by "looking into" the formation from the E_k position might simplify presentation of the data. This effective resistivity is defined as,

$$R_{eff}/R_m = (1 - d/D_i)R_i/R_m + (d/D_i)R_t/R_m \quad . \quad . \quad . \quad . \quad . \quad . \quad . \quad . \quad . \quad . \quad . \quad . \quad . \quad . \quad . \quad . \quad . \quad . \quad (4)$$

Thus R_{eff}/R_m ranges between R_i/R_m and R_t/R_m, its value varying inversely with D_i/d.

All of the b_k data for a given pair of values of e/d and R_s/R_m were fitted to a cubic equation in log (R_{eff}/R_m) using the method of least squares. The resulting analytical equations were plotted and compared to the original data. Smoothing, particularly at the ends of the curves, was done by hand. Values of b_k at a set of fixed values of R_{eff}/R_m were then cross plotted vs e/d and R_s/R_m, and each of the resulting curves smoothed. Final curves of b_k vs $\log(R_{eff}/R_m)$ were then drawn from these cross plots.

Despite several attempts, it was not found practical to fit the b_c data by the method of least squares to any

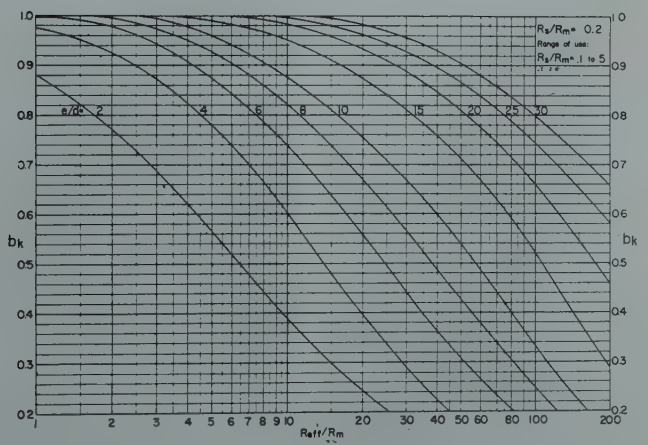

FIG. 4—ELECTROKINETIC POTENTIAL DEPARTURE CURVES FOR $R_s/R_m = 0.2$.

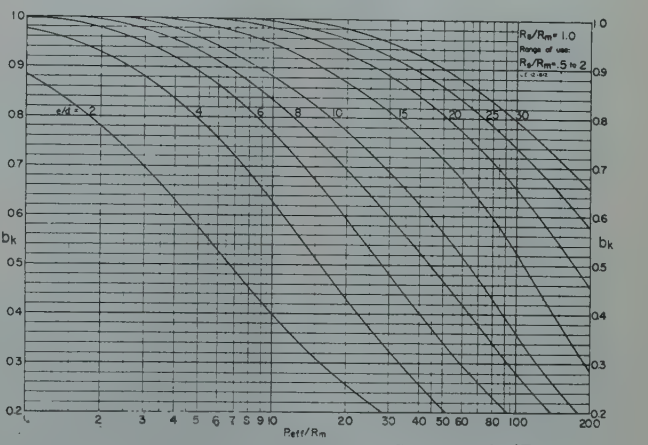

FIG. 5—ELECTROKINETIC POTENTIAL DEPARTURE CURVES FOR $R_s/R_m = 1.0$.

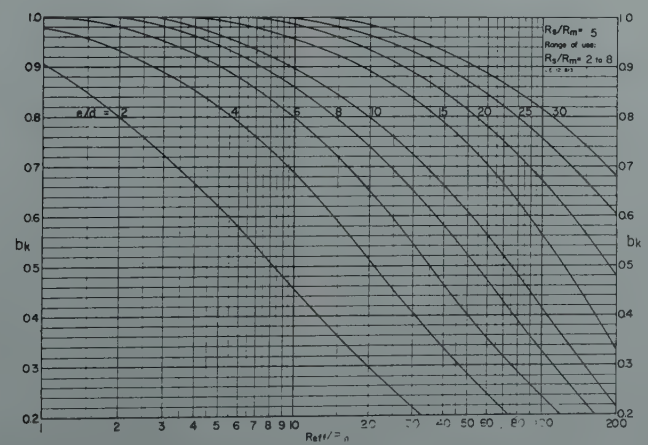

FIG. 6—ELECTROKINETIC POTENTIAL DEPARTURE CURVES FOR $R_s/R_m = 5.0$.

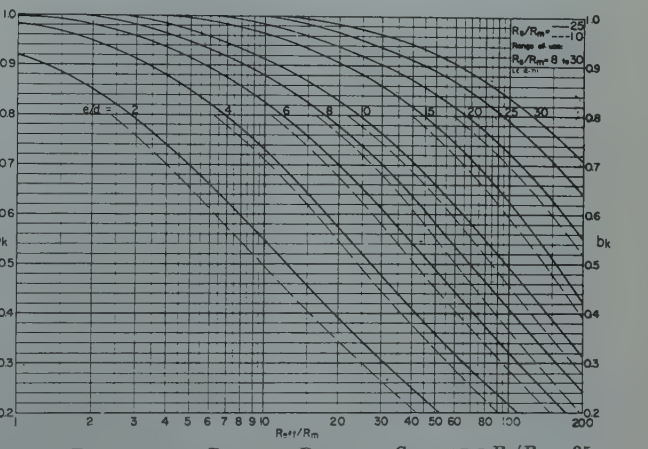

FIG. 7—ELECTROKINETIC POTENTIAL DEPARTURE CURVES FOR $R_s/R_m = 25$.

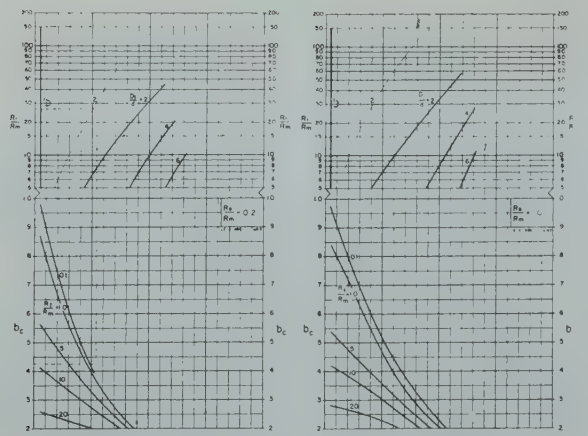

FIG. 8 ELECTROCHEMICAL POTENTIAL DEPARTURE CURVES FOR $e/d = 2$.

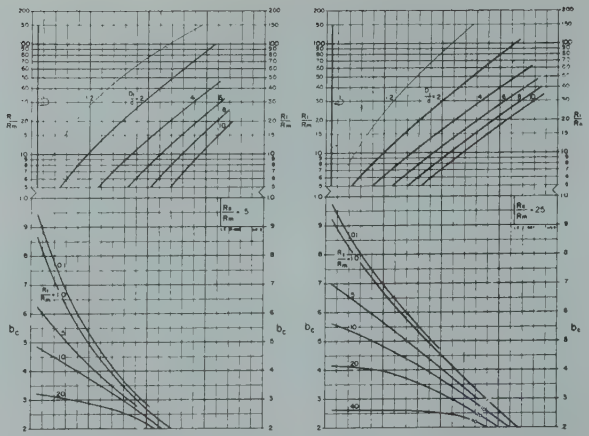

FIG. 9 ELECTROCHEMICAL POTENTIAL DEPARTURE CURVES FOR $e/d = 2$.

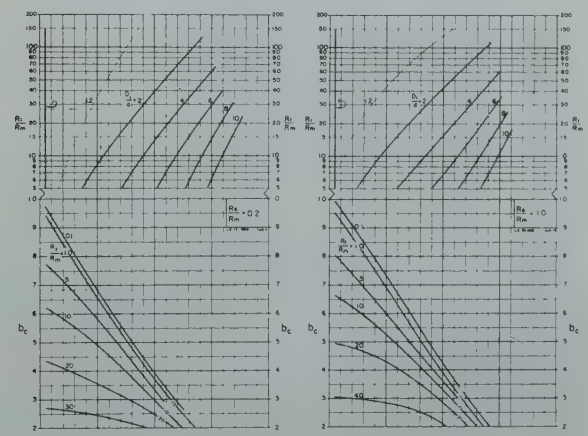

FIG. 10—ELECTROCHEMICAL POTENTIAL DEPARTURE CURVES FOR $e/d = 4$.

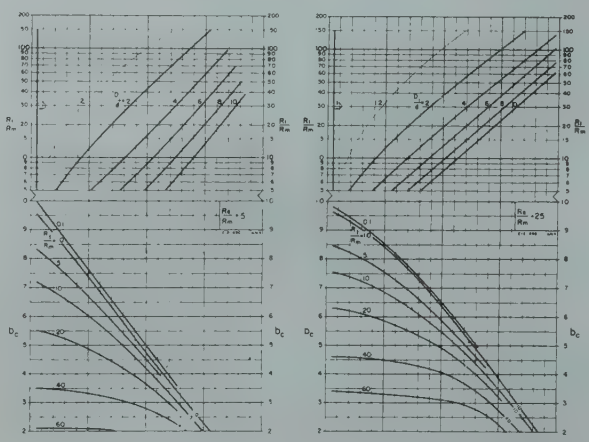

FIG. 11—ELECTROCHEMICAL POTENTIAL DEPARTURE CURVES FOR $e/d = 4$.

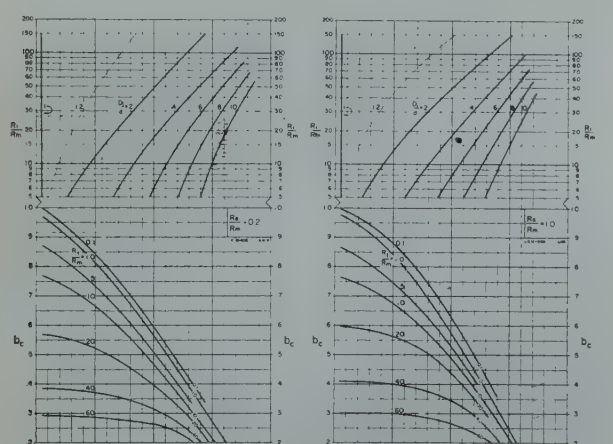

FIG. 12—ELECTROCHEMICAL POTENTIAL DEPARTURE CURVES FOR $e/d = 6$.

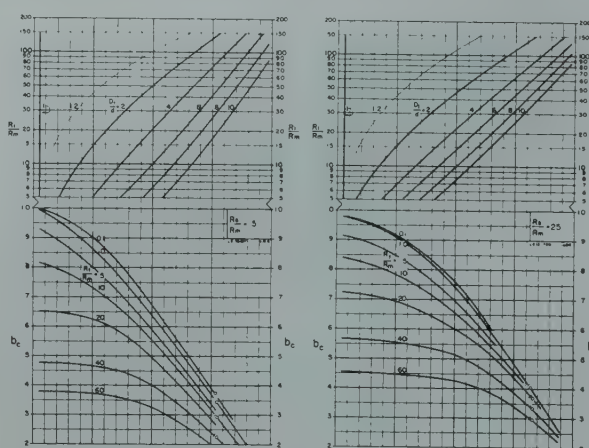

FIG. 13—ELECTROCHEMICAL POTENTIAL DEPARTURE CURVES FOR $e/d = 6$.

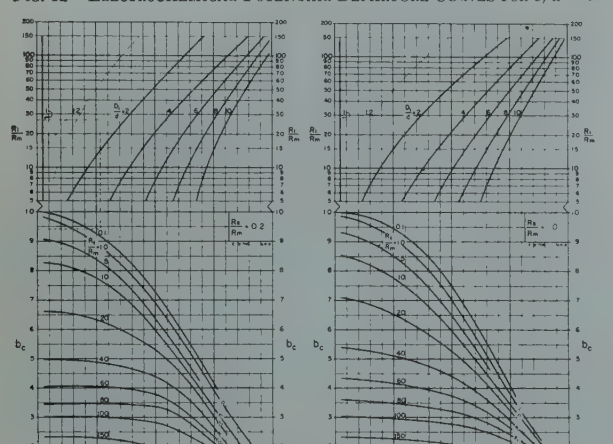

FIG. 14—ELECTROCHEMICAL POTENTIAL DEPARTURE CURVES FOR $e/d = 8$.

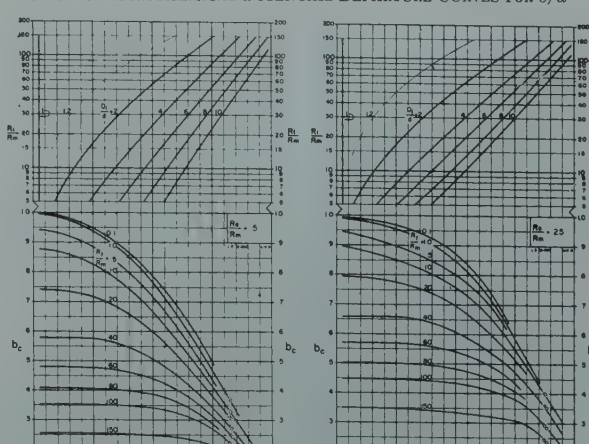

FIG. 15—ELECTROCHEMICAL POTENTIAL DEPARTURE CURVES FOR $e/d = 8$.

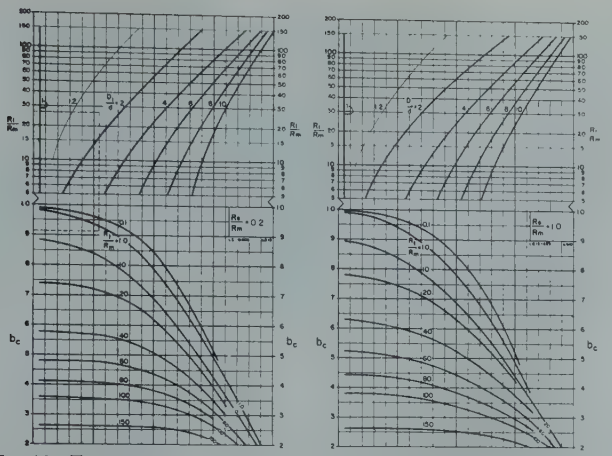

FIG. 16—ELECTROCHEMICAL POTENTIAL DEPARTURE CURVES FOR $e/d = 10$.

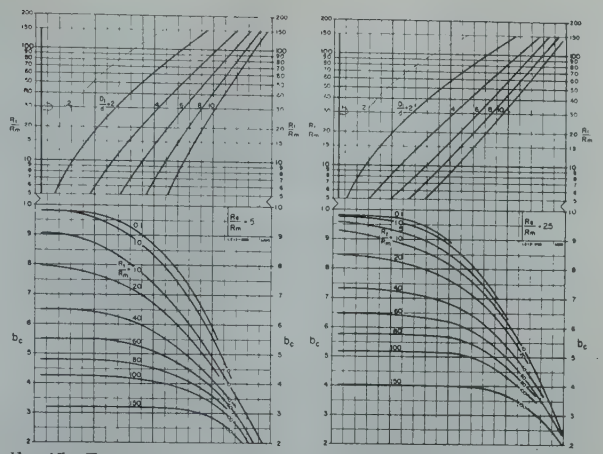

FIG. 17—ELECTROCHEMICAL POTENTIAL DEPARTURE CURVES FOR $e/d = 10$.

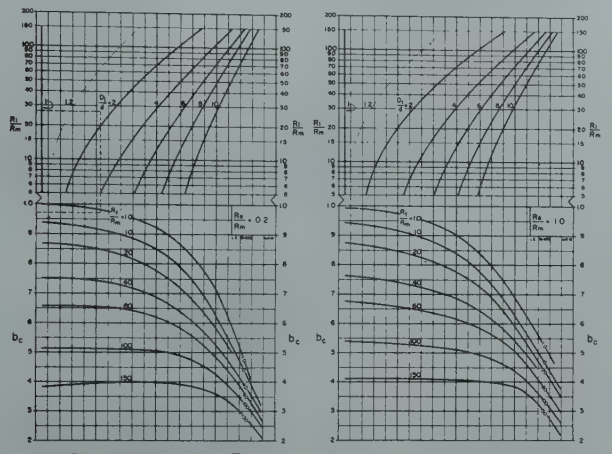

FIG. 18—ELECTROCHEMICAL POTENTIAL DEPARTURE CURVES FOR $e/d = 15$.

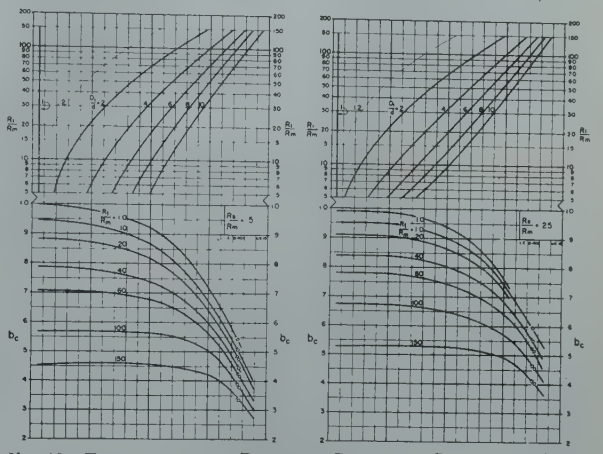

FIG. 19—ELECTROCHEMICAL POTENTIAL DEPARTURE CURVES FOR $e/d = 15$.

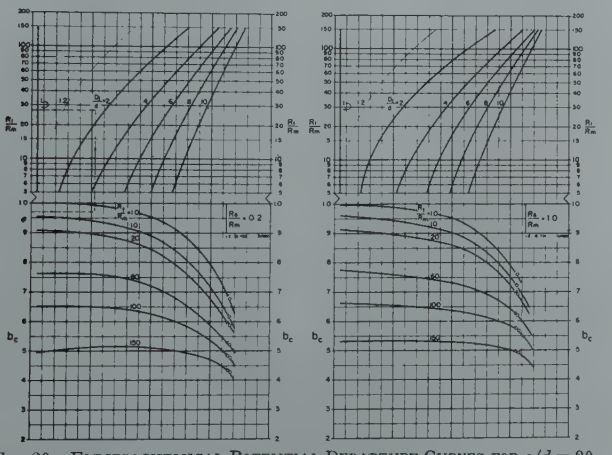

FIG. 20—ELECTROCHEMICAL POTENTIAL DEPARTURE CURVES FOR $e/d = 20$.

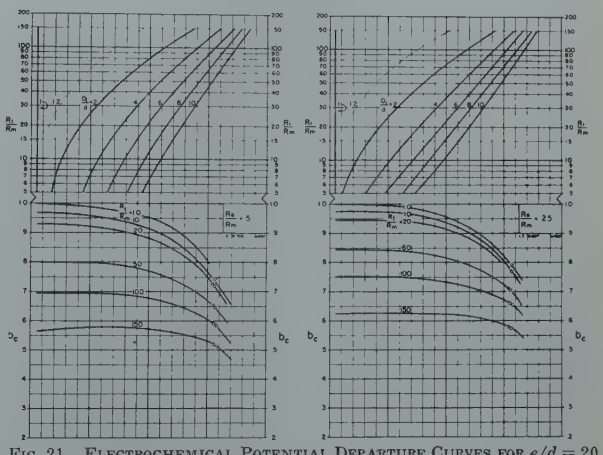

FIG. 21—ELECTROCHEMICAL POTENTIAL DEPARTURE CURVES FOR $e/d = 20$.

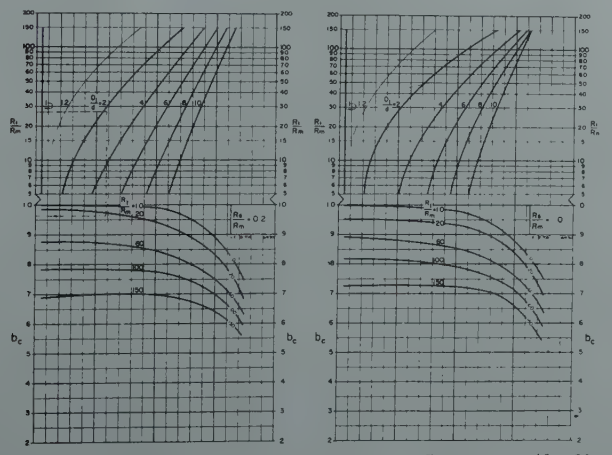

FIG. 22—ELECTROCHEMICAL POTENTIAL DEPARTURE CURVES FOR $e/d = 30$.

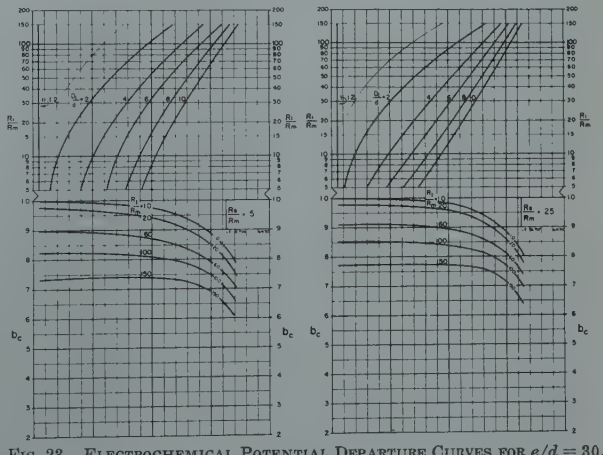

FIG. 23—ELECTROCHEMICAL POTENTIAL DEPARTURE CURVES FOR $e/d = 30$.

empirical formula. The b_c data were fitted entirely by eye.

The data were separated first according to e/d, as this variable is easiest to evaluate from an electric log. R_s/R_m served as a second break point by a similar argument. It then appeared that the b_c data could be expressed by an equation of the form,

$$b_c^* = f(R_t/R_m, S) \quad . \quad . \quad . \quad . \quad . \quad . \quad . \quad . \quad . \quad (5)$$

where b_c^* refers to values of b_c at fixed e/d and R_s/R_m, and is independent of R_i/R_m and D_i/d individually, and S is a function of D_i/d and R_i/R_m but not of R_t/R_m. Using this assumption, the presentation shown in the accompanying departure charts was developed. The unlabeled horizontal axis in the b_c charts is the arbitrary variable, S, in Eq. 5. The actual fitting was done by simultaneously varying the shapes of the D_i/d and R_t/R_m vs S curves to obtain the best fit. These curves were then made self-consistent by cross plotting against e/d, R_t/R_m, and D_i/d.

The departure curves finally obtained are presented in Figs. 4 through 23*.

PRECISION

The original analog data were compared with the final departure charts and the normalized deviation calculated as,

$$\text{dev.} = 100 \ (b_{\text{chart}} - b_{\text{analog}})/b_{\text{chart}} \quad . \quad . \quad . \quad (6)$$

The root mean square deviation for the 1,193 original data points compared to the charts is 5.4 per cent. This could be improved to 4.0 per cent by omitting 165 b_c points with $R_i/R_t < 1$, and $D_i/d > 2$. This suggests that for $R_i/R_t < 1$, the assumptions of Eq. 5 tend to become invalid.

The average absolute difference between the chart and analog reduction factor, b, is 0.016. The maximum for any single point is 0.18. The maximum normalized deviation is 35 per cent for a point with $b_c = 0.25$. Both maxima occur at $R_i/R_t < 1$.

The fit of the data ($b_{\text{analog}} - b_{\text{chart}}$) shows no significant trend with formation parameters except at low R_i/R_t as noted earlier. However, the deviation defined in Eq. 6 increases as the reduction factor becomes smaller, because it is expressed as a per cent of the reduction factor.

Fig. 3 shows one of the b_c charts with the analog data points as well as the smoothed curves representing the original values of D_i/d and R_t/R_m. The fit of these curves is typical.

The accuracy of these charts in use will depend upon both ability to accurately evaluate formation and borehole parameters from the logs and also upon whether the situation under study falls within the range of conditions used with the analog to obtain the charts. It is not anticipated that the error would increase very rapidly for modest extrapolations beyond the original data, except for low R_i/R_t values.

In addition, the method of presentation was selected with the objective of not only retaining as much of the precision of the original data as possible, but also of permitting use with as much accuracy with as little effort as practical. Thus, for the b_c data the value of e/d, certainly the easiest formation parameter to estimate, determines the correct page. The correct chart is determined by R_s/R_m, also readily evaluated. Of the remaining formation parameters, D_i/d is the most difficult to determine. However, the arrangement of the b_c charts permits estimation of the importance of this variable and of the error likely to be introduced by a poor guess.

CONCLUSIONS

1. The reduction of the SP by formation and borehole geometry and resistivity effects can be accurately modeled on an analog computer.
2. The resulting analog data can be presented in simplified form for field use while still retaining the precision of the data.
3. The formation parameters affect b over the range of these parameters studied in the following manner:
   a. b_c and b_k decrease markedly with decreasing e/d.
   b. b_c decreases markedly with increasing D_i/d.
   c. b_k is unaffected by D_i/d when $R_i = R_t$. When $R_i \neq R_t$, b_k is affected relatively more and more by R_i than R_t as D_i/d increases.
   d. b_c and b_k decrease with increasing R_t/R_m and R_i/R_m.
   e. b_c and b_k decrease slightly with decreasing R_s/R_m.

ACKNOWLEDGMENT

The authors wish to acknowledge the help and cooperation offered by H. Guyod and J. Pranglin throughout this project. A. U. Elser helped with the calculations.

REFERENCES

1. Doll, H. G.: "The SP Log: Theoretical Analysis and Principles of Interpretation", *Trans.* AIME (1948) **179**, 146.
2. Guyod, H.: "Electrical Analog of Resistivity Logging", *Geophysics* (July, 1955) **XX**, 3, 615.
3. Wyllie, M. R. J.: "A Quantitative Analysis of the Electro-Chemical Component of the SP Curve", *Trans.* AIME (1949) **186**, 17.

★★★

*Figs. 4 through 23, Copyright 1957, California Research Corp., printed by permission.

A Model for the Mechanism of Oil Recovery from the Porous Matrix Due to Water Invasion in Fractured Reservoirs

J. S. ARONOFSKY*
MEMBER AIME
L. MASSÉ
MAGNOLIA PETROLEUM CO.
DALLAS, TEX.
S. G. NATANSON
IRAQ PETROLEUM CO., LTD.
LONDON, ENGLAND

INTRODUCTION

The first step in a quantitative analysis of the mechanism of oil displacement by water in a fractured reservoir is usually conceded to be the solution of the differential equation describing the saturation distribution of two immiscible fluids flowing in a porous medium, where the capillary pressure is taken into account. In such a system the production mechanism may consist of displacement of oil both by the flow of water due to natural or artificially imposed pressure gradients and by imbibition, which implies a flow of water not due to external pressure gradients. Owing to the presence of the two oil displacement mechanisms, the mathematical model given by the differential equation intended to describe the system may not properly represent the behavior of the physical system. In fact, in the reservoir the rate of water advance may be very slow, and in the case of a fractured reservoir with a great number of large fractures, the pressure difference determining the flow of water through the matrix may be much less than 1 lb/psi over lengths of a few feet. In such a case, imbibition (the exchange between oil in the matrix and water in the fractures resulting from capillary forces) may become, with time, a significant element of the production mechanism.

It occurred to the authors, however, that without going into a physical analysis of the process of production, it might be possible by means of simple abstract reasoning to throw some light on the variation of recovery with time under conditions occurring in a highly fractured oil reservoir with rising water table.

The object of this paper is to present both the reasoning and its application to a reservoir of the highly fractured type. Specifically, the analysis given here was undertaken to try to explain the increase of recovery (as defined later) with time as observed in this reservoir, without having to assume unlikely variations in the reservoir parameters with depth. This attempt has been successful as will become clear upon comparison of the computed recoveries with the actual field data.

ABSTRACT MODEL

Let us consider a small volume, dv, of porous matrix saturated with oil at time, $t = 0$. Let the process of oil displacement by water start at time, $t = t_o$. At some time, t, the process will have terminated. Then a volume of oil equal to or smaller than the original oil contained in the matrix will have been produced. The first basic assumption that describes the model and guides the forthcoming reasoning is that the oil production from the small volume, dv, is a continuous monotonic function of time and that it converges to a finite limit. Such an assumption is not inconsistent with the results of laboratory waterflood tests as well as with results of imbibition tests where this is, in fact, observed. The second basic assumption is that none of the properties which determine the rate of convergence change sufficiently during the process to affect this rate or the limit.

Let it be assumed that the form of the function of time relative to production from the matrix volume, dv, is given by

$$\frac{V_o(t)}{V_i(t)} = R(1 - e^{-\lambda t}) \quad , \quad (1)$$

where $V_o(t)$ is the volume of oil produced up to that time t. R is the limit toward which the recovery converges, λ is a constant giving the rate of convergence, and $V_i(t)$ is the volume of oil originally in place in the volume, dv.

It should be noted that recovery at time t will be understood here to be

$$r = \frac{V_o(t)}{V_i(t)}.$$

It follows that r tends to R as t tends to infinity.

CONSTRUCTION OF RESERVOIR FROM ABSTRACT MODEL

Let the reservoir consist of a series of identical blocks of porous matrix stacked vertically and separated by fractures. Let each of these blocks satisfy the conditions of our abstract model. These conditions are: (1) that recovery is a continuous monotonic function of time converging to a finite limit, and (2) none of the properties that determine the rate of convergence change sufficiently to affect the rate or the limit. Let water be rising in fractures so that oil production from any part of the block starts when the water comes in contact with it.

TOTAL RECOVERY FROM THE RESERVOIR COMPARED TO RECOVERY FROM A SINGLE MODEL ELEMENT

As stipulated in Eq. 1, in the case of the abstract model,

$$r = R(1 - e^{-\lambda t}) \quad . \quad . \quad . \quad (2)$$

Original manuscript received in Society of Petroleum Engineers office on July 11, 1957. Revised manuscript received Nov. 26, 1957. Paper presented at 32nd Annual Fall Meeting of Society of Petroleum Engineers in Dallas, Tex., Oct. 6-9, 1957.

*Presently associated with Socony Mobil Oil Co., Inc., New York, N. Y.

In the case of the reservoir, the recovery is found as follows. Assume that N identical blocks are stacked vertically and that the block of rank j is submerged in water at time t when the water level has reached the height, $Z_j = Z(t_j)$. If V_{oj} is the volume of oil produced by the block of rank j, then,

$$V_o = \sum_{j=1}^{N} V_{oj} = \sum_{j=1}^{N} r_j V_{ij},$$

where r_j is the recovery from block j and V_{ij} is the volume of oil initially in this block.

If $V_o(t)$ is computed for time t, then,

$$r_j = R(1 - e^{-\lambda(t-t_j)}),$$

since block j has been submerged only for a time interval equal to $t - t_j$.

Then if N blocks are submerged at time t,

$$V_o(t) = \sum_{j=1}^{N} R\,(1 - e^{-\lambda(t-t_j)})\, n \triangle Z_j,$$

where

$$n \triangle Z_j = V_{ij}.$$

If we now allow the number of blocks to increase indefinitely, we get

$$V_o(t) = \lim_{N\to\infty} R \sum_{j=1}^{N} (1 - e^{-\lambda(t-t_j)})\, n \triangle Z_j$$

$$= n R \int_o^{Z(t)} (1 - e^{-\lambda(t-t_j)})\, dZ\,(t_j)\,.$$

If the velocity of advance of the water table is uniform and equal to a, then $Z = at$, and

$$V_o(t) = a\,n\,R\left(t + \frac{1}{\lambda}e^{-\lambda t} - \frac{1}{\lambda}\right) \quad . \quad . \quad . \quad . \quad . \quad . \quad . \quad (3)$$

The volume of the original oil in place in the invaded region is given by $V_i(t) = a\,n\,t$.

Thus

$$r = R\left[1 - \frac{1}{\lambda t}(1 - e^{-\lambda t})\right] \quad (4)$$

The comparison of the recoveries in time, as given by Eq. 2 and 4, is best done by means of the graph in Fig. 1.

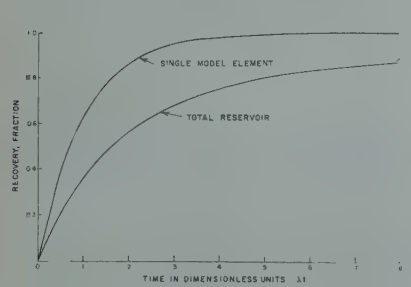

FIG. 1—RECOVERY IMBIBITION.

RESULTS OF COMPARISON

From Fig. 1 it is immediately seen that the recovery from the reservoir is lower than that from a single model element at any time before the limit is reached. The difference between the two recoveries converges to zero as each recovery converges to R; the value of the difference at any given time depends uniquely on λt and R. It should be stressed further that in case of constant velocity of advance of the water table, the rate of advance does not affect the difference.

The importance of these results may best be appreciated when expressed in terms of field experience. In fact they mean that oil recoveries obtained at various times of the past history of a fractured field will show an increasing trend, provided that production from the fractures is sufficiently slow. It should be emphasized that this basic result is valid even if the continuous monotonic function converging to a limit (which expresses the relation between time and recovery in the abstract model) is something other than the assumed exponential function. However, in such a case, the relation between the recoveries for the field and the model would be different. As long as the function is not specified, the quantitative analysis of this relation is not possible. Should this function be of the assumed exponential form, however, a number of quantitative results of practical interest can be obtained. It is in fact possible, knowing recoveries with time from the past history and the history of the water table movement, to extrapolate recoveries into the future and calculate the ultimate value of recovery. That, in turn, allows a comparison between field estimates of recovery and the values of residual oil obtained in laboratory tests. The following application is for the case of an actual reservoir.

APPLICATION TO AN ACTUAL FIELD

General Considerations

Some 20 waterflood tests made on large core samples showed that the variation of residual oil values is very small in spite of large variations in permeabilities. These ranged from a fraction of a millidarcy to several hundred millidarcies. It was considered that the variation in residual oil was sufficiently small to be ignored.

It should be pointed out that the nonhomogeneity of the rock does not quite fit the idealized model discussed. However, it was found that large changes in viscosity and in differential pressure did not affect the value of the residual oil. This, to some extent, justifies the second assumption made in determining the abstract model. Although expression (1) may not lead to the best fit to recovery in the case of imbibition, it was considered good enough for our purpose.

To summarize, it is believed that the actual reservoir considered here corresponds fairly well to the theoretical reservoir previously described.

Field Data Available

Thirty-two values of recovery (from the matrix alone) obtained from the material balance calculations, carried out at regular intervals throughout the history preceding gas cap development of the actual reservoir, were available. These are plotted in Fig. 5. It should be noted that by adjusting porosities, interstitial water content and other constants in the material balance equation, one would obtain different values of recoveries. The available set of recoveries should only be considered as an example. The form of the curve is correct, but the absolute values of the recoveries are obtained from this curve by multiplying by a constant factor.

Forty values of water level (in the fractures) as a function of time at regular intervals, obtained from field measurements during the past history of the field, are plotted in Fig. 3.

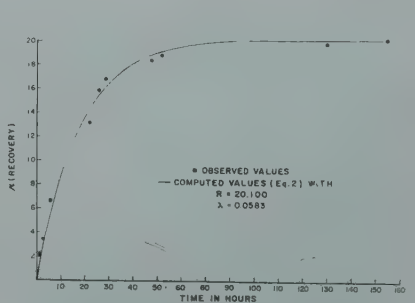

FIG. 2—IMBIBITION CURVE.

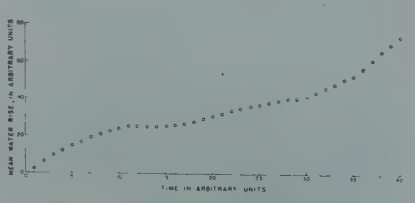

FIG. 3—RISE OF WATER TABLE.

Evaluation of λ for the Actual Reservoir

Should $Z(t)$ be a linear function of t, Eq. 3 reveals that r depends uniquely on R and λ. Thus having a number of values of r for various times, one could fit expression (3) to these data by a suitable choice of R and λ. Since the given $Z(t)$ is not a linear function of t, one has to devise a suitable treatment.

Let $Z_i = Z(t_i)$, where Z_i is the position of the water level at time, t_i. Then V_o is given by

$$V_o = n \int_o^{Z_i} R(1 - e^{-\lambda(t_i - t)})\, dZ$$

and

$$r = \frac{R}{Z_i} \int_o^{t_i} (1 - e^{-\lambda(t_i - t)})\, Z'(t)\, dt \,. \quad . \quad . \quad . \quad . \quad . \quad . \quad . \quad . \quad . \quad . \quad . \quad (6)$$

To evaluate this integral it is necessary to know the function, $Z(t)$. As a matter of interest, the case where $Z = at + bt^2$ was numerically evaluated for a pair of values of the parameters a and b; the results are plotted in Fig. 4 (Curve 3).

The values of the derivative, $Z'(t)$, which appear in Eq. 6 were obtained by interpolation and smoothing of the given values of $Z(t)$ and by numerical differentiation. The values of r/R were then obtained from Eq. 6 for various values of λ. If the field recoveries for each time period are plotted against r/R so obtained, and if these recoveries are consistent with the model assumed, then a straight line should result.

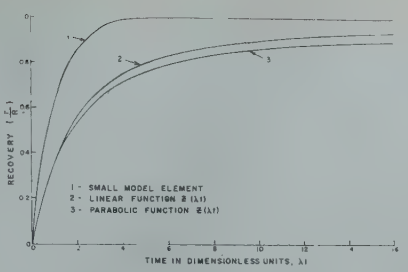

Fig. 4—Numerical Evaluation of $Z = at + bt^2$.

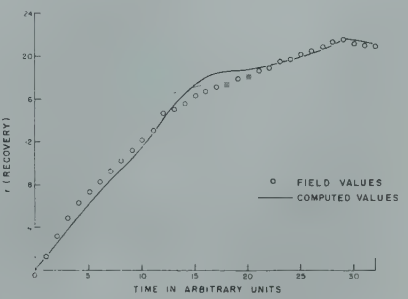

Fig. 5—Field Recoveries.

For each value of λ, such a plot was made, and the slope was determined by least squares methods. The value of λ selected was the one which gave the best fit on the least squares criterion.

Fig. 5 shows the result of the computations carried out in this manner compared to the field recoveries.

CONCLUSIONS

1. The considerable variation in observed recoveries in a fractured reservoir with time has been explained.

2. A method of extrapolating field recoveries has been presented.

3. It has been found that the mechanism of oil production from water invasion in a fractured reservoir may be a very lengthy process.

ACKNOWLEDGMENT

The authors wish to thank the Magnolia Petroleum Co. and the Iraq Petroleum Co., Ltd., for permission to publish this paper. They are also grateful to B. J. Dotson of Magnolia Petroleum Co. for the experimental data from which Fig. 2 was drawn. ★★★

Properties of Cementing Compositions at Elevated Temperatures and Pressure

GREG CARTER
JUNIOR MEMBER AIME
DWIGHT K. SMITH
MEMBER AIME

HALLIBURTON OIL WELL CEMENTING CO.
DUNCAN, OKLA.

T. P. 8001

ABSTRACT

Studies have been conducted on the properties of many deep well cementing compositions to determine their strength behavior over curing periods to 180 days at elevated temperatures and 3,000 psi pressure. This pressure results in essentially the same compressive strength as that obtained with much higher pressures in accordance with the findings of an API subcommittee.[1] These different compositions include API Classes A, E, and F cements containing additives such as retarders, bentonite, heavy weight materials and pozzolans. All compositions except mixtures of pozzolans and hydrated lime show from mild to severe degrees of strength loss over a temperature range from 230 to 320° F after setting. Pozzolan-lime compositions actually gain in strength with time at these high temperatures.

Other chemical and physical properties evaluated to observe their interrelationship with strength loss show very little correlation except in permeability. As retrogression in strength increases, the permeability of set cement increases. X-ray diffraction patterns on the set products indicate the formation of certain compounds having little or no strength value in those cementing compositions where strength loss was more severe.

Original manuscript received in Society of Petroleum Engineers office on Aug. 16, 1957. Revised manuscript received Jan. 15, 1958. Paper presented at 32nd Annual Fall Meeting of Society of Petroleum Engineers in Dallas, Tex., Oct. 6-9, 1957.

[1]References given at end of paper.

Discussion of this and all following technical papers is invited. Discussion in writing (three copies) may be sent to the offices of the *Journal of Petroleum Technology*. Any discussion offered after Dec. 31, 1958, should be in the form of a new paper.

INTRODUCTION

As a result of the growing trend toward deep well completions, a study has been made on the properties of the various cementing slurries presently in use at elevated temperatures and pressure. The strength of these compositions is of prime importance in selecting the most suitable material for use at high temperatures, to determine WOC time and the proper time to perforate with a minimum of shattering. Of primary interest in this investigation was the strength behavior of various compositions currently in use, and the effect of additives on cement after long periods of curing under severe conditions.

Earlier investigators[1,2,3] have pointed out that the strength of some cements will increase with increasing curing temperature to about 220 to 240° F, but at higher temperatures a loss in strength occurs at extended time intervals. Studies by the API Mid-Continent District Study Committee on Oil Well Cements[1] outlined a testing procedure whereby field conditions of temperature and pressure could be simulated in the laboratory.[4] It was observed that retarded cements undergo changes at elevated temperatures and some lose as much as 50 per cent of their early strength when cured at high temperatures. The scope of these tests was limited to curing periods of 1 to 28 days; additives were not covered in this study.

Saunders and Walker[2] found that the use of additives influenced the strength behavior of cements at high temperatures, but studies were conducted only to a seven-day curing period. Ludwig and Pence[3] conducted an investigation of two types of cements under elevated pressures and temperatures in an effort to explain the causes of this loss in strength phenomenon. It was observed that with retrogression in strength there were other physical and chemical changes which took place as the cement aged.

Today there are a number of cementing compositions available for use at well depths below 10,000 ft. Since all these earlier investigations were limited in curing time as well as the number and type of compositions studied, it was believed that a more extensive study should be conducted on the properties of cements at elevated temperatures, and this work should include those compositions actually in general field use at this time.

SCOPE OF INVESTIGATIONS

The first object of this study was to define clearly the temperature and time at which retrogression began and over what period of time this loss in strength extended. The second consideration was to analyze each composition for surface area, chemical analysis, permeability and X-ray diffraction pattern to obtain further information as to the cause of this behavior.

For this basic study, seven different cementing compositions were initially selected, with variations of these resulting in 15 actual test slurries.

1. Retarded-type oil well cements —five brands.
2. Retarded cements with bentonite.
3. Portland cements (API Class A) with chemical retarder.
4. Portland cements (API Class A) with bentonite and retarder.
5. Portland cements (API Class A) with pozzolans (three types) and retarder.
6. Pozzolan-lime compositions with and without retarder.
7. Portland cements, with diatomaceous earth and retarder.

After establishment of the time and temperature range over which the loss in strength occurred in these various compositions, a second series of tests was made on a more limited basis with selected additives. Here, the primary consideration was to determine the effects of different types of retarders and slurry weight increasing additives. The latter are very important in deep wells where it is desired to have the cement at or near the same weight as the drilling fluid in the hole at the time of cementing. The curing of high density cement slurries which contained different chemical retarders was restricted to 14,000 and 16,000-ft well conditions, which generally correspond to temperatures of 290 and 320° F along the Gulf Coast.

DESCRIPTION OF TESTING PROCEDURES

Preliminary tests were made to establish the thickening time of each of the compositions selected for study. Since the primary interests of these tests were in wells below 10,000 ft, pumpability measurements were made under casing cementing conditions from 12,000 to 16,000 ft (Table 1). When the pumpability exceeded 3 hours, tests were discontinued since this is normally as long as actually needed to place the cement at these depths. While a few of these basic compositions lacked the desired 3 hours pumpability, compressive strength tests were made at higher temperatures to study the loss in strength.

In studying the effects of retarded cement and weight materials, all of the compositions were designed to give a 3-hour pumpability by the addition of the necessary chemical retarders (Table 2).

The curing of the long-range compressive strength specimens was in the standard 2 × 2 × 2-in. brass cube molds. Sufficient individual specimens were prepared to have duplicates of each cementing composition. In a few instances rechecks were made to observe the degree of reproducibility that could be obtained. Specially constructed autoclaves, which would hold eight of these 2-in. molds, were used for all tests (Fig. 1). Water was used as the curing medium in the autoclaves which were submerged in oil baths and subjected to the temperatures of 200, 230, 260, 290, and 320° F. All slurries were cured under 3,000 psi curing pressure, which had been found to give approximately the maximum pressure effect on the strength of cements.[1] The application of pressure and temperature was according to API Test Schedules[4] 5S, 6S, 7S, 8S, and 9S. These maximum test pressures and temperatures were maintained until specimens were ready to be tested to destruction at ages of 1, 3, 7, 28, 60, 90, and 180 days.

X-ray diffraction patterns were made on all specimens of cements tested under different curing conditions to study changes in the chemical composition of the set cement. Chemical analysis, fineness tests, and permeability determinations were also made to study the inter-relation, if any, of these factors with loss in strength (Tables 3 and 4).

TABLE 1—THICKENING TIMES OF CEMENTING COMPOSITIONS
(Time — Hours:Minutes)

Composition	Water gal/sk	Slurry Weight lb/gal	Static temp. (°F) / Cementing temp. (°F)	Well Depth (ft)* 260 / 172 (12,000)	290 / 206 (14,000)	320 / 248 (16,000)
1. Retarded Cement A	4.50	16.25		3:00+	3:00+	1:38
2. Retarded Cement B	4.50	16.25		3:00+	3:00	1:45
3. Retarded Cement C	4.50	16.25		3:00+	3:02	1:42
4. Retarded Cement D	4.50	16.25		3:00+	3:08	1:40
5. Retarded Cement E	4.50	16.25		3:00+	2:50	1:33
6. Retarded Cement D— 4 Per cent Gel	5.90	15.20		3:00+	3:00+	1:45
7. API Class A Cement — 0.5 Per cent Lignin Retarder	5.20	15.60		3:00+	2:19	1:29
8. API Class A Cement—0.7 Per cent Lignin Retarder— 12 Per cent Gel	12.30	12.60		3:00+	2:50	2:11
9. API Class A Cement— Pozzolan X—0.5 Per cent Lignin Retarder	5.75	14.15		3:00+	3:00+	2:06
10. API Class A Cement— Pozzolan Y—0.5 Per cent Lignin Retarder	5.34	15.00		3:00+	3:00+	2:30
11. API Class A Cement— Pozzolan Z—0.5 Per cent Lignin Retarder	5.70	14.20		3:00+	3:00+	2:44
12. Pozzolan X— 15 Per cent Hydrated Lime	4.55	14.40		3:00+	1:52	1:13
13. Pozzolan X— 15 Per cent Hydrated Lime 0.5 Per cent Lignin Retarder	4.55	14.40		3:00+	3:00+	2:29
14. Pozzolan Y— 15 Per cent Hydrated Lime	4.75	15.20		2:31	1:42	1:01
15. API Class A Cement— 0.7 Per cent CMHEC Retarder 20 Per cent Diatomaceous Earth	13.50	12.40		3:00+	3:00+	2:02

*API RP 10B Casing Schedules

TABLE 2—THICKENING TIMES OF CEMENTING COMPOSITIONS WITH WEIGHT MATERIAL AND RETARDERS
(Time—Hours:Minutes)

Composition	Water gal/sk	Slurry Weight lb/gal	Static temp. (°F) / Cementing temp. (°F)	Well Depth (ft)* 290 / 206 (14,000)	320 / 248 (16,000)
1. Retarded Cement D	4.50	16.3		3:08	1:40
2. Retarded Cement D—Barite— Lignin Retarder	5.80	18.0		3:00+	3:00+
3. Retarded Cement D—Barite— CMHEC Retarder	5.80	18.0		3:00+	3:00+
4. Retarded Cement D—Ilmenite Ore— Lignin Retarder	3.10	19.9**		3:00+	3:00+
5. Retarded Cement D—Ilmenite Ore— CMHEC Retarder	5.10	18.0		3:00+	3:00+
6. Pozzolan X—Lime—Barite— Lignin Retarder	7.56	18.0		3:00+	3:00+
7. Pozzolan X—Lime—Ilmenite Ore— Lignin Retarder	4.55	18.0		3:00+	3:00+

*API RP 10B Casing Schedules.
**A reduction of water was necessary since the added retarder gave a low viscosity. For a proper viscosity (10-15 poises), only 3.1 gal of mixing water was required for the cement.

FIG. 1—CURING VESSELS AND MOLDS USED TO CURE CEMENT SPECIMENS UNDER DIFFERENT TEMPERATURES AND PRESSURES.

In the selection of the test compositions, five brands of retarded API Classes E and F cements were chosen from various manufacturers throughout the U. S. All were tested with the recommended 4.5 gal of water which corresponds to a 16.2 lb/gal slurry weight.

To observe the effects of bentonite in cement at these high temperatures, tests were made with retarded cement, API Class A cement, and an API Class B cement, all of which contained various percentages of gel. Pozzolans were also included in these studies, with tests being made on three different types blended individually with Class A portland cement in equal proportions by absolute volume. One of these was a fly-ash-type pozzolan, while the other two were of natural origin. Two per cent bentonite plus the necessary amount of retarder to allow the proper thickening time was blended with each of the three pozzolan-cement compositions.

For extremely deep well cementing, blends of pozzolans and hydrated lime have been used frequently. To study these compositions, a natural and a fly-ash-type pozzolan were selected from two different origins and blended with approximately 15 per cent hydrated lime. Data were obtained with and without chemical retarders to determine how they compared with the strengths of other materials at these high temperatures. To complete the 15 basic materials, a blend of Class A portland cement with 20 per cent diatomaceous earth plus a chemical retarder was included.

In studying the differences in retarders and heavy weight additives, two each of the more common materials used for these purposes were evaluated.

A lignin compound and CMHEC (carboxymethyl hydroxyethyl cellulose) were selected for comparison of retarders under high temperatures while a regular grind of drilling mud barite and a uniform particle gradation of an illmenite ore were compared as weight materials for high density cements.

DATA AND RESULTS

Thickening Times

Each of the compositions studied was tested to determine what placement time could be expected under the various test conditions. Test data in Tables 1 and 2 illustrate the various thickening time values which were obtained under depth and temperature conditions ranging from 12,000 to 16,000 ft and 260 to 320° F, respectively. At 14,000 and 16,000 ft there was a considerable variation in the thickening times of the 15 basic compositions; however, all were tested for strength over the entire temperature range. This variation in pumpability was particularly true at 16,000 ft, where some compositions lack the necessary pumpability for placement and only five had a thickening time of over 2 hours without the addition of extra retarder.

Compressive Strengths

A composite summary of all the test data on the 15 basic compositions is presented in the bar graph of Fig. 2. Here the respective strengths are shown on each composition at temperatures of 200, 230, 260, 290, and 320°F. Strength values represented by the bar graphs are shown for 1, 3, 7, 28, 60, and 90 days for each temperature condition of curing, except at 230° F where the 90-day values were not obtained. Tables 5 and 6 show the tabulated strengths of these 15 compositions after 1 day and 90 days of curing.

Most cementing compositions reached their maximum strength at 200° F in three to seven days, and showed very little change after curing for periods up to 180 days, with the exception of pozzolanic cements. With these materials the setting process is slower and the strength continued to increase even after 90 days of curing.

At 230° F the element of retrogression in strength was observed in some cementing compositions and became more pronounced at higher temperatures. Those compositions which contained pozzolans, portland cement and retarder continued to increase slowly in strength to 260° F, then began to retrogress at 290 and 320° F. The pozzolan-lime compositions, both with and without retarder, showed no evidence of loss in strength at any temperature and continued to increase slowly beyond 90 days. In those tests conducted for 180 days, this same increase in strength was noted.

This retrogression factor seems to depend on time and temperature in those cementing compositions where it occurs. The major loss in strength seems to take place with or without additives in the first 28 days with only minor changes beyond this time. At 290° F and above, this loss appears to take place in the first seven days.

Some of the compositions tested showed only moderate loss in strength, while in others this loss was very great. A few cementing materials were unaffected and actually gained in strength at the higher temperatures. A more specific break-

TABLE 3—CHEMICAL ANALYSIS

Composition	Oxide Analysis							Clinker Composition Loss Free Basis						Sieve Analysis Per cent	Surface Area Wagnor
	SiO_2	Fe_2O_3	Al_2O_3	CaO	MgO	SO_3	LOI	C_3S	C_2S	C_4AF	C_3A	$CaSO_4$	MgO	Passing 325	Cm^2/Gm
1. Retarded Cement A	22.8	4.5	5.0	64.2	0.5	1.5	0.7	44.0	32.2	13.7	5.6	2.6	1.5	89.0	1732
2. Retarded Cement B	24.3	3.1	3.1	65.3	0.9	1.3	1.3	52.1	31.4	9.6	3.1	2.2	0.9	71.9	1478
3. Retarded Cement C	23.2	5.0	4.2	64.0	1.2	2.0	0.7	42.7	34.4	15.2	2.7	3.4	1.2	79.1	1520
4. Retarded Cement D	21.2	4.8	5.8	63.5	1.0	2.1	0.4	46.0	26.1	14.6	7.0	3.6	1.0	74.5	1429
5. Retarded Cement E	21.2	6.0	4.9	63.1	1.1	2.0	0.2	44.4	27.3	18.2	3.9	3.4	1.1	89.0	1704
6. API Class A Cement	22.2	2.8	5.8	65.6	1.9	1.8	0.7	50.0	26.0	9.0	11.0	3.0	1.0	91.9	1771
7. Pozzolan X	47.12	23.12	17.87	3.96	1.22	0.98	1.98	—	—	—	—	—	—	84.9	3386*
8. Pozzolan Y	45.40	13.70	16.70	9.1	2.20	0.00	0.04	—	—	—	—	—	—	74.7	—
9. Pozzolan Z	65.92	22.32**	—	4.42	2.24	0.00	2 81	—	—	—	—	—	—	81.0	—

*Blaine
**As Iron and Aluminum Oxide

down of these results is illustrated in Fig. 3 and is as follows.

Retarded Cements

Each of the five brands of retarded cements gained in strength for its first three days and showed very little change at 200° F for periods up to six months. The average strength of all five cements was approximately 9,000 psi.

At 260° F a gain in strength was noted for the first seven days, then retrogression became pronounced. This loss continued for periods up to 90 days, where a leveling-off occurred. In most instances, this loss was not as serious as at higher curing conditions.

At 290 and 320° F, each of the five brands of cement began to retrogress after 24 hours, attained a maximum strength loss and showed little change after 90 days of curing. The average strength at 290° F in 90 days was 2,650 psi, while at 320° F this average dropped to 2,045 psi.

These latter values represent a loss of 77 per cent of the one-day strength.

The addition of a lignin retarder to common portland cement produced results almost identical to the five retarded brands of cement tested. This represents a good comparison between these two types of cements, which have a wide variation in chemical compositions.

Portland Cement with Pozzolans

The addition of 50 per cent pozzolan by absolute volume to an API Class A cement with sufficient retarder to allow placement in wells to 14,000 ft produced results similar to retarded cements. With the three types of pozzolans tested with portland cement and 2 per cent bentonite, the percentage loss was not as great as with retarded cement. It is possible that this loss was partly due to the presence of bentonite rather than to the nature of the pozzolan cement, although no data are presented without the presence of bentonite. Portland cement with pozzolans plus 2 per cent bentonite averaged about 2,500 psi compressive strength at 320°F in 90 days, which was somewhat higher than the average for the retarded cement.

Bentonite

The effects of bentonite on the retrogression of strength were evaluated with one brand of retarded cement, an API Class A cement, and an API Class B cement. The presence of bentonite produced more pronounced loss in strength than any other single additive except diatomaceous earth.

Bentonite had an extremely detrimental effect on the strength of cements at temperatures above 230° F.

TABLE 4—PERMEABILITY OF SET CEMENT—MD

Composition	Curing Time — Days, 290°F 3	290°F 7	290°F 14	320°F 3	320°F 7	320°F 14
1. Retarded Cement D	0.0241	0.0116	0.0178	0.0967	8.0537	—
2. Retarded Cement D—4 Per cent Gel	0.1285	0.0482	0.0409	0.3503	23.3190	21.0937
3. API Class A Cement — 0.7 Per cent Lignin Retarder—12 Per cent Gel	0.4113	0.1827	0.1398	0.7282	12.4322	—
4. API Class A Cement—Pozzolan X—0.5 Per cent Lignin Retarder	0.0003	0.0061	0.0075	0.0028	0.0207	0.0290
5. API Class A Cement—Pozzolan Y—0.5 Per cent Lignin Retarder	0.0021	0.0031	0.0014	0.0003	0.0065	0.0081
6. Pozzolan X—15 Per cent Hydrated Lime—0.5 Per cent Lignin Retarder	0.0087	0.0038	0.0007	0.0103	0.0182	0.0019
7. Retarded Cement D—Illmenite Ore—Lignin Retarder	0.0019	0.0030	0.0041	0.0392	8.9846	—
8. API Class A Cement—0.7 Per cent CMHEC Retarder—20 Per cent Diatomaceous Earth	0.1065	0.0344	0.0453	0.0060	0.0548	0.0522

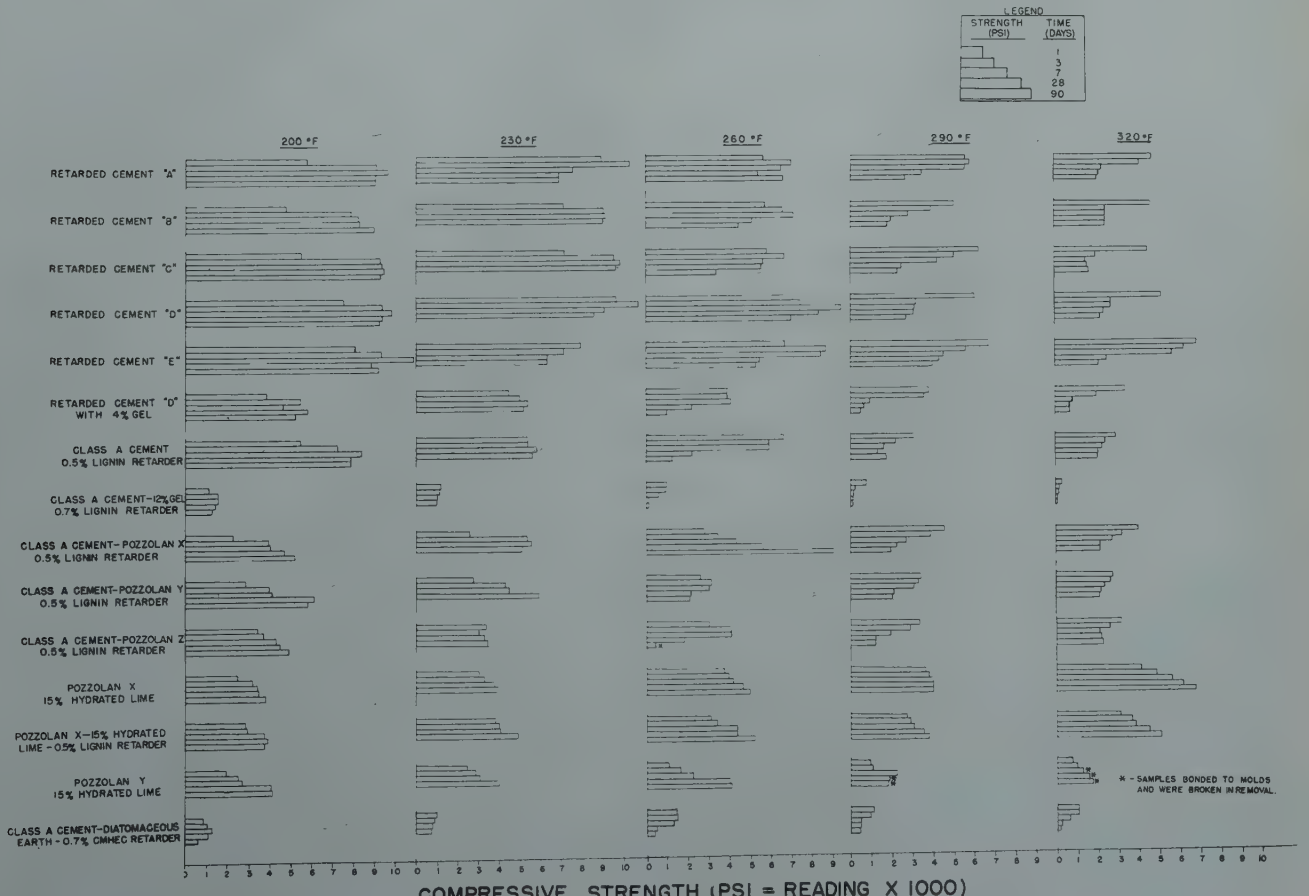
LEGEND
STRENGTH (PSI)
TIME (DAYS)
1
3
7
28
90
200 °F
230 °F
260 °F
290 °F
320 °F
RETARDED CEMENT "A"
RETARDED CEMENT "B"
RETARDED CEMENT "C"
RETARDED CEMENT "D"
RETARDED CEMENT "E"
RETARDED CEMENT "D" WITH 4% GEL
CLASS A CEMENT 0.5% LIGNIN RETARDER
CLASS A CEMENT-12% GEL 0.7% LIGNIN RETARDER
CLASS A CEMENT-POZZOLAN X 0.5% LIGNIN RETARDER
CLASS A CEMENT-POZZOLAN Y 0.5% LIGNIN RETARDER
CLASS A CEMENT-POZZOLAN Z 0.5% LIGNIN RETARDER
POZZOLAN X 15% HYDRATED LIME
POZZOLAN X—15% HYDRATED LIME - 0.5% LIGNIN RETARDER
POZZOLAN Y 15% HYDRATED LIME
CLASS A CEMENT-DIATOMACEOUS EARTH - 0.7% CMHEC RETARDER
* - SAMPLES BONDED TO MOLDS AND WERE BROKEN IN REMOVAL.
0 1 2 3 4 5 6 7 8 9 10
COMPRESSIVE STRENGTH (PSI = READING X 1000)

Fig. 2—Summary of the Compressive Strengths at Elevated Temperatures and Pressure.

At 260° F one brand of retarded cement with 4 per cent bentonite had dropped from about 7,000 psi in one day to aproximately 1,000 psi in 90 days. At 290 and 320° F this loss was much more rapid and had reduced the strength to about 500 psi with this same cement. Data not included herein indicated this same behavior in other brands of retarded cements.

With percentages of bentonite greater than 4 per cent in portland cement, the loss of strength was more rapid and of a greater magnitude. Eight per cent bentonite produced a greater loss in strength at 260° F in retarded cement than did 4 per cent.

Retrogression of portland cement, which contained high percentages of bentonite plus a lignin dispersant and retarder, was more severe than with retarded cement. At temperatures of 260° F and above, this type of cementing composition had lost almost its entire strength in 28 days, with values of less than 50 psi. While 260° F is generally the upper temperature limit for high percentages of bentonite in cement, it did become apparent that bentonite was significantly detrimental to the strength of cements at high temperatures.

Pozzolan-Lime Compositions

This composition was the only one of those studied that actually showed no evidence of strength loss at high temperatures and extended periods of time. The early strength gain was not as great in these compositions as with retarded cements, but at higher temperature the 28 to 90-day strengths were appreciably higher than for any of the other evaluated compositions. Comparing the two tested pozzolans, fly ash and natural pozzolan, there seemed to be little difference in strength at lower temperatures. At higher temperatures the natural pozzolan showed an extremely high bonding effect to the brass curing molds. In removing these specimens at 290 and 320° F after curing at 7, 28, and 90 days, a breakage occurred in the specimen and the strength values shown are not representative of the actual strength of the material.

Heavy Weight Additive

Limited data were obtained to study effects of two different types of heavy weight additives. Regular drilling mud barite and a special grade of illmenite ore were compared in retarded cements and pozzolan-lime compositions at 290 and 320° F, since this was the temperature at which the loss in strength became most critical. There seemed to be no appreciable loss in strength caused by the addition of either of these materials. The use of barite produced much lower strengths in both compositions, but this was probably due to higher quantities required to get the desired weight of 18 lb/gal and the additional mixing water. To obtain a heavy weight slurry using the illmenite ore required very little material or added mixing water and as a result, produced higher strengths than barite in both retarded cements and pozzolan-lime compositions.

Chemical Retarders

The two retarders, a lignin compound and CMHEC, were studied in combination with the heavy weight additives in pozzolan-lime slurries and in one brand of retarded cement. A comparison between these seems to show very little effect on retrogression in strength; however, the higher water requirements for CMHEC produced somewhat lower strengths. The lignin retarder actually dispersed the slurries and required less water to obtain the same initial slurry viscosity.

Diatomaceous Earth

In the one composition tested with portland cement containing 20 per cent diatomaceous earth plus CMHEC retarder, a rather severe strength loss occurred at temperatures above 230° F. The actual values were very similar to the results with 12 per cent bentonite in common portland.

X-Ray Diffraction Studies

After making strength tests, patterns were run on set samples of the hydration compounds formed with time and temperature. As retrogression in strength occurred, various compounds were detected by this analysis. In those cements where retrogression appeared to be the greatest a particular compound was detected and identified as dicalcium silicate alpha hydrate. Literature references by other investigators[6] indicate this compound has no cementitious value and would explain possible causes for loss in strength as noted. Additional work is being conducted on this phase and will possibly be presented at a later date.

Permeability

The permeability of the set cement to water at different time intervals at 290 and 320° F are presented in Table 4. These conditions were selected since this is the temperature

TABLE 5—24 HOUR COMPRESSIVE STRENGTH—PSI
(Pressure—3,000 psi)

Composition	CURING TEMPERATURE — °F 200	230	260	290	320
1. Retarded Cement A	5,765	8,500	5,710	5,500	4,710
2. Retarded Cement B	4,700	7,000	5,700	5,000	4,690
3. Retarded Cement C	5,465	7,100	5,760	6,200	4,475
4. Retarded Cement D	7,490	9,400	7,150	6,000	5,140
5. Retarded Cement E	8,050	7,800	6,675	6,700	6,850
6. Retarded Cement D—4 Per cent Gel	3,815	4,400	3,930	3,750	3,325
7. API Class A Cement — 0.5 Per cent Lignin Retarder	5,425	5,700	6,650	3,050	2,885
8. API Class A Cement — 0.7 Per cent Lignin Retarder — 12 Per cent Gel	1,070	1,075	980	670	230
9. API Class A Cement—Pozzolan X—0.5 Per cent Lignin Retarder	2,195	2,500	2,775	4,500	3,910
10. API Class A Cement — Pozzolan Y — 0.5 Per cent Lignin Retarder	2,850	2,900	2,610	3,400	2,710
11. API Class A Cement — Pozzolan Z — 0.5 Per cent Lignin Retarder	3,435	3,250	3,050	3,300	3,075
12. Pozzolan X — 15 Per cent Hydrated Lime	2,450	3,000	3,950	3,600	4,110
13. Pozzolan X — 15 Per cent Hydrated Lime 0.5 Per cent Lignin Retarder	2,865	3,800	3,435	3,700	3,075
14. Pozzolan Y — 15 Per cent Hydrated Lime	1,950	2,400	1,180	900	735
15. API Class A Cement — 0.7 Per cent CMHEC Retarder — 20 Per cent Diatomaceous Earth	880	1,000	1,295	1,100	1,025

TABLE 6—90 DAY COMPRESSIVE STRENGTH — PSI
(Pressure — 3,000 psi)

Composition	CURING TEMPERATURE — °F 200	260	290	320
1. Retarded Cement A	9,300	6,500	2,625	2,005
2. Retarded Cement B	9,100	4,485	1,750	2,445
3. Retarded Cement C	9,250	3,410	2,230	1,590
4. Retarded Cement D	9,200	7,010	2,625	2,145
5. Retarded Cement E	9,150	5,375	3,910	2,045
6. Retarded Cement D — 4 Per cent Gel	5,200	1,100	410	695
7. API Class A Cement — 0.5 Per cent Lignin Retarder	8,100	1,300	1,695	1,950
8. API Class A Cement — 0.7 Per cent Lignin Retarder — 12 Per cent Gel	1,300	40	50	65
9. API Class A Cement — Pozzolan X-0.5 Per cent Lignin Retarder	5,100	9,000	1,875	2,010
10. API Class A Cement — Pozzolan Y-0.5 Per cent Lignin Retarder	5,800	1,950	1,990	2,035
11. API Class A Cement — Pozzolan Z-0.5 Per cent Lignin Retarder	5,000	500*	1,985	2,265
12. Pozzolan X — 15 Per cent Hydrated Lime	3,800	5,000	4,000	6,735
13. Pozzolan X — 15 Per cent Hydrated Lime 0.5 Per cent Lignin Retarder	4,000	5,100	3,740	5,010
14. Pozzolan Y — 15 Per cent Hydrated Lime	4,200	4,100	1,500*	2,100*
15. API Class A Cement — 0.7 Per cent CMHEC Retarder — 20 Per cent Diatomaceous Earth	600	400	410	50

*Specimen bonded to mold and broke during removal

range where strength retrogression appears to be the most severe. All measurements were found to be less than 1 md with a few exceptions. At 290° F the permeabilities were lower for the same time interval than at 320° F. The retarded cement with or without bentonite increased rapidly between these two temperatures and had the highest values at 320° F of all compositions tested. Portland cement with 12 per cent bentonite was fairly soft and the packing effect at the time of testing may not give a comparative permeability to the other compositions. Pozzolan-lime compositions produced the lowest permeability values of all those studied. In general, the permeabilities of the set cement decreased as the strength of the cement increased and where retrogression was the greatest corresponding permeabilities were noted.

Composition	Effect of temperature on strength	Average compressive strength — 180 days 200° F	260° F	320° F
Retarded cement (ave. 5 brands)	Loss	9200	5400	2040
Retarded cement plus 4 per cent gel	Loss	5200	965	600
Pozzolan-portland cement-retarder	Loss	5300	5400	2100
Portland Cement 12 per cent gel-retarder	Loss	1120	40	65
Pozzolan-lime-retarder	Gain	4000	4800	4700
Portland-diatomaceous earth-retarder	Loss	800	400	50

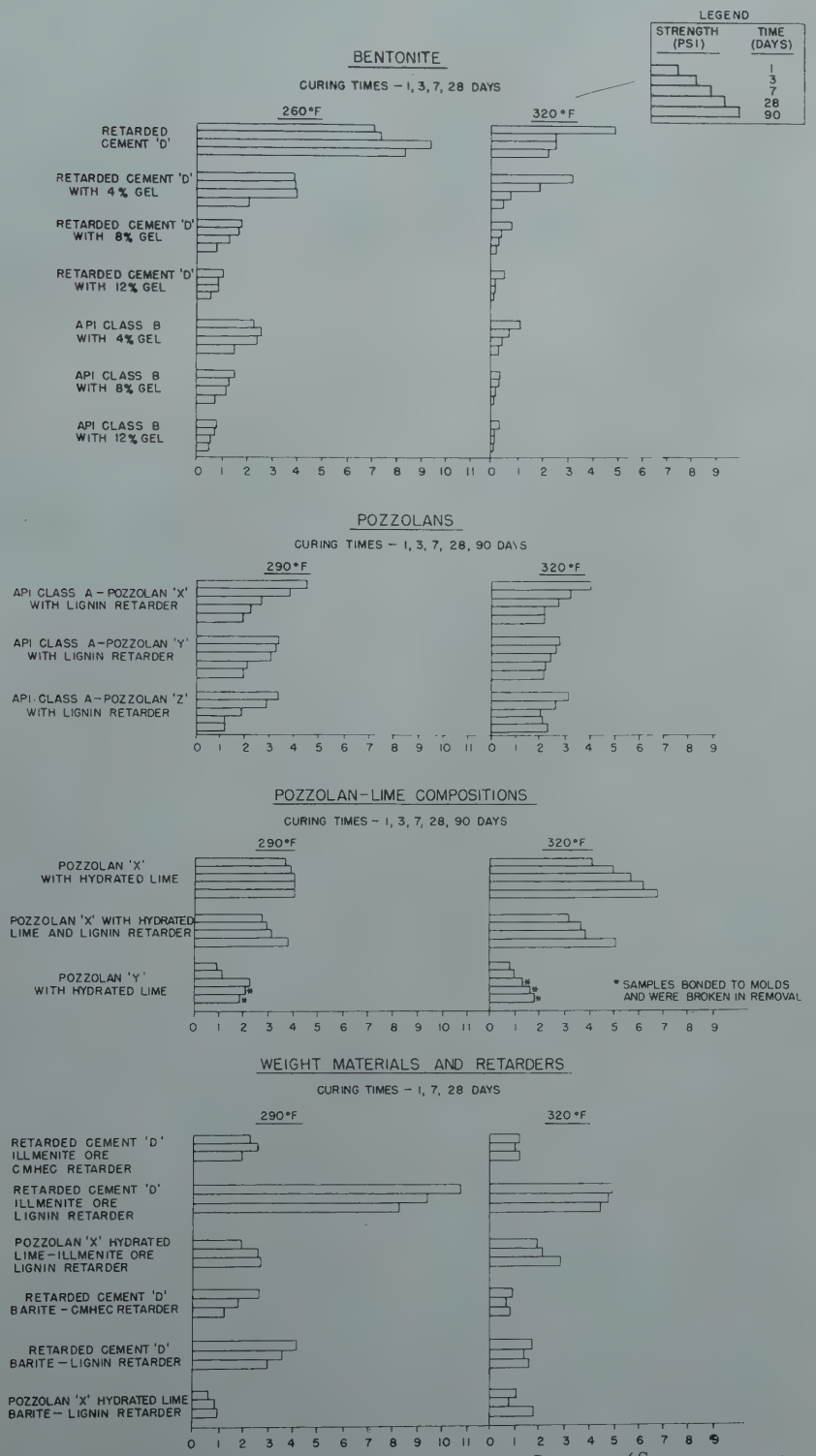
LEGEND
STRENGTH (PSI)
TIME (DAYS)
1
3
7
28
90
BENTONITE
CURING TIMES – 1, 3, 7, 28 DAYS
260°F
320°F
RETARDED CEMENT 'D'
RETARDED CEMENT 'D' WITH 4% GEL
RETARDED CEMENT 'D' WITH 8% GEL
RETARDED CEMENT 'D' WITH 12% GEL
API CLASS B WITH 4% GEL
API CLASS B WITH 8% GEL
API CLASS B WITH 12% GEL
POZZOLANS
CURING TIMES – 1, 3, 7, 28, 90 DAYS
290°F
320°F
API CLASS A – POZZOLAN 'X' WITH LIGNIN RETARDER
API CLASS A – POZZOLAN 'Y' WITH LIGNIN RETARDER
API CLASS A – POZZOLAN 'Z' WITH LIGNIN RETARDER
POZZOLAN–LIME COMPOSITIONS
CURING TIMES – 1, 3, 7, 28, 90 DAYS
290°F
320°F
POZZOLAN 'X' WITH HYDRATED LIME
POZZOLAN 'X' WITH HYDRATED LIME AND LIGNIN RETARDER
POZZOLAN 'Y' WITH HYDRATED LIME
* SAMPLES BONDED TO MOLDS AND WERE BROKEN IN REMOVAL
WEIGHT MATERIALS AND RETARDERS
CURING TIMES – 1, 7, 28 DAYS
290°F
320°F
RETARDED CEMENT 'D' ILLMENITE ORE CMHEC RETARDER
RETARDED CEMENT 'D' ILLMENITE ORE LIGNIN RETARDER
POZZOLAN 'X' HYDRATED LIME – ILLMENITE ORE LIGNIN RETARDER
RETARDED CEMENT 'D' BARITE – CMHEC RETARDER
RETARDED CEMENT 'D' BARITE – LIGNIN RETARDER
POZZOLAN 'X' HYDRATED LIME BARITE – LIGNIN RETARDER

FIG. 3—EFFECT OF ADDITIVES ON STRENGTH OF CEMENT (STRENGTH, PSI = READING × 1,000).

CONCLUSIONS

1. Loss in strength occurs in many of the cementing compositions used in high temperature wells. The critical temperature range appears to begin at 230°F while the more severe range seems to be at temperatures above 260°F. As the temperature increases above 260°F this retrogression phenomenon progresses more rapidly. In general, very little retrogression in strength was noted between 7- and 90-day strengths at 290 and 320°F.

2. All five of the retarded cements showed only slight deviation in strength between brands. The presence of certain additives in some cementing compositions produces severe retrogression effects, while some have very little or no effect on either retarded cements or pozzolan-lime compositions. A summary of 180-day strength values of the 15 basic compositions at three temperatures are shown in the table above.

3. While the strength of many of those compositions which showed retrogression are thought to be adequate for oil well cementing, it is possible that some of the many variable factors, such as mud contamination during the placement of cement slurry in a well, could produce a weakened set cement which would be much more susceptible to high temperature retrogression.

4. Test data with the two weight materials, barite and illmenite, show no serious evidence of strength retrogression in 28 days at 290 or 320°F as a result solely of the material itself.

5. Two of the more commonly used retarders do not appear to be affected by the high temperature strength loss.

6. The ratio of solids to the amount of mixing water appears to be a factor in affecting the strength of cements at high temperatures. For

example, two of the highest water-requiring additives, bentonite and diatomaceous earth, produced the greatest loss in strength.

7. There appears to be no correlation between the type of cement, chemical analysis, fineness or pumpability on the loss in strength.

8. X-ray diffraction studies detect the formation of a compound (dicalcium silicate alpha hydrate) which has little or no strength properties in those compositions where the severest loss in strength occurs.

9. Permeabilities of the set cement followed a similar trend to the compressive strength and were the greatest where retrogression was the severest. Those compositions having the greatest strengths likewise produced the lowest permeability.

ACKNOWLEDGMENT

The authors wish to express their appreciation to the Halliburton Oil Well Cementing Co. for permission to prepare and publish this paper. Appreciation is also extended to those of this organization who helped obtain data and offered suggestions for the preparation of this paper.

REFERENCES

1. "Effects of High Temperatures and Pressures on Strength of Oil Well Cements", The Mid-Continent Dist. Study Committee on Cementing Practices and Testing of Oil Well Cements, Spring Meeting, API, Oklahoma City, Okla. (1954).
2. Saunders, C. D., and Walker, W. A.: "Strengths of Oil Well Cements and Additives Under High Temperature Well Conditions", Paper 390-G presented at AIME Fall Meeting, San Antonio, Tex. (Oct., 1954).
3. Ludwig, N. C., and Pence, S. A.: "Properties of Portland Cement Pastes Cured at Elevated Temperatures and Pressures", *Jour.*, American Concrete Institute (Feb., 1956) **27,** No. 6, 673.
4. *Recommended Practices for Testing Oil Well Cements*, 5th Ed., API RP 10B, 1956.
5. Morgan, B. E., and Dumbauld, G. K.: "Measurement of the Permeability of Set Cement", *Trans.* AIME (1952) **195,** 323.
6. Kalousek, G. L.: "The Reaction of Cement Hydration at Elevated Temperatures", *Proc.*, Third International Symposium on the Chemistry of Cement, London (1952) 351.

DISCUSSION

B. E. MORGAN
MEMBER AIME

HUMBLE OIL & REFINING CO.
HOUSTON, TEX.

The presentation of this paper is apt to cause some confusion and anxiety about the effectiveness of certain cementing compositions in oil and gas wells, especially in connection with the use of bentonite in portland cements. It seems advisable, therefore, to offer a few comments about the proper use of bentonite in portland cements.

To begin, let me express appreciation to the authors for the extensive results presented in their paper. Their paper contains more laboratory data on several cementing compositions than have been published previously, but the information in the paper is not new. In addition to references cited, Dumbauld and Morgan presented in 1953 a limited amount of strength data on cements containing bentonite cured at temperatures ranging from 100 to 320° F. These early results and the data presented today are in fairly good agreement despite the fact that Carter and Smith used considerably more water in the cement containing 12 per cent bentonite and 0.7 per cent lignin retarder than we did, and, more water than we consider to be realistic for this composition.

To remove any possible misunderstanding about what we consider to be the proper use of bentonite in cements, the following is from the paper, "Recent Developments in the Use of Bentonite in Cements," which was published in *Drilling and Production Practice*, API (1953).

"Data presented in Table 5 indicate that modified cements containing 12 to 16 per cent bentonite and 0.25 to 0.75 per cent calcium lignosulfonate develop sufficient strength and impermeability to be used in wells having temperatures ranging from about 100 to 275° F. Near 275° F, the strength starts to decrease and the permeability starts to increase. This phenomenon has been noted in all portland cements, both regular portland and slow setting with and without bentonite added, but it is more critical in cement containing bentonite because the ultimate strength of the cement has already been reduced by the large amount of water which is added with the bentonite. For these reasons, modified cements have not been used in wells with formation temperatures above about 250°F. Higher strengths and slightly lower permeabilities are obtained by a reduction in the amount of bentonite used, as shown in Table 6, but the slurry weight must be increased. No troubles which might be attributed to failure of the modified cement to set properly have been experienced in the primary cementing of many wells with formation temperatures near 250°F at depths between about 9,000 and 13,000 ft."

The first conclusion of this paper reads as follows:

"Laboratory data and extensive field experience show that the properties of cements containing bentonite are satisfactory for use in wells with formation temperatures ranging from about 100 to 250° F. Cements containing 8 to 12 per cent bentonite have been used successfully in several thousand wells during the past four years."

To conclude, we wish to emphasize three points:

1. The data in the present paper and those published four years ago on the strength properties of bentonite-containing cements are in fairly good agreement. Accordingly, no change is needed in the existing recommendations for the proper use of bentonite in cements.

2. Bentonite-containing cements possess satisfactory properties for both the primary cementing and the squeeze cementing of wells with formation temperatures in the range of about 100 to 250°F.

3. Bentonite cements may not possess satisfactory set properties for the primary cementing of casing in wells having formation temperatures in excess of about 250°F; therefore, bentonite should not be added to cements to be used in primary cementing operations in deep, high-temperature wells. In squeeze-cementing operations it is likely that satisfactory set properties are obtained with bentonite-containing cements in wells having temperatures somewhat in ex-

cess of 250° F, because much of the water is apt to be filtered from the cement slurries before they set. It seems logical, however, to avoid the use of bentonite-containing cements at well temperatures above about 250° F in both primary and squeeze-cementing operations if other cementing compositions are available which possess the desired filtration rate, thickening time, and set properties.

AUTHORS' REPLY to B. E. MORGAN

These comments on the use of bentonite in cements are certainly appreciated. Morgan is correct in stating that the retrogression behavior in bentonite cements is not new, yet we know of no prior long-term strength data as shown herein. We also feel that the effects of the other admixtures on the strength of cements are new to the industry, as some of them have only been available for deep well cementing a short period of time.

Actually this paper is a continuation of the work by C. D. Saunders and W. A. Walker on the "Strengths of Oil Well Cements and Additives Under High Temperatures" presented at the AIME Fall Meeting in San Antonio, Tex., in 1954. Their paper was presented as a progress report with no definite conclusions being made until further testing could be completed.

As pointed out in the introduction, other data have been published but these investigations were limited in the curing time or the number and type of compositions tested. Since many cementing compositions have shown a tendency to lose their strength at high temperatures, it was the intention of this paper to obtain data with all types of cementing compositions over long periods of time to show what actual strength values would be expected and to give reasons for the cause of this behavior. ★★★

Process Variables of In Situ Combustion

WILLIAM L. MARTIN
MEMBER AIME
JOHN D. ALEXANDER
JUNIOR MEMBER AIME
JOHN N. DEW
MEMBER AIME

CONTINENTAL OIL CO.
PONCA CITY, OKLA.

ABSTRACT

This paper describes the results of a laboratory investigation conducted to obtain data for an evaluation of the in situ combustion process as a method of producing crude oil from reservoirs. Air and fuel requirements, rates of advance, combustion temperatures, and coke and fluid distributions are presented. The mechanism of oil recovery by in situ combustion is discussed.

Five crude oils ranging in gravity from 10.9 to 34.2° API were produced from a semiadiabatic, unconsolidated sand pack by in situ combustion. Experimental conditions were varied over a wide range in order to determine the inter-relationships of process variables. The minimum air flux requirement for self-sustained combustion was found to be less than 10 scf/hr-ft². The rate of advance of a self-sustained combustion zone was found to be nearly proportional to the air flux at the combustion front.

The effects of pressure and injected air flux were studied in a series of experiments using a 21.2° API crude. A minimum air requirement was observed at an air flux of 20 scf/hr-ft². The oil saturation consumed as fuel averaged 5.5 per cent of pore volume. The effect of air pressure was found to be small for experiments having high combustion efficiencies.

This study should promote a better understanding of the problems and mechanisms involved in laboratory investigations and field applications of the in situ combustion process. The data presented will be useful in the interpretation of results of field tests. When tempered with volumetric sweep efficiencies, the data can be used in making preliminary economic appraisals of the process as applied to reservoirs containing high porosity unconsolidated media.

Original manuscript received in Society of Petroleum Engineers office on Aug. 7, 1957. Revised manuscript received Dec. 30, 1957. Paper presented at 32nd Annual Fall Meeting of Society of Petroleum Engineers in Dallas, Tex., Oct. 6-9, 1957.

INTRODUCTION

The purpose of this work was to obtain laboratory data for an evaluation of the in situ combustion process as a method of producing crude oil from reservoirs.

In situ combustion basically consists of (1) injecting air into a reservoir through selected input wells to create an air sweep through the reservoir, (2) igniting the crude at the injection well, and (3) propagating the combustion front through the reservoir by continued air injection. By this means, oil is swept toward producing wells in the area. The fuel for combustion is supplied by heavy residual material (coke) which has been deposited on the sand grains during distillation and cracking of the crude oil ahead of the combustion front.

Recovery of petroleum by a combustion or heat wave process is not a new idea. F. A. Howard was granted a patent in 1923 on a process in which air and a combustible gas were pumped into an injection well and ignited.[1] Russian engineers reported on field experiments with a crude oil gasification process in 1935[2]. Other known early field tests include those conducted near Bartlesville and Ardmore, Okla., in 1942.[3] More recently completed field tests include an inverted seven-spot by Sinclair Oil Co. in the Delaware-Childers field, Nowata County, Okla.[4]; a three-well and an inverted five-spot test by Magnolia Petroleum Co. in Jefferson County, Okla.[5,6]; and a test by California Research Corp. in the Irvine-Furnace field in Kentucky. The Worthington Corp. has completed a test in cooperation with the Forest Oil Corp. in Clark County, Ill.[7]

Several field tests are now in progress. Sinclair has acquired a 600-acre lease in the Humboldt-Chanute field, Allen County, Kans., and is under way with a large-scale operation. Three field tests are under way in California. The General Petroleum Corp. is conducting an inverted five-spot pattern test in the South Belridge field in Kern County under a cooperative agreement with 11 other companies, including Continental Oil Co. California Research Corp. is conducting a four-well pattern test in Midway-Sunset field near Maricopa, and Richfield Oil Corp. is under way with a test in the Ojai field in Ventura County.

Although the published information is valuable concerning results of field tests, little laboratory data other than that reported by Kuhn and Koch[5] are available to aid in appraising the tests from a technical or economic standpoint. Engineering data needed to evaluate the process include the amount of air required per barrel of oil recovered, minimum injection rates which will support combustion, rates of advance, air required per unit volume of reservoir cleaned, amount of oil recovered, and amount of oil consumed as fuel. The present laboratory investigation was undertaken to provide these data for that portion of the reservoir swept by the combustion zone.

The first phase of this investigation was exploratory in nature and was conducted at injection pressures less than 100 psig. Data were ob-

[1]References given at end of paper.

tained over a wide range of experimental conditions in an effort to observe, qualitatively, the effect of some of the many variables that affect the in situ combustion process. At times several air flow rates were studied during a single experiment. During the second phase of the work, the effects of pressure and injected air flux were studied by means of long-term, stabilized experiments conducted at constant inlet pressure and exit gas flow rate.

DESCRIPTION OF APPARATUS

The two phases of the experimental work were conducted in two discrete, but basically similar, laboratory apparatus.

The simulated reservoirs consisted of vertical stainless steel tubes packed with unconsolidated sand and fitted with the necessary controlling and recording equipment. The first tube was 4 ft long and 4.85 in. in diameter with a wall thickness of 1/16 in. A porous stainless steel plate at the bottom of the tube prevented sand production. Eleven thermocouples in wells spaced at 4-in. intervals were used to measure temperatures at the center of the sand pack. Eleven additional thermocouples were placed against the outside of the tube opposite the wells. A thermocouple at the top gave an indication of the ignitor temperature.

The ignitor heater consisted of a coil of nichrome wire wound on a ceramic cone attached to the top of the apparatus. Five other heaters were wound around the tube so that the wall temperature of 8-in. intervals could be controlled by adjusting a Variac connected to each heater.

Fig. 1 shows a schematic flow diagram of the second apparatus. It was basically similar to the first except that provision was made for experimentation at elevated pressures. The second tube was 6 ft long and 5¾ in. in diameter with a wall thickness of 0.035 in. It was supported within a steel pressure jacket designed to withstand 1,000 psi. During an experiment, the pressure in the jacket was maintained equal to the injection pressure in the pack. The pressure difference across the tube wall was limited to 100 psi.

Sand pack temperatures were measured in a central ¼-in. thermowell with a thermocouple probe consisting of four thermocouples spaced at 4-in. intervals. The outside tube wall temperatures were measured with thermocouples placed at 4-in. intervals along the tube length. Six-

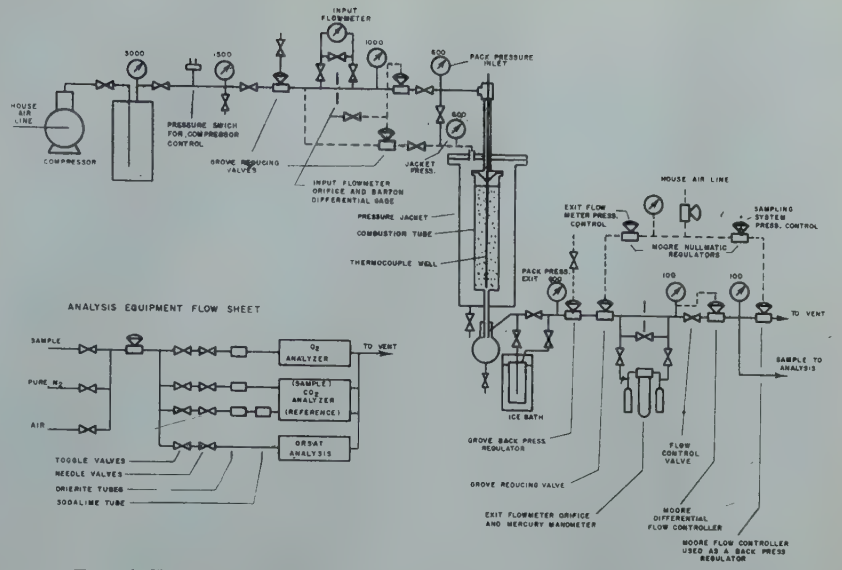

FIG. 1—FLOW SHEET FOR LABORATORY IN SITU COMBUSTION APPARATUS.

teen heaters were wound around the tube, each controlling the tube wall temperature of a 4-in. interval.

Other details of the air supply and flow control and measuring systems are included in the flow sheet (Fig. 1).

DESCRIPTION OF MATERIALS

The unconsolidated sand packs were prepared with Blackhawk E grade sand obtained from the Standard Silica Corp., Ottawa, Ill., and used as received. The sand was packed to the same reference levels in the tubes by slowly pouring in sand from the top while vibrating the tube. The porosities resulting from this technique averaged 36 per cent. The permeability to air of the clean sand before and after burning was about 10 darcies.

The five crude oils studied in the first phase of the investigation ranged in gravity from 10.9 to 34.2° API. ASTM distillation and viscosity data are shown in Table 1. The crude used during the second phase was the 21.2° API gravity crude described in Table 1. This crude had a carbon-hydrogen weight ratio of 7.23.

EXPERIMENTAL PROCEDURE

The tubes were charged with a known weight of sand which was packed to a definite volume as described. Frequently, a previously used pack was reused. After the gas permeability was measured, the pack was evacuated and saturated with water. A known weight of crude was then flooded through the pack, and gas permeability was established with a gas drive at room temperature.

The ignition procedure for the constant-flux experiments included an initial heating of the sand face during a nitrogen drive. This was continued until a temperature gradient was established similar to those previously observed during combustion. Combustion actually began when the injected gas was changed from nitrogen to air. This ignition procedure decreased the tendency for liquid block formation and promoted early stabilization of the experiment.

Pack temperatures were recorded

TABLE 1—VISCOSITY AND ASTM DISTILLATION DATA

Crude Type	10.9° API	18.3° API	21.2° API	28.9° API	34.2° API
Temperature, °F			Viscosity, Centistokes		
100	2,970	2,590	113.7	13.1	9.50
210	—	29.3	12.7	3.28	2.69
Volume Per Cent Distilled			Boiling Point, °F		
IBP	195	214	270	145	149
5	232	275	334	228	233
10	254	334	405	290	274
15	424	—	454	—	—
20	486	498	492	414	369
25	535	—	526	—	—
30	560	601	552	520	471
35	584	—	(33%) 564*	—	—
40	595	630*	—	592	557*
45	607	—	—	—	—
50	620	—	—	654*	—
55	630	—	—	—	—
60	634	—	—	—	—
65	628*	—	—	—	—

*Cracking temperature

continuously on a multipoint recorder. The outside temperatures at all levels were maintained slightly less than the corresponding inside temperatures by manually adjusting the tube wall heater Variacs. This type of control provided semiadiabatic conditions with a slight radial heat loss to the surroundings.

During the experiments, cumulative oil and water production, pressure drop across the pack, pressure at pack inlet, and the location of the combustion front were all plotted against cumulative run time so that a graphical picture of the progress of the run was available. Fig. 2 shows most of these data for Run 15.

RESULTS

In general, correlations attempted with the short-term exploratory data showed trends in fair agreement with the data obtained in the second phase; however, correlations of the exploratory data have been omitted in favor of the more representative constant-flux data. Table 2 gives data from the exploratory phase of the investigation. Table 3 gives the initial fluid saturations, experimental conditions, and material balance data from the constant flux runs. Table 4 gives process data obtained under stabilized combustion conditions during the constant flux runs.

Combustion Front Advance

Fig. 3 shows three successive temperature profiles of the sand-packed tube which were measured during Run 1. The first maximum on each of these curves is indicative of the location of a high temperature zone which accumulated while the ignitor was maintained at a high temperature and the air rate was low. The second maximum on each curve developed when the air injection rate was increased after the initial heating period. The latter peaks were used to locate the combustion front and measure its rate of advance.

Fig. 4 shows the location of the combustion front and the high temperature zone created by the ignitor heater as these two zones moved through the sand pack. It is evident from Figs. 3 and 4 that the rate of advance of the first zone is less than that of the combustion zone. Under the prevailing conditions, heat in the first zone moved more slowly by convection and conduction than the combustion front moved by the in situ generation of heat assisted by convection and conduction.

Rates of advance of combustion

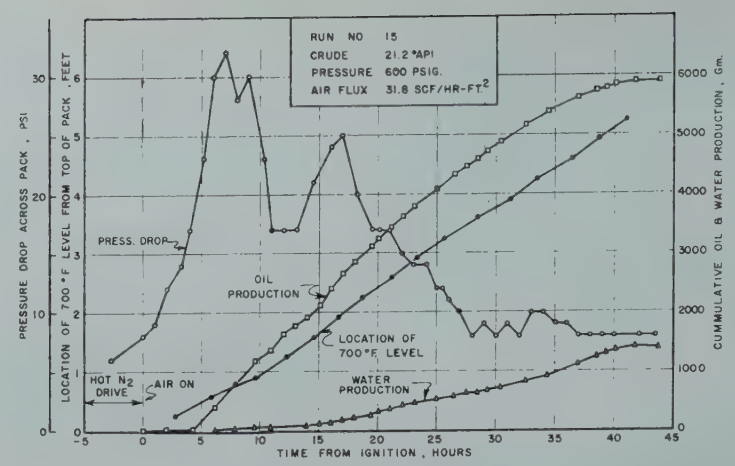

Fig. 2—Experimental Data, Run No. 15.

TABLE 2—COMBUSTION DATA—EXPLORATORY EXPERIMENTS

Run	Crude Oil Gravity, °API	Saturation at Ignition, Per cent of Porosity		Exit Flux scf/hr — ft²	Average Injection Pressure, psig	Approximate Combustion Temperature, °F	Rate of Advance, ft/day	Oxygen to Carbon scf/hr — ft²
		Oil	Water					
1	28.9	70.5	8.4	250	26	850	12.5	12.4
2	28.9	56.6	9.5	255	17	725	4.7	1.4
3	28.9	52.7	13.2	131	21	750	3.5	1.7
				128	13	650	2.6	1.1
4	10.9	63.2	8.7	75	90	1,000	5.0	10.1
				8.9	96	850	0.7	1.5
				23.2	96	850	2.8	3.5
				107	95	950	10.8	10.9
5	18.3	72.5	7.8	60.0	44	950	3.4	7.4
				32.2	26	850	2.6	3.8
				16.8	6	750	1.2	1.9
6	18.3	66.0	15.6	18.3	34	800	1.9	2.6
				74.4	48	900	6.8	10.1
7	18.3	44.1	20.2	23.2	18	825	2.5	3.2
				38.6	10	850	3.3	4.0
8	18.3	53.5	18.4	21.2	70	825	2.8	3.2
				9.9	56	625	0.9	1.0
9	34.2	47.6	15.5	20.1	8	750	2.4	2.1
10	34.2	42.1	17.2	18.6	65	750	2.5	1.9
				10.4	65	625	0.7	1.0
11	34.2	43.3	18.1	20.1	64	750	3.2	2.5
				20.6	64	625	0.8	1.1
12	21.2	75.0	10.7	21.5	27	800	2.8	2.8

TABLE 3—EXPERIMENTAL CONDITIONS AND MATERIAL BALANCE DATA—CONSTANT FLUX EXPERIMENTS — 21.2° API CRUDE

Run	13	14	15	16	17	18[1]
Pressure at Combustion Front, psig	80	80	600	600	600	600
Fluid Content at Ignition						
Grams of Oil	4,689	5,068	6,408	5,135	5,851	5,692
Grams of Water	824	1,925	922	1,000	884	860
Saturations at Ignition, Vol. per cent of Porosity						
Oil	52.3	56.6	76.2	61.0	69.6	67.7
Water	9.0	19.7	10.0	10.9	9.6	9.4
Oil Produced						
Wt. per cent of Charge at Ignition	86.6	90.2	92.2	90.4	89.9	—
Vol. per cent of Porosity	45.3	50.9	70.5	55.2	62.4	—
Estimated Oil Burned						
Wt. per cent of Charge	10.6	9.32	8.54	10.2	8.52	—
Vol. per cent of Porosity	5.08	4.83	5.62	5.70	5.29	—
Carbon-Hydrogen Ratio of Burned Residuum, lb/lb	9.0[2]	9.0[2]	8.54	9.64	12.3	—
Oil Material Balance Check, Wt. per cent	96.7[3]	99.9[3]	100.7	100.7	104.4	—

[1]Interrupted
[2]Assumed
[3]Based on assumed C/H ratio

TABLE 4—PROCESS DATA—CONSTANT FLUX EXPERIMENTS—21.2° API CRUDE

Run	13	14	15	16	17	18
Injected Air Flux, scf/hr-ft²	29.5	29.7	31.8	63.5	125	10.7
Produced Gas Flux, scf/hr-ft²	28.2	28.3	30.0	60.6	121	10.0
Rate of Advance of the Combustion Front, ft/day	2.90	3.26	3.05	5.17	8.39	0.854
Average Combustion Temperature, °F	825	800	775	800	850	650
Average CO_2 in Exit Gas, Vol. per cent	10.8	10.7	10.9	9.9	7.7	11.4
Average CO in Exit Gas, Vol. per cent	3.2	4.1	3.4	3.3	2.0	3.1
Average O_2 in Exit Gas, Vol. per cent	3.3	2.2	1.9	3.9	8.6	1.0
Carbon Burned, lb/100 lb of sand cleaned	0.99	0.94	1.11	1.23	1.10	1.24
Residue Burned, Vol. per cent of porosity	5.08	4.81	5.69	6.23	5.49	6.42
Oxygen Consumed to Carbon Oxides, scf/hr-ft²	3.51	3.63	3.78	7.00	10.52	1.29
Total Oxygen Consumed, scf/hr-ft²	5.25	5.59	6.07	10.93	15.74	2.13
Oxygen Consumed to Carbon Oxides, scf/ft³ of sand cleaned	29.1	26.7	29.8	32.5	30.1	36.3
Total Oxygen Consumed, scf/ft³ of sand cleaned	43.4	41.2	47.9	50.8	45.1	59.8
Oxygen Consumed, per cent of oxygen injected	84.9	90.1	91.4	82.3	60.3	95.6
Air Required, scf/ft³ of sand cleaned	245	219	251	295	358	301
Average Instantaneous GOR, scf/bbl	5,000	5,600	4,400	5,800	6,800	5,100
Minimum Cumulative GOR, scf/bbl	6,500	5,700	4,600	7,400	8,100	6,600
Cumulative GOR at GOR=10,000, scf/bbl	6,800	6,200	5,100	7,500	8,300	6,800
Cumulative GOR at GOR=20,000, scf/bbl	7,200	6,700	5,400	7,800	9,000	7,200

tronts were obtained from slopes of plots similar to Fig. 4 and are presented in Tables 2 and 4 along with corresponding combustion data. The exploratory data are representative of constant flux conditions of several hours' duration, but usually more than one flux was investigated during an exploratory run.

During the constant flux experiments, no sharp combustion peaks were observed because radial heat losses were better controlled and rates of advance were generally lower. In these experiments, the rate of advance of the combustion front was obtained by following the progression of a temperature level known to be representative of combustion conditions.

Fig. 5 shows the effect of injected air flux on the rate of advance of the combustion front. It may be seen that the rate of advance increases almost linearly with increasing flux above a flux of about 30 scf/hr-ft^2. Below this flux of 30, the rate of advance drops off rapidly with a decrease in flux. The most efficient flux is indicated by the point of tangency at 20 scf/hr-ft^2 of a line through the origin. It is of interest that these more precise data substantiate the data obtained in the shorter time intervals during the exploratory work. The effect of pressure on the rate of advance appears to be small. It is also indicated that an increase in water saturation at low levels increases the rate of advance.

Fig. 6 shows the linear relationship between the rate at which oxygen is consumed and the rate of advance of the combustion front. The oxygen converted to carbon oxides was obtained from gas analysis data. The total oxygen consumed was calculated as the difference between the oxygen supplied and the free oxygen produced. It has been assumed that the oxygen not appearing in any form in the produced gases was reacted to form water or oxygenated products, such as organic acids and alcohols. The presence of oxygenated compounds in the produced water was indicated by its color, odor, and low pH.

Combustion Efficiency

The percentage of the injected oxygen which is consumed in passing through the front is a measure of the efficiency of the combustion process. This percentage is calculated by dividing the rate at which oxygen is consumed by the rate of oxygen injection. Fig. 7 shows the percentage consumed as a function of the in-

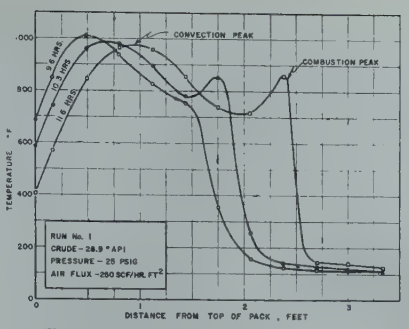

Fig. 3—Temperature Profiles, Run No. 1.

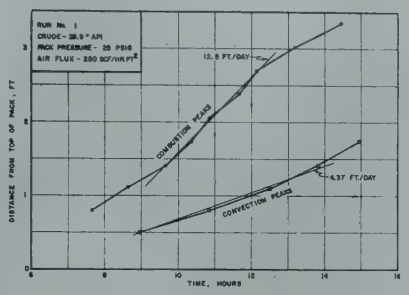

Fig. 4—Advance of High Temperature Zones, Run No. 1.

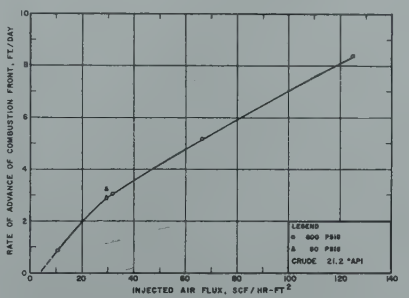

Fig. 5—Effect of Injected Air Flux on the Rate of Advance.

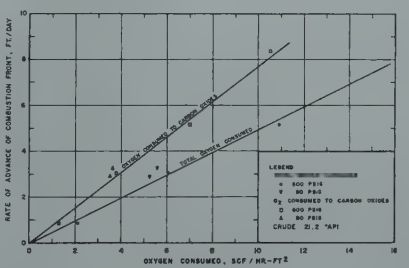

Fig. 6—Effect of Oxygen Consumed on the Rate of Advance of the Combustion Front.

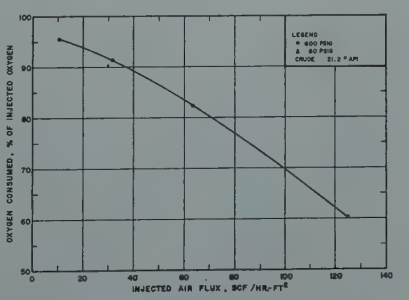

Fig. 7—Effect of Injected Air Flux on Oxygen Consumed as Percentage of Oxygen Injected.

jected air flux during the runs with 21.2° API crude. The combustion temperature for these runs ranged from 650 to 850°F with the average temperature about 800°F. This curve shows that the combustion efficiency increases as the flux is decreased for temperatures greater than 650°F.

As seen in Fig. 7, the combustion efficiencies for the 80 psig runs were less than the efficiency for the 600 psig run at the same air flux. This effect of pressure is due to decreased residence time and the kinetics of combustion. The effect of pressure on the kinetics of combustion becomes even more important when combustion efficiencies are lower. The difference in efficiencies observed between the two 80 psig runs is attributed to water saturation.

Minimum Rate of Self-Sustained Combustion

To maintain isothermal combustion in any situation, heat must be liberated by combustion at a rate equal to the net rate of heat loss to the surroundings. The data obtained in this investigation indicate that it is not possible to maintain stabilized, self-sustained combustion in sand packs by burning residual material at temperatures less than about 600°F due to the kinetics of combustion. Therefore, it is concluded that the minimum rate of self-sustained combustion for unconsolidated sand packs is that required to replace heat losses that occur at about 600°F.

The minimum air flux in any given situation is that required to provide the minimum rate of self-sustained combustion. The minimum rate of advance of a self-sustained combustion front in any given situation is that resulting when air is supplied at the minimum flux.

Minimum Air Flux

No self-sustained combustion front was observed at air rates less than 9.0 scf/hr-ft^2. During Run 8, the air flux was deliberately reduced from 10 to 4.0 scf/hr-ft^2. The temperature of the combustion zone declined steadily from 625 to 400°F, and the concentration of carbon oxides in the exit gases declined from 12.6 to 0.3 per cent in 12 hours. It was apparent that the flux of 4 scf/hr-ft^2 was less than that required for self-sustained combustion.

Combustion was re-established and maintained by adding a small amount of heat to the zone from the wall heaters. On raising the exit flux to 10.4 scf/hr-ft^2, combustion was ob-

served to be self-sustained at about 625°F.

An estimate of the minimum air flux required to support combustion in unconsolidated sand was calculated from experimental temperature gradients by assuming (1) that 100 per cent combustion efficiency was obtained, (2) that the controlling heat loss from the combustion zone was to the cooler sand just ahead, (3) that convective heat transfer was negligible, and (4) that the steady-state law of conduction would describe the heat loss under conditions of constant advance, temperature, and flux. The minimum flux so calculated was 4.0 scf/hr-ft². A value between 4 and 10 scf/hr-ft² is believed to be satisfactory for engineering calculations involving the heavier crude oils in unconsolidated reservoirs.

Minimum Rates of Advance

Experimental rates of advance as low as 0.7 ft/day with exit gas rates of 9 to 10 scf/hr-ft² are listed in Table 2. It is probable that even lower self-sustained rates could have been demonstrated with the improved apparatus. The combustion zone progresses through an oil sand by burning the residual material from the sand grains. The rate of advance of a combustion front is therefore inversely proportional to the amount of residual material laid down by the crude if the air flux and the rate of combustion remain constant. The minimum rate of advance is fixed by the amount of residual fuel that must be removed at the minimum air flux.

Calculations show that roughly 0.6 lb of residuum must be burned to raise the temperature of 100 lb of sand from 75 to 600°F in the absence of heat losses. Under these conditions, a minimum air flux of 4.0 scf/hr-ft² is sufficient to produce a rate of advance of about 1.0 ft/day in unconsolidated sand. This rate would be the theoretical maximum self-sustained rate of advance for a minimum air flux of 4 scf/hr-ft.² However, experimental data indicate that heat losses are minimized at a rate of advance of 2 ft/day. For this case, it would thus be necessary to supply air at a flux of 8 scf/hr-ft² to insure self-sustained combustion.

Air Requirements

Fig. 8 is a plot of the air required per cubic foot of sand cleaned as a function of the injected air flux. This curve shows a minimum air requirement of about 240 scf/ft³ of sand cleaned at a flux of about 20

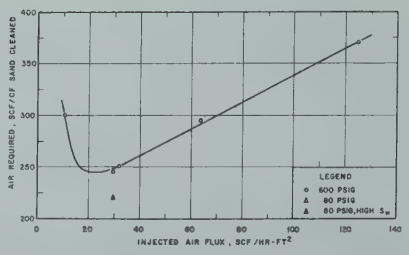

Fig. 8—Effect of Injected Air Flux on the Air Required per Cubic Foot of Sand Cleaned.

scf/hr-ft². The increase in air required as the flux was increased from 30 was due to the decreased efficiency shown in Fig. 7. The sharp increase in air requirements at low fluxes is supported by the data obtained in the exploratory runs. The data point representing data taken at 80 psig is in agreement with the 600 psig data obtained at similar water saturations. An increase in water saturation from 9 to 20 per cent decreased the air requirement for the 80 psig runs from 245 to 219 scf/ft³.

During exploratory runs, the exit gas produced per unit volume of sand pack intervals cleaned was calculated from the rate of advance and exit flux data given in Table 2. A plot similar to Fig. 8 resulted in scattered data points, but a minimum value of about 150 scf of exit gas per cubic foot of sand pack cleaned was observed at a flux of 20 scf/hr-ft².

When residual material is not present in sufficient quantity to insure a high combustion temperature (about 800 to 1,000°F), the kinetics of combustion will prevent the oxygen in air supplied at high rates from being entirely consumed as it passes through the front. This excess air is not used efficiently, although benefit is gained from movement of heat by convection. A scattering of air requirement data was obtained during the experiments with 28.9° API crude oil in early runs at high rates. The average fuel consumption was only 0.2 lb of carbon per 100 lb of sand. Air requirements as high as 1,300 scf/ft³ of sand cleaned were obtained at a flux of 255 scf/hr-ft². At a flux of 200 scf/hr-ft², the average air requirement for this crude was about 1,000 scf/ft³ of sand. This is enough air to move the combustion zone at a rate of about 5 ft/day by convection alone if radial heat losses were eliminated. The same air rate would be used efficiently with a low gravity crude oil, and a much faster rate of advance and lower air requirement per unit of sand cleaned would be observed.

Calculations assuming no heat loss and a heat of combustion of 500 Btu/scf of oxygen burned indicate that the theoretical minimum amount of air required to clean a cubic foot of unconsolidated sand by combustion at 750°F is about 135 scf/ft³. Calculations also show that the theoretical minimum amount of air or other gas required to move a heat wave by convection alone is about 10 scf/lb of sand or about 1,050 scf/ft³ of sand pack cleaned.

Gas-Oil Ratios

The ratios of air injected to oil produced ranged from 4,000 to 37,000 scf/bbl under conditions of stabilized combustion during the exploratory experiments. Fig. 9 shows the instantaneous and cumulative gas-oil ratio vs the percentage of pack cleaned for Run 13 of the constant flux experiments. The instantaneous GOR averaged 5,000 scf/bbl during the period of stabilized combustion. The cumulative GOR for Run 13 was a minimum of 6,500 scf/bbl when the front had cleaned 76 per cent of the pack and was 7,200 scf/bbl when the instantaneous GOR reached 20,000 scf/bbl.

Data from other runs show that the time required for initial oil production decreases as the initial oil saturation increases. With very high initial saturations, the instantaneous GOR starts at a lower value and increases with time. The air required and oil burned per cubic foot of sand cleaned does not change appreciably with oil saturation. Thus, an increase in initial oil saturation decreases the GOR's in tube runs, but the instantaneous GOR is less sensitive to initial oil saturation than the cumulative. Both are important because they give an indication of the

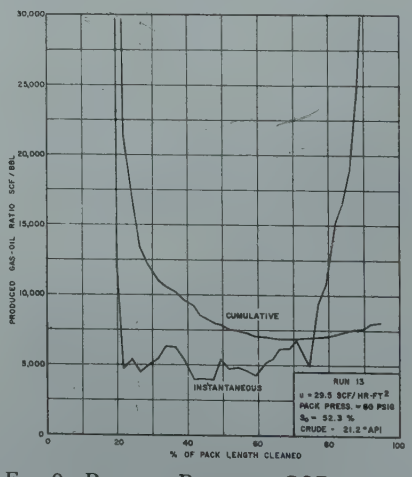

Fig. 9—Plot of Produced GOR vs Per Cent of Pack Length Cleaned, Run No. 13.

cost of oil displaced by combustion. Data in Table 4 show how cumulative and average instantaneous gas-oil ratios varied with air flux.

Oil Produced

Oil recoveries for the constant flux experiments ranged from 86.6 to 92.2 per cent of that in place at ignition. The gravity of the produced oil increased gradually during the latter stages of all runs, because heavy components were used for fuel and lighter hydrocarbons were produced by cracking and distillation. As the combustion front approached the end of the tube, a light oil or distillate was produced. Presumably, a condensate zone forms ahead of the combustion front.

Fuel Requirements

Tables 3 and 4 present data concerning the residual material used as fuel during runs with 21.2° API crude oil. Although the data vary slightly from run to run, an average value of approximately 1.17 lb of carbon per 100 lb of sand cleaned was observed. Table 2 gives exploratory data on oxygen converted to carbon oxides. Plots of these data indicate some effect of air flux on fuel requirements. The constant flux runs show these trends to a lesser degree. Although rationalizations can be made to explain the inflections observed, no definite conclusions seem justified at this time.

The effect of injected air flux on the amount of 21.2° API oil burned was slight and may be deduced from the data in Tables 3 and 4. The amount of crude consumed as fuel averaged 5.5 per cent of pore volume.

The carbon-hydrogen ratio of the fuel consumed was calculated by dividing the total weight of carbon burned, as determined from gas analysis, by the total weight of hydrogen burned, as determined from the combustion water produced. The data show that the carbon-hydrogen ratio increases with combustion temperature and air flux.

Saturation Distributions

Exploratory Run 12 was interrupted when the combustion zone had progressed about 1 ft into the sand pack (about 30 per cent of pack length) in order to obtain data on the distribution of crude oil, residual material, and water near the combustion zone. The pack was allowed to cool under pressure, slowly depressured, and then sampled throughout its length by digging out the sand.

The sand samples were analyzed for oil and water content by the Bureau of Mines method.[8] Samples of the extracted sand were ignited to determine the amount of insoluble residue or coke present. These data are shown in Fig. 10. The data from other interrupted runs resulted in similar shaped curves with about the same amount of residual material and water but with differing oil saturations.

Inspection of Fig. 10 shows that the oil saturation (based on a 21.2° API gravity) increased rapidly to 32 per cent in the 8-in. interval ahead of the burning zone, appeared to level out in the interval of increasing water saturation, and then increased rapidly to about 50 per cent of pore space at the end of the pack. Water saturation was detected about 6 in. from the burning zone and increased rapidly to about 16 per cent, approximately 14 in. ahead of the zone. It is of interest that the maximum coke content of the sand by analysis checks the run average amount of carbon burned as indicated by the Orsat data during this experiment; thus, the coked zone contributes most of the heat liberated by combustion.

Fig. 10 also shows a longitudinal temperature profile of the pack at the time the run was terminated. The maximum concentration of coke or residual material was observed at a point which had reached a temperature of about 700°F. Water saturation began where the temperature of the sand had never exceeded the boiling temperature of water. There was a leveling out of the temperature profile where water saturation increased which reflects the effects of vaporization and condensation of water being driven down the tube.

DISCUSSION

Mechanism of In Situ Combustion

The events which occur as a high temperature combustion front approaches a given point in porous media containing oil and water are as follows. The temperature increases gradually until the condensation and vaporization point of water is reached. The water vapor in the sweep gas condenses, and a residual water saturation is maintained by liquid flow. The residual water then begins to vaporize and is moved away by the sweep gas at a rate corresponding to the rate at which heat is being transferred from the combustion zone. Some oil is moved out by distillation and the increased gas flow resulting from the vaporization of water. When all the water has been vaporized, the temperature at the point increases. During this time, the viscosity of the oil in place decreases, and the volumes of oil and gas are increased by thermal expansion. These effects result in additional flow of liquid oil from the point. In addition to liquid flow, vaporization of oil will occur as component vapor pressures exceed the prevailing pressure. When temperatures approach 600°F, most of the original oil saturation will have been moved away from the point. The residual material begins to crack, forming lighter hydrocarbons and coke. Combustion will be occurring at rates controlled by process variables. If the combus-

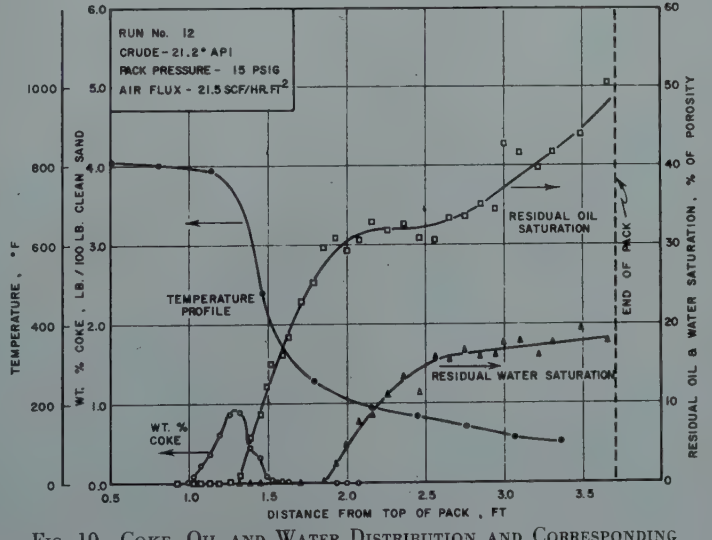
RUN No. 12
CRUDE - 21.2° API
PACK PRESSURE - 15 PSIG
AIR FLUX - 21.5 SCF/HR.FT²
TEMPERATURE PROFILE
RESIDUAL OIL SATURATION
RESIDUAL WATER SATURATION
WT. % COKE
END OF PACK
TEMPERATURE, °F
WT. % COKE, LB./100 LB. CLEAN SAND
RESIDUAL OIL & WATER SATURATION, % OF POROSITY
DISTANCE FROM TOP OF PACK, FT

Fig. 10—Coke, Oil and Water Distribution and Corresponding Temperature Profile, Run No. 12.

tion zone temperature is less than 600°F, considerable hydrogen will be burned. The resulting water vapor is carried by the sweep gas until it condenses ahead of the zone. As temperatures increase from 600°F, the residual material has more of an opportunity to crack before it is burned. Under these conditions more hydrogen will be recovered in the produced hydrocarbons, and the ratio of carbon to hydrogen consumed as fuel will be increased.

Liquids are moved away from an advancing combustion front in part by vaporization and in part by flow. Vaporization occurs at a rate corresponding to the rate of heat transfer from the zone to the liquids. If the heat transferred from a combustion zone causes excessive vaporization, liquid saturations will build up in cooler portions of the porous matrix and gas permeability blocks will develop. These blocks can reduce the air flux to levels below that required for self-sustained combustion. Permeability blocks were a technical difficulty often encountered following the ignition of crude oils in tube runs and may be important during field applications of the process.[5]

The most striking feature of the saturation distributions and the temperature profile shown in Fig. 10 is the short length of the combustion zone and the resulting high temperature gradient at the advancing front. The transition from hot, cleaned sand to relatively cool sand containing oil and water occurred over a distance of approximately 1 ft. At low rates of advance, the amount of preheat received by the porous matrix prior to the arrival of the combustion zone should increase with distance traversed by the front. This should result in a decrease in the residual material and air flux required for sustained combustion.[9] The effects of preheat would appear to be small at rapid rates of advance. It seems logical also that losses to over and underburden will be minimized in many field applications because of the relatively rapid velocities of advancing in situ combustion zones as compared with the rate of heat loss by thermal conduction.

Advance of Combustion Fronts

The propagation of a high energy combustion zone through an oil reservoir is the most rapid method of thermal recovery. Experimental and theoretical data show conclusively that such a combustion zone moves more rapidly than heat can be moved by the combined processes of conduction through the solid matrix and convective heat transfer by gases flowing at similar rates. In addition to being faster, the use of in situ combustion energy results in substantial savings in the amount of air required to advance the front through a unit of reservoir space. With rapid rates of advance, the exploratory data and calculations indicate that an advance by burning only requires about 20 per cent of the gas injection required to advance a heat wave by convection from the sweep gas. We do not wish to imply, however, that the latter technique is without advantage, since recycle of produced combustion gas can often be accomplished with a minimum of compression costs.

There may be a fairly narrow range of crude oil types which will provide the optimum amount of carbon or residual material for propagation of an in situ combustion wave. The methods proposed by Sinclair appear to be applicable to light crudes.[10] These methods involve injecting fuel gas and/or reducing the oxygen content of injected gas so that the rate of advance of the combustion zone is the same as the rate of movement of heat by convection.

If, on the other hand, one burns very heavy crude oils, excess heat is developed in the combustion zone because of the relatively large amount of residue laid down by these crudes. This excess heat is of no apparent value to the process, yet the front cannot be advanced without consuming the residue. This requires large quantities of additional air. With very heavy crudes, it may develop that the air required per unit of sand cleaned will make the process unattractive and means of reducing the air requirements will have to be developed.

For a given crude oil, the rate of advance of a combustion front appears to be directly proportional to the rate of formation of carbon oxides and the rate of total oxygen conversion. But the relationship between the rate of advance and the air flux is influenced by many inter-related variables, such as the combustion efficiency and the amount of residual material burned per unit of sand cleaned. The length of the combustion zone, the pressure and temperature, the reactivity of the residuum, and the air flux affect combustion efficiencies. The effect of process variables on the combustion characteristics and distributions of fluids and solids in combustion zones are important and are amenable to laboratory investigation.

It is apparent that the minimum rate of advance of a combustion front is related to the amount of residual material on the sand grains. For a given minimum air flux, minimum rates of advance decrease as the amount of residual material increases. In view of the many variables affecting minimum rates of advance, they may be defined as those rates which result when air is supplied at the minimum flux required for sustained combustion.

Minimum Air Rates

The instantaneous heat loss from the zone and the ratio of residual fuel to rock solids are the important variables relative to the definition of a minimum air rate. Preheat will tend to reduce the heat loss from a burning zone, thereby reducing the amount of residual material and air required to propagate and maintain the zone at combustion temperatures. At low rates of frontal advance, the amount of preheat experienced by a combustion zone could conceivably increase with distance traveled from the place of ignition. It should also increase with pressure because of the higher vaporization temperature of water ahead of the zone. Therefore, minimum air fluxes and residual material requirements may be lower in petroleum reservoirs than they are in laboratory experiments. Ideally, this point has significance over a relatively short but critical portion of a conventional five-spot pattern, i.e., the area out to about halfway between injection and production wells. It is encouraging to note that the effects expected in the field are in the proper direction for a workable process.

An estimate of the minimum air flux required for sustained combustion was obtained by heat transfer calculations and substantiated by experimentation. The indicated minimum flux of 4.0 scf/hr-ft^2 is applicable to unconsolidated sand packs only. Tube runs with consolidated media will require a higher air flux to compensate for higher thermal conductivity of the rock. Under field conditions, the minimum air flux will depend largely upon reservoir properties and the prevailing thermal gradients.

Total Air Requirements

Two extreme modes of operation exist for in situ combustion, i.e., heat

propagation with combustion controlling at low fluxes and heat propagation with convection controlling at high fluxes. It is possible to operate under self-sustaining conditions at either extreme, but the total air or gas requirements per unit of sand cleaned will be different.

The total air requirements with combustion controlling are affected by the characteristics of the crude oil, the porous matrix, and the combustion efficiency. A figure in the order of 250 scf/ft³ of unconsolidated sand seems appropriate for design and evaluation calculations.

Fuel Requirements

The propagation of a heat wave through a petroleum reservoir requires an amount of fuel which is largely fixed by the heat capacity of the porous matrix, the heat transferred with the zone, and the heat losses from the zone as it moves between wells. A reservoir having a low oil saturation, if subjected to a combustion drive, would most certainly yield less oil than one having a higher initial saturation of the same crude oil.

Tube runs do not necessarily give an absolute measure of the amount of oil which might be consumed in a field application of the process. Analog data reported by Vogel and Krueger[9] indicate that fuel requirements are affected by numerous variables, including the rate of advance and the distance the front has progressed away from the place of ignition (preheat). The work reported here did not include enough long-term data to evaluate the effect of distance moved in sand-packed tubes.

Data on oil burned may be found in Table 3. It should be noted that the data expressed in per cent of porosity cleaned are representative of the sand packs used in these experiments. The effect of porosity on the amount of oil burned was not determined, but the heat capacity and thermal conductivity of the gross matrix will be inversely proportional to porosity; thus, more oil will be required to heat a unit of low porosity sand than will be required for a unit of high porosity sand. The oil consumed, expressed in per cent of porosity, will be increased as the porosity is decreased by two effects: (1) more oil is required for fuel and (2) the oil burned will occupy a correspondingly larger portion of the available space. Low porosities will therefore limit the applicability of the process.

CONCLUDING REMARKS

This study should promote a better understanding of the problems and mechanisms involved in laboratory investigations and field applications of the in situ combustion process. The data presented will be useful in the planning, operation, and interpretation of field tests. These data, tempered with volumetric sweep efficiencies, can be used as a guide in making preliminary economic and technical appraisals of the process for reservoirs containing high porosity unconsolidated media; however, indiscriminate application can lead to erroneous results and conclusions. Estimation procedures based on the application of laboratory data to field conditions will be subject to considerable uncertainty until several large-scale field projects have been completed and evaluated.

The results of this work and the following conclusions apply strictly to the experimental conditions under which the data were obtained.

CONCLUSIONS

1. The minimum rate of stabilized, self-sustained in situ combustion of residual material in unconsolidated sand packs during air injection is that required to maintain a temperature level of about 600° F.

2. The minimum air flux which must be maintained to provide this minimum rate of self-sustained in situ combustion is about 4 scf/hr-ft² for adiabatic experiments with unconsolidated sand.

3. An in situ combustion zone advances through a sand pack by burning residual material; thus, with high combustion efficiencies, the rate of advance of a combustion zone is nearly proportional to the rate at which air is supplied to the zone and inversely proportional to the amount of residual material deposited.

4. The minimum self-sustained rate of advance, in a given situation, is that resulting when air is supplied at the minimum flux. The minimum rate of advance of an in situ combustion front in semiadiabatic, sand-packed tubes is 0.7 ft/day or less, depending on the properties and quantity of the residual material.

5. Total air requirements are dependent on the rate at which air is supplied to the front. A minimum air requirement is indicated at an air flux of 20 scf/hr-ft² in unconsolidated sand packs containing a specific 21.2° API crude.

6. In situ combustion experiments in unconsolidated sand packs containing a specific 21.2° API crude can be maintained satisfactorily at air fluxes above the minimum with a fuel consumption of about 1.2 lb of carbon per 100 lb of sand cleaned, which corresponds to about 5.5 per cent of pore volume.

7. The amount of hydrogen associated with the carbon burned during in situ combustion decreases as the combustion temperature and air flux at the front are increased.

8. It is indicated that the effect of pressure on in situ combustion is small for conditions where high combustion efficiencies exist and the kinetics of combustion are not controlling.

ACKNOWLEDGMENTS

The authors wish to express their appreciation to the management of Continental Oil Co. for permission to publish this paper. The authors also wish to thank all those who assisted in the collection of data and helped with the solution of special problems related to this work.

REFERENCES

1. Howard, F. A.: "Method of Operating Oil Well," U. S. Patent 1,473,348, to Standard Development Co. (Nov. 6, 1923).
2. Sheinman, A. B., Dubrovai, K. K., Sorokin, N. A., Charvigin, M. M., Zaks, S. L., and Zinchenko, K. F.: "Gasification of Crude Oil in Reservoir Sands—Part I," *Pet. Engr.* (Dec., 1938), **10,** 27; Part II, *Ibid.* (Feb., 1939), 91, 94, 96, 98, and 100.
3. Gibbon, Anthony: "Thermal Principle Applied to Secondary Oil Recovery," *The Oil Weekly* (Nov. 6, 1944), **115,** 170, 172.
4. Grant, B. F., and Szasz, S. E.: "Development of an Underground Heat Wave for Oil Recovery," *Trans.* AIME (1954), **201,** 108.
5. Kuhn, C. S., and Koch, R. L.: "In-Situ Combustion—Newest Method of Increasing Oil Recovery," *Oil and Gas Jour.* (Aug. 10, 1953), **52,** 92, 113, 114.
6. Koch, R. L., Gleason, J. F., Jr., and Boston, W. G.: "In-Situ Combustion Field Tested Again," *Oil and Gas Jour.* (Dec. 6, 1954), **53,** 102.
7. Walter, H.: "Application of Heat for Recovery of Oil: Field Test Results and Possibility of Profitable Operations," *Jour. Pet. Tech.* (Feb., 1957) **IX,** No. 2, 16.
8. Rall, C. G., and Taliaferro, D. B.: "A Method for Determining Simultaneously the Oil and Water Saturations of Oil Sands," RI 4004 USBM (1946).
9. Vogel, L. C., and Krueger, R. F.: "An Analog Computer for Studying Heat Transfer during a Thermal Recovery Process," *Trans.* AIME (1955) **204,** 208.
10. Smith, Robert L., and Watson, Kenneth M.: "Oil Recovery Process," U. S. Patent 2,642,943 (June 23, 1953).

★★★

The Effect of Fluid-Flow Rate and Viscosity on Laboratory Determinations of Oil-Water Relative Permeabilities

C. R. SANDBERG
MEMBER AIME
L. S. GOURNAY
R. F. SIPPEL

MAGNOLIA PETROLEUM CO.
DALLAS, TEX.

ABSTRACT

The effect of fluid-flow rate and fluid viscosity on oil-water relative permeability determinations was studied using the "dynamic flow technique." In this work relative permeability curves were obtained for homogeneous small core samples from several sandstone outcrop formations. Radio-tracers were used for the determination of fluid saturation and for the detection of saturation gradients. Cobalt-60 in the form of cobaltous chloride was used as a water-phase tracer in some of the experiments. Iodine-131 in the form of iodobenzene and Mercury-203 in the form of mercury diphenyl were used as oil-phase tracers in other experiments. Flow rates for each phase were varied within a range of 2.5 to 140.6 ml/hr. Oil-phase viscosities under flowing conditions were varied from 0.398 to 1.683 cp.

The relative permeabilities obtained were found to be solely a function of saturation and independent of flow rate, provided there was no saturation gradient induced in the core sample by "boundary effect." Even though equilibrium with respect to flowing conditions was obtained at the lower flow rates, where a saturation gradient exists, this equilibrium is of a "contingent"-type rather than the "steady-state" equilibrium implicit in the relative permeability concept. The only effect of increasing the oil or non-wetting phase viscosity was to decrease the flow rate required for the elimination of the boundary effect.

Fairly good agreement between experimentally determined and calculated values of the boundary effect was obtained when the non-wetting oil phase was the only flowing phase.

Original manuscript received in Society of Petroleum Engineers office on July 25, 1956. Revised manuscript received Dec. 16, 1957. Paper presented at Petroleum Branch Fall Meeting in Los Angeles, Oct. 14-17, 1956.

INTRODUCTION

In the characterization of reservoir rock, as well as in the solution of reservoir production problems, it is most desirable to have reliable relative permeability measurements for the rock and fluids of interest. Many techniques have been developed for the laboratory determination of the relative permeability of both large and small core samples. In varying degree, difficulties attend the use of all of the methods. Each of the methods requires the metered flow of fluids of known viscosity through the core sample under conditions wherein the pressure drop in the individual flowing phases can be measured or closely approximated. Since the relative permeability is a function of the saturation and distribution of the flowing fluids, some means of obtaining such information is also required.

The laboratory determination of the relative permeability of a sample should give the same relative permeability saturation relationship that would exist if the sample were in place in the oil reservoir. The attainment of this objective is complicated by the fact that the use of small core samples for laboratory measurements is usually necessary. As a result, errors in measuring the relative permeability arise from boundary effects at either the fluid input or output ends of the sample; no significant boundary effect is anticipated at the sides of the sample normal to direction of fluid flow. At the input end of the sample a boundary effect exists if the flow fluids are not commingled as they would be in the reservoir. At the output end of the sample a boundary effect exists as a result of discontinuity of the capillary properties of the system. Here the flowing fluids leave the small flow channels and enter a collecting system having much enlarged flow channels. Thus, there is a tendency for the wetting phase to be retained by the core sample because of the attraction of the core sample for the wetting fluid.

No reference is made to these boundary effects in either Darcy's equation or in the relative permeability concept. As a consequence the saturation effect peculiar to the input end of the core sample may cause an error in the effective permeability measurement, since some portion of the core sample must be utilized for commingling of the flow fluids. At the output portion of the core sample a saturation gradient or a saturation change along the axis of flow results. Since relative permeability is a function of fluid saturation, this saturation gradient may cause a variable permeability measurement, especially since extent and character of the saturation gradient can vary with fluid-flow rate.

The most convenient method of minimizing the boundary effect, especially at the output end of the sample, is to flow the fluids of interest through the core sample at such high rates that the capillary forces are insignificant as compared to the viscous forces involved in the fluid flow. Since recent work of a preliminary nature has indicated that fluid dispersion in the porous medium increases with the flow rate, the high flow minimizes the boundary effect at the input end of the core sample by enhancing the mixing of the fluids.

The use of this dynamic flow technique, which is the technique used for the experiments reported in this paper, depends upon the knowledge of the existence and extent of any saturation gradients in the core sample.

There are many methods of measuring average fluid saturation within a core sample, but there are only a few methods presently available for directly determining saturation gradients. The techniques which have been reported in the literature include electrical resistivity, X-ray absorption, gamma-ray absorption, neutron diffraction and the use of radioactive tracers.[1] The principal advantage of the radio-tracer technique, which is the one utilized for the experiments reported in this paper, lies in its inherently high resolving power. The use of a suitable tracer in one of the flowing phases along with a sensitive, well-collimated detector system enables saturation measurement over small portions of the core sample. Thus, the conventional small samples, in which the boundary effects may control the fluid-flow process, may be easily studied. Although the complex nature of the radio-tracer technique makes its use undesirable for routine work, it is well suited for the study of multiphase flow under ideal conditions. Such studies should enable one to set-up the necessary flow conditions for obtaining relative permeabilities on a routine basis using the more usual techniques for saturation measurement.

EXPERIMENTAL PROCEDURE

Flow System

The dynamic method was used for introducing and removing the fluids from the plexiglas mounted core sample. Both the wetting and non-wetting phases flowed directly into the sample without the use of a mixing head. A neoprene fluid entry gasket as shown in Fig. 1 was used to keep the oil and water phases separate before their entry into the sample. One set of concentric circles was used for the water phase; the other set of concentric circles was used for the oil phase. Dye studies showed that this entry system very effectively commingled both fluid phases within the first ½ cm of the core sample. The effluent end of the sample was maintained at atmospheric pressure without the use of porous end pads.

[1]References given at end of paper.

Fig. 1 — Gasket for Separation of Brine and Oil in Flow Cell.

For some of the experiments, pressure gauges, which were connected between the input and output lines for each phase, measured the pressure drop across the core sample for each phase. In other experiments two pressure taps were introduced for measuring oil-phase pressures at additional points along the core sample. The taps consisted of 1/32-in. holes drilled through the plexiglas core mount to the sample surface. The pressure gauges were Wiancko variable induction bridge-type, capable of measuring a maximum pressure difference of 10 psi. The extremely small volume take-up, 0.001 ml/10 psi, and the fast response of these gauges make them particularly suitable to this type measurement. The outputs of the gauges were fed to a six-channel Foxboro Dynalog recorder. This Wiancko-Foxboro combination proved to be extremely stable over long periods of time. The maximum zero drift encountered was 1 per cent over a period of one week.

The volume flow rate of each phase flowing through the core sample was obtained directly from the settings of Ruska constant rate positive displacement pumps. The flow rate could be varied from 2.5 to 140.6 ml/hr. The viscosity of the fluids at the temperature of the flow experiments was measured with modified Ostwald pipettes. Core sample temperature was measured using a resistance thermometer in contact with the sample. This temperature was recorded continuously on one channel of the Foxboro recorder.

All components of the flow system which came in contact with the corrosive saline aqueous flow solution were constructed of inert materials such as Saran, plexiglas, or neoprene. Both the flow apparatus and the displacement pumps were contained in constant temperature air baths which were controlled to within ± 0.05°C.

Fluid Saturation Determination

An ideal radio-tracer for fluid-flow experiments should have the following properties.

1. Gamma-ray energy between 0.2 and 1.5 mev in order to penetrate the core sample structure.
2. A half-life of 30 days or longer so that frequent renewal of the tracer is unnecessary.
3. A specific activity greater than 40 millicuries/gm is desirable so that concentrations of the tracer can be restricted to 1 gm/liter of solution.
4. The tracer should be preponderantly soluble (distribution ratio 100:1) in one phase.
5. Adsorption of the tracer on the porous medium should be a minimum.

Cobalt-60 in the form of cobaltous chloride was used as a tracer in the aqueous phase in some of the experiments. In other experiments either Iodine-131 in the form of iodobenzene or Mercury-203 in the form of mercury diphenyl were used as an oil-phase tracer. The properties of these radio-isotopes are summarized in Table 1.

None of these isotopes are ideal tracers. Radio-cobaltous chloride is a suitable water-phase tracer for water-wet sandstones having less than 5 per cent clay and iron oxide content. This limitation is a result of the tendency for cobalt ion to adsorb on these materials in sandstones giving false saturation values.

Although it is easy to synthesize oil-phase tracer compounds from Iodine-131, the short half-life of this radioisotope makes its use inconvenient. Mercury-203 has suitable half-life buts its γ energy is lower than is desirable.

For both the radio-cobalt and iodine tracers a conventional Geiger-Muller counting system may be used. A scintillation counter was necessary for use with the lower energy Mercury-203 tracer compound. The counting head developed for use with this material, as well as for the Iodine-131 experiments, consisted of a 1½ × 1½-in. cylindrical, thallium activated, sodium iodide crystal which

TABLE 1 — PROPERTIES OF THE RADIOISOTOPES USED FOR TRACER PREPARATION

Radioisotope	Energy (mev)	Half-life	Specific Activity Millicuries/gm
Cobalt-60	1.17, 1.33	5.3 years	34
Iodine-131	0.720	8 days	500
Mercury-203	0.286	43.5 days	100

was mounted on a Dumont 6292 photo-multiplier tube. The output from this tube was passed through a cathode follower preamplifier and was further amplified with an Atomic Instrument Co. Model 204B linear amplifier. A Model 510 single-channel pulse height analyzer was then utilized for selecting the energy region of interest. A conventional scaler was used to count the output from the pulse height analyzer. A Model 300 Beva Laboratory power supply was used to supply the high voltage to the photo-multiplier tube. This counting system proved to be exceedingly stable over periods of time as long as six months.

In order to determine the tracer activity, and thus the fluid saturations over small regions of the core sample, a movable collimating system was employed. Hevimet, a tungsten alloy which has a high coefficient of gamma-ray absorption, was used to form a slit between the detector and the core sample. In most of the experiments a slit 4 mm × 5 cm in cross section was used. This size permitted measurement of the average fluid saturations in 8-mm segments along the flow axis of the core sample. An electrical gear drive was used to move the detector and shield. With this mechanism the slit could be positioned to within 0.5 mm of any desired point on the core sample. The gamma-ray detector was shielded from scattered radiation by a shield assembly containing either lead or mercury as an absorber.

As the counting assembly was moved step-wise along the length of the core sample, the counting rate profile obtained included the sum of the count of the tracer in the flow solution plus background count. The background count consists of cosmic radiations and low level radiation from flow solution storage units in the flow equipment. When Cobalt-60 was used as a tracer, an additional count resulted from the adsorbed Cobalt-60 on the internal sample surface. To obtain the counting rate that would be indicative of fluid saturation, the sources of radiation other than those resulting from fluid saturation had to be evaluated and subtracted from the observed counting rate.

The background count was obtained by scanning the core sample in the flow equipment with all flow reservoirs and lines installed before any tracer solution was passed through the sample. The correction for background as a function of position was then subtracted from the count rate profiles obtained in the course of the fluid-flow experiments. In order to obtain the count equivalent to 100 per cent saturation of the core sample by the tracer fluid, a standard sample identical to that used for the flow experiments was utilized. This sample was saturated with exactly one pore volume of the tracer solution, placed in the flow system and scanned. The count obtained at any point in this scan minus the previously determined background count would be that expected for a 100 per cent saturated core sample at that point in the course of the fluid-flow experiments.

In the Cobalt-60 runs the difference in the count between that obtained from the flow experiment core sample after many pore volumes of tracer solution had been passed through it and the count from the standard sample was assumed to be due to adsorption of the tracer. This count as a function of position was used to correct fluid saturation determination counts in the course of the flow experiments.

Core Samples

Samples from four consolidated sandstone outcrops were selected for the flow experiments on the basis of their physical characteristics and chemical composition. The samples and pertinent properties are listed in Tables 2 and 3.

An attempt was made to select homogeneous core samples for the flow experiments to insure that any saturation gradients detected would be a result of boundary effects and not of irregularities in the porous structure of the core samples. In order to check the homogeneity of the core samples, random samples from the outcrop were inspected microscopically. Permeabilities, porosities, and capillary-pressure curves were also obtained for several plugs taken from the outcrop. When all of these determinations were in close agreement, the outcrop sandstone was considered reasonably homogeneous and suitable for the flow experiments. For the relative permeability experiments core samples of 1-in. diameter and 4- to 6-in. long were diamond drilled from the quarry blocks using an air-cooled drill. The samples were extracted for 48 hours in a mixture of 60 volume per cent carbon tetrachloride and 40 volume per cent methanol, dried to constant weight and then mounted in plexiglas.

TABLE 2—PHYSICAL CHARACTERISTICS OF CORE SAMPLES

Sample No.	Formation	Permeability (liquid) md	Per Cent Porosity
2703	Aris	757	27.8
2866	Crawford	645	28.8
3812	Torpedo	485	25.9
M929	Mueller	413	24.5

TABLE 3—X-RAY DIFFRACTION ANALYSIS OF CORE SAMPLES

Sample Number	Formation	Quartz (wt %)	Clay Minerals (wt %)	Iron Oxide Fe_2O_3(Wt %)
2703	Aris	95.8	3.7	0.5
2866	Crawford	96.4	3.4	0.2
3812	Torpedo	96.0	2.3	1.1
M929	Mueller	99.9	0.1	0

Flow Fluids

A 5 per cent sodium chloride solution was used for the aqueous phase in all of the flow experiments. When Cobalt-60 was used as a tracer, 20 millicuries of radioactive cobaltous chloride was added to a liter of the salt solution. Two per cent of "cold" cobaltous chloride was also added as a carrier in order to reduce statistically the adsorption of "hot" cobalt ions on the porous media. This tracer solution was kept at a pH of five or less to prevent precipitation of cobaltous hydroxide.

N-heptane (n-C_7H_{16}), n-tetradecane (n-$C_{14}H_{30}$) and Soltrol-C (a narrow boiling range naphtha) were used as hydrocarbon phases. These hydrocarbons were de-peroxidized by treatment with potassium permanganate in order to help insure that the core samples remained predominantly water wet throughout the course of the flow experiments. In the experiments where radio-iodobenzene or radio-mercury diphenyl were used as tracers, approximately 25 millicuries of the tracer compound was added to a liter of flow solution.

EXPERIMENTAL RESULTS

The Effect of Fluid-Flow Rate on Relative Permeability Determinations

In all of the relative permeability determinations the core sample was initially completely saturated with the aqueous wetting phase. The water desaturation relative permeability of the samples to the brine and to the hydrocarbon was then measured as the saturation of the hydrocarbon was progressively increased by decreasing the water-to-oil flowing ratio until a minimum water saturation was reached. The water resaturation cycle was obtained by reversing this process. At each flowing ratio the sample was scanned as the total fluid-flow rate was varied over a range within the limits of 2.5 to 140.6 ml/hr. Usually the permeability values were obtained at low flow rates and then the flow rate was progressively increased until the high-

est rate practicable was reached. Pressure drops were measured either over the entire core sample or between pressure taps placed so as to give pressure drops over the middle third of the core sample length.

Under certain saturation conditions the measured values of relative permeability were found to be directly related to fluid-flow rate. In general, the values of relative permeabilities for both phases were found to increase with an increase in a fluid-flow rate so as to approach a maximum value asymptotically.

This rate effect, which has been reported in the literature,[2] was obtained under a variety of flowing conditions for all of the sandstone samples.

Typical data are presented in Fig. 2 for the Aris sandstone, with brine and Soltrol-C as the flowing phases. The logarithm of the per cent relative permeability in the course of the initial water desaturation is plotted as a function of the average per cent water saturation in the core sample for a high and low flow rate. A semilog plot is used here, and in all such plots throughout this paper, as a means of amplifying the low permeability end of the scale. The overall pressure differential for the oil phase was used in the calculation of the permeabilities for both phases. Relative permeabilities obtained for a total flow rate of 115 ml/hr are designated by the solid points. Values obtained for a total flow rate of 10 ml/hr are shown as open points. The ratio numbers indicate the brine-Soltrol-C flowing ratio utilized in obtaining the point. High and low flow rate points at the same flowing ratio are tied together by dotted lines. Here, as was observed for all samples, the maximum relative permeabilities for both phases were obtained at the higher flow rates. For example, at a water saturation level of 60 per cent the low flow rate permeability for oil is 42.4 per cent of its high rate value and the permeability for water is only 14.7 per cent of its high rate value.

The rate effect can be seen in more detail in Figs. 3 and 4 where the relative permeability for each phase is shown as a function of flow rate. In Fig. 3 the water-flow rate is used as the abscissa because the bulk of the flowing fluids consist of brine as is shown by the brine-Soltrol-C index numbers. In Fig. 4, where the bulk of the flowing fluid is Soltrol-C, the oil-flow rate is used as an abscissa. The brine relative permeabilities are shown as solid lines and the Soltrol-C relative permeabilities are shown as dashed lines. It can be seen that the relative permeabilities for both phases increase with increasing flow rate until a maximum value is approached. Since the fluid saturation changed with flow rate, and core sample was uniformly saturated only at the asymptotic values of relative permeability, no saturation data are shown in these plots.

It should be noted that the relative permeability of the water phase increased very slightly with flow rate when the brine-Soltrol-C flowing ratios of 80, 40, 5 and 1 were used as contrasted with the marked increase in the oil-phase permeabilities with increased rate. The rate effect on the oil phase may be a result of some tendency for the oil phase to flow in slugs. Such a possibility at flowing ratios of 80 and 50 is indicated by the fact that a pulsation in the oil-phase pressure measurement was always observed at these flowing ratios.

Saturation profiles obtained in the course of the experiments are shown in Figs. 5, 6, and 7. The profiles plotted in Fig. 5 were obtained at the start of the water desaturation at the high brine-Soltrol-C ratios of 80 and 50. The per cent water saturation is plotted as the abscissa, and the distance in centimeters from the core sample input end is plotted as the ordinate. The highest flow rate, 112.5 ml/hr for water, is indicated by the solid points and the lowest

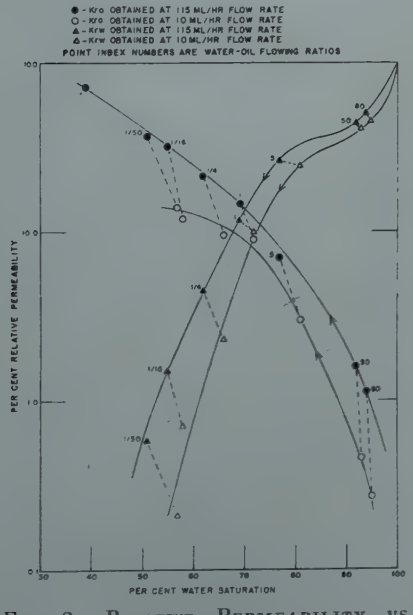
●-Kro OBTAINED AT 115 ML/HR FLOW RATE
○-Kro OBTAINED AT 10 ML/HR FLOW RATE
▲-Krw OBTAINED AT 115 ML/HR FLOW RATE
△-Krw OBTAINED AT 10 ML/HR FLOW RATE
POINT INDEX NUMBERS ARE WATER-OIL FLOWING RATIOS
PER CENT RELATIVE PERMEABILITY
PER CENT WATER SATURATION

Fig. 2—Relative Permeability vs Water Saturation, Aris Sandstone, Core Sample No. 2703K. Initial Water Desaturation (Brine-Soltrol-C).

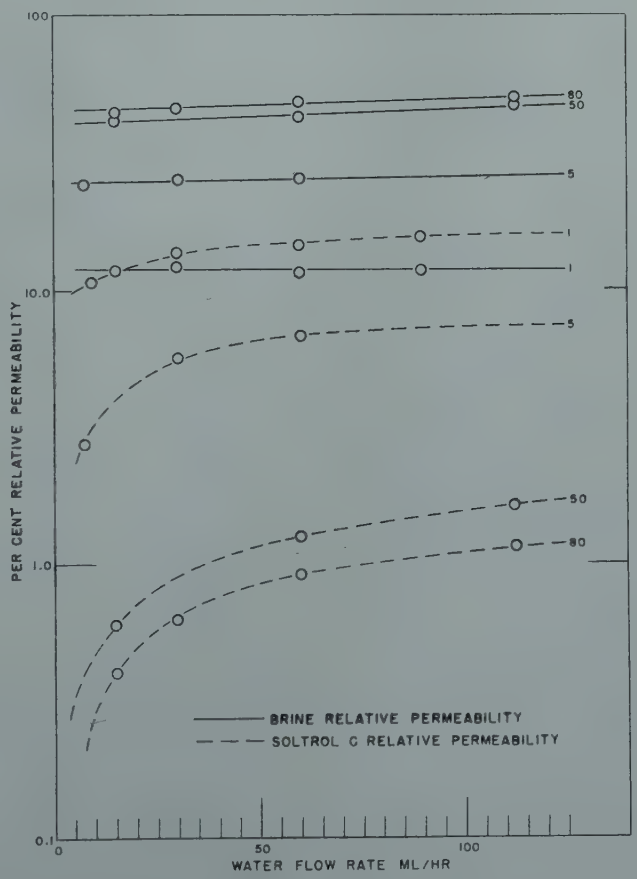

Fig. 3—Relative Permeability vs Water Flow Rate, Aris Sandstone, Core Sample No. 2703K. Initial Desaturation Curve Index Numbers are Water-oil Flowing Ratios.

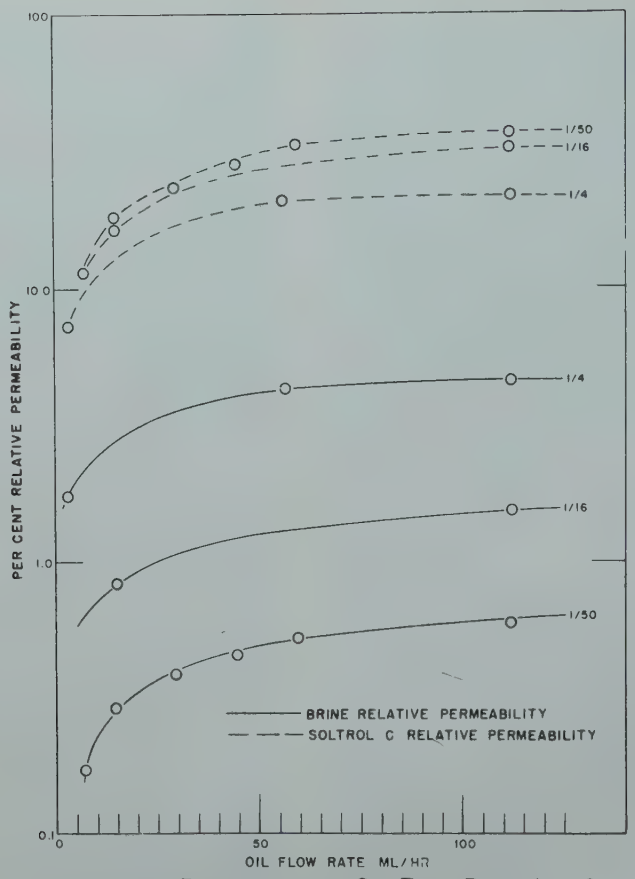

FIG. 4—RELATIVE PERMEABILITY VS OIL FLOW RATE, ARIS SANDSTONE, CORE SAMPLE NO. 2703K. INITIAL DESATURATION CURVE INDEX NUMBERS ARE WATER-OIL FLOWING RATIOS.

flow rate, 15 ml/hr, is indicated by the open points. The slight tendency towards a higher water saturation at the lower flow rate may be indicative of a saturation gradient of magnitude less than the accuracy of measurement. Within the possible error of measurement, there does not appear to be any marked saturation gradient or end effect at the flow rates shown. The same situation may exist for the 5:1 brine-Soltrol-C flowing ratios as shown in Fig. 6. It should be pointed out that saturation gradients were observed in other outcrop samples in this saturation region. For the 1:4 and 1:16 flowing ratios at low flow rates there is a marked saturation increase between the input and output ends of the core sample.

The fact that the low flow rate gradient is somewhat greater for the 1:4 flowing ratio than for the 1:16 flowing ratio (despite the higher water saturation) results from the lower oil-flow rate, 3.75 ml/hr for the 1:4 case, as compared with 15 ml/hr in the 1:16 case. The effect of flow rate is shown in even more detail in Fig. 7 for the 1:50 brine-Soltrol-C flow ratios. Here the 13 per cent saturation gradient at the output end decreases with increasing flow rate until the core sample is uniformly saturated. For core samples having a lower specific permeability a saturation gradient of as much as 30 per cent was observed between the input and output ends of the core samples under low flow rate conditions.

This saturation gradient which exists at low flow rate and correspondingly low pressure gradients is an indication of the existence of a boundary effect at the output end of the core sample. Although it has been shown in detail for only one relative permeability experiment, similar gradients were obtained in the relative permeability determinations for all of sandstones. Further, similar results were obtained regardless of whether the curves were obtained in the initial water desaturation cycle as in previous data or in the resaturation cycles.

Because of the large attractive forces between the brine-wetting phase and the solid surface, a certain amount of energy must be expended to remove the wetting phase from the porous system. This energy must be supplied to the hydrocarbon non-wetting phase in order to displace the wetting phase at the output end of the core sample. The saturation profiles of Figs. 6 and 7 indicate that insufficient energy is being applied to the non-wetting phase at the low flow rates to overcome these wetting forces. Consequently, the measured pressure differential for both phases cannot be indicative of the pressure gradient exclusively due to viscous flow. The measured pressure

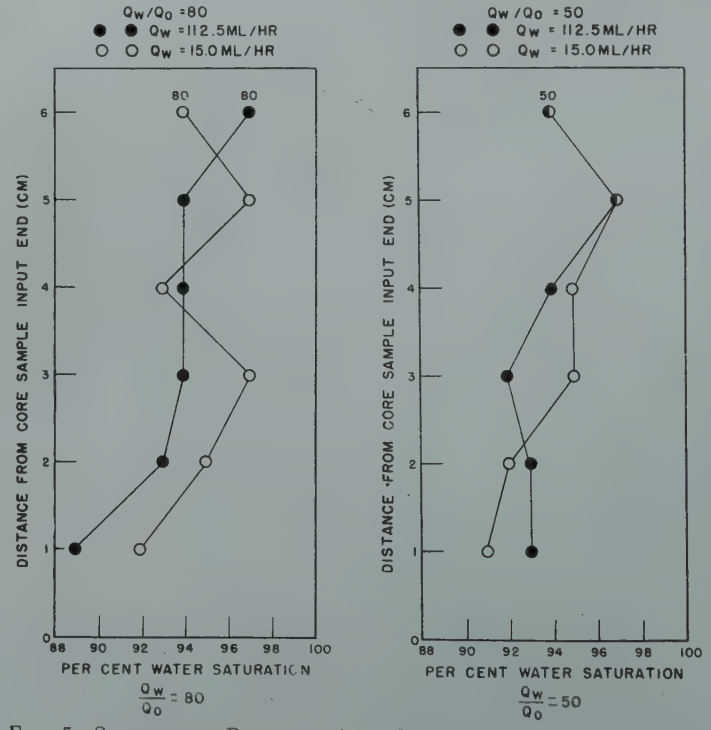

FIG. 5—SATURATION PROFILES, ARIS SANDSTONE, CORE SAMPLE NO. 2703K. INITIAL WATER DESATURATION (BRINE-SOLTROL-C).

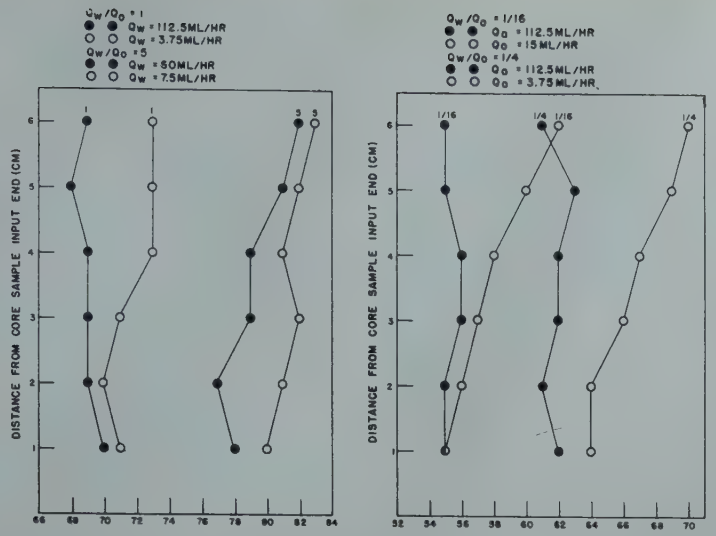

FIG. 6—SATURATION PROFILES, ARIS SANDSTONE, CORE SAMPLE NO. 2703K. INITIAL WATER DESATURATION (BRINE-SOLTROL-C).

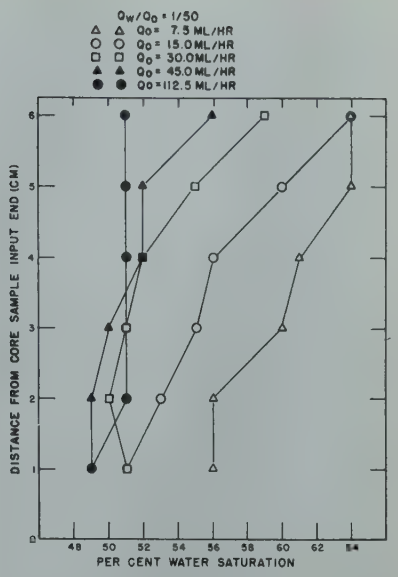
Qw/Qo = 1/50
Qo = 7.5 ML/HR
Qo = 15.0ML/HR
Qo = 30.0ML/HR
Qo = 45.0 ML/HR
Qo = 112.5 ML/HR
DISTANCE FROM CORE SAMPLE INPUT END (CM)
PER CENT WATER SATURATION

FIG. 7—SATURATION PROFILES, ARIS SANDSTONE, CORE SAMPLE NO. 2703K. INITIAL WATER DESATURATION (BRINE-SOLTROL-C).

gradient is the sum of that resulting from changes in capillary pressure along the sample due to the wetting forces and an average pressure gradient due to viscous flow. Only at high flow rates or at high water saturations, where the capillary pressure is small, does the viscous pressure gradient, which is the only gradient specified in Darcy's equation, become a predominant portion of the total pressure gradient. Thus, the saturation profiles, together with a plot of relative permeability vs flow rate, define the flow rate necessary to obtain an accurate and useful measurement of the relative permeability for a particular core sample.

Stabilized flow conditions, i.e., a pressure drop for each of the flowing phases which remained constant in time, was obtained in all of the permeability measurements regardless of whether or not saturation gradients were present. A comparison of the flow conditions at the same average saturation value for experiments where a saturation gradient was present (in contrast with those where no saturation gradient existed) showed that a lower flow rate was obtained for each of the flowing phases for a unit pressure drop when a saturation gradient was present, or a lower value of relative permeability for each of the flowing phases when the saturation gradient was present. It thus appears that although flow conditions were stabilized for all experiments, a contingent equilibrium exists when a saturation gradient is present rather than the steady-state equilibrium implicit in the relative permeability concept.

THE USE OF OIL-PHASE PRESSURE TAPS

Reference was made in the discussion of the flow apparatus to the use of a perforated neoprene gasket at the inflow face of the core sample to facilitate injection of oil and water. Fluids injected in this manner did not come in contact with each other prior to their entry into the core sample. Thus, pressure differential gauges connected across the sample measured the pressure drop of the given phase along the axis of flow. Although pressure measurements by this method are very convenient, they may not be representative of the pressure drop in the course of fluid flow. The gasket must necessarily cover part of the inflow face in order to maintain a barrier between the two phases. This reduces the effective cross sectional area of the sample at the inflow face and the resulting choking effect may introduce an erroneous pressure drop into a dynamic pressure measurement. Still another source of error in pressure measurement may be a consequence of the fact that the ratio of the entry areas available to the flowing phases remains constant even though the flowing ratio is changed in the course of a relative permeability determination.

To evaluate the magnitude of pressure drop encountered at the inflow face and its effect on relative permeability measurements, the oil-phase pressure was measured at two taps along the length of the core sample as well as from the input line of each phase. It was possible to determine the pressure drop over a known length of the sample without the disturbing influence of the fluid entry gasket. Relative permeability measurements were then made at rates sufficiently high so that no saturation gradient was noted. The pressure tap data yielded permeabilities consistently (though only slightly) higher than those obtained using the pressure measured at the input face of the sample.

It was hoped that the use of these pressure taps would enable the obtaining of reliable relative permeability measurements when a saturation gradient was present in the core sample. In all cases, when using these taps as a basis of pressure measurement, the presence of a saturation gradient in the core sample lowered the water- and oil-phase relative permeabilities even though the core was apparently uniformly saturated between the pressure taps. The extent of lowering, however, was usually a small fraction of that encountered when the intermediate pressure taps were not used.

These investigations indicated that for absolute measurements of relative permeabilities the use of pressure taps is desirable, especially if the entry or exit phases of the core samples are restricted in any manner.

THE EFFECT OF FLUID VISCOSITY ON RELATIVE PERMEABILITY-SATURATION RELATIONSHIP

Aris sandstone was used in the study of the effect of fluid viscosities and viscosity ratios on the measurement of relative permeability. After a water desaturation and resatura-

tion cycle, the single-cycle hysteresis disappeared and the sample reached conditions of stability and reproducibility. Relative permeability measurements were then made using an aqueous brine having a 0.833 cp viscosity and Soltrol-C as the oil phase having a viscosity of 1.147 cp. These measurements were repeated after the Soltrol-C was replaced by normal heptane of 0.398 cp viscosity and then by normal tetradecane of 1.683 cp viscosity. The resulting relative permeability data are plotted in Fig. 8. Although the oil-phase viscosity was varied from 0.398 to 1.683 cp and the oil to water viscosity ratio was varied from 0.48 to 2.02, the permeability-saturation relationship for this sample was, within experimental error, unchanged. It was found, however, that as oil viscosity was decreased higher flow rates were necessary to remove the saturation gradient. These data would, therefore, indicate an independence of relative permeability measurements on viscosity of the flowing fluids, provided that capillary end effects in the core sample are negligible.

COMPARISON OF EXPERIMENTAL AND CALCULATED SATURATION GRADIENTS

For two immiscible fluids flowing through a porous medium the following equation has been derived.[3] It is based on Darcy's law for each of the flowing phases and the assumption that the capillary pressure for the system is the difference between the pressures of the flowing phases.

$$L = \int_{S}^{1} \left(\frac{dP_c}{dS_w} \Big/ \frac{q_o \mu_o}{k_o A} - \frac{q_w \mu_w}{k_w A} \right) dS_w$$

If the effective permeability for each of the flowing phases as a function of saturation is known along with the capillary-pressure curve for the core sample of interest, it should be possible to calculate the saturation gradient at a particular flow rate from the above equation. Such calculations have been reported for oil-water[4] and oil-gas[5] systems.

Rather good agreement between observed and calculated saturation distributions was obtained at the high oil saturation region of the relative-permeability curve where only the oil phase was flowed. Under these conditions the equation is simplified considerably since the water term drops out.

Some typical results for this calculation are shown in Fig. 11 for the 413-md Mueller sandstone. The water desaturation cycle relative-permeability curve and the capillary-pressure curve for this sandstone are shown in Figs. 9 and 10. As is shown in Fig. 11 the measured saturation gradient with *n*-tetradecane as the flowing phase is greater in extent than the calculated gradient. This was the case for all of the core samples studied. As would be expected the extent of the gradient decreased with an increase in oil-flow rate.

ACCUARCY AND PRECISION IN THE RELATIVE PERMEABILITY DETERMINATIONS

At the present time no estimation can be made for the accuracy of permeability-saturation relationships. This must be the case until all the variables involved in such determina-

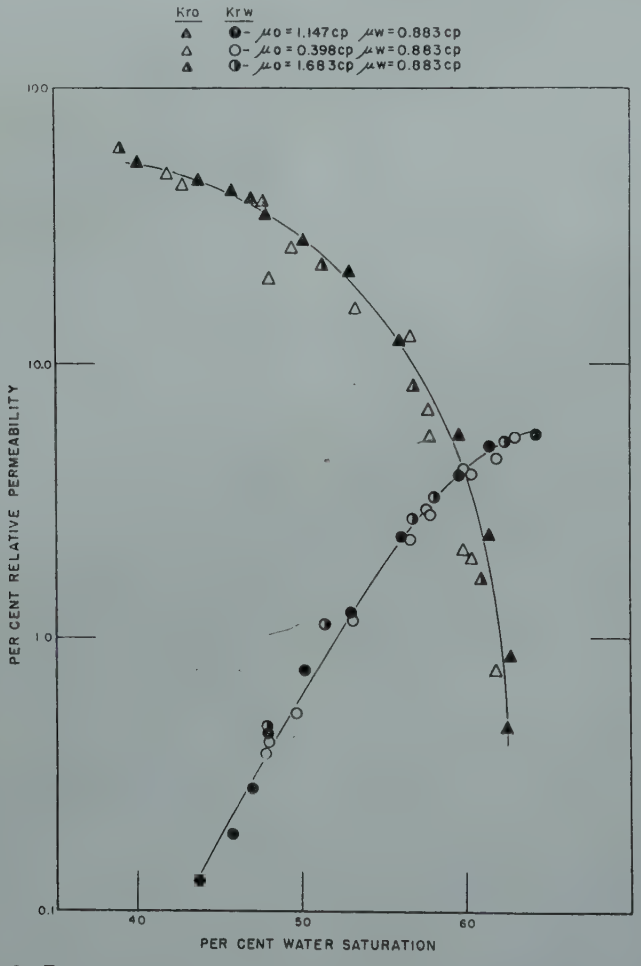

FIG. 8—RELATIVE PERMEABILITY VS WATER SATURATION, ARIS SANDSTONE, CORE SAMPLE NO. 2703K. HIGH FLOW RATE CONDITIONS.

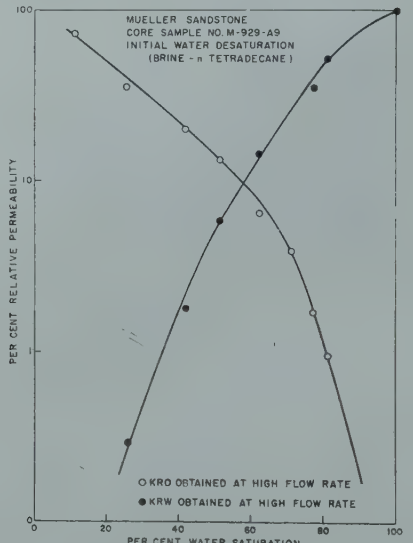

FIG. 9—RELATIVE PERMEABILITY VS WATER SATURATION.

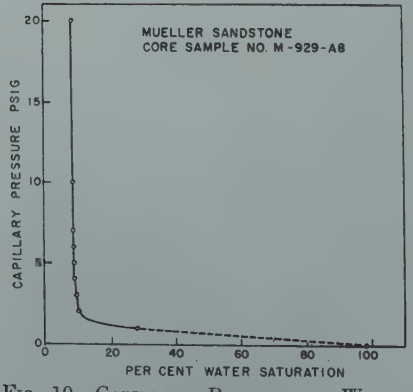

FIG. 10—CAPILLARY PRESSURE VS WATER SATURATION.

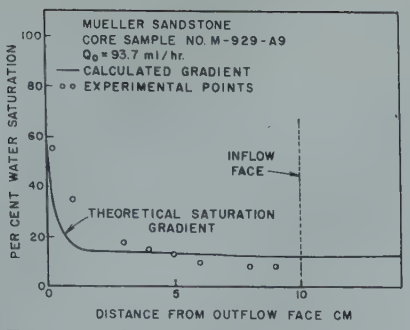

FIG. 11 — COMPARISON OF CALCULATED AND EXPERIMENTAL BOUNDARY EFFECT.

tions can be evaluated. Since core samples utilized for this study were strongly water-wet, thus eliminating wettability considerations, the principal source of error in the foregoing studies probably lies in the correlation of measured pressure drops with flowing conditions.

In contrast, the precision of the individual measurements required for the determinations can be readily evaluated. Fluid-flow rate is the most precisely measured variable in the permeability determination having a precision of better than 0.1 per cent. Core sample dimensions are precise to ± 0.5 per cent, while pressure measurement and viscosity determinations have a ± 1 per cent precision. The average fluid saturation of the core sample was determined for each relative-permeability data point. Tracer counts were made at a minimum of six stations along the length of the core sample. The accuracy of saturation measurement at each station was dependent upon the precision with which the counter was positioned and the total number of counts obtained at each station. Using the counter arrangements and tracer activities specified previously in this paper, a probability of 90 per cent existed that the maximum error at each station would be no more than ± 1.8 saturation per cent. The over-all water saturation utilized for each relative permeability point was then taken as the average of the saturations of the six or more equally spaced stations. Reliable error or precision of this average saturation would then be less than ± 0.72 saturation per cent.

As an independent check of the saturation measurements, it was noted that the radio-tracer saturations obtained at the low saturation end of the relative-permeability curves always closely checked that obtained in conventional capillary-pressure determinations for the sample material.

CONCLUSIONS

1. The relative permeability of porous medium to water and oil, as obtained by the dynamic flow technique, is a function of saturation and independent of flow rate, at all rates in excess of that required to saturate uniformly the core sample. Insufficient data are presently available for generally correlating the permeability of porous media with the minimum flow rate required to eliminate the boundary effect.

2. For a uniformly saturated core sample the relative permeability to either phase is independent of the non-wetting phase viscosity.

3. The outlet boundary effect as calculated from a capillary-pressure curve and the effective permeability of the non-wetting phase agrees with that experimentally observed when only the non-wetting phase is flowing.

ACKNOWLEDGMENT

The authors are indebted to J. W. Whalen and L. B. Lipson for their development of the neoprene entry gasket. They also wish to thank S. R. Faris and P. P. Reichertz for their many helpful comments and to express their appreciation to the Magnolia Petroleum Co. for permission to publish this paper.

REFERENCES

1. Josendal, V. A., Sandiford, B. B., and Wilson, J. W.: "Improved Multiphase Flow Studies Employing Radioactive Tracers," *Trans.* AIME (1952), **195**, 65.
2. Osoba, J. S., Richardson, J. G., Kerver, J. K., Hafford, J. A., and Blair, P. M.: "Laboratory Measurements of Relative Permeability", *Trans.* AIME (1951), **192**, 47.
3. Elkins, L. F.: Unpublished Communication (1943); Pirson, Sylvain J.: *Elements of Oil Reservoir Engineering* (1950) 328.
4. Caudle, B. H., Slobod, R. L., and Brownscombe, E. R.: "Further Developments in the Laboratory Determination of Relative Permeability", *Trans.* AIME (1951), **192**, 145.
5. Richardson, J. G., Kerver, J. K., Hafford, J. A., and Osoba, J. S.: "Laboratory Determination of Relative Permeability", *Trans.* AIME (1952) **195**, 187. ★★★

A Study of Anomalous Pressure Build-Up Behavior

G. L. STEGEMEIER
STUDENT MEMBER AIME
C. S. MATTHEWS
MEMBER AIME

UNIVERSITY OF TEXAS
AUSTIN, TEX.
SHELL OIL CO.
HOUSTON, TEX.

ABSTRACT

In one field in South Texas, approximately 75 per cent of the pressure build-up results show a characteristic "hump" (i.e., the pressure builds up and then falls off) which makes interpretation by standard methods impossible. Correlation of size and time of hump with formation permeability, well productivity index, and method of completion led to the tentative conclusion that the humps were caused by segregation of gas and oil in the wellbore after closing-in. This conclusion was confirmed by performance of simple laboratory bubble-rise experiments, by theoretical bubble-rise time calculations, and by a detailed calculation of PVT behavior in the wellbore of a particular well on which accurate surface and bottom-hole pressure measurements were made.*

The hump behavior has since been found to occur in many other fields. The cause, however, is not the same in all cases. In some of these the hump is traceable to leaks in the tubing which allow influx of gas from the annulus after closing-in. In other cases the hump is traceable to leaks in the device separating pay horizons in dually completed wells.

It is concluded that the recording of both surface and bottom-hole pressures is desirable in wells which show an anomalous build-up behavior. A number of field examples is discussed where use of both sets of measurements enables the cause for anomalous behavior to be found, and a reasonable interpretation of bottom-hole pressure to be made.

INTRODUCTION

Theoretically the pressure build-up in an infinite reservoir should be a linear function of ln $[(t + \triangle t)/\triangle t]$ where t is the production time and $\triangle t$ is the closed-in time. Some of the variations from this behavior are well known, such as the curved portion immediately after shut-in which results from after-production and skin effect, and the flattened end portion which results from boundary effects in a limited reservoir. The effect of stratified producing zones and irregular geometrical drainage patterns may also contribute unusual characteristics to build-ups. However, the effect of still another phenomenon—that of movement of fluids within the wellbore—has been neglected in most build-up studies to date. Fluid movements within the wellbore after shut-in occur as a result of after-production, packer failures, leaks in the casing or tubing, or buoyancy of the gas phase when both gas and liquid are present in the well. Each of these movements can influence the pressure build-up, sometimes sufficiently to negate use of the data for computing permeability or stabilized build-up pressure. Examples of each of these phenomena are discussed below.

FIELD OBSERVATIONS ON HUMP BUILD-UPS

In approximately 75 per cent of the wells in a medium-sized field in South Texas the pressure build-up curves rise to a maximum and then decline to what appears to be a stabilized reservoir pressure as shown in Fig. 1. Similar behavior has also been observed in wells in other fields in Texas and Louisiana. Because of the possibility of such behavior being a mechanical failure of the pressure bomb, two bombs were run in tandem into one well which had been known to exhibit this behavior. When both bombs recorded identical curves with the characteristic hump, it was inferred that the unusual build-up is a result of well or forma-

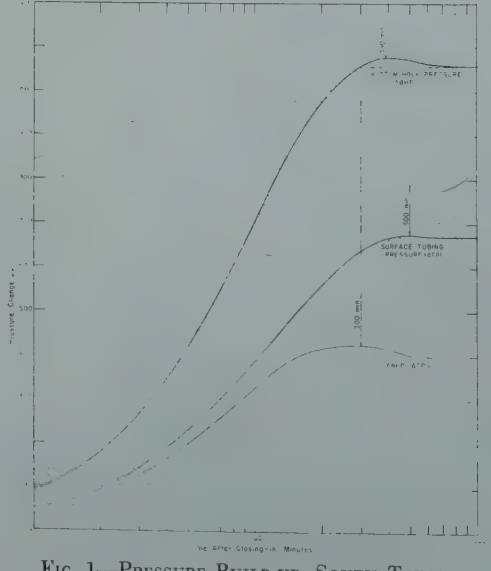

FIG. 1—PRESSURE BUILD-UP, SOUTH TEXAS WELL 1.

Original manuscript received in Society of Petroleum Engineers office on July 15, 1957. Revised manuscript received Jan. 13, 1958. Paper presented at 32nd Annual Fall Meeting of Society of Petroleum Engineers in Dallas, Tex., Oct. 6-9, 1957.

*This possibility had been suggested to one of the authors by A. B. Dyes of The Atlantic Refining Co. in 1950.

ion behavior, rather than a recording instrument failure.

In order to understand more fully the mechanism involved in these build-ups, a statistical study of 120 of these humping build-ups in one South Texas field was made. The results indicate that the humps may be as large as 180 psi, have an average size of about 45 psi, and always occur at the end of or shortly after the typical "swans-neck" part of build-up. The time of occurrence generally varies from 100 to 1,000 minutes after shut-in, with the greatest number of curves humping at 300 to 400 minutes. In all cases in which the hump is later than 300 minutes, the steep part of the build-up is also late and there is a sizeable rate of build-up within 350 minutes of the maximum.

Apparently, there is no correlation in this field between this unusual behavior and rate of production previous to shut-in, cumulative production, GOR, bottom-hole pressure, magnitude of pressure build-up, or structural position. However, core data indicate that humping does not generally occur in wells having an average permeability greater than 200 md. Similarly, wells with moderate permeability (50 to 100 md) may have anomalies which appear and disappear throughout the life of the well.

A plot of magnitude of hump vs productivity index (PI) is shown in Fig. 2. This plot shows that the humps are larger in wells with low PI's. In addition, for any given well, the humps get larger as the PI's get smaller. Thus, there is a possible relationship between presence of a skin zone (which would give a low PI) and size of hump.

The presence or absence of a packer has a considerable effect on size and time of humping. The average size in wells having a packer is about 60 psi, whereas it is only 10 psi in wells without packers. The average time of humping is about 350 minutes in packed wells, and 500 minutes in non-packed wells.

Summarizing all the facts obtained from this statistical study, it appears that for a hump to appear in the build-up it is necessary that the formation be only moderately permeable and have a low productivity index. The humps appear earlier and are of larger size when the annulus is packed-off.

A physical explanation of many of the humps may be given in terms of a phase redistribution within the wellbore involving rise of the gas phase through the oil and counter flow of oil downward*; however, before any application of this phenomenon is made to a well, a discussion of the theoretical effect of phase redistribution will be made.

*This possibility was suggested to one of the authors by A. B. Dyes of The Atlantic Refining Co. in 1950.

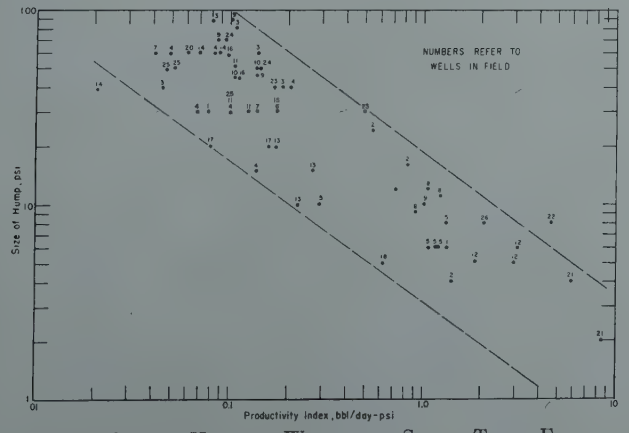

FIG. 2—SIZE OF HUMP IN WELLS IN A SOUTH TEXAS FIELD.

THEORETICAL AND EXPERIMENTAL STUDIES ON PHASE REDISTRIBUTION

STATIC THEORY AND EXPERIMENTS

To illustrate the theory, suppose a frictionless piston separates a liquid phase above and a gas phase below in a cylinder. Assume the gas is weightless, the liquid incompressible, and the pressure at the top is A. The gas trapped below the piston then is at pressure A, plus the pressure due to the fluid head of the liquid, P. When the cylinder is inverted so that the gas phase is at the top, the following pressures result. (1) Since the liquid is incompressible, the piston will not move and the gas will occupy the same volume; consequently, the gas will remain at the same pressure as before, $(A + P)$. (2) The pressure at the bottom is now the pressure exerted by the gas on the top of the piston $(A + P)$ plus the fluid head, P, making the total pressure $(A + 2P)$. Thus, by changing the relative position of the phases in the column the absolute pressure at both top and bottom is changed. The difference between the top and bottom pressure remains constant, however, and equal to the weight of the fluids between the two points divided by the cross-sectional area.

The experiment described above was made in the laboratory, and the results were found to be in good agreement with the above theory.

DYNAMIC EXPERIMENTS

Following this static-phase-demonstration experiment, a second experiment, which more closely simulated wellbore performance, was carried out using equipment shown in Fig. 3. The column was almost filled with glycerine, and with Valve B open and Valve C closed, air was introduced through the core at the base of the column.

When the air bubbles were sufficiently dispersed throughout the column, the air supply (Valve A), and

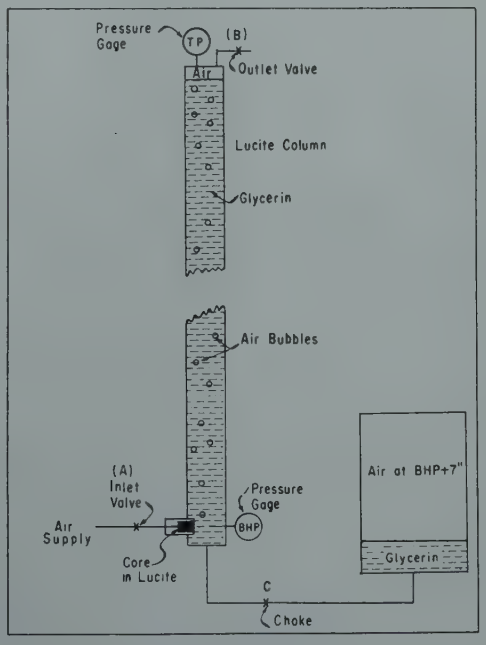

FIG. 3—A DYNAMIC PHASE-REDISTRIBUTION EXPERIMENT.

the outlet at the top of the column (Valve B) were closed simultaneously. A total pressure build-up at both top and bottom of about 13 in. of water was observed, due simply to bubble rise.

An explanation of the pressure rise in this case may be seen by considering the bubbles at the bottom to be compressed by the fluid head just as the gas is compressed below the piston. The subsequent rise of gas through the liquid lessens the pressure on the bubble due to fluid head, but because the gas cannot expand in the closed system, it exerts a pressure on the liquid at the gas-liquid interface. This pressure is transmitted to the bottom, and when added to the hydrostatic pressure, gives an additional pressure associated with bubble rise.

Several runs of this type were made in which the amount of gas initially at the top of the column and then the volume of bubbles contained in the liquid were varied. It was found that (1) the pressure build-up due to bubble rise is inversely proportional to some power of the top gas volume, and (2) the pressure build-up is directly proportional to the total volume of bubbles in the column.

In order to reproduce more closely the effect of a pressure build-up in a well, an inverted flask containing both glycerine and air was attached to the bottom of the column, this flask being analogous to the porous reservoir around the wellbore. Again air was flowed through the core and into the bottom of the column. This time the top valve was open, Valve C was slightly cracked, and the air pressure in the flask was adjusted to a value slightly above the flowing bottom-hole pressure. When a steady-state dispersion of bubbles throughout the column was reached, the air supply was shut-off and the top valve was closed. This time the pressure build-up resulted both from influx from the reservoir and from the bubble rise; however, the pressure build-up from bubble rise shortly after shut-in was so much greater than that from influx that the bottom-hole pressure rose above the reservoir pressure (see Fig. 4). This occurred because the liquid in the column was unable to flow back into the reservoir fast enough to prevent the anomalously high bottom-hole pressure caused by bubble rise. After rising above reservoir pressure the liquid in the column began to flow back into the reservoir until the bottom-hole pressure declined to the reservoir pressure.

This model is an analog of a well having a high skin factor, simulated by the partly closed valve, and a considerable quantity of bubbles entrapped in the borehole liquid at shut-in.

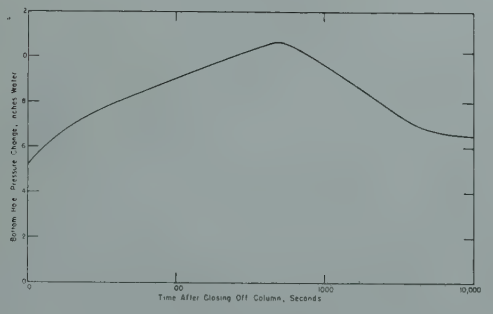

FIG. 4—AN EXPERIMENTAL PRESSURE HUMP CAUSED BY BUBBLE RISE.

ANOMALIES RESULTING FROM PHASE SEGREGATION

ASSUMPTIONS USED IN CALCULATING WELL BEHAVIOR

Temperature—Calculations take into account the effect of temperature gradient in a well on the volumetric properties of gases, but neglect the effect of changing temperature on liquid properties.

Supersaturation—Unless otherwise specified, the gas and oil are assumed to be in equilibrium at all times.

Friction loss in tubing—The pressure drop in the tubing due to friction was negligible in all cases considered in this report.

BASIC CALCULATIONS

An approximation of the limiting upward velocity of bubbles is needed to determine the length of time during which phase redistribution may be expected to occur. These limiting values were taken from the correlation of Peebles and Garber.[1]

TIME OF BUBBLE RISE IN A SOUTH TEXAS WELL

Assuming that no very small bubbles (i.e., radius < 0.0015 ft) occur, the minimum rate of rise obtained from this correlation is 0.35 ft/sec. Thus, the maximum time of rise in a 7,900-ft South Texas well is 377 minutes. The maximum rate of bubble rise is 0.55 ft/sec, which leads to a minimum rise time of 240 minutes.

Earlier it was stated that the humps in the South Texas field never were more than 350 minutes removed from a sizable rate of pressure build-up. To cause a sizable rate of build-up a considerable quantity of gas bubbles must have been entering the bottom of the hole within 350 minutes of humping. The time required for such gas to rise to the top is 240 to 377 minutes, the right order of magnitude to account for the hump.

ANALYSIS OF BEHAVIOR OF SOUTH TEXAS WELL 1

PRESSURE BEHAVIOR

Bottom-hole pressure (BHP) build-up data on Well 1 in a South Texas field were obtained by using the Shell Development Co.'s BHP telemetering device. This device allowed pressure to be measured to within less than 0.5 psia on an accurate time scale.

Fig. 1 shows the change in BHP (BHP after shut-in minus flowing BHP) and the change in tubing pressure (tubing pressure after shut-in minus flowing tubing pressure). The difference between these two curves is also plotted in Fig. 1. This difference curve is seen to rise, reach a maximum, and then decline to a constant value. Since the friction loss at any time is negligible, the value of the difference curve is proportional to the amount of fluid which has entered after shut-in between the BHP bomb and the tubing head, regardless of the phase distribution. Any increase in the difference curve indicates an increase in mass of material in the tubing, and, conversely, a decrease indicates an outward flow of material from the tubing. Because this well has a packer, the fluid leaving the tubing can flow only into the formation.

In view of these observations it is possible to analyze the pressure behavior shown in Fig. 1. The difference

[1]References given at end of paper.

curve rises after shut-in, indicating a normal after-production into the wellbore; however, at 300 minutes the difference curve reaches a maximum. This time coincides with the time at which the BHP curve first reaches the eventual stabilized pressure. As one might expect, the direction of flow after the BHP exceeds the stabilized BHP is from the tubing into the formation. This is seen in the fact that the difference curve decreases after the 300-minute point. The BHP continues to rise even after the pressure at this point exceeds the stabilized formation pressure because the pressure rise caused by rise of the gas occurs at a greater rate than the pressure decrease due to outflow. However, since no more gas is entering the tubing, the rate of pressure increase due to bubble rise finally decreases, and at 390 minutes equals the rate of pressure decrease due to outflow. This is the point at which the BHP reaches a maximum and begins its decline. After this time the tubing pressure will continue to increase, this rise being attributable to rise of the gas bubbles which last entered the tubing. When most of the gas has risen to the surface (500 minutes) the tubing pressure will finally begin to decline because of continued negative after-production. The final state of build-up is a stabilization of all three curves to constant values.

TOTAL PRESSURE RISE CAUSED BY PHASE SEGREGATION

The effect of phase redistribution on the South Texas Well 1 build-up discussed previously will now be computed by: (a) finding the amount of gas and oil in the tubing at the time of closing-in, (b) finding the rate and amount of after-production, (c) calculating the pressure increase caused by this after-production, and (d) attributing the difference between the observed and calculated pressure increase to phase redistribution.

The amount of gas and oil in the tubing at time of closing-in is calculated by the method discussed in Appendix 1. The results indicate that at time of closing-in there were 2,910 ft of gas (at tubing conditions) and 4,990 ft of liquid in the tubing.

The rate and amount of after-production are calculated in Appendix 2. Rate results are shown in Fig. 5. The initial rate is about 20 ft/min, but this drops rapidly to about 1 ft/min at the end of 200 minutes. Note that the results do not follow the often-used assumption that the rate of influx is proportional to the rate of change of BHP. However, the mass rate of influx is proportional to the rate of change of the *difference* between tubing and bottom-hole pressure. To a good approximation the total volumetric rate of influx is also proportional to the rate of change of this same difference. This suggests that tubing, casing, and BHP's should be measured during build-up when it is desired to make calculations of after-production for pressure build-up interpretation. Then by using the difference between top-hole and bottom-hole pressures one can calculate the rate of after-production accurately.

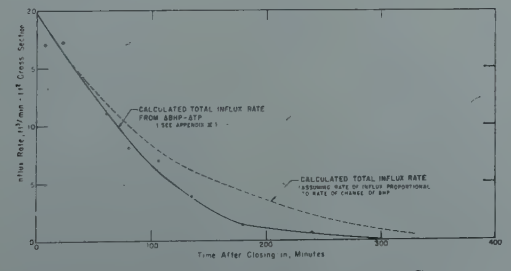
CALCULATED TOTAL INFLUX RATE FROM ΔBHP-ΔTP (SEE APPENDIX B)
CALCULATED TOTAL INFLUX RATE ASSUMING RATE OF INFLUX PROPORTIONAL TO RATE OF CHANGE OF BHP
Time After Closing in, Minutes

FIG. 5—RATE OF AFTER-PRODUCTION, SOUTH TEXAS WELL 1.

Knowing the amount of after-production in any period, one may calculate the pressure increase caused by the addition of this volume of fluid to the volume of fluid in the tubing. This is the pressure increase due to compression. This influx also increases the BHP by virtue of its weight, which is reflected directly in the difference between tubing-head and bottom-hole pressure. If there were no disturbing factors, the pressure increase due to compression plus the pressure increase due to weight of this after-production should equal the total increase in BHP. However, Curves A or B in Fig. 6 show that the sum of difference curve (which gives the pressure increase due to weight) and the pressure increase due to compression (obtained from Appendix 2) is always less than the BHP increase. This is true regardless of whether the gas in the tubing is assumed to go into solution or not. This indicates that another factor is causing a change in BHP. A plot of this factor (the difference between observed and calculated BHP) is also shown in Fig. 6 by Curves C and D. The curve for the case of solution equilibrium in the tubing (Curve C) closely resembles the experimental curve of pressure rise due to rise of bubbles. This analysis indicates that there may be a maximum total pressure increase due to bubble rise alone of about 300 psi. However, a large part of this increase is masked by the pressure build-up, and only a small part (20 psi) appears as a hump in this case.

DISCUSSION OF HUMPING BUILD-UP

It is believed that the preceding detailed analysis of behavior of South Texas Well 1 demonstrates the validity of the concept that phase segregation within the wellbore can cause an anomalous hump in the pressure build-up curve. The time required for bubble rise is of the right order of magnitude to account for the phenomenon. The difference curve indicates that liquid is pushed back into the formation.

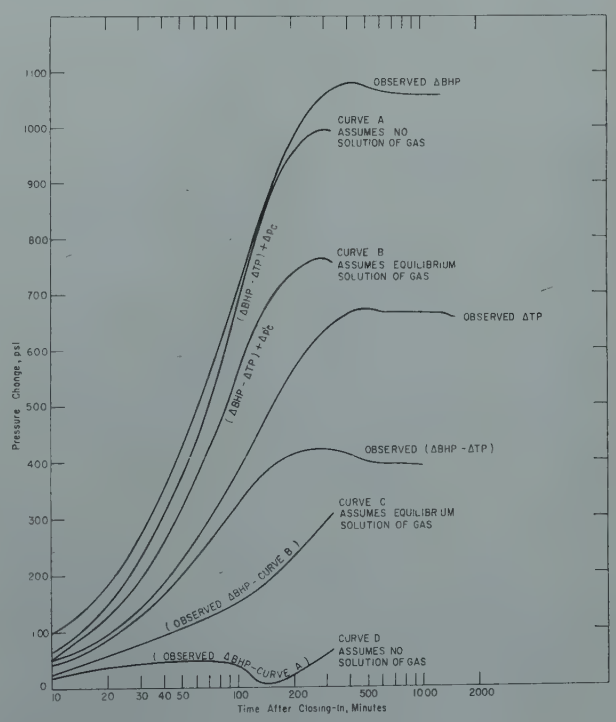
OBSERVED ΔBHP
CURVE A ASSUMES NO SOLUTION OF GAS
CURVE B ASSUMES EQUILIBRIUM SOLUTION OF GAS
OBSERVED ΔTP
OBSERVED (ΔBHP - ΔTP)
CURVE C ASSUMES EQUILIBRIUM SOLUTION OF GAS
CURVE D ASSUMES NO SOLUTION OF GAS
(ΔBHP - ΔTP) + ΔPc
(OBSERVED ΔBHP - CURVE B)
(OBSERVED ΔBHP - CURVE A)
Pressure Change, psi
Time After Closing-In, Minutes

FIG. 6—PRESSURE BEHAVIOR IN SOUTH TEXAS WELL 1.

The fact that wells without packers have smaller humps than wells with packers seems reasonable in view of our experiments with bubble-columns. There it was found that the amount of the pressure build-up caused by bubble rise diminished as the initial gas volume in the wellbore increased. Since the wells without packers have much more gas initially in the wellbore than wells with packers, they should have smaller humps. It was also observed that wells without packers had the hump later than wells with packers. This is reasonable because more influx will be required to bring the pressure in the wellbore up to that required to balance the reservoir pressure.

Having concluded that bubble rise is probably the cause for most of the hump anomalies at this South Texas field, an examination of an anomaly slightly different than found in South Texas Well 1 was made.

Analysis of Behavior of South Texas Well 2

An example of a well in which phase redistribution influences the build-up, but is not large enough to cause the BHP to exceed the reservoir pressure, is shown in Fig. 7 for South Texas Well 2. The difference curve for this well shows a maximum at about the same time as that for South Texas Well 1, indicating that wellbore conditions were similar at time of closing-in. However, the continued slow rise in pressure in Well 2, which tends to mask the hump, indicates that the formation permeability around this well is somewhat lower than that around Well 1.

On comparing the behavior of Well 2 with Well 1, it appears that there is probably an optimum permeability for humping; formations of low permeability will still be building up at the time of separation of most of the gas so that the hump may be partially masked, as in Well 2. In formations of high permeability and no skin effect, equilibrium can always exist between wellbore and formation with the result that no hump will occur. The optimum conditions appear to be found in formations of moderate permeability where there is a considerable skin effect.

ANOMALIES RESULTING FROM TUBING OR PACKER LEAKS

Analysis of Behavior of North Texas Well A

This well exhibits a behavior slightly different from the two previous examples, as shown in Fig. 8. The phase redistribution build-up occurs early, the tubing pressure reaching a maximum at about 120 minutes. This time the BHP exceeds the adjacent reservoir pressure so much that it reaches a maximum and humps even though the well has not built up to average reservoir pressure. Following the temporary decrease, the build-up continues toward the stabilized reservoir pressure with the complication that a slow leak in the tubing head causes this pressure to decrease. To balance this decrease in tubing pressures, the difference curve increases, i.e., the well loads with liquid. Because the rate of this loading (after-production) will influence the BHP, it appears that a straight-line portion is not reached during this build-up.

Analysis of Behavior of Williston Basin Well 1*

Three build-up curves on two wells in a Williston Basin field showed an anomaly caused by leakage between zones of different pressure. These wells were completed in two zones which were separated by a

*This anomaly and its explanation were brought to our attention by A. Hols of the Shell Oil Co.

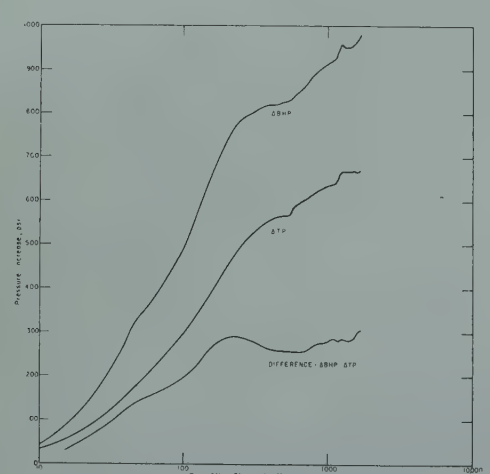

Fig. 7—Pressure Build-up, South Texas Well 2.

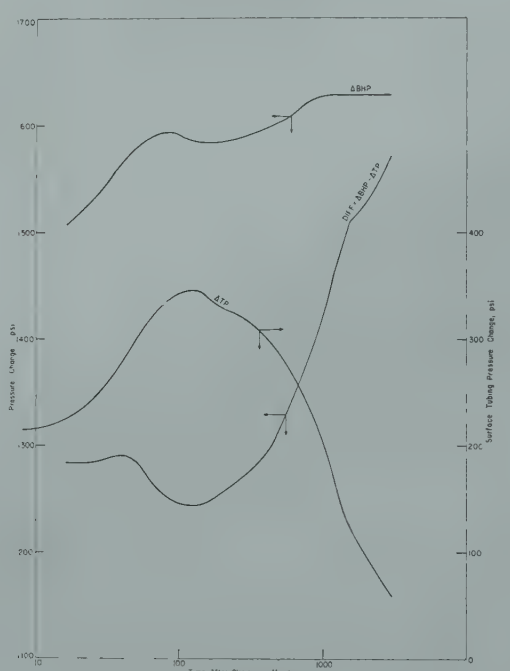

Fig. 8—Pressure Build-up, North Texas Well A.

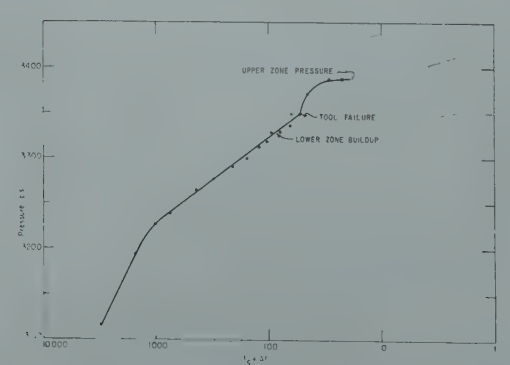

Fig. 9—Effect of Packer Failure on Pressure Build-up, Williston Basin Well 1 (Upper Zone Packed-off).

casing packer. The tubing contained a nipple which allowed selective production of either zone through the tubing. In Well 1 initial production was obtained from the lower zone, a choke being used to seal off the upper zone. After some months it was decided to switch the productive interval to the upper zone to conform to a recommended drainage pattern. Prior to this switch a build-up survey was conducted on the lower zone. Results are shown in Fig. 9. When the pressure differential between zones became small, the packing in the choke failed. Since the upper zone had already built up the annulus pressure, there was a rapid rise in pressure, as shown.

After the choke was pulled, a separation tool was run for an upper zone recompletion. A build-up survey conducted some months later gave results very similar to those shown in Fig. 9. When the pressure differential between zones became small the packing in the separation tool failed, which again caused an anomalous rise in pressure.

Analysis of Behavior of West Texas Well A

The West Texas Well A build-up had an unusually high tubing pressure build-up in addition to other difficulties which will be subsequently discussed. Since this was very much greater than the bottom-hole build-up, it appears that high pressure gas leaked from the casing into the tubing, thereby causing the tubing to unload. Such a redistribution can theoretically change the BHP if outflow from the well to the formation is restricted. A theoretical example (see Fig. 10) is calculated to show how a phase redistribution due to a tubing leak can affect the BHP. In this example the densities of gas and oil are assumed constant, and the casing volume is taken as five times the tubing volume.

As shown in Fig. 10 the liquid level will rise 500 ft in the casing as the liquid levels in tubing and casing equalize ($x = 500$ ft). Since the number of moles of gas does not change, the new average gas pressure can be calculated to be 1,842.6 psi. The final BHP can be calculated from this and from the gradients. It is found in this manner that if there is no outflow, the final BHP will increase by 103.7 psi because of the leak. Thus, such a leak could seriously affect the slope of a pressure build-up curve.

CONCLUSIONS

Phase redistribution within the wellbore can influence BHP behavior considerably, often leading to humps and irregularities. Optimum conditions for the formation of humps are encountered in formations of moderate permeability with some skin effect. Tubing and packer leaks can also cause humps. Measurement of surface tubing and casing pressure during build-up can be of aid in helping to unravel the cause of apparently anomalous behavior. Development of a bottom-hole tool which would allow the well to be shut-in near the bottom just above the pressure bomb would eliminate many anomalies.

As was noted in Fig. 5, because of disturbing effects of bubble rise and of compression of the fluid in the wellbore, the rate of influx after closing-in may not be proportional to the rate of change of BHP. In this light our method of making inflow calculations should be re-examined.

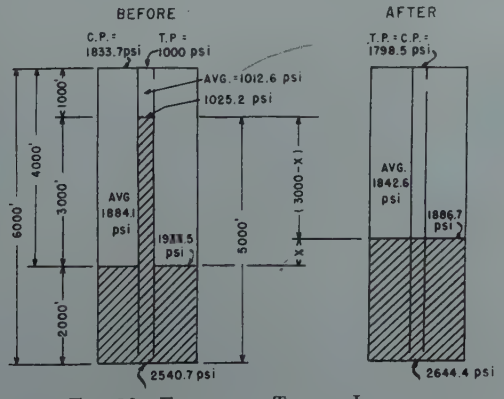

Fig. 10—Effect of Tubing Leak on Pressure Build-up.

NOMENCLATURE*

BHP = bottom-hole pressure

GOR = gas-oil ratio, scf of gas produced per barrel tank oil

GLR = gas-liquid ratio, the ratio in a small interval of tubing of total volume of gas (free and dissolved) when measured at standard conditions to volume of stock-tank oil, scf/bbl

TP = tubing pressure

G = gas after-production into bottom of tubing ft^3/ft^2 cross section

H = height of a point in wellbore above bottom of pay, ft

$\triangle H$ = incremental height in wellbore, ft

H_o = height of oil column in wellbore, ft

L = liquid after-production into bottom of tubing, ft^3/ft^2 cross section

$\triangle p$ = pressure drop, or difference, psia

$\triangle p_c$ = pressure rise due to compression of fluid in the wellbore by after-production, psia

V_g = total volume of gas in tubing at time of closing-in, ft^3/ft^2 cross section

V_{or} = the volume occupied by oil when saturated with gas at some temperature and pressure relative to its volume at bubble point conditions.

REFERENCES

1. Peebles and Garber: "Studies on the Motion of Gas Bubbles in Liquids," *Chem. Eng. Prog.* (1953), **49**, 88.
2. Gilbert: "Flowing and Gas-Lift Well Performance," *Drill. and Prod. Prac.*, API (1954), 126.
3. Perrine: "Analysis of Pressure Build-Up Curves," *Drill. and Prod. Prac.*, API (1956), 482.
4. West, W. J., Garvin, W. W., and Sheldon, J. W.: "Solution of the Equations of Unsteady State Two-Phase Flow in Oil Reservoirs," *Trans.* AIME (1954), **201**, 217.
5. Mueller, T. D., Warren, J. E., and West, W. J.: "Analysis of Reservoir Performance K_g/K_o Curves and a Laboratory K_g/K_o Curve Measured on a Core Sample," *Trans.* AIME (1955), **204**, 240.

APPENDIX 1

GAS AND OIL IN TUBING AT TIME OF CLOSING-IN

It is possible to approximate the volume of gas and oil in the tubing at flowing conditions assuming PVT

*See AIME symbols List in *Trans.* AIME (1957) **207**, 368, for other symbol definitions.

equilibrium at all points, neglecting friction drop, and assuming that the GLR* (the ratio of standard cubic feet of free and dissolved gas to barrels tank oil) is the same in any interval in the column.

With the above assumptions one may solve, by trial and error, for a curve of pressure vs depth which fits the known surface and bottom-hole flowing pressure. For South Texas Well 1 it was found that the calculated curve of pressure vs depth fits the observed end points when a gas-liquid ratio equal to 455 scf/STB is used (the flowing GOR was 700). In the final calculation the effect of a temperature gradient from 246 to 130° F at tubing head was included. These results were only slightly different from those assuming constant temperature of 246° F in the flowing tubing system.

From this same set of calculations the gas saturation at any level, and, therefore, the total amount of gas, can also be found. For South Texas Well 1 it was found that there are 2,910 ft of free gas and 4,990 ft of liquid in the tubing under flowing conditions.

It is realized that the assumption of a constant gas-liquid ratio throughout the tubing is not necessarily true. However, the method seems to give reliable results in South Texas wells, as will be discussed more fully in Appendix 2. At this point it should be mentioned, however, that the curve of pressure vs depth obtained above has a shape similar to the curves obtained by Gilbert[2] from field measurements.

APPENDIX 2

RATE AND AMOUNT OF AFTER-PRODUCTION

Rate of After-production

The difference between the change in bottom-hole pressure and the change in tubing pressure may be related directly to the amount of material flowing into the well. If the flowing gas-oil ratio is assumed to persist after shut-in**, the incremental difference relationship is:

$$\frac{\Delta(\Delta p)}{\Delta t} = \frac{\Delta(\Delta \text{BHP} - \Delta \text{TP})}{\Delta t} = 0.433\left[\rho_g \frac{\Delta G}{\Delta t} + \rho_o \frac{\Delta L}{\Delta t}\right],$$

where

$$\frac{\Delta L/\Delta t}{\Delta G/\Delta t} = \frac{B_o\, 5.61}{B_g\,(\text{GOR} - R_s)} = \frac{\text{rate of oil after-production at tubing conditions}}{\text{rate of free gas after-production, at tubing conditions}}.$$

By solving these two equations simultaneously we may obtain $\Delta L/\Delta t$ and $\Delta G/\Delta t$. By summing the ΔL's and the ΔG's we obtain the total liquid and gas after-production, L and G.

Using this method of calculation, the net liquid after-production is found to be 1,218 ft (1,317-ft positive after-production and 99-ft negative). Fig. 5 gives a plot of rate of total influx vs time in minutes.

If a gradient survey had been made while the bomb was being removed from South Texas Well 1, it would have been possible to check on some of these calculations by comparing the calculated and measured gas-oil interface in the tubing. Although no gradient survey was available on South Texas Well 1, one was available on South Texas Well 2, which may be closely compared since the two wells have similar GOR, rate of production, and depth. In this well the amount of gas was ascertained to be 1,700 ft at the end of the build-up. In the previous calculation for South Texas Well 1 the amount of gas at the beginning of shut-in was found to be 2,910 ft. Subtraction of the net after-production of 1,218 ft of liquid gives the height of gas remaining at the end of the South Texas Well 1 build-up—1,692 ft. The fact that this calculated height checks closely with that found by gradient survey in Well 2 indicates that these calculations are approximately correct.

Compression Caused by After-production

Knowing the cumulative volume of oil and gas flowing into the well at any time, the compression of the gas phase and the consequent increase in tubing head pressure can be calculated from

$$p_2 - p_1 = \Delta p_c = \frac{p_1 V_g}{V_g - (L + G)} - p_1, \quad . \quad (1)$$

where V_g is the volume of gas in tubing when flowing, ft³/ft² area; p_1 is the flowing gas pressure at tubing head; and p_2 is the final gas pressure at tubing head.

If it is decided to take solution of gas into account, G is replaced by G' in the above equation, where $G' = G -$ (decrease in gas volume due to solution − increase in oil volume) $= G - (\Delta V_1 - \Delta V_2)$.

The volume of gas going into solution per unit cross sectional area is:

$$\Delta V_1 = \left[\frac{dR_s}{dp}\right] \frac{\Delta p H_o B_g}{5.61\, B_o}.$$

The increase in oil volume per unit cross sectional area is:

$$\Delta V_2 = \left[\frac{dV_{or}}{dp}\right] \frac{\Delta p H_o}{V_{or}},$$

where R_s is the dissolved gas, H_o is the feet of oil in tubing, and Δp is the average pressure change.

Results of these calculations are used in plotting Fig. 6, where $\Delta p'_c$ is obtained from Eq. 1 by substituting G' for G. ★★★

*Note that the gas-liquid ratio (GLR) is not the same as the flowing gas-oil ratio (GOR) at steady state. The GOR at standard conditions of the total fluid entering the tubing at the bottom must be the same as the GOR at standard conditions of the total fluid leaving the tubing at the top. Because of liquid hold-up the GLR at standard conditions in the tubing is not the same as the flowing GOR. It is possible, for example, to have many feet of water in the tubing, and yet never produce any liquid water.

**Using calculations of pressure and saturation distribution in a depletion-type reservoir, made on the IBM 701 computer by Perrine[3], West, Garvin, and Sheldon[4], and Mueller, Warren, and West[5], it was found that the flowing GOR (when measured at surface conditions) is very nearly constant throughout a flowing reservoir. Therefore, when the reservoir is closed-in, the outlying gas and oil should continue to flow in at the same GOR.

Factors Affecting the Rate of Deposition of Cement in Unfractured Perforations During Squeeze-Cementing Operations

G. W. BINKLEY
JUNIOR MEMBER AIME
G. K. DUMBAULD
MEMBER AIME
R. E. COLLINS

HUMBLE OIL & REFINING CO.
HOUSTON, TEX.

T. P. 8005

ABSTRACT

A mathematical analysis has shown that the primary factors affecting the deposition of cement in unfractured perforations during squeeze-cementing operations are: the properties of the cement slurry, the geometry of the perforations, and the filtration time. The validity of the analysis has been substantiated by laboratory investigations.

The information presented in this paper makes possible the prediction of the rate of deposition of cement in and about unfractured perforations under given squeeze-cementing conditions, the proper filtration time to control the amount of deposition to any desired value, and the deposition properties needed in cement slurries to restrict to any desired degree the formation of nodes of cement solids inside the casing.

INTRODUCTION

The deposition of solids against a permeable medium by the process of filtration is an important property of a cement slurry. General recognition of the role of filtration in the use of cement in wells is evident in view of the fact that several patents on low-water-loss cements have been issued during the past few years.

In the conventional, high-pressure squeeze-cementing technique, a large volume of cement slurry is usually displaced into the area surrounding the perforated interval after the formation has been fractured hydraulically.[1] Near the end of the job, the pumping rate is slowed or stopped intermittently in an effort to obtain a high pressure in the wellbore. The way in which a high pressure is obtained is not understood thoroughly, but it is believed to be caused by the deposition of a rigid mass of compacted cement particles either in the fractures of the formations or inside the casing opposite the perforated interval. In a method of squeeze-cementing introduced several years ago, a small amount of cement slurry is squeezed into the perforations at a low pressure to avoid fracturing the formation.[2,3] The filling of the unfractured perforations with cement particles by the process of filtration is important to the success of this technique.

Early in the development of this low-pressure squeeze-cementing technique, laboratory and field-size experiments showed that conventional, neat cement slurries were unsatisfactory if the tubing was extended into or through the perforated section of the casing.[4,5] The extremely high filtration rate of neat cement slurries caused the deposition of a compacted mass of cement inside the casing and made it impossible to remove excess cement by reverse circulation and difficult to withdraw the tubing. Because the need for cements with a reduced filtration rate was obvious and urgent, modified cements containing 12 per cent bentonite were used until research was completed on modified cements containing 25 per cent bentonite.[6] These modified cements were useful in the solution of the immediate problem, but the following questions remained unanswered: (1) what is the optimum filtration rate of cement slurries for this application, (2) how long should the squeeze pressure be applied, and (3) how great are the effects of squeeze pressure and well temperature on the rate of deposition? Furthermore, the relationship of the filtration properties of cement slurries to the dimensions of the perforations and the wellbore was unknown. In order to obtain information relative to these basic considerations, a systematic evaluation of all the factors involved in the deposition of cement during low-pressure squeeze-cementing operations was initiated. Although the work was directed toward an evaluation of the factors influencing the deposition of cement in the low-pressure squeeze-

Original manuscript received in Society of Petroleum Engineers office on July 18, 1957. Revised manuscript received Feb. 3, 1958. Paper presented at 32nd Annual Fall Meeting of Society of Petroleum Engineers in Dallas, Tex., Oct. 6-9, 1957.

[1]References given at end of paper.

Discussion of this and all following technical papers is invited. Discussion in writing (three copies) may be sent to the offices of the *Journal of Petroleum Technology*. Any discussion offered after Dec. 31, 1958, should be in the form of a new paper.

cementing technique, much of the information is applicable in high-pressure squeeze-cementing operations.

The initial phase of the present investigation was a study of the properties of cement slurries that influence the deposition of cement by filtration. This phase included a theoretical study to determine what properties were important in defining the deposition of solids from cement slurries and laboratory tests to determine characteristic values of these properties. The second phase was the application of these general filtration principles to the specific case of the deposition in unfractured perforations. After mathematical relationships between the slurry properties defined in the first phase of the investigation and the geometry of perforations were developed, the validity of these correlations was investigated by making tests under conditions simulating those encountered in the squeeze cementing of unfractured perforations. The mathematical analysis, the results of the tests to evaluate its validity, and ways to use the information to predict the deposition of cement in squeeze-cementing operations are presented in this paper.

MATHEMATICAL ANALYSIS

The most pertinent features of a mathematical analysis of the factors affecting the rate of deposition of solids in unfractured perforations by filtration are presented in the following discussion.

Development of the Law of Filter Cake Formation

In a suspension, such as a cement slurry, the fraction by volume of solids, f, is defined as:

$$f = \frac{V_s}{V_s + V_l} = \frac{V_s}{V}, \quad \ldots\ldots\ldots \quad (1)$$

where V_s, V_l and V are the volumes of the solids, liquid, and suspension, respectively. If the composition of the slurry is unchanged by the filtration process, the thickness of the filter cake, dS, having a porosity, ϕ, which is deposited when a volume of filtrate, dQ, passes through a given plane permeable surface of area, A, may be expressed by the following equation:

$$dS = \frac{f}{1 - f - \phi} \cdot \frac{dQ}{A}. \quad \ldots\ldots\ldots \quad (2)$$

The "deposition constant", ω, is defined as

$$\omega = \frac{f}{1 - f - \phi}, \quad \ldots\ldots\ldots \quad (3)$$

and the "law of filter cake formation" may be written in the form:

$$\frac{dS}{dt} = \omega q, \quad \ldots\ldots\ldots \quad (4)$$

where q is the volumetric flow rate of filtrate per unit area of surface, and dS/dt is the rate of increase of filter cake thickness.

Growth of a Plane Filter Cake

If a filter press arranged to contain a slurry in contact with a plane permeable surface of area, A, is used to obtain a pressure differential between the suspension and the exterior of the permeable filtering surface, the filtrate begins to pass through the permeable surface, and the residual solids form a filter cake on the permeable surface. If the compressibilities of the filter cake, the filtrate, and the permeable surface are neglected, and the flow obeys Darcy's law, then Darcy's law and the law of continuity may be combined to give:

$$\frac{\partial}{\partial x}\left[\frac{k}{\mu}\frac{\partial P}{\partial x}\right] = 0 \quad \ldots\ldots\ldots \quad (5)$$

as the differential equation which describes the pressure distributions. Here, k is the permeability of the filter cake, and μ is the viscosity of the filtrate. If the assumptions are made that the permeability of the filter cake is uniform and that the pressure drop through the permeable filtering surface is negligible, boundary conditions may be set and proper integrations made. The integrated form and Darcy's law then are used to give.

$$q = \frac{k \triangle P}{\mu S}, \quad \ldots\ldots\ldots \quad (6)$$

where $\triangle P$ is the pressure differential. After this value of q is inserted into Eq. 4, it is integrated with $S = 0$ at $t = 0$, and the following equation results:

$$S = \sqrt{\frac{2k\omega \triangle P}{\mu}}\, t^{\frac{1}{2}}, \quad \ldots\ldots\ldots \quad (7)$$

for the growth of the filter cake thickness with the filtration time, t. From Eqs. 6 and 7 it can be shown that the rate of filtration as a function of time is

$$q = \sqrt{\frac{k \triangle P}{2\omega\mu}}\, t^{-\frac{1}{2}} \quad \ldots\ldots\ldots \quad (8)$$

When Eq. 8 is multiplied by the area, A, and integrated with respect to t with $Q = 0$ at $t = 0$, the cumulative volume of filtrate as a function of filtration time is obtained:

$$Q = \sqrt{\frac{2kA^2 \triangle P}{\omega\mu}}\, t^{\frac{1}{2}} \quad \ldots\ldots\ldots \quad (9)$$

The simultaneous solution of Eqs. 7 and 9 gives

$$k = \frac{\mu Q S}{2At \triangle P}, \quad \ldots\ldots\ldots \quad (10)$$

and

$$\omega = \frac{AS}{Q} \quad \ldots\ldots\ldots \quad (11)$$

Eqs. 10 and 11 may be used with data from filter press experiments to calculate k and ω, where $t = T_f$—i.e., filtration time of the experiments. Also, if f, the fraction by volume of solids in the suspension, is known, the porosity of the filter cake can be determined by means of Eq. 3.

Rate of Deposition of Solids in Unfractured Perforations

For an analysis of the filling of an unfractured perforation with solids deposited from a suspension by filtration, the geometry of the perforation is considered to be as shown in Fig. 1. In this analysis the filter cake, the filtrate, and the formation are considered to be incompressible. Also, the depth of the perforation is considered to be large in relation to its diameter. When the depth of the perforation is at least four times greater than the diameter, the depth of the perforation has a negligible effect upon the deposition process. For an approximate analysis, the filtration process is divided into two portions, one in which radial filtration predominates and a second in which linear filtration predominates.

If the pressure drop in the formation is assumed to be negligible, the following expression is obtained for q at the suspension-filter cake interface during the radial filtration stage through the use of Darcy's law and the equation of continuity.

$$q = \frac{-k \triangle P}{\mu(a - S) \ln\left[1 - \frac{S}{a}\right]} \quad \ldots\ldots \quad (12)$$

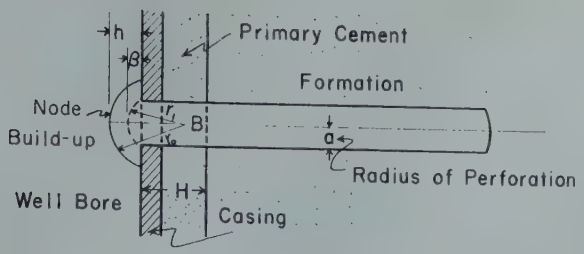

FIG. 1—GEOMETRY OF PERFORATION.

When this expression for q is inserted into Eq. 4, the following equation is obtained:

$$\frac{dS}{dt} = -\frac{k\omega\triangle P}{\mu}\left[\frac{1}{(a - S)\ln\left[1 - \frac{S}{a}\right]}\right] \quad . \quad (13)$$

When Eq. 13 is integrated with $S = 0$ at $t = 0$ and $S = a$ at $t = T_1$, the time to fill by radial filtration that portion of the perforation bounded by the porous formation is obtained.

$$T_1 = \frac{\mu}{\omega k\triangle P}\left[\frac{a^2}{4}\right] \quad . \quad (14)$$

In the second stage the portion of the perforation bounded by the primary cement and the casing is being filled, and the flow in this part of the perforation is essentially linear. It is assumed that the primary cement sheath is completely impermeable. However, deviation from linear flow occurs in the region of the perforation bounded by the formation. This flow can be approximated by replacing this part of the perforation with a disk of radius, a, and thickness, εa (i.e., a fraction, ε, of the perforation radius) through which the flow is linear. When Darcy's law is applied, the following equation for q is obtained:

$$q = \frac{k\triangle P}{\mu(S + \varepsilon a)} \quad . \quad (15)$$

When this is inserted into Eq. 4, the expression,

$$\frac{dS}{dt} = \frac{k\omega\triangle P}{\mu}\left[\frac{1}{S + \varepsilon a}\right], \quad . \quad (16)$$

is obtained. When Eq. 16 is integrated with the conditions $S = 0$ at $t = 0$ and $S = H$ at $t = T_2$, where H is the combined thickness of the cement sheath and casing,

$$T_2 = \frac{\mu}{k\omega\triangle P}\left[\frac{H^2}{2} + \varepsilon aH\right] \quad . \quad (17)$$

is obtained for the time required for the second stage of plugging.

Thus, the total time required to build a filter cake flush with the inside of the casing is

$$T = T_1 + T_2 = \frac{\mu}{k\omega\triangle P}\left[\frac{H^2}{2} + \frac{a^2}{4} + \varepsilon aH\right]. \quad (18)$$

It is necessary to determine the empirical constant, ε, from the fitting of Eq. 18 to experimental observations. A value of 0.25 was found to fit the results of many experiments conducted under a variety of test conditions.

The variables related to the deposition properties of a cement slurry occur only in the grouping, $\mu/k\omega\triangle P$, hereafter called the "composition factor". The value of this factor for a particular slurry can be obtained from the results of filtration experiments in a high-pressure filter press by use of the following equation, which is obtained by combining Eqs. 10 and 11.

$$\frac{\mu}{k\omega\triangle P} = \frac{2T_1}{S^2} \quad . \quad (19)$$

RATE OF DEPOSITION OF SOLIDS INSIDE THE CASING FOLLOWING PERFORATION FILL-UP

After a perforation is filled flush to the inside casing face, continued application of squeeze pressure causes the deposition of solids to form a node of filter cake over the perforation. A rigorous analysis of the formation and growth of a node inside the casing to predict the shape and size of the node as a function of time presents extreme difficulties and is impractical. The analysis is greatly simplified if the shape of the node is assumed. From observation of nodes it appears reasonable to assume that the node is spherical at every stage of growth. Also, it seems reasonable to assume that the lateral growth occurs at the same rate as the vertical growth. With these assumptions, the following relationship between the height and the radius of curvature of the node is obtained:

$$r_o = \frac{h^2 + (a + h)^2}{2h} \quad . \quad (20)$$

A sketch illustrating the geometry of the node and defining the symbols used is shown in Fig. 1. Note that for zero node height, $h = 0$, the radius of curvature, r_o, is infinite. Spherical flow of the filtrate is assumed to exist between the node surface and a spherical surface intersecting the edge of the perforation. The radius of curvature of this surface is denoted by r_1 in the sketch. The radius, r_1, can be expressed in terms of r_o by

$$r_1 = \sqrt{(r_o - h)^2 + a^2} \quad . \quad (21)$$

In this spherical region the pressure must satisfy the equation,

$$r\frac{\partial^2}{\partial r^2}(rP) = 0 \quad . \quad (22)$$

which has a solution of the form,

$$P = A + \frac{B}{r} \quad , \quad (23)$$

A and B being constant with respect to r. Here r is the radial coordinate of the spherical coordinate system with the center at Point B in the sketch.

The flow of filtrate within the perforation is assumed to be approximately linear from the surface of radius, r_1, and a plane at the distance, εa, below the plane of contact of formation and primary cement. This is the same ε introduced in the previous section. The height β of the surface of radius r_1 above the casing face is given by

$$\beta = r_1 - \sqrt{r_1^2 - a^2}. \quad (24)$$

Thus, a linear pressure gradient exists over the distance, $H + \beta + \varepsilon a$.

When the linear flow and spherical flow are combined, the flow rate per unit area into the node is obtained:

$$q = \left(\frac{k\triangle P}{\mu}\right) \times \left(\frac{1}{(H + \beta + \varepsilon a)\frac{r_o^2}{r_1^2} + \frac{r_o^2}{r_1} - r_o}\right) \quad . \quad (25)$$

Combining Eq. 25 with the deposition law gives

$$\frac{dh}{dt} = \left(\frac{k\omega\triangle P}{\mu}\right) \times \left(\frac{1}{(H + \beta + \varepsilon a)\frac{r_o^2}{r_1^2} + \frac{r_o^2}{r_1} - r_o}\right) \quad . \quad (26)$$

When r_o, r_1, and β are expressed in terms of h, Eq. 26 can, in principle, be integrated to give h as a function of time. However, it is much more practical to do the

integration numerically on a high speed digital computer, such as the Bendix G-15.

Note that when Eq. 26 is integrated with $h = 0$ at $t = 0$, the result gives the time elapsed from fill-up to a height of node, h. The time required for fill-up, as given by Eq. 18, must be added in order to have the total squeeze time.

The above integration has been done on the Bendix G-15 computer with the value of ε taken as 0.25. The results, including fill-up time, are plotted in Fig. 2 as

$$\frac{T}{(\mu/k\omega\triangle P)a^2} \text{ vs } \frac{H}{a},$$

with h/a as the parameter. Note that T is the total filtration time. Thus, on the given curves of Fig. 2 at $h/a = 0$ the value of T is the time required for filling the perforation flush to the inside of the casing.

Consistent cgs units have been assumed throughout the mathematical analysis just presented; however, the factors related in Fig. 2 may be expressed either in consistent cgs units or in the usual field units.

LABORATORY INVESTIGATION

The mathematical analysis just discussed showed that all of the variables related to the deposition properties of the cement slurry are contained in the composition factor, $\mu/k\omega\triangle P$. This analysis showed also that the permeability, k, and the deposition constant, ω, may be determined by measuring the filter cake thickness, S, and the cumulative volume of filtrate, Q, obtained when a cement slurry in contact with a plane permeable surface of area, A, is subjected to a given pressure differential, $\triangle P$, for a given time, T_f. The objective of the laboratory tests to be described was to determine the effect of temperature and pressure differential on the deposition constants and the permeabilities of cement slurries.

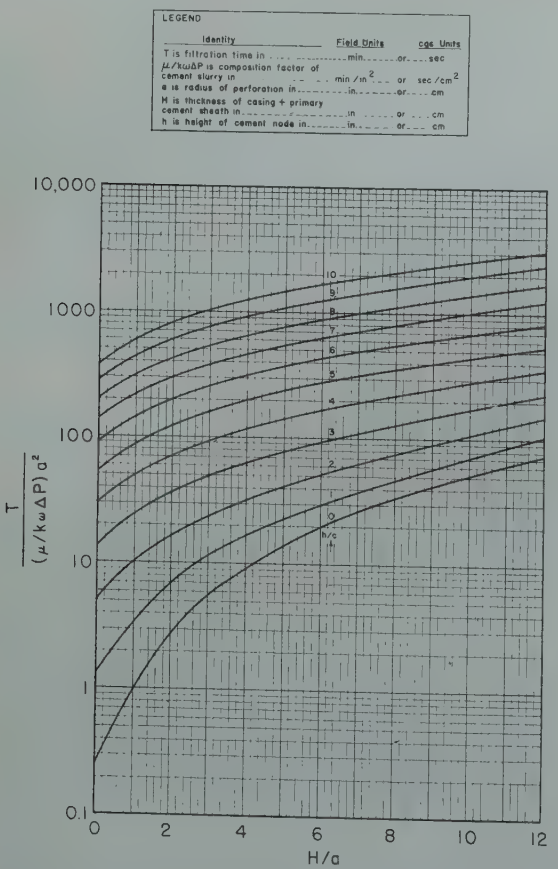

FIG. 2—RELATIONSHIP BETWEEN CEMENT PROPERTIES AND PERFORATION GEOMETRY WHICH AFFECT THE DEPOSITION OF SOLIDS IN AND ABOUT UNFRACTURED CYLINDRICAL PERFORATIONS.

EFFECT OF TEMPERATURE AND PRESSURE DIFFERENTIAL ON THE PERMEABILITIES OF THE FILTER CAKES AND ON THE DEPOSITION CONSTANTS OF CEMENT SLURRIES

Two cementing compositions which are presently used in the field in low-pressure squeeze-cementing operations were tested. These compositions were the modified portland cements containing either 12 or 25 per cent bentonite.[6]

PROCEDURE

A 1-qt Waring blendor was utilized to mix the cement slurries. A Baroid high-pressure, high-temperature filter cell, modified so that the deposited filter cake could be removed, was used to measure the filtration rates and deposition properties of the slurries. Also, the top valve stem was altered so that the filter cell could be connected to a nitrogen cylinder.

The tests were made at room temperature (78°F) and at 180°F with several pressure differentials between 100 and 1,500 psi. If the test temperature was above room temperature, the filter cell containing the test slurry was heated to the desired temperature before pressure was applied. At the completion of the filtration period the deposited filter cake was removed from the cell and washed under a gentle stream of water until no more deposited solids were removed. The thickness of the cake was measured to the nearest 1/32 in. The cumulative volume of filtrate to the nearest 0.5 cc was observed and recorded.

From the filtration data the permeability of the deposited filter cake and the deposition constant of each cement slurry were calculated using Eqs. 10 and 11, respectively.

RESULTS

The effect of pressure differential on the permeabilities of cement filter cakes deposited at temperatures of 78 and 180°F by each of the two cement compositions is shown in Fig. 3. It is evident that the permeability decreases as pressure differential increases. At a pressure differential of 800 psi the filter cake permeabilities begin to level off, and above 1,000 psi the effect of pressure is very slight. Fig. 3 shows also that for pressure differentials in excess of 800 psi the permeability of the cement filter cakes is approximately the same at 78 and 180°F. This indicates that the permeability of a deposited cement filter cake is not dependent upon temperature.

The effect of pressure differential at temperatures of 78 and 180°F on the deposition constants of the cement slurries is presented in Fig. 4. This figure shows that the values of the deposition constants decrease slightly with increasing pressure differential, but above about 800 psi the effect of pressure differential is negligible. It is also evident that the deposition constant of each of the cement slurries is independent of the test temperature.

EFFECT OF TEMPERATURE AND PRESSURE DIFFERENTIAL ON THE COMPOSITION FACTORS OF MODIFIED PORTLAND CEMENTS

Additional tests were made with the modified portland cements containing either 12 or 25 per cent bentonite and varying concentrations of calcium lignosul-

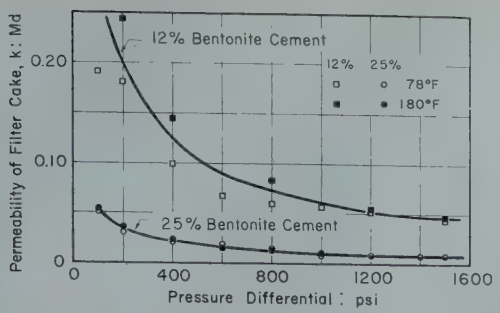

FIG. 3—EFFECT OF PRESSURE ON PERMEABILITIES OF MODIFIED CEMENT FILTER CAKES AT 78 AND 180° F.

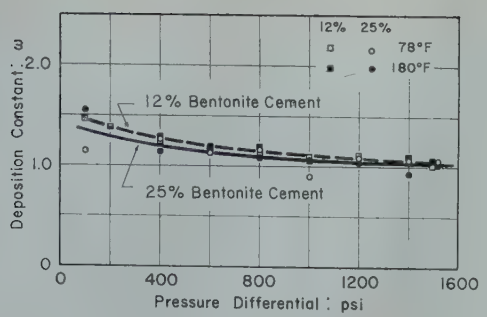

FIG. 4—EFFECT OF PRESSURE ON DEPOSITION CONSTANTS OF MODIFIED CEMENT SLURRIES AT 78 AND 180° F.

fonate. In these tests the laboratory mixing was adjusted to give as nearly as possible slurries having the same filtration rates as those obtained in the field, so that the information developed could be used as a guide for field work.

PROCEDURE

A 5-qt Waring blendor was employed for preparing the cement slurries. The same Baroid high-pressure, high-temperature filter cell (described in the previous section) was utilized to determine the filtration rates and deposition properties of the cement slurries. These tests were conducted at pressure differentials of 800 psi and above.

In order to obtain filtration results in the laboratory which were comparable to those obtained in the field, the volume of slurry prepared for each test was just sufficient to cover the mixing assembly in the bottom of the blendor. The mixing procedure was as follows. The calcium lignosulfonate was added to the mix water and agitated vigorously for one minute, the dry blend of cement and bentonite was added while the blendor was set at a slow speed, and then the blendor was turned to the maximum speed for two minutes. Because the violent agitation caused some air to be entrained in the slurry, the slurry was placed in a plastic jar and evacuated for 10 minutes prior to making the filtration test.

The filtration tests were made in the same manner as described previously. In tests conducted at 250°F, the filtrates were collected in a stainless steel cylinder immersed in an ice bath and maintained at a pressure of 50 psi.

Samples of filtrate were collected from several modified cement slurries filtered at 78, 180, and 250°F. The viscosities of these samples and that of tap water were measured with an Ostwald viscosimeter at several temperatures.

From the filtration data the permeability of the deposited filter cake, the deposition constant, and the composition factor of each slurry were calculated using Eqs. 10, 11, and 19, respectively.

RESULTS

The data presented in Table 1 show the effect of temperature and pressure differential on the filtration and deposition properties of modified cement slurries. To illustrate the effect of temperature on the composition factors of the two modified portland cements, pertinent data from Table 1 are presented graphically in Fig. 5. These data show that at pressure differentials of 800, 1,000, and 1,400 psi the composition factors are approximately the same at a given temperature, and that the effect of temperature is related to the change in the viscosity of the filtrate with temperature. The similarity of the curves for the composition factors and for the viscosity of water, plotted in Fig. 5, vividly demonstrates that changes in the composition factor result primarily from changes in the viscosity of the filtrate.

The viscosities of the filtrate samples which were collected from the modified cement slurries were found to be the same as that of water when they were compared at the same temperatures.

Since the effect of temperature on the product, $k\omega\triangle P$, is slight, and since the viscosity of the filtrate is the same as that of water, the value of the composition factor, $\mu/k\omega\triangle P$, at a given squeeze-cementing temperature can be calculated from a value measured at any temperature. This is done by multiplying the measured value of $\mu/k\omega\triangle P$ by the ratio of μ_f/μ_t, where μ_f is the viscosity of water at the squeeze-cementing temperature, and μ_t is the viscosity of water at the temperature of the test.

COMPARISON OF PREDICTED AND EXPERIMENTALLY OBSERVED RATES OF DEPOSITION OF CEMENT IN UNFRACTURED PERFORATIONS

After the composition factor of the cement slurry is determined, the information presented in Fig. 2 may be used to predict the rate of deposition of cement in unfractured perforations. The objective of the tests to be described was to determine the validity of the correlations in Fig. 2 in predicting the filling of an unfractured perforation with cement and the subsequent building of a node of cement over the perforation.

PROCEDURE

To simulate an unfractured perforation, a test setup similar to the one shown in Fig. 6 was used. As depicted in this figure, a sandstone core was cemented with Hydromite inside a short section of 4½-in. drill pipe with a steel plate welded over one end. The plate and core were drilled to a depth of approximately 4½ in. to simulate a well perforation. In order to have a thickness, H, of known dimensions, a section of pipe equal in length to the combined thickness of the steel plate and Hydromite was fitted tightly through the drilled steel plate on several of the core targets.

In these simulated squeeze-cementing tests, which were conducted at 78°F, a 22-in. length of 4½-in. ID aluminum pipe was fastened to the perforated end of the core target and filled with the test slurry. Nitrogen pressure was applied to the surface of the cement slurry for a given period of time to deposit a filter cake in the perforation. At the completion of the test the perforated target was disconnected from the reservoir, the area around the perforation was washed under a gentle stream of water, and the height of the deposited cement filter cake in relation to the inside face of the steel plate was measured to the nearest 1/32 in.

TABLE 1—EFFECT OF TEMPERATURE AND PRESSURE DIFFERENTIAL ON FILTRATION AND DEPOSITION PROPERTIES OF MODIFIED NORMAL PORTLAND CEMENT SLURRIES

(Prepared in a 5-qt Waring blendor to simulate field mixing)

Additives (wt. per cent of Cement)			Filtration Data using Baroid Filter Cell								Composition Factor
Bentonite	Calcium Lignosulfonate	Water Content Gal Water per Sack Cement	API Water Loss at 78° F (cc/30 min[1])	Test Temperature (°F)	Pressure Differential $\triangle P$ (psi)	Filtration Time, T_f (min)	Volume of Filtrate Q (cc)	Filter Cake Thickness S (in.)	Deposition Constant ω	Permeability Filter Cake k (md)	$\frac{\mu}{k\omega\triangle P}$
12	0.6	10	82[a]	78	800	10	39	0.75	1.16	0.042	35.8
12	0.6	10	80	78	1,000	10	38	0.78	1.27	0.034	32.3
12	0.6	10	80	78	1,400	10	42.5	0.80	1.13	0.028	31.4
12	0.7	10	71	180	800	5	44	0.88	1.20	0.044	13.0
12	0.7	10	74	180	1,000	5	49	0.86	1.05	0.038	13.8
12	0.7	10	72	180	1,400	5	51	0.92	1.08	0.031	11.7
12	1.6	10	47[b]	250	800	5	50.5	0.85	1.00	0.032	14.3
12	1.6	10	45	250	1,000	5	52	0.96	1.15	0.030	10.7
12	1.6	10	—	250	1,400	5	62	1.00	0.97	0.027	10.0
25	1.2	16	43[c]	78	800	15	22.5	0.36	0.968	0.008	225.6
25	1.2	16	39	78	1,000	15	22	0.36	0.982	0.006	228.3
25	1.2	16	42.5	78	1,400	15	24	0.38	0.939	0.005	212.1
25	1.4	16	38	180	800	10	32	0.50	0.942	0.009	79.7
25	1.4	16	38	180	1,000	10	33.5	0.52	0.930	0.008	75.0
25	1.4	16	36.5	180	1,400	10	35	0.53	0.913	0.006	71.7
25	1.6	16	33.5	250	800	10	43	0.64	0.900	0.011	46.3
25	1.6	16	32	250	1,000	10	46	0.64	0.840	0.009	48.6
25	1.6	16	32	250	1,400	10	46.5	0.69	0.890	0.007	42.0

[1]API water loss results reported on field slurries prepared with small, batch-type mixer:
[a]Cement containing 12 per cent bentonite + 0.6 per cent calcium lignosulfonate: 90 cc/30 min.
[b]Cement containing 12 per cent bentonite + 1.2 per cent calcium lignosulfonate: 45 cc/30 min.
[c]Cement containing 25 per cent bentonite + 1.2 per cent calcium lignosulfonate: 38 cc/30 min.

Prior to squeezing the perforated core, the composition factor of the test slurry was determined by filtering a portion of the slurry in the Baroid high-pressure, high-temperature filter cell. Using the composition factor obtained and the correlations in Fig. 2, the filtration time for the test was calculated.

RESULTS

The results of the simulated squeeze-cementing tests are presented in Table 2. For convenience in evaluating the difference between the calculated and measured node build-up, certain data from Table 2 are plotted in Fig. 7.

It is noted from Fig. 7 that each test result is within 0.25 in. of that predicted by calculation. Tests 1, 2, 6, 10, and 12 show excellent agreement. It is believed that the excessive node build-up on Tests 4 and 5 occurred because the Hydromite cement between the perforated steel plate and the sandstone core was cracked. The results which showed the measured node height to be less than the predicted node height may have resulted from removal of a part of the node in the washing process. The fact that the top portion of a cement cake is soft and hence poorly defined makes it difficult to measure the node height accurately. This same difficulty is experienced, of course, in measuring the cement filter cake thickness, S, used in the calculation of the composition factor. In view of the possible errors in these measurements, the data presented in Table 2 and in Fig. 7 are

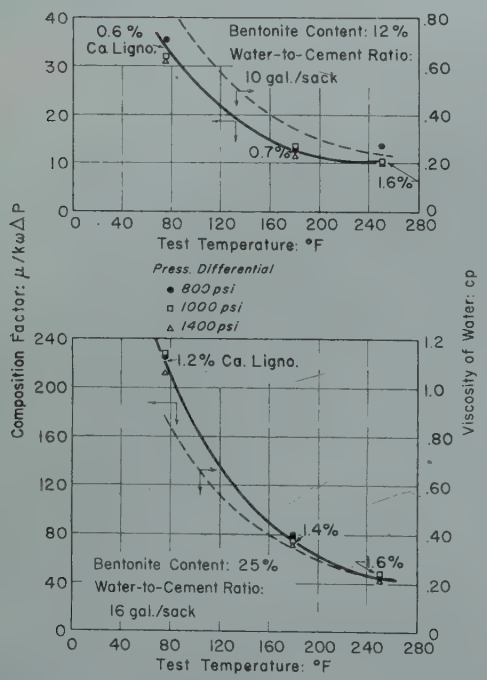

FIG. 5—EFFECT OF TEMPERATURE AND PRESSURE ON THE COMPOSITION FACTORS OF MODIFIED CEMENTS CONTAINING 12 AND 25 PER CENT BENTONITE.

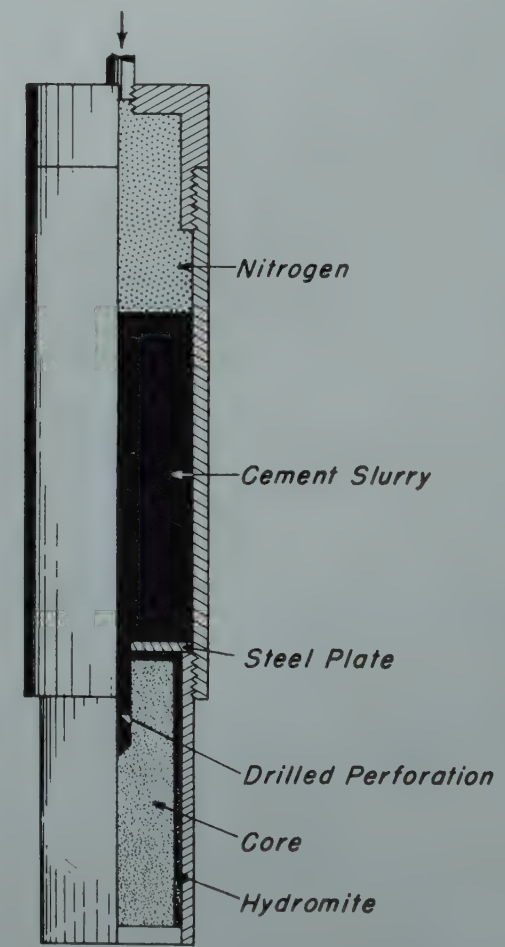

FIG. 6—TEST EQUIPMENT TO SIMULATE SQUEEZE CEMENTING OF UNFRACTURED PERFORATIONS.

believed to substantiate adequately the theory of cement deposition in unfractured perforations during squeeze-cementing operations.

USE OF RESULTS TO CALCULATE THE RATE OF DEPOSITION OF CEMENT IN SQUEEZE-CEMENTING OPERATIONS AND TO SELECT CEMENTS FOR FIELD USE

The results of this investigation show that the primary factors affecting the rate of deposition of cement in unfractured perforations are: (1) the composition factor of the cement slurry, (2) the geometry of the perforations, and (3) the filtration time. These three factors are related to each other as shown in Fig. 2.

The value of the composition factor, $\mu/k\omega\triangle P$, for pressure differentials of 800 psi and above depends primarily on the squeeze-cementing temperature. The temperature dependence arises principally as a result of the variation in viscosity of the filtrate, μ, with temperature. If the viscosity of the filtrate is the same as that of water, a temperature correction can be easily made in the manner previously described.

It should be emphasized that the value of the composition factor for a cement slurry is very sensitive to the method of mixing. Therefore, the most accurate composition factor can be obtained from tests on a sample of the field-mixed slurry in a Baroid high-pressure filtration assembly. This test should be made with a minimum pressure differential of 800 psi.

The importance of the geometry of the perforations must be emphasized because of its effect on the rate of node build-up during squeeze-cementing operations. The most important characteristic of the perforation geometry is the combined thickness of the primary cement sheath and the casing wall, H. Although this thickness is never known precisely, it is known within certain limits which are defined by the size of the casing and the size of the borehole. It is rarely, if ever, the same for all perforations because the casing may be off-center and the diameter of the borehole may be irregular. Consequently, the value of H for any perforation can be known only within a certain range. The minimum value for H results when the casing is against the borehole wall, in which case H is equal to the thickness of the casing. On the other side of the borehole, the thickness of the cement sheath and of the casing is the maximum value of H.

From the correlation of the three primary factors as depicted in Fig. 2, the following pertinent information relative to the rate of deposition of cement in unfractured perforations during a squeeze-cementing operation can be calculated: (1) the node build-up under a given set of conditions for a squeeze-cementing operation, (2) the proper filtration time to control the amount of node build-up, and (3) the composition factors needed in cement slurries to restrict the amount of node build-up.

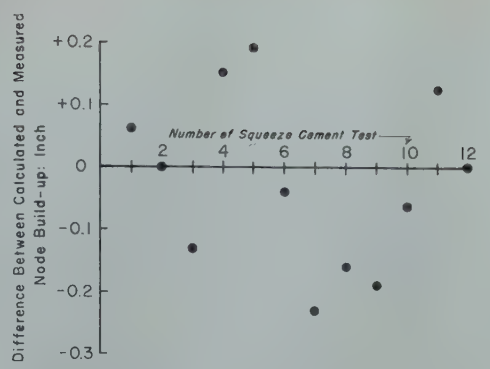

FIG. 7—DIFFERENCE BETWEEN CALCULATED AND MEASURED NODE BUILD-UP IN AND ABOUT PERFORATIONS SQUEEZE CEMENTED WITH MODIFIED CEMENT SLURRIES.

Since modified cements containing either 12 or 25 per cent bentonite are currently used in permanent-type squeeze-cementing operations, these compositions were selected to develop the information presented in Figs. 8 and 9.

Fig. 8 shows the node build-up which is obtained when modified cements containing either 12 or 25 per cent bentonite are used to squeeze-cement 0.5-in. diameter perforations through 5½-in., 17-lb casing in 7⅞-in. hole. For example, when the casing is centered the node build-up after a filtration time of 45 minutes is about 0.3 in. at 120°F and about 0.8 in. at 280°F with modified cement containing 12 per cent bentonite, and no node is developed with modified cement containing 25 per cent bentonite. When the casing is against one side of the hole, the node build-up is about 0.8 in. at 120°F and about 1.25 in. at 280°F with modified cement containing 12 per cent bentonite, and about 0.3 in. at 120°F and 0.6 in. at 280°F with modified cement containing 25 per cent bentonite. These calculations indicate excessive node build-up is to be expected when modified cement containing 12 per cent bentonite is used, and excessive node build-up can be avoided by the use of modified cement containing 25 per cent bentonite. In general, these results are in agreement with field experience.

Fig. 9 shows the deposition properties of cements, as defined by the composition factor, required to restrict the node build-up to what is considered to be a safe limit, 0.25 in., under the following conditions: 0.5-in. diameter perforations through 5½-in., 17-lb casing in 7⅞-in. hole subjected to a filtration time of 45 minutes

TABLE 2—NODE BUILD-UP IN AND ABOUT PERFORATIONS SQUEEZE-CEMENTED WITH MODIFIED NORMAL PORTLAND CEMENT SLURRIES
(Squeeze Pressure: 1,000 lb/in.² and Test Temperature: 78° F)

Test No.	Additives (wt. per cent of Cement)			Geometry of Perforation		Calculated Node Height on Perforation, h_c (in.)	H/a	h_c/a	Composition Factor, $\frac{\mu}{k\omega\triangle P}$	Filtration Time, T (min)	Measured Node on Perforation, h_m (in.)	$h_m - h_c$
	Bentonite	Calcium Lignosulfonate	Water Content Gal. Water per Sack Cement	Casing Wall Thickness + Cement Sheath, H (in.)	Radius of Perforation, a (in.)							
1	12	0.6	10	1.50	0.50	0	3.0	0	56.7	77.8	+ 0.06[1]	+ 0.06
2	12	0.6	10	1.27	0.39	0	3.26	0	16.0	12.2	0	0
3	25	1.2	16	1.69	0.50	0	2.34	0	64.6	25.3	− 0.13	− 0.13
4	25	1.2	16	0.64	0.40	0	1.61	0	80.1	26	+ 0.15	+ 0.15
5	25	1.2	16	0.78	0.38	0	2.04	0	80.1	51.2	+ 0.19	+ 0.19
6	12	0.6	10	0.85	0.36	0.79	2.35	2.19	25.1	75	+ 0.75[1]	− 0.04
7	10	0.3	10	1.87	0.25	0.54	7.50	2.25	6.0	29	+ 0.31[1]	− 0.23
8	10	0.5	10	1.87	0.25	0.54	7.50	2.25	15.7	75.5	+ 0.38[1]	− 0.16
9	8	0.0	10	1.87	0.25	0.57	7.50	2.30	3.0	15	+ 0.38[1]	− 0.19
10	12	0.7	10	0.625	0.25	0.81	2.50	3.28	14	45[2]	0.75	− 0.06
11	12	0.4	10	0.55	0.25	1.13	2.20	4.53	8.5	55	1.25	+ 0.12
12	12	0.4	10	0.55	0.25	1.13	2.20	4.53	8.5	55	1.13	0

[1]These cores had a pipe insert of length H as described in text.
[2]Temperature of squeeze-cement test was 180° F.

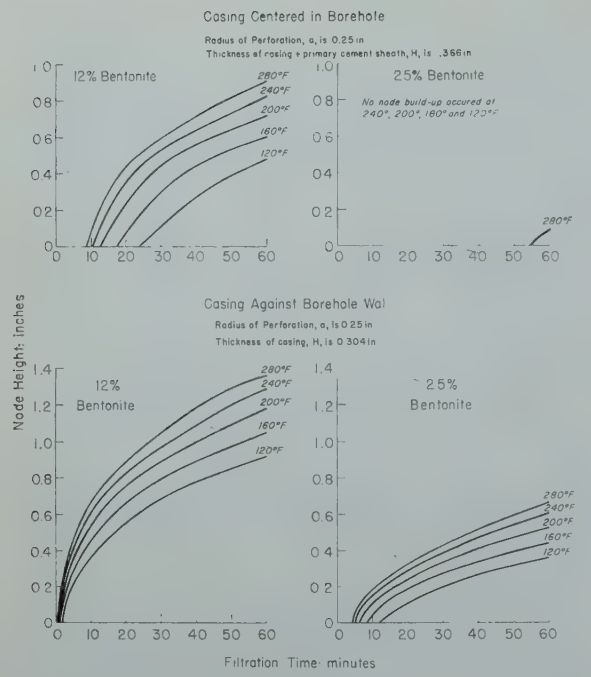

FIG. 8—EFFECT OF FILTRATION TIME AND TEMPERATURE ON HEIGHT OF NODE DEPOSITED INSIDE 5½-IN. CASING CEMENTED IN 7⅝-IN. HOLE DURING SQUEEZE-CEMENTING OPERATIONS WITH MODIFIED CEMENTS.

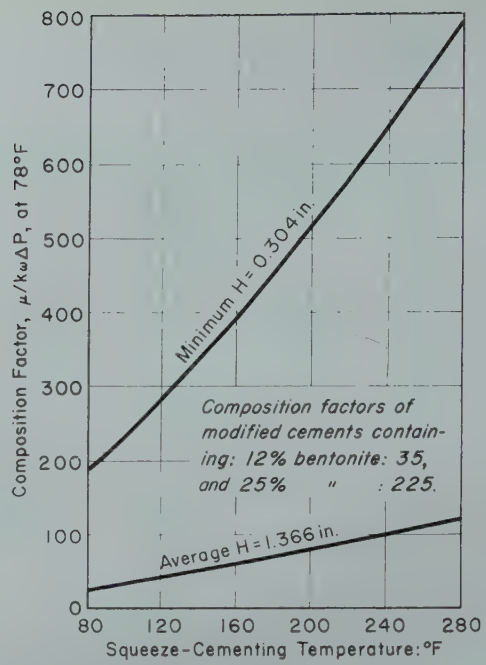
Composition Factor, μ/kωΔP, at 78°F
Minimum H = 0.304 in.
Composition factors of modified cements containing: 12% bentonite: 35, and 25% " : 225.
Average H = 1.366 in.
Squeeze-Cementing Temperature: °F

FIG. 9—COMPOSITION FACTORS REQUIRED TO RESTRICT NODE BUILD-UP TO 0.25 IN. AT VARIOUS SQUEEZE-CEMENTING CONDITIONS.

5½-in. casing cemented in 7⅝-in. hole in which radius of perforation, *a*, is 0.25 in., height of cement node, *h*, is 0.25 in., thickness of casing plus primary cement sheath, *H*, is as shown, and filtration time is 45 minutes.

at different temperatures. Similar calculations can be made for other conditions. This information is useful as a guide in the selection of the range of composition factors needed to perform squeeze-cementing jobs. High values for the composition factors are needed when the filtration time is long, the H is small, and the squeeze temperature is high. Cements having higher composition factors than that obtainable with modified cement containing 25 per cent bentonite are needed to limit node build-up to less than 0.25 in. in wells where the casing is not centered.

CONCLUSIONS

The results of a mathematical analysis of the deposition of solids by filtration in cylindrical, unfractured perforations and of laboratory tests to substantiate the mathematical analysis indicate that the following conclusions are valid in the squeeze-cementing of unfractured perforations in wells.

1. The primary factors affecting the rate of deposition of cement in unfractured perforations are the properties of the cement slurry, the geometry of the perforations, and the filtration time. The relationship of these factors to each other is defined adequately by the correlation presented in Fig. 2.

2. The properties of a cement slurry which influence the deposition of solids by filtration are the permeability of the deposited filter cake, k, the viscosity of the filtrate, μ, and a factor called the deposition constant, ω, which is related to the volume of filter cake deposited by a volume of filtrate. When these properties are grouped with the pressure differential applied to cause filtration, $\triangle P$, the composition factor, $\mu/k\omega\triangle P$, of the slurry is obtained. The value of the composition factor is determined experimentally by measuring the thickness of the filter cake deposited when a cement slurry is filtered through a permeable medium with a pressure differential of at least 800 psi for a known time.

3. The combined thickness of the casing and the impermeable cement sheath surrounding the casing is the most significant geometrical variable of the perforation. Because of the importance of this variable, the centering of the casing during the primary cementing job, the size and shape of the borehole, and the effectiveness of the primary cementing job affect the performance of subsequent squeeze-cementing operations in wells.

4. The information presented can be used to predict the rate of deposition of cement in and about unfractured perforations under given squeeze-cementing conditions, the proper filtration time to control the amount of deposition, and the composition factor needed in cement slurries to restrict node build-up.

ACKNOWLEDGMENT

The authors wish to express their appreciation to B. E. Morgan for his thoughts and guidance during the development of this work, and to the personnel of the Well Completion Group of Humble's Petroleum Engineering Div. for their assistance and close cooperation in this project. Appreciation is also extended to the management of the Humble Oil & Refining Co. for permission to publish this paper.

REFERENCES

1. Howard, George C., and Fast, C. R.: "Squeeze Cementing Operations", *Trans.* AIME (1950) **189,** 53.
2. Huber, T. A., Allen, T. O., and Abendroth, G. F.: "Well Completion Practices", presented at API meeting, Los Angeles, Calif. (Nov. 14, 1950).
3. Huber, T. A., and Tausch, G. H.: "Permanent-Type Well Completion", *Trans.* AIME (1953), **198,** 11.
4. Huber, T. A., Tausch, G. H., and Dublin, J. R., III: "A Simplified Cementing Technique for Recompletion Operations", *Trans.* AIME (1954) **201,** 27.
5. Huber, T. A., and Tausch, G. H.: "Permanent-Type Well Completion Developments", *Drill. and Prod. Prac.,* API (1955) 103.
6. Morgan, B. E., and Dumbauld, G. K.: "Bentonite Cements Proving Successful in Permanent-Type Squeeze Operations", *World Oil* (Nov., 1954) **139,** No. 6, 220. ★★★

A Method for Predicting Pressure Maintenance Performance For Reservoirs Producing Volatile Crude Oil

R. H. JACOBY
MEMBER AIME
V. J. BERRY, JR.
JUNIOR MEMBER AIME

PAN AMERICAN PETROLEUM CORP.
TULSA, OKLA.

ABSTRACT

When dry gas is injected into a reservoir containing a volatile crude oil, a significant amount of the reservoir liquid phase may become vaporized. The resultant rich gas phase, when subsequently produced, contributes to tank oil production. This contribution assumes greater importance, the more volatile the oil involved. Oil recovery may be substantially greater than that predicted by conventional frontal-drive methods, which do not consider the vaporization equilibrium between the reservoir oil phase and the injected gas.

A calculation method has been developed to account for vaporization of the reservoir liquid phase during gas-injection operations, and for the tank oil production which results from this factor. Recovery performance calculations are presented for a reservoir containing a highly volatile oil. Tank oil recovery is calculated to be about twice that predicted by the use of the conventional frontal-drive equations. In contrast to usual pressure maintenance performance results, in which the gas-oil ratio rises at an increasing rate after gas breakthrough, the predicted gas-oil ratio rises rapidly to about 12,000 scf/bbl and then rises much less rapidly. During gas injection, most of the reservoir liquid phase contacted is evaporated by the dry injection gas. The gas-oil ratio during this period is dependent upon reservoir pressure. The higher the operating pressure, the lower the gas-oil ratio. The predicted behavior is in accordance with laboratory PVT tests made to simulate the vaporization behavior. In addition to recovery performance predictions, results of the calculation procedure include complete wellstream composition data of value in the design of gasoline plant facilities often used in connection with gas-injection operations.

Original manuscript received in Society of Petroleum Engineers office on Aug. 30, 1957. Revised manuscript received Feb. 5, 1958. Paper presented at 32nd Annual Fall Meeting of Society of Petroleum Engineers in Dallas, Tex., Oct. 6-9, 1957.

INTRODUCTION

In the cycling of gas-condensate reservoirs, dry gas is injected to maintain reservoir pressure during wet gas production and to thereby eliminate or reduce ultimate loss of liquids due to retrograde condensation within the reservoir. Gas injected into crude oil reservoirs has a dual function. It displaces oil to the producing wells and at the same time serves to partially or fully maintain reservoir pressure. Oil shrinkage which would occur upon pressure reduction is thereby minimized or eliminated. Accepted calculation methods are available[1,2] for predicting recovery performance of either gas-condensate reservoirs or crude oil reservoirs which are being subjected to gas injection. In gas-condensate reservoirs, any retrograde liquid formed does not flow, and it is necessary to account only for the vaporization equilibrium between this liquid and the injected gas. Conversely, in normal crude oil reservoirs, both the oil and gas phases flow, but it has not been considered necessary to account for any vaporization of the reservoir liquid which might occur upon contact with the dry injection gas.

Recently, high shrinkage reservoir fluids known as "volatile oils" have been found in increasing amounts. These oils are characterized by tank oil gravities above 45° API, solution gas-oil ratios above 1,000 scf/bbl, and reservoir volume factors above two. Special techniques have been devised for predicting depletion performance of reservoirs containing such oils.[3,4,5,6] One of the characteristics of reservoirs producing volatile oils is that the reservoir gas phase carries a significant amount of oil which is recoverable as stock-tank liquid. This unusual vaporization behavior implies that an appreciable amount of reservoir liquid would be vaporized upon contact of the oil with dry injection gas. In a gas-injection operation, tank oil recovery would be obtained not only through frontal displacement of the reservoir liquid by the injected gas, but also through production of the rich gas phase. This means that not only are improved methods needed to predict recovery of such oils from reservoirs undergoing gas injection, but it would also be expected that high oil recoveries might be obtained by such operations.

When relatively dry gas is injected into a volatile oil reservoir, phase equilibrium between the injected gas and the reservoir oil will tend to be established. Initially the most volatile components, such as propane, the butanes and the pentanes, will account for most of the material transferred from the oil phase to the gas phase. As the partially stripped oil phase is contacted with additional dry injection gas, the heavier intermediate components, such as the hexanes, the heptanes and the octanes, will gradually transfer to the gas phase in increasing amounts. This is because the supply of lighter components in the oil phase dwindles due to the stripping action of the injected gas. This stripping action will usually continue to be effective down

[1]References given at end of paper.

through the heavier components, such as the decanes, since even they are relatively volatile at the high temperature and pressure conditions commonly encountered in volatile oil reservoirs. The result of the above-described vaporization process is that significant amounts of stock-tank oil components will be transferred to the reservoir gas phase for a long period. This reservoir gas can be produced at the surface, yielding high gravity tank oil at moderately low gas-oil ratios (10,000 to 20,000 scf/bbl).

In order to predict the behavior of such a process, it is necessary to account for the transfer of individual hydrocarbon components from one phase to the other in addition to accounting for the two-phase flow characteristics of the reservoir rock. The use of multicomponent flash calculations together with a material balance and the fractional flow equation offers a means of calculating the performance of such a system.

In formulating such a calculation method to describe the behavior of a petroleum reservoir the following basic assumptions have been made for simplification. These assumptions are usually used in reservoir performance predictions. (1) The reservoir is homogeneous with respect to porosity, permeability, interstitial water content, and oil and gas compositions, (2) relative permeability data measured on small cores in the laboratory describe the basic two-phase flow characteristics of the reservoir, and (3) equilibrium exists between the oil and gas phases.

In the case of primary depletion performance of a volatile oil reservoir, it is adequate to treat the heptanes and heavier fraction (C_{7+}) as a single component having fixed properties at a given pressure. However, in gas-injection operations this fraction will change appreciably in composition and properties at constant pressure due to the stripping action of the dry gas. It is therefore desirable to account for the vaporization of individual components of as high a molecular weight as undecane (C_{11}). It will be shown later that this upper limit is satisfactory for a typical volatile oil, since the still heavier components do not vaporize appreciably at reservoir conditions. These heavier components may be considered without much error to act as a single component since they are not significantly involved in the stripping action.

The purposes of this paper are: (1) to show that multi-component flash calculations using available *K*-values (equilibrium vaporization ratios) adequately predict the vaporization behavior of a volatile oil which is repeatedly contacted with dry gas, (2) to present a stepwise calculation scheme believed suitable for predicting the gas-injection performance of reservoirs producing volatile crude oil, and (3) to present an example performance prediction calculation, demonstrating the unusual recovery performance of such reservoirs under gas injection and the inadequacy of conventional methods of prediction.

PROCEDURE

Experimental Vaporization Test

To test the reliability of multicomponent flash calculations for describing the stripping action of dry gas on a volatile oil, a laboratory experiment was made to simulate a gas-injection operation. The original reservoir fluid composite (to be used later in example recovery calculations) was made by recombining separator oil and gas samples in a high pressure windowed cell. A fractional analysis of the reservoir composite is given in Table 1. The composite was then brought to a pressure of 4,500 psia and a temperature of 250° F. The amounts of the oil and gas phases were adjusted (by removal of some of the oil) so that the relative proportions of the two phases were approximately the same as would be encountered in the reservoir after primary depletion to that pressure. The following stepwise procedure was then repeated 17 times. A small measured amount of the gas phase was withdrawn and an appropriate amount of dry natural gas (96 per cent methane) was injected. Rather than withdraw both oil and gas (both would flow out from the reservoir in a gas-injection operation) only gas phase was removed from the cell. The total cell volume was then increased a suitable amount to reduce the volume per cent liquid phase remaining. This was done to simulate the reduction in oil volume which would be caused by frontal displacement of liquid by injected gas in the reservoir. Frontal displacement calculations were made to determine the amount of liquid which would be expected to be displaced at each step. In this way, this experiment was expected to give data on the relative amounts of reservoir oil and gas remaining at each stage of a typical gas-injection operation. The gas and oil volumes in the cell were observed after each cycle of removing and injecting gas. These data were converted to gas saturations in percentage of total hydrocarbon pore volume.

The laboratory experiment was next simulated by a series of multicomponent flash calculations. The experimental volumes of gas removed were used in these calculations. The required injected gas volumes were calculated by trial to match the experimentally observed total mixture volumes.

The calculations to simulate the laboratory experiment were made in two different ways. In the first calculation, all hydrocarbons above hexane were considered as a single "grouped" C_{7+} component having the appropriate average, but fixed, properties. In the second calculation the C_{6+} fraction was fractionated into individual cuts corresponding approximately to the normal hydrocarbons up through undecane. Each cut had a boiling range of 50°F and is listed in Table 1 according to its mid-boiling point. The residue was considered to be a single, grouped C_{12+} component with fixed properties.

Example Reservoir Performance Calculation

To show the unusual producing characteristics of a volatile oil reservoir under a gas-injection operation, the reservoir performance calcula-

TABLE 1—FLUID COMPOSITIONS

	Molecular Weight	Density at 60°F, gm/cc	Original Reservoir Fluid Composition	Reservoir Composite At Start of Gas Drive	Residue (Injection) Gas Composition
Nitrogen			.0167	.0168	.0272
Methane			.6051	.6062	.8595
Carbon Dioxide			.0218	.0218	.0278
Ethane			.0752	.0752	.0717
Propane			.0474	.0474	.0135
iso-Butane			.0138	.0138	.0003
n-Butane			.0274	.0273	
iso-Pentane			.0046	.0046	
n-Pentane			.0251	.0250	
150° F *n*-BP cut	90	.6684	.0199	.0198	
200° F *n*-BP cut	103	.7075	.0245	.0245	
250° F *n*-BP cut	115	.7423	.0241	.0240	
300° F *n*-BP cut	134	.7703	.0169	.0168	
350° F *n*-BP cut	146	.7771	.0142	.0141	
400° F *n*-BP cut	193	.7957	.0102	.0101	
425° F plus cut	302	.8346	.0531	.0526	

tion method to be described in this section has been applied to an actual reservoir. The example reservoir is the same reservoir for which the primary depletion performance was predicted in a previous paper.[3] This reservoir occurs in the Smackover limestone in North-central Louisiana at a depth of about 10,000 ft. Reservoir temperature is 246° F. The original reservoir pressure was 5,070 psia and a bottom-hole sample of oil, which was believed to be representative of original reservoir fluid, had a bubble-point pressure of 4,836 psia.

It was anticipated that maximum benefit from gas injection would be obtained at the highest practical operating pressure, therefore, 4,500 psia was chosen as the pressure to be maintained for the performance calculations. Since it was considered likely that a natural gasoline plant would be used in such a project and that some make-up dry gas would be required to maintain pressure, a dry residue-type gas of constant composition was used for injection gas in the calculations. The residue (injection) gas composition is given in Table 1.

The correlation of Hinshaw[7] was used as the basic source of K-values. With these data it was possible to obtain a good fit to the experimental, equilibrium flash vaporization data for the original bottom-hole sample[3] by interpolating between convergence pressures and by a slight adjustment of the methane K-value near the bubble-point pressure. The K-value for a 500° F mid-boiling point fraction was used for the 425° F-plus (C_{12+}) residue in the calculations. Published correlations[8,9,10] were used to calculate gas viscosities and oil- and gas-phase densities. A small correction was applied to all calculated oil densities to make them consistent with the few available experimentally measured densities. A simple correlative device was used to obtain oil viscosity. It has been noted that for a series of related oil phases, viscosity correlates well with density regardless of pressure, temperature, or composition. This observation is consistent with the published crude oil viscosity correlation of Beal.[11] The oil-phase viscosity data from the primary depletion performance were plotted vs density and this plot was used to obtain oil viscosities from calculated oil densities in the gas-injection calculation.

The remaining data required for the gas-injection performance calculation were gas-oil relative permeabilities and interstitial water content (30 per cent pore volume). The data used were the same as used for the depletion performance study.[3] The primary surface separator conditions chosen were 500 psia and 65° F. Stock-tank conditions of 14.7 psia and 70° F were assumed. It was not considered necessary to fit K-values for these conditions to experimental data on the actual fluids. These latter K-values were selected on the basis of convergence pressure calculated using Hadden's[12] method.

The fractional analysis and relative proportions of the reservoir oil and gas phases at 4,500 psia were obtained by recalculating the primary depletion performance[3] in three steps from the bubble-point pressure of 4,836 to 4,500 psia. The calculated gas saturation at 4,500 psia was sufficiently high so that the calculated gas-drive performance did not include the formation of an oil bank.

The reservoir recovery performance was calculated on the basis of 1 bbl of hydrocarbon pore space as follows (the scheme is illustrated in Fig. 1). An increment of the existing reservoir fluid was removed, the volumetric proportions of gas and oil in the increment being dictated by the two-phase flow relationship for the reservoir rock. An increment of injection gas was then added to the remaining reservoir mixture and a multi-component flash calculation was made with the new composite at reservoir conditions. The increments of fluid removed and injected were chosen by trial and error to meet the following restrictions.

1. The volumetric proportions in which oil and gas were removed corresponded to the average of the bottom-hole gas-oil ratios at the start and finish of a step. These ratios were determined by the gas and oil relative permeabilities corresponding to the wellbore gas saturations at the start and finish of the particular calculation step. This oil and gas mixture constituted the wellstream composite produced for the step.

2. The calculated volume of the reservoir composite at reservoir conditions was equal to the unit hydrocarbon pore volume at the end of each step.

3. The average reservoir gas saturation at the end of each step was related to the wellbore (outlet) gas saturation according to the saturation gradient predicted from the frontal-drive equations.[2]

Flash calculations were made for each increment of wellstream composite to determine the amount and composition of tank oil and primary separator overhead gas produced in each step. Producing gas-oil ratio data were computed from these results.

To illustrate the importance of performing all reservoir flash calculations with a detailed breakdown of the heavy fraction of the oil, example performance calculations were made in two ways. In the first calculation, all components heavier than hexane were considered as one component (C_{7+}) with fixed properties. In the second calculation, a more detailed fractional analysis of the C_{6+} fraction was used. The C_{12+} fraction was considered to have fixed properties and to behave as a single component. An additional reservoir performance calculation was also made using conventional methods[2] to illustrate the inadequacy of conventional gas-drive performance prediction methods. In this case the reservoir oil data used were conventional differential vaporization data[3] and no account was taken of the interaction between the dry injection gas and the rich reservoir liquid phase.

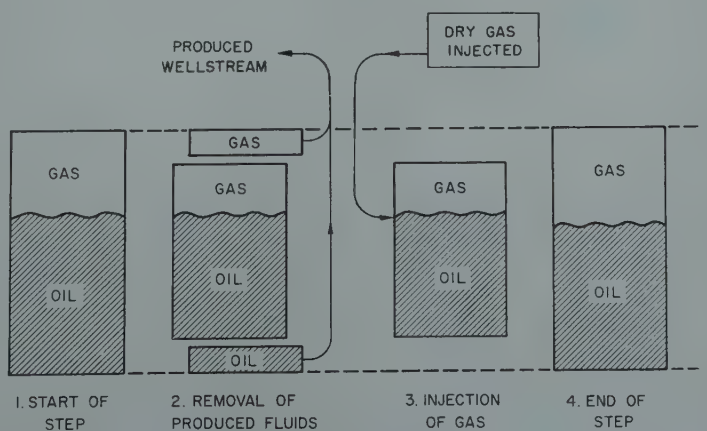

FIG. 1—MATERIAL BALANCE SCHEME USED FOR RESERVOIR PERFORMANCE PREDICTIONS.

TABLE 2—COMPOSITION OF RESERVOIR OIL AND GAS
(Mol Fractions)

Component	Start of Gas Drive at 4,500 psia	Cumulative Standard Cubic Feet of Injection Gas Per Barrel of Hydrocarbon Pore Space: 253	286	359	458	588	753	955	1136	1344	1585	2257
Reservoir Gas Phase												
Nitrogen	.0252	.0246	.0246	.0245	.0245	.0245	.0245	.0246	.0248	.0249	.0255
Methane	.7389	.7522	.7538	.7574	.7616	.7670	.7741	.7818	.7884	.7956	.8027	.8213
Carbon Dioxide	.0230	.0239	.0240	.0242	.0244	.0248	.0251	.0255	.0258	.0261	.0264	.0270
Ethane	.0752	.0745	.0744	.0742	.0740	.0738	.0735	.0732	.0730	.0728	.0726	.0721
Propane	.0417	.0369	.0364	.0353	.0338	.0320	.0299	.0276	.0258	.0239	.0221	.0179
iso-Butane	.0112	.0095	.0093	.0088	.0083	.0076	.0067	.0058	.0051	.0043	.0036	.0019
n-Butane	.0210	.0180	.0177	.0169	.0159	.0147	.0132	.0116	.0102	.0088	.0074	.0041
iso-Pentane	.0032	.0028	.0027	.0026	.0025	.0023	.0021	.0019	.0017	.0015	.0012	.0007
n-Pentane	.0162	.0144	.0142	.0137	.0131	.0123	.0112	.0100	.0090	.0079	.0067	.0038
150°F *n*-BP cut	.0111	.0102	.0101	.0098	.0094	.0089	.0083	.0075	.0069	.0061	.0054	.0033
200°F *n*-BP cut	.0119	.0112	.0111	.0109	.0106	.0102	.0096	.0089	.0082	.0074	.0066	.0043
250°F *n*-BP cut	.0093	.0091	.0090	.0089	.0088	.0086	.0083	.0079	.0075	.0069	.0064	.0045
300°F *n*-BP cut	.0051	.0051	.0051	.0051	.0051	.0051	.0050	.0049	.0047	.0045	.0042	.0033
350°F *n*-BP cut	.0029	.0031	.0031	.0031	.0032	.0032	.0032	.0033	.0032	.0032	.0032	.0028
400°F *n*-BP cut	.0014	.0015	.0015	.0015	.0016	.0016	.0017	.0017	.0018	.0018	.0018	.0018
425° plus cut	.0027	.0030	.0030	.0031	.0032	.0034	.0036	.0039	.0041	.0044	.0048	.0057
Reservoir Oil Phase												
Nitrogen	.0116	.0113	.0113	.0113	.0112	.0112	.0112	.0113	.0113	.0114	.0114	.0117
Methane	.5239	.5334	.5346	.5370	.5402	.5440	.5489	.5546	.5591	.5640	.5692	.5825
Carbon Dioxide	.0211	.0219	.0220	.0222	.0224	.0227	.0230	.0234	.0237	.0239	.0242	.0248
Ethane	.0752	.0745	.0744	.0742	.0740	.0738	.0735	.0732	.0730	.0728	.0726	.0721
Propane	.0509	.0450	.0443	.0430	.0412	.0390	.0365	.0336	.0314	.0292	.0270	.0219
iso-Butane	.0154	.0130	.0127	.0121	.0113	.0104	.0092	.0080	.0070	.0060	.0050	.0025
n-Butane	.0313	.0269	.0264	.0252	.0238	.0219	.0197	.0173	.0153	.0132	.0111	.0061
iso-Pentane	.0055	.0048	.0047	.0045	.0043	.0040	.0037	.0032	.0029	.0025	.0021	.0012
n-Pentane	.0305	.0272	.0268	.0259	.0247	.0231	.0212	.0188	.0169	.0148	.0127	.0072
150°F *n*-BP cut	.0252	.0231	.0229	.0223	.0214	.0203	.0189	.0171	.0156	.0139	.0122	.0074
200°F *n*-BP cut	.0322	.0304	.0301	.0295	.0287	.0275	.0259	.0240	.0222	.0201	.0179	.0115
250°F *n*-BP cut	.0331	.0324	.0322	.0319	.0314	.0307	.0296	.0281	.0266	.0248	.0227	.0161
300°F *n*-BP cut	.0241	.0244	.0244	.0244	.0243	.0241	.0237	.0231	.0224	.0215	.0202	.0158
350°F *n*-BP cut	.0210	.0220	.0221	.0223	.0226	.0229	.0231	.0232	.0232	.0230	.0225	.0200
400°F *n*-BP cut	.0155	.0167	.0168	.0171	.0175	.0181	.0187	.0193	.0198	.0202	.0205	.0205
425°F plus cut	.0835	.0930	.0943	.0971	.1010	.1063	.1132	.1218	.1926	.1387	.1487	.1787
Bottom-hole gas-oil ratio, (vol./vol.)	0.92	1.13	1.86	3.26	5.89	10.29	19.1	35.7	56.5	87.8	140	389
Reservoir gas saturation (per cent)	23.5	34.3	35.6	37.7	40.0	42.5	45.0	47.6	49.5	51.4	53.3	57.5

Effect of Reservoir Operating Pressure

It is known qualitatively that the oil content of reservoir gas varies markedly with pressure above 3,000 psia. Therefore, it was deemed important to show some measure of this effect without having to make the full performance calculations for a series of pressures. This was done by taking the reservoir gas compositions (at various pressures) from the previously reported primary depletion study[3] and flashing them at surface separator conditions. The calculated separator gas-oil ratios directly reflect the relative richness of the reservoir gas phase at the various pressures, and, therefore, will indicate how the efficiency of oil recovery by vaporization into the injected gas varies with operating pressure.

RESULTS AND DISCUSSION

Experimental Vaporization Test

The results of the laboratory vaporization test are presented in Fig. 2. This figure shows the vaporization behavior during a gas-injection operation in a PVT cell, in terms of gas saturation (in per cent hydrocarbon pore volume) after the injection of various amounts of dry gas. The two calculated vaporization histories are also shown. In the first, the heavy hydrocarbons (C_{7+}) were grouped together and handled as one component. In the second case all the heavy hydrocarbons lighter than C_{12} were treated individually. The results of the second calculation fit the experimental data well. Conversely, the first calculation predicts *complete vaporization* of the liquid phase, which is not consistent with the experimental data. From these results it is concluded that the vaporization of a volatile oil which is repeatedly contacted with dry gas can be adequately predicted with multi-component flash calculations which consider the individual vaporization behavior of the normal hydrocarbons up to undecane (C_{11}). This result also adds confidence to the use of multi-component flash calculations in the reservoir performance calculation method described earlier.

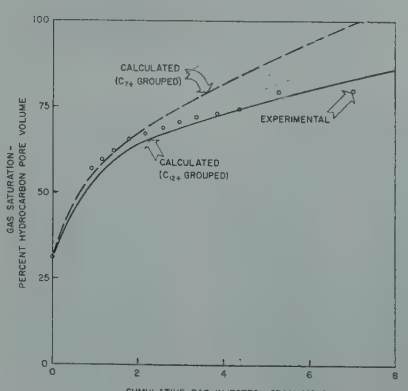

Fig. 2—Comparison of Calculated and Experimental Oil Vaporization.

Example Reservoir Performance Calculation

The results of the example reservoir gas injection performance calculations are shown in Figs. 3, 4, and 5. These figures show the cumulative tank oil production, separator gas-oil ratio, and cumulative separator gas production, respectively, as functions of cumulative dry gas injection volume. Results are presented for the calculations based both on treatment of the C_{7+} hydrocarbon fraction as a single component and on treatment of the C_{12+} hydrocarbons as a single component. Conventional frontal-drive performance predictions are also shown for comparison.

Predicted tank oil recoveries (Fig. 3) at a cumulative gas injection equivalent to one hydrocarbon pore volume are 0.155, 0.120, and 0.088 bbl/bbl of hydrocarbon pore space for the three calculations, respectively. In view of the previous discussion, the predicted recovery of 0.120 bbl/bbl of hydrocarbon pore space is believed reliable. The calculation based upon a grouped C_{7+} fraction is believed to over-estimate recovery, since it predicts that continued dry gas injection will result in *complete evaporation* of the reservoir liquid phase. The above-described compari-

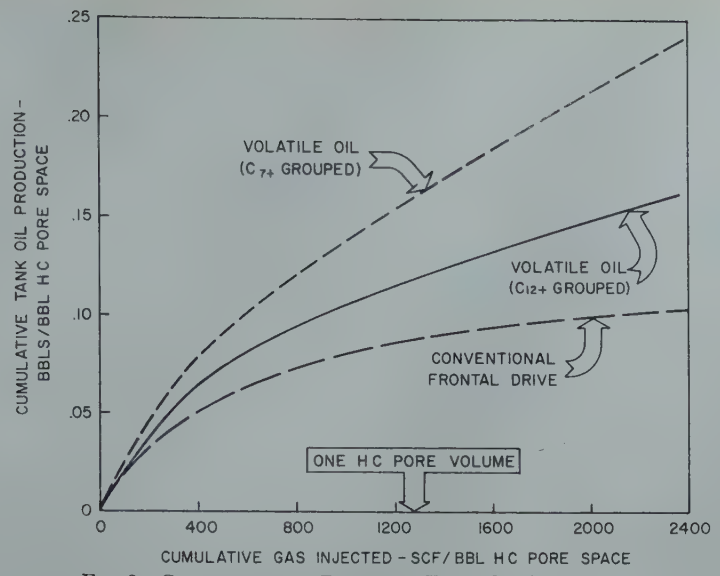

FIG. 3—COMPARISON OF PREDICTED TANK OIL PRODUCTION (EXAMPLE RESERVOIR).

son with laboratory data shows that this predicted complete vaporization is not realistic. Conversely, since the conventional frontal-drive prediction methods do not account for that portion of the oil recovered by vaporization into the dry injection gas, the results of such calculations will underestimate recovery. The error involved will depend largely upon the volatility of the reservoir fluid and upon the amount of dry gas which contacts oil at the specific reservoir conditions.

Results given in Fig. 4 show even more strikingly the differences in predicted performance for the three calculation methods compared. Calculations based on a grouping of the C_{7+} fraction show an initial rapid rise in gas-oil ratio following gas breakthrough, which occurs at a cumulative gas injection of about 350 scf/bbl of hydrocarbon pore space. Gas breakthrough is followed by a period of substantial oil production at a constant producing gas-oil ratio of about 12,000 scf/bbl. This result is not believed to be realistic. An examination of the details of the calculation shows that this constant gas-oil ratio is a result of considering that the C_{7+} fraction of the reservoir oil behaves as a single component.

The gas-oil ratio performance calculated by the method based upon an individual treatment of the heavy components through undecane (C_{11}) is believed realistic, in view of the success in duplicating laboratory vaporization performance. The gas-oil ratio computed by this latter method shows a rapid rise immediately after gas breakthrough. This rise is followed by a period of oil production at more slowly rising gas-oil ratios. This means that a normally attractive yield of liquid products from the reservoir may continue for some time beyond gas breakthrough. The oil recovery realized by the time the producing gas-oil ratio reaches 20,000 scf/bbl* is predicted to be 0.145 bbl/bbl of hydrocarbon pore space. This is more than twice the recovery of 0.068 bbl predicted by the conventional frontal-drive methods. These two recovery figures are chosen at the same producing gas-oil ratios, and are, therefore, believed to reflect more realistically than those figures quoted earlier, the degree to which conventional prediction methods will underestimate recovery from volatile oil reservoirs. This higher predicted recovery is solely a result of accounting for vaporization of the reservoir liquid phase. In the conventional frontal-drive calculation, the predicted rapid rise in producing gas-oil ratio after gas breakthrough results from failure to account for the vaporization of hydrocarbons into the injected gas.

Fig. 5 shows the predicted cumulative separator gas production volumes vs cumulative injection gas volume, and, therefore, includes information from which the amount of make-up gas required to maintain reservoir pressure can be determined. Both the calculations accounting for the detailed phase behavior give nearly identical results. The results indicate approximately 20 per cent less gas produced than is predicted by the conventional frontal-drive method, when compared at the same cumulative gas-injection volume.

To summarize the results of the performance predictions, Table 3 shows cumulative oil recovery, injected gas volume, produced gas volume, and the ratio of cumulative injected gas to produced oil for each of the calculations. The comparison is made for a producing gas-oil ratio of 20,000 scf/bbl. This tabulation shows that although the cumulative oil recoveries predicted by the three methods of calculation differ by as much as a factor of four, the cumulative ratios of injected gas to produced oil differ by only about 30 per cent. It is speculated that the three methods would predict ratios

*A gas-oil ratio of 20,000 scf/bbl was chosen arbitrarily as a basis for comparison of the calculation methods. At a lower comparison gas-oil ratio, the calculated recoveries differ less, whereas, at a higher comparison gas-oil ratio they differ more.

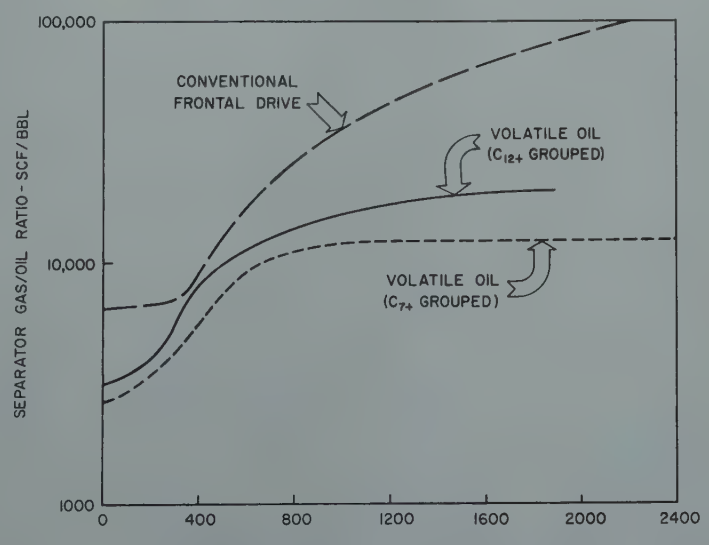

FIG. 4—COMPARISON OF PREDICTED SEPARATOR GAS-OIL RATIO (EXAMPLE RESERVOIR).

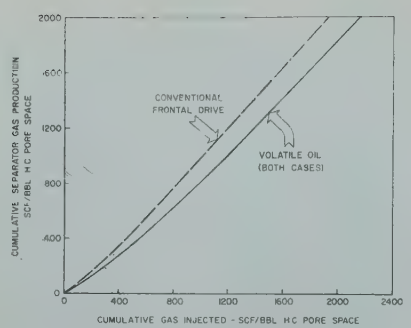

FIG. 5—COMPARISON OF PREDICTED SEPARATOR GAS PRODUCTION (EXAMPLE RESERVOIR).

differing by no more than this amount if a similar comparison were made for any other reservoir, whether it contained a volatile oil or not. On the basis of the comparison shown in Table 3, the expected net cost of gas handling per barrel of oil recovered for a particular project might be nearly the same regardless of the method of performance calculation employed. However, the total oil recovery which could be credited against plant investment will be underestimated by conventional performance calculations.

The method proposed in this paper yields information regarding compositions of the wellstream and of the produced oil and gas. This information, which is not available in advance of production when the conventional frontal-drive methods are used, is of particular value in the design of plant facilities normally used in connection with gas-injection operations. Where composition data are needed for the same purpose for reservoirs not containing volatile oils, the method described here can also be used to advantage. The method may also be applied to the prediction of recovery from a reservoir undergoing limited gas injection such that reservoir pressure is allowed to decline.

From the above results and discussion it is concluded that conventional frontal-drive methods are inadequate to predict the oil recovery performance of volatile oil reservoirs being subjected to gas injection. Furthermore, it is also concluded that conventional frontal-drive methods will underestimate the total oil which can be recovered from such reservoirs by gas injection.

EFFECT OF RESERVOIR OPERATING PRESSURE

The results of the separator calculations using reservoir gas for several different operating pressures appear in Fig. 6. These data are the initial gas-oil ratios which would be observed for different reservoir operating pressures, and, therefore, reflect the relative level of producing gas-oil ratios throughout the entire operation. They indicate that producing gas-oil ratios increase sharply as operating pressure is decreased. As the gas-oil ratio increases, the amount of gas which must be handled to produce a barrel of oil increases. Therefore, it can be concluded that the efficiency of oil recovery by gas injection into volatile oil reservoirs falls off with increasing rapidity as operating pressure is lowered.

CONCLUSIONS

On the basis of the information presented in this paper, the following conclusions are believed justified.

1. The vaporization of a volatile oil which is repeatedly contacted with dry gas can be adequately predicted with multi-component flash calculations which consider the individual vaporization behavior of the normal hydrocarbons up to undecane (C_{11}).

2. Conventional frontal-drive methods are inadequate to predict the oil recovery performance of volatile oil reservoirs being subjected to gas injection.

3. Conventional frontal-drive methods will underestimate the total oil which can be recovered from such reservoirs by gas injection.

4. The efficiency of oil recovery by gas injection into volatile oil reservoirs falls off with increasing rapidity with a decrease in operating pressure.

TABLE 3—COMPARISON OF RESULTS OF EXAMPLE RESERVOIR PERFORMANCE PREDICTIONS
(Basis of Comparison: Producing gas-oil ratio of 20,000 scf/bbl)

Calculation Method	Cumulative Oil Recovery* (bbl)	Cumulative Separator Gas Production* (scf)	Cumulative Gas Injected* (scf)	Cumulative Injection Gas-Oil Ratio** (scf/bbl)
Volatile Oil (C_{7+} Grouped)***	0.247	2,157	2,475	10,020
Volatile Oil (C_{12+} Grouped)	0.145	1,535	1,790	12,360
Conventional Frontal Drive	0.068	600	630	9,250

*Per barrel of hydrocarbon pore space.
**Cumulative volume of injection gas per barrel of oil recovered.
***Producing gas-oil ratio reaches 20,000 scf/bbl only after complete vaporization of reservoir liquid phase

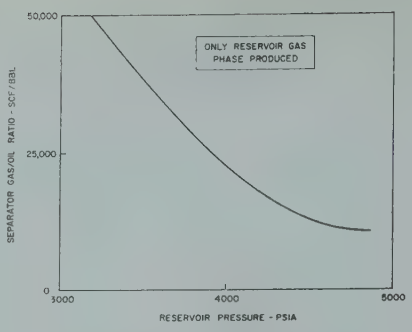

FIG. 6—EFFECT OF RESERVOIR PRESSURE ON SEPARATOR GAS-OIL RATIO (EXAMPLE RESERVOIR).

REFERENCES

1. Standing, M. B., Lindblad, E. N., and Parsons, R. L.: "Calculated Recoveries by Cycling from a Retrograde Reservoir of Variable Permeability," *Trans.* AIME (1948) **174,** 165.
2. Craig, F. F., Jr., and Geffen, T. M.: "The Determination of Partial Pressure Maintenance Performance by Laboratory Flow Tests," *Trans.* AIME (1956) **207,** 42.
3. Jacoby, R. H., and Berry, V. J., Jr.: "A Method for Predicting Depletion Performance of a Reservoir Producing Volatile Crude Oil," *Trans.* AIME (1957), **210,** 27.
4. Cook, A. B., Spencer, G. B., and Bobrowski, F. P.: "Special Considerations in Predicting Reservoir Performance of Highly Volatile Type Oil Reservoirs," *Trans.* AIME (1951) **192,** 37.
5. Reudelhuber, F. O., and Hinds, R. F.: "A Compositional Material Balance Method for Prediction of Recovery from Volatile Oil Depletion Drive Reservoirs," *Trans.* AIME (1957) **210,** 19.
6. Brinkman, F. H., and Weinaug, C. F.: "Calculated Performance of a Dissolved Gas Drive Reservoir by a Phase Behavior Method," *AIChE Jour.* (1957) **3,** 29.
7. Hinshaw, D. F.: "Correlation of the Vapor Liquid Equilibrium Constants of Hydrocarbons," PhD Thesis, University of Michigan, 1955.
8. Carr, N. L., Kobayashi, Riki, and Burrows, D. B.: "Viscosity of Hydrocarbon Gases Under Pressure," *Trans.* AIME (1954) **201,** 264.
9. Standing, M. B.: *Volumetric and Phase Behavior of Oil Field Hydrocarbon Systems,* Reinhold Pub. Co., N. Y. (1952) 35.
10. Brown, G. G., Katz, D. L., Oberfell, G. G., and Alden, R. C.: "Natural Gasoline and the Volatile Hydrocarbons," Natural Gasoline Association of America, Tulsa, Okla. (1948), 38.
11. Beal, C.: "The Viscosity of Air, Water, Natural Gas, Crude Oil and Its Associated Gases at Oilfield Temperatures and Pressures," *Trans.* AIME (1946) **165,** 94.
12. Hadden, S. T.: "Convergence Pressure in Hydrocarbon Vapor-Liquid Equilibrium," Chem. Engr. Prog. Sym. No. 7, Applied Thermodynamics (1953) 53.

★★★

Pressure Measurements During Formation Fracturing Operations

J. K. GODBEY
H. D. HODGES

MAGNOLIA PETROLEUM CO.
DALLAS, TEX.

ABSTRACT

In order to better understand the fracturing process, bottom-hole pressures were measured during a number of typical fracturing operations. A recently developed system was used that allows simultaneous surface recording of both the bottom-hole and wellhead pressures on the same chart.

The results from six fracturing treatments are summarized on the basis of the pressure data obtained. Although no complete analysis is attempted, the value of accurate pressure measurements is emphasized. Important characteristics of the bottom-hole pressure record do not appear at the wellhead because of the damping effect of the fluid-filled column. In four of the six treatments described, the formations apparently fractured during the initial surge of pressure with only crude oil in the well. The properties of the fluids used during the treatments are given and the fluid friction losses are obtained directly from the pressure records. This technique is also shown to be adequate for determining when various fluids, used during the process, enter the formation.

INTRODUCTION

Hydraulic fracturing for the purpose of increasing well productivity is now accepted in many areas as a regular completion and workover practice. Numerous articles have appeared in the literature discussing the various techniques and theories of hydraulic fracturing[1]. In general, three basic types of formation fractures are recognized today. These are the horizontal fracture, the vertical fracture, and fractures along natural planes of weakness in the formation[2]. Any one or all three of these fracture types may be present in a fracturing operation. However, with only the wellhead pressure record as a guide, it is difficult at best to determine if the formation actually fractured, and is almost impossible to determine the type of fracture induced. These difficulties arise in part because the wellhead pressure record, especially when fracturing through tubing, does not accurately reflect the pressure variations occurring at the formation. Several factors contribute to this effect and preclude the possibility of using the wellhead pressure as a basis for accurately calculating the bottom-hole pressure. These factors are:

1. The compressibilities of the fluids which damp the pressure variations.
2. The changes in the densities of the fluids or apparent densities of the sand-laden fluids.
3. The flowing friction of the various fluids and mixtures, which is dependent on the flow rates and the condition of the tubing, casing, or wellbore.
4. The non-Newtonian characteristics of a sand-oil mixture and its dependence upon the fluid properties, the concentration of sand, and the mesh size used.
5. The unknown and variable temperatures throughout the fluid column.

Because of these reasons it was determined that in order to obtain a more accurate knowledge of the nature of fracturing, the bottom-hole pressure must be measured along with the pressure at the surface during a fracturing treatment. Even with accurate pressure data, a reliable estimate of the nature of fracturing is still dependent upon knowledge of the tectonic conditions. However, the hydraulic pressure on the formation is basic to any approach to a complete analysis.

In order to accomplish this objective a system was developed to record the wellhead and bottom-hole pressures simultaneously at the surface. By recording both pressures on a dual pen strip-chart recorder, it was possible to greatly expand the time scale so that rapid pressure variations would be faithfully recorded. By such simultaneous recording, time discrepancies inherent in separate records are eliminated, thus overcoming one of the most difficult problems associated with bottom-hole recording systems.

This paper illustrates the results obtained by using this system during six typical fracturing operations. All of these tests were taken in wells that were treated through tubing. By a direct comparison of the wellhead and bottom-hole pressures, the importance of obtaining complete pressure information during a fracturing treatment is emphasized.

THE INSTRUMENTATION AND PROCEDURES

The bottom-hole pressure measuring instrument consisted of a pressure-sensing element, a telemetering section, and a lead-filled weight or sinker bar. The pressure-sensing element used was an isoelastic Amerada pressure-gauge element. By using an isoelastic element, no temperature compensation was necessary in the tests described, since the temperature was believed to be well below the maximum temperature limit of 270°F. The rotary output shaft of this helical Bourdon tube element was coupled to a precision miniature potentiometer. The rotation of the pressure-gauge shaft thus changed the resistance presented by the potentiometer

Manuscript received in Society of Petroleum Engineers office on July 31, 1957. Paper presented at 32nd Annual Fall Meeting of Society of Petroleum Engineers in Dallas, Tex., Oct. 6-9, 1957.
[1]References given at end of paper.

to a telemetering oscillator. This special electronic oscillator received its power from the surface through the single conductor logging cable, and in turn transmitted a signal over the same conductor to the surface. The frequency of the oscillator signal was proportional to the bottom-hole pressure and was converted at the surface into a voltage suitable for recording. The entire bottom-hole pressure measuring instrument was 1½ in. in diameter and approximately 10 ft long. The instrument was supported in the well by a 3/16-in., single conductor, armored cable.

A special perforated sub with a stop-bar was attached to the lower end of the tubing before it was lowered into a well. After the tubing was set in the casing, the pressure gauge was lowered by means of the cable to the zone to be fractured, and was allowed to rest on the stop-bar in the sub. In some cases a single packer was used between the tubing and casing, in which case the special sub was placed below the packer. When straddle packers were used, the special sub was placed just above the lower packer.

After the instrument was lowered to the zone, the supporting cable was sealed at the wellhead with a modified two-stage Bowen packer. After the fracturing treatment, the instrument was retrieved during the idle period of the treatment operation. By using this procedure, no lubricator was necessary for injecting or retrieving the instrument.

A circular chart pressure recorder was used to measure the wellhead pressure. This recorder was modified by the addition of a precision potentiometer on the pen shaft, so that the wellhead pressure might also be recorded on the dual pen strip-chart recorder. This system allowed the pressure variations to be observed at the wellhead as well as in the instrument truck.

The two pressure signals were used to drive the two pens on the single recorder independently. The recorder chart was driven by a synchronous motor through a gear changing mechanism which permitted several accurately controlled speeds to be selected. In most cases, a chart speed of 1 in./min was found to be fast enough to record the pressure variations encountered.

The pressure scales on the recorder could be adjusted independently for both the wellhead and bottom-hole pressures by separate electrical control circuits. However, in all cases the ranges were made equal for both pressure measurements. In this way, the variations in static head, friction losses, and other pressure variations could be compared directly on the final record. A useable chart width of 10 in. allowed pressure readings to be taken directly from the chart with an accuracy of better than 1 per cent of full-scale reading.

The actual fracturing treatments described in this paper are similar in most respects. In each case, the wells were over-flushed with two tubing volumes of lease crude oil, both before and after the sand laden fracturing fluid was introduced. The variations in procedure involved only the nature and volume of the fracturing fluids used and the amount of sand they carried. In each case a 20 to 40 mesh Ottawa sand was used.

DATA

Simultaneous bottom-hole and surface pressure records were made during six attempted fracturing operations. Data from these operations are contained in Figs. 1 and 2. Each of these operations is described separately as follows.

From the bottom-hole pressure record of Well A, Fig. 1, it is evident that the formation apparently fractured under the initial pressure surge. This is indicated by the sharp decline in pressure at three minutes on the time axis. This decline is undoubtedly caused by the sudden movement of liquid and the increase in pressure drop from friction losses. It will be noted that no indication of this fracture is shown on the surface pressure record. Apparently, the fracture remained open during the remainder of the record, since the bottom-hole pressure remained less than the initial peak. This apparent fracture occurred with only the lease crude breakdown oil in the well. The maximum bottom-hole pressure of 3,830 psig checks closely with the overburden pressure based upon an assumed value of 1 psi/ft of depth since the perforations were between 3,539 and 3,566 ft. The static head is equal to the difference between the two measured pressures during shut-down periods. In this case, taking a minimum at 23.3 minutes, the static head is approximately 1,300 psi. The difference between the bottom-hole and surface pressures in the interval immediately following the apparent fracture averages about 400 psi. By taking the sum of the static head and the pressure difference during the injection of the breakdown oil, a friction loss on the order of 1,700 psi is determined. Similar calculations can be made to determine the loss of pressure due to flowing friction at any other time on the record. From this example the great effect of friction on the resultant pressure on the formation can be clearly seen, and is even more pronounced when the injected fluid is more viscous. From the time the sand-oil mixture reaches the formation until the start of the flush, the friction accounts for 1,100 to 1,400 psi loss in pressure above the static head;

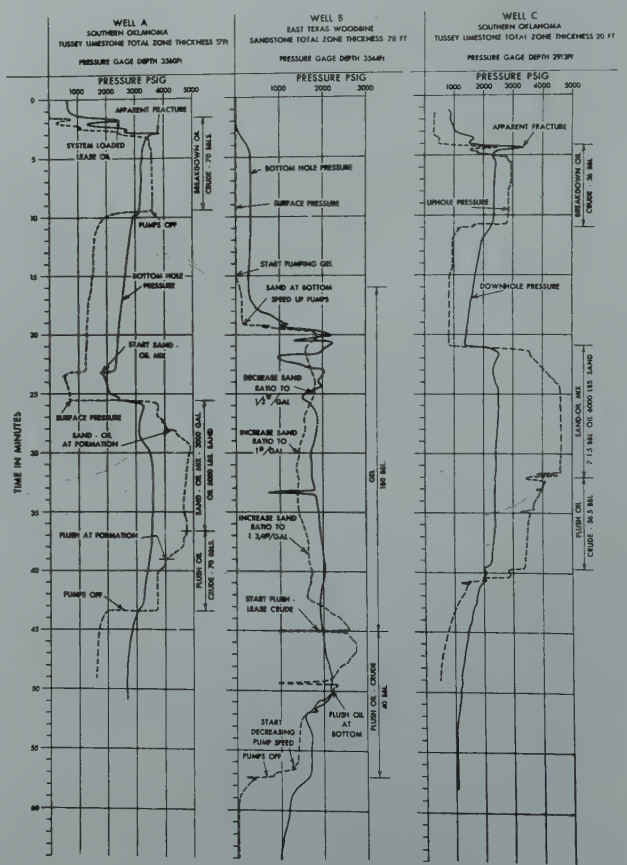

FIG. 1—SURFACE AND BOTTOM-HOLE PRESSURE RECORDS TAKEN DURING FRACTURING TREATMENTS.

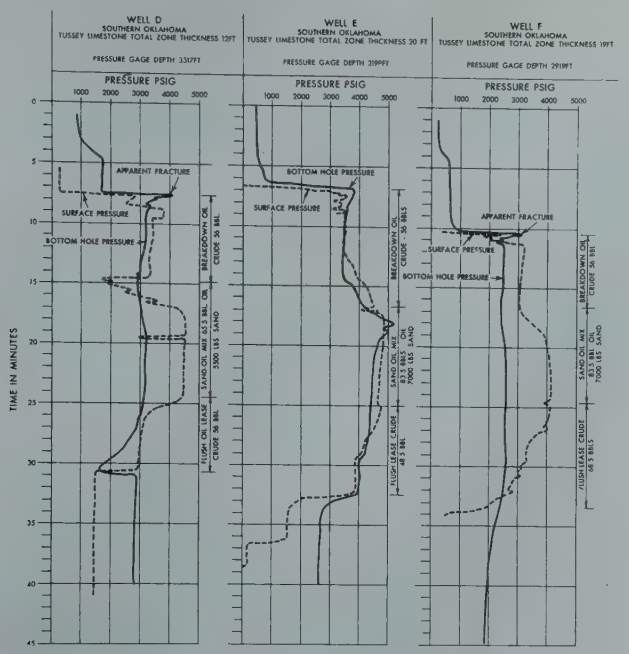
WELL D
SOUTHERN OKLAHOMA
TUSSEY LIMESTONE TOTAL ZONE THICKNESS 12FT
PRESSURE GAGE DEPTH 3317FT
WELL E
SOUTHERN OKLAHOMA
TUSSEY LIMESTONE TOTAL ZONE THICKNESS 20 FT
PRESSURE GAGE DEPTH 3199FT
WELL F
SOUTHERN OKLAHOMA
TUSSEY LIMESTONE TOTAL ZONE THICKNESS 19FT
PRESSURE GAGE DEPTH 2919FT
PRESSURE PSIG
1000 2000 3000 4000 5000
TIME IN MINUTES
APPARENT FRACTURE
SURFACE PRESSURE
BOTTOM HOLE PRESSURE
BREAKDOWN OIL CRUDE 56 BBL
SAND OIL MIX 83.5 BBL OIL 5500 LBS SAND
FLUSH OIL LEASE CRUDE 56 BBL
BREAKDOWN OIL CRUDE 56 BBLS
SAND OIL MIX 83.5 BBL OIL 7000 LBS SAND
FLUSH LEASE CRUDE 48.5 BBLS

FIG. 2—SURFACE AND BOTTOM-HOLE PRESSURE RECORDS TAKEN DURING FRACTURING TREATMENTS.

or from 2,400 to 2,700 psi total pressure loss. The higher pumping rates during this period increase the friction losses although the bottom-hole pressure remains about the same.

The passage of the fluid interfaces into the formation can be picked out from the two pressure records. The passage of the crude-oil to sand-oil interface is evidenced by the minimum on the bottom-hole record and the sharp increase in the surface record. If we take the total load volume of the tubing and divide it by the time from the start of the interface into the tubing to the assumed interface passage, we obtain a flow rate comparable to that obtained by averaging the total fluid used during the time of injection. This gives a reasonable check on the above interpretation of the record. The passage of the lease-oil interface at 39 minutes is evidenced by the declining bottom-hole pressure and the break in the surface pressure. Again, a volume calculation checks very closely with this point.

The pressure records of Well B, Fig. 1, show no sharp break-back in the bottom-hole pressure under the initial pressure surge as in the previous case. However, break-backs and a regaining of formation pressure at 20.5, 22, 25, and 33.5 minutes are observed. These temporary decreases in bottom-hole pressure are interpreted to represent the opening of fractures of limited extent. When the fractures are pressured-up by the injected fluid, the pressure increases to near the original value. This well had been previously fractured, which provides a plausible explanation for this particular type of break-back in pressure. Since the formation was highly permeable, the tubing would not hold a load of lease oil; therefore the survey started with a load of gel in the well. Nevertheless, it is possible to pick out the points at which sand as well as the flush oil entered the formation. These are indicated on the record at 19 and 50 minutes, respectively. The large pressure break-backs are not present on the surface pressure record. In a like manner the drops in the surface pressure at 45 and 49 minutes are not recorded on the bottom-hole pressure record. These drops in wellhead pressure were caused by a switching of tanks and a momentary slowing of the pumps, respectively. The bottom-hole pressure remained above the surface pressure most of the time during the gel injection. The surface pressure became greater than the bottom-hole pressure during the first part of the flush because of the increase in flow rate.

In Well C, Fig. 1, the sharp break-back in bottom-hole pressure again indicates an apparent fracture on the initial pressure surge. A sharp peak in the surface pressure is also noted in this record. However, the distinguishing feature of the formation pressure record is that a maximum pressure was reached just before the formation fractured. On the surface record subsequent pressures greatly exceed the pressure indicated by the break-back peak. The maximum bottom-hole pressure exceeded the overburden pressure as calculated in the case of Well A. This indicates the probable fracturing of the formation with lease crude oil in the well. The loss in bottom-hole pressure during the injection of the sand-oil exceeded the hydrostatic head by approximately 2,200 psi. Again, the increased surface pressure resulted in no increase in bottom-hole pressure during this period. The passage of the various interfaces into the formation can be located as in the previous examples.

The record obtained on Well D, Fig. 2, again shows an apparent fracture occurring with the initial pressure surge. This fracture is indicated only slightly on the surface record. The maximum formation pressure again exceeded the probable overburden pressure at the time of fracture. This record strikingly illustrates that the wide variations of the surface pressure due to changes in pump speeds have very little effect on the bottom-hole pressure. The decrease in bottom-hole pressure from 25 to 30 minutes was caused by the intense vibration of the borehole instrument. These vibrations were introduced by the non-synchronous operation of the pumps and cannot be considered as an accurate measure of the bottom-hole pressure in this region.

In the records of Well E, Fig. 2, the occurrence of a fracture is in doubt. The gradual break-back in the bottom-hole pressure following the initial surge may indicate some increase in formation permeability, but this increase is not sufficient to prevent the pressure from increasing to another peak. The second peak, at 18 minutes on the record, is the maximum bottom-hole pressure recorded. However, little increase in permeability is indicated in the subsequent portion of the record. It is interesting to note that although the bottom-hole pressure greatly exceeded the over-burden pressure in this case, no major fracturing is indicated.

The records of Well F, Fig. 2, again show an apparent fracture occurring during the initial pressure surge. It is very apparent in this record that the bottom-hole pressures remained essentially constant after the fracture even though various fluids and surface pressures were used. This levelling-off of the bottom-hole pressure curve is characteristic of all the records taken which show an apparent fracture. Because of the exceedingly flat pressure characteristic shown in this record, it is difficult to detect the passage of the various interfaces into the formation.

Samples of the fluids and mixtures used in all of these tests were collected in sealed containers at the time of the treatment. A summary of the fracture surveys as well as the properties of the fluids used are shown in Table 1. Because the exact formation temperature was not known in each case, the gravities and viscosities were determined at several standard temperatures. The temperatures shown in the table were closely

TABLE 1—SUMMARY OF FRACTURE SURVEYS AND PROPERTIES OF FLUIDS USED

Summary of Fracture Surveys							Properties of Fracturing Fluids							
Well	Depths of Casing Perforations (ft) From	To	Pressure Gauge Depth (ft)	Maximum BHP (psig)	Average Injection Rate (BPM)	Apparent Fracture	Fluids Used	Specific Gravity 60° F	80° F	Gravity (°API) 60° F	80° F	Viscosity (cp) 60° F	80° F	100° F	210° F
A	3,539 3,550 3,558	3,546 3,552 3,566	3,560	3,830	8.3	Yes	Lse. Crude Frac. Oil		0.865 0.933		32 20		11.5 300	6 130	
B[1]	3,577	3,655	3,544	2,230	5.3	No	Lse. Crude Gel.		0.84 0.85		37 35		7 70-95[2]	3	
C	2,935	2,955	2,991	3,400	8.8	Yes	Lse. Crude Frac. Oil	0.8761 0.9210		30.03 22.14		69.0 549.0		24.4 80.0	4.9 7.3
D	3,298	3,310	3,317	4,140	9.4	Yes	Lse. Crude Frac. Oil	0.8741 0.9160		30.40 22.98		80.0 381.0		33.0 139 0	4.9 12.6
E	3,152 3,164	3,158 3,170	3,198	5,200	9.9	No	Lse. Crude Frac Oil[3]	0.9130 0.9160		23.48 22.98		600 315		7° 5 92.5	6.7 10.7
F	2,874 2,900	2,889 2,904	2,919	3,110	10.1	Yes	Lse. Crude Frac. Oil	0.8771 0.9180		29.85 22.64		95.0 549		32.0 84.9	5.9 7.3

[1]Well had been previously subjected to a fracturing treatment.
[2]Estimated from operation, since this is a function of shear rate and mixing time.
[3]Contains low fluid loss additive.

controlled and the viscosity measurements were taken using a Brookfield Synchro-Letric viscometer. The fracturing oil and gel viscosities were measured without the sand in suspension. The gel viscosity could not be accurately measured because of the nature of the fluid; however, an approximate range of values is given.

Although an effort was made to obtain accurate data during these treatments, some parameters could not be adequately controlled or measured. For a complete analysis, especially to include the properties of the fluids used in fracturing, such variables as the surface and bottom-hole temperatures and injection flow rates should be measured in addition to the pressures.

INTERPRETATIONS

By a direct comparison of surface and bottom-hole pressures, the following information may be obtained: (1) the maximum pressure exerted against the formation, a rapid pressure decline implying fracturing, (2) the hydrostatic head of the fluid column when the fluid is not flowing, (3) whether the improved permeability of the formation was maintained, (4) the fluid pressure loss experienced because of flowing friction in the tubing, (5) passage of various fluid interfaces into the formation, and (6) pressures obtained with various fracturing fluids entering the formation.

The damping effect of the fluid-filled column is best illustrated in the detection of the rapid change in permeability of the formation caused by a fracture. When the well is fluid filled, previous to applying pump pressure, the gauge records a pressure equal to the hydrostatic head of the fluid column. If pressure is applied at the wellhead and no fluid movement results, the difference between the two pressures still represents the static head. However, if a fracture occurs, the fluid moves rapidly into the formation, thus reducing the bottom-hole pressure because of the rapid increase in the flowing friction through the tubing. Under ideal conditions the wellhead pressure should be maintained constant to produce this effect. In the cases illustrated, the rapid drop in formation pressure is very pronounced, even though the surface pressure may increase during this interval. The maximum pressure at the formation, in the case of a fracture which is maintained open throughout the treatment, will occur immediately preceding the actual fracture. If the permeability of the formation is maintained, the pressure at the formation will remain below the level required to initiate the fracture. This maximum formation pressure followed by the rapid decline to a lower pressure, is not reproduced in the surface pressure records in this distinctive form. Therefore, the actual bottom-hole pressure is of utmost importance if initiation of a fracture is to be detected.

In the case where the formation opens, then closes, or a limited fracture is incurred, the pressure at the formation would show a decrease and then an increase as the friction losses (and consequent pressure drop in the tubing) successively increase and decrease with flow rate. For the case where no fracture occurs, the pressure at the formation should follow the trend of the wellhead pressure with a slight deviation due to friction losses and changes in hydrostatic head with various fluids. The effect of pressure on flow rate, and, hence, the friction losses, would be controlled primarily by the permeability of the formation.

In order to analyze the result of the passage of a fluid interface into the formation, we must consider first the effect of the movement of the interface down the tubing. Normally, for fluids used in a fracturing operation, the contrast in viscosity of the fluids is much greater than the contrast in their density. Therefore, the variation in pressures with the passage of an interface down the tubing is governed mostly by the change in friction losses. For a constant flow rate there will be a linear increase or decrease in the difference between the wellhead and bottom-hole pressures, depending upon whether the change is from a less viscous to a more viscous fluid or vice versa. Upon entry of the interface into the formation, the pressure difference will tend to become constant, thus marking the interface.

Since the differences in the surface and bottom-hole pressures under flowing conditions depend greatly upon the viscosity and the resultant friction losses, the surface pressure can be expected to rise considerably when changing from a low viscosity fluid to a high viscosity fluid while maintaining a relatively constant flow rate. The rise in surface pressure in this case does not effect an increase in the bottom-hole pressure since the added pressure is used to overcome the friction losses in the tubing. This effect is noted in the examples given where the fluid is changed from a lease crude to a more viscous frac oil.

By obtaining the actual pressure on the formation during a fracture treatment, and if the inherent tectonic stresses are known, it should be possible to determine the type of fracture induced.

CONCLUSIONS

The observation of both the wellhead and bottom-hole pressures during fracturing operations is necessary to a complete understanding and possible improvement of this process. With specific reference to the fracturing

treatments through tubing presented in this paper, the following conclusions are of particular interest.

1. Bottom-hole pressures cannot be accurately determined from surface pressure measurements.

2. The actual pressure exerted against a formation in most cases is relatively constant. The long fluid columns tend to dampen surface pressure fluctuations.

3. In four of the six wells tested, fracturing was apparently induced by the thin load oil rather than the thick sand-oil mixture.

4. The increased surface pressure required to displace the thick sand-oil mixture is not necessarily transmitted to the formation. The high friction losses concomitant with the flow of a viscous oil may actually reduce the pressure exerted on the formation. From the records presented the actual friction loss can be calculated.

5. Because of the high friction losses, it is possible to have bottom-hole pressures considerably less than the surface pressures.

6. If the tectonic stresses can be determined, it should be possible to estimate the nature and extent of fracturing by obtaining accurate bottom-hole pressures.

7. In most cases it is possible to detect the passage of the interface of two fracturing fluids into the formation from the bottom-hole pressure record.

Through the use of a continuous surface recording bottom-hole pressure gauge, a better insight into the characteristics of well fracturing has been obtained. It is anticipated that the accumulation of additional data in various areas and under different conditions will provide the necessary information to allow better control and improved practices in the application of the fracturing process.

ACKNOWLEDGMENTS

The authors wish to express their appreciation to the management of Magnolia Petroleum Co. for permission to publish this paper. Acknowledgment of the field help in conducting these tests is also made to H. V. Hardin and M. E. Miller of the Healdton Dist., Magnolia Producing Dept. The help extended by J. J. Bresenham, Jr., of the Magnolia Petroleum Co. Engineering Dept., in the collection of data for this paper is also gratefully acknowledged.

REFERENCES

1. Hurst, R. E., Moore, J. M., and Ramsey, D. E.: "Development and Application of 'Frac' Treatments in the Permian Basin", *Trans.* AIME (1955) **204,** 58.
2. McGuire, W. J., Jr., Harrison, E., and Kieschnick, W. F., Jr.: "The Mechanics of Formation Fracture Induction and Extension", *Trans.* AIME (1954) **201,** 252.
3. Wilsey, L. E., and Bearden, Wm. G.: "Reservoir Fracturing — A Method of Oil Recovery from Extremely Low Permeability Formations", *Trans.* AIME (1954) **201,** 21.
4. Hubbert, M. K., and Willis, D. G.: "Mechanics of Hydraulic Fracturing". *Trans.* AIME (1957), **210,** 153. ★★★

Use of Chemicals to Maintain Clear Water for Drilling

J. P. GALLUS
J. L. LUMMUS
J. E. FOX, JR.

PAN AMERICAN PETROLEUM CORP.
TULSA, OKLA.

ABSTRACT

Fresh water or brine drilling fluids may be kept free of suspended drilled solids by the addition of a water soluble acrylamide-carboxylic acid copolymer at the flowline. Addition of from .01 to 0.2 lb/bbl of the polymer solution to drilling fluids containing less than 5 per cent clay solids by weight causes the solids to flocculate and settle rapidly to the bottom of the pits. Solutions of the polymer injected at the pump suction reduce the loss of water to permeable formations without impairing the permeability to oil. The use of drilling fluids clarified with the polymer has resulted in increased drilling rates, extended bit life, and lower drilling fluid costs.

INTRODUCTION

Field experience and the results of a number of investigations have established that the accumulation of solids in drilling fluid reduces drilling rate.[1-5] Drilling with water makes possible higher drilling rates than can be achieved with mud but in many areas drilling with water may not be feasible because of the possibility of encountering high formation pressures or hydratable formations. To combat these conditions, the drilling fluid must possess certain physical properties such as viscosity, density, fluid loss, etc., which require the presence of solids.

The current trend in drilling fluid treatment is to maintain as low a percentage of solids as is possible without harmfully affecting the mud properties needed for drilling. Mechanical separating devices such as wet cyclones and decanting-type centrifuges are proving to be an economical means of controlling the percentage of solids and thereby maintaining low solids muds. Also, special muds have been developed for the purpose of retarding the hydration of drilled solids so that they may be more easily removed by shale shakers or settling pits.

In some areas, such as West Texas, the characteristics of some formations will permit drilling with water. However, because of the dispersion of drilled solids, it is usually not possible to maintain clear water even with the aid of mechanical separators, or by utilizing large settling pits. For this reason the commonly used term "water drilling" is a misnomer since the water usually contains some solids.

Because of the improved drilling rates and other benefits which might be effected, a laboratory and field study was made of the use of flocculating agents for maintaining clear water for drilling.

PROCEDURE

Laboratory—Solids Settling

Two techniques were employed to determine the effectiveness of flocculating agents in settling solids from drilling mud.

First, the rate of fall of solids was measured in graduated beakers containing mud treated with various flocculating agents. Natural gum, oil-in-water emulsions prepared with ethoxylated nonyl phenols and diesel oil, and a powdered synthetic acrylamide-carboxylic acid copolymer* (hereinafter referred to as "polymer") were tested as flocculating agents in both fresh water and salt saturated muds containing 4 per cent solids. The polymer was not added in the powder form directly to the muds but was first dissolved in water in a concentration of 3.5 lb/bbl. The polymer solution was then added directly to the mud. The concentration of the flocculating agents, including the polymer, was varied. High rates of fall of the solids indicated high flocculating efficiency.

A second technique consisted of measuring the time in minutes required to obtain clear water at the pump suction after addition of the various flocculating agents at the flowline. These tests were made using a model mud circulating system having a total volume of approximately 10 gal. The natural fresh water and brine muds used contained 4 per cent solids. A sketch of the circulating system appears in Fig. 1. The circulating rate

Original manuscript received in Society of Petroleum Engineers office on Sept. 5, 1957. Revised manuscript received Feb. 18, 1958. Paper presented at 32nd Annual Fall Meeting of Society of Petroleum Engineers in Dallas, Tex., Oct. 6-9, 1957.

[1]References given at end of paper.

Discussion of this and all following technical papers is invited. Discussion in writing (three copies) may be sent to the offices of the *Journal of Petroleum Technology*. Any discussion offered after Dec. 31, 1958, should be in the form of a new paper.

*Sold under the trade-mark SEPARAN 2610, by the Dow Chemical Co.

used during tests was equivalent to 10 bbl/min in an average-size field mud system. A small centrifugal pump powered by an electric motor served as a slush pump.

Laboratory—Fluid Loss

The effect of the polymer on fluid loss was measured by standard API filtrate tests and by flow rate tests through sandstone cores measuring 1 and 2 in. in diameter, and ½ to 28 in. in length. Permeability of the cores varied from 10 to 1,500 md. Some of the cores were treated with ethyl silicate to eliminate clay effects during permeability tests. Comparison of the permeabilities of the cores to water with the permeabilities to water after exposure to the polymer solution indicated the plugging effect. The polymer was used in a concentration of 0.175 lb of the dry powder per barrel of water. During some tests the faces of the cores were continuously scraped to prevent surface coating.

Depth of plugging was also determined by measuring permeabilities as successive increments were sliced from the end of a sandstone core 8-cm long. First, the permeability to distilled water was determined. Then 8.5 ml of the polymer solution was injected and the mean water permeability measured in the direction counter to which the polymer solution had been injected. Segments of core were then removed from the plugged face of the core and the permeability of the remaining part was measured. Permeabilities were measured with a differential pressure of from 10 to 80 psi.

Other permeability measurements were made on cores which were saturated with oil before injection of the test fluids. The purpose of these tests was to investigate the behavior of the polymer in the presence of oil and also to observe the effect on oil permeability.

Field

A 1 per cent aqueous solution (3.5 lb/bbl) of the polymer was mixed in a large volume tank or in manifolded drums suitably positioned to permit gravity feed to the mud system. Aspirator-type solids dispersers and mechanical or air agitators were employed in dissolving the polymer.

To clarify the solids-laden fluid discharging from the wells, a continuous stream of the polymer solution was introduced just below the shale shaker where the fluid from the flowline discharged into the pits. Here, sufficient agitation was available to provide adequate dispersion of the polymer solution in the mud.

The polymer solution was added at a sufficient rate to maintain clear fluid at the pump suction. Rate of injection was dependent on both quantity and nature of solids in the fluid and was varied from ½ to 4 lb of polymer in solution per hour. Solids such as bentonite which dispersed readily in the mud (referred to as high yield solids in this report) required the higher quantities of polymer. Solids such as kaolinite or shale which did not disperse well (referred to as low yield solids) required the lower quantities of polymer.

When practical, the fluid discharging from wells was circulated through earthen reserve pits to take advantage of the large settling area and obviate otherwise frequent jetting of the steel circulating pits to remove settled solids. Fig. 2 shows a typical fluid circulating system used during field tests. When it was not possible to circulate through a reserve pit, the settling pit was jetted when solids accumulated sufficiently to begin flowing into the suction pit.

To reduce fluid loss to permeable formations, the polymer solution was injected directly into the pump suction line. The quantity injected varied from 1 to 6 lb in solution per hour depending upon the permeability of the formations penetrated. Where available, electric logs of adjacent wells were consulted for indications of depths where permeable strata might be encountered. Seventeen field tests were conducted.

RESULTS

Laboratory

The results of typical settling rate tests in graduated beakers are presented graphically in Fig. 3. The periods of time required to obtain clear water in the model circulating system after adding various flocculating agents, including the acrylamide-carboxylic acid copolymer, to mud containing 4 per cent solids are shown in Table 1.

Figs. 4, 5, and 6 show the effects of the polymer on the permeability of sandstone cores. The return water permeability of natural Nellie Bly sandstone in the 1,000-md range measured from 2 to 5 per cent of the original permeability after exposure to water containing 0.175 lb of polymer per barrel. The mean water permeability of Nellie Bly sandstone cores, with clays made water insensitive with ethyl silicate, measured approximately 10 per cent of the original water permeability after exposure to the same solution of the polymer. Experiments conducted to determine depth of plugging indicated that the "plugged zone" comprised approximately one-half of a test core 8-cm long (Fig. 6). Fig. 7 is a graphical presentation of these same data.

Ninety-seven per cent of the mean relative permeability to oil was recovered by backflowing oil through a Turkey Mountain sandstone core in which clays had been made water insensitive and the core exposed to a

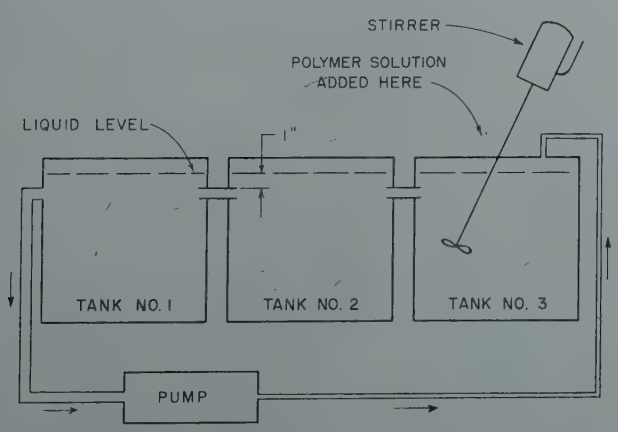

Fig. 1—Diagram of Laboratory Circulating System Used to Compare Flocculating Agents.

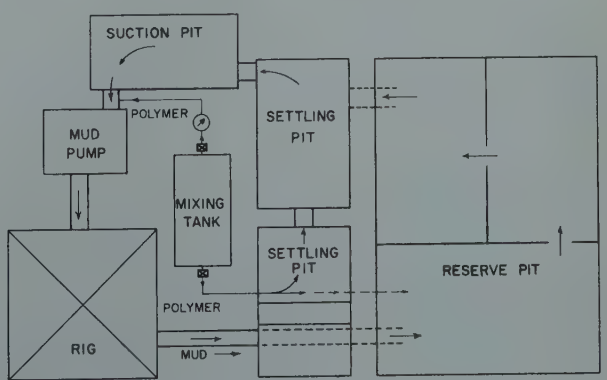

Fig. 2—Flow System when Using Flocculating Agent.

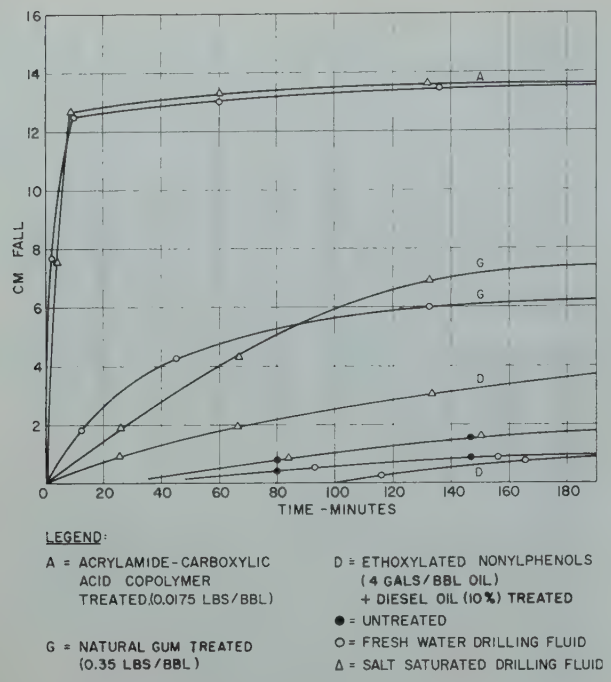

FIG. 3—SOLIDS SETTLING RATES IN FRESH WATER AND SALT-SATURATED DRILLING FLUIDS.

polymer solution of 0.175 lb/bbl of water. Similar results were obtained using native state oilfield cores.

No visible filter cakes were formed on cores exposed to the polymer-treated water or brine.

FIELD

Table 2 is a tabulation of field tests where the polymer was used for settling out solids from water and brine and preventing fluid loss to permeable formations in wells ranging in depths from 234 to 11,160 ft.

Fig. 8 (Field Test No. 2) compares the drilling rate obtained on a well in Andrews County, Tex., where the drilling water was clarified with the polymer and the drilling rate of two wells drilled in the same area without benefit of the polymer treatment. The three wells compared were drilled with the same rig operated by the same crew.

Fig. 9 compares the drilling rate of a well in Midland County, Tex. (Field Test No. 14), drilled with water clarified with the polymer from a depth of 8,535 to 9,800 ft with the drilling rates for the same interval in four adjacent wells which were drilled with conventional drilling mud. Utilizing the polymer-treated system, a 43 per cent increase in drilling rate and a 37 per cent decrease in drill bit requirements was observed. The five wells compared were drilled with the same rig and crew.

Water requirements, which are high in some areas such as New Mexico and West Texas, have been reduced by as much as 50 per cent.

Some typical savings in cost realized by drilling with clear water treated with the polymer are shown in Table 3.

TABLE 1—PERFORMANCE OF FLOCCULATING AGENTS IN A MODEL CIRCULATING SYSTEM

Drilling Fluid	Flocculating Agent	Optimum Concentration of Flocculating Agent	Time in Minutes to Obtain Clear Water at Pump Suction
Water	Acrylamide Carb. acid Copolymer	0.0175 lb/bbl	0.5
Brine	Acrylamide Carb. acid Copolymer	0.0175 lb/bbl	0.5
Water	Ethoxylated nonyl phenols + diesel oil	4 gal/bbl oil 10 Per cent	8.0
Brine	Ethoxylated nonyl phenols + diesel oil	4 gal/bbl oil 10 Per cent	6.5
Water	Natural gum	0.35 lb/bbl	7.5
Brine	Natural gum	0.35 lb/bbl	7.0
Water	None	No clear water obtained	—
Brine	None	——	4,800.0

DISCUSSION

Rapid flocculation and rapid sedimentation are requisites for clear water drilling operations as the drilling

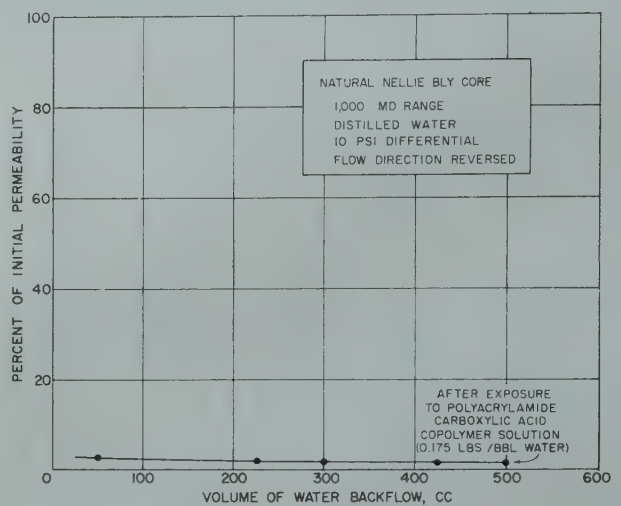
PERCENT OF INITIAL PERMEABILITY
VOLUME OF WATER BACKFLOW, CC
NATURAL NELLIE BLY CORE
1,000 MD RANGE
DISTILLED WATER
10 PSI DIFFERENTIAL
FLOW DIRECTION REVERSED
AFTER EXPOSURE TO POLYACRYLAMIDE CARBOXYLIC ACID COPOLYMER SOLUTION (0.175 LBS /BBL WATER)

FIG. 4—EFFECT OF ACRYLAMIDE-CARBOXYLIC ACID COPOLYMER ON RETURN WATER PERMEABILITY.

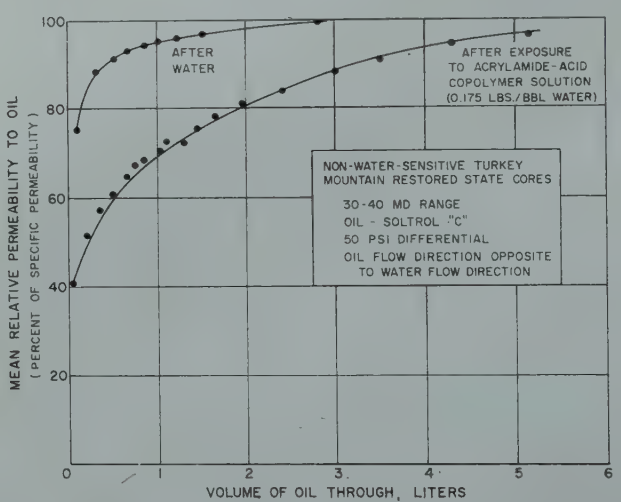
MEAN RELATIVE PERMEABILITY TO OIL (PERCENT OF SPECIFIC PERMEABILITY)
VOLUME OF OIL THROUGH, LITERS
AFTER WATER
AFTER EXPOSURE TO ACRYLAMIDE-ACID COPOLYMER SOLUTION (0.175 LBS./BBL WATER)
NON-WATER-SENSITIVE TURKEY MOUNTAIN RESTORED STATE CORES
30-40 MD RANGE
OIL - SOLTROL "C"
50 PSI DIFFERENTIAL
OIL FLOW DIRECTION OPPOSITE TO WATER FLOW DIRECTION

FIG. 5—EFFECT OF ACRYLAMIDE-CARBOXYLIC ACID COPOLYMER ON RETURN MEAN RELATIVE PERMEABILITY TO OIL.

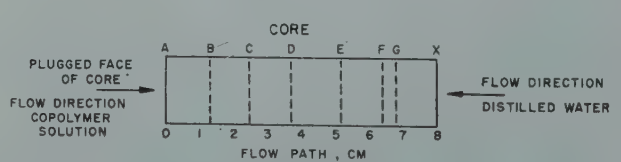

PERMEABILITY TESTS (DISTILLED WATER)

FLOW PATH	LENGTH OF FLOW PATH, CM	K, MD
X TO A	8.0	0.84
X TO B	6.7	0.95
X TO C	5.6	1.22
X TO D	4.3	1.30
X TO E	2.9	2.33
X TO F	1.7	4.23
X TO G	1.2	9.21

FIG. 6—DEPTH OF PLUGGING BY ACRYLAMIDE-CARBOXYLIC ACID COPOLYMER.

fluid emerging from the well must be clarified, while in motion, during the relatively short period of time in which the mud passes from the flowline to the pump suction.

As shown in Table 1, the optimum concentration of the polymer to obtain maximum flocculating efficiency was found to be approximately 0.0175 lb/bbl of mud. Overtreatment with as much as three times this amount did not impair or improve flocculating efficiency.

The data were obtained using natural fresh water and brine drilling fluids containing 4 per cent clay solids by weight in a model circulating system. Clear water was obtained at the pump suction in 0.5 minutes upon treatment of both the fresh water and the brine drilling fluids with 0.0175 lb/bbl of the polymer in an aqueous solution as compared to from 6.5 to 8 minutes when treating with higher concentrations of the other flocculating agents tested. Fig. 3 is a comparison of the flocculation efficiency of the same agents under static conditions.

The mechanism by which the polymer acts as a flocculating agent differs from some of the more common mud flocculating agents such as calcium hydroxide and calcium sulfate. The polymer, in addition to causing clay particles to group together, effects direct bonding between particles by virtue of the affinity for and adsorption on solids by the amide and carboxyl groups. This property promotes formation of larger groups of particles and effects more efficient flocculation. The adsorption is essentially an irreversible process.

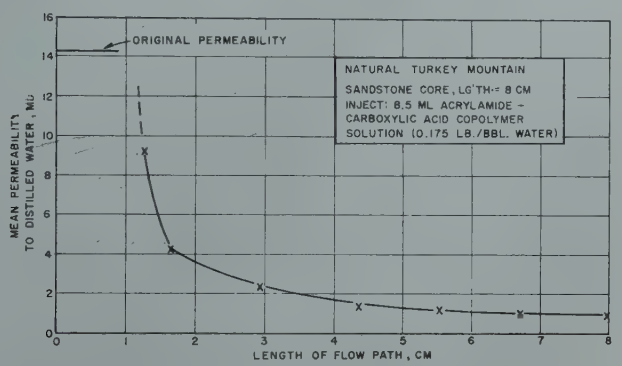
ORIGINAL PERMEABILITY
NATURAL TURKEY MOUNTAIN SANDSTONE CORE, LGTH= 8 CM
INJECT: 8.5 ML ACRYLAMIDE - CARBOXYLIC ACID COPOLYMER SOLUTION (0.175 LB./BBL. WATER)
MEAN PERMEABILITY TO DISTILLED WATER, MD
LENGTH OF FLOW PATH, CM

FIG. 7—DEPTH OF PLUGGING BY ACRYLAMIDE-CARBOXYLIC ACID COPOLYMER.

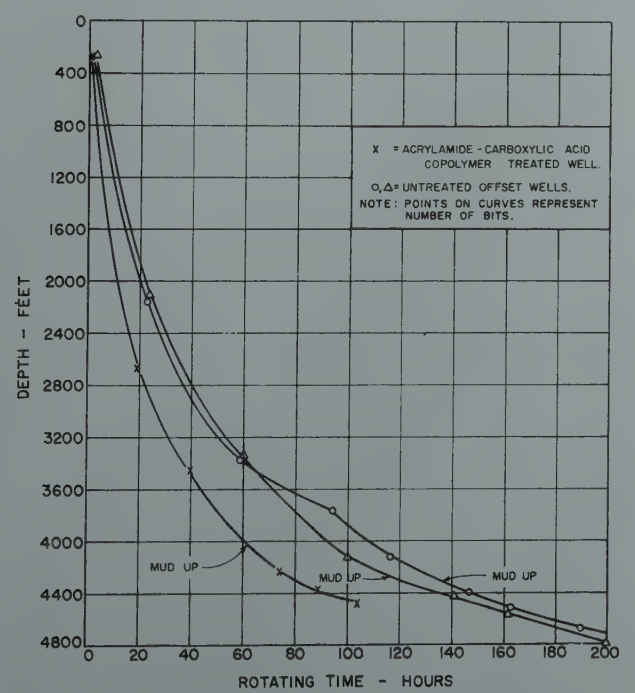
X = ACRYLAMIDE - CARBOXYLIC ACID COPOLYMER TREATED WELL.
O, Δ = UNTREATED OFFSET WELLS.
NOTE: POINTS ON CURVES REPRESENT NUMBER OF BITS.
MUD UP
MUD UP
MUD UP
DEPTH - FEET
ROTATING TIME - HOURS

FIG. 8—EFFECT OF TREATMENT WITH ACRYMALIDE-CARBOXYLIC ACID COPOLYMER ON DRILLING RATES IN ANDREWS COUNTY, TEX.

TABLE 2—RESULTS OF FIELD TESTS USING AN ACRYLAMIDE-CARBOXYLIC ACID COPOLYMER

Test No.	Area	Depths (ft)	Results
1	Winkler County, Tex.	459- 3,559	Trip time reduced six hours Drilling time reduced 35 per cent Bit life increased 25 per cent
2	Andrews County, Tex.	352- 4,050	Drilling time reduced 39 per cent Bit life increased 18 per cent Trouble-free trips
3	Scurry County, Tex.	4,995- 7,560	Reduced fluid loss to formations 80 per cent Reduced mud costs 50 per cent
4	Winkler County, Tex.	550- 8,747	Reduced drilling time 41 per cent Increased bit and pump liner life 26 per cent
5	Scurry County, Tex.	2,730- 6,750	Reduced fluid loss to formations 95 per cent Increased penetration rate 34 per cent Increased bit life 19 per cent
6	Scurry County, Tex.	4,460- 7,000	Reduced fluid loss to formations 50 per cent Increased penetration rate 31 per cent Increased bit life 22 per cent
7	Andrews County, Tex.	5,500-11,160	Drilled 1,000 ft deeper than adjacent wells with water
8	Lipscomb County, Tex.	3,460- 6,135	Saved $2,000 on mud costs Regained circulation by slugging 20 lb of polymer
9	Lipscomb County, Tex.	365- 3,493	Reduced seepage 66 per cent Increased penetration rates and bit life
10	San Juan County, N. M.	263- 5,020	Drilled to 5,020 ft in 11 days (fastest drilling rate recorded in area). Stopped water loss to formations
11	San Juan County, N. M.	234- 4,700	Prevented water seepage. Reduced drilling time. Increased bit and pump liner life 26 per cent
12	Lipscomb County, Tex.	1,719- 3,115	Saved nine bits. Saved 128 rotating hours
13	Andrews County, Tex.	5,435-10,710	Saved 13 bits. Saved 85 rotating hours over 5,000-ft interval
14	Andrews County, Tex.	8,550- 9,800	Saved 2⅛ bits, 22 hours drilling time over 1,250-ft interval. Chemical cost $25. Savings $2,000
15	Lea County, N. M.	4,250- 4,770	Reduced fluid seepage from 40 to 0 bbl/hr. Reduced drilling time, increased bit and pump liner life.
16	Cleveland County, Okla.	925- 2,735	Inadequate fluid volume and settling area prevented maintenance of clear water at pump. Highly bentonitic solids required reserve pit circulation.
17	Alberta, Canada	2,100- 7,800	Reduced drilling time nine days to 7,800 ft. Good bore conditions.

As a result of its affinity for and adsorption on solids, the polymer does not remain long in the circulating fluid. The polymer must be continuously injected into the drilling fluid system as a dilute aqueous solution. The need for continuous injection presented no problem in the field. A single batch prepared daily and allowed to flow slowly into the mud system continuously while drilling proved to be a satisfactory means of maintaining clear water at the pump suction.

The addition of the polymer to water in concentrations of from 0.02 to 0.3 lb/bbl did not reduce the filtrate rate through Whatman No. 52 filter paper as measured by the standard API fluid loss test. It was subsequently found, however, that the permeability to water of sandstone cores was appreciably reduced on exposure of cores to solutions containing from 0.0175 to 0.175 lb/bbl of the polymer.

The property of the polymer for reducing formation

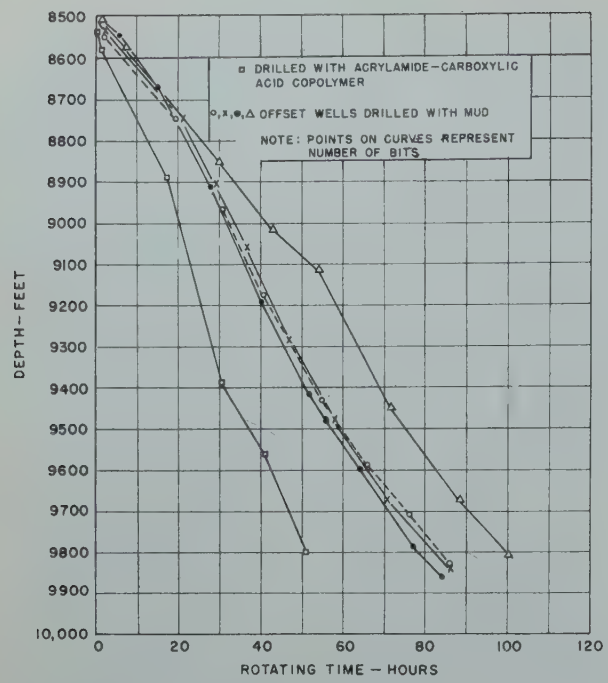

FIG. 9—EFFECT OF TREATMENT WITH ACRYLAMIDE-CARBOXYLIC ACID COPOLYMER ON DRILLING RATES IN MIDLAND COUNTY, TEX.

permeability to water without impairing the permeability to oil is illustrated in Figs. 4, 5, and 6. Without this property, clarified water drilling would be neither economical nor desirable as both the excessive loss of drilling fluid and damage to the permeability of oil-bearing zones could not be tolerated in many wells.

The mechanism by which formation permeability is reduced probably is a result of the large molecules of the polymer plugging the rock pores by adsorbing to the pore walls. The plugging tendency of the polymer was observed in consolidated cores having a permeability as high as 1,500 md. The depth of plugging achieved on exposure of formations to the polymer solution has not been completely investigated, although Figs. 6 and 7 indicate that the plugged zone would extend at least a short distance into the formation.

These laboratory results show that the addition of a water solution of an acrylamide-carboxylic acid copolymer to drilling fluids containing less than 5 per cent clay solids by weight causes the solids to flocculate and settle rapidly. The results further show that treatment of low solids drilling fluids with from 0.0175 to 0.175 lb of polymer per barrel of fluid will provide clear water at the pump suction. It is also shown that treatment with the polymer solution reduces the permeability of formations to water by as much as 90 to 98 per cent without impairing the oil productivity of these formations.

The 17 field trials conducted using the polymer for the purpose of removing suspended solids from the drilling water and preventing fluid loss to permeable formations were, in general, successful. Penetration rates were increased an average of 50 per cent, bit life was extended approximately 25 per cent, and mud costs were reduced by as much as 50 per cent. Examples are shown in Tables 2 and 3, and Figs. 8 and 9.

Table 3 shows typical savings realized through the use of the polymer. The total savings realized on the five wells selected varied from $2,500 to $9,000. The cost of using the polymer ranged from $300 to $500 per

TABLE 3—TYPICAL SAVINGS REALIZED THROUGH USE OF ACRYLAMIDE CARBOXYLIC ACID COPOLYMER

(Rig time charge: $1,000.00 per day—Bit cost: $200.00 each)

Field Test No.	Area	Depths (ft)	Principal Effects	Total Cost Savings
1	Winkler County, Tex.	459- 3,559	Reduced trip time—Six hours Reduced drilling time—35 Per cent Increased bit life—25 Per cent	$2,500.00
5	Scurry County, Tex.	4,995- 7,560	Reduced water loss—80 Per cent Reduced total mud costs—50 Per cent	$4,000.00
7	Scurry County, Tex.	2,730- 6,750	Reduced water loss—95 Per cent Increased penetration rate—34 Per cent Increased bit life—19 Per cent	$4,100.00
9	Andrews County, Tex.	5,500-11,160	Obtained $0.50/ft footage price reduction from contractor	$2,500.00
20	Alberta, Canada	2,100- 7,800	Reduced drilling time—Nine days	$9,000.00

well. Maintenance costs averaged from $15 to $50 per day.

These field results indicated that the use of the polymer to provide clear water for drilling increased penetration rates and bit life and sharply reduced mud costs.

Other benefits were experienced early in Field Test No. 1 in Winkler County, Tex., in that the first round trip at 1,750 ft required only two hours. Usually the first trip in the redbeds requires from four to nine hours because of the pipe dragging in the bore. The reason for this fast trip time is believed to be a result of the low fluid loss properties of the polymer solution in that little or no filter cake was deposited to hinder the movement of the drill string. It was observed that there was less sloughing of the redbeds during this and subsequent tests in the same area as compared to results obtained with conventional drilling fluids which is an indication that the polymer was retarding the hydration of the redbeds.

Field Test No. 3 was conducted in Scurry County to substantiate the plugging effect of the polymer observed in the laboratory. Gel chemical mud and lost circulation materials are usually required in this area because fluid loss to permeable formations by seepage is severe from the surface down and becomes excessive below 5,000 ft. On the test well a polymer solution was injected into the pump suction line at a rate of 1.3 to 4 lb of polymer per hour. As a result of this treatment, loss of fluid to permeable formations was reduced by 80 per cent. The generally troublesome shale section between 6,100 and 7,500 ft was penetrated without difficulty. On this well the mud cost was reduced to approximately one-half of the average for 13 other wells drilled in the area with conventional drilling fluids.

In another well (Field Test No. 5) in the same field the loss of drilling fluid to permeable zones was reduced with the polymer to 5 per cent of the normal fluid loss.

The ability of the polymer to reduce sharply fluid loss to permeable rock was observed in other wells in Texas, Oklahoma, and New Mexico. For example, in Test No. 8 on a well in the Texas Panhandle, circulation was completely lost and upon injection of a slug of concentrated polymer solution (approximately 20 lb of polymer in 10 bbl of water) full returns were regained immediately.

Field Test No. 4 in Winkler County is of particular interest as this hole which was drilled with clear water treated with the polymer was sufficiently free of filter cake, bit cuttings and cavings to permit setting of casing without mudding up.

Field Test No. 16 was unsuccessful because of insufficient pit volume for settling of the flocculated solids. In this test circulation was possible only through two 250-bbl capacity steel mud pits since the reserve pit, which would have provided sufficient settling space, was below the level of the steel pits. When sufficient pit volume is not available for settling the flocculated solids, the frequency of jetting to remove solids is too high for efficient operation. Where the use of a large reserve pit is impractical or impossible, wet cyclone separators or other mechanical separating devices which are capable of reducing the solids content of the drilling fluid may aid in reducing the frequency of jetting.

The low cuttings carrying capacity of the solids-free drilling fluid was found to be a disadvantage in areas where hole washouts occurred.

When these washouts occur, the bit cuttings and flocculated solids tend to accumulate on bottom when circulation is stopped. The solids, however, are easily removed upon resumption of circulation and have in no case shown a tendency to cause the drill string to stick.

In these field tests, conversion from clear water drilling to mud drilling was necessary at various drilling depths for such reasons as (1) the need for improving the bit cuttings carrying capacity to keep the hole clean or to provide samples of adequate size for geological inspection, (2) a higher fluid density to combat anticipated formation pressures, and (3) to combat loss of circulation with bridging materials.

If it is necessary to convert to mud after using the polymer, injection of polymer solution may be discontinued one to two hours or 100 to 200 ft before adding clay. The polymer completely disappears in a relatively short time because of adsorption to solids.

The polymer has been found to be both practical and economical for providing clear water for drilling in areas where water drilling is feasible and indications are that this treating chemical will become more widely used in the near future.

CONCLUSIONS

1. The addition of a water solution of a synthetic acrylamide-carboxylic acid copolymer to drilling fluids containing less than 5 per cent clay solids by weight causes the solids to flocculate and settle rapidly.

2. Treatment of low solids drilling fluids with from 0.0175 to 0.175 lb of polymer per barrel of fluid provides clear water at the pump suction for drilling.

3. Treatment with the polymer solution reduces the permeability of the formations tested in the laboratory to water by 90 to 98 per cent without formation of visible filter cakes.

4. Exposure of the oil-bearing formations tested in the laboratory to water treated with the polymer does not impair the permeability of the formations to oil.

5. The use of the polymer in applicable areas to provide clear water for drilling increases drilling rate and bit life and lowers mud costs.

6. The loss of water to permeable formations, other than loss to vugs, caverns or fractures, while drilling may be effectively controlled by addition of from 1 to 4 lb of polymer per hour at the pump suction.

REFERENCES

1. Gray, George R., and Kellogg, W. C.: "A Cross-section of Typical Mud Problems", *World Oil* (Aug. 1, 1955) 102.
2. Waddell, R. W.: "Drilling Fluid Must Be Fitted to Requirements of Hole", *Drilling* (Nov. 1953) 73.
3. Bell, J. S.: "Fluid Choice Is Great Factor in Economic Drilling Rate", *Drilling* (Nov. 1953) 81.
4. Wheless, N. H., and Howe, Jack L.: "Low Solids Muds Improve Rate of Drilling, Cut Hole Time", *Drilling* (Aug., 1953) 70.
5. Eckel, John R.: "Effect of Mud Properties on Drilling Rate", *Drill. and Prod. Prac.*, API (1954) 119. ★★★

Miscible Fluid Displacement in Porous Media

JAMES W. LACEY
ARTHUR L. DRAPER
GEORGE G. BINDER, JR.
MEMBER AIME

THE CARTER OIL CO.
TULSA, OKLA.

ABSTRACT

An experimental investigation of miscible fluid displacement has been made in linear porous media under highly adverse mobility ratio conditions. Various refined oils were displaced at field rates by liquid propane in both horizontal and vertical models 9 to 36 ft in length.

In horizontal tests, mixed zones or transition zones form between the two liquids early in the displacements. Initially, the zones grow rapidly. In 2-in. diameter models, the mixed regions become nearly stable zones from 6- to 20-ft long. From then on these quasi-stable zones apparently grow only by molecular diffusion.

The lengths of the quasi-stable zones appear to be almost independent of the core material in which displacements are made and increase with increasing rates of injection and oil/solvent viscosity ratios. The lengths of the quasi-stable zones measured in 2-in. diameter models at viscosity ratios and injection rates anticipated in the field indicate that essentially piston-like displacements of oil by solvent would occur. However, the mixed zone lengths increase markedly as the model diameter increases.

In vertical displacements controlled by gravity drainage, only short transition zones form. The entire lengths of these zones can be accounted for by molecular diffusion. Therefore, in reservoirs having characteristics allowing a high degree of gravity drainage, nearly complete oil recovery should be attainable by miscible fluid displacement.

INTRODUCTION

The oil industry is faced with an ever increasing cost for finding new oil reservoirs. This, coupled with the fact that conventional methods of oil recovery usually leave from 1 to 3 bbl of oil in the ground for every barrel produced, has aroused considerable interest in developing more efficient methods. An integral part of the mechanism of many of these new methods of recovery is a miscible fluid displacement in which oil is displaced by a much less viscous material such as liquid propane. A number of investigators have explored the mechanics of miscible fluid displacement,[1,2,3,4,5,6] but in the experiments reported many of the important factors have been varied only over a limited range far removed from normal oilfield values.

This paper presents the results of an experimental study of oil displacement by liquid propane at field rates from linear, natural-sandstone models of various sizes. Both horizontal and vertical flow tests were made.

[1]References given at end of paper.

Original manuscript received in Society of Petroleum Engineers office Sept. 15, 1957. Revised manuscript received March 17, 1958. Paper presented at 32nd Annual Fall Meeting of Society of Petroleum Engineers in Dallas, Tex., Oct. 6-9, 1957.

EXPERIMENTAL APPARATUS AND PROCEDURE

Refined oils with viscosities varying over a wide range were displaced at several rates by liquid propane from both horizontal and vertical flow systems. The behavior of the displacement was observed by propane-oil analyses of the effluent and, when possible, by differential pressure measurements along the cores. A schematic flow diagram of the apparatus used to conduct the experiments is shown in Fig. 1.

The cores used in the tests were 9-ft lengths cut from natural consolidated sandstone and turned to the desired diameter. These were cast in steel tubing with a low melting point (160°F) alloy which expands on solidification. Flanges welded to the ends of the steel pipes permitted sealing the ends or butting one core to another. Pressure seals were maintained with O-rings.

The cores were cleaned by flushing

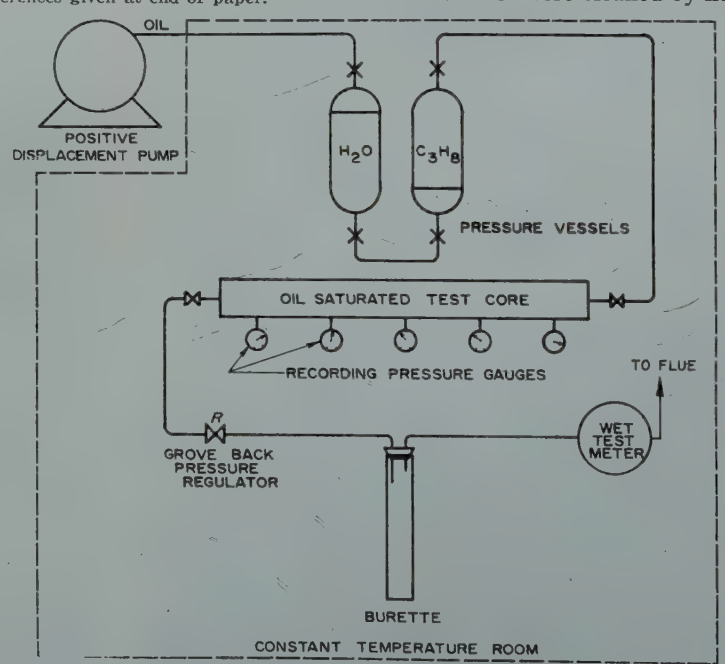

FIG. 1—SCHEMATIC FLOW DIAGRAM OF EXPERIMENTAL APPARATUS.

with acetone and pentane and drying with nitrogen. Connate water was established by saturating the cores with brine and flooding with Primol until brine production ceased. The viscous oil was replaced by the desired oil either by direct flushing or pentane extraction followed by drying and resaturation.

A positive displacement pump was used to inject liquid propane into the core at a constant rate. The rate was adjusted in each experiment to obtain the desired linear velocity in the core. A Grove back-pressure regulator on the core outlet kept the pressure within the sandstone in excess of the propane vapor pressure. After the produced liquids passed through the back-pressure regulator and dropped to atmospheric pressure, the oil was collected and measured in a burette and the propane was metered as a gas.

Accurate temperature control was necessary during those tests in which the leading edge of the propane front was followed by recording pressure drops across 1-ft increments of the model. Temperature variations were held within $\pm$ 0.1°F. The pressure measurements were made with Baldwin absolute and Statham differential strain gauges.

HORIZONTAL FLOW TESTS

The Quasi-stable Transition Zone

Constant rate oil displacements by liquid propane from horizontal, 2-in. diameter cores of various lengths revealed the following characteristics of an adverse mobility ratio, miscible fluid displacement. A zone of mixing forms between the oil and the propane which is too large to be accounted for by longitudinal molecular diffusion. The center of the mixed zone seems to travel at the average flow velocity. The rate of growth of the mixed zone continually decreases until further growth is not detectable. The quasi-stable zone is, presumably, still increasing slowly due to molecular diffusion.

The stabilization of the mixed zone was directly observed in a liquid propane displacement of a 180-cp refined oil from a 22-ft long, 2-in. diameter, Bartlesville sandstone core. The displacement was conducted at a constant flooding rate of 2 in./day. Pressures were recorded continuously at 1-ft intervals along the core, and the time at which the pressure drop across an increment began to decline signaled the first propane invasion of that increment. A typical sample of the data obtained during the experiment is shown in Fig. 2. The pressure drop across an increment is plotted as a function of the calendar date. The time at which propane invasion of this particular 1-ft increment of the core began is precisely defined.

The location of the farthest propane advance, as a function of time, can be combined with the volume injected at any time to give the curve shown in Fig. 3. In this figure, the propane penetration beyond its position in a piston-like displacement is shown. It will be seen that the propane, after a high initial penetration rate, slows down and finally moves essentially at the injection rate. The horizontal portion of the curve represents the part of the experiment in which piston-like displacement was achieved and the length of the mixed zone between the oil and the propane was quasi-stable.

Fig. 4 shows the propane concentration in the effluent plotted as a function of the propane injected. The distance between the 100 per cent oil concentration and the 100 per cent propane concentration in the effluent is the length of the quasi-stable transition zone.

The pressure profiling technique for detecting the stabilization of the mixing zone could not be used in the low-viscosity oil experiments because the pressure gradients were too small. An alternate technique requiring multiple experiments proved satisfactory. The zone was known to be nearly stable when the same length of transition zone, as measured by effluent analysis, resulted from similar experiments made in cores of different length. A typical set of data is shown in Fig. 5 where quasi-stable zones 12.5 ft in length were observed in both 10- and 18-ft cores when 1.3-cp oil was displaced by liquid propane at a rate of 8.5 in./day.

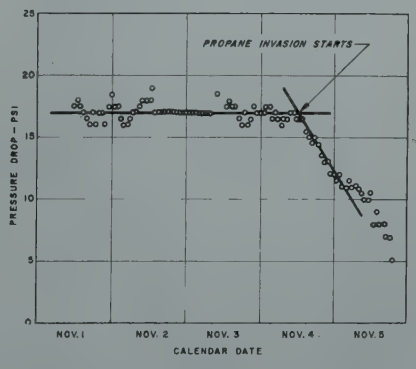

Fig. 2—Propane Tracing by Pressure Measurement.

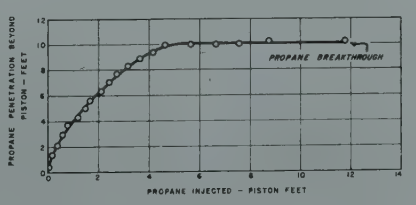

Fig. 3—Propane Penetration into 180-cp Oil. Rate—2in./day; Core—2 in. × 22 ft, Bartlesville Sandstone.

The Effect of Core Material

The effect of core material variation on the length of the stable transition zone was determined by displacing Soltrol-C by propane at a rate of 2.0 $\pm$ 0.1 in./day in Bandera, Bartlesville and Torpedo sandstones. These materials have permeabilities of 10, 50, and 1,500 md, respectively. The detailed properties of the core materials are given in Table 1, and the properties of the fluids used are given in Table 2. The lengths of the quasi-stable transition zones measured in these three sandstones ranged from 6.5 to 7.0 ft. Thus, for the materials tested, this zone size is practically independent of the core material.

The Effect of Oil Viscosity

The effect of oil viscosity on the length of the quasi-stable transition zone was measured by displacing various oils from Bartlesville sandstone cores at 2 in./day. Fig. 6 presents the results of these tests and shows that the length of the transition zone increases as the oil viscosity increases.

The Effect of Injection Rate

The effect of injection rate on the quasi-stable, transition zone length

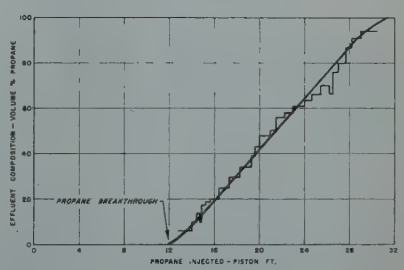

Fig. 4—Effluent Composition—Propane Displacing 180-cp Oil. Rate—2 in./day; Core—2 in. × 22 ft, Bartlesville Sandstone.

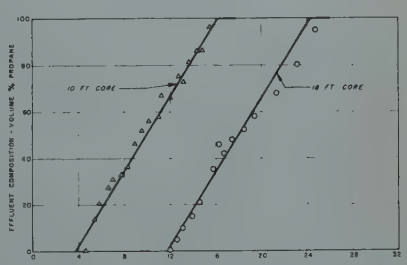

Fig. 5—Quasi-stable Transition Zones Produced from Cores of Different Length. Rate—8.5 in./day; Cores—2 in. Diameter Bandera Sandstone.

TABLE 1—SUMMARY OF CORE PROPERTIES

Core Material	Dry Air Permeability (md)	Porosity (per cent)	Connate Water (per cent PV)
Bandera Sandstone	10	15	33
Bartlesville Sandstone	50	22	35
Torpedo Sandstone	1,500	27	27

TABLE 2—SUMMARY OF FLUID PROPERTIES

	Viscosity at 75° F	Density at 75° F gm/ml
Propane	0.1	.497
Soltrol	1.3	.785
Primol	160.0	.890
Bright Stock	3,000.0	—

was measured in Bandera sandstone cores by displacing Soltrol-C with propane at rates ranging from 2 to 16 in./day. These rates cover the range ordinarily found in the field. The experimental results (Fig. 7) show that the zone length increases as the injection rate increases.

The Effect of Core Diameter

The effect of core diameter on the zone length was investigated by displacing 180-cp oil by liquid propane at a rate of 2 in./day from a piece of Bartlesville sandstone (6 in. in diameter and 36 ft in length) and comparing the results with a previous test run under the same conditions in a 2-in. diameter model. The 6-in. diameter core was formed by joining two 18-ft models with a short piece of 1/16-in. diameter tubing. The progress of the propane through the core was followed by measuring incremental pressure drops along the core. Unlike the experiment in the 2-in. core in which the propane formed a nearly stable 20-ft transition zone, the mixing zone in the 6-in. core did not stabilize within the available core length.

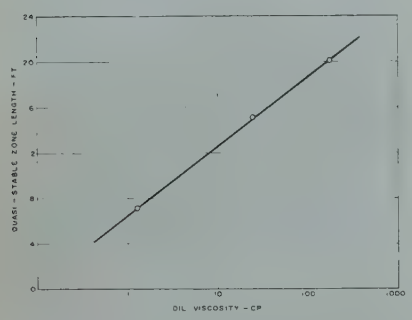

FIG. 6—EFFECT OF OIL VISCOSITY ON QUASI-STABLE ZONE LENGTH. PROPANE DISPLACING OIL FROM 2-IN. DIAMETER BARTLESVILLE SANDSTONE AT 2 IN./DAY.

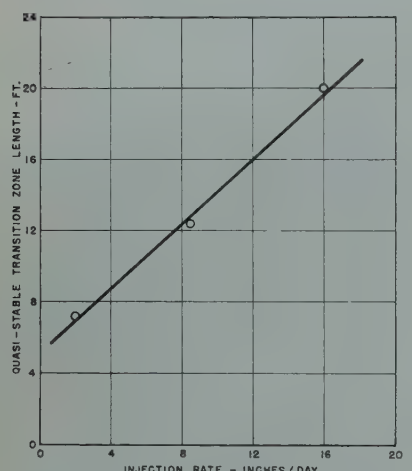

FIG. 7—EFFECT OF INJECTION RATE ON THE LENGTH OF THE QUASI-STABLE TRANSITION ZONE. PROPANE DISPLACING SOLTROL-C FROM 2 IN. × 18-FT BANDERA SANDSTONE.

To see if gravity segregation was a major factor in the behavior of the 6-in. diameter model, a test was made in which adding carbon tetrachloride to the propane reduced the density difference between the oil and solvent to 0.1 from 0.38 gm/ml. The results of these two tests were very similar and are plotted in Fig. 8 together with the results of the comparable test in the 2-in. diameter core.

In spite of the complications introduced in these tests by joining cores with small diameter flow lines and adding carbon tetrachloride to the propane, several facts are obvious. These are as follows: (1) under test conditions, increasing the core diameter from 2 to 6 in. caused a drastic increase in the length of the mixed zone, and (2) there is some indication that gravity segregation was not a significant factor in this increase.

It is believed that variations in permeability are a prime factor in this apparent effect of diameter on miscible fluid displacement. Even small permeability variations would initiate fingering and channeling of the less viscous propane. Due to the highly adverse mobility ratio, once oil is by-passed by solvent there is very little pressure gradient to cause it to flow. The primary mechanism of recovery of the by-passed oil is probably molecular diffusion. Thus, the poorer performance in the large diameter model indicates that the distance across which diffusion must occur probably increases as the model diameter increases.

VERTICAL FLOW TESTS

If oil is being displaced vertically downward by solvent and fingering exists at the front, the vertical pressure gradient in the solvent finger can be expected to be equal to the vertical pressure gradient in the oil immediately surrounding the finger. This pressure gradient equality is expressed by

$$\frac{\rho_s}{1{,}033} - \frac{V_s f \mu_s}{k_s} = \frac{\rho_o}{1{,}033} - \frac{V_o f \mu_o}{k_o}, \quad \ldots\ldots\ldots\ldots (1)$$

where ρ_o, (ρ_s) is oil (solvent) density, gm/ml; V_o, (V_s) is oil (solvent) flow velocity within the porous medium, cm/sec; f is porosity; μ_o, (μ_s) is oil (solvent) viscosity, cp; and k_o, (k_s) is permeability of oil (solvent) containing portion of rock, darcies.

The first term on each side of Eq. 1 expresses the contribution of the fluid density to the pressure gradient in units of atm/cm. The second term is the pressure gradient consumed by flow as given by the Darcy equation. Solving Eq. 1 for V_s gives

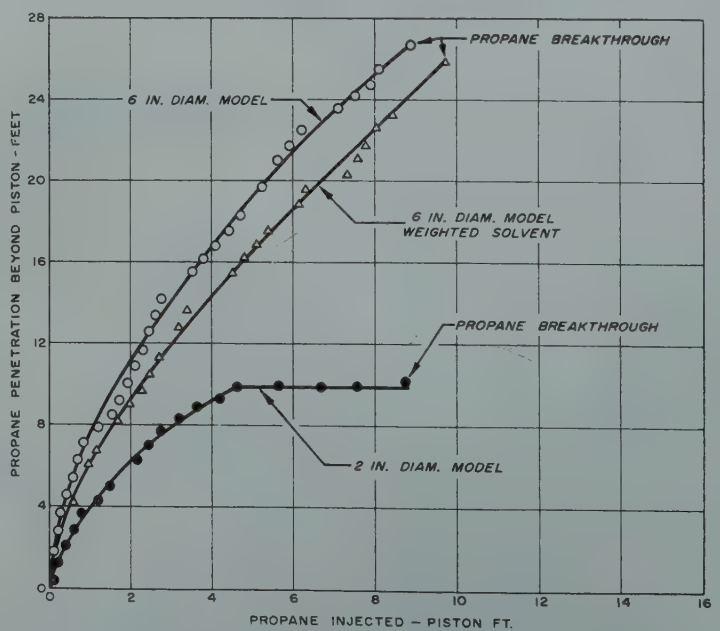
PROPANE BREAKTHROUGH
6 IN. DIAM. MODEL
6 IN. DIAM. MODEL WEIGHTED SOLVENT
PROPANE BREAKTHROUGH
2 IN. DIAM. MODEL
PROPANE PENETRATION BEYOND PISTON - FEET
PROPANE INJECTED - PISTON FT.

FIG. 8—EFFECT OF CORE DIAMETER ON PROPANE PENETRATION INTO 180-CP OIL. RATE—2 IN./DAY, BARTLESVILLE SANDSTONE.

$$V_s = V_o(k_s/k_o)(\mu_o/\mu_s) - (k_s/1{,}033 f\mu_s)(\rho_o - \rho_s) \quad . \quad . \quad . \quad . \quad . \quad . \quad . \quad . \quad . \quad . \quad (2)$$

Substituting $V_s = V_o = V$ and rearranging gives,

$$V = (\rho_o - \rho_s)/1{,}033\, f(\mu_o/k_o - \mu_s/k_s) \quad . \quad . \quad . \quad . \quad . \quad . \quad . \quad . \quad . \quad . \quad (3)$$

Solving Eq. 3 for V gives the maximum flow velocity for stable displacement. At higher flow velocities, fingers will form and grow. At lower velocities, fingers previously formed at higher velocities will shrink and disappear. This equation is similar to one developed by Hill[7].

Five tests were made in which propane displaced oil vertically downward through 2-in. diameter, 9-ft Torpedo sandstone cores. The viscosity of the displaced oil and the injection rate were varied. The results of the tests are given in Table 3. The mixed zone lengths as determined by effluent analysis are listed in Column 4 and show two distinct differences between the Soltrol-C and 25-cp oil tests. First, at corresponding rates the mixed zone lengths for the more viscous oil displacements are longer than those for the less viscous tests. Second, the zone length in the less viscous oil displacement decreases with increasing velocity while the length in the more viscous oil displacement increases with increasing velocity. The explanation for this apparently contradictory behavior is evident from the comparison of information listed in Columns 6 and 7, which shows that longitudinal molecular diffusion alone can account for the mixed zone lengths in the less viscous oil tests but not in the more viscous tests. The diffusional penetration of propane was calculated by standard techniques for a propane concentration of 0.1 volume per cent. Previously measured values for the effective diffusivity in Torpedo sandstone of propane into Soltrol-C and 25-cp oil were 0.8 and 0.08 cm²/day, respectively. The rates in the less viscous tests were well below the rate at which fingering would be expected according to Eq. 3. If any portion of the Torpedo sandstone had a permeability lower than 940 md, fingering would be expected according to Eq. 3 even at 2 in./day, the lowest rate used in the more viscous oil tests. It is believed that the Torpedo sandstone used in these tests was sufficiently heterogeneous to fulfill this condition.

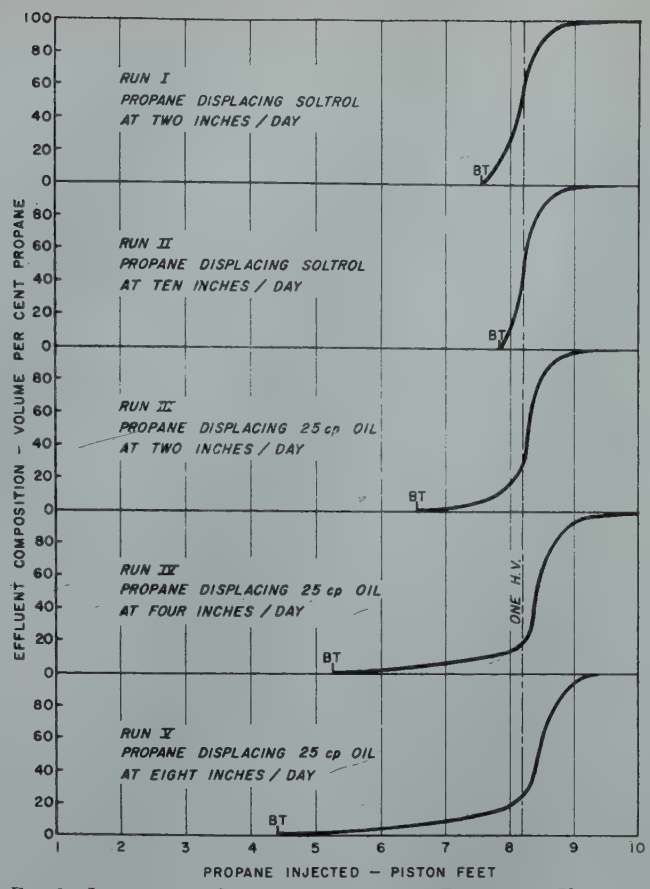

FIG. 9—LENGTH AND COMPOSITION OF MIXED ZONES FROM VERTICAL TORPEDO SANDSTONE CORES.

The analysis of the effluent from the vertical cores for the five experiments is shown in Fig. 9. The propane concentration in the outflowing stream is shown as a function of the piston position of ideal displacement. The figure shows that lengthening of the mixed zone in the more viscous displacements takes place principally in the oil-rich region.

CONCLUSIONS

The experiments made with the test cores in a horizontal position showed that, of all parameters investigated, variations in core diameter had the greatest effect on the length of the mixed zone between oil and solvent. From this work, the following conclusions may be drawn.

1. Under test conditions, increasing core diameter from 2 to 6 in. caused a drastic increase in the length of the mixed zone.

2. Test results obtained on small laboratory models cannot be extended directly to the field.

From the experiments made with the test cores in a vertical position, the following conclusion is made. Those reservoirs which have properties allowing a high degree of gravity drainage can be exploited efficiently by a miscible-type process. Furthermore, these tests have indicated that Eq. 3 is probably valid for indicating when these conditions exist.

TABLE 3—VERTICAL FLOW TEST RESULTS
(Torpedo Sandstone)

Run	Oil	Injection Rate (in./day)	Mixed Zone Length (ft)	Elapsed Time Until Breakthrough (days)	Propane Penetration at Breakthrough (ft)	
					Experimental	Calculated for Diffusion Alone
1	Soltrol-C	2	1.45	47.4	0.7	0.8
2	Soltrol-C	10	0.82	10.3	0.4	0.4
3	25-cp oil	2	2.10	43.1	1.7	0.3
4	25-cp oil	4	4.00	.....	.....	.....
5	25-cp oil	8	5.10	.....	.....	.....

REFERENCES

1. Everett, J. P., Gooch, F. W., Jr., and Calhoun, J. C., Jr.: *Trans.* AIME (1950) **189,** 215.
2. Henderson, J. H., Gove, N. B., Ledbetter, H. J., and Griffith, J. D.: *Trans.* AIME (1953) **198,** 33.
3. Offeringa, J., and van der Poel, C.: *Trans.* AIME (1954) **201,** 310.
4. von Rosenberg, D. V.: *AIChE Jour.* (March, 1956) **2,** 55.
5. Hall, H. N., and Geffen, T. M.: *Trans.* AIME (1957) **210,** 48.
6. Koch, H. A., Jr., and Slobod, R. L.: *Trans.* AIME (1957) **210,** 40.
7. Hill, S.: *Chemical Engineering Science* (1952) **1,** 247. ★★★

Effect of Flow Rate on Paraffin Accumulation in Plastic, Steel, and Coated Pipe

F. W. JESSEN
MEMBER AIME
JAMES N. HOWELL*

THE UNIVERSITY OF TEXAS
AUSTIN, TEX.

INTRODUCTION

The accumulation of paraffin deposits in tubular goods has been recognized as a major production problem since the inception of the petroleum industry. This problem is not limited to any particular geographical area nor is it limited to a specific type of crude oil.[1] Generally speaking, "paraffin" deposition pertains to the deposition of any predominately organic material in flow lines, and possibly even at the sand face, which would hamper the production of oil. In some fields, a continuous effort is required to remove deposits of paraffin and in order to accomplish this, many unique methods have been devised. The best solution to this problem, however, is to prevent the formation of such deposits. One method which has been tried in a number of fields is the use of plastic pipe.

The purpose of this investigation is to compare the relative effectiveness of several plastic materials to aid in the reduction or prevention of paraffin accumulations in surface flow lines.

COMPOSITION OF PARAFFIN DEPOSITS

By definition, paraffin deposits are those materials which are insoluble in crude oil at the prevailing producing conditions of temperature and pressure. Such deposits[2,3] usually consist of small particles of petroleum wax intermixed with resins, asphaltic material, and crude oil. They may also contain a variety of foreign materials such as sand, silt, water, various metal oxides, sulfates and carbonates of iron, barium, and calcium.

The petroleum waxes deposited in flow strings usually consist of both a "hard" and a "soft" wax fraction. These waxes are largely aliphatic hydrocarbons with smaller amounts of aromatic and naphthenic compounds. Nathan[4] has classified the hard and soft wax fractions. The aliphatic hydrocarbons present are those of high molecular weight with high melting points. Reistle[3] pointed out that these high molecular weight compounds first separate from the oil due to a sharp decrease in solubility as the melting point increases.

The identification of the resins and asphaltic materials rests, at present, on an arbitrary solubility procedure. Under certain conditions, materials which are insoluble in pentane (ASTM D-893) are defined as resins and asphalts. Subgrouping of these materials is made on decreasing solubility in benzene and carbon disulfide.[5]

Shock[1] found some correlation between the solvent response and the pentane insoluble content of paraffins; higher pentane insoluble fractions are less soluble in any of the commonly used commercial solvents.

PARAFFIN CONTROL METHODS

The methods used in oil fields to prevent and remove paraffin accumulations can be grouped into four general classes: (1) operative methods, (2) physical methods, (3) chemical methods, and (4) combination of any of these. Operative methods attempt to prevent the formation of paraffin deposits while the other methods are concerned primarily with the removal of these deposits.

Plastic coated pipe has been used for a number of years to prevent corrosion in wells, and in many instances paraffin deposits have been greatly reduced. Field observations have indicated that plastic coated pipe not only reduced paraffin accumulation but in some cases eliminated deposition completely; however, data are needed to demonstrate the relative effectiveness of plastic materials.

Deposition Apparatus

The pipe used to determine the effect of velocity on rates of deposition was ¾- and 2-in. nominal diameter, and 5 ft in length. Steel, butyrate, rigid PVC, kralastic resin-type plastic pipes, epoxy coated pipe, PVC lined glass fiber pipe, and aluminum pipe were tested. Steel pipe was used as a control.

Fig. 1 is a schematic diagram of the apparatus showing the relative position of the separate units making up the equipment.

In order to facilitate the installation and removal of the test pipes in the apparatus, O-ring seals capable of sustaining pressures of 50 psi were provided at each end.

Test pipes were submerged in a cold water bath maintained at or below room temperature by circulating water through copper cooling coils packed in ice. A hot water bath equipped with immersion-type heaters, stirrers, and a thermoregulator was used to maintain the temperature of the oil prior to introduction into the piping manifold. The capacity of the oil reservoir was 30 gal.

A 33-gal/min centrifugal pump, capable of producing turbulent flow velocities in the test pipes, was used to circulate the oil through the system when using ¾-in. pipe; and a 70-gal/min centrifugal pump was used in later tests using 2-in. pipe. A by-pass arrangement made it pos-

Original manuscript received in Society of Petroleum Engineers office Aug. 20, 1957. Revised manuscript received March 11, 1958.

*Presently associated with The Shell Oil Co., New Orleans, La.

[1]References given at end of paper.

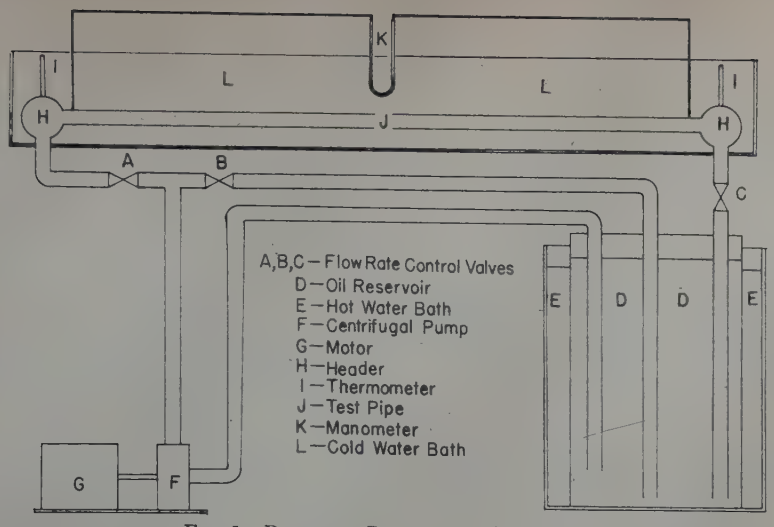

FIG. 1—PARAFFIN DEPOSITION APPARATUS.

sible to obtain variations in flow rates through the piping system and also provided a means for stirring the oil in the oil reservoir, thus assuring uniform temperature of the oil and complete solution of the paraffin.

Pressure differentials across the test sections were measured by means of a manometer and a meter was used to check the total flow. Fig. 2 shows the arrangement of the piping.

CONTACT ANGLE APPARATUS

Conact angle measurements were made using Stegemeier's procedure.[6]

CLOUD POINT

The cloud point of the crude oils was determined using the method described by Howell and Jessen.[7]

DETERMINATION OF RATES OF PARAFFIN DEPOSITION

As shown in Fig. 1, flow rates were controlled by Valves B and C. During low rates of flow, part of the fluid circulated by the pump was bypassed through Valve B into the oil reservoir. Proper manipulation of Valves B and C made it possible to adjust the flow to any described rate into the upstream header and through the individual test sections of pipe. Prior to each run, Valve A was closed and Valve B opened in order to circulate the oil and thus dislodge and dissolve from the bottom of the storage reservoir any paraffin that may have settled between runs.

Velocity of flow in the test pipe sections was determined by measuring the pressure differential across each pipe with a manometer.

The difference between the inlet and outlet oil temperatures was only 1 to 2° F. This difference in temperature was constant throughout each experimental run. Undoubtedly the temperature drop at the inner wall of the pipes was much greater.

At the completion of a run, which normally required a period of about three hours, the test pipes were removed from the apparatus and the deposited paraffin (which was rather uniform throughout the section) was cleaned from the pipes by pushing a tight fitting rubber "squeegee" through the pipes several times. Normal pentane was used to transfer the paraffin from beakers into standard ASTM 100-ml centrifuge tubes. An excess of pentane was then added to bring the total volume to 100 ml. The mixture was shaken and centrifuged at 1,500 rpm for 20 minutes. The solid separated was recorded as the paraffin deposited.

Before the test pipes were reinstalled for the next run, they were thoroughly cleaned inside and out by wiping several times with a kerosene-saturated rag and then dried with a clean, dry cloth.

DISCUSSION OF RESULTS

Rates of deposition were obtained by using kerosene and two refined microcrystalline waxes (Figs. 3 and 4) in order to determine the effects of the melting point upon the rate of deposition. Greatest deposition at any velocity for the two systems took place in the solution containing the paraffin with the lowest melting point. At first, this appears contrary to what might be expected since the greatest deposition more likely should take place in the solution containing the highest melting point paraffin; that is, the least soluble.

Although both solutions were prepared so as to have the same cloud point of 120° F, there was a marked difference in the concentration of paraffin due to the solubilities in kerosene. A kerosene solution saturated with wax having a melting point of 200° F contained 0.57 gm/100 ml at 120°F, while a solution saturated with wax having a melting point of 186° F contained 2.01 gm/100 ml at the same temperature. Upon cooling to 110° F, the temperature at which these runs were made, the solubilities decreased to 0.23 and 0.84 gm/100 ml, respectively, for the 200 and 186° F melting point waxes. The change of solubility from 120 to 110° F results, therefore, in 0.34 gm/100 ml free wax in suspension in the solution containing the 200° F melting point wax compared to 1.17 gm/100 ml for the 186° F melting point wax solution. Therefore, the difference in the rates of deposition for these two solutions may be attributed to the concentration of free wax in suspension at the temperature

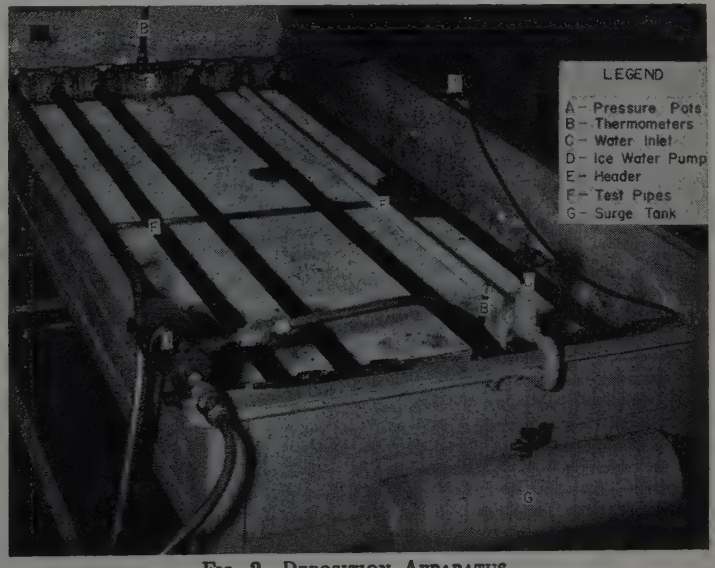

FIG. 2—DEPOSITION APPARATUS.

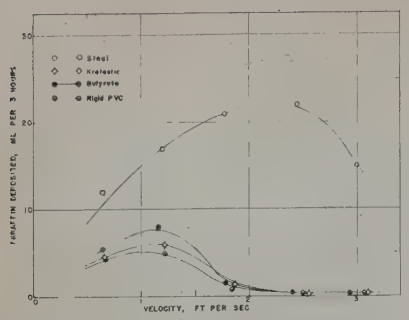

FIG. 3—EFFECT OF VELOCITY ON RATE OF DEPOSITION FOR 200° F MP WAX IN KEROSENE AT 110° F. CLOUD POINT OF SOLUTION IS 120° F.

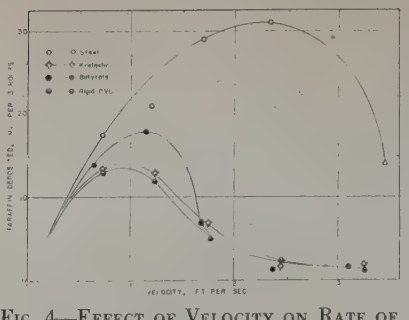

FIG. 4—EFFECT OF VELOCITY ON RATE OF DEPOSITION FOR 186° F MP WAX IN KEROSENE AT 110° F. CLOUD POINT OF SOLUTION IS 120° F.

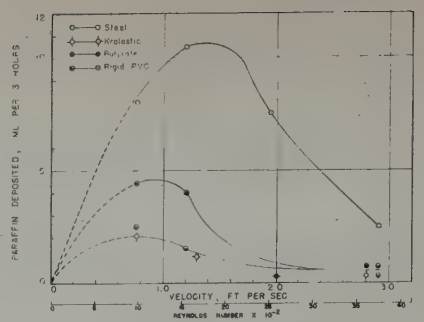

FIG. 5—EFFECT OF VELOCITY ON RATE OF DEPOSITION OF BIG FOOT CRUDE OIL AT 102° F AND WATER TEMPERATURE OF 70° F.

of the runs. Predictions concerning possible paraffin accumulation in oilfield tubular goods must be based upon a thorough knowledge of the concentration and melting point of the paraffin in solution in the crude oil.

Rate of paraffin deposition vs flow rate was determined for crude oils from several fields* known to deposit paraffin. Analyses of the different oils are given in Table 1.

The rate of paraffin deposition at all velocities and temperatures was greatest in steel pipe but considerable paraffin deposition was also found in butyrate pipe. The least amount of paraffin accumulation was noted in the rigid PVC and kralastic plastic pipes. All plastic pipe tested showed less tendency for accumulation of paraffin than did steel or aluminum pipe.

In experiments using 2-in. pipe size, the 3-M plastic lined fiber glass pipe showed consistently lower quantities of deposit than did the other resin-coated pipe or plastic pipe. Again, more deposition occurred in the steel and aluminum pipe, although the wide variation apparent when using ¾-in. pipe was not noted.

A gradual increase in the rate of paraffin deposition was obtained with increased velocity, the maximum rate being reached when the flow changed from viscous to turbulent flow. At higher velocities the rate of deposition decreased rapidly. Results of flow tests on Big Foot crude oil, Fig. 5, illustrate the typical shape of the curves obtained.

At Reynolds numbers greater than 4,000, the plastic pipe surfaces were free of any paraffin accumulation; however, since some oil remained on the inside of the pipes after draining, the paraffin was determined analytically in the manner previously described.

Figs. 6 and 7 show paraffin deposition-velocity curves for crude oil from well No. DU-24-1, located on the eastern end of the Delhi field, which was reported experiencing considerable difficulty from paraffin deposits. Figs. 8 and 9 represent data on crude oil taken from well No. DU-184-1, located in the western portion of the field. These wells are equipped with Tube-Kote tubing in order to reduce paraffin accumulation which occurs at low withdrawal rates.[8] At rates above 200 BOPD rapid deposition of paraffin in the tubing is prevented. A rate of 200 BOPD through 2-in. tubing corresponds to a Reynolds number of 2,042 which is the approximate velocity at which turbulent flow begins. Maximum rate of deposition was obtained in the laboratory at a velocity corresponding to a Reynolds number of 846. A Reynolds number of 2,042 determined from the field data (200 BOPD through 2-in. tubing) corresponds to a linear velocity of 1.45 ft/sec in the laboratory apparatus. At this linear velocity, paraffin deposition in the ¾-in. plastic pipe was substantially reduced.

The tendency for the rate of paraffin deposition to increase with velocity to velocities approximately equal to the transition velocity (Reynolds number 1,980) is clearly shown in Fig. 10 on the curve for the rate of paraffin deposition in the steel pipe. Not much difference was noted in the relative effectiveness in any of the plastic pipes for reducing deposition.

High viscous drag was obtained at relatively low flow rates in the more viscous fluids. This may account for the fact that no deposition was obtained from the Oklahoma crude oil which had a viscosity of 29.5 cp compared to an average of 4 cp for the other crude oils examined. Even though a velocity of 5.1 ft/sec, corresponding to a Reynolds number of 678, was reached, no measurable deposition was obtained from this crude oil when flowing through ¾-in. pipe. Use of 2-in pipe enabled test observations over a range of Reynolds numbers up to 1,500. In every instance, paraffin deposition was substantially lower than with other crude oils used in the flow experiments through 2-in. pipe. Whether this smaller amount of accumulation was occasioned solely by the viscous drag is questionable since this particular crude oil had a much higher asphaltic content.

Two possible mechanisms for paraffin deposition may be considered. First, deposition of paraffin from the crude oil at the pipe walls; that is, growth of the paraffin particles in place at pipe surfaces, and second, paraffin crystals may occur or be present in the oil and these may subsequently be deposited. The first mechanism for paraffin deposition seems to be the controlling factor since the greatest deposition was obtained from the crude oils when maintained at temperatures above or near the cloud point prior to cooling in the piping system. For example, the temperature of the oil in Fig. 8

*Big Foot field, Frio County, Tex.; Delhi field, Franklin Parish, La.; Howard Glasscock field, Howard County, Tex.; Prentice field, Yoakum County, Tex.; and the Camp N. W. pool, Okla.

TABLE 1 — ANALYSIS OF CRUDE OILS

	Camp NW Pool	Howard Glasscock	Delhi DU-184-1	Delhi DU-24-1	Big Foot	Prentice
Gravity, °API (60°F)	26	29.9	40	39	38	30.5
Viscosity, cp (100°F)	29.5	10.2	3.2	4.3	4.0	3.5
Cloud Point, °F	78	97	105	119	113	97
Paraffin Wax, per cent	2.11	3.39	4.35	4.32	3.79	2.21
Pentane Insolubles, per cent	3.73	1.18	1.37	1.19	0.552	3.41
Benzene Insolubles, per cent	0.157	1.128	0.00	0.00	0.0018	0.115
Melting Point of Paraffin Wax, °F	125	121	122	128	120	133

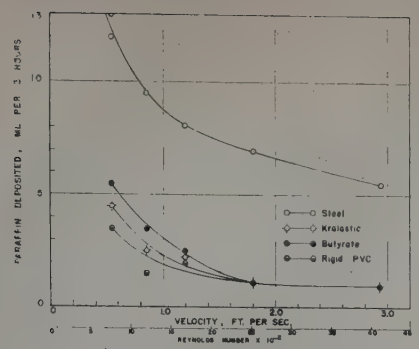

FIG. 6—EFFECT OF VELOCITY ON RATE OF DEPOSITION OF DELHI DU-24-1 CRUDE OIL AT 108° F AND WATER TEMPERATURE OF 70° F.

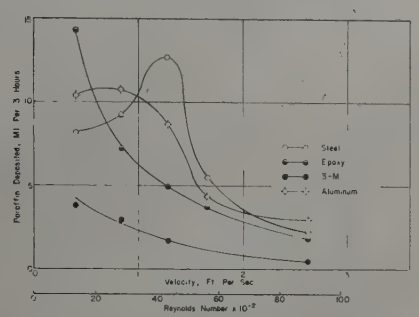

FIG. 7—EFFECT OF VELOCITY ON RATE OF DEPOSITION (2-IN. PIPE) OF DELHI DU-24-1 CRUDE OIL AT 105° F AND WATER TEMPERATURE OF 70° F.

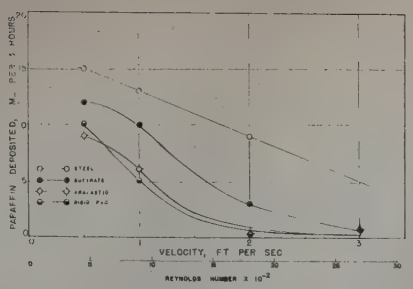

FIG. 8—EFFECT OF VELOCITY ON RATE OF DEPOSITION OF DELHI DU-184-1 CRUDE OIL AT 106° F AND WATER TEMPERATURE OF 80° F.

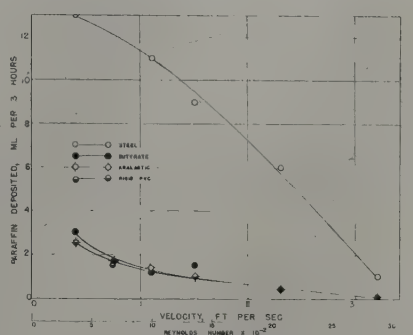

FIG. 9—EFFECT OF VELOCITY ON RATE OF DEPOSITION OF DELHI DU-184-1 CRUDE OIL AT 90° F AND WATER TEMPERATURE OF 70° F.

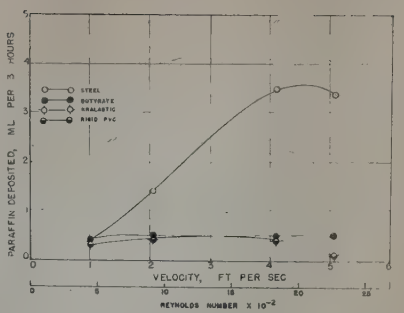

FIG. 10—EFFECT OF VELOCITY ON RATE OF DEPOSITION OF HOWARD GLASSCOCK CRUDE OIL AT 85° F AND WATER TEMPERATURE OF 70° F.

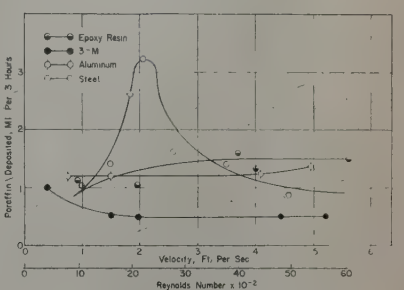

FIG. 11—EFFECT OF VELOCITY ON RATE OF DEPOSITION (2-IN. PIPE SIZE) OF HOWARD GLASSCOCK CRUDE OIL AT 88° F AND WATER TEMPERATURE OF 70° F.

was 1° F higher than the cloud point, while in Fig. 9 the temperature of the oil was 15° F below the cloud point before introduction into the test pipes. In the first instance deposition could be possible only by growth of the paraffin particles at pipe walls, while in the latter case deposition would be possible by both mechanisms. There was not much difference in rates of paraffin deposition within the steel pipe at these temperatures; however, approximately three times as much paraffin was deposited in the plastic pipes at low velocities when the temperature of the oil was maintained slightly above the cloud point as when the oil temperature was controlled at 15° F below the cloud point even though the final oil temperature was 16° F lower.

There is, of course, another factor which may explain this difference in the quantity of paraffin deposited, namely, the lower heat conductivity of the plastic pipe. That is, when operating with oil temperatures above the cloud point, initial solid phase occurrence is postulated to take place directly on the wall of the pipe and, therefore, it is reasonable to expect that deposition should be much greater on steel than on plastic. On the other hand, when operating at initial oil temperatures below the cloud point, a solid phase is presumed present and deposition would not be dependent solely on the cooling at the inner walls of the pipe, but may be controlled by the adhering tendency of the solid on the exposed surface.

Occurrence of a gradual build-up in the deposition rate may be explained on the basis of mass transfer of the paraffin particles. Less paraffin is carried past a given point on the pipe wall in a specified interval of time during low rates of flow. As the flow is increased, more and more paraffin is carried by the moving oil stream providing a greater opportunity for deposition upon the surface of the pipe. However, the viscous drag exerted by the stream tends to remove the accumulation and, at high velocities, becomes equal to or may exceed the shear stresses within the deposited paraffin and literally tear the paraffin deposit apart. Paraffin deposited at high rates of flow was observed to be considerably harder than paraffin deposited at lower rates of flow. The increase in both viscous drag and shearing stresses in the paraffin deposits at high rates of flow possibly accounts for the gradual decrease in deposition rate at higher velocities rather than a sudden and complete elimination of paraffin deposition as would be expected if the shearing stress of the paraffin remained constant and was suddenly exceeded by the viscous drag of the flow stream.

The maximum rate of deposition with the steel pipe took place at somewhat higher velocities than for plastic pipes. To explain this apparent irregularity, it is necessary to consider the role of thermal conductivity of the pipe materials and the effects of temperature upon the adherence of the paraffin deposited.

The loss of temperature of the crude oil is the major factor involved in the formation of paraffin deposits. The hardness of the paraffin deposit is also directly related to the temperature of the deposit. Paraffin deposits are more crystalline at lower temperatures and, therefore, are more tightly held together. Steel, having the greatest thermal conductivity of any of the materials tested, permitted the greatest loss of heat from the oil and, as a result, a lower temperature at the inner pipe wall. The attainment of higher velocities in the steel pipe before the the maximum rate of deposition was reached may further be explained by the variation in physical characteristics of the paraffin deposit formed.

The relative wettability of the butyrate, kralastic, and rigid PVC plastic materials as reflected by the contact angle measurements on the plastic materials of saturated solutions of different melting point paraffins in kerosene is shown in Fig. 14. The contact angle increased slightly with the melting point of the paraffin wax in solution, indicating that crude oils

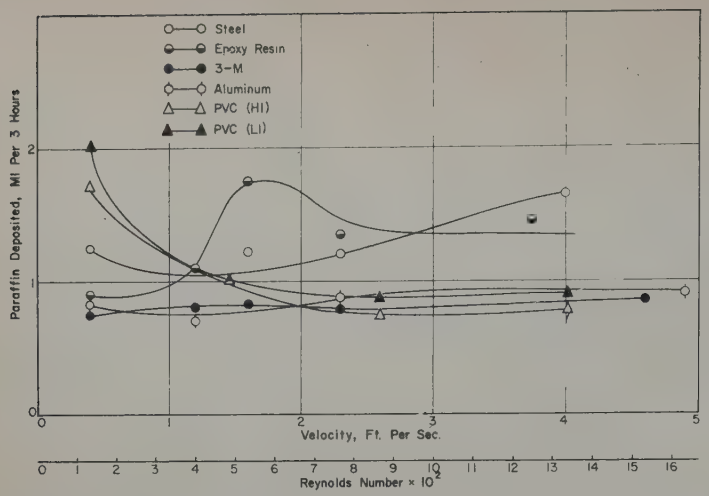

FIG. 12—EFFECT OF VELOCITY ON RATE OF DEPOSITION (2-IN. PIPE SIZE) OF OKLAHOMA CRUDE OIL, DENNY NO. 2, AT 85° F AND WATER TEMPERATURE OF 65° F.

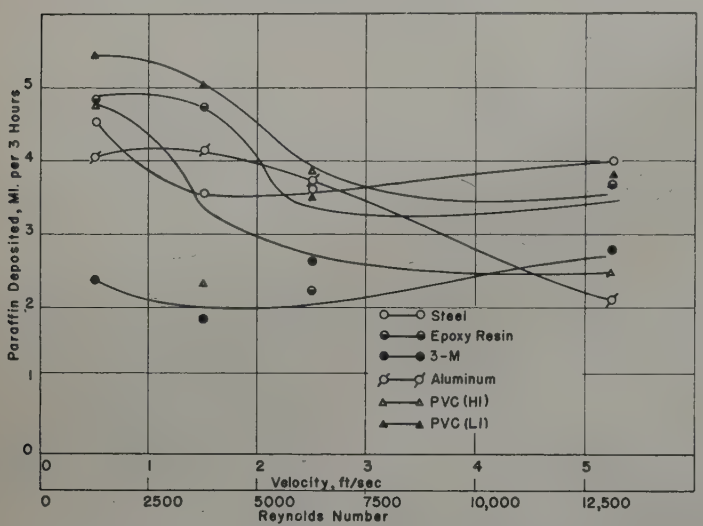

FIG. 13—EFFECT OF VELOCITY ON RATE OF DEPOSITION OF PRENTICE FIELD CRUDE OIL AT 87° F AND WATER TEMPERATURE OF 67° F.

containing high melting point paraffin waxes would tend to wet these materials to a lesser degree than crude oils containing lower melting point paraffins.

Table 2 shows the relative wettability of various plastic materials by the crude oils used in this investigation. The contact angles of these crude oils agreed fairly well with those found when using a saturated solution of kerosene and 122° F melting point paraffin wax. The variation in contact angle on any one plastic material was small except for the Camp N. W. pool and the Howard Glasscock field crudes. This may be due to differences in composition since the latter crudes contained greater amounts of asphaltic constituents.

CONCLUSIONS

1. Rate of paraffin deposition in steel pipe varies with flow rate, reaching a maximum just prior to change from viscous to turbulent flow and decreasing with increased turbulence.

2. Deposition of paraffin on various kinds of plastic pipe shows the same general pattern with regard to flow rate. The amount of accumulation noted, however, was appreciably less in every instance.

3. When cooling of the oil from temperatures above the cloud point takes place at the pipe wall, an increased deposit of paraffin results, as compared with that obtained when the oil has been cooled below the cloud point prior to circulation through the pipe.

4. The rate of accumulation of paraffin on plastic pipe seems related to the degree of wettability by the crude oil.

5. Although plastic pipe may not entirely eliminate paraffin deposits, the rate of deposition on plastic pipe or plastic lined pipe is substantially lower than on steel or aluminum pipe.

TABLE 2 — CONTACT ANGLES OF CRUDE OILS ON PLASTIC MATERIALS

Fluid	PVC	Kralastic	Butyrate	3-M	Epoxy Resin
Delhi DU-24-1	17	Spreads	Spreads	Spreads	Spreads
Delhi DU-184-1	17	Spreads	Spreads	Spreads	Spreads
Camp NW Pool	20	12	10	Spreads	Spreads
Howard Glasscock	17	9	2-3	Spreads	Spreads
Big Foot	17	Spreads	Spreads	Spreads	Spreads
Water	74	70	52	68	53

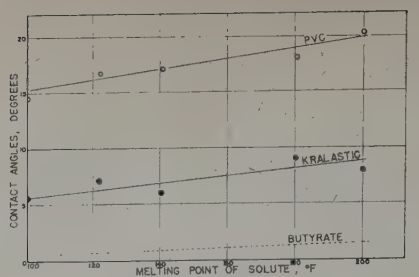

FIG. 14—VARIATION OF CONTACT ANGLES FOR SATURATED KEROSENE SOLUTIONS AT 75° F.

ACKNOWLEDGMENTS

The authors wish to acknowledge with thanks the help of Wesley W. Smith and Charles Fraser who assisted with some of the laboratory work. They are indebted to the Carlon Products Corp., Cleveland, Ohio, for financial assistance on the project and for permission to publish the results presented in this paper.

REFERENCES

1. Shock, D. A., Sudbury, J. D., and Crockett, J. J.: "Studies of the Mechanism of Paraffin Deposition and Its Control," *Jour. Pet. Tech.* (Sept., 1955) **VII**, No. 9, 23.
2. Bowers, E. F., and Renfro, H.: "Paraffin Removal in South Texas," *Oil and Gas Jour.* (1947) **46**, No. 4, 134.
3. Reistle, C. E., Jr.: "Paraffin and Congealing-Oil Problems," *Bull.*, USBM (1927) **7**, 348.
4. Nathan, C. C.: "Solubility Studies on High Molecular Weight Paraffin Hydrocarbons Obtained from Petroleum Rod Waxes," *Trans.* AIME (1955) **204**, 151.
5. Gruse, W. A., and Stevens, D. R.: *Chemical Technology of Petroleum*, McGraw-Hill Book Co., Inc., N. Y. (1942) Chap. XXII.
6. Stegemeier, G. L.: "The Relationship of Relative Permeability to Contact Angles," MS Thesis, The University of Texas (Jan. 1954).
7. Howell, J. N., and Jessen, F. W.: "Determination of the Viscosity-Temperature Relationship for Crude Oils with the Ultra-Viscoson," *Trans.* AIME (1956) **207**, 330.
8. Private communication: L. F. Ellison, Sun Oil Co., Delhi, La. (April 12, 1955).

★★★

The Effect of Partial Penetration on Pressure Build-Up in Oil Wells

ROBERT G. NISLE

PHILLIPS PETROLEUM CO.
BARTLESVILLE, OKLA.

ABSTRACT

The classic theory of pressure build-up in shut-in oil wells as developed by Horner and van Everdingen is based on two-dimensional radial symmetry in the well-reservoir system. Such symmetry does not exist in the case of a well which partially penetrates the producing formation. As a result of this lack of symmetry the use of the classic theory in such cases become questionable.

In this paper the mathematical theory has been extended to include the case of partially penetrating wells. Numerical solutions illustrating the application of the equations are presented. The effect of partial penetration on pressure build-up is shown by a comparison of synthetic pressure build-up curves derived from the numerical solution of the equation for partially penetrating wells for various degrees of penetration. It is shown that partial penetration is detectable from the characteristic shape of the pressure build-up curve and that formation productivity may be calculated from the pressure build-up data in a manner identical to that described by the classic theory.

INTRODUCTION

The use of pressure build-up data on shut-in oil wells is a well-established technique for the measurement of reservoir productivity. The work of Horner[1] and van Everdingen[2] is well known. Since the publication of their pioneering work, others[3,4] have elaborated and extended the technique. These authors have dealt exclusively with the case of wells that completely penetrate the producing formation. Two-dimensional radial symmetry is achieved, thereby, and the problem is greatly simplified.

This ideal situation is seldom encountered in practice. But, in spite of this, the technique is often employed anyway. The question, therefore, arises: how much confidence can be placed in the results of such calculations when the data are taken on wells that only partially penetrate the producing formation? It is the purpose of this work to answer this question. Only the single-phase fluid case will be considered.

van Everdingen[2] has presented a rigorous solution of the two-dimensional case, but because of mathematical complexity, this solution has not proved to be particularly useful. Horner[1] utilized Kelvin's point source solution in two dimensions and showed that it is a sufficiently good approximation for oil reservoir studies.

The geometry of the well and the producing formation is illustrated in Fig. 1. Geometrically the formation may be described as an infinite slab. The infinite slab is defined as the solid (the porous medium in this case) bounded by two parallel planes. Thus, the slab extends to very great distances in both the positive and negative directions of two of the coordinate axes, but is finite in

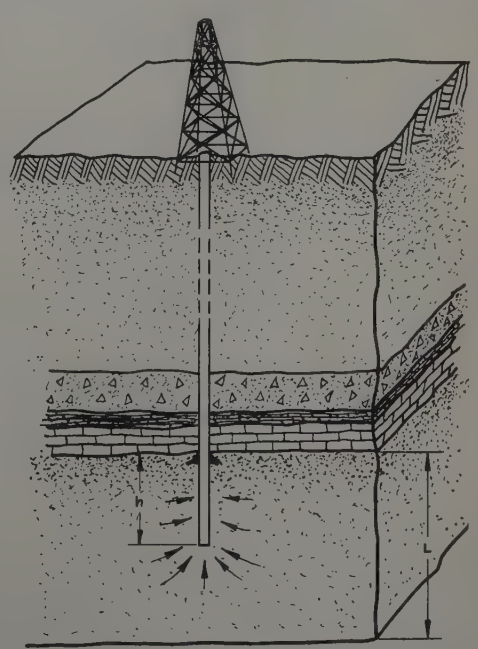

FIG. 1 — A PARTIALLY PENETRATING WELL IN A RESERVOIR INFINITE IN EXTENT IN THE HORIZONTAL PLANE BUT HAVING A FINITE THICKNESS.

Original manuscript received in Society of Petroleum Engineers office Sept. 10, 1957. Revised manuscript received March 7, 1958.

[1]References given at end of paper.

Discussion of this and all following technical papers is invited. Discussion in writing (three copies) may be sent to the offices of the *Journal of Petroleum Technology*. Any discussion offered after Dec. 31, 1958, should be in the form of a new paper.

both the positive and negative directions along the third coordinate axis.

The partially penetrating well problem has been studied by Muskat[7] for steady-state conditions. He calculated steady-state pressure distributions and steady-state productive capacity in barrels per day. These results give no indication of the influence of partial penetration on the pressure build-up curve which is a transient effect. Another approach is, therefore, required. The point source concept, as previously indicated, is sufficiently accurate, and therefore, provides an alternative approach.

MATHEMATICAL DERIVATION

The mathematical derivation of the equation for a partially penetrating well in an infinite slab will begin with Fourier's equation in three dimensions. This equation in turn is derivable from the continuity equation, the equation of state, and Darcy's equation. This derivation is readily available.[7]

Solution of the Basic Differential Equation

The basic differential equation[5] is

$$\frac{\partial^2 p}{\partial x^2} + \frac{\partial^2 p}{\partial y^2} + \frac{\partial^2 p}{\partial z^2} = \frac{1}{K}\frac{\partial p}{\partial t}, \quad . \quad . \quad . \quad . \quad . \quad . \quad . \quad (1)$$

where

$$1/K = \frac{cuf}{k}. \quad . \quad . \quad . \quad . \quad . \quad . \quad . \quad . \quad . \quad . \quad . \quad (2)$$

The solution of Eq. 1 in the Kelvin[6] instantaneous point source form is given by Carslaw and Jaeger[5]. It is

$$\triangle p(r,t) = \frac{Q}{8fc(\pi Kt)^{3/2}} exp^{\frac{-r^2}{4Kt}}. \quad . \quad . \quad . \quad . \quad . \quad (3)$$

From this equation, all other solutions are obtainable by summation.

Continuous Infinite Line Source

This case is solved by finding the solution for the instantaneous infinite line source first. Integration of the latter solution over the interval 0 to T yields the required continuous infinite line source solution. The first integration is carried out over the space variable.

Suppose the line to be parallel to the z-axis, passing through the point (x', y'). Then, if $r^2 = (x - x')^2 + (y - y')^2 + (z - z')^2$, it follows from Eq. 3 that

$$\triangle p(\text{line}) = \frac{Q}{4fc(\pi Kt)} exp^{-\frac{(x-x')^2 + (y-y')^2}{4Kt}} \frac{1}{\sqrt{\pi}} \int_{-\infty}^{\infty} exp^{-\frac{(z-z')^2}{4Kt}} \frac{dz'}{\sqrt{4Kt}} \quad . \quad . \quad . \quad . \quad . \quad . \quad (4)$$

The integral in Eq. 4, together with the normalizing factor $\frac{1}{\sqrt{\pi}}$ is the error function and is equal to one. Hence,

$$\triangle p(\text{line}) = \frac{Q}{4fc(\pi Kt)} exp^{-\frac{(x-x')^2 + (y-y')^2}{4Kt}}. \quad . \quad . \quad . \quad . \quad . \quad . \quad . \quad . \quad . \quad . \quad (5)$$

Eq. 5 is the solution for the instantaneous infinite line source.

Let the liquid withdrawal rate be q. Then the total withdrawal, Q, in the time interval, dt, is

$$Q = q\,dt. \quad . \quad . \quad . \quad . \quad . \quad . \quad . \quad . \quad . \quad . \quad . \quad (6)$$

Let $r^2 = (x - x')^2 + (y - y')^2$, and substitute Eq. 6 in Eq. 5. Then, the solution for the continuous infinite line source is,

$$\triangle p(\text{line}) = \frac{q}{4fc\pi K}\int_0^T exp^{-\frac{r^2}{4K(T-t')}} \frac{dt'}{(T-t')}. \quad . \quad . \quad . \quad . \quad . \quad . \quad . \quad . \quad . \quad . \quad . \quad (7)$$

In order to integrate Eq. 7 make the coordinate transformation

$$v = \frac{r^2}{4K(T-t')}.$$

Then Eq. 7 may be written,

$$\triangle p(\text{line}) = \frac{q}{4\pi Kfc}\int_{\frac{r^2}{4KT}}^{\infty} \frac{\varepsilon^{-v}}{v}\,dv \quad . \quad . \quad . \quad . \quad . \quad (8)$$

The integral in Eq. 8 is by definition the exponential integral (Ei). q in Eq. 8 is the withdrawal rate per unit length of the infinite line source, hence $qh = -q_o$ if $-q_o$ = total withdrawal over a portion, h, of the infinite line source. If the pressure in the medium is other than zero, Eq. 8 may be written,

$$p(r,t) = P_o - \frac{q_o u}{4\pi kh} Ei\left(\frac{-cufr^2}{4kT}\right), \quad . \quad . \quad . \quad (9)$$

where Eq. 2 has been substituted for $1/K$. This is the form of the solution used by Horner.

Instantaneous Line Source of Length, h, in a Semi-Infinite Medium

The development is based on Eq. 3. The geometry is shown in Fig. 2. The positive z direction is taken as shown and the boundary condition to be satisfied is $\frac{dp}{dz} = 0$ in the bounding plane, taken to be the x-y plane. The introduction of the positive image $(+Q)$ of length h and located as shown in Fig. 2 accomplishes this result. The solution of this case is obtained by integrating along this line source from $-h$ to $+h$, thus,

$$\triangle p(h) = \frac{Q}{4fc(\pi Kt)} exp^{-\frac{(x-x')^2 + (y-y')^2}{4Kt}} \frac{1}{\sqrt{\pi}} \int_{-h}^{+h} exp^{-\frac{(z-z')^2}{4Kt}} \frac{dz'}{\sqrt{4Kt}}. \quad . \quad . \quad . \quad . \quad . \quad . \quad . \quad . \quad (10)$$

Introduce the coordinate transformation,

$$v = \frac{z - z'}{\sqrt{4Kt}},$$

then

$$\triangle p(h) = -\frac{Q\ exp^{-\frac{(x-x')^2 + (y-y')^2}{4Kt}}}{4fc(\pi Kt)} \frac{1}{\sqrt{\pi}} \int_{\frac{z+h}{\sqrt{4Kt}}}^{\frac{z-h}{\sqrt{4Kt}}} exp^{-v^2}\,dv. \quad . \quad . \quad . \quad . \quad . \quad . \quad . \quad . \quad . \quad . \quad (11)$$

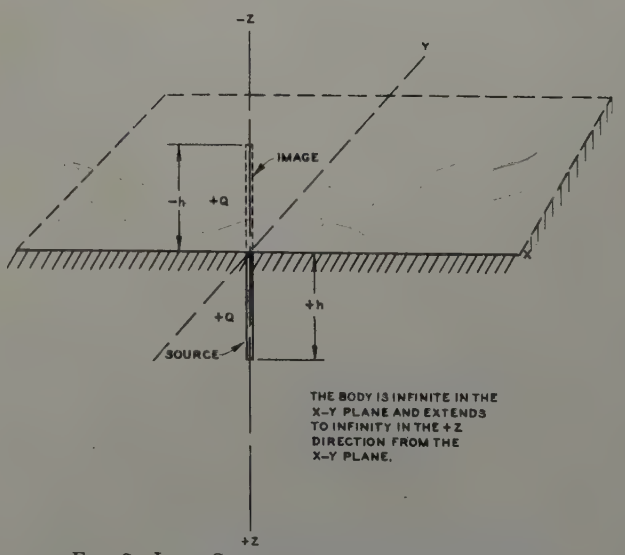

Fig. 2—Line Source in Semi-Infinite Medium.

This integral involves error functions and the solution may, therefore, be expressed formally, thus,

$$\Delta p(h) = \frac{Q}{4fc(\pi Kt)} exp^{\frac{-r^2}{4Kt}} \tfrac{1}{2}\left[erf\frac{z+h}{\sqrt{4Kt}} - erf\frac{z-h}{\sqrt{4Kt}}\right]. \quad . \quad . \quad . \quad . \quad . \quad . \quad . \quad . \quad . \quad . \quad . \quad . \quad . \quad (12)$$

Values of the error functions in the parentheses may be obtained from published tables[5]. In Pierce's tabulation the error function has been normalized over the interval 0 to ∞. Hence, the factor, ½, has been introduced into Eq. 12 in order to permit the use of published tabulations.

Partially Penetrating Source in an Infinite Slab

This case is treated by a straight forward extension of the previous development. The geometry is shown in Fig. 3. The boundry conditions are

$$\frac{dp}{dz} = 0 \text{ at } z = 0 \text{ and } z = L \quad . \quad . \quad . \quad . \quad . \quad . \quad . \quad . \quad . \quad . \quad . \quad . \quad . \quad (13)$$

In order to satisfy conditions (Eq. 13) an infinite set of images is required as indicated in Fig. 3. Each of these images may be represented by an integral of the type used in Eq. 10. Each of these integrals may be transformed as in Eq. 11 and the results expressed as in Eq. 12. The solution of the partially penetrating case may therefore be written directly from the results of the previous case.

$$\Delta p = \frac{Q\ exp^{\frac{-r^2}{4Kt}}}{4fc(\pi Kt)}\left[\tfrac{1}{2}\left(erf\frac{z+h}{\sqrt{4Kt}} - erf\frac{z-h}{\sqrt{4Kt}}\right)\right.$$

$$+\tfrac{1}{2}\sum_{n=1}^{n=\infty}\left(erf\frac{z-(2nL-h)}{\sqrt{4Kt}} - erf\frac{z-(2nL+h)}{\sqrt{4Kt}}\right.$$

$$\left.\left. + erf\frac{z+(2nL+h)}{\sqrt{4Kt}} - erf\frac{z+(2nL-h)}{\sqrt{4Kt}}\right)\right]. \quad (14)$$

Eq. 14 is the solution of the case of an instantaneous source of length, h, in an infinite slab of thickness, L.

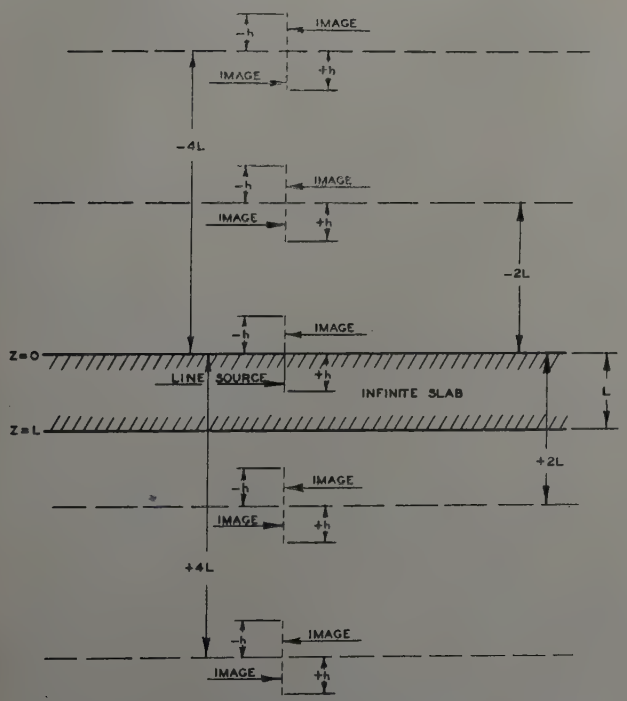

Fig. 3—Partial Penetraton in an Infinite Slab.

It will be noted that when $h = L$, the integration extends from $-\infty$ to $+\infty$. This case reduces in the limit to Eq. 4. Furthermore, this situation assures the convergence of the summation in Eq. 14. The error function is known to converge for the limits $-\infty$ and $+\infty$. The summation must converge, therefore, because the summation involves only a non-overlapping sequence of finite limits lying within the range $-\infty$ to $+\infty$.

Partially Penetrating Continuous Line Source

This case is solved as in the previous cases by integration from time equal zero to time equal T. Here again the solution may be written directly from the previous results. For convenience certain substitutions are made as follows. $b = h/L$, $d = z/L$, $\frac{1}{K} = \frac{cuf}{k}$, B = formation volume factor, and q_o = surface volume production rate.

$$\Delta p(r,t) = \frac{q_o uB}{4\pi kh}\int_o^T exp^{-\frac{cuf\,r^2}{4k(T-t)}}\left[\tfrac{1}{2}\left[erf\right.\right.$$

$$\left(\frac{cuf\ (z+h)^2}{4k(T-t)}\right)^{\frac{1}{2}} - erf\left(\frac{cuf(z-h)^2}{4k(T-t)}\right)^{\frac{1}{2}}\left.\right] + \tfrac{1}{2}\sum_{n=1}^{n=\infty}$$

$$\left[erf\left(\frac{cuf(2n+b-d)^2L^2}{4k(T-t)}\right)^{\frac{1}{2}} - erf\right.$$

$$\left(\frac{cuf(2n-b-d)^2L^2}{4k(T-t)}\right)^{\frac{1}{2}} + erf\left(\frac{cuf(2n+b+d)^2L^2}{4k(T-t)}\right)^{\frac{1}{2}}$$

$$\left.\left. - erf\left(\frac{cuf(2n-b+d)^2L^2}{4k(T-t)}\right)^{\frac{1}{2}}\right]\right]\frac{dt}{T-t} \quad . \quad . \quad . \quad (15)$$

Eq. 15 is the formal representation of the integration which must be performed in order to obtain the pressure drop due to a continuous source of length, h, in an infinite slab of thickness, L. It is apparent that the analytical solution of Eq. 15 presents certain difficulties. In order to examine the effect of partial penetration on pressure build-up curves, therefore, numerical methods will be necessary. The numerical solution of Eq. 15 is treated in the following section.

NUMERICAL CALCULATIONS

It is not apparent from an examination of Eq. 15 how partial penetration affects a pressure build-up curve. In order to investigate this question, numerical calculations must be employed over a suitable range of values of the parameters. The range used is more conveniently expressed if some of the terms in Eq. 15 are regrouped.

Let

$$Y = L\sqrt{\frac{cuf}{4k}}$$

$$m_1(n) = 2n + b - d$$
$$m_2(n) = 2n - b - d$$
$$m_3(n) = 2n + b + d$$
$$m_4(n) = 2n - b + d$$

and

$$F(T) = \frac{exp^{-\frac{cuf\,r^2}{4kT}}}{2T}\left[\left(erf\ Y\frac{(d+b)}{\sqrt{T}} - erf\ Y\frac{(d-b)}{\sqrt{T}}\right)\right.$$

$$+\sum_{n=1}^{n=\infty}\left(erf\frac{Ym_1(n)}{\sqrt{T}} - erf\frac{Ym_2(n)}{\sqrt{T}} + erf\frac{Ym_3(n)}{\sqrt{T}}\right.$$

$$\left.\left. - erf\frac{Ym_4(n)}{\sqrt{T}}\right)\right] \quad . \quad . \quad . \quad . \quad . \quad . \quad . \quad . \quad . \quad . \quad . \quad . \quad (16)$$

TABLE 1—PARAMETERS IN THE NUMERICAL EVALUATION OF EQ. 16

$Y = 50, 100, 200$
$b = 0.2, 0.4, 0.6, 0.8$
$d = 0.0$
$d = 0.2, 0.5$ ($b = 0.6$ only)
$r = 10$ cm, $L = 3{,}000$ cm
$\overline{Q} = 50$, $P_o = 3{,}000$ psi

The integral in Eq. 15 may now be calculated graphically by plotting $F(T)$ vs T and finding the area under the curve from 0 to T for any desired value of T. This process runs into difficulty in the region around $T = 0$. Fortunately, there is a way out. For small values of T, the term in the brackets in Eq. 16 approaches one and the integral in Eq. 15 approaches the exponential integral. For these values of T, therefore, published tables[9] may be used. For larger values of T, the exponential term in Eq. 16 approaches one when r is small. In this work, therefore, the term in brackets in Eq. 16 was calculated by the Datatron digital computer for several sets of parameters, as shown in Table 1.

Graphs of $F(T)$ vs T were constructed from these calculations and the areas under the curves between the times, T (minimum) and T were measured with a planimeter. These values of the integral, when added to the value of the exponential integral at T (minimum), give the values of the integral in Eq. 15 at the desired times, T. These values of the integral in Eq. 15, as a function of the time, T, have been designated "pressure drawdown coefficients" (D_c). D_c was plotted as a function of time and penetration ratio on large work sheets and used to construct the synthetic pressure build-up curves. An example of such a plot is given in Fig. 4.

TABLE 2—SYNTHESIS OF PRESSURE BUILD-UP CURVES

$Y = 200$ $b = 0.4$ $T = 4 \times 10^5$ sec
$\overline{Q} = 50$ $P_o = 3{,}000$ psi

Pressure Drawdown Coefficient						$\frac{\Delta T}{T + \Delta T}$
$D_c\ (T + \Delta T)$	$D_c(\Delta T)$	Diff.	ΔP	P	ΔT (Sec)	
11.02	6.63	4.39	219	2,781	600	1.49×10^{-3}
11.02	7.74	3.28	164	2,836	1,800	4.48×10^{-3}
11.04	9.83	1.21	60	2,940	24,000	5.66×10^{-2}
11.10	10.40	.70	35	2,965	90,000	1.84×10^{-1}
11.25	10.90	.35	17	2,983	300,000	4.3×10^{-1}
11.38	11.18	.20	10	2,990	600,000	6.0×10^{-1}

The pressure build-up curves are synthesized by reading D_c from the curves at time ΔT and $(T + \Delta T)$, and applying the principle of superposition. An example of such calculation is shown in Table 2. In this table $D_c\ (T + \Delta T)$ and $D_c\ (\Delta T)$ are read from the chart. Their difference is multiplied by $\overline{Q}$ to give ΔP, where $\overline{Q} = \frac{q_o u B}{4\pi k h}$. The pressure, P, is obtained by subtracting ΔP from P_o. ΔT is the assumed shut-in time and the remaining column in the table is calculated in the usual manner.

The resulting synthetic pressure build-up curves are shown in Figs. 5, 6, and 7.

Fig. 8 shows the effect of different producing times prior to shut-in, Fig. 9 shows the effect of making the measurement at different depths in the well, and Fig.

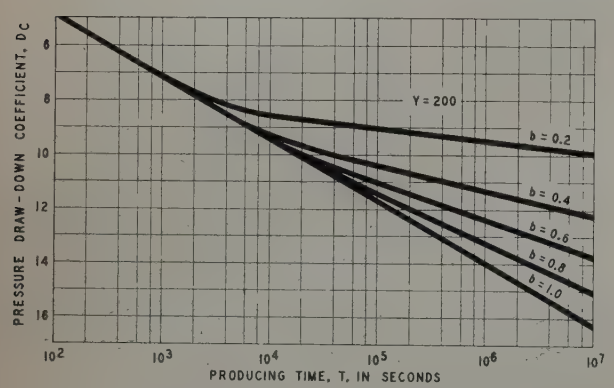

FIG. 4—PRESSURE DRAWDOWN COEFFICIENT VS TIME.

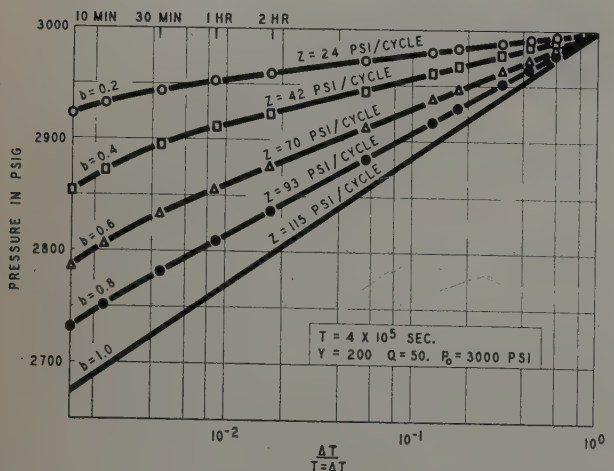

FIG. 5—SYNTHETIC PRESSURE BUILD-UP CURVES SHOWING EFFECT OF PARTIAL PENETRATION.

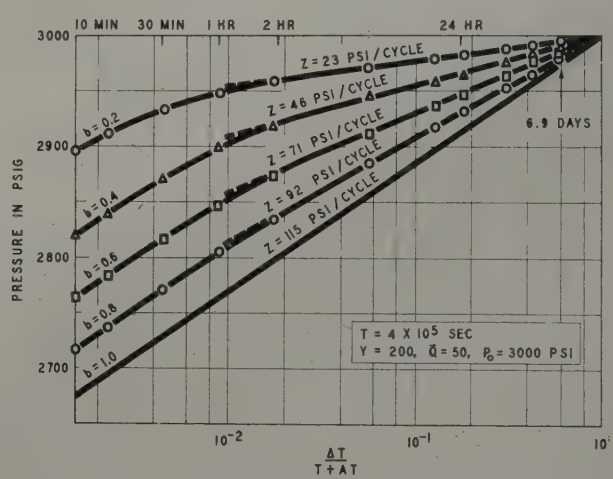

FIG. 6—SYNTHETIC PRESSURE BUILD-UP CURVES SHOWING EFFECT OF PARTIAL PENETRATION.

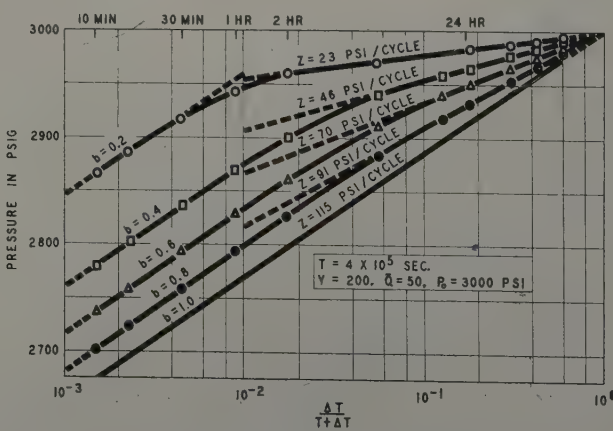

FIG. 7—SYNTHETIC PRESSURE BUILD-UP CURVES SHOWING EFFECT OF PARTIAL PENETRATION.

10 shows the effect of the quantity, $Y = L\sqrt{\frac{cuf}{4k}}$.

DISCUSSION

It will be noted that all these curves have two features in common: (1) at early times the slope of the pressure build-up curve approaches that for 100 per cent penetration, and (2) at late times the slope becomes very nearly b times the slope for 100 per cent penetration. Table 3 shows this comparison.

The curves that have been synthesized are based on the condition that the production rate per unit length of exposed formation is constant. That is, q_o/h in the term $\frac{q_o uB}{4\pi kh}$ in Eq. 15 is constant. Thus, if the early part of these curves is used in the usual way to calculate a value for kh, a value which represents the productivity of the well, not the formation, will be obtained since h is the well penetration. Formation productivity can be obtained by using a production rate adjusted for the penetration. Assume for the moment that a well is producing at some specific rate q_1, then

$$\frac{q_1}{h} L = \frac{q_1}{b} = q_L ,$$

where q_L is the production rate if the penetration were 100 per cent.

Now bZ is the penetration ratio times the slope of the early part of the build-up curve, which is shown to be the slope of the late part in Table 3. Therefore, the use of the late part of the build-up curve (slope = bZ) and the given production rate, q_1, is equivalent to introducing a correction for penetration to the production rate. Hence,

$$kL = \frac{162.5\ q_1\ B}{bZ},$$

where kL is the productivity of the formation. Therefore, one need not be concerned regarding the degree of penetration, if the formation productivity is desired, in cases where the early part is obscured by afterflow; a situation, incidentally, which is nearly universal.

If well productivity is desired, some knowledge of the penetration ratio, b, is necessary. In this case it would be desirable to make a correction for afterflow[9].

The synthesized pressure build-up curves illustrate the effect of partial penetration for the range of parameters used. For values of $L\sqrt{\frac{cuf}{4k}}$ outside the range used here, the effect of partial penetration can be deduced from the results given. Since L appears to the first power, it predominates over cuf and k which occur as square roots. But the worst conditions, as illustrated in Fig. 5, are probably due to a small L. This is just the situation when partial penetration is least likely to occur. At the other extreme, illustrated in Fig. 7, the initial straight part extends to later times. Thus, the principles discussed herein may be applied when L is large and partial penetration is most likely to occur. Furthermore, if afterflow is not present, or if present and a correction is made, and if the complete build-up curve is

TABLE 3—COMPARISON OF SLOPES OF BUILD-UP CURVES AT LATE TIMES
(All slopes in psi per cycle)

b =	0.2	0.4	0.6	0.8	1.0	Fig. No.
bZ 100 =	23	46	69	92	115	
Y = 50,	24	42	70	93		6
Y = 100,	23	46	71	92		7
Y = 200,	23	46	70	91		8

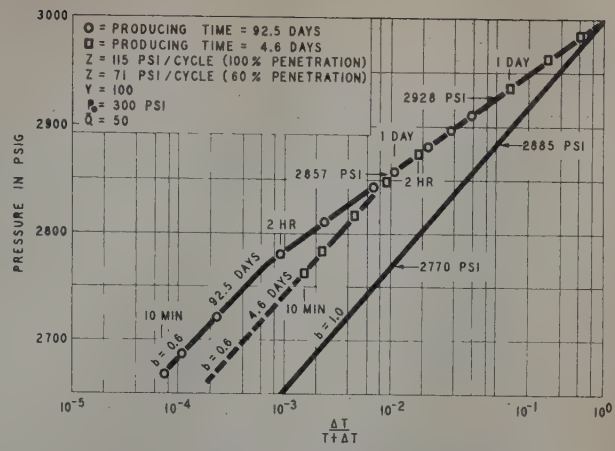

FIG. 8—SYNTHETIC PRESSURE BUILD-UP CURVES SHOWING EFFECT OF PRODUCING TIME BEFORE SHUT-IN.

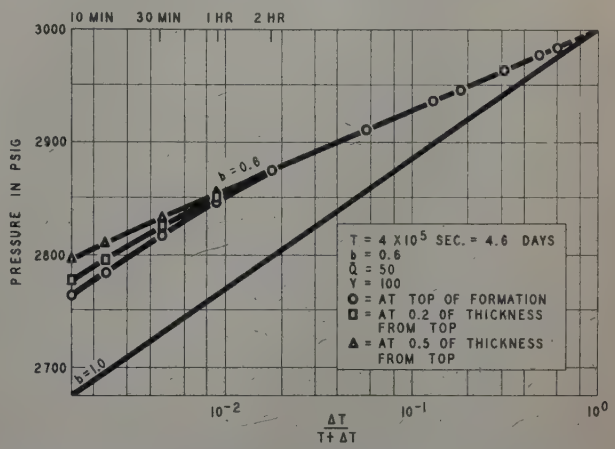

FIG. 9—SYNTHETIC PRESSURE BUILD-UP CURVES SHOWING VARIATION IN PRESSURE AT DIFFERENT LEVELS BELOW FORMATION TOP.

available, then a means is provided for calculating the penetration ratio from the ratio of the slope of the late part to that of the early part of the build-up curve. From this calculated penetration ratio and the known producing interval the effective formation thickness may be obtained by a simple calculation.

It should be noted that there are grave practical difficulties to this procedure, however. For instance, afterflow is a major obstacle even when a correction is attempted, since such a correction does not always produce the desired result. The analysis simply shows that in principle, at least, it ought to be possible to calculate the penetration ratio from build-up data.

One further point should be mentioned in connection with the use of Eq. 15. It will be noted that the pressure change varies with the z coordinate. This means that the wellbore is not at constant pressure from top to bottom. But neither is this true in an actual well, because of fluid head. In this connection the classic theory assumes a uniform wellbore pressure, whereas the pressure difference between top and bottom of the well might be as much as 50 psi or more in very thick formations. Fig. 9 shows that this situation is no more serious for the equations developed here than in the classic case.

CONCLUSIONS

On the basis of the results presented here the following conclusions are presented.

1. Partial penetration does not invalidate the use of

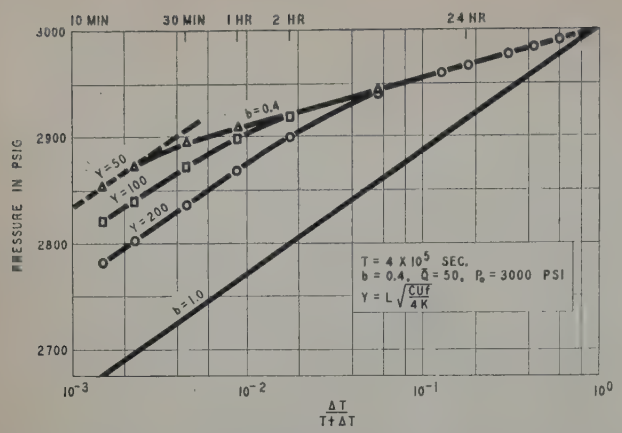

FIG. 10—SYNTHETIC PRESSURE BUILD-UP CURVES SHOWING EFFECT OF QUANTITY (Y).

the classic theory for the calculation of reservoir productivity from pressure build-up data.

2. Partial penetration does produce a characteristic shape of the pressure build-up which differs from the classic form, and this difference may be utilized to estimate the penetration ratio and hence the effective formation thickness.

NOMENCLATURE*

(All units metric unless otherwise stated.)

f = porosity
h = length of producing interval, or length of line source
L = formation thickness, or thickness of infinite slab
p = the general pressure, atmospheres
P_o = initial formation pressure, atmospheres
q = production rate per unit length of line source, or producing interval
Q = total production
r = radial coordinate, spherical or cylindrical polar
t, T = time
u = viscosity
x, y, z = cartesian coordinates
Z = slope of the straight part of the pressure build-up curve

*See AIME Symbols List in *Trans.* AIME (1956) 207, 363, for other symbol definitions.

$$b = h/L$$

$$1/K = \frac{cuf}{k}$$

$$d = z/L$$

$$\overline{Q} = \frac{q_o uB}{4\pi kh}$$

$$Y = L\sqrt{\frac{cuf}{4k}}$$

ACKNOWLEDGMENTS

The author wishes to thank the management of Phillips Petroleum Co. for permission to publish this material. In addition, the author takes this opportunity to express his appreciation in particular to those who rendered valuable assisance in the preparation of this material: to M. R. Dean who reviewed the manuscript and made many valuable suggestions, R. O. Shelton and J. D. Tucker of the Mathematical Engineering Branch of the Research and Development Dept. for their assistance in making the numerical calculations of Eq. 16, and to Morea Prentice who prepared the graphical integrations.

REFERENCES

1. Horner, D. R.: *Proc.* Third World Pet. Congress, Sec. II, E. J. Brill, Leiden (1951) 503.
2. van Everdingen, A. F.: "The Skin Effect and its Influence on the Productive Capacity of a Well," *Trans.* AIME (1953) **198,** 171.
3. Thomas, G. B.: "Analysis of Pressure Build-Up Data," *Trans.* AIME (1953) **198,** 125.
4. Miller, C. C., Dyes, A. B., and Hutchinson, C. A., Jr.: "The Estimation of Permeability and Reservoir Pressure from Bottom-Hole Pressure Build-Up Characteristics," *Trans.* (1950) **189,** 91.
5. Carslaw, H. S., and Jaeger, J. C.: *Conduction of Heat in Solids,* Oxford Univ. Press, London (1947).
6. Kelvin, Lord: Mathematical and Physical Papers, **II,** 41.
7. Muskat, M.: *Physical Principles of Oil Production,* McGraw-Hill Book Co., N. Y. (1949) Sec. 5.4 and 5.5, Chap. 4.
8. Peirce, B. O.: *A Short Table of Integrals,* Ginn and Co., 3rd Ed., Boston (1929) 116.
9. *Tables of Sine, Cosine, and Exponential Integrals,* Federal Works Agency (WPA) Supt. of Doc., Washington, D. C., **I, II.**
10. Gladfelter, H. E., Tracy, G. W., and Wilsey, L. E.: *Oil and Gas Jour.* (May 23, 1955) 126. ★★★

Hydraulic Fracturing – Fracture Flow Capacity vs Well Productivity

H. K. van POOLLEN
MEMBER AIME
JOHN M. TINSLEY
CALVIN D. SAUNDERS
MEMBER AIME

HALLIBURTON OIL WELL CEMENTING CO.
DUNCAN, OKLA.

ABSTRACT

In the past few years much consideration has been given to the evaluation of the effect of hydraulic fracturing on the productivity of wells. Generally, these studies included the evaluation of fracturing materials, fracture extension and formation damage due to the use of various fracturing fluids. Only little consideration has been given to the characteristics, and in particular the flow capacity, of the fracture itself and its effect on well productivity.

This paper presents the results of laboratory investigations pointed toward the evaluation of the efficiency of various fractures with special emphasis on the flow capacity of these fractures. Data presented in this paper are the results of both an electrical model study and physical testing. Under consideration are (1) effect of overflush, (2) premature production of well after treatment, (3) "tailing-in" with coarse sand near the end of the treatment, (4) effect of propping agent size and concentration, (5) reduction in effective fracture permeability caused by formation caused by formation fines, silt and clays, and (6) effect of various fluids on formation strength and competency.

The results of this investigation indicate that the flow capacity of a fracture is affected by any or all of the various parameters mentioned above. The authors believe that a better understanding and utilization of these factors should result in more efficient formation fracturing.

Original manuscript received in Society of Petroleum Engineers office July 15, 1957. Revised manuscript received April 8, 1958. Paper presented at 32nd Annual Fall Meeting of Society of Petroleum Engineers in Dallas, Tex., Oct. 6-9, 1957.

INTRODUCTION

Hydraulic fracturing has become almost a standard practice of many companies for stimulating production from old and new wells. Although most companies utilize this service, techniques of application vary widely between companies and areas.

Probably too often when a well in an area responds favorably to a particular technique all future wells in the same area are treated in a similar manner. Possibly a modification of the technique would result in a further production increase. Variables, of which many are extremely difficult to evaluate from field results, hamper the selection of procedure changes.

Attempts are being made by a number of organizations to analyze statistically treating techniques from production data. This is a very worthy and necessary approach but very possibly laboratory investigations may aid in evaluating some of the variables which tend to affect the results of a fracturing treatment. Some of the factors cannot be studied from practical field experience and only laboratory tests can show the possibilities which might exist.

One of the factors which appears to be of major concern today is the flow capacity of the created fracture and how it can be changed. Papers on this general subject have been primarily concerned with the size of propping agent and the extent of fracture. Papers have also been written on the possible permeability damage to formations by fracturing fluids. In addition, it might be possible that another type of flow restriction is prevalent. This would be a restriction of flow through a sand-packed fracture caused by foreign materials integrating within the propping agent.

This paper presents preliminary data obtained in an attempt to evaluate the effect of some factors affecting flow through sand-packed fractures.

No attempt is being made to offer a fracturing technique adaptable to all areas and conditions, but to furnish data tending to show the possible effects which might be caused by variations in procedures and materials.

PROPPING AGENT PERMEABILITIES

A hydraulically induced fracture containing sand as a propping agent may theoretically be classified as a packed-sand system. The flow of fluids through such packed systems has been the subject of much research. Although there have been numerous methods proposed for the evaluation of such systems, most writers agree on the general properties affecting their flow capacity or permeability. These properties include porosity, particle size, sphericity and the roughness of the particle. In some methods of evaluation the particle size and sphericity terms are combined to produce an equation which is a function of the surface area of the particles.

In this study the permeability of various fracturing sands was both measured and calculated.

The apparatus for the permeability measurements consisted of a 52-in. Lucite tube with a 2.5-in. ID. A screen and drain plug were fitted in the bottom of this tube to retain and hold the sand in place while allowing fluid flow. Two pressure taps consisting of thin, highly perforated

tubes were extended across the entire cross section of the flow area. These pressure taps were spaced 25 in. apart with the lower tap being 5 in. from the bottom of the test section. A constant fluid head device was fitted to the upper portion of the flow column.

The procedure used for the evaluation of sand permeability was as follows. The Lucite tube was filled with dry sand. Special care was taken to insure that even distribution of all sized grains was obtained through the depth of the tube. After filling the column, the sand was packed with the aid of a high-speed vibrator. A vacuum was then placed on the upper portion of the column and air free water was allowed to flow upward into the sand body at a very slow rate. The amount of water needed to fill the voids in the sand body was used for determining the porosity of the bed. After complete saturation of the column, water was allowed to flow under constant head downward through the test section. The permeability was calculated using Darcy's law:

$$K = \frac{\mu L Q}{A \Delta P}, \quad . \quad . \quad . \quad . \quad (1)$$

where μ is viscosity of fluid, cp; Q is flow rate, ml/sec; ΔP is pressure drop, atm; L is length over which pressure drop was measured, cm; A is cross sectional area of sand column, cm^2; and K is permeability, darcies.

The calculated value of permeability was obtained with the use of the Kozeny-Carman equation:

$$K = \frac{\phi^3}{k S_o^2 (1-\phi)^2}, \quad . \quad (2)$$

where K is permeability, cm^2 (K in darcies $= 1.01234 \times 10^8 \times K$ in cm^2); k is Kozeny-Carman constant; S_o is specific surface area, cm^2/cm^3; and ϕ is porosity, fraction.

Extensive research has been done in evaluating the Kozeny-Carman constant. According to Carman[1] the constant k can be written in the form,

$$k = k_o \left\{\frac{L_e}{L}\right\}^2, \quad . \quad . \quad . \quad . \quad (3)$$

where k_o is a "shape factor" believed by Carman to have a probable average value of 2.5. The term $\left\{\frac{L_e}{L}\right\}^2$ has been commonly referred to as the "tortuosity" by Rose and Bruce[2]. Carman has suggested that $\left\{\frac{L_e}{L}\right\}^2$ has a value of 2.0 in all unconsolidated porous media. From Eq. 3 if k_o has a value of 2.5 and $\left\{\frac{L_e}{L}\right\}^2$ a value of 2.0 the value of k will be 5.0. From results of work done by Wyllie and Gregory[3] the measured values of k appear to be in reasonable accord with the value of 5.0 ± 10 per cent for aggregates of irregular particles or spheres at an experimental porosity of about 40 per cent. The preceding constants were used in the following calculations.

The surface areas were calculated using the equation,

$$S_o = \frac{6}{d_m} = \frac{6}{\text{mean diameter, cm}}, \quad (4)$$

and for mixed sizes,

$$S_o = X_1 (S_o)_A + X_2 (S_o)_B + \ldots X_n (S_o)_n. \quad . \quad . \quad . \quad . \quad . \quad (5)$$

These equations for surface area are based on the use of spheres; however, it was necessary to use a sphericity factor with the angular sands. Sphericity is defined as the surface area of a sphere having a volume equal to that of the particle divided by the surface area of the particle. The sphericity of most angular particles is stated by Brown[4] to have a value of 0.7 to 0.8.

Table 1 shows the screen analyses together with the calculated and measured permeabilities of typical propping sands. It will be noted in some cases there is quite a large difference between the measured and calculated value of permeability. This is probably due to the method used in evaluating the surface areas of the sand since none of these sands can truly be classified as perfect spheres. It may also be seen upon examination of these sands that the roundness or sphericity factor decreases somewhat in the smaller grain sizes.

Table 2 shows the reduction in permeability of packed columns containing 20- to 40-mesh sand to which was added various amounts of a fine Mill Creek sand. As may be seen in these results, small amounts of fine sand appreciably reduced the original permeability of the packed column.

TABLE 2—SCREEN ANALYSES AND PERMEABILITY RESULTS OF BLENDED 20-40 AND FINE MILL CREEK SANDS

	Per Cent Passed and Retained		
Screen Size	20-40 Round Sand	10% Fine Mill Creek Sand	20% Fine Mill Creek Sand
On 20	0.25	0.33	0.39
Through 20 on 25	4.25	7.57	
	36.55		
Through 25 on 30		21.66	20.68
Through 30 on 40	49.00	64.19	52.68
Through 40 on 50	12.80	5.26	4.29
Through 50 on 60	0.85	0.50	0.59
Through 60 on 70		0.52	1.23
	0.35		
Through 70 on 80		0.52	1.56
Through 80 on 100	—	1.25	4.37
Through 100 on 140	—	1.18	4.44
Through 140 on 200	—	0.29	1.90
Through 200 on 325	—	0.04	0.22
Through 325 on Pan	—	0.01	0.09
Sphericity	1.00	1.00[a]	1.00[a]
		0.80[b]	0.80[b]
Porosity	0.35	0.31	0.28
Calculated Permeability—darcies	157.00	73.50	30.90
Measured Permeability—darcies	121.00	71.50	25.80

[a]Used for all particles larger than 60 mesh.
[b]Used for all particles smaller than 60 mesh.

EFFECT OF FRACTURES ON PRODUCTIVITY

In the following discussion and analyses the following assumptions are made. The formation is homogeneous and isotropic (constant permeability, constant porosity); the fluids are incompressible and homogeneous; the system is in a steady state of flow with a radial drainage boundary, and the effect of gravity is ignored. These assumptions will definitely limit the numerical results of this study; however, certain trends will be similar to those in actual field cases, and the effects of fracture contamination, overflush, and sand gradation can nevertheless be demonstrated.

From an analysis of electrical model studies, trends were derived concerning the effect of various fractures on productivity[5]. The results of

TABLE 1—SCREEN ANALYSES AND PERMEABILITY RESULTS

	Per Cent Passed and Retained					
Screen Size	8-12 Angular	10-20 Angular	10-20 Round	10-30 Round	20-40 Round	40-60 Round
Through 6 on 8	32.60	0.11	—	—	—	—
Through 8 on 10	51.50	5.05	—	—	—	—
Through 10 on 12	15.35	21.35	0.15		—	—
Through 12 on 14	0.40		3.80		—	—
		69.59				
Through 14 on 16	—	—	13.47	12.97	—	—
Through 16 on 18	—	2.70	29.50		—	—
Through 18 on 20	—	0.67	34.73		0.25	—
Through 20 on 25	—	—	13.08			—
				79.60	36.55	
Through 25 on 30	—	—	0.70			0.70
Through 30 on 40	—	—	3.65	6.83	49.00	30.15
Through 40 on 50	—	—	1.05	0.50	12.80	39.18
Through 50 on 60	—	—	0.15	—	0.85	12.40
Through 60 on 70	—	—	—	—		8.10
					0.35	
Through 70 on 80	—	—	—	—		3.40
Through 80 on 100	—	—	—	—	—	6.32
Sphericity	0.80	0.80	1.00	1.00	1.00	1.00
Porosity	0.36	0.36	0.32	0.33	0.35	0.32
Calculated Permeability—darcies	2,156.00	921.00	353.00	238.50	157.00	43.80
Measured Permeability—darcies	1,745.00	881.00	325.00	191.00	121.00	45.00

[1]References given at end of paper.

these analyses are presently shown in Fig. 1 for horizontal fractures. Productivity ratios with and without fractures are plotted against the ratio, $\frac{Kh \text{ fracture}}{Kh \text{ formation}}$ for varying bed thicknesses. The Kh is defined as the product of the permeability (K) and the thickness (h) of either fracture or formation. It may be noted that the plotted points do not fall on a smooth curve but deviate from it. The reason for this deviation is that the flow pattern will vary with different bed thicknesses.

Also shown in Fig. 1 is a curve which is calculated by the equation,

$$\frac{Q_f}{Q_o} = \frac{\ln r_e/r_w}{(Kh)_o} \div \left(\frac{\ln r_f/r_w}{(Kh)_o + (Kh)_f} + \frac{\ln r_e/r_f}{(Kh)_o} \right), \quad \ldots \ldots \quad (6)$$

where Q_o is well productivity before fracturing, Q_f is well productivity after fracturing, r_e is radius of drainage, r_f is radius of horizontal fracture, r_w is radius of wellbore, $(Kh)_o$ is Kh of unfractured formation, and $(Kh)_f$ is Kh of fracture.

In the derivation of Eq. 6 the assumptions are made that the effective Kh of the fractured formation between r_w and r_f is equal to $(Kh)_o + (Kh)_f$ and that all flow is in horizontal planes only. A deviation factor should therefore be applied to make the equation more realistic. However, as may be seen in Fig. 1 the deviation is seldom over 10 per cent for which reason Eq. 6 shall be used in the following discussions.

Data from the electrical model studies based on vertical fractures are graphically shown in Fig. 2. A similar trend can be observed as in the case of the horizontal fractures. In this case, however, productivity ratios are independent of the thickness of the formation, and the Kh of the fracture is proportional to the radius of drainage.

In Fig. 3 are shown the calculated productivity ratios of fractures using different volumes and grades of propping sand. The conditions for these calculations were that the wells are on a 10-acre spacing with a 6-in. wellbore, that the extent of the fractures is 0.2 r_e = 66 ft, that the bed thickness is 50 ft, that the permeability is 50 md, and that the fracturing fluids cause no formation damage. Only horizontal fractures are shown; however, the trends will be quite similar with vertical fractures. This figure demonstrates that the productivity due to fracturing increases as the size of propping agent and/or thickness of fracture increases.

Fig. 4 shows the productivity changes for fractures using 20-40 mesh sand with varying amounts of contamination by a fine Mill Creek sand. It can be seen that a considerable decrease in well productivity occurs when the fracturing sand is contaminated with finer sand. How propping sand might become contaminated after being placed in the formation will subsequently be discussed.

Fig. 5 shows the effects of (1) overflush, (2) tailing-in with a coarser sand, and (3) the fact that major production increases may be due to penetration through zones of low permeability (wellbore damage).

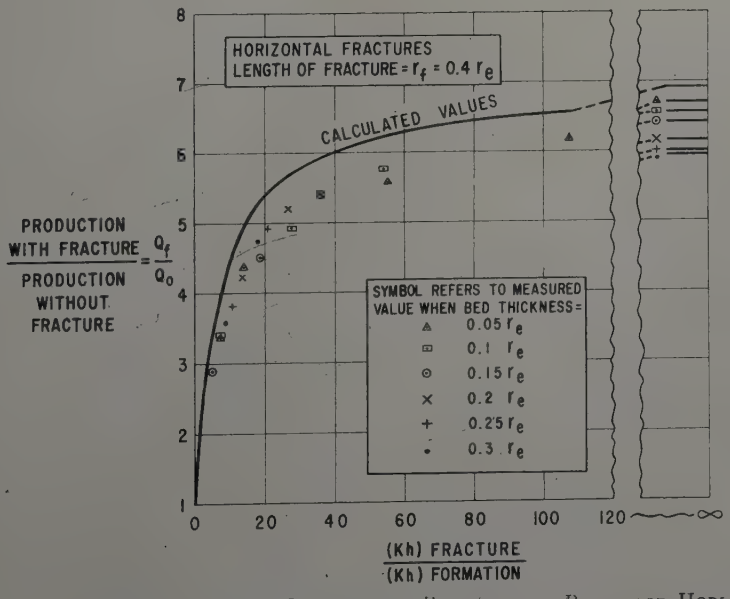

FIG. 1—EFFECT OF FLOW CAPACITY ON PRODUCTIVITY RATIO FOR HORIZONTAL FRACTURES.

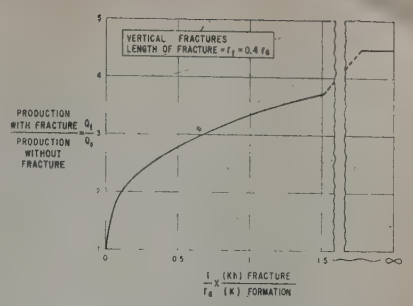

FIG. 2—EFFECT OF FLOW CAPACITIES ON PRODUCTIVITY RATIO FOR VERTICAL FRACTURES.

In the case of overflush, the assumptions were made that the entire body of fracturing fluid and sand was moved radially outward, thus extending the fracture. The per cent of overflush is the per cent of the fluid which was originally used to place the sand in the fracture. The characteristics of the overflush fluid were assumed to be identical to the characteristics of the sand-carrying fluid. Also, it is assumed that the fractures have "healed" in those places from which propping sand has been displaced.

In the case in which the regular 20-40 mesh sand was tailed-in with 10-20 mesh angular sand, the total amount of sand used remained constant.

The left scale depicts the productivity change after fracturing a well which is surrounded by a damaged zone 2 ft deep with a permeability of 5 md, which is 10 per cent of the original. When a 0.01-ft thick fracture with 20-40 mesh sand is made, the productivity will increase 3.44 times. If only 1 per cent of the 20-40 mesh sand is replaced by 10-20 mesh angular sand (tail-in), the productivity will increase 6.48 times the original productivity. The productivity increase will follow an upward trend with increased per cent of 10-20 mesh angular as a tail-in.

When overflush is used, it can be noted that the productivity increase will be less than if no overflush had been used under the existing conditions. As a matter of fact, the productivity ratio will decrease from 3.44 to 1.03 when the overflush is only as little as 1 per cent of the fluid used to carry the sand. This effect is particularly noticeable in the case of a damaged formation. If the damage (in our case 2 ft deep and 90 per cent loss of permeability) were completely removed by some means, the productivity would increase 3.6 times.

On the right scale in Fig. 5 is shown the effect of both overflush

and tailing-in with coarse sand where no damage exists surrounding the wellbore. It can be noted that with a fracture with 20-40 mesh sand and 0.01 ft thick, the productivity can be increased 1.34 times. With 1 per cent tail-in of 10-20 mesh sand, the productivity can be increased to 1.85 whereas with 1 per cent overflush the productivity increase will be only 1.12.

Under certain conditions the propping sand may be produced shortly after treatment of the well. One reason for such behavior may be that inadequate time was allowed for the fracture to close sufficiently and retain the sand in place (premature production). In such cases the results should be similar to those shown in the cases of overflush.

The following general conclusions may be drawn from Fig. 5: (1) a major increase in productivity may be due to breaking through a damaged zone, (2) beneficial effects may be obtained by tailing-in with coarser sand, and (3) overflush and premature production may be detrimental to fracturing results.

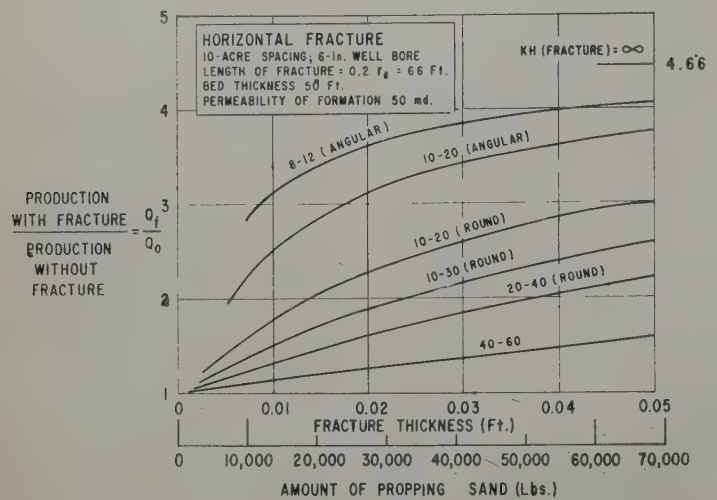

FIG. 3—EFFECT OF FRACTURE THICKNESS ON PRODUCTIVITY RATIO FOR TYPICAL PROPPING SANDS.

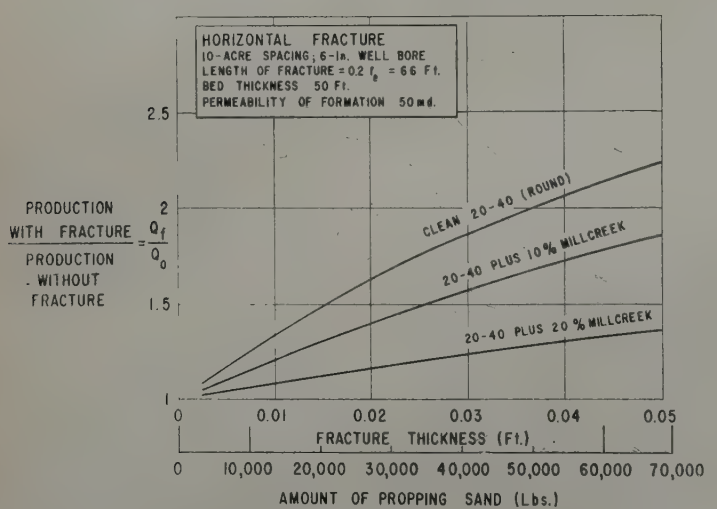
HORIZONTAL FRACTURE
10-ACRE SPACING; 6-In. WELL BORE
LENGTH OF FRACTURE = 0.2 r_e = 66 Ft.
BED THICKNESS 50 Ft.
PERMEABILITY OF FORMATION 50 md.
CLEAN 20-40 (ROUND)
20-40 PLUS 10% MILLCREEK
20-40 PLUS 20% MILLCREEK
PRODUCTION WITH FRACTURE / PRODUCTION WITHOUT FRACTURE = Q_f/Q_o
FRACTURE THICKNESS (Ft.)
AMOUNT OF PROPPING SAND (Lbs.)

FIG. 4 - PROPPING SAND CONTAMINATION ON PRODUCTIVITY RATIO.

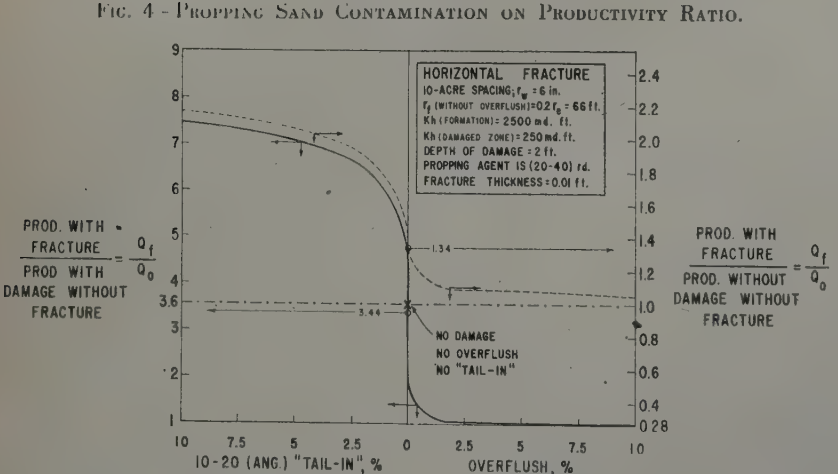
HORIZONTAL FRACTURE
10-ACRE SPACING; r_w = 6 in.
r_e (WITHOUT OVERFLUSH) = 0.2 r_e = 66 ft.
Kh (FORMATION) = 2500 md. ft.
Kh (DAMAGED ZONE) = 250 md. ft.
DEPTH OF DAMAGE = 2 ft.
PROPPING AGENT IS (20-40) rd.
FRACTURE THICKNESS = 0.01 ft.
1.34
3.44
NO DAMAGE
NO OVERFLUSH
NO "TAIL-IN"
PROD. WITH FRACTURE / PROD WITH DAMAGE WITHOUT FRACTURE = Q_f/Q_o
PROD. WITH FRACTURE / PROD. WITHOUT DAMAGE WITHOUT FRACTURE = Q_f/Q_o
10-20 (ANG.) "TAIL-IN", %
OVERFLUSH, %

FIG. 5—EFFECT OF WELLBORE DAMAGE, OVERFLUSH, AND TAILING-IN ON PRODUCTIVITY.

FLUID EFFECT ON FORMATIONS

The following series of tests were conducted for the purpose of determining the effect of various fluids on the competency and strengths of different formations. The fluids used were those commonly applied as fracturing fluids or in conjunction with the fracturing treatment.

Formation segments were immersed in these fluids under line vacuum. Observations were made on the competency of formations after such immersion. The results of these observations are listed in Table 3 together with the formation characteristics and the clay minerals found present.

In Table 4 are listed the compressive strengths of formations after immersion in the different fluids. The compressive strengths shown are average values measured on cylindrical cores ¾ in. in diameter and ¾ in. long. The flat faces of these cores were capped with gypsum cement to obtain an even bearing surface. It is realized that the size and shape of these samples are not in accord with the ASTM recommendation; however, the trend should be similar. The ¾-in. cores were used because of the availability of formation material.

From both Tables 3 and 4 the conclusion can be derived that both the competency and the compressive strength of a formation may be affected when immersed in water-base fluids. Also, it might be noted that when the cementitious material of the formation is soluble in the treating fluid, complete disintegration may result with an accompanying release of insoluble fine particles. Disruption of formations was also noted in the presence of clays which incur a volume change upon contact with certain fluids.

CONCLUSIONS

The general results of this examination indicate the results of a fracturing treatment are very dependent

upon the flow capacity of the produced fracture. Any method which causes a flow restriction within the propped fracture can appreciably reduce the possible production increase. Restriction of flow through a propped fracture can be caused in part by the following.

1. *Overflush* — Removal of propping agent by overflush from the close proximity of the wellbore may allow excessive healing or closing of the fracture in this area.

2. *Premature production after treatment* — This can also cause removal of propping agent leaving conditions similar to overflush.

3. *Release of formation fines from fracture surfaces* — Such fines can become integrated within the propping agent, thus reducing the effective permeability. Even small percentages can be very detrimental.

4. *Fluid effect on competency and strength* — Use of an improper fracturing fluid and/or other fluids in conjunction with the treatment can cause partial to complete disintegration of some fracture surfaces, thus releasing fines, silts and clays.

Productivity increases may be improved by the following.

1. *Large propping agent* — The use of as large a propping agent as practical for the particular well conditions should give superior results.

2. *Tail-in* — If sufficiently large sand cannot be used throughout, the use of a large sand at the end of the treatment can be very beneficial.

As previously stated, the presentation given here is based on preliminary laboratory evaluations. Therefore, the numerical values shown should not be used directly but the purpose of this paper is to indicate the possible effects on various factors only.

TABLE 3—EFFECT OF VARIOUS FLUIDS ON COMPETENCY

	Formation Depth, ft	A 6,800	B 6,885	C 9,165	D 6,330	E 1,166	F 1,192
Formation Characteristics and Clay Minerals	Permeability, md	10	15	3	6	2	11
	Porosity, Per Cent	—	—	15	10	22	20
	Solubility, Per Cent	less 1	less 1	3	50	17	18
	Salt Content, Mg/100 gm	60	80	120	60	300	230
	Chlorite	small	small	small	—	—	—
	Illite	small	small	small	small	small	small
	Kaolinite	small	small	small	small	small	small
	Montmorillonite	*	*	—	—	large	large
Effect of Immersion	Water	N	S	N	N	P	P
	10 Per Cent NaCl Solution	N	N	N	N	S-L	S
	2 Per Cent $CaCl_2$ Solution	N	N-S	N	N	L	S
	2 Per Cent HCl	N	S	N	S-L	—	P
	7½ Per Cent HCl	—	—	—	—	—	L
	7½ Per Cent HCl + Surfactant	N	N	N	C	S-L	S
	15 Per Cent HCl	N	N	S	L-P	P-C	S
	15 Per Cent HCl + 10 Per Cent $NaHF_2$	N	P	P	—	L-P	—

*Probably mixed layer illite-montmorillonite, montmorillonite-chlorite.
N = No detrimental effect noted.
S = Small amount of fines released.
L = Large amount of fines released.
P = Partially disintegrated.
C = Completely disintegrated.

TABLE 4—EFFECT OF VARIOUS FLUIDS ON COMPRESSIVE STRENGTH

	Formation Depth, ft	G 2,608	H 1,192	I 6,279	J 6,786	K 6,845	L 540	M 1,201	N 1,166	O 9,059	P —
Formation Characteristics and Clay Minerals	Permeability, md	less 1	11	less 1	less 1	3	—	22	2	12	9
	Porosity, Per Cent	8	20	9	13	20	—	22	22	17	14
	Solubility, Per Cent	85	18	14	12	2	Less 1	18	18	2	1
	Salt Content, Mg/100 gm	120	230	80	40	60	260	210	280	55	145
	Chlorite	—	—	small	—	small	trace	—	—	small	small
	Illite	trace	small	small	small	small	small	small	small	small	small
	Kaolinite	—	small	small	small	small	small	small	small	—	small
	Montmorillonite	—	large	*	*	*	—	large	large	small	—
Compressive Strength After Immersion	Kerosene	16,580	1,818	10,249	8,832	4,982	598	3,537	1,719	9,948	13,193
	Water	16,087	P	9,654	8,179	3,775	369	4,019 (P-C)	P-C	9,714	12,756
	10 Per Cent NaCl	—	1,141	—	—	—	396 (P)	—	842 (P)	6,567	—
	2 Per Cent $CaCl_2$	—	1,078	—	—	—	C	—	1,078 (P)	6,875	—
	2 Per Cent HCl	—	555	—	—	—	435	—	716 (P)	10,134	—
	7½ Per Cent HCl	12,600	276	3,988	5,944	—	365	1,488 (P)	344 (P)	—	13,394
	7½ Per Cent HCl + Surfactant	12,470	253	7,527	8,145	4,574	310	582 (P)	365	9,753	11,540
	15 Per Cent HCl	15,050	247	—	—	—	510	802 (P)	317 (P)	9,352	—
	15 Per Cent + 10 Per Cent $NaHF_2$	8,551	—	6,929	7,541	3,501	392 (P)	1,762 (P)	—	—	11,363

*Mixed layer illite-chlorite, illite-montmorillonite.
N = No detrimental effect noted.
S = Small amount of fines released.
L = Large amount of fines released.
P = Partially disintegrated.
C = Completely disintegrated.

ACKNOWLEDGMENT

The authors wish to express their appreciation to the Halliburton Oil Well Cementing Co. for permission to prepare and present this paper. Appreciation is also extended to those of this organization who helped obtain data and offered suggestions for the preparation of this paper.

REFERENCES

1. Carman, P. C.: *Trans.* Inst. Chem. Engrs., London (1937), **15**, 150.
2. Rose, W. D., and Bruce, W. A.: *Trans.* AIME (1949) **186**, 127.
3. Wyllie, M. R. J., and Gregory, A. R.: *Ind. and Engr. Chem.* (1955) **47**, 1379.
4. Brown, G. G.: *Unit Operations*, John Wiley & Sons, N. Y., 2nd Ed. (1951) 214.
5. van Poollen, H. K.: "Productivity vs Permeability Damage in Hydraulically Produced Fractures", Paper No. 906-2G, Spring Meeting of SW Dist. API, 1957. ★★★

Calculation of Linear Waterflood Behavior Including the Effects of Capillary Pressure

JIM DOUGLAS, JR.
P. M. BLAIR
JUNIOR MEMBERS AIME
R. J. WAGNER

HUMBLE OIL & REFINING CO.
HOUSTON, TEX.
THE RICE INSTITUTE
HOUSTON, TEX.

ABSTRACT

The calculation of the behavior of an oil reservoir during a water flood has long been an important problem to reservoir engineers. Buckley and Leverett derived the differential equation which describes the displacement of oil from a linear porous medium by an immiscible fluid, but this equation could not be solved by the methods of classic mathematics. Consequently, in order to integrate the equation over the length of the reservoir, they neglected the effects of capillary pressure.

In the present paper, a numerical method has been developed for determining the behavior of a linear water flood with the inclusion of capillary pressure. The differential equation which was derived for the case of incompressible fluids is second order and non-linear. This differential equation was approximated by an implicit form of difference equation which is second order correct in both time and distance. An electronic digital computer was used to perform the numerical solution of the difference equation.

INTRODUCTION

The problem of calculating the flow and distribution of fluids in an oil reservoir subjected to a water flood has long challenged the reservoir engineer. The ability to solve this problem would provide a valuable tool for the design and study of field waterflooding programs. One of the first contributions in this field was made by Buckley and Leverett,[1,2] who developed a method of calculating waterflood performance in a linear reservoir. Their technique was limited by the practical necessity of excluding quantitative consideration of capillary pressure. It is the purpose of this paper to describe a method for calculating the behavior of a linear water flood with capillary pressure considered. This method, although limited to the linear case, should serve as a step toward the solution of the two- or three-dimensional waterflooding problem which would better describe actual reservoirs.

The treatment of the problem has assumed that the reservoir is linear and homogeneous, that both oil and water are incompressible, and that gravitational forces may be neglected, and that water is injected into one end of the reservoir and oil and water are produced from the other. Though these assumptions may not be directly applied to natural reservoirs, they are closely approached in many laboratory core tests.

The physical problem has been represented mathematically by means of a differential equation and suitable boundary conditions. The inclusion of capillary pressure effects causes the differential equation to be second order and non-linear, and it is not amenable to solution in terms of known functions. Nevertheless, the problem may be solved by numerical methods. The authors have successfully calculated several cases from the start of water injection through to depletion of the hypothetical reservoir using realistic capillary pressure and relative permeability characteristics that were chosen so as to put the method to a test.

DIFFERENTIAL EQUATION

In two- or three-dimensional problems involving the two-phase flow of incompressible fluids through a porous medium, the equations describing the flow can be combined until only two dependent variables remain, the pressure in one phase, and the saturation of one phase. These variables appear in two simultaneous partial differential equations which are derived on the basis of the conservation of mass and Darcy's law as applied to two-phase flow. For a linear reservoir, this system of differential equations can be reduced to a single, non-linear, second order, parabolic differential equation for one dependent variable, the saturation of one phase.

For incompressible water and oil, it can be shown that the conservation of mass for the two phases requires that

$$\frac{\partial q_w}{\partial \xi} = -\phi \frac{\partial s_w}{\partial \tau}, \quad \ldots \ldots \ldots \quad (1)$$

$$\frac{\partial q_o}{\partial \xi} = -\phi \frac{\partial s_o}{\partial \tau}, \quad \ldots \ldots \ldots \quad (2)$$

where q_w and q_o are the water and oil flow rates per unit cross-section, s_w and s_o their saturations, ϕ, the porosity, and ξ and τ, dimensional space and time variables.

Darcy's law, as extended to two-phase flow including the effect of capillary pressure,[3] is as follows:

$$q_w = -\frac{k_w}{\mu_w} \frac{\partial p_w}{\partial \xi}, \quad \ldots \ldots \ldots \quad (3)$$

Original manuscript received in Society of Petroleum Engineers office July 15, 1957. Revised manuscript received Feb. 13, 1958. Paper presented at 32nd Annual Fall Meeting of Society of Petroleum Engineers in Dallas, Tex., Oct. 6-9, 1957.
[1]References given at end of paper.

$$q_o = -\frac{k_o}{\mu_o}\frac{\partial p_o}{\partial \xi}, \quad \ldots \quad (4)$$

where k refers to the effective permeability with respect to a phase, μ, to the viscosity of the phase, and p to the pressure in a phase. In the displacement process under consideration, the water saturation at each point in the core is always increasing, and under these conditions the effective permeabilities to each phase depend only on the fluid saturations. Likewise, under these conditions, the capillary pressure,

$$p_c = p_o - p_w , \quad \ldots \quad (5)$$

depends only on the fluid saturation. For brevity, let

$$s = s_o = 1 - s_w \quad \ldots \quad (6)$$

The differential equation satisfied by s may now be derived from the above relations. First, it follows from Eqs. 1 and 2 that

$$q_w(\xi,\tau) + q_o(\xi,\tau) = Q(\tau) , \quad \ldots \quad (7)$$

where $Q(\tau)$ is the total flow rate per unit of cross-sectional area at time τ. Although no material simplification of the problem is effected by using a constant rate, it is convenient to do so, and throughout the remainder of the discussion this will be assumed; i.e.,

$$q_w(\xi,\tau) + q_o(\xi,\tau) = Q \quad \ldots \quad (8)$$

If p_o is replaced by $p_w + p_c$ in Eq. 4 and then Eqs. 3 and 4 are substituted into Eq. 8, it can be seen that

$$\frac{\partial p_w}{\partial \xi} = -\frac{Q}{\frac{k_o}{\mu_o} + \frac{k_w}{\mu_w}} - \frac{\frac{dp_c}{ds}}{1 + \frac{k_w\mu_o}{k_o\mu_w}}\frac{\partial s}{\partial \xi} \quad \ldots \quad (9)$$

It then follows from Eqs. 1, 3, and 9 that

$$\frac{\partial}{\partial \xi}\left[\frac{k_w k_o \frac{dp_c}{ds}}{k_w\mu_o + k_o\mu_w}\frac{\partial s}{\partial \xi}\right] + \frac{d}{ds}\left[\frac{Q}{1 + \frac{k_o\mu_w}{k_w\mu_o}}\right]\frac{\partial s}{\partial \xi} = \phi\frac{\partial s}{\partial \tau}. \quad \ldots \quad (10)$$

Eq. 10 may be put into the dimensionless form,

$$\frac{\partial}{\partial x}\left[g(s)\frac{\partial s}{\partial x}\right] + h(s)\frac{\partial s}{\partial x} = \frac{\partial s}{\partial t}, \quad \ldots \quad (11)$$

where

$$g(s) = \frac{k_w k_o \frac{dp_c}{ds}}{QL(k_w\mu_o + k_o\mu_w)}, \quad \ldots \quad (12)$$

$$h(s) = \frac{d}{ds}\left[\frac{1}{1 + \frac{k_{ro}\mu_w}{k_{rw}\mu_o}}\right], \quad \ldots \quad (13)$$

by the change of variables

$$x = \xi/L , \quad \ldots \quad (14)$$

$$t = Q\tau/L\phi , \quad \ldots \quad (15)$$

L being the length of the reservoir.

If the dependence of $\frac{dp_c}{ds}$ on s is expressed in the form $\frac{\frac{dp_c}{ds}}{\left[\frac{dp_c}{ds}\right]_{\text{char.}}} = \gamma(s)$, where $\gamma(s)$ is a dimensionless capillary pressure gradient and $\left[\frac{dp_c}{ds}\right]_{\text{char.}}$ is a "characteristic" value of the slope of the capillary pressure curve, then $g(s)$ may be put in the form

$$g(s) = \left[\frac{K\left(\frac{dp_c}{ds}\right)_{\text{char.}}}{QL\mu_o}\right]\frac{k_{ro}k_{rw}\gamma(s)}{\left[k_{rw} + k_{ro}\left(\frac{\mu_w}{\mu_o}\right)\right]}.$$

This form, which is essentially the same as presented by Rapoport and Leas,[9] shows that, in addition to the relative permeability and dimensionless capillary pressure gradient characteristics of the porous medium, the saturation profile at any time depends also on the value of the two dimensionless groups,

$$\frac{\mu_w}{\mu_o} \text{ and } \frac{QL\mu_o}{K\left[\frac{dp_c}{ds}\right]_{\text{char.}}}.$$

Eq. 11 is the fundamental differential equation for the saturation of oil, and its solution gives a complete description of the physical problem being studied. It is possible by transforming the dependent variable to simplify the form of the equation with regard to the numerical procedure to follow. Denote the maximum oil saturation (i.e., that oil saturation for which s_w is equal to the connate water saturation) by $s_{\max}$ and the residual oil saturation by s_{res}, and let

$$r = r(s) = \frac{1}{Z}\int_{s_{\max}}^{s} g(\zeta)\,d\zeta \quad \ldots \quad (16)$$

where

$$Z = \int_{s_{\max}}^{s_{\text{res}}} g(\zeta)\,d\zeta \quad \ldots \quad (17)$$

Then, in terms of r, Eq. 11 becomes

$$\frac{\partial^2 r}{\partial x^2} + \alpha(r)\frac{\partial r}{\partial x} = \beta(r)\frac{\partial r}{\partial t}, \quad \ldots \quad (18)$$

where

$$\alpha(r) = \frac{1}{Z}\frac{d}{dr}\left[\frac{1}{1 + \frac{k_{ro}\mu_w}{k_{rw}\mu_o}}\right], \quad \ldots \quad (19)$$

$$\beta(r) = \frac{1}{Z}\frac{ds}{dr} \quad \ldots \quad (20)$$

To complete the specification of the problem, an initial condition on s and boundary conditions at the two ends $x = 0$ and $x = 1$ of the reservoir must be given. At $t = 0$, let

$$s(x,0) = s_{\max} \quad \ldots \quad (21)$$

This corresponds to the initial condition

$$r(x,0) = 0 \quad \ldots \quad (22)$$

The boundary at $x = 0$ will be the inflow face for the injected water. This requires that

$$q_o(0,t) = 0 \quad \ldots \quad (23)$$

This implies that

$$\frac{\partial p_o}{\partial x} = 0 \quad \ldots \quad (24)$$

From Eqs. 3, 5, 8, 14, and 24,

$$\frac{\partial p_c}{\partial x} = \frac{dp_c}{ds}\frac{\partial s}{\partial x} = \frac{LQ\mu_w}{k_w}. \quad \ldots \quad (25)$$

This is equivalent to

$$\frac{\partial r(0,t)}{\partial x} = \frac{1}{Z\left[1 + \frac{k_{rw}\mu_o}{k_{ro}\mu_w}\right]} \quad \ldots \quad (26)$$

It has been observed in laboratory experiments that before any water is produced at the outflow face the water saturation in the neighborhood of the outflow face builds up to essentially its maximum value.[4,7] Moreover, the water saturation there remains at this maximum value from then on throughout the remainder of the flood. This can be expressed mathematically as follows:

$$q_w(1,t) = 0 \qquad \text{if } s(1,t) > s_{\text{res}} \quad \ldots \quad (27)$$

and

$$s(1,t) = s_{\text{res}} \qquad \text{if } s(1,t') = s_{\text{res}} \quad \ldots \quad (28)$$

for some $t' < t$.

Let t^* be the first time such that $s(1,t) = s_{res}$. Then, Eqs. 27 and 28 can be converted to the following:

$$\frac{\partial r(1,t)}{\partial x} = \frac{-1}{Z\left[1 + \frac{k_{ro}\mu_w}{k_{rw}\mu_o}\right]}, \qquad t < t^* \quad , \quad (29)$$

$$r(1,t) = 1, \qquad t \geq t^* \quad . \quad (30)$$

This completes the reduction of the physical problem to a mathematical problem. Collecting, we obtain the following system:

$$\text{(a)} \qquad \frac{\partial^2 r}{\partial x^2} + \alpha(r)\frac{\partial r}{\partial x} = \beta(r)\frac{\partial r}{\partial t},$$

$$\text{(b)} \qquad r(x,0) = 0,$$

$$\text{(c)} \qquad \frac{\partial r(0,t)}{\partial x} = \frac{1}{Z\left[1 + \frac{k_{rw}\mu_o}{k_{ro}\mu_w}\right]} = v[r(0,t)],$$

$$\text{(d}_1\text{)} \qquad \frac{\partial r(1,t)}{\partial x} = \frac{-1}{Z\left[1 + \frac{k_{ro}\mu_w}{k_{rw}\mu_o}\right]} = y[r(1,t)], \quad t < t^*,$$

$$\text{(d}_2\text{)} \qquad r(1,t) = 1, \qquad t \geq t^* \quad . \quad . \quad . \quad . \quad . \quad (31)$$

Since the system (Eq. 31) will be solved by an approximate method, it is valuable to have a redundant relation that must be satisfied to use as a measure of the correctness of the approximation. An over-all material balance may be used for this relationship quite satisfactorily. The water balance is

$$Q\tau = \int_o^\tau q_w(L,\tau_1)\,d\tau_1 + \phi\int_o^L [s_w(\xi,\tau) - s_{wi}]d\xi,$$

. . . . . (32)

where s_{wi} is the initial water saturation. For $t < t^*$, this may be reduced to

$$t = \int_o^1 \{1 - s_{cw} - s[r(x,t)]\}dx \quad , \quad t < t^* . \quad (33)$$

For $t \geq t^*$, it can be shown that

$$q_w(1,t) = Q\left[1 + Z\frac{\partial r(1,t)}{\partial x}\right]. \quad . \quad . \quad . \quad . \quad (34)$$

and that Eq. 32 becomes

$$t^* = Z\int_{t^*}^t \frac{\partial r(1,t_1)}{\partial x}\,dt_1 + \int_o^1 \{1 - s_{cw} - s[r(x,t)]\}dx .$$

. . . . . (35)

DIFFERENCE EQUATION

The fundamental differential Eq. 31(a) is a quasi-linear parabolic differential equation and is not amenable to the techniques of solution common to classic mathematical physics; however, it is possible to approximate its solution by finite difference techniques. The difference analog of Eq. 31(a) to be employed in this paper is a modified Crank-Nicolson difference equation.[5] This difference relation is discussed in detail in the literature[5] for a slightly simpler, but still non-linear, parabolic differential equation; in particular, its advantages over other commonly used difference relations are pointed out. Moreover, it is derived completely there; thus, only a description and its final form will be given here.

Let $\Delta x = 1/I$ and $\Delta t > 0$, and let $x_i = (i-1)\,\Delta x$, $i = 0, 1, \ldots, I+2$, and $t_n = n\Delta t$, $n = 0, 1, \ldots$. Denote by $w_{i,n}$ the value of the solution of the difference equation (i.e., the approximation to r) at the point (x_i, t_n). Define the first x-difference of $w_{i,n}$ to be

$$\Delta_x w_{i,n} = \frac{w_{i+1,n} - w_{i-1,n}}{2\,\Delta x}, \quad . \quad . \quad . \quad . \quad . \quad . \quad (36)$$

and its second x-difference to be

$$\Delta_x^2 w_{i,n} = \frac{w_{i+1,n} - 2w_{i,n} + w_{i-1,n}}{(\Delta x)^2} \quad . \quad . \quad . \quad (37)$$

The first difference is an approximation to the first derivative and the second difference to the second derivative.

The modified Crank-Nicolson equation for Eq. 31(a) may be obtained as follows. Assume that the values of $w_{i,j}$ are known for $j = 0, 1, \ldots, n$ and that the values of $w_{i,n+1}$ are not yet known. Replace the second derivative $\frac{\partial^2 r}{\partial x^2}$ by the average of the second difference at the times t_n and t_{n+1}:

$$\frac{\partial^2 r}{\partial x^2} \rightarrow \tfrac{1}{2}\,[\Delta_x^2 w_{i,n+1} + \Delta_x^2 w_{i,n}] \quad . \quad . \quad . \quad . \quad (38)$$

similarly, let

$$\frac{\partial r}{\partial x} \rightarrow \tfrac{1}{2}\,[\Delta_x w_{i,n+1} + \Delta_x w_{i,n}] \quad . \quad . \quad . \quad . \quad . \quad (39)$$

Also, let

$$\frac{\partial r}{\partial t} \rightarrow \frac{w_{i,n+1} - w_{i,n}}{\Delta t} \quad . \quad . \quad . \quad . \quad . \quad . \quad . \quad . \quad (40)$$

This leaves only the choice of r in the coefficients $\alpha(r)$ and $\beta(r)$ to be made. It is desirable that an approximation to the value of r at the point $(x_i, t_{n+\frac{1}{2}})$ be used, since Eqs. 38 and 40 are centered there, and that this approximation leave the algebraic equations that must be solved at each time step linear. As shown in Ref. 5, this may be done by defining

$$w^*_{i,n+\frac{1}{2}} = w_{i,n} + \frac{\Delta t[\Delta_x^2 w_{i,n} + \alpha(w_{i,n})\Delta_x w_{i,n}]}{2\beta(w_{i,n})},$$

. . . . . (41)

and letting

$$r \rightarrow w^*_{i,n+\frac{1}{2}} . \quad . \quad . \quad . \quad . \quad . \quad . \quad . \quad . \quad . \quad (42)$$

Hence, the difference equation may be written as follows:

$$\Delta_x^2 w_{i,n+1} + \Delta_x^2 w_{i,n} + \alpha(w^*_{i,n+\frac{1}{2}}) \times [\Delta_x w_{i,n+1} + \Delta_x w_{i,n}] = 2\beta(w^*_{i,n+\frac{1}{2}})\left[\frac{w_{i,n+1} - w_{i,n}}{\Delta t}\right]. \quad . \quad . \quad . \quad (43)$$

The above relation is to be satisfied for $i = 1, \ldots I+1$, when $t < t^*$ and for $i = 1, \ldots, I$ when $t \geq t^*$.

The initial condition and the boundary conditions must also be translated into difference form. The initial condition is

$$w_{i,0} = 0 \quad . \quad . \quad . \quad . \quad . \quad . \quad . \quad . \quad . \quad . \quad (44)$$

The problem of evaluating r in $v(r)$ and $y(r)$ may be solved in the same way as before. Let

$$w^{**}_{i,n+1} = w_{i,n} + \frac{\Delta t[\Delta_x^2 w_{i,n} + \alpha(w_{i,n})\Delta_x w_{i,n}]}{\beta(w_{i,n})}, \quad . \quad . \quad (45)$$

and replace the boundary conditions by

$$\Delta_x w_{1,n+1} = v(w^{**}_{1,n+1}) \quad , \quad . \quad . \quad . \quad . \quad . \quad . \quad (46)$$

$$\Delta_x w_{I+1,n+1} = y(w^{**}_{I+1,n+1}) \quad , \quad t < t^* \quad , \quad . \quad . \quad . \quad (47)$$

$$w_{I+1,n+1} = 1 \quad , \qquad t \geq t^* \quad . \quad . \quad . \quad . \quad . \quad . \quad (48)$$

Note that the number of points at which $w_{i,n+1}$ is evaluated decreases by one when t surpasses t^*. The linear algebraic equations to be solved at each time step can be treated by a form of Gaussian elimination.[6]

It is necessary in the material balance check to evaluate some integrals numerically. The saturation integral in Eqs. 33 and 35 can be handled quite well by Simpson's rule. The integral,

$$\int_{t^*}^{t} \frac{\partial r(1, t_1)}{\partial t}\, dt_1 \quad ,$$

arising in Eq. 35 can be approximated by the trapezoidal rule after approximating $\frac{\partial r(1,t)}{\partial t}$ by

$$\frac{w_{I-1,n+1} - 4w_{I,n+1} + 3w_{I+1,n+1}}{2\,\Delta x} \quad , \quad . \quad . \quad . \quad . \quad (49)$$

a formula resulting from interpolating the last three values by a parabola.

DESCRIPTION OF CALCULATIONS

Calculations of the fluid saturations in a linear, homogeneous reservoir have been made for five values of the dimensionless rate parameter, $\frac{QL\mu_o}{K\left[\frac{dp_c}{ds}\right]_{\text{char.}}}$. These values are 0.0159, 0.159, 1.59, 7.95, and 15.9. In all these cases, the viscosity ratio was held constant at $\frac{\mu_w}{\mu_o} = \frac{1}{2}$ and the calculations were continued in each case until the water-oil ratio exceeded 100 to 1.

These calculations were carried out to serve as examples of the type of results possible by application of the numerical procedures presented herein. They apply only for one-dimensional flow with a water-to-oil viscosity ratio of one-half, and for the particular relative permeability and dimensionless capillary pressure data used, which are shown in Figs. 1 and 2, respectively. The equations for these curves are

$$k_{ro} = 1.4256(s - 0.216) \quad ,$$

$$k_{rw} = 1.6329(0.7 - s)^2 \quad ,$$

$$\frac{p_c}{\left[\frac{dp_c}{ds}\right]_{s_{\text{char.}}}} = \left[\frac{0.05669}{(0.7 - s)^2} - 0.242\right].$$

The reason for using such reservoir characteristics was to investigate the feasibility of making the calculations with data that cause the integral, Z, to be unbounded. With such data, the transformation of the dependent variable from s to r is accomplished by integrating nearly, but not quite, to connate water saturation.

In order to prepare the data for use in the computer, the following relations were obtained:[8]

$$s = 0.7 - 0.43372\, r^3 + 3.0819\, r^6 - 10.592\, r^9 + 14.256\, r^{12} - 6.79618\, r^{15} \quad ,$$

$$\frac{k_{rw}}{k_{rw} + [\frac{1}{2}]k_{ro}} = (0.6291\, r^3 - 3.4696\, r^6 + 12.229\, r^9 - 16.178\, r^{12} + 7.7895\, r^{15})^2 \quad .$$

From these two relations all the other pertinent functions (α, β, y, and v) may be derived.

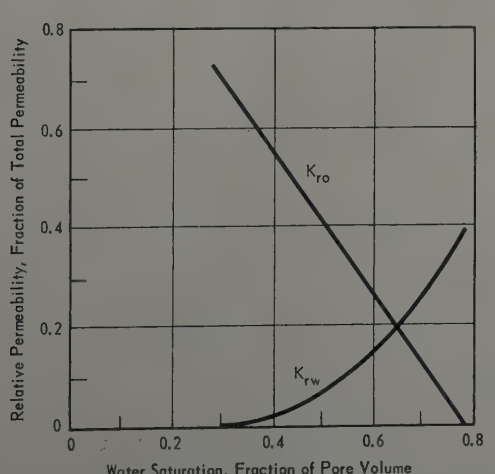

FIG. 1—RELATIVE PERMEABILITIES OF THE HYPOTHETICAL RESERVOIR.

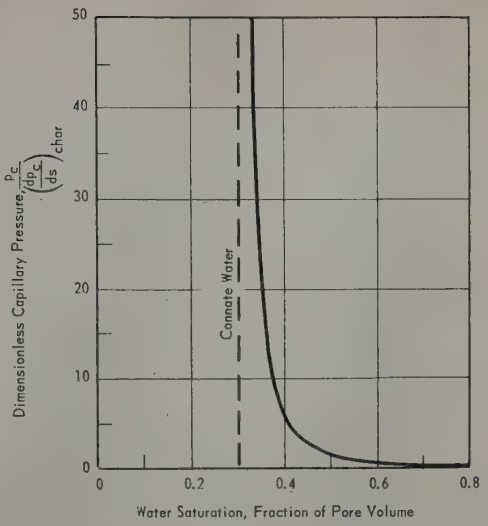

FIG. 2—DIMENSIONLESS CAPILLARY PRESSURE OF THE HYPOTHETICAL RESERVOIR.

After the calculations were made, it was noted that two discrepancies existed in the data. First, since $g(s)$ vanishes for $s = s_{res}$, the derivatives of s with respect to r should be infinite for $s = s_{res}$. Obviously the polynominal representation above does not describe this behavior. The fitting of the curve in this manner induces an inconsistency between Eqs. 25 and 26 as s approaches s_{res} at the inflow face. The other difficulty arises from the shape of the capillary pressure curve at residual oil saturation. It can be shown from consideration of the boundary conditions (Eq. 25) for saturations near that at residual oil that dp_c/ds must be infinite at this saturation. The curve used in the examples did not have this property. As a result, $r(0,t)$ tended to rise above one; this was prevented in the calculation by limiting r to a greatest value of one. As a result neither of these limitations in the data should have had an appreciable effect on the calculation.

The calculations required 260 operations (logical and arithmetic) per distance increment per time step on a machine which ran this calculation at a rate of 13,000 operations per second. Since about 1,200 time steps were needed to deplete the reservoir and a Δx of 0.02 was sufficiently small for Cases I, II, and III, they were calculated in 25 minutes each (including output time) and had material balance errors (by Simpson's rule) at water breakthrough of 0.21, 0.14, and 1.6 per cent, respectively. A Δx of 0.005 was necessary in Cases IV and V in order to hold the error at water breakthrough to 1.4 and 7.2 per cent, respectively. These cases took 100 minutes each. In all cases the time increment began at 0.0001 and was doubled every 200 time steps until it reached 0.0016, at which value it remained until the end of the case. Any of the errors quoted can be reduced by using smaller distance and time increments.

DISCUSSION OF RESULTS

The results of the example calculations are shown in Figs. 3 through 13. In Figs. 3 through 7 are shown

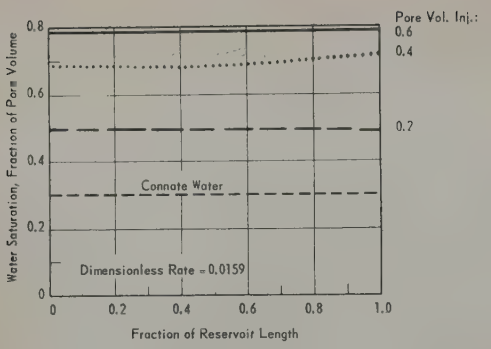

FIG. 3—SATURATION DISTRIBUTIONS FOR CASE I.

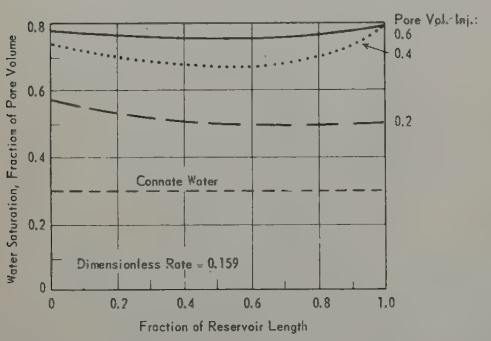

FIG. 4—SATURATION DISTRIBUTIONS FOR CASE II.

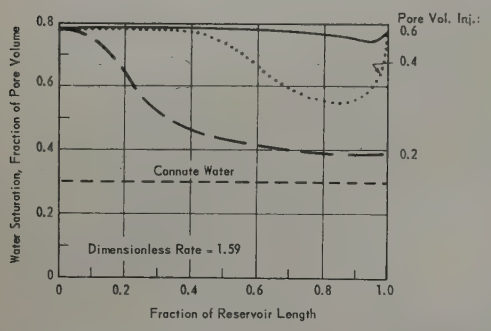

FIG. 5—SATURATION DISTRIBUTIONS FOR CASE III.

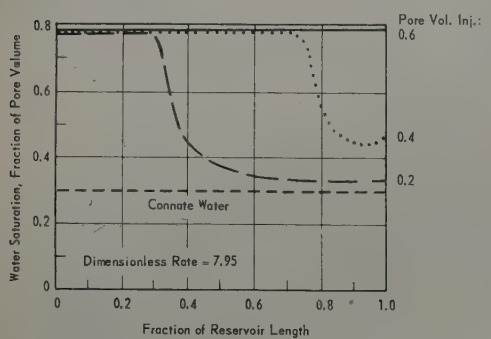

FIG. 6—SATURATION DISTRIBUTIONS FOR CASE IV.

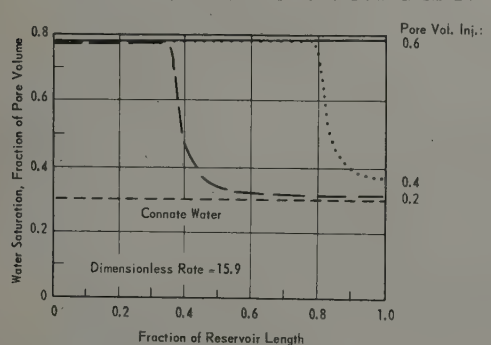

FIG. 7—SATURATION DISTRIBUTIONS FOR CASE V.

the saturation distributions for the five cases at three different stages of the flood. At the two lowest dimensionless rates (Figs. 3 and 4), the capillary forces move the water into the core fast enough that no steep saturation gradients exist. The next highest rate (Fig. 5) results in larger saturation gradients, though the front is still spread over a considerable portion of the reservoir. The increase in water saturation at the outflow face as a result of the discontinuity of the medium there is clearly shown by this case. Figs. 6 and 7 show how the water front gets steeper with increasing rate.

To show a comparison of the steepness of the fronts, the saturation distributions for the four highest rate cases are compared at 0.2 and 0.4 pore volume injected in Figs. 8 and 9, respectively. Also shown there for comparison are saturation distributions calculated by the Buckley-Leverett method, in which it is assumed that the capillary pressure gradient is zero at all saturations. This case corresponds to a dimensionless rate of infinity. It can be seen that as the dimensionless rate is increased, the front gets steeper and approaches the Buckley-Leverett curve. Fig. 10 shows the saturation distribution along the reservoir for all cases, except the low rate case, just at the point of water breakthrough.

A plot of oil recovery as a function of cumulative water injection, Fig. 11, shows that for dimensionless

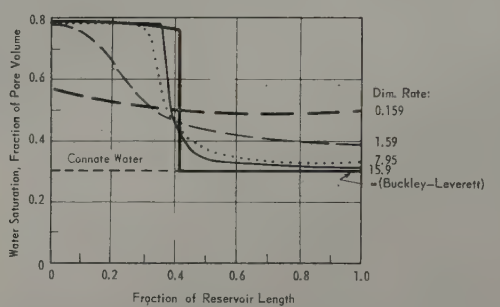

FIG. 8—SATURATION DISTRIBUTIONS FOR FOUR CASES AT 0.2 PORE VOLUME OF WATER INJECTED.

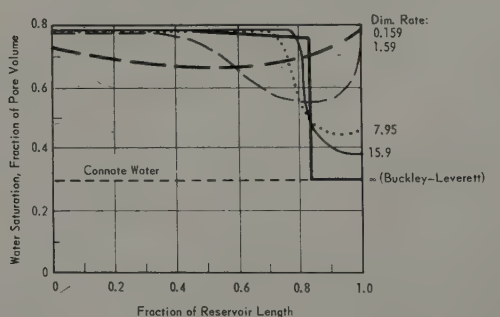

FIG. 9—SATURATION DISTRIBUTIONS FOR FOUR CASES AT 0.4 PORE VOLUME OF WATER INJECTED.

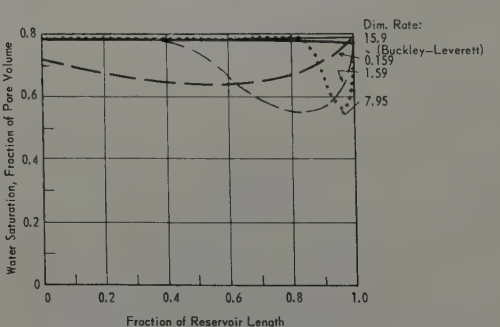

FIG. 10—SATURATION DISTRIBUTIONS FOR FOUR CASES AT WATER BREAKTHROUGH.

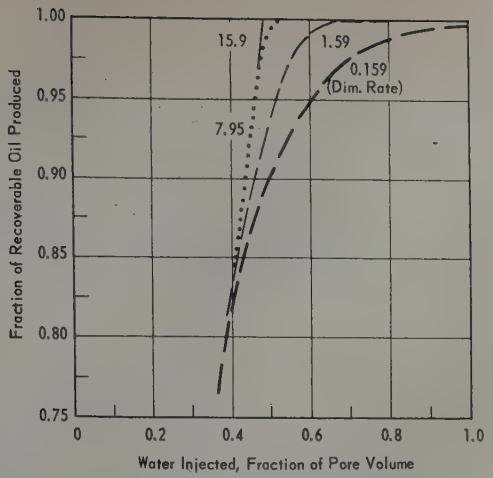

FIG. 11—PRODUCTION CURVES FOR FOUR CASES AFTER WATER BREAKTHROUGH.

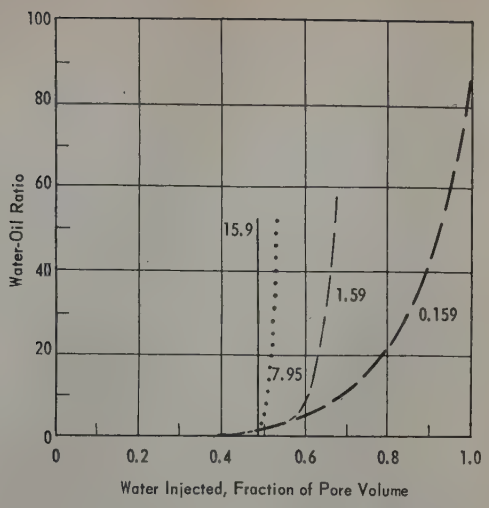

FIG. 12—COMPARISON OF WATER-OIL RATIOS.

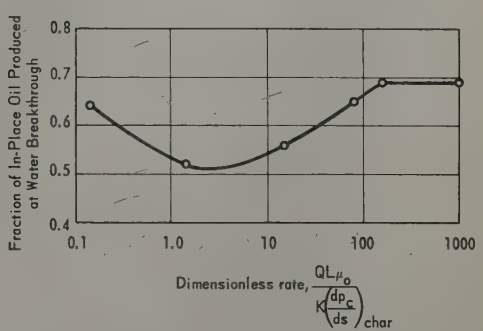

FIG. 13—VARIATION IN OIL RECOVERY AT WATER BREAKTHROUGH AS A FUNCTION OF DIMENSIONLESS RATE.

rates less than 15.9 the efficiency increases appreciably with increasing rate. However, for rates from 15.9 to ∞ there is no difference in the production curve.

The water-oil ratios, when plotted against injected volume as in Fig. 12, show that for rates less than 15.9 the ratios for the higher rate runs rise more rapidly after water breakthrough than do those for the lower rates.

If the calculated oil recoveries at breakthrough are plotted as a function of the dimensionless rate, as is done in Fig. 13, it can be seen that for rates from approximately 1 to 16 this recovery increases with increasing rate. At the higher rates, which would generally obtain in field floods, the breakthrough recovery is essentially independent of the dimensionless rate group. This dependence of breakthrough recovery upon rate for a homogeneous system such as was studied is due to capillary pressure effects, and has been discussed by Rapoport and Leas. The results presented in Fig. 12 demonstrate the same increase in recovery at breakthrough with increasing rate that they noted, provided the rates are in a certain range (1 to 16 in this case). However, at lower values of the dimensionless rate parameter, the breakthrough recovery passes through a minimum and then increases with decreasing rate. This behavior results from the fact that there are two distinct effects of capillary pressure. One of these is the "spreading" of the invading water front by capillary forces. The other is the well-known "end effect"[2] and was included in the differential system presented in this paper as the boundary condition at the outflow face. At extremely low rates in water-wet systems the latter effect would predominate and prevent the production of water until all the recoverable oil had been produced. This was not shown in the data of Rapoport and Leas because their systems were oil-wet.

CONCLUSIONS

Linear, two-phase flow through homogeneous porous solids is described by a second-order, quasi-linear, parabolic differential equation derived from fundamental flow equations, including capillary-pressure concepts. The calculations described in this paper demonstrate that this differential equation can be approximated by an implicit form of difference equation which is second order correct in both time and distance, and that from this approximation a complete saturation distribution history can be calculated. The calculations are of such length that it is necessary to run them on a high-speed computer.

NOMENCLATURE

g = permeability-capillary-pressure function, defined by Eq. 12
h = flow function, defined by Eq. 13
I = number of distance increments
K = total permeability, darcies
k = effective permeability, darcies
L = length of reservoir, cm
p = pressure, atmospheres
Q = total flow rate per unit cross-section, cc/cm^2
q = flow rate per unit cross-section, cc/cm^2
r = dependent variable of differential equation
s = saturation
t = dimensionless time, defined by Eq. 15
v = inflow boundary condition, defined by Eq. 31(c)
w = dependent variable of difference equation
x = dimensionless distance, defined by Eq. 14
y = outflow boundary conditions, defined by Eq. 31(d_1)
Z = normalizing integral defined by Eq. 17
α = coefficient of differential equation, defined by Eq. 19
β = coefficient of differential equation, defined by Eq. 20
μ = viscosity, cp
ξ = distance along the reservoir, cm
τ = time, seconds
ϕ = porosity

SUBSCRIPTS

c = capillary
cw = connate water
i = distance index
j = time index (particular)
n = time index (general)
o = oil
r = relative
w = water
1 = variable of integration

SUPERSCRIPTS

$*$ = (on w) predicted value at $t = n + \frac{1}{2}$
$*$ = (on t) time of water breakthrough
$**$ = predicted value at $t = n + 1$
$'$ = a particular value of t

ACKNOWLEDGMENT

The authors wish to express their appreciation to several members of the Humble Production Research Div. for their assistance with this work, and particularly to D. N. Turner for assistance in programming the calculations for the computer.

REFERENCES

1. Buckley, S. E., and Leverett, M. C.: "Mechanism of Fluid Displacement in Sands, *Trans.*, AIME (1942) **146,** 107.
2. Leverett, M. C.: "Capillary Behavior in Porous Solids," *Trans.*, AIME (1941) **142,** 152.
3. Muskat, Morris: *Physical Principles of Oil Production,* McGraw-Hill Book Co., N. Y. (1949).
4. Richardson, J. G., Kerver, J. K., Hafford, J. A., and Osoba, J. S.: "Laboratory Determination of Relative Permeability," *Trans.*, AIME (1952) **195,** 187.
5. Douglas, J., Jr.: "The Application of Stability Analysis in the Numerical Solution of Quasi-Linear Parabolic Differential Equations," to be published.
6. Bruce, G. H., Peaceman, D. W., Rachford, H. H., Jr., and Rice, J. D.: "Calculations of Unsteady-State Gas Flow Through Porous Media." *Trans.* AIME, (1953) **198,** 79.
7. Perkins, F. M., Jr.: "An Investigation of the Role of Capillary Forces in Laboratory Water Floods," *Trans.* AIME (1957) **210,** 409.
8. Rachford, H. H., Jr., and Schultz, W. P.: "Some Useful Tables for Approximating Smooth Curves by Fifth-and-Lower Degree Polynomials," *Trans.* AIME (1955) **204,** 289.
9. Rapoport, L. A., and Leas, W. J.: "Properties of Linear Waterfloods," *Trans.* AIME (1953) **198,** 139. ★★★

A Theoretical Description of Water-Drive Processes Involving Viscous Fingering

P. van MEURS
JUNIOR MEMBER AIME
C. van der POEL

KONINKLIJKE/SHELL-LABORATORIUM
AMSTERDAM, NETHERLANDS

ABSTRACT

From observations of the linear displacement of oil by water from a porous medium as visualized in transparent models, new insight into the mechanism of viscous fingering, as occurring in the case of unfavorable oil-water viscosity ratios, has been obtained.

A mathematical description of the observed phenomena leads to formulas expressing both oil production and pressure drop across the formation as a function of cumulative water injection with the oil-water viscosity ratio as a parameter.

Theoretical results are compared with those obtained from scaled laboratory experiments in sand-filled tubes in which water was injected at the one end and production was obtained from the other end.

In the second part of the paper the same principles are used to calculate a more realistic production scheme in which production of oil and water is obtained from wells regularly distributed over the field. Results show satisfactory agreement with production data of an actual oil field.

Application of the theory is extremely simple as only a limited number of readily available parameters have to be known and results are presented in an analytical form.

INTRODUCTION

When oil is displaced from a porous medium by water having a viscosity lower than the oil, the oil-water interface is essentially unstable and has the tendency to break up into what are called "fingers" or "streamers". This viscous fingering has been noted before by Engelberts and Klinkenberg[1] and has recently been demonstrated in transparent models by van Meurs[2].

It is highly questionable whether it is at all possible to perform relative permeability measurements in the laboratory reproducing the same distribution of water and oil in the cores as present in practice. Therefore, we based our descriptive theory on an idealized model which was "tailored" to the fingering mechanism as observed in transparent models under scaled conditions.

This approach was the more attractive, as a highly simplified model had already yielded an adequate description of the process. Though we are aware our theoretical approach can be extended in several ways, it is given here in its simplest form to explain the fundamental principles and to avoid complicated formulas.

SIMPLEST CASE OF A LINEAR DRIVE

Observations and Theoretical Model

In Fig. 1 a series of photographs shows how water penetrates into a formation saturated with an oil which is considerably more viscous than the water. The technique for obtaining these photographs, using transparent models, has already been described[2]. The fingers can be clearly observed and are seen to be mainly parallel to the flow direction. Note that the contours of these fingers are not smooth but show protrusions of water enclosing oil pockets.

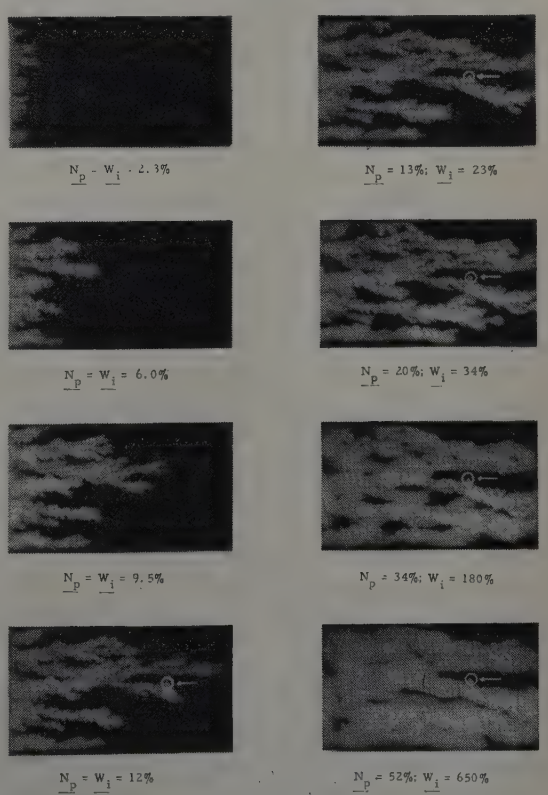

FIG. 1—LINEAR DISPLACEMENT OF HIGHLY VISCOUS OIL BY WATER, SHOWING THE IMMOBILITY OF THE WATER PROTRUSIONS (ARROW). OIL-WATER VISCOSITY RATIO —80.

Manuscript received in Society of Petroleum Engineers office July 17, 1957. Paper presented at 32nd Annual Fall Meeting of Society of Petroleum Engineers in Dallas, Tex., Oct. 6-9, 1957.
[1]References given at end of paper.

These protrusions do not advance in the direction of flow; see for instance the protrusion in Fig. 1 indicated by an arrow. This means that the fluid flow both in the protrusions and in the oil pockets is greatly hampered.

Between the water fingers macroscopic areas remain which have not been contacted by water. They are evidently outside the water protrusions and the oil flow proceeds unhindered.

For purposes of calculation we will idealize this flow mechanism in the following way: (1) the displacement process is of a one-dimensional character in the region where both oil and water are present, (2) oil flow outside the water fingers as well as water flow in the center proceeds unhindered, (3) in the edge zone of the water fingers both the water in the water protrusions and the oil in the enclosed pockets are completely prevented from flowing into the flow direction, and (4) the fractions of both immobile oil and water in a cross section of the formation are independent of time and place.

Let us consider a unit cross section of the formation large enough to contain sufficient fingers to be representative of the total cross section. Such a cross section can be divided into the following areas (see also Fig. 2): (1) the area outside the water fingers where oil flows unhindered, (2) the sum of the center areas of the water fingers where the water flows unhindered, and (3) the area consisting of the edge zones of all the water fingers of the cross section. In this area both oil and water are immobile.

The sizes of these areas will be characterized by means of oil and water saturations.

All immobile water of Area 3 expressed as a fraction will be denoted as S_{wm}. This means that S_{wm} is the immobile water saturation averaged over the unit cross section. In the same way we define S_{or} by averaging the saturation of immobile oil over this cross section. If we denote the average water saturation of the cross section by S_w, the size of Area 2 where the water flows unhindered is equal to $S_w - S_{wm}$.

Likewise, the size of Area 1 where the oil flows unhindered equals $S_o - S_{or}$, or with $S_o + S_w = 1$, the size of Area 1 may also be written as $1 - S_{or} - S_w$.

Calculation of Oil Production Performance

If we define the amount of water flowing through the unit cross section as q_w (dimension, $L\,t^{-1}$), then

$$q_w = u_w(S_w - S_{wm}) \quad . \quad . \quad . \quad . \quad . \quad . \quad . \quad . \quad (1)$$

in which u_w is the volumetric velocity of the water in Area 2.

As the flow in this area was assumed to be unhindered, u_w obeys Darcy's law for a single phase.

$$u_w = -\frac{k}{\mu_w}\frac{\partial p_w}{\partial x}, \quad . \quad . \quad . \quad . \quad . \quad . \quad . \quad . \quad . \quad (2)$$

p_w being the pressure in the water phase.

For the amount of oil passing the cross section we find likewise,

$$q_o = u_o\ (1 - S_{or} - S_w) \quad , \quad . \quad . \quad . \quad . \quad . \quad . \quad (3)$$

with

$$u_o = -\frac{k}{\mu_o}\frac{\partial p_o}{\partial x}. \quad . \quad . \quad . \quad . \quad . \quad . \quad . \quad . \quad . \quad (4)$$

Since macroscopic parts of the oil-saturated formation are by-passed by the penetrating water fingers, it is understandable that the difference, p_c, between pressures in oil and water phase will be approximately constant as long as the finger edges do not interfere. This will be true up to high water saturations. Consequently, $p_o - p_w$ = constant, and

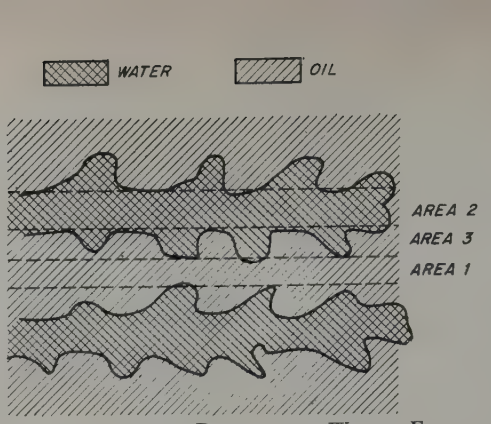

Fig. 2—Idealized Picture of Water Fingers Showing Protrusions and Oil Pockets.

$$\frac{\partial p_o}{\partial x} = \frac{\partial p_w}{\partial x} \quad . \quad . \quad . \quad . \quad . \quad . \quad . \quad . \quad . \quad . \quad . \quad (5)$$

From Eqs. 2, 4, and 5, it follows that

$$u_w = Mu_o \quad . \quad . \quad . \quad . \quad . \quad . \quad . \quad . \quad . \quad . \quad . \quad (6)$$

The total amount of fluid passing the cross section is

$$q = q_o + q_w \quad , \quad . \quad . \quad . \quad . \quad . \quad . \quad . \quad . \quad . \quad . \quad (7)$$

and owing to assumed incompressibility of both oil and water phase, q is only a function of time and not of place.

For the fractional water flow, f_w, we find with Eqs. 1, 3, 6, and 7,

$$f_w = \frac{q_w}{q} = \frac{M(S_w - S_{wm})}{(M-1)(S_w - S_{wm}) + B}, \quad . \quad (8)$$

with

$$B = 1 - S_{or} - S_{wm} \quad . \quad . \quad . \quad . \quad . \quad . \quad . \quad . \quad . \quad (9)$$

The equation of continuity for the water phase is

$$\frac{\partial q_w}{\partial x} + \phi\frac{\partial S_w}{\partial t} = 0 \quad . \quad . \quad . \quad . \quad . \quad . \quad . \quad . \quad (10)$$

or

$$\frac{\partial f_w}{\partial X} + \frac{\partial S_w}{\partial W_i} = 0 \quad , \quad . \quad . \quad . \quad . \quad . \quad . \quad . \quad (11)$$

in which $W_i = \frac{\int q\,dt}{\phi L}$ equals the cumulative water injection as a fraction of the pore volume. L is the length of the formation and $X = \frac{x}{L}$ is the dimensionless distance along the flow direction taken from the point of water injection.

From Eq. 8 it follows that f_w is a function of S_w only; therefore, we can write for Eq. 11,

$$\frac{df_w}{dS_w}\frac{\partial S_w}{\partial X} + \frac{\partial S_w}{\partial W_i} = 0. \quad . \quad . \quad . \quad . \quad . \quad . \quad . \quad . \quad (12)$$

Differentiating Eq. 8 gives

$$f_s = \frac{df_w}{dS_w} = \frac{MB}{[(M-1)(S_w - S_{wm}) + B]^2} \quad . \quad (13)$$

The general solution of this differential equation is

$$X = \omega(S_w) + \frac{df_w}{dS_w}W_i. \quad . \quad . \quad . \quad . \quad . \quad . \quad . \quad (14)$$

We assume the initial water front (at $t = 0$ or $W_i = 0$) to be undisturbed and perpendicular to the flow direction; thus

$$\omega(S_w) \equiv 0 \quad . \quad . \quad . \quad . \quad . \quad . \quad . \quad . \quad . \quad . \quad . \quad (15)$$

Substitution of Eqs. 13 and 15 in Eq. 14 results in

$$X = \frac{MBW_i}{[(M-1)(S_w - S_{wm}) + B]^2} \quad , \quad . \quad . \quad (16)$$

and we find for the water saturation distribution in the region where both oil and water flow, that

$$S_w = S_{wm} - \frac{B}{M-1} + \frac{\sqrt{MB}}{M-1}\sqrt{\frac{W_i}{X}} \quad . \quad . \quad (17)$$

We now discuss the range of saturations where Eqs. 16 and 17 are valid. First of all it is clear that S_w cannot increase above $1 - S_{or}$ (see Fig. 3). From Eq. 16 we see that this critical value is reached at a distance, X_1, given by

$$X_1 = \frac{W_i}{MB} \quad . \quad . \quad . \quad . \quad . \quad . \quad . \quad . \quad . \quad . \quad . \quad (18)$$

In the foregoing treatment it has been assumed that there is no flow perpendicular to the main direction of flow (x direction). This assumption is roughly confirmed by the qualitative observation that fingers are not seen to deviate appreciably from the mean direction of flow.

Still, before breakthrough, this assumption can never be everywhere correct. Especially at the top of the fingers there should also be a component of the pressure gradient in directions perpendicular to the X-axis. This is also observed visually, for this is the very spot where the mentioned protrusions are formed. This phenomenon calls for a more detailed inspection.

The formation of water protrusions at the finger tips requires a certain amount of water; however, once filled, these protrusions do not constitute a passageway for the water; this requires S_w to exceed S_{wm} (see also Eq. 1, which breaks down for $S_w < S_{wm}$). Therefore, we must cut-off the theoretical water saturation distribution (Eq. 17) at a point, X_c, where the saturation is larger than S_{wm}. This critical water saturation is S_c (see also Fig. 4). Obviously, the vertical cut-off as given in Fig. 4 is an idealization; the real change may be somewhat more gradual. To find the cut-off point we reason as follows.

The amount of water entering the unit cross section in one second at X_c is used to fill the formation to the critical saturation, S_c. If we denote the velocity at which S_c is propagated by v_c, this amount has to be equal to $\phi v_c S_c$

$$(q_w)_{S_w = S_c} = \phi\, v_c S_c \quad . \quad . \quad . \quad . \quad . \quad . \quad . \quad . \quad . \quad (19)$$

Now the velocity at which the critical saturation propagates is defined

$$v_c = \left(\frac{dx}{dt}\right)_{S_w = S_c} \quad . \quad . \quad . \quad . \quad . \quad . \quad . \quad . \quad . \quad (20)$$

or using the definitions of X and W_i,

$$v_c = \frac{q}{\phi}\left(\frac{dX}{dW_i}\right)_{S_w = S_c} \quad . \quad . \quad . \quad . \quad . \quad . \quad . \quad . \quad (21)$$

or using Eq. 14,

$$v_c = \frac{q}{\phi}\,(f_s)_{S_w = S_c} \quad . \quad . \quad . \quad . \quad . \quad . \quad . \quad . \quad . \quad (22)$$

Substitution of Eq. 22 in Eq. 19 gives for the condition at the cut-off boundary,

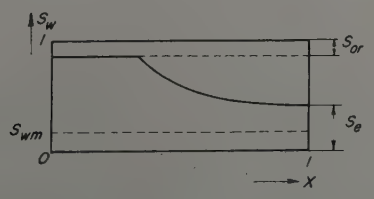

FIG. 3 — SCHEMATIC REPRESENTATION OF WATER SATURATION DISTRIBUTION AFTER BREAKTHROUGH.

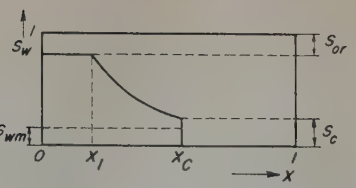

FIG. 4 — SCHEMATIC REPRESENTATION OF WATER SATURATION DISTRIBUTION BEFORE BREAKTHROUGH.

$$\left(\frac{q_w}{q} = f_w = \frac{df_w}{dS_w} S_w\right)_{S_w = S_c} \quad . \quad . \quad . \quad . \quad . \quad . \quad (23)$$

Using Eqs. 8 and 13, we find from Eq. 23 the water saturation at the cut-off point

$$S_c = S_{wm} + \sqrt{\frac{BS_{wm}}{M-1}}, \quad . \quad . \quad . \quad . \quad . \quad . \quad . \quad (24)$$

and for X_c, substituting Eq. 24 in Eq. 16, gives

$$X_c = \frac{MBW_i}{[B + \sqrt{B(M-1)S_{wm}}]^2} \quad . \quad . \quad . \quad . \quad . \quad (25)$$

Breakthrough will occur when the critical saturation, S_c, arrives at the outflow end of the formation. At that moment the total cumulative production, W_i, equals the breakthrough recovery, N_{pb}. Therefore, if we substitute in Eq. 25, $X_c = 1$, $W_i = N_{pb}$, we find

$$N_{pb} = \frac{A^2}{MB}, \quad . \quad . \quad . \quad . \quad . \quad . \quad . \quad . \quad . \quad . \quad (26)$$

where

$$A = \sqrt{(M-1)BS_{wm}} + B \quad . \quad . \quad . \quad . \quad . \quad (27)$$

Eq. 26 shows that for $M = \infty$, $N_{pb} = S_{wm}$, i.e., breakthrough occurs at the moment when the minimum saturation is established throughout the formation.

The cumulative oil recovery after breakthrough, N_p, is easily found by integrating the water saturation present in the formation (see Fig. 3)

$$N_p = X_1\,(1 - S_{or}) + \int_{X_1}^{1} S_w dX \quad ,$$

or using Eqs. 17 and 18,

$$N_p = S_{wm} + \frac{1}{M-1}\,(2\sqrt{W_i MB} - W_i - B).$$

$$. \quad . \quad . \quad . \quad . \quad . \quad . \quad . \quad . \quad . \quad . \quad . \quad . \quad . \quad . \quad . \quad . \quad . \quad . \quad (28)$$

In these equations N_p like W_i is expressed in fractions of the pore volume.

From Eq. 28, all recoveries after breakthrough can be easily calculated. Eq. 28 is valid up to the moment that $X_1 = 1$, or for $W_i \leq MB$. For $W_i \geq MB$ the recovery is $N_p = 1 - S_{or}$.

How the oil produced varies with viscosity ratio, M, and gross production, W_i, is illustrated in Fig. 5. Here the curves are calculated from Eq. 28 for $S_{wm} = S_{or} = 0.15$. The breakthrough recoveries according to Eq. 26 are indicated as well.

The dotted lines in Fig. 5 indicate the oil production reached at the economic limit of the water cut (f_t). Curves are given for values of $f_t = 0.95$, 0.98 and 0.99, respectively.

The relation between f_t and ultimate recovery, N_{pu}, which has been used to calculate these curves, can easily be found from Eqs. 8, 17, and 28 by eliminating S_w and W_i and substituting $X = 1$. This results in

$$N_{pu} = S_{wm} + B\,\frac{M - f_t\,(M-1)}{[M - f_t\,(M-1)]^2} \quad (28a) \quad . \quad .$$

From Fig. 5 it is seen that for intermediate oil-

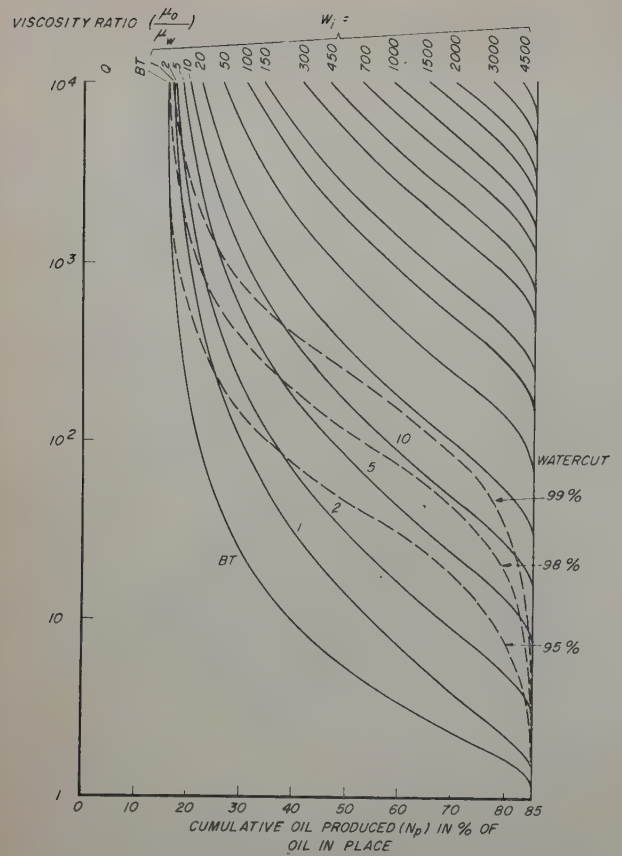

FIG. 5 — OIL PRODUCED AS A FUNCTION OF VISCOSITY RATIO, CALCULATED, FOR $S_{or} = S_{wm} = 0.15$ FOR BREAKTHROUGH (BT), AND VARIOUS VALUES OF GROSS PRODUCTION GIVEN IN MULTIPLES OF OIL IN PLACE.

water viscosity ratios ($M \approx 100$) the limit to which production can be carried on profitably has an enormous effect on the final recovery.

CALCULATION OF THE PRESSURE DROP ACROSS THE FORMATION

Pressure drops across the formation are easily calculated from the foregoing results by using Darcy's equation,

$$\Delta p = \frac{\mu L}{k} \int_0^1 u dX. \quad . \quad . \quad . \quad . \quad . \quad . \quad . \quad . \quad (29)$$

If we neglect the pressure difference between oil and water phase, μ and u represent either the water viscosity and the water velocity in Area 2 (where the water flows unhindered) or the oil viscosity and oil velocity in Area 1.

Before water breakthrough we find

$$\Delta p = \frac{\mu_w L}{k} \int_0^{X_1} u_w dX + \frac{\mu_w L}{k} \int_{X_1}^{X_c} u_w dX + \frac{\mu_o L}{k} \int_{X_c}^{1} u_o dX ,$$

and together with Eqs. 1, 3, 6, 7, 17, 18, and 25, this results in

$$P = 1 - W_i \left[MB \left(\frac{1}{A^2} - \frac{2}{3A^3} - \frac{1}{3M^2B^2} \right) \right],$$

$$. \quad (30)$$

for $0 \leq W_i \leq \frac{A^2}{MB}$,

where P is a dimensionless pressure drop,

$$P = \frac{\Delta p k}{q \mu_o L} \quad . \quad (31)$$

and A is again

$$A = \sqrt{(M-1)BS_{wm}} + B \quad . \quad (27)$$

After water breakthrough the pressure drop is given by

$$\Delta p = \frac{\mu_w L}{k} \int_0^{X_1} u_w dX + \frac{\mu_w L}{k} \int_{X_1}^{1} u_w dX$$

or

$$P = \frac{1}{3} \frac{W_i}{M^2B^2} + \frac{2}{3} \sqrt{\frac{1}{MBW_i}}, \quad . \quad (32)$$

for $\frac{A^2}{MB} \leq W_i \leq MB$.

After the saturation, $1 - S_{or}$, has reached the outflow end the pressure drop is finally given by substituting $W_i = MB$ in Eq. 32.

$$P = \frac{1}{MB} \quad . \quad (33)$$

for $W_i \geq MB$.

COMPARISON WITH EXPERIMENTAL RESULTS

Recoveries calculated by means of Eqs. 26 and 28 are compared with results of scaled model experiments carried out by Croes and Schwarz[3] in horizontal sand-filled tubes at a varying oil-water viscosity ratio in Fig. 6.

The value which must be substituted for the residual oil saturation, S_{or}, follows easily from the final recoveries obtained with low-viscosity oils; the experiments of Croes and Schwarz show a value of $S_{or} = 0.15$.

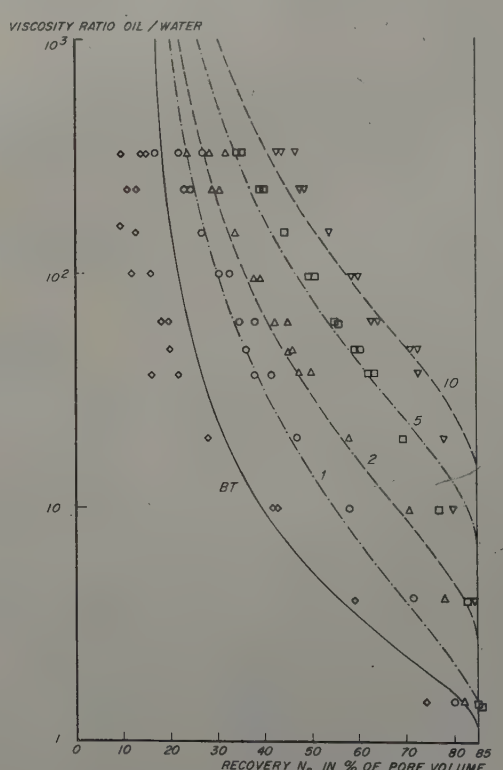

FIG. 6 — RESULTS OF WATERFLOODING EXPERIMENTS, ACCORDING TO CROES AND SCHWARZ[3], COMPARED WITH THEORY. DRAWN LINES ARE THEORETICAL FOR $S_{wm} = S_{or} = 0.15$ FOR BREAKTHROUGH (BT) AND $W_i = 1, 2, 5,$ AND 10 PORE VOLUMES.

The value of S_{wm} does not follow directly from the experiments. The best fit between theoretical and experimental results was obtained with $S_{wm} = 0.15$.

Fig. 6 shows good agreement for recoveries between 0.20 and 0.75; experimental breakthrough recoveries are often lower than the calculated values. This is not unrealistic since every inhomogeneity in the formation will tend to decrease the breakthrough recovery. Almost immediately after breakthrough, however, the discrepancy between theory and experiment was found to lie within the experimental error.

At recoveries over 75 per cent the theoretically predicted values are seen to be high. This is due to the fact that the capillary pressure difference, p_c, has been assumed to be a constant. For high water saturations it is known, however, that p_c increases with increasing saturation. This fact could be accounted for theoretically, but would give rise to far more complicated formulas and is therefore omitted for the time being.

A further check of the theory has been made by measuring the pressure drop across a model tube as a function of W_i and comparing the experimental results with those offered by the theory.

The experiments were carried out for values of $M = 3.15$ and 7.0. The injection rate was chosen high ($q = 15.3 \times 10^{-2}$ cm/sec) in order to minimize capillary effects. Fig. 7 illustrates the agreement between the experimental data and the theoretical curves for $S_{wm} = 0.15$ and $S_{or} = 0.10$.

All available experimental data (those presented here, as well as others) could be described theoretically with a value of $S_{wm} = 0.15$. The values of S_{or} in the used (loose) sands showed more variation, i.e., from 0.07 up to 0.15.

PRODUCTION PERFORMANCE OF A FIELD WITH LINEARLY ENCROACHING EDGE WATER PRODUCED BY EVENLY DISTRIBUTED WELLS

Specification of the Theoretical Model Reservoir

The production in an actual field differs appreciably from that just described, since oil is recovered from wells more or less regularly distributed over the entire field. Especially at the moment of the first water production, oil recoveries will be much smaller than predicted by the formulas derived so far as a consequence of an early water breakthrough in the wells situated close to the flank.

We will now calculate the production performance of a linear water-drive field with a regular grid of wells. In order to make the problem dependent on one space coordinate only (to render it linear), we will introduce a theoretical model with an infinite number of regularly spaced wells covering the whole field.

Let us consider an idealized oil field produced by linearly encroaching edge water under the following conditions: (1) the field has a rectangular shape and a constant thickness, (2) edge water is encroaching from one side of the rectangle, (3) the production is obtained from an infinite number of regularly distributed wells, (4) the formation is homogeneous, (5) the wells are closed in upon reaching a predetermined water-cut value, (6) all producing wells have the same gross production rate, (7) gravity and capillary effects are negligible, and (8) initial oil saturation is 100 per cent.

Points 1, 2, and 3 make the problem linear, which

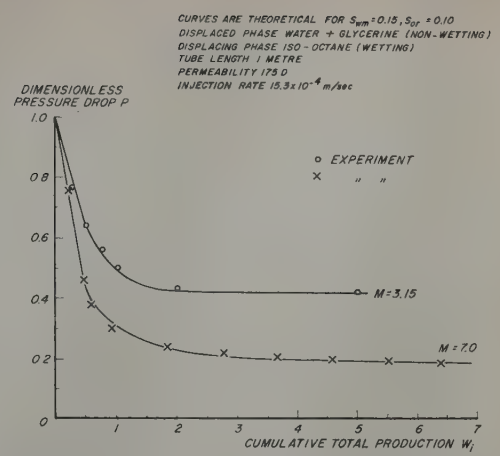
CURVES ARE THEORETICAL FOR S_{wm} = 0.15, S_{or} = 0.10
DISPLACED PHASE WATER + GLYCERINE (NON-WETTING)
DISPLACING PHASE ISO - OCTANE (WETTING)
TUBE LENGTH 1 METRE
PERMEABILITY 175 D
INJECTION RATE 15.3 x 10⁻⁴ m/sec
DIMENSIONLESS PRESSURE DROP P
o EXPERIMENT
× " "
M = 3.15
M = 7.0
CUMULATIVE TOTAL PRODUCTION W_i

Fig. 7—Calculated Pressure Drops Compared with Results of Linear Displacement Experiments.

is necessary to make possible a theoretical treatment. In almost any theoretical treatment Point 4 must be assumed; in practice, however, large inhomogeneities will be most common. Especially will water breakthrough occur earlier in inhomogeneous formations, which means that the results of our calculation applied to an inhomogeneous field will be on the optimistic side for the first stage of the production history. There is experimental evidence, however, that the ultimate recovery is not much affected, at all events, not at high viscosity ratios[2].

In Point 6 it is assumed that all wells have the same gross production rate. In a real oil field this will not be strictly valid. The wells closer to the original oil-water interface will have a larger production rate than the wells nearer the crest. Also the wells which produce both oil and water will have a higher gross production rate than the others. On the other hand, the well spacing nearer the water front will often be larger than at the crest, which partly offsets this effect.

The sole object of Point 8, i.e., assuming the initial oil saturation to be 100 per cent, is to keep the formulas more simple. When the results of this paper are applied to an actual oil field having a connate water saturation, cumulative oil productions are found expressed as a fraction of the oil in place, and not of the total pore volume.

We may expect our theoretical model to describe oil production fairly accurately, in particular at higher viscosity ratios. Small deviations may be expected in an early stage of the producing life of an inhomogeneous field.

Determination of the Water Saturation Distribution

Fig. 8 indicates how the formation can be split into three regions. In Region 1 the wells have been abandoned; the wells produce both oil and water in Region 2 and clean oil in Region 3. The lower portion is a sketch of the water saturation distribution at the same moment as represented above.

The first problem is to determine this saturation distribution as a function of the cumulative gross production. We shall consider this problem separately for the various regions.

Region 1

Here we have the same situation as described in a

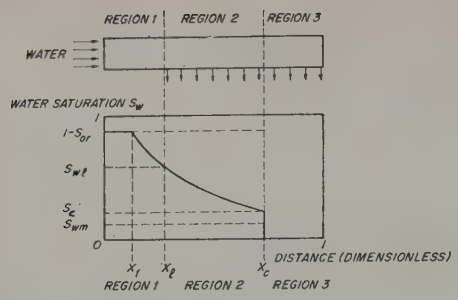

FIG. 8—ILLUSTRATION OF HOW FORMATION CAN BE SPLIT INTO THREE REGIONS (TOP), ACCOMPANIED BY DIAGRAM (LOWER) SHOWING WATER SATURATION DISTRIBUTION.

previous section; oil is displaced by water injected at one side of the formation ($X = 0$), and production is obtained from the other side ($X = X_l$).

Therefore, the water saturation distribution between X_1 and X_l, i.e., in Region 1, is given again by Eq. 17, where

$$X_1 = \frac{W_i}{MB}, \quad \ldots \quad (18)$$

and $X_l = f_{sl} W_i$ (see Eq. 14). For values of X smaller than X_1 the water saturation is equal to $1 - S_{or}$.

REGION 2

Through every cross section in this region both oil and water flow simultaneously. Eqs. 1 and 3 are also valid in Region 2, but the sum of q_w and q_o, denoted by q_t, this time depends on X, owing to withdrawal of fluid through the wells in this region. Since all producing wells in the field are assumed to have the same gross production rate, q_t decreases linearly with increasing X.

At the end of the field (for $X = 1$) $q_t = 0$ and for $X = X_l$, q_t must equal q. Therefore, in Regions 2 and 3,

$$q_o + q_w = q_t = q \frac{1 - X}{1 - X_l}. \quad \ldots \quad (34)$$

With Eqs. 1 and 3 this becomes in Region 2,

$$u_w(S_w - S_{wm}) + u_o(1 - S_{or} - S_w) = q \frac{1 - X}{1 - X_l}. \quad \ldots \quad (35)$$

By means of this equation we can calculate the fractional water flow, f_w. The result is identical to that for Region 1,

$$f_w = \frac{M(S_w - S_{wm})}{(M - 1)(S_w - S_{wm}) + B}. \quad \ldots \quad (8)$$

Therefore, also $f_s = \frac{df_w}{dS_w}$ is identical in both regions.

Equality of the pressure gradients in water and oil phases again gives,

$$u_w = Mu_o \quad \ldots \quad (6)$$

The equation of continuity is more complicated in Region 2 than in Region 1 since we must take account of the fluid produced by the wells. We find that

$$\frac{\partial S_w}{\partial W_i} + F \frac{u_w}{q}(S_w - S_{wm}) + \frac{\partial}{\partial X}\frac{u_w}{q}(S_w - S_{wm}) = 0. \quad \ldots \quad (36)$$

F is the fraction of the fluid flowing through the cross section at coordinate X, which is produced per unit time and unit length by the wells situated at coordinate X:

$$F = -\frac{1}{q_t}\frac{dq_t}{dX}, \quad \ldots \quad (37)$$

or with Eq. 34,

$$F = \frac{1}{1 - X} \quad \ldots \quad (38)$$

Substitution of Eqs. 6, 35 and 38 in Eq. 36 results in

$$(1 - X_l)\frac{\partial S_w}{\partial W_i} + f_s(1 - X)\frac{\partial S_w}{\partial X} = 0 \quad \ldots \quad (39)$$

This differential equation governing the saturation distribution in Region 2 is comparable to Eq. 10, valid in Region 1. It is easy to see that for $X = X_l = f_{sl} W_i$, both equations become identical. The solution of Eq. 39 is

$$X = 1 - (1 - W_i f_{sl})^{f_s/f_{sl}} \quad \ldots \quad (40)$$

or

$$S_w = S_{wm} - \frac{B}{M - 1} + \frac{1}{M - 1}\sqrt{\frac{MB}{f_{sl}}}\sqrt{\frac{\ln\frac{1}{1 - W_i f_{sl}}}{\ln\frac{1}{1 - X}}} \quad \ldots \quad (41)$$

This equation becomes identical to the corresponding Eq. 17 for $X = X_l = W_i f_{sl}$.

Eq. 41 is valid between X_l and X_c, which still have to be determined. According to Eqs. 8 and 13 it follows for $X = X_l$ and $S_w = S_{wl}$, that

$$f_l = \frac{M(S_{wl} - S_{wm})}{(M - 1)(S_{wl} - S_{wm}) + B}$$

and

$$f_{sl} = \frac{MB}{[(M - 1)(S_{wl} - S_{wm}) + B]^2}.$$

Elimination of S_{wl} from these two equations results in

$$f_{sl} = \frac{1}{MB}[f_l + M(1 - f_l)]^2. \quad \ldots \quad (42)$$

For $X = X_c$ the water saturation is S_c, which is found from the same boundary conditions (Eq. 19) as used in the previous section. We now have to use the appropriate equations valid for Region 2 instead.

It is easily found that Eq. 24,

$$S_c = S_{wm} + \sqrt{\frac{BS_{wm}}{M - 1}}, \quad \ldots \quad (24)$$

is valid in Region 2 as well.

Hence, using Eq. 40, we find

$$X_c = 1 - (1 - W_i f_{sl})^{f_{sc}/f_{sl}} \quad \ldots \quad (43)$$

with

$$f_{sc} = \frac{MB}{[B + \sqrt{B(M - 1)S_{wm}}]^2}$$

or

$$f_{sc} = \frac{MB}{A^2}. \quad \ldots \quad (44)$$

To recapitulate we give the complete saturation distribution as follows.

For $0 \leq X \leq X_1$:

$$S_w = 1 - S_{or}$$

with

$$X_1 = \frac{W_i}{MB}.$$

For $X_1 \leq X \leq X_l$:

$$S_w = S_{wm} - \frac{B}{M - 1} + \frac{\sqrt{MB}}{M - 1}\sqrt{W_i/X}$$

with

$$X_i = W_i f_{sl},$$

$$f_{sl} = \frac{1}{MB}[f_i + M(1 - f_i)]^2.$$

For $X_i \leq X \leq X_c$:

$$S_w = S_{wm} - \frac{B}{M-1} + \frac{1}{M-1}\sqrt{\frac{MB}{f_{sl}}}\sqrt{\frac{\ln \frac{1}{1 - W_i f_{sl}}}{\ln \frac{1}{1-X}}}$$

with

$$X_c = 1 - (1 - W_i f_{sl})^{f_{sc}/f_{sl}}$$

and

$$f_{sc} = \frac{MB}{[B + \sqrt{B(M-1)S_{wm}}]^2}.$$

For $X_c \leq X \leq 1$:

$$S_w = 0.$$

Oil Production Performance

The cumulative oil production, N_{pt}, of the total field is again given by

$$N_{pt}(W_i) = \int_0^1 S_w(X, W_i)\, dX.$$

Using the results of the previous section we find for the cumulative oil production as function of cumulative gross production:

$$N_{pt} = -\frac{MB}{M-1}X_1 + \frac{2}{M-1}\sqrt{\frac{MB}{f_{sl}}}X_i + \left(S_{wm} - \frac{B}{M-1}\right)X_c + \frac{1}{M-1}\sqrt{\frac{\pi MB}{f_{sl}}}y_i(\operatorname{erf} y_c - \operatorname{erf} y_i), \quad . \quad . \quad . \quad . \quad . \quad . \quad . \quad . \quad (45)$$

where M is oil-water viscosity ratio,

$B = 1 - S_{or} - S_{wm}$,

$$f_{sl} = \frac{1}{MB}[f_i + M(1 - f_i)]^2,$$

$$f_{sc} = \frac{MB}{[B + \sqrt{B(M-1)S_{wm}}]^2},$$

$$X_1 = \frac{W_i}{MB},$$

$$X_i = W_i f_{sl},$$

$$X_c = 1 - (1 - W_i f_{sl})^{f_{sc}/f_{sl}},$$

$$y_i = \sqrt{\ln \frac{1}{1 - X_i}},$$

$$y_c = \sqrt{\ln \frac{1}{1 - X_c}} = \sqrt{\frac{f_{sc}}{f_{sl}}}\, y_i,$$

$$\operatorname{erf} y = \frac{2}{\sqrt{\pi}}\int_0^y e^{-\alpha^2}\, d\alpha,$$

W_i is cumulative water injection in pore volumes, and N_{pt} is cumulative oil production in pore volumes.

Oil Productions of Separate Wells

In the following we will calculate the cumulative oil productions of the separate wells, both at the moment of water breakthrough and when the economic limit of the water cut is reached.

In order to simplify the problem we have assumed that with respect to oil production performance our idealized field with an infinitely dense well spacing is representative of a real oil field with a regular well pattern. If this approximation is permitted, we may use the same reasoning the other way round, i.e., in order to calculate the cumulative oil production of the separate wells we may integrate the oil produced by a region of our theoretical model and allot the amounts to one well in the actual field.

Suppose we have an oil field with n rows of wells between the water front and the crest, the well spacing being λ. We want to know the amounts of oil produced by the wells 1, 2, . . . i, . . . n. ($n\lambda = 1$) and we assume that these amounts are equal to the amounts of oil produced between $\lambda i - \lambda$ and λi ($i = 1, 2, \ldots n$) in our theoretical model. During a certain time every well produces clean oil; this we call Period A. Afterwards a well produces oil and water until the economic limit is reached (Period B).

Period A

The total amount of fluid (oil) flowing through the cross section at coordinate X is $q_i = q\,\frac{1 - X}{1 - X_i}$ (see Eq. 34). The amount of oil produced between X and $X + dX$ during a time dt is $-\frac{dq_i}{dX}\,dX\,dt$ or $\frac{q}{1 - X_i}\,dX\,dt$. At the end of Period A, $t = t_c$; $X = X_c$; $W_i = W_{ic}$. According to Eq. 43,

$$X_c = X = 1 - (1 - W_{ic} f_{sl})^{f_{sc}/f_{sl}}$$

or

$$\ln \frac{1}{1 - W_{ic} f_{sl}} = \frac{f_{sl}}{f_{sc}} \ln \frac{1}{1 - X}. \quad . \quad . \quad . \quad . \quad (46)$$

The cumulative oil production at the moment of water breakthrough obtained between X and $X + dX$ expressed as a fraction of the total pore volume is

$$\frac{1}{\phi L}\int_0^{t_c} \frac{q}{1 - X_i}\,dX\,dt = \int_0^{W_{ic}} \frac{q}{1 - W_i f_{sl}}\,dX\,dW_i$$

(see Eq. 14).

After integration and using Eq. 46 it becomes $\frac{dX}{f_{sc}} \ln \frac{1}{1 - X}$. The cumulative oil production at water breakthrough obtained from well No. i is then

$$\int_{\lambda i - \lambda}^{\lambda i} \frac{1}{f_{sc}} \ln \frac{1}{1 - X}\, dX$$

or

$$\frac{1}{f_{sc}}\left[\lambda + \lambda \ln \frac{1}{1 - \lambda(i-1)} - \frac{1 - \lambda i}{\lambda} \ln\left(1 + \frac{\lambda}{1 - \lambda i}\right)\right]. \quad . \quad . \quad . \quad . \quad . \quad . \quad . \quad . \quad . \quad . \quad . \quad . \quad (46a)$$

This amount of oil is expressed as a fraction of the pore volume of the total field. However, it is more convenient to express the production of the separate wells as a fraction of the pore volume corresponding to their allotted area. Therefore we must divide Eq. 46a by λ, and so find for the cumulative oil production of well No. i at the moment of water breakthrough (N_{ib}):

$$N_{ib} = \frac{1}{f_{sc}}\left[1 + \ln \frac{1}{1 - \lambda(i-1)} - \frac{1 - \lambda i}{\lambda} \ln\left(1 + \frac{\lambda}{1 - \lambda i}\right)\right]_{i = 1 \ldots n} \quad . \quad . \quad . \quad . \quad . \quad . \quad . \quad . \quad . \quad . \quad . \quad (47)$$

or

$$N_{ib} = \frac{F(\lambda, i)}{f_{sc}} \quad \ldots \quad (48)$$

with

$$F(\lambda, i) = \left[1 + \ln \frac{1}{1 - \lambda(i-1)} - \frac{1 - \lambda i}{\lambda} \ln\left(1 + \frac{\lambda}{1 - \lambda i}\right)\right]_{i = 1 \ldots n} \quad \ldots \quad (49)$$

PERIOD B

The wells produce oil and water during Period B. The economic limit marks the end of Period B, then $t = t_l$; $X = X_l$; $W_i = W_{il}$; and $X_l = X = f_{sl}\, W_{il}$. The total amount of fluid flowing through a cross section at X is $q_t = q\,\frac{1 - X}{1 - X_l}$ (see Eq. 34). Fraction F of the fluid, which is produced per unit length and per unit time, is $F = \frac{1}{1 - X}$ (see Eq. 38).

The amount of oil produced between X and $X + dX$, and during time, dt, expressed as a fraction of pore volume of the total field, is $\frac{1}{\phi L} F\, u_o\, (1 - S_{or} - S_w)\, dX\, dt$. With Eqs. 6, 35, 38, and 41, this becomes

$$\frac{1}{\lambda}\frac{1}{M-1}\left[\sqrt{MB\, f_{sl}}\,\frac{\sqrt{\ln \frac{1}{1 - X}}}{\sqrt{\ln \frac{1}{1 - W_i f_{sl}}}\,(1 - W_i f_{sl})} - \frac{1}{M-1}\frac{1}{1 - W_i f_{sl}}\right] dX\, dW_i,$$

now expressed as a fraction of the pore volume belonging to one well. Integration from water breakthrough to the moment when the economic limit is reached gives

$$\frac{1}{\lambda}\frac{1}{M-1}\left[2\sqrt{MB}\left(\frac{1}{\sqrt{f_{sl}}} - \frac{1}{\sqrt{f_{sc}}}\right) - \left(\frac{1}{f_{sl}} - \frac{1}{f_{sc}}\right)\right] \ln \frac{1}{1 - X}\, dX \quad \ldots \quad (50)$$

The cumulative oil production of well No. i (after breakthrough) is

$$\frac{1}{M-1}\left[2\sqrt{MB}\left(\frac{1}{\sqrt{f_{sl}}} - \frac{1}{\sqrt{f_{sc}}}\right) - \left(\frac{1}{f_{sl}} - \frac{1}{f_{sc}}\right)\right]\left[1 + \ln \frac{1}{1 - \lambda(i-1)} - \frac{1 - \lambda i}{\lambda} \ln\left(1 + \frac{\lambda}{1 - \lambda i}\right)\right], \quad \ldots \quad (51)$$

and the total cumulative oil production of well No. i being the sum of Eqs. 47 and 51,

$$N_{il} = D \cdot F(\lambda, i) \quad \ldots \quad (52)$$

with

$$D = \frac{1}{f_{sc}} + 2\,\frac{\sqrt{MB}}{M-1}\left(\frac{1}{\sqrt{f_{sl}}} - \frac{1}{\sqrt{f_{sc}}}\right) - \frac{1}{M-1}\left(\frac{1}{f_{sl}} - \frac{1}{f_{sc}}\right). \quad \ldots \quad (53)$$

Application to an Actual Oil Field

In this section the theory developed is applied to an actual field. Eq. 45 presents a relation between the cumulative oil production and the cumulative gross production of the total field.

The field is produced by a strong water drive. The total productive area is 8.5 km^2 and the net sand bulk volume is 220.8×10^6 m^3.

The field is shut-off at the crest by a fault; down structure there is a natural water front. The angle of dip is ca 6°. The formation consists of nearly unconsolidated sand intersected by numerous thin layers of low permeability. A representative average porosity is assumed to be 35 per cent; the average permeability is several darcies. Crude viscosity at reservoir conditions is ca 250 cp. The formation water has a viscosity of 0.6 cp., making the viscosity ratio ca 400. The connate water saturation is estimated at 18 per cent. The following empirical relation between the cumulative oil production and the cumulative gross production of the field was found.

$$N_{pt} = \frac{1}{\alpha} \ln (W_t + \beta) + \gamma, \quad \ldots \quad (54)$$

where N_{pt} is cumulative oil production, W_t is cumulative gross production, and α, β, and γ are constants.

Assuming that this formula remains valid at high water cuts, we may extrapolate the production performance according to this formula. The result of this extrapolation is presented in Fig. 9. The dashed line represents production data of the field expressed as a fraction of the oil originally in place (estimated at 63.37×10^6 m^3). The dotted black line is the extrapolation of the production data according to Eq. 54:

$$N_p = 0.141^{10} \log (W_t - 0.12) + 0.225.$$

In order to check the validity of this extrapolation, a scaled model experiment has been done in the semi-technical model simulating the field. The main part of this model consisted of a rectangular box ($3.3 \times 1.5 \times 0.24$ m). Water can be injected through a manifold into the oil-saturated sand pack in the reservoir. Water and oil were produced through eight wells by means of proportioning pumps (Fig. 10). The permeability of the sand pack was 400 darcies; oil viscosity, 400 cp; water viscosity, 1 cp.; and injection rate, 1.9×10^{-2} cm^3/cm^2 sec. Production from the edge wells was half as great as that from the central wells.

The production curve for this experiment is also given in Fig. 9. It is clear that there is good agreement between the results of the model experiment and the practical data as well as the extrapolation according to Eq. 54.

We will now use these results to check the theory presented. The parameters of Eq. 45 have been given the following values: $M = 400$; $f_t = .99$; $S_{or} = .20$; and $S_{wm} = .15$.

A residual oil saturation of 20 per cent is assumed to be reasonable for a loose sand. The minimum water saturation, S_{wm}, is given the same value as was found to be valid for scaled model tube experiments in the previous section. Since the calculation work involved in using Eq. 45 is tedious and time consuming, it has

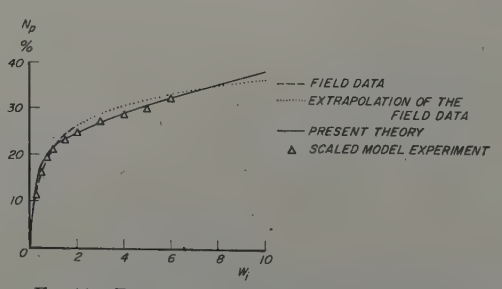

FIG. 9—PRODUCTION PERFORMANCE, WATER-DRIVE FIELD.

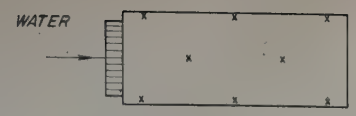

FIG. 10—ILLUSTRATING WELL PATTERN IN SEMI-TECHNICAL MODEL.

been programmed for a digital computer. The result of this computation, using the already-mentioned parameter values, is shown also in Fig. 9. We see that both the actual production performance (inclusive of extrapolation) and the result of the semi-technical model experiment correspond well with the behavior theoretically predicted.

As a second application we shall calculate the cumulative oil productions of the separate wells at water breakthrough and when the economic limit is reached for the same field. This is done by means of Eqs. 48 and 52. The field is produced by (on an average) eight rows of wells. Hence, in Eqs. 48 and 52 we can put $n = 8$ and $\lambda = 0.125$. Using the same parameter values as before we get $\frac{1}{f_{sc}} = 0.1824$, and $D = 0.3833$. Table 1 gives the values for N_{ib} and N_{il}.

From Eqs. 48 and 52 we deduce the two following important general rules: (1) the ratio of ultimate cumulative oil production to breakthrough cumulative oil production is the same for every well in the field, and (2) the ratio between the ultimate cumulative oil productions of two different wells in the field is identical to the ratio between their breakthrough cumulative oil productions.

The data of Table 1 show that the first ratio is 2.1 in the case of our field. However, since the theoretical value may be somewhat optimistic for the first stage of the production history, this figure is possibly on the low side.

From Table 1 we also learn that the crest wells of the field will produce almost 50 times as much oil as the wells close to the water front. The field is in too early a production stage to check the results from Table 1 for the crest wells. It would be interesting, however, to check theoretical predictions for the wells closer to the original water front. Unfortunately, at the moment of writing this paper, the data at the disposal of the authors were insufficient for doing so.

DISCUSSION OF THE INFLUENCE OF VARIATIONS IN THE VALUES OF THE PARAMETERS

The question may arise concerning the effect of changes in the chosen values of the parameters. In practice large variations occur in the value of the oil-water visosity ratio. However, in a very early stage of the producing life of a field, the proper value will be available with sufficient accuracy. The residual oil saturation can be obtained from a floodpot test in which a low-viscosity oil is displaced by water until the residual saturation is reached. The influence of a chosen value of the residual saturation upon the production performance of high-viscosity oil fields is, moreover, very small. For instance, in the field case given we have assumed a residual saturation of 20 per cent. However, if we had taken values of 15 or 25 per cent, the effect upon the calculated productions would have been in the order of 1 per cent.

The water-cut value at the economic limit depends on the specific circumstances of the oil field, which can be accurately calculated of the oil field, which can be accurately calculated if all data are available. Moreover, the value chosen is only important for the obtainable ultimate recovery of the field. The theoretical production performance of the field turns out to be almost identical for a wide range of values of f_t; the curve is only continued further (to higher recoveries) for higher values of f_t.

TABLE 1—CUMULATIVE OIL PRODUCTION AT WATER BREAKTHOUGH, N_{ib}, AND ULTIMATE CUMULATIVE OIL PRODUCTION, N_{il}, OF THE SEPARATE WELLS AS A FRACTION OF THEIR ALLOTTED PORE VOLUMES

i	$f(\lambda,i)$	N_{ib}	N_{il}
1	.0648	.012	.025
2	.2076	.038	.080
3	.3755	.069	.144
4	.576	.105	.221
5	.830	.151	.318
6	1.172	.214	.449
7	1.693	.309	.649
8	3.079	.562	1.179

Determination of the minimum water saturation, S_{wm}, presents a greater difficulty. The physical meaning of this parameter is the saturation of the immobile water corresponding to the edge region of the water fingers. It is, however, reasonable to assume that this saturation is identical in oil fields and scaled model experiments. Very fortunately all scaled model experiments investigated so far could be described within the accuracy of measurement with a value of the minimum water saturation of 15 per cent. Also, the application of the method to the production performance of the actual field showed a good fit with the production data when S_{wm} was assumed to be 15 per cent. However, since the applicability of scaled model experiments on displacement processes in consolidated porous structures is somewhat questionable, there is a possibility that for those cases another value of S_{wm} must be chosen.

CONCLUSIONS

1. The theory presented describes the effect of viscous fingering on the production performance of the water-drive process with simple analytical equations.
2. Production performance and pressure drops calculated according to the theory agree well with measurements in sand-filled tubes under scaled conditions.
3. The theory developed allows predicting the production performance of a water-drive field with regularly spaced wells. The only data which have to be known are the oil-water viscosity ratio, residual oil saturation, minimum water saturation, and the water-cut value at the economic limit of the wells.
4. With this theory it is possible to calculate the cumulative oil productions of the separate wells as a function of their distance to the original water front, both at water breakthrough and at the economic limit.

NOMENCLATURE

$A = \sqrt{(M-1)\,BS_{wm}} + B$ (constant)

$B = 1 - S_{or} - S_{wm}$ (constant)

$D = \frac{1}{f_{sc}} + 2\frac{\sqrt{MB}}{M-1}\left(\frac{1}{\sqrt{f_{sl}}} - \frac{1}{\sqrt{f_{sc}}}\right) - \frac{1}{M-1}\left(\frac{1}{f_{sl}} - \frac{1}{f_{sc}}\right)$

F = fraction of the flowing fluid produced per unit time and unit length

$f_w = \frac{q_w}{q}$ = fractional water flow = water cut

f_t = value of the water cut at the economic limit

$f_s = \dfrac{df_w}{dS_w}$

f_{st} = value of f_s at the economic limit

f_{sc} = value of f_s at the moment of water breakthrough

i = serial number of well; $i = 1 \ldots . n$

k = single-phase (specific) permeability

L = length of formation in direction of flow

M = oil-water viscosity ratio

n = number of rows of wells

N_{ib} = cumulative oil production from well No. i at the moment of water breakthrough expressed as a fraction of the pore volume allotted to well No. i

N_{it} = ultimate cumulative oil production of well No. i expressed as a fraction of the pore volume allotted to well No. i

N_p = cumulative oil production (in pore volumes or oil in place)

N_{pb} = recovery at water breakthrough (in pore volumes)

N_{pt} = cumulative oil production of the total field expressed as a fraction of the total pore volume or oil in place

N_{pu} = cumulative oil production in pore volumes at the economic limit of the water cut

N_{pw} = cumulative water production (in pore volumes or oil in place)

p_o = pressure in oil phase

p_w = pressure in water phase

p_c = capillary pressure difference

Δp = pressure drop

$P = \dfrac{\Delta pk}{q\mu_o L}$ = dimensionless pressure drop

q = water injection rate of the field

q_o = amount of oil flowing through a unit cross section of the formation (per unit time)

q_w = amount of water flowing through a unit cross section of the formation (per unit time)

q_t = amount of fluid (oil + water) flowing through a unit cross section of the formation

S_o = oil saturation

S_w = water saturation

S_{wm} = immobile water saturation (constant)

S_{or} = immobile oil saturation = residual oil saturation (constant)

S_c = critical water saturation (at the front) (constant)

t = time

t_t = moment when economic limit is reached

t_c = moment of water breakthrough

u_o = darcy single-phase flow velocity for oil

u_w = darcy single-phase flow velocity for water

v_c = speed of propagation of saturation, S_c; $v_c = \left(\dfrac{dX}{dW_i}\right) S_w = S_c$

W_i = cumulative gross production of the total field expressed as a fraction of the total pore volume, $W_i = \dfrac{\int q dt}{\phi L}$

x = distance from original water front

X = dimensionless distance from original water front, $X = \dfrac{x}{L}$

X_1 = coordinate where $S_w = 1 - S_{or}$

X_t = coordinate where economic limit is reached

X_c = highest value of X where water occurs

$y = \sqrt{\ln \dfrac{1}{1 - x}}$

$y_t = \sqrt{\ln \dfrac{1}{1 - X_t}}$

$y_c = \sqrt{\ln \dfrac{1}{1 - X_c}}$

λ = dimensionless well distance = real well distance/L

μ_o = absolute viscosity of oil

μ_w = absolute viscosity of water

ϕ = porosity

REFERENCES

1. Engelberts, W. F., and Klinkenberg, L. J.: "Laboratory Experiments on the Displacement of Oil by Water from Packs of Granular Materials", *Proc.*, Third World Petr. Congress, The Hague (1951) Part II, 544.
2. van Meurs, P.: "The Use of Transparent Three-Dimensional Models for Studying the Mechanism of Flow Processes in Oil Reservoirs", *Trans.* AIME (1957) **210**, 295.
3. Croes, G. A., and Schwarz, N.: "Dimensionally Scaled Experiments and the Theories on the Water-Drive Process", *Trans.* AIME (1955), **204**, 35. ★★★

Laboratory Studies of Five-Spot Waterflood Performance

L. A. RAPOPORT
C. W. CARPENTER, JR.
W. J. LEAS
MEMBERS AIME

THE JERSEY PRODUCTION RESEARCH CO.
TULSA, OKLA.

ABSTRACT

A program of scaled flow model experiments has been undertaken to study the performance of five-spot water floods. The modeling procedures are discussed and the construction and operation of the flow models are described. The tests were specifically designed to investigate the effects of injection rate and of oil-to-water viscosity ratio on oil recovery. The areal sweep of five-spot water floods was also studied, and direct comparisons between five-spot and linear flooding behavior have been established to permit better utilization of core analysis results for purposes of field waterflood evaluations.

INTRODUCTION

For a long time reservoir engineering procedures have been confined to the consideration of idealized, one-dimensional or linear systems.[1,2,3] However, direct application of the linear waterflood mechanism to the evaluation of actual field performance is justifiable only for the purposes of rough approximation. To obtain a realistic analysis of field behavior, it is necessary to account for reservoir geometry and well distribution, and to take into consideration the configuration of the flow of fluids between injection and producing wells.

In the past it has been attempted to account for the complex nature of the fluid movement in the reservoir by associating each well pattern with a certain "sweep-efficiency constant", e.g., a sweep efficiency of 72 per cent for the conventional five-spot pattern.[4] More recently, methods of waterflood evaluation have been improved by the introduction of variable sweep-efficiency factors, defining the areal coverage as a function of cumulative water injection and viscosity or "mobility" ratio.[5,6,7] These variable sweep-efficiency factors, derived from miscible fluid displacement experiments, require the assumption of piston-like displacement of oil by water. This implies that only one fluid, either oil or water, is moving at any one point of the reservoir at any moment. Such an assumption, however, is incompatible with the bulk of the experimental evidence and also theoretical considerations which indicate that usually in the area invaded by water, both oil and water are flowing in varying proportions, in accordance with the relative permeability characteristics of the porous medium.[1,3]

Another recent approach toward the evaluation of five-spot flooding behavior involves correlations of the areal sweep efficiency (observed in immiscible fluid experiments) with a "mobility ratio," based on the consideration of the "average" relative permeability to the displacing fluid.[8] Combination of these correlations with a modification of the Buckley-Leverett frontal-drive equation leads to a computational procedure for predicting the recovery performance of areal water floods. While of considerable interest, this approach has no complete theoretical justification and, therefore, does not entirely clarify the features of five-spot water floods.

Rigorous, theoretical treatment of waterflood behavior in two- or three-dimensional systems as encountered in the reservoir, including proper consideration of relative permeability and capillary-pressure functions, is as yet beyond the scope of analytical or computational methods. The behavior of such water floods can, however, be studied by means of scaled flow model experiments, which is the approach followed in these investigations. The flow model experiments described in this paper simulate a uniform, horizontal formation of constant thickness with fully penetrating wells. The system under consideration is entirely liquid saturated and not influenced by compressibility effects, which is representative of the situation achieved after gas fill-up under practical conditions. Gravity segregation effects are assumed to be negligible, which implies a relatively thin reservoir formation and/or low vertical permeability.

THEORETICAL CONSIDERATIONS

For a flow system of uniform thickness with no appreciable effects of gravity segregation, the analysis of water-oil displacement can be confined to a two-dimensional treatment based on the consideration of a "slice" of unit thickness. Referring to previously established derivations,[9] the displacement of oil by water in such a system can be described by the following, dimensionless equations:

$$\frac{\partial U_X}{\partial X} + \frac{\partial U_Y}{\partial Y} = 0 \quad . \quad . \quad . \quad . \quad . \quad . \quad . \quad . \quad . \quad (1)$$

$$\frac{\partial S}{\partial W_i} + F' \left[U_X \frac{\partial S}{\partial X} + U_Y \frac{\partial S}{\partial Y} \right] - \frac{\sigma \sqrt{k\phi}}{q\mu_w} \frac{1}{c}$$

$$\left[\frac{\partial}{\partial X} \left[\left(\Psi J' \frac{\partial S}{\partial X} \right) \right] + \frac{\partial}{\partial Y} \left(\Psi J' \frac{\partial S}{\partial Y} \right) \right] = 0 \quad . \quad . \quad . \quad (2)$$

Eq. 1 may be visualized as defining the components

Original manuscript received in Society of Petroleum Engineers office Sept. 25, 1956. Revised manuscript received April 3, 1958. Paper presented at Petroleum Branch Fall Meeting in Los Angeles, Calif., Oct. 14-17, 1956.
[1]References given at end of paper.

of a dimensionless flux or velocity distribution function, U_x and U_y, in terms of the (dimensionless) coordinates and the saturation at any point of the flow system. Eq. 2, then, defines the saturation at any point as a function of cumulative injection, W_i.

Eq. 2 indicates that areal flooding behavior depends specifically upon q, the rate of injection per unit sand thickness. More generally, it is seen that the displacement of oil by water in a two-dimensional flow system is largely governed by the dimensionless group of parameters,

$$\frac{q\mu_w}{\sigma\sqrt{k\phi}} = C_2 \quad . \quad . \quad . \quad . \quad . \quad . \quad . \quad . \quad . \quad . \quad . \quad (3)$$

This group C_2, may be designated as the "capillary pressure coefficient" because its value defines the relative importance of the capillary forces in the displacement of oil by water. It is seen that for a given value of C_2, all porous flow systems of given geometry, operated under similar boundary conditions, and characterized by the same oil-to-water viscosity ratio, and the same F, Ψ and J-functions, will yield the same flooding behavior, i.e., the same relation between cumulative water injection and oil production. Thus, Group C_2 represents a scaling factor which can be used to relate the results of flow model experiments to field performance. The scaling factor, C_2, represents an extension to two-dimensional flow systems of the scaling factor previously derived for linear systems, which may be expressed[3] as $C_1 = Lu\,\mu_w/\sigma\sqrt{k\phi}$.

It will be noted that with increasing values of the scaling factor, C_2, the relative importance of the capillary-pressure term in Eq. 2 decreases and may eventually become negligible. For sufficiently high rates of injection, or for scaling factors greater than a certain "critical" value, the water-oil displacement (Eq. 2) can, therefore, be expected to reduce to the simplified form,

$$\frac{\partial S}{\partial W_i} + F'\left[U_x\frac{\partial S}{\partial X} + U_Y\frac{\partial S}{\partial Y}\right] = 0 \quad . \quad . \quad . \quad . \quad (4)$$

Under these conditions, the water-oil displacement is no longer influenced by capillary effects and is independent of rate of injection. Extending the terminology employed in previous studies on linear flow systems,[3] two-dimensional water-oil displacements that are independent of rate may be qualified as "stabilized".

Another observation of considerable importance is that Eqs. 1 and 2 are obviously independent of the over-all dimensions of the flooded system.* Thus, it is inferred that the recovery performance of five-spot water floods is independent of well spacing. This does not imply that five-spot flooding performance, particularly as regards injectivity, is independent of the ratio of well diameter to well spacing. However, tests preliminary to these studies have indicated that variations in well diameter have little if any effect on recovery.

In the light of these theoretical aspects of water-oil displacement, the experimental program was subdivided into two phases: (1) investigations of the effect of rate on five-spot flooding behavior and evaluation of the range of practical conditions under which stabilized flooding behavior can be expected, and (2) studies of the recovery performance of stabilized five-spot water floods at various oil-to-water viscosity ratios and comparisons of linear waterflood performance with that of stabilized five-spot water floods. In general, the approach followed consisted of attempting the simulation of representative field conditions, rather than scaling specific reservoir cases.

*In this connection it may be noted that the scaling factor, C_2, derived by mathematical analysis is independent of dimensions, i.e., of the distance between wells, and thereby differs from the one proposed in Ref. 8.

EQUIPMENT AND PROCEDURES

Description of Flow Model

In order to obtain an areal flow model suitable for the present studies, an unconsolidated porous medium was packed in a chrome-plated steel box having inside dimensions of 32 × 16 × 2 in. (see Fig. 1). A transparent Lucite cover plate and the use of colored fluids permitted observation of the movement of the oil-water interface. A flexible copper sheet, sealed against the bottom plate of the model framework and inflated to about 100 psi, compacted the powders forming the porous medium of the model. Appropriate reinforcements in the model framework absorbed the stresses imposed by compaction pressure.

The model contains 19 fully penetrating wells (fine-mesh, nickel screen liners ⅛ in. in diameter), arranged to allow the selection of various flood patterns and to facilitate auxiliary operations such as saturation, flushing, and cleaning of the model. Teflon O-rings seal the liners to plastic wellheads on the top plate of the model.

The linear-flow system used in conjunction with the model was a flooding cell of Lucite tubing of 3.8-cm ID, and an effective length of 30.7 cm. Brass pistons inserted at each end of the tube and sealed by Teflon O-rings compacted the powders contained in the flooding cell. A network of grooves machined on the face of the compaction pistons insured evenly distributed flow over the cross section of the flooding cell. Particular precautions were taken to have identical porous media in the linear cell and the areal model, and also to ensure that the wettability characteristics of both systems remained unchanged throughout the tests.

Properties of Porous Media and Fluid Systems

The porous medium used in the model and linear flooding cell for the bulk of the studies consisted of a packing of graded glass beads, 120 microns in diameter, rendered preferentially oil-wet by dri-film treatment. Use of graded powders was found desirable to prevent segregation of particles during the packing, thus avoiding formation of heterogeneities in the flow systems. Application of dri-film was found to produce stable, oleophyllic surface characteristics, permitting preserva-

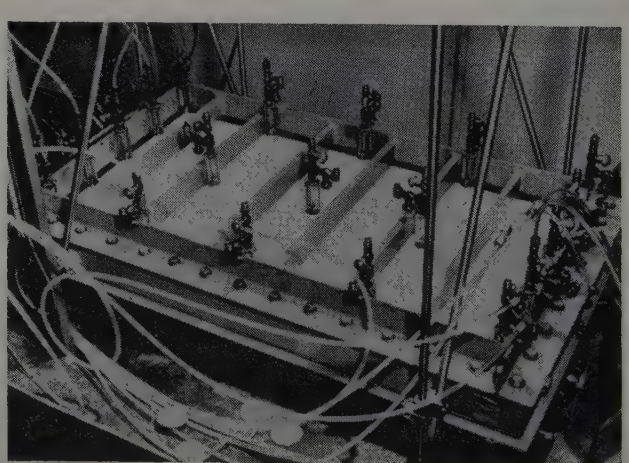

Fig. 1—Areal Flow Model.

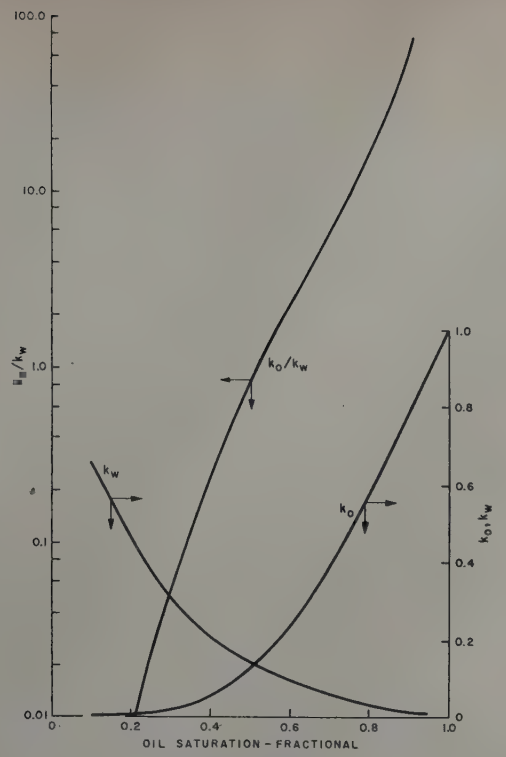

FIG. 2—RELATIVE PERMEABILITIES, DRI-FILMED GLASS BEAD PACKING.

tion of the same flow properties throughout the test program.

The porosity of the glass-bead packing was 39 per cent and the specific permeability to oil, about 11.4 darcies. The relative permeability characteristics of this packing (determined under dynamic, steady-state conditions and rechecked by computation from waterflood experiments[10]) are presented in Fig. 2. The *J*-curve, obtained from capillary displacement of oil by water, is included in Fig. 7.

Some of the results presented for purposes of comparison were obtained with a model packing of 200/230-mesh Alundum powder. This powder, of 70-micron average particle size, yielded a packing of 50 per cent porosity and 7,500-md permeability.

All the flooding experiments were performed in the absence of connate water. The fluids employed were solutions of sugar and chromium-potassium-sulfate (chrome alum) in distilled water to represent the aqueous phase, and various refined white oils varying in viscosity from 1 to 120 cp. The sugar was added to adjust the water viscosity (and hence the "viscosity level") of the fluid system, and the chrome alum was the color agent permitting observation of the oil-water displacement. All the oils were checked for contaminants (polar compounds) which, if present, could alter the surface properties of the porous medium and produce fluctuations in the values of interfacial tension throughout the test program. Fluid contamination was checked by interfacial tension measurements before and after filtering the fluids through activated alumina. Interfacial tension measurements were also conducted on the effluents from the flow systems during the flooding experiments. In all cases the interfacial tension of the various fluid systems was 43 ± 1 dyne/cm.

PROCEDURES

Throughout most of the studies the flow model was used to represent one-half of a five-spot element, and in some experiments two complete five-spot units were simulated. Each flooding test was conducted at a constant rate of injection. A combination of Moore null-matic pressure controllers and differential flow regulators was used to adjust and maintain injection rates within ± 5 per cent of any pre-set value. All tests were conducted in a thermostatically controlled room at 23 ± 0.2° C. Produced effluents were taken to oil-water separators which, in turn, overflowed into graduated cylinders. The accuracy of the volumetric oil and water production measurements obtained in this manner is estimated to be ± 1 per cent of pore volume.

At the completion of each flood the flow system was flushed with several pore volumes of pure heptane and then with distilled water to remove the sugar and chrome alum solution. The flow system was then dried with compressed air or nitrogen in preparation for the next test.

RESULTS AND DISCUSSION

The flooding experiments in the flow model and in the linear cell were conducted at oil-water viscosity ratios ranging from 0.1:1 to 95:1. In each case the fluid system employed in the linear cell was the same as in the flow model. A summary of the fluid characteristics, rates of injection, and values of scaling factor characterizing the flooding experiments in the flow model packed with glass beads is presented in Table 1. For the sake of convenience, the rates of injection in this table, as well as in Figs. 3 through 6, are expressed in usual "field units" namely, B/D/ft of sand thickness (per well). In order to permit correlation of the present results with those of previous investigations,[6,7,8] the values of mobility ratio corresponding to each of the viscosity ratios employed, and calculated on the basis proposed by Craig, *et al*,[8] are also listed in Table 1.

EFFECT OF RATE ON FIVE-SPOT FLOODING BEHAVIOR

Series of tests employing different porous media and oil-to-water viscosity ratios were conducted in the flow model to investigate the effect of injection rate on five-spot flooding behavior. The test results performed in the 200/230-mesh Alundum powder packing at an oil-water viscosity ratio of 0.9:1 are presented in Fig. 3. For low values of injection rate, from 1.75 to 22.0 B/D/ft, oil recoveries and flooding efficiency are seen to be markedly influenced by injection rate, increasing with increasing rates of injection. However, the effect of rate on flooding performance becomes less pro-

TABLE 1—SUMMARY OF FIVE-SPOT WATERFLOOD TESTS
(Glass-Bead Packing)

Oil-water viscosity ratio (fractional)	Water viscosity (cp)	Mobility ratio (fractional)	Injection rate into model (for half five-spot) (cc/min)	Injection rate per ft sand thickness (for full five-spot) (B/D/ft)	Scaling factor* $\frac{q\mu_w}{\sigma\sqrt{k\phi}}$
0.1	84.00	18.2	35.0	3.85	1.14×10^{-3}
1.0	8.22	2.9	1.0	0.11	3.12×10^{-4}
1.0	8.60	2.9	10.6	1.17	3.47×10^{-3}
1.0	8.20	2.9	120.0	13.20	3.73×10^{-2}
1.0	8.17	2.9	120.0	13.20	3.73×10^{-2}
5.4	7.60	1.0	80.0	8.80	2.31×10^{-2}
5.4	7.90	1.0	78.0	8.60	2.45×10^{-2}
5.4	7.90	1.0	12.0	1.32	3.61×10^{-3}
5.4	7.90	1.0	27.0	2.97	8.11×10^{-3}
15.7	1.12	0.64	150.0	16.50	6.39×10^{-3}
15.7	1.13	0.64	170.0	18.70	7.30×10^{-3}
40.0	1.11	0.52	110.0	12.10	4.64×10^{-3}
40.0	1.10	0.52	90.0	9.90	3.42×10^{-3}
40.0	1.11	0.52	75.0	8.25	3.17×10^{-3}
95.0	1.10	0.40	90.0	9.90	3.76×10^{-3}

*These values of scaling factor are obtained by expressing q in B/D/ft (per well), μ_w in cp, σ in dyne/cm, k in md, and ϕ, fractional.

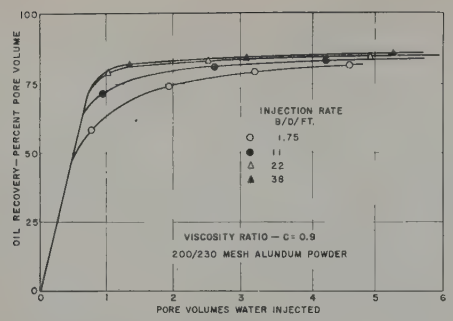

FIG. 3—EFFECT OF INJECTION RATE ON FIVE-SPOT FLOODING BEHAVIOR.

nounced with increasing rates and is eventually negligible for sufficiently high rates of injection. Identical results are obtained in the floods conducted at rates of injection of 22 and 38 B/D/ft, indicating that the five-spot flooding behavior in this porous medium becomes independent of rate, or stabilized, for rates of injection in excess of 22 B/D/ft. Thus, the critical value of the scaling factor, $q\mu_w/\sigma\sqrt{k\phi}$, is equal to (or slightly less than) 7.4×10^{-3}.*

The results of similar rate tests, conducted at an oil-water viscosity ratio of about 1:1 in the glass-bead packing, are presented in Fig. 4. It will be noted that the results presented in Fig. 4 were obtained using a high viscosity fluid system, corresponding to a water viscosity of 8.6 cp. Thus, stabilization is obtained at much lower rates (1.17 B/D/ft) than with the low viscosity fluid system employed in the 200/230-mesh Alundum powder packing (Fig. 3). However, the value of the scaling factor required to attain stabilized five-spot flooding behavior in the glass-bead packing is seen to be of the same order of magnitude as that required for the Alundum powder (3.5×10^{-3}).

Several tests were conducted to investigate the effect of injection rate on flooding behavior at higher viscosity ratios. Fig. 5 shows the flooding curves obtained for an oil-water viscosity ratio of 18:1 in the 200/230-mesh Alundum at injection rates of 6 and 18 B/D/ft. Since identical results were obtained at both rates, it is concluded that stabilized flooding behavior is obtained at this viscosity ratio for rates in excess of 6 B/D/ft, i.e., for values of scaling factor higher than 2×10^{-3}. The results of water floods at two different rates in the glass-bead packing for an oil-water viscosity ratio of 40:1 are shown in Fig. 6. Here, stabilized flooding is seen to be insured for rates in excess of 8.25 B/D/ft or for values of scaling factor greater than 3.2×10^{-3}.

The described data confirm that stabilized five-spot flooding behavior, anticipated on a theoretical basis, is actually observed for finite, relatively small values of the scaling factor. An additional finding is that for a given porous medium the critical value of scaling factor required to reach stabilized flooding behavior appears to decrease with increasing oil-water viscosity ratios (as could be generally expected from theoretical considerations).

In a rigorous sense the critical values of five-spot scaling coefficient derived from the present model experiments are applicable only to porous media possessing the same J-function as the materials used in this study. However, an extension of the present results to a wider range of porous media appears justifiable. To this effect

*As in Table 1, this value of scaling factor is obtained by expressing q in B/D/ft, μ_w in cp, σ in dyne/cm, and f, fractional.

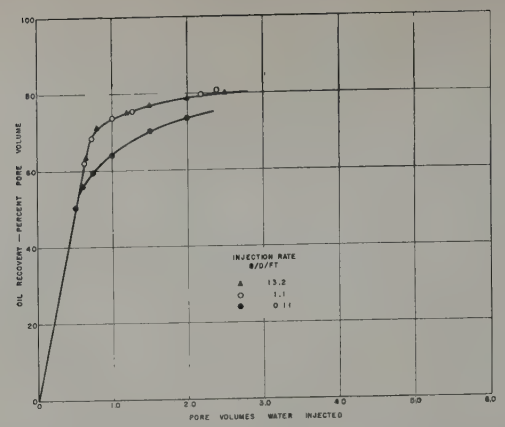

FIG. 4—EFFECT OF INJECTION RATE ON FIVE-SPOT FLOODING BEHAVIOR (VISCOSITY RATIO — C = 1.0), GLASS BEAD PACKING.

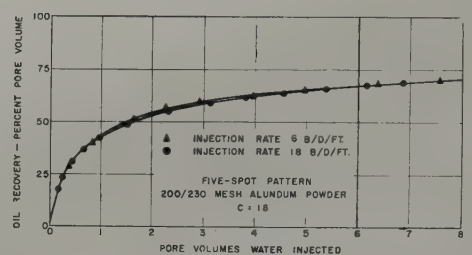

FIG. 5—EFFECT OF INJECTION RATE ON FIVE-SPOT FLOODING BEHAVIOR (STABILIZED CONDITIONS).

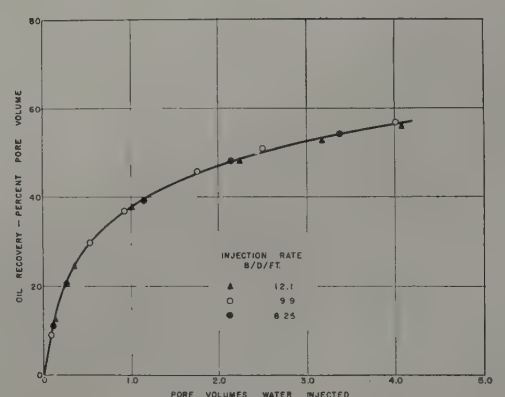

FIG. 6—EFFECT OF INJECTION RATE ON FIVE-SPOT FLOODING BEHAVIOR (VISCOSITY RATIO — C = 40), GLASS BEAD PACKING.

it will be noted from Eq. 2 that the relative importance of capillary forces in the displacement of oil by water is proportional to the derivative or slope, J', of the J-function. For purposes of first approximation, then, it may be considered that the critical values of scaling coefficient required to achieve stabilized flooding behavior increase also in direct proportion to the derivative of the J-function. For purposes of illustration, the J-function and its derivative applying to the glass-bead packing, together with the J- and J'-functions applying to various natural core materials, are presented in Figs. 7 and 8. As can be seen (Fig. 8), the J-function derivatives for a number of reservoir materials are less than five times greater than the J-function derivative characterizing the glass-bead model packing. This finding, then, indicates that for many natural reservoir materials, the critical value of scaling coefficient can be expected

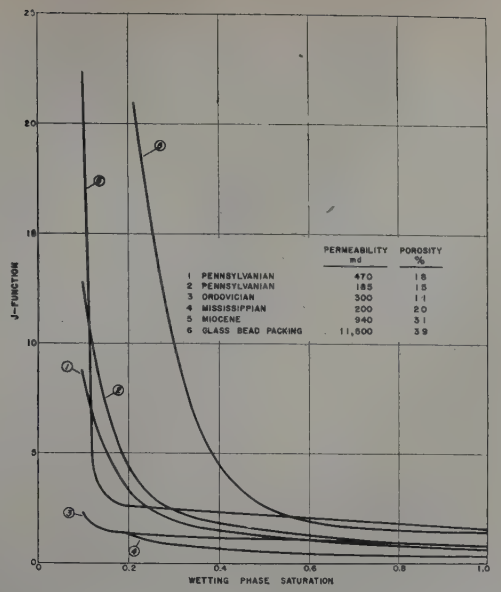

FIG. 7—*J*-FUNCTIONS FOR THE MODEL'S GLASS BEAD PACKING AND VARIOUS NATURAL POROUS MEDIA.

to be smaller than 1.75×10^{-2} (i.e., smaller than $5 \times 3.5 \times 10^{-3}$).

The flow model results regarding the stabilization of five-spot water floods gain particular significance if considered in the light of practical field conditions. For example, in formations of about 20 per cent porosity and 100-md effective permeability, the rates of injection usually maintained during a flooding operation are of the order of 10 B/D/ft of sand thickness. Assuming a water viscosity of 0.9 cp and an oil-water interfacial tension of 32 dyne/cm, the given conditions correspond to a scaling coefficient of 6.3×10^{-2}. This value is considerably greater than the critical values of scaling coefficient derived from the results of the flow model experiments and from consideration of the *J*-curves applying to various natural reservoir materials. Thus, it can be inferred that five-spot water floods under field conditions are likely to be stabilized and that (aside from effects of gas compressibility) field waterflood recoveries are independent of rate of injection. This important conclusion should be supplemented by theoretical considerations, based on Eq. 2, which indicate that five-spot flooding behavior is also independent of well spacing.

In order to qualify these statements properly, it is stressed that they imply consideration of homogeneous porous formations of relatively small thickness and/or low vertical permeability. With reference to such formations, flow model experiments are most likely to be representative of field performance if conducted under conditions simulating stabilized flooding behavior. Such conditions were insured in all the tests described hereafter that were carried out to investigate areal coverage, effects of viscosity ratio, and correlations between five-spot and linear flooding behavior.

AREAL COVERAGE

Visual observation of the waterflood sweep in the flow model was made possible by the chrome alum which gave a deep blue shade to the area invaded by the flood water. As reported by other investigators, the water-invaded zone was found to be radial during the initial flooding stages, then stretched into a squared-

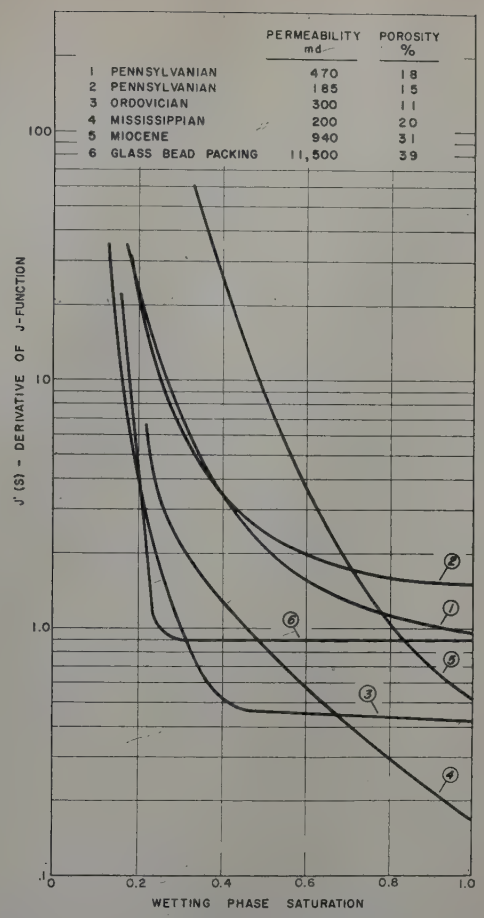

FIG. 8—DERIVATIVE OF *J*-FUNCTION FOR THE MODEL'S GLASS BEAD PACKING AND VARIOUS NATURAL POROUS MEDIA.

off pattern, and finally developed a cusp toward the producing wells.[7,8] With increasing oil-to-water viscosity ratios this cusp became more pronounced and began to form at an earlier flooding stage, resulting in an overall decrease of areal coverage at the moment of water breakthrough.

The observed relationship between areal coverage at water breakthrough and oil-to-water viscosity ratio is presented in Fig. 9. For purposes of comparison, Fig. 9 includes also the correlation between areal coverage and mobility ratio obtained by Dyes, *et al*[7] (in immiscible fluid displacements), together with a replot of the present data on the basis of the "average" mobility ratio as defined by Craig, *et al*[8]. As may be seen, the present data follow fairly closely (but do not coincide with) the general trend of the earlier results.[7,8]

An additional observation of particular interest pertains to the growth of the water-invaded zone after the moment of water breakthrough. This growth was found to be quite rapid, even in the floods involving high viscosity oils. Complete coverage of the five-spot area by the invading water was observed in all cases, occuring after injection of about 1 pore volume in the floods of low viscosity oil and after injection of 2 to 3 pore volumes in the floods involving highly viscous oils.

The visual examination of the fluid movement in the model also revealed some of the more detailed aspects of the flood pattern development. At low oil-to-water viscosity ratios (below a value of about 15:1), the water-invaded zone in the porous body was delineated by a sharp, smooth front, behind which the water ap-

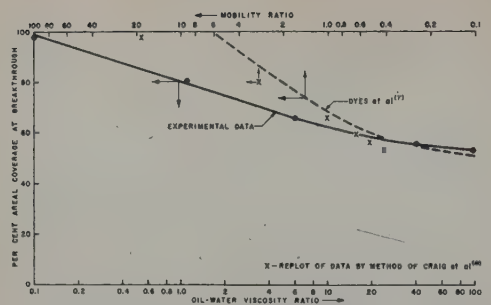
MOBILITY RATIO
PER CENT AREAL COVERAGE AT BREAKTHROUGH
EXPERIMENTAL DATA
DYES et al
X-REPLOT OF DATA BY METHOD OF CRAIG et al
OIL-WATER VISCOSITY RATIO

FIG. 9—EFFECT OF VISCOSITY RATIO ON AREAL COVERAGE IN FIVE-SPOT FLOODS.

peared to be very finely and uniformly distributed. With increasing oil-to-water viscosity ratios, the advancing water front became somewhat less defined, exhibiting local fingering. Concurrently, the water-invaded zone gained a less uniform, more filigreed appearance with a detectable gradation of shading and density from the front back to the injection well, indicating higher water saturations in the vicinity of the injection well. In all cases, however, the individual stringers or water filaments within the water-invaded zone were found to grow quite rapidly into a continuous, fairly uniform body, after injection of about 1 pore volume of water.

COMPARISON OF FIVE-SPOT AND LINEAR WATERFLOOD PERFORMANCE

Detailed investigations of stabilized flooding behavior in the five-spot flow model and in the linear flow system were conducted using the dri-filmed glass-bead packing. The relationships between oil recovery and cumulative injection for different oil-water viscosity ratios are presented in Fig. 10. In this figure, the dashed lines represent the linear flooding curves while the solid lines are those of the five-spot system. For each of these systems the oil recovery at water breakthrough is seen to decrease rapidly with increasing viscosity ratio, and, in general, increasing amounts of water are required to reach any given recovery as the viscosity ratio increases. However, the trend of the curves in Fig. 10 suggests that the ultimate waterflood oil recovery is independent of the viscosity ratio. These results are consistent with the theory of stabilized, (linear) water floods.

The curves of Fig. 10 reveal the effects of geometry on flooding behavior. For a given oil-to-water viscosity ratio the oil recovery at water breakthrough is always higher in the linear floods than in the five-spot, and the spread between the recoveries at water breakthrough for the two systems increases with increasing viscosity ratios. However, after the moment of water breakthrough, the five-spot flooding curves exhibit in each case a steady rise, and the recovery obtained from the five-spot becomes equal to and, subsequently, even slightly greater than that of the corresponding linear flood. The trends derived from these findings are supported by the observations of sweep efficiency. The lower oil recoveries at water breakthrough in the five-spot are, of course, due to the fact that only a portion of the total reservoir area is covered by the flood water at the moment of water breakthrough (Fig. 9). The subsequent rapid increase of the five-spot recoveries is consistent with the observation of fast growth of areal coverage after the moment of water breakthrough. Finally, the general trend toward the same ultimate recovery for both the five-spot and the linear flow systems is in agreement with the observation of complete

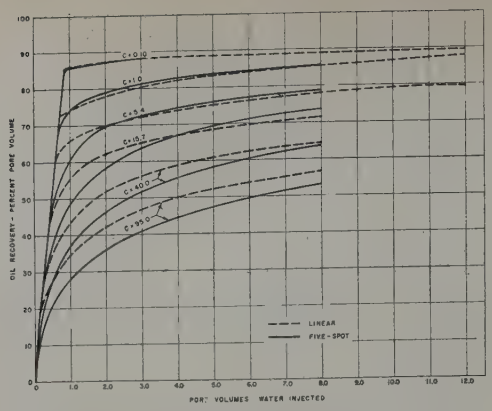

FIG. 10—COMPARISONS OF FIVE-SPOT AND LINEAR WATER FLOODS, GLASS BEAD PACKING.

areal coverage (achieved in the flow model in all cases) after injection of a few pore volumes.

An unexpected finding, for which no explanation seems available at present, is the cross-over of the five-spot and linear flooding curves. The cumulative injection required to reach the point of intersection is seen to increase systematically with increasing oil-water viscosity ratios. In Fig. 10 this intersection is clearly observed at three different viscosity ratios (1:1, 5.4:1, and 15.7:1), and it is likely that a similar phenomenon would have occurred at the higher viscosity ratios if greater amounts of water had been injected. The possibility that the cross-over of the linear and five-spot flooding curves might be a result of insufficiently controlled experimentation was investigated by means of additional tests on a different packing (400-mesh Alundum powder), and also by conducting linear water floods (simulated by an elongated line drive) in the areal flow model. The results of these tests confirmed the cross-over of the areal and linear waterflood curves, thereby stressing further the high flooding efficiency of the five-spot.

The data obtained from the present study provide a convenient means for evaluating other approaches proposed in the literature for correlating linear and five-spot flooding behavior. It appeared of particular interest to compare the experimental five-spot flooding curves of the glass-bead packing with those calculated on the basis of relative permeability data (Fig. 2) in accordance with the procedure and the areal coverage correlations proposed by Craig, *et al.*[8] This comparison is shown in Fig. 11. As may be seen, there is no good agreement nor even a systematic, correlative trend between the calculated and the experimental five-spot flooding curves. A detailed discussion of this discrepancy is beyond the scope of this paper. However, it may be recalled that the calculation procedure[8] implies two (arbitrary) assumptions. On one hand, it is assumed that the mobility of the water-invaded region can be determined by considering the relative permeability to water associated with the average water saturation, while in reality the mobility at any point of the swept region is the sum of both the oil and the water mobilities. On the other hand, the computational method implies that for a given cumulative injection the average saturation of the swept region is the same in the five-spot as in a linear system. In an effort to clarify this assumption the average water saturation of the water-invaded area in the five-spot and in the linear system at the moment of water breakthrough (obtained by combining Figs. 9 and 10) has been plotted in Fig. 12 as

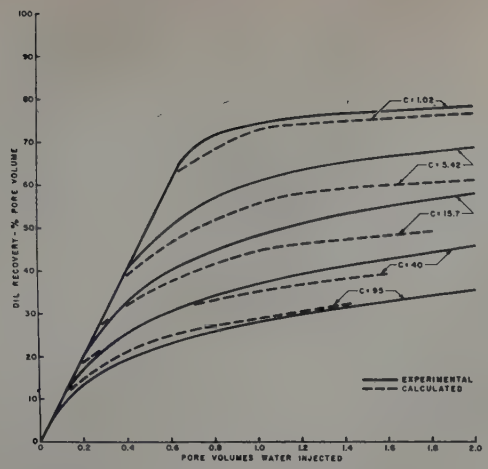

FIG. 11—COMPARISON OF EXPERIMENTAL AND CALCULATED FIVE-SPOT FLOODING BEHAVIOR.

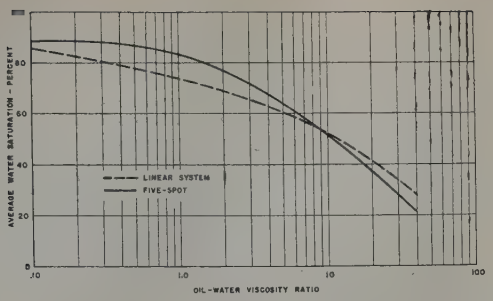

FIG. 12—AVERAGE WATER SATURATION OF WATER-INVADED AREA AT WATER BREAKTHROUGH.

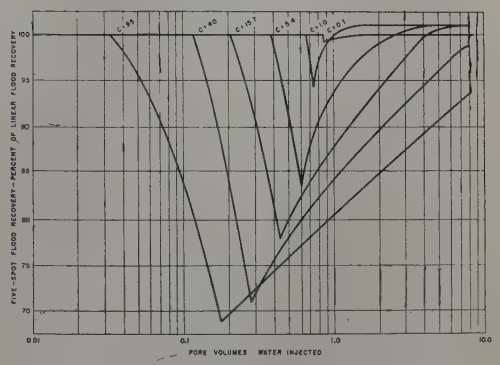

FIG. 13—CORRELATION BETWEEN LINEAR AND FIVE-SPOT FLOODING BEHAVIOR.

a function of the oil-water viscosity ratio. The observed separation between the two curves of Fig. 12 indicates that generally the average saturation of the water-invaded area in the five-spot is different from, and not directly related to, the average saturation existing in the linear system at the same flooding stage. This observation suggests that the areal sweep at successive flooding stages cannot be used as a direct factor of proportionality in correlating linear and five-spot flooding performance. A further deterrent to such a scheme is the fact that recoveries in the five-spot become higher than in the linear floods (Fig. 10); this phenomenon could not possibly be accounted for by using an areal coverage factor which is necessarily less than (or equal to) unity.

In attempting to make practical use of the direct comparison of linear and five-spot flooding behavior, it will be kept in mind that the flooding curves in Fig. 10 are not representative of porous media having relative permeability characteristics different from those of the unconsolidated medium used in these model studies. However, the correlative trends indicated by these curves may be used as a guide for approximating five-spot flooding performance on the basis of linear (laboratory) flooding results. For this purpose it is convenient to express the five-spot recoveries at various oil-to-water viscosity ratios as a fraction of the corresponding linear flood recoveries, as illustrated in Fig. 13. Of the various "correlation" or "correction curves" shown in Fig. 13, the particular one to be employed for a given five-spot waterflood prediction can then be selected by seeking the viscosity ratio that corresponds to the best match between one of the linear flooding curves of the model material and the linear flooding performance of the core material under consideration.

CONCLUSIONS

1. The performance of areal, five-spot array water floods has been studied in a program of scaled flow model experiments. All the areal and associated linear flooding experiments were conducted in homogeneous, preferentially oil-wet porous media, in the absence of free gas and under conditions where gravity effects are negligible.

2. The study of the effect of injection rate on oil recovery in five-spot water floods has shown that for sufficiently high rates, as usually encountered under field conditions, the flooding behavior (in sufficiently homogeneous systems) can be expected to be rate-independent or stabilized.

3. It has been confirmed that the sweep of five-spot water floods does not remain confined to a portion of the reservoir area and that complete areal coverage is achieved in all cases after injection of 1 to 2.5 pore volumes of water.

4. The recovery performance of stabilized five-spot water floods, studied over a wide range of oil-to-water viscosity ratios, has been compared with that of linear floods. The linear floods always yield a greater recovery at the moment of water breakthrough; however, after water breakthrough the recovery of the five-spot floods soon reach and even slightly surpass that of the linear system.

5. It was not possible to derive a simple relationship between areal sweep and recovery performance of five-spot water floods. However, direct correlations have been established between the recovery performance of linear and five-spot water floods. These correlations are suggested as a tool for rapid approximate evaluations.

NOMENCLATURE

Subscripts o and w pertain to oil and water, respectively.

S = water saturation, dimensionless fraction
x,y,z = spatial coordinates, cm
t = time, sec
L = principal dimension, size of five-spot, cm
$X = x/L$, $Y = y/L$ = dimensionless space coordinates
W_i = cumulative water injection, pore volume
q = rate of water injection per unit sand thickness, cc/cm/sec

ϕ = porosity, dimensionless fraction

k = specific permeability, darcies

σ = water-oil interfacial tension, dyne/cm

μ_o, μ_w = viscosities of oil and water, cp

$c = \mu_o/\mu_w$ = oil-water viscosity ratio

$u = u_o + u_w$ = total, two-phase unit flux, rate of flow per unit cross-sectional area, cc/sm^2/sec

$U = \dfrac{u}{q/L}$ = velocity distribution function, dimensionless

U_x, U_y = components along axes of coordinates of velocity distribution function, dimensionless

k_{ro}, k_{rw} = relative permeabilities to oil and water, dimensionless functions of saturation

$F = \left[1 + \dfrac{k_{ro}}{k_{rw}} \dfrac{\mu_w}{\mu_o}\right]^{-1}$ = dimensionless function of saturation

$F' = \dfrac{dF}{dS}$ = derivative of ϕ with respect to saturation

$\Psi = k_{ro} F$ = dimensionless function of saturation

$J(S) = \dfrac{Pc}{\sigma}\left(\dfrac{k}{\phi}\right)^{\frac{1}{2}}$ = capillary retention function, dimensionless function of saturation

$J'(S) = \dfrac{dJ}{dS}$ = derivative of J with respect to saturation, dimensionless function of saturation

REFERENCES

1. Buckley, S. E. and Leverett, M. C.: "Mechanism of Fluid Displacement in Sands", *Trans.* AIME (1942) **146,** 107.
2. Dykstra, H. and Parsons, R. L.: "The Prediction of Oil Recovery by Waterflood", *Secondary Recovery of Oil in the United States,* 2nd Ed., API (1950).
3. Rapoport, L. A. and Leas, W. J.: "Properties of Linear Water Floods", *Trans.* AIME (1953) **198,** 139.
4. Muskat, Morris: *Physical Principles of Oil Production,* McGraw-Hill Book Co., Inc., N. Y. (1949) 657.
5. Aronofsky, J. S.: "Mobility Ratio—Its Influence on Flood Patterns during Water Encroachment", *Trans.* AIME (1952) **195,** 15.
6. Slobod, R. L. and Caudle, B. H.: "X-Ray Shadowgraph Studies of Areal Sweep-out Efficiencies", *Trans.* AIME (1952) **195,** 315.
7. Dyes, A. B., Caudle, B. H. and Erickson, R. A.: "Oil Production after Breakthrough—as Influenced by Mobility Ratio", *Trans. AIME* (1954) **201,** 81.
8. Craig, F. F., Jr., Geffen, T. M. and Morse, R. A.: "Oil Recovery Performance of Pattern Gas or Water Injection Operations from Model Tests", *Trans.* AIME (1955) **204,** 7.
9. Rapoport, L. A.: "Scaling Laws for Use in Design and Operation of Water-Oil Flow Models", *Trans.* AIME (1955) **204,** 143.
10. Johnson, E. F., Bossler, D. P. and Nauman, V. O.: "The Calculation of Relative Permeability from Displacement Experiments", paper 1023-G, presented at AIME Third Biennial Secondary Recovery Symposium in Wichita Falls, Tex. (May 5-6, 1958) ★★★

A Laboratory Study of Laminar and Turbulent Flow in Heterogeneous Porosity Limestones

CHARLES R. STEWART
WILLIAM W. OWENS
MEMBERS AIME

PAN AMERICAN PETROLEUM CORP.
TULSA, OKLA.

ABSTRACT

Reservoir performance predictions based on laboratory core test data assume that fluid flow is laminar for the laboratory test. A study has been made to determine the validity of this assumption for laboratory tests on various types of porosity found in producing limestone formations.

Data are presented which show that turbulence and slippage can occur during laboratory tests on heterogeneous-type porosity limestones, thus causing serious errors in measured single-phase permeabilities and two-phase relative permeability characteristics. In single-phase flow tests it is possible to eliminate turbulence and correct for slippage or to eliminate both factors by controlling test conditions. It is not always possible to control test conditions and thereby eliminate turbulence and slippage in two-phase flow tests. A correction method is presented which can be used to calculate the true two-phase laminar flow relative permeability characteristic even though turbulence and slippage exist.

INTRODUCTION

It is customary to make use of Darcy's law and modifications of this law, together with laboratory data on formation core samples to predict the performance of producing reservoirs. Such predictions are based on an assumption that fluid flow is in the laminar or streamline region for the laboratory test.

It was the purpose of this investigation to determine the extent to which turbulent flow may occur in laboratory fluid flow tests on heterogeneous porosity limestones. Considering that turbulent flow conditions might exist in some laboratory fluid flow tests, additional emphasis was placed on the development of a method to correct for turbulence when laminar flow conditions could not be attained.

Original manuscript received in Society of Petroleum Engineers office Oct. 4, 1957. Revised manuscript received Mar. 4, 1958. Paper presented at Oklahoma Conference on Fluid Flow at the University of Oklahoma, Norman, Okla., Sept. 24, 1957.

FLUID FLOW CONCEPTS FOR POROUS MEDIA

The Influence of Pore Geometry on Fluid Flow

One of the more important factors influencing fluid flow in porous media is the geometry of the pore space which includes such characteristics of the pores as size, shape, distribution, roughness, uniformity, etc. In general, oil- and gas-producing formations can be divided into two broad types on the basis of pore geometry. One has been called sandstone-type porosity media, which is characterized by a small range in pore size, uniformity in shape of the pores, smooth pore surfaces and a regular and uniform distribution of pores. The other type has been called heterogeneous porosity media and is usually limited to the dolomites and limestones. This type is characterized by a wide variation in the size, shape, and distribution of the pores and rough, irregular pore surfaces. It is therefore apparent that conditions are much more favorable for turbulent flow* in heterogeneous-type porosity media than in sandstone-type porosity media.

*For simplicity, the words "turbulent" and "turbulence" will henceforth be used to mean flow which does not obey the laminar flow equations.

Interrelationship Between Turbulence and Gas Slippage

In studying the problem of turbulent flow in laboratory tests on porous media, it is necessary to be aware of the interrelationship between slippage and turbulence for gas flow. As a result of slippage or the Klinkenberg effect[3], apparent permeabilities to gas are greater than the true value because there is no stationary layer of gas in contact with the walls of the flow channels. Gas slippage decreases as the mean free path of the gas molecules decreases. Since the mean free path of any gas decreases with increasing density, increases in static pressure result in lower apparent gas permeabilities. However, a reduction in gas permeability can also be due to turbulence. Therefore, in studying only turbulent flow in porous media, it is necessary to hold gas density, and slippage, constant or to reduce slippage to a negligible value by operating at high static pressures.

Presentation of Laminar and Turbulent Flow Data

A graphical relationship between permeability and a pseudo-Reynolds number, $N_{\prime\prime}$, will be used to show the two types of fluid flow, i.e., laminar and turbulent. The usual graphical method for such a description has been the use of friction factor-Reynolds number charts[4]. On such a logarithmic diagram, the laminar region appears as a straight line having a slope of 45 degrees. As the friction factor decreases and the Reynolds number increases, the turbulent region is reached and appears as a deviation from the 45-degree slope line. However, in petroleum engineering literature resistance of por-

[3]References given at end of paper.

ous media is expressed in either darcy or millidarcy units; therefore, a relationship involving permeability seems more desirable. The pseudo-Reynolds number, which will be used with permeability to differentiate between laminar and turbulent flow, is simply the linear velocity times density divided by viscosity. It will be noted that a diameter term is absent from the general form of the Reynolds number equation, but this does not invalidate its use to study turbulence in porous media. It does mean, however, that no comparison can be made between different cores. In the graphical presentations, laminar flow is indicated when the observed permeability does not change for varying values of N_p. When turbulence begins to affect flow, the observed permeability decreases as N_p increases.

APPARATUS AND PROCEDURE

The apparatus used for the flow tests on heterogeneous-type porosity core samples has been described in a previous publication[2]. The test fluids used were dry, pure gases and a relatively pure hydrocarbon liquid in the range of C_{10} to C_{12} having a viscosity and density of approximately 1.3 cp and 0.75 gm/cc, respectively. The gases used were carbon dioxide, nitrogen, air and helium.

Tables 1 and 2 present the physical characteristics of eight core samples used in this study. The test results on these samples are characteristic of the results obtained on a total of 21 samples tested.

Two separate procedures were used for the tests on the heterogeneous porosity-type cores. For the single-phase flow tests, the pore space of each sample was completely filled with air, and permeabilities were determined at various values of pressure differential under a condition of constant arithmetic mean pressure. The one exception were the tests on Sample 1 where the single-phase permeabilities were determined using both air and C_{10}-C_{12}. For the two-phase flow tests, a number of external gas drives were performed on each sample (see Table 2). For each test, gas was injected at constant pressure into the 100 per cent oil-saturated core, and gas and oil were produced at constant downstream pressure. Cumulative volumes of gas and oil were recorded vs cumulative time.

TABLE 1 — SINGLE-PHASE FLOW DATA IN HETEROGENEOUS POROSITY LIMESTONES (Fig. 1)

Formation	Core No.	Test fluid $C_{10}-C_{12}$	Length (cm)	Cross-sectional area, (cm^2)	Porosity (per cent)	Laminar permeability (md)	Diff. pressure range, (atm)	Mean pressure (atm abs)	Maximum test (N_p)
Panhandle oolitic	1	Air	12.6	61	11	22	0.01-0.8	4.0	1
Strawn reef	2	Air	24.0	62	12	390	0.001-0.07	7.7	12
Cordova outcrop	3	Air	25.0	56	26	35	0.03-6.6	1.5-4.3	25
Canyon reef	4	Air	12.4	62	13	30	0.005-1.0	7.8	36
Devonian chert	5	Air	13.5	60	31	10	0.005-1.0	7.8	5
Pennsylvanian reef	6	Air	26.0	56	19	200	0.005-0.5	7.7	32

TABLE 2 — TWO-PHASE FLOW TEST DATA, HETEROGENEOUS POROSITY LIMESTONES

Formation	Core No.	Run No.	Gas used	Pressure drop (atm)	Outlet Pressure (atm abs)	Specific gas permeability (md)	Specific oil permeability (md)
Wolfcamp Limestone	7	1	Air	0.16	13.0	215	720
		2	CO_2	0.16	1.0	362	720
		3	Air	0.16	1.0	448	720
Porosity = 26 per cent		4	He	0.16	1.0	670	720
Permeability = 725 md		5	He	0.08	1.0	700	720
		6	He	0.08	0.50	725	720
Palo Pinto Reef	8	1	N_2	1.0	13.0	21	39
		2	CO_2	1.0	1.0	29	39
		3	Air	1.0	1.0	33	39
		4	He	1.0	1.0	42	39
Porosity = 14 per cent		5	He	1.0	0.5	46	39
Permeability = 39 md		6	He	1.0	0.07	—	39

METHODS OF CALCULATION

The calculation procedure used for the single-phase flow permeabilities was the standard procedure described in API Code No. 27. For the two-phase flow tests, which were external gas drives, gas permeability at average gas saturation was calculated from the instantaneous gas velocity at arithmetic average pressure. The gas velocity was calculated from the slope of the cumulative gas volume vs cumulative time curve. Gas permeabilities calculated in this manner for sandstones have been compared to those obtained by the Penn. State steady-state method. This comparison leads to the conclusion that gas permeabilities calculated from external gas-drive data give a valid representation of the relation between gas permeability and gas saturation. The oil permeabilities were calculated from the gas permeability and k_g/k_o as calculated by the Welge method[5].

The pseudo-Reynolds number, N_p, which is equal to $V\rho/\mu$, was determined at arithmetic mean pressure from the fluid velocity, V, in centimeters per second (i.e., volumetric flow rate divided by the product of cross-sectional area, fractional porosity, and fractional saturation) and the fluid density, ρ, in grams per cubic centimeter, and viscosity, μ, in poises. The units of this pseudo-Reynolds number are reciprocal centimeters.

RESULTS AND DISCUSSION

Single-Phase Flow Tests

The Frequency and Magnitude of Turbulence

To investigate the frequency and magnitude of turbulence in heterogeneous porosity-type media, flow tests were performed on 21 individual large-diameter core samples from eight producing limestone formations and one outcrop. Typical results are presented in Fig. 1. This figure shows the permeability reductions as a function of the pseudo-Reynolds number. The permeability reductions have been calculated by dividing the observed permeability by the laminar flow permeability and expressing this ratio as a percentage. Laminar flow is represented by the region where 100 per cent permeability exists for various values of N_p. Turbulence begins in the region where permeability ratios are less than 100 per cent. Except for Core No. 3, the arithmetic mean core pressure for each sample was held constant. Constant mean pressure also means constant density for any given gas and, therefore, all

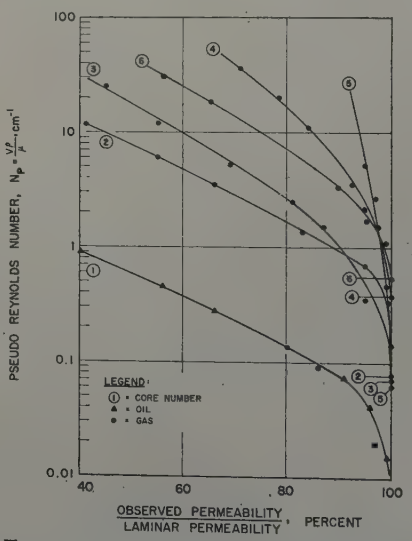

FIG. 1 — TURBULENCE IN SINGLE-PHASE PERMEABILITY MEASUREMENTS, HETEROGENEOUS POROSITY LIMESTONES.

permeability changes, except Core No. 3, are due to turbulence and not gas slippage.

The test data for Core No. 3 substantiate the introductory discussion concerning the importance of holding gas slippage constant in studying turbulent flow. The permeability reductions for this core shown in Fig. 1 are due to both turbulence and changes in gas slippage. The mean pressure for the tests on Core No. 3 varied from 1.5 to 4.3 atm abs, yet the per cent permeability vs N_p curve is quite similar to the curves for the other samples. It is believed that gas slippage was of small magnitude in all other tests, for which data are presented in Fig. 1, because mean test pressures were from approximately 4 to 8 atm abs. That slippage was not significant for the tests on Core No. 1 is verified by the fact that a single curve fits the test data which include runs using oil where slippage does not occur.

The physical characteristics of the core samples, together with the values of mean pressure, range of pressure differentials, and maximum test pseudo-Reynolds number for the tests shown in Fig. 1, are presented in Table 1. It can be observed that considerable variation in single-phase gas permeability was obtained over the range of laboratory test conditions. These variations in permeability are attributed to turbulence of various magnitudes during the permeability measurements. It is predicted that these cores would exhibit turbulence of similar magnitude during two-phase flow.

TURBULENCE WITH SLIPPAGE

The test data previously discussed resulted from tests in which slippage effects were present but were held constant. Before undertaking a study of two-phase flow, it appeared pertinent to repeat the same type of single-phase tests and allow slippage to vary to determine in what way it would influence the test results. One of the samples of Strawn reef limestone was selected for testing. The results of these tests are presented in Fig. 2. The curves of this figure present the experimentally determined variation in gas permeability as a function of N_p for four separate conditions of constant gas slippage, i.e., constant mean pressure and constant density. The general shape of these curves and their position relative to the mean test pressures show that both slippage and turbulence are affecting the measured permeability.

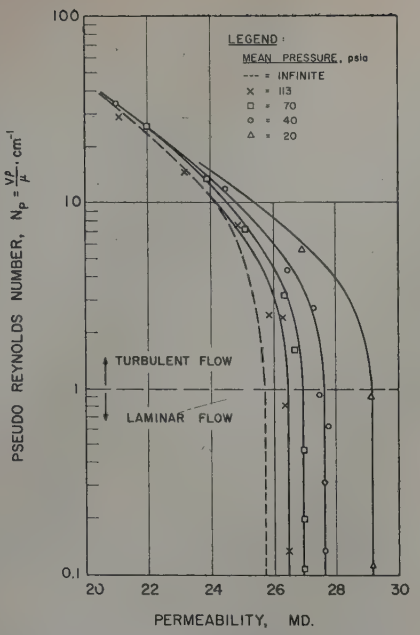

FIG. 2—SLIPPAGE AND TURBULENCE IN AIR PERMEABILITY MEASUREMENTS, STRAWN REEF LIMESTONE.

The region of laminar flow with slippage extends over the range of N_p from 0.1 to 1.0. In this range the permeability is a function of the mean free path or density and is independent of N_p. In fact, the relationship between permeability and mean pressure in this region gives a typical Klinkenberg curve.

The turbulent region of Fig. 2 is in the region of N_p values above 1.0, where the permeability for any constant mean pressure condition decreases for increasing values of N_p. In the range of N_p from 1.0 to 30, both turbulence and slippage affect the measured permeability and the curves for each constant mean pressure condition show separate relationships of permeability vs N_p. In this region, it is visualized that laminar flow with slippage may exist in some of the flow channels, while turbulent flow exists in others. For N_p values greater than 30, it appears that a single curve represents the relationship between permeability and N_p. In this region, flow in all the channels is turbulent and the effect of slippage has disappeared. In fact, it is difficult to visualize a condition of slippage when flow is turbulent. Turbulence involves the movement of large masses of gas, whereas slippage is a phenomenon depending upon the movement of individual molecules.

TURBULENCE — NO SLIPPAGE

The sample of Strawn reef limestone used in the previous study has

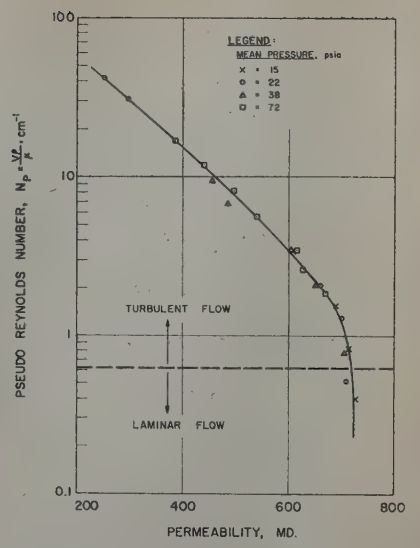

FIG. 3—TURBULENCE IN AIR PERMEABILITY MEASUREMENTS, WOLFCAMP LIMESTONE.

a pore space composed of low permeability intergranular material and a higher permeability system of solution cavities or vugs. This is the type of pore geometry in which fluid flow is affected by both turbulence and slippage. However, not all limestones have this type of pore geometry. Fig. 3 presents the results of a study on a fractured limestone where flow was affected by turbulence alone. Gas permeabilities were measured at various values of mean pressure and N_p. As shown in Fig. 3, the experimental points for four separate values of mean pressure, or mean gas density, fall on a smooth curve of permeability vs N_p. Slippage effects were too small to be measurable in this sample of fractured Wolfcamp lime. Previous studies of thin sections from plastic impregnated portions of this sample revealed that it has a hairline fracture system. The permeability of this fracture system is responsible for almost all of the permeability of the core. The fracture width is large compared to the molecular mean free path of the gas molecules, and slippage is consequently too low to be measured. The laminar region of flow for this sample probably exists in the region of N_p values below 0.6. Increases in the value of N_p beyond 0.6 result in turbulent flow.

TWO-PHASE FLOW TESTS

TURBULENCE — NO SLIPPAGE

The previously described sample of Wolfcamp lime, which has been shown to be free of slippage effects, has been used to study turbulence alone during two-phase flow of gas and oil. Six external gas-drive tests

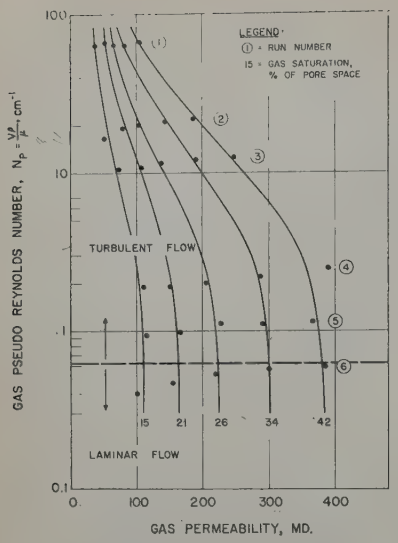

FIG. 4 — TURBULENCE IN EXTERNAL GAS DRIVES, WOLFCAMP LIMESTONE CORE NO. 7.

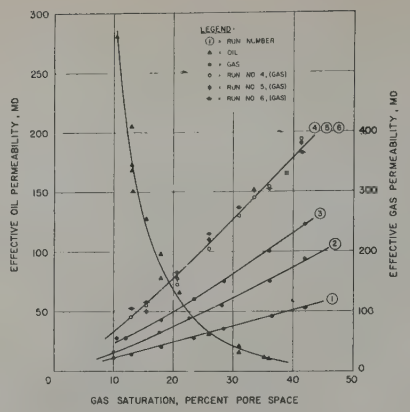
LEGEND
① = RUN NUMBER
▲ = OIL
● = GAS
○ = RUN NO. 4, (GAS)
ϕ = RUN NO. 5, (GAS)
◆ = RUN NO. 6, (GAS)
EFFECTIVE OIL PERMEABILITY, MD
EFFECTIVE GAS PERMEABILITY, MD
GAS SATURATION, PERCENT PORE SPACE

FIG. 5 — TURBULENCE IN EXTERNAL GAS DRIVES, WOLFCAMP LIMESTONE.

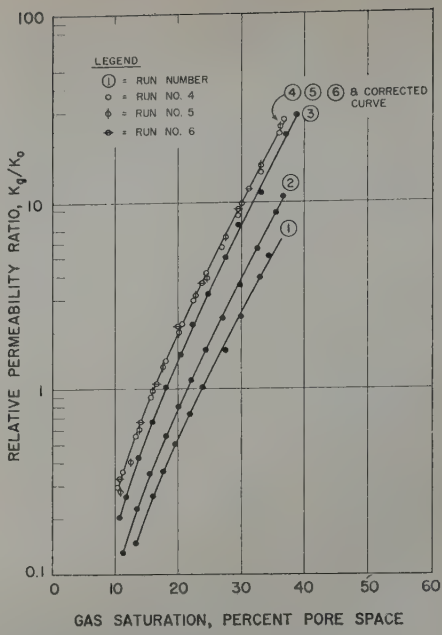
LEGEND
① = RUN NUMBER
○ = RUN NO. 4
ϕ = RUN NO. 5
◆ = RUN NO. 6
④ ⑤ ⑥ & CORRECTED CURVE
RELATIVE PERMEABILITY RATIO, K_g/K_o
GAS SATURATION, PERCENT PORE SPACE

FIG. 6 — TURBULENCE IN EXTERNAL GAS DRIVES, WOLFCAMP LIMESTONE.

were performed on this core. Gas density and, therefore, the magnitude of turbulence, was varied by using three different gases and by varying the test pressure. Table 2 presents data on the test conditions applying to the six external gas drives on this core sample. Fig. 4 presents the results of these six separate external gas drives. The instantaneous effective gas permeability for each run was calculated at five values of gas saturation—15, 21, 26, 34 and 42 per cent pore space. The values of N_p for each run were also calculated at each value of saturation.

Several pertinent deductions can be made from Fig. 4. These two-phase flow data show two regions of flow (laminar and turbulent) similar to those which are evident in single-phase flow. The turbulent region of Fig. 4 is estimated to be in the region of N_p values above approximately 0.6. In this region the permeability to gas for any one constant gas saturation decreases as the pseudo-Reynolds number increases. For values of N_p below 0.6 the flow is laminar and changes in the pseudo-Reynolds number have no effect on the gas permeability. The test data of Fig. 4 are presented in the conventional manner in Fig. 5, which shows the relationship between effective fluid permeabilities and gas saturation for Runs 1 through 6 (Table 2). The important points brought out by this figure are (1) while the effective gas permeability relationships for the various tests are different, the effective oil permeability relationships are almost identical, and (2) the effective gas permeability relationships for Runs 4, 5 and 6 are best represented by a single curve. This fact leads to the prediction that, although Run 6 appears to be the only one free of turbulence (Fig. 4), Runs 4, 5 and 6 should show no appreciable difference in their k_g/k_o characteristics (i.e., the ratio of gas to oil permeability vs gas saturations).

In summary, it is observed that calculated k_g/k_o characteristics using data in the laminar region of Fig. 4 will give the true characteristics for this core sample. Conversely, the calculated k_g/k_o characteristics using data obtained under turbulent flow conditions will be erroneous due to reduced permeability in the gas phase. Fig. 6 presents the calculated k_g/k_o relationships vs gas saturation for the six runs on the Wolfcamp core. This figure shows that reductions in gas permeability due to turbulence in the gas phase result in corresponding reductions in the k_g/k_o relationship. The true k_g/k_o relationship for this rock is represented by the k_g/k_o curve for Run 6, where gas flow was in the laminar region. As predicted previously, there is also no practical difference in the k_g/k_o characteristics for Runs 4, 5 and 6.

TURBULENCE WITH SLIPPAGE

A core sample which showed slippage effects for single-phase gas flow was also tested using the same technique previously described. Table 2 presents data on the test conditions applying to six external gas-drive tests performed on this sample of Palo Pinto reef limestone.

Fig. 7 presents the results of these gas-drive tests, which show the same type relationships as presented for the Wolfcamp lime. However, there is one significant difference. Both slippage and turbulent effects are evident. Above a N_p value of approximately 1.5, gas permeability is affected by turbulence for all values of gas saturation such as observed in Fig. 4. Below an N_p of about 1.5, it is believed that turbulence is absent and slippage effects are present.

The channel flow concept, which has been accepted as applying to an external-drive displacement mechanism, confirms the belief that slippage effects are present in the region of N_p values below 1.5. According to this concept, injected gas first sweeps out the largest flow channels. As gas saturation is increased, progressively smaller pore openings are filled with gas until finally the minimum average gas flow channel diameter is reached at the irreducible wetting liquid saturation. Since gas slippage depends in part upon the flow channel diameter, slippage effects should increase with increases in the average gas saturation during an external gas drive[3,6]. This is exactly what is shown in Fig. 7 for the region of N_p values less than 1.5. For 12 per cent average gas saturation, the gas permeability is not affected by a change in N_p. For 36 per cent gas saturation, the increase in gas permeability is approximately 10 per cent when N_p is reduced from 1.5 to 0.5. The gas permeability data for Runs 4, 5 and 6 were plotted as a function of reciprocal mean pressure and resulted in excellent linear relationships or Klinkenberg curves. Average pore diameters were calculated using the Klinkenberg curves. These calculations showed

that average pore diameters of the gas-conducting pores varied from 16 microns at the beginning of a run to 7 microns at 36 per cent gas saturation. These values for average pore diameter agree with values cited by Rose[7] for producing formations.

None of the external gas drives presented in Fig. 7 represents the true flow behavior of the Palo Pinto reef core. For high values of N_p, the calculated k_g/k_o characteristics will be in error due to turbulence in the gas phase, which produces apparent gas permeabilities lower than the true value. At low values of N_p, gas permeabilities are higher than the true values due to slippage, and the calculated k_g/k_o characteristics will again be in error. The test data on this core again show that oil flow was in the laminar region for all tests.

In addition to the previously described external gas-drive tests on the Wolfcamp and Palo Pinto reef cores, similar tests were performed on samples of Strawn reef limestone, oolitic dolomite, and Cordova shell-stone outcrop. The tests on these three samples were not sufficient in number to allow a plot of N_p vs gas saturation as shown in Figs. 4 and 7. However, the same type relationship shown by Fig. 5 was obtained. Again oil flow was in the laminar region for all tests on these cores. It is apparent from the test results shown that almost any gas permeability relationship can be observed depending upon the applied test conditions. It is also apparent that laminar flow without slippage must prevail in two-phase flow tests in order to obtain valid results or that a method must be devised for correcting for slippage and turbulence.

The test data which have been presented lead to the following conclusions. Turbulence and slippage can exist during laboratory flow tests on heterogeneous porosity limestones for usual test conditions. Measured single-phase permeabilities and two-phase permeability characteristics can be seriously in error due to turbulence and slippage. In single-phase flow tests it should be possible to eliminate turbulence and correct for slippage or to eliminate both factors by controlling the test conditions. To eliminate turbulence, it is necessary only to reduce the flow velocity until laminar flow conditions prevail. If slippage occurs, the determination of several laminar flow gas permeabilities at different values of gas density allows a precise determination of the

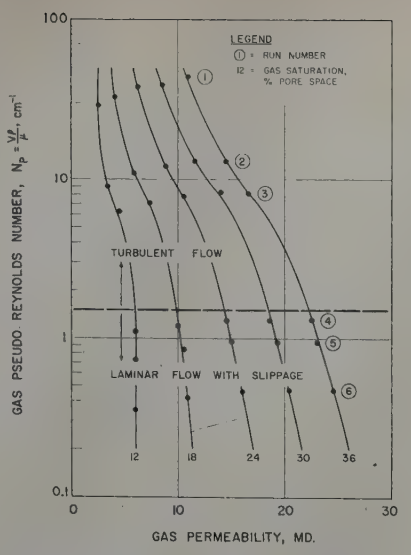

Fig. 7 — Turbulence and Slippage in External Gas Drives, Palo Pinto Reed Core No. 19.

true fluid permeability. It is also possible to eliminate slippage by conducting tests at high static pressures where the effect of slippage is negligible.

Further, it is concluded that it is not always possible to eliminate both turbulence and slippage in two-phase flow tests by controlling test conditions. If slippage is to be removed by operating at high static pressure, then conditions favorable for turbulent flow exist. It is not possible in all types of heterogeneous porosity limestones to counteract the conditions favorable for turbulence by reducing the pressure differential and, therefore, the flow velocity. Pressure differentials must be above a certain limit depending upon the capillary characteristics of the particular limestone core being tested. If the pressure differential is reduced below this limit, serious errors can be introduced due to the stabilized zone and capillary end effects. However, a correction method is presented which can be used to calculate the true laminar flow relative permeability characteristic even though turbulence and slippage exist during a laboratory test.

Method for Correcting Two-Phase Flow Data

Rose[7] has proposed a method for calculating the correct gas relative permeability for an external gas drive where slippage alone affects the gas permeability. The basis of this method is the use of a specified base gas permeability (measured at 100 per cent gas saturation). The permeability must be measured using the same gas and under identical conditions of mean free path as would occur in the external gas drive. It is proposed that Rose's method can be extended to correct also for the presence of turbulence. Such a proposal requires that the base gas permeability be measured with the same gas at the same pressure differential and static pressure applying to the two-phase test. Inherent in this method is at least one assumption, i.e., that laminar flow prevails in the oil phase, which is the condition that existed for the external gas drives on the Wolfcamp and Palo Pinto core tests. This empirical method gives results that are consistent with present concepts of fluid flow in porous media. The detailed steps of applying this method to external gas-drive tests where turbulence occurs are as follows.

1. Measure specific permeabilities to gas and oil at 100 per cent fluid saturation using the same gas and the same oil at the density and pressure drop to be used in the gas drive.

2. Using the external-drive experimental data, calculate the apparent effective gas permeability, apparent k_g/k_o, and effective oil permeability at various gas saturations.

3. Using the appropriate base permeabilities measured in (1), calculate the true gas relative permeability, k_g/k, and oil relative permeability, k_o/k, vs average gas saturation relationships.

4. Using (3), calculate the true k_g/k_o vs gas saturation relationship.

Application of Method to Test Data

The stated calculation procedure, through Step 3, was applied to test results for the Wolfcamp and Palo Pinto core samples. Fig. 8 shows a typical result for Runs 1, 3, 4, 5 and 6 on the Wolfcamp core. The base permeability values used for the calculation of the results are tabulated in Table 2. It is evident that the extreme variation in gas permeability relationships for the tests on the Wolfcamp core sample has been changed, within practical limits, to a single relationship of gas permeability vs gas saturation. The percentage relative fluid permeabilities shown in Fig. 8 can now be used to calculate the corrected k_g/k_o relationship. This corrected k_g/k_o curve is almost identical with the k_g/k_o curve for the helium gas drive (No. 6 in Fig. 6). Referring to Fig. 4, the k_g/k_o relationship for this external drive is in the

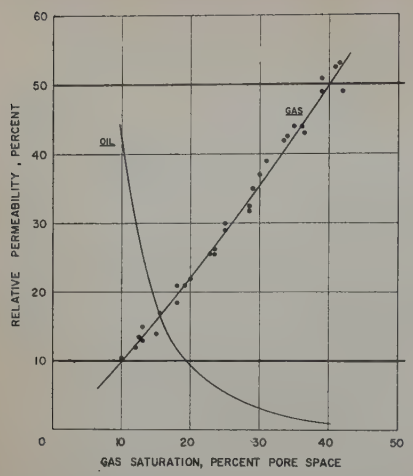

FIG. 8—CORRECTED GAS RELATIVE PERMEABILITY, RUNS 1 THROUGH 6, WOLFCAMP LIMESTONE.

region of laminar flow for this sample.

For the Palo Pinto reef sample, the corrected k_g/k_o relationship is presented by the dashed curve in Fig. 9. This corrected curve is located between the curves for Runs 3 and 5. Referring to Fig. 7, Run 3 is in the turbulent region where the k_g/k_o relationship is erroneously low because of lowered gas permeability. Conversely, Run 5 is in the region where gas slippage results in a k_g/k_o relationship which is erroneously high.

In summary, a correction method can be used to calculate the true relative permeability characteristics of a core even though turbulence and slippage were present during a laboratory flow test.

CONCLUSIONS

1. Turbulence and slippage can exist during laboratory flow tests on heterogeneous porosity limestones for usual test conditions. Measured single-phase permeabilities and two-phase permeability characteristics can be seriously in error due to turbulence and slippage.

2. In single-phase flow tests it should be possible to eliminate turbulence and correct for slippage or to eliminate both factors by controlling the test conditions. However, it is not always possible to eliminate both turbulence and slippage in two-phase flow tests by controlling test conditions.

3. A correction method has been developed which can be used to calculate the true relative permeability characteristics of a core even though turbulence and slippage were present during a laboratory flow test.

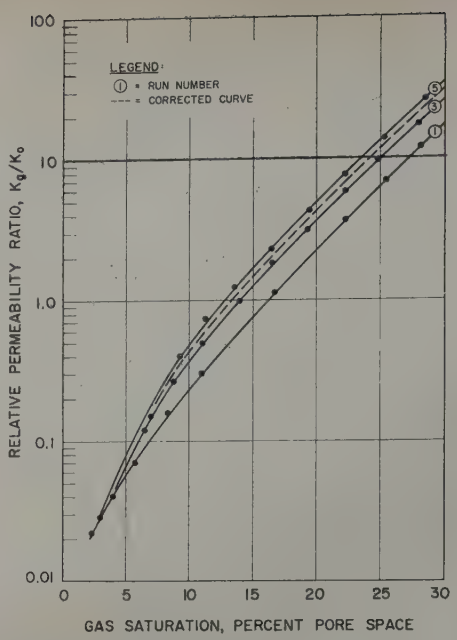

FIG. 9—SLIPPAGE AND TURBULENCE IN EXTERNAL GAS DRIVES, PALO PINTO REEF LIMESTONE.

REFERENCES

1. Muskat, Morris: *Flow of Homogeneous Fluids*, McGraw-Hill Book Co., Inc., N.Y. (1936).
2. Stewart, C. R., Craig, F. F. and Morse, R. A.: "Determination of Limestone Performance Characteristics by Model Flow Tests", *Trans.* AIME (1953) **198**, 93.
3. Klinkenberg, L. J.: "The Permeability of Porous Media to Liquids and Gases", *Drill. and Prod. Prac.*, API (1941) 200.
4. Fancher, G. H. and Lewis, J. A.: "Flow of Simple Fluids Through Porous Materials", *Ind. Eng. Chem.* (1933) **25**, 1139.
5. Welge, H. J.: "A Simplified Method for Computing Oil Recovery by Gas or Water Drive", *Trans.* AIME (1952) **195**, 91.
6. Yuster, S. T.: "Homogeneous Permeability Determination", *Drill. and Prod. Prac.*, API (1946) 356.
7. Rose, W. D.: "Permeability and Gas-Slippage Phenomena", *Drill. and Prod. Prac.*, API (1948) 209. ★★★

Comparison Between the Predicted and Actual Production History of a Condensate Reservoir

J. K. RODGERS — GULF RESEARCH & DEVELOPMENT CO.
N. H. HARRISON — PITTSBURGH, PA.
S. REGIER* — GULF OIL CORP.
MEMBER AIME — TULSA, OKLA.

ABSTRACT

This paper presents comparisons of data obtained from a laboratory reservoir study and from a calculated behavior prediction with the actual production history of a condensate reservoir.

A small non-commercial discovery was depleted under closely controlled conditions and the well fluids were sampled at frequent intervals. Data on the reservoir and production variables were accumulated on a fixed schedule. A laboratory reservoir study was made using the initial well fluid samples as charging stock. The production procedures and operating conditions were held constant throughout the study wherever possible and in general paralleled the field work. The well fluid compositions and the cumulative recoveries as a function of the reservoir pressure were also calculated using conventional flash vaporization procedures and equilibrium constants.

Comparisons based on the composition of the well fluid show good agreement, the laboratory study agreeing within experimental accuracy with the field work and the calculated data comparing equally well. The gas-oil ratios are also in good agreement, but with somewhat greater deviations at the higher pressures.

In the over-all picture, it is believed that a model study can predict within experimental accuracy the production history of a condensate reservoir. Better equilibrium constants for the heavier hydrocarbons are needed in order to attain improved composition accuracy by calculation.

Original manuscript received in Society of Petroleum Engineers office July 31, 1957. Revised manuscript received April 21, 1958. Paper presented at 32nd Annual Fall Meeting of Society of Petroleum Engineers in Dallas, Tex., Oct. 6-9, 1957.

*Presently associated with the Warren Petroleum Corp., Tulsa, Okla.

Discussion of this and all following technical papers is invited. Discussion in writing (three copies) may be sent to the offices of the *Journal of Petroleum Technology*. Any discussion offered after Dec. 31, 1958, should be in the form of a new paper.

INTRODUCTION

In Aug., 1955, a gas condensate well was completed in San Juan County, Utah, that was initially thought capable of good commercial production. These conclusions were derived principally from core data and electric logs, which indicated good permeability, porosity and gas content. However, after the usual series of potential tests it was found that the reservoir pressure had declined some 22 per cent, and it was obvious that the zone tapped was but a small pocket or trap.

It became apparent that, with a controlled depletion of a small reservoir, a unique opportunity was available to compare laboratory and calculated studies with an actual field depletion and to further the present knowledge of condensate reservoirs.

FIELD WORK

The Coalbed Canyon Well No. 1 was conventionally completed in the Paradox limestone formation to a total depth of 5,912 ft. The producing zone from 5,762 to 5,806 ft was perforated with four jet shots per ft. The wellhead and field equipment were also conventional, the major items consisting of a two-pass indirect fired line heater, a high- and a low-pressure separator with the necessary controls and accessories, gas meters, back-pressure regulators, flare stacks and condensate stock tanks.

The initial testing of this well consisted of a series of flow potential and pressure build-up tests during which some 30 MMcf of gas was produced. The reservoir pressure declined from an estimated 2,300 to 1,782 psig during this period, from which it was concluded that the reservoir was very small.

In order to approach steady-state conditions in the reservoir and so provide optimum conditions for making comparisons, the field depletion was programmed to approach, if possible, constant production conditions. Bi-hourly readings were taken of the tubing pressure, the pressure and temperature of the separators, oil and gas rates, and other pertinent operating data. The gas rate, as indicated by the orifice meter, was held constant by the adjustment of the choke in the line heater. The temperature of the first stage separator was held constant by adjustment of the line heater jacket temperature. Practical considerations of production made the maintenance of a constant gas rate impossible. The test started with a gas rate of 4 MMcf/D and a separator pressure of 250 psig. This rate was maintained until the choke was fully opened. The gas rate then declined with the falling tubing pressure and production was continued until the rate was about 2

MMcf/D. The separator pressure was then lowered to 100 psig, and the choke adjusted to re-establish the gas rate at 4 MMcf/D. This same procedure was repeated with the separator pressure at 50 psig. The second-stage separator was operated at 20 psig throughout the test. Because of the low potential of the well and the desire to deplete the reservoir to a low pressure, it was necessary to use lower flow rates during the last part of the test. The gas rate had dropped to 1.5 MMcf/D when the well was finally shut in.

At daily intervals the water production was measured by draining the separators. Oil samples were flashed from the high- and low-pressure separators and their gravities determined. The shrinkage factor and the production rate of the high-pressure separator liquid and the gravity of the high- and low-pressure separator gases were measured.

At less frequent intervals the tubing pressure was checked with a dead-weight gauge in order to have a running calibration on the tubing gauge, a 12-in. precision instrument. The separator fluids were sampled at flowing tubing pressures of 1,314, 1,147, 797, 603, 380, 248, 137, and 104 psig. Simultaneously, flowing reservoir pressures were measured while the separator samples were being taken.

The well was shut in for pressure build-up tests twice during the depletion, the first one being for a 72-hour period and the second for 219 hours. Pressure build-up data were also taken for 60 days following the final shut-in of the well.

LABORATORY APPARATUS

The heart of the model reservoir is a high-pressure cell of 4-liter capacity. The cell is equipped with a three-way valve, a safety disc rated at 7,500 psig, one arm of a Wheatstone-bridge circuit used as a "hot wire" to facilitate determining the gas-oil interface and an insulated wire probe for locating the oil-mercury interface. For volume variance mercury is injected through a valved line connected to the bottom of the cell.

The separation system is composed of three stages, stacked vertically to permit thorough drainage of the produced liquids. The high-pressure and intermediate-pressure separators are windowed cells of 30-cc capacity machined from blocks of steel and tested to 5,000 psi. The third stage is a precision graduated glass cylinder for collecting the liquids and directly determining the amount produced. All three separators are immersed in individual thermostatically controlled baths to maintain any desired constant temperature. The gas outlets of the separators are connected through back-pressure regulators to a bank of storage vessels so manifolded that the separator gases can be collected separately or mixed together. In these studies, the gases from the intermediate- and low-pressure separators were mixed and collected separately from that of the high-pressure separator. The collection system is connected to sampling apparatus for sample removal and to a vacuum pump for evacuation.

Other accessory equipment includes accurately calibrated pressure gauges, a dead-weight tester and bypass valves for venting the gas pressure in the separators.

Analyses of the fluids were made on a low temperature distillation apparatus. The determination of nitrogen was made by the method recommended by the NGAA.

LABORATORY PROCEDURE

Five model production studies were made in the laboratory with each study consisting of several runs.

The correct amounts of gas and liquid, as calculated from the field GOR, were determined for charging the 4-liter cell to somewhat above the dewpoint pressure. The gas was expanded into calibrated cylinders to atmospheric pressure, measured, and then condensed into the cell by cooling it with liquid nitrogen. Liquid was displaced into the cell at above bubble-point pressure by a calibrated piston pump using mercury as the displacing liquid. The cell was then placed in a thermostatically controlled oil bath at reservoir temperature and rocked to assure attainment of equilibrium.

Before starting a run, the three-stage separator system was flushed and filled with natural gas and the gas collection system evacuated. Effluent from the gas phase in the cell was slowly fed into the first-stage separator until the operating pressure, 750 psig, was attained. A back-pressure regulator then maintained this pressure throughout the run. When sufficient liquid had accumulated in the first stage, it was manually bled into the second stage where an operating pressure of 50 psig was maintained. Liquid from this stage was then bled into the third stage at atmospheric pressure and collected in the precision graduated cylinder. At the end of each run, which was determined by reaching a predetermined reservoir pressure or the limits of the collection systems, the reservoir was "shut in", the separators drained of all liquid and the gas then vented to the respective collection systems. Gas and liquid volumes were measured and samples taken for analysis.

Each study consisted of essentially three parts: (1) depletion to dew point, (2) depletion from the dew point to a predetermined pressure, and (3) displacement of the reservoir residue fluids at the predetermined pressure.

The first part consisted of a constant volume depletion to the dewpoint pressure of the reservoir. This established a common starting point for all the studies, and through the analyses of the produced fluids provided a check of the accuracy of the charge and a means of determining if equilibrium had been attained.

The second part of each study consisted of depleting the reservoir from the dew point to a predetermined pressure. For the five studies these pressures were approximately 80, 60, 40, 20, and 10 per cent of the dewpoint pressure. In this part of the study, it was on occasion necessary to make the pressure depletion in several steps because of the limits of the collection systems. Consequently, each run was specified in pressure range so that it coincided precisely with the same run from the other studies. Thus, each run was made in the same manner as the coinciding runs and gave duplication of conditions and experimental data. These runs provided the data from which the cumulative production could be calculated as well as GOR's and composition of the well fluids.

The third part of each study was the displacement of the reservoir fluids at constant pressure. Mercury was injected into the reservoir to maintain a constant pressure as the fluids were removed. The gas phase was completely displaced, passed through the separator system and the products collected and measured in an identical manner to that used for the constant volume runs.

The gas-oil interface was located by a hot wire Wheatstone-bridge circuit in the cell head; the oil-mercury interface by an insulated probe in the cell head. Amounts of mercury injected determined the volume of the gas phase and of the oil phase formed by retrograde condensation.

Samples of each phase were taken for analysis. Data from this part of the study provided the compressibility factors of the well fluid and the determination of the *K*-values of the hydrocarbons at the coincident pressure and temperature.

Throughout all the studies the operating conditions of the three separators were 750, 50 psig, and atmospheric pressure, and their temperatures were 65, 65, and 60° F, respectively. On the last study, though, where the reservoir was depleted to 200 psig, it was necessary to lower the separator pressure; this was done in two steps. On next to the last run, separator pressures were 250, 20 psig, and atmospheric pressure; on the final run, they were 100 psig, atmospheric, and atmospheric, respectively.

CALCULATION PROCEDURE

The second method of predicting the recoveries obtainable from a condensate reservoir is by calculation. From an initial volume, pressure, temperature and composition of the reservoir fluid, vapor-liquid equilibrium constants and standard flash vaporization procedures, it is possible to determine the recoveries of the various components as the pressure of a reservoir declines.

In order to derive the calculated volumes and compositions of the produced fluids during the life of a field, the following simplifying assumptions are required.

1. The flowing bottom-hole pressure is the equilibrium pressure and the dew point of the reservoir fluid flowing into the wellbore. The static bottom-hole pressure is the shut-in equilibrium pressure of the reservoir and determines the amount of well fluid produced during any pressure decrement.

2. The condensate which accumulates in the reservoir through the retrograde region as the pressure declines will remain immobile. Thus, in order to produce any part of this condensate, re-vaporization must occur before any of these hydrocarbons can move into the wellbore.

3. All condensate which forms in the wellbore will be produced with the gas from which it originated.

4. The average composition of the well fluid produced during any pressure decrement is the arithmetic average value of the initial and final fluid produced during any pressure step.

5. No liquid hydrocarbons exist in the reservoir under the initial reservoir conditions of temperature and pressure.

Regarding the fifth assumption, the initial samples taken for the purpose of determining the composition of the reservoir fluid were obtained at a pressure of 2,217 psig. It was found that the reservoir fluid was saturated at that pressure. Thus, it was indeterminate whether the reservoir had been saturated at its original estimated pressure of 2,300 psig. Through the laboratory determination, as discussed, a dew point of 2,217 psig was established for the initial reservoir samples. By use of this dew point for both the laboratory and the calculation studies, a common basis for comparison of data was established. The reservoir was thus assumed to be undersaturated at 2,300 psig.

The calculation of a reservoir depletion is based essentially on data available early in the life of the reservoir. The pertinent items concerning the Coalbed Canyon Well No. 1 are as follows: (1) estimated original reservoir pressure, 2,300 psig; (2) reservoir temperature, 134° F; (3) dewpoint pressure, 2,217 psig; (4) pore volume of the reservoir, 658,000 cu ft, which was obtained by a material balance using the fluid produced during the drill-stem tests as the basis for the estimate; and (5) composition of the well fluid, which is listed as follows.

Component	Mol Per Cent
Nitrogen	0.99
Methane	77.41
Ethane	11.48
Propane	5.31
iso-Butane	0.97
n-Butane	1.33
iso-Pentane	0.59
n-Pentane	0.38
Hexanes	0.54
Heptanes +	1.00
TOTAL	100.00
Mol Wt C_{7+}	116.4
Sp Gr C_{7+}	0.7443

Accurate phase behavior characteristics of the hydrocarbons are essential in order to predict recoveries. The procedure used in developing applicable equilibrium factors (or *K*-values) were based on methods developed and published elsewhere in the literature. The procedure in developing these equilibrium factors for this study consisted in general of the following steps. First, the properties of the heptanes-plus fraction in the well fluid were examined. A review of the true boiling point distillation curve, the molecular weight, specific gravity and characterization factor indicated that equilibrium factors developed for octanes would give relatively good results for the heptanes-plus fraction. Second, the apparent convergence pressure of 3,340 psia was determined using the method suggested by Hadden.[1] The third step was the development of the minimum equilibrium values obtained from empirical correlations.[2] After several attempts, a smooth set of equilibrium factors was developed as shown in Fig. 6 by using the NGAA equilibrium factors[3] from 0 to 500 psia, the minimum *K*-values as calculated in Step 3, the values determined from the dewpoint composition at 2,217 psia, and the apparent convergence pressure selected previously. Fig. 6 is the plot of log K − Log P, normally developed for hydrocarbon systems. Equilibrium factors for nitrogen were developed through a cross plot of data published by Jacoby and Rzasa[4] on the non-hydrocarbon constituents of the reservoir fluids.

Compressibility factors were unavailable for the calculation study. Approximate values were developed by flashing the initial fluid composition to various pressures in the life of the project.[5] The vapor phase obtained from these calculations was then treated in the usual manner by application of the reduced pressure and temperature curves cited in the literature[6] for the determination of compressibility factors.

The procedure used in the calculated depletion of Coalbed Canyon Unit No. 1 was begun by determining the gas volume produced from 2,300 to 2,217 psia. As this step was above the dew point, the composition of the gas remained constant and the decrement was made through the use of the gas laws alone. All the pressure decrements from the dewpoint pressure to the abandonment pressure require treatment of the changing volume of condensate in the reservoir as the pressure decreases, in addition to the effects resulting from the production of the reservoir gas. The calculation procedure, in general, consists of making an estimate of the amount and the average composition of the fluid produced during any pressure step. This estimated fluid is then subtracted by components from the total fluid remaining in the reservoir from the previous pressure decrement.

By making a conventional flash calculation of the reservoir fluid, the distribution of the components between the liquid and vapor phases can be obtained. A comparison of the physical volume of the combined liquid and vapor to the pore volume of the reservoir will reveal the accuracy of the produced volume of fluid

[1]References given at end of paper.

already estimated. A comparison of the estimated and calculated composition at the final pressure of each decrement should also be made. If the estimate of fluid production or the final composition of any decrement do not agree reasonably well with the calculated values, this procedure should be repeated until a satisfactory comparison is made before continuing to the next step.

DISCUSSION

The well fluid compositions obtained by laboratory studies and calculations are compared with the actual field samples in Figs. 1 through 5. The curves drawn on these figures represent the smoothed reservoir composition with which the laboratory and calculated data are compared. An examination of these figures will, in general, reveal good agreement between these studies and the field samples.

There were small discrepancies between the composition of the well fluid charged to the laboratory apparatus and the value used as the initial fluid in the calculated study, which introduced a difference in composition throughout the whole of the two studies. The trends of the two studies are, however, quite similar.

Compositional comparisons of methane, ethane and propane are shown in Fig. 1. The methane and ethane are in very good agreement throughout the whole pressure range. The propane shows some slight variance, the laboratory and calculated work agreeing quite well with each other but being slightly higher than that of the reservoir data in the middle pressure range.

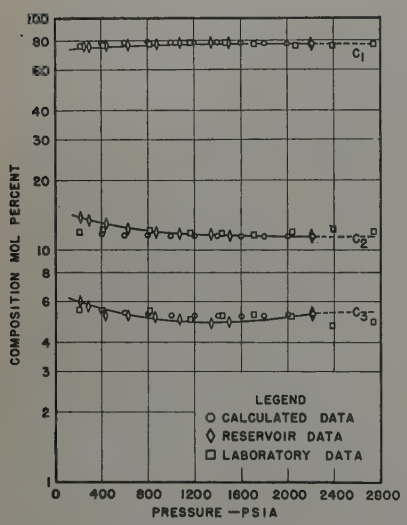

Fig. 1—Comparisons of the Well Fluid Compositions.

The conformity of iso- and normal butane and pentane components, as shown in Figs. 2 and 3, were somewhat less favorable due to the erratic points in the analyses obtained on the laboratory and reservoir samples. Sharp separation of the iso- and normal components of butane and pentane is known to be a difficult operation on the low-temperature distillation apparatus in use today.

The scattering of the points on these curves is believed to be due to this lack of resolution and, for this reason, the isomers of the components are combined and shown in Fig. 4. An improvement in the results is apparent.

In Fig. 5 the comparison of the hexane compositions was good in the upper-pressure range, but below 1,500 psi, the laboratory points scattered at random, and the calculated data are high.

The comparison of the heptane-plus data indicates that considerable improvement in the calculated composition could be made. As stated previously, from all of the indicated properties of the heptane-plus fraction the *K*-values for octane should have been satisfactory. The appearance of the data on the curve clearly shows the need for improved techniques in establishing proper equilibrium data. Except at the very lowest pressures, agreement between the laboratory and the reservoir data is good. The comparison of the nitrogen composition data indicate a common trend even though the data are somewhat scattered. These determinations were made by the NGAA method.

The equilibrium factor curves shown in Fig. 6 are those used for the calculation study. The points plotted are those values obtained from the laboratory work. The agreement of the data is only fair. The laboratory data develop a family of curves that are of somewhat different shape than those used in the calculated study. The methane and hexane curves are both lower, the ethane and propane in reasonable agreement, and the butanes and pentanes are considerably higher in the upper-pressure region. The heptane-plus data are considerably higher in the mid-pressure region with best agreement at the highest pressure. The poor resolution of the butane and pentane isomers made combination necessary for these calculations. These data follow the trends of the laboratory well-fluid compositions. In most of the cases where the laboratory work shows a component with a higher concentration than the calculated study, the indicated equilib-

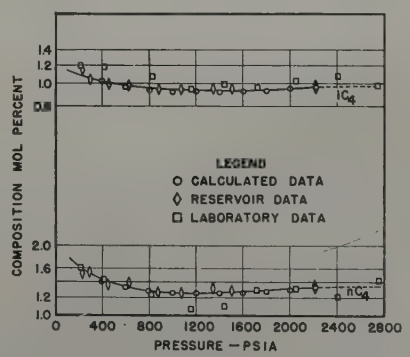

Fig. 2—Comparisons of the Well Fluid Compositions.

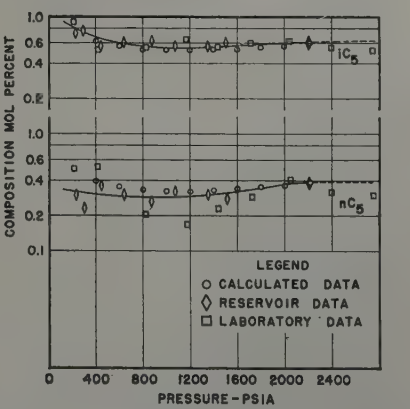

Fig. 3—Comparisons of the Well Fluid Compositions.

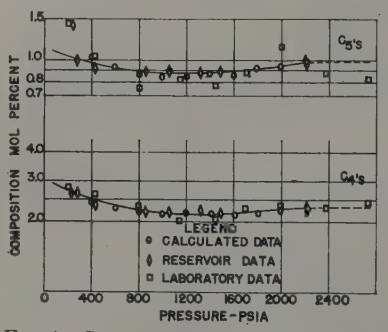

Fig. 4—Comparisons of the Well Fluid Compositions.

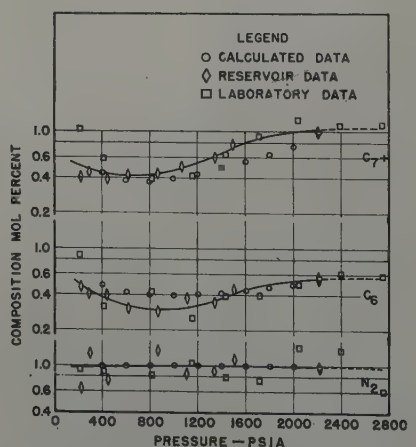

Fig. 5—Comparisons of the Well Fluid Compositions.

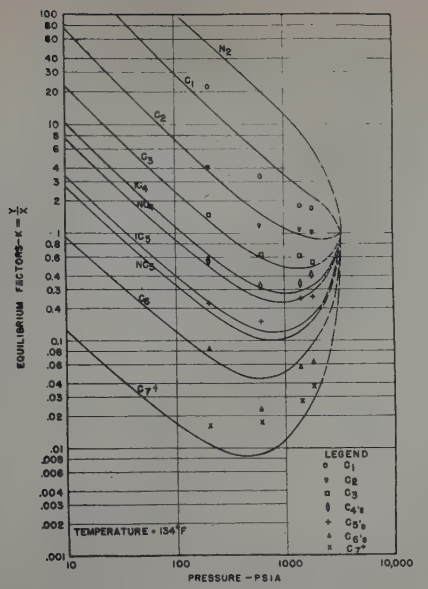

FIG. 6—COMPARISON OF THE EQUILIBRIUM FACTORS.

rium constants are correspondingly lower.

Fig. 7 is a comparison of compressibility factors. The curve is calculated from the well-fluid composition and the reduced temperature and pressure data of the components. The points shown are those derived from the laboratory work. The agreement is good.

The data shown in Fig. 8 are a plot of the produced gas vs pressure/compressibility (P/Z). The actual and calculated volumes are compared with the original estimated values. The agreement is very good, with the deviations of the actual and calculated volumes from the straight line signifying the effects of the retrograde condensation in the reservoir.

Fig. 9 is a comparison of the calculated and laboratory GOR in the reservoir at the reservoir temperature and pressure.

Fig. 10 is the comparison of the high-pressure separator gas-stock tank oil ratio as derived in the laboratory with that found in the field. The agreement of the two was favorable.

CONCLUSIONS

From the comparison made between the results of the laboratory and calculated studies and the values obtained during the controlled depletion of the reservoir itself, several conclusions have been drawn. First, the laboratory depletion study closely reproduced the data obtained from the reservoir as the field was depleted, thereby indicating that within the accuracy of the equipment, laboratory studies can reproduce the

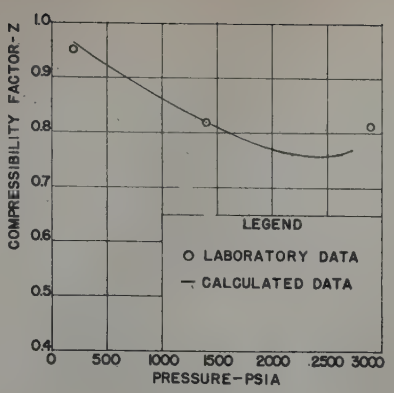

FIG. 7—COMPRESSIBILITY FACTOR OF THE WELL FLUID.

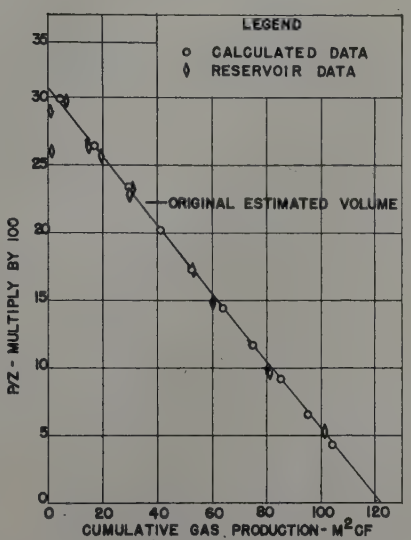

FIG. 8—GAS CONTENT OF RESERVOIR.

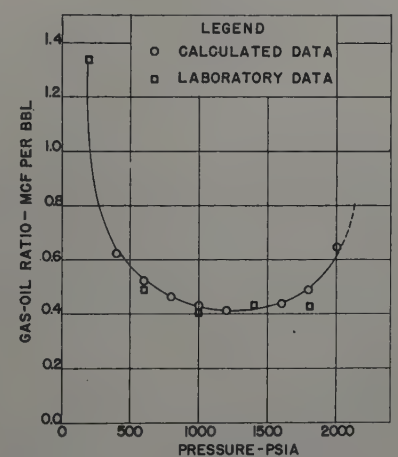

FIG. 9—GAS-OIL RATIO OF RESERVOIR FLUIDS.

conditions of a condensate reservoir through the life of such a system. Secondly, compositions and volumes through the life of a condensate reservoir can be predicted by calculations provided representative equilibrium factors are available. Thirdly, improved procedures for developing the equilibrium factors for the heavier hydrocarbons would improve the over-all accuracy of the calcula-

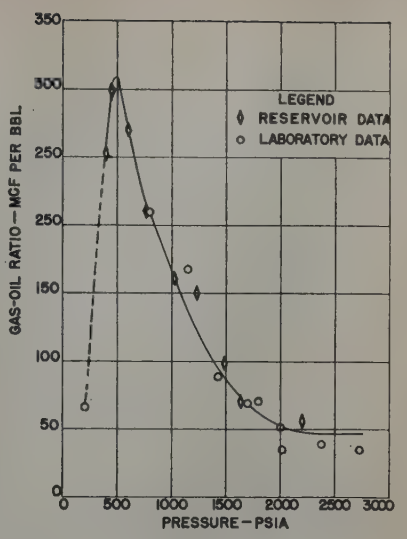

FIG. 10—SEPARATOR GAS-OIL RATIO OF WELL FLUID.

tion method. Fourthly, by use of one of the various electronic computers, the calculation method can be far more rapid than the laboratory method and is a good method for quickly obtaining approximate results. Finally, further laboratory studies will be required to advance the present knowledge of the equilibrium factors of the heavier hydrocarbons.

ACKNOWLEDGMENTS

The authors wish to express their appreciation to the Gulf Research and Development Co. and to the Tulsa Div. of the Gulf Oil Corp. for permission to publish this paper. A part of this work has been submitted by one of the authors to the University of Tulsa as a thesis.

REFERENCES

1. Hadden, S. T.: "Convergence Pressure in Hydrocarbon Vapor-Liquid Equilibria", *Chem. Eng. Prog.* (1953) Symposium Series 49, No. 753.
2. Hadden, S. T.: "Vapor-Liquid Equilibria in Hydrocarbon Systems", *Chem. Eng. Prog.* (Jan. and Feb., 1948) **44.**
3. NGAA: *Equilibrium Ratio Data Book*, Tulsa, Okla.
4. Jacoby, R. H., and Rzasa, M. J.: "Equilibrium Vaporization Ratios for Nitrogen, Methane, Carbon Dioxide, Ethane and Hydrogen Sulfide in Absorber Oil-Natural Gas and Crude Oil-Natural Gas Systems", *Trans.* AIME (1952) **195,** 99.
5. Allen, F. H., and Roe, R. P.: "Performance Characteristics of a Volumetric Condensate Reservoir", *Trans.* AIME (1950) **189,** 83.
6. Standing, M. B.: *Behavior of Oil Field Hydrocarbon Systems*, Reinhold Publishing Co., N. Y. (1952).
7. Brown, G. G., Katz, D. L., Oberfell, G. G., and Alden, R. C.: "Natural Gasoline and the Volatile Hydrocarbons", NGAA (1948) Tulsa, Okla.

★★★

Estimation of Ultimate Recovery from Solution Gas-Drive Reservoirs

W. L. WAHL
L. D. MULLINS
E. B. ELFRINK
MEMBERS AIME

MAGNOLIA PETROLEUM CO.
DALLAS, TEX.

INTRODUCTION

In the past few years several articles and papers presenting results of solution gas-drive depletion calculations have appeared in the literature[1,5]. Such calculations are of interest to the oil industry, for investment decisions must often be made before much is known about a reservoir. At other times, an estimate of the possible benefits to be realized from alternate production methods is desirable, and theoretical depletion calculations can serve as a floor or reference level from which to work. In any case, an estimate of ultimate oil recovery based upon engineering data is commonly required.

An engineer confronted with the problem of obtaining, for a specific reservoir system, an estimate of ultimate oil recovery by solution gas-drive depletion usually will be forced to perform the calculations himself. This is despite the quantity of data in the literature. Rarely will either experience or the literature provide results from a reservoir system similar in all important respects to the one under consideration, and calculated results are not so plentiful that satisfactory interpolation procedures can be devised. Performing the calculations, however, is a tedious, time-consuming task unless an electronic computer is available, and, in practice, time and manpower are not always available for this purpose.

A quick, simple, consistent method was needed for reducing the uncertainty in estimated oil recovery from solution gas-drive reservoirs when only minimum information about the reservoir system is available.

Original manuscript received in Society of Petroleum Engineers office Sept. 15, 1957. Revised manuscript received April 16, 1958. Paper presented at Southern California Petroleum Section Fall Meeting in Los Angeles, Oct. 17-18, 1957.

[1]References given at end of paper.

PROCEDURE

Method of Calculation

The usual requisite assumptions were made so that the material balance equation could be used to calculate data for the charts. The following assumptions were made: (1) the reservoir is homogeneous and isotropic; (2) oil recovery is due entirely to solution gas drive and neither a gas cap nor a water drive nor gravity drainage is present; (3) the initial reservoir pressure is the bubble-point pressure of the reservoir fluid; (4) initial total liquid saturation is 100 per cent of pore space; (5) interstitial water saturation remains at the initial value as the reservoir pressure declines from the bubble-point pressure to atmospheric pressure; (6) equilibrium gas saturation is 5 per cent of pore space; and (7) oil and gas saturations are uniformly distributed throughout the reservoir at all times. There are no saturation gradients due to a wellbore, nor is the geometry of the reservoir system considered.

The material balance equation was written in the form of a differential equation[1] which was integrated to determine the change in oil saturation for an assigned pressure drop. Formal integration was not possible, so recourse was made to the Runge-Kutta method[2] of numerical integration. All computations were performed on IBM equipment.

Numerical integration yielded the change in oil saturation within the reservoir as the pressure declined from the bubble-point pressure to atmospheric pressure. The initial oil saturation minus the change in oil saturation yielded the oil saturation at atmospheric pressure. The oil originally in place was obtained by dividing the initial oil saturation by the initial formation volume factor (differential liberation) while the oil in place at atmospheric pressure was obtained by dividing the final oil saturation by the formation volume factor at atmospheric pressure. Ultimate oil recovery, expressed as a percentage of the initial oil in place, was obtained by dividing the difference between the oil initially in place and the oil in place at atmospheric pressure by the oil initially in place and multiplying by 100.

PVT Data

Charts were based upon 135 solutions to the material balance equation. PVT properties of the reservoir fluids were variables in this equation and had to be known as functions of pressure. The required PVT data might have been obtained from either actual reservoir fluid systems or correlated data. However, correlated PVT data were developed and employed in the calculations for the following reasons: (1) it is doubtful that 135 sets of PVT data could have been obtained for the values of variables investigated in this study, and (2) results of recovery calculations from randomly obtained PVT data could not be correlated as well as results from selected PVT data.

The PVT data used to develop the

correlations consisted primarily of Mid-Continent and Gulf Coast crude oil systems although Canadian and South American systems were represented. Data from approximately 75 fluid systems were used, but only part of the data were utilized for any one correlation. When only minimum information about a fluid system is available, the correlations presented in Figs. 10 thru 14 may prove useful.

The correlation of oil formation volume factor (B_o) vs bubble-point pressure is shown in Fig. 10. Suppose B_o and the bubble-point pressure for a reservoir fluid locate a point somewhere on one of the curves. Then B_o will decrease along this curve with decreasing pressure. Since B_o and the bubble-point pressure generally will not locate a point exactly on one of the curves, it is necessary to interpolate for values.

Solution gas-oil ratio (R_s) vs bubble-point pressure curves are presented in Fig. 11. Procedure is similar to that for estimating oil formation volume factor. Corresponding values of solution gas-oil ratio and bubble-point pressure locate a point somewhere on one of the curves, and solution gas-oil ratio then decreases along the curve with decreasing pressure. Interpolation between curves may be necessary.

A curve for reciprocal gas formation volume factor vs reservoir pressure is shown in Fig. 12. Data

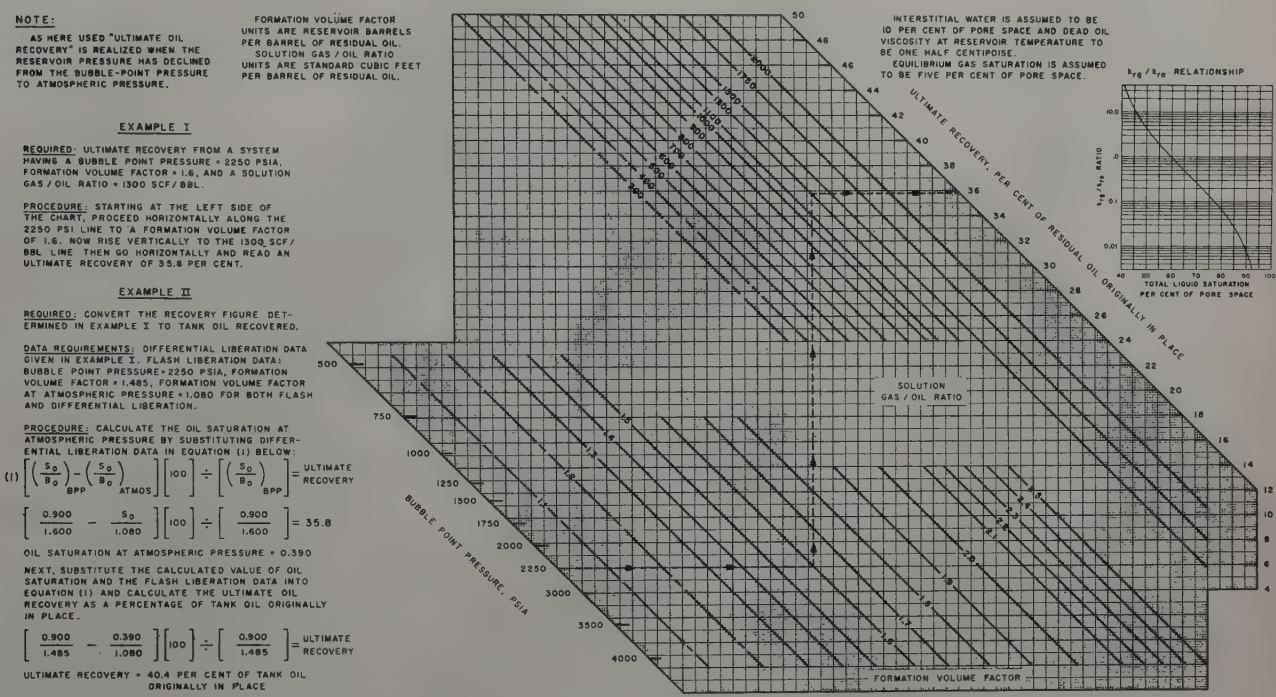
NOTE:
AS HERE USED "ULTIMATE OIL RECOVERY" IS REALIZED WHEN THE RESERVOIR PRESSURE HAS DECLINED FROM THE BUBBLE-POINT PRESSURE TO ATMOSPHERIC PRESSURE.
FORMATION VOLUME FACTOR UNITS ARE RESERVOIR BARRELS PER BARREL OF RESIDUAL OIL.
SOLUTION GAS / OIL RATIO UNITS ARE STANDARD CUBIC FEET PER BARREL OF RESIDUAL OIL.
EXAMPLE I
REQUIRED: ULTIMATE RECOVERY FROM A SYSTEM HAVING A BUBBLE POINT PRESSURE = 2250 PSIA, FORMATION VOLUME FACTOR = 1.6, AND A SOLUTION GAS / OIL RATIO = 1300 SCF / BBL.
PROCEDURE: STARTING AT THE LEFT SIDE OF THE CHART, PROCEED HORIZONTALLY ALONG THE 2250 PSI LINE TO A FORMATION VOLUME FACTOR OF 1.6. NOW RISE VERTICALLY TO THE 1300 SCF/BBL LINE THEN GO HORIZONTALLY AND READ AN ULTIMATE RECOVERY OF 35.8 PER CENT.
EXAMPLE II
REQUIRED: CONVERT THE RECOVERY FIGURE DETERMINED IN EXAMPLE I TO TANK OIL RECOVERED.
DATA REQUIREMENTS: DIFFERENTIAL LIBERATION DATA GIVEN IN EXAMPLE I. FLASH LIBERATION DATA: BUBBLE POINT PRESSURE = 2250 PSIA, FORMATION VOLUME FACTOR = 1.485, FORMATION VOLUME FACTOR AT ATMOSPHERIC PRESSURE = 1.080 FOR BOTH FLASH AND DIFFERENTIAL LIBERATION.
PROCEDURE: CALCULATE THE OIL SATURATION AT ATMOSPHERIC PRESSURE BY SUBSTITUTING DIFFERENTIAL LIBERATION DATA IN EQUATION (I) BELOW:
(I) $\left[\left(\frac{S_o}{B_o}\right)_{BPP} - \left(\frac{S_o}{B_o}\right)_{ATMOS}\right]\left[100\right] \div \left[\left(\frac{S_o}{B_o}\right)_{BPP}\right] =$ ULTIMATE RECOVERY
$\left[\frac{0.900}{1.600} - \frac{S_o}{1.080}\right]\left[100\right] \div \left[\frac{0.900}{1.600}\right] = 35.8$
OIL SATURATION AT ATMOSPHERIC PRESSURE = 0.390
NEXT, SUBSTITUTE THE CALCULATED VALUE OF OIL SATURATION AND THE FLASH LIBERATION DATA INTO EQUATION (I) AND CALCULATE THE ULTIMATE OIL RECOVERY AS A PERCENTAGE OF TANK OIL ORIGINALLY IN PLACE.
$\left[\frac{0.900}{1.485} - \frac{0.390}{1.080}\right]\left[100\right] \div \left[\frac{0.900}{1.485}\right] =$ ULTIMATE RECOVERY
ULTIMATE RECOVERY = 40.4 PER CENT OF TANK OIL ORIGINALLY IN PLACE
INTERSTITIAL WATER IS ASSUMED TO BE 10 PER CENT OF PORE SPACE AND DEAD OIL VISCOSITY AT RESERVOIR TEMPERATURE TO BE ONE HALF CENTIPOISE.
EQUILIBRIUM GAS SATURATION IS ASSUMED TO BE FIVE PER CENT OF PORE SPACE.
ULTIMATE RECOVERY, PER CENT OF RESIDUAL OIL ORIGINALLY IN PLACE
k_{rg}/k_{ro} RELATIONSHIP
k_{rg}/k_{ro} RATIO
TOTAL LIQUID SATURATION PER CENT OF PORE SPACE
SOLUTION GAS / OIL RATIO
BUBBLE POINT PRESSURE, PSIA
FORMATION VOLUME FACTOR

FIG. 1—CHART FOR ESTIMATING ULTIMATE RECOVERY FROM SOLUTION GAS-DRIVE RESERVOIRS.

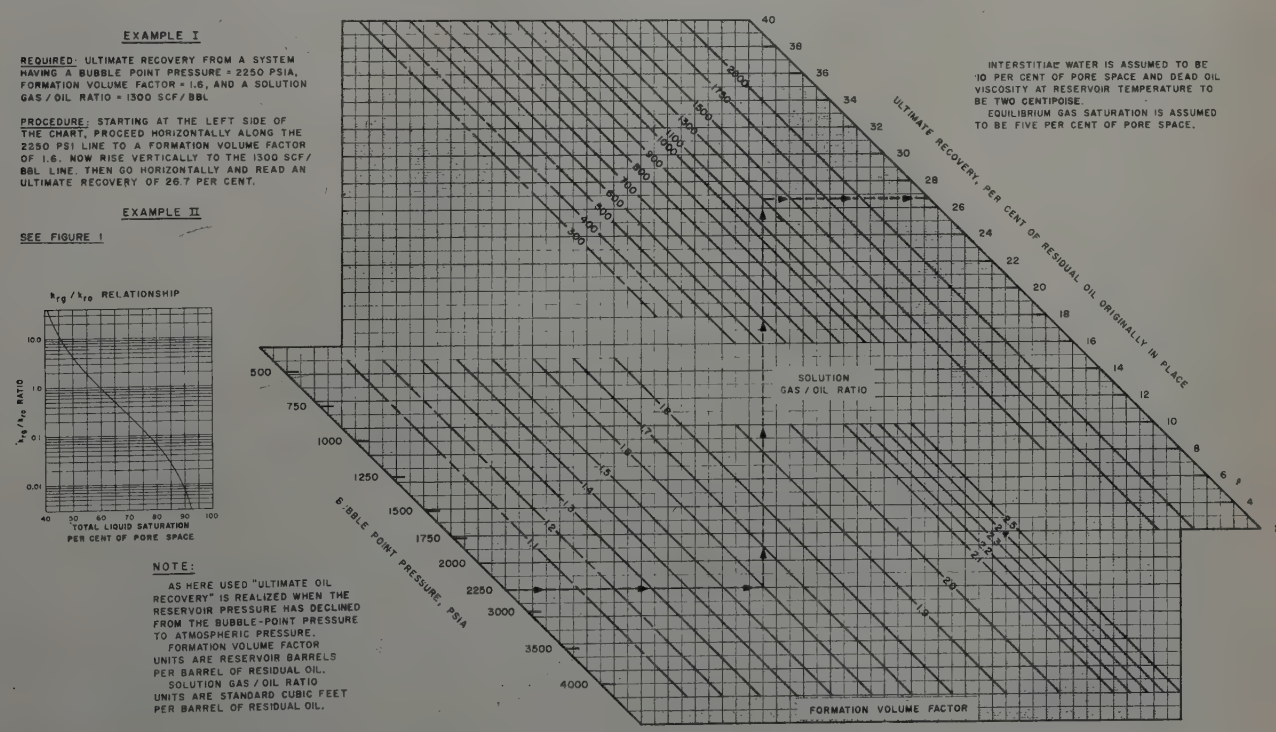
EXAMPLE I
REQUIRED: ULTIMATE RECOVERY FROM A SYSTEM HAVING A BUBBLE POINT PRESSURE = 2250 PSIA, FORMATION VOLUME FACTOR = 1.6, AND A SOLUTION GAS / OIL RATIO = 1300 SCF / BBL
PROCEDURE: STARTING AT THE LEFT SIDE OF THE CHART, PROCEED HORIZONTALLY ALONG THE 2250 PSI LINE TO A FORMATION VOLUME FACTOR OF 1.6. NOW RISE VERTICALLY TO THE 1300 SCF/BBL LINE, THEN GO HORIZONTALLY AND READ AN ULTIMATE RECOVERY OF 26.7 PER CENT.
EXAMPLE II
SEE FIGURE 1
k_{rg}/k_{ro} RELATIONSHIP
k_{rg}/k_{ro} RATIO
TOTAL LIQUID SATURATION PER CENT OF PORE SPACE
NOTE:
AS HERE USED "ULTIMATE OIL RECOVERY" IS REALIZED WHEN THE RESERVOIR PRESSURE HAS DECLINED FROM THE BUBBLE-POINT PRESSURE TO ATMOSPHERIC PRESSURE.
FORMATION VOLUME FACTOR UNITS ARE RESERVOIR BARRELS PER BARREL OF RESIDUAL OIL.
SOLUTION GAS / OIL RATIO UNITS ARE STANDARD CUBIC FEET PER BARREL OF RESIDUAL OIL.
INTERSTITIAL WATER IS ASSUMED TO BE 10 PER CENT OF PORE SPACE AND DEAD OIL VISCOSITY AT RESERVOIR TEMPERATURE TO BE TWO CENTIPOISE.
EQUILIBRIUM GAS SATURATION IS ASSUMED TO BE FIVE PER CENT OF PORE SPACE.
ULTIMATE RECOVERY, PER CENT OF RESIDUAL OIL ORIGINALLY IN PLACE
SOLUTION GAS / OIL RATIO
BUBBLE POINT PRESSURE, PSIA
FORMATION VOLUME FACTOR

FIG. 2—CHART FOR ESTIMATING ULTIMATE RECOVERY FROM SOLUTION GAS-DRIVE RESERVOIRS.

for the curve were obtained in the following manner.

Gas gravities as functions of pressure were obtained from PVT analyses of reservoir fluids. Gas gravities were used to determine pseudo-critical temperatures and pressures from published correlations.[3] Pseudo-critical temperatures and pressures in turn permitted the pseudo-reduced temperatures and pressures to be calculated because pressure histories and temperatures of the fluid systems were known. Published correlations[4] were employed to determine compressibility factors which, in turn, permitted the reciprocal formation volume factors to be calculated as functions of pressure.

The reservoir fluids used as the basis for Fig. 12 had bubble-point pressures ranging from 1,485 to 4,000 psia and represented reservoirs having temperatures ranging from 132 to 284° F.

Fig. 13 shows gas-saturated oil viscosity vs solution gas-oil ratio.

Gas viscosity vs reservoir pressure is presented in Fig. 14. Gas gravity and pressure data were obtained from analyses of reservoir fluids, and the method of Carr, Kobayashi and Burrows[3] was used to compute the gas viscosity at reservoir conditions as a function of pressure. PVT data from which the correlation was developed had bubble-point pressures ranging from 1,146 to 4,200 psia

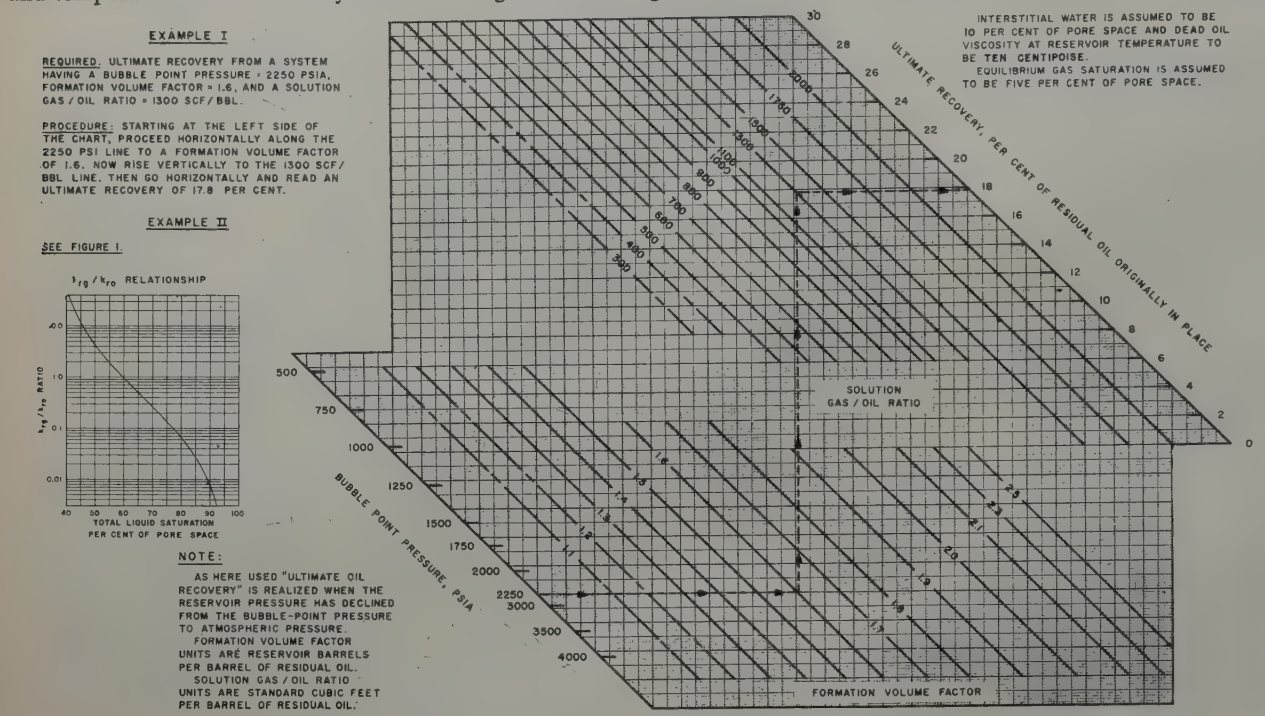
EXAMPLE I
REQUIRED: ULTIMATE RECOVERY FROM A SYSTEM HAVING A BUBBLE POINT PRESSURE = 2250 PSIA, FORMATION VOLUME FACTOR = 1.6, AND A SOLUTION GAS / OIL RATIO = 1300 SCF / BBL.
PROCEDURE: STARTING AT THE LEFT SIDE OF THE CHART, PROCEED HORIZONTALLY ALONG THE 2250 PSI LINE TO A FORMATION VOLUME FACTOR OF 1.6, NOW RISE VERTICALLY TO THE 1300 SCF / BBL LINE, THEN GO HORIZONTALLY AND READ AN ULTIMATE RECOVERY OF 17.8 PER CENT.
EXAMPLE II
SEE FIGURE 1.
k_{rg}/k_{ro} RELATIONSHIP
TOTAL LIQUID SATURATION PER CENT OF PORE SPACE
NOTE:
AS HERE USED "ULTIMATE OIL RECOVERY" IS REALIZED WHEN THE RESERVOIR PRESSURE HAS DECLINED FROM THE BUBBLE-POINT PRESSURE TO ATMOSPHERIC PRESSURE.
FORMATION VOLUME FACTOR UNITS ARE RESERVOIR BARRELS PER BARREL OF RESIDUAL OIL.
SOLUTION GAS / OIL RATIO UNITS ARE STANDARD CUBIC FEET PER BARREL OF RESIDUAL OIL.
INTERSTITIAL WATER IS ASSUMED TO BE 10 PER CENT OF PORE SPACE AND DEAD OIL VISCOSITY AT RESERVOIR TEMPERATURE TO BE TEN CENTIPOISE.
EQUILIBRIUM GAS SATURATION IS ASSUMED TO BE FIVE PER CENT OF PORE SPACE.
ULTIMATE RECOVERY, PER CENT OF RESIDUAL OIL ORIGINALLY IN PLACE
SOLUTION GAS / OIL RATIO
BUBBLE POINT PRESSURE, PSIA
FORMATION VOLUME FACTOR

FIG. 3—CHART FOR ESTIMATING ULTIMATE RECOVERY FROM SOLUTION GAS-DRIVE RESERVOIRS.

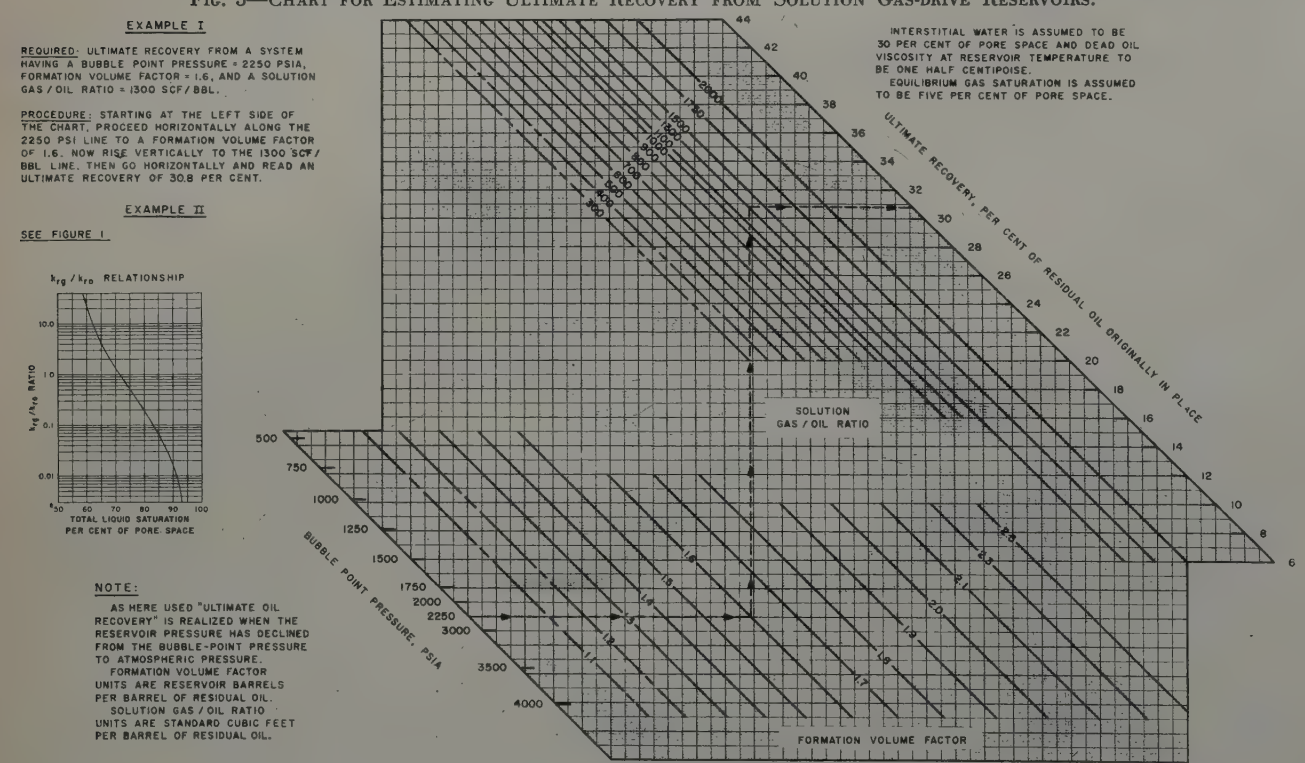
EXAMPLE I
REQUIRED: ULTIMATE RECOVERY FROM A SYSTEM HAVING A BUBBLE POINT PRESSURE = 2250 PSIA, FORMATION VOLUME FACTOR = 1.6, AND A SOLUTION GAS / OIL RATIO = 1300 SCF / BBL.
PROCEDURE: STARTING AT THE LEFT SIDE OF THE CHART, PROCEED HORIZONTALLY ALONG THE 2250 PSI LINE TO A FORMATION VOLUME FACTOR OF 1.6, NOW RISE VERTICALLY TO THE 1300 SCF / BBL LINE, THEN GO HORIZONTALLY AND READ AN ULTIMATE RECOVERY OF 30.8 PER CENT.
EXAMPLE II
SEE FIGURE 1
k_{rg}/k_{ro} RELATIONSHIP
TOTAL LIQUID SATURATION PER CENT OF PORE SPACE
NOTE:
AS HERE USED "ULTIMATE OIL RECOVERY" IS REALIZED WHEN THE RESERVOIR PRESSURE HAS DECLINED FROM THE BUBBLE-POINT PRESSURE TO ATMOSPHERIC PRESSURE.
FORMATION VOLUME FACTOR UNITS ARE RESERVOIR BARRELS PER BARREL OF RESIDUAL OIL.
SOLUTION GAS / OIL RATIO UNITS ARE STANDARD CUBIC FEET PER BARREL OF RESIDUAL OIL.
INTERSTITIAL WATER IS ASSUMED TO BE 30 PER CENT OF PORE SPACE AND DEAD OIL VISCOSITY AT RESERVOIR TEMPERATURE TO BE ONE HALF CENTIPOISE.
EQUILIBRIUM GAS SATURATION IS ASSUMED TO BE FIVE PER CENT OF PORE SPACE.
ULTIMATE RECOVERY, PER CENT OF RESIDUAL OIL ORIGINALLY IN PLACE
SOLUTION GAS / OIL RATIO
BUBBLE POINT PRESSURE, PSIA
FORMATION VOLUME FACTOR

FIG. 4—CHART FOR ESTIMATING ULTIMATE RECOVERY FROM SOLUTION GAS-DRIVE RESERVOIRS.

and reservoir temperatures ranging from 95 to 284° F.

k_{rg}/k_{ro} Ratio

All variables except one in the material balance equation are functions of reservoir pressure, the exception being the relative permeability ratio, k_{rg}/k_{ro}, which must be known as a function of saturation in order to solve the equation. Relative permeability data from field measurements on sandstone reservoirs were examined with the objective of developing a k_{rg}/k_{ro} ratio-saturation correlation which could be used in this study. It was found that when interstitial water saturation was treated as a parameter in the correlating procedure, an equation could be written which expressed the k_{rg}/k_{ro} ratio as a function of oil saturation alone. The equation is

$$k_{rg}/k_{ro} = \xi\,(0.0435 + 0.4556\xi)$$

and

$$\xi = \frac{1 - S_{gc} - S_w - S_o}{S_o - C},$$

where S_{gc} is equilibrium gas saturation, a constant = 0.05 in these calculations; S_w is interstitial water saturation, fraction of pore space; S_o is

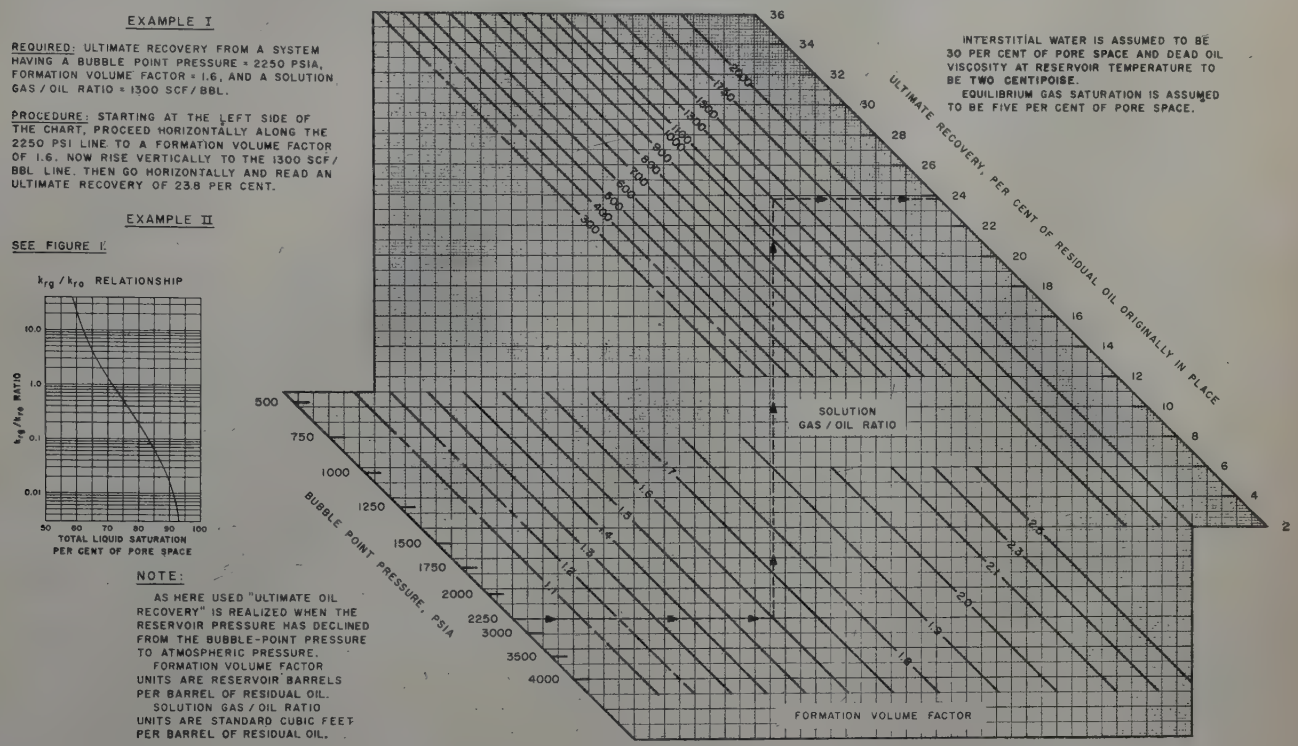
EXAMPLE I
REQUIRED: ULTIMATE RECOVERY FROM A SYSTEM HAVING A BUBBLE POINT PRESSURE = 2250 PSIA, FORMATION VOLUME FACTOR = 1.6, AND A SOLUTION GAS / OIL RATIO = 1300 SCF / BBL.
PROCEDURE: STARTING AT THE LEFT SIDE OF THE CHART, PROCEED HORIZONTALLY ALONG THE 2250 PSI LINE TO A FORMATION VOLUME FACTOR OF 1.6. NOW RISE VERTICALLY TO THE 1300 SCF / BBL LINE. THEN GO HORIZONTALLY AND READ AN ULTIMATE RECOVERY OF 23.8 PER CENT.
EXAMPLE II
SEE FIGURE 1.
k_{rg}/k_{ro} RELATIONSHIP
k_{rg}/k_{ro} RATIO
TOTAL LIQUID SATURATION PER CENT OF PORE SPACE
NOTE:
AS HERE USED "ULTIMATE OIL RECOVERY" IS REALIZED WHEN THE RESERVOIR PRESSURE HAS DECLINED FROM THE BUBBLE-POINT PRESSURE TO ATMOSPHERIC PRESSURE.
FORMATION VOLUME FACTOR UNITS ARE RESERVOIR BARRELS PER BARREL OF RESIDUAL OIL.
SOLUTION GAS / OIL RATIO UNITS ARE STANDARD CUBIC FEET PER BARREL OF RESIDUAL OIL.
INTERSTITIAL WATER IS ASSUMED TO BE 30 PER CENT OF PORE SPACE AND DEAD OIL VISCOSITY AT RESERVOIR TEMPERATURE TO BE TWO CENTIPOISE.
EQUILIBRIUM GAS SATURATION IS ASSUMED TO BE FIVE PER CENT OF PORE SPACE.
ULTIMATE RECOVERY, PER CENT OF RESIDUAL OIL ORIGINALLY IN PLACE
SOLUTION GAS / OIL RATIO
BUBBLE POINT PRESSURE, PSIA
FORMATION VOLUME FACTOR

FIG. 5—CHART FOR ESTIMATING ULTIMATE RECOVERY FROM SOLUTION GAS-DRIVE RESERVOIRS.

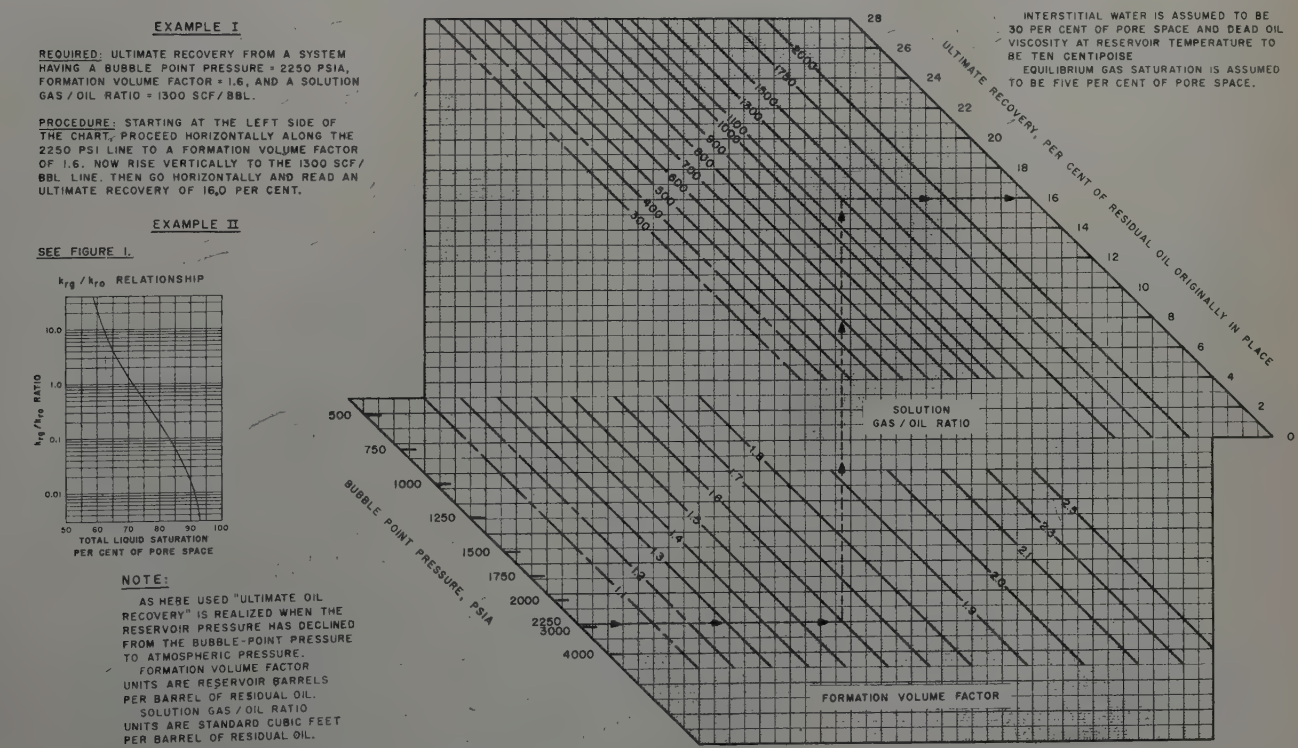
EXAMPLE I
REQUIRED: ULTIMATE RECOVERY FROM A SYSTEM HAVING A BUBBLE POINT PRESSURE = 2250 PSIA, FORMATION VOLUME FACTOR = 1.6, AND A SOLUTION GAS / OIL RATIO = 1300 SCF / BBL.
PROCEDURE: STARTING AT THE LEFT SIDE OF THE CHART, PROCEED HORIZONTALLY ALONG THE 2250 PSI LINE TO A FORMATION VOLUME FACTOR OF 1.6. NOW RISE VERTICALLY TO THE 1300 SCF / BBL LINE. THEN GO HORIZONTALLY AND READ AN ULTIMATE RECOVERY OF 16.0 PER CENT.
EXAMPLE II
SEE FIGURE 1.
k_{rg}/k_{ro} RELATIONSHIP
k_{rg}/k_{ro} RATIO
TOTAL LIQUID SATURATION PER CENT OF PORE SPACE
NOTE:
AS HERE USED "ULTIMATE OIL RECOVERY" IS REALIZED WHEN THE RESERVOIR PRESSURE HAS DECLINED FROM THE BUBBLE-POINT PRESSURE TO ATMOSPHERIC PRESSURE.
FORMATION VOLUME FACTOR UNITS ARE RESERVOIR BARRELS PER BARREL OF RESIDUAL OIL.
SOLUTION GAS / OIL RATIO UNITS ARE STANDARD CUBIC FEET PER BARREL OF RESIDUAL OIL.
INTERSTITIAL WATER IS ASSUMED TO BE 30 PER CENT OF PORE SPACE AND DEAD OIL VISCOSITY AT RESERVOIR TEMPERATURE TO BE TEN CENTIPOISE
EQUILIBRIUM GAS SATURATION IS ASSUMED TO BE FIVE PER CENT OF PORE SPACE.
ULTIMATE RECOVERY, PER CENT OF RESIDUAL OIL ORIGINALLY IN PLACE
SOLUTION GAS / OIL RATIO
BUBBLE POINT PRESSURE, PSIA
FORMATION VOLUME FACTOR

FIG. 6—CHART FOR ESTIMATING ULTIMATE RECOVERY FROM SOLUTION GAS-DRIVE RESERVOIRS.

oil saturation, fraction of pore space; and C is a constant = 0.25 in these calculations.

The k_{rg}/k_{ro} ratio vs saturation curves calculated with the equation are shown in Fig. 15. Since every value of interstitial water saturation yields a different k_{rg}/k_{ro} ratio curve, Fig. 15 shows the k_{rg}/k_{ro} ratio vs total liquid saturation with interstitial water as a parameter. These curves are the result of a data correlation. As such, they exhibit trends observed in data, but, obviously, they do not duplicate nor are they characteristic of all k_{rg}/k_{ro} ratio curves.

DISCUSSION

The nine charts for estimating ultimate oil recovery from solution gas-drive reservoirs are presented in Figs. 1 through 9. Each chart incorporates a sample calculation to demonstrate the method of operation. For these charts, the interstitial water saturation determines the relative permeability ratio-total liquid saturation relationship. Values of bubble-point pressure, oil formation volume factor, and solution gas-oil ratio shown

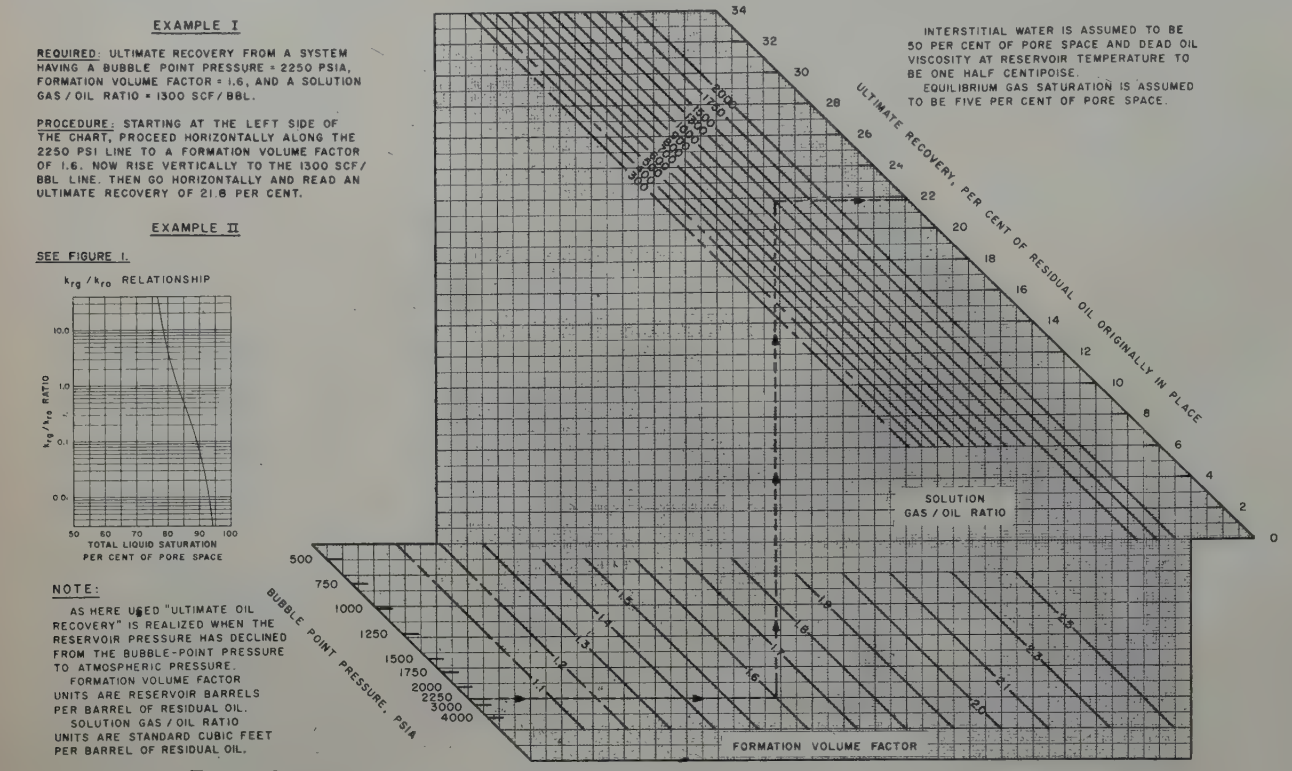
EXAMPLE I
REQUIRED: ULTIMATE RECOVERY FROM A SYSTEM HAVING A BUBBLE POINT PRESSURE = 2250 PSIA, FORMATION VOLUME FACTOR = 1.6, AND A SOLUTION GAS / OIL RATIO = 1300 SCF / BBL.
PROCEDURE: STARTING AT THE LEFT SIDE OF THE CHART, PROCEED HORIZONTALLY ALONG THE 2250 PSI LINE TO A FORMATION VOLUME FACTOR OF 1.6. NOW RISE VERTICALLY TO THE 1300 SCF / BBL LINE. THEN GO HORIZONTALLY AND READ AN ULTIMATE RECOVERY OF 21.8 PER CENT.
EXAMPLE II
SEE FIGURE 1.
k_{rg}/k_{ro} RELATIONSHIP
k_{rg}/k_{ro} RATIO
TOTAL LIQUID SATURATION PER CENT OF PORE SPACE
NOTE:
AS HERE USED "ULTIMATE OIL RECOVERY" IS REALIZED WHEN THE RESERVOIR PRESSURE HAS DECLINED FROM THE BUBBLE-POINT PRESSURE TO ATMOSPHERIC PRESSURE.
FORMATION VOLUME FACTOR UNITS ARE RESERVOIR BARRELS PER BARREL OF RESIDUAL OIL.
SOLUTION GAS / OIL RATIO UNITS ARE STANDARD CUBIC FEET PER BARREL OF RESIDUAL OIL.
INTERSTITIAL WATER IS ASSUMED TO BE 50 PER CENT OF PORE SPACE AND DEAD OIL VISCOSITY AT RESERVOIR TEMPERATURE TO BE ONE HALF CENTIPOISE.
EQUILIBRIUM GAS SATURATION IS ASSUMED TO BE FIVE PER CENT OF PORE SPACE.
ULTIMATE RECOVERY, PER CENT OF RESIDUAL OIL ORIGINALLY IN PLACE
SOLUTION GAS / OIL RATIO
BUBBLE POINT PRESSURE, PSIA
FORMATION VOLUME FACTOR

FIG. 7—CHART FOR ESTIMATING ULTIMATE RECOVERY FROM SOLUTION GAS-DRIVE RESERVOIRS.

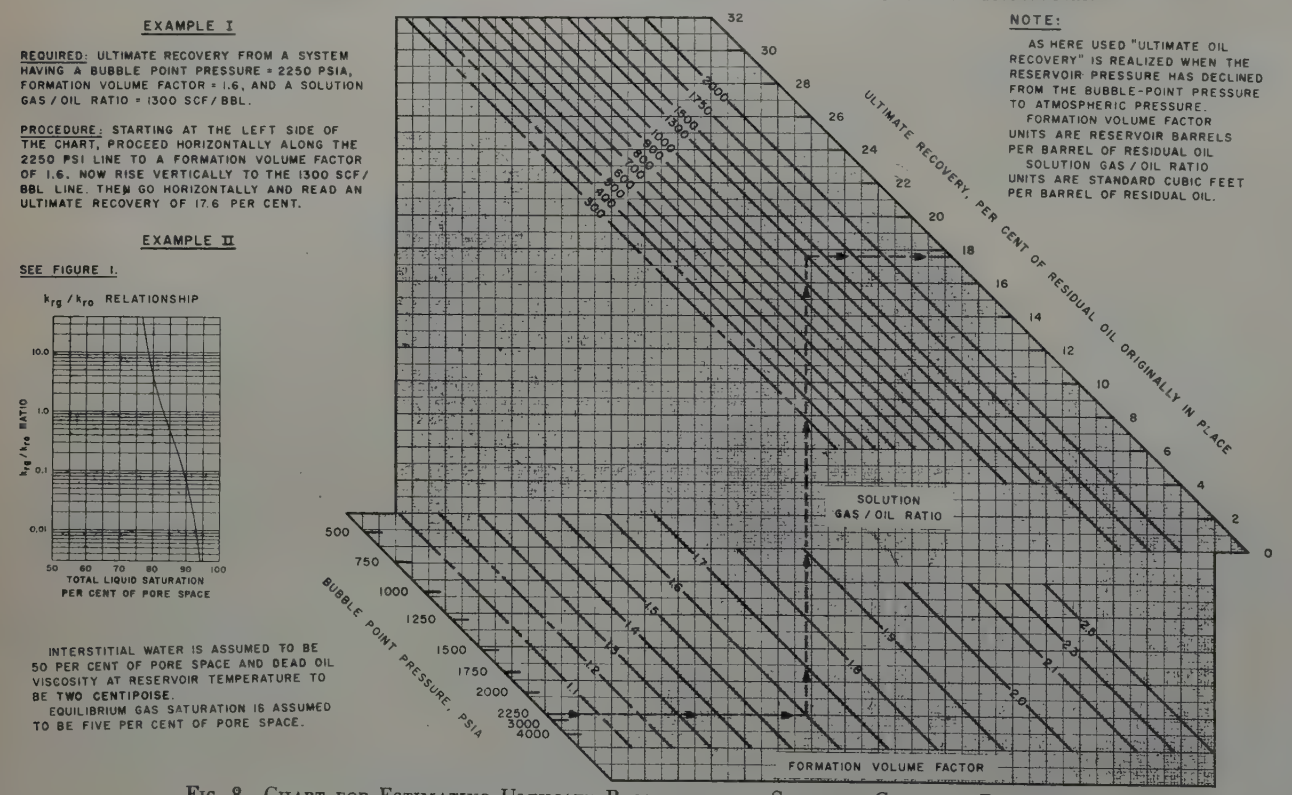
EXAMPLE I
REQUIRED: ULTIMATE RECOVERY FROM A SYSTEM HAVING A BUBBLE POINT PRESSURE = 2250 PSIA, FORMATION VOLUME FACTOR = 1.6, AND A SOLUTION GAS / OIL RATIO = 1300 SCF / BBL.
PROCEDURE: STARTING AT THE LEFT SIDE OF THE CHART, PROCEED HORIZONTALLY ALONG THE 2250 PSI LINE TO A FORMATION VOLUME FACTOR OF 1.6. NOW RISE VERTICALLY TO THE 1300 SCF / BBL LINE. THEN GO HORIZONTALLY AND READ AN ULTIMATE RECOVERY OF 17.6 PER CENT.
EXAMPLE II
SEE FIGURE 1.
k_{rg}/k_{ro} RELATIONSHIP
k_{rg}/k_{ro} RATIO
TOTAL LIQUID SATURATION PER CENT OF PORE SPACE
INTERSTITIAL WATER IS ASSUMED TO BE 50 PER CENT OF PORE SPACE AND DEAD OIL VISCOSITY AT RESERVOIR TEMPERATURE TO BE TWO CENTIPOISE.
EQUILIBRIUM GAS SATURATION IS ASSUMED TO BE FIVE PER CENT OF PORE SPACE.
NOTE:
AS HERE USED "ULTIMATE OIL RECOVERY" IS REALIZED WHEN THE RESERVOIR PRESSURE HAS DECLINED FROM THE BUBBLE-POINT PRESSURE TO ATMOSPHERIC PRESSURE.
FORMATION VOLUME FACTOR UNITS ARE RESERVOIR BARRELS PER BARREL OF RESIDUAL OIL
SOLUTION GAS / OIL RATIO UNITS ARE STANDARD CUBIC FEET PER BARREL OF RESIDUAL OIL.
ULTIMATE RECOVERY, PER CENT OF RESIDUAL OIL ORIGINALLY IN PLACE
SOLUTION GAS / OIL RATIO
BUBBLE POINT PRESSURE, PSIA
FORMATION VOLUME FACTOR

FIG. 8—CHART FOR ESTIMATING ULTIMATE RECOVERY FROM SOLUTION GAS-DRIVE RESERVOIRS.

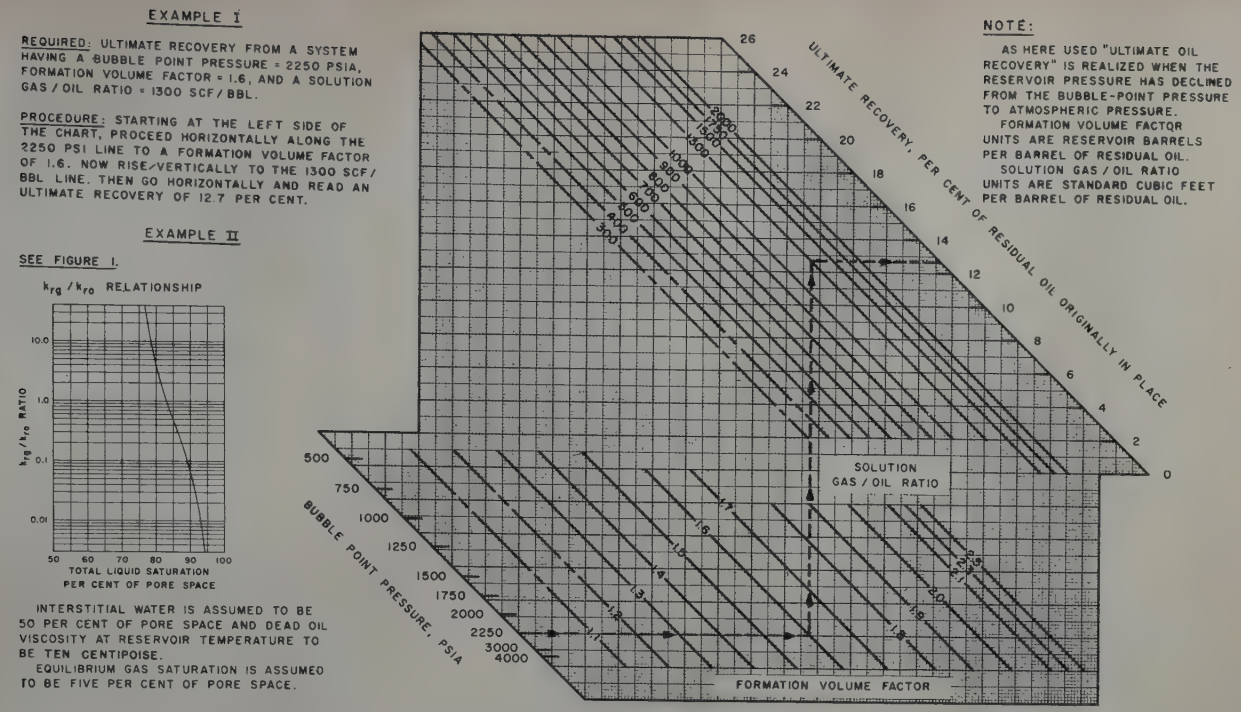
EXAMPLE I
REQUIRED: ULTIMATE RECOVERY FROM A SYSTEM HAVING A BUBBLE POINT PRESSURE = 2250 PSIA, FORMATION VOLUME FACTOR = 1.6, AND A SOLUTION GAS / OIL RATIO = 1300 SCF / BBL.
PROCEDURE: STARTING AT THE LEFT SIDE OF THE CHART, PROCEED HORIZONTALLY ALONG THE 2250 PSI LINE TO A FORMATION VOLUME FACTOR OF 1.6. NOW RISE VERTICALLY TO THE 1300 SCF / BBL LINE. THEN GO HORIZONTALLY AND READ AN ULTIMATE RECOVERY OF 12.7 PER CENT.
EXAMPLE II
SEE FIGURE 1.
k_{rg}/k_{ro} RELATIONSHIP
k_{rg}/k_{ro} RATIO
TOTAL LIQUID SATURATION PER CENT OF PORE SPACE
INTERSTITIAL WATER IS ASSUMED TO BE 50 PER CENT OF PORE SPACE AND DEAD OIL VISCOSITY AT RESERVOIR TEMPERATURE TO BE TEN CENTIPOISE.
EQUILIBRIUM GAS SATURATION IS ASSUMED TO BE FIVE PER CENT OF PORE SPACE.
NOTE:
AS HERE USED "ULTIMATE OIL RECOVERY" IS REALIZED WHEN THE RESERVOIR PRESSURE HAS DECLINED FROM THE BUBBLE-POINT PRESSURE TO ATMOSPHERIC PRESSURE.
FORMATION VOLUME FACTOR UNITS ARE RESERVOIR BARRELS PER BARREL OF RESIDUAL OIL.
SOLUTION GAS / OIL RATIO UNITS ARE STANDARD CUBIC FEET PER BARREL OF RESIDUAL OIL.
ULTIMATE RECOVERY, PER CENT OF RESIDUAL OIL ORIGINALLY IN PLACE
SOLUTION GAS / OIL RATIO
BUBBLE POINT PRESSURE, PSIA
FORMATION VOLUME FACTOR

FIG. 9—CHART FOR ESTIMATING ULTIMATE RECOVERY FROM SOLUTION GAS-DRIVE RESERVOIRS.

on the charts, but not used in the calculations, were obtained by interpolation. Formation volume factors of 1.1 and 1.2 bbl/bbl and solution gas-oil ratios of 300 and 400 scf/bbl were obtained by extrapolation; these values are shown as dashed lines on the charts. Locations of the 4,000-psi point on the pressure axes were obtained by extrapolation.

Values of formation volume factor and solution gas-oil ratio necessary for use of the charts should be obtained from a differential analysis. If only flash (equilibrium) data are available, differential data must be estimated from the flash data. At present, there are no correlations available for this purpose, but an empirical relationship between flash and differential formation volume factors is presented in Fig. 16. A similar relationship between flash and differential solution gas-oil ratio is presented in Fig. 17.

Maximum solution gas-oil ratio shown on the charts is 2,000 scf/bbl. This limit was imposed because the straight material balance approach to primary depletion calculations is not adequate for high gas-oil ratio fluid systems. The free reservoir gas contains components which separate as liquids in the stock tank, and a different approach to estimating recovery is desirable.

The meaning of ultimate oil recovery has been restricted here to that oil recovered as the reservoir pressure declined from the bubble-point pressure to atmospheric pressure. If the reservoir fluid is undersaturated at the initial reservoir pressure, the total recovery would be the sum of (1) the recovery due to fluid expansion as the reservoir pressure decreased from the initial value to the bubble-point pressure, and (2) the ultimate oil recovery estimated by means of one of the charts.

Charts may be used to estimate only the ultimate oil recovery—the final answer. They cannot be used to estimate recovery as a function of pressure decline, for the assumption of an initial total liquid saturation equal to 100 per cent of pore space prohibits it.

Ultimate oil recovery figures are expressed in terms of residual oil. The reason for this is that differential liberation was presumed to occur within the reservoir, and the end product of a differential liberation is residual oil. However, ultimate oil recovery may be obtained as a percentage of the stock-tank oil initially in place by performing the necessary calculations. All data necessary to compute the reservoir oil saturation at atmospheric pressure are available in this paper. When both differential and flash liberation data are available or can be estimated, the tank oil recovered can be determined. A calculation of this type is shown in Fig. 1.

Ultimate oil recovery on the charts is expressed as a percentage of the initial oil in place, which depends upon the oil formation volume factor and the reservoir oil saturation. Since the fractional reservoir oil saturation is the quantity one minus the water saturation minus the gas

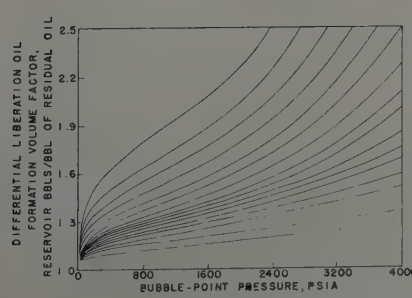

FIG. 10—TYPICAL OIL FORMATION VOLUME FACTOR CURVES VS BUBBLE-POINT PRESSURE.

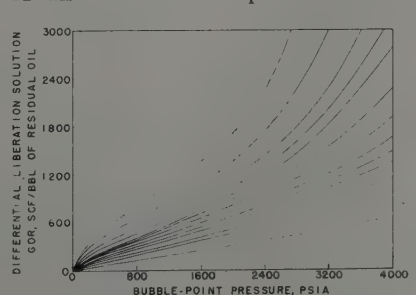

FIG. 11—TYPICAL SOLUTION GAS-OIL RATIO CURVES VS BUBBLE-POINT PRESSURE.

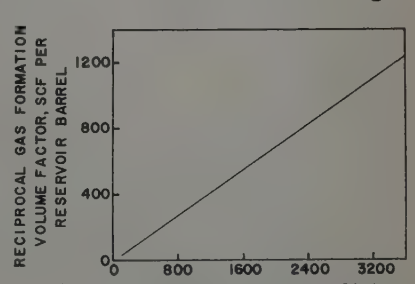

FIG. 12—RECIPROCAL GAS FORMATION VOLUME FACTOR VS RESERVOIR PRESSURE.

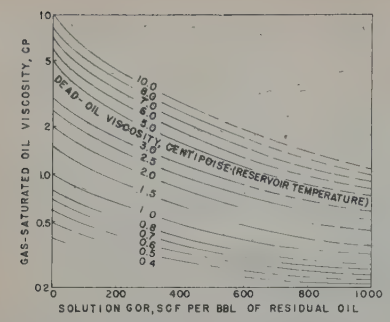
GAS-SATURATED OIL VISCOSITY, CP
DEAD-OIL VISCOSITY, CENTIPOISE (RESERVOIR TEMPERATURE)
SOLUTION GOR, SCF PER BBL OF RESIDUAL OIL

FIG. 13—GAS-SATURATED OIL VISCOSITY VS SOLUTION GAS-OIL RATIO.

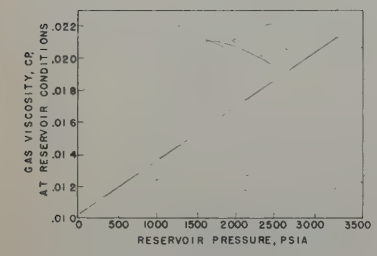

FIG. 14—GAS VISCOSITY VS RESERVOIR PRESSURE.

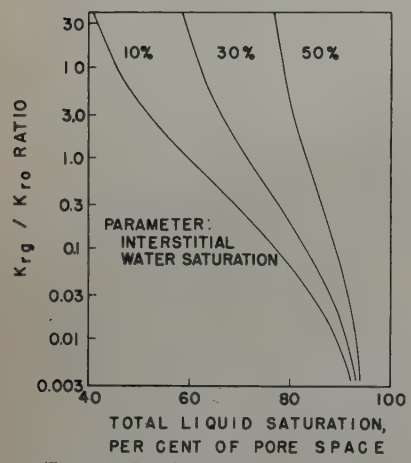

FIG. 15—k_{rg}/k_{ro} VS TOTAL LIQUID SATURATION.

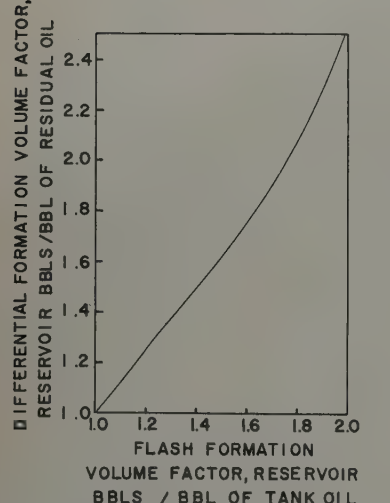
DIFFERENTIAL FORMATION VOLUME FACTOR, RESERVOIR BBLS/BBL OF RESIDUAL OIL
FLASH FORMATION VOLUME FACTOR, RESERVOIR BBLS / BBL OF TANK OIL

FIG. 16—EMPIRICAL RELATIONSHIP BETWEEN FLASH AND DIFFERENTIAL LIBERATION FORMATION VOLUME FACTORS.

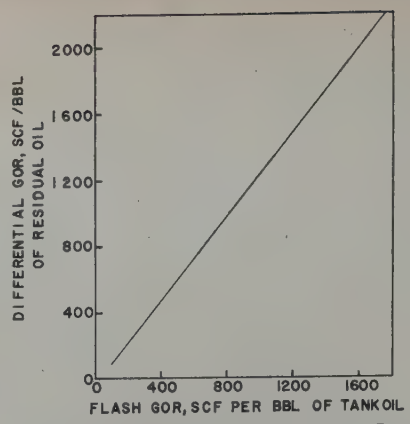

FIG. 17—EMPIRICAL RELATIONSHIP BETWEEN FLASH AND DIFFERENTIAL LIBERATION SOLUTION GAS-OIL RATIOS.

saturation, it is apparent that water saturation is directly involved in calculating the ultimate oil recovery figures on the charts.

Maximum deviation from the calculated value of ultimate oil recovery is one-half recovery per cent for all charts. However, recovery figures obtained by means of the charts should be regarded as estimates since properties of reservoir systems, as well as hydrocarbon systems, depart in varying degree from the assumed properties listed earlier. Additional data for constructing the charts would have been desirable in order to more thoroughly check them, but results obtained compare very well with results of similar depletion calculations presented by Muskat.[1] However, in describing the systems he investigated, Muskat did not provide sufficient information in all cases so that recovery from identical systems can be estimated from the charts. Even so, those systems for which a comparison could be checked within two recovery per cent. The reservoir systems used for the charts are listed in Table 1.

Interstitial water saturation and dead-oil viscosity of an actual reservoir system may not correspond exactly to any one of the charts. In this case, interpolation will be necessary. Consider the following system.

Interstitial water saturation	20 per cent pore space
Dead-oil viscosity	1 cp
Oil formation volume factor	1.6 bbl/bbl
Solution gas-oil ratio	1,300 scf/bbl
Bubble-point pressure	2,250 psia

The above values of B_o, R_s and bubble-point pressure are found on all charts, but there is no chart for 20 per cent interstitial water saturation or dead-oil viscosity of 1 cp. The method to be described is suggested as a suitable interpolation procedure.

Use each of the nine charts to determine ultimate oil recovery for the given values of B_o, R_s and bubble-point pressure. Values so obtained are given in the following table.

Table 1—Reservoir Systems Used to Develop Ultimate Oil Recovery Charts

Bubble-point Pressure, (psia)	Differential solution gas-oil ratio, scf/bbl of residual oil	Differential oil formation volume factor, res. bbl/bbl of residual oil	Oil formation volume factor at atmospheric pressure, res. bbl/bbl of residual oil
750	100	1.10	1.06
750	500	1.30	1.08
1,500	500	1.30	1.07
1,500	1,000	1.30	1.07
1,500	1,000	1.50	1.09
2,250	1,000	1.50	1.08
2,250	1,000	1.80	1.11
2,250	1,500	1.50	1.08
2,250	1,500	1.80	1.11
2,250	2,000	1.80	1.11
3,000	1,500	1.80	1.09
3,000	1,500	2.10	1.11
3,000	2,000	1.80	1.09
3,000	2,000	2.10	1.11
3,000	2,000	2.50	1.13

Dead-oil viscosity, (cp)	Ultimate oil recovery for interstitial water saturation		
	10 per cent	30 per cent	50 per cent
10	17.8	16.0	12.7
2	26.7	23.8	17.6
½	35.8	30.8	21.8

Now plot ultimate oil recovery vs interstitial water saturation with dead-oil viscosity as the parameter. From the curves read values of ultimate oil recovery at 20 per cent interstitial water saturation for dead-oil viscosities of 10, 2, and ½ cp. These values are as follows.

Dead-oil viscosity, (cp)	Ultimate oil recovery (per cent)
10	17.0
2	25.5
½	33.6

Next, plot dead-oil viscosity vs ultimate oil recovery and read an ultimate oil recovery of 29.4 per cent for a dead-oil viscosity of 1 cp.

ACKNOWLEDGMENT

The authors wish to thank P. R. McGee, O. D. Ferris, A. S. Lee, and J. T. Nipper for programming calculations for the computer.

REFERENCES

1. Muskat, Morris: *Physical Principals of Oil Production*, McGraw-Hill Book Co., Inc., N. Y. (1949).
2. Scarborough, James B.: *Numerical Mathematical Analysis*, 2nd Ed., The Johns Hopkins Press, Baltimore (1950).
3. Carr, N. L., Kobayashi, R., and Burrows, D. B.: *Trans.* AIME (1954) **204**, 264.
4. Natural Gasoline Supply Men's Association Data Book (1951).
5. Arps, J. J., and Roberts, T. G.: *Trans.* AIME (1955) **204**, 120. ★★★

The Use of High-Speed Computers for Predicting Flood-Out Patterns

D. G. McCARTY
MEMBER AIME
E. C. BARFIELD
JUNIOR MEMBER AIME

HUMBLE OIL & REFINING CO.
HOUSTON, TEX.

ABSTRACT

Two-dimensional analyses offer considerable promise in providing the basic information required to effect more precise control of petroleum reservoir performance. This paper describes a method for conducting some engineering analyses of this type using a high-speed digital computer. The general approach is to (1) develop a representative numerical model of the reservoir and (2) employ a suitable numerical technique to solve the basic equation of flow and to develop the required engineering information for the particular case represented by the model.

This technique has been used to calculate pattern performance in connection with several field projects involving water injection into oil reservoirs. This type of analysis involves sequentially (1) calculating the pressure distribution in the reservoir and (2) tracking the progress of the interface between the displaced and displacing fluids in a step-wise manner to provide a depletion history of the operation.

The particular analysis presented in this discussion is subject to the restriction that the mobility of the displaced and displacing fluids be equal and assumes that the fluids are incompressible and that gravity and capillary pressure do not affect the shape of the flood pattern. Complete two-dimensional flexibility is maintained with regard to definition of reservoir rock and fluid characteristics, placement of physical restraints and boundary conditions, investigation of flow characteristics in the reservoir, and movement of the displaced and displacing fluid interface.

The results of these studies indicate that the high-speed digital computer is well suited for conducting reservoir performance studies in two-space dimensions and that dependable numerical techniques are available for making such analyses.

INTRODUCTION

One of the problems facing petroleum engineers is that of providing more precise engineering control over reservoir operations at all stages during the depletion cycle. The most direct approach to this problem is to simulate the reservoir with some type of physical or mathematical model and use the information developed from the behavior of the prototype to predict the performance of the actual reservoir. This principle is, of course, not new, and a variety of simulation techniques have been developed to provide information on the behavior of oil and gas reservoirs.

One straightforward refinement of present reservoir analysis techniques is the progress from one-dimensional reservoir models to those where the reservoir can be represented in two- and three-space dimensions. Multi-dimensional reservoir analyses are desired in order to show not only *what* is happening in the reservoir but in addition to show *where* in the reservoir the various phenomena of interest are occurring.

Thus far, two-dimensional analyses have been confined predominantly to potentiometric and electrolytic model studies.[1,2] However, when large numbers of wells are involved and where large-scale models are required, such problems become very tedious and instrumentation problems become acute.[3] It is possible through use of numerical methods and general purpose digital computers to avoid many of the instrumentation difficulties and to relax some of the restrictions of previous techniques. The purpose of this paper is to discuss some recent experiences with the use of high-speed digital computers for predicting pattern performance in fluid injection operations and to describe the numerical procedures which have been used for making such analyses.

THE NUMERICAL MODEL

The problem of representing the reservoir with an appropriate numerical model is composed of at least two important considerations. The first requires that an adequate description of the reservoir mechanism be formulated in the form of the basic differential equation describing the process. The second consideration is definition of the physical characteristics of the reservoir. The latter requires that representative basic data be obtained, examined, and interpreted to provide sufficient detailed definition of the pertinent physical properties throughout the system.

The Differential Equation

One of the basic assumptions made for the purpose of performing the two-dimensional studies being dis-

Original manuscript received in Society of Petroleum Engineers office Aug. 15, 1957. Revised manuscript received Feb. 21, 1958. Paper presented at 32nd Annual Fall Meeting of Society of Petroleum Engineers in Dallas, Tex., Oct. 6-9, 1957.

[1]References given at end of paper.

cussed here was that a distinct oil-water interface is formed and a single fluid, either water or oil, respectively, is flowing in the predominantly water-saturated or oil-saturated regions of the reservoir. Then, for single-phase flow in regions on either side of the interface, the basic differential equation which describes the pressure distribution in the reservoir is

$$\frac{\partial^2 p}{\partial x^2} + \frac{\partial^2 p}{\partial y^2} = \frac{c\phi\mu}{k}\frac{\partial p}{\partial t}, \quad \ldots\ldots\ldots \quad (1)$$

if the effects of gravity are negligible.

Eq. 1 extended to incorporate varying fluid mobility and formation thickness can be written

$$\frac{\partial}{\partial x}\left(\frac{kh}{\mu}\frac{\partial p}{\partial x}\right) + \frac{\partial}{\partial y}\left(\frac{kh}{\mu}\frac{\partial p}{\partial y}\right) = c\phi h\frac{\partial p}{\partial t}. \quad \ldots \quad (2)$$

In the studies discussed here, both the water and oil were assumed to be incompressible and their mobilities equal. Under these conditions the analysis becomes simpler, and computational requirements are greatly reduced. Eq. 2 then reduces to

$$\frac{\partial}{\partial x}\left(kh\frac{\partial p}{\partial x}\right) + \frac{\partial}{\partial y}\left(kh\frac{\partial p}{\partial y}\right) = 0 \quad \ldots \quad (3)$$

which is Laplace's equation modified to permit use of variable coefficients.

Numerical methods for solving partial differential equations such as Eq. 3 usually involve replacing the derivatives by finite differences and solving the resulting difference equations to obtain the pressure distribution. A convenient procedure which may be used in formulating the difference equations is to start with a grid network which can be superimposed over a scaled map of the reservoir. This grid or integration net serves as a reference framework for formulating the appropriate difference equations. An example of this procedure is shown in Fig. 1. For a typical set of grid intersections adjacent to a typical point, i, j, a difference equation analog of Eq. 3 for a square mesh ($\Delta x = \Delta y$) is

$$(kh)_{i+\frac{1}{2},j}\,(p_{i+1,j} - p_{i,j}) - (kh)_{i-\frac{1}{2},j}\,(p_{i,j} - p_{i-1,j}) + (kh)_{i,j+\frac{1}{2}}\,(p_{i,j+1} - p_{i,j}) - (kh)_{i,j-\frac{1}{2}}\,(p_{i,j} - p_{i,j-1}) - q_{i,j} = 0, \quad \ldots\ldots\ldots \quad (4)$$

where $q_{i,j}$ has been added to permit injection or withdrawal of fluid from a grid intersection if a producing or injection well is located at this point. The coefficients, $kh_{i+\frac{1}{2}}$ and $kh_{j+\frac{1}{2}}$, apply to the intervals between the i and $i+1$ intersections and between the j and $j+1$ intersections, respectively.

Defining the Reservoir

The superimposed grid network referred to in the previous paragraph can also be employed as a reference framework to define the physical characteristics of the reservoir. A technique which has been found to be convenient for preparing basic data is to construct detailed isopachous and isopermeability maps from well logs, laboratory core analyses, and well testing information. Then by superimposing the integration net on these maps, appropriate values of permeability and thickness can be assigned to each grid point. These basic data "matrices" then compromise the catalog of basic data used throughout the reservoir engineering analysis.

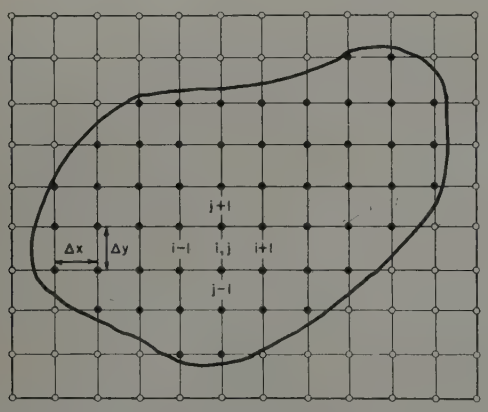

Fig. 1 — Typical Numerical Model Showing Field Boundary and Reference Notation.

Another requirement for defining the physical system being studied is imposition of the appropriate boundary and initial conditions. One frequently encountered problem is the reservoir whose boundaries are closed to the flow of fluids. For problems of this type, the physical boundary can be simulated by assigning zero permeability to all intervals outside the limits of the reservoir. In Fig. 1, this would correspond to assigning zero permeability to all intervals involving any of the open-circled intersections.

If the region of interest is completely symmetrical with respect to its surroundings, a reflection boundary may be specified to insure no flow across the regional boundaries. Cases arise where other than closed-boundary situations have to be handled, such as the influx of water across a particular portion of the field boundary. In cases such as these, appropriate constants or functions have to be introduced into the calculation to produce the proper magnitudes of flow at these boundaries.

One other restriction or boundary condition which must be placed on the model is the production or injection rate assigned to those mesh points in the model which represent either production or injection wells. The q term in Eq. 4 permits the use of any grid intersection as a production or injection point.

COMPUTATION PROCEDURE

The pattern performance computation can be subdivided into three major parts: (1) pressure computation, (2) front movement and (3) adjustment of the production-injection schedule. For a mobility ratio of 1, the pressure distribution is a unique function of the production-injection schedule, and the pressure computation is repeated only where the adjustment called for in Part 3 is made. An adjustment is made in the production-injection schedule each time a production well is flooded and removed from the pattern or each time an injection well is added. On the other hand, accuracy of flood front movement requires that points on the flood front be advanced in rather small distance increments. The result of this is that the front movement computations are generally made more frequently than are Parts 1 and 3. This sequence of events is illustrated in Fig. 2 for a hypothetical case. The entire pattern performance calculation can be handled automatically within the computer and a flow chart of the procedure is included as Fig. 3.

Pressure Computation

The numerical technique used for most of the pressure distribution calculations was the "alternating direction implicit" procedure (ADIP) proposed by Peaceman and Rachford.[4] This method has received considerable study, and its characteristics are fairly well known. Also, the works of Peaceman, *et al*, indicated this method to be one of the most efficient from the standpoint

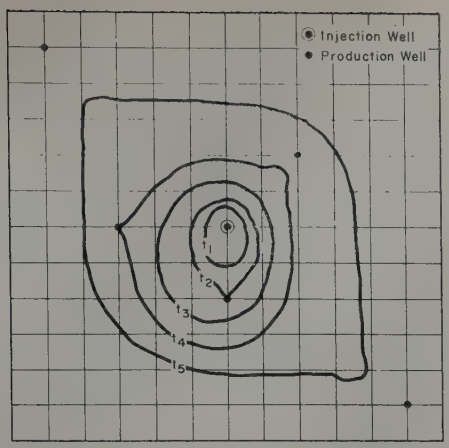

FIG. 2—HYPOTHETICAL FLOOD PATTERN SHOWING ADVANCING FRONT AND PROGRESSIVE FLOODING OF WELLS.

of computational requirements.[4,5] When used for solving the Laplace difference equation, the ADIP is an iterative technique in which successively more refined values of pressure continuously replace older values until convergence to the solution to any desired accuracy is achieved. It has been shown that the procedure requires approximately $(2 \ln N)/N^*$ as many numerical operations for solution to the Laplace equation as does the best previously known iterative procedure.

Basically the ADIP is a two-step process involving two difference equations rather than the usual one. In the case where it is used to iterate to the solution of the Laplace equation, each step of iteration is considered as a time step of a corresponding unsteady-state problem. Thus, if we consider the equation,

$$\frac{\partial^2 p}{\partial x^2} + \frac{\partial^2 p}{\partial y^2} = \frac{\partial p}{\partial t}, \quad \ldots \quad (5)$$

the ADIP requires for the first step that one of the second derivatives be replaced with a second difference expressed in terms of the unknown values of p while the other second derivative term is to be evaluated in terms of p's at the known time level. The second step is performed in a similar manner reversing the positions of the second derivative terms with respect to known and unknown values of p. The resulting difference equations would be

$$\left[\frac{p_{i-1,j} - 2p_{i,j} + p_{i+1,j}}{\Delta x^2}\right]^{(n+1)} + \left[\frac{p_{i,j-1} - 2p_{i,j} + p_{i,j+1}}{\Delta y^2}\right]^{n} = \frac{p_{i,j}^{(n+1)} - p_{i,j}^{n}}{\Delta t}, \quad \ldots \quad (6)$$

and

$$\left[\frac{p_{i-1,j} - 2p_{i,j} + p_{i+1,j}}{\Delta x^2}\right]^{(n+1)} + \left[\frac{p_{i,j-1} - 2p_{i,j} + p_{i,j+1}}{\Delta y^2}\right]^{(n+2)} = \frac{p_{i,j}^{(n+2)} - p_{i,j}^{(n+1)}}{\Delta t}, \quad \ldots \quad (7)$$

where the superscripts n, $n+1$, and $n+2$ refer to time levels. If $\Delta x = \Delta y$, the equations can be written in more convenient form,

$$[p_{i-1,j} - (2+\gamma)p_{i,j} + p_{i+1,j}]^{(n+1)} + [p_{i,j-1} - (2-\gamma)p_{i,j} + p_{i,j+1}]^{n} = 0, \quad \ldots \quad (8)$$

and

$$[p_{i-1,j} - (2-\gamma)p_{i,j} + p_{i+1,j}]^{(n+1)} + [p_{i,j-1} - (2-\gamma)p_{i,j} + p_{i,j+1}]^{(n+2)} = 0, \quad \ldots \quad (9)$$

*Where N^2 is the number of points in the model.

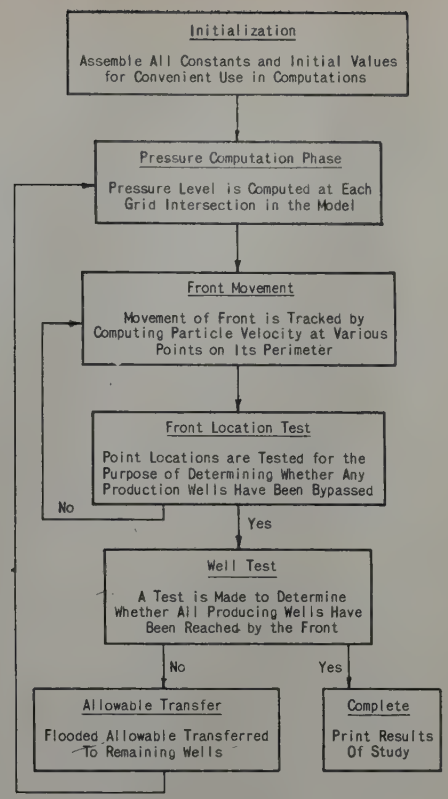
Initialization
Assemble All Constants and Initial Values for Convenient Use in Computations
Pressure Computation Phase
Pressure Level is Computed at Each Grid Intersection in the Model
Front Movement
Movement of Front is Tracked by Computing Particle Velocity at Various Points on Its Perimeter
Front Location Test
Point Locations are Tested for the Purpose of Determining Whether Any Production Wells Have Been Bypassed
No
Yes
Well Test
A Test is Made to Determine Whether All Producing Wells Have Been Reached by the Front
No
Yes
Allowable Transfer
Flooded Allowable Transferred To Remaining Wells
Complete
Print Results Of Study

FIG. 3—SIMPLIFIED FLOW DIAGRAM OF CALCULATION PROCEDURE.

where $\gamma = \dfrac{\Delta x^2}{\Delta t} = \dfrac{\Delta y^2}{\Delta t}$.

Now, if the same procedure is applied to formulate the two-part iteration step for Eq. 3, the following equations result.

$$\left[(kh)_{i-\frac{1}{2},j}\, p_{i-1,j} - [(kh)_{i-\frac{1}{2},j} + (kh)_{i+\frac{1}{2},j} + \gamma]p_{i,j} + (kh)_{i+\frac{1}{2},j}\, p_{i+1,j}\right]^{(n+1)} + \left[(kh)_{i,j-\frac{1}{2}}\, p_{i,j-1} - [(kh)_{i,j-\frac{1}{2}} + (kh)_{i,j+\frac{1}{2}} - \gamma]\, p_{i,j} + (kh)_{i,j+\frac{1}{2}}\, p_{i,j+1}\right]^{n} - q_{i,j} = 0, \quad \ldots \quad (10)$$

and

$$\left[(kh)_{i,j-\frac{1}{2}}\, p_{i,j-1} - [(kh)_{i,j-\frac{1}{2}} + (kh)_{i,j+\frac{1}{2}} + \gamma]\, p_{i,j} + (kh)_{i,j+\frac{1}{2}}\, p_{i,j+1}\right]^{(n+2)} + \left[(kh)_{i-\frac{1}{2},j}\, p_{i-1,j} - [(kh)_{i+\frac{1}{2},j} + (kh)_{i-\frac{1}{2},j} - \gamma]\, p_{i,j} + (kh)_{i+\frac{1}{2},j}\, p_{i+1,j}\right]^{(n+1)} - q_{i,j} = 0, \quad \ldots \quad (11)$$

where γ now functions as an iteration parameter and where $q_{i,j}$ has been added to permit injection or production at point i, j. Although a discussion of the role of the iteration parameter in numerical processes is beyond the scope of this paper, the use of optimum values of γ can have an important bearing on the rate of convergence of the process. Therefore, it is usually efficient to make an estimate of the best value or sequence of values to use in a particular problem and to adjust these as necessary if the rate of convergence of the calculation is abnormally slow.[4]

Eq. 10 is said to be implicit in the x-direction while Eq. 11 is implicit in the y-direction. The second-

bracketed term of each equation represents either the initial values or the values calculated during the previous iteration.

To solve for pressure distribution in a typical problem, the following procedure is given.

1. Eq. 10 is written row by row for each point in the model. This results in a set of simultaneous equations for each row which can be arranged into a matrix of tridiagonal form and solved fairly conveniently by an elimination technique (see Eq. 14).

2. Similarly and after completion of the pressure computation for all rows in the model, Eq. 11 is written column by column for each point in the model. The resulting sets of equations are solved for new pressure values throughout the model as in the previous step. Computed pressure values from Step 1 become the known values for Step 2 and vice versa.

These two steps complete one iteration step, and this sequence of operations is repeated as many times as necessary until convergence is attained.

For computing convenience, the numerical model is completely reproduced within the computer. The model then takes the form of five data matrices. (The term data matrix applies to the block of information formed by specifying the value of the reservoir data parameter at corresponding points in the integration net.) These five matrices are: (1) x-direction permeability corresponding to intervals between grid points in the x-direction; (2) y-direction permeability corresponding to y-direction mesh intervals; (3) reservoir thickness at grid intersections in the model; (4) a q-matrix which contains the production or injection rate corresponding to each point in the model (this value is, of course, zero for all points not representing injection or production wells); and (5) a p-matrix which always contains the current value of reservoir pressure at each point in the model.

Fig. 4 shows how these matrices are fitted to the integration net to form the desired model. Values of h for use in the coefficients kh of Eqs. 10 and 11 are obtained by interpolation.

With the data arranged as shown in Fig. 4 and with permeability values of zero assigned at all mid-points in the integration net outside the boundaries of the reservoir, it is possible to perform the entire pressure distribution computation with one pair of difference equations which applies equally to all interior and boundary points. To illustrate, Eq. 10 can be written,

$$(A_i p_{i-1,j} - B_i p_{i,j} + C_i p_{i+1,j})^{(n+1)} = D_i, \quad . \quad (12)$$

by making substitutions,

$$A_i = (kh)_{i-\frac{1}{2}}$$
$$B_i = -[(kh)_{i-\frac{1}{2}} + (kh)_{i+\frac{1}{2}} + \gamma]$$
$$C_i = (kh)_{i+\frac{1}{2}}$$
$$D_i = q_{i,j} - \Big[(kh)_{i,j-\frac{1}{2}}\, p_{i,j-1} - [(kh)_{i,j-\frac{1}{2}} + (kh)_{i,j+\frac{1}{2}} - \gamma] + (kh)_{i,j+\frac{1}{2}}\, p_{i,j-1}\Big]^n .$$

Eq. 12 is written for all points along a typical row or column (e.g., Row 2 of Fig. 4). The basic set of simultaneous equations for an $N+1$ point row will take the form,

$$\begin{aligned} A_o + B_o p_o + C_o p_1 &= D_o \\ A_1 p_o + B_1 p_1 + C_1 p_2 &= D_1 \\ A_2 p_1 + B_2 p_2 + C_2 p_3 &= D_2 \\ \cdots\cdots\cdots\cdots\cdots\cdots\cdots\cdots & \quad (13) \\ A_N p_{N-1} + B_N p_N + C_N &= D_N, \end{aligned}$$

where the A_o and C_N terms are always zero.

As zero permeability has been assigned to all mid-points of the integration net outside the reservoir, solution of the above set of equations produces non-zero values of p only for points within the reservoir.

The set of equations can be solved[4] using a non-iterative technique as follows.

$$p_N = g_N, \; p_i = g_i - \frac{C_i p_{i+1}}{w_i}, \; 0 \leqslant i \leqslant N\text{-}1, \quad (14)$$

where

$$w_o = B_o, \; w_i = B_i - \frac{A_i C_{i-1}}{w_{i-1}}, \qquad 1 \leqslant i \leqslant N$$

$$g_o = \frac{D_o}{w_o}, \; g_i = \frac{D_i - A_i g_{i-1}}{w_i}.$$

The values of g_i and w_i are computed in order of increasing i followed by the evaluation of p_i in order of decreasing i.

A check on the progress of the pressure calculation can be obtained by solving Eq. 15 for each point in the model after each double step.

$$(kh)_{i+\frac{1}{2},j}\,(p_{i+1,j} - p_{i,j}) - (kh)_{i-\frac{1}{2},j}(p_{i,j} - (p_{i-1,j}) + (kh)_{i,j+\frac{1}{2}}\,(p_{i,j+1} - p_{i,j}) - (kh)_{i,j-\frac{1}{2}}(p_{i,j} - p_{i,j-1}) - q_{i,j} = \delta \quad . \quad (15)$$

The value, δ, is squared and accumulated for all points in the mesh. As the correct solution to the problem requires that δ equal zero for each point in the mesh, the procedure given provides a convenient means of monitoring the progress of the calculations. The computation can generally be considered complete when the rate of change in the magnitude of this number becomes insignificant for several double steps.

Fig. 5 summarizes the essential steps from the start of the problem through completion of the pressure computation phase. The final result is the steady-state pressure distribution for a particular schedule of production and injection rates.

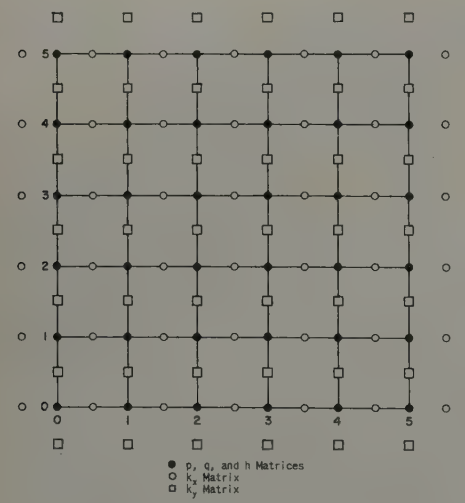

FIG. 4—ARRANGEMENT OF DATA MATRICES FOR MACHINE COMPUTATIONS.

BOUNDARY MOVEMENT COMPUTATION

Both manual and automatic methods have been employed for tracking movement of the flood front through the reservoir. The procedure is essentially the same in either case and is based upon computing the particle velocity at various points on the flood front. The velocity of each point is multiplied by a specified time interval, and this product is added to the coordi-

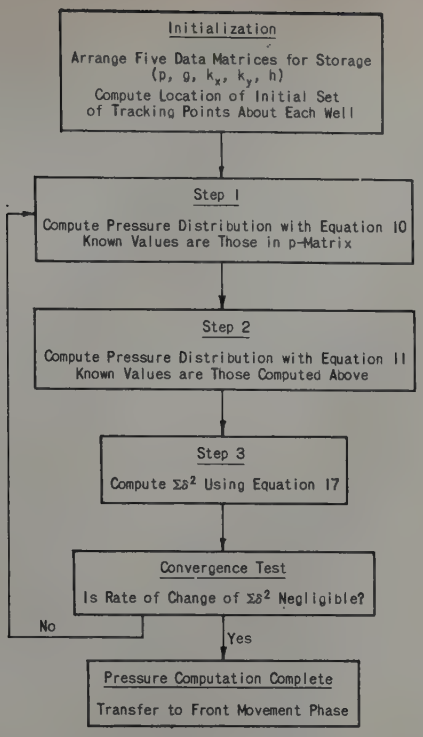
Initialization
Arrange Five Data Matrices for Storage (p, g, k_x, k_y, h)
Compute Location of Initial Set of Tracking Points About Each Well
Step 1
Compute Pressure Distribution with Equation 10
Known Values are Those in p-Matrix
Step 2
Compute Pressure Distribution with Equation 11
Known Values are Those Computed Above
Step 3
Compute $\Sigma\delta^2$ Using Equation 17
Convergence Test
Is Rate of Change of $\Sigma\delta^2$ Negligible?
No
Yes
Pressure Computation Complete
Transfer to Front Movement Phase

FIG. 5—FLOW DIAGRAM FOR PRESSURE COMPUTATION.

nates of the point to determine its new location. The process is followed repeatedly until the front reaches or floods out a production well. When wells are flooded by the displacing fluid, they are generally shut in, and the allowable is either transferred to other producing wells in accordance with the field rules or dropped from the production schedule if transfer is not possible. At this time, the pressure distribution is recalculated, and the boundary movement is repeated until another well is flooded. This process is continued to depletion of the reservoir.

In the automatic tracking procedure,[6] the velocity calculation, front movement, and allowable transfer is all handled internally by the computer. The problem is started by spacing an arbitrary number of points evenly around a small circle about each injection well. The movement of each point is tracked stepwise throughout the history of the project. The location of the front may be constructed by connecting the points having a common time level. Experience has shown that approximately 50 points per well are sufficient for accurate front location in most problems.

After the pressure distribution is calculated the x and y components of velocity are computed at each grid intersection in the model, e.g.,

$$v_{x,i} = (p_{i+\frac{1}{2}} - p_{i,-\frac{1}{2}}) \frac{k_{x,i}}{\mu\phi S_{od}\Delta x} \quad . \quad . \quad . \quad . \quad . \quad (16)$$

The maximum velocity computed is used to determine a time interval which will restrict the movement of any point to some specified maximum distance during the step. This action insures that local velocity gradients will not severely affect the accuracy of the tracking procedure. The velocity at which any point is moving is determined by bilinear interpolation between velocities at the four surrounding intersections. New point location is obtained by multiplying the component velocities of the point by the time interval and adding the products to the coordinates of the point at the previous time level.

$$x_{t+1} = x_t + v_{x,t}\,\Delta t$$
$$y_{t+1} = y_t + v_{y,t}\,\Delta t \quad . \quad . \quad . \quad . \quad (17)$$

Each time a point is moved its new location is compared with the locations of the production wells. If any point falls within a specified radius about any production well, the well is considered to have been reached by the flood front. When a well is invaded, a choice is made as to whether the well will continue to be produced or will be shut in and its allowable disposed of in some manner (such as transferred to another well). All of the factors involved in allowable transfer such as well capability, field rules, and the like must be specified in advance in order for the computation to follow the actual sequence of events properly.

When all wells have been flooded, this situation is recognized by the computer, and the calculations are halted. Fig. 6 illustrates the flow of computations during this phase of the problem.

DISCUSSION OF RESULTS

Most of the field studies which have been performed to date have involved (1) selection of optimum injection patterns, (2) evaluation of performance of reservoir flooding operations, or (3) evaluation of pilot waterflood projects. To illustrate the first application, Figs. 7 and 8 show two patterns obtained during the study of an actual reservoir. The contours represent equal-time lines for each pattern. Some of the problems peculiar to each pattern are apparent in the illustrations. For example, considering the end-to-end pattern, a large "pocket" of oil is left trapped in one area of the field where the flood fronts do not coalesce

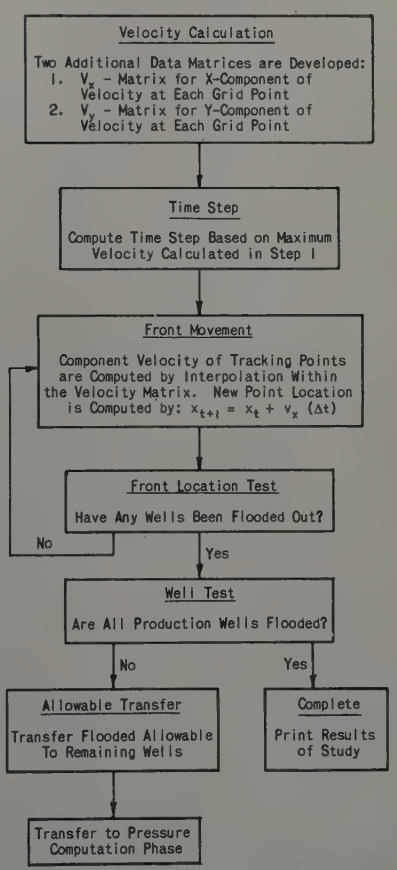
Velocity Calculation
Two Additional Data Matrices are Developed:
1. V_x - Matrix for X-Component of Velocity at Each Grid Point
2. V_y - Matrix for Y-Component of Velocity at Each Grid Point
Time Step
Compute Time Step Based on Maximum Velocity Calculated in Step 1
Front Movement
Component Velocity of Tracking Points are Computed by Interpolation Within the Velocity Matrix. New Point Location is Computed by: $x_{t+1} = x_t + v_x\,(\Delta t)$
Front Location Test
Have Any Wells Been Flooded Out?
No
Yes
Well Test
Are All Production Wells Flooded?
No
Yes
Allowable Transfer
Transfer Flooded Allowable To Remaining Wells
Complete
Print Results of Study
Transfer to Pressure Computation Phase

FIG. 6—FLOW DIAGRAM FOR FRONT MOVEMENT.

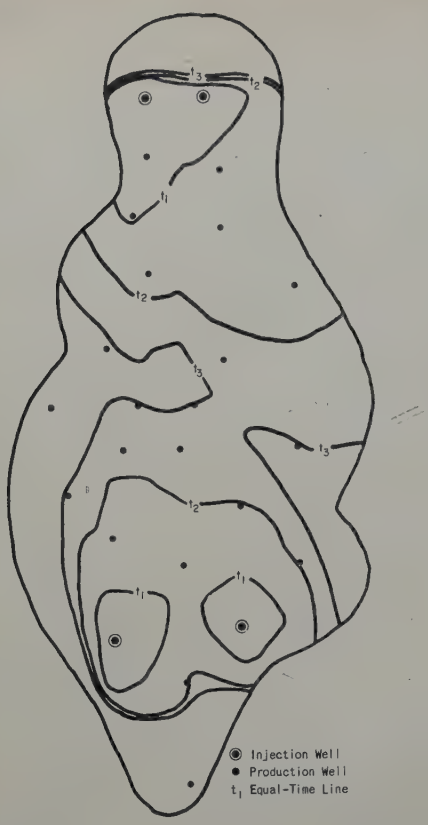

FIG. 7—TYPICAL FLOOD PATTERN RESULTING FROM FIELD STUDY.

FIG. 8—TYPICAL FLOOD PATTERN RESULTING FROM FIELD STUDY.

evenly. The peripheral-type pattern invades a lesser volume of the reservoir before flooding all wells and also indicates early flooding of the better located production wells.

In the preceding example, the reservoir was represented with a rectangular integration net containing approximately 1,400 grid points, approximately 1,000 of which were contained within the productive area of the reservoir. As there was a total of 25 injection and production wells in the reservoir, this arrangement resulted in an average density of approximately 40 grid points per well. When scaled to reservoir dimensions, the mesh interval between grid points was about 315 ft. The results of this study indicated that this size integration net provided sufficient definition of the reservoir and permitted accurate tracking of the water-oil front movement.

A large commercial computer (IBM 704) was used for the calculations described. The computing time required for the initial pressure distribution calculation was approximately 15 minutes. After the first pressure calculation was completed, results of the preceding calculation could be used as the initial pressure distribution estimate for the cases which followed. The more realistic starting pressure distribution greatly reduced the number of iterations required, and all succeeding calculations of pressure distribution required approximately 20 per cent as much time as the initial calculation. The total machine time including all pressure and front movement computations required to complete the problem was approximately three hours.

An attempt was made to duplicate the results of the study illustrated in Figs. 7 and 8 on a much smaller electronic computer. The integration net used in the latter problem included 256 grid points of which approximately 150 were included within the field boundaries. The point density in this case was approximately six per well, and the mesh interval in the numerical model represented approximately 900 ft in the reservoir. The small computer did not have sufficient storage capacity to permit inclusion of the automatic boundary movement program, and only the pressure computation was made on the computer. Approximately 60 hours of computing time was required to develop one pressure distribution. Subsequent attempts to move the flood front indicated that the grid density used in this example was too small to provide accurate duplication of the results developed using the finer grid.

Another pattern performance study involved evaluating the flood performance of a portion of a large pressure maintenance project to explore the effect of altering the reservoir injection pattern. In this case, the well density in the reservoir was rather high, and the use of a 1,500-point integration net provided less than five grid points per well which, in most cases, meant there was only one grid point between wells along a coordinate axis. An attempt to solve the problem using the 1,500-point grid was unsuccessful as the scarcity of pressure information between wells prevented accurate front movement. Consequently, the model was enlarged to 6,000 points by halving the mesh interval. This resulted in a point density of about 16 points per well, and the mesh interval represented 500 ft in the reservoir. With this finer grid, the experience was comparable to that obtained on the previous problem. The pressure computation for the 6,000-point grid required approximately 55 minutes per case on the large computer.

A second variation of the basic pattern performance problem arose in connection with evaluating the per-

formance of an isolated five-spot waterflood operation. The pilot flood was located within a very large productive area, and interpretation of field performance was complicated by an anisotropic reservoir permeability situation known to be characteristic of this area. This situation was further indicated by the very rapid breakthrough of injected water in some wells far removed from the injection area and delayed breakthrough in other wells very close to the injection area.

In this particular case, all reservoir properties were considered to be uniform except for permeability, which was assumed to be several times greater in one direction than along the normal to this axis. An analytic solution to Laplace's equation was used to compute pressure, and the contribution of each well in the system was accumulated using the superposition principle to provide the pressure values at points of interest. Front movement was computed automatically in the manner described previously. The orientation of the axis of greater permeability and the ratio of the permeabilities were varied until the best match of time and order of water breakthrough into the producing wells was obtained. All computations including the front movement were performed on the large computer, and the entire analysis was completed in approximately three hours.

Fig. 9 illustrates the results of the pilot waterflood study. It can be seen that the indicated pattern performance of this five-spot and the probable ratio of the amount of oil flooded from the lease to that produced from the pilot area varies considerably from that usually observed in similar operations where the reservoir is more homogeneous. The experience emphasizes the hazard of basing quantitative appraisals of field performance on results obtained from idealized cases.

CONCLUSIONS

The extension of analyses to include studies of reservoir performance in two space dimensions should result in a marked improvement in reservoir engineering. Such analyses improve the dependability of reservoir performance predictions and provide field and other operating personnel with additional engineering information of value in conducting production operations.

The results of these studies indicate that the high-speed digital computer is well suited for studying reservoir performance in two and three space dimensions and that dependable numerical techniques are available for making many such analyses. Experience to date with both large and small computers indicates that the large computer is the more practical of the two for reservoir-scale, two-dimensional calculation work.

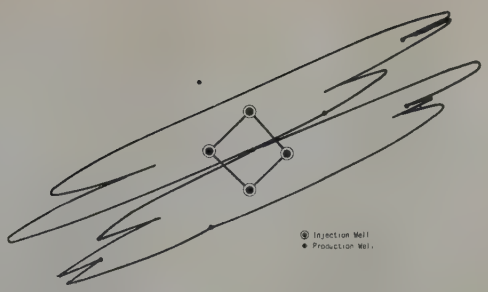

FIG. 9—CALCULATED FLOOD PATTERN IN ANISOTROPIC FIVE-SPOT PILOT FLOOD.

NOMENCLATURE

k = permeability
h = thickness
μ = fluid viscosity
p = pressure
q = production or injection rate
C = compressibility
ϕ = porosity
v = front velocity
S_{od} = fraction of oil displaced
t = time
γ = iteration parameter
N = number of points along typical row or column
δ = residual, measure of convergence
x = distance coordinate
y = distance coordinate
A, B, C, D = coefficient terms defined in text
i = subscript indicating i^{th} grid intersection in x-direction
j = subscript indicating i^{th} grid intersection in y-direction
n = superscript indicating n^{th} time step

REFERENCES

1. Lee, B. D.: "Potentiometric Model Studies of Fluid Flow in Petroleum Reservoirs", *Trans.* AIME (1948) **174**, 41.
2. Muskat, M.: "Theory of Potentiometric Models", *Trans.* AIME (1949) **179**, 216.
3. Odeh, A. S., Bradley, H. B. and Heller, J. P.: "Scale Limitations in Potentiometric Model Construction", *Trans.* AIME (1956) **207**, 200.
4. Peaceman, D. W. and Rachford, H. H., Jr.: "The Numerical Solution of Parabolic and Elliptic Differential Equations", *J. Soc. Ind. Appl. Math.* (1955) **3**, 28.
5. Douglas, J., Jr.: "On the Numerical Integration of $u_{xx} + u_{yy} = u_t$ by Implicit Methods", *J. Soc. Ind. Appl. Math.* (1955) **3**, 52.
6. Collins, R. E. and Simons, L. H.: "Calculation of Water Flood Sweep Patterns for Unit Mobility Ratio" (to be published). ★★★

Fluid Dynamics During an Underground Combustion Process

L. A. WILSON
R. J. WYGAL
D. W. REED
R. L. GERGINS
J. H. HENDERSON
MEMBER AIME

GULF RESEARCH & DEVELOPMENT CO.
PITTSBURGH, PA.

ABSTRACT

This paper presents a method of predicting the production history of an underground combustion recovery process. A rigorous solution of the thermodynamics and hydrodynamics involved is beyond the scope of this report. However, a practical scheme to appraise combustion recovery performance has been worked out. By prudent assumptions, regarding the attainment of steady-state conditions, a trial-and-error solution, which satisfies both material balance and three-phase relative permeability requirements has been evolved and tested.

As a combustion zone moves through a formation the interstitial water, the water of combustion and a portion of the oil will be vaporized. These vapors will move downstream to a cooler region of the formation where they will condense. Part of the remaining oil will be displaced by the imposed gas drive and what remains behind will be consumed as fuel. The fluids will distribute themselves downstream in a manner which will satisfy the three-phase relative permeability characteristics of the formation. Three distinct zones will exist ahead of the combustion zone: (1) a zone termed a water bank which contains three mobile phases, oil, water and gas; (2) a region containing two mobile phases, oil and gas, called the oil bank; and (3) a zone having the fluid saturation distribution which existed prior to combustion.

The mobile water will impose a water flood on the oil in the region containing three flowing phases. The process can be visualized as a simultaneous water flood and combustion-supported gas drive. It is possible to estimate the saturation distributions in the water bank and oil bank as well as the production history for any combustion temperature if the porosity, three-phase relative permeability characteristics, oil viscosity and initial saturations are known. This has been done for injection pressures ranging from 1 to 100 atm, oil viscosities of 10 to 1,000 cp and porosities from 20 to 40 per cent. Several of these calculations have been checked in the laboratory, with the result indicating rather good agreement between the predicted and observed production histories.

The analytical and experimental techniques are described and the comparison of predicted and observed performance presented.

Original manuscript received in Society of Petroleum Engineers office Oct. 12, 1957. Revised manuscript received March 14, 1958. Paper presented at 32nd Annual Fall Meeting of Society of Petroleum Engineers in Dallas, Tex., Oct. 6-9, 1957.

INTRODUCTION

Considerable research by the oil industry during the past 10 years has been directed toward the thermal recovery of crude oil. Of all schemes considered, the one receiving the most attention is in situ combustion. This is a process in which part of the oil is actually burned within the reservoir rock. The uniqueness of the process lies in its potential. Theoretically, this potential generates from the following: (1) it may open the door to vast reserves previously not economically producible, (2) it may induce increased production rates where low rates are now realized and (3) it may give high over-all recovery efficiency.

The general idea of the process has received considerable attention in the literature [1-5] and the following brief description is intended for orientation only.

In situ combustion can be visualized by considering a linear system, one end of which represents the injection well and the other the producing well. The formation at the inlet end is raised to ignition temperature by placing a gas or electric heater at the face of the formation or by the ignition of thermite, charcoal or similar material. While heating, the water and part of the oil in the heated region is vaporized and moved out into the reservoir by the injection of gas containing oxygen. In addition, part of the oil is displaced as liquid by the imposed gas drive. The oil not displaced is modified to an immobile, coke-like material (hereafter referred to as coke) by the high temperatures existing immediately ahead of the combustion zone. This coke is used as fuel, and the combustion front advances through the formation at a temperature which is probably in excess of 800°F. As the combustion front advances it will drive ahead all interstitial oil not rendered immobile and all interstitial water plus the water formed by the combustion of hydrogen. As a result the sand behind the combustion zone is freed of all oil and water.

Although the general description of the process has been outlined in the literature, there has been no consideration of the behavior of the fluids moving downstream from the combustion front. It is the purpose of this paper to present a technique

[1]References given at end of paper.

for predicting this behavior and for estimating production history during an underground combustion process.

DEVELOPMENT OF THE BANK CONCEPT

Intuitive reasoning leads one to the conclusion that the detailed fluid behavior must be quite complex. As the leading edge of the high temperature zone advances, a fractionation of the oil must occur. Likewise, the water is vaporized, and when these fluids reach cooler regions condensation will occur. This condensation for the oil will in effect be fractional condensation where the heavier materials condense nearer the combustion zone. Thus, the lighter ends of the oil will be condensing and mixing with the essentially unmodified oil existing at the point of condensation.

The combined effect of the added heat and solvation would result in viscosity gradients in the oil. However, the experimental evidence indicates that the temperature ahead of the combustion front declines rapidly to the original reservoir temperature, particularly in the early phases of the process. This can also be shown mathematically to be true for the case of a non-condensable gas. This means that a marked reduction in oil viscosity will occur for only a short interval ahead of the combustion front. Under these circumstances, the displaced fluids from the combustion front move into cooler regions where the mobility is low. This lack of mobility results in increased liquid saturation at the expense of gas saturation. The result is a marked increase in the resistance to gas flow. The early experiments confirmed this liquid build-up or "bank" and it has also been observed by other investigators.[1]

The process has been considered for the case of constant injection pressure. If the mean pressure ahead of the combustion front is practically the same as the injection pressure and the viscosities of the fluids are not appreciably changed, the dynamic behavior of the gas, oil and water can be estimated from considerations of Darcy's law and a material balance.

The application of these two fundamental principles results in the prediction of three distinct zones ahead of the combustion front. The first, nearest the front, contains three mobile phases, oil, water and gas. The second, immediately downstream from the first, contains two mobile phases, oil and gas. The third, immediately downstream from the second, contains two mobile phases and represents the reservoir conditions after gas driving and just prior to the inception of combustion. Hereafter, these zones will be referred to as the water bank, oil bank and zone of initial conditions, respectively. Subscripts 1, 2 and 3, respectively, will be used to distinguish the various symbols applicable to these three zones.

The following assumptions must be made:

1. All fluids are flowing at the original reservoir temperature.
2. The effects of fractional condensation ahead of the combustion zone are neglected and the original fluids are flowing in all zones.
3. The mean pressure is practically identical to the injection pressure.
4. No gravity segregation occurs.
5. The combustion front advances at essentially constant temperature.
6. The saturation gradient of each fluid in the banks is negligible.
7. The heat losses to surroundings are negligible.
8. The ratio of water produced to fuel consumed remains constant.

The following data must either be assumed or known from auxiliary experiments: (1) the difference between the initial reservoir temperature and the peak temperature of the combustion front (assumed here to be 538°C or about 1,000°F, (2) the calorific value of the fuel (assumed here to be 10,500 cal/gm), (3) the ratio of water produced to fuel consumed (assumed here to be 1.3 vol/vol), and (4) the ratio of standard volumes of air per volume of oil required for combustion (assumed here to be 10,500 scc/cc).

These figures are based on the carbon-hydrogen ratio of a typical coke formed during the combustion process.

ANALYTICAL METHOD FOR CALCULATING PRODUCTION HISTORY

The general procedure for the calculations involves the following steps:

1. Calculate the fluid saturations in the water bank.
2. Determine the velocity of the front of the water bank with respect to the velocity of the flame front.
3. Calculate the oil and gas saturations in the oil bank.
4. Determine the velocity of the front of the oil bank with respect to the velocity of the flame front.
5. Estimate the lengths of the banks and the actual pressure distribution for the particular system in question as a function of distances burned.
6. Calculate the flame front velocity and the rates of fluid production at each of the assumed distances burned.
7. Calculate cumulative production as a function of time.

Step 1—Calculating the Saturations in the Water Bank

If the saturation gradient in the water bank is to be small, the volumetric rate of each fluid moving in the downstream section of the bank must be equal to the volumetric rate moving as a result of the advance of the flame front. The rate* at which oil moves from the flame front will be

$$q''_{o1} = v_f A \phi S_{o1} - \frac{v_f A (1-\phi) \rho_s C_s \Delta T}{\Delta H_c \rho_o} \quad . \quad . \quad . \quad . \quad (1)$$

The heat capacities of the oil, gas and water have been neglected in Eq. 1 because they represent only about 30 per cent of the total heat capacity and tend to be cyclic in that the oil, gas and water moving into a cold zone give up their heat.

The rate of oil movement in the downstream section of the bank will be that which can be caused by the pressure gradient established by the injected gas, or

$$q_{o1} = q_{g1} \frac{k_{ro}}{k_{rg}} \frac{\mu_g}{\mu_o} \quad . \quad . \quad . \quad (2)$$

These two oil rates must be equal, or

$$q_{o1} = q''_{o1} \quad . \quad . \quad . \quad . \quad . \quad (3)$$

Now, with the assumption that the mean pressure is the same as the injection pressure, the gas rate can be calculated for any injection pressure and rate of advance. The air rate required for combustion (standard cc/sec) can be obtained by using the expression,

$$q_{sc} = \frac{v_f A (1-\phi)(\rho_s)(C_s)(\Delta T)(10{,}500)}{\Delta H_c \rho_o} \quad . \quad . \quad . \quad . \quad . \quad . \quad . \quad . \quad . \quad (4)$$

Now,

$$q_{g1} = q_{sc} \frac{p_{sc}}{\overline{p}} \quad . \quad . \quad . \quad (5)$$

*Throughout this development the double primes will indicate liquid rates dependent upon the advancing combustion zone. No primes will be used when the rates are those resulting from the pressure gradient imposed by the gas.

At any assumed gas saturation different oil saturations can be arbitrarily assumed and the amount of oil which can be moved with the gas can be calculated. Using the same conditions, the amount of oil which must be moved if there is to be no change in oil saturation (thus maintaining the material balance) can be calculated by Eq. 1. At each assumed gas saturation there will be one oil saturation at which $q_{o1} = q''_{o1}$. This is determined by plotting oil saturation vs $(q_{o1} - q''_{o1})$. These calculations are repeated for several gas saturations.

By a similar analysis one can see that the rate at which the water can be moved by the gas phase must be equal to the rate at which it is being moved by the advancing combustion zone, or

$$q_{w1} = q''_{w1} \quad . \quad . \quad . \quad . \quad . \quad (6)$$

Now,

$$\frac{q_{o1}}{q_{w1}} = \left(\frac{k_{ro}}{k_{rw}}\right)_1 \frac{\mu_w}{\mu_g} \quad . \quad . \quad (7)$$

The water being moved forward by the combustion zone is that originally present plus the water of combustion. That is,

$$q''_{w1} = v_f A\phi S_{w1} + \frac{v_f A(1-\phi)(\rho_s)C_s(\Delta T)(1.3)}{\Delta H_c \rho_o} \quad . \quad . \quad (8)$$

At each assumed gas saturation there will be one water saturation where $q_{w1} = q''_{w1}$. This is determined by plotting water saturation vs $(q_{w1} - q''_{w1})$. These calculations are then repeated for several gas saturations.

To this point the calculations have determined the oil and water saturations at various assumed gas saturations which satisfy both the conditions of uniform saturation in the bank and the three-phase relative permeability characteristics of the medium in which the bank forms. But it is also known that the sum of the saturations must be 100 per cent, or

$$S_{g1} + S_{o1} + S_{w1} = 100 \quad . \quad (9)$$

Therefore, the saturation distribution which satisfies Eq. 9 must be obtained. This can be done by summing the oil saturation at which $(q_{o1} - q''_{o1})$ is zero at any assumed gas saturation, the water saturation at which $(q_{w1} - q''_{w1})$ is zero at the same gas saturation and the gas saturation itself. By plotting $S_{g1} + S_{o1} + S_{w1}$ vs the gas saturation, the gas saturation at which the total saturation is 100 is obtained; this gas saturation necessarily satisfies the relative permeability relationships, the material balance and the flow equations.

Now, from a plot of the gas saturation at which $q_{o1} = q''_{o1}$ vs oil saturation, the oil saturation which satisfies the assumed conditions can be found. From a similar plot of water saturation vs gas saturation at which $q_{w1} = q''_{w1}$, the water saturation can be found.

In Table 1 the method of calculation is tabulated. At each assumed gas saturation, oil and water saturations are assumed and $(q_{o1} - q''_{o})$ and $(q_{w1} - q''_{w})$ are determined. Fig. 1 is a plot of $(q_{w1} - q''_{w1})$ as a function of water saturation at various gas saturations. At each gas saturation a water saturation is found at which $q_{w1} = q''_{w1}$ and the condition of uniform water saturation is satisfied. Fig. 2 is a similar plot for the oil saturations.

Fig. 3 is a plot of total saturation where $q_{o1} = q''_{o1}$ and $q_{w1} = q''_{w1}$ for any gas saturation as a function of gas saturation. Where this curve crosses the 100 per cent saturation line it defines the gas saturation that satisfies the conditions of uniform saturation, material balance and Darcy's law. Knowing this gas saturation, the corresponding oil and water saturations can be read from Fig. 4.

The described calculations will determine the three-phase saturation distribution in the water bank. Table 2 shows for sandstones of varying porosity the calculated saturation distributions in this bank. The three-phase relative permeability data used were those determined for Berea sandstone at the Gulf Laboratories (on the drainage cycle) by methods described elsewhere.[6] The residual water saturation for this sand was found to be 20 per cent. It can be seen that the water saturations in the water bank are all above the residual and all phases have mobility.

Step 2—Determining the Velocity of the Water Bank

The volumetric flow rate of the water in the oil bank is equal to the rate of water flow in the water bank augmented or diminished by water moved out or left behind as a result of the differences in saturation in the two banks. That is,

$$q_{w2} = q_{w1} + v_w A\phi(S_{w2} - S_{w1}) \quad . \quad (10)$$

Now, if the interface between the oil and water banks is at the point where the water saturation approaches the irreducible, q_{w2} is zero. Then Eq. 10 becomes

$$q_{w2} = 0 = q_{w1} + v_w A\phi(S_{w2} - S_{w1}). \quad . \quad . \quad . \quad . \quad . \quad . \quad . \quad (10a)$$

Solving for v_w there results

$$v_w = \frac{q_{w1}}{A\phi(S_{w1} - S_{w2})} \quad . \quad (11)$$

Eq. 11 can be solved directly for v_w. The velocity of the water bank can be expressed as

$$v_w = Cv_f. \quad . \quad . \quad . \quad . \quad (12)$$

Step 3—Calculating Oil and Gas Saturations in the Oil Bank

The volumetric flow rate of the oil and gas in the oil bank is equal to the rate at which these fluids move in the water bank plus what is pushed out or left behind as a result of the saturation differences in the two banks. Analytically this is given by Eqs. 13 and 14.

$$q_{g2} = q_{g1} + v_w A\phi(S_{g2} - S_{g1}) \quad . \quad (13)$$

$$q_{o2} = q_{o1} + v_w A\phi(S_{o2} - S_{o1}) = q_{o1} + v_w A\phi(S_{w1} - S_{w2} - S_{g2} + S_{g1}) \quad . \quad . \quad . \quad . \quad . \quad . \quad . \quad . \quad . \quad . \quad (14)$$

Dividing Eq. 13 by Eq. 14 results in an expression for q_{g2}/q_{o2}.

$$\frac{q_{g2}}{q_{o2}} = \frac{q_{g1} + v_w A\phi(S_{g2} - S_{g1})}{q_{o1} + v_w A\phi(S_{w1} - S_{w2} - S_{g2} + S_{g1})} \quad . \quad . \quad . \quad . \quad . \quad . \quad . \quad . \quad . \quad . \quad (15)$$

An independent relationship for the same ratio is

$$\frac{q_{g2}}{q_{o2}} = \left(\frac{k_{rg}}{k_{ro}}\right)_2 \frac{\mu_o}{\mu_g} \quad . \quad . \quad (16)$$

Combining Eqs. 15 and 16 gives

$$\frac{q_{g1} + v_w A\phi(S_{g2} - S_{g1})}{q_{o1} + v_w A\phi(S_{w1} - S_{w2} - S_{g2} + S_{g1})} = \left(\frac{k_{rg}}{k_{ro}}\right)_2 \frac{\mu_o}{\mu_g} \quad . \quad . \quad . \quad . \quad . \quad . \quad (17)$$

Eq. 17 can be solved for the gas saturation, S_{g2}, by assuming gas saturations and determining the corresponding gas-oil relative permeability ratios until the satisfying conditions are established.

Step 4—Determining the Velocity of the Oil Bank

A material balance made on the oil bank and the zone of initial saturations existing downstream from the oil bank (i.e., conditions in the reservoir before combustion commenced but after gas driving) gives

$$q_{g3} = q_{g2} + v_o A\phi(S_{g3} - S_{g2}) \quad . \quad . \quad . \quad . \quad . \quad . \quad . \quad (18)$$

and

$$q_{o3} = q_{o2} + v_o A\phi(S_{o3} - S_{o2}). \quad . \quad . \quad . \quad . \quad . \quad . \quad . \quad . \quad (19)$$

By dividing Eq. 18 by Eq. 19, an expression is obtained for q_{g3}/q_{o3}.

$$\frac{q_{g3}}{q_{o3}} = \frac{q_{g2} + v_o A\phi(S_{g3} - S_{g2})}{q_{o2} + v_o A\phi(S_{o3} - S_{o2})} \quad . \quad . \quad . \quad . \quad . \quad . \quad . \quad . \quad (20)$$

TABLE 1—CALCULATIONS FOR THREE-PHASE SATURATION DISTRIBUTIONS

Gas saturation (S_g)	Oil saturation (S_o)	Water saturation (S_w)	Gas-oil relative permeability ratio	gas-water relative permeability ratio	Oil rate due to gas drive (q_{o1})	water rate due to gas drive (q_{w1})	Oil rate due to moving flame front (q_{o1}'')	water-rate due to moving flame front (q_{w1}'')	$q_{o1} - q_{o1}''$	$q_{w1} - q_{w1}''$
10	70		0.0061		1.52787		0.01793		1.50994	
	60	30	0.0067	11	1.39104	0.08473	0.01466	0.01622	1.37638	0.06851
	50	40	0.0115	0.94	0.81043	0.99149	0.01140	0.01949	0.79903	0.9720
	40	50	0.0165	0.195	0.56485	4.77949	0.00853	0.02276	0.55632	5.72873
	30	60	0.0305	0.062	0.30557		0.00486	0.02602	0.30071	
	20	70	0.215	0.0232	0.4335		0.00159	0.02929	0.04176	
		25		46		0.02026		0.01459		0.00567
		27.5		21		0.04438		0.01540		0.02898
15	70		0.05		0.18640		0.01793		0.16847	
	60		0.0562		0.16584		0.01466		0.15118	
	50		0.0708		0.13164		0.01140		0.12024	
	40		0.102		0.09137		0.00813		0.08324	
	30		0.236		0.03949		0.00486		0.03463	
	20		0.9		0.01036		0.00159		0.00877	
		25						0.01459		
		27.5						0.01540		
		30		68		0.01371		0.01622		−0.00251
		32.5		37		0.02519		0.01704		0.00815
		35		13.7		0.06803		0.01785		0.05018
		40		5.8		0.16069		0.01949		0.14120
		50		1.17		0.79658		0.02258		0.7740
17.5	70		0.077		0.12104		0.01793		0.10311	
	60		0.084		0.11095		0.01466		0.09629	
	50		0.10		0.0932		0.01140		0.08180	
	40		0.143		0.06517		0.00813		0.05704	
	30		0.335		0.02782		0.00486		0.02296	
	20		1.49		0.00626		0.00159		0.00467	
		30		91		0.01024		0.01622		−0.00598
		32.5		44		0.02118		0.01704		0.00414
		35		21		0.04438		0.01785		0.02653
		37.5		11.2		0.08321		0.01867		0.06454
20	70		0.124		0.07516		0.01793		0.05723	
	60	20	0.135		0.06904		0.01466	0.01225	0.05438	
	50	30	0.160	125	0.05825	0.00746	0.1140	0.01622	0.04685	−0.00876
	40	40	0.221	10.6	0.04217	0.08792	0.00813	0.01949	0.03404	0.06843
	30	50	0.523	2.3	0.01782	0.40522	0.00486	0 02276	0.01296	0.38246
	20	60	2.74	0.7	0.00340	1.33143	0.00159	0.02602	0.00181	1.30541
		32.5		66		0.01412		0.01704		−0.00292
		35		35		0.02663		0.01785		0.00878
30	50	20	0.836		0.01115		0.01140	0.01225	−0.00025	
	40	30	0.995	300	0.00937	0.00311	0.00813	0.01622	0.00124	−0.01311
	30	40	1.685	25.2	0.00553	0.03698	0.00486	0.01949	0.00067	0.01749
	25	50	2.824	5.2	0.00330	0.17923	0.00323	0.02276	−0.00007	0.15647
		35		70		0.01331		0.01785		−0.00454
		37.5		40		0.02330		0.01867		0.00463
40	50		3.39		0.00275		0.01140		−0.00865	
	40	20	4.0		0.00233		0.00813	0.01225	−0.00580	
	30	30	6.1	580	0.00153	0.00161	0.00486	0.01622	−0.00333	−0.01461
	20	40	16.4	49.5	0.00057	0.01883	0.00159	0.01949	−0.00102	−0.00066
		50		10.1		0.09228		0.02276		0.06952
		35		140		0.00666		0.01785		−0.01119
25	50	32.5	0.339	106.45	0.02749	0.00876	0.01140	0.01704	0.01609	−0.00828
	40	35	0.489	56.90	0.01906	0.01638	0.00813	0.01785	0.01093	−0.00147
	30	37.5	0.985	31.43	0.00946	0.02965	0.00486	0.01867	0.00460	0.01098
	25		1.692		0.00551		0.00323		0.00228	
Check										
32.6	29.1	38	2.167	50	0.00430	0.01865	0.00457	0.01883	−0.00027	−0.00018

Porosity = 20 per cent
Velocity of combustion front = 0.5 ft/day = 0.000176 cm/sec
Air required = 51.8 cc/sec ft²
Oil viscosity = 100 cp
Air viscosity = 0.018 cp
Water viscosity = 1 cp
Injection pressure = 1 atm

Now q_{g3}/q_{o3} can also be expressed by

$$\frac{q_{g3}}{q_{o3}} = \left(\frac{k_{rg}}{k_{ro}}\right)_3 \frac{\mu_o}{\mu_g} \quad . \quad . \quad (21)$$

Combining Eqs. 20 and 21 gives

$$\frac{q_{g3}}{q_{o3}} = \frac{q_{g2} + v_o A\phi(S_{g3} - S_{g2})}{q_{o2} + v_o A\phi(S_{o3} - S_{o2})} = \left(\frac{k_{rg}}{k_{ro}}\right)_3 \frac{\mu_o}{\mu_g} \quad . \quad . \quad . \quad . \quad . \quad . \quad (22)$$

Solution of Eq. 22 gives the velocity of the front of the oil bank, v_o. This velocity can be expressed as

$$v_o = C' v_f \quad . \quad . \quad . \quad . \quad (23)$$

The calculations which have been made cover a range of injection pressures, oil viscosities and formation porosities. The initial saturation distribution in each case was 20 per cent water, 20 per cent gas and 60 per cent oil. The results of these calculations are shown in Table 2.

Initially it was assumed that the mean pressure is practically the same as the injection pressure. Fig. 5 is a plot of fluid saturations as a function of pressure. It can be seen that the saturations tend to a constant value as the injection pressure increases. The oil saturation changes 4 per cent of pore volume as the pressure is increased from 10 to 100 atm. This corresponds to a change in mobility of only 20 per cent. The gas saturation changes 3.5 per cent of pore volume for the same increase in pressure; this represents a change in mobility of 50 per cent. These data indicate that even a relatively large difference between the mean pressure and the injection pressure would result in a small change in saturation, particularly at pressures above 10 atm. Thus, the initial assumption may be justified.

Step 5—Calculating the Pressure Distribution

In any specific case the pressure distribution can be calculated in the following manner. In the early stages of the process, the system contains the three regions, i.e., the water bank, oil bank and zone of initial conditions. It is assumed that some definite short distance has been burned. The lengths of the water bank and oil bank can be calculated by Eqs. 24 and 25, respectively.

$$L_1 = (C - 1)\, L_B \quad . \quad . \quad (24)$$

and

$$L_2 = (C' - C)\, L_B \quad . \quad . \quad (25)$$

The length of the zone of initial conditions is equal to the total length of the system less the sum of the lengths of the distance burned, the water bank and the oil bank.

In the previous development it was

assumed that the mean pressure in the different zones was identical. Actually, of course, this is not true. Therefore, it is assumed that the continuity of the gas phase is defined by

$$q_{g1}\,\bar{p}_1 = q_{g2}\,\bar{p}_2 = q_{g3}\,\bar{p}_3 \quad . \quad (26)$$

Now Eq. 26 can be written

$$\frac{k_{g1}A\Delta p_1\bar{p}_1}{\mu_g L_1} = \frac{k_{g2}A\Delta p_2\bar{p}_2}{\mu_g L_2} = \frac{k_{g3}A\Delta p_3\bar{p}_3}{\mu_g L_3} \quad . \quad (27)$$

From Table 2 it can be seen that the gas saturations in the water bank and oil bank are about the same. Realizing this, a weighted mean effective permeability to gas can be used to estimate the pressure drop through these zones. This weighted mean effective permeability to gas is defined by

$$k_{ge} = \frac{L_1 k_{g1} + L_2 k_{g2}}{L_1 + L_2} \quad . \quad (28)$$

Eq. 27 can now be written

$$\frac{\Delta p_{1,2}\,\bar{p}_{1,2}}{\Delta p_3\,p_{g3}} = \frac{k_{g3}\,(L_1 + L_2)}{k_{ge}\,L_3}, \quad . \quad (29)$$

where $\Delta p_{1,2}$ is pressure drop through the water bank and oil bank and $\bar{p}_{1,2}$ is mean pressure in the water bank and oil bank. The right-hand member of Eq. 29 can now be numerically evaluated.

Experimental evidence has shown the pressure drop through the burned zone to be negligible. Therefore, the total pressure drop through the system is the difference between the injection and production pressures and will be equal to the sum of the pressure drop through Zones 1, 2 and 3.

$$\Delta p_T = \Delta p_{1,2} + \Delta p_3 \quad . \quad (30)$$

where Δp_T is total pressure drop through the system.

Arbitrary values of $\Delta p_{1,2}$ are assumed and the corresponding values of $\bar{p}_{1,2}$, $\bar{p}_{g3}$ and Δp_3 established. This evaluates the left-hand member of Eq. 29 for each of the assumed values of $\Delta p_{1,2}$. The value of $\Delta p_{1,2}$, which gives numerical identity to the two sides of Eq. 29 is the pressure drop through the water bank and oil bank.

The pressure drop in the individual bank is determined in an analogous manner. In this case Eq. 29 would be written as Eq. 29a and Eq. 30 would be written as Eq. 30a.

$$\frac{\Delta p_1\bar{p}_1}{\Delta p_2\bar{p}_2} = \frac{k_{g2}L_1}{k_{g1}L_2} \quad . \quad . \quad . \quad (29a)$$

$$\Delta p_{1,2} = \Delta p_1 + \Delta p_2. \quad . \quad (30a)$$

In this manner the pressure distribution can be evaluated for any position of the flame front.

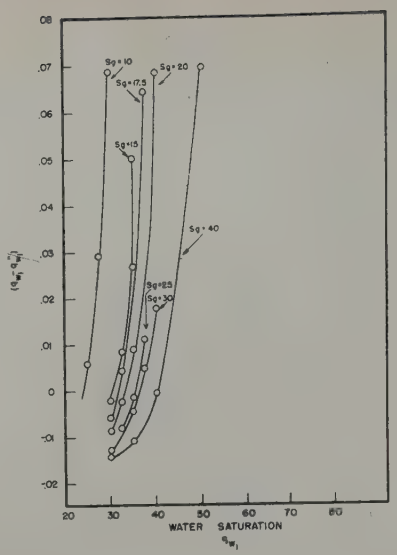

FIG. 1—$(q_{w1} - q''_{w1})$ VS S_{w1} FOR VARIOUS GAS SATURATIONS.

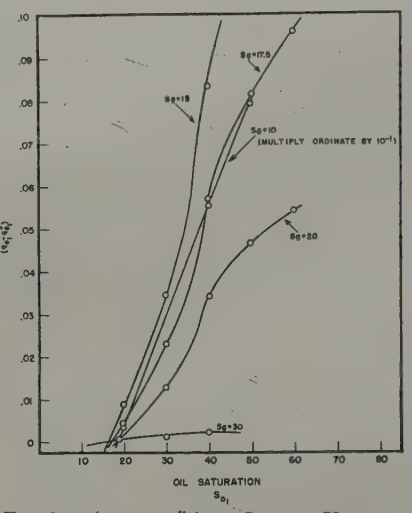

FIG. 2—$(q_{o1} - q''_{o1})$ VS S_{o1} FOR VARIOUS GAS SATURATIONS.

STEP 6—CALCULATING THE FLAME FRONT VELOCITY AND THE FLUID PRODUCTION RATES

Once the pressure distribution has been established, the gas rate in the water bank can be evaluated by

$$q_{g1} = \frac{k_{g1}A\Delta p_1}{\mu_g L_1} \quad . \quad . \quad . \quad (31)$$

Knowing q_{g1}, the velocity of the flame front can be evaluated using Eqs. 4 and 5.

The oil rate through the water bank can also now be evaluated,

$$q_{o1} = \frac{k_{o1}A\Delta p_1}{\mu_o L_1} \quad . \quad . \quad . \quad (32)$$

The rate of fluid production at any time is the rate of oil flow in the zone which is at the end of the system. That is, when the zone of initial conditions is producing, the gas production rates can be calculated using Eqs. 31, 13 and 18. Similarly, oil

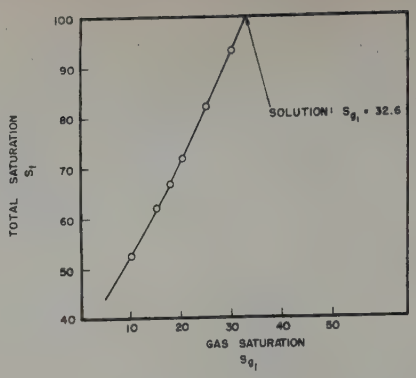

FIG. 3—TOTAL SATURATION VS S_{g1} WHEN $q_{w1} = q''_{o1}$ AND $q_{w1} = q''_{w1}$.

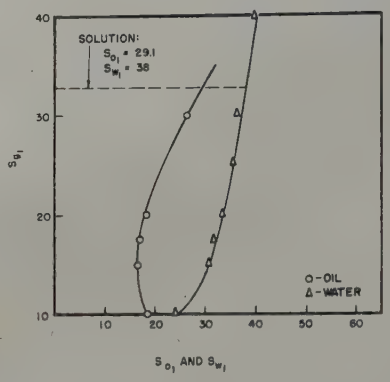

FIG. 4—S_{g1} VS S_{o1} AND S_{w1} WHEN $q_{o1} = q''_{o1}$ and $q_{w1} = q''_{w1}$.

production rates can be evaluated using Eqs. 32, 14 and 19. No water is produced until the water bank has reached the producing end of the system.

During the production of the oil bank the gas production rates can be estimated using Eqs. 31 and 13 and the oil production rates can be evaluated using Eqs. 32 and 14.

When the water bank is producing the gas production rates are evaluated from Eq. 31, the oil production rates from Eq. 1 and the water production rates from Eq. 8.

The producing gas-oil and water-oil ratios at any time can be calculated analogously.

STEP 7—CALCULATING CUMULATIVE PRODUCTION AS A FUNCTION OF TIME

The predicted cumulative production can be calculated by graphically integrating the curve of $1/v_f$ vs distance burned. This gives the time required to burn that distance. Then this time is plotted vs the instantaneous production rate at the distance burned. Graphical integration of this curve results in the cumulative production at any time.

PREDICTED PRODUCTION HISTORIES

The production history of a linear

TABLE 2 — SATURATION DISTRIBUTIONS

Porosity (ϕ)	Injection pressure (P_i, atm)	Oil viscosity (μ_o, cp)	Three-mobile phase zone			Oil bank zone			Initial conditions				
			S_{g1}	S_{o1}	S_{w1}	S_{g2}	S_{o2}	S_{w2}	S_{g3}	S_{o3}	S_{w3}	C	C'
40	2	10	30	25	45	—	—	—	20	60	20	2.095	—
40	5	10	23.5	29.8	48	23.9	56.1	20	20	60	20	1.98	—
40	10	10	19.2	30.3	50.7	19.6	60.4	20	20	60	20	1.89	—
40	51	10	12	32	56	12.5	68.8	20	20	60	20	1.76	8.69
40	101	10	11.5	30.5	58	12	68	20	20	60	20	1.72	10.1
40	1	100	22.9	38.4	38.4	19.2	60.8	20	20	60	20	2.49	—
40	5	100	13.5	47.7	38.9	12.4	67.6	20	20	60	20	2.45	10.3
40	10	100	11.4	49.2	39.4	10.9	69.1	20	20	60	20	2.43	10.0
40	50	100	8.1	52.0	40.5	7.7	72.3	20	20	60	20	2.33	8.10
40	100	100	6.3	54.0	39.7	6.3	73.7	20	20	60	20	2.39	6.90
40	1	1,000	11.1	61.4	27.5	10.5	69.5	20	20	60	20	4.65	9.47
40	5	1,000	8.2	61.6	30.2	7.68	72.3	20	20	60	20	3.68	7.61
40	10	1,000	6.9	62.4	30.7	6.18	73.8	20	20	60	20	3.56	6.98
40	51	1,000	3.7	65.3	31	3.5	76.5	20	20	60	20	3.49	5.97
40	101	1,000	3.4	66.8	29.8	3.0	77.0	20	20	60	20	3.79	5.86
30	5	10	26.6	26.3	47.3	26.8	53.2	20	20	60	20	2.15	—
30	11	10	20.8	28.5	50.7	21.1	58.9	20	20	60	20	2.02	—
30	1	100	25.5	37.4	37.1	21.9	58.1	20	20	60	20	2.84	—
30	5	100	15.8	44.7	39.9	14.2	65.8	20	20	60	20	2.58	10.2
30	11	100	11.6	45.9	42.5	11.9	68.1	20	20	60	20	2.39	9.91
30	6	1,000	8.1	60.2	31.7	8.8	71.2	20	20	60	20	3.68	8.04
30	11	1,000	7.0	61.9	31.1	8.6	71.4	20	20	60	20	3.83	7.76
20	5	10	32.5	19.6	48.2	30.2	49.8	20	20	60	20	2.40	—
20	11	10	26.7	22.5	50.8	24.2	55.8	20	20	60	20	2.29	—
20	1	100	32.6	29.1	38.0	24.1	55.9	20	20	60	20	3.20	—
20	5	100	20.4	40.0	41.0	15.5	64.5	20	20	60	20	2.89	12.7
20	11	100	12.9	47.0	40.1	13.3	66.7	20	20	60	20	2.97	10.9
20	6	1,000	13.0	49	38	9.0	71.0	20	20	60	20	3.2	9.19
20	11	1,000	8.75	58.6	32.7	7.5	72.5	20	20	60	20	4.12	8.61

system for several values of the controlling parameters has been calculated. The following values were assumed.

Length	100 ft
Area	1 ft²
Porosity	40 per cent
Absolute permeability	10 darcies
Injection pressure	100 atm
Producing pressure	1 atm

The relative permeability characteristics previously described were assumed to be valid. Figs. 6 through 8 show the results for oils exhibiting viscosities at reservoir temperatures of 100, 500 and 1,000 cp, respectively.

The velocity of movement of the combustion zone decreases with increasing oil viscosity. For the specific cases considered, the time required to burn completely through the system was slightly less than five days for the 100-cp oil, a little over 19 days for the 500-cp oil and almost 26 days for the 1,000-cp oil.

The production data are shown as rates; this type of plot shows clearly the arrival of the banks. After water production commences the WOR is constant in each case but decreases with increasing oil viscosity from about 0.973 for the 100-cp oil to about 0.708 for the 1,000-cp oil.

The general pattern of the producing gas-oil ratio, R, is the same in each case. That is, it is high until the arrival of the oil bank when it drops sharply before increasing again after the arrival of the water bank. The numerical value of R during the production of each of the zones depends upon the oil viscosity. However, the cumulative gas-oil ratio, R_p, for each case is the same — about 6,500 scf/bbl. This figure can be obtained on the basis of heat requirements alone.

At any porosity there is a definite mass of rock which must be heated to the peak temperature. To achieve this temperature a portion of the oil in place must be burned. That oil not burned will be produced. The gas required is the amount of air necessary to burn the fraction of oil consumed. The graphs in Fig. 6 through 8 are for systems of 40 per cent porosity at initial oil saturations of 60 per cent V_p. The cumulative injected gas-produced oil ratio (R_{pi}) obtained for this system is about 6,500 scf/bbl.

The R_{pi} and WOR will change as the porosity changes. As the porosity decreases there is more rock to heat but less oil present in a cubic foot of the rock. Thus, more of the available oil must be burned to supply the heat. In addition, the higher oil consumption requires that additional oxygen be injected. Hence the R_{pi} will increase sharply as the porosity decreases. The extent to which this occurs can be estimated solely on the basis of heat requirements. This has been done for an oil saturation of 60 per cent V_p and the results are shown graphically in Fig. 9. The R_{pi} increases rapidly at the lower porosities; below a limiting porosity a combustion front cannot be propagated.

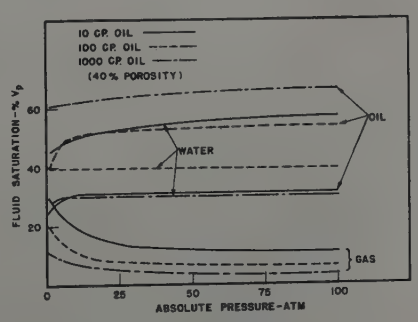

FIG. 5 — EFFECT OF PRESSURE AND OIL VISCOSITY ON FLUID SATURATIONS IN WATER BANK.

As a result of the larger amount of oil that is consumed at lower porosities, more water of combustion will be formed. Therefore, the WOR will also increase with a decrease in porosity.

EXPERIMENTAL PROCEDURE AND EQUIPMENT

Several experiments have been performed in the laboratory to assess these calculations. The injected air was passed through a drying column before it entered the test cell. The product liquids were measured volumetrically and the product gases by a wet-test meter. The effluent gas stream passed first through an ice bath and then through the wet-test meter.

The test cell was designed as shown in Fig. 10. The cell was constructed of 0.040-in. stainless steel with an inside diameter of 2.875 in. and was wrapped with 1/32 in. of mica. Around the mica was placed 3/16 in. of asbestos millboard. All this was enclosed in a ⅜-in. ceramic heater-form. Two sets of open thermocouple wells were placed longitudinally along the tube every 3 in. and 180° apart. The wells were so designed that sheathed thermocouples could be inserted through the wells and positioned along the center line of the cell. Of each set of diametrically opposed thermocouples, one was used for recording the temperature on a recording potentiometer and the other was part of the heater control system.

Helices of resistance wire were

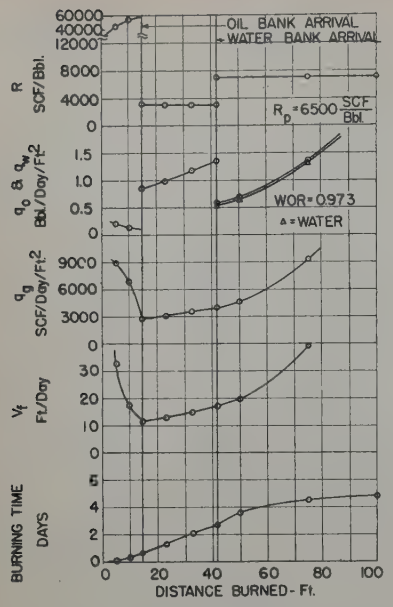

FIG. 6—PRODUCTION HISTORY FOR 100-CP OIL. $\phi = 40$ PER CENT, $k = 10$ DARCIES, $p_i = 100$ ATM, $\Delta P = 99$ ATM, AND $L = 100$ FT.

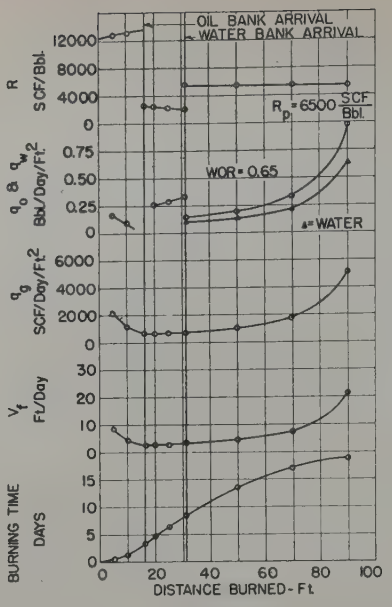

FIG. 7—PRODUCTION HISTORY FOR 500-CP OIL. $\phi = 40$ PER CENT, $k = 10$ DARCIES, $p_i = 100$ ATM, $\Delta P = 99$ ATM, AND $L = 10$ FT.

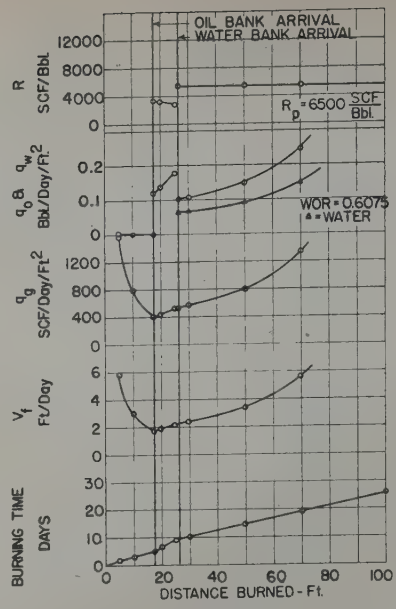

FIG. 8—PRODUCTION HISTORY FOR 1,000-CP OIL. $\phi = 40$ PER CENT, $k = 10$ DARCIES, $p_i = 10$ ATM, $\Delta P = 99$ ATM, AND $L = 100$ FT.

wrapped on the heater-form so that their heating region was 3 in. of tube length. The heater straddled the thermocouple wells. Another set of thermocouples was placed at 90° to those previously mentioned and positioned against a 1-in. square of stainless steel located on the asbestos millboard just under the heater-form. These thermocouples bucked those positioned along the center line through a relay. The relay controlled the heaters. In operation the heaters would come on if the temperature along the center line was 1.5 to 2°F higher than the temperature under the heater-form. The heater would remain on until the differential was less than this. Another series of thermocouples was placed alongside those positioned under the heater-form to record this temperature.

All the experimental work has been done using an unconsolidated sand. This sand is made by crushing Berea sandstone and is available commercially (Cleveland Quarries Co., Amherst, Ohio). The sand exhibits apparent particle sizes from less than 200 mesh to larger than 18 mesh.

In the early experiments the tubes were initially packed to contain four distinct zones. These were a region containing coked sand and charcoal representing the burned-out area and used as fuel to start combustion, a water bank, an oil bank and a region representing the zone of initial conditions. In setting up these zones it was assumed that the combustion zone had advanced 10 cm. With this assumption it was possible to calculate the lengths of the water bank and the oil bank because the theory predicts the lengths of these zones relative to the distance burned. It had been previously established that, by carefully tamping a mixture of oil, water and crushed Berea sandstone into the tubes, a porosity of about 37 per cent could be obtained with an absolute permeability of about 10 darcies. Hence, in setting up the experiments sufficient oil, water and sand were mixed to give the desired length of each zone. The ratio of oil and water to sand were such that the saturations predicted by the method would be obtained in each zone. The water and sand were first mixed and the oil then added to this mixture. Combustion was initiated by bringing the charcoal to a glow with a Bunsen flame and then starting air injection. During this ignition phase, all effluent gases were produced through a thermowell at the interface between the water bank and the coked sand. When the thermocouple at this interface indicated a peak temperature, the end of the tube was opened and the exhaust gases directed through the entire tube.

In the later experiments the cells were packed at the uniform saturations existing prior to combustion and ignition was accomplished as previously described.

EXPERIMENTAL RESULTS

The general features of the bank concept have been verified by the numerous tests conducted. Early fears were that the oversimplified theory would rule out any experimental verification. However, the observation of distinct saturation banks and the validity of the production rate predictions have encouraged further work on both theory and experiment.

Two factors of much concern in the empirical check of the theory were (1) the use of three-phase relative permeability data from consolidated sand to check the combustion performance in unconsolidated sand and (2) the pronounced thermal effect downstream from the combustion zone.

THREE-PHASE RELATIVE PERMEABILITY

In order to make the numerical prediction of production performance, it was necessary to have three-phase relative permeability information in the region of low gas saturations. Published data on three-phase behavior are markedly scarce and particularly so for this saturation region. The three-phase results of Corey[6] *et al*, provided data in the region of low gas saturation but only for consolidated Berea sand. In lieu of other data these were used while efforts were continued to provide three-phase flow information for the actual crushed Berea sand used in the combustion tests.

The sensitivity of the prediction to the three-phase relative permeability was investigated. Since three-phase flow behavior is extremely difficult to

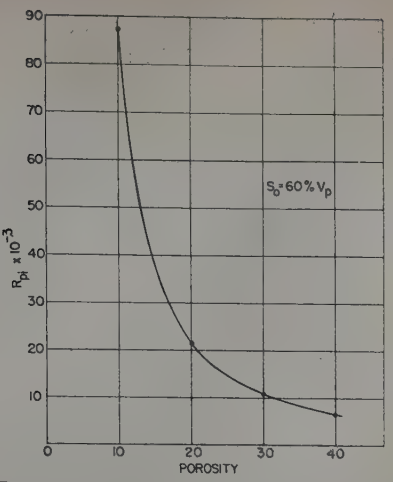

FIG. 9—CUMULATIVE INJECTED AIR-PRODUCED OIL RATIO AS A FUNCTION OF POROSITY FOR BURNING AT 1,000°F ABOVE RESERVOIR TEMPERATURE.

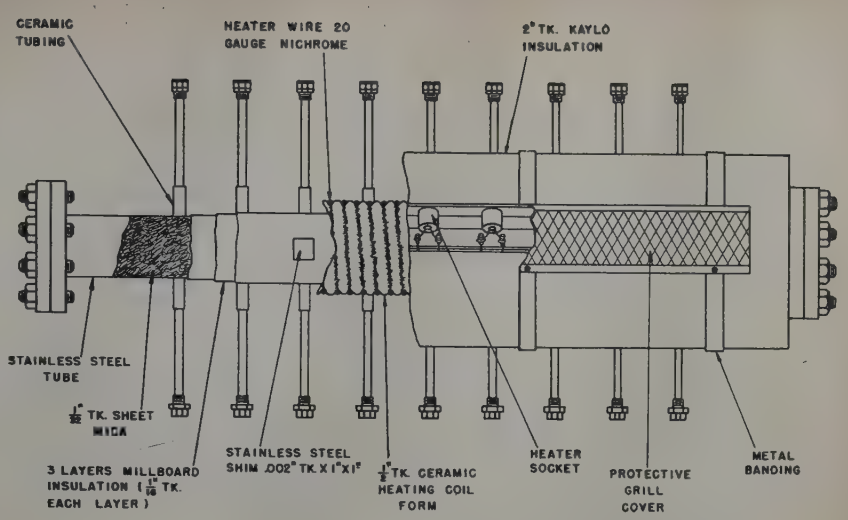
CERAMIC TUBING
HEATER WIRE 20 GAUGE NICHROME
2" TK. KAYLO INSULATION
STAINLESS STEEL TUBE
1/16" TK. SHEET MICA
3 LAYERS MILLBOARD INSULATION (1/16" TK. EACH LAYER)
STAINLESS STEEL SHIM .002" TK. X 1" X 1"
1/4" TK. CERAMIC HEATING COIL FORM
HEATER SOCKET
PROTECTIVE GRILL COVER
METAL BANDING

FIG. 10—DETAIL OF COMBUSTION TUBE ASSEMBLY.

measure on unconsolidated sand, the method of Corey[6,7] was used to predict the three-phase flow behavior of a system of packed spheres from the data of Wyllie and Gregory.[8] The saturations which must exist in the water and oil banks for this pack are shown in Table 3 along with those computed for like combustion conditions using the relative permeability behavior for consolidated Berea sand.

These values probably bracket the range of three-phase flow conditions which might be experienced in practice, the one set being characteristic of a highly consolidated sand and the other an extreme example of unconsolidated material.

Early in the history of the experimental combustion work it became evident that, during the period of production not dominated by thermal effects, the observed production rates were very close to those predicted using the three-phase behavior of consolidated Berea sand. This rather surprising occurrence has since been partially explained by study of the capillary pressure and relative permeability characteristics of the crushed Berea sand used in the combustion tests. Both tests showed the character of the crushed Berea to be much like that of the consolidated Berea. This is illustrated by Fig. 11 which shows both the capillary pressure and the relative permeability to gas for the crushed and consolidated sand. Further exploration of the flow properties of the crushed sand is in progress since it is such a crucial item in the performance prediction.

THERMAL EFFECTS AHEAD OF COMBUSTION ZONE

To force a manageable solution, the temperature downstream from the combustion zone was initially assumed to be the original reservoir temperature and the combustion tube or reservoir was assumed to be adiabatic. These two incompatible conditions were troublesome in attempting to check the theory experimentally. The second requirement has been fulfilled reasonably well by the equipment used. However, it now appears mandatory that the downstream temperature effect be incorporated in the theory and it certainly is desirable that it be accounted for in field predictions.

Predictions have been made of the thermal effect to be expected for linear and radial flow systems when a negligible contribution by conduction was assumed, but heat loss was taken into account. Although for a radial system of reservoir dimensions the heated zone downstream may be virtually negligible, it becomes a prohibitively large fraction of the total length of a laboratory system. For example, at a practical rate of advance a linear reservoir system which had burned for 3 ft would result in a significantly heated zone downstream which would be 4 ft in length. In the experimental work a region was observed ahead of the combustion front in which the temperature approached the temperature of condensed steam. This "steam plateau" observed by others[3] seemed to have little effect on the producing rates until it neared the production end of the experimental combustion tube. The high resistance to flow of the viscous oil in the oil bank (which remained at ambient temperature during the test) dominated the production performance until the water bank arrived at the producing end of the system. Shortly after the arrival of the water bank, the zone of increased temperature neared the end of the tube and the rates of oil, water and gas production increased far beyond the predicted values. Since the total length of the packed tube was only 8.5 ft, the only valid data checking the theory are those obtained during the time the combustion zone traversed the first one-third of the tube. Work is currently in progress to incorporate the downstream temperature increase into the prediction of performance.

Successful combustion tests were made using oils having viscosities of 89, 177 and 500 cp at 85°F. Fig. 12 shows a typical experimental history in terms of production rates vs distance burned. The plot shows the arrival of the oil and water banks and, particularly for the case of oil production rate, good agreement between the observed and predicted values. The arrival of the water bank presages the arrival of the elevated temperature zone at the end of the system. This terminates the dominance of the production history by the oil bank. The sharp increase in observed production rates reflect the breakdown in the agreement between the predicted and observed performance shortly after the arrival of the water bank.

TABLE 3—COMPARISON OF CALCULATED FLUID SATURATIONS USING RELATIVE PERMEABILITY CHARACTERISTICS OF CONSOLIDATED AND UNCONSOLIDATED MATERIAL

Water Bank	Consolidated Berea sand	Unconsolidated glass beads
S_{g1}	11.6	18.4
S_{o1}	51.6	68.8
S_{w1}	36.8	12.8
Oil bank		
S_{g2}	10.9	18.2
S_{o2}	69.1	81.8
S_{w2}	20.0	0
Residual water per cent	20.0	0

Injection pressure = 7 atm
Porosity = 37 per cent
Oil viscosity = 177 cp

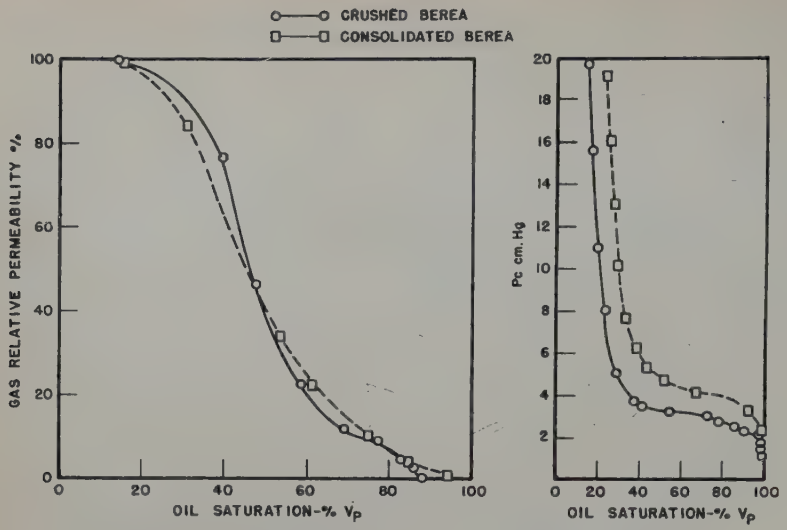

FIG. 11—GAS RELATIVE PERMEABILITY AND CAPILLARY PRESSURE CHARACTERISTICS FOR CONSOLIDATED AND CRUSHED BEREA SANDSTONE.

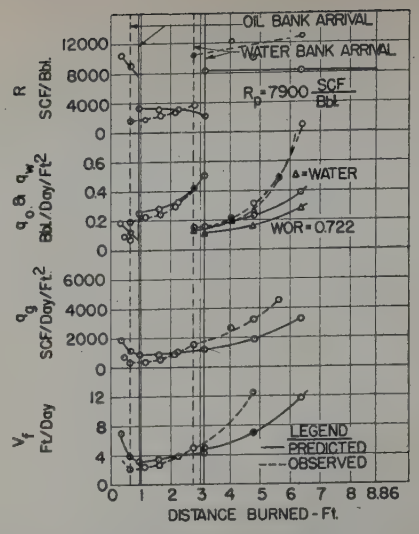

FIG. 12—PREDICTED AND OBSERVED PRODUCTION HISTORY FOR 177-CP OIL. $\phi = 37$ PER CENT, $k = 10$ DARCIES, $p_i = 7$ ATM, $\Delta P = 6$ ATM, AND $L = 8.86$ FT.

The graphic behavior of Fig. 12 was that of a system in which the banks were initially present and based on a burned distance of 10 cm as previously described. Other experiments have been done on systems in which the banks formed spontaneously. This provided support for the bank concept and gave similar checks on the arrival of the oil and water banks and of the oil production rates.

CONCLUSIONS

A method has been proposed whereby oil recovery by underground combustion may be theoretically and empirically predicted if the characteristics of the reservoir rock and the saturations and nature of its contained fluids are known. Initial tests have demonstrated the basic promise of the method of analysis and have shown the direction in which further work must be aimed to improve the performance prediction.

To use the proposed method of evaluating a combustion recovery technique, the following three factors should be better understood.

1. The role of three-phase flow in the prediction must be further evaluated and three-phase flow data must be procured for a number of systems.

2. The effect of the increased temperature zone downstream must be incorporated in the numerical solution of production history to make the experimental verification quantitatively significant.

3. The conversion of the linear performance to pattern performance on a reservoir scale must be effected.

NOMENCLATURE*

C_s = specific heat of sand (0.25 cal/gm °C)

C = ratio of the velocity of the front of the water bank to the velocity of the combustion zone

C' = ratio of the velocity of the front of the oil bank to the velocity of the combustion zone

ΔH_c = heat of combustion of oil (10,500 cal/gm)

k_{gn} = effective gas permeability in Zone n, darcies

k_{ge} = mean effective gas permeability, darcies

L_B = length of burned zone

L_1 = length of water bank

L_2 = length of oil bank

Δp = pressure differential, atm

P_{sc} = pressure at standard conditions, 1 atm

q_{sc} = air rate required for combustion scc/sec

R_{pi} = cumulative injected gas-produced oil ratio

ΔT = difference between peak temperature and initial reservoir temperature (538°C)

μ_o/μ_g = oil-gas viscosity ratio (μ_g = 0.018 cp)

v_f = rate of advance of combustion zone, cm/sec

v_w = velocity of front of water bank, cm/sec

v_o = velocity of front of oil bank, cm/sec

WOR = producing water-oil ratio

ρ_s = density of sand (2.65 gm/cc)

ρ_o = density of oil (0.9 gm/cc)

Subscripts 1, 2 and 3 refer to the water bank, oil bank and zone of initial conditions, respectively.

Double primes refer to fluid rates caused by the advancing combustion zone. No primes are used when the fluid rate is that caused by the pressure gradient imposed by the gas.

*Symbols not included in the following nomenclature can be found in "Letter Symbols for Petroleum Reservoir Engineering and Electric Logging," published in the Oct., 1956 issue of JOURNAL OF PETROLEUM TECHNOLOGY and *Petroleum Transactions* Vol. 207.

REFERENCES

1. Kuhn, C. S. and Koch, R. L.: "In Situ Combustion — Newest Method of Increasing Oil Recovery", *Oil and Gas Jour.* (Aug. 10, 1955) **52**, 92.
2. Grant, B. F. and Szasz, S. E.: "Development of Underground Heat Wave for Oil Recovery", *Trans.* AIME (1954) **201**, 108.
3. Hester, D. V. and Menzie, D. E.: "Development of Subsurface Combustion Drive", *Pet. Engr.* (Nov., 1954) **26**, B82.
4. Garbus, R.: "New Idea in Thermal Oil Recovery", *Pet. Engr.* (April, 1956) **28**, B83.
5. Smith, R. L. and Watson, K. M.: "Oil Recovery Process", U. S. Pat. No. 2,642,943 (June 23, 1953) Sinclair Oil & Gas Co.
6. Corey, A. T., Rathjens, C. H., Henderson, J. H. and Wyllie, M. R. J.: "Three-Phase Relative Permeability", *Trans.* AIME (1956) **207**, 349.
7. Corey, A. T.: "The Interrelation Between Gas and Oil Relative Permeabilities", *Prod. Monthly* (Nov., 1954) **19**, 38.
8. Wyllie, M. R. J. and Gregory, A. R.: "Fluid Flow Through Unconsolidated Porous Aggregates", *Ind. & Eng. Chem.* (1955) **47**, 1379. ★★★

Reservoir Rock Wettability—Its Significance and Evaluation

J. E. BOBEK
JUNIOR MEMBER AIME
C. C. MATTAX
M. O. DENEKAS

JERSEY PRODUCTION RESEARCH CO.
TULSA, OKLA.

ABSTRACT

Investigations in recent years have shown that rock wettability can exert a profound influence on the displacement of oil by water from oil producing reservoirs. Core analyses frequently show oil recoveries from preferentially water-wet rock to be significantly greater than those from preferentially oil-wet rock. Thus, an accurate prediction of water-drive or waterflood oil recovery is dependent on the evaluation of reservoir rock wettability.

Laboratory and field studies have been undertaken to examine and develop methods which may be used to measure rock wettability, to investigate factors which may alter the wettability of reservoir rock, and to determine the wettability of specific reservoirs. It has been found that measurement of the rate and volume of spontaneous imbibition of the wetting phase by a rock is a reliable and reproducible test for semi-quantitative determination of preferential rock wettability. Laboratory tests have shown that the wettability of reservoir rock may depend on both the crude oil composition and the rock type. Field and laboratory tests have indicated that coring fluids and core handling techniques can cause significant changes in the wettability of rock surfaces. However, a few fluids, brine in particular, appear not to affect core wettability and may be used when coring to determine reservoir wettability. Core handling and packing procedures have been developed which preserve core wettability during storage and laboratory testing. The wettability characteristics of six reservoirs have been evaluated by wettability tests performed in the field on fresh cores cut with brine or special water-base muds. The tests indicated that all six reservoirs are water wet; however, the degree differed from one reservoir to another.

Original manuscript received in Society of Petroleum Engineers office Aug. 5, 1957. Revised manuscript received April 1, 1958. Paper presented at 32nd Annual Fall Meeting of Society of Petroleum Engineers in Dallas, Tex., Oct. 6-9, 1957.

Discussion of this and all following technical papers is invited. Discussion in writing (three copies) may be sent to the offices of the *Journal of Petroleum Technology*. Any discussion offered after Dec. 31, 1958, should be in the form of a new paper.

INTRODUCTION

Although surface properties of reservoir rock and interfacial characteristics of rock, crude oil, and water systems have been discussed for many years, the full significance of these properties to the production of oil is still in the process of evaluation. It is known, however, that one surface characteristic—preferential wettability of the reservoir rock—is of paramount importance when the reservoir is being produced by waterflood or water-drive mechanisms.

The importance of rock wettability has been pointed out by several authors[1,2,3,4] who have found that preferentially water-wet cores flood more efficiently than oil-wet cores; that is, more oil is recovered from water-wet cores in the early flooding stages than from oil-wet cores. Other authors[5,6] indicate that waterflood oil recovery from cores of intermediate wettability may be greater than that from either strongly water-wet or strongly oil-wet cores. These recent investigations emphasize that the true wettability of a reservoir must be known before the performance of waterflood or water-drive reservoirs can be accurately evaluated.

When reservoir wettability is to be determined by core analysis, precautions must be taken to maintain the original wettability which can be altered readily during coring[3] and testing.[7] In the coring operation the core may be partially or completely penetrated by the drilling fluid which, if it contains surface active materials, may drastically change the wettability of the core. Also, improper core handling during storage and testing may change its wettability because of evaporation of fluids or exposure to oxygen or surface active contaminants. One purpose of this paper is to discuss methods for obtaining, preserving, and testing cores without altering their original wettability. In addition, the results of wettability tests on fresh and preserved cores from six reservoirs are presented where special precautions were taken to obtain samples without altering their wettability during the coring operation.

[1]Reference given at end of paper.

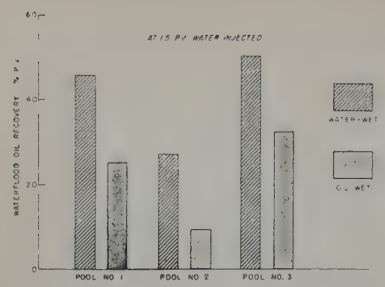

FIG. 1—EFFECT OF WETTABILITY ON PREDICTED FIELD WATERFLOOD BEHAVIOR.

IMPORTANCE OF WETTABILITY

The importance of wettability in oil production can be illustrated by practical examples. Two sets of engineering calculations were made of the waterflood oil recovery behavior of three reservoirs. Both sets accounted for such things as areal pattern efficiency and reservoir stratification. They differed only in that one set of calculations assumed the reservoirs as oil-wet, while the other assumed them water-wet. Calculation of the oil-wet recovery behaviors was based on core analyses of aged, oil-wet cores, while calculation of water-wet oil recovery behaviors was based on tests of cores which had been cleaned by heating at 400°C to render them strongly water wet. Comparisons of the calculated waterflood behaviors for the three reservoirs are shown in Fig. 1. As indicated in Fig. 1, when the pools were assumed water wet, the calculated oil recovery at 1.5 pore volumes of water injected was 1.5 to 2.8 times greater than when the pools were assumed oil wet. If any of the three reservoirs considered in Fig. 1 were water wet, water flooding could be a very profitable process. However, if the reservoirs were oil wet, a water flood would be less profitable for Pools 1 and 3 and would probably be uneconomic for Pool 2. In particular, Pool 2 exemplifies a reservoir for which the selection of the best producing mechanism could very well be governed by the preferential wettability of the reservoir, if its wettability were known with some certainty.

MEASUREMENT OF WETTABILITY

The term "preferential wettability" as it is applied to a rock surface and the two liquid phases—water and oil—may be defined qualitatively by considering the behavior of the water and oil when they are placed in contact on the rock surface. Thus, if water tends to displace oil from the rock surface, the rock will be termed preferentially water wet. Similarly, if oil tends to displace the water, the rock will be termed preferentially oil wet. (The shorter terms "water wet" and "oil wet" will be used hereafter to indicate "preferentially water wet" and "preferentially oil wet", respectively.)

Wettability has been defined frequently in terms of the contact angle between the fluid interface and the solid surface. However, in porous media a direct measurement of contact angles is impractical, if not impossible. Furthermore, in porous media wettability and its effects on fluid flow behavior are manifested primarily through the capillary pressure-fluid saturation relationship. Thus, it is believed that the most useful methods for measuring core wettabilities are those based on the observation of different types of capillary-pressure phenomena.

CONSOLIDATED CORES

At present, imbibition tests seem the most satisfactory quick method for evaluating core wettability. Displacement of non-wetting fluid from a core sample by spontaneous invasion, or "imbibition," of the wetting fluid is a process which depends primarily upon capillary pressure as a driving force. (In turn, the capillary pressure is proportional to the cosine of the contact angle.)

Gatenby and Marsden[8] have shown that rock wettabilities determined by imbibition tests agree qualitatively

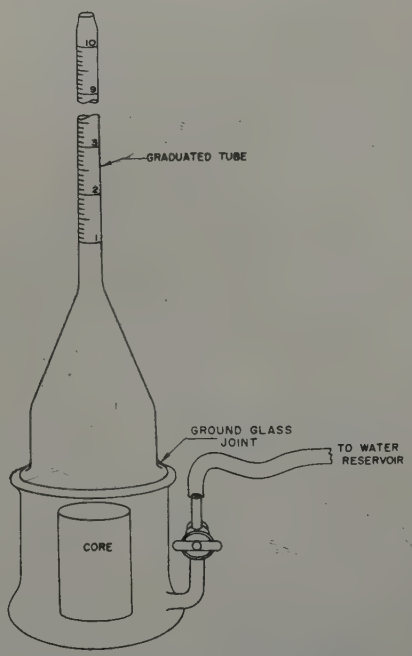

FIG. 2—APPARATUS FOR DETERMINATION OF IMBIBITION RATES (WATER-WET CORES).

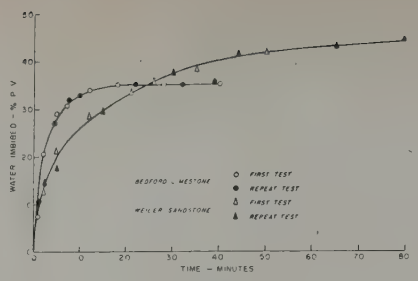

FIG. 3—REPRODUCIBILITY OF IMBIBITION DATA.

with wettabilities determined by capillary-pressure measurements. However, as yet a theoretical correlation between imbibition and contact angle of wetting has not been defined.

The imbibition behavior of a rock depends to some extent on the permeability of the rock, the viscosities of the imbibing and displaced fluids, and the initial water and oil saturations of the rock. It has been shown experimentally that these factors exert much less influence on imbibition behavior than does the preferential wettability of the imbibing rock. Furthermore, in practice, the effects on imbibition of variations in the properties of the rock-fluid system are taken into account since imbibition data are usually analyzed by comparing the behavior of the rock sample of unknown wettability with "reference" imbibition data. Reference imbibition data are obtained on the same rock sample after it has been cleaned (to make it completely water wet) and saturated with a refined white oil of the same viscosity and at the same saturation as the oil initially contained by the rock.

The volumetric apparatus used in water imbibition tests in these studies is shown in Fig. 2. Moore and Slobod[5] have described a similar apparatus. For oil imbibition tests the apparatus is inverted.

Data which show that the imbibition process is reproducible are shown in Fig. 3. These curves are the results of repeated imbibition tests on an outcrop limestone core and an outcrop sandstone core using a purified white oil and distilled water. The cores were heated at 400°C for 24 hours prior to each test to remove organic materials from the core surfaces. The reproducibility of the data for each core indicates the validity of heating as a cleaning process to obtain a surface with reproducible wetting characteristics and demonstrates the precision of the imbibition test technique as a means of determining preferential wettability.

Good precision may be obtained

also in imbibition tests on cores which imbibe less readily than the muffled cores. These tests are discussed in the Rock-Crude Oil Interaction section of this paper.

Unconsolidated Cores

The wettability of unconsolidated material may be determined qualitatively by microscopic observation of fluid movement in the sand. This method has proved especially valuable for well-site testing. To test for water wettability, a thin layer of sand is spread on a microscope slide. Oil saturation is increased by adding a refined white oil of proper viscosity. Droplets of water are then placed on the surface of the sand, and movement of the fluids is observed. If the water moves readily into the sand as a bank and displaces oil from the surface of the sand grains, the sample is water wet. In this test it is also helpful to observe the shape and location of the residual crude oil in the water-invaded region. If the sand is water wet, the oil will form spherical droplets, indicating that the oil is the non-wetting phase. A similar procedure is used to test for oil wettability.

Waterflooding tests may be used to confirm the wettability of unconsolidated sand samples. The ratio of the permeability to water in the presence of residual oil to the permeability to oil in the presence of connate water will be normally less than 0.3 in water-wet media, but will be near unity in oil-wet media. Thus, by measuring the permeability of a core before and after water flooding, its wettability can be determined qualitatively.

ROCK-CRUDE OIL INTERACTION

The inorganic constituents of reservoir rock are generally considered to be strongly water wet. Imbibition tests using clean reservoir rock and refined oils have also demonstrated this (Fig. 3). If, however, all reservoir core samples were strongly water wet, no wettability problem would be involved in reservoir work. Two obvious questions, therefore, are: (1) do variations in wettability occur in reservoirs? and (2) if so, how can they be explained?

As a relatively simple approach to a study of the possible variations in the wettability of reservoir rocks, seven natural, but cleaned, rock samples were saturated completely, under vacuum, with eight different crude oils—making a total of 56 rock-crude oil combinations. A representative cross section of results of imbibition wettability tests on these combinations is shown in Table 1. Here, a strongly water-wet core is indicated by WWW; a moderately water-wet core by WW; a slightly water-wet core by W; a neutral core by N and a slightly oil-wet core by O. The assignment of these semi-quantitative wettability designations to specific rock-crude oil systems is based on the relative amount of imbibition and the amount of reduction in the slope of the crude oil imbibition curve from that obtained using a purified white oil. Imbibition data using crude oils were found to be nearly as reproducible as those obtained with refined oils.

The most obvious conclusion to be drawn from these data is that different degrees of wettability can exist for various core-crude systems. It will be noted also that, in general, the wettability of sandstone is more readily altered by crude oil than that of limestone. More specifically: (1) the same core material can be affected differently by different crudes and (2) the same crude oil can cause different wettability effects in various cores. Therefore, apparently the core and the crude oil interact in some manner which causes a change in the wetting properties of the core matrix.

Three factors which might cause the changes in imbibition observed in the rock-crude oil exposure tests are: (1) plugging by agglomerates from the crude oil, (2) film formation at the oil-water interface, or (3) adsorption of crude oil onto the rock surface. Plugging should be caused largely by the crude oil alone, irrespective of the mineral in contact with it. Film formation at oil-water interfaces essentially should be caused only by the crude oil when placed in contact with water. Since the same crude oil behaves differently with various rocks, the mechanical effects of plugging and film formation do not explain the observed variations. Adsorption of components from the crude oil onto the mineral surface seems the most plausible explanation of the observed imbibition changes. Later material to be presented in this paper also indicates that the formation of and changes in the organic layer adsorbed on the rock surfaces may be the major cause of wettability changes.

To investigate further the cause of changes in wettability, a study has been made of the effect on rock wettability of specific fractions of crude oils. These fractions were obtained by a number of techniques such as distillation, chromatography and deasphalting. Each fraction was diluted in a neutral solvent and then used to saturate a core. After the core had been exposed to this solution, its imbibition rate was determined. Evidence to date indicates that components in the higher molecular weight ranges, and also probably polar in nature, decrease water wettability of minerals most strongly. Small fractions, on the order of 2 per cent of some crudes, decreased the wettability of minerals appreciably. Adsorption seems the most likely process to explain this effect.

TABLE I—EFFECT OF CRUDE OILS ON ROCK WETTABILITY

Core Type	Formation	Abqaiq	Bradford	Elk Basin	Loudon	LL-453
Limestone	Abqaiq	WW	N	W	WW	N
	Bedford outcrop	WWW	WW	WWW	WW	N
Sandstone	LL-370	N	N	N	W	N
	LL-453	O	N	N	N	N

INSTABILITY OF ROCK WETTABILITY

The results of waterflood and related tests on core material are often inconsistent both with the results of tests on other cores from the same reservoir and with the behavior which might be expected on the basis of the performance history of the reservoir. These inconsistencies can often be traced to changes in the wettability of the core material before or during core tests. These changes may occur while the well is being cored, during core storage, or while handling the core material. In coring, for example, penetration of the core by some drilling fluid filtrates has been shown to alter drastically its wettability.

While Coring

A series of tests was performed with three commonly used drilling muds to determine their effects on core wettability. The tests were run on strongly water-wet core samples. Prior to exposure to the drilling fluid filtrates, reference water imbibition data were obtained on the cores using refined oil and distilled water. After exposure of the cores to the filtrates, the water saturation in the cores was reduced by flushing with refined oil and the imbibition behavior of the cores was again observed. The results of tests with the three drilling muds are shown in Fig. 4. The treated

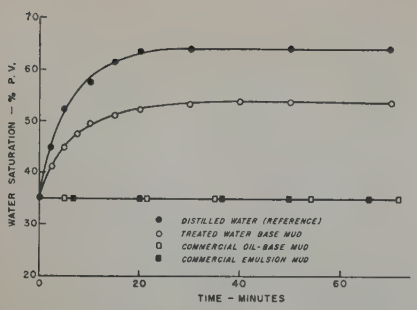

FIG. 4—IMBIBITION CURVES SHOWING ADVERSE EFFECTS OF COMMONLY USED DRILLING FLUIDS ON ROCK WETTABILITY.

water-base mud, which was sampled from the surface returns in the drilling of a well approximately 5,000 ft in depth, contained bentonite, caustic, lime, and quebracho as well as lost circulation material and natural muds. This fluid reduced the water wettability of the test plug, although the rock would still be considered moderately water wet. On the other hand, in laboratory tests both the commercial oil-base and the oil-emulsion muds completely inhibited water imbibition. Subsequent oil imbibition tests indicated that the rock exposed to the emulsion mud was neutral in wettability and that oil-base mud caused complete inversion from water-wet to oil-wet behavior. It is apparent that careful selection and stringent control of coring fluids are necessary if the core is to have the same wettability as the reservoir rock.

It would also seem that consideration should be given to possible wettability changes that may arise from temperature and pressure reduction which usually accompany removal of the rock sample from the reservoir. To our knowledge, no conclusive evidence has been obtained which would clarify this topic.

While Handling and Testing

Wettability changes in core material after it has been recovered at the surface are also frequently observed.[7] Such changes are usually due to weathering during long-term storage in an oxidizing atmosphere or to "drying out" of the core, in which cases some non-volatile components of the residual crude tend to deposit on the pore walls and the core frequently becomes oil wet. The effects of weathering can best be illustrated by comparing the wettability of weathered cores with that of fresh-cut cores. This comparison is discussed later under the heading "Well-Site Tests".

In the laboratory as well, the rock may be exposed to an environment which alters its wettability. The use of fluids which contain surface active materials is a frequent source of trouble. Tests have indicated that reasonably good quality light oils in the C_{10} to C_{12} range may contain enough polar impurities to reduce significantly the wettability of a water-wet rock. It has also been observed that the use of solvent extraction procedures to remove crude oil from a core almost invariably changes its wettability. This effect has been observed by others and offers a serious objection to the use of extractive techniques preliminary to core tests whose results are dependent on the wettability of the rock.

The use of a flooding cell in which a rubber sleeve is in direct contact with the test core is not to be recommended since the core may be contaminated by oil soluble components of the rubber.

These examples of changes in core wettability which result from the use of established routines, reagents, and equipment indicate the sensitivity of the core surface properties to test conditions. The need for careful control of the environment of the core through each stage of its recovery and use should be emphasized. In many instances, to obtain and maintain a carefully preserved sample may require but little more effort than is usually expended on routine core samples.

PRESERVATION OF CORE WETTABILITY

While Coring

One of the most challenging problems encountered in attempts to preserve the wettability of core material is selecting and controlling the composition of the drilling fluid used in the coring operation. The sizeable effects on core wettability of many commonly used muds (Fig. 4) have made it necessary to conduct experimental tests on a large number of drilling fluids and fluid components in order to select coring fluids with minimum wettability effects which, at the same time, are practical from the standpoint of current drilling practice.

The results obtained with oil-base and oil-emulsion muds discouraged further investigation of these mud types. Thus, this investigation was primarily concerned with an evaluation of water-base muds. Furthermore, since a large percentage of the more frequently used muds contain, in various combinations, a relatively limited number of component materials, it was desirable to concentrate most effort on a study of individual drilling fluid components. These components may be classed as colloids, thinners, weighting agents, and lost circulation materials. Suitable studies on a limited number of materials in each of the above classes should yield information allowing the formulation of non-contaminating drilling fluids from non-contaminating components.

The components selected for testing were dissolved in or leached with distilled water. The concentrations of solutions of the reasonably soluble components were adjusted to duplicate those usually encountered in field practice. Subsequently, a test core of known wettability was completely saturated with the aqueous solution. The saturation of the aqueous phase was reduced by flushing with refined oil and the water imbibition behavior of the core was observed.

Results representative of those obtained in tests of the drilling fluid components are presented in Table 2. These data were obtained in tests on water-wet limestone and sandstone and on oil-wet sandstone. It will be noted that rock salt, carboxymethylcellulose (CMC), bentonite, and barite had no effect on the wettability of the strongly water-wet cores. Also, lime had no effect on the limestone core and but slightly increased the water-wettability of the sandstone core. The other components which are shown alter wettability of either the water-wet sandstone or the water-wet limestone. Hence, these are not recommended for use in coring to obtain samples for use in the evaluation of wettability.

Tests on water-wet cores alone cannot yield sufficient information to allow the selection of a proper coring fluid for use in evaluating reservoir wettability. In the choice of a coring mud one must consider that either water-wet or oil-wet behavior of the reservoir is possible. Consequently, drilling mud components were also tested for effects on wettability of oil-wet rocks. Only those components which did not decrease wettability of water-wet cores were selected for tests on oil-wet cores. The selection of the oil-wet system, however, was somewhat arbitrary because not enough is known about naturally occurring oil-wet systems to synthesize them properly in the laboratory. In these tests the system chosen was muffled Weiler sandstone exposed to Elk Basin crude oil. While there is some question as to appli-

cability of results obtained on this system to all coring operations, the results give considerable insight into the action of drilling fluids on oil-wet rock surfaces.

The sandstone cores were saturated with the crude, and after standing one day were flushed with the filtered solutions of mud components. They were immersed in oil to determine if the degree of oil wettability had been altered. Cores flushed with brine were found to remain oil wet whereas those flushed with bentonite, CMC, and lime did not imbibe oil. These latter cores were then flushed with oil to reduce the water saturation and were immersed in water. The cores consistently imbibed water indicating that they were no longer oil wet but water wet (see Table 2). Thus, the oil wettability of the rock had been completely reversed by the lime, CMC, and bentonite solutions.

A limited number of additional experiments using bentonite solutions of controlled basicity have indicated that the wettability of the oil-wet system is not reversed if the solution pH is lowered into the near neutral or acidic range.

From these experiments one can conclude that ideally, brine (or water) should be used in coring a reservoir to obtain samples for reservoir wettability evaluation. However, in cases where the pH of the fluids can be properly controlled, bentonite muds can be used.

Control of contamination in muds during a field coring operation usually requires cleaning of surface lines, tanks, pumps and casing before the coring begins. Most of the cleaning may be satisfactorily accomplished by flushing the system with several volumes of water or brine, although special cleaning of the mud system may be required if large residues of oil-base or emulsion-base muds persist. That control of mud contamination is practical has been demonstrated in several coring operations which will be discussed later. The results of wettability tests on the muds used in one of the coring operations are shown in Fig. 5. The mud samples tested were taken from

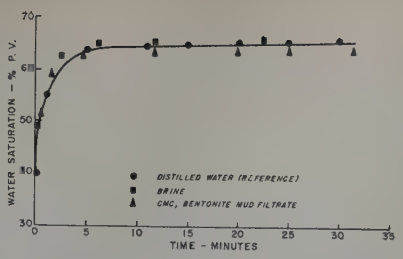

FIG. 5 — ROCK WETTABILITY UNALTERED BY SELECTED DRILLING FLUIDS.

the surface returns in coring to obtain wettability samples of an oil-producing limestone formation. The imbibition data shown were obtained on limestone test cores exposed to the mud samples. It will be noted that the test data are quite close to reference data obtained on the same test cores using pure liquids. Thus, these two drilling fluids probably did not alter the wettability of the reservoir core.

DURING STORAGE AND TESTING

The solution of problems encountered in preservation of the core wettability after recovery of the core at the surface is considerably less difficult than the solution of those involved in coring. It has been found that suitable packing of core material immediately after removal from the barrel will prevent changes in wettability for several months. Two methods of packing have been found satisfactory. In one, the core material is imersed in deoxygenated formation brine or suitable synthetic brine, contained in glass-lined steel tubes or in epoxy resin or polyester plastic tubes which can be sealed against content leakage and against the entrance of oxygen. In the other packing procedure, the cores are wrapped in Saran or polyethylene film and aluminum foil. Subsequently, the package is coated with a thick layer of paraffin. By either procedure, the cores are protected from oxygen and prevented from drying out.

Both packing procedures have been used successfully for storage of core material. Controlled water imbibition tests on samples from two pools indicated that when properly stored, no significant change in wettability occurred over an eight-month period. Test data on 18 fresh and 16 preserved samples from each pool are presented in Fig. 6 ("fresh" refers to well-site core tests). Additional evidence confirming the utility of the two packing procedures will be presented in the following section.

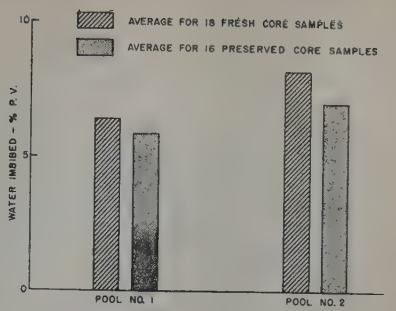

FIG. 6—EFFECT OF STORAGE ON CORE WETTABILITY.

Precautions which should be taken in laboratory handling and testing of core material require little discussion. Contamination from flooding cells containing rubber sleeves may be prevented by using an innerliner of tubular polyethylene film. Although the film necessitates the use of somewhat greater sleeve pressures, it in no way interferes with the normal cell operation. Additional precautions relate, in the main, to control of the purity of fluids to which the cores are exposed. Materials of questionable purity should be tested by interfacial tension measurement or, better, by investigation of possible effects of materials on the imbibition behavior of reference core material. If impurities are present, they can usually be removed by passing the contaminated fluid through an adsorption column containing activated alumina.

WELL-SITE TESTS

The most important practical objective of this program has been to develop and apply methods for determining reservoir wettability. To date, the wettabilities of six reservoirs have been determined by measurements on core material obtained from the reservoirs under carefully controlled conditions. Information gained from laboratory studies concerning wettability testing techniques, coring fluid composition and methods of core storage already discussed were applied in these special coring operations. The results of wettability tests on fresh and preserved cores from these reservoirs are given in Table 3.

Well-site wettability tests were performed on fresh core samples from each of the six reservoirs. The cores

TABLE 2—EFFECTS OF WATER-BASE MUD COMPONENTS ON THE WETTABILITY OF OIL-WET OR WATER-WET CORES

Component	Wettability of test cores after exposure to filtrate		
	Water-wet limestone	Water-wet sandstone	Oil-wet sandstone
Rock-salt	No change	No change	No change
Starch	Slightly less water-wet	Slightly less water-wet	----------
CMC	No change	No change	Water-wet
Bentonite	No change	No change	Water-wet
Tetrasodium pyrophosphate	No change	Less water-wet	----------
Calcium lignosulfonate	No change	Less water-wet	----------
Lime	No change	Slightly more water-wet	Water-wet
Barite	No change	No change	----------

TABLE 3—WETTABILITY OF FRESH, PRESERVED AND WEATHERED CORES

Reservoir	Formation	Coring fluid	Wettability		
			Fresh*	Preserved	Weathered
1	Limestone	Brine	W	W	----
		Bentonite-CMC-water	W	W	----
		Water-base mud	----	----	0
		Oil-base mud	----	0	----
2	Limestone	Brine	W	W	----
		Bentonite-CMC-water	W	W	----
		Water-base mud	----	----	N
3	Unconsolidated sand	Bentonite-CMC-water	WW†	WW	0
		Oil-base mud	----	N	0
4	Unconsolidated sand	Bentonite-water	WW†	WW	0
5	Sandstone	Bentonite-water	W	W	----
		Water-base mud	----	----	W
6	Sandstone	Brine	WW	WW	----

*Well-site test results
†Estimated from microscopic wettability tests

used in the well-site tests were obtained by coring the formation with brine or with a water-base mud whose composition was controlled to minimize the possibility of altering rock wettability during the coring operation (see Column 3, Table 3). Of the reservoirs in which special coring operations were undertaken to determine reservoir wettability, two were limestone reservoirs, two unconsolidated sand reservoirs, and two consolidated sandstone reservoirs. The wettability of the consolidated cores was determined by the imbibition test while the wettability of the unconsolidated sand was determined by microscopic examination and confirmed by waterflooding tests. As indicated in Table 3, core samples from all six reservoirs were water wet, but to varying degrees.

Fresh core material from each of the six reservoirs was preserved by methods previously discussed, and subsequent laboratory tests revealed that they had remained water wet (Column 5, Table 3). This is further confirmation of the reliability of the core packaging methods.

Table 3 also lists the results of laboratory tests on preserved samples from two wells cut with oil-base mud. These cores were found to be either neutral or oil wet. Comparison of these results with tests of fresh cores taken from the same reservoirs under controlled conditions further points out the hazards of coring with oil-base mud when the primary objective is to determine reservoir wettability.

The last column in Table 3 lists test results of weathered cores from five of the reservoirs. Comparing these results with those obtained on fresh and preserved core samples from the same reservoirs showed that in all but one case the weathered cores underwent a major change in wettability. Therefore, weathered cores should not be used in tests to determine reservoir wettability.

PRACTICAL APPLICATIONS

A program may be outlined which will greatly increase the probability that core samples possessing a wettability representative of that in the reservoir will be obtained. The first step is to core the formation with a fluid whose composition is controlled to minimize contamination which could change rock wettability. The best coring fluid from the wettability standpoint is brine or fresh water. The original drilling mud should be completely displaced from the casing and surface equipment by brine or water before coring is started. If, because of operating difficulties, coring cannot be performed with brine, a water-base mud whose composition is restricted to bentonite, CMC, barite, and water with a pH near neutral will probably be satisfactory. Although this mud may cause some alteration in rock wettability, the change will not be as great as when using an oil-base mud.

Next, the wettability of the fresh core should be immediately determined at the well site, or the cores should be carefully stored for later testing at the laboratory. In order that reliable core analysis data will be obtained at either the well site or laboratory, precautions should be taken at each step of the testing program to insure that wettability is not altered by contamination, oxidation, or evaporation.

Unless the necessary effort is put forth to obtain and test cores possessing wettability characteristics similar to those in the reservoir, core analysis results such as waterflood oil recovery, capillary pressure, and relative permeability will be in error and can lead to grossly erroneous conclusions concerning the reservoir behavior.

CONCLUSIONS

1. Wettability can have an important influence on oil recovery by water flood or water drive. Waterflood oil recovery predictions based on core analysis data frequently show oil recoveries from water-wet rock to be higher than those from oil-wet rock by 15 per cent of the original oil in place.

2. The preferential wettability of a reservoir rock is largely controlled by compounds adsorbed at the rock surface.

3. Coring of water-wet reservoir rock with commonly used oil-base muds may change the wettability of a water-wet core to neutral or oil wet.

4. In laboratory tests core wettability is not altered by coring with brine or fresh water.

5. Weathering of fresh water-wet cores will frequently cause the grain surfaces to become oil wet. Therefore, weathered cores should not be used to determine the wettability of the reservoir.

6. Wettability of fresh cores can be preserved for several months by proper storage.

7. Fresh cores taken from six reservoirs under carefully controlled conditions were found to be water wet in varying degrees.

ACKNOWLEDGMENT

The authors express their appreciations to the management of The Jersey Production Research Co. for permission to publish this paper. They are indebted also to Mrs. Madelen Rey and Miss Jan Eastham who obtained much of the data presented.

REFERENCES

1. Newcombe, J., McGhee, J. and Rzasa, M. J.: "Wettability Versus Displacement in Water Flooding in Unconsolidated Sand Columns", *Trans.* AIME (1955) **204,** 227.
2. Kinney, P. T. and Nielsen, R. F.: "Wettability in Oil Recovery", *World Oil* (1951) **132,** No. 4, 145.
3. Jennings, N. Y., Jr.: "Surface Properties of Natural and Synthetic Porous Media", *Prod. Monthly* (1957) **21,** No. 5, 20.
4. Coley, F. N., Marsden, S. S. and Calhoun, J. C., Jr.: "A Study of the Effect of Wettability on the Behavior of Fluids in Synthetic Porous Media", *Prod. Monthly* (1956) **20,** No. 8, 29.
5. Moore, T. F. and Slobod, R. L.: "Effect of Viscosity and Capillarity on Displacement of Oil by Water", *Prod. Monthly* (1956) **20,** No. 10, 20.
6. Kennedy, H. T., Burja, E. O. and Boykin, R. S.: "An Investigation of the Effects of Wettability on the Recovery of Oil by Water Flooding", *Jour. Phys. Chem.* (1955) **59,** 867.
7. Richardson, J. G., Perkins, F. M. and Osoba, J. S.: "Differences in Behavior of Fresh and Aged East Texas Woodbine Cores", *Trans.* AIME (1955) **204,** 86.
8. Gatenby, W. A. and Marsden, S. S.: "Some Wettability Characteristics of Synthetic Porous Media", *Prod. Monthly* (1957) **22,** No. 1, 5. ★★★

Porosity Balance Verifies Water Saturation Determined From Logs

M. P. TIXIER
MEMBER AIME

SCHLUMBERGER WELL SURVEYING CORP.
HOUSTON, TEX.

ABSTRACT

In several log interpretation methods, water saturation is evaluated by use of the ratio of the readings of a short spacing resistivity device and a long spacing resistivity device plus information on the mud filtrate and connate water resistivities, which is often derivable from the SP. These methods are valid over a certain range of conditions, usually specified by moderate invasion and R_{xo} greater than R_t. Since these methods involve no explicit evaluation of the formation factor, F, the saturation so found may be used in the standard Archie equation to derive a computed formation factor which, as a check, may be compared with the formation factor known from other independent measurements. Discrepancies in the two values of formation factor generally indicate that the ratio method is not within its range of applicability. If the computed F is too low, the corresponding S_w is too low; if the computed F is too great, the corresponding S_w is too great. By means of this "porosity balance" check, and some knowledge of the probable conditions of invasion, the interpretation can often be improved.

The porosity balance check is discussed for the cases of the Induction-Electrical Log Interpretation Method, the Rocky Mountain Method, and the R_{xo}/R_t Method. For the first method, a discussion is also given for the case of shaly sands.

INTRODUCTION

Although many logging tools are available to obtain a practical value of porosity, the only logging method reflecting the water saturation is electrical logging.

Water saturation is commonly computed from electrical log data by means of the basic Archie formula,

$$S_w = \left(\frac{F R_w}{R_t}\right)^{\frac{1}{2}}, \quad \ldots\ldots\ldots \quad (1)$$

where F is the formation factor, R_w the resistivity of the formation water, and R_t the true resistivity of the formation.

One difficulty in this procedure is a possible error in the evaluation of R_t from the logs— for example, in the case of very deep invasion. There is no possibility, inherent in the procedure, which would provide a check of the accuracy of R_t and, hence, of the computed saturation.

Original manuscript received in Society of Petroleum Engineers office Feb. 13, 1958. Revised manuscript received May 19, 1958. Paper presented at Fourth Annual Joint Meeting of Rocky Mountain Petroleum Sections in Denver, Colo., March 3-4, 1958.

Other approaches have been proposed which are based essentially on the ratio of the readings made with two different devices: one device, with a short radius of investigation, provides a value close to the resistivity of the invaded zone; the second device, with a long radius of investigation, gives a value close to the true resistivity of the bed. By these methods, the determination of saturation is made independently of any direct knowledge of the formation factor. Therefore, if the formation factor (or porosity) is known from other sources (core analysis, neutron log, MicroLog . . .), it becomes possible to take advantage of this additional information in order to check the value of saturation derived from these latter methods.

Inasmuch as this proposed check procedure relies on a knowledge of the value of formation factor or porosity, it has been deemed appropriate to call this verification a porosity balance.

The purpose of this paper is to discuss the principle and the application of the porosity balance, depending on the method of interpretation being used.

Basis of the Method

There are in existence three interpretation methods by means of which the water saturation can be found without a knowledge of the formation factor (or porosity). As just stated, they are based on the fact that the *ratio* of the two resistivities (one measuring the resistivity close to the hole, the other measuring the resistivity far from the hole) is independent of the formation factor since it affects the two resistivity measurements in the same way.

Chronologically, the resistivity ratio methods are: (1) the Rocky Mountain Method, which has been used since 1943 and was explained in a paper in 1949;[1] (2) the R_{xo}/R_t Method or Shaly Sand Method, presented in 1954, which permits the calculation of the water saturation in both clean and shaly sands[2]; and (3) the Induction-Electrical Log Method, presented in 1957 for the interpretation of the induction-electrical log combination.[3]

Each method requires certain definite conditions in order for the interpretation to be reliable. The porosity balance method will let us know whether these conditions are fulfilled.

In clean formations we know that the fundamental Archie relation (Eq. 1) must always be verified. This relation can be rewritten:

[1]References given at end of paper.

$$F = \frac{R_t}{R_w} S_w^2 \quad . \quad . \quad . \quad . \quad . \quad . \quad . \quad . \quad . \quad . \quad . \quad (2)$$

In Eq. 2 we can admit that R_w is reasonably well known, from the SP or from direct measurements on samples of connate water. The check of the value of S_w, found from any of the three ratio resistivity methods, is to enter it into Eq. 2 and to compare the value thus computed for F with the known, true value of F.

In the case of Methods 1 and 2, R_t in Eq. 2 is taken equal to the R_t value used in the application of the method. For Method 3, R_t is taken equal to R_{IL}, or is derived from R_{IL} by means of a procedure described later.

Obviously, if the resistivity ratio method used to obtain S_w is applied in a case where all conditions of application are fulfilled, the water saturation so found will be correct. Therefore, the formation factor derived from Eq. 2 will also be correct and should check with an independent knowledge of this formation factor (or porosity). When the two values of formation factor are different, we may conclude: (1) if the computed F is lower than the true F, the value of S_w given by the resistivity ratio method is too low, and (2) if the computed F is higher than the true F, the value of S_w given by the resistivity ratio method is too high.

A more detailed discussion will be given on the application of the porosity balance method for each of the three resistivity ratio methods just given.

PART I — Porosity Balance for Induction-Electrical Log Interpretation

In a recent paper,[3] a simple method was presented for the interpretation of the induction-electrical log in fresh mud. A practical chart* (Fig. 12 of Ref. 3, reproduced here as Fig. 1) was presented on which the ratio R_{16}/R_{IL} is plotted against either the corrected SP reading or against the value of R_{mf}/R_w. The indications of the chart serve to determine whether oil or water production can be expected from a given bed. In addition, approximate scales on the chart indicate the order of magnitude of the water saturation, S_w.

As stated in the paper,[3] some knowledge of the depth of filtrate invasion is necessary for a correct application of the chart. In particular, the invasion diameter, D_i, must be not less than $2d$ nor greater than $10d$ (where d is the hole diameter).

A further basic requirement for the use of the chart is that the invaded zone resistivity, R_{xo}, be higher than the uncontaminated zone resistivity, R_t. This condition is generally fulfilled when R_{mf}/R_w is high, as in the case of fresh muds and saline connate waters, and provided the water saturation is not too low. Whereas this is the situation prevailing in most cases, exceptions are not uncommon, mostly in regions where connate waters are comparatively fresh; and, as a result, R_{mf}/R_w is low. Printed on the chart are limiting values below which use of the chart is not recommended.

Finally, the chart is intended for the case of fairly homogeneous beds. The interpretation may be made difficult if the bed is broken by thin hard streaks. The presence of thin highly resistive streaks within the bed or near its boundaries may spuriously increase the average short normal reading over the bed, whereas the induction log reading remains practically unaffected.

It follows that the chart may be misleading when the proper conditions for its application are not fulfilled. For example, on the Gulf Coast very shallow invasion (less than $2d$) may be found in the Frio and Miocene. In the Mid-Continent very deep invasion is often found in consolidated rocks. Water sands that are hardly invaded or very deeply invaded will appear as oil- or gas-bearing on the interpretation chart. To be able to recognize such cases is of great interest.

The value of R_t to be used in Eq. 2 is selected in the following manner.

1. If the readings R_{16}/R_{IL} vs R_{mf}/R_w plot well below the critical line on the interpretation chart, it is provisionally concluded that the bed is oil- or gas-bearing and that the invasion depth lies within the $2d$ to $10d$ limits. In this case R_{IL} can be taken, to a first approximation, as equal to R_t because, when the formation is oil- or gas-bearing and the invasion is not too deep, the usual increase in R_{IL} due to the fresh mud invaded zone is approximately compensated for by the decrease in resistivity contributed by the salt-water annulus.*

2. If the plotted point falls within the water zone (shaded area on the chart), it is provisionally concluded that the bed is water bearing. R_{IL} in this case is generally greater than R_t. The value of R_t can be derived from R_{16}/R_{IL} and the SP using the theoretical chart** of Fig. 2. The SP gives R_{mf}/R_w, which in a clean water-bearing sand is equal to R_{xo}/R_t. The observed value of R_{16}/R_{IL} may be represented in Fig. 2 by a line of 45° slope which intersects the curve of given R_{xo}/R_t at two points, corresponding to two different depths of invasion. Local experience will usually suffice to indicate which is the correct point. The coordinates of this point define the values R_{xo}/R_{IL} and R_{xo}/R_{16}, from which R_t is readily derived since R_{xo}/R_t is known. (Furthermore, if R_{xo} is known, R_{xo}/R_t, and hence R_t, can be obtained from a direct plot on Fig. 2 and checked against the R_{xo}/R_t found from the SP.)

When the value of F derived from Eq. 2 does not check with the known value, one is led to ask in what

*Schlumberger Log Interpretation Chart D-12.

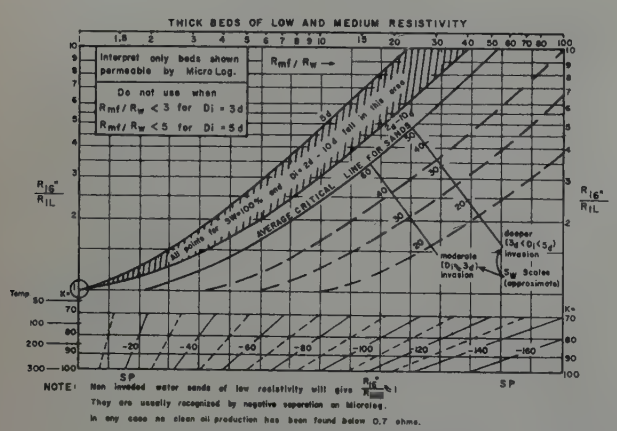

FIG. 1—INDUCTION-ELECTRICAL LOG INTERPRETATION CHART (40-IN. INDUCTION—16-IN. NORMAL).

*The "annulus" is a region containing a high saturation of formation water which tends to accumulate between the invasion front and the oil- or gas-bearing uncontaminated zone. This annular region of low resistivity has noticeable effect only in the case of low initial water saturation; i.e., relatively high hydrocarbon saturation.

**Schlumberger Log Interpretation Chart B-10.

manner do the conditions affecting R_{16} and R_{IL} violate the listed requirements and, also, in what manner is it possible to arrive at a more correct value of the saturation. In the following, various possible cases will be discussed.

Clean Formations

I. F computed through Eq. 2 is lower than the true value of F

This indicates that the saturation value derived from the chart is too low. This may happen mostly when the invasion diameter is smaller or greater than the limiting values compatible with the chart; i.e., $2d$ and $10d$. In the former case, R_{16} is too low and in the latter case R_{IL} is too high.

The existence of shallow invasion is usually expected in very porous formations and is generally known from local experience. Sometimes its effects can be observed even on the MicroLog. Negative separation may sometimes occur in water sands because the 2-in. micronormal "sees" past the invaded zone, and its reading is lowered by the effect of R_o.

The existence of deep invasion may be expected in low porosity formations when high water loss mud is used or when the log is made a long time after the formation is drilled.

It is quite often possible to check whether we are in a situation of very deep or very shallow invasion. If invasion is deep, R_{16}, after correction for borehole effect and adjacent formations, should be close to R_i, invaded zone resistivity. Thus, it is possible to derive from it an approximate value of the formation factor, using Chart C-16 (Schlumberger book of log interpretation charts). If the invasion is shallow, R_{16} after correction is quite different from R_i, because of the effect of the uncontaminated zone, and the value obtained through Chart C-16 would be far from the true value of F. The check, accordingly, will consist in computing a value of F from R_{16} (corrected) and comparing it to the true value of F; according to whether both values are close or different, it will be concluded that the invasion is deep or shallow.

A. $D_i < 2d$—R_{16} too Low

In this case R_{IL} is practically equal to R_t. If a good knowledge of F or the porosity is available in advance, then the correct procedure is to compute S_w from Eq. 1 using R_{IL} as R_t.

B. $D_i > 10d$—R_{IL} too High

Here, R_{IL} is necessarily greater than R_t. However, taking R_{IL} equal to R_t in Eq. 2, and using the value of S_w given by the chart of Fig. 1, still provides a computed value of F which *is lower* than the true value. This fundamental point has been checked on numerous typical cases.

But, *if Eq. 1 is used, with $R_t = R_{IL}$, and with the true value for F, the value computed for S_w will be too low.*

The proposed procedure to improve the interpretation is to try a lower value of R_{IL} than that read from the log. This selected value corresponds to a somewhat reduced depth of invasion, all other conditions being the same. R_{16} is practically unaffected because, even after this hypothetical reduction, the invasion still remains very deep. Therefore, using the same R_{16} and the new R_{IL}, we determine a new S_w from the interpretation chart (Fig. 1) and recheck the porosity balance. If the new value of S_w falls below the critical line, R_{IL} is taken equal to R_t in Eq. 2. If the new value falls in the water zone, the value of R_t to be used in Eq. 2 should be determined from R_{16}/R_{IL} and R_{mf}/R_w by means of Fig. 2, as previously explained.

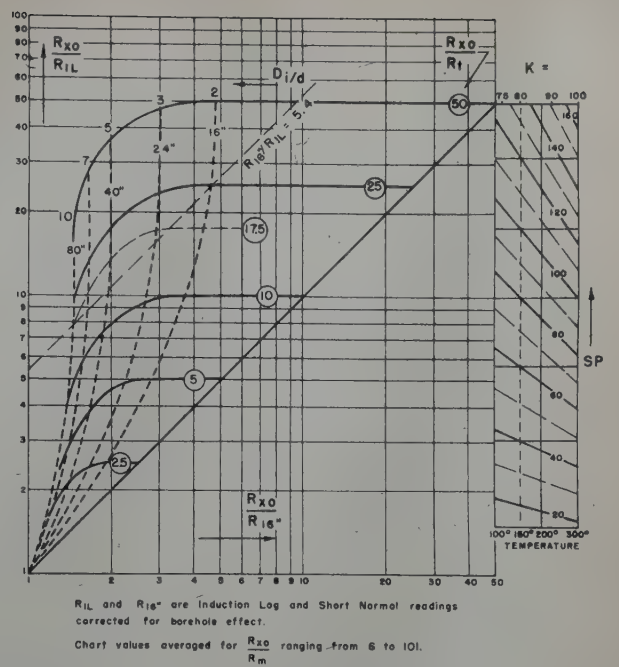

Fig. 2—Values Computed for 40-in. Induction and 16-in. Normal Supposing No Annulus of Formation Water is Present (Hole: 8-in. Thick Beds and Case of $S_w > 60$ per cent).

By successive trials, a value of R_{IL} and corresponding values of R_t and S_w can be found which will satisfy the porosity balance. The value of S_w thus arrived at is likely to be a good approximation to the true value.

Examples of Computed F too Low

A. Very Shallow Invasion

This case is the one most effectively resolved by the porosity balance check. Let us take an induction-electrical log (Fig. 3) typifying conditions often found in the Gulf Coast.

R_{16} (corrected for borehole) = 1.5	$R_{mf} = 0.85$
$R_{IL} = 1.0$	$R_{mf}/R_w = 17$
$R_{16}/R_{IL} = 1.5$	$(K = 80)$
SP = − 100 mv	$R_w = 0.05$

Fig. 1 gives $S_w = 20$ per cent for $5d$ invasion or $S_w = 25$ per cent for $3d$ invasion. An average S_w is 22.5 per cent, which would be characteristic of an oil or gas sand. If this interpretation is correct, then R_{IL} should be approximately equal to R_t; and Eq. 2 gives $F = (1/0.05) \times (.225)^2 = 1$. A formation factor of 1 is impossible, and we know from the foregoing discussion that a S_w of 22.5 per cent is much too low. In this case an exact knowledge of the formation factor is unnecessary to prove that this solution is incorrect.

Now, if we know from other sources that the sand porosity is 35 per cent, corresponding to a formation factor of about 6, S_w will be computed simply through Eq. 1 taking $R_{IL} = R_t$; namely,

$$S_w^2 = \frac{F R_w}{R_t} = \frac{6 \times 0.05}{1.0} = 0.30, \text{ and}$$

$S_w = 55$ per cent.

B. Very Deep Invasion

The porosity balance may be of great help in this case; *but the porosity and, hence, the formation factor must be accurately known.* Fig. 4 shows schematically a North Texas log.

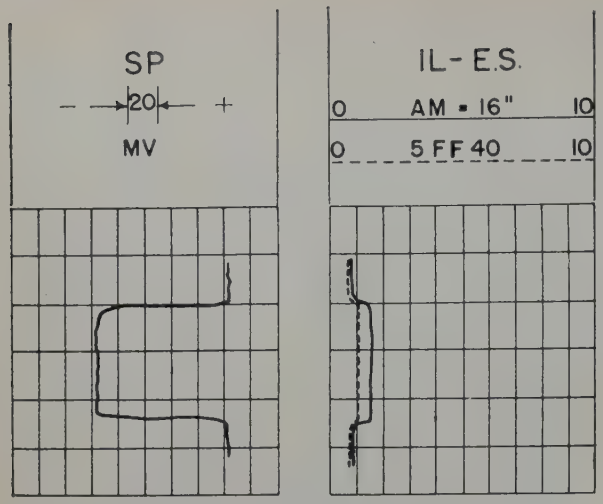

FIG. 3—INDUCTION-ELECTRICAL LOG OF A GULF COAST SAND—CASE OF VERY SHALLOW INVASION.

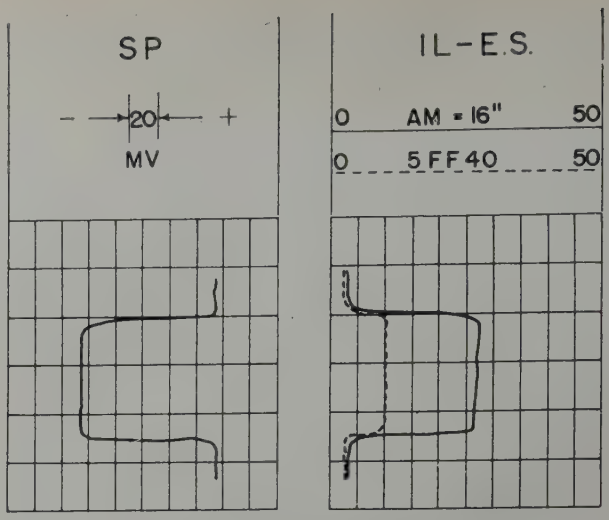

FIG. 4—INDUCTION-ELECTRICAL LOG IN A NORTH TEXAS WELL—CASE OF DEEP INVASION.

R_{16} (corrected for borehole) = 27
R_{IL} = 10
R_{16}/R_{IL} = 2.7
SP = − 100 mv
According to the MicroLog, F = 30.

R_{mf} = 1.4
R_{mf}/R_w = 17.5
(K = 80)
R_w = 0.08

Since, in this instance, we are in a region where invasion is known to be deep, the deeper invasion scale will preferably be used in Fig. 1 to determine S_w. Thus, we get S_w = 35 per cent.

Eq. 2 gives $F = 10/0.08 \times (0.35)^2 = 15$.

We see that application of the chart results in a lower formation factor than that obtained from the MicroLog. The saturation value given by the chart (35 per cent) is, therefore, too low.

Use of Eq. 1 with $R_t = R_{IL} = 10$ would give $S_w = (30 \times .08/10)^{\frac{1}{2}}$ or 50 per cent. But, because of the deep invasion, R_{IL} is greater than R_t, therefore, this value of 50 per cent is also too low.

Since R_{IL} is too high, let us use a fictitious value of $R_{IL} = 5$ ohm, leaving R_{16} and the SP as found. We have $R_{16}/R_{IL} = 27/5 = 5.4$, and the point falls within the water zone.

In order to check the formation factor corresponding to this water saturation of 100 per cent, we have to process R_{IL} through the chart of Fig. 2. The 45° line, started from 5.4, will cut $R_{xo}/R_t = R_{mf}/R_w = 17.5$ around $R_{xo}/R_{IL} = 8$. Then, $R_{xo}/R_{IL} \div R_{xo}/R_t = R_t/R_{IL} = 8/17.5$; thus,

$$R_t = \frac{8}{17.5} R_{IL} = \frac{8 \times 5}{17.5} = 2.3,$$

which is almost identical with the R_o value calculated through $R_o = F R_w$; i.e., $30 \times 0.08 = 2.4$.

Finally, we obtain $F = (2.3/0.08) \times (1)^2 = 28.5$. This value of F, obtained with S_w = 100 per cent, is quite close to the value of F derived from the MicroLog. Consequently, there is no doubt that this sand is a water sand.

II. F COMPUTED THROUGH EQ. 2 IS HIGHER THAN THE TRUE VALUE OF F

In this case the value of S_w found from the chart is too high. This may happen mostly when R_{xo} is less than R_t or when R_{16} is too high.

A. R_{mf}/R_w is Low

As a result, R_{xo} is generally smaller than R_t when the formation is oil bearing. (It may also occur occasionally for high R_{mf}/R_w ratios if the water saturation is exceedingly low, but this case is rare.)

In fact, computations have shown that, after the proper corrections for mud column and bed thickness are made, R_{16} is practically always higher than R_{IL}, whatever the ratio R_{xo}/R_t. There seems to be no obvious and sure criterion for recognizing whether R_{xo} is lower or greater than R_t and, therefore, if the chart is applicable or not. This is why it is clearly mentioned on the chart that it should not be used for specified low values of R_{mf}/R_w. Since these limitations cannot be spelled out quite accurately because they may vary somewhat with the values of the other parameters involved, it is always useful to try the porosity balance method, even if R_{mf}/R_w is above, but close to, the indicated limiting values. In many instances, the formation factor computed from Eq. 2 will be obviously too high, according to local experience, and the interpretation given by the chart will undoubtedly be too pessimistic.

In these cases, the use of Eq. 1 is recommended. When $R_{xo} < R_t$ and there is some invasion, although R_{16} will still be lower than R_t after bed thickness and borehole correction*, it will be a better approximation to R_t than R_{IL}.

Fig. 5 is taken from a log in Beaver County, Okla.

R_{16} = 66 (corrected)
R_{IL} = 25
R_{16}/R_{IL} = 2.65
SP = − 60 mv

R_{mf} = 0.48 at 125°F
R_w = 0.085 from SP
R_{mf}/R_w = 5.7

The MicroLateroLog (not shown) gives an average value of 17 for R_{xo}, so that F = 25, assuming a residual oil saturation of 15 per cent. In Fig. 1, with R_{16}/R_{IL} = 2.65 and R_{mf}/R_w = 5.7, we find S_w = 100 per cent.

For application of the porosity balance, we will use a value of R_t derived from R_{IL} by means of Fig. 2, according to the outlined procedure. The value found for R_t is 23. Then Eq. 2 gives $F = 23/0.085 = 270$, which is far above the value given by the MicroLateroLog, Therefore, S_w should be appreciably lower than 100 per cent.

A more exact value can be obtained by using the Archie formula, with F = 25, and $R_t = R_{16}$; i.e., 66 (in this instance R_{xo} is most likely to be lower than R_t, and the short normal to read closer to R_t than the induction log).

Finally, $S_w = (25 \times 0.085/66)^{\frac{1}{2}}$ or 18 per cent. The

*Since no charts have been published giving bed thickness and borehole corrections for $R_{xo} < R_{16}$, Schlumberger Log Interpretation Chart B-13 (no invasion or $R_{xo} = R_t$) is the most appropriate for correcting R_{16} in this case.

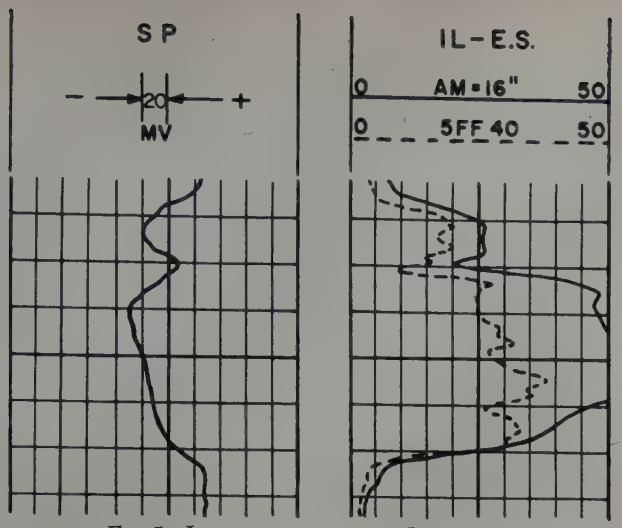

FIG. 5—INDUCTION-ELECTRICAL LOG IN THE MORROW SAND, OKLA.

sand produced condensate on the formation tester and also on a drill-stem test.

B. R_{16} too High

The short normal reading may be unduly increased because of thin resistive streaks within or adjacent to the bed under consideration.

Again, in this case, when the computed F is higher than the true F, a better S_w value should be expected from the application of Eq. 1 with $R_{IL} = R_t$.

SHALY SANDS

In the referred paper,[3] a procedure was given whereby, if the shaliness were not too great, the interpretation chart (Fig. 1) could be used to determine the approximate saturation of shaly sands. It is of interest to also check against the results of such a determination.

Electrical log interpretation in shaly sands, as a rule, is more delicate and less accurate than in clean sands (see Ref. 2).

The presence of interstitial shales decreases the contrasts between resistivity values due to variations in porosity and saturation. Furthermore, the interpretation requires an accurate measurement of R_{xo} with the MicroLog, which is sometimes difficult and even impossible, particularly in the case of very shallow invasion. (The knowledge of porosity from other sources, for example core analysis, is not of great help; R_{xo} cannot be computed from the porosity value, since it depends also on the shale content, which is unknown.)

Application of the proposed method in the case of shaly sands is also less reliable for the same reasons. In order to understand the procedure to be proposed, it is advisable to return to the case of a clean formation.

Here, it is known that $S_w^2 = F R_w/R_t$ and $S_{xo}^2 = F R_{mf}/R_{xo}$, where S_{xo} is the water saturation in the flushed zone; hence,

$$\frac{R_{mf}}{R_w} = \frac{R_{xo}}{R_t} \times \left(\frac{S_{xo}}{S_w}\right)^2 \quad . \quad . \quad . \quad . \quad . \quad . \quad . \quad . \quad (3)$$

Assuming that the SSP of a clean formation can be taken equal to $-K \log R_{mf}/R_w$, it results that

$$\text{SSP} = -K \log \left[\frac{R_{xo}}{R_t} \times \left(\frac{S_{xo}}{S_w}\right)^2\right].$$

The solution of this equation is given graphically by Chart D-4 (of the log interpretation charts) reproduced here as Fig. 6, where R_{xo}/R_t is plotted in ordinates and SSP or R_{mf}/R_w is plotted in abscissae.

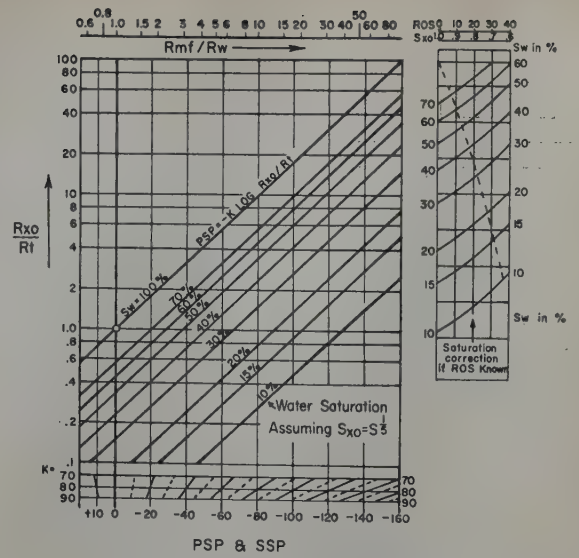

FIG. 6—SATURATION DETERMINATION.
(For Larger Reproduction, See Fig. 10, Ref. 3.)

A similar equation can be written for the pseudostatic SP of a shaly formation:

$$\text{PSP} = -K \log \left[\frac{R_{xo}}{R_t} \times \left(\frac{S_{xo}}{S_{wa}}\right)^2\right],$$

where S_{wa} is an "apparent" water saturation. This value of S_{wa} can be also obtained from Fig. 6, by entering R_{xo}/R_t in ordinates and PSP in abscissae. Furthermore, the PSP can be expressed through $-K \log R_{mf}/R_{wa}$, where R_{wa} is an apparent connate water resistivity.

Entering this value into the cited equation,

$$-K \log \frac{R_{mf}}{R_{wa}} = -K \log \left[\frac{R_{xo}}{R_t} \times \left(\frac{S_{xo}}{S_{wa}}\right)^2\right]$$

or

$$\left(\frac{S_{wa}}{S_{xo}}\right)^2 = \frac{R_{xo}}{R_{mf}} \times \frac{R_{wa}}{R_t}.$$

We also have

$$F_a = \frac{R_{xo}}{R_{mf}} \quad . \quad . \quad . \quad . \quad . \quad . \quad . \quad . \quad . \quad . \quad . \quad . \quad (4)$$

Thus,

$$F_a = \frac{R_{xo}}{R_{mf}} = \frac{R_t}{R_{wa}} \times \left(\frac{S_{wa}}{S_{xo}}\right)^2 \quad . \quad . \quad . \quad . \quad . \quad (5)$$

Eq. 5 for a shaly sand is the equation corresponding to Eq. 2 for a clean formation and suggests a corresponding porosity balance check of the F_a computed from S_{wa} in Eq. 5 with the F_a found from Eq. 4.

In fact, Eq. 5 can be used in a check of S_{wa}, just as Eq. 2 is used in the case of clean sands. However, the use of Eq. 5 requires computation of F_a from the ratio R_{xo}/R_{mf}, determination of R_{wa} from the PSP, and computation of the ratio, S_{wa}/S_{xo}.

As a result of this check, more accurate values of S_w can be found in the following cases.

I. COMPUTED F_a TOO LOW (S_{wa} TOO LOW)

A. Too Shallow Invasion—R_{16} too Low

In this case the shaly sand interpretation chart (Fig. 6) should be used with R_{IL} taken as R_t. (R_{xo}/R_t vs PSP and SSP.)

NOTE: The value of R_{xo} can be affected by R_t because of low invasion.

B. Too Deep Invasion—R_{IL} too High

R_{IL} reads higher than R_t. A new value which is lower than that taken off the log can be selected for R_{IL}, and

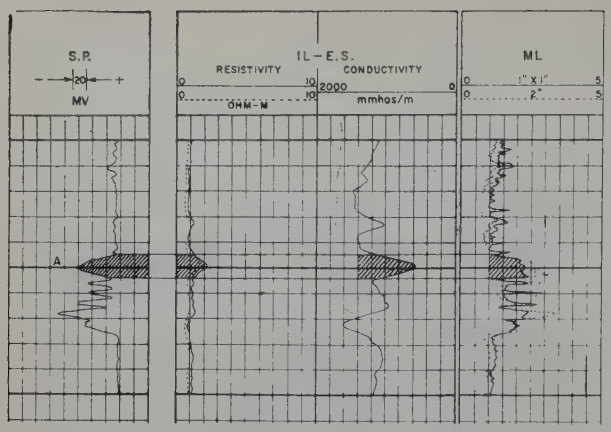

FIG. 7—SAND-SHALE SERIES IN A SOUTH LOUISIANA WELL—SHALLOW INVASION IN A SHALY SAND.

the procedure is the same as that described for clean sands.

Example of Computed F_a too Low

Fig. 7 shows a sand-shale series in South Louisiana, Bed A.

$R_{16} = 2.2$ PSP = − 55 mv
$R_{IL} = 1.9$ SSP = −110 mv
$R_{16}/R_{IL} = 1.15$ $R_{mf} = 1.2$ at 140°F
From the PSP, $R_{wa} = 0.23$ at 140° F.

The average value of R_{xo} over the interval is 5.3. Entering $R_{16}/R_{IL} = 1.15$ and PSP = − 55 mv into the interpretation chart (Fig. 1) gives $S_{wa} = 38$ per cent (and less than 20 per cent for S_w).

From Eq. 4, $F_a = 5.3/1.2 = 4.4$. From Eq. 5, $F_a = (1.9/0.23) \times (0.38)^2/(0.8)^2 = 1.9$, with $S_{xo} = 0.8$.

Since F_a derived from Eq. 5 is less than F_a derived from Eq. 4, the value of S_{wa} is too low also. The reason for this is that R_{16} is too low because of too shallow invasion. Under this condition, $R_{IL} = R_t$.

The correct procedure now is to use Fig. 6 with $R_{xo} = 5.3$ and $R_t = 1.9$, or $R_{xo}/R_t = 2.8$, which gives $S_w = 50$ per cent.

This is quite a reasonable value which, with shaly sands, may correspond to a good production. In fact, after perforation the interval gave 75.4 bbl of oil and 280,000 cu ft/day of gas.

II. COMPUTED F_a TOO HIGH (S_{wa} TOO HIGH)

A. R_{mf}/R_w is Low

In this case, R_{16} can be taken as R_t and the ratio R_{xo}/R_t vs PSP and SSP should be used with Fig. 6 (standard shaly sand interpretation).

B. R_{16} too High

R_{IL} can be used as R_t and the ratio R_{xo}/R_t vs PSP and SSP should be used with Fig. 6. This case is not likely to be seen often.

SUMMARY

CLEAN FORMATIONS

I. F COMPUTED THROUGH EQ. 2 LOWER THAN TRUE F: S_w TOO LOW

A. R_{16} too Low (too shallow invasion)—Use Archie formula, Eq. 1.

B. R_{IL} too High (very deep invasion)—Try successively decreasing values of R_{IL} until Eq. 2 is satisfied.

II. F COMPUTED HIGHER THAN THE TRUE F: S_w TOO HIGH

A. R_{mf}/R_w is Low—Use Archie formula with $R_t = R_{16}$ (corrected).

B. R_{16} too High—Use Archie formula with $R_t = R_{IL}$.

SHALY SANDS

I. F_a DERIVED FROM EQ. 5 LOWER THAN F_a DERIVED FROM MICROLOG: S_{wa} IS TOO LOW

A. R_{16} too low (too shallow invasion) — Use Fig. 6 and regular shaly sand procedure, taking $R_{IL} = R_t$. (This may still give a value for S_w not necessarily correct since R_{xo} from the MicroLog may be affected by R_t.)

B. R_{IL} too High (too deep invasion) — Try successively decreasing values of R_{IL} until values of F_a from Eqs. 4 and 5 agree.

II. F_a DERIVED FROM EQ. 5 HIGHER THAN F_a DERIVED FROM MICROLOG: S_{wa} IS TOO HIGH

A. R_{mf}/R_w is Low—Use Fig. 6 and regular shaly sand method, taking $R_{16} = R_t$.

B. R_{16} too High—Use Fig. 6 and regular shaly sand method, taking $R_{IL} = R_t$.

REMARKS

The use of the porosity balance can prevent many errors. It provides a way to check whether the application of Fig. 1 is permissible or not. When it is recognized that this chart would give too optimistic results (S_w too low), some local experience will most often indicate whether this is due to too shallow invasion (Case IA) or to too deep invasion (Case IB). If this chart, on the contrary, would be pessimistic (S_w found too high), the amplitude of the SP will generally indicate whether this is due to $R_{xo} < R_t$ (Case IIA) or R_{16} too high (Case IIB).

The respective advantages of the new interpretation given by Fig. 1 and of the standard interpretation used in the past can be pointed out by the use of the porosity balance in the cited difficult cases.

In Cases IA (shallow invasion) and IIB (R_{16} too high), the best results will be obtained by taking R_t equal to the induction log reading and using the standard method of interpretation through Eq. 1.

In Case IIA ($R_{xo} < R_t$) the standard method of interpretation would have called for the use of the induction log as R_t whereas the 16-in. normal reading (corrected) is actually the best approximation to R_t.

In Case IB (deep invasion), the standard method would give an incorrect value of saturation. A better result can be often obtained by means of Fig. 1 and successive trials of various R_{IL} values.

A good porosity control is, of course, necessary for a correct application of the porosity balance in clean sands, especially in the case of deep invasion. The MicroLog is also indispensable for the application of the method in shaly sands.

PART II — Porosity Balance for the Rocky Mountain Method

The Rocky Mountain Method is the oldest resistivity ratio method. Judged by modern standards, many aspects of the method are empirical; it is doubtful if we could explain the choice of the various parameters in the same fashion.

The water saturation in this method is given by the relation,

$$S_w = \frac{R_t}{R_t} \times \frac{R_w}{R_z}, \quad \ldots \ldots \ldots \quad (6)$$

where R_t is given by a short normal corrected for hole effect, as if the bed were non-invaded*; R_t is given by

*Schlumberger Log Interpretation Chart B-2 or B-4.

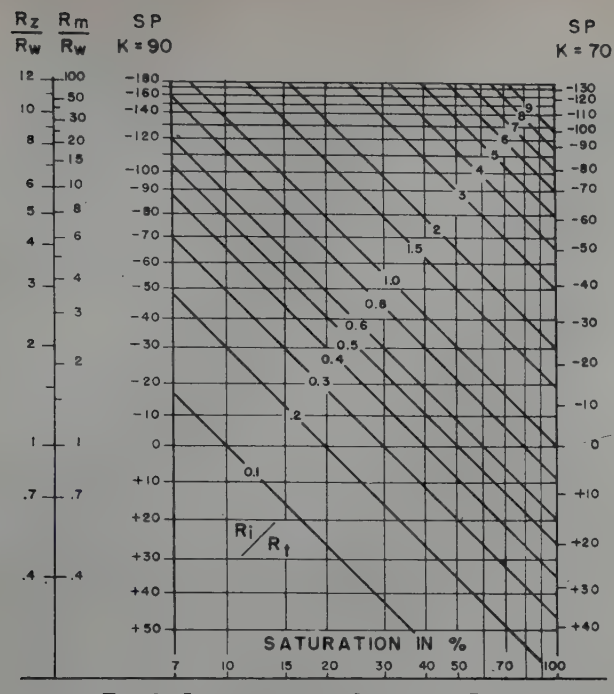

FIG. 8—INTERPRETATION CHART FOR ROCKY MOUNTAIN METHOD.

the lateral, or the induction log, corrected for both hole effect and average invasion, R_w is connate water resistivity; and R_z is resistivity of the water in the invaded zone, made up of a mixture of connate and filtrate waters. A graphical solution of Eq. 6 is given in Fig. 8.*

For this method, the principle of the porosity balance check can be explained as follows.

The formation factor is computed by Eq. 2.

$$F = \frac{R_t}{R_w} \quad S_w^2 \quad . \quad . \quad . \quad . \quad . \quad . \quad . \quad . \quad . \quad . \quad (2)$$

Carrying the value of S_w from Eq. 6 into Eq. 2 gives

$$F = \frac{R_t}{R_w}\left(\frac{R_i}{R_t}\cdot\frac{R_w}{R_z}\right)^2 = \frac{R_w}{R_t}\left(\frac{R_i}{R_z}\right)^2 = \frac{R_i^2}{R_t}\cdot\frac{R_w}{R_z^2}\cdot$$

$$. \quad (7)$$

If the value of F computed through Eq. 2 is *lower* than the true F, Eq. 7 shows that R_i^2/R_t is too low—accordingly R_i/R_t is too low, and S_w, from Eq. 6, is also too low. Conversely, if F computed is higher than the true F, S_w given by the method is too high.

Eqs. 6 and 7 furthermore show that the check should be quite sensitive, since any relative error in R_t entails the same relative error in S_w and F. Furthermore, any relative error in R_i entails the same relative error in S_w, but twice as great a relative error in F.

We have found that the Rocky Mountain Method is of great utility in medium and hard formations when $R_{16}/R_m > 10$, and when the formation under investigation is very thick. One should recall that this method was introduced when neither MicroLog nor Micro-Laterolog was available; its great advantage was the fact that no formation factor value was necessary in order to arrive at a value of water saturation.

From experience it has been found that this method gives good results when the invasion diameter, $D_i \approx 5d$. Errors will be found if the invasion is shallow or very deep. In both cases the method is generally too optimistic. We will study these cases first.

*Schlumberger Log Interpretation Chart D-8.

1. F COMPUTED THROUGH EQ. 2 IS LOWER THAN THE TRUE VALUE OF F.

This indicates that the water saturation derived from Fig. 8 is too low.

A. D_i Small—The Short Normal Reading is too Low

The existence of shallow invasion is usually expected in very porous formations. For this reason, the condition $R_{16}/R_m > 10$ is required before using this method in order to eliminate most of the very porous formations.

It may also happen that the formation is tight and has no permeability; therefore, no invasion has taken place. This may happen even though a definite SP is recorded in front of such formations. Nowadays, the MicroLog permits the elimination of such cases.

It is obvious that with shallow invasion the long lateral curve will give a value close to the true resistivity if the formation is thick enough and no interference from adjacent formations takes place. The correct procedure is to compute S_w from the Eq. 1, using the long lateral reading (after correction) as R_t.

B. D_i Large—The Lateral Reading is too High

Deep invasion often takes place in formations of low porosity, especially when high water-loss muds are used or when the log is made a long time after the formation is drilled.

Since the lateral reading is high, it will yield too low value for S_w when used as R_t in Fig. 8.

The best procedure to obtain a better interpretation is to try a lower value for R_t. This selected value corresponds to a smaller invasion, all other conditions being the same. R_{16} is practically unaffected because even after this hypothetical reduction invasion is still relatively deep. Therefore, by using the same R_i and a new value of R_t, we determine a new S_w from Fig. 8 and recheck the porosity balance.

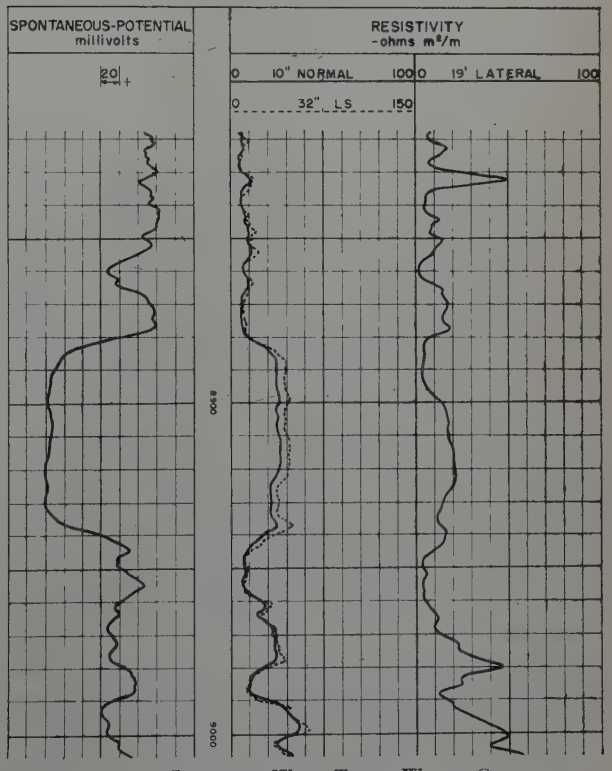

FIG. 9—LOG IN A WEST TEXAS WELL—CASE OF DEEP INVASION.

By successive trials, a value of R_t and of S_w can be found to satisfy the porosity balance. The new value of S_w thus arrived at is likely to be a good approximation to the true value.

It should also be remembered that the direct application of Eq. 1 to obtain the water saturation will yield an incorrect solution if we insert the erroneous value of R_t found from the lateral.

Example of Computed F too Low

Case of Deep Invasion—Inasmuch as this case is the most troublesome, the following example from West Texas is given as an illustration (Fig. 9).

R_m = 0.9 at BHT
Bit size: 7⅞ in.
R_{10} = 26
R_{10} = 21 (at 8,920 ft)
SP = −120 mv (K = 80)
R_w = 0.025

The neutron (not shown) gives in this interval a porosity of 7 to 10 per cent.

R_{10}/R_m = 29
R_{10}/R_m = 23
R_t/R_m = 33
R_t/R_m = 19
] see Schlumberger Chart B-4
R_t/R_t = 1.74, with SP = − 120 mv and K = 80, gives
S_w = 17.5 per cent
$F = (17.1/0.025) \times (0.175)^2 \approx 21$, corresponding to Φ = 19 per cent.

This calculated formation factor of 21 is many times smaller than the one derived from the neutron porosity ($90 < F < 205$). This is a typical case of deep invasion.

Using a true resistivity of 3 ohm, the Rocky Mountain Method gives S_w = 100 per cent and F = 120. Such a formation factor, corresponding to Φ = 9 per cent, gives good agreement with the information from the neutron. The limestone curve available in this well yields a porosity of the same order as the neutron log.

II. F COMPUTED THROUGH EQ. 2 GREATER THAN THE TRUE VALUE OF F

In this case the value of S_w found from Fig. 8 is too high.

A. Short Normal Reading too High

In oil- and gas-bearing formations where little or no invasion takes place, the short normal approaches R_t instead of R_t. When the sand has a low water saturation, R_t is large, and greater than the invaded zone resistivity (R_t) would have been had the sand been invaded by mud filtrate. This condition of little or no invasion may not be known beforehand, and a blind application of the Rocky Mountain Method gives S_w and F too high. The correct procedure here is to use the standard relation Eq. 1.

B. Induction Log too Low

If an induction log is used to obtain R_t, it is possible that when R_{mf}/R_w is low the induction log value may be too low because $R_{xo} < R_t$ (see Part I, II-A).

PART III — Porosity Balance for R_{xo}/R_t Method

This method, which is applicable both for clean and shaly formations, gives correct results when R_{xo} can be determined accurately from the MicroLog or the Micro-Laterolog and R_t from a deep investigation device. It has then proved of great utility in soft sands. It is also useful in case of salty muds in hard formations: since little or no mud cake exists, a good value of R_{xo} can be obtained with the MicroLaterolog, and the Laterolog is used for an approach to the measurement of R_t.

The interpretation, with this method, is based on Eq. 3, already presented in Part I.

$$\frac{R_{mf}}{R_w} = \frac{R_{xo}}{R_t}\left(\frac{S_{xo}}{S_w}\right)^2 \quad \ldots\ldots\ldots \quad (3)$$

where S_{xo} is the water saturation in the flushed zone.

The value of F, for a clean sand, is related to R_{xo} through

$$F = \left(\frac{R_{xo}}{R_{mf}}\right) S_{xo}^2 \quad \ldots\ldots\ldots \quad (8)$$

and to R_t through Eq. 2,

$$F = \left(\frac{R_t}{R_w}\right) S_w^2 \quad \ldots\ldots\ldots \quad (2)$$

Combining Eqs. 8 and 2 gives Eq. 3.

Since these three equations are not independent, it is obvious that the value of F derived from R_{xo}, as given by the MicroLog or MicroLaterolog, cannot be used for the porosity balance check. An independent way of obtaining porosity must be available, such as core analysis, sonic log, neutron log . . . Furthermore, the porosity balance gives an independent check of S_w *only in clean formations.*

The main chart of Fig. 6*, which gives a praphical solution to Eq. 3, was established with the assumption that $S_{xo} = S_w^{1/5}$.

Eq. 3 can be written,

$$S_w = \left(\frac{R_{xo}}{R_t} \cdot \frac{R_w}{R_{mf}}\right)^{5/8} \quad \ldots\ldots\ldots \quad (9)$$

Transferring this value into Eq. 2 gives

$$F = \frac{R_t}{R_w}\left(\frac{R_{xo}}{R_t} \cdot \frac{R_w}{R_{mf}}\right)^{5/4} = \left(\frac{R_{xo}^5}{R_t}\right)^{1/4} \cdot \left(\frac{R_w}{R_{mf}}\right)^{5/4} \cdot \frac{1}{R_w} \cdot \quad \ldots\ldots\ldots \quad (10)$$

When F computed through Eq. 2 is found lower than the true F value, Eq. 10 shows that $(R_{xo}^5/R_t)^{1/4}$ is too low, hence R_{xo}/R_t is too low, and also S_w, according to Eq. 3. Conversely, if F is found higher than the true F, S_w given by the method is too high.

The porosity balance check, in this case, is not as sensitive as with the Rocky Mountain Method. A relative error in R_{xo} entails about an equal relative error in F, but a relative error in R_t causes a relative error in F which is about one-fourth as large.

I. F COMPUTED THROUGH EQ. 2 IS LOWER THAN THE TRUE VALUE OF F.

A. Erroneous R_{xo}

It is obvious that if the MicroLog or MicroLaterolog is used in conditions where an erroneous value of R_{xo} is obtained, a wrong value for S_w will result. This can be the case in hard formations when the MicroLog or the MicroLaterolog values used are too low because mud cake thicknesses are not negligible. Fortunately, this case can be recognized without much difficulty when R_t is less than the value given by the short normal; in this case the R_{xo} value should be as great as, or greater than, the short normal reading. If an independent value of porosity is available, one can calculate from it a "synthetic" R_{xo} which will point out the error in the indication of the microdevice.

B. Shallow Invasion

In a water sand with shallow invasion, the value found for R_{xo} may be too low, giving S_w too low. When this happens, the calculated F is often so low as to be

*Schlumberger Log Interpretation Chart D-4.

ridiculous, and the error is obvious. An independent knowledge of F is not often needed in this case.

C. Deep Invasion

In hard formations that are deeply invaded, the value found for R_t may be too high. At the same time R_{xo} may be too low, as just explained (see IA). Such accumulation of errors will give a ridiculous value for F. Taking $R_{xo} = R_{16}$ will improve the situation; if there is an independent knowledge of F, the presence of deep invasion can be accounted for.

II. F COMPUTED THROUGH EQ. 2 IS HIGHER THAN THE TRUE F.

In this case the value of S_w found by Fig. 8 is too high.

A. R_{xo} too High

This may take place in oil- and gas-bearing formations that have not been flushed properly by the mud filtrate. This occurs in highly permeable sands of the Gulf Coast where filtrate segregation takes place easily. It is also found in tight limestone matrices where the invasion takes place mostly in fractures and fissures. In these cases pessimistic interpretation can result if a good porosity control is not available. The standard relation (Eq. 1) should be used in this case.

B. Induction Log too Low

If an induction log is used to obtain R_t, it is possible that when R_{mf}/R_w is low the induction log value may be too low because $R_{xo} < R_t$ (see Part I, II-A).

CONCLUSIONS

Porosity balance is intended to provide a check of saturation values derived from logs by means of one of the resistivity ratio methods: (1) Induction-Electrical Log Method, (2) Rocky Mountain Method, and (3) R_{xo}/R_t Method.

The porosity balance check consists of computing a value of the formation factor, using the saturation value found by the application of one of the cited methods, and comparing this computed formation factor with the formation factor (or equivalently the porosity) derived from other independent sources. In general, if the computed formation factor is too low the corresponding value of saturation is too low; if the computed formation factor is too high, the corresponding value of saturation is too high.

The systematic use of the porosity balance can prevent the making of large errors and, in most cases, will provide a good verification of the water saturation calculated from the logs. In many cases, when discrepancies exist, the check makes it possible to improve the interpretation.

It is obvious that such a check is not possible by use of the standard relation (Eq. 1) alone, since any knowledge of the value of F has already been used in the determination of S_w ($S_w = \sqrt{F R_w/R_t}$).

The correct measurement of porosity for the knowledge of the corresponding formation factor cannot be over-emphasized.

ACKNOWLEDGMENT

The author wishes to express his appreciation to M. Martin and F. Segesman for their valuable assistance in the preparation of this paper. The release by the oil companies of data and examples used in this paper is also appreciated.

REFERENCES

1. Tixier, M. P.: "Electric Log Analysis in the Rocky Mountains", *Drill and Prod Prac.* API (1949) 316.
2. Poupon, A., Loy, M. E. and Tixier, M. P.: "A Contribution to Electrical Log Interpretation in Shaly Sands", *Trans.* AIME (1954) **201**, 138.
3. Dumanoir, J. L., Tixier, M. P. and Martin, Maurice: "Interpretation of the Induction-Electrical Log in Fresh Mud", *Trans.* AIME (1957) **210**, 202.

★★★

Streaming Potential and the SP Log

M. GONDOUIN
JUNIOR MEMBER AIME
C. SCALA

SCHLUMBERGER WELL SURVEYING CORP.
RIDGEFIELD, CONN.

ABSTRACT

Published laboratory data have established that very significant streaming potentials can exist across mud cakes subjected to pressure differentials such as exist between a mud column and formation fluids. Since shale is similar in kind and in properties to a well-formed mud cake, it appeared possible that streaming potentials might also arise across shales. A practical consequence would be that the streaming potential contribution to the SP would be smaller than might otherwise be assumed since the SP is measured with respect to the "shale base line". The resultant contribution would be the difference between the streaming potential across the shale and that across the mud cake.

In order to investigate this possibility, a laboratory apparatus was devised for measuring streaming potentials under pressure conditions normally encountered in wells. Reported data on streaming potentials across mud cakes were verified. More important, appreciable streaming potentials were found across shale samples. As in the case of mud cakes, the shale potentials varied with the concentration and nature of the impregnating electrolyte. Dependence on pressure was in a different relation than that for mud cakes, possibly because of the lower compressibility of shales. The differences in streaming potentials between the shales and mud cakes were generally small, although they might vary considerably in practice depending on the relative electrokinetic properties of the particular shale-mud cake combination. A "poorly effective" shale with a "very effective mud cake" would produce the largest negative addition to the electrochemical component of the SP.

Results of field experiments with pressurized wells were considered in the light of the laboratory results.

INTRODUCTION

Field experiments wherein the pressure of the mud column in a borehole was varied have often indicated the presence of a streaming potential, but its magnitude was not easily predictable and its sign sometimes changed from one formation to another in the same well.[1] In the interpretation of SP logs from standard surveys, nevertheless, the correct value of R_w is very frequently obtained, within the limits of field accuracy, using only the simple electrochemical expression of the SP provided that proper corrections are made for bed thickness, ion activity, etc.[2] Accordingly, it was apparent that the streaming potential component of the SP in a borehole was considerably more complex than commonly assumed and clarification was indeed necessary

The close similarity in nature and constitution of a shale to a well-compacted mud cake suggested that a streaming potential might also exist across shales as pointed out by M. P. Tixier in 1953 and as recently emphasized by Wyllie.[3] The practical consequence would be that the streaming potential across the mud cake would be canceled, at least in part, on electrical logs since the SP is recorded with respect to the shale potential as a base line. This appeared to be a plausible explanation for many of the effects observed but no supporting data were available. In 1955 preliminary experiments at low pressures were conducted in our laboratories which supported the hypothesis of the shale streaming potential and formed the basis for later studies at borehole pressures.*

EARLY LOW PRESSURE EXPERIMENTS

The early experiments were conducted primarily to determine the possibility of a streaming potential across shales. The shale used was a compact type designated as No. 7 from Reagan County, Tex. (Permian). Cut samples were saturated for over one month in .2 to 2.0-N NaCl solutions. In order to eliminate all electrode polarization effects, a dynamic method was used. A transient pressure of about 1 atm was applied across

Original manuscript received in Society of Petroleum Engineers office Sept. 15, 1957. Revised manuscript received May 29, 1958. Paper presented at 32nd Annual Fall Meeting of Society of Petroleum Engineers in Dallas, Tex., Oct. 6-9, 1957.

Discussion of this and all following technical papers is invited. Discussion in writing (three copies) may be sent to the offices of the *Journal of Petroleum Technology*. Any discussion offered after Dec. 31, 1958, should be in the form of a new paper.

[1] References given at end of paper.

*After the present paper was written and submitted for publication, it was brought to our attention that K. D. Shenck in his recent MS thesis entitled "An Investigation of the Streaming Potential Developed in Formations of Low Permeabilities" also showed the existence of a sizeable streaming potential across shale samples. (U. of Oklahoma, 1955.)

the sample and the resulting transient streaming potential was recorded. The resistivity of the shale samples was also determined. All results are presented in Table 1.

It was immediately obvious that the streaming potential across shale was far from negligible ($\sim +.17$ mv/atm for a .2-N NaCl solution).

It has been shown by Wyllie[4], that due to compressibility, the streaming potential across a mud cake is not directly proportional to the pressure difference P, but varies according to

$$E_k = k P^y , \quad . \quad . \quad . \quad . \quad . \quad . \quad . \quad . \quad . \quad . \quad . \quad (1)$$

where the exponent y has an average value of .75 when P is expressed in psi. This relationship was verified later by several experimenters including ourselves. According to Eq. 1, a typical streaming potential* across a mud cake at 100 atm is only about + 16 mv for a .2-N NaCl filtrate. If the limited data on shale could be extrapolated linearly to high pressures, the value for 100 atm would be + 17 mv. It was therefore conceivable that the streaming potential across shales could largely offset the streaming potential across the mud cake. Further study was definitely justified.

The present paper describes laboratory and field measurements of the streaming potential of shales under a broader range of pressures and from a variety of different shales. The effect of this source of potential on the SP curve is discussed.

TECHNIQUES OF MEASUREMENT AT HIGH PRESSURES

In order to measure the streaming potential at high pressures, a different apparatus was necessary. A high input impedance measuring circuit had to be used. Electrode polarization was a factor and for this reason it was preferable to use an alternating voltage signal which is considerably less affected by electrode polarization than a DC signal. This was accomplished by superimposing to the large static pressure difference on the sample studied a small alternating pressure, dP, of constant amplitude and frequency. The alternating electrokinetic emf, dE_k, produced was amplified and recorded as a function of the static pressure. The results could then be expressed as dE_k/dP vs P. This method gave excellent results. Since dP was known with good precision, the curve of E_k vs P could be readily constructed by integration of dE_k/dP.

A direct measurement of the static streaming potential, E_k vs P_{static}, was also possible by using reversible Ag-AgCl electrodes to minimize electrode polarization. However, the measurements were less accurate (± .1 mv) than by the alternating pressure method.

All laboratory experiments were at 75° F except where otherwise noted.

Sample Mounting

Shale disks of ⅞-in. diameter and ⅛ to ¾-in. thick were cut from field cores. Because of the tendency of the shale to cleave under pressure, the disks were cut with the shale bedding plane to be perpendicular to the direction of fluid flow in measurements. The disks were then cemented with Hysol inside one end of a machined Hysol holder (Fig. 1, part 6). The holder dimensions were 1-3/16 in. in diameter and 1½-in. long with a ½-in. axial hole to connect one face of the shale disk to the high pressure solution. Both faces of the disks were ground flat. Finally, the mounted samples were equilibrated in NaCl solution for several weeks at 70°C.

Pressure Bomb

The mounted sample was then inserted in a pressure bomb (Fig. 1), made of aluminum and entirely lined with a nylon jacket to insulate electrically the salt solution contained in the bomb from the aluminum housing.

The shale sample formed the partition between the two watertight compartments of the bomb. An Ag-AgCl electrode was placed in each compartment and connected to an insulated and watertight terminal on the aluminum housing. In order to avoid fracturing the shale when applying pressure, the face of the mounted shale sample was supported by a sintered steel disk resting on a shoulder of the pressure bomb body. Due to the high permeability and low electrical resistivity of the steel disk, no appreciable streaming potential could be generated across it and its mechanical strength was more than sufficient to resist the force applied to the shale sample by the imposed pressure.

Both compartments of the bomb were filled with the same NaCl solution and a thin rubber diaphragm was used to close each fluid chamber. The outer face of the rubber diaphragm closing one of the compartments was then submitted to the pressure of a nitrogen gas tank through a flexible pressure hose. The other compartment of the bomb was left at atmospheric pressure. A pressure reducer on the gas tank permitted the static pressure applied across the shale to be adjusted at any selected value between 0 and 1,000 psi. The static pressure was read on a Bourdon gauge connected to the gas line.

Alternating Pressure Devices

The bomb assembly was bolted horizontally to the platform of a modified shaker. The acceleration of the platform was a nearly pure sinusoidal function of time with a maximum amplitude of ± 30 g at a shaking frequency of 6.8 cps. This acceleration applied to the column of fluid in the bomb produced a sinusoidally

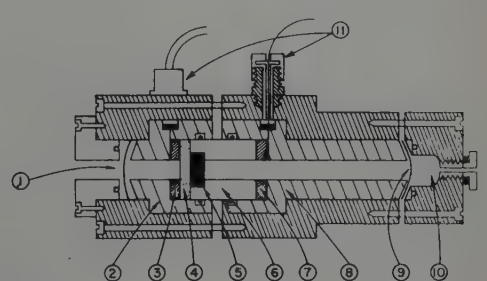

FIG. 1 — HIGH PRESSURE STREAMING POTENTIAL CELL.

Low Pressure Side
1. Rubber diaphragm
2. Nylon jacket
3. Ag-AgCl electrode
4. Sintered steel disk
5. Shale disk

High Pressure Side
6. Hysol holder
7. Ag-AgCl electrode
8. Nylon jacket
9. Rubber diaphragm
10. Gas chamber
11. Pressure-tight electrode connectors

*By definition, the sign of the streaming potential is the polarity of the electrode on the low pressure side. In a borehole, a positive streaming potential so defined would be recorded as a negative deflection since the measuring electrode is on the high pressure or mud side.

TABLE 1—RESULTS OF EARLY EXPERIMENTS, SHALE NO. 7—PERMIAN FROM TEXAS

NaCl Concentration of filtering fluid	Streaming Potential coefficient (mv/atm)	resistivity (Ωm) Shale
.2 N	.17	28
.5 N	.15	23
1.0 N	.14	17
2.0 N	.09	11

Sample dimensions: ¼ x ¼ x 7/16 in.
Transient pressure difference: 1 atm

varying pressure in the fluid calculable from the shaking speed and the length of the fluid column. By changing the pulley on the motor, the maximum amplitude of the pressure could be changed from ± .085 to ± .232 atm. A schematic of the pressure bomb, shaker and recording equipment assembly is shown in Fig. 2.

AC Recording Equipment

The electrical terminals of the bomb housing were connected by a low-noise coaxial cable to a chopper stabilized, low frequency amplifier with a gain of 1,000, (EMR Model No. 62A). A 20 μfd capacitor was placed in series in the input circuit. The output of the amplifier was connected through an electronic band-pass filter tuned at the frequency of the shaker to a Tektronix oscilloscope No. 535. The sinusoid appearing on the scope was then photographed with a Polaroid Land Camera. It was checked that no appreciable signal was introduced either by the cable or by the streaming potential across the sintered steel disk.

The over-all gain of the recording channel was measured in order to convert the signal amplitude on the photograph to millivolts. From the calibrated sweep frequency of the Tektronix scope, the period T of the shaker could be readily measured on the picture. The amplitude, A, of the alternating displacement of the shaking tube was measured carefully. The acceleration, γ, of the shaker could then be calculated exactly using the equation of longitudinal sinusoidal motion, namely $\gamma = \gamma_o \sin (2\pi t/T)$. Knowing the length, L, of the fluid column comprised between the two rubber diaphragms of the pressure bomb and the density, ρ, of the fluid, the alternating pressure was given by $\gamma P = L\rho\gamma_o$. The streaming potential coefficient*, dE_k/dP, was therefore completely derivable from the photograph. Measurements were made for each value of the static pressure in the range of 0 to 1,000 psi at 100-psi intervals.

DC Measuring Equipment

A vibrating reed electrometer, Applied Physics Corp. Model 30M, was connected across the 20 μfd capacitor in the input circuit of the AC recording channel. Due to the large time constant of the electrometer, it was practically insensitive to the alternating streaming potential produced by shaking, but any additional DC streaming potential produced when changing the static pressure was readily indicated.

The Ag-AgCl electrodes were found to be stable within ± 0.1 mv and the measured static streaming potential was generally about 1 to 2 mv/100 psi static pressure.

The sign of the streaming potential was also indicated on the electrometer. The results of the static measurements were compared to those obtained with the AC recording channel.

*E_k is sufficiently linear with pressure to assume $\Delta E_k/\Delta P = dE_k/dP$.

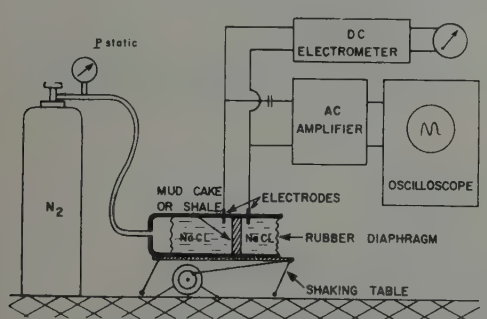

Fig. 2—Schematic of High Pressure Streaming Potential Apparatus Assembly.

Resistivity Measurements

The resistivity of each shale sample was measured with a two-electrode cell and a bridge. The cell was calibrated with NaCl solutions of known resistivity. The shale resistivity of some samples was also known from previous measurements with an inductive-type conductivity meter.

Permeability Measurements

With a slight modification of the pressure bomb it was possible to measure the permeability of the mounted shale sample. The rubber diaphragm on the low pressure end of the bomb was removed and the low pressure compartment connected to a calibrated glass capillary tube. The NaCl solution in the low pressure compartment was colored with Rhodamine B. The rise of the colored fluid in the capillary tube at various pressures was observed on a mirror-scale graduated in millimeters.

The permeability, K, was calculated from a plot of the level in the capillary vs time. The same plot also yielded an approximate value of the diffusivity coefficient $K/\mu(c + c')\,\phi$, where $c + c'$ is the apparent compressibility of the water in the pore space, μ the viscosity and ϕ the porosity. This parameter governs the progression of the fluid pressure front into the shale as shown in the Appendix.

Precautions were taken to avoid any rapid temperature variation in the room and the temperature inside the bomb was recorded within ± .5° C during the measurement. The absence of a leak at the O ring seal between the mounted sample and the bomb lining was checked by replacing the mounted shale sample by a solid Hysol plug of the same dimensions.

Base Exchange Capacity Measurements

The base exchange capacity per 100 gm of ground shale sample was measured for a few shales using the standard ammonium acetate method.

The porosity of the shale was estimated from direct measurements on solid shale plugs with a gas porosimeter and from measurements of grain volume on ground shale samples. From these data, the base exchange capacity per unit pore volume and the corresponding b factor of Hill and Milburn's method[5] were calculated.**

Membrane Potential Measurements

Some of the shale samples were tested as ion exchange membranes between two NaCl solutions. The ideality of the various shales was expressed qualitatively by plotting the ratio $K_{sh} = E/\log(a_1/a_2)$ vs the activity of the most concentrated solution in the manner described in Ref. 2. From these plots, the ratio $K_{sh}/59$ for a concentration of .1 N and 1 N was taken as an index of the efficiency of the shale under consideration. A fracture in the shale would seriously reduce this ratio.

LABORATORY MEASUREMENTS

Shale Samples

The streaming potential of 16 shale samples, for the most part at three different concentrations of the filtering NaCl solution, is shown in Fig. 3. The origin and

**The b factor is an index of the shaliness of the rock and is related to the base exchange capacity per pore volume (CEC/PV) by the expression $b = -.135\ (CEC/PV) - .0055$. It is therefore related to the fixed charge concentration, A, of the rock or m_R of Ref. 6.

characteristics of the shales are listed in Table 2. It was found that the static pressure had practically no effect on the magnitude of the streaming potential coefficient of shales, as shown by the linear increase of E_k with pressure (Fig. 4), and it must be inferred that the compressibility of shale in the pressure range studied was too small to affect its electrokinetic properties.

A comparison with earlier experimental results on Shale No. 7 is shown in Fig. 5. There is very good agreement in spite of the completely different methods of measurement used.

Returning to Fig. 3, it is seen that the streaming potential coefficient generally increases with the solution resistivity but not linearly. An expression of the form,

$$dE_k/dP_{(mv/atm)} = A(R_{mf})^n, \quad . \quad . \quad . \quad . \quad . \quad (2)$$

with $.15 < A < .7$ and $n \sim .3$, appears to be more suitable. This indicates that the surface conductance of the shale plays an important part. It appears in Fig. 3 that for most of the shales studied the streaming potential coefficient for a 1-Ωm solution resistivity is on the average about .25 mv/atm ($A_{av} = .25$ in Eq. 2). However, considerable departure from this "average" value is found for Shales 1-B and 29, showing that the type of shale can be of great consequence in the actual magnitude of the potential.

In an attempt to correlate the electrokinetic properties of shale with other properties, the base exchange capacity per pore volume or the b factor, of various shales are listed in Table 3. Also, the degree of ideality as indicated by electrochemical membrane potential measurements, which can be taken as an index of shaliness, is compared to the magnitude of the streaming potential coefficient. There does not seem to be any direct correlation between the variations of the shale streaming potential and the indices of shaliness.* Listed also are the permeabilities in .2-N NaCl solution since permeability is a distinguishing feature between a sandy shale and a shaly sand.

*Recent experimental results, to be published elsewhere, indicate that the electrokinetic properties of shales are dependent primarily on the transference number, t_w, of water, whereas the membrane behavior of shale is more dependent on the transference number, t_1 of Na^+ ions. t_w and t_1 are not directly related to each other, therefore it is not too surprising that no good correlation was found between "shaliness" or "membrane ideality" and dE_k/dP.

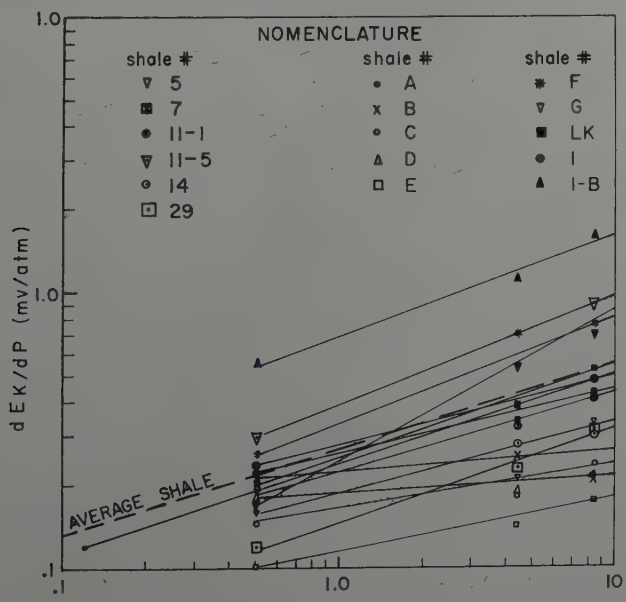

FIG. 3—dE_k/dP vs FLUID RESISTIVITY.

TABLE 2—ORIGIN AND AGE OF SHALE SAMPLES USED IN STREAMING POTENTIAL MEASUREMENTS

Shale No.	Locality or Field	State	Age or Depth (ft)
A	Centralia	Illinois	1,394
B	Hobbs Wildcat	New Mex.	8,603
C	Colorado County	Texas	9,057
D	Neves	Montana	7,067
E	Hovenweep	Utah	5,880
F	Stockholm	Oklahoma	4,155
G	Williams	New Mex.	11,235
LK	Houston County	Texas	?
1	Clark County	Illinois	Pennsylvanian 464
1-B	Clark County	Illinois	Pennsylvanian 468
5	Montgomery County	Texas	Eocene (Wilcox)
7	Reagan County	Texas	Permian (Spraberry)
11-1	Houston County	Texas	Upper Cretaceous (Woodbine)
11-5	Navarro County	Texas	Upper Cretaceous (Woodbine)
14	San Luis Obispo County	California	Middle Miocene
29	Sydney	Nebraska	Cretaceous

MUD CAKE SAMPLES

In order to compare directly the streaming potential of shales with that of mud cakes, a mud cake was formed on the sintered steel disk of the pressure bomb by filling the larger compartment of the bomb with an actual bentonite mud obtained from the field, and applying gas pressure to force filtrate through the porous steel disk. For this, the pressure bomb was placed vertically and the rubber diaphragms were not used. Once the cake was formed, both chambers were filled with a NaCl solution, the mud cake was equilibrated with the salt solution for several days and the streaming potential was measured as before. This laboratory produced mud cake was designated No. 1. A description of the mud used is given in Table 4.

The results of dynamic and static streaming potential measurements are indicated in Fig. 6. A plot of dE_k/dP vs P_{static} shows that, contrary to the results obtained with shales, the streaming potential coefficient varies with static pressure, Fig. 6. As a first approximation, the decrease of dE_k/dP can be considered as proportional to the static pressure, which leads to an equation of the form given by Wyllie, Eq. 1, for the variation of streaming potential with pressure. This result can

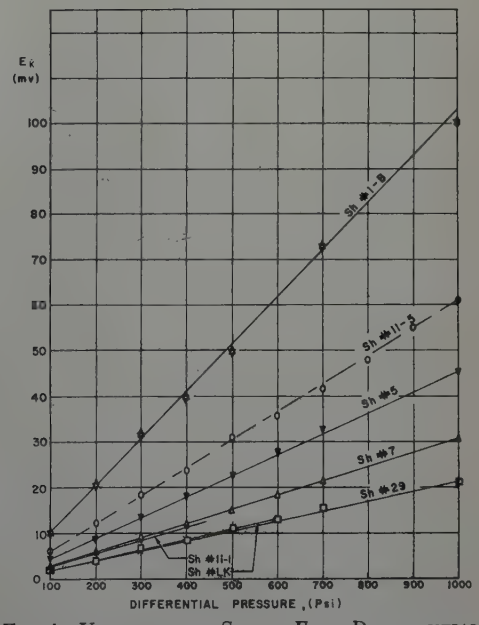

FIG. 4—VARIATION OF STATIC E_k vs DIFFERENTIAL PRESSURE FOR VARIOUS SHALES IN 0.01-N NaCl.

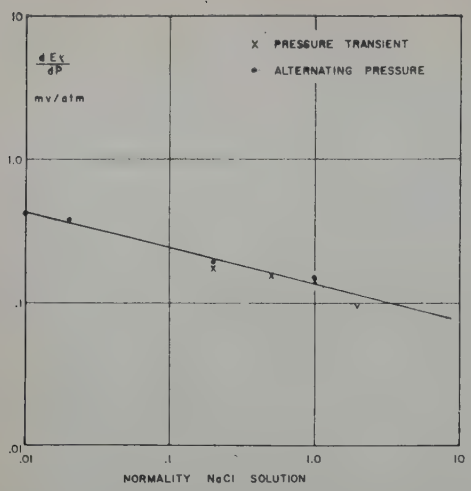

FIG. 5—STREAMING POTENTIAL OF SHALE NO. 7 VS CONCENTRATION OF NaCl SOLUTION. DIFFERENTIAL PRESSURE 14 PSI IN PRESSURE TRANSIENT METHOD, AND UP TO 1,000 PSI IN ALTERNATING PRESSURE METHOD.

also be confirmed by the plotting of the experimental values of E_k (static) vs P_{static}. The exponent y in Eq. 1 was found to be less than 1.0 in agreement with Wyllie's values.

A similar experiment was performed on a well-compacted mud cake formed under the conditions of pressure and temperature of the borehole. The mud cake, designated No. 2, was cut and mounted in exactly the same manner as the shale samples, and was equilibrated with NaCl solutions for the same length of time. Although the sample broke at 300 psi, the results that were obtained are in line with those of the artificially produced mud cake. The plot of dE_k/dP vs P for this mud is also shown in Fig. 6. For this mud cake the exponent y was about .79.

INFLUENCE OF THE VALENCE OF THE CATION

The electrokinetic potential is a function of the zeta (ζ) potential which for a given permeable membrane depends on the valence and size of the ions in the solution. In particular, it has been shown by Oakes and Burcik[7] that lanthanum (La^{+++}) ions depress the ζ-potential of clays, and at increasing concentrations the sign of the streaming potential is actually reversed.

Two of our shale samples (Nos. 7 and 29) were equilibrated with $LaCl_3$ solution and the streaming potential measured as before, except that the filtering fluid was a $LaCl_3$ solution. The results are indicated in Table 5. They are in qualitative agreement to those of Oakes and Burcik for mud cakes, and the sign reversal for a $LaCl_3$ concentration near .1 N is quite conspicuous. For divalent ions, such as Ca^{++} and Mg^{++}, the streaming potential would also be reduced but would not actually change sign in the usual range of concentrations. Although this experiment is only of academic interest since $LaCl_3$ is not expected in the mud filtrate, it shows that the streaming potential in shale exhibits the characteristics found with mud cakes.

EFFECTS OF TEMPERATURE

The effect of temperature on the streaming potential coefficient of shales was not investigated but the data obtained on mud cakes by Wyllie[4] indicated that this effect is probably not too important.

A significant effect of temperature on the SP log is a systematic base-line shift towards the positive direction. In consequence of the shale streaming potential, a base-line shift towards the negative direction would normally be expected as the depth (and therefore the differential pressure) increases. Such a shift is observed occasionally but not as commonly as a shift in the positive direction. It was therefore believed that some other phenomenon was masking the expected effect. For example, the potential with respect to ground of the SP measuring lead electrode is dependent on temperature and might therefore vary with depth in a manner to compensate the shale potential.

TABLE 4—CHARACTERISTICS OF MUD USED FOR MUD CAKE NO. 1

Type of Mud	Bentonite, Caustic-Quebracho
Weight:	10.2 lb/gal
Viscosity:	37 sec
Water Loss:	17 cc/30 min
R_m @ 75°F:	0.85 Ωm
R_{mf} @ 75°F:	0.60 Ωm
R_{mc} @ 75°F:	1.68 Ωm

The thermodynamically reversible potential of any metallic electrode with respect to the electrolyte in which it is immersed is given by the common equation.

$$E = E_{oT,P} + \frac{RT}{zF} \ln a_m \quad . \quad . \quad . \quad . \quad . \quad . \quad . \quad (3)$$

For a lead electrode in a mud containing a mixture of many ions, the exact electrode reaction is not readily predictable. The temperature coefficient of the potential depends on the over-all heat of the electrode reaction.

The magnitude of the temperature effect was determined for lead electrodes in a particular mud by a simple experiment. Here, two lead electrodes were placed respectively in two beakers containing identical mud samples (Aquagel-tannex-soda ash pH 8.5, R_m = .58 Ωm at 25°C) connected through a mud bridge. One beaker was maintained at a constant low temperature; the other was heated to various predetermined temperatures. The potential of the electrode in the heated beaker became more positive with increase in temperature. The temperature coefficient, roughly constant over a 40°C range, was approximately 0.31mv/°C. The temperature coefficients for muds of pH 10.5 and 12.5 were 0.19 and 0.13, respectively.

Another source of temperature dependence was studied. The shale in contact with mud filtrate acts as an electrode capable of exchanging ions with the mud filtrate. The exchange reaction and the corresponding emf at the junction shale/mud filtrate depend on temperature in a similar way to the contact emf between a metallic electrode and an electrolyte. This was recently observed with synthetic ion exchange membranes by Tyrell, Taylor and Williams[8] who called the phenomenon a "Seebeck effect" (by analogy with the Seebeck effect at the junction of metallic thermocouples). The emf is expressed by an equation similar to Eq. 3, where a_m in this case is the activity of the exchangeable ion in the mud filtrate.

The magnitude of the temperature dependence of the exchange potential with shale membranes was measured using the cell,

$$\mathrm{Ag/AgCl/NaCl}_{T_1}(C_1)\mathrm{/Shale/\ NaCl}_{T_2}(C_1)$$
$$\mathrm{NaCl}_{T_1}(C_1)\mathrm{/Ag/AgCl.}$$

TABLE 5—SHALE AND MUD CAKE STREAMING POTENTIALS WITH $LaCl_3$ SOLUTIONS

Concentration	.01N	.02N	.025N	.04N	.05N	.06N*	.08N*	.2N
dE_s/dP (mv/atm)								
Shale No. 7	+.16	+.11	—	—	—	0	—	−.13
Shale No. 29	—	+.34	—	—	—	—	0	−.20
Mudcakes**	—	—	+.68	+.47	+.31	—	0	—
ζ/ζ_0								

*Calculated.
**Data from Oakes and Burcik[7]. ζ_0 is Zeta potential at infinite dilution.

TABLE 6—PERMEABILITY OF SHALES (millidarcies)

Shale No.	.02 N NaCl	.2 N NaCl	1 N NaCl
A	—	2×10^{-6}	1×10^{-5}
C	3×10^{-4}	4×10^{-4}	—
D	6×10^{-4}	—	—
E	—	7×10^{-6}	—
F	—	8×10^{-4}	—
G	—	2×10^{-6}	—
LK	10^{-6}	7×10^{-6}	—
1-B	9×10^{-5}	—	—
14	—	4×10^{-4}	—
29	4×10^{-3}	—	—

Since the two Ag/AgCl electrodes are immersed in two identical salt solutions kept at the same temperature and the difference in transference numbers of Na^+ and Cl^- does not vary appreciably with temperature, the emf measured corresponds only to that of the cell, $NaCl_{T_1}(C_1)$/shale/$NaCl_{T_2}(C_1)$. The results are plotted in Fig. 7 for NaCl concentrations of .01 N, .1 N, and 1.0 N (8, .9 and .1 Ωm, respectively) and are compared with the results obtained on synthetic ion exchange membranes.[8] The experiment was repeated with a cell where the shale membrane had been replaced by a 10-ft column of .4-Ωm mud. The same order of emf values was obtained showing that a long mud column acted as an ion exchanger electrode. Summarizing, the change in emf due to the effect of temperature on the junction, clay/mud filtrate might produce a positive base-line drift of about 15 mv for a 100°F temperature difference in a 1-Ωm mud.

In conclusion, it is apparent from these experiments that the positive emf from temperature changes with depth in a borehole at the junctions lead/mud and mud filtrate/shale may offset the negative shale base-line drift of the shale streaming potential with temperature.

FIELD MEASUREMENTS

Numerous measurements[4,9,10,11] of streaming potential have been made in wells where the mud column had been put under an additional pressure or where the mud level in the hole had been lowered. But in most cases the change in SP with mud pressure was recorded only on front of permeable formations with the result that only the mud cake streaming potential was measured. However, in special instances the SP log was run over a complete section including shales and sands. Then it was observed repeatedly that a negative shift of the entire log occurred even when all precautions were taken to keep the potential of the ground SP electrode constant. The phenomenon was noted as early as 1934 by A. A. Perebinossoff in Pechelbronn, France. Another example, from California, is shown in Fig. 8. In 1941, during an experimental test run in cooperation with the Shell Oil Co., a streaming potential of about −7 mv was observed in front of a shale section for a 700-psi increase in mud pressure.

By applying an alternating pressure of about 100 psi at 0.5 cps with a suitable arrangement of the mud pump, a vibrated SP log was obtained in 1948. A striking feature was that the amplitude of the alternating streaming potential was roughly of the same order over the whole section, which included shale streaks 5 to 10-ft thick (Fig. 9).

Finally, in a recent field experiment with two SP electrodes placed respectively in front of a shale bed and in front of a permeable zone, an SP change of −8 mv was observed in front of the mud cake for a 400-psi increase in mud pressure, and −4 mv in front of the shale for the same pressure difference. The change in the SP value referred to the shale base line was therefore only −4 mv for a 400-psi additional pressure. The mud resistivity was 1.9 Ωm at 75°F.

The difficulty of performing a sufficient number of controlled experiments in the field with all significant parameters known accurately is very great and accordingly usable experiments are few. Nevertheless, as previously mentioned, the large number of cases where the water resistivity calculated on the basis of an electrochemical SP alone have agreed with production data indicates that the electrokinetic contribution is often small. Since laboratory measurements show a very significant electrokinetic potential for most mud cakes, a compensating potential such as from the shale is here also indicated.

Of course, specific cases where the mud cake streaming potential is unusually high or the shale streaming potential unusually low will exhibit a very significant residual electrokinetic SP component. The example of Fig. 8, for instance, presents such a combination. The shale streaming potential (.32 mv/atm) is rather low for a 5.8-Ωm mud, while the mud cake streaming potential is somewhat above average.

As pointed out by Wyllie, one special case of residual streaming potential on the SP log is in depleted reservoir sands. There the fluid pressure might be much lower in the sand than in the adjacent shales since the very low permeability of shale would prevent fast reestablishment of the pressure equilibrium. Consequently, the higher differential pressure across the mud cake than across the shales should result in the mud cake stream-

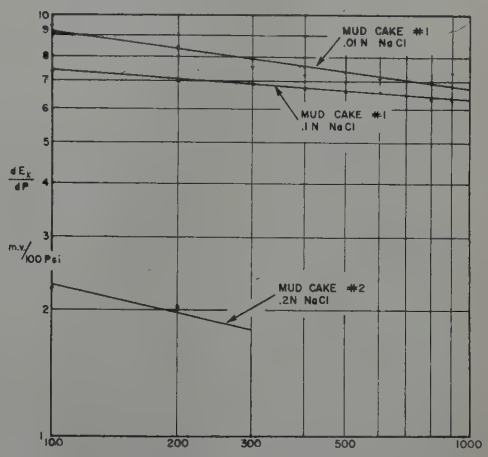

FIG. 6—VARIATION OF dE_k/dP WITH STATIC PRESSURE FOR MUD CAKES 1 AND 2.

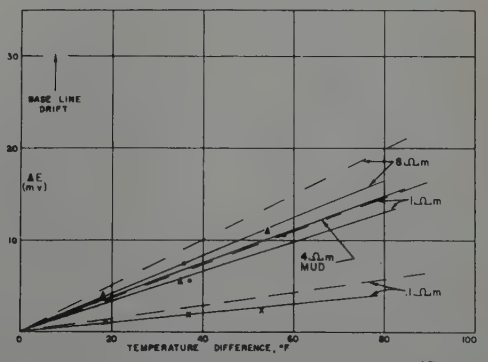

FIG. 7—VARIATION OF POTENTIAL MUD/SHALE WITH TEMPERATURE. FULL LINES ARE MEASURED DATA FOR NaCl/SHALE NO. 28: X — .01 N; O — .1 N; □ — 1 N; AND Δ — 4ΩM MUD DASHED LINES ARE DATA FOR NaBr/CATIONIC RESIN (PERMAPLEX C10) FROM REF. 8 FOR CORRESPONDING CONCENTRATIONS.

ing potential, E_{mc}, being larger than E_{sh}, across the shale. The pressure difference between shale and sand would also give rise to a streaming potential, E_{int}, at the shale-sand interface. However, the magnitude of E_{int} would be much smaller than either E_{sh} or E_{mc} because of the generally low resistivity of connate waters.

DISCUSSION

It is shown in Fig. 10 that although a definite residual streaming potential between mud cake and shale exists at low pressure, at high pressure the compaction of the mud cakes may decrease it and even reverse its sign. The pressure corresponding to an exact compensation (cross-over point) might be about 1,600 psi for a 1-Ωm mud filtrate with an "average mud cake" and an "average shale". Such a pressure is of the same order as the difference between formation pressure and mud column pressure in some deep wells (10,000 ft). For shallower wells and lower pressures the compensation may not be exact, but then both mud cake and shale streaming potentials are smaller so that even partial compensation would leave only a few millivolts for the streaming potential component of the SP. For muds fresher than 1 Ωm, the cross-over point should occur at a higher pressure, and under ordinary conditions there will be some residual negative streaming potential component whose magnitude will depend on the electrokinetic properties of both the mud cake and the shale.

To evaluate the extent of the compensation between shale and mud cake streaming potentials with actual field muds, a statistical study was made by combining

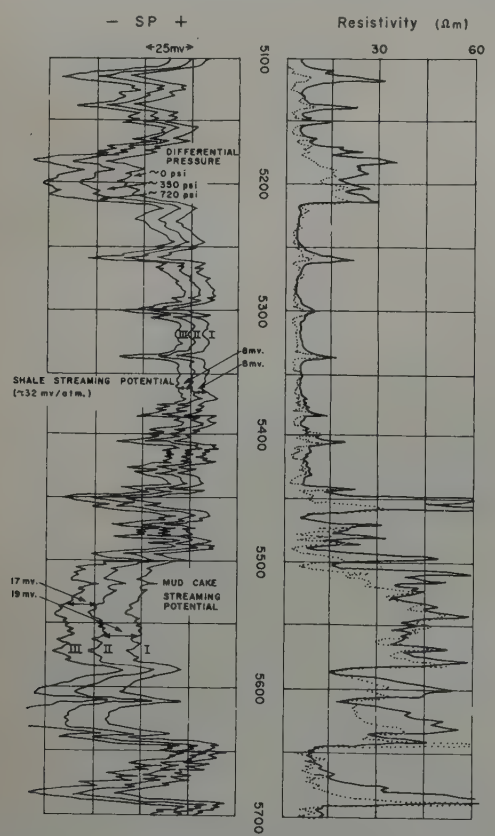

FIG. 8—DIFFERENTIAL SP EXPERIMENTS (CALIF., 1939). MUD DENSITY — 1.16, RESISTIVITY — 5.8 Ωm. (I) MUD LEVEL AT 706 FT. (II) HOLE FILLED, INCREASING PRESSURE TO ABOUT 24 ATM. (III) ADDITIONAL MUD PRESSURE OF ABOUT 25 ATM.

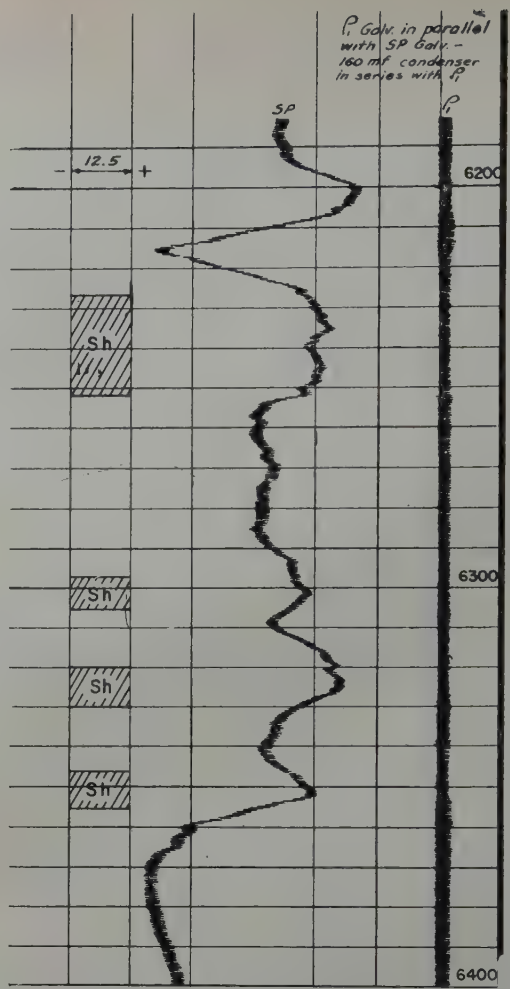

FIG. 9—VIBRATED SP FIELD EXPERIMENT. PRESSURE VARIATIONS AT 0.5 CPS BETWEEN 40 AND 150 PSI. CURVE ON LEFT IS THE SP RECORDED WITH RESULTING SUPERPOSED 0.5-CPS SP VARIATIONS. CURVE ON RIGHT HAS THE NORMAL SP VARIATIONS FILTERED OUT.

Pressure 25-50 psi to 150 psi and back to 25-50 psi
Frequency 0.5 cps
(N in mud pit)

our data on shale streaming potentials with those on mud cakes obtained by Moore[12] on 31 field muds from various parts of the country, and ranging in resistivity from .18 Ωm to 3.79 Ωm. The values of E_k at 100, 300, 500, 800, and 1,000 psi were calculated for each one of our 14 shales and subtracted successively from each of the E_k values measured by Moore on his 31 field muds at the same pressure. The result for each value of the pressure was a set of $14 \times 31 = 434$ residual potentials ($E_{mc} - E_{sh}$) corresponding to the electrokinetic components of the SP which would be observed in the hypothetical case of a well drilled into shale formations with any one of Moore's field muds.

These residuals were then tabulated in 5-mv increments and the number of residuals in each interval was plotted vs the mean value of the interval. The smoothed out statistical curves obtained in this manner are shown in Fig. 11. It appears immediately that the compensation is quite fair, with a maximum number of cases corresponding to a value of the electrokinetic component of the SP between − 5 and − 10 mv.

Other factors (such as a slight amount of shale in so-called "clean sands", or departure from ideal behavior of the shales, or the effect of invasion, etc. . . .)

which have been neglected in the formulation of the simple SP equation tend to reduce the amplitude of the SP. Accordingly, a small residual electrokinetic potential may frequently, by partial cancellation of these second-order terms, lead to a final SP value closer to the theoretical electrochemical value.

The SP shift in front of shales as well as in front of sands observed in field experiments as in Fig. 8, when an additional pressure is applied to mud column, is now easy to understand. Cases where the same increase in mud pressure may sometimes produce a *decrease* in the SP in front of certain formations and an *increase* in front of others may be explained as follows. The streaming potential component of the SP, $\Delta E_k = (E_{mc} - E_{sh})$, plotted vs differential pressure in Fig. 10 exhibits a maximum. (The pressure corresponding to the maximum is that for which dE_k/dP is the same for mud cake and shale.) When a well is submitted to an additional mud pressure besides the initial differential hydrostatic pressure, the following phenomena are to be expected: (1) for low initial differential hydrostatic pressure, the effect of an additional mud pressure is to *increase the SP* (Region A in Fig. 10); (2) for a higher initial differential hydrostatic pressure, the *SP remains practically unaffected* by limited changes in mud pressure (Region B in Fig. 10); (3) for a still higher initial differential hydrostatic pressure, any pressure increment results in a *decrease of the SP* (Region C in Fig. 10). All three phenomena have been observed in the field, although attention has been given primarily to the first one.

The displacement of the frequency peak on the statistical curves of Fig. 11 as a function of the differential pressure also strongly indicates that the electrokinetic component of the SP ($E_{mc} - E_{sh}$) first increases with pressure, passes through a maximum and then decreases.

One possible explanation for the streaming potential of some mud cakes being lower than that of shales at very high compaction pressures beyond the cross-over point where the two would normally be assumed similar may be that the clay particles in most "low water-loss" muds are mixed with organic colloids (starch, CMC, tannex, etc.) which tend to make the total charge density per unit volume of clay lower in the compacted mud cake than in the shale. This explanation is borne out by the experimental results of Salisch[13] who found that the streaming potential across mud cakes was lowered by the addition of starch, all other mud constituents remaining the same.

Finally, the wide variations between the electrokinetic properties of different shales and different mud

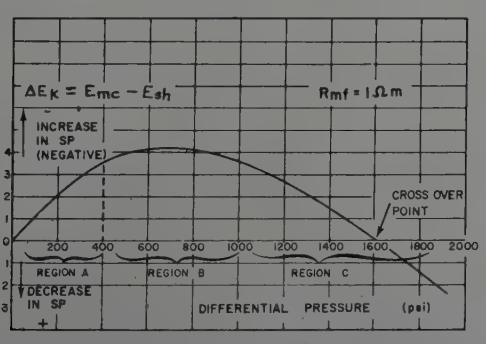

FIG. 10—ELECTRO-FILTRATION COMPONENT OF THE SP LOG VS DIFFERENTIAL PRESSURE. CALCULATED FOR AN AVERAGE SHALE AND MUD CAKE AND $R_{mf} = 1\ \Omega M$.

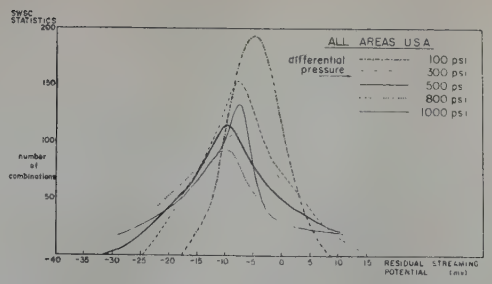

FIG. 11—STATISTICAL DISTRIBUTION OF RESIDUAL STREAMING POTENTIAL COMPONENT OF THE SP.

cakes explains why in certain cases a very significant electrokinetic component of the SP is present. For instance, the combination of a shale such as No. 29 with a very active mud cake such as Wyllie's No. 15-natural mud from Venezuela ($E_k = -44$ mv at 500 psi for a 2.3-Ωm mud) would result in a streaming potential component of $-44 + 2.7 = -41.3$ mv on the SP log.

CONCLUSIONS

The existence of a streaming potential across shales as well as across mud cakes has been proved by both laboratory and field experiments, and has been shown to account for many unexplained features of the SP log. In particular, it shows that in many cases the over-all contribution of electrokinetic phenomena to the SP log is minor and tends to compensate for the second-order terms which are neglected in the usual expression of the electrochemical SP.

There may be instances where, due to a particular combination of shale and mud cake properties or to an unusual pressure distribution (depleted sand), the electrokinetic component of the SP is not negligible.

For high resistivity muds and high differential pressures (1,500 psi), the extent of the compensation will depend primarly on the electrokinetic properties of both mud cakes and shales. Unless these are known, it may be necessary to rely on local field experience in particular formations drilled with a given type of mud. However, it is not advisable to apply the same "streaming potential correction" in all cases since the correction may change radically when a new type of mud is used.

For low resistivity muds ($R_{mf} \leqslant 1\ \Omega m$) both the streaming potentials in front of mud cakes and in front of shales are small and their difference may not be significant on the SP log.

ACKNOWLEDGMENTS

The authors wish to acknowledge the contributions of R. Blizard and E. Cook who performed the earlier experiments, and of the able assistance of A. Heim and A. Kermabon in some of the laboratory measurements and of G. K. Gillies and C. Johnston in the field experiments.

Particular credit is due G. L. Simard and M. Martin for their continued help and guidance during this investigation, and acknowledgment is made of the technical advice of M. Ferre. The cooperation of the oil companies in furnishing shale cores and log data is appreciated. The Shell Oil Co. in particular is to be thanked for its interest and for making a field experiment possible.

Stimulating discussions were held with M. R. J. Wyllie, H. Hill, and L. DeWitte. It is a pleasure to acknowledge their very pertinent comments and criticisms.

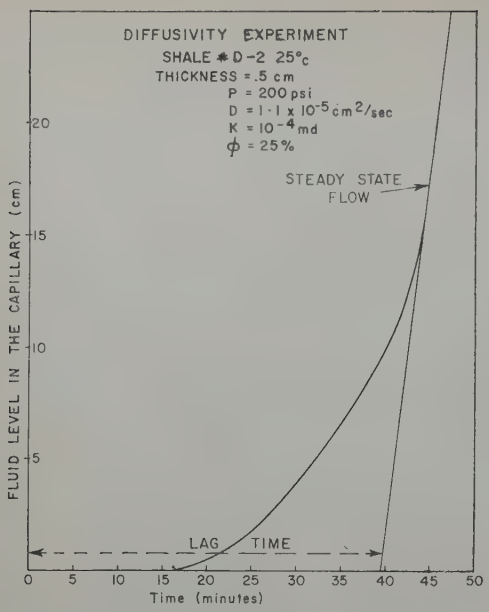
DIFFUSIVITY EXPERIMENT
SHALE # D-2 25°c
THICKNESS = .5 cm
P = 200 psi
D = 1·1 x 10⁻⁵ cm²/sec
K = 10⁻⁴ md
ϕ = 25%
STEADY STATE FLOW
LAG TIME
FLUID LEVEL IN THE CAPILLARY (cm)
Time (minutes)
0 5 10 15 20 25 30 35 40 45 50
5 10 15 20

FIG. 12—EXPERIMENTAL CURVE OF CUMULATIVE FLUID FLOW THROUGH SHALE VS TIME.

REFERENCES

1. Pirson, S. J.: *Bull.*, Mineral Industries Experimental Sta., Pennsylvania State College (1948) 52.
2. Gondouin, M., Tixier, M. P. and Simard, G. L.: *Trans.* AIME (1957), **210,** 58.
3. Wyllie, M. R. J.: *Fundamentals of Electric Log Interpretation*, 2nd Ed., Academic Press, N. Y. (1957).
4. Wyllie, M. R. J.: *Trans.* AIME (1951), **192,** 1; also Natl. Conf. on Clays and Clay Techn.—Univ. of Calif., Berkeley (1952).
5. Hill, H. J. and Millburn, J. D.: *Trans.* AIME (1956) **207,** 65.
6. DeWitte, L.: *Trans.* AIME (1955) **204,** 103.
7. Oakes, D. T., and Burcik, E. J.: *Proc.*, Fourth Natl. Conf. on Clays and Clay Materials, National Academy of Sciences, National Research Council (1956) Pub. 456, 225.
8. Tyrell, H. J. V., Taylor, D. A. and Williams, C. M.: *Nature* (April 7, 1956) 669.
9. Schlumberger, C. and M., and Leonardon, E. G.: *Trans.* AIME (1934) **110,** 273.
10. Gillingham, W. J.: Mineral Ind. Exp. Sta., Penn. State College, *Bull.* 21.
11. Sauvage, R.: "Relationship Between SP and Mud Pressure", Burma (1934) unpublished.
12. Moore, D. W.: MS Thesis, U. of Oklahoma (1955).
13. Salisch, H. A.: "An Experimental Investigation of Factors Affecting the Electrokinetic Component of the SP Curve", MS Thesis, U. of Oklahoma (1954).
14. Van Everdingen, A. F. and Hurst, W.: *Trans.* AIME (1949) **186,** 305.
15. Carslaw, H. S. and Jaeger, J. C.: *Conduction of Heat in Solids*, Oxford (1947).
16. Crank, J.: *The Mathematics of Diffusion*, Oxford (1956).
17. Fatt, I.: *Trans.* AIME (1958) **213,** 64.
18. Barrer, R. M.: *Diffusion In and Through Solids*, Cambridge (1941).
19. Terzaghi, K.: *Economic Geology*, 50th Anniv. Vol., Part 2, 575.
20. Despic, A. and Hills, G. J.: *Trans.* Farad. Soc. (1957) **53,** 1262.
21. Helfferich, F. and Ocker, H. D.: Zeitschrift fur Physikalische Chemie (1957) **10,** 374.

APPENDIX

NON STEADY STATE-PRESSURE DISTRIBUTION OF THE FLUID FLOWING INTO A SHALE

In the evaluation of $E_{k\ \text{shale}}$ under the borehole conditions it was implied that all of the pressure drop between mud and formation pressures occurred in the portion of the shale bed in equilibrium with the mud filtrate. In order to substantiate this assumption the relative positions of the spatial pressure distribution and of the diffusion front in shale are calculated. It is shown that both fronts progress approximately at the same rate.

ASSUMPTIONS

Both the fluid and the pore space are compressible. The flow obeys Darcy's law. The filtrate has the same compressibility, density and viscosity as the formation water. For simplicity we will assume a linear flow into a semi-infinite medium bounded by a plane surface. The case of a radial flow into an infinite medium bounded internally by a cylindrical surface has been treated[14,15], but it is felt that a plot of the corresponding solution would take considerably more time and would not differ too much from the simple solution of a linear flow. At any rate, the main effect of the radial distribution would be to make the pressure front more abrupt and to slow down its rate of progression.

The following basic equations are for linear flow.

Darcy's Law: $$Q = \frac{K}{\mu}\frac{\partial P}{\partial x} \quad . \quad . \quad . \quad . \quad . \quad . \quad . \quad . \quad (1)$$

Material balance equation:

$$\frac{\partial(\rho Q)}{\partial x} = \frac{\partial(\rho\phi)}{\partial t} \quad . \quad . \quad . \quad . \quad . \quad . \quad . \quad . \quad . \quad . \quad (2)$$

Compressibility equations:

$$\rho = \rho_o e^{c'P} \quad \text{(for water)}) \quad , \quad . \quad . \quad . \quad . \quad . \quad . \quad (3)$$

and

$$\phi = \phi_o e^{cP} \quad \text{(for the shale pore space)} \ ,$$

with $$P = P_x - P_F \quad . \quad . \quad . \quad . \quad . \quad . \quad . \quad . \quad . \quad . \quad (4)$$

where Q is the rate of flow into the shale, P_x the fluid pressure inside the shale at a distance of x from the wall, P_F the formation pressure, K the shale permeability, μ the fluid viscosity, t the time, ρ the fluid density, ϕ the shale porosity, and c' and c the compressibility coefficients of the fluid and of the pore space, respectively.

Then,

$$P = \frac{1}{c + c'}\log_e \frac{\phi\rho}{\phi_o\,\rho_o}, \quad . \quad . \quad . \quad . \quad . \quad . \quad . \quad . \quad (5)$$

and by differentiating with respect to x and substituting into Darcy's law,

$$Q = \frac{K}{\mu(c + c')\phi\rho}\frac{\partial(\phi\rho)}{\partial x} \quad . \quad . \quad . \quad . \quad . \quad . \quad . \quad (6)$$

Then the material balance equation becomes

$$\frac{\partial}{\partial x}\left(\frac{K}{(c+c')\phi\mu}\frac{\partial(\phi\rho)}{\partial x}\right) = \partial\left(\frac{\rho\phi}{\partial t}\right) . \quad . \quad . \quad . \quad (7)$$

But for relatively small values of P, it is possible to approximate $\phi\rho$ by

$$\phi\rho = \phi_o\,\rho_o\,[1 + (c + c')\,P] \quad . \quad . \quad . \quad . \quad . \quad (8)$$

Differentiating with respect to x and to t the material balance equation becomes

$$\frac{\partial}{\partial x}\left[\frac{K}{\mu(c + c')\phi}\frac{\partial P}{\partial x}\right] = \frac{\partial P}{\partial t}, \quad . \quad . \quad . \quad . \quad . \quad . \quad (9)$$

which is identical to the common differential equation of diffusion,

$$\frac{\partial}{\partial x}\left[D\frac{\partial C}{\partial x}\right] = \frac{\partial C}{\partial t}, \quad . \quad . \quad . \quad . \quad . \quad . \quad . \quad . \quad (10)$$

in which the concentration C has been replaced by the pressure P, and where the diffusion coefficient,

$$D = \frac{K}{\mu\,(c + c')\phi} = \frac{K}{\mu\,(c + c')\phi_o\,e^{cP}}, \quad . \quad (11)$$

which will be called the "diffusivity" coefficient of the fluid into the shale.

The solution of Eq. 10 when D is an exponential function has been given by Crank[16], but in the low pressure range $P = 200$ psi and for compressibilities of pore space of the order of 50×10^{-5} cc/cc/atm (assuming that the shale pore space compressibility is of the same order of magnitude as that measured on sandstone by Fatt[17]) the term $e^{cP} = 1.01$ so that D remains practically independent of P.

$$D \approx \frac{K}{\mu(c + c')\phi_o} \quad . \quad . \quad . \quad . \quad . \quad . \quad . \quad . \quad . \quad (12)$$

Then the solution of Eq. 10 becomes simply

$$P = (P_m - P_F) \operatorname{erf} \frac{x}{2\sqrt{Dt}} \quad . \quad . \quad . \quad . \quad . \quad (13)$$

where $P_m - P_F$ is the total differential pressure.

The evaluation of D on shales can be made directly using the "time-lag" method developed by Barrer[18] for the measurement of diffusion coefficients.

In the permeability measurement the rise of the colored fluid in the glass capillary is plotted as a function of the time elapsed after application of the pressure difference across the shale membrane. The type of curve obtained is shown in Fig. 12. The permeability K is obtained from the slope of the straight-line portion (steady-state flow) and it can be shown that the diffusivity coefficient is related to the lag time L by

$$D \approx \frac{h^2}{6L}, \quad . \quad . \quad . \quad . \quad . \quad . \quad . \quad . \quad . \quad . \quad . \quad (14)$$

where h is the thickness of the shale membrane.

The values of D obtained on three different shales of permeabilities ranging from 10^{-4} to 10^{-6} md varied from 10^{-5} to 10^{-6} cm^2/sec. These values are in excellent agreement with those measured by Terzaghi[19] on surface clays. Using our experimental data for K, D and ϕ_o in Eq. 12 one can calculate $(c + c')$. The values obtained are at least one order of magnitude larger than the compressibilities of reservoir rocks measured by Fatt[17]. Even so, the term e^{cP} remains close enough to the value of 1 that D can be taken as constant in the 200-psi pressure range used in the experiment. For high pressures, however, the term e^{cP} must be taken into account. As a result, the pressure front is slightly more abrupt than for a constant D. It is seen that the pressure drop is contained entirely in a zone very close to the face of the formation (Fig. 13).

The cumulative flow, Q_t, can also be calculated by

$$Q_t = \int_o^t \left(\frac{k}{\mu}\frac{\partial P}{\partial x}\right)_{x=o} dt \quad . \quad . \quad . \quad . \quad . \quad . \quad . \quad . \quad (15)$$

or, with a constant D,

$$Q_t = 2K/\mu \frac{\Delta P}{\sqrt{\pi D}} \sqrt{t} \quad . \quad . \quad . \quad . \quad . \quad . \quad . \quad (16)$$

If one assumed a piston-like displacement of the formation water by the mud filtrate, the corresponding

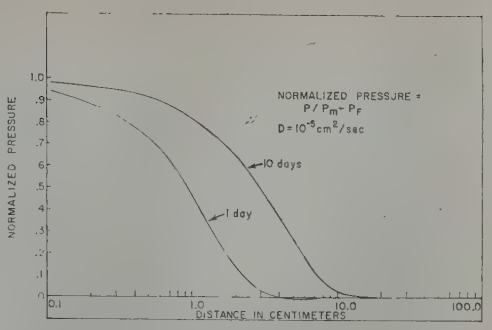

FIG. 13—PRESSURE DISTRIBUTION IN SHALE (LINEAR FLOW).

depth of invasion into low permeability shale would be only 8×10^{-2} cm after one day for $D = 10^{-5}$ cm^2/sec and $K = 10^{-6}$ md; but at these very low flow rates other effects such as mixing due to "channeling" and ionic diffusion from the concentrated formation water into the dilute mud filtrate appreciably extend the "invaded" zone in the shale.

The diffusion coefficient, D', for shale at the formation temperature is not known, but one can calculate its order of magnitude from the shale conductivity, K, and fixed charge concentration, A, using the Nernst-Einstein equation.

$$D' = \frac{RT}{zF^2}\lambda \quad , \quad . \quad . \quad . \quad . \quad . \quad . \quad . \quad . \quad . \quad . \quad (17)$$

where λ is the equivalent conductance of the shale,

$$\lambda = \frac{K(\Omega^{-1}\ \text{cm}^{-1})}{A(\text{eq/cc of shale})} \quad , \quad . \quad . \quad . \quad . \quad . \quad (18)$$

and z the valence of the diffusing ion. This neglects the electro-osmotic contribution to the shale conductivity, but this effect is quite small at high concentrations. The fixed charge concentration, A, at high concentrations can be evaluated from measurements of the base exchange capacity. An average BEC value of about 11 meq/100 gm of shale, with a shale density of 2.5 gives $A \approx .275 \times 10^{-3}$ eq/cc. An average shale conductivity at a bottom-hole temperature of 350°K may be taken as about 10×10^{-3} mho/cm. D' given by Eq. 17 is therefore,

$$D' = \frac{8.3 \times 350°\text{K}}{(96{,}500)^2} \times \frac{10 \times 10^{-3}}{.275 \times 10^{-3}}$$
$$= 1.1 \times 10^{-5}\ \text{cm}^2/\text{sec}.$$

This figure is in general agreement with the values measured on synthetic ion exchange membranes[20,21]. Ionic diffusion alone, even in the absence of any pressure gradient, accounts for a penetration of the invasion front into the shale as deep as that of the pressure front. When other factors such as mixing due to microscopic channeling, as commonly observed in porous rocks, and swelling of the clay matrix are taken into account, it seems quite reasonable to assume that the portion of the shale in equilibrium with the mud filtrate extends over the entire zone where a pressure gradient exists.

★★★

The Cutting Carrying Capacity of Air At Pressures Above Atmospheric

KENNETH E. GRAY
JUNIOR MEMBER AIME

THE CALIFORNIA CO.
VENICE, LA.

ABSTRACT

The turbulent flow drag coefficients, or friction factors, have been experimentally determined for the cuttings normally encountered in drilling operations.

The gas law and average drag coefficients for characteristically flat particles (limestones and shales) and for angular to sub-rounded particles (sandstones) were used to extend Newton's equation to a more useful form. The resulting equations are expressions for the slip velocity of a particle as a function of the particle size and shape, the bottom-hole injection pressure, and the bottom-hole temperature.

The velocities necessary to lift actual rock cuttings as observed in the laboratory were compared with velocities predicted from the derived equations. Results indicate that there is no single correct circulating velocity and that the commonly used 3,000 ft/min linear velocity may be sufficient to lift only very small particles. The advantage, in terms of horsepower requirements, of cycling high pressure air to obtain lower compression ratios was shown.

INTRODUCTION

A promising departure from standard rotary hydraulic drilling is air or gas drilling. In many instances the rate of penetration and bit life increases resulting from this method have been very substantial. Further the application of air drilling in areas of lost circulation or water sensitive pay zones has been highly successful.

PURPOSE

For the drilling contractor, the practical question remains, "How much air pressure and volume should I have?" It is necessary to have a reasonable knowledge of the air velocities and pressures required in air drilling operations for the proper design and most advantageous use of surface equipment and for adequate removal of cuttings from the borehole. Based on experience, most operators agree that at least 3,000 ft/min linear velocity is necessary for satisfactory hole cleaning.[1]

Original manuscript received in Society of Petroleum Engineers office July 19, 1957. Revised manuscript received April 21, 1958. Paper presented at 32nd Annual Fall Meeting of Society of Petroleum Engineers in Dallas, Tex., Oct. 6-9, 1957.
[1]References given at end of paper.

It was the purpose of this investigation to evaluate the drag coefficients, or friction factors, for the cuttings normally encountered in drilling operations, i.e., sandstones, limestones and shales, and to utilize the values obtained to develop an expression for the minimum velocities and pressures (hence the volumes) necessary to lift these cuttings.

THEORY

Several investigators[2,3,4] have done extensive work on the ability of drilling mud to lift bit cuttings. They conclude that the ability of a drilling mud to lift cuttings is dependent on the density difference between the rock being drilled and the drilling mud, the cutting size and shape, the mud flow constants, and the flow state (laminar, transitional or turbulent) of the mud. However, drilling muds are not true fluids but have a variation of viscosity with velocity in laminar flow and a constant apparent viscosity in turbulent flow.

A survey of the literature revealed that no experimental work had been done to determine the velocities necessary to lift actual rock cuttings using a compressible fluid such as air or gas. In 1953, Nicolson[5] stated that in air drilling fluid mechanics the particles could be assumed spherical in shape and that a constant drag coefficient of 0.5 could be used due to the highly turbulent flow of the circulating air. By equating the turbulent resistance on the particle to the gravitational force on the particle, he obtained the expression,

$$V_s = 2.67 \left(\frac{D \rho_s}{\rho_f} \right)^{\frac{1}{2}} , \quad . \quad . \quad . \quad . \quad . \quad . \quad . \quad . \quad (1)$$

where V_s is slip velocity of spherical particle, ft/sec; D is particle diameter, in.; ρ_s is particle density, lb/ft^3; and ρ_f is fluid density, lb/ft^3.

However, as stated earlier, most operators seem to agree that adequate hole cleaning can be obtained by circulating a sufficient volume of air to give a linear velocity of 3,000 ft/min in the annular space.

BASIC EQUATION

The velocity with which a solid particle freely falls through a fluid will increase until the accelerating force, gravity, is equal to the resisting forces, buoyancy due to the fluid displaced by the particle and friction due to the relative motion of the particle through the fluid. When the accelerating and resisting forces become equal,

the solid continues to fall at a constant maximum or terminal velocity unless additional forces upset this balance. It is this terminal velocity, commonly called slip velocity, which is of interest in air drilling, and it is given by

$$V_s = \sqrt{\frac{4(\rho_s - \rho_f)gD}{3\rho_f f_D}}, \quad \ldots\ldots\ldots \quad (2)$$

where g is the gravitational constant, (32.2 ft/sec^2) and f_D is the drag coefficient.

Eq. 2, which holds true for laminar, transitional, or turbulent flow is frequently termed Newton's law. It expresses the maximum velocity for falling spheres in a fluid of infinite extent in terms of a variable friction factor or drag coefficient, f_D. The complete derivation is given in the Appendix.

The drag coefficient, f_D, is a function of the Reynolds number, R_e, and when D, ρ_f, or V_s is unknown, Eq. 2 must be solved by a trial-and-error procedure because these terms appear in both the friction factor and the Reynolds number. However, the trial-and-error procedure when solving for V_s may be eliminated by a method outlined by Brown[6], as shown in the Appendix.

Wall Effect on Slip Velocity

If the fluid is confined in an annulus or otherwise so that it may not be regarded as infinite in extent, the projected area of the falling particle is not negligible with respect to the cross-sectional area of the annular space through which it is moving. The effect is to increase the resistive force on the particle, and the apparent slip velocity calculated from the annular dimensions and flow rate is lower than the theoretical slip velocity of that particle in a fluid of infinite extent. Actually, slip velocity is the relative velocity between the particle and the fluid and is, therefore, the same in either case.

For an annulus, an empirical correction or "wall effect" factor by which V_s may be modified has been suggested.[2]

For turbulent conditions,

$$V_a = \frac{V_s}{1 + D/d}, \quad \ldots\ldots\ldots \quad (3)$$

where V_a is the apparent slip velocity, V_s is the theoretical slip velocity, and d is the equivalent diameter of the annulus (four times hydraulic radius).

Effect of Particle Shape on Slip Velocity

If the particle is not spherical in shape, the slip velocity, V_s, is some value less than that required for a perfectly spherical particle. It has been customary to multiply the V_s for a spherical particle by the sphericity, ϕ, in order to determine the actual slip velocity for an irregularly shaped particle. The sphericity[6] (ϕ) is the surface area of a sphere having the same volume as the particle divided by the surface area of the particle.

$$\phi = \frac{D_{avg}}{D_s}\left(\frac{1}{n}\right), \quad \ldots\ldots\ldots \quad (4)$$

where n is ratio of specific surfaces, D_{avg} is average screen size, and D_s is diameter of sphere having same volume as particle.

The application of the correction factor sphericity, ϕ, is useful when the particle in question is of a regular shape such as a cube, cylinder or disk. However, it is difficult to apply to an irregular particle such as a rock cutting due to the difficulty in evaluating the ratio of specific surfaces, n.

Referring to the Stanton diagram shown in Fig. 1, it appears that the drag coefficient, f_D, for a given set of conditions, should be essentially constant in highly turbulent flow. Furthermore, for the condition of turbulent flow, the drag coefficient is, for all practical purposes, independent of viscosity. The magnitude of f_D for a given system should be a function of the characteristic shape of the particle being lifted, that is, its deviation from spherical shape. It follows, then, that by evaluating f_D for a given shape of rock particle, the problem of determining the sphericity of that particle may be circumvented.

APPARATUS AND PROCEDURE

Apparatus

The apparatus used in this investigation is shown in Figs. 2 and 3. Transparent Lucite tubing having an ID of 4 in. and a wall thickness of 0.25 in. was used to represent the annular space of a borehole. The drill pipe, represented by 1.5-in. pipe, was rigidly centered in the annular space as shown in Fig. 2. The over-all length of the flow string was approximately 20 ft.

The pressure lines were placed inside the drill pipe rather than into the plastic tubing so as not to weaken the Lucite flow string.

The injection and back pressures were indicated on the duplex gauge; the pressure drop between the point of cutting injection and various points up the flow-string could be read on the mercury manometer.

The back-pressure valve consisted of 1-in. rubber tubing in a short piece of pipe slightly large in diameter (see Fig. 3). Air forced into the annular space between the tubing and the pipe caused the rubber tubing to "neck down" and restrict the flow of air through the system, yet allow rock cuttings to pass through the valve. By controlling the pressure exerted on the rubber tubing by means of a 0- to 200-psi regulator (the back-pressure regulator shown in Fig. 2) the desired back pressure could be held on the system.

Procedure

1. A sample of rock cuttings, having been sized with Tyler screens, was placed in the lubricator, and air from the storage tanks was passed through the orifice meter at a low rate.

2. The back-pressure valve was adjusted to restrict the flow rate to a very small value.

3. The injection pressure was then increased and the back pressure steadily decreased until the cuttings were

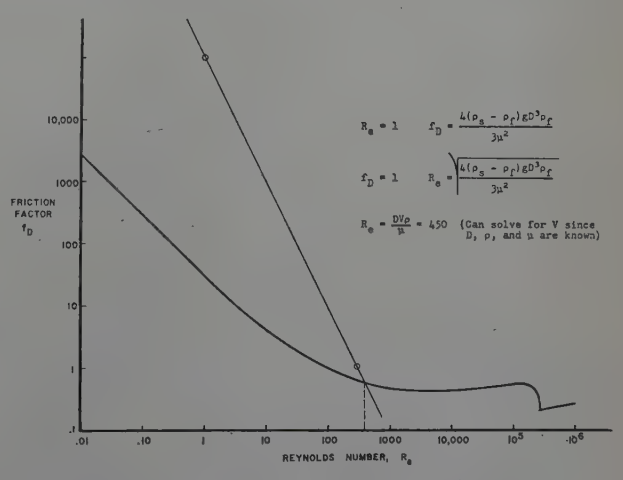

Fig. 1—Friction Factor vs Reynolds Number for Spherical Particles.

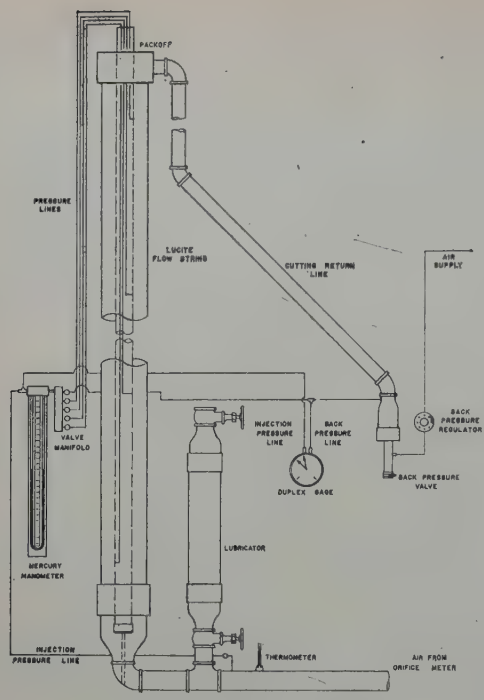

FIG. 2—AIR DRILLING APPARATUS.

suspended in the flow string. The movement of the cuttings up or down the annulus could be easily controlled with the back-pressure valve.

4. While the cuttings were suspended, the orifice meter readings, flowing temperature, and the injection and back pressures were recorded.

5. In addition, the pressure drops between the injection point and the various positions up the flow string were recorded.

This procedure was repeated at flowing back pressures ranging from 0 to 81 psig.

6. To evaluate f_D for a characteristic cutting shape, the apparent velocity, V_a, calculated from flow data and the geometry of the flow string, was corrected for wall effect to give a V_a in an infinite fluid system (V_a would then be numerically equal to V_s). This value for V_a was substituted into Eq. 2 and f_D calculated for that trial. The resulting values for f_D were averaged, and this average value was then used as the theoretical f_D for that cutting shape in subsequent use of Eq. 2.

Each experimental value for f_D obtained in the listed manner was for an air stream of a specific density and velocity. Although f_D is a function of the velocity at which the flowing fluid is passing the cuttings, after turbulent flow has been established f_D is not greatly influenced by increases in the velocity of the air stream. On this basis it was assumed that in turbulent flow, cuttings which are characteristically flat, or flake-like (such as limestone or shale) would have the same constant drag coefficient. Rounded particles such as sandstone cuttings would have some other constant drag coefficient.

EXPERIMENTAL RESULTS

Table 1 gives a summary of the experimental data taken and the calculations made to compare observed and theoretical slip velocities of limestone and sandstone particles. The percentage deviation was calculated using V_a and V_s (theoretical).

EXTENSION OF BASIC EQUATION

Having experimentally established a drag coefficient of 1.40 for flat particles (shales and limestones) and 0.81 for angular to sub-rounded particles (sandstones), Eq. 2 may be further simplified.

$$V_s = \sqrt{\frac{4(\rho_s - \rho_f)gD}{3\rho_f f_D}} \quad \ldots\ldots\ldots \quad (2)$$

Recalling from the gas law that

$$Pv = \frac{ZRT}{M}, \quad \ldots\ldots\ldots\ldots \quad (5)$$

where v is specific volume, ft³/lb; P is pressure, psia; R is gas constant, 10.73; T is temperature, °R; M is molecular weight; and Z is deviation factor.

Thence

$$\rho_f = \frac{1}{v} = \text{lb/ft}^3 = \frac{PM}{ZRT} \quad \ldots\ldots\ldots \quad (6)$$

Using the average experimentally determined f_D of 1.40 for flat particles (limestone or shales) and remembering that for air: $M = 29$, $R = 10.73$, and $Z = 1.0$ (at 100°F, Z ranges from 1.00 to .996 as P ranges from atmospheric to 500 psia).

$$\rho_f(\text{air}) = \frac{P(29)}{(1)(10.73)(T)}.$$

By substituting ρ_f and f_D into Eq. 2, the following equation is obtained.

$$V_s = 1.6\left[D\left(\frac{.371T\rho_s}{P} - 1\right)\right]^{\frac{1}{2}}, \quad \ldots \quad (7)$$

where T is bottom-hole temperature, °R, and P is bottom-hole injection pressure, psia. Eq. 7 may be very closely approximated by

$$V_s = \left(.9456\,\frac{DT\rho_s}{P}\right)^{\frac{1}{2}} \quad \ldots\ldots\ldots \quad (8)$$

A similar procedure for sandstone particles, using an f_D of 0.81 will yield the equations:

$$V_s = 2.1\left[D\left(\frac{.371T\rho_s}{P} - 1\right)\right]^{\frac{1}{2}}, \quad \ldots \quad (9)$$

and

$$V_s = \left(1.445\,\frac{DT\rho_s}{P}\right)^{\frac{1}{2}} \quad \ldots\ldots\ldots \quad (10)$$

The density of sand, lime or shale falls within a limited range. The bottom-hole injection temperature will

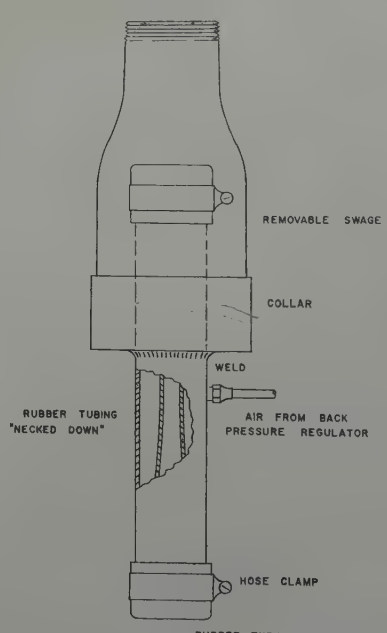

FIG. 3—BACK-PRESSURE VALVE.

be somewhat lower than the temperature of the compressed air due to the temperature drop caused by the expansion of air across the bit jets. The temperature drop due to air expansion may be determined, but as will be shown, knowledge of its exact magnitude is not necessary.

By substituting average values for ρ_s and arbitrary values for T, Eqs. 7 or 8 and 9 or 10 may be used to construct curves showing slip velocity, V_s, as a function of bottom-hole injection pressure with particle diameter as a parameter. Fig. 4 shows such a plot for the lime and shale particles using a ρ_s of 175 lb/ft^3 and a bottom-hole temperature of 100°F. Fig. 5 shows a plot for sandstone particles using a ρ_s of 162 lb/ft^3 and a bottom-hole temperature of 100°F.

Eqs. 7 through 10 are essentially insensitive to changes in ρ_s or T since both ρ_s and T are large numbers and appear in a square root term. The values for slip velocity read from Figs. 4 or 5 could be easily corrected for other densities or bottom-hole temperatures. For example, if the bottom-hole temperature were 150°F instead of 100°F as shown on the figures, the correction factor would be $(610/560)^{\frac{1}{2}} = 1.04$. Thus, for the example given, an error of 50° results in an error of 4 per cent for the slip velocity, V_s.

DISCUSSION OF EXPERIMENTAL RESULTS

The assumption that the drag coefficient for a characteristic cutting shape should be a constant in turbulent flow was verified within reasonable limits of accuracy. As a result, the actual velocities, V_a, compared quite favorably with the theoretical velocities, V_s. This is especially heartening in view of the fact that gas volume measured with an orifice meter may be in error by a substantial amount.

DISCUSSION OF EXPERIMENTAL RESULTS IN TERMS OF AIR DRILLING OPERATIONS

Eq. 2 was derived using as one assumption that the fluid be incompressible. Actually, it is only necessary to know the density of the lifting fluid at the most critical point, namely, at the bottom of the hole. Thus in Eqs. 7 through 10 the density is taken into account by virtue of P, the bottom-hole injection pressure and T, the bottom-hole temperature.

The slip velocities reported herein must be considered as *minimum* values inasmuch as they were obtained when the velocity of the cuttings relative to the borehole was zero. In actual drilling the cuttings must have a net velocity up the hole equal to or greater than the drilling rate.

Linear Velocity Requirements

Figs. 4 and 5 indicate that there is no single correct circulating velocity and that the commonly used 3,000 ft/min linear velocity of free air is sufficient to lift only very small particles, especially if they are angular to sub-rounded in shape. For example, Fig. 5 shows that at atmospheric pressure, a linear velocity of 3,000 ft/min (50 ft/sec) will suspend a sandstone particle having a diameter of slightly more than 0.2 in. Considering a pressure correction alone, the 50 ft/sec velocity would be equivalent to a velocity of about 7.4 ft/sec at 100 psia. Yet Fig. 5 shows that at 100 psia, a minimum velocity of approximately 18 ft/sec is necessary to lift the cutting. This strongly illustrates the fact that the lifting power of air is proportional to the density and square of the velocity, the effect of velocity being much greater.

Thus, even by ignoring friction losses and temperature effects, a linear velocity of 3,000 ft/min is sufficient to lift only the very small particles in a system having a bottom-hole pressure as low as 100 psia. Perhaps this partly explains why air drilled cuttings are usually of dust proportions. High-speed motion pictures of a rock bit drilling at atmospheric pressure reveal puffs of powder plus chips near the penetrating tooth as these particles are suddenly detached from the main body of the formation. It would seem that the larger chips remain at or near the bottom of the hole until they are broken up by grinding action of the drill pipe, and by striking each other, the walls of the hole, or the tool joints until they are sufficiently small to be lifted up the hole by the available air velocity. This is not to imply that the size of the cuttings and penetration rate are necessarily related.

TABLE 1—SUMMARY OF EXPERIMENTAL DATA TAKEN AND CALCULATIONS MADE TO COMPARE OBSERVED AND THEORETICAL SLIP VELOCITIES OF LIMESTONE AND SANDSTONE PARTICLES.

Type particle	Q	Q'	V_a	D	D/d	$V_s = V_a(1 + D/d)$	ρ_{f_i}	ρ_s	$f_D = \frac{3.778\ D(\rho_s - \rho_{f_i})}{V_s^2\ \rho_{f_i}}$	V_s Theoretical	V_a Theoretical	Per cent deviation
Sand-	91.6	93.7	23.3	.079	.0372	24.2	.0748	161	1.037	27.5	26.5	12.10
stone	115	95	23.6	.079	.0372	24.5	.0927	lb/ft^3	.82	24.7	23.8	.84
	169	65.5	16.25	.079	.0372	16.85	.1468		1.09	16.85	16.25	.00
	116	116	28.8	.079	.0372	29.9	.0765		.667	27.1	26.1	10.35
	144	141	35.0	.112	.0527	36.9	.0783		.606	31.9	30.3	15.50
	154.5	149	37.0	.158	.0743	39.8	.0795		.722	37.7	35.1	5.41
	250	95.8	23.8	.158	.0743	25.6	.200		.695	24.7	22.1	7.69
	321	64.5	16.0	.158	.0743	17.2	.382		.803	17.2	16.0	.00
								avg.	.805			avg. 6.49
Lime-	207	54.1	13.42	.158	.0743	14.4	.293	164	1.52	15.0	13.98	4.28
stone	205.7	59.4	14.72	.158	.0743	15.8	.278	lb/ft^3	1.33	15.44	14.38	2.08
	263	55.6	13.80	.158	.0743	14.8	.362		1.167	13.5	12.6	9.53
	301	48.5	12.03	.224	.1053	13.3	.475		1.56	14.05	12.7	5.83
	245.5	71.9	17.83	.224	.1053	19.7	.261		1.298	18.92	17.15	3.52
	177.7	110.4	27.42	.224	.1053	30.3	.1225		1.168	27.6	25.0	9.60
	327.5	51.25	12.7	.317	.1480	14.6	.489		1.782	16.47	14.35	11.80
	251	70.25	17.42	.317	.1480	20.0	.274		1.693	22.0	19.2	9.38
	204	103.7	25.73	.317	.1480	29.5	.1925		1.110	29.7	25.9	.77
								avg.	1.400			avg. 7.10

Q = scf/min

Q' = ft^3/min at injection pressure and flowing temperature

$V_a = \frac{Q'}{.0672 \times 60}$

D = particle diameter, in.

d = equivalent diameter = ID Lucite − OD drill pipe

ρ_{f_i} = fluid density at injection pressure and flowing temperature

Theoretical $V_s = K\left[D\left(\frac{.371 T \rho_s}{P} - 1\right)\right]^{\frac{1}{2}}$

$K = 2.1$ for sandstone
$K = 1.6$ for limestone

Theoretical $V_a = \frac{V_s}{(1 + D/d)}$

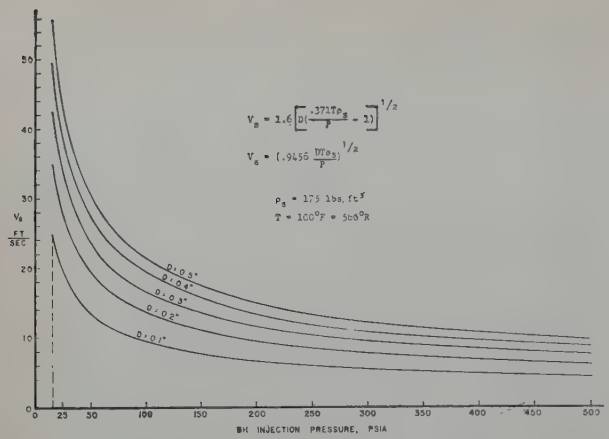

FIG. 4—SLIP VELOCITY VS BOTTOM-HOLE INJECTION PRESSURE FOR LIMESTONE AND SHALE.

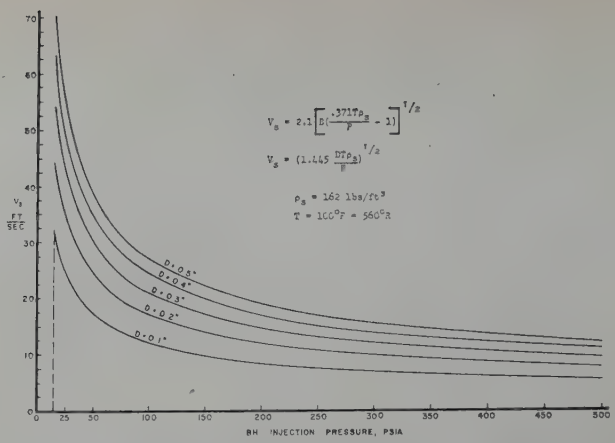

FIG. 5—SLIP VELOCITY VS BOTTOM-HOLE INJECTION PRESSURE FOR SANDSTONE.

HORSEPOWER REQUIREMENTS

Referring again to Figs. 4 and 5, note that the slip velocity decreases rapidly as the injection pressure increases from atmospheric to 200 psia. Further increases in pressure have a relatively small effect on slip velocity. The horsepower requirements, however, are not so obvious.

Suppose, after sustaining certain pressure losses in the surface connections, in the drill pipe and across the bit, the apparatus previously shown is operating at 100-psia bottom-hole injection pressure and ejecting cuttings to the atmosphere (it is universal practice to eject the cuttings to the atmosphere) while for another case the system is operating at the same pressure drop, namely 85 psia, but the bottom-hole injection pressure is 500 psia and the outlet pressure is 415 psia. Assume that limestone cuttings having a diameter of 0.20 in. are being lifted. From Fig. 4, the slip velocities are 13.6 and 6.05 ft/sec, respectively, for injection pressures of 100 and 500 psia. The cross-sectional area of the annular space of the apparatus shown in Fig. 2 is 0.0672 ft^2.

Volume_{100} = 54.8 ft^3/min at 100 psia = 347 scf/min
Volume_{500} = 24.4 ft^3/min at 500 psia = 772 scf/min
(Note that these volumes correspond to free air linear velocities of 5,170 and 11,500 ft/min, respectively.)
The compression ratio in each case is

$$R_{100} = \frac{100}{14.7} = 6.80,$$

and

$$R_{500} = \frac{500}{415} = 1.21\ ,$$

and the isothermal horsepower requirements are given by

$$\text{hp} = .1479\ Q \log R_c\ , \quad . \quad . \quad . \quad . \quad . \quad . \quad . \quad (11)$$

where Q is scf/min delivered, and R_c is the compression ratio.

$$\text{hp}_{100} = .1479\ (347)\ (.832) = 42.7 \text{ hp}$$

$$\text{hp}_{500} = .1479\ (772)\ (.082) = 9.37 \text{ hp}$$

The air delivered per horsepower input in each case is: (1) at 100 psia, 347/42.7 = 8.14 scf/min per hp input; and at 500 psia, 772/9.37 = 82.4 scf/min per hp input. Thus, it can be seen that even though it would be necessary to inject slightly more than twice the amount of air at 500 psia as would be necessary at 100 psia, the air can be delivered 10 times cheaper at the higher pressure due to the lower compression ratio. Inasmuch as compressor costs are a direct function of compression ratio, it would seem to be advantageous to cycle high-pressure air in order to take advantage of the lower compression ratios where conditions for such operations are favorable. To prevent loss of pressure while a connection is being made, a drillpipe float could be used.

Admittedly, this illustration is over-simplified, for in actual operations it would be necessary to consider, in addition to the possibility of encountering water, the fact that particle slip effectively increases the volume of suspended cuttings and that considerable flow resistance is encountered in the drill pipe and bit, and in the cuttings loaded air stream in the annulus. The example is merely to point out the possible advantage to be gained by cycling high pressure air. The advantages of a closed system would increase, although not linearly, with the higher pressures necessary in deeper holes. At shallow depths where low pressures are adequate, the compression ratio would still be low, and the closed system would be less attractive.

It is of interest also that both friction losses and drillpipe erosion are functions of the square of the velocity of the moving air stream; both should be reduced by the lower flow rates inherent in high pressure cycling.

CONCLUSIONS AND RECOMMENDATIONS

Slip velocities, calculated from experimentally determined drag coefficients, had deviations ranging from 0 to 15 per cent with an average of 6.49 per cent for sandstone and 0 to 11.8 per cent with an average of 7.10 per cent for limestone.

The commonly used 3,000 ft/min linear velocity of free air is sufficient to remove only the very small rock particles from the borehole.

Horsepower requirements may be lowered by cycling high pressure air to take advantage of lower compression ratios. However, it would be necessary to remove all the cuttings and dust from the air prior to its being returned to the compressors for repressuring. It is recommended that a cyclone separator, to be used in conjunction with a high pressure filter system or water spray, be developed for this application.

ACKNOWLEDGMENTS

This investigation was carried out at the U. of Tulsa, and the author wishes to express his gratitude to that institution for the use of laboratory facilities and to

the Pan American Petroleum Corp. for the financial support which made this project possible.

Special thanks are due Carl Gatlin for his guidance and constructive criticism throughout the investigation.

REFERENCES

1. McLaughlin, Philip L.: *Slim Hole Facts With Data On Air Drilling*, Cardwell Mfg. Co., Wichita, Kans., 1955.
2. Williams, C. E., Jr. and Bruce, G. H.: *Trans.* AIME (1951) **192**, 111.
3. Hall, H. N., Thompson, H. and Nuss, F.: *Trans.* AIME (1950) **189**, 35.
4. Pigott, R. J. S.: *Drill. and Prod. Prac.*, API (1941) 91.
5. Nicolson, K. M.: *Drill and Prod. Prac.*, API (1953) 300.
6. Brown, G. G. & Associates: *Unit Operations*, John Wiley & Sons, Inc. N.Y. (1950).

APPENDIX

The derivation of the basic equation for slip velocity is based upon the following assumptions: (1) the solid is a non-porous, incompressible spherical particle; (2) the fluid is incompressible and of sufficient extent to eliminate the effects of the confining walls; (3) the accelerating force is derived from a uniform gravitational field; and (4) other particles do not affect the motion of the particle under consideration, that is, the particle is falling freely.

The resultant force tending to move the particle downward is the summation of the following forces:

$$F' = ma = mg - wg - F'_R, \quad . \quad . \quad . \quad . \quad . \quad . \quad . \quad (12)$$

where F' is resultant force on particle, m is particle mass, a is acceleration of particle dV/dT, g is gravitational constant, mg is gravitational force on the particle, wg is buoyant force on the particle, and F'_R is resisting force due to friction effects or that required to accelerate the fluid being displaced.

All of the terms can be evaluated except the resisting force, F_R'. Newton[6] developed an expression for the resisting force as follows:

$$F'_R = \frac{(f')\,A\rho_f\,V^2}{2}, \quad . \quad . \quad . \quad . \quad . \quad . \quad . \quad . \quad (13)$$

where ρ_f is fluid density, V is particle velocity, f' is general friction factor, and A is representative area. For a sphere, the representative area, A, is the projected area, $\pi D^2/4$, and

$$F'_R = \frac{(f_D)\,\pi\,D^2\rho_f V^2}{8}, \quad . \quad . \quad . \quad . \quad . \quad . \quad . \quad (14)$$

where f_D is the friction factor, or drag coefficient, for the specific application of Eq. 13, namely, to spheres.

By substituting Eq. 14 into Eq. 12 the steady-state maximum falling velocity, or slip velocity, may be computed.

$$m\frac{dV}{dT} = mg - wg - F'_R \quad . \quad . \quad . \quad . \quad . \quad (15)$$

$$\left(\frac{\pi D^3}{6}\right)\rho_s\frac{dV}{dT} = \left(\frac{\pi D^3}{6}\right)g(\rho_s - \rho_f) - f_D\frac{\pi D^2\rho_f V^2}{8}$$

$$. \quad . \quad . \quad . \quad . \quad . \quad . \quad . \quad . \quad . \quad . \quad . \quad (16)$$

$$\frac{dV}{dT} = \frac{(\rho_s - \rho_f)g}{\rho_s} - \frac{3f_D\rho_f V^2}{4D\rho_s}. \quad . \quad . \quad . \quad . \quad (17)$$

Eq. 17 may be integrated for the velocity, V, at any time, T. However, the maximum velocity may be obtained directly, since for the condition of maximum velocity, V_s, the acceleration, dV/dT, is equal to zero.

$$\left(\frac{\rho_s - \rho_f}{\rho_s}\right)g = \frac{3f_D\rho_f V_s^2}{4D\rho_s}. \quad . \quad . \quad . \quad . \quad . \quad (18)$$

$$V_s^2 = \frac{4(\rho_s - \rho_f)gD}{3\rho_f f_D} \quad . \quad . \quad . \quad . \quad . \quad . \quad . \quad . \quad (19)$$

$$V_s = \sqrt{\frac{4(\rho_s - \rho_f)gD}{3\rho_f f_D}}, \quad . \quad . \quad . \quad . \quad . \quad (20)$$

where V_s is slip velocity, ft/sec.

When V_s is desired, the trial-and-error procedure may be eliminated as shown by the following equations. Solving Eq. 20 for f_D and writing it in logarithmic form gives,

$$f_D = \frac{4(\rho_s - \rho_f)gD}{3V_s^2\rho_f}, \quad . \quad . \quad . \quad . \quad . \quad . \quad . \quad (21)$$

$$\log f_D = \log\frac{4(\rho_s - \rho_f)gD}{3\rho_f} - 2\log V_s, \quad . \quad (22)$$

and the Reynolds number,

$$\log R_e = \log\frac{D\rho_f}{\mu} + \log V_s, \quad . \quad . \quad . \quad . \quad (23)$$

where μ is the viscosity, and the other nomenclature is the same as previously given.

Eliminating $\log V_s$ between these equations gives

$$\log f_D = -2\log R_e + \log\frac{4(\rho_s - \rho_f)\ gD^3\rho_f}{3\mu^2}$$

$$. \quad . \quad . \quad . \quad . \quad . \quad . \quad . \quad . \quad . \quad . \quad . \quad (24)$$

This is an equation between f_D and R_e in which V_s does not appear, and may be plotted on a graph of f_D vs R_e with a slope of (-2) and passing through the points,

$$R_e = 1;\ f_D = \frac{4(\rho_s - \rho_f)\ gD^3\rho_f}{3\mu^2},$$

and

$$f_D = 1;\ R_e = \sqrt{\frac{4(\rho_s - \rho_f)\,gD^3\rho_f}{3\mu^2}} \quad . \quad . \quad . \quad (25)$$

The intersection of the straight line of Eq. 24 with a plot of f_D vs R_e (Stanton diagram) gives the desired value of the Reynolds number incorporating the value of V_s. The value of V_s can then be computed directly from the value for R_e, since D, ρ_f and μ are known (see Fig. 1). ★★★

The Injection of Detergent Slugs in Water Floods

J. J. TABER | GULF RESEARCH & DEVELOPMENT CO.
PITTSBURGH, PA.

ABSTRACT

A major obstacle to the use of wetting agents in secondary recovery by water flooding is the adsorption of the agents on the sand. As a result of adsorption, the surfactant always lags behind the floodwater front. Consideration of the chromatographic theory of adsorption indicates that the detergents will not lag as much if used in very high concentrations. An investigation was made of the possibility of using high concentrations economically by flowing slugs of wetting agents followed by normal flood water. The experiments consisted of adsorption studies on Alundum powder and Berea sandstone. Flow tests on a 12-in. Alundum core and 22-in. Berea core were used to determine rate of detergent movement. The results of the flow experiments indicate that the relative rate of surfactant advance is, indeed, sensitive to the concentration of the agent. A 10 per cent slug moved with a rate that was 78 to 95 per cent as fast as the rate of advance of the flood water. By contrast, one with 25 ppm (the number of parts of commercial detergent in a million parts of water on a weight basis) concentration moved less than one-fourth as fast as the flood water, and calculations indicate that in very long porous systems the rate of movement of the lower concentrations will be a small fraction of the rate of advance of the flood front.

The results of the adsorption studies were utilized to calculate the rate of advance of the detergent when only the initial concentration was known. The calculated rates showed substantial agreement with the experimental flow tests in the high concentration ranges. The adsorption results were also used to estimate the cost of the materials for a slug-type surfactant flood in the field.

In addition to the faster rates of movement, the concentrated detergent slugs removed much more oil than the dilute solutions. However, the effectiveness of the slug process depends on many variables. The quantity of oil removed is increased markedly by increasing the flooding rate. The efficiency is also influenced by the type of crude, type of reservoir rock and initial water saturation. Therefore, a careful analysis of each reservoir system is required before the economic value of the process can be determined.

INTRODUCTION

It is well known that the displacement of oil by invading water during water flooding is far from complete. It is generally agreed that the unrecovered oil is retained in the porous medium by the capillary forces which may be relatively large compared to the forces generated by the flowing water. Therefore, it was logical that some early workers should turn to surface-active materials to reduce the capillary forces to facilitate the release of oil. As early as 1927,[1] a patent was granted for the use of surface-active materials in water flooding. In 1932, when soap solutions were passed through Bradford and Venango sands, it was reported that the results were inconclusive, erratic and that "further investigation is needed to determine exactly the function of the solution and to obtain a clearer insight into the phenomena involved."[2] Some of the modern scientific reports conclude with a similar statement,[3] showing that the lack of agreement on the mechanism of oil removal by wetting agents is still very widespread even though several comprehensive studies have been reported.[4-5]

Although there is a lack of agreement as to the general effectiveness of the detergents for water flooding, most investigators do agree that all of the common detergents are strongly adsorbed onto the solid surfaces of the reservoir. In the early calculations it appeared that all additives would be lost before reaching much of the formation area which contained the additional oil to be removed. Experiments indicated that if the usual small waterflood concentrations of wetting agents were used, the rate of advance of detergent through the formation would be only a small fraction of the rate of advance of the flood front. Indeed, some investigators[4] felt that the use of wetting agents would never be economically feasible because of their adsorption. For example, Dunning[5] estimated that the wetting agent in concentrations of 25 ppm, would advance only 0.05 times as fast as the flood front. Ojeda, *et al*,[6] found that a surfactant in a concentration of 10 ppm moved less than 0.01 times as fast as the flood front. It is significant, however, that both investigators found that increased concentrations of wetting agents moved faster, relative to the flood front, than solutions at the lower concentrations. Ojeda showed that an extrapolation of his data indicated a relative rate of 0.5 at 1 per cent concentration, while Dunning[5] estimated a relative rate of 0.46 for a 1 per cent concentration.

It was obvious that these concentrations could not be used for continuous injection because the cost of the injected detergent would far exceed the value of additional oil produced. Traditionally, detergents are used in very low concentrations for they show good

Original manuscript received in Society of Petroleum Engineers office Jan. 22, 1958. Revised manuscript received July 9, 1958. Paper presented at Fourth Annual Meeting of Rocky Mountain Petroleum Sections in Denver, Colo., March 3-4, 1958.

[1]References given at end of paper.

detersive properties in the range of a few parts per million and vast quantities of water can be treated economically if the concentration is kept very low.

Preston and Calhoun[7] were the first to point out that it is not necessary to treat all the injected water with the surfactants since the basic principles of chromatography should apply to the system. Therefore, the detergent could be injected for a time and then moved through the formation by the untreated water. A careful evaluation of this process has been published by Johnson[8] who concluded that the chromatographic process should be economic for removing additional oil only if used in a narrow range of concentrations; the maximum concentration being about 0.1 per cent. However, all the aforementioned authors placed severe restrictions on operation of the process. They based calculations on the minimum quantity of detergent that must be injected to move the detergent from the injection well to the producing well at its initial concentration. One of the objectives of this paper is to show that much higher concentrations can be used more effectively if this restriction is removed.

THEORETICAL

There is a sound theoretical basis for predicting that the wetting agents will move faster at higher concentrations. Utilizing a theory of chromatography developed by DeVault,[9] Preston and Calhoun[7] have related the concentration of the detergent to its rate of advance relative to the rate of movement of the water flood.

One of their equations is

$$R = \frac{1}{1 + \dfrac{Pf(c)}{c}} \quad . \quad . \quad . \quad . \quad . \quad . \quad . \quad . \quad . \quad (1)$$

where R is rate of advance of the leading edge of the surfactant divided by the rate of advance of flood front; P is $\rho\ (1 - \phi)/\phi$, where ρ is the grain density and ϕ is the porosity of the porous medium; c is initial concentration of solution injected; and $f(c)$ is the functional notation of an adsorption isotherm.

If the adsorption of the detergent onto the porous solid follows the form of one of the standard isotherms, it is possible to substitute the constants from the isotherm into Eq. 1. For example, the Langmuir isotherm gives

$$R = \frac{1}{1 + \dfrac{PKa}{1 + Kc}} \quad . \quad . \quad . \quad . \quad . \quad . \quad . \quad . \quad . \quad (2)$$

where K and a are constants in the Langmuir isotherm (see Appendix).

Examination of Eqs. 1 and 2 indicates that R will increase as c increases and approach unity as c becomes very large. Therefore, according to theory, any relative speed of wetting agent advance approaching unity can be achieved by increasing the concentration of the agent. The chromatographic theory as utilized by Preston and Calhoun in Eq. 1 applies only to the concentration of the solution as it is initially injected. As the bank of detergent moves through the porous medium it is attenuated by the adsorption-desorption process, mixing with the connate water, loss to the oil phase, and the annular thinning resulting from radial flow. The simple theory will account for the reduction in concentration which is caused by the adsorption-desorption process alone. As soon as the concentration of the slug falls below this initial injection value, the slug will move more slowly in accordance with Eq. 1. However, as yet there is no straightforward theory to describe the ever-decreasing rate that will occur.

Therefore, previous workers[7,8] have assumed that the full-strength material should be produced at the producing well. The amount required for injection can be determined from the same theory. The expression for the radial case which was derived from Preston and Calhoun's theory in terms of the Langmuir isotherm is,

$$V_m = \pi(X_d)^2\, h\phi P \left[\frac{K^2 ac}{(1 + Kc)^2}\right], \quad . \quad . \quad . \quad . \quad . \quad (3)$$

where V_m is the minimum volume of solution of concentration, c, to be injected so that it will emerge at the same concentration at point X_d, the latter being the distance between the injection well and a specified distance into the formation. If experimental values for the adsorption at high concentrations are substituted into Eq. 3, it is found that very large quantities of detergent will be required to move the full-strength slug from the injection well to the producing well. However, if low concentrations are used (less than 50 ppm), the relative rate of detergent movement (R value) will be so low that scores of reservoir pore volumes of flood water would be required to move the detergent through the bulk of the reservoir. Therefore, the maximum effectiveness can be achieved by using a high concentration, but choosing X_d to be some reasonable distance into the formation. This distance may be far short of the producing well. Even though the R value will fall after this point is passed, it will always be much higher than if a low concentration, with its attendant low R value, were used. Indeed, it appears that one should choose as high a concentration as possible for the initial slug. We have not gone beyond concentrations of 10 per cent because higher concentrations may become too viscous for easy injection.

In addition to the increased relative velocity of the detergent zone, other benefits should accrue from the presence of a high surfactant concentration at the oil-water interface. Workers at Pennsylvania State U.[6,10] have shown that the residual oil after water flooding is a decreasing function of $\Delta P/\sigma_{ow}$. Thus, for a given pressure difference, the oil removal increases as the interfacial tension (σ_{ow}) decreases. Extremely low values of interfacial tension can be obtained only with relatively high concentrations of surfactant. In another case, Moore and Blum[11] observed visually that a very sharp reduction of interfacial tension caused much more oil to be removed than if the interfacial tension gradually reduced. Thus, it would appear that highly concentrated surfactant should be present at the leading edge of the flooding water if wetting agents are to effect additional recovery.

EXPERIMENTAL METHODS AND MATERIALS

The surfactant used in most of the experiments was Triton X-100 (Rohm and Haas Co., Philadelphia, Pa.) a non-ionic detergent of the polyoxyethylated-phenol type. It has been used and described by other investigators involved in adsorption and oil displacement studies.[12,13] In addition, Pluronic L-62 (Wyandotte Chemical Corp., Wyandotte, Mich.) was used in one of the flow tests. It is a polyoxypropylene-polyoxyethylene type of non-ionic detergent.

The Adsorption of Detergents on Alundum and Berea Sandstone

The unconsolidated Alundum for the adsorption

studies was an Alundum cement (Norton Co., Worcester, Mass.) designated as RA 1084. It was washed three times by shaking with distilled water, the solid and liquid being separated by a centrifuge between washings. Soluble material and the very fine particles were removed by this process. Known concentrations of Triton X-100 were equilibrated with the Alundum by shaking for one hour. The samples were then centrifuged and the supernatant liquid analyzed for detergent concentration by the surface tension method. A calibration curve was prepared by determining the surface tension of various concentrations down to 1 ppm. In the region below the critical micelle concentration the plot of surface tension vs the log of concentration is linear. The equilibrium concentrations after adsorption were diluted to this range and the surface tension was then determined. The amount of detergent adsorbed was determined by the difference between the equilibrium concentration and the original concentration.

The adsorption of the surfactant on natural porous media was accomplished by the unique device pictured in Fig. 1. The 1-in. Berea sandstone plugs were encased in aluminum foil prior to their enclosure in the Hassler sleeve. The flasks were constructed by joining a neck of heavy-walled glass tubing to Erlenmeyer flasks. Teflon stopcocks were also attached to the flasks. The glass necks of the flasks fit into the Hassler sleeve and are held by the outer end plates with a gentle pressure against the core. When mounted in this fashion, glass, Teflon and aluminum are the only materials making contact with either the core or the surfactant solution. These precautions were necessary because rubber or plastics interfere with the ultraviolet spectrophotometric analysis that was used to determine the concentration of the surfactant in solution. In operation the surfactant solution was placed in one of the flasks and the equipment assembled. The entire unit was then inverted and the solution was forced through the core by modest air pressure or gravity. After the solution passed through the core, the apparatus was inverted to allow flow in the reverse direction. This procedure was repeated several times until equilibrium between the adsorbed and dissolved detergent was established. The solution was analyzed before and after the adsorption experiment by ultraviolet spectrophotometry. Prior to the experiment it was necessary to flush the sandstone with distilled water to remove the soluble material which absorbs radiation in the same ultraviolet band as Triton X-100.

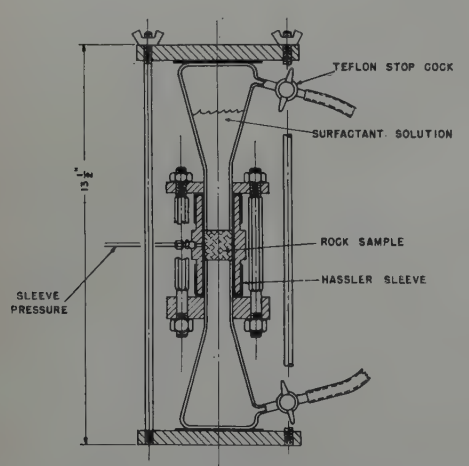

FIG. 1—APPARATUS FOR ADSORPTION STUDIES ON CONSOLIDATED POROUS MEDIA.

The rest of the interference was eliminated by using a differential peak analysis, i.e., the peak height between two low points was determined. The Triton X-100 peak occurs at 275.5 $m\mu$. Readings were also taken at 245 and 295 $m\mu$. The final value for Triton X-100 adsorption is essentially the height of the Triton X-100 peak above the background adsorption line which connects the two other points.

THE EXPERIMENTAL DETERMINATION OF THE RATE OF DETERGENT MOVEMENT IN CONSOLIDATED ALUNDUM AND BEREA SANDSTONE

The Alundum core used for the flow tests was 22-cm long and had a cross-sectional area of 6.30 cm². The properties of the core are given in Table 1. The core was mounted in a Lucite tube and sealed at the ends with O-rings and Lucite end plates. The apparatus, illustrated in Fig. 2, included a constant-pressure pump controlled by a capacitance switch which was activated by air pressure on a water column under pump pressure. To eliminate the chance of air dissolving in the flood solution, a rubber diaphragm was installed between the flooding fluid and switch column. The flood water passed through a short Alundum core filter to eliminate plugging of the test core. A calibrated pipette with a three-way stopcock was used to inject with air pressure the slugs of wetting agent. The pressure drop across the core was measured by a mercury manometer connected at the inlet of the end plate. Produced oil and effuent water passed through a graduated collection tube which was used to measure produced oil, as well as to determine the rate of efflux for permeability calculations. The tube was arranged so that an air bubble could be injected into the effluent stream in order to determine the time for 1 ml of effluent water to be discharged. A bubbler device was used to detect the presence of wetting agent in the effluent water. The end of a capillary tube was immersed in a small trap in the flow line. The rate at which a number of bubbles discharged under a constant pressure was recorded. A decrease in the time for a number of bubbles to discharge indicated a drop in surface tension of the effluent water caused by the presence of the wetting agent. This device was sensitive to very small concentrations of surfactants in the range of a few parts per million.

The Berea sandstone core used for the determination of the R value had a permeability of 115 md prior to the experiment. Its length was 57 cm and the cross-sectional area was 8.45 cm². It was coated with Armstrong Adhesive (Houghton Laboratories, Inc., Olena, N. Y.) and then molded in Hysol epoxy resin. The apparatus was similar to that described in Fig. 2. The chief difference was the substitution of a constant-rate pump for the constant-pressure pump. A millipore filter was placed in the system to filter the distilled water before it entered the core. The arrival of the slug at the output end of the core was detected again by monitoring the effluent stream for the change in surface tension. In addition, samples of the effluent were collected for analysis so that the concentration profile of the emerging slug could be determined.

DISPLACEMENT OF CRUDE OIL BY SURFACTANT SOLUTIONS

Berea sandstone samples were used for the studies involving the displacement of crude oil by surfactants. The samples were 1 in. in diameter and 1- to 2-in. long. The cores were mounted in sleeve-type core holders

TABLE 1—RESULTS OF FLOODING EXPERIMENTS ON ALUNDUM CORE SATURATED WITH SOLTROL AND WATER

Test No.	Initial S_o (Per cent of V_p)	Initial S_w (Per cent of V_p)	Oil produced by water (Per cent of original)	Oil produced by surfactant (Per cent of residual)	R factor	Conc. of surfactant (ppm)	Average P (cm Hg)	Average Q (cc/min)	Remarks
1.(A)	100		78.4	4.8	0.243	25	24.3	0.778	25 ppm Triton X-100 flood solution
2.(B)	20.5	79.5		3.5	0.740	10,000	24.4	0.610	5 ml 1 per cent Triton X-100 slug in 25 ppm Triton X-100 flood solution
3.(C)	100		53.7	0.1	0.678	10,000	24.4	0.600	5 ml 1 per cent Triton X-100 slug in distilled water flood
4.(D)	100		63.0	0.03	0.457	1,000	20.6	0.196	5 ml 0.1 per cent Triton X-100 slug in 10 ppm Hyamine 2389 flood solution
5.(X)		100			0.740 (High R value caused by bactericide)	1,000	25.5	0.225	5 ml 0.1 per cent Triton X-100 slug in 100 ppm Hyamine 2389 flood solution
6.(E)	100		76.0	8.2	0.844	100,000	24.4	0.505	5 ml 10 per cent Triton X-100 slug in 25 ppm Hyamine 2389 flood solution
7.(F)	100		69.4	3.73	0.779	100,000	23.8	0.962	1.45 ml 10 per cent Pluronics L-62 slug in distilled water flood
8.(G)	100			77.0 (15 per cent more than average of col. 4)	0.870	100,000	22.4	1.250	1.45 ml 10 per cent Triton X-100 slug heading distilled water flood
9.(H)	71	29		61.5	0.83	100,000	24.2	0.625	1.45 ml 10 per cent Triton X-100 slug heading distilled water flood

Description of core:

Length	— 22 cm
Diameter	— 2.83 cm
Area of cross section	— 6.30 cm^2
Bulk volume	— 138.7 cm^3
Porosity	— 22.5 per cent
Permeability (Klinkenberg extrapolation)	— 270 md

which were equipped with Teflon end plugs. The associated flow equipment was similar to Fig. 2 so that slugs could be injected at various stages during a water flood. Produced oil and water were separated in a graduated collector. The oil produced by the surfactant slugs was measured volumetrically and in some cases checked by gravimetric techniques.

Most samples were saturated first with 2.5 per cent brine and then flooded with a West Texas crude oil until no more water could be removed. The resulting water saturations (Tables 2 and 3) were higher than the normally expected connate water saturation for Berea cores. Therefore, some samples were prepared by reducing the brine content of the cores by a blotting technique until the desired saturation range was achieved. The samples were then evacuated briefly and saturated with oil. The results of these saturations are given by Runs 3 and 4 in Table 2.

EXPERIMENTAL RESULTS

Adsorption Studies on Alundum Powder and Berea Sandstone

The amount of Triton X-100 adsorbed by Alundum powder at various concentrations is illustrated by Fig.3. The curve, usually referred to as an adsorption isotherm, indicates a maximum adsorption at about 250 ppm. Beyond this point, the adsorption falls off and then flattens out. Although this maximum in the adsorption isotherm is not observed in most classical studies, it has recently been reported by others who have studied the adsorption of detergents on various substances.[14,15] A more recent paper[16] dealing with the adsorption of non-ionics on quartz reports that the adsorption passes through a maximum for some surfactants, but not necessarily for all of them. If the decrease in the adsorption above 200 to 300 ppm were generally true, it would make the proposed slug technique even more attractive.

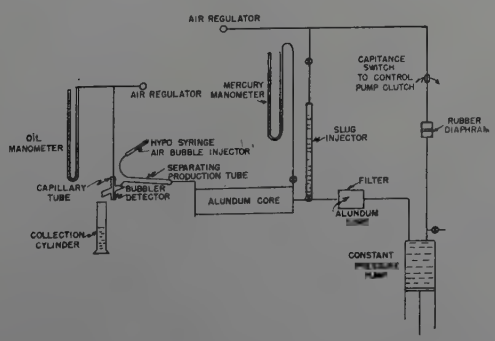

FIG. 2—SCHEMATIC DIAGRAM OF APPARATUS FOR FLOOD TESTS.

The adsorption of Triton X-100 on the Berea sandstone samples followed more traditional patterns. The isotherm is plotted in Fig. 4. It shows that the adsorption was studied from an equilibrium concentration of about 100 ppm up to 92,000 ppm. In the lower concentration range the adsorption increases with concentration until an equilibrium concentration of 700 ppm was reached. This early portion of the curve follows either the standard Langmuir or Freundlich isotherm forms; it indicates monomolecular adsorption is occurring. Above 800 ppm the adsorption rises quickly and levels off at an absolute value of about 8×10^{-4} gm of detergent adsorbed per gram of Berea sandstone. When

TABLE 2—THE RECOVERY OF OIL BY SURFACTANT SLUGS OF 10 PER CENT TRITON X-100 AND 1-M NaOH AT SLOW RATES

Test No.	Type of sandstone	Initial S_o	S_{or} after brine flood	Additional oil removed by slug: Per cent pore volume	Additional oil removed by slug: Per cent residual
1	Berea	61.3	37.2	3.8	10.2
2	Berea	62.2	(Slug in first)	8.8*	22.0*
3	Berea	77.3	44.7	5.7	12.8
4	Berea	74.2	34.1	5.2	15.2
5	N. Texas	61.9	39.0	12.7	32.6**
6	N. Texas	71.7	32.9	5.5	16.7

*Based on the difference between the final oil saturation of 31.1 per cent and an S_{or} of 39.9, which is the average of all S_{or} values for Berea in Tables 2 and 3.

**Recovery may have been influenced by some evolution of gas in core during test.

TABLE 3—THE EFFECT OF SODIUM HYDROXIDE CONCENTRATION ON THE RECOVERY OF OIL BY SURFACTANT SLUGS

Slug composition	Initial S_o	S_{or} after brine flood	Oil produced by slug: per cent pore volume	Oil produced by slug: per cent Residual
10 per cent Triton X-100	64.9	42.6	2.8	6.6
10 per cent Triton X-100 1-M NaOH	61.3	37.0	3.8	11.4
10 per cent Triton X-100 0.01-M NaOH	67.0	40.2	4.2	10.0
10 per cent Triton X-100 10^{-4}-M NaOH	64.7	44.6	4.4	9.8
10 per cent Triton X-100 10^{-6}-M NaOH	65.5	38.8	3.4	8.8

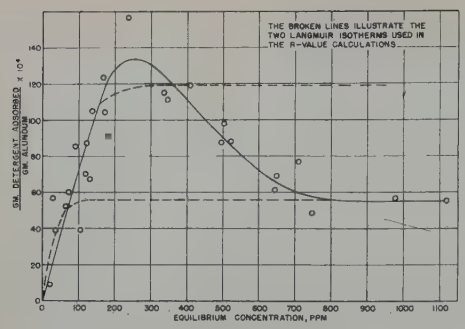
THE BROKEN LINES ILLUSTRATE THE TWO LANGMUIR ISOTHERMS USED IN THE R-VALUE CALCULATIONS
GM. DETERGENT ADSORBED X 10⁴ / GM. ALUNDUM
EQUILIBRIUM CONCENTRATION, PPM

FIG. 3—THE ADSORPTION OF TRITON X-100 ON ALUNDUM.

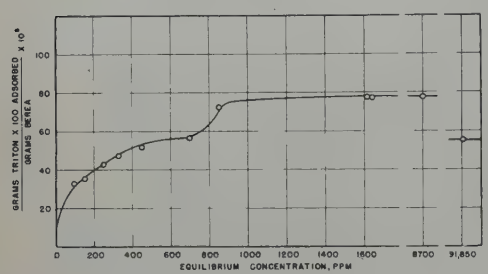

FIG. 4—THE ADSORPTION OF TRITON X-100 ON BEREA SANDSTONE.

an initial concentration of approximately 100,000 ppm or 10 per cent detergent (the proposed concentration of the slug to be used in water flooding) was used, the adsorption fell back to the value of the plateau established at the lower concentrations. Of course, the determination of the absolute adsorption in the very high concentration range is not as precise as for low concentrations because the adsorption value is dependent upon the difference between two large numbers. However, the maximum deviation that could be expected in the spectrophotometric results would still yield an adsorption value below the higher plateau observed in the middle range of concentrations. It is this relatively small adsorption observed at the very high concentrations that provides the physical basis for the much higher R values of the highly concentrated slug.

RESULTS OF FLOW EXPERIMENTS ON LONG CORES AND CALCULATION OF THE R VALUES

The results of the flow experiments with the consolidated Alundum are given in Table 1. The R value for the tests carried out under the most similar conditions is plotted against concentration in Fig. 5. The figure demonstrates that the rate of advance of the slug increases as the concentration of the slug is increased. The 10 per cent slugs moved more than 80 per cent as fast as the flood water. The dilute slugs moved at much smaller relative rates. Although the conditions of the slug flooding were not identical from test to test, the increased rate of the slug with increasing surfactant concentration was consistently observed.

The flow experiments on the long Berea sandstone core gave a similar result. The 10 per cent slug moved through the core and emerged after slightly more than one pore volume of fluid had been produced. The actual R values were calculated to be 0.92 and 0.95.

The R values were calculated from the adsorption isotherms by utilizing Eqs. 1 and 2. For Alundum, the values were calculated by allowing the isotherm to approximate Langmuir isotherms as shown in Fig. 3. It was assumed that the effective adsorption for R value calculations would lie somewhere between the two limiting isotherms that are plotted in Fig. 3. The constants in Eq. 2 were determined by plotting the Langmuir isotherms in the linear form and evaluating constants K and a. For the lower limiting isotherms the constants are 2.34×10^4 and 5.66×10^{-3}, respectively. In order to compare the R values calculated from the adsorption isotherm with those observed in the flow experiments, it was necessary to correct for the difference in surface areas of the two solid materials. The Kozeny-Carman surface area of the Alundum core was calculated to be 164 cm²/gm, while the powder was 4,070 cm²/gm. Therefore, it was necessary to multiply P in Eq. 2 by 164/4,070.

The calculated R values for Alundum are given in Fig. 5 while those obtained from the Berea isotherm are shown in Fig. 6. The latter was determined directly from the Berea isotherm by using Eq. 1. A similar calculation for the Alundum isotherm gives values which are close to the upper curve in Fig. 5.

It can be seen that the R values for both Alundum and Berea range from very low to approximately unity. The agreement between the experimental relative rates and the calculated values is substantial at the higher concentrations, but the calculated values fall off faster than the experimental points as the concentration falls below 1 per cent. The higher experimental R values at the lower concentrations indicate that the limited theory of adsorption as applied by Preston and Calhoun is inadequate. According to their theory, the front of the detergent zone is self-sharpening, i.e., the concentration should rise very rapidly as soon as any is detected in the effluent stream. Therefore, our experimental procedure was designed to sense the earliest arrival of small quantities of detergent. More complete theories now being developed by workers in this laboratory indicate that the effect of miscible mixing of the detergent zone with water and the failure to achieve adsorption equilibrium become appreciable in the relatively short system used in the laboratory. The effect of the mixing and diffusion is to move smaller concentrations of the

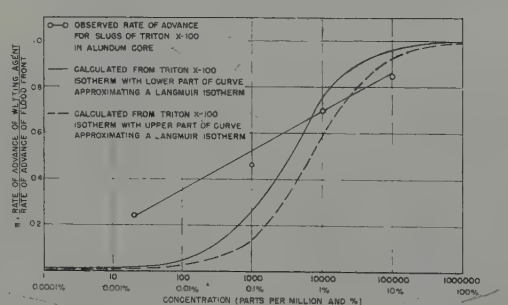
OBSERVED RATE OF ADVANCE FOR SLUGS OF TRITON X-100 IN ALUNDUM CORE
CALCULATED FROM TRITON X-100 ISOTHERM WITH LOWER PART OF CURVE APPROXIMATING A LANGMUIR ISOTHERM
CALCULATED FROM TRITON X-100 ISOTHERM WITH UPPER PART OF CURVE APPROXIMATING A LANGMUIR ISOTHERM
R = RATE OF ADVANCE OF WETTING AGENT / RATE OF ADVANCE OF FLOOD FRONT
CONCENTRATION (PARTS PER MILLION AND %)

FIG. 5—RATE OF ADVANCE OF TRITON X-100 AT VARIOUS CONCENTRATIONS OF DETERGENT.

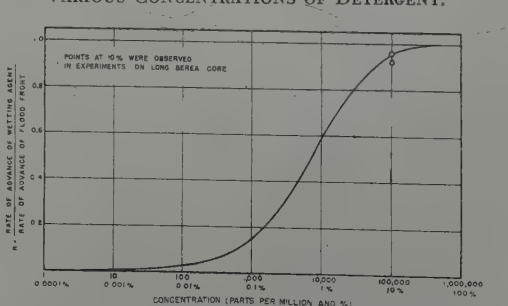
POINTS AT 10% WERE OBSERVED IN EXPERIMENTS ON LONG BEREA CORE
R = RATE OF ADVANCE OF WETTING AGENT / RATE OF ADVANCE OF FLOOD FRONT
CONCENTRATION (PARTS PER MILLION AND %)

FIG. 6—RATE OF ADVANCE OF TRITON X-100 CALCULATED FROM ADSORPTION OF THE DETERGENT ON BEREA SANDSTONE.

detergent ahead of the main zone, thus giving rise to higher R values. However, in extremely long systems such as underground reservoirs, the mixing becomes less important than the adsorption phenomena because a stabilized detergent front with a relatively sharp concentration gradient develops. Therefore, in the low concentration regions the calculated curves in Figs. 5 and 6 should be more applicable to field conditions than the experimental results.

The significant result of all of the adsorption studies and the flow experiments is the fact that detergents can be moved through a porous medium with rates that are more than half the rate of the flowing water, only if they are used in very high concentrations.

Oil Removal by Surfactant Slugs

The additional soltrol oil removed by the various slugs is listed in Table 1. The additional oil removed by 1 per cent or stronger slugs ranged from 0.1 to 15 per cent of the residual oil remaining after a brine flood. The average was a modest 7.6 per cent. However, the Alundum core was a water-wet system and other workers have claimed that detergent flooding is effective only in an oil-wet system.[11] Also, we know that some of the oil is actually dissolved in the aqueous phase and thus cannot be measured in the oil phase in the separator.

Recent attempts in other laboratories to improve the recovery via wetting agents have demonstrated that wetting agents alone, even though concentrated, may not be sufficient to obtain high recoveries. However, when sodium hydroxide was added to a non-ionic detergent, recoveries approaching 100 per cent of the oil in place were achieved.[17] This finding appeared to be very favorable. If the detergent-alkali mixture would function in the slug mode of operation, tremendous additional quantities of oil could be recovered. Therefore, a study of the displacement of crude oil by caustic detergent solutions was undertaken. The results of several of the tests on the 1-in. plugs are given in Table 2. It will be noted at once that the recoveries are far less than 100 per cent. However, our experience has shown that the following conditions will contribute to low recoveries: (1) low flooding rates, (2) high water saturation at the start of the water floods, (3) loss of crude oil to the slug itself, and (4) a complete water flood prior to the slug flood. All of these conditions were operating to yield lower recoveries than reported by the other workers who conducted their experiments at much faster rates.

The flooding rate appears to be one of the most important variables in the displacement experiments. The tests in Table 2 were carried out at the low rate of about 3 ft/day. When the rate was increased, the recovery increased substantially. Thus, the recovery will be greater in regions nearer the injection and producing wells where the rates are greater. The results in Table 2 represent the recovery that can be expected in the central part of the reservoir.

Table 2 shows that when cores were prepared with more realistic water saturations the recovery improved (Runs 3 and 4 compared to Run 1). Run 2 shows that better recovery is achieved when the slug is injected prior to any water flood. For all experiments except Run 2, the slug was injected after a complete water flood had taken place. The reason for the latter procedure is that in any slug program in the reservoir, the slug can operate only on the by-passed oil. Even if an R value of one is achieved, the slug will not be at the front because the oil is actually displaced by the bank of connate water that builds up ahead of the injected fluid.

The loss of the crude oil to the strong slug solution may be significant. Gravimetric checks of the oil residuals indicated that more oil was removed from the core than was measured in the separator. The difference was due, in part, to the solubilization of the crude oil by the powerful surfactant slugs. In some cases, the oil dissolved by the slug amounted to a few per cent of the residual.

A brief investigation of the sodium hydroxide requirements was made by carrying out the same type of flooding tests with varying concentrations of sodium hydroxide. The results, given in Table 3, indicate that the sodium hydroxide need not be more concentrated than 0.01 molar (0.04 per cent). However, the recoveries by the 1-molar solutions were affected more by the previously mentioned loss of crude oil to the slug. The amount of crude dissolved in the slugs increased with increasing sodium hydroxide content.

Cost of the Surfactant Slug Process

The above results indicate that the adsorption problem can be overcome and that more oil can be recovered by using concentrated surfactant slugs mixed with sodium hydroxide. However, when attempting to assess the economic value of the process, it is more difficult to reach definite conclusions. The chief stumbling block is the lack of information on the oil removal by the slugs under actual operating conditions.

To arrive at some estimate of the cost of the process, it was assumed that a slug of sufficient size should be injected to move at full strength for 100 ft into the reservoir in a typical 10-acre, five-spot pattern. Beyond 100 ft the concentration will fall and the R value will diminish. However, the R value will remain relatively high until the concentration of the advancing slug falls to the parts per million range. This should not happen until the surfactant has almost reached the producing well. According to Table 2 the amount of additional oil recovered by such a slug should approach 5 per cent of the pore volume of the reservoir. In regions near the injection well much more oil will be displaced because of the high rates, but 5 per cent over-all should be a good conservative estimate. Therefore, in the 10-acre, five-spot with a sand of 20 per cent porosity the slug should produce 775 bbl of oil per foot of formation. On the basis of current prices the cost of the chemical materials would be about 46 cents/bbl of additional oil recovered. The normal waterflooding cost in addition to the detergent cost should remain essentially unchanged. Because of the high R values, the amount of water injected would be no greater than the water injected during the life of a normal flood. The additional oil would be recovered late in the flood, but the improved injection rates that should be observed throughout the flood would provide for an early increase in the rate of oil production.

A discussion of the use of concentrated slugs of detergents for water floods would be incomplete without consideration of the results of slug injections in field trials. However, none of the reported field trials has been carried out as discussed in this report. Either the detergent has been much too dilute or, if a concentrated slug was used, it was much too small to be effective. The volume of the 10 per cent slug which will move at full strength for 100 ft would be 192 cu ft/ft of forma-

tion. When injected, the slug would extend from the injection well to a point 17.5 ft into the reservoir. By contrast, the slugs used in the Grover flood[18] consisted of only 10 gal of detergent for the entire producing zone. Obviously, a slug of such small volume would be reduced to a fraction of an inch in thickness before it had penetrated any significant distance into the formation. Its concentration would fall off to the range of a few parts per million before it could remove additional oil.

CONCLUSIONS

1. The results of the adsorption and flow studies indicate that the rate of advance of a detergent solution in a porous medium can be roughly predicted if the concentration of the detergent and the adsorption isotherm on the medium is known.

2. Concentrated slugs of detergents can be moved through the reservoir with speeds that approach 95 per cent of the rate of the flood advance.

3. Additional oil can be removed by the slugs—the exact amount depends on the conditions. With mixtures of NaOH and non-ionic detergents it is possible to remove additional oil equal to 5 per cent of the pore volume of the sandstone. This is true even after a complete water flood has passed.

4. The slugs must be concentrated and of sufficient volume to progress a significant distance into the formation.

5. Utilizing the result of both the adsorption and flow tests, it is estimated that the chemical alone will cost 46 cents for each additional barrel of oil recovered. More detailed laboratory experience with natural reservoir materials might decrease this estimate.

NOMENCLATURE

R = rate of advance of the leading edge of the surfactant zone relative to the rate of the water flood. Specifically, the rate of detergent advance divided by the linear flooding rate
c = concentration of the surfactant in the aqueous solution
ρ = grain density of the porous medium
ϕ = porosity of the porous medium
$f(c)$ = functional notation for the adsorption isotherm, i.e., the grams of detergent adsorbed per gram of solid at the equilibrium concentration (c)
K,a = constants in the Langmuir adsorption isotherm
X_d = distance from point of injection
V_m = minimum volume of solution of concentration c to be injected so that it will arrive at the same concentration at point X_d
h = formation thickness
$P = \rho(1 - \phi)/\phi$
S_o = oil saturation
S_{or} = residual oil saturation

ACKNOWLEDGMENTS

The author wishes to thank Nancy B. Sussman, R. E. Klob and G. E. Johnson for their valuable assistance in much of the experimental work described in this paper.

REFERENCES

1. Atkinson, H.: U. S. Patent No. 1,651,311 (1927).
2. Barnes, K. B.: "Preliminary Experiments in Oil Recovery —Soap Solution Tests", *Bull.*, Penn. State U., Mineral Ind. Exp. Sta. (1932) No. 11, 79.
3. Guereca, R. A. and Butler, H. S.: "Screening Surface Active Agents for Oil Displacing Ability", *Prod. Monthly* (1955) **19,** 21.
4. Kennedy, H. T. and Guerrero, G. T.: "The Effect of Surface and Interfacial Tensions on the Recovery of Oil by Water Flooding", *Trans.* AIME (1954) **201,** 124.
5. Dunning, H. N. and Hsiso, L.: "Experiments with Detergents as Water Flooding Additives", *Prod. Monthly* (1954) **18,** 24.
6. Ojeda, E., Preston, F. W. and Calhoun, J. C., Jr.: "Correlation of Oil Residuals Following Surfactant Floods", *Prod. Monthly* (1953) **18,** 20.
7. Preston, F. W. and Calhoun, J. C., Jr.: "Application of Chromatography to Petroleum Production Research", *Prod. Monthly* (1952) **16,** No. 5, 22.
8. Johnson, C. E., Jr.: "Evaluation of Surfactants for Oil Field Flooding", *Jour. Am. Oil Chem. Soc.* (1957) **34,** 209.
9. DeVault, D.: "The Theory of Chromatography", *Jour.* ACS (1943) **65,** 532.
10. Paez, J., Reed, P. and Calhoun, J. C., Jr.: "Relationships Between Oil Recovery, Interfacial Tension and Pressure Gradient in Water-Wet Porous Media", *Bull.*, Penn. State U., Mineral Ind. Exp. Sta. (1954) No. 64, 115.
11. Moore, T. F. and Blum, H. A.: "Wettability in SAA Water Flooding", *Oil and Gas Jour.* (1952) **51,** 108.
12. Dunning, H. N., Gustafson, H. J. and Johansen, R. T.: *Ind. Engr. Chem.* (1954) **46,** 591.
13. Dunning, H. N. and Johansen, R. T.: "Laboratory Evaluation of Water Additives for Petroleum Displacement", RI 5352, USBM (July, 1957).
14. Hsiso, L. and Dunning, H. N.: "A Comparative Study of Non-Ionic Detergent Adsorption by Radiotracer, Spectrophotometric and Surface Tension Methods", *Jour. Phys. Chem.* (1955) **59,** 362.
15. Fava, A. and Eyring, H.: "Equilibrium and Kinetics of Detergent Adsorption — A Generalized Equilibration Theory", *Jour. Phys. Chem.* (1956) **60,** 890.
16. Dunning, H. N.: "Adsorption of Polyoxyethylated Detergents on Quartz", presented before the Pet. Chem. Div., ACS, Atlantic City (Sept. 17-21, 1956).
17. Riesberg, J. and Doscher, T. M.: "Interfacial Phenomena in Crude-Oil-Water Systems", *Prod. Monthly* (1956) **21,** 43.
18. Dunning, H. N., Johansen, R. T., Walker, C. J. and Powell, J. P.: "What Detergent Injection Did at Grover Water Flood", *Oil and Gas Jour.* (Sept., 1955) **54,** 115.

APPENDIX

DETERMINATION OF CONSTANTS K AND a IN THE LANGMUIR ISOTHERM

$$f(c) = \frac{Kac}{1 + Kc} = \frac{x}{m},$$

where x is grams detergent adsorbed and m is mass of adsorbent. To determine a and K the isotherm is plotted in the linear form,

$$\frac{c}{x/m} = \frac{1}{a}c + \frac{1}{aK},$$

where a is obtained from the slope of the plot of $\frac{c}{x/m}$ vs c and K from the intercept. ★★★

Application of Numerical Methods to Predict Recovery From Thin Oil Columns

H. H. RACHFORD, JR. — HUMBLE OIL & REFINING CO., HOUSTON, TEX.
R. D. TAYLOR — NEW ORLEANS, LA.
JIM DOUGLAS, JR. — THE RICE INSTITUTE, HOUSTON, TEX.
P. M. DYKE — HUMBLE OIL & REFINING CO., HOUSTON, TEX.
JUNIOR MEMBERS AIME

ABSTRACT

The performance of a water-drive reservoir having a gas cap depends primarily on the movement of the gas-oil and oil-water contacts. The movement of the contacts during production depends in turn on fluid withdrawals and how the reservoir pressure changes as fluids are produced from the reservoir; that is, on how effectively the aquifer maintains pressure by replacing withdrawals.

Inasmuch as pressure changes, fluid withdrawals, contact positions, and produced gas-oil and oil-water ratios are interdependent, the analysis and prediction of the performance of a reservoir produced in a given way must take into account this interdependence throughout depletion.

This paper presents an analysis which, within the limitations of the assumptions made, yields an engineering approach to predicting future performance based on reservoir pressure and production history. The most significant assumption is the method of extrapolation of future gas-oil and water-oil ratios. The extrapolation procedure smoothly increases both ratios to preselected values as the remaining oil column undergoes a specified decrease in thickness. This preselection is made on the basis of previous field experience in depletion of similar reservoirs under similar conditions. For computing future performance a volumetric balance is combined with the differential equation defining pressure distribution in the aquifer to obtain positions of water-oil and gas-oil contacts. From these positions are extrapolated produced water-oil and gas-oil ratios. Reservoir performance can be investigated when oil production rates are dependent upon various factors including the performance of the reservoir itself. Examples of practical application of the procedure are included.

INTRODUCTION

To predict performance of water-drive reservoirs with gas caps and thin oil columns, it is necessary to describe the motions of the fluids within the reservoir during the entire production period to depletion. These motions depend on the pressure changes and on the withdrawal of oil, gas and water. Production of oil from the oil zone primarily causes water to move in to take its place; production of gas from the cap tends to cause oil to migrate into its place. In addition, the volumes of oil and gas remaining in the reservoir depend on changes in the pressure, since a decrease in pressure causes fluid expansion, gas liberation and oil shrinkage.

A method of relating the future pressure to total withdrawals is used to describe the motions of fluids within the reservoir under conditions arising in possible modes of production. The analysis is based on two relationships and will reduce the problem to one amenable to digital computation. The first of these concerns the dependence of the pressure distribution in the entire aquifer furnishing the water drive upon the total reservoir withdrawals. This dependence is dictated by the permeability distribution and the extent of the aquifer; at present, such information is most readily obtained from the performance history by means of the resistance-capacitance reservoir analyzer. The second relation involves withdrawals, pressure in the reservoir, and movement of oil, gas, and water within the reservoir. The analysis is subject to certain simplifying assumptions that are necessary to permit solution of the problem.

A comparison of the methods of this paper with those presently practiced is pertinent. One method of analysis is to use the reservoir analyzer to predict reservoir behavior based on aquifer characteristics determined from production history. Inasmuch as the total withdrawal rate depends upon the gas-oil and water-oil ratios, which depend in turn upon, among other things, the positions of the gas-oil and water-oil contacts, these ratios must be assumed in advance. In this paper these ratios are, instead, related to the computed positions of gas-oil and water-oil contacts. Thus, our method can be applied to problems in which the oil production rate is limited by produced gas-oil ratio, or to problems in which it is desired to determine the variable gas injection rate that will maintain the gas-oil or water-oil contact stationary. These problems cannot be worked satisfactorily on the analyzer. Another method presently used is based on a paper by Hurst.[4] Since his procedure is dependent upon using the solution of the heat flow equation, which requires constant permeability within the aquifer, and our procedure recognizes variations of permeability in

Original manuscript received in Society of Petroleum Engineers office Sept. 15, 1957. Revised manuscript received June 9, 1958. Paper presented at 32nd Annual Fall Meeting of Society of Petroleum Engineers in Dallas, Tex., Oct. 6-9, 1957.

[4]References given at end of paper.

the aquifer, the relation between withdrawals and pressure variation is more realistic in our case.

Two examples of the application of the method of the paper to actual reservoirs follow a description of the method. It can be seen from figures presenting the results that there exist a number of effects which may be overlooked in simpler reservoir analyses. In particular, the pressure rises in Reservoir A toward the end of the life of the field after the gas cap has been produced. This results because the corresponding decrease in total reservoir withdrawals allows water influx from the aquifer to repressurize the reservoir. Also, the effect of increased water production on the pressure is observed. For the case in which gas is being returned, the rapid increase in total withdrawal rate, which is a consequence of the assumed constant oil production rate and the rise in produced water fraction toward the end of the producing life, depresses the pressure and thereby decreases the required injection rate. This decrease further increases the net reservoir withdrawals and leads to the abrupt pressure decline shown.

ANALYSIS OF PRESSURE PERFORMANCE OF THE AQUIFER

It is assumed that the aquifer can be represented as a porous body with permeability and thickness properties which can be described in terms of a single distance variable, the radial distance from the reservoir. This implies a circular symmetry such that, if the aquifer is described in polar coordinates (r, Θ), all the derivatives of the dependent variable, pressure, with respect to angle Θ are zero. It is further assumed that the water in the aquifer follows the classical equation of state, which is $d\sigma/dp = c\,\sigma$, where σ is density, c the constant compressibility, and P the pressure, in consistent units. The aquifer is assumed to be bounded on the outside by radius r_R where the permeability, K, goes to zero, and on the inside by radius r_w, the radius of the reservoir across which is assumed to flow all water entering the reservoir from the aquifer. To relate pressure changes in the aquifer to withdrawals across radius r_w, it is necessary to write the general equation of flow in and out of an annular zone bounded by radius r and $r + dr$.

Flow out of zone toward reservoir in time $d\theta$ is

$$\frac{2\pi K_r r h_r}{\mu}\left(\frac{\partial P}{\partial r}\right)_r d\theta$$

and flow into zone toward reservoir in time $d\theta$ is

$$\frac{2\pi K_{r+dr}(r+dr)h_{r+dr}}{\mu}\left(\frac{\partial P}{\partial r}\right)_{r+dr} d\theta \quad . \quad . \quad (1)$$

where K_r, h_r, and $\left(\frac{\partial P}{\partial r}\right)_r$ are permeability, thickness, and pressure gradient, respectively, at radius r. The water viscosity, μ, is assumed constant. Writing input − output = accumulation in symbols gives

$$\frac{2\pi}{\mu}\left[\sigma_{r+dr}\,(K_{r+dr})\,(h_{r+dr})\,(r+dr)\left(\frac{\partial P}{\partial r}\right)_{r+dr} - \sigma_r K_r h_r r\left(\frac{\partial P}{\partial r}\right)_r\right] d\theta = 2\pi r\phi h_r(d\sigma)(dr) \quad . \quad . \quad (2)$$

where ϕ is the porosity, which is assumed to be constant. In the limit as $dr \to 0$, and assuming that terms of the order of $c\left(\frac{\partial P}{\partial r}\right)^2$ are small compared with $\frac{\partial^2 P}{\partial r^2}$,

$$\frac{r}{\phi\mu ch}\frac{\partial}{\partial r}\left(Krh\frac{\partial P}{\partial r}\right) = r^2\frac{\partial P}{\partial \theta} \quad . \quad . \quad . \quad . \quad . \quad (3)$$

A useful variable change is made by setting $r = r_R e^{-u}$, whereupon Eq. 3 becomes

$$\frac{\partial}{\partial u}\left(k\frac{\partial P}{\partial u}\right) = r_R^2\phi\,\mu\,che^{-2u}\left(\frac{\partial P}{\partial \theta}\right), \quad . \quad . \quad . \quad (4)$$

where $Kh = k$.

The boundary conditions on Eq. 4 may be determined as follows. At $r = r_R$, the outer boundary of the aquifer, the radial flow is zero. A sufficient mathematical condition to express this fact is

$$k_{u=0}\left(\frac{\partial P}{\partial u}\right)_{u=0} = 0; \quad . \quad . \quad . \quad . \quad . \quad . \quad . \quad . \quad . \quad (5)$$

At the inner boundary, r_w, a rate of water influx $I(\theta)$ reservoir volumes per unit time takes place; thus,

$$I(\theta) = \frac{2\pi k_{r_w}}{\mu}\left(\frac{\partial P}{\partial u}\right)_{u=\log\frac{r_R}{r_w}} \quad . \quad . \quad . \quad . \quad . \quad (6)$$

The function $I(\theta)$ depends on net withdrawals from the reservoir and the fluid expansion within the reservoir. If at time θ the total compressibility of fluids in the reservoir is C_F, volume per unit pressure change, and $W(\theta)$ is the rate of withdrawal from the reservoir of the total reservoir volume of oil, gas and water, then the rate of influx $I(\theta)$ *is* $W(\theta)$ decreased by the rate of expansion of reservoir fluids, or

$$I(\theta) = -W(\theta) - C_F\left(\frac{\partial P}{\partial \theta}\right) \quad . \quad . \quad . \quad . \quad . \quad . \quad (7)$$

Thus, the inner boundary condition becomes,

$$W(\theta) + C_F\left(\frac{\partial P}{\partial \theta}\right)_{u=\log\frac{r_R}{r_w}} = \frac{2\pi k_{r_w}}{\mu}\left(\frac{\partial P}{\partial u}\right)_{u=\log\frac{r_R}{r_w}} \quad . \quad . \quad . \quad . \quad . \quad . \quad . \quad . \quad . \quad . \quad . \quad . \quad . \quad (8)$$

A second change of variable should be made. Approximation of the solution of Eqs. 4, 5 and 8 by numerical methods will require approximating derivatives of P with u and θ by differences in pressure over small intervals of u and θ. Such differences will always be small compared with the values of P itself. Therefore, to obtain suitable accuracy in the numerical computation, a function z is defined as

$$z = \frac{P_{\text{orig}} - P}{P_{\text{orig}} - P_m}, \quad . \quad . \quad . \quad . \quad . \quad . \quad . \quad . \quad . \quad . \quad (9)$$

where P_{orig} is the original reservoir pressure, and P_m is the least pressure to which it is desired to carry out calculations. The function z is initially zero everywhere in the aquifer and has the property that small changes in P from P_{orig} are reflected as more significant changes in z.

Substitution of z into Eqs. 4, 5 and 8 yields the differential system,

$$\frac{\partial}{\partial u}\left(k\frac{\partial z}{\partial u}\right) = r_R^2\,\phi\,\mu\,che^{-2u}\left(\frac{\partial z}{\partial \theta}\right), \quad . \quad . \quad . \quad (10)$$

$$k_{u=0}\left(\frac{\partial z}{\partial u}\right)_{u=0} = 0, \quad . \quad . \quad . \quad . \quad . \quad . \quad . \quad (11)$$

and

$$\frac{-W(\theta)}{P_{\text{orig}} - P_m} + C_F\left(\frac{\partial z}{\partial \theta}\right)_{u=\log\frac{r_R}{r_w}} = \frac{2\pi}{\mu}k_{r_w}\left(\frac{\partial z}{\partial u}\right)_{u=\log\frac{r_R}{r_w}} \quad . \quad . \quad . \quad . \quad . \quad . \quad . \quad . \quad . \quad . \quad . \quad . \quad . \quad (12)$$

To obtain a numerical approximation to the solution of Eq. 10 subject to boundary conditions (Eqs. 11 and 12), it is necessary to write difference analogs of Eqs. 10, 11 and 12, which are algebraic equations that can

be solved numerically and whose solution converges to that of the differential system. To write such a set of analogs, a distance grid is set up by considering z as a function of u and θ at the points $(i + \frac{1}{2})\,\Delta u$, $n\Delta\theta$, $i = 0, 1, \ldots, j$, $n = 1,2, \ldots$.

The number, j, of intervals into which the u-axis is to be divided is

$$\frac{\left(\log \frac{r_R}{r_w}\right)}{\Delta u} .$$

For the purpose of notation, $z([i + \frac{1}{2}]\Delta u,\ n\Delta\theta)$ is written as $z_{i,n}$.

The derivatives of Eq. 10 will be approximated at the point u_i, $\theta_{n+\frac{1}{2}}$ so as to relate the value of $z_{i,n+1}$ to the value of $z_{i,n}$. The approximations of the terms of Eq. 10 are

$$\frac{\partial}{\partial u}\left(k\frac{\partial z}{\partial u}\right)_{i,n+\frac{1}{2}} \cong \frac{1}{2(\Delta u)^2}\,[k_{i+\frac{1}{2}}\,(z_{i+1,n+1} - z_{i,n+1}) - k_{i-\frac{1}{2}}\,(z_{i,n+1} - z_{i-1,n-1}) + k_{i+\frac{1}{2}}\,(z_{i+1,n} - z_{i,n}) - k_{i-\frac{1}{2}}\,(z_{i,n} - z_{i-1,n})], \quad . \quad . \quad . \quad . \quad . \quad . \quad . \quad . \quad . \quad . \quad (13a)$$

and

$$\left(\frac{\partial z}{\partial \theta}\right)_{i,n+\frac{1}{2}} \cong \frac{z_{i,n+1} - z_{i,n}}{\Delta\theta}, \quad . \quad . \quad . \quad . \quad . \quad (13b)$$

where $k_{i+\frac{1}{2}}$ is the value of k at $u_{i+\frac{1}{2}} = (i + 1)\Delta u$. Making these substitutions in Eq. 10 yields

$$\frac{\Delta\theta}{2(\Delta u)^2}\,[k_{i+\frac{1}{2}}\,(z_{i+1,n+1} - z_{i,n+1}) - k_{i-\frac{1}{2}}\,(z_{i,n+1} - z_{i-1,n+1}) + k_{i+\frac{1}{2}}\,(z_{i+1,n} - z_{i,n}) - k_{i-\frac{1}{2}}\,(z_{i,n} - z_{i-1,n})] = r_L^2\phi\,\mu c h e^{-2u_i}\,(z_{i,n+1} - z_{i,n}). \quad . \quad . \quad . \quad . \quad . \quad . \quad (13c)$$

The difference analog of boundary Eq. 11 is

$$k_{-\frac{1}{2}}\,(z_{-1} - z_0) = 0 . \quad . \quad . \quad . \quad . \quad . \quad . \quad . \quad . \quad . \quad (14a)$$

This condition may be satisfied either by setting $z_{-1} = z_0$ or $k_{-\frac{1}{2}} \equiv 0$. For ease of computation, the latter choice was made. Thus,

$$k_{-\frac{1}{2}} \equiv 0 \quad . \quad . \quad . \quad . \quad . \quad . \quad . \quad . \quad . \quad . \quad . \quad . \quad (14b)$$

The difference analog of Eq. 12 is

$$\frac{-W_{n+\frac{1}{2}}\Delta\theta}{P_{orig} - P_m} + C_{F_n}\,(z_{j,n+1} - z_{j,n}) = \frac{2\pi k_{j-\frac{1}{2}}}{\mu\Delta u}\,(z_{j,n+1} - z_{j-1\,n+1})\,\Delta\theta . \quad . \quad . \quad . \quad . \quad (15)$$

The system (Eqs. 13c, 14b and 15) can be written in the form

$$\left.\begin{aligned} &B_0\,z_{0,n+1} + C_0 z_{1,n+1} = D_{0,n} \\ &A_1\,z_{0,n+1} + B_0 z_{1,n+1} + C_0 z_{2,n+1} = D_{1,n} \\ &A_i z_{i-1,n+1} + B_i z_{i,n+1} + C_i z_{i+1,n+1} = D_{i,n} \\ &A_i z_{j-1,n+1} + B_{j,n+1} z_{j,n+1} = D_{j,n} , \end{aligned}\right\} \quad . \quad . \quad . \quad . \quad . \quad . \quad . \quad . \quad . \quad . \quad . \quad . \quad (16)$$

where the coefficients A_i, B_i, and C_i, $i \neq j$, depends only on the values of k, and the parameters Δu, $\Delta\theta$, r_R, ϕ, μ, c and h. The coefficient B_j depends, in addition, on C_F, which is discussed in the next section. The set of $D_{i,n}$ depend upon the parameters listed above as well as upon the values of $z_{i,n}$, for $i = 0, 1, \ldots, j$.

The set of simultaneous equations (Eq. 16) can readily be solved. Because the matrix of coefficients of Eq. 16 is tridiagonal, the solution of the equations by Gaussian elimination is both practical and easy, regardless of the size of j. A particularly efficient method of handling the work on computing machines is described in Ref. 1.

Here the question should arise as to whether or not the numerical values obtained by the repeated stepwise solution of Eq. 16 bear any relationship to the solution of the differential system of Eqs. 10, 11 and 12. To answer this question requires a process referred to as a convergence proof showing that the difference between the solution of Eqs. 10, 11 and 12 and the numerical solution of Eqs. 13c, 14b and 15 is bounded by a constant which decreases uniformly in magnitude as Δu and $\Delta\theta$ are decreased. This proof is beyond the scope of this paper; however, it can be referred to in the literature.[3]

The only remaining problem in evaluating the solution for successive steps, given the set of $W_{n+\frac{1}{2}}$, is the computation of C_{F_n} which depends on pressure; the amount of oil, gas and water in the reservoir at time θ_n; and the properties of the oil and gas. The pressure-dependent gas and oil properties used in this paper are (1) $\gamma(P_k)$—Mcf of gas per barrel of reservoir gas at pressure, P_k; (2) $\beta(P_k)$—barrels of stock-tank oil per barrel of reservoir oil at pressure, P_k; and (3) $\lambda(P_k)$—barrels of reservoir gas liberated per barrel of reservoir oil at pressure, P_k.

The compressibility C_{F_n} can be evaluated from the given functions, provided the volumes of reservoir oil, N_n bbl, and reservoir gas, G_n bbl, are known. If at time θ_n, G_n bbl of gas are present of which $G_n - \lambda_n N_n = V_n$ bbl are free gas not liberated from the oil present, then the rate of volume change with pressure of the quantity of gas whose volume at standard conditions is $V_n\gamma_n$, a constant, is

$$\frac{dV_n}{dP} = -\left(\frac{G_n - \lambda_n N_n}{\gamma_n}\right)\left(\frac{d\gamma}{dP}\right)_n = -\,(G_n - \lambda_n N_n)\left(\frac{d\log\gamma}{dP}\right)_n \quad . \quad . \quad . \quad . \quad (17)$$

Similarly, the rate of change of oil volume with pressure is

$$\frac{dN_n}{dP} = -\frac{N_n}{\beta}\left(\frac{d\beta}{dP}\right)_n = -\,N_n\left(\frac{d\log\beta}{dP}\right)_n . \quad (18)$$

The rate of change of liberated gas volume with pressure is

$$\frac{d(N_n\lambda_n)}{dP} = N_n\left[\left(\frac{d\lambda}{dP}\right)_n - \lambda_n\frac{d\log\beta}{dP}\right)_n\Bigg]. \quad (19)$$

Thus, the total rate of volume change with pressure is:

$$C_{F_n} = -\,(G_n - \lambda_n N_n)\left(\frac{d\log\gamma}{dP}\right)_n + N_n\left[\left(\frac{d\lambda}{dP}\right)_n - (1 + \lambda_n)\left(\frac{d\log\beta}{dP}\right)_n\right] + c\,\Omega_n , \quad . \quad . \quad . \quad . \quad . \quad . \quad . \quad . \quad . \quad . \quad (20)$$

where $c\Omega_n$ is the water compressibility, bbl/psi.

All that remains to calculate C_{F_n} are the relations between N_{n+1} and N_n, and G_{n+1} and G_n.

$$N_{n+1} - N_n = q_{o_{n+\frac{1}{2}}}\,\Delta\theta - N_n\left(\frac{d\log\beta}{dP}\right)_n\Delta P_n ,$$

and

$$G_{n+1} - G_n = q_{g_{n+\frac{1}{2}}}\,\Delta\theta - \Bigg[(G_n - \lambda_n N_n)\left(\frac{d\log\gamma}{dP}\right)_n + N_n\left\{\lambda_n\left(\frac{d\log\beta}{dP}\right)_n - \left(\frac{d\lambda}{dP}\right)_n\right\}\Bigg]\Delta P_n , \quad . \quad . \quad (21)$$

where $q_{o_{n+\frac{1}{2}}}$ and $q_{g_{n+\frac{1}{2}}}$, which are taken as negative quantities, are the reservoir oil and gas rates in reservoir barrels per unit time, respectively. If $q_{w_{n+\frac{1}{2}}}$ is the water

withdrawal rate in reservoir barrels, the total withdrawal rate, W, is given by

$$W_{n+\frac{1}{2}} = q_{g_{n+\frac{1}{2}}} + q_{o_{n+\frac{1}{2}}} + q_{w_{n+\frac{1}{2}}} \quad . \quad . \quad . \quad . \quad . \quad (22)$$

The relation between Q_g and Q_o, the production rates of total gas (free plus dissolved) in Mcf per day and stock-tank liquid (including condensate) in barrels per day, respectively, and q_g and q_o is given by the solution of the relations,

$$Q_o = Y q_g \gamma + q_o \beta ,$$

and

$$Q_g = q_g \gamma + q_o (\beta r_{do} - \lambda\gamma) ,$$

where Y is the condensate ratio, bbl/Mcf, and r_{do} is the original dissolved gas ratio, Mcf/STB. The solution is

$$q_g = \frac{Q_o (r_{do} \beta - \gamma\lambda) - \beta Q_g}{\gamma Y (r_{do} \beta - \gamma\lambda) - \beta\gamma} ,$$

$$q_o = \frac{Q_g - q_g \gamma}{r_{do} \beta - \lambda\gamma} .$$

The pressure performance of the aquifer may now be computed provided G_o, N_o, Ω_o, the set of production rates by time intervals for gas, oil, and water, and the aquifer properties in terms of a set $k_{i-\frac{1}{2}}$ $(i = 1, \ldots j)$ are given. The values of k are most easily obtained by matching the observed reservoir pressure data to production data by adjusting for appropriate values of k on an electric reservoir analyzer.[2]

FLUID MIGRATION

The computation described thus far is sufficient to predict all future pressure behavior and oil and gas volumes within the reservoir, given the future withdrawal rates. However, the primary purpose of the present calculations is to enable prediction of performance to depletion of gas-cap, water-drive reservoirs. The future oil production rate may be assumed by predicting future allowables. The future gas and water withdrawals, on the other hand, depend on the produced gas-oil ratios and water fractions. The ratios and fractions in turn depend on a number of factors including the thickness of the oil column and the gas cap, the production rate, and completion intervals.

For this study it is assumed that the gas-oil ratio and water fraction produced in the time interval from n to $n + 1$ can be related solely to the thickness of the oil and gas columns at time $n\Delta\theta$. With this assumption, the problem of prediction has two parts: to find the position of the gas-oil and water-oil contact and to express quantitatively the gas-oil ratio and water fraction as a function of these positions.

The original positions of the contacts, volumes of oil and gas, and the geometry of the reservoir are assumed to be known. It is assumed that the properties of the reservoir may be described in terms of a single distance variable x, the vertical distance measured above the initial oil-water contact. The reservoir area, $A(x)$, is the function used to describe the geometry. The void volume available to hydrocarbons is decreased by the connate water saturation, which also is a function of the height x, $S_w(x)$. Thus, the total hydrocarbon volume in the reservoir is given by

$$\text{hydrocarbon volume} = \int_0^{x_t} \phi(x)\, A(x)\, [1 - S_w(x)]\, dx ,$$

where x_t is the value of x corresponding to the top of the reservoir and $\phi(x)$ is the porosity averaged over the reservoir at position x. The function $\phi(x)$ is given by

$$\phi(x) = \begin{cases} \phi_1 , & x_{go} \le x \le x_t \\ \phi_2 , & 0 \le x \le x_{go} \end{cases} \quad , \quad . \quad . \quad . \quad . \quad . \quad (24)$$

where x_{go} is the original position of the gas-oil contact and ϕ_1 and ϕ_2 are defined by

$$G_0 = \phi_1 \int_{x_{go}}^{x_t} A(x)\, [1 - S_w(x)]\, dx \quad . \quad . \quad (24a)$$

and

$$N_0 = \phi_2 \int_0^{x_{go}} A(x)\, [1 - S_w(x)]\, dx \quad . \quad . \quad . \quad (24b)$$

In producing the reservoir, changes in the contacts occur. Fig. 1 shows five zones which may form during the production. Zone 1 is the gas zone, which has never been invaded by oil and is, therefore, filled only with gas and connate water. Zone 2, containing oil remaining residual after gas displacement, will be formed if the gas-oil contact is falling, because gas will not completely displace oil. If x_{g_M} is the highest point attained at any time by the gas-oil contact, then Zone 2 lies between x_{g_n} and x_{g_M} at time $n\Delta\theta$. If x_{g_m} is the minimum value of x_g, then Zone 3, containing residual gas by oil displacement, lies between x_{g_m} and x_{g_n}. Zone 4 is the oil zone that has never been invaded by either gas or water; however, it may contain gas by virtue of liberation from the oil. Zone 5 is a watered-out region between the lowest point attained by the water-oil contact, x_{o_m}, and the position x_{o_n}. During the movement of hydrocarbons, the connate water is assumed immobile; thus, the water saturation retains the original distribution $S_w(x)$ except below x_{o_n}, where S_w is set equal to $1 - S_{so} - S_{sg}$, S_{so} being the residual oil in Zone 5 and S_{sg} the residual gas in Zone 5. Although other zones are possible, they are of minor importance and are not considered.

The stepwise procedure for calculation of positions of gas-oil and oil-water contacts at time $(n + 1)\ \Delta\theta$ from their positions at time $n\Delta\theta$ requires calculating the reservoir volumes of oil and gas for time $(n +)\Delta\theta$. The procedure for this is as follows.

1. Apply Eq. 20 to find C_{F_n} from known values of all the parameters at time $n\Delta\theta$.

2. Use Eq. 22, with the production rates for time period, $n\Delta\theta$ to $(n + 1)\ \Delta\theta$, to determine $W_{n+\frac{1}{2}}$.

3. Solve the system of Eq. 16. This yields a value of $z_{j,n+1}$, which yields $P_{j,n+1}$, from which $\Delta P_n = P_{j,n+1} - P_{j,n}$ is determined.

4. Substitute ΔP_n into Eq. 21 to determine values for N_{n+1} and G_{n+1}.

Once the volume of reservoir oil and gas is known at time $(n + 1)\ \Delta\theta$, the new gas-oil contact $x_{g_{n+1}}$ may be

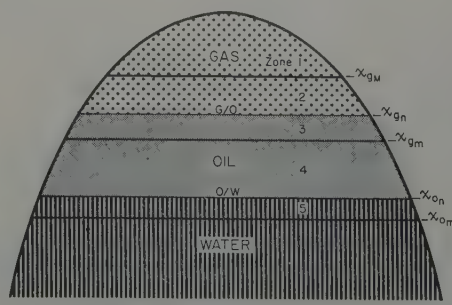

FIG. 1—SCHEMATIC REPRESENTATION OF RESERVOIR.

obtained by solving the following set of equations for the variable limits $x_{g_{n+1}}$ and $x_{o_{n+1}}$.

$$G_{n+1} = \int_{x_{o_m}}^{x_{o_{n+1}}} S_{5g_n}\phi(x)\,A(x)\,dx + \int_{x_{o_{n+1}}}^{x_{g_m}} \phi(x)\,dx + \int_{x_{g_m}}^{x_{g_{n+1}}} S_{3g_n}\phi(x)\,A(x)\,dx + \int_{x_{g_{n+1}}}^{x_{g_m}} S_{2g_n}\phi(x)\,A(x)\,dx + \int_{x_{g_m}}^{x_t} S_{1g_n}\phi(x)\,A(x)\,dx, \quad . \quad . \quad . \quad . \quad . \quad . \quad . \quad (25a)$$

and

$$N_{n+1} = \int_{x_{o_m}}^{x_{o_{n+1}}} S_{5o_n}\phi(x)\,A(x)\,dx + \int_{x_{o_{n+1}}}^{x_{g_m}} S_{4o_n}\phi(x)\,A(x)\,dx + \int_{x_{g_m}}^{x_{g_{n+1}}} S_{3o_n}\phi(x)\,A(x)\,dx + \int_{x_{g_{n+1}}}^{x_{g_M}} S_{2o_n}\phi(x)\,A(x)\,dx, \quad . \quad . \quad . \quad . \quad . \quad . \quad . \quad (25b)$$

where $S_{\alpha g_n}$ and $S_{\alpha o_n}$ signify the average gas and oil saturations, respectively, within zone α at time $n\Delta\theta$.

To solve for the new contacts, it is necessary to specify the values of saturation in the several intervals. The water saturation $S_w(x)$ is the same for all time for $x_{o_n} < x < x_t$ and corresponds to that determined from the capillary distribution calculated from capillary pressure measurements. Other saturations are summarized in Table 1.

S_{org} and S_{orw} (Table 1) are the residual oil by gas displacement and by water displacement, respectively, and S_e is the equilibrium gas saturation.

The intent of these assumptions was twofold: (1) to simplify solving Eq. 25 to permit a reasonable solution time, and (2) provide a description of the saturation behavior within the defined zones that is consistent with the accuracy of the other assumptions made in the problem.

In brief, the saturations summarized in Table 1 can be described qualitatively in terms of the mobile and immobile phases. The gas saturation in Zone 1 is all the volume not occupied by connate water. The oil in Zone 2 is a fixed or immobile phase and is at the residual saturation of oil flushed by gas, corrected for oil shrinkage. The gas in Zone 2 occupies the volume not occupied by oil or water. The gas in Zone 3 is the fixed phase that results when the mobile gas phase of Zones 1 and 2 is displaced by oil. Its saturation is taken to be the equilibrium gas saturation, corrected for re-solution of gas in the oil should the pressure increase above the average pressure at which the gas in Zone 3 was deposited. Also, the saturation is not permitted to rise above the equilibrium gas saturation, as it is assumed that migration of gas to the gas cap will occur should the oil trapped in Zone 3 liberate gas. The oil in Zone 3 is that volume not occupied by gas or water. In Zone 4, the gas is the fixed phase that results from evolution from the oil present. Should sufficient gas be evolved that the gas saturation would exceed the equilibrium gas saturation, then by virtue of the fact that the oil column is considered to be thin, the excess is considered to migrate to the cap, and the gas saturation is maintained at S_e. Should any migration occur and should this be followed by a rise in pressure, the Zone 4 gas-oil equilibrium is corrected by the amount of the loss of gas to the cap of the excess of gas above S_e. This is important if the pressure increases after substantial gas liberation and migration to the cap have occurred. Zone 4 oil occupies the volume not occupied by gas or water. In Zone 5, both the oil and gas are fixed phases. The oil is taken to be that remaining residual after water displacement, corrected for the average shrinkage between the original pressure and the pressure P_n. The gas is that liberated from the residual oil, but is not allowed to exceed S_e.

TABLE 1 — SATURATION VALUES

Zone	S_{o_n}	S_{g_n}
1.	0	$1 - S_w(x_{g_n})$
2.	Min $\begin{cases} S_{org} \\ S_{org} \cdot \beta(P_M)/\beta(P_n) \end{cases}$	$1 - S_{2o} - S_w(x_{g_n})$
	P_M was pressure when $x_g = x_{g_M}$	Min $\begin{cases} S_e \\ S_e + S_{3o_{n-1}}[\lambda_n - \lambda(P_m)] \end{cases}$
		P_m was pressure when $x_g = x_{g_m}$.
3.	$1 - S_{3g_n} - S_w(x_{g_m})$	Min $\begin{cases} S_e \\ S_{4o_n}\lambda_n - Pos[(1 - S_e - S_w (x_{g_n})\lambda_M - S_e] \end{cases}$
4.	$1 - S_{4g_n} - S_w(x_{g_n})$	λ_M is maximum value of λ to step n
5.	Min $\begin{cases} S_{orw} \\ S_{orw} \cdot \dfrac{\beta(P_m)}{\overline{\beta}(P_n)} \end{cases}$	Min $\begin{cases} S_e \\ S_{5o_{n-1}}\lambda_n - Pos[S_{5o_m}\ \lambda_m - S_e] \end{cases}$
	where $\beta(P_m)$ was β when $x_o = x_{o_m}$, $\overline{\beta}(P_n)$ is $\frac{1}{2}[\beta(P_n) + \beta(P_{orig})]$	where m refers to time when $x_o = x_{o_m}$

Eqs. 25a and 25b may now be solved; every term in the integrand is evaluable at time $n\Delta\theta$. Rewriting the equations, using definitions of Eq. 24 for ϕ^1 and ϕ^2, yields a set of equations which may be solved by iteration:

$$G^*_{n+1} = \int_{x_{o_m}}^{x^*_{o_{n+1}}} S_{5g_n}\phi(x)A(x)dx + \int_{x^*_{o_{n+1}}}^{x_{g_m}} S_{1g_n}\phi(x)A(x)dx + \int_{x_{g_m}}^{x^*_{g_M}} S_{3g_n}\phi(x)A(x)dx + \int_{x^*_{g_m}}^{x_{g_M}} [1 - S_w(x)]\phi(x)A(x)dx - \int_{x^*_{g_{n+1}}}^{x_{g_M}} S_{2o_n}\phi(x)A(x)\,dx + \int_{x_{g_M}}^{x_t} [1 - S_w(x)]\phi(x)A(x)\,dx, \quad . \quad . \quad . \quad . \quad . \quad . \quad . \quad . \quad . \quad . \quad . \quad . \quad . \quad . \quad . \quad (26a)$$

and

$$N^*_{n+1} = \int_{x_{o_m}}^{x^*_{o_{n+1}}} S_{5o_n}\phi(x)A(x)\,dx + \int_{x^*_{o_{m+1}}}^{x_{g_M}} [1 - S_w(x)]\phi(x)A(x)\,dx - \int_{x^*_{o_{n+1}}}^{x_{g_m}} S_{4g_n}\phi(x)A(x)\,dx + \int_{x_{o_m}}^{x^*_{g_{n+1}}} [1 - S_w(x)]\phi(x)A(x)\,dx - \int_{x_{g_m}}^{x^*_{g_{n+1}}} S_{3g_n}\phi(x)A(x)dx + \int_{x^*_{g_{n+1}}}^{x_{g_M}} S_{2o_M}\phi(x)A(x)\,dx, \quad . \quad . \quad . \quad . \quad . \quad . \quad . \quad . \quad . \quad . \quad . \quad . \quad . \quad . \quad . \quad (26b)$$

where $x^*_{o_{n+1}}$ and $x^*_{g_{n+1}}$ are the trial parameters for the iteration. To obtain a solution, a relationship must be applied to determine a Δx_o and Δx_g from the differences, $G_{n+1} - G^*_{n+1}$ and $N_{n+1} - N^*_{n+1}$. Such a relationship may be derived by differentiating Eq. 26 with respect to the independent variables, x_g and x_o. From Eqs. 26a and 26b,

$$\begin{cases} G = f_1(x_o, x_g) , \\ N = f_2(x_o, x_g) \end{cases} \quad . \quad . \quad . \quad . \quad . \quad . \quad . \quad . \quad . \quad (27)$$

To first order correctness

$$\begin{cases} \Delta G = \dfrac{\partial f_1}{\partial x_o} \Delta x_o + \dfrac{\partial f_1}{\partial x_g} \Delta x_g , \\ \Delta N = \dfrac{\partial f_2}{\partial x_o} \Delta x_o + \dfrac{\partial f_2}{\partial x_g} \Delta x_g ; \end{cases} \quad . \quad . \quad . \quad . \quad . \quad (28)$$

and, since the correction ΔG is that which should be added to G^* to improve it,

$$\begin{cases} \Delta G = G_{n+1} - G^*_{n+1} \\ \Delta N = N_{n+1} - N^*_{n+1} \end{cases} \quad . \quad . \quad . \quad . \quad . \quad . \quad . \quad (29)$$

With certain restrictions on the behavior of f_1 and f_2 it can be shown that the process converges. Substitution of the derivatives of the f-functions of Eq. 27 (from differentiating Eqs. 26a and 26b with respect to the variable limits; i.e., the starred terms) and solution of Eq. 28 for the corrections, Δx_g and Δx_o, yields

$$\Delta x_g = \frac{(G_{n+1} - G^*_{n+1})(S_{5o_n} - S_{4o_n}) - (N_{n+1} - N^*_{n+1})(S_{3g_n} - S_{4g_n})}{A(x_{g_n})\,\phi(x_{g_n})[(S_{3g_n} - S_{2g_n}) - (S_{5o_n} - S_{4o_n}) - (S_{3o_n} - S_{2o_n})(S_{5g_n} - S_{4g_n})]} ,$$

and

$$\Delta x_o = \frac{(N_{n+1} - N^*_{n+1})(S_{3g_n} - S_{2g_n}) - (G_{n+1} - G^*_{n+1})(S_{3o_n} - S_{2o_n})}{A(x_{o_n})\phi(x_{o_n})[(S_{3g_n} - S_{2g_n})(S_{5o_n} - S_{4o_n}) - (S_{3o_n} - S_{2o_n})(S_{5g_n} - S_{4g_n})]} . \quad . \quad . \quad . \quad . \quad . \quad . \quad . \quad (30)$$

In practice, the solution of Eq. 26a is accomplished by calculating G^*_{n+1} and N^*_{n+1} for x_{o_n} and substituting into Eq. 30 to yield Δx_g and Δx_o. The $x^*_{g_{n+1}}$ and $x^*_{o_{n+1}}$ are obtained from Eq. 30a:

$$\begin{aligned} x^*_{g_{n+1}} &= x_{g_n} + \Delta x_g , \\ x^*_{o_{n+1}} &= x_{o_n} + \Delta x_o \end{aligned} \quad . \quad . \quad . \quad . \quad . \quad . \quad . \quad . \quad (30a)$$

The value of $x^*_{o_{n+1}}$ is then checked against x_{o_m} to determine whether at this step x_o will be less than x_{o_m}, and, if so, the values of S_{5o} and S_{5g} of Eq. 30 are replaced by zero. Similarly, $x^*_{g_{n+1}}$ is checked to see whether it exceeds x_{g_M} or is less than x_{g_m}. If $x^*_{g_{n+1}} > x_{g_M}$ then S_{2o} is replaced by zero, and S_{2g} by S_{1g} in Eq. 30. If $x^*_{g_{n+1}} < x_{g_m}$, then the values of S_{3g} and S_{3o} are replaced by S_{4g} and S_{4o}, respectively, in Eq. 30. The solution of Eq. 30 with these changes is then recomputed if, and only if, any changes were necessary, and the values so obtained are substituted into Eq. 30a to obtain $x_{g_{n+1}}$ and $x_{o_{n+1}}$. This procedure constitutes taking only one step of iteration and is permissible provided the time step, $\Delta\theta$, during computation is kept small, so that errors introduced by the first order approximations of Eq. 28 are small.

A word should be said about a special case which arises at the lower boundary of Zone 5. Initially, the water saturation is 1 at $x_o = 0$. When water displacement begins, the residual oil saturation S_{orw} is assumed to exist below the water-oil contact. However, as x_o moves up from zero, S_{orw} is considered as S_{5o} for $x_o > 0$; therefore, the integral, $\int_0^{x_{o_n}} S_{5o}\phi(x)\,A(x)\,dx$, will include more oil than was originally present in that interval. To handle this problem, the value of x_{o_r} was found corresponding to $1 - S_w(x_{o_r}) = S_{orw}$ and x_{o_r} was assumed to be the starting point for moving the oil-water boundary. The integrals of $\int_{x_{o_m}}^{x_{o_n}} S_{5o}\phi(x)A(x)\,dx$ were evaluated as $\int_{x_{o_m}}^{o} S_{5o}\phi(x)\,A(x)\,dx +$

$$\int_{o}^{x_{o_r}} [1 - S_w(x)]\phi(x)\,A(x)\,dx + \int_{x_{o_r}}^{x_{o_n}} S_{5o}\phi(x)\,A(x)\,dx .$$

It was recognized that should x_{o_m} be moved below zero, an error is made in the oil content of Zone 5 between 0 and x_{o_r}. However, a case in which x_{o_m} becomes negative appears unlikely.

To summarize the method of computing, given as a function of time the production rates of oil, gas and water, and the values of all variables at time $n\Delta\theta$:

1. Apply Eq. 22 to determine $W_{n+\frac{1}{2}}$.
2. Apply Eq. 20 to determine C_{F_n}.
3. Solve Eq. 16 for $z_{i,n+1}$, $i = 0, 1, \ldots, j$, and $\Delta P_n = P_{j,n+1} - P_{j,n}$.
4. Solve Eq. 21 for N_{n+1} and G_{n+1}.
5. Evaluate Eqs. 30 and 30a; compare new x values with limits x_{o_m}, x_{g_n}, and x_{g_M}; change any appropriate saturations; and re-solve Eqs. 30 and 30a for $x_{o_{n+1}}$ and $x_{g_{n+1}}$.

This stepwise procedure follows the movement of the gas-oil contact and oil-water contact and calculates the aquifer pressure as a function of time and distance from the reservoir.

PREDICTION

The procedure just described assumes the water, gas, and oil production rates to be given for each time interval. This is the situation during production history. To predict behavior into the future, these rates must either be specified in advance or predictable at each step of the computation. As was pointed out in the previous section, it was assumed that the oil production rates would be specified as a function of time and the position of the contacts and other properties derivable from the instantaneous results of the computations. The gas and water rates would then be related to the oil rate through the gas-oil ratio and the produced water fraction.

The gas-oil ratio must depend on the thickness of both the oil and gas columns in such a way that it increases as the oil column thins and decreases to zero as the gas column approaches zero. To choose a function with these properties, ρ, defined as the ratio q_g/q_o is taken to be

$$\rho_{n+\frac{1}{2}} = \frac{(x_t - x_{g_n})}{(x_t - x_{g_\pi})}\left[\frac{A_n}{x_{g_n} - x_{o_n}} + B_n\right] , \quad (31)$$

where the subscript π refers to the latest time for which production data are available. For a constant gas column thickness, A and B are coefficients of a linear function in $\dfrac{1}{x_g - x_o}$ which passes through ρ_π and terminates at ρ_f, the value of ρ at the final oil column thickness, x_f. To determine these constants, values must be specified for

GOR_f, the final gas-oil ratio in standard cubic feet of free plus dissolved gas per barrel of condensate-free stock-tank oil, and for x_f. Then,

$$\rho_\pi = \frac{A_n}{x_{g_\pi} - x_{o_\pi}} + B_n,$$

and

$$\rho_f = \frac{A_n}{x_f} + B_n, \quad \ldots\ldots\ldots \quad (32)$$

where ρ_f is related to GOR_f by

$$\rho_f = \frac{\lambda y + \beta(GOR_f - r_{so})}{\gamma} \quad \ldots\ldots \quad (33)$$

Hence,

$$A_n = \frac{\rho_f - \rho_\pi}{\dfrac{1}{x_f} - \dfrac{1}{x_{g_\pi} - x_{o_\pi}}},$$

and

$$B_n = \rho_\pi - \frac{A_n}{x_{g_\pi} - x_{o_\pi}}.$$

The water fraction is treated similarly by assuming the final produced water fraction in the reservoir to be w_f at the time the oil column thickness has attained the value x_f.

If y is the water-oil ratio of the fluids leaving the reservoir, then $y_f = \dfrac{w_f}{1 - w_f}$, and if $y_{n+\frac{1}{2}}$ is taken as

$$y_{n+\frac{1}{2}} = \left(\frac{x_{g_\pi} - x_{o_\pi} - \delta}{x_{g_n} - x_{o_n} - \delta}\right) y_\pi, \quad \ldots\ldots \quad (34)$$

where δ is a parameter that sets $y_{n+\frac{1}{2}} = y_f$ for $x_{g_n} - x_{o_n} = x_f$. Solution of Eq. 34 for δ yields

$$\delta = \frac{(x_{g_\pi} - x_{o_\pi})\, y_\pi - y_f x_f}{y_\pi - y_f}.$$

From Eqs. 31 and 34, the relationships

$$q_{g_{n+\frac{1}{2}}} = \rho_{n+\frac{1}{2}}\, q_{o_{n+\frac{1}{2}}} \quad \ldots\ldots\ldots \quad (35a)$$

and

$$q_{w_{n+\frac{1}{2}}} = y_{n+\frac{1}{2}}\, q_{o_{n+\frac{1}{2}}} \quad \ldots\ldots\ldots \quad (35b)$$

specify total reservoir withdrawals, given the oil withdrawal rate, $q_{o_{n+\frac{1}{2}}}$. Given an allowable $E_{n+\frac{1}{2}}$ bbl per time period, the oil rate $q_{o_{n+\frac{1}{2}}}$ is related by

$$q_{o_{n+\frac{1}{2}}} = \frac{E_{n+\frac{1}{2}}}{\rho_n \gamma_n y_n + \beta_n}, \quad \ldots\ldots\ldots \quad (36)$$

where $Y_n = Y_o\ Pos\left[1 - \dfrac{GR_n}{\gamma_n G_n}\right]$; Y_o is the original condensate richness, bbl/Mcf, and GR_n is the total gas return to time $n\Delta\theta$, Mcf. The function $Pos\,(v)$ is defined

$$Pos\ (v) = \begin{cases} v, & v \geq o, \\ o, & v < o. \end{cases}$$

Now, with the allowable $E(\theta)$ a specified function of time, applications of Eqs. 31, 34, and 36 provides sufficient relationships to yield a value of $W_{n+\frac{1}{2}}$ from Eq. 22. This procedure permits predicting ahead in time until either the reservoir pressure is depleted or until $x_{g_n} - x_{o_n} \leq x_f$.

GAS RETURN

Two possible purposes of gas return may readily be considered—to prevent rise of the gas-oil contact above x_{g_π} or to prevent rise of the water-oil contact above x_{o_π}. For each case the rate of gas return, $L_{n+\frac{1}{2}}$, res. B/D, is computed such that $L_{n+\frac{1}{2}}\,\Delta\theta$ is the reservoir volume that should be filled by gas at that step.

For maintaining the gas-oil contact,

$$L_{n+\frac{1}{2}}\,\Delta\theta = Pos\,[A(x_{g_n})(x_{g_\pi} - x_{g_n})\phi(x_{g_n})(S_{gg} - S_{iw})],$$

where $i = 1$ if $x_{g_n} = x_{g_M}$, and $i = 2$ if $x_{g_n} < x_{g_M}$.

For maintaining water-oil contact,

$$L_{n+\frac{1}{2}}\,\Delta\theta = Pos\,[A(x_{o_n})(x_{o_\pi} - x_{o_n})\phi(x_{o_M})(S_{so} - S_{wo})],$$

where the symbol $Pos\ (\ )$ has the same significance as in Eq. 36. If gas is being returned, $q_{g_{n+\frac{1}{2}}} = \rho_{n+\frac{1}{2}}\, q_{o_{n+\frac{1}{2}}} - L_{n+\frac{1}{2}}$.

TREATMENT OF THE INPUT DATA

The fluid properties related to pressure, γ, β and λ, are sufficient to characterize the oil behavior. The required reservoir geometry properties are $A(x)$ and $S_w(x)$. These five relationships, the aquifer properties, and associated constants are all the data required for the solution outlined in the foregoing sections.

The functions chosen for matching the oil properties are $\gamma(z)$, $\dfrac{1}{\beta}(z)$ and $\dfrac{1}{1+\lambda}(z)$. A fifth-degree polynomial is fitted to each of these by the method outlined in Ref. 5.

The function $A(x)$ is often sufficiently smooth that it may be adequately matched by the method of Ref. 5. However, $S_w(x)$ is a very difficult function to match, having the shape shown in Fig. 3. To obtain a suitable match for $S_w(x)$, a function $\xi\left(\dfrac{x}{x_t}\right)$ was defined as

$$\xi\left(\frac{x}{x_t}\right) = [1 - S_w(x)]\ A(x)\left[\frac{1 + a\dfrac{x}{x_t}}{b\dfrac{x}{x_t}}\right], \quad (37)$$

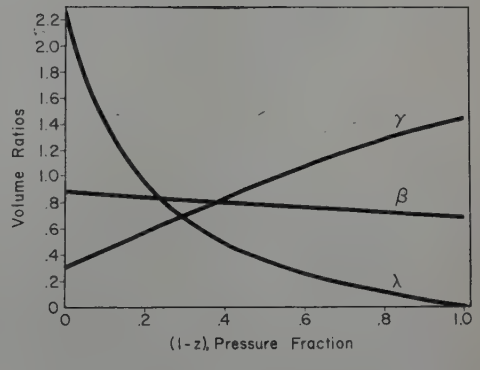

FIG. 2—RESERVOIR A, FLUID CHARACTERISTICS.

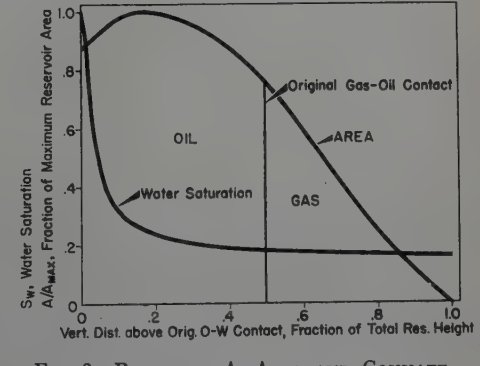

FIG. 3—RESERVOIR A, AREA AND CONNATE WATER SATURATION.

where $\xi\left(\frac{x}{x_t}\right)$ is matched by a fifth-degree polynomial in $\frac{x}{x_t}$. The product $A(x)\ [1 - S_w(x)]$ was chosen for the match because in evaluating Eq. 26, $\int A(x)\ [1 - S_w(x)]dx$ appears frequently. The multiplier $\frac{1 + a\frac{x}{x_t}}{b\frac{x}{x_t}}$ was chosen because it smooths out the function $[1 - S_w(x)]$ in the neighborhood of $x = 0$, provided a and b are properly chosen. They are evaluated as follows.

$$a = \frac{9\left(1 - S_w, \frac{x}{x_t} = 0.1\right)}{\left(S_w, \frac{x}{x_t} = 0.1\right) - \left(S_w, \frac{x}{x_t} = 1.0\right)} - 1 ,$$

and

$$b = 10\left(1 - S_w, \frac{x}{x_t} = 0.1\right)\left(\frac{a}{10} - 1\right).$$

The integral of the approximation for $A(x)\ [1 - S_w(x)]$ is obtained from

$$\int_{x_1}^{x_2} \frac{b\frac{x}{x_t}}{1 + a\frac{x}{x_t}}\,\xi\left(\frac{x}{x_t}\right)dx \cong\cong \int_{x_1}^{x_2} [1 - S_w(x)]A(x)\,dx\,. \quad \ldots\ldots\ldots\ldots\ldots\ldots \quad (38)$$

If $X = \frac{x}{x_t}$, integration of Eq. 38 is performed as follows.

Let $\xi(X) = B_0 + B_1X + B_2X^2 + \ldots + B_5X^5$, whereupon Eq. 38 becomes

$$\int_{x_1}^{x_2}[1 - S_w(x)]\ A(x)\ dx \cong x_t \int_{X_1}^{X_2} \frac{B_0X + B_1X^2 + \ldots + B_5X^6}{1 + aX}$$

$$dX = \Big[\ H_0 \log (1 + aX) + H_1(1 + aX) + H_2(1 + aX)^2 + \ldots + H_6(1 + aX)^6\Big]_{1 + aX_1}^{1 \pm aX_2} , \ldots\ldots \quad (38a)$$

where the H-vector is related to the B-vector by the matrix multiplication:

H_0	$= \frac{x_t b}{a}$	−1	1	−1	1	−1	1	B_0/a
H_1		1	−2	3	−4	5	−6	B_1/a^2
H_2		0	½	−3/2	3	−5	15/2	B_2/a^3
H_3		0	0	1/3	−4/3	10/3	−20/3	B_3/a^4
H_4		0	0	0	¼	−5/4	15/4	B_4/a^5
H_5		0	0	0	0	1/5	−6/5	B_5/a^6
H_6		0	0	0	0	0	1/6	

APPLICATION OF COMPUTING PROCEDURE TO PREDICTION OF RESERVOIR PERFORMANCE

The procedure discussed in the foregoing section was developed for comparing the performance of gas-cap, water-drive reservoirs produced with and without gas return. In this study, the purpose of returning gas to such reservoirs is to replace part of the free or cap gas that is being produced so as to prevent loss of recoverable oil through migration of oil into the gas cap and the attendant wetting by oil of oil-free sand in the cap. In order to place a value on preventing such oil loss, it is necessary to determine the cost of gas injection. This in turn depends on how much gas will be required at what pressure, and the additional oil recovery must be sufficient to pay the cost of injection and yield a return on the investment. Application of the foregoing procedure should provide a reasonable prediction of performance that serves as a physical basis for making this economic study.

It is the purpose of this section to show an application of the computing procedure to be two reservoirs which were considered for a gas injection program. Reservoir A is characterized by an original gas-cap volume which is of the same size as the reservoir oil volume and a moderate-sized aquifer which feeds the reservoir through a substantial constriction. Reservoir B has a gas cap which is large by comparison with the reservoir oil volume and a permeable aquifer which, insofar as can be determined from production history, is essentially infinite in extent.

The required geometry for the reservoirs is shown in Figs. 3 and 4. Along the abscissa is plotted the vertical height in the reservoir above the original water-oil contact, as a fraction of the maximum height of the reservoir. Along the ordinate are plotted the reservoir area as a fraction of the maximum area and the original water saturation as fraction of total pore volume.

The properties of the reservoir fluids as characterized by γ, β and λ are given for Reservoir A in Fig. 2. These relationships for Reservoir B are quite similar.

The results of interest are presented in Figs. 5, 6, 7 and 8. Figs. 5 and 7 are plots of pressure, gas-oil ratio, water fraction, and cumulative injected gas for Reservoirs A and B, respectively. In each of these, comparison is made of future performance with and without gas injection. For these examples the oil production rates were taken to be constant, although this was recognized as not being a realistic mode of operation. It could, in fact, have been chosen arbitrarily or as a declining function of time or to depend on the pressure, column thickness, or any other variable being computed. The motion of the gas-oil and oil-water contacts is shown in Figs. 6 and 8.

The depletion performance of the reservoirs appear normal. Reservoir A shows a marked pressure sensitivity to total withdrawals, giving rise to widely different pressure performances for the two modes of operation. On the other hand, pressure in Reservoir B is relatively insensitive to changes in withdrawals, and initiation of injection makes no important change in the

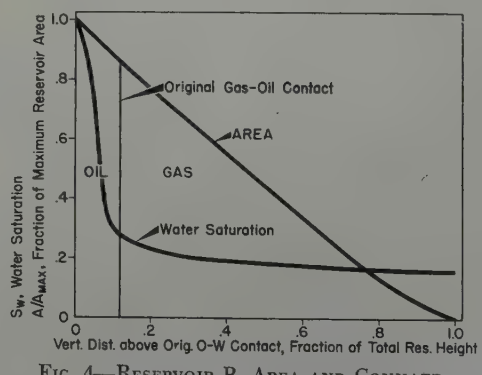

FIG. 4—RESERVOIR B, AREA AND CONNATE WATER SATURATION.

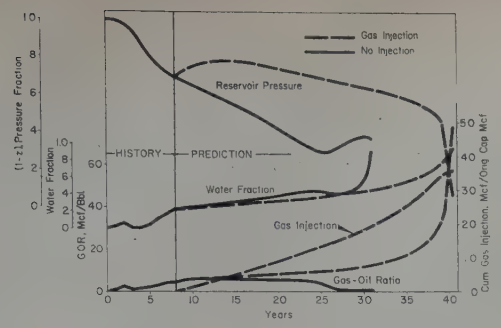

FIG. 5—RESERVOIR A, HISTORY AND PREDICTED PERFORMANCE.

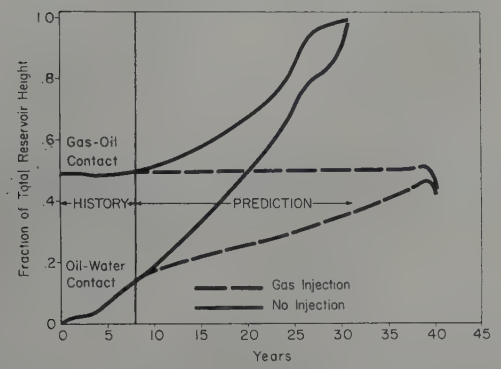

FIG. 6—RESERVOIR A, HISTORY AND PREDICTED POSITION OF CONTACTS.

pressure behavior. The strongly differing response of the two reservoirs to the injection of gas emphasizes the need for studying individual reservoir performance by applying the method outlined in the foregoing section. It can be seen that, under the assumptions controlling predicted gas-oil ratio, the relative size of the gas cap and the oil zone significantly influence differences in performance when the cap size is and is not maintained. From the injection program, Reservoir A experiences about a one-third increase in recovery, whereas recovery from Reservoir B is doubled. Further, the amount of gas, the time schedule of its injection, and the injection pressure required to maintain gas-cap size depend materially on the aquifer characteristics and the compressibility of fluids within the reservoir.

Thus, to analyze the economics of proposed injection programs necessitates acquiring the type of information developed by applying the method of this paper individually for each reservoir considered under a number of possible modes of operation. Within the limitations of the assumptions, these results will provide a physical basis for designing an optimum injection program and determining its economic value.

Although examples presented treat a particular problem, it should be emphasized that the analysis and its

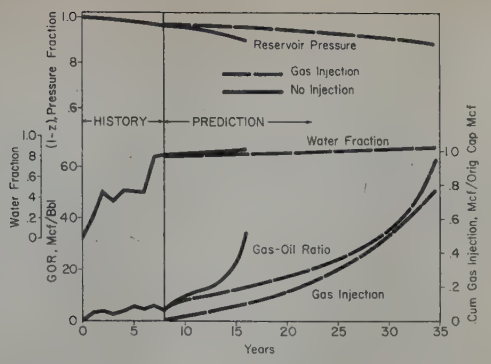

FIG. 7—RESERVOIR B, HISTORY AND PREDICTED PERFORMANCE.

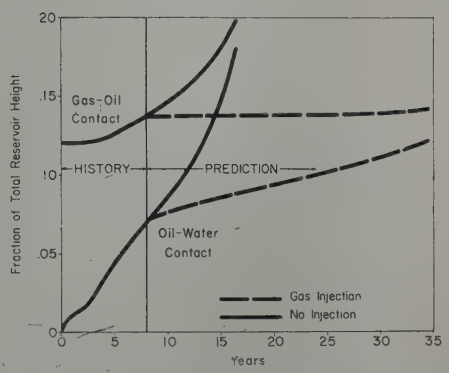

FIG. 8—RESERVOIR B, HISTORY AND PREDICTED POSITION OF CONTACTS.

derived procedure provide a substantial degree of flexibility in treating resevoir problems wherein a gas zone and a water zone confine a thin oil column. The complex, inter-related influences of pressure changes, water influx, and gas expansion are described quantitatively in a way that facilitates taking into account such variations in modes of production as gas injection, water injection, and a dependence of the future rates of fluid withdrawals on the future performance of the reservoir.

REFERENCES

1. Bruce, G. H., Peaceman, D. W., Rachford, H. H., Jr., and Rice, J. D.: "Calculations of Unsteady-State Gas Flow Through Porous Media", *Trans.* AIME (1953) **198,** 79.
2. Bruce, W. A.: "An Electrical Device for Analyzing Oil Reservoir Behavior", *Trans.* AIME (1943) **151,** 112.
3. Douglas, J., Jr.: "Application of Stability Analysis in the Numerical Solution of Quasi-Linear Parabolic Differential Equations" (to be published).
4. Hurst, W.: "Water Influx into a Reservoir and its Application to the Equation of Volumetric Balance", *Trans.* AIME (1943) **151,** 57.
5. Rachford, H. H., Jr. and Schultz, W. P.: "Some Useful Tables for Approximating Smooth Curves by Fifth-and-Lower Degree Polynomials," *Trans.* AIME (1955) **204,** 289.

★★★

Producing Wells on Casing Flow—An Analysis of Flowing Pressure Gradients

P. B. BAXENDELL
MEMBER AIME

COMPANIA SHELL DE VENEZUELA, LTD.
MARACAIBO, VENEZUELA

ABSTRACT

The Cretaceous limestone wells of the Mara/Maracaibo Dist. of Venezuela are extremely prolific producers. To maintain production on cessation of natural flow, large scale gas-lift operations were commenced involving high production rates on casing flow. For the design of these gas-lift installations it was essential to have some knowledge of the pressure gradients involved in casing flow, so that the required injection pressures, optimum gas injection rates, etc., could be forecast.

This paper presents a method of calculating these annular pressure gradients. Basically the method makes use of an energy balance equation coupled with an empirical energy loss factor derived from field data. The calculations have been put in a form suitable for "punch card-type" calculating machines.

A set of gradient curves for Mara/Maracaibo conditions covering flow rates up to 12,000 B/D, and GOR's of 500 to 2,000 cu ft/bbl is presented. From these curves the flowing BHP can be predicted from surface data and the vertical flow performance under varying conditions of gas injection can be estimated.

The method has been applied to La Paz and Mara gas-lift operations for over three years and has given consistently accurate results.

INTRODUCTION

The Cretaceous limestone fields of the Mara/Maracaibo area in Venezuela are characterized by the presence of widely distributed fissure systems. Under these conditions individual wells frequently have extremely high potentials and such wells are generally flowed on the casing-tubing annulus in order to reduce the pressure loss in vertical flow. To maintain production on cessation of natural flow, an extensive gas-lift system was planned.

As a first approach to this gas-lift design problem, an attempt was made to construct a set of empirical flowing gradient curves from the available subsurface pressure data. Such a method has been used successfully for tubing-flow conditions in California by Gilbert[1]. Unfortunately, the empirical construction of casing-flow gradient curves presents additional difficulties, as pressure bombs cannot be run in the casing-tubing annulus against high rates of flow. Thus, the full flowing gradients cannot be defined by actual measurement and the best that can be done is to obtain spot pressures at the tubing shoe. Under these conditions a vast accumulation of BHP data is required to construct a set of gradients.

In the La Paz and Mara fields the majority of the available flowing pressure measurements fall into a relatively narrow GOR range, in the neighborhood of the solution ratio. While there appeared to be reasonable prospects of constructing gradient curves for this limited range, measurements at higher GOR's, which were of major interest for gas-lift operations, were relatively few and the prospects of constructing empirical curves correspondingly remote.

As an alternative approach, the possibilities of a mathematical analysis of vertical flow conditions were investigated.

May and Laird[2,3] in 1934 presented an excellent analysis of the vertical-flow conditions in the Anglo-Iranian Oil Co.'s fields. Their analysis was based on an energy-balance equation and calculated the losses due to kinetic energy, friction and slippage separately. By combining these losses with the total calculated available energy, the required depth-pressure traverse could be deduced. On applying the method to La Paz conditions, good results were obtained for tubing flow at high tubing-head pressures. However, for lower wellhead pressures (300 psi and under) the discrepancy between calculated and measured values increased appreciably. It was considered that this was probably due to energy losses caused by slippage or liquid hang-up in a continuous gas phase, for which it was difficult to visualize any analytical approach.

In 1952 Poettmann and Carpenter[4] presented a method of pressure gradient calculation which, while based on an energy-balance equation similar to that employed by May and Laird, made no attempt to evaluate the various components making up the total energy loss resulting from irreversibilities of flowing fluids. Instead, they proposed a method of analysis which assumed that all significant losses for multiphase flow could be correlated in a form similar to that of the Fanning equation for frictional losses in single-phase flow. They then derived an empirical relationship linking measurable field data with a factor which, when applied to the standard form of the Fanning equation, would enable the energy losses to be determined. The total available

Original manuscript received in Society of Petroleum Engineers office Oct. 30, 1957. Revised manuscript received July 1, 1958. Paper presented at Second Annual Regional Meeting of Venezuela Petroleum Sections in Caracas, Nov. 6-9, 1957.
[1]References given at end of paper.

energy could be calculated in a similar manner to that used by May and Laird and, knowing the distribution of the losses, a depth-pressure traverse could be drawn.

On publication of the paper, the method was applied in Venezuela to construct a set of tubing-flow gradient curves for producing conditions in the Lake Maracaibo concessions. The results proved encouraging when checked against field data and it was decided to investigate the possibilities for annular flow. The following principal difficulties were immediately apparent: (1) the energy loss factor correlation of Poettmann and Carpenter has to be extended to cover higher production rates, (2) the annular cross section has to be converted into terms of an equivalent circular conduit in order to fit the equation form, and (3) the crescent shaped annulus (i.e., tubing lying against casing wall) might affect the slippage characteristics and invalidate the low flow rate end of the energy loss factor correlation.

This paper describes the approach to these problems and the method ultimately employed to construct a full set of flowing pressure gradient curves for casing-flow conditions in the La Paz and Mara fields.

THE BASIC ENERGY EQUATION ANALYSIS

Using the same nomenclature as used by Poettmann and Carpenter, the energy balance based on 1 lb of flowing fluid can be expressed as follows, assuming that no external work is done by the fluid in flow.

$$\int_{P_1}^{P_2} V\,dP + \Delta h + \Delta(v^2/2g) + W_f = 0 \quad . \quad . \quad . \quad (1)$$

where V is specific volume of flowing fluid, ft³/lb; P is pressure, psia; Δh is difference in head above datum, ft; $\Delta(v^2/2g)$ is difference in kinetic energy of 1 lb of flowing fluid between initial and final states of flow; and W_f is total energy losses due to irreversibilities of the fluid in flow.

Of these terms the value of the kinetic energy function is small as compared to the other functions in the energy balance and is neglected. Further, assuming that the energy losses can be correlated with the Fanning equation, W_f can be written,

$$W_f = 4f\bar{v}^2\Delta h/2gD \quad . \quad . \quad . \quad . \quad . \quad . \quad . \quad . \quad (2)$$

where f is used as the correlating function for total energy loss, whether due to friction or otherwise, and D is the inside diameter of the pipe in feet. The velocity, $\bar{v}$, is assumed constant and equal to the integrated average value between limits, P_1 and P_2.

Substituting in Eq. 1 we have

$$\int_{P_1}^{P_2} V dP + \Delta h + 4f\bar{v}^2\Delta h/2gD = 0 \quad . \quad . \quad . \quad . \quad . \quad (3)$$

or converting to field units,

$$\frac{1}{M}\int_{P_1}^{P_2} V_m dP + \Delta h + fQ^2\bar{V}_m{}^2\Delta h/7.413 \times 10^{10}D^5 = 0 \quad . \quad . \quad . \quad . \quad (4)$$

or

$$\Delta h = \frac{\frac{1}{M}\int_{P_2}^{P_1} V_m\,dP}{1 + fQ^2\bar{V}_m^2/7.413 \times 10^{10}D^5} \quad . \quad . \quad . \quad . \quad (5)$$

where V_m is cubic feet of gas and oil, at pressure P, per barrel of stock-tank oil; M is total mass of gas and oil, in pounds, associated with 1 STB; Q is production, STB/D; and $\bar{V}_m$ is the integrated average value of V_m between pressure limits, P_1 and P_2.

By dividing Eq. 5 into ΔP the following expression for pressure gradient results.

$$\Delta P/\Delta h = \bar{\rho} + \bar{K}\bar{\rho} \quad . \quad . \quad . \quad . \quad . \quad . \quad . \quad . \quad . \quad (6)$$

where $\bar{\rho}$ is the integrated average density over the pressure range ΔP, and $\bar{K} = fQ^2M^2/7.413 \times 10^{10}\bar{\rho}^2D^5$ and the full equation becomes

$$\Delta P/\Delta h = \bar{\rho} + fQ^2M^2/7.413 \times 10^{10}\bar{\rho}D^5 \quad . \quad . \quad (7)$$

CORRELATION OF ENERGY LOSS FACTOR, f, WITH FIELD DATA

To establish a correlation linking the energy loss factor, f, with field data, Poettmann and Carpenter retained the analogy with single-phase flow and the Fanning equation, by correlating f against the product of diameter, density and velocity, Dpv, which corresponds to the numerator of the Reynolds number. The viscosity term, which forms the denominator of the Reynolds number, cannot be evaluated for two-phase flow conditions and is ignored. A logical development, for as Poettman and Carpenter point out: "The fact that viscosity is not one of the variables involved in the vertical multiphase flow is both fortunate and to be expected. This is because of the fact that the degree of turbulence is of such a magnitude that, of the total energy loss, W_f, that portion resulting from viscous shear is negligible." Various other workers in this field have made the same observation.

There were two reasons why the correlation established by Poettman and Carpenter could not be applied directly to the La Paz conditions: (1) the correlation was only established for rates of flow very much lower than the La Paz conditions, and (2) the annular section has to be converted into terms of an equivalent circular conduit in order to fit the equation form. This latter problem requires some amplification. The basic equation for tubing flow has been shown to be

$$\frac{\Delta P}{\Delta h} = \bar{\rho} + \frac{fQ^2M^2}{7.413 \times 10^{10}\bar{\rho}D^5} \quad . \quad . \quad . \quad . \quad . \quad . \quad (7)$$

Converting into the annular flow form, this becomes

$$\frac{\Delta P}{\Delta h} = \bar{\rho} + \frac{fQ^2M^2}{7.413 \times 10^{10}\bar{\rho}(D_1^2 - D_2^2)^2 D_e} \quad . \quad . \quad (8)$$

where D_1 is the internal diameter of the casing, ft; D_2 is the external diameter of the tubing, ft; and D_e is the equivalent hydraulic diameter of the annulus.

Similarly, the correlating parameter $D\rho v$ becomes $D_e\rho v$.

While a variety of forms exist for establishing the equivalent hydraulic diameter for non-circular conduits, it was felt that for a complex cross-sectional area of this type (complicated by collars and upsets) it would, if possible, be better to avoid any such evaluation, which would introduce an element of possible error.

The form of the basic equation (Eq. 8) has as variables only two terms which can not be evaluated from the field data, i.e., f and D_e. Furthermore, the conditions investigated in La Paz were concerned with flow in an annulus of fixed size, i.e., 2⅞-in. tubing and 7-in. casing, and thus D_e, though unknown, must be constant. Consequently, the parameters chosen for correlation of energy-loss factor with field data were mass flow rate MQ and the term f/D_e. Both these terms can be

evaluated by applying field data to Eq. 8. Following are the stages in this evaluation.

Evaluation of $\bar{\rho}$

In order to evaluate $\bar{\rho}$ a set of pressure-density curves covering the GOR range encountered in field conditions must be constructed. Using the standard PVT analysis for a representative well, a pressure-density curve can be drawn directly for the GOR at which the analysis sample was taken. Theoretical pressure-density curves for other GOR's can be constructed from the basic PVT data as follows.

If Y (1b) is the mass of 1 bbl of tank oil plus solution gas, d (1b/ft^3) is density of gas at standard conditions, X (ft^3/bbl) is excess GOR, then $Y + Xd$ (lb) is the total mass corresponding to 1 bbl of tank oil.

Further, disregarding temperature effect: the volume of 1 bbl of tank oil plus solution gas is $5.615\ V_t/C_b$ (ft^3), and the volume of excess gas is X/V (ft^3), where V_t is relative total volume (compared to volume at saturation pressure), C_b is shrinkage factor from saturation pressure to standard tank conditions, and V is expansion factor from considered pressure to standand conditions. Therefore, the total volume corresponding to 1 bbl of tank oil will be $5.615\ (V_t/C_b) + X/V$ (ft^3), and the density is

$$\frac{Y + Xd}{5.615\ (V_t/C_b) + X/V}\ (\text{lb/ft}^3).$$

All these terms are obtainable directly from the standard PVT analysis and hence the pressure-density curves over the required GOR range can be constructed.

Fig. 1 shows a set of pressure-density curves constructed for La Paz conditions. From these curves the value of $\bar{\rho}$ between any pressure limits can be derived by graphical integration.

Evaluation of M

M is the total mass of gas and oil, in pounds, associated with 1 bbl of stock tank oil in the flow string. It is dependent on the GOR. As already shown, the total mass corresponding to 1 bbl of tank oil is $(Y + Xd)$ lb.

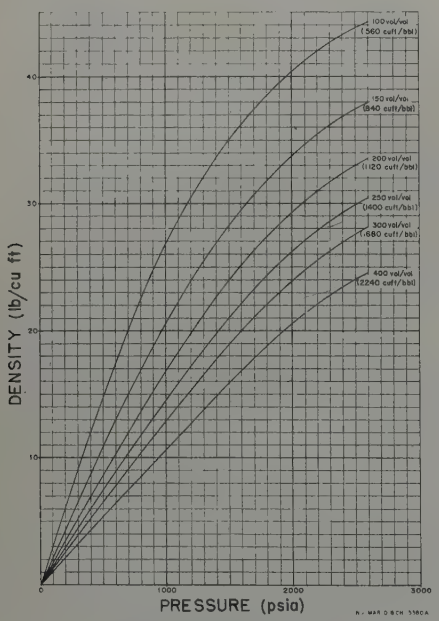

Fig. 1—Pressure-density Curves, La Paz Conditions.

Derivation of $\Delta P/\Delta h$ from Field Flowing Pressure Data

As a preliminary step, an attempt was made to arrange the available flowing pressure data in the form of pressure vs rate curves for varying depth and GOR's. As previously stated, the majority of the pressure data available fall into a relatively narrow range of GOR (around the solution ratio). Consequently, it was found that it was only possible to establish reasonable trends of pressure vs rate for a few limited cases of depths and GOR. These specific cases were selected to establish the energy-loss factor correlation. Arranging the data in this form, rather than considering each individual pressure reading, had the advantages that (1) field results could be weighed and anomalies rejected before applying them to the calculated form, and (2) ΔP readings could be taken from the curves at selected rates, thus ensuring a good spread of MQ values on the correlation graph.

From the pressure vs rate curves, values of ΔP for various production rates were read directly. The integrated values of ρ, over the pressure limits so read, were then established by graphically integrating the pressure-density curve over these limits. The values of mass flow rate, QM, corresponding to each selected oil rate and GOR were calculated as described. Having thus established values for $\bar{\rho}$, QM and $\Delta P/\Delta h$, these values were substituted in the original form of Eq. 8 and solved for f/D_e. The corresponding values of QM and f/D_e were then plotted (Fig. 2). A reasonable correlation curve was obtained from these readings.

CALCULATION OF THE CURVES

The energy equation form (Eq. 8) was used throughout. The correlation established in Fig. 2 justified calculation over a range of MQ values from 600,000 to 5 million lb/day (approximately 1,700 to 14,000 B/D dependent on GOR).

Metric units are employed in La Paz and Mara fields and it was decided to construct gradients at the following rates: 300, 400, 500, 700, 900, 1,100, 1,500 and 2,000 m^3/day, each at GOR's of 100, 150, 200, 250, 300 and 400 vol/vol (corresponding to a range of flow rates in U.S. units of approximately 1,800 to 12,500 B/D at GOR's from 560 to 2,250 cu ft/bbl).

Points on these curves were to be calculated at intervals of 200-psi pressure differential over a range of 200 to 2,600 psi, requiring a total of 624 separate calculations of gradient.

Fortunately, the given form of energy equation was suitable for mechanized calculation on punch-card machines and a considerable saving in time and effort was achieved.

The calculation was done in the following manner:

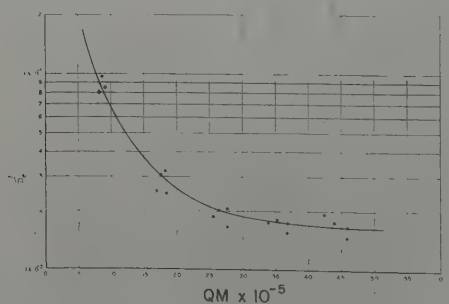

Fig. 2—Correlation Curve.

(1) for each rate and GOR for which a gradient curve was required, a value of QM was calculated, (2) using these values of QM, the corresponding values of f/D_e were read from Fig. 2, and (3) a set of values for ρ in increments of 200 psi were taken from Fig. 1 for each GOR.

This was the information supplied to the machines, which then calculated the gradient over 200-psi pressure increments for each set of values and each production rate (QM). Succeeding values of gradients were then averaged mechanically and divided into the pressure increment (200 psi) to convert the gradient value into feet. These depth values were then summed cumulatively to give the depth corresponding to each point on the full pressure range of 200 to 2,600 psi.

Table 1 represents the final machine form for each individual gradient curve.

The curves were then plotted directly on a pressure vs depth scale. The plotted curves originate at a pressure of 200 psi. In order to convert to a conventional gradient form, as used by Gilbert[1], they were extrapolated back to zero pressure and arranged with a common origin on the depth-pressure parameters. An example of this type of curve is shown in Fig. 3*.

REVERSED CURVATURE

As noted originally by Poettmann and Carpenter, the condition occasionally arises where the calculated pressure traverse in the low pressure range is concave downwards, instead of concave upwards as is usually the case in the calculated gradient curves and as appears to be always the case in measured traverses. This departure only occurs in the extreme low pressure end and has been adjusted by Poettmann and Carpenter by extrapolating the concave upwards trend back to zero pressure, ignoring the anomalous readings. This same procedure has been used in calculations of tubing-flow traverses in Venezuela and has been found to give satisfactory correlation with practical results. In most cases the departure is slight, and the extrapolation is obvious and presents no difficulty.

These reversal of curvature anomalies appeared as expected in the present analysis and were corrected by extrapolation. The anomalies became more marked with increasing rate.

This is to be expected from the form of the basic energy equation, which for any fixed mass flow rate can be expressed as $dp/dh = \rho +$ Constant$/\rho$, and consequently will have a point of inflection in the gradient curve at the low pressure (low density) end. With increased rates the value of the constant increases and the inflection point progresses to correspondingly higher pressures.

OPTIMUM GAS-OIL RATIOS

The optimum GOR's derived from these gradient curves at varying casinghead pressures conform well with the limited data available on this subject. Fig. 4

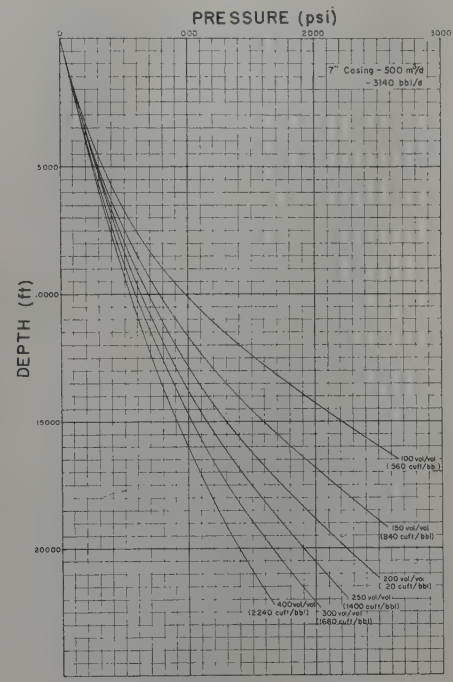

FIG. 3—PRESSURE VS DEPTH CURVE.

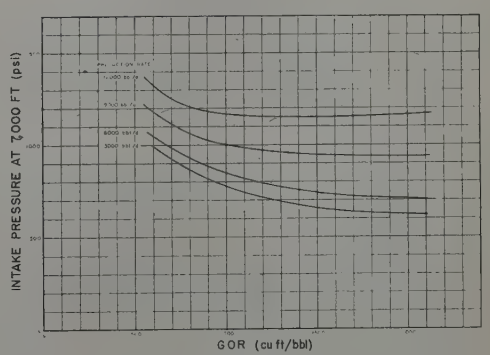

FIG. 4—INTAKE PRESSURE VS GOR AT 7,000 FT. 7 × 2⅞-IN. ANNULAR FLOW, CASINGHEAD PRESSURE—200 PSI.

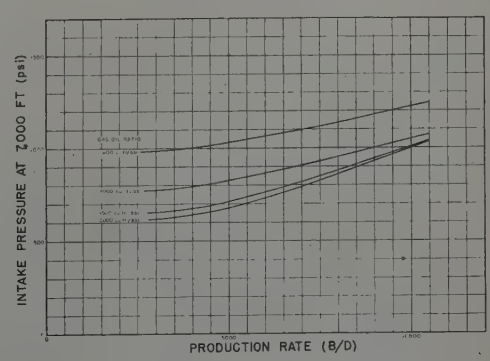

FIG. 5—INTAKE PRESSURE VS PRODUCTION RATE AT 7,000 FT. 7 × 2⅞-IN. ANNULAR FLOW, CASINGHEAD PRESSURE—200 PSI.

*Space will not permit publication of the full set of calculated curves. However, they are available from the author on request.

TABLE 1—MACHINE FORM FOR INDIVIDUAL GRADIENT CURVE

Eg. GOR = 150 vol/vol[3], Rate = 700 M³/D
= 842 cu ft/bbl = 4,400 B/D
Value QM = 1,522,550 lb/day
f/D_e = 0.0365

Pressure (psi)	Density (lb/cu ft)	Gradient (psi/ft)	Distance between pressure points (200 ÷ average gradient)	Cumulative depth (ft)
200	4.43	0.0691	—	0
400	8.71	0.0800	2,684	2,684
600	12.83	0.1023	2,194	4,879
800	16.87	0.1272	1,743	6,621
1,000	20.50	0.1506	1,440	8,061
1,200	23.81	0.1725	1,238	9,299
1,400	26.80	0.1924	1,096	10,395
1,600	29.47	0.2104	993	11,388
1,800	31.80	0.2262	916	12,304
2,000	33.81	0.2398	858	13,163
2,200	35.45	0.2510	815	13,978
2,400	36.80	0.2602	783	14,760
2,600	38.00	0.2684	757	15,517

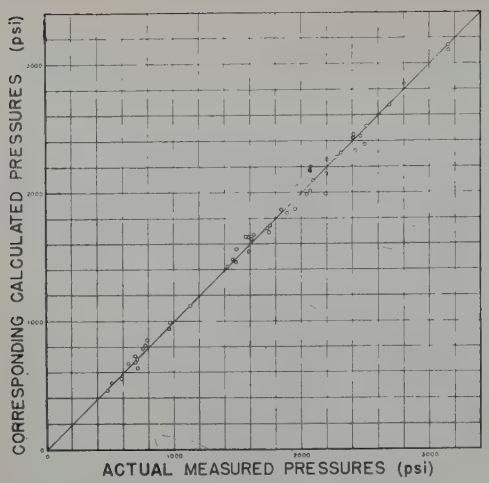

FIG. 6—CHECK MEASUREMENTS CALCULATED VS MEASURED READINGS.

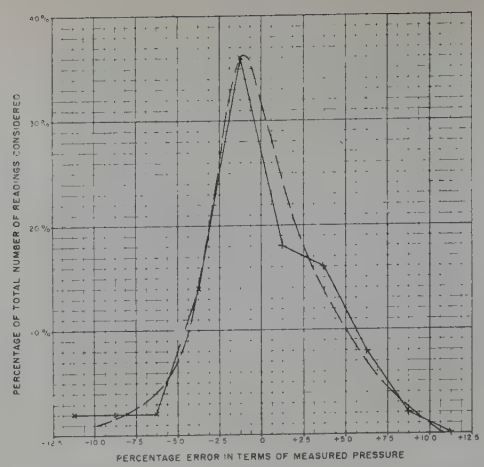

FIG. 7—FREQUENCY OF DEPARTURE OF CALCULATED PRESSURE FROM MEASURED PRESSURE.

shows a typical plot of intake pressure at 7,000 ft vs GOR for rates of flow of 3,000, 6,000, 9,000 and 12,000 B/D at a casinghead pressure of 200 psi.

The slope of these curves is of interest as explaining certain gas-lift anomalies. In several La Paz producers it had been observed that increasing the input GOR did not apparently improve production even when operating below what was considered to be the over-all optimum ratio. It can be seen from the curves that even at low flow rates the approach to the optimum is such that an increase in over-all GOR in the range 1,500 to 2,000 cu ft/bbl makes very little difference to the intake pressure. This is clearer if the curves are redrawn in the form shown in Fig. 5.

ACCURACY OF THE CURVES

In order to establish a check on the validity of the calculated curves a total of 50 flowing BHP surveys were examined. These surveys were made in La Paz and Mara Cretaceous wells and varied in rate between 1,700 and 14,000 B/D.

The anticipated flowing BHP's were then read from the charts and checked with the pressure bomb measurements. The results of these check readings are shown graphically in Fig. 6.

The frequency of departure is shown graphically in Fig. 7. This shows the percentage of the total number of readings falling into separate subdivisions of 2.5 per cent error. It appears that an accuracy of better than 5 per cent is expectable; 60 per cent of the total readings have an error of under ± 2.5 per cent.

Considering the broad approximations made in the method of analysis, this apparent accuracy is surprising. The fact that the gradient curves have been in regular use in gas-lift string design and general flowing performance problems in the La Paz and Mara fields for over three years is perhaps a better indication of their accuracy.

ACKNOWLEDGMENT

The author wishes to express his appreciation to the managers of Compañiá Shell de Venezuela, Ltd., for their permission to publish this paper. He also wishes to thank F. H. Poettmann for his very valuable comments.

REFERENCES

1. Gilbert, W. E.: "Flowing and Gas-lift Well Performance", Spring Meeting Pacific Coast Dist., API (1954).
2. May, C. J. and Laird, A.: "The Efficiency of Flowing Wells", *Jour. Inst. Pet. Tech.* (1934).
3. May, C. J.: "Efficiency of Flowing Wells", *Trans.* AIME (1935) **114**, 99.
4. Poettmann, F. H. and Carpenter, P. G.: "The Multiphase Flow of Gas, Oil, and Water Through Vertical Flow Strings, with Application to the Design of Gas-lift Installations", *Drill. and Prod. Prac.*, API (1952) 257. ★★★

Velocity Log Characteristics

A. A. STRIPLING | MAGNOLIA PETROLEUM CO.
DALLAS, TEX.

INTRODUCTION

This paper discusses the characteristics of the velocity logs now available to the petroleum industry, and some of their advantages and limitations.

The velocity log was designed as an aid to the geophysicist to determine velocity layering in the earth and to provide fast, accurate and economical vertical travel time data. After a number of logs had been made, studies were carried out on their use in correlating strata in adjacent wells. It was found that adjacent strata usually show sufficient velocity contrast to make it possible to correlate these from well to well, even in areas where electric or radioactive logs fail.[1]

In addition, velocity logs have been useful in the determination of porosity and thickness of reservoir rock.[2] These uses for velocity logs require an understanding of the characteristics of the log in response to the changes in velocity and in borehole conditions encountered normally in logging.

GENERAL DISCUSSION OF INSTRUMENTATION

The measurement made in velocity logging is more accurately described as a measurement of time rather than velocity. Ideally the log is obtained by measuring the length of time required for compressional sound waves to travel through a fixed distance in the formation. In practice, the time measurement may be made accurately but the distance through which the waves have traveled may vary slightly. Changes in borehole diameter are responsible largely for the difficulty in maintaining a fixed distance, especially if the diameter variations are so abrupt and frequent that the borehole instrument cannot follow contours of the hole.

Several service companies have velocity logging equipment available or under development which have different transmitters, receivers, and measuring systems. While these differences are important, there are actually only two systems in use at the present time (Fig. 1).[3,4] The first system initiates a pulse at a transmitter and detects it at a single receiver. The transmitter and receiver are separated by a fixed distance, called the spacing. The time measured is that between the initiation of the pulse and the first arrival of acoustical energy at the receiver.

The second system uses two receivers and a transmitter. The receivers are separated by a fixed distance and the time between arrivals of energy at the two receivers is measured. Here, the spacing is the distance between receivers.

The two systems have much in common for it is possible to record both logs simultaneously. Usually the transmitter is an electro-mechanical transducer which produces discrete

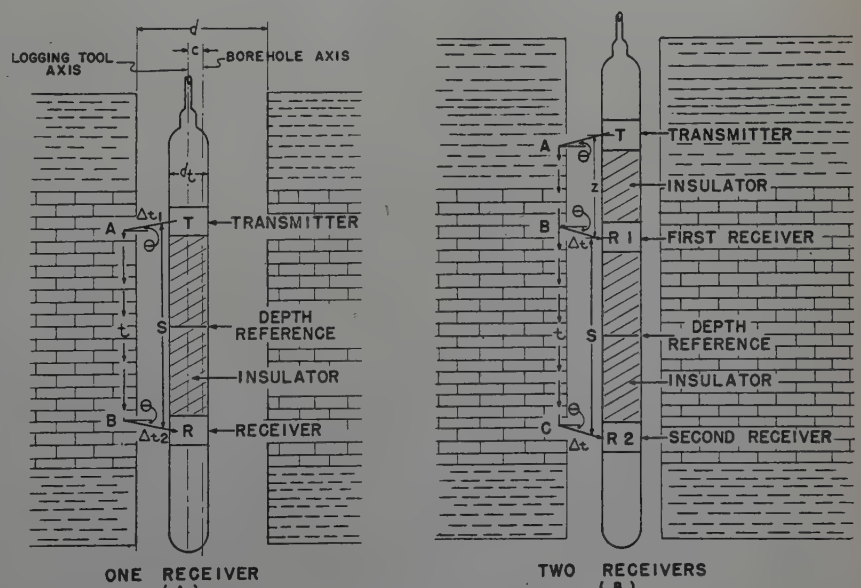

FIG. 1—BOREHOLE INSTRUMENTS FOR VELOCITY LOGS.

Original manuscript received in Society of Petroleum Engineers office May 23, 1958. Revised manuscript received Aug. 4, 1958.
[1]References given at end of paper.
Discussion of this and all following technical papers is invited. Discussion in writing (three copies) may be sent to the offices of the *Journal of Petroleum Technology*. Any discussion offered after Dec. 31, 1958, should be in the form of a new paper.

acoustical pulses in the frequency range from 10 to 20 kilocycles/sec. In some instruments the pulse repetition rate is slow and point-by-point measurements are made. In others the repetition rate is on the order of 20 times a second. Even with this high repetition rate point-by-point measurements are made, but they are so closely spaced that an essentially continuous record results at normal logging speeds.

Energy from the transmitter is coupled to the borehole wall through the drilling fluid. Velocity logs may be made in any type drilling fluid except gas or air. Gas-cut muds decrease the efficiency of the acoustical coupling.

The one- and two-receiver logs of a true-gauge hole are practically identical; however, very few wells are true gauge over their entire depth. In general the single-receiver log will measure too much travel time or too low velocity opposite washed-out zones. The two-receiver log will be distorted for a distance equal to its spacing at the boundaries of washed-out zones. The reasons for these characteristics will be given in the discussion that follows.

CHARACTERISTICS OF SINGLE-RECEIVER SYSTEMS

Correction Necessary for Mud Path

One version of single-receiver logging instruments is shown in Fig. 1A. The instrument may have bumpers to reduce noise caused by instrument drag against the side of the borehole. The distance between the transmitter and receiver is the spacing, S. The depth reference is midway between the transmitter and receiver. The time measurement, t, is made from the initiation of the pulse to the arrival of acoustical energy at the receiver. The velocity may be approximated by dividing the spacing by the time (S/t). However, a closer approximation would result if t were decreased by the sum of the mud-travel times, Δt_1 between the transmitter and the borehole wall and Δt_2, between the borehole wall and the receiver. Formation velocity V_f can be written,

$$V_f = S/[t - (\Delta t_1 + \Delta t_2)] \quad . \quad (1)$$

Eq. 1 is sufficiently accurate only when Δt_1 and Δt_2 are small. This condition is realized when the logging instrument is close to the borehole wall.

If the distance from the logging instrument to the borehole wall is large, additional corrections are necessary . Let us assume that simple refraction theory is applicable. Let the diameter of the hole be d and of the logging tool d_t. The axis of the tool is assumed to be parallel to the axis of the borehole, but may be displaced from it by a distance, c. The velocity of the mud will be denoted by V_m and of the formation V_f. It is assumed that $V_f > V_m$.

When the transmitter pulses, the resulting waves progress outward in all directions. If the receiver is too close to the source (S too small), the first waves to reach the receiver will travel in a direct path through the mud. If S is increased, the indirect wave, which travels partly through the formation, will arrive at the receiver first. The quantities that determine which wave arrives first are spacing, length of mud path and velocities, V_m and V_f. Only the indirect wave is of interest in velocity logging.

The earliest arrival time is measured. The ray path of least time will be TABR (Fig. 1A), which can be broken into three parts to determine the travel time for each segment. The first part TA is the incident ray refracted along the interface at the critical angle, θ. AB travels through the formation with velocity V_f and BR is the emergent ray detected by the receiver. By Snell's law, $\sin \theta = V_m/V_f$, and the total travel time along the refraction path is

$$t = \frac{TA}{V_m} + \frac{AB}{V_f} + \frac{BR}{V_m} \quad . \quad (2)$$

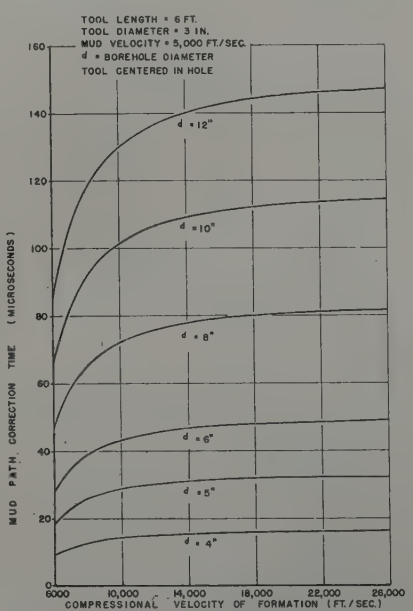

Fig. 2—Mud Path Correction Time as a Function of Compressional Velocity of Formation. (One-receiver Log).

It is desirable to express Eq. 2 in terms of the assigned dimensions. It also would be more convenient to express the path through the formation not as a variable distance AB, but as the fixed distance, S. If this is done, Eq. 2 becomes

$$t = \frac{S}{V_f} + \frac{[d - (d_t + 2c)]}{V_m}\sqrt{1 - \left(\frac{V_m}{V_f}\right)^2} \quad . \quad (3)$$

It can be seen from Eq. 3 that t is made up of formation travel and mud-path times. Mud-path time is not a constant since d, c and V_f may vary during the logging operation. Fig. 2 is a plot of correction time vs formation velocity for a series of hole sizes. The positive correction necessary to make AB $= S$ and the negative correction for mud path are combined and called "mud-path correction time". Since the plot is made on the assumption that $c = 0$, the correction is maximum. In practice, the value of c for a true-gauge hole may be estimated by assuming the logging tool to be against the wall of the hole (unless centralizers are used). In washed-out sections it is difficult to estimate c.

Radius of Investigation

In well log interpretation it is highly desirable to know the lateral extent of the measurement, or "radius of investigation" of the logging sonde. In electric logging, for example, it can be shown that the long spacings are less affected by borehole irregularities and invaded zones than the short spacings. Interpretation methods utilize this fact by comparing logs of various spacings.

In acoustic velocity logging the radius of investigation will be determined by the least travel-time path for refracted waves leaving the transmitter to arrive at the receivers. Reasoning intuitively, one might assume that the wave path very near the borehole wall is physically the shortest and, hence, the path of least travel time. This reasoning might lead one to conclude that the log is influenced only by the rock within a few inches of the borehole wall. Although not completely unsound, this reasoning is subject to modification.

The wave lengths of the acoustic energy may be calculated from the relationship, $\lambda = V/n$, where λ is wave length, V the velocity through the formation and n the wave frequency. In sedimentary rocks, V varies from approximately 5,000 to 25,000 ft/sec. Frequencies used in logging tools now available are from

10 to 20 kilocycles/sec. Therefore, λ ranges from 0.25 to 2.5 ft (1 ft is probably a good average value). Acoustic energy within this range of wave lengths will not be confined to a small region immediately adjacent to the borehole wall. Experiments made in the laboratory indicate that a thickness of at least 3λ is necessary to support a compressional wave over an appreciable distance. In these experiments, brass plates varying in thickness from a fraction to several wave lengths were used. Each plate was mounted firmly on a thick, silver bar whose acoustic impedance closely matched the brass plate and whose compressional velocity was less than that of brass. This was done to obtain a condition similar to an invaded zone with a formation of lower velocity behind it.

If the results of these experiments are applicable to the field measurements, then the lateral extent of acoustic waves in velocity logging ranges from 0.75 to 7.5 ft from the borehole wall, with 3 ft as an average value. This distance depends mainly on the wave length of the transmitted energy. The wave length, in turn, is determined by the frequency of the transmitted wave and its velocity.

Our experience in logging through casing illustrates the point. Formation velocities either higher or lower than casing velocity may be measured in a cased hole provided the casing is bonded rigidly to the formation by cement. If the casing is not cemented, acoustic energy is transmitted through it, but not through the surrounding formation. In this situation, casing velocity only is recorded on the log.

Further evidence supporting the conclusion that the radius of investigation is greater than a few inches has been found on field logs in the Gulf Coast area. The acoustic velocity through gas sands has been measured in several wells. Normally, the velocity through a gas sand is lower than the velocity through a water sand of the same porosity. However, when mud filtrate invasion is deep, the velocities are the same. When invasion is shallow, the "thin" invaded zone does not support the compressional wave and the lower velocity through the gas sand is measured.

In the example just cited, the invaded zone was a higher velocity zone adjacent to the borehole wall. The apparent velocity on the log depended upon whether or not this zone would transmit a measurable compressional wave over a distance equal to the Z spacing (Fig. 1B). An interesting variation occurs when the velocity gradient is reversed and the zone of low velocity is adjacent to the borehole wall. This situation occurs when certain shales are drilled with water-base mud. The shale formation swells and becomes altered with the result that lower acoustic velocity will be found in the region near the wall. It is possible to measure this lower velocity by providing a short spacing from the transmitter to the first receiver. However, if this spacing is increased, the shortest travel time is through the unaltered formation and a higher velocity is measured. Under these conditions, a logging sonde with a long Z spacing has a greater radius of investigation and the velocity measured is that of the unaltered shale.

Response at Interface Between Thick Beds

A thick bed may be defined as any bed whose vertical thickness is greater than the spacing, S. If there is a sharp interface between thick homogeneous beds, as illustrated in Fig. 3, the change from the first velocity, V_1, to the second, V_2, will appear to occur over a vertical distance equal to S. The bed boundary may be picked as 0.5 S below the velocity break at A.

In order to compute the response just described, it is convenient to assume that S is divided into n increments, each ΔS. As the tool traverses the boundary, assume that y increments are in the zone having velocity V_1, and that $n - y$ increments are in the zone having velocity V_2. The travel time through the first interval is $y\,\Delta S/V_1$, and the time through the second interval is $(n - y)\Delta S/V_2$. The time, t, over the spacing S is $y\Delta S/V_1 + (n - y)\,\Delta S/V_2$. Since the log is a record of this time, the response at this position has been determined. The response across the boundary may be determined by letting y vary from 0 to n.

Still more specifically, assume S to be 6 ft, V_1 to be 10,000 ft/sec in shale and V_2 to be 20,000 ft/sec in limestone. Then the travel time in the shale will be 100 microseconds/ft, and in the limestone, 50 microseconds/ft. When the entire tool is within the shale zone, the travel time over the spacing will be 600 microseconds. When the transmitter is 5 ft above the interface and the receiver is 1 ft below it, the time over the spacing will be 550 microseconds, and when the tool is lowered another foot, the time will be 500 microseconds. Successive displacements into the limestone will show the time decreasing 50 microseconds/ft until the tool is wholly within the limestone. At this position, the time over the spacing will be 300 microseconds. The velocity over the 6-ft interval at any position may be determined by dividing 6 ft by the time in seconds across the interval.

In the field example illustrating the response of the velocity log at bed boundaries, the thickness of the bed and the location of the boundaries may be seen on the MicroLaterolog. The high resistivity on the MicroLaterolog correlates with high velocity. True bed thickness in this example is 25 ft. On the velocity log, the high-velocity excursion begins at 3,383 ft and ends at 3,414 ft. By applying the one-half spacing rule ($0.5S = 3$ ft in this example), one finds the bed boundaries to be at 3,386 and 3,411 ft.

Response of the Velocity Log to Thin Beds Bounded by Homogeneous Thick Beds

A thin bed may be defined as one of uniform velocity whose vertical thickness is equal to or less than the spacing S of the logging instrument. Three thin beds are illustrated in Fig. 4. The vertical dimensions

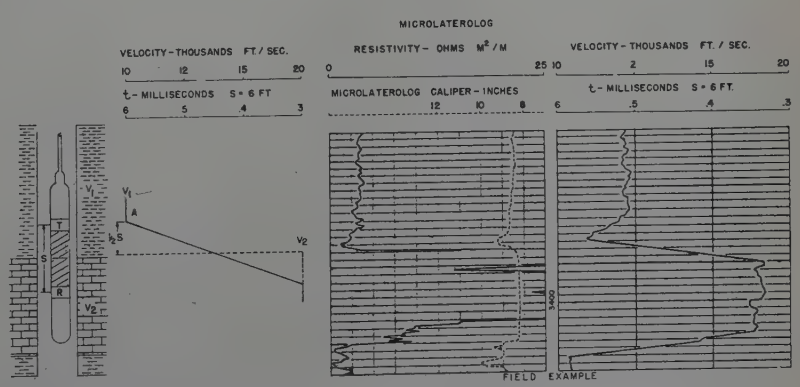

Fig. 3—Beds Thicker than the Spacing. (One- or Two-receiver Log.)

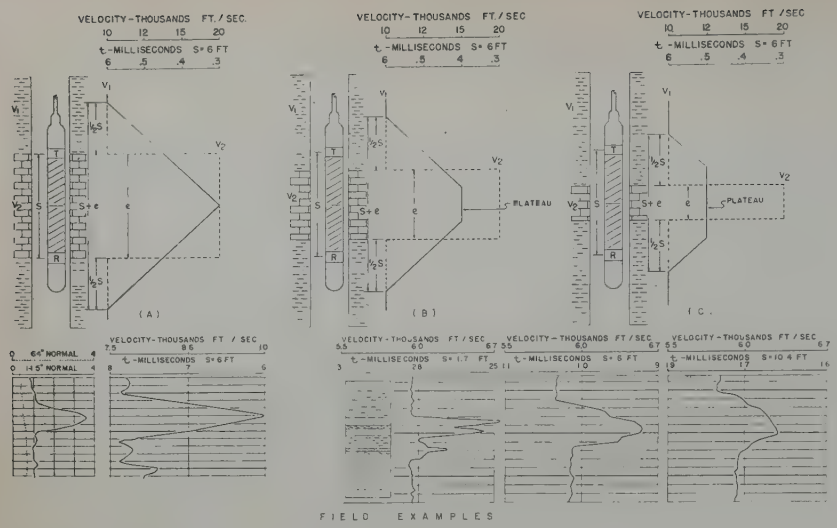

FIG. 4—RESPONSE TO ISOLATED THIN BEDS. (ONE-OR TWO-RECEIVER LOG.)

in the figure may be tabulated in terms of S.

Fig. 4	e	Plateau	Maximum Apparent Velocity
A	S	Point	V_2
B	$\frac{2}{3}S$	$\frac{1}{3}S$	Less than V_2
C	$\frac{1}{3}S$	$\frac{2}{3}S$	Less than V_2

It may be seen from these data that the vertical extent of each plateau is $S - e$.

In determining bed thickness for an isolated thin bed, the points where the log first departs from adjacent bed velocity are used. These points will be separated by a distance, $S + e$. The bed boundaries will lie between these points, $0.5S$ from each. It should be noted that this is not the same as measuring between mid-points on the excursions. Confusion may arise also if the vertical extent of the velocity plateaus is used to determine bed thickness. This is so because of the inverse relationship, the thinner the bed the thicker its plateau.

In Fig. 4B and 4C, the thin beds have been assigned a velocity, V_2, and the adjacent beds velocity, V_1. The minimum travel time (velocity plateau) occurs when the entire thin bed is within the spacing. The minimum travel time may be computed by addition, $e/V_2 + (S-e)/V_1$. This minimum travel time is recorded at the plateau. V_1 and e may be determined from the log, and since S is known, it is theoretically possible to compute V_2.

Field examples have been selected to illustrate these points. In the lower left corner of Fig. 4, the response to a bed of higher resistivity is recorded. The bed thickness is so close to the spacing of the 64-in. normal that this log does not show its boundaries. The 14.5-in. normal shows the bed thickness to be 7 ft. The velocity log has a peak value and also indicates the bed thickness to be 7 ft.

In the lower right corner of Fig. 4 are three velocity logs of different spacing through the same section. The high-velocity bed is composed of very thin limestone stringers with adjacent thick shale beds. As the spacing increases (from left to right) the indicated velocity decreases and the apparent bed thickness increases.

RESPONSE OF THE VELOCITY LOG TO A SEQUENCE OF THIN BEDS

In the figures discussed previously the symmetry of velocity logs has been illustrated. In Fig. 5A this symmetry is repeated for a sequence of thin beds. The centers of the plateaus are directly opposite the centers of their respective beds. Also the center of the low-velocity anomaly on the log is opposite the center of the low-velocity bed. In this figure only two velocities, V_1 and V_2, were considered.

In Fig. 5B alternation of V_1 and V_2 is again considered, but the beds are thinner. In this case the vertical resolution of beds thinner than the spacing is no longer apparent. For example, there is no direct indication on the log of the presence of the center bed of velocity, V_2.

Fig. 5C shows the same beds as Fig. 5B but with different velocities. It would be difficult to determine bed boundaries from the log. Although the bed boundaries are not clearly resolved, the indicated velocities are correct for the given spacing. No bed, however thin, has been omitted from the measurement. As is the case in other logging systems, better bed resolution may be obtained with shorter spacing.

RESPONSE OF THE ONE-RECEIVER LOG TO CAVITIES

When the borehole is enlarged abruptly, the distance from transmitter and receiver to the wall is increased. Therefore, mud-path travel time is increased and the travel time on the log is greater than if no cavity were present. The apparent velocity recorded on the log is lower than the true velocity of the formation; this is a systematic error. It is difficult to correct even if a caliper log is available because the distance between the tool and borehole wall is unknown.

A characteristic response to thin cavities is illustrated in Fig. 6A. In the construction of the figure, travel times were assumed to be 200 microseconds/ft in the drilling mud, 50 microseconds/ft in the limestone beds and 100 microseconds/ft in the

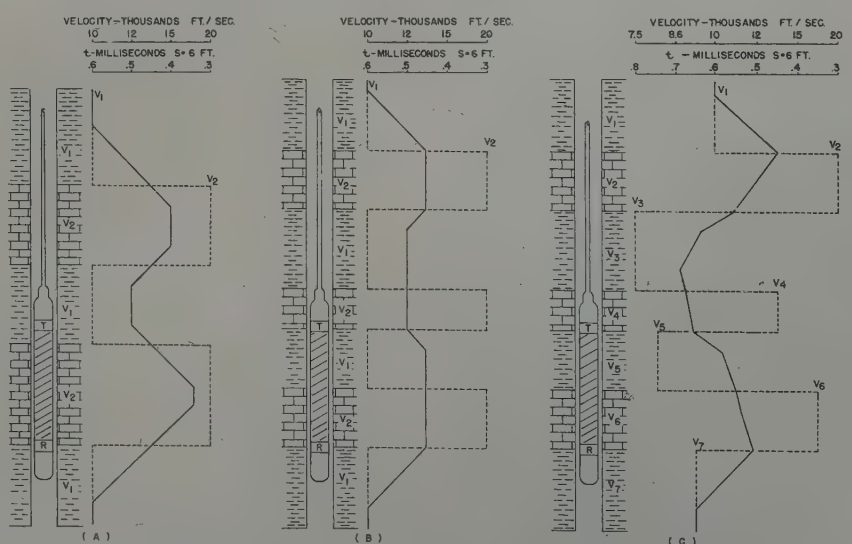

FIG. 5—RESPONSE TO A SEQUENCE OF THIN BEDS. (ONE-OR TWO-RECEIVER LOG.)

shale. The increase in borehole radius was chosen as 1 ft, shale bed thickness 2 ft and instrument spacing 6 ft. The theoretical curve was plotted by moving the tool in small increments and determining the shortest possible travel time over any path from transmitter to receiver. Two maxima were observed, one when the receiver was at Point A, and one when the transmitter was at Point B. When the receiver is at Point A the travel time over Path F_1BA is equal to the travel time over Path $F_1F_2F_3A$. Movement of the receiver either upward or downward will decrease the time measurement. Similar reasoning establishes a maximum travel time measurement when the transmitter is at Point B.

Obviously, the contour of the borehole will affect the response just described. Various travel times in the formation may occur and will combine to determine the curve shape.

CHARACTERISTICS OF THE TWO-RECEIVER SYSTEM

Measurement Between Receivers Eliminates Necessity for Mud-path Correction

The ray path taken by the sound wave, described in a previous section, can also be applied to the two-receiver system. The incident ray continues through the formation where it is refracted into the mud all along the borehole. This refracted wave is detected first at the receiver nearest the transmitter and later at the second receiver. The arrival of the sound wave at the first receiver initiates the time measurement and the arrival of the wave at the second receiver ends it. Therefore, if the mud-path travel time from borehole to receiver is the same for each receiver, the effect of mud-path travel time is eliminated from the measurement. The importance of this can be recognized when one realizes that it is no longer necessary to make a correction to the log even though the distance from the instrument to the borehole wall varies. The velocity may be determined from this log by S/t, where S is the distance between receivers and t is the time between arrivals of the sound waves at the two receivers.

Response of the Two-Receiver Log to Cavities

As the two-receiver logging tool moves past an abrupt change in borehole diameter the necessary condition for accurate formation travel time measurement is no longer satisfied. If the first receiver only is within the enlarged section, there is extra mud path between this receiver and the wall. This has the effect of delaying the start of the measurement. Consequently, too short a time is recorded and the apparent velocity on the log is too high. If the cavity is thicker than the spacing, both receivers may be in the enlarged section as the logging instrument moves through it. During this time, the distance from the receivers to the wall will be approximately equal and good measurements will be made. Finally, the first receiver will be in the smaller section of the hole while the second receiver is in the enlarged section. The situation is now reversed, because the time measurement is too long and the apparent velocity too low.

Fig. 6B illustrates this important characteristic of the two-receiver log. It is evident that the excursions on the computed log are not characteristic of the formations. Velocity measurements are distorted for a distance of $0.5S$ both above and below the boundaries of the cavity. This applies to a thick cavity as well as to the thin cavity in the illustration.

Despite this distortion, the errors involved are equal and opposite. The travel time measurement obtained by integrating the log over the distance $S + e$ will be accurate.

Field examples in Fig. 6 show a caliper log and the two types of velocity logs. The effective thickness of the cavity is about 2 ft. The spacing is 6 ft for both velocity logs. Note that the distance between the two maximum time measurements (velocity minima) is about 5 ft for the one-receiver log. This corresponds closely to the theoretical log shown in Fig. 6A. The distance between these points is a function of the spacing, but not necessarily equal to it.

On the field example for the two-receiver log, there is one maximum and one minimum time measurement. The vertical distance between them is equal to the spacing; this will be true in all cases where the cavity thickness is less than the spacing. The cavity is not located half way between these two points; however, the upper and lower boundaries of the cavity may be located by the one-half spacing rule illustrated in Fig. 6B.

A comparison of one- and two-receiver logs is shown in Fig. 7. These logs were recorded simultaneously in a well having a section of Pennsylvanian shales and limestones. The shales washed out, leaving large cavities as shown by the caliper log. The time measurements from the two-receiver log checked very closely with measurements from a conventional geophone survey. Time measurements on the one-receiver log proved to be too long through this section.

CONCLUSIONS

The measurement made in velocity logging is more accurately described as a measurement of time rather than velocity. There are two systems available: (1) the borehole instrument has a transmitter (acoustic

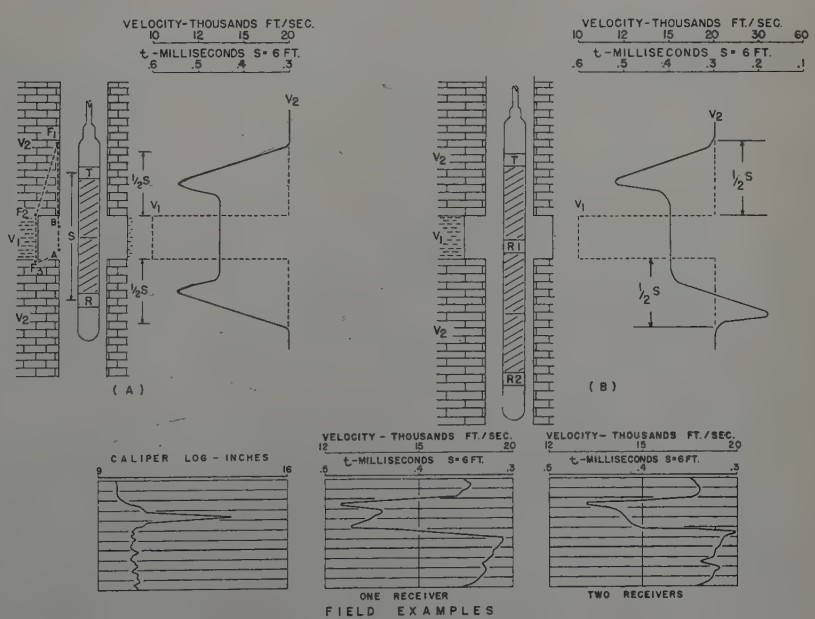

Fig. 6—Response of the Logs to a Thin Cavity.

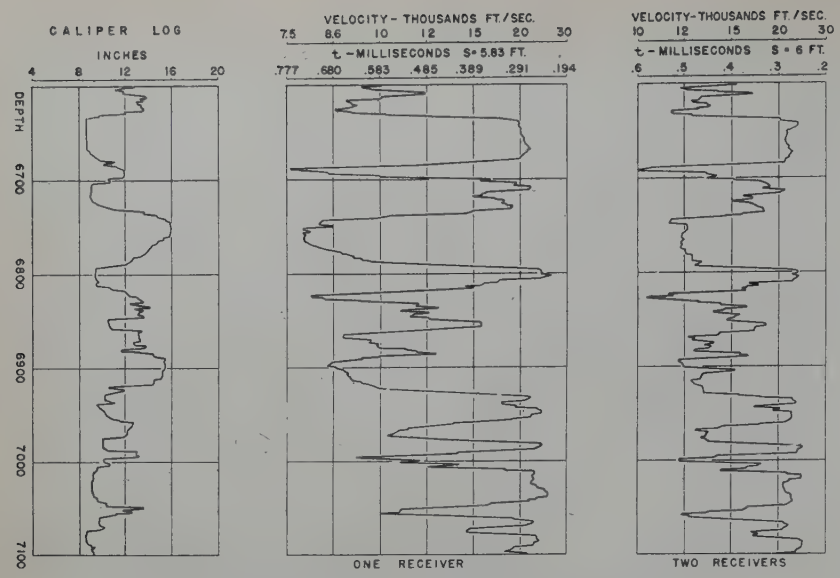

FIG. 7—COMPARISON OF ONE- AND TWO-RECEIVER LOGS THROUGH A WASHED-OUT SECTION, GRADY COUNTY, OKLA.

pulse generator) and a single receiver. These are separated by a fixed distance and the measurement made is the time required for a pulse leaving the transmitter to be detected at the receiver; and (2) the borehole instrument has a transmitter and two receivers in vertical alignment. In this system a measurement is made of the time between arrivals of acoustic energy at the two receivers.

The two-receiver velocity log is more accurate than the single-receiver log because it eliminates the necessity for mud travel-time correction. In true gauge sections of the borehole, logs obtained with the two systems are practically identical, differing only through borehole cavities and in sections where the velocity has been altered by swelling of shales or by filtrate invasion.

The velocity log obtained with either system is symmetrical and is affected only by the properties of the material within the spacing. The logs are distorted at the boundaries of cavities. With the two-receiver system, the errors introduced by this distortion are self-compensating, and thus the vertical travel time based on the distorted readings is correct.

The radius of investigation of the velocity log depends primarily on the wave length of the acoustic energy transmitted through the formation, and secondarily on conditions near the borehole wall. In general, this radius is about three wave lengths, or from 0.75 to 7.5 ft for logging tools in use at present.

The boundary between adjacent thick beds may be found by measuring a distance equal to one-half the log spacing from the point where the log first responds to the influence of the adjacent bed toward that bed.

Studies of various combinations of thin beds (bed thickness less than tool spacing) show that in some cases the log defines bed boundaries clearly; in others, the results are such that boundary determinations are obscured.

ACKNOWLEDGMENTS

The author wishes to acknowledge the contributions made by J. E. Berry, W. G. Hicks, F. C. Karal, Jr., and J. Zemanek, Jr. The figures were drawn by R. L. Atkins. The author also wishes to thank the management of Magnolia Petroleum Co. for permission to publish this paper.

REFERENCES

1. Breck, H. R., Schoellhorn, S. W., and Baum, R. B.: "Velocity Logging and Its Geological and Geophysical Applications", *Bull.*, AAPG (Aug., 1957) **V**, No. 8, 41.
2. Hicks, W. G. and Berry, J. E.: "Application of Continuous Velocity Logs to Determination of Fluid Saturation of Reservoir Rocks", *Geophysics* (July, 1956) **XXI**, No. 3, 739.
3. Vogel, C. B.: "A Seismic Velocity Logging Method", *Geophysics* (July, 1952) **XVII**, No. 3.
4. Summers, G. C. and Broding, R. A.: "Continuous Velocity Logging", *Geophysics* (July, 1952), **XVII**, No. 3.

★★★

Spacing of Natural Gas Wells

R. C. CRAZE
MEMBER AIME

HUMBLE OIL & REFINING CO.
HOUSTON, TEX.

ABSTRACT

The discovery of a new gas reservoir demands that the planning of a sound well-spacing program be initiated early in the development stage. It is the purpose of this discussion to illustrate by actual field examples the application of basic well-spacing principles, previously developed for oil reservoirs, to the problem of well spacing in natural gas fields. These studies are presented for the field use of geologists and engineers who are concerned with the initial planning of the proper development of the newly discovered gas reservoir.

INTRODUCTION

The phenomenal growth of a vigorous natural gas industry emphasizes the increasing importance of natural gas as a source of energy, fuel, and raw materials to our nation's economy. Since 1945 marketed production of natural gas for the U. S. has increased 2½ times to a record high of 10.6 trillion cu ft during 1957. As major participants in the gas industry, we share an added interest to develop and produce our natural gas reserves with constantly improved efficiency.

The subject of well spacing is vitally important to the gas industry, for the well itself plays a significant role in the development of the natural gas reservoir and in control of the recovery process. Maximum utilization of wells is an integral part of sound conservation practices.

The discovery of a new gas reservoir demands that careful choice of well location and well spacing be made and that the planning of a sound well spacing program be initiated early on the development stage. With the drilling of the first development well, efforts of the geologist and engineer must be directed toward acquisition of adequate technical evidence upon which a firm recommendation for a spacing program may be based. With this technical appraisal as a foundation, operators and state regulatory agencies jointly can go far in providing a framework for sound development of gas fields to achieve a program of conservation that avoids the unnecessary well.

WELL-SPACING CONCEPTS

Through laboratory and field investigations of the mechanism of the recovery of oil and gas, of fluid behavior, and of effective control of reservoir and well, a crystallization of ideas regarding reservoir behavior has emerged as a well-developed technology. Associated with a better understanding of the fundamental principles underlying reservoir and well behavior has been the growth of concepts concerning the role of wells and their spacing in the development and operation of an oil or gas reservoir.

In addition to serving as outlets for the withdrawal of fluids from the reservoir, wells are recognized as having two other important functions: (1) providing access to the reservoir to obtain information concerning the characteristics of the reservoir and its fluids, and (2) serving as a means by which the natural or induced recovery mechanism may be effectively controlled. Beyond a minimum number of wells required to fulfill these two functions, additional wells will not increase recovery. With particular emphasis upon well spacing in oil reservoirs, many studies of the well spacing-recovery relationship have evolved the concept that the ultimate oil recovery is essentially independent of the well spacing.[1]

These fundamental concepts are no different when regarding the role of wells and their spacing in the natural gas reservoir. They are equally applicable to the consideration of well spacing in gas reservoirs. For the gas reservoir, the problem of well spacing then revolves around the question of drainage and the degree or extent to which a well may drain gas from its surrounding reservoir environment.

Theoretical and Experimental Work

During the past 30 years, theoretical and experimental work carried on to study the physical principles involved in the flow of fluids through porous media has shed light upon the matter of drainage. Fundamental mathematical equations have been derived to describe the mechanism of flow of oil and gas through porous rocks.

With the recent advent of high-speed digital computers, attempts have been made with mounting success to develop solutions, employing numerical techniques, to mathematical expressions that describe more rigorously the physical behavior and mechanism involved in the unsteady-state flow of compressible fluids, such as a gas, through porous rock. In 1953, Bruce, Peaceman, Rachford and Rice[2] published a stable numerical procedure for solving the equation for production of gas at constant rate. The results of these calculations are significant with respect to this matter of drainage, for they indicated (1) that depletion of the gas reservoir resulted in a drop in pressure at the extremity of the

Original manuscript received in Society of Petroleum Engineers office April 1, 1958. Revised manuscript received July 24, 1958. Paper presented at Gas Technology Symposium in Shreveport, La., April 17-18, 1958.

[1]References given at end of paper.

reservoir, and (2) that in a continuous sand body gas can be drained from a very large area in a predictable length of time.

FIELD EVIDENCE OF DRAINAGE

Although theoretical and experimental work regarding drainage has been invaluable in the development of present thinking, it is to the field that many investigators have turned for proof of drainage and its implications in the well-spacing question—whether it relates to an oil or to a gas reservoir.

Woodbine Basin Study

An outstanding example of pressure interference is found in the Woodbine formation in East Texas where more than a dozen major oil and gas pools draw on the Woodbine formation for water drive. Studies of the performance of these reservoirs have given direct evidence of pronounced pressure interference between pools and of the mass movements of water over distances of many miles. An area-wide investigation of the pressure behavior throughout the Woodbine sand by Bell and Shepherd,[3] and by Rumble, Spain, and Stamm,[4] indicated that by 1946-47 the influence of the Mexia-Powell fault line field production was felt about 70 to 80 miles from the fault line fields and that the influence of the East Texas field had extended westward some 65 miles (Fig. 1). Here was proof of the extent to which movement of a fluid may occur in a continuous sand body.

Interfield Interference

With the study of Woodbine Basin as general background, one may turn more specifically to the behavior patterns of the Navarro Crossing, Oakwood, and Southwest Oakwood fields, a group of gas fields located in the south central portion of the basin. The pressure-production histories of these fields bring into focus the interfield interference that occurred during the course of development and production from the area, and shed further light upon the degree of continuity within the Woodbine formation and magnitude of distances over which interfering effects and pressure reactions may be experienced. This in turn provides basis for certain conclusions regarding the spacing of gas wells for effective depletion of these gas reserves.

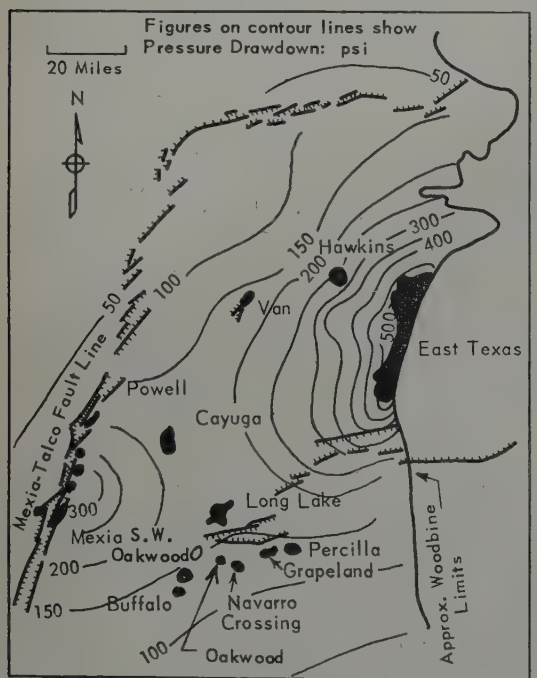

Fig. 1—Pressure Loss in Woodbine Basin (Jan. 1, 1947).[3,4]

Navarro Crossing

The Navarro Crossing field, 14 miles south of Long Lake field in northwestern Houston County, Tex., was discovered April 8, 1938, with the completion of Humble's H. H. Dailey No. 1.

Situated in the upper portion of the Woodbine sand formation of Cretaceous age, the reservoir was found to comprise a large gas cap overlying a thin oil column. The permeability of the sand was 1,100 md and its porosity 21 per cent. The reservoir was first produced as an oil field, but nearly immediate difficulties were encountered in avoiding extremely high GOR's and large quantities of water. Following a Railroad Commission hearing, a revision of field rules permitted proration of both gas and oil wells on the basis of gas production, and Navarro Crossing began operation as a gas reserve March 10, 1945. From an initial reservoir pressure of 2,700 psi at − 5,615 ft, the pressure declined to 2,552 psi by early 1945 (Fig. 2) as a result of withdrawals of oil, gas and water from the field itself and as a result of the production of other nearby fields drawing upon the basin for their water drive. Since the institution of gas sales from Navarro Crossing, the pressure has declined steadily to 2,230 psi as of May 1, 1957.

Oakwood

Evidence of interfield interference is presented in the pressure behavior of the Oakwood field, located in the northeast portion of Leon County, Tex., 1.5 miles west of Navarro Crossing and 13 miles south of Long Lake. Oakwood was discovered April 3, 1939, with the completion of Humble's E. F. Swift Heirs No. 1, one year after discovery of the Navarro Crossing field. As at Navarro Crossing, the Oakwood reservoir, producing from the Woodbine sand, likewise had a large gas cap, a very thin oil column, and an effective water drive. One month after completion of the discovery well, an initial shut-in subsurface pressure of 2,660 psi was measured in Swift Heirs No. 1 at the datum of − 5,615 ft. It is notable that this pressure was 40 psi below an estimated normal pressure for this depth (2,700 psi), and was nearly identical to the aver-

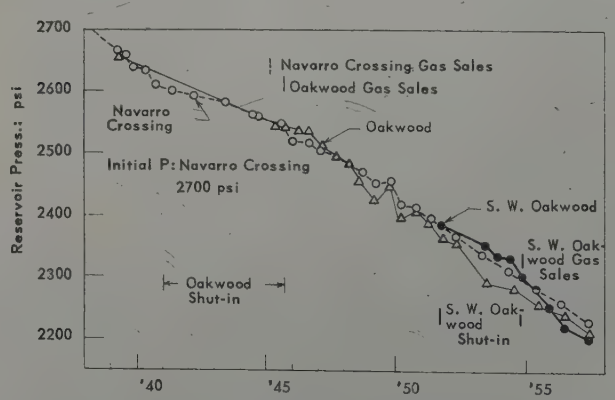

Fig. 2—Pressure Behavior, Navarro Crossing, Oakwood, Southwest Oakwood Gas Fields.

age reservoir pressure observed at Navarro Crossing at that time (Fig. 2).

During 1939, two oil wells and two gas wells were drilled in the field. The gas wells were shut in at the end of 1939 for lack of commercial market. The oil wells continued to produce as high GOR wells until Jan. 25, 1941, when they were reclassified as gas wells and shut in. All wells at Oakwood remained shut in until Sept. 15, 1945, when completion of a commercial gas gathering system permitted gas production for commercial sale. Just prior to reopening the field, an average subsurface pressure of 2,544 psi was observed in two wells July 11, 1945. This pressure was 90 psi less than that measured in the same two wells six years earlier, although the field had produced but very little oil and gas during the first 1½ years and had remained shut-in for the latter 4½ years. It was also significant that 2,544 psi at Oakwood compared very closely with a reservoir pressure of 2,547 psi measured Aug. 1, 1945, in 16 wells at Navarro Crossing. It was indicated that, despite shut-down, the pressure at Oakwood continued to fall along the trend observed at adjacent Navarro Crossing as the latter continued to produce. It is reasonable to conclude that the pressure decline at Oakwood, while it remained shut in, was the result of the interfering effects of withdrawals of fluids (oil, gas, and water) not only from nearby Navarro Crossing, but also from other gas and oil reservoirs producing from the common Woodbine aquifer in the larger regional vicinity of Oakwood. This interference established the continuity of the Woodbine formation and emphasized the fact that pressure communication over large distances was possible.

SOUTHWEST OAKWOOD

Discovery of the Southwest Oakwood gas field Sept. 19, 1951, in northeast Leon County, provided more dramatic evidence of interference and pressure communication between fields producing regionally from a common basin. This reservoir is 5 miles west of Oakwood, 10 miles west of Navarro Crossing, 6 miles northeast of Buffalo and 13 miles southwest of Long Lake. It is a low-relief, faulted anticline, with gas production obtained from the Lewisville section of the Woodbine sand. The formation has a permeability of 250 md and a porosity of 23 per cent. One month after completion of the discovery well, Humble's Lester Foran No. 1 (now Southwest Oakwood Gas Unit 1, Well No. 1), an initial reservoir pressure of 2,384 psi was observed in that well at a datum of − 5,519 ft (Fig. 2). This was about 270 psi below the normal estimated original pressure that existed in that portion of the Woodbine basin prior to production.

Development of this field proceeded on 640-acre spacing, and by the latter part of 1954 six wells had been completed. During that entire period since discovery, all wells drilled remained shut in following their initial potential test because of lack of commercial gas outlet. It was not until Nov. 15, 1954, that production of gas for commercial sale began. Throughout this initial shut-in period of more than three years, measurements of subsurface pressures were made in wells as they were completed. All measurements indicated a declining pressure trend in the reservoir even though no gas had as yet been produced from the field. The last survey, Nov. 1, 1954, two weeks before production began, showed a pressure of 2,304 psi, representing a decline of 80 psi over the three year shut-in period. As shown in Fig. 2, this pressure behavior at Southwest Oakwood closely paralleled the pressure trends at Oakwood and at Navarro Crossing. In fact, the 2,304 psi on Nov. 1, 1954 almost equaled the pressure at Navarro Crossing.

The interfering effects of withdrawals of gas from surrounding fields upon the pressure behavior at Southwest Oakwood may be more readily seen in Fig. 3. Here the pressure variations for Southwest Oakwood are presented for a four-year period from Sept., 1951 to the middle of 1955. This interval covers the shut-in period occurring during the first three years at Southwest Oakwood. Also presented are monthly rates of gas withdrawals from Navarro Crossing, Oakwood, Buffalo and Long Lake. Closer examination of pressure variations at Southwest Oakwood shows that the reservoir pressure of this shut-in field responded to peak winter gas withdrawals from those fields by more rapid rate of pressure decline. Cut-backs in gas production during summer months resulted in moderation of the overall downward trend in pressure. The response in pressure behavior of the Southwest Oakwood reservoir during the extended shut-in period to gas withdrawals from surrounding fields 5 to 13 miles away reflects the magnitude of the interfield interference occurring in this portion of the Woodbine Basin and certainly gives proof of the great distances over which pressure communication can occur in a continuous sand body.

DELAYED DEVELOPMENT AND STEP-OUT WELLS

Positive evidence of drainage and mass movement of reservoir fluids over considerable distances may be found in the case histories of delayed development and step-out wells. The following examples in actual field operations are cited where later drilled step-out wells or delayed development wells in remote portions of a continuous reservoir rock have given ample proof of fluid migration having occurred from these remote areas toward the centers of continued withdrawals of gas from earlier drilled completions. The physical depletion of gas that has occurred in these later developed areas has been confirmed by the definite reduction in reservoir pressure initially observed upon completion of these more recent wells, by their reduced potentials or deliverability, and by their production characteristics similar to or identical with those of earlier drilled wells.

OAKWOOD

It has been pointed out that the Oakwood field was partially developed in 1939 with two oil wells and two

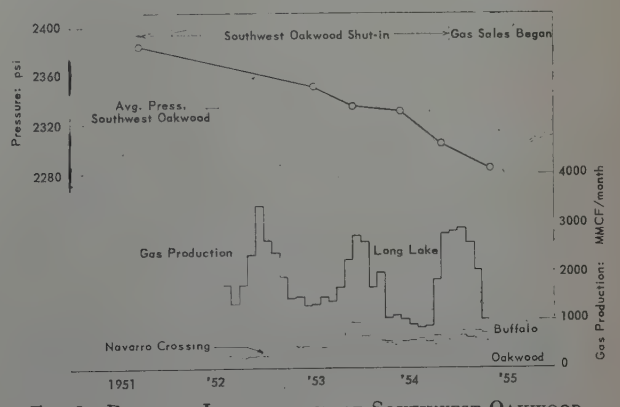

FIG. 3—PRESSURE INTERFERENCE AT SOUTHWEST OAKWOOD.

gas wells in the Woodbine sand. The gas wells were soon shut in for lack of market. The oil wells continued to produce until Jan., 1941, when they were reclassified as gas wells and shut in. The field remained shut in until Sept. 15, 1945, when a gas market outlet was obtained. Just prior to reopening the field, Humble's Leone Plantation No. 1 was completed on July 23, 1945, as a gas well at a location 3,200 ft southeast of the nearest earlier drilled gas well. Five days earlier on July 18, 1945, during a drill-stem test, a pressure of 2,550 psi was measured in this well (Fig. 4). This pressure was 150 psi below the initial pressure of 2,700 psi established for this field at the − 5,615-ft datum, and nearly identical to the average pressure of 2,544 psi, observed at that time in two earlier completed wells. Hence, despite the fact that the field had been shut in for the past 4½ years and had produced but very little oil and gas since its discovery in 1939, the pressure over the entire reservoir had declined uniformly by 90 psi during the six-year interval because of withdrawals from nearby Navarro Crossing and from other fields producing from the common Woodbine aquifer. The uniformity of pressure response over an area of at least 740 acres surrounding George Hailey No. 1, the nearest earlier drilled well to Leone Plantation No. 1, indicates that adequate drainage of gas from this reservoir could be accomplished by well spacings considerably in excess of 320 acres/well.

SOUTHWEST OAKWOOD

Again looking at intrafield behavior as individual wells are completed, the progressive development of the Southwest Oakwood field provides conclusive indications of the large distances over which gas can move within a continuous reservoir. Shortly after discovery on Sept. 19, 1951, an initial pressure of 2,384 psi was observed in Humble's S. W. Oakwood Gas Unit 1, Well 1. This pressure, 270 psi below the normal estimated original pressure at the datum of − 5,519 ft, reflected the interfering effects of withdrawals of gas from neighboring fields producing from the common aquifer. As development of the reservoir proceeded from south to north on a 640-acre spacing pattern, initial pressures were measured in each well soon after completion. The trend of these pressures, shown in Fig. 5, exhibits a continuous decline, even though the field remained shut in from Sept. 19, 1951, its discovery date, until Nov., 1954, when gas production was initiated for sale. Gas Unit Wells 11, 13 and 14 were completed after gas production began. Each of these

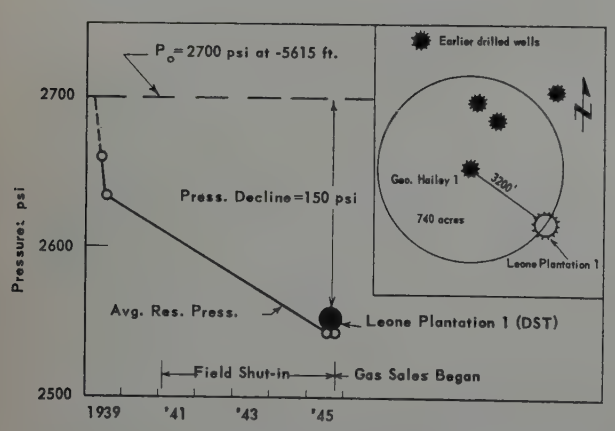

FIG. 4—INITIAL PRESSURE IN STEP-OUT WELL, OAKWOOD GAS FIELD.

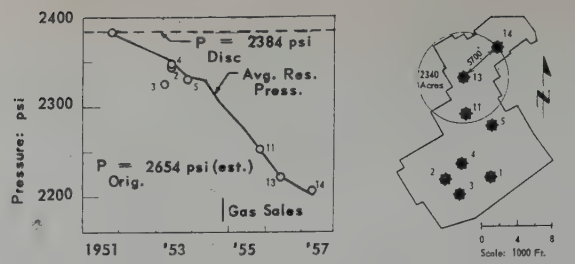

FIG. 5—INITIAL PRESSURES IN STEP-OUT WELLS, SOUTHWEST OAKWOOD FIELD.

initial pressures was progressively lower than the pressure of 2,384 psi measured in the discovery well, and the trend of these pressures followed nearly identically the trend of the average reservoir pressure decline, both during the initial shut-in period and following the opening of the field to gas production. This behavior indicates the uniformity of the pressure communication throughout the entire reservoir formation and the degree to which the pressure in remote areas responds to withdrawals of gas from earlier drilled portions of the reservoir.

One specific example of the extent to which drainage can occur in a gas reservoir is seen in the case of Southwest Oakwood Gas Unit 14, Well 1, in the extreme north end of the field. This well was completed March 26, 1957, at a distance of 5,700 ft from Gas Unit 13, Well 1, the nearest prior drilled well. Two months after its completion, Gas Unit 14, Well 1, exhibited an initial pressure of 2,208 psi, 176 psi below the pressure in the discovery well, and almost identical to the pressure of 2,214 psi observed in the nearest well. It is indicated that the closest well, Gas Unit 13, Well 1, was draining quite effectively an area of more than 2,300 acres. This in itself is proof of the great distances over which gas can move in a continuous porous medium and is an indication that the developed pattern of 640 acres/well for this reservoir was more than sufficient to effect recovery of gas.

In this field, as well as at Oakwood, the uniformity of pressure distribution over the entire structure, both in the step-out areas and in the earlier developed areas, gives ample testimony to the uniformity of gas recovery from all parts of the reservoir, whether the field is developed on spacings less than 320 acres/well or on wider spacings of 640 acres or more.

CARTHAGE FIELD, LOWER PETTIT FORMATION

The progressive development of the Lower Pettit reservoir of the Carthage gas field, Panola County, Tex., supplies an interesting example of intercommunication throughout a large productive limestone formation as evidenced by subsurface pressures measured upon completion of successive wells. The Carthage field comprises a structure formed by a broad, low-relief nose plunging from the western flank of the Sabine uplift. Gas is produced from 10 different reservoirs in the field. The major reservoir, Lower Pettit zone, was discovered Dec. 22, 1936, with gas production obtained from a gray, fossiliferous to crystalline porous limestone of Lower Cretaceous age at depths ranging from approximately − 5,600 to − 6,300 ft. This reservoir is continuous over the entire Carthage field and covers approximately 280,000 acres. Development proceeded with the drilling of gas wells on standard 640-acre units with a 10 per cent tolerance. The original

reservoir pressure was estimated to be 3,265 psi at the datum of − 5,750 ft.

As the field was developed, initial subsurface pressures were measured in many of the individual wells shortly after completion. Comparisons between initial pressures in step-out wells or in later drilled infill locations with the original reservoir pressure and with pressures observed concurrently in earlier drilled surrounding wells provide positive evidence of pressure communication and the occurrence of gas movement over large distances in this limestone formation. Examination of such pressure behavior was conducted for several areas in the Lower Pettit zone of this field, and for various time periods in its development history. One such example is cited here as offering typical evidence of intrafield communication and the extent to which a well will drain gas.

This example, Fig. 6, comprises a group of six wells in the north-central portion of the field. Wells 1 through 5 were drilled earlier from Oct., 1945, to July, 1948, whereas Well 6 was drilled into the interwell area in April, 1950, at a distance of 4,300 ft from Well 3, the nearest of the surrounding wells. An initial pressure of 2,717 psi was measured in Well 6 immediately following its completion. This pressure was 548 psi below the estimated original reservoir pressure and only about 230 psi above the average pressure of the five surrounding wells and the average pressure of the entire Lower Pettit zone for that date. It is obvious that drainage had occurred in the reservoir formation surrounding the interspaced well and that the other wells had contributed to this interference. It is indicated that withdrawal of gas from Well 3, the nearest earlier drilled well, had resulted in pressure drawdown over an area of more than 1,330 acres.

From the evidence presented by pressure draw-downs at completion of step-out or interspaced wells in the Carthage Lower Pettit zone, it is demonstrated that drainage has occurred over areas two to three times greater than the 640-acre development pattern. It can be concluded that the 640-acre well spacing pattern here is more than adequate to provide complete drainage and uniform depletion of this gas reserve.

TRAWICK GAS FIELD

The Upper Pettit limestone reservoir in the Trawick field,[1] Nacogdoches and Rusk counties, Tex., also provides an excellent example of drainage over extremely wide areas in a gas field developed on 640-acre spacing. In this reservoir the average formation porosity is approximately 20 per cent, and the permeability is 134 md. The original reservoir pressure at − 7,050 ft was 3,984 psi. As development proceeded continuously, following discovery of the field in June, 1949, initial pressures were measured in each step-out well shortly after completion. It can be seen in Fig. 7 that each of the initial pressures in these step-out wells was substantially less than the original reservoir pressure and that these initial pressures, at the time of their measurement, agreed very well with the declining field average pressure. The almost identical trend in the progressive decline in the initial pressures of the step-out wells, compared with the trend of average reservoir pressure in the developed portion of the reservoir, indicates the uniform pressure response in previously undrilled portions of the reservoir to the effects of gas production from earlier developed areas. This decline in pressure in each step-out area gave positive indication that drainage had taken place in that portion of the reservoir.

As a specific example, Trawick Gas Unit 53 in the extreme northwest corner of the field was completed in Jan., 1955, with a measured initial pressure of 3,715 psi, 269 psi less than the original reservoir pressure and essentially identical to the field average pressure on that date. Gas Unit 53 was a step-out well approximately 6,500 ft from Gas Unit 47, the nearest producing well. It is indicated that withdrawal of gas from Gas Unit 47 resulted in pressure drawdown over an area of more than 3,000 acres. These initial pressure measurements in development wells at Trawick demonstrate conclusively that drainage has occurred over areas considerably greater than the 640-acre development pattern and that 640-acre well spacing is more than adequate to provide complete drainage and uniform depletion of this gas reservoir.

DETERMINATION OF GAS WELL SPACING

In the foregoing discussion evidence has been presented to show that drainage of gas can occur over great distances within a continuous reservoir. Rapid establishment of pressure communication and uniformity of pressure distribution throughout the entire reservoir, whether in remote portions developed at later dates or in earlier developed areas, have indicated the uniformity and effectiveness of gas recovery irrespective of the spacing employed. It is concluded, then, that the recovery of gas is independent of the well spacing—

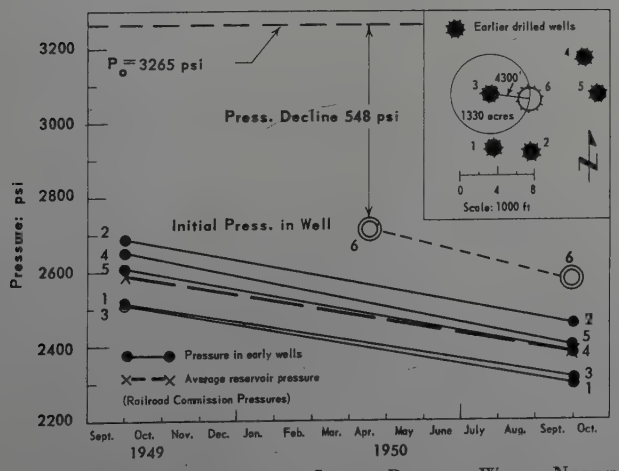

FIG. 6—INITIAL PRESSURE IN LATER DRILLED WELL, NORTH CENTRAL AREA, CARTHAGE GAS FIELD, LOWER PETTIT ZONE.

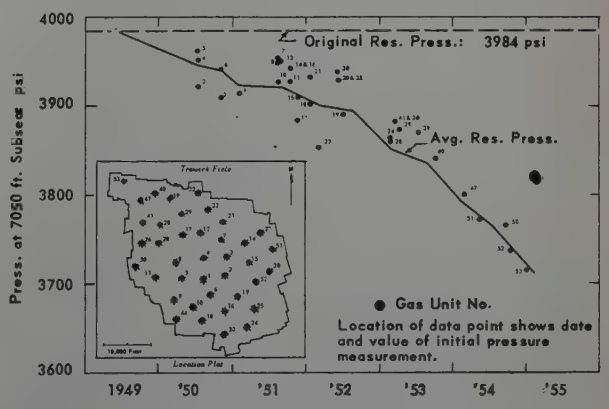

FIG. 7—INITIAL PRESSURES IN STEP-OUT WELLS, TRAWICK GAS FIELD.[1]

that the distance between wells is not one of the physical factors upon which gas recovery is dependent. Although distance of drainage is not a factor controlling ultimate recovery, geometry of the reservoir and location of wells with respect to such geometry are important.

With these conclusions in mind, then, the determination of the well-spacing program for a gas reservoir rests primarily upon the following considerations.

1. A sufficient number of wells must be drilled to provide adequate geologic information concerning structural configuration of the reservoir, continuity and characteristics of the reservoir rock and their distribution, both laterally and vertically, and total amounts of gas and water contained in the reservoir. This information may be obtained by coring, logging and testing strategically located wells.

2. Sufficient wells must be drilled to drain the reservoir under the type of drive operative and to permit effective control of the gas recovery mechanism throughout the entire process. This function of the well in its relation to efficient recovery of natural gas implies a geometric dependence, not a physical dependence, of recovery on well spacing. For those gas reservoirs operating under influence of a natural water drive, sufficient wells properly located and completed must be available to maintain adequate control of the displacing water and to assure effective flushing of gas from all parts of the reservoir. Likewise, in those reservoirs producing gas and natural gas liquids under pressure maintenance by gas injection and cycling, sufficient wells must be properly located to control the cycling process for maximum hydrocarbon recovery from the entire reservoir.

3. A sufficient number of wells must be provided that are physically capable of withdrawing gas at the desired rate of production for the reservoir under the available or chosen recovery mechanism. Further, this number of wells should be sufficient to produce this total volume of gas without incurring inefficient individual well performance.

Once an adequate number of wells has been drilled to provide the necessary geologic information, to drain the reservoir effectively, and to permit the desired rate of withdrawal without inefficient well performance, then additional producing wells beyond this minimum number are unnecessary to achieve the ultimate gas recovery. It is recognized that in many gas reservoirs variations in lease ownership and the right of individual operators to share proportionately in the field production of gas have introduced complicating factors in securing a proper spacing program for each field. A sound well-spacing pattern, coupled with a sound allocation program, is possible through acquisition and interchange of knowledge and through cooperative effort to eliminate the unnecessary well.

TECHNICAL EVIDENCE TO SUPPORT SPACING REQUEST

The goal of a sound well-spacing program is (1) to obtain adequate information regarding the reservoir characteristics and behavior, and (2) to provide a minimum number of wells to assure effective control of the naturally available or chosen recovery mechanism for maximum gas and hydrocarbon liquid recovery. Planning such a program requires first that factual data necessary for a quantitative evaluation of the proper well spacing for each field be accumulated as early as possible.

Accumulation of technical information sufficient to permit sound recommendations for a development program early in the life of a new reservoir is not easy. However, the foregoing discussion of drainage and the accompanying examples illustrating drainage occurrence in the field have provided clues as to the approaches by which evidence may be procured to serve as a basis for spacing recommendations.

Technical evidence to support a well-spacing program for a specific gas reservoir should be directed toward determining, first, the continuity of the reservoir rock. Continuity within the reservoir formation may be established by two principal types of evidence. First of these is geologic evidence which presents the geometric configuration of the productive formation, the lateral and vertical variations in lithology, and the degree of physical continuity of individual productive horizons. Studies of continuity should not be limited to the reservoir proper, but should also consider surrounding regional and basin features.

The second type of evidence to establish continuity comprises studies of pressure communication between areas or between wells. This information may be in the form of observed pressure variations that show interference between or among areas. It may also be in the form of reduced pressures observed in step-out development wells or in later drilled interspaced wells. To obtain this information, accurate subsurface pressure measurements must be made in all gas wells immediately upon completion. Initial pressure measurements in development wells, as illustrated in this paper, provide ample evidence of reservoir continuity and fluid movement and serve as primary arguments for wider spacing of natural gas wells. Information regarding a well's producing ability, potential and productivity and decline characteristics may also be utilized in interpretation of pressure data and their implications with respect to drainage.

Another consideration in the planned spacing program involves the number and location of wells required to control the recovery process and to produce the reservoir at the desired rate of withdrawal without sacrifice in the capability of the well itself to produce efficiently. This requires data on the properties and behavior of the contained reservoir fluids. With such information at hand, it is then important that the naturally available reservoir drive be identified early and a determination made as to the probable recovery mechanism, whether natural or induced, under which the production of natural gas and its associated hydrocarbon liquids will be obtained. With the recovery process established, determination of the minimum number of wells and their location with respect to reservoir geometry to achieve effective control of the recovery mechanism can be made.

One further step involves determination of the desired rate of withdrawal of gas from the reservoir and the number of wells necessary to provide this rate of withdrawal and yet at the same time maintain each well within its capability to produce its share of the field allowable efficiently. Productivity factor measurements obtained by conventional flow tests on individual wells give an index to the productive ability of a well. Flow tests should be made on the initial well upon its completion and on each additional well as development proceeds. Interpretation of these data can assist in se-

lecting the rate at which an individual well can withdraw gas efficiently.

SUMMARY

Associated with an improved understanding of the fundamental principles underlying reservoir and well behavior has been the growth of concepts concerning the role of wells and their spacing in the development and operation of an oil reservoir. For the natural gas reservoir these concepts are no different. They are equally applicable in any consideration of well spacing in gas reservoirs. Maximum utilization of wells is an integral part of sound conservation practices whether the wells produce oil or gas.

In addition to serving as an outlet for production, the natural gas well has two primary functions, (1) providing access to the reservoir to obtain necessary information, and (2) serving as the means to control effectively the natural or induced recovery mechanism. Beyond a minimum number of wells required to fulfill these functions, additional wells will not increase recovery.

Case histories involving interference and drainage observable in step-out wells during development or in delayed drilling of interspaced wells have given ample evidence that gas, as a highly mobile fluid, can move throughout an intercommunicating and continuous porous reservoir over distances far exceeding any spacing normally employed in gas fields today. This supports the conclusion that a gas well can drain a large area effectively in both limestone and sandstone formations. It would appear prudent during development of the new pool to employ wide initial spacing to obtain with a minimum number of wells the maximum information necessary to determine the final spacing for effective control of the recovery. Initial wide spacing should lend a flexibility to the development of the gas reservoir that would minimize the possibility of drilling unnecessary wells. The savings in energy, material and capital by eliminating unnecessary wells will encourage a more intensive exploration for and development of new gas reserves. In addition, these savings may be utilized in more widespread application of conservation projects designed to increase the recovery of gaseous and liquid hydrocarbons.

The trend toward wider well spacing in new gas reservoirs is entirely proper and justifiable on the basis of growing technologic evidence. In Texas, for example, the Railroad Commission issued spacing rules on 40 gas fields during 1957. Twelve, or 30 per cent, of these called for 640-acre spacing; 23 fields, or 57.5 per cent, were permitted 320-acre spacing; and five fields were granted 160-acre spacing. In Mississippi, a statewide rule provides a minimum of 320-acre spacing for gas wells.

Technological advances fostered by industry and applied to the development and production of our natural gas reserves go hand in hand with the evolution of sound conservation practices. This program cannot remain static but must continue to keep pace with the growth of exploration and production effort in the area of natural gas. It would seem plausible at this time to examine the permissible spacing rule structure and to establish statewide rules that would promote effective development of new gas reserves on initial wide spacing, spacing wider than that normally employed in practice today. Along with this, it would be appropriate to provide a sound allocation of gas allowables designed to encourage wider spacing of gas wells rather than to penalize it. Jointly, this could go far toward the development of new gas reserves in this area and would do much to stimulate a more effective recovery of this vital resource. It would thereby enable the industry to meet the increasing demands of the nation with an adequate supply of natural gas at lower cost.

ACKNOWLEDGMENT

The author wishes to acknowledge the contributions of B. M. Sullivan and M. O. Langham of the Humble Oil & Refining Co. who directly assisted in the preparation of several of the case histories cited here. The author further expresses his appreciation to his associates who reviewed the manuscript and whose constructive suggestions and counsel were most helpful.

REFERENCES

1. Craze, R. C. and Glanville, J. W.: "Plan Your Well Spacing Early", *Oil and Gas Jour.* mid-year report (July 30, 1956) **54**, No. 65, 216.
2. Bruce, G. H., Peaceman, D. W., Rachford, H. H., Jr. and Rice, J. D.: "Calculations of Unsteady-State Gas Flow Through Porous Media", *Trans.* AIME (1953) **198**, 79.
3. Bell, J. S. and Shepherd, J. M.: "Pressure Behavior in the Woodbine Sand", *Trans.* AIME (1951) **192**, 19.
4. Rumble, R. C., Spain, H. H., and Stamm, H. E., III: "A Reservoir Analyzer Study of the Woodbine Basin", *Trans.* AIME (1951) **192**, 331. ★★★

Reservoir Analysis for Pressure Maintenance Operations Based on Complete Segregation of Mobile Fluids

JOHN C. MARTIN
MEMBER AIME

CREOLE PETROLEUM CORP.
MARACAIBO, VENEZUELA

ABSTRACT

A brief review is presented of the past performance of a number of large, thin, highly permeable reservoirs with low dips in the Bolivar Coastal fields of Venezuela. The performance of these reservoirs indicates that the fluids are segregated vertically within the sand section by gravity. With this assumption, equations are developed which describe the performance under pressure maintenance operations. Methods of solving these equations and results of simple example calculations are presented.

Example calculations indicate that under pressure maintenance conditions injected gas tends to flow preferentially along the top of the sands and that encroaching water has a tendency to flow preferentially along the bottom. The expected performance of segregated fluids is discussed and compared with that of fluids which are uniformly distributed in any sand section.

INTRODUCTION

The field performance of a number of reservoirs described herein indicates that the fluids are segregated vertically within the sand section by the force of gravity. Thus, it was felt that any method used to predict the future performance of these reservoirs should consider the effects of segregation in the sand sections. A study of the available information on some of the reservoirs suggests that increased recoveries may be expected if the reservoir pressure is maintained by either crestal gas injection or flank water injection.

To predict future performance of reservoirs under pressure maintenance operations, a method of analysis was needed which would account for segregation of fluids in the sand sections. Several methods of analysis have been developed to take into account the segregation of fluids in the reservoir as a whole.[1,2] To our knowledge no method considers segregation of the fluids within sand sections in the manner indicated by the past performance of several reservoirs in the Maracaibo Basin. This paper outlines part of the work done in studying some of these reservoirs and contains a description of their performance characteristics. The analysis presented is restricted to pressure maintenance conditions, since space limitations prevent a full discussion of the development of the mathematical relations and the various methods of solving them. Only a sketch of the development of the mathematical relations is given. The various methods of solving these relations are pointed out, but the actual determination of solutions to various problems are omitted except for one example. It is felt that these results may aid in the study of reservoirs outside the Maracaibo Basin.

Some concepts on which the present analysis is based are outlined by D. N. Dietz.[3] However, the analysis presented herein includes several factors not considered by Dietz: (1) variations in permeability and in the cross section, (2) various shapes of the cross section, and (3) the production of fluids. Also, the mathematical development presented by Dietz differs considerably from our corresponding analysis.

RESERVOIR CHARACTERISTICS

The reservoirs under consideration, large and thin, with low dip and high permeability, are large to the extent that they contain from 0.5 to over four billion bbl of oil initially in place. The section thicknesses vary from 100 to 400 ft and the lengths from 10,000 to 40,000 ft. Thus, a length-wise cross section of the producing formation appears to be long and thin. The dip angles vary from 0 to 6 degrees and the average permeabilities vary from 0.5 to over three darcies. The reservoirs contain from 20 to 50 per cent shale interlaminated with the productive sands. Most shale breaks within the major sands do not correlate from one well to the next, and correlation is often difficult, even between wells drilled from the same location. However, it is often possible to correlate the shale breaks between major sands for some distance.

Herein we are concerned with the performance of reservoirs containing oil of gravities over 20° API. Past reservoir performance indicates good pressure communication and, in cases where pressure sinks have developed, large amounts of fluid migration have occurred. Few of the reservoirs have had initial gas caps, but also, few have been found to be highly undersaturated. Due to gravity segregation, secondary gas caps usually form before the pressure has been reduced more than 25 per cent of its initial value. The effect of gravity has not only been apparent on a reservoir-wide basis, but has also caused segregation of the reservoir fluids in productive sections. Proof of this is found from the results of selective well tests, workovers, and electric and various other types of logs. Evidence that

Original manuscript received in Society of Petroleum Engineers office July 17, 1957. Revised manuscript received June 2, 1958. Paper presented at 32nd Annual Fall Meeting of Society of Petroleum Engineers in Dallas, Tex., Oct. 6-9, 1957.
[1]References given at end of paper.

the indicated segregation can take place within relatively short times was found from theoretical calculations.[4]

Further insight into the characteristics of these reservoirs can be obtained by considering the performance of crest wells, which are usually completed with the entire producing section open to production. With the formation of a secondary gas cap, a high GOR develops which can be reduced by shutting off the upper sands. It is not uncommon to reduce the GOR from 2,000 to 400 ft³/bbl. Calculations indicate that if there were no shale breaks, the GOR could not be effectively controlled by shutting off the upper sands. Thus, the shale breaks cover sufficient areas to prevent gas coning. The GOR after a gas shut-off workover is often considerably lower than one would expect if it is assumed that the gas does not segregate to the top of the section. Thus, there are indications that even at the crest of the structure the gas segregates to the top of the producing interval. This is in spite of the many shale breaks present.

Certain reservoirs have partial water drives. There is strong evidence that the water tends to flow along the bottom of the reservoir and in most cases it is possible to reduce the WOR of a well by shutting off the lower sands.

The over-all field performances indicate that the shale breaks extend over sufficiently large areas to remove much of the harmful effects of gas and water coning, while at the same time their areal extent is sufficiently limited so that the fluids can segregate under the force of gravity.

LIMITATIONS AND ASSUMPTIONS IN CALCULATING RESERVOIR PERFORMANCE DURING PRESSURE MAINTENANCE OPERATIONS

The analysis is limited to reservoirs which have the same characteristics as those described in the preceding section. In addition, the following assumptions are made.

1. The fluids are segregated by the force of gravity and only one phase is free to flow at any point. Thus, below the water-oil contact only water is free to flow and above the gas-oil contact only gas is free to flow.
2. The reservoir pressure is maintained and all fluid characteristics can be considered constant.
3. The total withdrawals in reservoir volumes are equal at all times to the sum of the fluid injection and water influx.
4. The effects of capillarity can be neglected. Thus, the transition zones from water to oil and from oil to gas are neglected.
5. The effects of the wells are neglected to the extent that the production is taken directly out of each elemental volume.
6. The permeability of the sands is assumed to be constant in the horizontal direction perpendicular to the direction of flow.
7. The velocities of the flows in the vertical direction are very small compared to the velocities of the flows along the axis of the reservoir.
8. The dip angles and the slopes of the contact between the fluids are small.

RESERVOIR EQUATIONS

The reservoir equations employed herein are based on relations governing the average velocity of flow of each phase and the equations of continuity. The equations governing the average velocity of flow of each phase are:

$$\bar{v}_a = -\frac{\bar{k}_a}{\mu_a}\left[\frac{\partial p_{ab}}{\partial x} - g\rho_a\frac{\partial(H - Hs_a)}{\partial x} - \alpha g\,\rho_a\right] \quad . \quad (1a)^*$$

$$\bar{v}_b = -\frac{\bar{k}_b}{\mu_b}\left[\frac{\partial p_{ab}}{\partial x} - g\rho_b\frac{\partial(H - Hs_a)}{\partial x} - \alpha g\,\rho_b\right] \quad . \quad (1b)^*$$

Eqs. 1a and 1b are very similar to Darcy's law. The average permeability functions are analogous to the effective permeabilities in that they can be expressed as functions of s_a, and the effective permeabilities can be expressed as functions of the saturation of one phase. Plots of the functions, $\bar{k}_a$ and $\bar{k}_b$, do not generally have the same shape as the effective permeabilities. Fig. 1 presents the variations of $\bar{k}_a$ and $\bar{k}_b$ with s_a for three different permeability distributions for rectangular cross sections. Curve A corresponds to a sand section with a uniform permeability. Curve B is associated with a sand section in which the upper half has twice the permeability of the lower half, and Curve C is associated with a sand section where the reverse of Curve B is true. The permeability functions, $\bar{k}_a$ and $\bar{k}_b$, are dependent on the shape of the cross section as well as the permeability variations perpendicular to the bedding planes and in the direction of flow. Thus, the permeability functions for a rectangular cross section has a different shape than that for a circular cross section, and the permeability function can be functions of x.

Eqs. 1a and 1b contain the pressure along the contact between the two phases, while in Darcy's law, the pressure is associated with the point under consideration. By utilizing a mean pressure, Darcy's law can be written so that the capillary effects introduce terms somewhat analogous to those in Eqs. 1a and 1b which contain $\frac{\partial(H - Hs_a)}{\partial x}$.[5] It should be noted that the terms containing $\frac{\partial(H - Hs_a)}{\partial x}$ in Eqs. 1a and 1b are a result of the change in the contact between the two fluids with distance and the change in H with distance and are not a result of capillary effects.

The equations of continuity can be expressed:*

$$\frac{\partial(A\bar{v}_a)}{\partial x} + \frac{\partial q_a}{\partial x} = -\bar{\phi}A\frac{\partial \bar{S}_a}{\partial t_D}, \quad . \quad . \quad . \quad . \quad . \quad (2)$$

$$\bar{v} = \frac{A_i\bar{v}_i}{A} - \frac{1}{A}\int_{x_i}^{x}(1 + R_b)\frac{\partial q_a}{\partial x}\,dx, \quad . \quad . \quad (3)$$

and

$$\bar{v} \equiv \bar{v}_a + \bar{v}_b \quad . \quad . \quad . \quad . \quad . \quad . \quad . \quad . \quad . \quad . \quad . \quad (4)$$

By knowing the rates of production of Phases a and b, Eq. 3 can be evaluated. Thus, $\bar{v}$ will be considered as a known function of x and t. Since $\bar{S}_a$ is a function of s_a and x, Eqs. 1 through 4 constitute five equations containing five dependent variables and two independent variables. The dependent variables are $\bar{v}_a$, $\bar{v}_b$, $\bar{v}$, p_{ab} and s_a, while the independent variables are x and t. Variables $\bar{v}_a$, $\bar{v}_b$ and p_{ab} can be eliminated from the relations given by Eqs. 1 through 4. The resulting relation expressed in non-dimensional form is

$$\frac{\partial}{\partial X}\left\{\frac{A\bar{v}}{A_i\bar{v}_i}F + \frac{AB}{A_i}\left[\frac{1}{\alpha L}\frac{\partial(H - Hs_a)}{\partial X} + 1\right]G\right\} + \frac{1}{A_i\bar{v}_i}\frac{\partial q_a}{\partial X} = -\frac{A}{A_i}\frac{\partial \bar{S}_a}{\partial t_D} \quad . \quad . \quad . \quad . \quad . \quad . \quad . \quad . \quad (5)$$

*The derivation of Eqs. 1a, 1b, 2 and 3 is given in Appendix A.

Since $\bar{v}$ is a known function of X and t_D, Eq. 5 is a partial differential equation containing one unknown, s_a.

Eq. 5 places no restrictions on the ratio in which the two phases are produced. We shall investigate the result of assuming that the entire section is open to production and that draw-downs of the wells are very small.

The presence of the wellbores is neglected and flow is assumed to be in one direction only. In considering the ratio of the produced fluids, we shall not neglect the wellbores and shall assume that the flow remains in one direction except near the wells into which the fluid is drawn. Based on these assumptions, the ratio of Phase *b* to Phase *a* drawn into the wellbores is

$$R_b = \left(\frac{\mu_a}{\mu_b}\right)\left(\frac{\bar{k}_b}{k_a}\right).$$

In deriving equations of continuity, the production was assumed to be distributed so that it was taken directly from each elemental volume. Thus, the rate of change of production with distance can be determined and the ratio of the rate of production of Phase *b* to the rate of total fluid production at any point is

$$\frac{R_b \frac{\partial q_a}{\partial X}}{(1+R_b)\frac{\partial q_a}{\partial X}} = \frac{R_b}{1+R_b} = R_b F \quad . \quad . \quad . \quad . \quad (6)$$

From Eqs. 6 and 25 the following relation can be obtained.

$$\frac{\partial q_a}{\partial X} = -F\frac{\partial(A\bar{v})}{\partial X} \quad . \quad . \quad . \quad . \quad . \quad . \quad . \quad . \quad (7)$$

Substituting Eq. 7 into Eq. 5 and simplifying, yields

$$\frac{A\bar{v}}{A_i\bar{v}_i}\left(\frac{\partial F}{\partial s_a}\frac{\partial s_a}{\partial X} + F'\right) + \frac{\partial}{\partial X}\left\{\frac{AB}{A_i}\left[\frac{1}{\alpha L}\frac{\partial(H - Hs_a)}{\partial X} + 1\right]G\right\} = -\frac{A}{A_i}\frac{\partial \bar{S}_a}{\partial t_D} \quad . \quad . \quad . \quad . \quad . \quad . \quad . \quad (8)$$

Eq. 8 represents a simplification of Eq. 5 for the case where the entire section is open to production.

Eqs. 5 and 8 are non-linear, second-order, partial differential equations—generally very difficult to solve. Fortunately, a number of solutions of these equations can be obtained which are useful in reservoir analyses and in the study of the general behavior of segregated flows.

In certain cases it is possible to obtain exact solutions of Eq. 5 where the contact between the two phases is independent of time or where it is characterized by an arbitrary shape which travels with a constant velocity. In other cases, the first and second derivatives of s_a with X are sufficiently small so that the contribution of the term, $\frac{H}{\alpha L}\frac{\partial s_a}{\partial X}$, in the factor multiplying G can be neglected. For these cases, Eqs. 5 and 8 can be approximated by

$$\frac{\partial}{dX}\left\{\frac{A\bar{v}}{A_i\bar{v}_i}F + \frac{AB}{A_i}\left[\frac{(1-s_a)H'}{\alpha L} + 1\right]G\right\} + \frac{1}{A_i\bar{v}_i}\frac{\partial q_a}{\partial X} = -\frac{A}{A_i}\frac{\partial \bar{S}_a}{\partial t_D} \quad . \quad . \quad . \quad . \quad . \quad . \quad . \quad (9)$$

$$\frac{A\bar{v}}{A_i\bar{v}_i}\left(F' + \frac{\partial F}{\partial s_a}\frac{\partial s_a}{\partial X}\right) + \frac{\partial}{\partial X}\left\{\frac{AB}{A_i}\left[\frac{(1-s_a)H'}{\alpha L} + 1\right]G\right\} = -\frac{A}{A_i}\frac{\partial \bar{S}_a}{\partial t_D} \quad . \quad . \quad . \quad . \quad . \quad . \quad . \quad (10)$$

Fortunately, Eqs. 9 and 10 can be used to obtain approximate solutions to a number of practical problems.

Eqs. 9 and 10 are first-order, linear, partial differential equations. Solutions of these equations can be obtained by evaluating the following systems of subsidiary, ordinary differential equations.[6,7] For Eq. 9:

$$\frac{dX}{\frac{A\bar{v}}{A_i\bar{v}_i}\frac{\partial F}{\partial s_a} - \frac{ABH'G}{\alpha L A_i} + \frac{AB}{A_i}\left[\frac{(1-s_a)H'}{\alpha L} + 1\right]\frac{\partial G}{\partial s_a}} = \frac{dt_D}{\frac{A}{A}\frac{\partial \bar{S}_a}{s_a}} = -\frac{ds_a}{\frac{A\bar{v}}{A_i\bar{v}_i}F' + \frac{F}{A_i\bar{v}_i}\frac{\partial(A\bar{v})}{\partial X} + \frac{1}{A_i\bar{v}_i}\frac{\partial q_a}{\partial X} + \frac{AB}{A_i}\left[\frac{(1-s_a)H'}{\alpha L} + 1\right]\left(G' + G\frac{dA}{dX}\right) + \frac{(1-s_a)ABG}{A_iL}\frac{d}{dX}\left(\frac{H'}{\alpha}\right)} \quad . \quad . \quad . \quad . \quad . \quad (11)$$

For Eq. 10:

$$\frac{dX}{\frac{A\bar{v}}{A_i\bar{v}_i}\frac{\partial F}{\partial s_a} - \frac{ABH'G}{\alpha L A_i} + \frac{AB}{A_i}\left[\frac{(1-s_a)H'}{\alpha L} + 1\right]\frac{\partial G}{\partial s_a}} = \frac{dt_D}{\frac{A}{A_i}\frac{\partial \bar{S}_a}{\partial s_a}} = -\frac{ds_a}{\frac{A\bar{v}}{A_i\bar{v}_i}F' + \frac{B}{A_i}\left[\frac{(1-s_a)H'}{\alpha L} + 1\right]\left(G' + G\frac{dA}{dX}\right) + \frac{(1-s_a)ABG}{A_iL}\frac{d}{dX}\left(\frac{H'}{\alpha}\right)} \quad . \quad . \quad . \quad . \quad . \quad (12)$$

Eqs. 11 and 12 can be evaluated numerically or graphically, and in certain cases they can be integrated analytically. In evaluating these equations numerically or graphically, we have found that in many cases the calculations can be reduced considerably by introducing the boundary conditions along with the integration.

The solution of Eq. 11 can often be used to determine a first approximation to the term, $\frac{\partial s_a}{\partial X}$, in Eq. 5. For these cases a second approximation to the solution of Eq. 5 can be determined as follows. Substitute the expression for $\frac{\partial s_a}{\partial X}$ obtained from the solution of Eq. 11 into Eq. 5. The resulting equation is a first-order, linear, partial differential equation which can be reduced to a system of ordinary differential equations in the same manner as Eqs. 9 and 10 were reduced to Eqs. 11 and 12. The solution of the system of ordinary differential equations yields a second approximation to the solution of Eq. 5. This process can be repeated to obtain successively higher approximations to the solutions of Eq. 5. It is, of course, necessary to use the highest approximation to determine the expression for $\frac{\partial s_a}{\partial X}$, which is substituted into Eq. 5.

The same procedure is followed when Eq. 12 is used to obtain iterative solutions of Eq. 8. The author has not investigated the range of convergence of this iterative process except by calculating a few examples. In these examples the process appears to converge satisfactorily provided $\frac{\partial s_a}{\partial X}$ is not large.

Unfortunately, proper application of the preceding

equations requires a certain amount of mathematical background together with an understanding of the physics involved. This is especially true in using Eqs. 11 and 12. In many cases, the proper interpretation of the results obtained from Eqs. 11 and 12 requires that discontinuities be introduced which are based on physical considerations.

SIMPLE EXAMPLES

To illustrate some characteristics of segregated flow, a few examples are considered. The first example concerns a sand with a rectangular cross section and with uniform thickness, dip angle, and permeability. A constant rate of flow of Phase *b* into the upper end displaces Phase *a* from the sand. We shall consider only flows which are characterized by a fluid contact which travels with a constant velocity and does not change its shape with time. The derivation of the equation governing this flow is presented in Appendix B, and the solution is

$$s_a = \frac{\alpha L}{H}\left\{1 + \frac{1 - \left(\frac{\mu_a}{\mu_b}\right)\left[\frac{k_b(S_{ar})}{k_a(S_{br})}\right]}{\frac{\alpha k_b(S_{ar})\, g\,(\rho_a - \rho_b)}{\mu_b \bar{v}}}\right\}(X - t_D + a_2) \quad . \quad . \quad . \quad . \quad . \quad . \quad . \quad . \quad . \quad . \quad . \quad (13)$$

Eq. 13 represents a tilted fluid contact which varies linearly with x and t_D, and moves with a non-dimensional velocity equal to one. The slope of the fluid contact is a constant and is equal to

$$H\frac{\partial s_a}{\partial x} = \alpha\left\{1 + \frac{1 - \left(\frac{\mu_a}{\mu_b}\right)\left[\frac{k_b(S_{ar})}{k_a(S_{br})}\right]}{\frac{\alpha k_b(S_{ar})\, g(\rho_a - \rho_b)}{\mu_b \bar{v}}}\right\} \quad . \quad (14)$$

Eq. 14 indicates that the slope of the fluid contact is a function of the mobility of the two fluids, the dip angle, the difference in density between the two fluids, and the velocity, $\bar{v}$. For $\bar{v} = 0$ the slope is horizontal. For cases where the mobility of Phase *b*, at points above the fluid contact, is greater than the mobility of Phase *a* below the fluid contact, the slope of the fluid contact decreases as $\bar{v}$ increases. For cases where $k_b(S_{ar})/\mu_b \leq k_a(S_{br})/\mu_a$, the slope of the fluid contact increases as $\bar{v}$ increases. The value of $\bar{v}$ at which the slope of the fluid contact is zero is

$$\bar{v}_c = \frac{\alpha g(\rho_a - \rho_b)}{\frac{\mu_a}{k_a(S_{br})} - \frac{\mu_b}{k_b(S_{ar})}} \quad . \quad . \quad . \quad . \quad . \quad . \quad (15)$$

The value of $\bar{v}$ given by Eq. 15 is equal to the so-called critical velocity which has been discussed by several authors.[3,8,9]

For values of $\bar{v}$ above the critical velocity, the slope of the fluid contact is negative and Eq. 13 represents the condition where Phase *a* is displacing Phase *b* in the down-dip direction. Since the development was carried out on a general basis it appears there is no quasi-steady-state solution of the form characterized by Eq. 27 for values of $\bar{v}$ greater than the critical value where Phase *b* displaces Phase *a*. Thus, for $\bar{v} > \bar{v}_c$, the shape of the fluid contact must be an ever-changing function of time.

Dietz[3] discussed the critical velocity and concluded that at the critical velocity the fluid contact will remain horizontal provided it is horizontal initially. The analysis presented in Appendix B does not support this contention since there appears to be no solution of Eq. 5 of the form required. Based on Eq. 13 one would expect $\frac{\partial s_a}{\partial x}$ to approach a constant value greater than zero for $\bar{v} < \bar{v}_c$. A flow of this nature appears to be what occurred in the results of model tests presented in Fig. 1a of Ref. 3. In this case Phase *a* displaced Phase *b* in the up-dip direction.

The second example concerns a reservoir with a uniform permeability in which gas is injected at the top. Initially there is a tilted gas-oil contact and at $t_D = 0$, gas is injected into the upper boundary at a constant rate. The production of fluids is distributed uniformly over the reservoir and the ratio of gas to total fluid production is given by Eq. 6. The various parameters are given in Table 1 and the results are presented in Fig. 2a. These results indicate a tendency for the gas to move along the top of the sand. The lines represent the gas-oil contact obtained by solving Eq. 12. In the small region where the slope of the gas-oil contact is large, Eq. 12 does not yield representative results because the term which was assumed to be small cannot be neglected in this region. The gas-oil contact in this small region shown in Fig. 2a was estimated from a study of Eq. 5.

The rapid movement of the gas along the top of the reservoir is characteristic of the flow obtained in cases where the fluids are segregated and the mobility of the driving phase is much greater than that of the driven phase. Due to the high mobility of the gas, the pressure gradients in the reservoir are reduced sharply as the upper sands are gassed out. As a result of the production of the reservoir fluids throughout the reservoir, the viscous or applied pressure gradients are gradually reduced in the down-dip direction. The movement of the gas along the top of the sands continues until the applied pressure gradient is approximately balanced by the gravitational pressure gradient in the dip-wise direction.

The general behavior indicated by Fig. 2a has been observed in small sand models. Unfortunately, sufficient data are not yet available for a given flow in a model to allow a quantitative comparison to be made between the theory and the model flow.

In certain pilot operations[10,11] where a gas or a low-density liquid has been injected, there is evidence that the low-density fluids moved through the upper sands only. In certain cases there is also evidence that the upper sands are not the most permeable. We have not yet investigated this matter in detail, however, there ap-

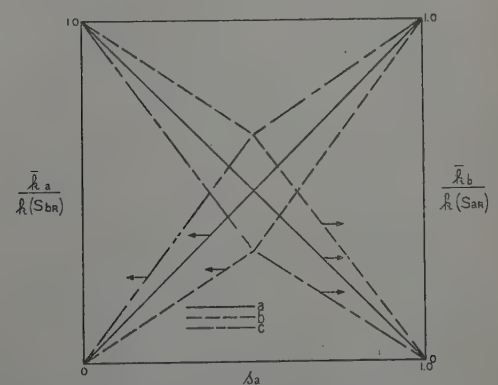

FIG. 1—PERMEABILITY FUNCTIONS.

TABLE 1—RESERVOIR PROPERTIES USED IN EXAMPLES

Symbol	Fig. 2	Fig. 3
L	10,000 ft	—
H	100 ft	—
α	6 degrees	0 degrees
μ_g	.0250 cp	—
μ_n	4.12 cp	2.22 cp
μ_w	.337 cp	.50 cp
$g\rho_o$	.325 psi/ft	—
$g\rho_g$	.039 psi/ft	—
$g\rho_w$	.433 psi/ft	—
$k_g(S_{or})/k_o(S_{gr})$	1.00	—
$k_o(S_{wr})/(S_{or})$	1.78	1.78
v_i	.30 ft/day	—

pears to be some indication that segregated flows sometimes occur even in closely spaced pilots.

In the third example, the reservoir has a uniform permeability and water is injected at the bottom at a constant rate. Initially there is a tilted water-oil contact, and the production of the fluids is distributed uniformly over the reservoir. The ratio of the oil produced to the total fluid produced is given by Eq. 6. The various parameters are given in Table 1 and the results, based on Eq. 12, are presented in Fig. 2b. These results indicate a tendency for the water to flow along the bottom of the reservoir. The rapid movement of the water through the lower portion of the sand continues until the applied pressure gradient is approximately balanced by the gravitational pressure gradient. In the region where the slopes of the water-oil contact are large, Eq. 12 does not yield representative results. In this small region, the shape of the water-oil contact was estimated from a study of Eq. 5.

In the fourth example, we shall consider a linear reservoir in which water is injected in one end and fluids are produced from the other. The upper half of the reservoir has a permeability one-half that of the lower half. The values of the various parameters are given in Table 1, and the results (based on Eq. 11) are presented in Fig. 3a. The results indicate that the tendency of the water to move along the lower portion of the sand is increased if the lower sands have a higher permeability than the upper sands. The finger of water which runs along the bottom of the lower sand is thicker in Fig. 3a than in Fig. 2b. This is due mainly to the different viscosities used in the two examples.

The fifth example is based on the same conditions as the fourth except that the upper half of the sand has twice the permeability of the lower. The movement of the water-oil contact is presented in Fig. 3b. These results were calculated from Eq. 11 and indicate a tendency for the water to flow along the bottom of the sand with the higher permeability. The results presented in Ref. 12 indicate that in some cases this is true. In several of our experiments, the water-oil contact assumed a shape similar to the dotted lines in Fig. 3b. Thus, it appears that at least both types of flow illustrated in Fig. 3b are possible, depending on the particular conditions.

In addition to Ref. 12 some experimental work on the effects of gravity on water flooding has been reported.[13,14] The results presented in Ref. 13 indicate that no appreciable effect of segregation was present in the tests. In view of the range of variables investigated, this is not surprising. The results presented in Ref. 14 indicate a considerable effect of gravity on the test results.

RESERVOIR ANALYSIS

The equations presented herein can be used in conjunction with other relations to predict the future performance of reservoirs under pressure maintenance operations. There are a number of methods by which this can be accomplished. We have used the method outlined here in calculations involving pressure maintenance by gas injection and by flank flood. The equations presented in the preceding sections can be used to predict the movements of the gas-oil and the water-oil contacts providing the various parameters are known and the flow is essentially along one axis.The parameters require a knowledge of the total withdrawal and the ratios at which the fluids are produced.

The total volume of fluid injected is determined by either the maximum producing capacity of the reservoir or a fixed production schedule. The ratios at which the fluids are produced should be based on the past performance of the reservoir and the position of the fluid contacts. Our results indicate that in certain cases the presence of shale lenses reduces the amount of gas and water coning to the extent that the ratios at which the fluids are produced can be predicted by neglecting coning.

To reduce the mathematics involved, the reservoir is broken down into a number of radial blocks as shown in Fig. 4. The rate of production is assumed to remain

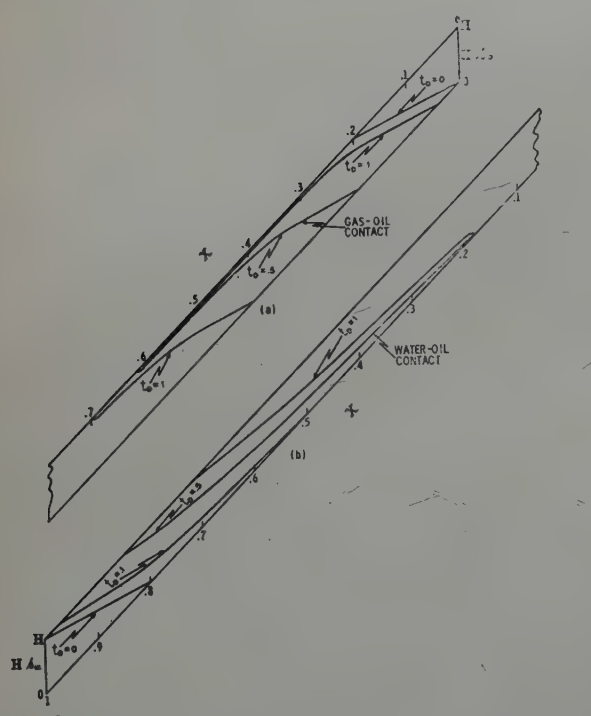

FIG. 2—CALCULATED MOVEMENTS OF GAS-OIL AND WATER-OIL CONTACTS. VERTICAL SCALE 9.6 TIMES HORIZONTAL SCALE.

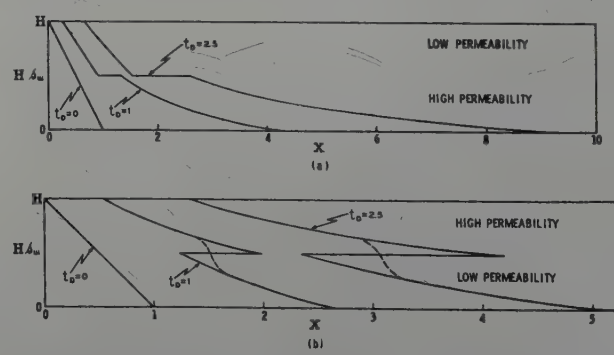

FIG. 3—CALCULATED MOVEMENTS OF WATER-OIL CONTACT. HORIZONTAL SCALE SMALLER THAN VERTICAL SCALE.

constant over a fixed time period. The following procedure is used to determine the performance during a time period.

1. Estimates of the fluid productions during the time period are based on the position of the fluid contacts, the characteristics and number of wells, and results of previous time period calculations.

2. The total velocity, $\bar{v}$, is calculated based on the estimated fluid productions.

3. The movements of the fluid contacts during the time period are calculated using Eq. 11 and/or Eq. 12. In regions where the slopes of the fluid contacts are not small, the slopes of the contacts are estimated based on a study of Eq. 5. This study may include steady-state, quasi-steady-state, or iterative solutions. Fortunately, in many cases, the region where the shape of the contact of the fluid must be estimated is only a small portion of the reservoir. Thus, in these cases only minor errors are usually introduced in the over-all performance.

4. The results of the calculated movements of the fluid contacts are used to determine the productions of the fluids during the time period. If these productions agree with the productions estimated in Step 1, the process is complete. If they are not in agreement the entire process is repeated until agreement is reached. The author has found that in many cases the agreement between estimated and calculated productions is obtained on the first trial.

A more elegant method than that just outlined is to treat $\bar{v}$ as being a function of s_a, x and t, and solve Eqs. 9 or 10 over the entire reservoir or over the individual blocks. In this case Eqs. 9 or 10 can be reduced to a system of ordinary differential equations similar to Eqs. 11 and 12. In this method the number of wells and their characteristics must be included in the relation for $\bar{v}$, and it is not necessary to divide the time into incremental periods.

TYPES OF PERFORMANCE

The examples presented in Figs. 2 and 3 illustrate some characteristics of segregated flow. The tendency for the gas to move along the upper sands of the reservoir can make pressure maintenance by gas injection unattractive in cases where there are no shale breaks to reduce coning, or in cases where the production from the upper sands cannot be shut-off. In cases where the production from various sands can be controlled by workovers, pressure maintenance by gas injection can sometimes offer a very attractive means of increasing the oil recovery.

The results presented in Fig. 2a are based on the assumption that the entire sand section is open to production. In this case, the gas-oil ratios of the wells in the upper portion of the reservoir are extremely high, and appreciable oil recovery is only obtained by cycling very large amounts of gas. In case it is possible to shut-off production from the sands at the top of the section, much less gas is required, and the thickness of the gassed-out top sand increases much more rapidly than is indicated in Fig. 2a.

If it is assumed that the fluids are not segregated by gravity in the sections, a different type performance under pressure maintenance by gas injection is obtained. For a reservoir with uniform permeability there would be little advantage in shutting off particular portions of the sands since all would produce at approximately the same GOR. In regions where the applied pressure is greater than the gravitational pressure, the GOR of any given well would increase continuously after the initial gas front has passed.

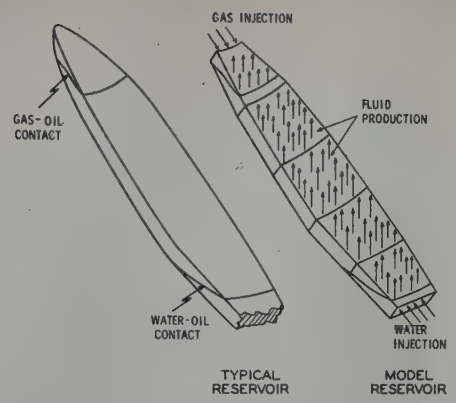

FIG. 4—RESERVOIR MODEL.

From case studies it appears that the calculated movement of gas along the reservoir top is considerably faster in a reservoir with segregated flow than movement of the initial gas front in the same reservoir if it is assumed that the fluids are uniformly distributed throughout the sand in any given section. The calculated performance of a reservoir, under the assumption that the fluids are segregated, can be more or less favorable than the calculated performance of the same reservoir under the assumption that the fluids are uniformly distributed in each section. This performance depends to a large extent upon the ability to shut-off the gassed-out sands.

The calculated performances for pressure maintenance by flank water injection are somewhat similar to those calculated for gas injection, providing the mobility of the water in the watered-out sands is considerably larger than that of the oil above the water-oil contact. In one case it was found that the water flowing along the bottom of the reservoir greatly reduced the pressure gradients within the reservoir; this provided favorable pressure communication.

CONCLUSIONS

1. The past performance of certain reservoirs in the Maracaibo Basin indicates that the fluids are segregated in the sands.

2. It has been possible to develop a theory which can be used as a basis for predicting future performance of reservoirs and which takes into account the segregation of the fluids in the sands.

3. The general flow patterns predicted by the methods presented herein are often quite different from that predicted by theories based on the assumption that the fluids are uniformly distributed in the sands.

4. While the results of the theory presented herein are in qualitative agreement with observed flows, much work remains to be done before the range of applicability is well defined.

NOMENCLATURE*

$$B = \frac{k_b(S_{ar})\, g(\rho_a - \rho_b)}{\mu_b \bar{v}_i}$$

*See AIME Symbols List in *Trans.* AIME (1956) 207, 363, for other symbol definitions.

$$F = \frac{1}{1 + \left(\frac{\mu_a}{\mu_b}\right)\left(\frac{\bar{k}_b}{\bar{k}_a}\right)}$$

$$G = \frac{\alpha \bar{k}_b}{k_b(S_{ar})} F$$

F', G' = the partial derivative of F and G, respectively, with respect to x assuming s_a is independent of x

$$H' \equiv \frac{dH}{dx}$$

$\bar{k}_a$ = average permeability in section to Phase a

$\bar{k}_b$ = average permeability in section to Phase b

L = length of reservoir

R_b = the ratio of Phase b to Phase a

$\bar{S}_a$ = average saturation of Phase a at any point along the x axis

$\bar{S}_b$ = average saturation of Phase b at any point along the x axis

S_{ar} = residual saturation of Phase a above the fluid contact

S_{br} = residual saturation of Phase b below the fluid contact

s_a = fraction of section occupied chiefly by Phase a

s_b = fraction of section occupied chiefly by Phase b

$\bar{v}$ = average velocity in section

$$X = \frac{x}{L}$$

x, y, z = coordinate axes (see Fig. 5)

z_1, z_2 = limits of integration (see Fig. 5)

α = dip angle

$\bar{\phi}$ = average porosity in section

SUBSCRIPTS

a = Phase a

b = Phase b

ab = refers to conditions along the contact of the two phases.

REFERENCES

1. Wooddy, L. D., Jr. and Moscrip, Robert, III: "Performance Calculations for Combination Drive Reservoirs", *Trans.* AIME (1956) **207,** 128.
2. Shreve, D. R. and Welch, L. W., Jr.: "Gas Drive and Gravity Drainage Analysis for Pressure Maintenance Operations", *Trans.* AIME (1956) **207,** 136.
3. Dietz, D. N.: "A Theoretical Approach to the Problem of Encroaching and By-Passing Edge Water", *Proc.* Kon. Neder. Adad. Wetenshaffen (1953) Series B-56, 83.
4. Martin, John C.: "Some Mathematical Aspects of Two-Phase Flow with Applications to Flooding and Gravity Segregation Problems", *Prod. Monthly* (April, 1958) 22.
5. Muskat, Morris: *Physical Principles of Oil Production,* McGraw-Hill Book Co., Inc., N. Y. (1949).
6. Ford, Lester R.: *Differential Equations,* McGraw-Hill Book Co., Inc., N. Y. (1955).
7. Sneddon, Ian N.: *Elements of Partial Differential Equations,* McGraw-Hill Book Co., Inc., N. Y. (1957).
8. Hill, M. A.: "Channelling in Packed Columns", *Chem. Engr. Sci.* (1952) **1,** No. 6.
9. van der Poel, C. and Killian, J. W.: "Attic Oil", paper 919-G presented at 32nd Annual Fall Meeting of SPE in Dallas, Tex. (Oct. 6-9, 1957).
10. Walter, H.: "Application of Heat for Recovery of Oil: Field Test Results and Possibility of Profitable Operation", *Jour. Pet. Tech.* (Feb. 1957) **IX,** No. 2, 16.
11. Kuhn, C. S. and Koch, R. L.: "In-Situ Combustion—Newest Method of Increasing Oil Recovery", *Oil and Gas Jour.* (Aug. 10, 1953).
12. Jordan, J. K., McCardell, W. M. and Hocott, C. R.: "Effect of Rate on Oil Recovery by Waterflooding", *Oil and Gas Jour.* (May 13, 1957).
13. Croes, G. A. and Schwarz, N.: "Dimensionally Scaled Experiments and the Theories on the Water-Drive Process", *Trans.* AIME (1955) **204,** 35.
14. Craig, F. F., Jr., Sanderlin, J. L., Moore, D. W. and Geffen, T. M.: "A Laboratory Study of Gravity Segregation in Frontal Drives", *Trans.* AIME (1957) **210,** 275.

APPENDIX A

The basic reservoir equations are derived with two types of relations being considered: (1) relations governing the average flow of each phase and(2) equations of continuity. The two phases are denoted by Phase a and Phase b, with Phase b being the lighter of the two.

The vertical velocities have been assumed small while the vertical permeability has not been assumed small. Thus, from Darcy's law for small dip angles,

$$\frac{\partial p_a}{\partial y} \approx g\rho_a \quad . \quad . \quad . \quad . \quad . \quad . \quad . \quad . \quad . \quad . \quad (16a)$$

$$\frac{\partial p_b}{\partial y} \approx g\rho_b \quad . \quad . \quad . \quad . \quad . \quad . \quad . \quad . \quad . \quad . \quad (16b)$$

The following results can be obtained by integrating Eqs. 16a and 16b.

$$p_a = p_{ab} - g\rho_a Hs_b + g\rho_a y \quad . \quad . \quad . \quad . \quad . \quad (17a)$$

$$p_b = p_{ab} - g\rho_b Hs_b + g\rho_b y \quad . \quad . \quad . \quad . \quad . \quad (17b)$$

The coordinate axes are shown in Fig. 5. The velocity of the flow in the x direction at any point below the contact of the two phases is

$$v_a = -\frac{k_a}{\mu_a}\left(\frac{\partial p_a}{\partial x} - \alpha g\rho_a\right) . \quad . \quad . \quad . \quad . \quad . \quad . \quad (18)$$

Similarly, the velocity of the flow in the x direction at any point above the contact of the two phases is

$$v_b = -\frac{k_b}{\mu_b}\left(\frac{\partial p_b}{\partial x} - \alpha g\rho_b\right) . \quad . \quad . \quad . \quad . \quad . \quad . \quad (19)$$

The following results can be obtained by substituting Eqs. 17a and 17b into Eqs. 18 and 19, integrating the resulting relations over the cross section and dividing by A.

$$\bar{v}_a = -\frac{1}{\mu_a}\left[\frac{\partial p_{ab}}{\partial x} - g\rho_a \frac{\partial (Hs_a)}{\partial x} - \alpha g\rho_a\right] \int\int \frac{k_a}{A}\, da$$

$$. \quad . \quad . \quad . \quad . \quad . \quad . \quad . \quad . \quad . \quad . \quad . \quad . \quad . \quad . \quad (20a)$$

$$\bar{v}_b = -\frac{1}{\mu_b}\left[\frac{\partial p_{ab}}{\partial x} - g\rho_b \frac{\partial (Hs_b)}{\partial x} - \alpha g\rho_b\right] \int\int \frac{k_b}{A}\, da$$

$$. \quad . \quad . \quad . \quad . \quad . \quad . \quad . \quad . \quad . \quad . \quad . \quad . \quad . \quad . \quad (20b)$$

Eqs. 20a and 20b are the same as Eqs. 1a and 1b except that $1 - s_a$ replaces s_b.

For cross sections such as illustrated in Fig. 5b the permeability functions, $\bar{k}_a$ and $\bar{k}_b$, can be expressed as

$$\bar{k}_a = \int_{H(1-s_a)}^{H} \frac{(z_2 - z_1)k_a}{A}\, dy \ ,$$

and

$$\bar{k}_b = \int_{0}^{H(1-s_a)} \frac{(z_2 - z_1)k_b}{A}\, dy \ .$$

These expressions indicate that for any given flow, $\bar{k}_a$ and $\bar{k}_b$ can be expressed as functions of only s_a and x.

The equations of continuity are found by equating the rate of change of saturation with time in an elemental volume to the rate of flow into the elemental volume. The elemental volume is the volume between any two positions along the x axis separated by an elemental distance, Δx (see Fig. 6). The change in the

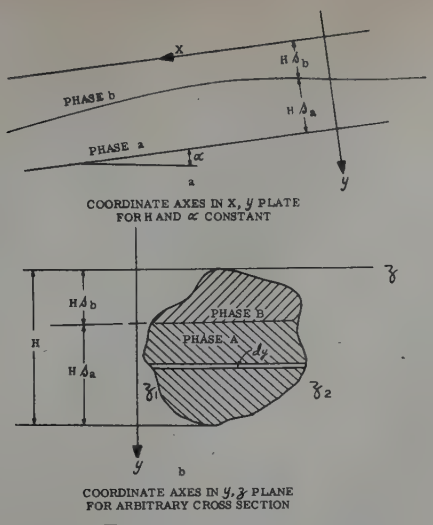
PHASE b
PHASE a
COORDINATE AXES IN X, y PLATE FOR H AND α CONSTANT
PHASE B
PHASE A
COORDINATE AXES IN y, z PLANE FOR ARBITRARY CROSS SECTION

FIG. 5—COORDINATE AXES.

amount of Phase a in the elemental volume during a small increment of time, Δt is

$$\left(\frac{\partial \bar{S}_a}{\partial t}\right) A\,\bar{\phi}\,\Delta x \Delta t \ .$$

The preceding expression must equal the difference between what flows into and out of the elemental volume during the time, Δt. In evaluating this difference, we must consider not only the volume of Phase a that flows through the two faces, but also the amount of production of Phase a during time, Δt. Taking these differences into account, the net flow into the elemental volume during time, Δt, is

$$\left[\bar{v}_a A - \left(\bar{v}_a + \frac{\partial \bar{v}_a}{\partial x}\Delta x\right)\left(A + \frac{\partial A}{\partial x}\Delta x\right)\right]\Delta t - \frac{\partial q_a}{\partial x}\Delta x \Delta t = -\left[\frac{\partial (A\bar{v}_a)}{\partial x} + \frac{\partial q_a}{\partial x}\right]\Delta x \Delta t \ .$$

The result of equating the two preceding expressions is

$$\frac{\partial (A\bar{v}_a)}{\partial x} + \frac{\partial q_a}{\partial x} = -A\,\bar{\phi}\frac{\partial \bar{S}_a}{\partial t} \ . \quad . \quad . \quad . \quad . \quad . \quad (21)$$

The equation of continuity for Phase a is Eq. 21. In a manner similar to that used in deriving the preceding equation, the equation of continuity for Phase b is

$$\frac{\partial (A\bar{v}_b)}{\partial x} + \frac{\partial q_b}{\partial x} = -A\,\bar{\phi}\frac{\partial \bar{S}_b}{\partial t} \ . \quad . \quad . \quad . \quad . \quad . \quad (22)$$

The average saturations at any point on the x axis are expressed by

$$\bar{S}_a = \frac{1}{A\,\bar{\phi}}\int\int \phi\, S_a da \ ,$$

and

$$\bar{S}_b = \frac{1}{A\,\bar{\phi}}\int\int \phi\, S_b da \ .$$

For cross sections as illustrated in Fig. 5b the preceding expressions may be reduced to

$$\bar{S}_a = \frac{1}{\bar{\phi}\,A}\left[A\,\bar{\phi}\,S_{ar} + (1 - S_{br} - S_{ar})\int_{H(1-s_a)}^{H} (z_2 - z_1)\,\phi\, dy\right],$$

and

$$\bar{S}_b = \frac{1}{\bar{\phi}\,A}\left[A\,\bar{\phi}\,S_{br} + (1 - S_{br} - S_{ar})\int_{0}^{H(1-s_a)} (z_2 - z_1)\,\phi\, dy\right].$$

Thus, the saturation functions, $\bar{S}_a$ and $\bar{S}_b$, are functions

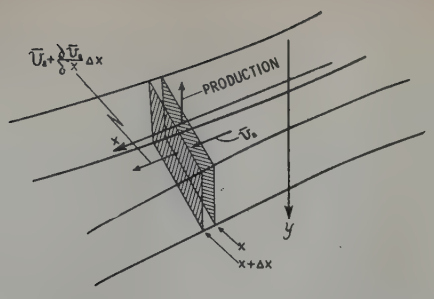

FIG. 6—ELEMENTAL VOLUME FOR RECTANGULAR CROSS SECTIONS.

of s_a and x for any given flow.

From the definition of s_a, s_b, $\bar{S}_a$ and $\bar{S}_b$ the following relations can be obtained:

$$s_a + s_b = 1 \ , \quad . \quad . \quad . \quad . \quad . \quad . \quad . \quad . \quad . \quad (23)$$

and

$$\bar{S}_a + \bar{S}_b = 1 \ . \quad . \quad . \quad . \quad . \quad . \quad . \quad . \quad . \quad . \quad (24)$$

The result of adding Eqs. 21 and 22 is

$$\frac{\partial (A\bar{v})}{\partial x} = -(1 + R_b)\frac{\partial q_a}{\partial x} . \quad . \quad . \quad . \quad . \quad . \quad (25)$$

The result of integrating Eq. 25 with respect to x is

$$\bar{v} = \frac{A_i \bar{v}_i}{A} - \frac{1}{A}\int_{x_i}^{x} (1 + R_b)\frac{\partial q_a}{\partial x}\, dx \quad . \quad . \quad . \quad (26)$$

APPENDIX B

The derivation of Eq. 13 is given, and the type of flow under consideration can be characterized by the following expression:

$$s_a = \bar{\psi}\,(\mathrm{X} - t_D) \ , \quad . \quad . \quad . \quad . \quad . \quad . \quad . \quad . \quad (27)$$

where $\bar{\psi}$ is an unknown function of $\mathrm{X} - t_D$ which is to be determined.

For the conditions of this problem Eq. 5 reduces to

$$\frac{\partial}{\partial \mathrm{X}}\left[F - B\left(\frac{H}{\alpha L}\frac{\partial s_a}{\partial \mathrm{X}} - 1\right)G\right] = -\frac{\partial s_a}{\partial t_D} \ . \quad (28)$$

The following relation can be obtained by substituting Eq. 27 into Eq. 28 and integrating the resulting relation.

$$\mathrm{X} - t_D + a_2 = \frac{HB}{\alpha L}\int_{s_{ai}}^{s_a} \frac{G}{BG + F - s_a - a_1}\, ds_a \ ,$$

$$. \quad . \quad . \quad . \quad . \quad . \quad . \quad . \quad . \quad . \quad . \quad . \quad . \quad . \quad (29)$$

where a_1 and a_2 are constants of integration.

In this example the function, s_a, varies from zero to one since Phase b completely displaces Phase a except for the immobile residual saturation of Phase a. Thus, for sections up dip of the fluid contact, $\bar{v}_a = s_a = 0$, and $\bar{v}_b = \bar{v}$. Similarly, for sections down dip of the fluid contact, $\bar{v}_b = s_b = 0$, and $\bar{v}_a = \bar{v}$. Under these conditions the constant a_1 is zero and Eq. 29 reduces to

$$s_a = \frac{\partial L}{H}\left(1 + \frac{1 - \left(\frac{\mu_a}{\mu_b}\right)\left[\frac{k_b(S_{ar})}{k_a(S_{br})}\right]}{\frac{\alpha k_b(S_{ar})\, g(\rho_a - \rho_b)}{\mu_b \bar{v}}}\right)(\mathrm{X} - t_D + a_2)$$

$$. \quad . \quad . \quad . \quad . \quad . \quad . \quad . \quad . \quad . \quad . \quad . \quad . \quad . \quad (30)$$

A relation similar to Eq. 30 can be obtained for the cases where $\bar{v}$ is negative and Phase a displaces Phase b. The types of flows are very similar to those given by Eq. 30. ★★★

The Deterioration of Miscible Zones in Porous Media

JOHN A. SIEVERT
JOHN N. DEW
MEMBER AIME
FRANCIS R. CONLEY
MEMBER AIME

CONTINENTAL OIL CO.
PONCA CITY, OKLA.

ABSTRACT

Recent literature shows that pronounced increases in oil recovery can result from the use of miscible systems in recovery operations. This literature also points out certain problems associated with maintaining miscibility, e.g., compositional changes resulting from alterations in pressure and temperature or from zone dilution. The purpose of the work described in this paper was to study miscible zones for possible use in waterflooding operations and examine the manner in which these zones break down. The fluid system selected for study was oil—tertiary-butyl alcohol—water, which, because of its narrow range of miscibility, is ideally suited for investigation in short, linear systems.

The laboratory-observed effects on oil recovery and zone stability of a number of variables are reported. Among the variables investigated were miscible zone size, viscosity ratio, length of travel, and interstitial water saturation.

Results obtained with this system show that interstitial water adversely affects recoveries because of premature phase break. Salinity of the water further aggravates this situation. This effect, although pronounced for this system, would probably occur in any fluid system containing an alcohol. As expected, viscosity ratio has a decided influence on recovery efficiency and zone stability. The results also show that use of a sufficient zone size, even though the system has poor phase characteristics, yields higher oil recoveries than are obtained from straight water floods. Length-of-travel studies showed a square root relationship between zone growth and path length for favorable viscosity ratios. No such clear-cut dependence was observed under unfavorable viscosity conditions.

INTRODUCTION

As new oil reserves have become increasingly more difficult and expensive to find and develop, the oil industry has devoted more and more time and money to finding more efficient methods for exploiting known reserves. The increasing number of water floods is one manifestation of this attempt to improve oil recoveries from existing fields. Since considerable quantities of oil are by-passed by the waterflood process, it is only a partial answer to the problem. The search continues.

Of late, several proposed processes have received the critical attention of investigators. Among them are gas drives, in situ thermal reactions and miscible displacements. The present paper is concerned with miscible displacements in conjunction with water floods.

Recent literature[1-7] reports that, under proper conditions, oil recoveries from LPG floods, propane sweeps, condensing gas drives, etc., approach 100 per cent of the oil in place in the region contacted by the flood. This literature also points out some of the problems associated with these processes, one of the main ones being the maintaining of miscibility. Compositional changes resulting from pressure and temperature variations or from zone dilution give rise to phase breaks and loss of miscibility, the conclusion being that, after loss of miscibility, much of the beneficial influence of the zone is lost.[2] The results of the subject work show that, if sufficient zone material exists ahead of a phase interface, considerable improvement in oil recovery can be obtained.

In order to increase our understanding of the behavior of miscible systems as they degenerate into immiscible processes, a laboratory system having rapid deterioration characteristics was needed. The fluid system oil—*tertiary*-butyl alcohol (TBA)—water possesses these properties and was the system investigated.

Although these fluids are different from those generally employed in miscible studies, an understanding of their behavior can be applied to other miscible slug processes. However, under conditions where mass transfer maintains a miscible system through multiple contacts, e.g., enriched gas drive or high pressure gas drive, the observed behavior of alcohol zones would not be applicable.

The variables of interest were zone size, viscosity ratio, length of travel, initial water saturation, rate and core characteristics. Of these, only the effects of the following on zone breakdown and oil recovery are reported in detail: (1) zone size, (2) path length, and (3) initial water saturation. The effects of viscosity ratio and core characteristics are discussed in conjunction with other variables. Although initial water saturation is not envisioned as important to the phase behavior of hydrocarbon systems, e.g., LPG, it is important in alcohol systems.

The properties of the fluids and cores used are given in Table 1. As previously stated, this fluid system was selected because of the limited range of miscibility

Original manuscript received in Society of Petroleum Engineers office Aug. 7, 1957. Revised manuscript received June 12, 1958. Paper presented at 32nd Annual Fall Meeting of Society of Petroleum Engineers in Dallas, Tex., Oct. 6-9, 1957.

[1]References given at end of paper.

of the three components. Although the oil and TBA and the TBA and distilled water are miscible in all proportions, a mixture of the three requires high concentrations of TBA to insure complete miscibility.

To increase the viscosity of the water, cane sugar was added. The presence of sugar alters the phase properties from those of pure water. At low concentrations of sugar solution and high concentrations of TBA, solid sugar is precipitated. As the concentration of sugar solution is increased, a point is finally reached at which the TBA and sugar solution become immiscible. The precipitated sugar then redissolves in the lower or aqueous layer. When the water concentration becomes sufficiently large, a region of limited solubility is again encountered. Fig. 1 illustrates these various aspects of the phase behavior for the fluid combinations used in the study. The phase diagram for a light Frio crude with distilled water is also shown for comparison. The presence of salt in the water causes further reductions in miscibility. This limited miscibility made possible the use of short, linear cores, since long travel paths were not necessary to obtain and observe zone breakdown.

EXPERIMENTAL

The several phases of the experimental program discussed herein were carried out by conducting vertical floods at a constant rate of 436 cm/day (14.3 ft/day) in consolidated Alundum cores fitted with Lucite header caps to permit observation of the core faces. The cores were initially 100 per cent oil saturated except for three floods which contained an initial water saturation. After each flood the cores were cleaned and their weight and air permeability checked prior to resaturation. The samples from each flood were analyzed by a refractometric method. Those samples which contained water were saturated with salt to effect an essentially quantitative separation between TBA and water prior to analysis. These data could be translated into oil recovery and zone growth behavior as functions of the specific variable studied.

RESULTS AND DISCUSSION

Results of the experiments will be discussed according to the variable of interest for both favorable and unfavorable viscosity ratios as it affected oil recovery and zone growth. A favorable viscosity ratio is defined as one in which the ratio of the viscosity of the displaced liquid to the viscosity of the displacing liquid is less than unity for both mixing regions, i.e., $\mu_o < \mu_{TBA} < \mu_w$. An unfavorable viscosity ratio is one in which the ratio of displaced-fluid viscosity to displacing-fluid viscosity is greater than unity, or $\mu_o > \mu_{TBA} > \mu_w$. As can be seen in Table 1, the viscosity levels, and hence the viscosity ratios, were held constant for all floods with favorable ratios. The same is true of the viscosity levels and ratios for all floods having unfavorable viscosity ratios.

It should be emphasized that the values in the results, such as pore volumes and lengths, cannot be directly transferred to field conditions. They apply only to the system used.

Effect of Zone Size on Oil Recovery

The limited literature[8,9] available on TBA slug displacements reports that zone size has an important effect on oil recovery; however, these investigations were of small zones over a narrow range. The data were further complicated by the presence of an initial water saturation. In order to extend the range of zone sizes and reduce the number of variables in any given run, floods with zone sizes ranging up to 1.27 pore volume (PV) were performed with no initial water

TABLE 1—PROPERTIES OF FLUIDS AND CORES USED DURING THE INVESTIGATION

PROPERTIES OF FLUIDS

	Favorable Combination			Unfavorable Combination		
	Oil	Tech. TBA	H_2O	Oil	Tech. TBA	Distilled H_2O
Per cent composition (wt)	5 per cent Nujol — 95 per cent Kerosene	100	41 per cent Sugar — 59 per cent Water	48 per cent Nujol — 52 per cent Kerosene	100	100
Density (gm ml^{-1})	0.80	0.78	1.18	0.83	0.78	0.99
Viscosity (cp at 25° C)	1.62	4.22	6.03	6.05	4.22	0.89
Viscosity ratio (μDisplaced)						
(μDisplacing)	0.38	0.70		1.43	4.74	

PROPERTIES OF CORES

Core number	Porosity in per cent	Pore volume (ml)	K_{air} in (md)	Diameter (cm)	Length (cm)
7917-SC2	20.8	152	237	5.50	30.7
7917-SC3	21.1	154	243	5.50	30.7
7919-SC1	25.3	314	373	5.08	61.2
7919-SC1—A	26.0	54.2	380	5.08	10.3
—B	25.4	259	362	5.08	50.4
—C	25.5	210	368	5.08	40.7
—D	25.4	157	368	5.08	30.5
—E	25.6	27.0	381	5.08	5.18
—F	25.6	106	367	5.08	20.4

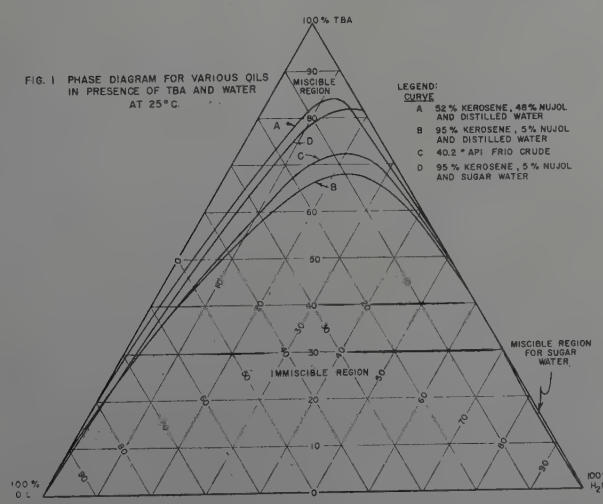

FIG. 1 PHASE DIAGRAM FOR VARIOUS OILS IN PRESENCE OF TBA AND WATER AT 25°C.

Fig. 1—Phase Diagram for Various Oils in Presence of TBA and Water at 25°C.

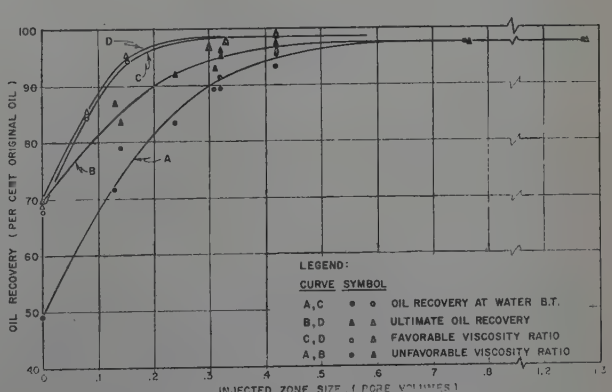
OIL RECOVERY (PER CENT ORIGINAL OIL)
INJECTED ZONE SIZE (PORE VOLUMES)
LEGEND:
CURVE SYMBOL
A,C • ○ OIL RECOVERY AT WATER B.T.
B,D ▲ △ ULTIMATE OIL RECOVERY
C,D ○ △ FAVORABLE VISCOSITY RATIO
A,B • △ UNFAVORABLE VISCOSITY RATIO

Fig. 2—Oil Recoveries as Functions of Initial Zone Size in a 30.7-cm Core for Favorable and Unfavorable Viscosity Ratios.

saturation. The water breakthrough and ultimate oil recoveries obtained from these floods using a 30.7-cm core are plotted as functions of zone size in Fig. 2.

FAVORABLE VISCOSITY RATIOS

As can be seen in Fig. 2, decreasing the zone size for favorable viscosity ratios had the effect of decreasing the ultimate oil recovery when the initial slug sizes were smaller than 0.30 PV. At sizes greater than this, little increase in ultimate oil recovery was observed with increased zone size.

For zone sizes larger than 0.30 PV, the ultimate recoveries, which approached 100 per cent of the oil in place, were obtained prior to water breakthrough. As the zone size was decreased from 0.30 PV, the behavior was similar to that observed for water floods with favorable viscosity ratios; namely, after water breakthrough oil production virtually ceased, leaving a residual oil saturation. This residual oil saturation increased with decreasing zone sizes until the residual of a water flood was obtained at an initial zone size 0.0 PV.

The observed separation and decline of these two curves at zone sizes smaller than 0.30 PV are interpreted to mean that the amount of TBA present was insufficient to traverse the path length of 30.7 cm and still maintain a buffer region containing sufficient TBA to prevent a phase break. That a phase break occurred at these zone sizes is supported by other evidence, namely, that at the time of water breakthrough, the water appeared as a separate phase at the outlet face and that the over-all composition of the effluent at water breakthrough was such that it fell within the immiscible region shown in Fig. 1. This same general behavior pattern was observed with unfavorable viscosity ratios except that subordinate oil production after water breakthrough played a more dominant role in determining the ultimate recovery values.

UNFAVORABLE VISCOSITY RATIOS

Fig. 2 also shows a plot of oil recovery as a function of zone size with the unfavorable fluid combination. At zone sizes below 0.6 PV, the oil recovery at water breakthrough became less than the ultimate recovery. This difference became greater as zone sizes were decreased until the recovery from a typical water flood was obtained at zero zone size. Ultimate oil recovery did not decline until the zone size became smaller than 0.5 PV, implying that increased recovery can be obtained even though phase break occurs if a sufficient quantity of slug material is injected to permit the existence of a substantial oil-alcohol mixing region ahead of the interface formed by the phase break. The observed differences between ultimate oil recovery and recovery at water breakthrough for zone sizes smaller than 0.6 PV are attributed to a phase break. Such a phase break should result in changes in the zone growth parameters at or near these same zone sizes.

EFFECT OF ZONE SIZE ON GROWTH

In order to describe the physical growth of the zone, certain zone parameters were defined (these quantities are listed at the end of the paper under Nomenclature). It will be noted that in this list, as well as in Fig. 3, the quantities are defined in terms of the 90 per cent and 10 per cent concentrations in the effluent. These points were used because the tails on the composition vs volume curves made it very difficult to measure the point at which the concentration of a given component reached 0 per cent or 100 per cent.

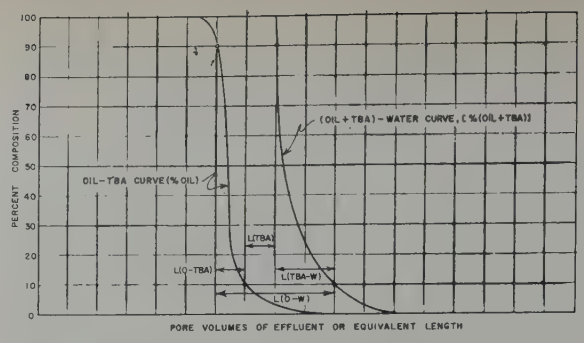

FIG. 3—ILLUSTRATION SHOWING THE DETERMINATION AND MEANING OF THE ZONE GROWTH PARAMETERS.

The numerical value of a given parameter was obtained by a difference method. An example will best serve to illustrate the method. Assume that one is trying to find the length of the oil-TBA mixing region, $L_{(O\text{-}TBA)}$, for a particular flood. This length lies between the 90 and 10 per cent oil concentration in the effluent. From a plot of composition vs volume of effluent, such as is typified by Fig. 3, the volume of effluent collected between the arrival of the selected compositions at the outlet face can be determined. By applying the appropriate factors, this volume difference can be converted to a length termed $L_{(O\text{-}TBA)}$.

It should be mentioned that in the case of small initial zone sizes the 10 per cent water concentration appeared in the effluent before the 10 per cent oil concentration. This resulted in negative values for the length of the TBA zone, $L_{(TBA)}$. The negative values have no meaning other than that the TBA zone was consumed and they give some measure of the penetration by the water phase into the oil-TBA region. It should also be pointed out that the viscosity gradients between any two components are constantly changing even when miscibility is maintained. In addition, when a phase break occurs, there is a sharp and abrupt change in the viscosity gradients. The size of the samples collected precluded measurement of these changes. Separate viscosity determinations carried out under equilibrium conditions indicate that these changes could be quite severe.

FAVORABLE VISCOSITY RATIOS

In Fig. 4 are plots of the various growth parameters for this series of floods. This figure shows that the curve for $L_{(TBA)}$ assumed negative values at zone sizes smaller than 0.19 PV. In addition, the curves for $L_{(O\text{-}TBA)}$; the length of the water-TBA region, $L_{(TBA\text{-}W)}$; the over-all length, $L_{(O\text{-}W)}$; and the change in over-all length, $\Delta L_{(O\text{-}W)}$, all show a change in slope near a zone size of 0.20 PV.

Any explanation of this behavior must take into account the fact that the curves for these quantities as functions of zone size all exhibit a change in behavior at or near the same zone size. In view of the phase behavior of the system, the negative nature of $L_{(TBA)}$ at zone sizes below 0.19 PV, the decline in ultimate oil recovery at zone sizes smaller than 0.30 PV, and the observance of two phases on the core face at water breakthrough, it was concluded that the observed

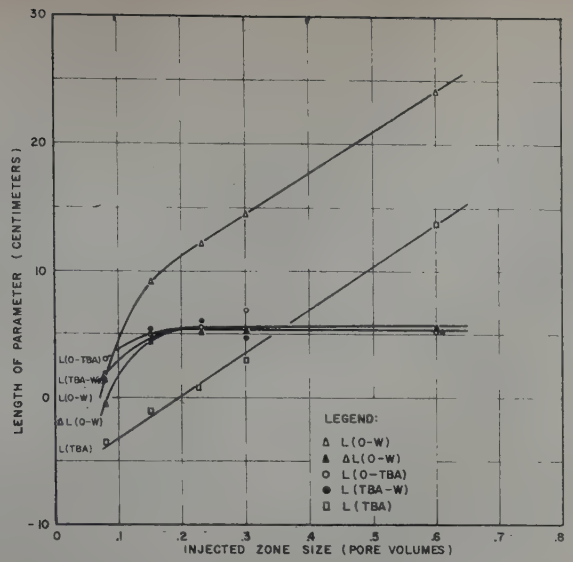

FIG. 4—ZONE PARAMETERS AS FUNCTIONS OF INITIAL ZONE SIZE FOR A 30.7-CM CORE AND FAVORABLE VISCOSITY RATIO.

changes were caused by a phase break with the resultant formation of an interface. A critical minimum zone size therefore exists below which miscibility cannot be maintained throughout the path length flooded. The oil recovery at zone sizes below this critical one then becomes a function of both a miscible-type and of an immiscible-type displacement and the path length over which each type is controlling. This is consistent with the observed decline in oil recoveries at the smaller zone sizes. A subordinate production due to a flushing action accounts for the small but definite separation between the ultimate-oil-recovery and oil-recovery-at-water-breakthrough curves.

Any mathematical expression for this balance between the two mechanisms will have to account for the benefits which may accrue from the oil-TBA mixing region ahead of the interface.

UNFAVORABLE VISCOSITY RATIOS

The same growth parameters were studied for unfavorable viscosity conditions and are plotted in Fig. 5. This figure shows that $L_{(TBA)}$ became negative at a zone size of 0.55 PV. The curves for $L_{(O-W)}$, $\Delta L_{(O-W)}$, and $L_{(TBA-W)}$ all show a change in slope near a zone size of 0.6 PV. This is the same zone size at which oil recovery at water breakthrough began declining with zone size decreases. All of this evidence shows the occurrence of a phase break at some zone size between 0.5 and 0.6 PV.

SUMMARY OF ZONE SIZE EFFECT

It was observed that a close agreement existed between the zone sizes at which growth parameters exhibited changes; those at which oil recoveries began declining, and those at which phase break was observed at the outlet face of the core. These changes reflect the effects of a phase break, and this is true for both favorable and unfavorable viscosity ratios. The results further show that a phase separation in the trailing edge of the zone does not result in a pronounced decrease in ultimate oil recovery until the zone size becomes so small that little or no oil-TBA region exists ahead of the phase-break-created interface.

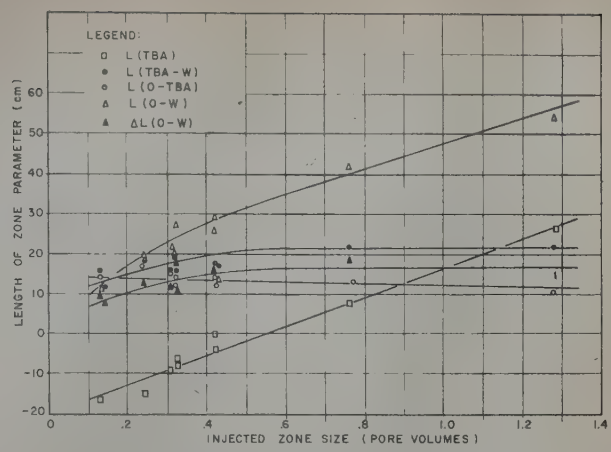

FIG. 5—GROWTH OF ZONE PARAMETERS AS FUNCTIONS OF INITIAL ZONE SIZE FOR A 30.7-CM CORE AND UNFAVORABLE VISCOSITY RATIO.

EFFECT OF PATH LENGTH ON OIL RECOVERY AND ZONE GROWTH

Once the effects of zone size were established, the zone growth as a function of path length was investigated. This was done to determine how the critical zone size changes with travel distance. To observe this growth, a zone size was chosen which, for favorable viscosity ratios, should have resulted in a phase break at approximately 55 cm of path length if the square root growth law predicted by von Rosenberg[10] is valid.

FAVORABLE VISCOSITY RATIOS

A constant-volume zone size was chosen for study at four path lengths with the same favorable viscosity ratios and levels as were used in the zone size studies. This constant volume zone would have had a length of 11.6 cm if no growth occurred. The various path lengths were obtained by successively cutting sections from an original 61.2-cm core. Oil recovery as a function of path length for these conditions is listed in Table 2. As expected, the table shows that the ultimate oil recovery and the oil recovery at water breakthrough were equal at all path lengths.

The growths of the zone parameters as functions of path length for these conditions are plotted in Fig. 6. In this figure, the curves are growth curves predicted on the basis of a square root dependence of zone growth on path length. Except for the curves for $L_{(O-W)}$ and $L_{(TBA)}$ the predicted curve for each growth parameter was obtained by multiplying the average experimental value of that parameter as observed at the 5.18-cm length by the square root of the ratio of the new path length to 5.18 cm. The predicted curve for $L_{(O-W)}$ was obtained by adding the initial zone size to the predicted value of $\Delta L_{(O-W)}$ computed as described. The predicted curve for $L_{(TBA)}$ was obtained by summing one-half of the predicted values of $L_{(O-TBA)}$ and $L_{(TBA-W)}$ at

TABLE 2—OIL RECOVERY AS A FUNCTION OF PATH LENGTH WITH FAVORABLE FLUID COMBINATION AND CONSTANT VOLUME ZONE

Path length (cm)	Fractional Pore volume of zone	Oil Recovery: Water breakthrough (per cent original oil) Experimental	Water breakthrough Average	Ultimate (per cent original oil) Experimental	Ultimate Average
5.18	2.21	98.9	97.4	98.9	97.4
		95.8		95.8	
10.4	1.10	99.4	98.0	99.4	98.0
		96.6		96.6	
30.5	0.38	99.9	100.0	99.9	100.0
		100.0		100.0	
61.2	0.19	99.2	97.3	99.2	97.3
		95.4		95.4	

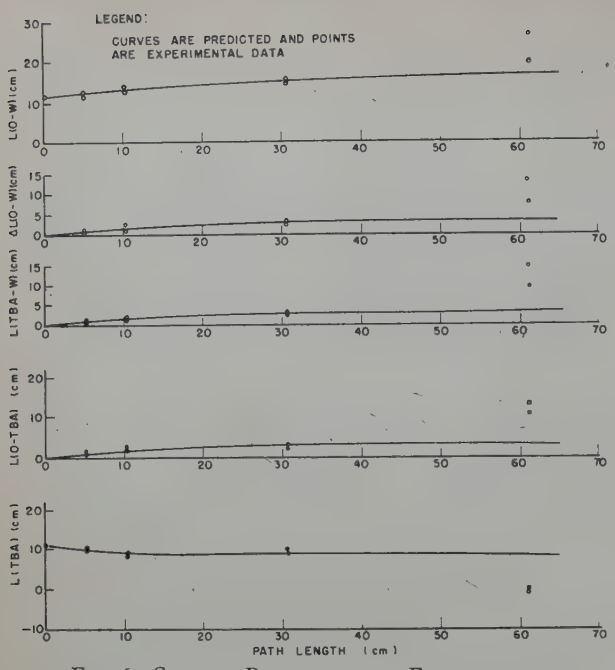

FIG. 6—GROWTH PARAMETERS AS FUNCTIONS OF PATH LENGTH FOR A CONSTANT VOLUME ZONE, FAVORABLE VISCOSITY RATIO AND CONSTANT INJECTION RATE.

any given path length and subtracting this sum from the initial zone length.

The experimental data points fit the predicted curve quite well for path lengths up to 30.5 cm., inclusive. The experimental data exhibit a positive deviation from the predicted values at 61.2 cm of length. It will be noted that the value for $L_{(TBA)}$ is negative at this path length, meaning that the buffer zone is gone and that oil and water dissolved in TBA have contacted and a phase separation has occurred.

That a phase break occurred at this longest path length (61.2 cm) is further substantiated by the fact that water appeared as a separate phase on the outlet face of the core at water breakthrough. Because the study of initial zone size effects showed that when two phases appeared in the effluent the over-all composition was in the immiscible region of the phase diagram, no composition calculations were performed for the path-length study.

In the discussion of zone size effects, it was shown that, for the 30.7-cm core, the zone underwent a phase separation at an initial zone size of 0.30 PV at these same favorable viscosity ratios. Assuming that the square root law is applicable to the minimum zone size necessary to maintain an intact zone, the path length at which zone breakdown would be expected would be 55.2 cm. The indications are that, since $L_{(TBA)}$ was slightly negative (-0.02 cm) at 61.2 cm, conditions were such that a phase break occurred at a path length slightly shorter than 61.2 cm.

In summarizing the effects of path length for the favorable viscosity conditions, we concluded that for the zone approximating the critical size the phase break occurred too late in the life of the flood to have a pronounced influence on ultimate oil recovery value for the path length used. If cores longer than 61.2 cm had been flooded with this initial zone size (11.6 cm), oil recoveries would have been expected to decline. Once phase break occurred, the rate of deformation of the zone increased above the square root growth rate

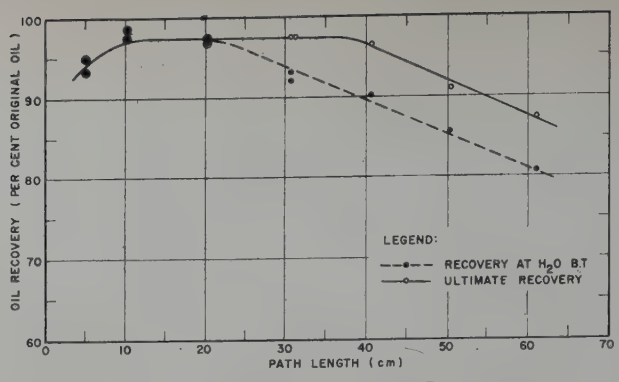

FIG. 7—OIL RECOVERY VS PATH LENGTH FOR CONSTANT VOLUME ZONE, UNFAVORABLE VISCOSITY RATIO AND CONSTANT RATE.

observed when miscibility was maintained throughout. The critical zone size required is proportioned to the square root of path length for a linear system with favorable viscosity ratios.

UNFAVORABLE VISCOSITY RATIOS

Fig. 7 shows the effect of path length on oil recovery for a constant volume zone with unfavorable viscosity ratios. Again, the same fluids were used in this study as were used in the study of zone size for unfavorable viscosity ratios. The length of this zone in the cores would have been 11.6 cm if no growth had occurred. Seven path lengths were used in this study. For short path lengths, the curves for oil recovery at water breakthrough and ultimate recovery are identical. Their mutual curve, as a function of path length, attains a maximum of 97.5 per cent at about 10 cm of length. Why the oil recovery curves should show a maximum at this path length is not at all obvious. It could be that the low pressures encountered with the 5.18-cm core ($P < 2$ psig) were not sufficient to cause the TBA to enter the inlet face at all points and that, once a finger of TBA broke through, most of the TBA followed this path, thereby by-passing some oil near the inlet face. In other words, fingering effects had become important. Very little oil had to be by-passed at this short path length to cause an appreciable decrease in the per cent oil recovered. The decrease in oil recovery at 5.18 cm shown in Fig. 7 was about 4 per cent of the oil in place, which is equivalent to the loss of 1.1 cc. At path lengths greater than 20 cm, the curves are separate, the curve for oil recovery at water breakthrough declining much more rapidly than the curve for ultimate oil recovery until a path length of 40 cm is attained. At this length, the curves appear to become parallel. It is expected that they would continue to decline with increasing path length, asymptotically approaching waterflood recoveries as a limit, since for an infinite path length any finite zone injected would be no more effective than a water flood.

Fig. 8 is a plot of the zone parameters as functions of path length for these viscosity conditions. It is noted that $L_{(TBA)}$ assumes negative values at a path length of 24 cm. Because of the tails on the composition curves below the 10 per cent composition points, the agreement between this value and the 20-cm path length at which incipient decline in oil recovery at water breakthrough occurs is considered good. The curves for $L_{(O-W)}$, $\Delta L_{(O-W)}$, and $L_{(TBA-W)}$ undergo a decrease in slope at a path length between 20 and 30 cm. The slope of the $L_{(O-TBA)}$ curve remains relatively uniform over the range of path lengths studied.

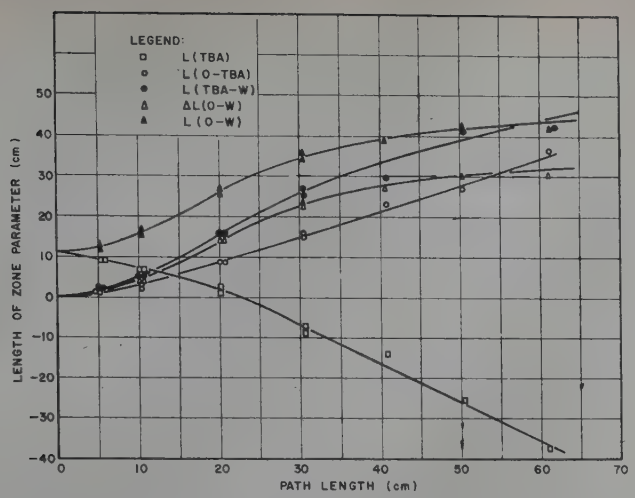

FIG. 8—ZONE PARAMETERS AS FUNCTIONS OF PATH LENGTH FOR UNFAVORABLE VISCOSITY RATIO AND CONSTANT RATE.

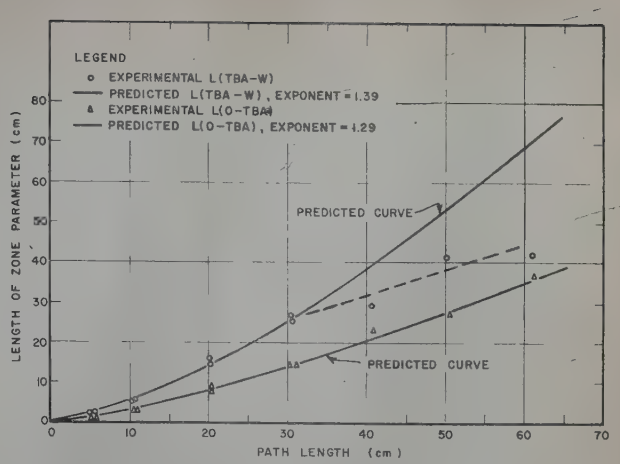

FIG. 9—FIT OF EXPERIMENTAL $L_{(O-TBA)}$ AND $L_{(TBA-W)}$ VALUES TO PREDICTED GROWTH CURVE FOR UNFAVORABLE VISCOSITY RATIO AND CONSTANT RATE.

An attempt to determine the dependency between the zone growth parameters and path length was made, since no known theoretical treatment for zone growth behavior under unfavorable viscosity conditions exists. It was found that a log-log plot of zone parameter vs path length resulted in a straight line with the exception of the last few points on the log $[L_{(TBA-W)}]$ curve. These points are for path lengths where phase break is expected. The slope for the oil-TBA curve was found to be 1.29, while the TBA-water curve had a slope of 1.39 in the miscible region.

Using these slopes as exponents for the path-length ratios, we predicted growth curves for each mixing region, as shown in Fig. 9. The experimental points for $L_{(O-TBA)}$ fit this predicted curve quite well; however, for path lengths greater than 30 cm, the data points for $L_{(TBA-W)}$ depart radically from the predicted curve. A curve drawn through these non-conforming points (dashed curve in Fig. 9) intersects the predicted curve at a path length of 30 cm. A similar treatment for $\Delta L_{(O-W)}$ showed its slope in a log-log plot against path length to be 1.53 and the intersection of a curve drawn through the non-conforming points with the predicted curve to be at 28.4 cm. These two values are considered to be in good agreement with the 25-cm length at which $L_{(TBA)}$ became zero. Because of the unfavorable viscosity ratios, these values are also in fair agreement with the 20-cm path length at which a separation between the oil-recovery-at-water-breakthrough curve and the ultimate-oil-recovery curve occurred. In the previous discussion, it was noted that such a separation occurred when phase break occurred. In this particular series of runs, phase separation was not observed at the 20-cm path length; but two phases were observed at the 30.5-cm path length. Hence, somewhere between these two path lengths a phase break occurred.

In the study of zone size effects, it was found that approximately 0.6 PV of zone material was necessary to maintain miscibility for a path length of 30.7 cm. By using the growth exponents determined from this series of floods, one can calculate that phase break should have occurred at about 25 cm of path length for the constant volume zone used in these floods. In view of this agreement, the observed behavior is attributed to a phase break in the trailing edge of the oil-TBA mixing region. The decrease in ultimate oil recovery was not coincident with the phase break, as was also observed in the zone size studies. The reason for this is that an appreciable mixing zone of oil and TBA exists ahead of the phase interface for zone sizes near the critical one.

These findings have implications in applications of similar processes. Since phase break in the trailing edge results in a relatively decreased rate of over-all zone growth under unfavorable viscosity conditions, it may be desirable to inject a slug of sufficient size to permit a substantial mixing zone to exist ahead of the phase-break-created interface but not necessarily sufficient to maintain complete miscibility throughout the entire displacement distance. Favorable viscosity ratios are still desired, since, in a linear flood at least, the fractional pore volume of material necessary to maintain miscibility decreases as distance increases. The growth of a mixing region in the systems observed was a function of the viscosity ratio between the components when that ratio was unfavorable. This conclusion is based upon the observation that the exponent of path length was different for each mixing region, that region having the more unfavorable viscosity ratio also having the larger exponent. This was not observed with favorable viscosity ratios.

Because of the phase characteristics of the system, the effects of an initial water saturation should play a dominant role in controlling the displacement efficiency. This facet of the process was investigated in three floods.

EFFECT OF INITIAL WATER SATURATION ON OIL RECOVERY AND ZONE GROWTH

The effect of initial water saturation (S_{wi}) on oil recovery is listed in Table 3. In this table, three runs with no S_{wi} are compared with the three runs which

TABLE 3—COMPARISON OF OIL RECOVERIES[1] AND ZONE STRETCHING OBTAINED FROM THE SAME CORE FOR EQUAL ZONE SIZES AND RATES WITH AND WITHOUT AN INITIAL WATER SATURATION

S_{wi} = 0.4 PV			S_{wi} = 0.0 PV		
Per cent oil recovery			Per cent oil recovery		
TBA breakthrough	Ultimate	$\Delta L_{(O-W)}$ / L	TBA breakthrough	Ultimate	$\Delta L_{(O-W)}$ / L
67.5	72.0	2.54	67.2	95.1	1.13
74.8	77.3	3.42	66.6	96.2	1.79
76.1	78.0	3.05	70.3	92.8	1.26
Average 72.8	75.8	3.00	68.0	94.7	1.39

[1]Oil recoveries are expressed as per cent of original oil in place.

had an S_{wi} of 0.4 PV, which was the only saturation studied. All other conditions were equal. Clearly, the effect of S_{wi} is to reduce the efficiency of the zone. The average recovery at TBA breakthrough was 72.8 per cent or 4.8 per cent higher when a S_{wi} existed than when none existed, but the average ultimate recovery dropped to 75.8 per cent vs 94.7 per cent when no water was initially present.

In order to explain these observations, it is necessary to mention two results obtained from indirectly related experiments. The first of these is that, when two phases exist, the TBA concentration is higher in the water phase than in the oil phase.[8] The second is that TBA is preferentially absorbed from the oil phase by Alundum. The increase in oil recovery at TBA breakthrough is a result of the combination of these two effects which act to increase the oil saturation ahead of the interface. Behind the interface is a solution of TBA in water. Very little dissolved oil is present, and oil production ceases.

The decrease in ultimate oil recovery from that obtained when no S_{wi} existed is due to the fact that both oil and water are immediately contacted by the TBA; and after only a very short distance has been traversed, phase separation occurs in the leading edge of the zone. Hence, the previously suggested oil recovery balance between immiscible and miscible displacement processes is highly in favor of the immiscible-type displacement. The net result is an ultimate oil recovery only slightly better than the 71 per cent obtained from a water flood.

Because the study of individual growth parameters was precluded by interstitial water production, the fractional zone stretching, $\frac{\Delta L_{(O\text{-}W)}}{L}$, was used as the measure of growth. When no water was present this ratio had a value of 1.39. When an initial water saturation existed this value increased to 3.00 or it more than doubled. The increase was caused by the fingering and flushing resulting from the formation of an interface.

Effect of Viscosity Ratio and Core Characteristics on Zone Growth

The effect of viscosity ratio on zone growth is illustrated in Fig. 10, where it is shown that for a constant path length, favorable viscosity ratios, as defined earlier, gave rise to a constant growth which was independent of viscosity ratio over the range investigated but which appeared to depend upon core characteristics. Fig. 10 is a plot of $L_{(O\text{-}TBA)}$ and $L_{(TBA\text{-}W)}$ vs log (viscosity ratio)

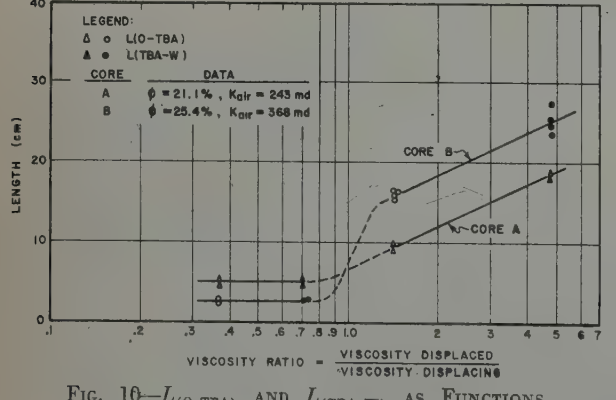

Fig. 10—$L_{(O\text{-}TBA)}$ and $L_{(TBA\text{-}W)}$ as Functions of Viscosity Ratio for Two Cores of Equal Length and Flooded at Equal Rates.

for two different cores of equal length and for zone sizes large enough to eliminate phase break. When the viscosity ratio became greater than unity, $L_{(O\text{-}TBA)}$ and $L_{(TBA\text{-}W)}$ exhibited different growth values which depended upon the viscosity ratios. The separation between the two curves occurred because of differing core characteristics. Assuming that the curves in Fig. 10 remain linear throughout the unfavorable region, one may determine that the length of a mixing region for unfavorable viscosity ratios is given by:

$$L = C + 18.1 \log \frac{\mu \text{ displaced}}{\mu \text{ displacing}},$$

where L is the length of the mixing region in centimeters and C is a constant whose value depends upon the particular core characteristics.

Many authors have reported no significant effect of pore geometry on miscible displacements. If this is true, then C should be a universal constant; however, Fig. 10 shows that it is not, since the extrapolations of the two curves in the unfavorable viscosity region intersect the ordinate for a viscosity ratio of unity at different points. Other work done at this laboratory substantiates that porous medium type has a significant effect on the behavior of miscible displacements. These discrepancies point out the need for further effort devoted to determining core effects.

In essence, what is yet needed is enough data to establish the critical zone size for a wide range of viscosity ratios as a function of path length and core characteristics. This would result in a family of curves, since the results of this study indicate that each viscosity ratio in the unfavorable region will yield a different growth exponent, which in turn will determine to what power the path-length ratio must be raised in the mathematical treatment of zone growth.

CONCLUSIONS

The following conclusions based on results obtained from linear miscible-zone displacements in short, cylindrical Alundum cores, are not necessarily applicable to field operations; they apply specifically to the systems used.

1. For a constant path length, zone size has an effect on oil recovery efficiency for sizes smaller than the critical one at which phase break occurs.
2. The ultimate recovery at zone sizes less than the critical size is a composite of that from an immiscible displacement and that from a miscible displacement.
3. The efficiency and zone stability and hence the critical zone size necessary to maintain miscibility are dependent upon viscosity ratio, path length, phase properties of the fluids and core characteristics.
4. At the viscosity level studied, the effect of viscosity on the growth of the mixing regions (oil-TBA and TBA-water) for a constant path length is negligible when the viscosity ratios are favorable, the amount of growth being a function of the core and fluid characteristics.
5. At the viscosity levels used, the growth of the mixing regions is dependent upon viscosity ratios, core characteristics, and fluid characteristics when the viscosity ratios are unfavorable. The more unfavorable the ratio, the greater is the growth for a given path length.
6. For given core characteristics, zone growth shows a square root dependence upon path length when viscosity ratios are favorable for the short-path lengths

studied. When they are unfavorable, the dependence upon path length is greater than the one-half power; the exact dependence being related to the viscosity ratio. For systems studied, it was greater than unity.

7. In the system studied, the deterioration of the zone was hastened by the presence of an initial water saturation, which, because of the phase behavior of the system, caused a phase break in the leading edge of the zone.

8. Deterioration of the trailing edge of a zone does not necessarily result in a decrease in ultimate oil recovery. An appreciable decrease is observed in those cases where zone breakdown occurs so early in the life of the flood that a substantial solvent-oil region cannot exist ahead of the phase-break-created interface.

ACKNOWLEDGMENTS

The authors express their appreciation to Stanley Frankel for his helpful comments and suggestions, to Byron Dyche for performing the experiments, and to the management of Continental Oil Co. for permission to present this paper.

NOMENCLATURE

L = calculated length a zone would occupy in a porous medium if no mixing occurred, cm

$L_{(O\text{-}TBA)}$ = length between the 90 per cent oil-10 per cent TBA and 10 per cent oil-90 per cent TBA concentrations in the effluent as measured at the outlet face, cm

$L_{(TBA\text{-}W)}$ = length between the 10 per cent water-90 per cent (oil + TBA) and 90 per cent water-10 per cent (oil + TBA) concentration points in the effluent as measured at the outlet face, cm

$L_{(O\text{-}W)}$ = length between the 90 per cent oil-10 per cent TBA and 90 per cent water-10 per cent (oil + TBA) concentration points in the effluent as measured at the outlet face, cm

$\Delta L_{(O\text{-}W)} = L_{(O\text{-}W)} - L$, cm

$L_{(TBA)}$ = length between the 10 per cent oil-90 per cent TBA and 10 per cent water-90 per cent (oil + TBA) concentration points in the effluent as measured at the outlet face, cm

REFERENCES

1. Jenks, Loren H., Campbell, John B. and Binder, George G., Jr.: "A Field Test of the Gas-Driven Liquid Propane Method of Oil Recovery", *Trans.* AIME (1957), **210**, 34.
2. Koch, H. A., Jr. and Slobod, R. L.: "Miscible Slug Process", *Trans.* AIME (1957) **210**, 40.
3. Hall, H. N. and Geffen, T. M.: "A Laboratory Study of Solvent Flooding" *Trans.* AIME (1957) **210**, 43.
4. Stone, H. L. and Crump, J. S.: "The Effect of Gas Composition Upon Oil Recovery by Gas Drive", *Trans.* AIME (1956) **207**, 105.
5. Morse, R. A.: "Recovery of Oil from Reservoirs", German Pat. No. 849534, Stanolind Oil and Gas Co., (July, 1952).
6. Morse, R. A., *et al*: "Secondary Recovery", U. S. Pat. No. 2,742,089, Stanolind Oil and Gas Co. (April 17, 1957).
7. Offeringa, J. and van der Poel, C.: "Displacement of Oil from Porous Media by Miscible Liquids", *Trans.* AIME (1954) **201**, 310.
8. Paulsell, W. G.: "The Effect of a Mutually Miscible Intermediate Phase on Immiscible Fluid Displacement in a Porous Media", MPE Thesis, U. of Oklahoma (1953).
9. Jones, R. F.: "Effects of Viscosity and Rates on Miscible Liquid Displacements in a Porous Medium", MPE Thesis, U. of Oklahoma (1954).
10. von Rosenberg, D. U.: "Mechanics of Steady State Single-Phase Fluid Displacement from Porous Media", *Jour.* AIChE (March, 1956) **2**, 55. ★★★

Field Results of South Belridge Thermal Recovery Experiment

C. F. GATES
MEMBER AIME
H. J. RAMEY, JR.
JUNIOR MEMBER AIME

GENERAL PETROLEUM CORP.
SANTA FE SPRINGS, CALIF.

ABSTRACT

Results of a field research project on the thermal recovery of oil by movement of a combustion front are presented. This field test was conducted in the South Belridge field, Calif. The test pattern was a single 2.5-acre five-spot pattern in the 700-ft deep Tulare sand.

Results of this project indicate the technical feasibility of producing high viscosity, low-gravity crude oils by thermal means. It was demonstrated that heavy oils could be moved rapidly over considerable distances by thermal drive, and that high percentage recoveries of oil could be effected. The bulk of the oil recovery came after arrival of the burning front at a production well. However, rapid corrosion and high-temperature failure of conventional pipe and equipment both below and above surface occurred. Stainless steels gave more satisfactory performance under these conditions than did conventional steels.

Oxygen was seldom observed in gas from wells ahead of the burning front, and it appears that the front was continuous throughout the life of the experiment.

INTRODUCTION

During late 1953 and early 1954, industry-wide attention was focused on the thermal recovery of oil by movement of a combustion front through an oil zone. Two separate Oklahoma field tests were described in publications by Kuhn and Koch[1], and Grant and Szasz.[2] To obtain basic information needed for making engineering and economic appraisals of commercial recovery of heavy oil by this thermal recovery method, a new field research project[3,4] was started May 31, 1955. Twelve oil companies contributed to this project with General Petroleum Corp. as operator.

Since combustion recovery experiments* with heavy oils in other areas had been conducted in small patterns,[2,5] an important purpose of this test was to determine whether the process could be operated in a pattern of near-commercial well spacing. The South Belridge field, located 30 miles north of Taft, Calif., was chosen because its oil sands are similar to many heavy oil sands which typically have low primary recovery and leave a large amount of oil in place. Such fields are not particularly suited for common secondary recovery methods.

DESCRIPTION OF TEST SITE

The test interval was a Tulare sand at a depth of about 700 ft. Nine test wells were drilled, cored and completed from Oct., 1955, through Jan., 1956. The initial pattern shown on the map, Fig. 1, consisted of an injection well (1I), four producing wells (1P-4P), and four observation wells (1T-4T). An old well (81) was also recompleted for use as an observation well. The area enclosed by the original four production wells was 2.5 acres; the distance from the injection well to each production well was 233 ft. During the combustion period, Well 5P was drilled to replace Well 2P, and Well 6P was drilled to replace Well 3P. The new wells were 25 ft beyond the old production wells along a diagonal from the injection well, and resulted in an increase in pattern area to 2.75 acres.

Isopachs are shown in Fig. 1. The average thickness of the oil sand in the test pattern was 30 ft. Fig. 2 presents two cross sections through the test pattern. Oil sand is represented by white and claystone by gray. The dashed lines indicate layers of conglomerate grading to claystone. The sand thickness was fairly uniform throughout the test pattern except in the 1P area. The sand body dips gently from the northwest to southeast, about 3 degrees from horizontal. The sand is unconsolidated, and grades from very fine material to pebbles as large as 2 in. in diameter.

Table 1 presents the average initial properties of the formation. The in-place porosity of 37 per cent was estimated from the porosity of coke-consolidated cores taken after combustion. Original core analyses data were adjusted to 37 per cent, giving pore volume saturations of 60 per cent oil, 37 per cent water, and 3 per

Manuscript received in Society of Petroleum Engineers office Sept. 15, 1958. Paper presented at Annual Fall Meeting of the Los Angeles Basin Petroleum Section in Los Angeles, Oct. 16-17, 1958.

[1]References given at end of paper.

*The recent literature contains many descriptions of field and laboratory studies of the combustion-drive thermal recovery method. Attention is directed to Refs. 6-15 for information on these studies.

Discussion of this and all following technical papers is invited. Discussion in writing (three copies) may be sent to the offices of the *Journal of Petroleum Technology*. Any discussion offered after Dec. 31, 1958, should be in the form of a new paper.

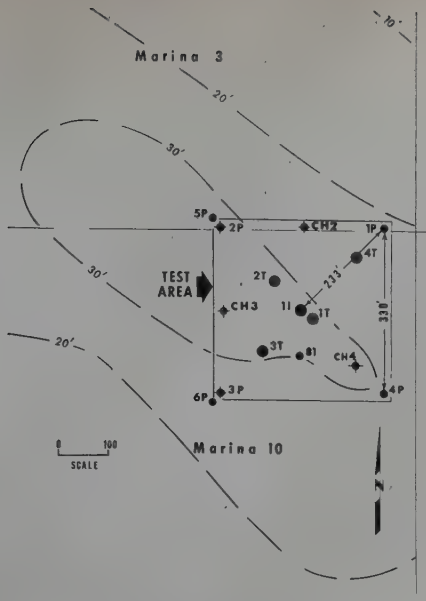

FIG. 1—ISOPACHOUS MAP OF 700-FT TULARE SAND, SOUTH BELRIDGE FIELD.

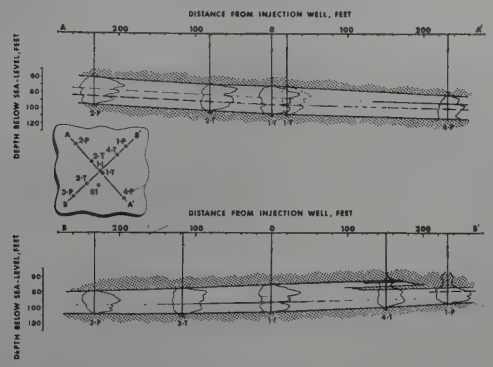
DISTANCE FROM INJECTION WELL, FEET
DEPTH BELOW SEA-LEVEL, FEET
DISTANCE FROM INJECTION WELL, FEET
DEPTH BELOW SEA-LEVEL, FEET

FIG. 2—CROSS SECTIONS OF OIL SAND THROUGH TEST PATTERN.

cent gas. The initial formation temperature was 87°F.

A schematic flow diagram of the major equipment used in the experiment is shown in Fig. 3. Air was compressed by three 350-bhp compressors which could supply 3.5 MMcf of air per day at 500 psi. The compressed air was injected through the central well. After ignition, the air passed through a very high permeability "burned" region in the sand to the "burning" front. There the air burned the residuum and coke remaining on the sand, about 15 per cent by weight of the initial oil. The rest of the oil, formation water, and the water of combustion were pushed ahead of the burning front. The combustion gases moved rapidly through and far out in front of the bank. Combustion gases were recovered at the producing wells along with oil and water which was being pushed ahead of the burning front.

Production wells were pumped initially, but after arrival of the burning front, the gas rates and well productivities were high enough so that wells flowed. Produced fluids passed from the wellhead to a separator. Oil and water passed to the tank farm for gauging. The separated gas passed through a back-pressure regulator

TABLE 1—INITIAL FORMATION PROPERTIES

Porosity, per cent	37
Oil saturation, per cent	60 (1,720 bbl/acre-ft)
Water saturation, per cent	37 (1,060 bbl/acre-ft)
Gas saturation, per cent	3
Total oil in test pattern, bbl (1P-5P-6P-4P)	145,000
Total water in test pattern, bbl	90,000
Oil gravity, °API	12.9°
Oil viscosity, cp at 87°F	2,700
Specific permeability to air, darcies	8

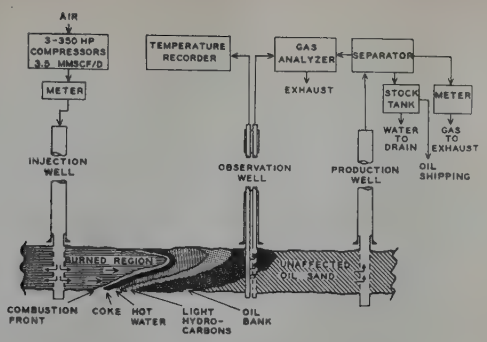

FIG. 3—FLOW DIAGRAM OF TEST.

to the meter runs. Gas was measured by orifice meters. At the start of air injection all exhaust gas was passed through a flame arrestor and flared to prevent accumulation of combustible gas in the test area.

In addition to the injection and production wells, five observation wells were located in the test pattern. Each observation well was cased to the top of the sand, and two strings of pipe were run to the bottom of the sand. One string of 2.5-in. pipe was slotted over the test interval to permit collection of gas samples. The other string was 2-in. pipe, capped at the bottom. This string permitted running a thermocouple cable to measure formation temperatures. The injection well and all production wells were completed with similar thermowells.

The air injection rate and the produced gas rates were regulated with volume and pressure controllers. All gas analyses were made with a mass spectrometer. Temperature readings were made with thermocouples.

Conventional pipe was used, with the exception of the injection well liner, replacement well liners, and observation well tubing strings, which were Type-304 stainless steel across the sand interval.

Fig. 4 is a photograph of the test site, facing southwest. Production Well 1P is shown in the center foreground. Wells 2P, 3P and 4P may be seen by moving in a counterclockwise direction from Well 1P. The injection well, 1I, is in the center of the picture under the derrick. The derrick was positioned over the injection well to permit installation of a 54-ft lubricator for running an electrical igniter into the well under pressure. The tank farm, consisting of eight 100-bbl tanks, may be seen to the left of the injection well. The building to the immediate right of the injection well is the operations building which contained instruments, an office and a shop. The building to the far right of the injection well is the compressor building. The observation wellheads appear within the square formed by the four production wells. The most distinct observation well is 4T, which may be seen on a direct line from the injection well to Well 1P in the immediate foreground.

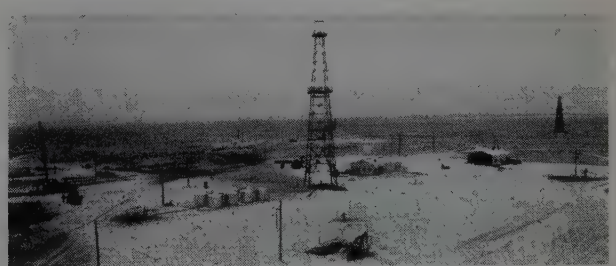

FIG. 4—AERIAL VIEW OF THE SOUTH BELRIDGE TEST AREA.

PRODUCTION BEFORE AIR INJECTION

Following completion in Oct., 1955, the four production wells and the injection well were pumped to establish the initial liquid and gas production rates. By the end of Feb., 1956, the average production per well was 5 B/D of oil, and negligible water and gas. The producing mean formation pressure was atmospheric. The oil production mechanism appeared to be mainly solution gas drive with no active water drive evident. A total of 3,680 bbl of oil were produced during this period.

AIR INJECTION RESULTS

Air injection was started March 1, 1956, and continued almost without interruption throughout the experiment. Air was injected at rates as high as 700 Mscf/D with a maximum pressure of 240 psi before ignition (Fig. 5). The calculated initial effective permeability to air averaged 50 md. No appreciable effect of air injection rate on liquid production rate was found. The gas production rate was relatively high in Wells 2P and 3P to the west but relatively low at Well 4P to the southeast, and practically insignificant at Well 1P to the northeast.

Besides being unevenly distributed, the total gas production rate from the pattern wells was only half of the injected air rate. Efforts to improve the distribution of gas flow by back-pressuring production Wells 2P and 3P sharply reduced the pattern gas and oil production rates and increased loss of air from the test pattern. Back-pressuring was discontinued.

Analysis of the gas from each of the four production wells indicated a substantial loss of oxygen but no substantial increase in carbon dioxide (Fig. 14). At the same time the formation temperature began to rise throughout the pattern. Apparently, oxygen was reacting with the crude oil and generating heat. Oxidation reactions of this type are well known. As with most oxidations, the reaction rate increases rapidly with temperature increase.

When the carbon dioxide content of the gas sampled at observation Well 1T (20 ft from the injection well) suddenly rose in early June, 1956, the air injection rate was cut back to avoid spontaneous ignition. But on June 15, 1956, the entire injection wellbore reached temperatures in excess of 1,000°F. Combustion had begun spontaneously at or near the injection well.

THERMAL RECOVERY RESULTS

Air Injection and Movement of "Burning" Front

The air injection rate and resultant location of the burning front along the major axes of the test pattern are shown in Fig. 5. The curve, on the top portion of Fig. 5, shows the cut-back of air injection rate following appearance of combustion gases at the time of ignition.

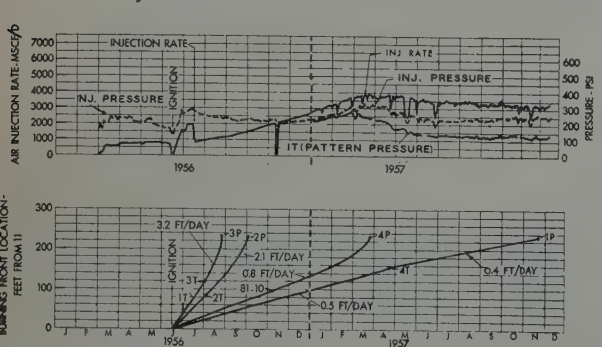

Fig. 5—Air Injection Rate and Pressure and Wellhead Pressure at Observation Well 1T. Burning Front Locations.

Previous experience, both in laboratory experiments and field tests,[1,2] indicated the immediate development of a fluid "block" upon ignition which could restrict air flow seriously. At South Belridge there was no measurable increase in injection pressure during the period immediately following ignition and air could be injected at any desired rate without abnormal pressure increases.

During the remainder of June and during July, 1956, the air injection rate was increased rapidly to move the burning front to the first observation well (1T) in two weeks' time. The immediate goal was to find whether a satisfactory ignition had taken place and if it would be necessary to use the igniter. The burning front arrived at Well 1T satisfactorily and the electrical igniter was never used.

On July 15, 1956, the air injection rate was reduced to the design level, and the design schedule was maintained after that time. As shown, the air injection rate was increased slowly until the compressor capacity was reached in late Feb., 1957. The air injection rate was then held at a level of approximately 3,500 Mscf/D. The injection pressure reached a maximum of 330 psi, about equal to hydrostatic pressure from the surface. The injection pressure is also shown in Fig. 5.

In Feb., 1957, it became apparent that pattern pressure was dropping despite an increase in injection pressure. The wellhead pressure of Well 1T, which was representative of the pressure at the other observation wells and the average pattern pressure, is shown on the top portion of Fig. 5. An analysis of test data indicated that plugging between Wells 1I and 1T had begun in Nov., 1956, and reached a maximum and constant level in Feb., 1957. No further loss in injectivity resulted. A neutron log run in Well 1I indicated a high liquid saturation near this wellbore. Apparently water and compressor lube oil had condensed in the formation. Although this fact had no important effect on the test, steps to avoid plugging the high-permeability burned region might be taken in other projects if injection pressure were a serious factor.

As a result of the air injection schedule, and the distribution of air permeability in the test area, the burning front moved through the test pattern as shown by the lower portion of Fig. 5. The points on the curves represent arrival of the front at the various wells in the test pattern. Arrival of the front was inferred from temperature measurements. The rate of advance of the front was markedly different in the four pattern quadrants. The front reached Well 3P in late Aug., 1956, or 73 days after ignition. The front then reached Well 2P in Oct., 1956, and Well 4P in late March, 1957. The front reached Well 4T in late April, 1957, but did not reach Well 1P until late Nov., 1957. The average velocity of the burning front ranged from 0.4 to 3.2 ft/day.

Fig. 6 illustrates typical temperature profiles measured during progress of the burning front by a well. The curve for Well 1I indicates the maximum temperatures recorded at ignition. The next profile shows temperatures measured at the nearest observation well (1T). The character of the temperature profile indicates burning was taking place in the top of the interval. The temperatures shown for Wells 2T, 81-10, and 3T, are

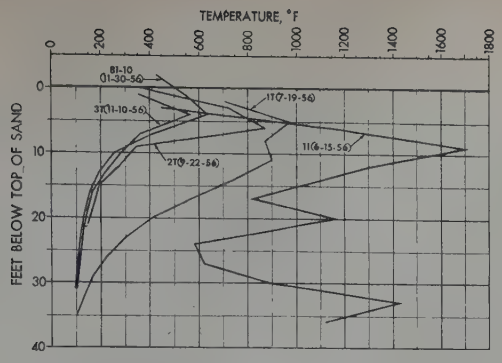

FIG. 6—TEMPERATURE PROFILES THROUGH SAND SECTION.

not as high as those at Wells 1I and 1T, but again, the hottest portion was in the top of the interval. Observation Wells 1T, 2T and 3T were sidewall cored at the end of the test. The thickness burned, as determined by core analysis, is described in the section, "Post Thermal Recovery Coring".

LIQUID AND GAS PRODUCTION

OIL AND WATER

Before air injection the production rate per well was about 5 B/D of oil and 0.1 B/D of water. Rates did not change appreciably as a direct result of air injection until ignition occurred. An increase in oil rate was measured at production wells within two weeks after ignition. No change in temperature, pressure drawdown, or oil gravity was noted at production wells at this time.

Fig. 7 presents oil gravity and production rate for Well 1P, the production well to the northeast of the injection well. The sudden, sharp rises in oil production rate shown during 1956 were the result of workover jobs which generally consisted of scratching perforations, swabbing and bailing. No appreciable quantity of sand was bailed from Well 1P or the other production wells during similar operations. However, it appeared that all production wells were subject to gradual plugging. Well workovers were scheduled more often than in normal operations in an attempt to minimize loss of oil from the pattern. Although not shown in Fig. 7, the water rate increased from 0.1 B/D before ignition but remained below 3 B/D during 1956.

In mid-Jan., 1957, both the oil and water production rates from Well 1P began to rise, accompanied by a rapid increase in oil gravity from 13° to 17.5° API. The increases in rate, gravity and water-cut were definite evidence of movement of the burning front toward this well. In late April, 1957, Well 1P was scratched, swabbed and bailed, resulting in an increase in oil rate to 70 B/D. At that time it appeared that movement of the front toward Well 1P was being hindered by a decline in pattern static pressure. After June, 1957, workovers consisted of injecting hot oil into the casing with the pumping unit shut down. Sharp increases in oil rate after June, 1957, shown by Figs. 7 and 10, were a result of "hot-oil" well treatment. The burning front finally reached Well 1P in late Nov., 1957.

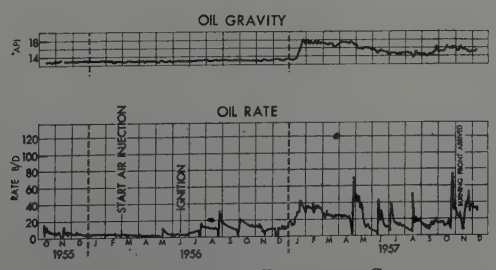

FIG. 7—OIL PRODUCTION RATE AND GRAVITY FOR PRODUCTION WELL 1P.

Fig. 8 presents similar information for production Wells 2P and 5P in the northwest quadrant. After a workover at the end of June, 1956, the oil rate at Well 2P increased rapidly to about 20 B/D. The water-cut, not shown in Fig. 8, began to increase rapidly by the end of July, 1956. The sharp rise in oil rate shown in early Sept., 1956, resulted from a workover. A gradual increase in oil gravity was noticed in Aug., 1956. The oil gravity reached 14.5° API in Oct., 1956, and remained at that level until Well 2P was abandoned.

The burning front reached Well 2P in early Oct., 1956. Thereafter, the oil rate rose rapidly to as high as 120 B/D. The well was put to flowing in early Nov., 1956. By that time, the water cut was 50 per cent. During November, the oil production rate declined rapidly to 10 B/D. Indications were that the liner and tubing had failed as a result of high temperatures and corrosive conditions in the wellbore. In early Dec., 1956, a 4.75-in. liner was run in Well 2P and the well was put to flowing. The oil production rate increased gradually through Feb., 1957. At the end of February, Well 2P plugged and the casing failed above the production zone. Attempts to return Well 2P to production failed and a cement plug was set and the well abandoned.

A considerable quantity of oil was produced from Well 2P after arrival of the burning front, and no apparent decline existed prior to abandoning this well. For this reason the well was replaced by drilling Well 5P 25-ft beyond Well 2P on a direct line from the injection well, or 258 ft from Well 1I. Well 5P was completed with a stainless steel slotted liner. Cores indicated that the top 10 ft of the interval had been burned at this location, and that average oil saturation of the interval was only 510 bbl/acre-ft, about one-third the initial oil saturation.* Yet this well started producing in mid-April, 1957, flowing 320 B/D of oil with approximately 20-psi drawdown. The oil production rate dropped to 90 B/D by mid-Sept., 1957. The well was shut in during late September, while Well 2P was reworked in an attempt to shut-off a gas leak from

*Cores taken during this and subsequent coring of "hot" intervals were warm to the touch when removed from the core barrel. It is quite possible that these cores were flushed and that oil saturations reported are too low. Core analysis results are presented as the best available information because it was not possible to determine whether, or to what degree, cores were flushed.

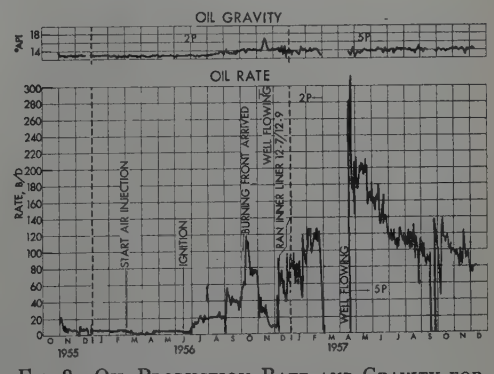

FIG. 8—OIL PRODUCTION RATE AND GRAVITY FOR PRODUCTION WELLS 2P AND 5P.

the pattern. Well 5P was returned to flowing the last week of Sept., 1957. Over half the recovery from the northwestern quadrant was realized after completion of Well 5P. The gravity of oil produced from this well remained about 14° API. No workovers of any kind were necessary despite the considerable cumulative oil production from this well.

Fig. 9 presents oil production rate and oil gravity for Wells 3P and 6P. The oil rate of Well 3P started to increase within 10 days after ignition and water production started rising significantly in mid-July, 1956. The burning front reached Well 3P about the end of Aug., 1956, only 73 days after ignition. The water-cut reached 50 per cent at the time of front arrival. The oil gravity began to rise in Aug., 1956, but like Well 2P, was never over 14° API for more than a few days. The maximum oil production rate reached after arrival of the burning front was 125 B/D, but the oil rate dropped rapidly and averaged only 50 B/D through the end of Sept., 1956.

Well 3P flowed during most of September, but the oil rate dropped to only 25 B/D during early Oct., 1956, and the well was bailed, scratched, and the pump replaced in mid-October. Liner damage was indicated by bailings, and by the fact that the well sanded almost immediately after the workover. It was shut in until Nov. 1, 1956. During early November efforts were made to clean out Well 3P and place it back on stream. During this workover, the mud column suddenly fell away and the well blew out. The well was brought under control and a cement plug was placed in the damaged liner. Air injection was stopped for three days during this well work.

Because of the high cumulative oil production from Well 2P after the arrival of the burning front, it appeared that considerable oil could yet be recovered from the Well 3P quadrant. Well 6P was completed as a replacement for Well 3P in mid-April, 1957. This well was 25 ft from Well 3P on a line from the injection well (258 ft from Well 1I). Cores from Well 6P indicated no burned sand, but the indicated oil saturation was low, only half the initial saturation. The well was put on the pump at 20 B/D in late April, 1957. It was swabbed in and put to flowing in late May, 1957, at a rate of 140 B/D, but declined to 30 B/D by Dec., 1957.

Fig. 10 shows oil production rate and gravity for Well 4P, the southeastern production well in the pattern. The sudden, sharp rises in oil rate during 1956 were the result of workovers. Although the water production increased with oil rate soon after ignition, the water cut did not rise appreciably until mid-Dec., 1956. The burning front reached the vicinity of Well 4P in late March, 1957. But considerable trouble with liner

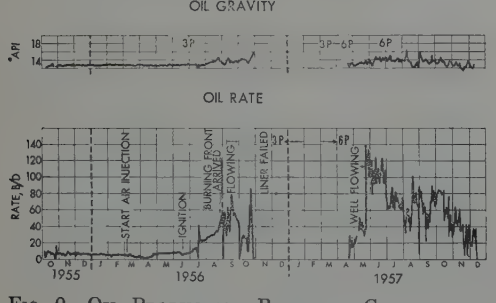

Fig. 9—Oil Production Rate and Gravity for Production Wells 3P and 6P.

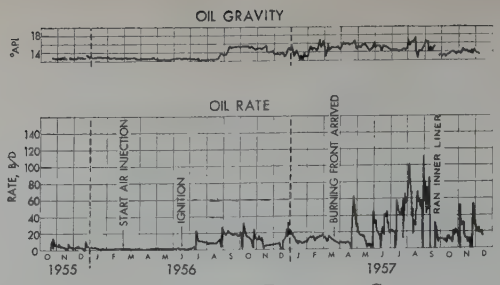

Fig. 10—Oil Production Rate and Gravity for Production Well 4P.

slot plugging was experienced. In mid-April, 1957, Well 4P was bailed and scratched. The oil production rate rose to 55 B/D, but declined rapidly. About June 1, 1957, hot-oil injection was started on a frequent basis. As a result the oil production rate improved steadily and the well was put to flowing in late July, 1957. The oil production rate reached 110 B/D. In early Sept., 1957, sand and coke production became serious, indicating that the liner had failed. The well was killed with mud and a stainless steel inner liner was run. Thereafter, the well produced at low oil and gas rates by pumping.

The oil gravity increased from 12.5° to 15.5° API in Aug. and Sept., 1956, six months before the apparent arrival of the burning front. The oil gravity averaged 15° API after arrival of the burning front.

Fig. 11 presents the oil production rate for the entire pattern. Just before ignition, the pattern oil rate was 20 B/D. During combustion the oil production rate was as high as 390 B/D and averaged 140 B/D, seven times the rate before ignition, despite the fact that Well 3P was down for five months and Well 2P was down for two months before being replaced. The thermal recovery process has demonstrated ability to move this viscous oil rapidly over great distances.

Table 2 summarizes oil recovery from the test pattern quadrants during combustion through Nov. 15, 1957. The total oil recovery from the pattern was 73,950 bbl compared to the initial pattern oil content of 145,000 bbl. This corresponds to an oil recovery of 51 per cent, or 880 bbl/acre-ft for the 84.2 acre-ft in the test pattern. The per cent recovery figures are based on the assumption that all production from a well originated in its respective quadrant. The 96 per cent recovery for the 2P and 5P quadrant indicates that some of the oil produced from Wells 2P and 5P must have moved from outside this quadrant.

With normal methods of production, a recovery of 10 to 15 per cent of the oil in place could be expected in the life of the field (40 to 60 years). Of course, the cost per barrel of oil was far higher for thermal recovery than for normal production.

GAS PRODUCTION

Fig. 12 presents the gas production rates from pattern production wells. The top plot of this figure presents

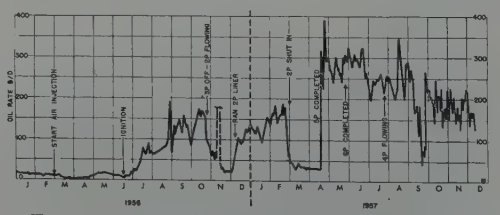

Fig. 11—Total Oil Production Rate From Entire Pattern.

TABLE 2—OIL PRODUCTION DURING COMBUSTION THROUGH NOV. 15, 1957

Quadrant	Barrels	Oil Recovery: Per cent of oil initially in quadrant	Oil Recovery: bbl/acre-ft
1P	8,360	29	490
2P + 5P	38,550	96	1,650
3P + 6P	17,250	41	710
4P	9,790	29	500
Totals	73,950	51	880

the gas production rate from Well 1P. Little gas was produced until a few months before arrival of the burning front late in Nov., 1957.

The second plot of Fig. 12 presents gas production rates from Wells 2P and 5P. The main feature of gas production from the 2P-5P quadrant was a rapid rise in gas rate coincident with arrival of the burning front in Oct., 1956. Thereafter the rate was restricted by the producing pressure used in flowing the wells.

The gas production rate from Wells 3P and 6P is shown in the third plot of Fig. 12. Gas production at Well 3P increased following arrival of the burning front in Sept., 1956. The erratic nature of gas production after arrival of the burning front was a result of production difficulties discussed in connection with liquid production. Gas production from Well 6P was not significant until this well was swabbed in and started flowing in late May, 1957. It appears that the burning front was near Well 6P at completion and moved rapidly into the well in May, 1957.

The last plot of Fig. 12 shows the gas production rate from Well 4P. The burning front reached Well 4P about March, 1957. The gas production rate varied after front arrival depending upon condition of the well.

Thus, a rapid increase in gas production rate was generally found at burning front arrival, but gas rates remained relatively constant after the initial rise. Another observation is that gas production rates from pattern wells were quite different, and the result was different burning front velocities toward the production wells.

Fig. 13 presents the total pattern gas production rate in Mscf/D and in per cent of the air injection rate. The gas production rate was only 20 per cent of the air injection rate from Dec., 1956, through Feb., 1957. At the end of February the gas production rate suddenly dropped to less than 5 per cent of the injection rate. This drop was coincident with abandonment of Well 2P. Moreover, the gas production from outlying wells also dropped. It appeared that gas was leaking from the 700-ft test zone to non-oil-bearing sands above the test zone.

When Wells 5P and 6P were placed on production

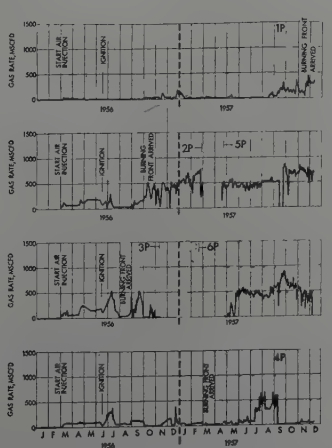

FIG. 12—GAS PRODUCTION RATES FROM PATTERN PRODUCTION WELLS.

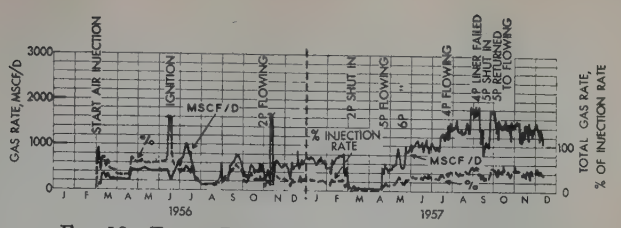

FIG. 13—TOTAL PATTERN GAS RATE PERFORMANCE.

in late April, 1957, the total pattern gas production rate increased. By Sept., 1957, the gas rate was 50 per cent of the injection rate. But a lack of gas production from outlying wells indicated a leak was still significant. After extensive investigation it appeared that Well 2P was the probable source of the leak. Well 2P was re-entered in mid-Sept., 1957. This job was difficult and expensive and illustrates conditions that may be encountered in working on damaged wells. After the cement plug was drilled out, milling on junk was started. At 500 ft mud circulation was lost and the well blew-in briefly before the blow-out preventer was closed. After a hole in the casing was plugged with cement, milling proceeded to 600 ft, where severe lost circulation again occurred. This time two successive cement jobs were unsuccessful. Cement and mud dropped so fast a vacuum was pulled on the wellhead. Finally, a third cement job appeared satisfactory and it was possible to hold pressure on the wellhead. The final tally was 2,500 bbl of mud and 1,000 sacks of cement used. Indications were that the leak was at least partially plugged and work was stopped. Outlying wells then began to show increasing gas production rates and by Oct., 1957, the total gas production rate, including both pattern and outlying wells, was 70 per cent of the air injection rate.

GAS ANALYSIS AND FUEL CONSUMPTION

Fig. 14 presents oxygen and carbon dioxide content of the produced gas from the pattern wells. After ignition the per cent oxygen dropped rapidly to zero for all production wells and remained there until burning front arrival. Correspondingly, the per cent carbon dioxide increased rapidly to about 15 per cent and remained at that level to near breakthrough of the burning front. Only occasional indications of oxygen were found in gas streams from wells ahead of the burning front. This leads to the conclusion that the injected air generally passed through the front, that the front was continuous, and that oxygen usage was almost complete.

Through Nov. 15, 1957, the fuel consumed as calculated from gas produced from pattern wells only, amounted to 5,380 bbl of oil. Because of the uncertainty of the composition of the gas which was *not* produced from the pattern, the total fuel consumption

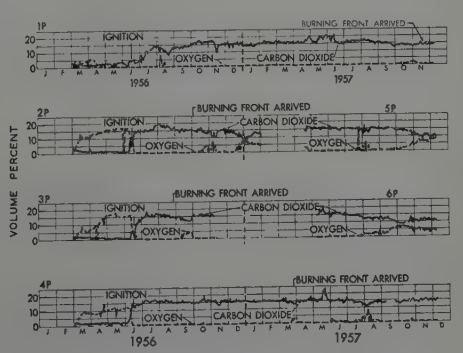

FIG. 14—CARBON DIOXIDE AND OXYGEN CONCENTRATION IN GAS FROM PRODUCTION WELLS.

could range from 15,700 to 22,600 bbl. It is believed that the best estimate of the total fuel consumed through Nov. 15, 1957 is 15,700 bbl, 14.7 per cent of the oil initially in place in the volume burned.

AIR-OIL, GAS-OIL RATIOS

The "current" ratio of injected air to produced oil, the current ratio of produced gas to oil, and the cumulative ratio of injected air to oil are shown in Fig. 15. The heavy solid line presents the cumulative ratio of injected air to produced oil. Because the cost of compressing air is one of the major factors in economic consideration of this process, this curve is significant. The cumulative ratio of injected air to produced oil was 19 Mscf/bbl at the end of the experiment. This value is probably high because of a gas leak from the pattern. The current ratio of injected air to produced oil was less than 15 Mscf/bbl for a large portion of the combustion phase, and particularly during the time that the major part of the total oil recovery was realized after mid-April, 1957. The current ratio of produced gas to oil for the entire pattern is shown by the lowest line in Fig. 15. During most of the combustion phase the current ratio of produced gas to oil was on the order of 5 Mscf/bbl.

OIL CHARACTERISTICS

Table 3 presents the average properties of the initial crude and thermal recovery oil. The gravity of the thermal recovery oil produced through Nov. 15, 1957, averaged 14.2° API. After burning front arrival, a condensate of 35° to 38° API gravity was produced with the gas in a concentration of 0.1 gal/Mscf. It is estimated that the total quantity of condensate exhausted with the produced gas would result in an increase in the average thermal recovery oil gravity by 1° API. It did not appear economically feasible to recover this condensate, however.

A significant change in oil viscosity accompanied the gravity increase. If it is assumed that the formation temperature in the vicinity of a "hot" production well during combustion was 160°F, a conservatively low estimate, viscosity information in Table 3 indicates a reduction from 2,700 cp for initial oil at the initial formation temperature to 54 cp, a reduction in viscosity by a factor of at least 50.

In regard to oil composition, both the gasoline and diesel oil cuts increased at the expense of the residua. Although a measurable improvement in produced oil resulted, such a change may not increase the commercial value of the crude. Refinery evaluations of the combustion crude indicated that it was compatible with other stocks, but would require additional processing.

The initial water cut of produced liquids was only 4 per cent. But, as the burning front approached a production well, the water-oil ratio increased because all

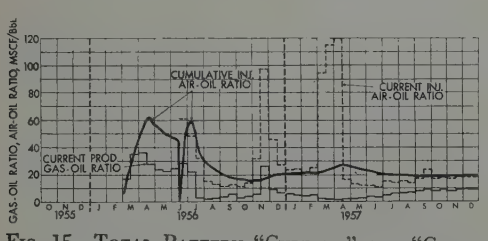

FIG. 15—TOTAL PATTERN "CURRENT" AND "CUMULATIVE" RATIOS OF INJECTED AIR TO PRODUCED OIL, AND CURRENT PRODUCED GAS-OIL RATIO.

TABLE 3—CHARACTERISTICS OF INITIAL OIL AND AVERAGE OIL PRODUCED BY THERMAL RECOVERY THROUGH NOV. 15, 1957

	Initial Oil	Thermal recovery oil
Average gravity, °API at 60°F	12.9	14.2
Viscosity of dead oil, cp at 87°F	2,700	800
120°F	540	200
160°F	120	54
Composition, volume per cent		
Gasoline	0.5	2.0
Diesel Oil	29.5	38.0
Residua	70.0	60.0

connate water and water of combustion was moved ahead of the high temperature burning front. Water-in-oil emulsion became increasingly severe. Emulsions as high as 40 to 50 per cent water were common. However, the water content of lease shipments was maintained below 2 per cent after March, 1957, by addition of emulsion-breaking chemicals.

POST THERMAL RECOVERY CORING

Starting in early Sept. through Nov., 1957, three core holes were drilled and observation Wells 1T, 2T and 3T were sidewall cored to determine the reduction in oil saturation and the vertical thickness burned within the test pattern. The locations of these core holes are shown in Fig. 1.

As a result of coring it appeared that 15 to 25 ft of the top of the interval was burned at Well 1T, the top 13 ft of the interval was swept by the burning front at Wells 2T and CH2, the top 10 ft was burned at Well CH3, 8 ft was burned in the top portion of the interval at Well 3T, while only 3 to 4 ft was burned near the top of the interval at Well CH4.

Figs. 16 and 17 present the results of core analyses and logs from these wells. The first column of graphs shows the oil saturation obtained from core analyses of sidewall samples. The second column presents the resistivity logs, while the third column presents neutron logs. The burned and not-burned intervals are noted on the shaded bands.

The oil saturation throughout the burned interval was found to be low in each well, often less than 2 to 3 per cent of pore volume. A coke deposit was generally found above and below the burned section. Coked sections were also found within the burned interval at Wells 1T and 2T. Generally, there appeared to be a few feet of a wet, depleted zone below the burned sand which may have resulted from a steam drive or evaporation of oil into the burned interval. The remainder of the unburned interval contained oil, but was depleted. The oil content of the not-burned portion of the interval ranged from 560 to 780 bbl/acre-ft. The average oil content of the unburned portion of the

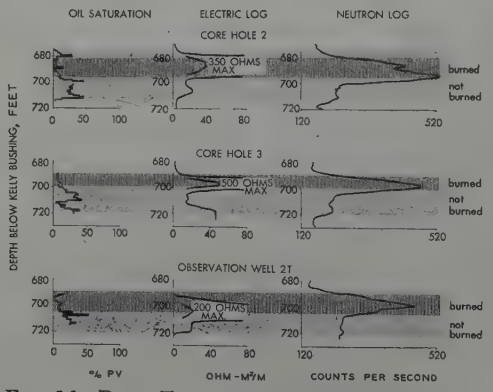

FIG. 16—POST THERMAL RECOVERY CORING AND LOGGING RESULTS FROM WELLS CH-2, CH-3 AND 2T.

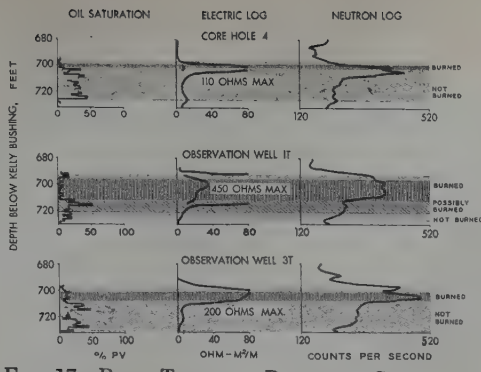

FIG. 17—POST THERMAL RECOVERY CORING AND LOGGING RESULTS FROM WELLS CH-4, 1T AND 3T.

interval for the six wells cored was 660 bbl/acre-ft, or about 38 per cent of the estimated initial oil content of 1,720 bbl/acre-ft. Again, it is possible that cores were flushed and the oil saturations reported might be too low.

Ignition studies of coke-bearing samples indicated coke deposits ranging from 1.0 to 5.4 lb/cu ft of bulk volume. Extremely high coke deposits of 8.9 to 14.2 lb/cu ft were found in several samples which appeared to be composed mainly of claystone or fine silt. The atomic hydrogen-to-carbon ratio of the coke was determined to be 1.67. The computed specific gravity of the coke varied considerably, but averaged 1.38.

The resistivity logs indicated extremely high resistivity for the burned interval; on the order of 100 to 500 ohm-m. The initial resistivity of the formation was approximately 50 ohm-m. Thus, the resistivity log was useful for determining the vertical location and thickness of the burned interval.

The neutron log also showed high deflection over the burned interval as a result of the low water and oil content of burned sand and consequent low hydrogen density.

Fig. 18 presents an interpretation of the location of the burned sand and residual oil saturations throughout the test area. This plot was prepared from "as received" core data and other information obtained during the test. The dashed lines represent lines of constant burned thickness. Average oil saturations of cores are shown for the *entire* sand interval. It is estimated that the burning front moved over 6.3 acres in areal extent, far beyond the test pattern area of 2.5 acres. The average thickness of the burned region appeared to be 10 to 15 ft, and the total volume burned was 56 acre-ft. The region outside the perimeter of the burned region is shown as an "oil bank" since there was a net efflux of oil from the burned region.

Table 4 presents a material balance on oil and water. When the sum of produced oil, fuel and apparent residual oil is subtracted from the original oil within the perimeter of the burning front, it appears that there was a net efflux of oil from the burned region of 73,880 bbl. Apparently, movement of the burning front displaced a quantity of oil outside the burned area which was equal in volume to that produced.

Restricting attention to the test pattern area enclosed by Wells 1P, 5P, 6P and 4P, shown in Fig. 18, the following conclusions may be reached. Of the 84.2 acre-ft of reservoir volume within the test pattern, 33.3 acre-ft were burned. Apparent average residual oil content of the test pattern was 715 bbl/acre-ft, about 40 per cent of the original oil content. This corresponds

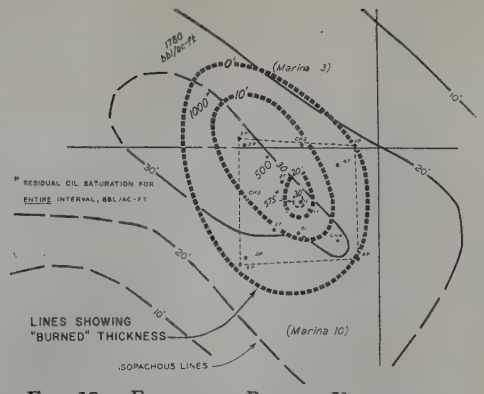

FIG. 18—ESTIMATED BURNED VOLUME AND RESIDUAL OIL CONTENT ON NOV. 15, 1957.

to a residual oil content of 60,440 bbl. Prorating the oil consumed as fuel between the test pattern area and the surrounding area results in an estimated fuel consumed within the test pattern of 9,300 bbl. The total oil produced, 80,580 bbl, fuel, and residual oil, exceeds the initial pattern oil content by 5,320 bbl.

SAFETY PRECAUTIONS

During the experiment, hot, burned intervals were cored and wells damaged by high temperatures and corrosive conditions were successfully repaired by conventional rotary drilling with mud circulation. Although lost circulation of mud and brief blowouts were encountered, no hazardous conditions resulted when adequate blowout preventers were used.

At the initiation of air injection, produced gas was passed through a flame arrestor and flared. Produced gases should be exhausted so as to avoid accumulation of explosive or toxic gases. Detection instruments and technical information on toxic and combustible gases were used by employees at the test site.

Oil can ignite spontaneously in a compressed air system. This possibility was reduced by avoiding (1) excessive use of lube oil through careful adjustments and maintenance of equipment, (2) accumulation of oil in the compressed air lines, and (3) volatile lube oils.

CONCLUSIONS

It is not possible to translate the cost of this research experiment generally into the cost for commercial developments. The instrumentation and technical supervision used was far in excess of what would be necessary for commercial development. Furthermore, it is difficult to determine to what degree conclusions are specific to the South Belridge field and the specific well pattern employed, and to what degree they are generally true. At this stage of development of the process, it is believed wise to consider most results specific to South Belridge, both in regard to the test sand and the well

TABLE 4—MATERIAL BALANCE ON OIL AND WATER THROUGH NOV. 15, 1957

	Oil (bbl)	Water (bbl)
1. Oil and water produced		
Period		
Normal production	3,680	175
Air injection	1,440	40
Combustion	75,460	42,590
Total	80,580	42,805
2. Oil consumed as fuel, bbl	15,650	
Water produced by combustion of fuel, bbl		16,250
3. Apparent residual fluid within perimeter of burning front, bbl	155,890	174,445
4. Apparent liquid moved outside perimeter of burned area, bbl	73,880	0

pattern used. As more field experience is accumulated, it should be possible to sort general truths from peculiarities of particular sites and experiments. Conclusions reached from the Belridge experiment include the following.

1. Air injection prior to ignition had no significant effect on oil rates.

2. "Slow" oxidation of the oil in the formation by air occurred at pressures of 200 psi and at formation temperature. The heat generated by this slow oxidation was sufficient to raise the formation temperature to the point that spontaneous ignition occurred near the injection well.

3. Immediately following ignition no serious fluid blocking near the injection well was experienced.

4. Oil production rates began to increase soon after ignition. The oil moved more readily than would be expected from oil production rates before ignition.

5. Wells must be able to produce at rates about equal to the rate of oil displacement. Frequent well stimulation work was necessary to maintain adequate oil rates.

6. The average oil rate during combustion was seven times the average rate before ignition.

7. Pattern oil recovery was about 880 bbl/acre-ft or 51 per cent of the oil in place initially.

8. It appears that the burning front was moved as far as 400 ft from the injection well, and that a total area of 6.3 acres was swept by the burning front.

9. The burned interval was limited to less than half the net sand interval over most of the burned region.

10. The oil content of the unburned portion of the interval was less than half the initial oil content.

11. Both resistivity and neutron logs were found useful in defining the vertical position of the interval burned.

12. The velocity of the burning front ranged between 0.4 and 3 ft/day between the injection and production wells with the air injection schedule employed during this test.

13. Oxygen was not observed in gas produced from wells ahead of the burning front. It appears that all the injected air passed through the burning front, with the possible exception of air which leaked from the test pattern. The burning front remained continuous throughout the life of the test.

14. The pressure in the burned region was essentially equal to the injection well pressure until the burned region near Well 1I became plugged, presumably by condensed water and lube oil from the compressors.

15. Burning resumed satisfactorily following a three-day shut down of air injection.

16. It was not possible to effect significant control of directional movement of the burning front in this test by throttling produced gas.

17. Gas production rates were high enough to flow producing wells after burning front arrival.

18. High temperatures and corrosive conditions in producing wells created extremely severe well maintenance problems which led to well failures. Stainless steel liners installed in replacement wells gave much better service than the conventional steel liners of the original wells.

19. The bulk of oil production came after the burning front reached the production wells.

20. The cumulative ratio of injected air to produced oil was 19 Mscf/bbl at the end of the experiment. This value may be high because of a gas leak from the pattern. The current ratio of produced gas to oil averaged about 5 Mscf/bbl.

21. When the burning front approached a production well, the water cut increased and water-in-oil emulsion became a serious problem.

22. Despite the high formation temperatures and permeability, the burned zone was cored and hot wells were worked over using conventional field practices. As with any other field in which gas pressure may cause a loss in fluid column density, or high permeability may result in appreciable fluid loss, blowout equipment should be used.

ACKNOWLEDGMENT

Acknowledgment is made to the management of the General Petroleum Corp. and contributing companies for permission to publish this investigation. The spirit of cooperation displayed by representatives of the contributors in appraising the operation and analyzing the results was particularly appreciated. Contributing companies were: Continental Oil Co., Chanslor-Western Oil & Development Co., Esso Research & Engineering Co., Gulf Oil Corp., Honolulu Oil Corp., Ohio Oil Co., Shell Development Co., Sunray Mid-Continent Oil Co., The Texas Co., Tidewater Oil Co. and Union Oil Co.

An experiment on this scale requires the efforts of many people. The valuable consultation of Magnolia Petroleum Co.'s Field Research Laboratory personnel who did pioneer laboratory and field work on the process was greatly appreciated. The following engineers assigned to the project deserve special mention: W. E. Dittman, E. T. Cozens, I. Sklar, F. A. Cuff, J. D. Beale and J. A. Teberg.

REFERENCES

1. Kuhn, C. S. and Koch, R. L.: *Oil and Gas Jour.*, (Aug. 10, 1953) **52,** 92.
2. Grant, B. F. and Szasz, S. E.: *Trans.* AIME (1954) **201,** 108.
3. "General Pete Starting Pilot Plan to Recover Heavy Oil", *Oil and Gas Jour.* (July 25, 1955) **54,** 132.
4. "Torch Applied to 'Fire Flood' Project", *Oil and Gas Jour.* (July 9, 1956) **54,** 62.
5. Koch, R. L., Gleason, J. F., Jr. and Boston, W. G.: *Oil and Gas Jour.* (Dec. 6, 1954) **53,** 102.
6. "Sinclair to Test New Oil Recovery Method", *Oil and Gas Jour.* (April 11, 1955) **53,** 81.
7. "Socal Tests 'Fire Drive' ", *Oil and Gas Jour.* (Aug. 22, 1955) **54,** 98.
8. "Experiment Ignited—Socal Testing Underground Combustion in Kern County", *Oil and Gas Jour.* (July 23, 1956) **54,** 69.
9. Walter, H.: *Jour. Pet. Tech.* (Feb., 1957) **IX,** No. 2, 16.
10. "Another Thermal Recovery Project—Third in the State—Has Been Started in California", *Pet. Week* (March 22, 1957) **4,** 31.
11. Wilson, L. A., Wygal, R. J., Reed, D. W., Gergins, R. L. and Henderson, J. H.: *Trans.* AIME (1958) **213,** 146.
12. Martin, W. L., Alexander, J. D. and Dew, J. N.: *Trans.* AIME (1958) **213,** 28.
13. McNiel, J. S., Jr., and Moss, J. T.: *Pet. Engr.* (July, 1958) **30,** No. 7, B-29.
14. "Texas Fireflood Solves Some Problems", *Pet. Week* (July 18, 1958) 22.
15. Breston, J. N.: *Jour. Pet. Tech.* (Aug., 1958) **X,** No. 8, 13.

★★★

Effect of Fractures on Sweep-out Pattern

A. B. DYES
MEMBER AIME
C. E. KEMP
B. H. CAUDLE
MEMBER AIME

THE ATLANTIC REFINING CO.
DALLAS, TEX.

ABSTRACT

It has been suggested that formation fractures created by well stimulation treatments will adversely affect sweep-out efficiency in injection operations. Fluid-flow model studies involving vertical fractures of various lengths and fluid systems of various mobility ratios have been carried out to study this subject. In addition, limited data have been obtained on one model containing a horizontal fracture. It was found that relatively long and highly conductive fractures (not generally obtained in fracturing operations) were required to affect the sweep-out efficiency substantially.

In a given case in the field an approximate distinction can be made between the presence of long conductive fractures and shorter or less conductive ones. This is done with pressure build-up analyses along with data on the relationship of fracture length and conductivity to well productivity. This type analysis shows that usually the fractures induced are either short or of limited conductivity and therefore do not damage sweep-out efficiency.

INTRODUCTION

Improved well productivity and injectivity can frequently be exploited in injection operations. Higher total throughput can yield improved economics. On occasion, the achievement of an increased productivity or injectivity in specific wells can bring about a more uniform sweep of the reservoir. Higher rates can be exploited particularly in water floods of "depleted" reservoirs where a rapid "fill-up" is desired and where low pressures contribute to low well productivity. The creation of fractures local to the wellbore is an excellent means for achieving these objectives. Even though fracturing has been employed in some floods with success,[1,2,3] there still seems to be some reluctance to employ this tool for fear of undue damage to the flood pattern and ultimate recovery. We therefore need to examine the influence which fractures of varying length may have on flood performance and then determine the length of fractures which obtain in the field with conventional fracture treatments.

A substantial influence of fractures on the recovery obtained at breakthrough of the injected fluid has been presented by Crawford and Collins for equal fluid mobilities for the line-drive pattern.[4,5] In addition, the influence which a fracture has on the production performance after breakthrough and on the ultimate recovery warrants consideration in reaching a conclusion concerning the use of induced fractures in flooding operations. This report presents this type of data for the five-spot injection pattern for several fluid mobilities.

In arriving at some conclusion concerning the fracture lengths obtained in field operations we must examine the performance characteristic most affected by the fracture. This is the change in the flow system as reflected in the change in productivity and pressure build-up behavior. A study of these changes is also presented in this report.

RESERVOIR ANALOGS

The X-ray shadowgraph technique, employing miscible displacement in porous models, has been used in the study of the influence of fractures on pattern sweep-out efficiency. The X-ray shadowgraph procedure is described in detail in an earlier report[6]. Fractures were represented by leaving the proper portion of the model surface exposed to either injection or production. This assumes the fracture resistance to be negligible compared to that of the formation. Actually the flow resistance in propped fractures obtained in the field is sometimes not negligible so that the results with this model indicate the maximum influence of the fracture.

Two types of models were necessary to represent vertical fractures in a five-spot flood. These pattern elements are illustrated in Fig. 1. In studying the influence of the horizontal fracture, only one well spacing length to thickness ratio of 50 was used.

The pool unit of a Carter Electric Analyzer was used in studying the influence of fractures on productivity and build-up behavior. The square drainage system of a well was represented by a network of 576 elements of equal volume and resistance. One-fourth of this drainage area was studied as a model unit using a network of 144 condensers and resistors. Vertical fractures were represented by a shunt directed from the well perpendicular to the drainage boundary. Horizontal fractures were represented by a circular shunt. Resistance of a shunt was varied in representing different conductivities for the fractures.

FRACTURE DIRECTION AND LENGTH

The direction at which a vertical fracture extends into the formation and its length and conductivity influence the sweep behavior. The two

Original manuscript received in Society of Petroleum Engineers office March 14, 1958. Revised manuscript received Aug. 27, 1958. Paper presented at Third Biennial Secondary Recovery Symposium in Wichita Falls, Tex., May 5-6, 1958.

[1]References given at end of paper.

FIG. 1—FRACTURED ELEMENTS OF A FIVE-SPOT. T—ELEMENTAL PATTERN WHERE FRACTURES "POINT" TOWARD OFFSET WELLS. B—ELEMENTAL PATTERN WHERE FRACTURES "POINT" BETWEEN OFFSET WELLS.

extremes in direction are illustrated for the five-spot in Fig. 1 where in one case the fractures "point" toward the offset wells and in the other case the fractures point between the offset wells.

For the favorable direction (between wells) a fracture length up to three-fourths of the distance between the well and the element boundary was shown to have little effect on the sweep-out behavior. This is illustrated in Fig. 2 for a system with a mobility ratio of about one. Such fractures could be employed for rate stimulation without harm to the flood.

In the event the fracture is directed in an unfavorable direction (toward an offset producing well), the breakthrough recovery is reduced. On the other hand the recovery after breakthrough is increased so that the total recovery approaches that of an unfractured pattern. This is illustrated in Fig. 3. A long fracture out to half the distance to the offset well does not harm ultimate recovery. However, the injection volume must be increased. For example, the volume injected for a fracture length of one-half is 20 per cent greater than that for the unfractured pattern. The throughput rate for the operation using fractures, however, would be about twice that of the unfractured case; thus more recovery could be obtained at any given time. A similar behavior is illustrated for a horizontal fracture with a length of one-half, Table 1.

Fractures of greater length and of limited conductivity would also be expected to yield similar results. A limited conductivity is expected to be the more normal result in field fracturing operations. If longer fractures of high conductivity are obtained in the unfavorable direction, the ultimate recovery can be reduced. This is illustrated for a fracture length of three-fourths in Fig. 3.

MOBILITY RATIO

Several earlier papers have reported the effect of fluid mobility ratios on flood pattern behavior in the absence of fractures.[7,8] For the fractured well case where the direction of the fracture (between wells) does not significantly influence the sweep behavior, the previous data can adequately describe the influence of the fluid mobilities on the operation. The effect of varying mobility ratios has been studied for the case in which the fracture direction is of significance (toward wells). The results for one particular fracture length of one-half are illustrated in Fig. 4. Favorable mobility ratios, expressed as mobility ratios less than one, reduce the throughput for a given recovery. Those greater than one add to the amount of throughput, with ratios greater than three reducing somewhat the ultimate recovery. With unfavorable mobility ratios a fracture length of one-half can still be used with little harm to the flood. The effect of mobility ratio and additional fracture lengths on flood behavior are illustrated in Table 1 for breakthrough and ultimate recovery.

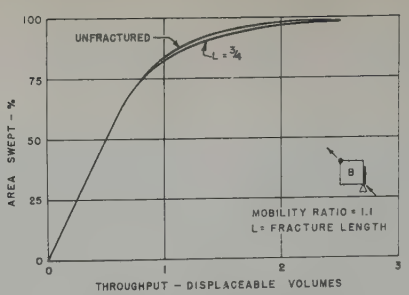

FIG. 2—SWEEP-OUT WITH FRACTURE OF FAVORABLE DIRECTION.

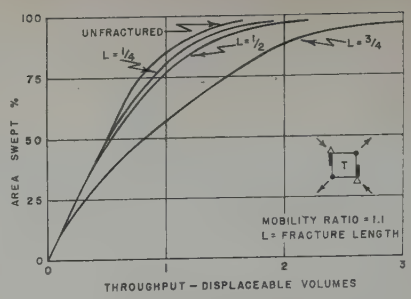

FIG. 3 — SWEEP-OUT WITH FRACTURE OF UNFAVORABLE DIRECTION.

FRACTURE LOCATION — INJECTION WELL OR PRODUCING WELL

A fracture placed in a producing well does not yield the same flow system as when placed in an injection well. Flood performance need not be the same for these cases. The flood performance for each fracture location was studied. These are summarized in Table 1. When the fracture is directed between offset wells the flood performance for each type of fractured well is about the same as for the unfractured reservoir. However, if the fracture is directed toward the offset well a more pronounced difference in flood behavior arises between the two fracture locations when the mobility ratio is other than one. With unfavorable mobility ratio (higher mobility in swept region) the flood behavior is more favorable with the fracture placed in the producing well than it is when the fracture is placed in the injection well. When the mobilities are favorable the location of a fracture in the injection well yields

TABLE 1—BREAKTHROUGH AND ULTIMATE RECOVERY, FRACTURED FIVE-SPOT

Well fractured	Fracture* element	Fracture length	Mobility ratio	Area Swept, per cent: Breakthrough	Area Swept, per cent: 90 per cent cut of injection fluid	Throughput at 90 per cent cut displaceable volumes
Injection	T	1/4	3	39	92	2.2
		1/4	1.1	45	96	1.7
		1/4	0.3	87	97	1.2
		1/4	0.1	93	98	1.0
		1/2	3	28	92	2.7
		1/2	1.1	37	96	1.8
		1/2	0.3	57	97	1.2
		1/2	0.1	88	98	1.1
		3/4	3	10	83	3.8
		3/4	1.1	14	93	2.3
		3/4	0.3	23	96	1.5
		3/4	0.1	33	97	1.2
Production	T	1/4	3	40	88	1.9
		1/4	1.1	43	95	1.6
		1/4	0.3	63	97	1.2
		1/4	0.1	78	98	1.1
		1/2	3	22	92	2.1
		1/2	1.1	24	96	1.7
		1/2	0.3	35	98	1.3
		1/2	0.1	38	98	1.2
		3/4	3	9	87	3.3
		3/4	1.1	13	94	2.3
		3/4	0.3	15	96	1.8
		3/4	0.1	18	98	1.8
Unfractured			3	56	92	2.2
			1.1	72	99	1.8
			0.3	83	99	1.3
			0.1	99	99	1.0
Injection	Radial (Horizontal)	1/2	1	30	95	2.5

*See Fig. 1.

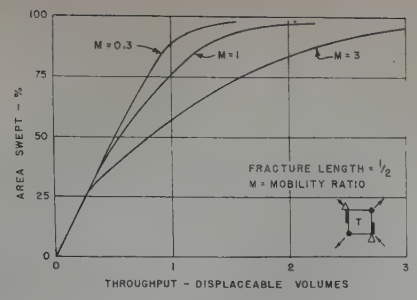

FIG. 4—INFLUENCE OF MOBILITY RATIO AND FRACTURE.

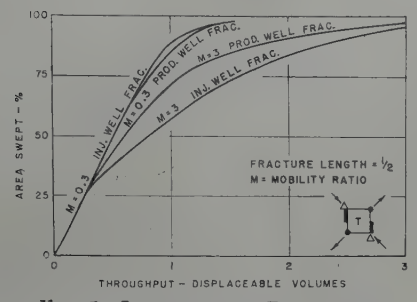
INJ. WELL FRAC.
M = 0.3 PROD. WELL FRAC.
M = 3 PROD. WELL FRAC.
M = 3 INJ. WELL FRAC.
M = 0.3
AREA SWEPT - %
FRACTURE LENGTH = ½
M = MOBILITY RATIO
THROUGHPUT - DISPLACEABLE VOLUMES

FIG. 5—INJECTION OR PRODUCTION WELL FRACTURE.

slightly better pattern results than when placed in the producer. These are illustrated in Fig. 5.

These statements refer to the more important performance as reflected by producing cut after breakthrough and ultimate recovery. The relatively unimportant breakthrough points shown in Table 1 sometimes show contradictory performance, reflecting a difficulty in picking the breakthrough point in the laboratory models using miscible phase displacement. There is no difficulty in determining the area swept as a function of throughput and in reflecting the production of any significant amount of injected material present in the producing stream.

No models were studied in which both the injection well and producing well were fractured. Neither well alone adversely affects the flood if the fracture length is less than half the distance between wells. It was, therefore, thought that this same length if divided between the two wells would also not adversely affect the flood.

FRACTURE INFLUENCE IN WELL PRODUCTIVITY

In reaching a conclusion concerning the use of fractures in flooding operations it is desirable to know the kind and extent of fractures which result from normal fracture treatments. Well productivity and pressure build-up tests which measure the effective flow near and far from the well can indicate the alteration in these flow regions resulting from fracturing operations. The development of the influence of various fractures on the productivity and build-up tests should make those tools useful for this purpose. A study of this was undertaken with an electrical analog model.

The kind of fracture, horizontal or vertical, and its length and conductivity relative to that of the formation control the magnitude of the increase to be obtained in a fractured well's productivity. The influence of these variables on productivity as obtained by the analog model is illustrated in Fig. 6. The ratio of the productivity of the fractured well to that of the unfractured well is illustrated for two significantly different fracture conductivities. The fracture conductivity (C) is expressed as the width of the fracture in feet times the permeability of the packed fracture divided by the permeability of the formation. It was considered that at conductivities over 10,000 the fracture resistance to flow is negligible and therefore no additional studies need be made for greater values. The unfractured well productivity value is for a well which has a ratio of well drainage radius (well spacing distance/2) to wellbore radius of 2,800. The curve of Fig. 6 can be used to approximate other ratios of radii of 2,000, 4,000 and 8,000 by multiplying the productivity ratio by .96, 1.05 and 1.15, respectively.

We could use these relationships to estimate fracture length providing that an estimate can be made of fracture conductivity and orientation (vertical or horizontal). These can be estimated satisfactorily in some cases. However, the most effective and reliable use, considering uncertainties in making the above estimates, is to set upper limits on fracture lengths by observing productivity increases and estimating a range of conductivities likely to bracket the actual one. This can be done best for lower productivity increases, i.e. two- to threefold.

For example, this study shows that considering fracture conductivities expected in most field operations, productivities up to about a twofold increase would indicate short fractures (less than 10 per cent penetration). This is true in the absence of damage or improvement at the well for horizontal or vertical fractures. Fracture conductivities expected in most field operations with conventional treatments (20 to 40 mesh

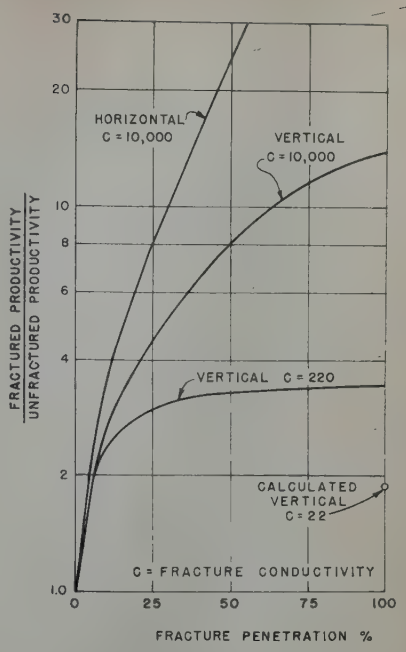
HORIZONTAL C = 10,000
VERTICAL C = 10,000
VERTICAL C = 220
CALCULATED VERTICAL C = 22
C = FRACTURE CONDUCTIVITY
FRACTURED PRODUCTIVITY / UNFRACTURED PRODUCTIVITY
FRACTURE PENETRATION %

FIG. 6—FRACTURED WELL PRODUCTIVITY.

sand) are in the range, 30 to 2,000.* This follows from (1) most formations fractured are in the 1- to 100-md range, (2) a 20- to 40-mesh sand pack has a permeability of 100,000 to 150,000 md, and (3) propped fracture widths are indicated by theoretical calculations and field observations to be a few tenths of an inch.

Increase in productivity greater than about twofold may arise from either relatively long, low conductivity fractures or from relatively short, high conductivity fractures or some intermediate combination. Unless good estimates of conductivity and orientation (vertical or horizontal) can be made in these cases, the fracture length cannot be estimated very well.

It is important to know whether or not a well has improvements or blockage local to the wellbore prior to fracturing if productivity changes are used to determine the presence of short or long fractures. For example, if a well has local blockage a several-fold change in productivity is possible through the establishment of a short fracture that effectively eliminates blockage. If no blockage were assumed, this might be erroneously

*Most notable exceptions occur in some high permeability Gulf Coast sands. This leads to very low conductivities (conductivity of fracture has been defined in this paper relative to formation permeability as conductivity = $\frac{\text{(md) fracture permeability} \times \text{width (feet)}}{\text{formation permeability (md)}}$) and even very long fractures give only about a twofold increase. In this case an upper limit on fracture length cannot be set, but for 20- to 40-mesh sand fractures the conductivity is probably too low to affect sweep-out seriously even for long fractures.

interpreted as indicative of a long fracture.

Similarly, if improvement were present prior to fracturing, a twofold increase in productivity would mean a long and relatively conductive fracture. If no improvement were assumed this would be erroneously interpreted as reflecting a short fracture. Productivity and build-up tests obtained prior to the fracture treatment can be used to evaluate any blockage or improvement that might exist around the well prior to fracturing by either of the methods now in use in the industry.[9,10]

FRACTURE INFLUENCE ON PRESSURE BUILD-UP

Build-up curves are used by the industry to measure the in-place permeability in regions near and far removed from the wellbore. The slope of the straight-line portion of the plot of pressure vs log time has been shown to be independent of reasonable changes in permeability near the wellbore.[9] As longer fractures are achieved with increasingly larger fracture fluid volumes and rates, the slope of the build-up curve must be changed from that of a radial flow system to, in the extreme, that of a linear flow system (100 per cent fracture penetration of high conductivity). The electrical analog model was used to examine the influence of fracture length and conductivity on the slope of pressure build-up curves.

Fig. 7 illustrates the change which occurs in the position of the build-up curve for vertical fractures of different lengths (case of highly conductive fractures). The change in slope is also a function of the conductivity of the fracture. This is illustrated for a completely penetrating vertical fracture in Fig. 8. For example, a completely penetrating fracture with a conductivity of 200 has the same effect as a highly conductive fracture of 30 per cent penetration.

Fractures that extend beyond a 15 per cent penetration alter the position and slope of the straight-line portion of the build-up curve. These changes need to be included in the determination of both the effective permeability of the formation and any calculation of final build-up pressures.

FRACTURES ACHIEVED IN THE FIELD

The sweep-out pattern studies indicate that fracturing can be em-

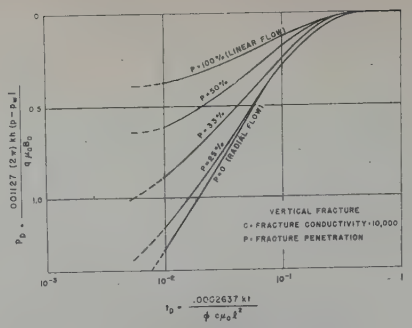

FIG. 7—FRACTURE PENETRATION ON PRESSURE BUILD-UP.

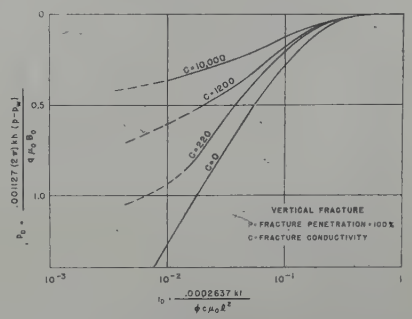

FIG. 8—FRACTURE CONDUCTIVITY ON PRESSURE BUILD-UP.

ployed in flooding operations without any harm to the flood provided the fracture is short (less than one-half if either injection or producing well is fractured or less than one-fourth if both are fractured). Pressure build-up tests (used mainly to establish the absence or presence of wellbore damage prior to fracturing) and productivity tests before and after the treatment will permit differentiation between long and short fractures in the fashion already discussed. Where it can be shown that conventional fracturing techniques result in short fractures, such treatments could be applied with confidence in improving a flooding operation.

An analysis of a large number of pressure build-up curves by an industry study group has shown that on the average, up to 1955, fracturing had achieved less than a twofold increase in productivity.[11] This indicates fractures which do no harm to flood pattern behavior. This is in line with our own observations on build-up analyses in our company. It has usually been difficult to establish a long, effectively conductive fracture. This is also suggested by an analysis of the mechanics of fracturing techniques. Some of the productivity increases reported in the survey[11] were in excess of twofold. Also probably an up-to-date survey would show more cases with greater increases because of the trend of using larger treatments. For these cases we cannot draw firm conclusions about sweep damage because it is more difficult to establish fracture length from well test data, and we have no sweep-out model results for limited conductivity fractures. It is obvious though that our infinite conductivity fracture sweep-out studies lead to a conservative conclusion. So, even fracture increases somewhat beyond twofold probably do not indicate sweep damage is to be expected. However, the prolonged maintenance of a high injection pressure with the water or gas being used in an injection operation may possibly create long and harmful fractures.

CONCLUSIONS

Short fractures (a fracture length up to about one-half), either horizontal or vertical, can be used in flooding operations for the pattern studied (five-spot) to gain an increase in injectivity or productivity without any serious harm to sweep-out pattern.

A long fracture (a fracture length greater than about one-half) does not harm the sweep if it is directed between producers. If it is directed towards a producer, the throughput volume necessary to attain a given recovery is increased. The ultimate recovery will not be significantly reduced until the fracture length exceeds three-fourths.

Productivity and pressure build-up tests obtained prior to and following a fracture treatment on a well can be used to differentiate between a short or long fracture in the reservoir in many cases.

Conventional fracture treatments seem to achieve only short fractures usually and consequently their use in flooding operations would not adversely affect the flood.

NOMENCLATURE*

Fracture length (L) = fraction of distance between fractured well and boundary of element in flood pattern (note reference lengths differ for the two elements of Fig. 1)

*See AIME Symbols List in *Trans.* AIME (1957) **207**, 363, for other symbol definitions.

Fracture penetration (P) = per cent of distance between well and drainage boundary in build-up analyses

Fracture conductivity (C) = measure of the effectiveness of the flow in fracture relative to flow capacity of formation expressed as permeability of fracture times the width of fracture in feet divided by formation permeability

Mobility ratio (M) = mobility (k_r/μ) of swept region divided by mobility of unswept region

q = flow rate, stock tank barrels per day

p_w = shut-in pressure at a time after shut in

t = shut in time, hours

l = one-half well spacing distance, ft

REFERENCES

1. Roark, G. E. and Lindner, J. D.: "Effects of Extensive Well Fracturing in a Waterflood Operation in the North Texas Strawn Sand", *Trans.* AIME (1955) **204,** 16.
2. Stegelman, Arthur, Jr.: "Considerations and Results of Hydraulic Fracturing in Waterflood Areas", *Prod. Monthly* (Jan., 1956) 28.
3. Paul, J. R. and Noble, C. W.: "Waterflood Project Performance Following Fracturing in Eastern Kansas", *Prod. Monthly* (April, 1955) 56.
4. Crawford, P. B. and Collins, R. E.: "Estimated Effect of Vertical Fractures on Secondary Recovery", *Trans.* AIME (1954) **201,** 192.
5. Crawford, P. B. and Collins, R. E.: "Analysis of Flooding Horizontally Fractured Thin Reservoirs", *World Oil* (1954) 139; Sept., 173; Oct., 214; Nov., 212; Dec., 197.
6. Caudle, B. H. and Slobod, R. L.: "X-Ray Shadowgraph Studies of Areal Sweep-Out Efficiencies", *Trans.* AIME (1952) **195,** 265.
7. Dyes, A. B., Caudle, B. H. and Erickson, R. A.: "Oil Production after Breakthrough — As Influenced by Mobility Ratio", *Trans.* AIME (1954) **201,** 81.
8. Craig, F. F., Jr., Geffen, T. M. and Morse, R. A.: "Oil Recovery Performance of Pattern Gas or Water Injection Operations from Model Tests", *Trans.* AIME (1955) **204,** 7.
9. Miller, C. C., Dyes, A. B. and Hutchinson, C. A., Jr.: "The Estimation of Permeability and Reservoir Pressure from Bottom-Hole Pressure Build-Up Characteristics", *Trans.* AIME (1950) **189,** 91.
10. Van Everdingen, A. F.: "The Skin Effect and Its Influence on the Productive Capacity of a Well", *Trans.* AIME (1953) **198,** 171.
11. API Mid-Continent Dist. Study Committee on Completion Practices: "Selection and Evaluation of Well-Completion Method", *Drill. and Prod. Prac.,* API (1955) 421. ★★★

Pressure Fall-Off in Water Injection Wells

P. HAZEBROEK
MEMBER AIME
H. RAINBOW
C. S. MATTHEWS
MEMBER AIME

SHELL DEVELOPMENT CO.

SHELL OIL CO.
HOUSTON, TEX.

ABSTRACT

A new theoretical treatment has been obtained for the behavior of pattern waterflood injection wells when closed in. Two cases are treated: Case 1 where oil and water are assumed to have the same properties, and Case 2 where they are different. In applying the method, one plots log $(p - p_e)$ vs closed-in time, where p is well-bore pressure at any time and p_e is static pressure. The value of p_e is determined by trial and error as that value which makes the plot linear at large time. A value for the permeability-thickness product can be determined from the intercept of this linear part, and a value of the skin factor from the injection pressure at time of closing in. Application of the method to data from water floods at three fields seems to give reasonable results. For the case of unit mobility ratio, it is proved that this new method should give the same value for permeability-thickness product as the conventional pressure build-up method. In addition, the new method gives correct values for static pressure, whereas the conventional method does not, often indicating negative static pressures. The new method may be used in cases where the surface pressure persists after closing in as well as in cases where it does not.

INTRODUCTION

It is of considerable interest and importance to be able to determine the characteristics of the reservoir in an area surrounding a water injection well. Thus, if we can determine early in the life of an injection well that there is a considerable "skin effect", remedial measures can be started before a full-scale pattern flood begins. Similarly, if it can be shown that a gradual buildup of skin effect is occurring with time, measures to free the water of plugging material can be taken. Determination of static pressure in the water-injection well may show that the water is entering a thief zone and not the desired reservoir. Finally, determination of the permeability of the sand around the injection well will allow estimation of the future relation between injection pressure and rate.

It should be possible to determine average reservoir permeability, skin effect and static pressure from pressure fall-off data. However, at the time we began work on this subject, it was thought that no adequate theory on which to base such determinations was available. According to the conventional method which considers the reservoir to be filled with one fluid of small compressibility (see Van Everdingen[1]*, Joers[2], and Nowak[3]), shut-in pressure is plotted vs log $[(t_c + \Delta t)/\Delta t]$ where t_c is injection time, and Δt is closed-in time. The physical significance of injection time, t_c, may well be questioned in this case, since in a reservoir completely filled with a single fluid (as required by this theory) and with input and output rates equal, the pressure behavior after an initial transient is independent of t_c. Attempts by our Tulsa area to use this theory led to negative values of static pressure in most cases.

Because of these limitations of the method discussed above, it was decided to attempt to develop a new theory of pressure behavior in water injection wells, one which would apply when there is a gas saturation, as is so often the case in water floods.

In the following treatment the assumptions and basic equations are given first, then the method of application of the equations. A complete example is given to clarify details of application. All difficult mathematics has been placed in the appendices so that the reader can follow the text without difficulty. However, if he wishes only to apply the results without knowing the basis for them, he can learn how to do this from reading only the sections entitled "Plotting of Experimental Results" and "Example."

ASSUMPTIONS AND BASIC EQUATIONS

Statement of Problem

It will be assumed that a horizontal layer of constant thickness contains in its pore system a mixture of oil, gas and water. While water is being injected into this pore system through a well at constant rate, an oil bank is built up, gas being expelled from the space taken by the oil as shown in Fig. 1. The saturations within each

Original manuscript received in Society of Petroleum Engineers office July 17, 1957. Revised manuscript received July 7, 1958. Paper presented at 32nd Annual Fall Meeting of Society of Petroleum Engineers in Dallas, Tex., Oct. 6-9, 1957.

[1]References given at end of paper.

*Van Everdingen did not claim that the theory he developed would apply to water injection wells. Joers and Nowak did make the claim.

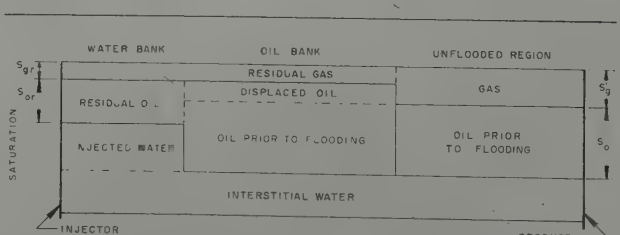

FIG. 1—FLUID SATURATIONS IN THE RESERVOIR.

bank are assumed to be constant. The assumption will be made that the boundary between the oil bank and water bank and likewise the outer boundary of the oil bank are of circular cross section, concentric with the well as shown in Fig. 2. The pressure at the outer boundary remains constant and equal to the gas pressure. The water-oil interface and the outer boundary move outward while water injection continues. After a time, t_c, water injection is stopped. It is required to find the change in bottom-hole pressure in the closed-in well.

First the case will be considered where the water and oil are assumed to have identical compressibility, viscosity and relative permeability. Then the case will be discussed where these physical properties are different for water and oil.

Equations for Case 1: Physical Constants of Water and Oil Are Assumed Equal

We consider first the pressure build-up in the formation during injection. In Appendix 1 it is shown that except in the beginning of the injection period the fluid behaves very nearly as if it were incompressible. The pressure distribution in the formation for an incompressible fluid is

$$p = p_e + \frac{i\mu}{2\pi kh} \ln \frac{r_e}{r}, \quad . \quad . \quad . \quad . \quad . \quad . \quad . \quad . \quad (1)^*$$

where the external boundary radius at injection time, t, is

$$r_e = \sqrt{it/\pi\phi h(S_g - S_{gr})} \quad . \quad . \quad . \quad . \quad . \quad . \quad . \quad (2)$$

Further, taking account of the skin factor, S, the bottom-hole injection pressure is

$$p_o = p_e + \frac{i\mu}{2\pi kh}\left[S + \ln \frac{r_e}{r_w}\right] \quad . \quad . \quad . \quad . \quad . \quad . \quad (3)$$

Let the well be closed in at time, $t = t_c$. Then the outer fluid radius has grown to a value which may be obtained from Eq. 2 by putting $t = t_c$. After the well is shut in, the compressibility has to be taken into account. Then the pressure in the formation satisfies the equation,

$$\frac{\partial^2 p}{\partial r^2} + \frac{1}{r}\frac{\partial p}{\partial r} = \frac{\phi\mu c}{k}\frac{\partial p}{\partial t} \quad . \quad . \quad . \quad . \quad . \quad . \quad . \quad (4)$$

After closing in, only the fluid remaining in tubing or casing flows into the formation, and this occurs at a decreasing rate. This amount of fluid is very small compared to the pore volume occupied by fluid in the formation. Further increase of r_e is almost entirely due to expansion of the compressed liquid in the formation and may be shown to be comparatively small. Hence, the pressure at distance r_e at time of closing in will not be much different from p_e and will revert again to p_e when the pressure stabilizes to p_e everywhere in the field. Hence, only a small error will be made when, after closing in, the pressure is assumed to be equal to p_e at the radius r_e at closing-in time.**

Thus, we take as boundary condition,

$$p = p_e \text{ at } r = r_e, \quad . \quad . \quad . \quad . \quad . \quad . \quad . \quad . \quad . \quad (5)$$

where r_e has now a fixed value.

In general, a surface pressure is required to maintain the injection rate, i. Regarding this pressure there

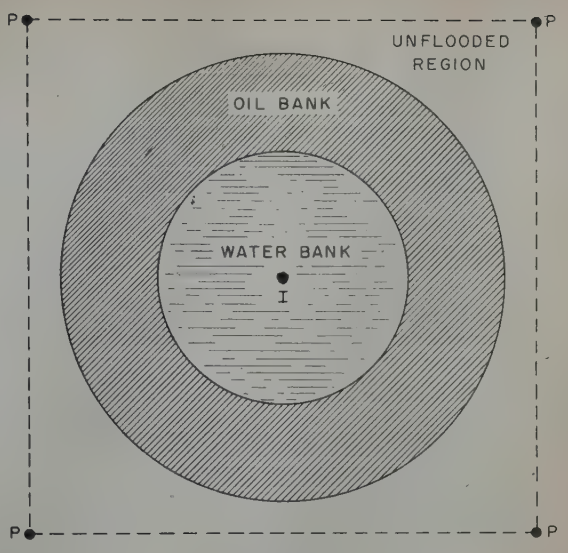

I = INJECTOR
P = PRODUCER

Fig. 2—Oil and Water Banks.

are two possibilities to be considered after the well has been closed in. (1) The surface pressure decreases slowly and the well stays filled up to the top for considerable closed-in times. This would happen in the case of high reservoir pressures. Afterflow into the formation would then result only from expansion of the water in the well as the pressure decreases. (2) The surface pressure drops to zero a short time after closing in, after which the fluid level starts to sink. In this case the volume of inflow into the formation at any time is for practical purposes equal to the volume between the top of the well and the water level of the wellbore column, the expansion of the water being comparatively negligible.

If the surface pressure during flowing time is p_h and the bottom-hole pressure p_o, we have as initial closed-in condition for the bottom-hole pressure for Case A,

$$p_w = p_o \text{ for } t = t_c, \quad . \quad . \quad . \quad . \quad . \quad . \quad . \quad . \quad (6)$$

and for Case B,

$$p_w = p_o - p_h \text{ for } t = t_c \quad . \quad . \quad . \quad . \quad . \quad . \quad . \quad (6a)$$

It is shown in Appendix 2 that

$$\frac{dp_w}{dt} = \chi\left[r\frac{\partial p}{\partial r}\right]_{r=r_w}, \quad . \quad . \quad . \quad . \quad . \quad . \quad . \quad . \quad (7)$$

where for Case A,

$$\chi = \frac{8kh\rho g}{\mu d_t^2 c(p_w - p_h)}, \quad . \quad . \quad . \quad . \quad . \quad . \quad . \quad . \quad (8)$$

and for Case B,

$$\chi = \frac{8kh\rho g}{\mu d_t^2}, \quad . \quad . \quad . \quad . \quad . \quad . \quad . \quad . \quad . \quad (8a)$$

Note that the quantity, $p_w - p_h$, in Eq. 8 is equal to the hydrostatic pressure, $\rho g z_o$. Finally the bottom-hole pressure and the formation pressure at the well are connected by

$$p_w = p(r_w) - S\left[r\frac{\partial p}{\partial r}\right]_{r=r_w} \quad . \quad . \quad . \quad . \quad . \quad . \quad (9)$$

Eq. 4, together with Eqs. 5, 6, 7, 8 and 9, completes the system of equations we must solve. From this system the following formula for the well pressure is derived in Appendix 3.

$$p_w = p_e + \frac{i\mu}{2\pi kh}\sum_{n=1}^{\infty} B_n e^{-x_n^2 \Delta t_D}, \quad . \quad . \quad (10)$$

*In the theoretical developments quantities are expressed in the cgs system of units. However, in equations which the engineer will use in applications of this work, quantities are expressed in common engineering units: psi, ft, B/D, cp, sec, and md. Factors to affect the necessary conversions have been made in equations he will use. The units given under "Nomenclature" are correct for use in these equations of application. (Eqs. 11, 12, 13, 15, 17, 21, 22, 24, 25 and 26).

**With this assumption liquid is still allowed to flow across the fixed boundary, r_e, due to expansion.

where B_n is defined in Appendix 3 by Eqs. 59, 60 and 61.

Method for Application of Case 1

We have found that observed values of the bottom-hole pressure, p_w, in an injection well closed in for time Δt can be fitted by a series of exponentials similar to the theoretical Eq. 10.

$$p_w(t) = p_e + \sum_n b_n e^{-\beta_n \Delta t} \quad . \quad . \quad . \quad . \quad (10a)$$

In actual examples usually only the first term, $b_1 e^{-\beta_1 \Delta t}$, is determined, this being sufficient to allow values of the permeability and the skin factor to be obtained in applications of the theory. If we compare this first term with the first term, $B_1 e^{-\alpha_1^2 \Delta t}$ in Eq. 10, we obtain

$$\frac{B_1}{b_1} \quad \frac{2\pi kh}{i\mu} \quad . \quad . \quad . \quad . \quad . \quad . \quad . \quad . \quad . \quad . \quad (11)$$

As shown in Appendix 3, this can be reduced to

$$kh = \frac{i\mu}{b_1} \cdot \frac{1 - C_1 - C_2}{(1 - C_3)^2} \cdot f(\theta) \ , \quad . \quad . \quad . \quad (12)$$

and knowing kh we can find S from Eq. 3, which is, in practical units,

$$S + \ln \frac{r_e}{r_w} \cong \frac{0.00708(p_o - p_e)}{i\mu/kh}, \quad . \quad . \quad . \quad (13)$$

where r_e may be calculated from

$$r_e = \sqrt{\frac{W_i(5.615)}{\pi\phi(S_g - S_{gr})h}} \quad . \quad . \quad . \quad . \quad . \quad . \quad (14)$$

Eqs. 12, 13 and 14 are written for the following practical system of units: k in md, h in ft, i in B/D, W_i in bbl, μ in cp, and b_1 in psi.

The quantities, C_1, C_2 and C_3, when expressed in practical units, become for Case A where the surface pressure persists after closing in,

$$\left.\begin{aligned} C_1 &= 194 \, \frac{d_t^2 \beta_1 b_1 c(p_w - p_h)}{i\rho} \\ C_2 &= 0 \\ C_3 &= \frac{p_o - p_e}{b_1} C_1 \end{aligned}\right\},$$

for Case B where the surface pressure drops to zero shortly after closing in,

$$\left.\begin{aligned} C_1 &= 194 \, \frac{d_t^2 B_1 b_1}{i\rho} \\ C_2 &= \frac{p_h}{b_1} C_1 \\ C_3 &= \frac{p_o - p_e}{b_1} C_1 \end{aligned}\right\} \quad . \quad . \quad . \quad . \quad . \quad . \quad . \quad . \quad (15)$$

and for both cases A and B

$$\theta = \frac{C_1(1 - C_3)}{2(1 - C_1 - C_2)} \, .$$

Here d_t is the diameter of tubing or casing expressed in inches, ρ is in gm/cc, c is in psi^{-1}, p is in psi, and β_1 is expressed in sec^{-1}. When β_1 is expressed in (hours)$^{-1}$ the factor (194) in C_1 should be replaced by 0.0538. The quantities p_w and p_h should be taken at time of closing in. Note that $p_w - p_h$ is constant for Case A.

In Case A and very often in Case B the quantities, C_1, C_2, C_3, and θ are small and $f(\theta)$ can be taken equal to $f(0) = 181$. This means that the effect of the after flow into the formation is negligible. In that case we have simply,

$$kh = 181 \, \frac{i\mu}{b_1}$$

Equations for Case 2: Physical Constants of Water and Oil Assumed Different

In this case, we have to restrict ourselves to the limiting assumption that after closing in, no water flows from the well into the formation. The general problem where water is allowed to flow into the formation, though soluble, yields formulas too unwieldy to be of practical use. The restricted problem corresponds to the case where θ is small in our first problem. We have observed that this occurs very frequently so the theory can still often be applied.

First, we consider the flowing period. It does not seem easy to obtain a rigorous solution when both oil and water are considered compressible. On the strength of the result we found for a single compressible fluid, it seems reasonable to assume that after a short time both fluids behave as if they were incompressible. If so, the pressures in the water and in the oil regions, p_1 and p_2, are easily found to be

$$\left.\begin{aligned} p_1 &= \frac{i\mu_w}{2\pi k_w h}\left[\ln \frac{r_e}{r} + (M - 1) \ln \frac{r_e}{r_o}\right] + p_e \ , \\ p_2 &= \frac{i\mu_w}{2\pi k_w h} M \ln \frac{r_e}{r} + p_e \ , \end{aligned}\right\} \quad . \quad (16)$$

where

$$M = \frac{k_w \mu_o}{k_o \mu_w} \quad . \quad . \quad . \quad . \quad . \quad . \quad . \quad . \quad . \quad . \quad (17)$$

is the mobility ratio of water and oil.

Next we consider the pressure behavior after closing in. We now assume the fluids to be compressible. The pressures satisfy Eq. 4 where the appropriate subscripts for water and oil should be put in. As in Case 1 the approximate assumption is made that r_e remains constant and equal to its value at closing-in time. In addition no flow is allowed to take place across the wellbore.

In Appendix 4 it is found that under such conditions,

$$p_w = p_e + \frac{i\mu_w}{2\pi k_w h} \sum_{n=1}^{\infty} B_n e^{-\alpha^2 n \Delta t_D} \ , \quad . \quad (18)$$

where B_n is defined in Appendix 4 by Eqs. 86 to 89.

Method for Application of Case 2

As in Case 1, only the first term of the series will be used. From the definition of B_1 we find

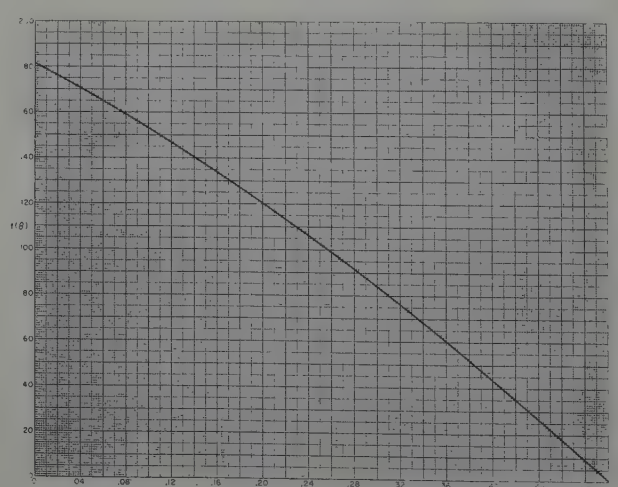

Fig. 3—Function for Calculating kh, Case 1.

$$k_w h = \frac{i\mu_w}{b_1} \cdot \frac{B_1}{2\pi}, \quad \ldots \quad (19)$$

hence

$$k_o h = \frac{i\mu_o}{b_1} \cdot \frac{1}{M} \cdot \frac{B_1}{2\pi}. \quad \ldots \quad (20)$$

In practical units of md, ft, B/D, cp and psi,

$$k_w h = \frac{i\mu_w}{b_1} (2F) \quad \ldots \quad (21)$$

and

$$k_o h = \frac{\mu_o}{\mu_w} \frac{k_w h}{M}, \quad \ldots \quad (22)$$

where

$$F = 141.2\, B_1. \quad \ldots \quad (23)$$

In order to obtain F we still have to know R_o, which may be obtained from the saturation data.

$$R_o = \frac{1}{\sqrt{\frac{V_o}{V_w} + 1}}, \quad \ldots \quad (24)$$

where at times prior to fill-up,

$$\frac{V_o}{V_w} = \frac{\text{volume oil bank}}{\text{volume water bank}} = \frac{S_o - S_{or}}{S_g - S_{gr}} \quad \ldots \quad (25)$$

A set of curves (Figs. 4, 5 and 6) have been constructed giving F as a function of M for assumed values of the parameters, R_o and γ. Each figure corresponds to a value of $\gamma(\gamma = 1, 2$ and $4)$ and gives curves corresponding to values, $R_o = 0.1,\ 0.2, \ldots,\ 0.9, 1$. Curves for the limiting case, $R_o = 0$, have been drawn for $\gamma = 2$ and $\gamma = 4$ when $M > 2$. These curves have been omitted for other values of γ and M because of their closeness to the curve, $R_o = 0.1$. The plotted value of F contains a number of conversion constants such that kh is obtained in md-ft when i is in B/D, μ is in cp, and b_1 is in psi.

It will be noticed that the quantities, C_1, C_2 and C_3, are not used in these calculations. The quantities entered into Eqs. 12 because of the afterflow from the wellbore into the formation which took place after

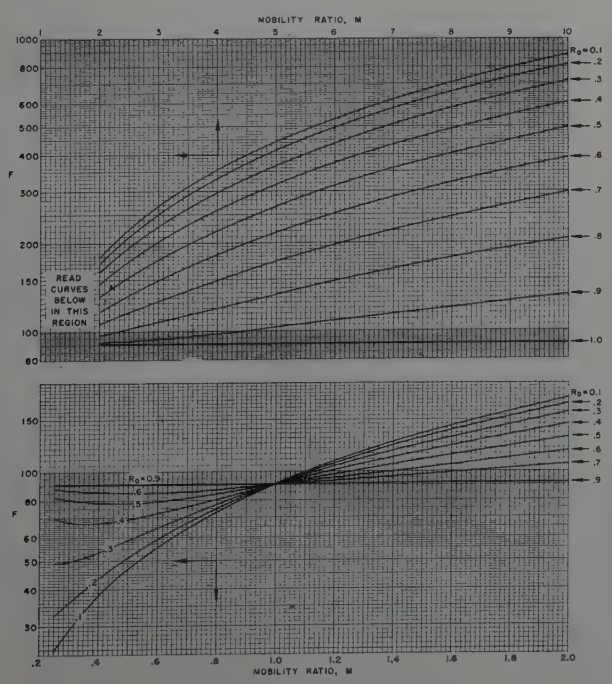

FIG. 4—FUNCTION FOR CALCULATING kh, CASE 2, $\gamma = 1$.

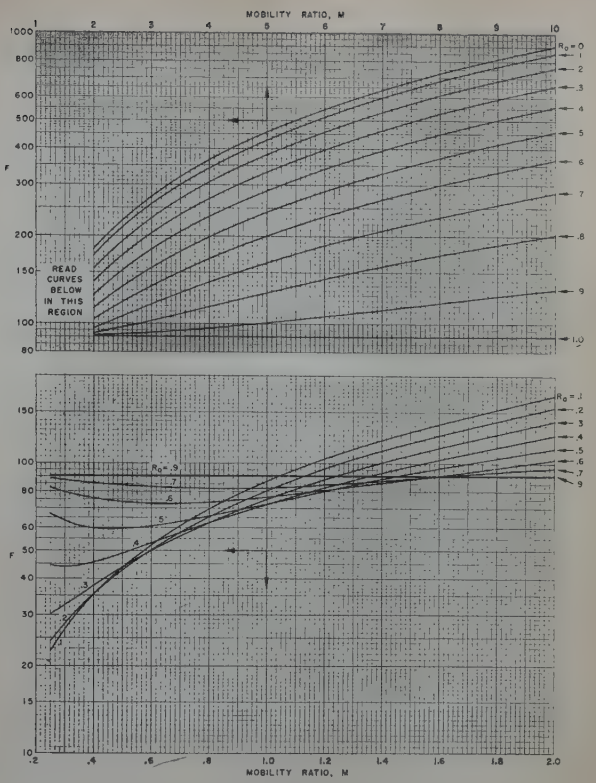

FIG. 5—FUNCTION FOR CALCULATING kh, CASE 2, $\gamma = 2$.

closing in at the surface. No afterflow was assumed to take place in Case 2 so that these quantities did not appear. However, it is suggested that C_1 be calculated for Case 2 to determine whether Case 2 is applicable. If C_1 is small, then the afterflow will be small for each unit drop in pressure. Tentatively, it is suggested that Case 2 be applied only when $C_1 \leq 0.1$.

An estimate of S for Case 2 may be obtained from the flowing bottom-hole pressure just before closing in.

$$p_o = \frac{i\mu_w}{2\pi k_w h}\left[S + \ln\frac{r_e}{r_w} + (M-1)\ln\frac{r_e}{r_o}\right] + p_e.$$

As $\ln\ (r_e/r_o) = (1/2)\ \ln[(V_o/V_w) + 1]$, we find in practical units,

$$S + \ln\frac{r_e}{r_w} = 0.00708\,\frac{(p_o - p_e)\,k_w h}{i\mu} - \frac{M-1}{2} \cdot \ln\left[\frac{V_o}{V_w} + 1\right]. \quad \ldots \quad (26)$$

PLOTTING OF EXPERIMENTAL RESULTS

As we have seen, in applying the theory it is necessary to determine p_e, b_1, and β_1 in the series (Eq. 10a) for $p_w(t)$. This may be done graphically as follows. We assume some reasonable value for p_e, then plot log $(p - p_e)$ vs t where p is the wellbore pressure at any time, t. If the result is not a straight line at large times, the value of p_e is changed and a new curve plotted. On semilog paper the new curve can be plotted without any additional computations by shifting the previous points a certain amount, Δp, in pressure at the same value of time. For example, in Fig. 7 Curve B shows values obtained for $p_e = 200$ psi. By mentally subtracting 30 psi from the value of $p - p_e$ for each point we plot Curve C, for which $p_e = 230$ psi.

It is sometimes difficult to tell when the best straight

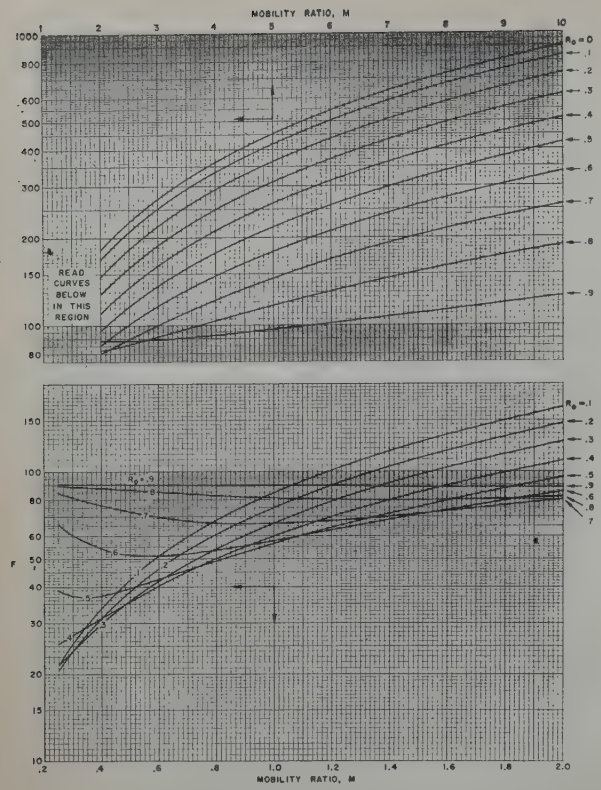

FIG. 6—FUNCTION FOR CALCULATING kh, CASE 2, $\gamma = 4$.

line is obtained. For example, a straight line can also be drawn through the last few points of Curve B in Fig. 7. We have found it helpful in such cases to "bracket" the best curve by curves of type A and B, Fig. 7.

When the assumed value of p_e is too high, the curve turns down, as in Curve A, Fig. 7. For too low a value of p_e the curve turns up as in Curve B, Fig. 7. The value of p_e which gives Curve C is the correct one. The intercept at $t = 0$ is b_1 and β_1 is obtained by multiplying the slope of the straight line by 2.303.

For cases where the surface pressure persists during shut in one need only plot log $(p' - p'_e)$ vs t, where p' is the surface pressure at any time and p'_e is the static surface pressure.

EXAMPLE

Fig. 8 shows an example pressure fall-off curve. The value of p_e was known for this well from a previous lengthy shut-in period. This value (32 psi) was used in plotting Fig. 8. We have the following data on this well.

$i = 1{,}020$ B/D
$h = 45$ ft
diameter casing = 6.366 in. (no tubing)
$p_o = 598$ psi
$p_h = 0$
cumulative injection = 6,097 bbl
$\mu_w = 0.9$ cp
$\rho = 1$ gm/cc
$r_w = 1$ ft*
$\phi = 0.3$
$S_{wc} = 0.30$
$S_g = 0.12$
$S_{gr} = 0$
$S_o = 0.58$
$S_{or} = 0.2$

*Estimated on basis of sand removed during swabbing.

$M = 4$ (estimated)

$$\frac{V_o}{V_w} = \frac{S_o - S_{or}}{S_g - S_{gr}} \simeq 3$$

CASE 1

From Fig. 8 we find $b_1 = 347$ psi and $\beta_1 = 1.45 \times 10^{-5}$ sec^{-1}. According to Eq. 15 we have for the case where the surface pressure drops to zero shortly after closing in,

$$C_1 = \frac{194 d_t^2 \beta_1 b_1}{\rho i} = \frac{194(6.366)^2\ 1.45 \times 10^{-5}\ (347)}{1(1{,}020)}$$

$$= 0.0386$$

$C_2 = 0$, since $p_h = 0$

$$C_3 = C_1 \cdot \frac{\Delta p_o}{b_1} = 0.0386\left[\frac{566}{347}\right] = 0.0628 .$$

Then

$$\theta = \frac{C_1(1 - C_2)}{2(1 - C_1 - C_2)} = \frac{0.0386(0.937)}{2(0.961)} = 0.0188 .$$

From Fig. 3, $f(\theta) = 176.5$. Therefore,

$$kh = \frac{i\mu}{b_1} \cdot \frac{(1 - C_1 - C_2)}{(1 - C_3)^2} \cdot f(\theta) = \frac{1{,}020(0.9)}{347} \cdot \frac{(0.961)}{(0.937)^2} \cdot 176.5 = 511 \text{ md-ft (Case 1)},$$

and

$$S + \ln \frac{r_e}{r_w} = \frac{0.00708(p_o - p_e)}{i\mu/kh}$$

$$= \frac{0.00708(566)}{1{,}020(0.9)/511} = 2.23 .$$

According to Eq. 14,

$$r_e = \sqrt{\frac{6097(5.615)}{\pi(0.3)(0.12)(45)}} = 82 \text{ ft} .$$

Therefore, $S = 2.23 - 2.303 \log (82/1) = -2.18$ (Case 1).

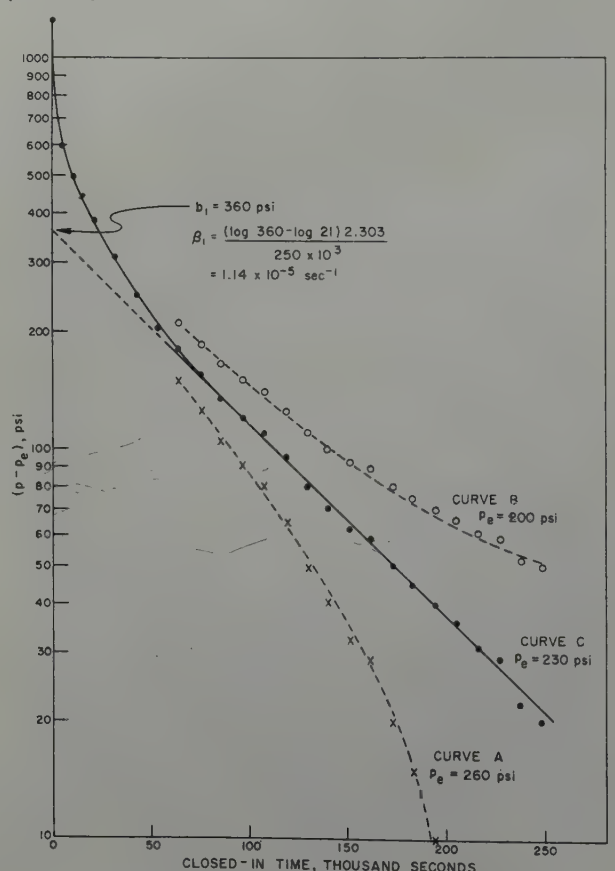
b_1 = 360 psi
$\beta_1 = \frac{(\log 360 - \log 21)\ 2.303}{250 \times 10^3}$
$= 1.14 \times 10^{-5}$ sec^{-1}
CURVE B
p_e = 200 psi
CURVE C
p_e = 230 psi
CURVE A
p_e = 260 psi
$(p - p_e)$, psi
CLOSED-IN TIME, THOUSAND SECONDS

FIG. 7—PRESSURE FALL-OFF CURVE.

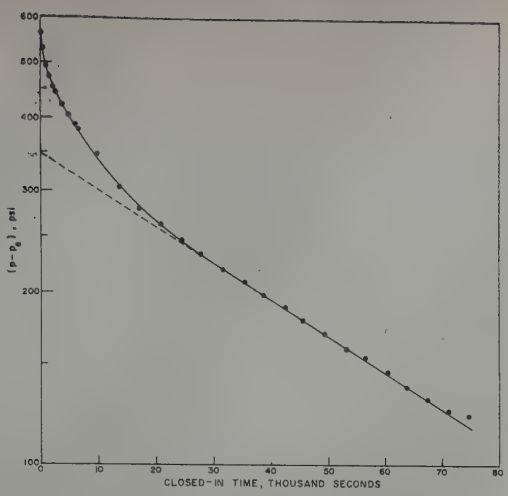

FIG. 8—PRESSURE FALL-OFF CURVE.

CASE 2

According to Eq. 24,

$$R_o = \frac{1}{\sqrt{\frac{V_o}{V_w} + 1}} = \frac{1}{\sqrt{4}} = 0.5 .$$

Further, $M = 4$ and $\gamma = 1$ since $c_o \cong c_w$ for most dead oils. Therefore, using Eq. 21, and reading F from Fig. 4, we obtain

$$k_w h = \frac{i\mu_w}{b_1} \cdot 2F$$

$$= \frac{1{,}020(0.9)}{347} \cdot 2(221)$$

$$= 1{,}170 \text{ md-ft (Case 2)} .$$

This value of $k_w h$ is 2.28 times as large as the value obtained for the single-fluid case (Case 1).

The skin effect is found from Eq. 26.

$$S = \frac{0.00708(566)\ 1{,}170}{1{,}020(0.9)} - \frac{4-1}{2} \ln 4 - \ln \frac{82}{1}$$

$$= 5.10 - 2.08 - 4.41$$

$$= -1.39 \text{ (Case 2)} .$$

FIELD RESULTS

Table 1 gives representative values of p_e, kh, and S calculated from the theories of Case 1 for Field 2 and from Cases 1 and 2 for Fields 1 and 3. The mobility ratio was not known for Field 2 so that Case 2 could not be applied there. A list of the constants used in obtaining the values in these tables is given in Appendix 5. The values shown in Table 2 under "Conventional Method", discussed in the "Introduction", were determined by our Tulsa area. In Table 1 for Field 1, Case 2, we took $k_w h \cong k_o h$, in agreement with flood-pot results.

The average value of $k_w h$ or $k_o h$ obtained at Field 1 from fall-offs on 20 wells was 396 md-ft. This leads to an average permeability to water or oil of about 11 md. The average air permeability at Field 1 was 65 md, and from relative permeability results the average permeability to water or oil at the appropriate water or oil-bank saturation is 6.5 md, in reasonable agreement with the above value.

Assuming that the mobility ratio and relative permeability at Field 2 is about the same as Field 1, we obtain an average water permeability of 9 md from fall-off results for Field 2 which compares with an air permeability of 152 md. Or, assuming a relative permeability to water of 0.1 at the water-bank saturation (as at Field 1), we obtain a permeability to water of 15 md, again in fair agreement with pressure fall-off results.

At Field 3 the average permeability to water obtained in well fall-offs is 136 md over an 80-ft interval. From core data we calculate an average air permeability of 1,300 md and a relative permeability to water of 0.15 at water-bank saturation. These figures lead to a water permeability of 195 md, in reasonable agreement with the fall-off data.

At Field 3 the static pressure around each injector was known from lengthy shut-in periods prior to injection. These values were used in plotting results for this field, and in every case led to a curve linear at large time as predicted by the theory (see Fig. 8 for an example). The fact that these independently determined values of p_e behaved as predicted lends confidence to use of this theory.

Table 2 gives a comparison of values determined by our Case 1 method and that determined by the conventional method of Van Everdingen[1] (1953) as used by Joers[2] (1954) and Nowak[3] (1955). The values of kh and S given by the two methods agree surprisingly well considering the vast difference in theory and treatment of data. The conventional method is somewhat more erratic. The negative values of static pressure given by the conventional method are, of course, meaningless, and probably indicate that all values of static pressure obtained by the conventional method are incorrect. A better static value might have been obtained by the method of Matthews and Brons[4] (1952).

All values shown in Table 2 are for the case where the surface pressure drops to zero within a few minutes after closing in. Equally good agreement between kh values was obtained for cases where the surface pressure persisted after closing in.

COMPARISON OF CONVENTIONAL AND PRESENT THEORY

As noted, Table 2 shows that values of kh obtained by the conventional procedure and by application of Case 1 are in most cases of the same order of magnitude. This seems rather surprising as, at first sight, there

TABLE 1—APPLICATION TO DATA FROM WATER FLOODS

		Case 1			Case 2		
Field	Well	p_e (psia)	kh (md-ft)	S	$k_w h$ (md-ft)	$k_o h$ (md-ft)	S
1	1	465	67	−4.2	120	120	−3.8
	2	277	367	−3.2	660	660	−1.0
	3	297	970	+11.6	1,750	1,750	+25.6
2	1	81	41	−1.3			
	2	30	430	−5.5			
	3	103	98	−4.0			
3	1	20	5,540	−0.5	13,400	111,700	+3.2
	2	35	3,960	−0.4	8,220	68,500	+2.7
	3	32	5,340	0	10,960	91,300	+2.4

TABLE 2—COMPARISON OF RESULTS FROM CASE 1 AND OLDER CONVENTIONAL METHOD

		Case 1			Conventional Method		
Field	Well	p_e (psia)	kh (md-ft)	S	p_e (psia)	kh (md-ft)	S
1	1	465	67	−4.2	−264	70	−4.6
	2	277	367	−3.2	−36	580	−1.5
	3	297	970	+11.6	263	3,000	+49.0
2	1	81	41	−1.3	−380	60	−0.8
	2	30	430	−5.5	−15	260	−2.2
	3	103	98	−4.0	−517	140	−2.0
3	1	20	5,540	−0.5	13	9,100	+2.7
	2	35	3,960	−0.4	−135	3,500	+1.3
	3	32	5,340	0	−8	6,000	+2.0

is no apparent connection between the two methods. The agreement may, however, be explained as follows if we restrict ourselves to the limiting case where flow into the wellbore after closing in is negligible. For this case we have shown in Appendix 3 that the well pressure after closed-in time, Δt, is given by

$$p_w(\Delta t) = p_e + \frac{i\mu}{2\pi kh} \sum_{n=1}^{\infty} B_n e^{-x_n^2 \Delta t_D} \quad . \quad (27)$$

where $\Delta t_D = \frac{k\Delta t}{\phi\mu c r_e^2}$, $B_n = \frac{2}{x_n^2 J_1^2(x_n)}$, and x_n are the zeros of $J_0(x)$. Eq. 27 may be written,

$$p_w(\Delta t) = p_e + \frac{i\mu}{4\pi kh} \ln \frac{\Delta t}{t_c + \Delta t} + \frac{i\mu}{2\pi kh} \cdot \left(\sum_{n=1}^{\infty} B_n e^{-x_n^2 \Delta t_D} - \frac{1}{2} \ln \frac{\Delta t_D}{t_{Dc} + \Delta t_D} \right) \cong p_e + \frac{i\mu}{4\pi kh} \ln \frac{\Delta t}{t_c + \Delta t} + \frac{i\mu}{2\pi kh} \left(Z(\Delta t_D) + \frac{1}{2} \ln t_{Dc} \right), \quad . \quad . \quad . \quad (28)$$

where

$$Z(\Delta t_D) = \sum_{n=1}^{\infty} B_n e^{-x_n^2 \Delta t_D} - \frac{1}{2} \ln \Delta t_D ,$$

and $\ln (t_{Dc} + \Delta t_D)$ has been replaced by $\ln t_{Dc}$, since Δt_D is small compared to t_{Dc}.

A numerical evaluation shows that $Z(\Delta t_D)$ is for practical purposes constant for values of $\Delta t_D < 0.2$. It may be shown that this constant is equal to $\ln 2 - (\frac{1}{2})\ C = 0.4045$, where C = Euler's constant = 0.5772. Hence, for $\Delta t_D < 0.2$ the slope of the curve of p vs $\ln [\Delta t/(t_c + \Delta t)]$ is $i\mu/4\pi kh$, and thus, for no influx through the wellbore after closing in, and for $\Delta t_D < 0.2$, the conventional method and the present method should lead to the same value of kh.*

Unfortunately there is flow across the wellbore on closing in, with the result that the pressure readings at early times are disturbed. Therefore, the conventional method cannot be used at very early times. One must wait until the influx through the wellbore is a small fraction of its original value. On the other hand the conventional method cannot be used for very long closed-in times ($\Delta t_D > 0.2$) because then $Z(\Delta t_D)$ is no longer constant (for very large times the sum of the last two terms in Eq. 28 is zero and $p_w(\Delta t) \to p_e$). Thus, the conventional method should give the correct value of kh if it is applied in the correct time interval; not too early, not too late. The conventional method should give incorrect values for p_e and therefore also for skin factor, S.

An illustrative example of what this means is shown in Fig. 9 for Well 13 at Field 1. The experimental points are shown as dots, together with the straight-line extrapolation through the latter points. This extrapolation leads to a value of p_e of -457 psia, as shown, and the slope of this line gives $kh = 80$ md-ft. Extrapolation according to our new method gives $p_e = 288$ psia and $kh = 58$ md-ft. These two values of kh are in reasonable agreement.

We may conclude that the conventional theory should theoretically give correct values of kh for the case

*The conventional method and the present method, when modified to reflect the condition of no flow across the outer boundary should also lead to the same value of kh for depletion-type reservoirs.

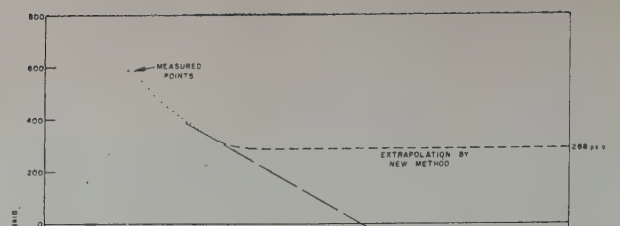

FIG. 9—COMPARISON OF THEORIES.

where oil and water have the same physical properties. In practice some error may be made when the conventional method is used because of indecision as to where the straight-line section is. The conventional theory leads to incorrect values of p_e, and therefore of skin factor, S. Finally, it is not possible to take the effects of mobility ratio into account in the conventional theory.

CONCLUSIONS

Application of this new theory to injection wells on Shell water floods seems to give reasonable values for reservoir parameters such as permeability, skin factor and static reservoir pressure. Values obtained for static reservoir pressure are much more reasonable than those given by conventional methods. The new method allows determination of reservoir parameters when there is a considerable gas saturation, as would be the case in the initial stages of flooding a reservoir depleted by solution gas drive. This permits early determination of whether the injection wells have been completed properly, or are in need of remedial measures. It is believed that this new theory will also be applicable to water floods after fill-up.

NOMENCLATURE**†

b_1 = constant in Eq. 10a, found as intercept on a plot such as Fig. 7, psia
B_1 = constant in Eqs. 10 and 18
$C_1 = 194 d_t^2 \beta_1 b_1 / i\rho$, dimensionless
$C_2 = 194 d_t^2 \beta_1 p_h / i\rho$, dimensionless
$C_3 = 194 d_t^2 \beta_1 \Delta p_o / i\rho$, dimensionless
d_t = inside diameter of tubing, if there is one, or of casing, in.
$f(\theta)$ = function for calculating kh, Case 1
F = function for calculating kh, Case 2
$M = k_w\mu_o / k_o\mu_w$ = water-to-oil mobility ratio
p_h = pressure at wellhead, psia
p_o = sand face injection pressure at time of closing in, psia
r_o = outer radius of water bank, ft
$R_o = r_o / r_e$
S_{wc} = interstitial water saturation at time of flooding
S = skin factor = (pressure drop across skin)/$(i\mu/2\pi kh)$ in consistent units
t_c = time at which well is closed in, sec
Δt = closed-in time, sec

See AIME Symbols List in *Trans.* AIME (1957) **207, 363, for other symbol definitions.
†See footnote for Eq. 1.

t_D = dimensionless time (see Eq. 51)
Δt_D = dimensionless closed-in time
t_{De} = time at which well is closed in, dimensionless
$\frac{V_o}{V_w} = \frac{\text{volume of oil bank}}{\text{volume water bank}}$, before fill-up
$= (S_o - S_{or})/(S_g - S_{gr})$
β_1 = constant in Eq. 10a, sec^{-1}
= (slope of straight line in Fig. 7) · (2.303)
$\theta = [C_1(1 - C_3)]/[2(1 - C_1 - C_2)]$
$\gamma = c_o/c_w$
$\chi = \frac{8kh\rho g}{\mu d_t^2 c(p_w - p_h)}$ or $\frac{8kh\rho g}{\mu d_t^2}$
$ei(x) = \int_x^\infty \frac{e^{-x}}{x}\,dx$

REFERENCES

1. Van Everdingen, A. F.: "The Skin Effect and Its Influence on the Productive Capacity of a Well", *Trans.* AIME (1953) **198**, 171.
2. Joers and Smith: "Determination of Effective Formation Permeabilities and Operation Efficiencies of Water-Input Wells", presented at 18th Penn. State Conf. on Pet. Prod. (1954).
3. Nowak, T. J. and Lester, G. W.: "Analysis of Pressure Fall-Off Curves Obtained in Water Injection Wells to Determine Injective Capacity and Formation Damage", *Trans.* AIME (1955) **204**, 96.
4. Matthews, C. S., Brons, F. and Hazebroek, P.: "A Method for Determination of Average Pressure in a Bounded Reservoir", *Trans.* AIME (1954), **201**, 182.
5. Van Everdingen, A. F. and Hurst, W.: "The Application of the Laplace Transformation to Flow Problems in Reservoirs", *Trans.* AIME (1949) **186**, 305.

APPENDIX 1

SOLUTION OF EQUATIONS DURING INJECTION

If water is injected into the formation at constant rate, i, the boundary condition at the well is $r\,(\partial p/\partial r) = -\,i\mu/2\pi kh$ at $r = r_w$. With the usual approximation, this may be replaced by

$$\lim_{r\to 0} r\frac{\partial p}{\partial r} = -\frac{i\mu}{2\pi kh} \quad . \quad . \quad . \quad . \quad . \quad . \quad . \quad (29)$$

At the interface, $r = r_e$, between the oil bank and the unflooded region the pressure is constant and equal to the assumed constant pressure, p_e, in the unflooded region,

$$p = p_e \text{ at } r = r_e \quad . \quad . \quad . \quad . \quad . \quad . \quad . \quad . \quad . \quad (30)$$

The radius, r_e, which increases with the amount of fluid injected, is a function of time. Equating the amount of fluid moving across the interface, $r = r_e$, in time dt to the increase of volume of the fluid bank, we get

$$\frac{dr_e}{dt} = -\frac{k}{(S_g - S_{gr})\phi\mu}\left[\frac{\partial p}{\partial r}\right]_{r=r_e} \quad . \quad . \quad . \quad . \quad (31)$$

We shall try to satisfy Eq. 4 and the boundary conditions (Eqs. 29, 30 and 31) by a solution of the type,

$$p = p_e + g(x) \quad , \quad . \quad . \quad . \quad . \quad . \quad . \quad . \quad . \quad (32)$$

where

$$x = \frac{\phi\mu c r^2}{4kt} \quad . \quad . \quad . \quad . \quad . \quad . \quad . \quad . \quad . \quad (33)$$

Then the partial differential Eq. 4 reduces to the ordinary differential equation,

$$\frac{d}{dx}\left[x\frac{dg}{dx}\right] + x\frac{dg}{dx} = 0\,,$$

which has the general solution,

$$g(x) = C_1 + C_2\,\text{ei}\,x\,,$$

The integration constants, C_1 and C_2, are determined by the boundary conditions (Eqs. 29 and 30), after which the solution reduces to

$$g(x) = \frac{i\mu}{4\pi kh}(\text{ei}\,x - \text{ei}\,x_e) \quad , \quad . \quad . \quad . \quad . \quad . \quad (34)$$

where

$$x_e = \phi\mu c r_e^2/4kt \quad . \quad . \quad . \quad . \quad . \quad . \quad . \quad . \quad . \quad (35)$$

It has still to be shown that Eq. 31 can be satisfied. Using Eqs. 33, 34 and 35, Eq. 31 becomes

$$x_e + t\frac{dx_e}{dt} = \frac{iuc}{4\pi kh(S_g - S_{gr})}e^{-x_e}.$$

The general solution of this equation is of the type $x_e = C/t$ for small t. Further, there is a special solution, x_e = constant = α, where α satisfies the equation,

$$\alpha e^{\alpha} = \frac{iuc}{4\pi kh(S_g - S_{gr})} \quad . \quad . \quad . \quad . \quad . \quad . \quad . \quad (36)$$

In order to decide which one of these solutions is valid we write x_e in the form,

$$x_e = \frac{\phi\mu c r_e^2}{4kt} = \frac{i\mu c}{4\pi kh(S_g - S_{gr})}\cdot\frac{\pi\phi h r_e^2(S_g - S_{gr})}{it}$$
$$= \frac{i\mu c V_t}{4\pi kh(S_g - S_{gr})\,it}$$

where V_t is the pore volume swept out at time t, and it is the amount of injected fluid. It is clear that the ratio V_t/it should be finite for all t, including the limiting value at $t = 0$. Hence, a solution of the type $x_e = C/t$ for t small cannot have physical meaning and the solution $x_e = \alpha$ should be adopted.

If we eliminate x from Eqs. 32 to 35, we find

$$p = p_e + \frac{i\mu}{4\pi kh}\left[\text{ei}\,\frac{\phi\mu c r^2}{4kt} - \text{ei}\,\frac{\phi\mu c r_e^2}{4kt}\right], \quad (37)$$

where r_e as a function of time is given by

$$r_e = \sqrt{\alpha\frac{4kt}{\phi\mu c}} \quad , \quad . \quad . \quad . \quad . \quad . \quad . \quad . \quad . \quad (38)$$

the constant, α, being determined by Eq. 36.

For sufficiently large times, Eq. 37 may be approximated by

$$p = p_e + \frac{i\mu}{2\pi kh}\ln\frac{r_e}{r} \quad . \quad . \quad . \quad . \quad . \quad . \quad . \quad (39)$$

Owing to the small value of c in the second member of Eq. 36, α is small and $e^{\alpha} \sim 1$. Then, putting $\alpha = i\mu c/4\pi kh(S_g - S_{gr})$ in Eq. 38, we get

$$r_e = \sqrt{it/\pi\phi h(S_g - S_{gr})} \quad . \quad . \quad . \quad . \quad . \quad (40)$$

or

$$it = \pi\phi h r_e^2(S_g - S_{gr}). \quad . \quad . \quad . \quad . \quad . \quad . \quad (41)$$

Referring to Fig. 1 it will be seen that Eqs. 39 and 41 are the same as those for an incompressible fluid. It follows that, except in the initial stage of injection, the liquid behaves as if it were incompressible.

APPENDIX 2

DERIVATION OF EQ. 7

We assume that the flow of water in the well after closing in can be considered as passing through a succession of steady states. Then the pressure gradient in

the water column at depth z in the injection wellbore is

$$\frac{dp}{dz} = \rho g \quad . \quad . \quad . \quad . \quad . \quad . \quad . \quad . \quad . \quad . \quad . \quad (42)$$

The density of the compressible water at pressure p is

$$\rho = \rho_0 e^{cp} \quad , \quad . \quad . \quad . \quad . \quad . \quad . \quad . \quad . \quad . \quad . \quad (43)$$

where ρ_o is the density at zero pressure. Substituting in Eq. 42 and solving the resulting differential equation, we get $e^{-cp} = \text{constant} - c\rho_0 gz$. At depth z_o of the reservoir the pressure is equal to p_w. Then, eliminating the integration constant we find

$$e^{-cp} - e^{-cp_w} = c\rho_0 g(z_0 - z) \quad . \quad . \quad . \quad . \quad . \quad (44)$$

We have to consider the two possibilities:

A. The well is completely filled up and the wellhead pressure is $p_h > 0$. Then, $p = p_h$ for $z = 0$. . . . (45)

B. The well is not completely filled up, the water level is at a depth, $z = z_1(t)$ below the surface and z increases with time. Then,

$$p = 0 \text{ for } z = z_1 > 0 \quad . \quad . \quad . \quad . \quad . \quad . \quad . \quad . \quad (46)$$

In case A the mass of water in the well is

$$M = \pi r_w^2 \int_o^{z_0} \rho dz.$$

Eliminating ρ by means of Eq. 42 we obtain

$$M = \frac{\pi r_w^2}{g} \int_{p_h}^{p_w} dp = \frac{\pi r_w^2 (p_w - p_h)}{g}.$$

The mass rate of flow into the formation due to expansion is

$$\frac{dM}{dt} = \frac{\pi r_w^2}{g}\left[\frac{dp_w}{dt} - \frac{dp_h}{dt}\right]. \quad . \quad . \quad . \quad . \quad . \quad . \quad (47)$$

Using Eq. 45, Eq. 44 becomes

$$e^{-cp_h} - e^{-cp_w} = c\rho_0 gz_0. \quad . \quad . \quad . \quad . \quad . \quad . \quad (48)$$

Differentiation with respect to t yields

$$e^{-cp_h}\frac{dp_h}{dt} = e^{-cp_w}\frac{dp_w}{dt}.$$

For the pressures under consideration, cp is small so that we can take $e^{-cp} \sim 1 - cp$. Therefore,

$$\frac{dp_h}{dt} = \left\{1 - c(p_w - p_h)\right\}\frac{dp_w}{dt}. \quad . \quad . \quad . \quad . \quad (49)$$

In the same way we get from Eq. 48, $p_w - p_h \sim \rho_0 gz_0$. Hence, $p_w - p_h$ is approximately constant and equal to hydrostatic pressure at reservoir depth. From Eqs. 47 and 49 we find,

$$\frac{dM}{dt} = \frac{\pi r_w^2 c(p_w - p_h)}{g}\frac{dp_w}{dt} \quad . \quad . \quad . \quad . \quad (50)$$

At this stage the density, ρ, in Eq. 43 can be taken approximately equal to ρ_0; hence, the volume rate of flow is

$$\frac{1}{\rho_0}\frac{dM}{dt} = \frac{\pi r_w^2 c(p_w - p_h)}{\rho_0 g}\frac{dp_w}{dt}.$$

This should be equal to the flow rate into the formation,

$$\frac{2\pi kh}{\mu}\left[r\frac{\partial p_f}{\partial r}\right]_{r_w}.$$

Equating the two rates and putting $r_w = d_t/2$ we obtain Eq. 7, where χ is defined by Eq. 8.

In Case B we find for the mass of the water in the well,

$$M = \frac{\pi r_w^2}{g} p_w \,,$$

and for the volume rate flow,

$$\frac{1}{\rho_0}\frac{dM}{dt} = \frac{\pi r_w^2}{\rho_0 g}\frac{dp_w}{dt},$$

which leads to Eq. 7 and to Eq. 8a for χ.

APPENDIX 3

SOLUTION OF EQUATIONS FOR CASE 1

The equations in this Appendix are developed explicitly for the case where the wellhead pressure drops to zero at time of shut in, Case B. The solution for the other case is almost identical.

We introduce dimensionless quantities

$$\left.\begin{aligned} P &= \frac{p}{i\mu/2\pi kh}, \quad \Delta t_D = \frac{k\Delta t}{\phi\mu c r_e^2}, \\ R &= \frac{r}{r_e}, \qquad A = \frac{8\phi ch\rho g r_e^2}{d_t^2}, \end{aligned}\right\} \quad . \quad . \quad . \quad (51)$$

By a familiar approximation we replace $(r\,\partial p/\partial r)_{r=r_w}$ in Eqs. 7 and 9 by $(r\partial p/\partial r)_{r\to 0}$ Then Eq. 4 and the initial and boundary conditions (Eqs. 6a, 9, 7 and 5), become

$$\frac{\partial^2 P}{\partial R^2} + \frac{1}{R}\frac{\partial P}{\partial R} = \frac{\partial P}{\partial(\Delta t_D)}, \quad . \quad . \quad . \quad . \quad . \quad . \quad (52)$$

$$P_w = P_o - P_h \text{ for } \Delta t_D = 0, \quad . \quad . \quad . \quad . \quad . \quad (53)$$

$$P_w = P(R_w) - S\left[R\frac{\partial P}{\partial R}\right]_{R\to 0}, \quad . \quad . \quad . \quad . \quad (54)$$

$$\frac{dP_w}{\Delta t_D} = A\left[R\frac{\partial P}{\partial R}\right]_{R\to 0}, \quad . \quad . \quad . \quad . \quad . \quad . \quad (55)$$

$$P = P_e \text{ for } R = 1 \quad . \quad . \quad . \quad . \quad . \quad . \quad . \quad (56)$$

Eliminating P_w from Eqs. 54 and 55 we find a boundary condition for P,

$$A\left[R\frac{\partial P}{\partial R}\right]_{R\to 0} = \frac{d}{d(\Delta t_D)}\left\{P(R_w) - S\left[R\frac{\partial P}{\partial R}\right]_{R\to 0}\right\}.$$

The equations can be solved by applying the Laplace transformation,

$$P^*(R, s) = \int_0^\infty e^{-s\Delta t_D} P(R, \Delta t_D) d\Delta t_D \,.$$

We solve first for P^* and then obtain P_w^* from Eq. 54. As the calculations are routine it is sufficient to give the result,

$$P_w^* = \frac{P_e}{s} + \left\{\frac{P_o - P_e - P_h}{s} - \frac{A}{s^2} + \frac{A}{s^2}\frac{\left[P_h + \frac{A}{s}\right]I_0(\sqrt{s})}{G(s)}\right\}, \quad . \quad . \quad . \quad . \quad . \quad . \quad . \quad . \quad . \quad . \quad . \quad (57)$$

where

$$G(s) = I_0(\sqrt{s})\left\{K_0(R_w\sqrt{s}) + S + \frac{A}{s}\right\} - K_0(\sqrt{s})\, I_0(R_w\sqrt{s}) \quad . \quad . \quad . \quad . \quad (58)$$

When in Eq. 57 the expression between braces is expanded in powers of s, it is found to have no pole at $s = 0$. It is a meromorphic function, its poles being the zeros of $G(s)$.

The time function, P_w, is found by applying Heaviside's expansion theorem to Eq. 57,

$$P_w = P_e + \sum_n B_n e^{-x_n^2 \Delta t_D},$$

where $x_n = i\sqrt{s_n}$ is real, s_n being the roots of $G(s) = 0$, and

$$B_n = \frac{A}{s_n^2}\frac{\left[P_h + \frac{A}{s_n}\right]I_0(\sqrt{s_n})}{\left[\frac{dG}{ds}\right]_{s=s_n}}.$$

As R_w is a small quantity, Eq. 58 for $G(s)$ may be replaced by

$$G(s) \sim I_0(\sqrt{s})\left\{ -\ln\left[\frac{\gamma}{2}R_w\sqrt{s}\right] + S + \frac{A}{s}\right\} - K_0(\sqrt{s})$$

as long as $R_w\sqrt{s} << 1$. After substitution for (dG/ds) and some algebraic manipulations, we find

$$B_n = \frac{\frac{2A}{x_n^2}\left[\frac{A}{x_n^2} - \frac{p_h}{i\mu/2\pi kh}\right]}{[J_0(x_n)]^{-2} - 1 + \frac{2A}{x_n^2}}, \quad \ldots\ldots (59)$$

where x_n are the roots of the equation,

$$J_0(x)\left[S + \ln\frac{2r_e}{\gamma r_w} - \frac{A}{x^2} - \ln x\right] + \frac{\pi}{2} Y_0(x) = 0, \quad \ldots\ldots (60)$$

and

$$A = 8\phi ch\rho g r_e^2/d_t^2 \quad \ldots\ldots (61)$$

AN EXPRESSION FOR kh AND S

From Eqs. 11 and 59 we have,

$$\frac{A}{x_1^2}\left[\frac{A}{x_1^2} - \frac{p_h}{i\mu/2\pi kh}\right] = \frac{\pi khb_1}{i\mu}\left[\frac{1}{J_0^2(x_1)} - 1 + \frac{2A}{x_1^2}\right]. \quad \ldots\ldots (62)$$

From the definition of Δt_D in Eq. 51 and from Eq. 10a,

$$\frac{\beta_1}{x_1^2} = \frac{k}{\phi\mu c r_e^2}. \quad \ldots\ldots (63)$$

Comparing with Eq. 61 we find,

$$kh = \frac{\mu d_t^2 \beta_1}{8\rho g}\frac{A}{x_1^2}. \quad \ldots\ldots (64)$$

This eliminates the product, $\phi c r_e^2$, the value of which is rather uncertain. Just before closing in, the bottom-hole pressure according to Eq. 3 was given by

$$p_o = \frac{i\mu}{2\pi kh}\left[\ln\frac{r_e}{r_w} + S\right] + p_e \quad \ldots\ldots (65)$$

Eliminating the unknown quantities, A, kh, and $S + \ln(r_e/r_w)$, from Eqs. 60, 62, 64 and 65, we obtain an equation for x_1

$$\left[\theta + \ln\frac{2}{\gamma} - \ln x_1\right] J_0^2(x_1) + \frac{\pi}{2} Y_0(x_1)J_0(x_1) - \theta = 0, \quad \ldots\ldots (66)$$

where

$$\theta = \frac{C_1(1 - C_3)}{2(1 - C_1 - C_2)}, \quad \ldots\ldots (67)$$

and, in cgs units,

$$C_1 = \frac{\pi d_t^2 \beta_1 b_1}{4\rho g i}$$
$$C_2 = \frac{p_h}{b_1} C_1 \quad \ldots\ldots (68)$$
$$C_3 = \frac{p_o - p_e}{b_1} C_1.$$

All quantities in the expressions for C_1, C_2 and C_3 are known, hence θ is known and Eq. 66 can be solved for x_1. When x_1 is known kh can be obtained from Eqs. 62 and 64.

$$kh = \frac{i\mu}{b_1}\frac{1}{\pi}\frac{1 - C_1 - C_2}{(1 - C_3)^2}\theta^2\left[\frac{1}{J_0^2(x_1)} - 1\right]. \quad \ldots\ldots (69)$$

Then, with this value of kh, $S + \ln(r_e/r_w)$ is determined from Eq. 65 as

$$S + \ln\frac{r_e}{r_w} = \frac{(p_o - p_e)}{i\mu/2\pi kh} \quad \ldots\ldots (70)$$

These formulas become Eqs. 12 and 13 when expressed in practical units. $f(\theta)$ in Eq. 12 is defined by, $f(\theta) = 282.4\,\theta^2[J_0^{-2}(x_1) - 1]$, and x_1 for given θ by Eq. 66. The factor 282.4 is a unit conversion factor.

For $\theta = 0$, $J_0(x_1)$ vanishes. It can be shown that for $\theta \to 0$, $f(\theta)$ approaches the limit, $f(0) = 181.2$. Further, it may be proved that for $\theta = 0$, $B_n = 2/x_n^2 J_1^2(x_n)$.

This is the solution when there is no after flow into the formation.

APPENDIX 4

SOLUTION OF EQUATIONS FOR CASE 2

We first introduce the dimensionless quantities,

$$P = \frac{p}{i\mu_w/2\pi k_w h}, \quad R = \frac{r}{r_e}, \quad \Delta t_D = \frac{k_o \Delta t}{\phi\mu_o c_o r_e^2} \quad \ldots\ldots (71)$$

Then the equations become

$$\frac{\partial^2 P_1}{\partial R^2} + \frac{1}{R}\frac{\partial P_1}{\partial R} = \lambda^2 \frac{\partial P_1}{\partial(\Delta t_D)}, \quad \ldots\ldots (72)$$

where

$$\lambda^2 = \frac{1}{M\gamma} \qquad \left[\gamma = \frac{c_o}{c_w}\right], \quad \ldots\ldots (73)$$

and

$$\frac{\partial^2 P_2}{\partial R^2} + \frac{1}{R}\frac{\partial P_2}{\partial R} = \frac{\partial P_2}{\partial(\Delta t_D)}, \quad \ldots\ldots (74)$$

with the conditions,

$$\left[\begin{aligned} P_1 &= -\ln R - (M - 1)\ln R_0 + P_e \\ P_2 &= -M\ln R + P_e \end{aligned}\right] \quad \text{for } \Delta t_D = 0, \quad \ldots\ldots (75)$$

$$\frac{\partial P_1}{\partial R} = 0 \qquad \text{for } R = 0, \quad \ldots\ldots (76)$$

$$\left.\begin{aligned} P_1 &= P_2 \\ M\frac{\partial P_1}{\partial R} &= \frac{\partial P_2}{\partial R} \end{aligned}\right\} \qquad \text{for } R = R_0 \quad \ldots\ldots (77)$$

$$P_2 = P_e \text{ for } R = 1. \quad \ldots\ldots (78)$$

For the solution, we again make use of the Laplace transformation. After some tedious but straightforward calculations we find for the bottom-hole pressure,

$$P_w^* = P_1^*(R_w) = \frac{P_e - (M - 1)\ln R_0 - \ln R_w}{s} - \frac{K_0(R_w\sqrt{s})}{s} - \frac{1}{s}\frac{M\lambda\phi_{00}K_1(\lambda R_0\sqrt{s}) - \phi_{10}K_0(\lambda R_0\sqrt{s})}{M\lambda\phi_{00}I_1(\lambda R_0\sqrt{s}) + \phi_{10}I_0(\lambda R_0\sqrt{s})}, \quad \ldots\ldots (79)$$

where

$$\left.\begin{aligned} \phi_{00} &= K_0(R_0\sqrt{s})\,I_0(\sqrt{s}) - I_0(R_0\sqrt{s})\,K_0(\sqrt{s}) \\ \phi_{10} &= K_1(R_0\sqrt{s})\,I_0(\sqrt{s}) + I_1(R_0\sqrt{s})\,K_0(\sqrt{s}) \end{aligned}\right\}. \quad \ldots\ldots (80)$$

Now, P_w^* is a meromorphic function of s. It can be verified that the quantity $P_w^* - (P_e/s)$ has no pole for

$s = 0$, hence the time function $P_w(\Delta t_D)$ can be obtained from Eq. 79 by Heaviside's expansion theorem.

$$P_w(\Delta t_D) = P_e + \Sigma B_n e^{s_n \Delta t_D},$$

where

$$B_n = -\frac{1}{s} \frac{M\lambda\phi_{00}K_1(\lambda R_0\sqrt{s}) - \phi_{10}K_0(\lambda R_0\sqrt{s})}{\frac{d}{ds}\left\{M\lambda\phi_{00}I_1(\lambda R_0\sqrt{s}) + \phi_{10}I_0(\lambda R_0\sqrt{s})\right\}}, \quad \ldots \quad (81)$$

$s = s_n$ being the nth root of the equation,

$$M\lambda\phi_{00}I_1(\lambda R_0\sqrt{s}) + \phi_{10}I_0(\lambda R_0\sqrt{s}) = 0 \quad . \quad (82)$$

From physical considerations it may be assumed that the roots of this equation are pure imaginary numbers, as complex roots would give rise to damped oscillatory terms. Hence, in order to calculate B_n we put $\sqrt{s} = ix$ or $s = -x^2$. Then,

$$\phi_{00} = -\frac{\pi}{2}\Phi_{00}, \quad \phi_{10} = i\frac{\pi}{2}\Phi_{10},$$

where

$$\Phi_{mn} = Y_m(R_0x)\, J_n(x) - J_m(R_0x)\, Y_n(x) \quad . \quad (83)$$

In this notation,

$$B_n = -\frac{2}{x} \frac{M\lambda\Phi_{00}Y_1(\lambda R_0x) - \Phi_{10}Y_0(\lambda R_0x)}{\frac{d}{dx}\left\{M\lambda\Phi_{00}J_1(\lambda R_0x) - \Phi_{10}J_0(\lambda R_0x)\right\}}, \quad \ldots \quad (84)$$

where $x = x_n$ is the nth root of the equation,

$$M\lambda\Phi_{00}J_1(\lambda R_0x) - \Phi_{10}J_0(\lambda R_0x) = 0 \quad . \quad . \quad . \quad (85)$$

The reduction of B_n to the formula given in the text is rather long and tedious. We shall not give the whole derivation but shall only clarify a few points where the algebra is not quite obvious.

After some calculations, the denominator in Eq. 84 is found to be equal to $[(M\lambda^2 - 1)\, R_0\Phi_{00} + \Phi_{11}]\, J_0(\lambda R_0x) - [(M - 1)\, \lambda R_0\Phi_{10} + M\lambda\Phi_{01}]\, J_1(\lambda R_0x)$.

Eliminating $J_1(\lambda R_0x)$ by use of Eq. 85, we get

$$\frac{J_0(\lambda R_0x)}{\Phi_{00}}\left\{(M\lambda^2 - 1)\, R_0\Phi_{00}^2 - \left(1 - \frac{1}{M}\right)R_0\Phi_{10}^2 + \Phi_{00}\Phi_{11} - \Phi_{01}\Phi_{10}\right\}.$$

The expression, $\Phi_{00}\Phi_{11} - \Phi_{01}\Phi_{10}$, may be reduced to $[Y_0(R_0x)\, J_1(R_0x) - J_0(R_0x)\, Y_1(R_0x)]\, [Y_0(x)\, J_1(x) - J_0(x)\, Y_1(x)] = 4/\pi^2R_0x^2$. Further, Φ_{10} may be eliminated by use of Eq. 85. Likewise, Φ_{10} may be eliminated from the numerator of Eq. 84. Further, λ is replaced by $1/\sqrt{\gamma M}$ according to Eq. 73. Then we find finally,

$$B_n = \frac{2\gamma M}{R_w^2x_n^2\left(1 - \gamma + \frac{4\gamma}{\pi^2R_0^2x_n^2\Phi_{00}^2}\right)J_0^2\left(\frac{R_0x_n}{\sqrt{\gamma M}}\right) - (M - 1)\, J_1^2\left(\frac{R_0x_n}{\sqrt{\gamma M}}\right)}, \quad \ldots \quad (86)$$

with x_n the roots of the equation,

$$\sqrt{\frac{M}{\gamma}}\Phi_{00}J_1\left(\frac{R_0x}{\sqrt{\gamma M}}\right) - \Phi_{10}J_0\left(\frac{R_0x}{\sqrt{\gamma M}}\right) = 0, \quad (87)$$

in which

$$\left.\begin{aligned}\Phi_{00} &= Y_0(R_0x)\, J_0(x) - J_0(R_0x)\, Y_0(x)\\ \Phi_{10} &= Y_1(R_0x)\, J_0(x) - J_1(R_0x)\, Y_0(x)\end{aligned}\right\} \quad . \quad (88)$$

$$\gamma = \frac{c_o}{c_w}. \quad \ldots \quad (89)$$

APPENDIX 5

CONSTANTS USED IN CALCULATIONS

Field	μ_w (cp)	μ_o (cp)	M	V_o/V_w	γ
1	0.9	3.5	4	1.35	1
2	1.0	—	—	—	—
3	0.9	30	4	3	1

★★★

Determination of Wettability by Dye Adsorption

O. C. HOLBROOK
GEORGE G. BERNARD
THE PURE OIL CO.
CRYSTAL LAKE, ILL.

ABSTRACT

A method has been developed for determining the relative water wettability (fraction of the surface wet by water) of porous media. This method involves the adsorption of methylene blue dye from an aqueous solution onto the solid surfaces of rock contacted by the injected dye solution. Experiments on Berea sandstone cores have shown that water-wet cores adsorb a large amount of dye from solution. In oil-wet cores, however, the injected aqueous dye solution is prevented from contacting the adsorptive surfaces by a film of oil and virtually no dye is adsorbed.

This method was tested by experiments on mixtures of water-wet and oil-wet sand. Using the dye adsorption method, it was possible to determine quantitatively the fraction of water-wet and oil-wet sand in such mixtures.

The dye adsorption test is readily applied to determining the relative water wettability of fresh oilfield cores. The cores are not extracted before testing. Observed values of the wettability of field cores tested to date have varied from 100 to 6 per cent water wet.

INTRODUCTION

Recent articles[1-5] have emphasized the important role that wettability plays in almost all phases of reservoir rock behavior. It has been shown that wettability has a profound effect on the interstitial water saturation, residual oil saturation, capillary pressure, relative permeability, waterflood behavior, and resistivity index of oilfield cores. A quantitative investigation of the effect of wettability on these core properties is severely handicapped by the lack of a simple technique for measuring the wettability of a porous medium. If such a technique were available, it would provide investigators with a means of gaining insight into the distribution of phases within a core.

A number of qualitative methods of estimating wettability are known. These include contact angle measurements, flotation tests and studies of displacement pressure,[6] imbibition[7] and relative permeability data.[1] Using these tests, it is usually possible to classify a core as water-wet, oil-wet, or some intermediate degree of wettability. One recently proposed method involving measurement of nuclear magnetic relaxation[8] offers promise of determining quantitatively the fractional wettability of cores. The equipment is rather elaborate and necessary treatment of the cores before testing probably alters the natural wettability. This latter point also applies to most of the cited qualitative methods.

This paper presents a new technique for determining water wettability of cores; it is based on measurements of the dye adsorption capacity of the core. This method has the advantage of requiring relatively simple equipment and involves minimum handling of the core before testing.

It is important to distinguish between the various concepts of wettability referred to in the literature. The term "wetting" is defined by Bartell[9] as that phenomenon which occurs when a solid and liquid phase come in contact in any manner so as to form a solid-liquid interface. A preferentially water-wet solid is defined by Jennings[10] in terms of the advancing contact angle in the solid water-oil systems. Brown and Fatt[5] regard fractional wettability as the fraction of the total surface area that is preferentially oil-wet or water-wet.

However, none of these definitions adequately describes the type wettability measured by the dye test. This calls for the introduction of a new term, "relative water wettability", which we define as the fraction of the total surface area of a core contacted by injected water.

DESCRIPTION OF METHOD

The ability of a porous medium (especially the clays) to adsorb large quantities of surfactants, dyes, etc., is well known. It is reasonable to assume that a substance can be adsorbed from solution onto a solid surface only if the solution contacts the surface. In this connection Shapiro[11] has shown by experiments on silica gel that completely dry gel will adsorb methyl red dye from a benzene solution. On the other hand, if a film of water more than several molecules thick is present on the silica gel, the adsorption capacity of the gel for the dye is drastically reduced. Thus, a study of the dye adsorption capacity of cores should give some clue as to the fluid distribution on the surface of the core.

TEST OF METHOD

As a qualitative check on this theory, dye adsorption tests were run on similar Berea sandstone cores (Table 1, Cores 1-5). Cores saturated initially with water and flooded with 0.01 per cent aqueous methylene blue adsorbed 0.58 mg dye/gm of core. Similar cores saturated initially with water, driven to irreducible water with oil, and then flooded with the same dye solution also adsorbed 0.58 mg dye/gm of core. Another core, treated with a 5 per cent Dri-Film solution, dried and saturated with oil (Soltrol) adsorbed no dye when the dye solution was injected. These tests confirm

Original manuscript received in Society of Petroleum Engineers office July 15, 1957. Revised manuscript received Aug. 1, 1958. Paper presented at 32nd Annual Fall Meeting of Society of Petroleum Engineers in Dallas, Tex., Oct. 6-9, 1957.

[1]References given at end of paper.

TABLE 1 — DYE ADSORPTION TESTS ON BEREA SANDSTONE CORES

Object	Core No.[1]	Concn. of Dri-Film solution (per cent)	Initial saturant	Subsequent treatment	Adsorption capacity, mg dye / gm core	Relative water wettability
Test of theory	1	0	water	none	0.58	1.00
	2	0	water	none	0.58	1.00
	3	0	water	Drive with Soltrol to irreducible water	0.60	1.00
	4	0	water		0.56	1.00
	5	5	Soltrol	none	0.00	0.00
Test of extraction	6	0	Kansas crude	Extract with chloroform and methanol, saturate with water	0.57	0.98
	7	0	Kansas crude	Extract with chloroform and methanol, heat to 950°F, saturate with water	0.51	0.88
	8	0	Kansas crude	Extract with benzene and methanol, saturate with water	0.49	0.84
Correlation of imbibition with wettability	9	0	water	none	0.71	0.96
	10	0.01	water	none	0.53	0.72
	11	0.1	water	none	0.57	0.77
	12	5.0	water	none	0.46	0.62
	13	0	water	Drive with Soltrol to irreducible water	0.76	1.00
	14	0	Soltrol	Drive with water to residual oil, then with oil to irreducible water	0.59	0.80
	15	0.1	Soltrol		0.18	0.24
	16	5.0	Soltrol		0 05	0.07

[1]Cores 1-8 were taken from the same block of Berea sandstone; average adsorption capacity, 0.58. Cores 9-16 were taken from the same block of Berea sandstone; average adsorption capacity, 0.74.

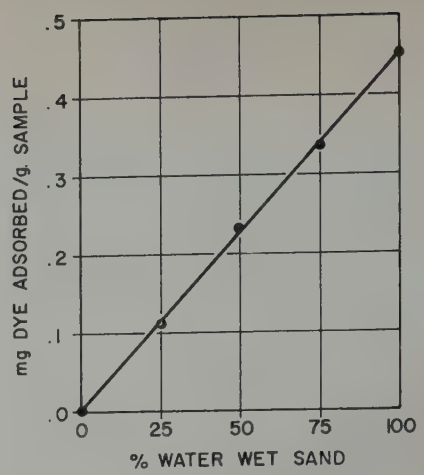

FIG. 1—DYE ADSORPTION TEST ON MIXTURES OF WATER- AND OIL-WET 250-MESH SAND.

qualitatively the ability of dye adsorption measurements to indicate the relative water wettability of oilfield cores.

A quantitative test of this method is ideally performed on a consolidated porous medium resembling as closely as possible an actual field core. No experimental procedure could be devised to accomplish this because of lack of a suitable standard for measuring wettability. Instead, tests were made on loose mixtures of different proportions of water-wet and oil-wet 250-mesh Ottawa sand. These tests are described in detail in the following section.

EXPERIMENTAL PROCEDURE

Careful attention was paid to the fluids with which these samples were first contacted because it has been shown[11] that the fluid with which a dry material is first contacted has a considerable influence on its subsequent wettability. The sand, saturated with water, was considered to be 100 per cent water-wet. Sand treated with a 5 per cent Dri-Film SC-87 solution in hexane, oven dried at 250°F for one hour and saturated with Soltrol was considered to be 100 per cent oil-wet. Mixtures of different proportions of these sands, saturated with their respective wetting fluids, were prepared as shown in Table 2. The weight of water-wet sand in each mixture (except Sample 5) was kept constant to insure that the equilibrium dye concentration for each mixture would be roughly the same. Each of the cited sand mixtures was shaken with 25 cc of 0.01 per cent aqueous methylene blue solution for 30 minutes, then centrifuged and the dye concentration was determined. The results were expressed as milligrams of dye adsorbed per gram of dry sand. The relative water wettability was determined by dividing the adsorption capacity of each sample by the adsorption capacity of the 100 per cent water-wet sample.

Several techniques for measuring dye concentration are available. In this work, the light transmittancy of the solution was determined in a Cenco-Sheard-Sanford Type B-2 Photelometer and the dye concentration was determined from a calibration curve.

RESULTS

Table 2 and Fig. 1 present the results of these tests. There is near perfect correlation between the dye adsorption capacities and the known proportion of water-wet sand in the mix. This technique, then, furnishes a quantitative estimate of the proportion of water-wet surface in the mix; this proportion we have defined as relative water wettability.

APPLICATION OF TEST TO FIELD CORES

The following procedure was devised for applying the dye test to the determination of the relative water wettability of fresh field cores. Two adjacent* 1 × 1 in. plugs were drilled parallel to the bedding plane from each fresh field core. The drill was lubricated with water of the same salinity as formation water. One plug was saturated with synthetic formation water by means of an evacuation procedure. The dye adsorption capacity of this plug was then determined by passing the dye solution through the freshly drilled and saturated plug. The resultant adsorption capacity (mg dye/gm of plug) was proportional to surface area of the plug contacted by the aqueous dye solution. The second plug was extracted with a mixture of chloroform and methanol and saturated with synthetic formation water. Subsequent work (see section entitled "Test of Extraction Procedure") showed that this treatment made the plug completely water-wet. After allowing time for the clays to rehydrate, the adsorption capacity of the second plug was determined. Assuming this plug was completely wet by the dye solution, the adsorption capacity would be proportional to its total exposed surface area. Division of the adsorption capacity of the fresh plug by the adsorption capacity of the extracted plug gave the fraction of the surface of the fresh plug that was water-wet, i.e., its relative water wettability. A detailed description of this procedure follows.

*We realize that there will be some differences between two adjacent plugs. For the purpose of this test, the assumption is made that these differences are negligible.

DETERMINATION OF DYE ADSORPTION CAPACITY

The core, saturated with the de-

TABLE 2—TESTS ON MIXTURES OF WATER-WET AND OIL-WET 250-MESH SAND

Sample No.	Dry weight of sand (gm) Water-wet	Oil-wet	Total	Per cent water-wet sand in mixture	Equilibrium dye Color	Conc (per cent)	mg of dye adsorbed per gm sample	Relative water wettability by dye test[1]
1	2	0	2	100	31.0	0.0064	0.45	1.00
2	2	0.67	2.67	75	31.0	0.0064	0.337	0.75
3	2	2	4.0	50	31.5	0.0064	0.231	0.51
4	2	6	8	25	31.0	0.0064	0.112	0.25
5	0	10	10	0	17.5	0.0100	0.00	0 00

[1] $\frac{\text{adsorption capacity of sample}}{\text{adsorption capacity of 100 per cent water-wet sample}}$

sired fluids, was placed in a conventional core holder and a filtered aqueous solution containing 0.01 per cent methylene blue and 0.5 per cent $CaCl_2$ was injected at a rate of about one pore volume per minute. $CaCl_2$ was added to prevent clays from dispersing and plugging the core. The effluent was collected in 25-cc increments (approximately 10 pore volumes) and its dye concentration was determined colorimetrically as previously described. This was continued until the dye concentration in the effluent reached 0.009 per cent. The test was discontinued at this point. The dye concentration of the solution entering the core was measured at the beginning and end of each test. The dye concentration was plotted against the volume of effluent as shown in Fig. 2. The area between the curves was integrated graphically and the results expressed as mg dye/gm of core.

Test of Extraction Procedure

There are several references in the literature[10] concerning the inability of conventional extraction procedures to make cores completely water-wet Accordingly, several tests of different extraction procedures were made on Berea sandstone cores saturated with a Kansas crude oil which previous work had shown to be very difficult to extract. In these tests the dry core was saturated with the oil and allowed to soak for at least 24 hours. The core was then extracted overnight, dried, saturated with brine and its dye adsorption capacity was determined. The results (Table 1, Cores 6-8) show that extraction with a mixture of three parts chloroform and one part methanol almost completely restored the cores to their initial dye adsorption capacities. It should be noted that this extraction procedure was found by Jennings[10] to be relatively ineffective in removing the oil-wet characteristics of some cores. Heating as a method of cleaning up cores could not be used since heat can destroy irreversibly part of the dye adsorption capacity of some clays.

Test on Field Cores

The relative water wettabilities of fresh cores from several different fields were determined using the dye adsorption technique to get some idea of the range of values encountered in actual practice. Table 3 shows the results obtained with the dye adsorption tests.

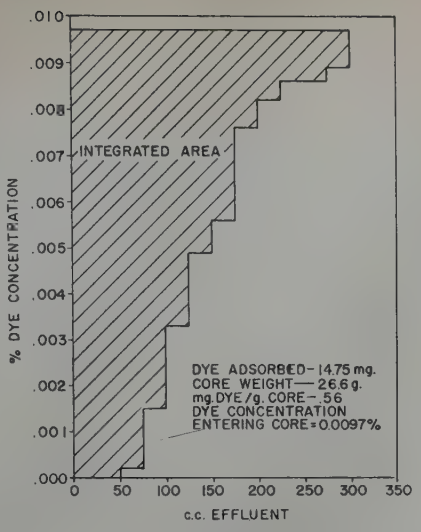

Fig. 2—Dye Adsorption Curve, Berea Core No. 7.

CORRELATION OF RELATIVE WATER WETTABILITY WITH WATER IMBIBITION

In order to investigate the utility of the dye test in studying flow behavior, an attempt was made to correlate qualitatively the relative water wettability with the water imbibition rate into Berea cores. These tests were performed on one group of cores initially containing air and on another group initially containing oil and irreducible water.

Experimental Procedure

Four adjacent 1 × 1 in. Berea cores were drilled. Three were treated with hexane solutions containing 0.01, 0.1 and 5.0 per cent Dri-Film SC-87. About 40 pore volumes of the treating solution were passed through each core. The cores were dried at 250°F for at least one hour after treatment. The imbibition rates were determined by contacting one face of each core with water and allowing the water to imbibe. The cores were removed periodically and their saturations were determined by weighing. After equilibrium was attained the cores were saturated with water and their dye adsorption capacities were determined as described previously.

To test this procedure on cores of different wettabilities containing oil and irreducible water, a second group of four adjacent 1×1 in. Berea cores was selected. These cores were treated as follows: (1) Core 13, saturated with brine; (2) Core 14, saturated with Soltrol; (3) Core 15, treated with 40 pore volumes of 0.1 per cent Dri-Film, dried, saturated with Soltrol; and (4) Core 16, treated with 40 pore volumes of 5 per cent Dri-Film, dried, saturated with Soltrol.

TABLE 3—WETTABILITY DETERMINATIONS ON FIELD CORES

Location of field	Adsorption capacity (mg dye/gm core) Fresh	Extracted	Relative water Wettability
Wyoming	0.05	0.85	0.06
California	0.39	0.56	0.70
Colorado[1]			
A	0.74	0.78	0.95
B	0.63	0.81	0.78
C	0.29	0.42	0.69
D	1.15	1.10	1.00

[1]Samples taken from the same well.

After this treatment, Core 13 was driven with Soltrol to irreducible water. Cores 14, 15 and 16 were driven with water to residual oil and then with Soltrol to irreducible water. To determine the imbibition curves each core was placed in a centrifuge tube having a graduated neck. The tube was filled with water and quickly inverted and the open end placed under water. The volume of oil displaced by the imbibing water collected in the neck of the centrifuge tube and was measured periodically. The tube was shaken before each reading to dislodge oil droplets from the surface of the core.

Results

In the water imbibition tests on dry cores the water imbibed most rapidly into the untreated core. Water imbibed at a somewhat slower rate into the cores treated with 0.01 and 0.1 per cent Dri-Film, and virtually no water was imbibed by the core treated with 5.0 per cent Dri-Film. The relative water wettabilities of these cores were 0.96, 0.72, 0.77 and 0.62, respectively. These water wettabilities show that all the cores were predominantly water-wet, even the one made strongly water repellent by Dri-Film treatment. Apparently, saturating the dry cores with water had forced them into a wettability condition in which the relative water wettability bore no relation to the preferential wettability. It was concluded that this experiment could best be performed on cores containing water and oil distributed on the core surfaces in accordance with the preferential wettability of the core.

The second set of water imbibition tests was run on cores containing oil and irreducible water. The results of the imbibition tests are shown in Fig. 3, and the dye adsorption capacities and fractional wettabilities are given in Table 1, Cores 13-16. The imbibition rates decrease in the following order: Core 13 > Core 14 > Core 15 > Core 16. The relative water wettabilities for these cores are 1.00, 0.80, 0.24 and 0.07, respectively. This shows a qualitative correlation between imbibition rate and water wettability.

DISCUSSION

Relative water wettability has been defined herein as the fraction of total core surface area contacted by flowing water. This area is assumed to be proportional to the quantity of methylene blue dye adsorbed. The amount of dye adsorbed is a function, among other factors, of the area exposed to the dye solution and the adsorptive capacity of the exposed surface. Since the clays constitute the major part of the surface area of a typical core, most dye adsorption probably takes place on the clay surface. Evidently, then, the test results actually show the fraction of the clay surface that is wet by water.

Clays can remove dye from solution through at least three mechanisms: adsorption, cation exchange and chemical reaction. While it would be interesting to know the basic dye adsorption mechanism, its nature does not affect the determination of water wettability. Regardless of the mechanism, if a fresh core removed 0.33 mg dye/gm and a similar extracted core removed 0.66 mg/gm, the relative water wettability would be 0.5.

Relative water wettability greater than 100 per cent has been observed on cores containing substantial amounts of montmorillonite. That is, the fresh cores adsorbed more dye than the extracted cores. This is believed to be caused by irreversible changes in the clay structure resulting from extraction and subsequent drying. Thus far, this behavior has been observed with cores from only one field.

The relative water wettabilities of similar cores measured during the imbibition experiments varied considerably, depending on the fluid which first contacted the dried core. For example, Cores 12 and 16 were treated with a 5 per cent Dri-Film solution and oven dried. Core 12 was then saturated with water and had a relative water wettability of 0.62. Core 16 was saturated with oil and had a relative water wettability of 0.07. This effect has been reported previously with respect to the relative permeability of cores. Geffen *et al*[12] give relative permeability curves on a core treated with Dri-Film. When initially saturated with water, the core exhibited a typically water-wet behavior. When initially saturated with oil, it gave a typically oil-wet behavior. This shows the importance of the first fluid with which a dry core is contacted in determining its subsequent wettability behavior.

It is generally assumed that the imbibition behavior of cores indicates their state of wettability. Under most conditions we have found this to be true. When cores contained both oil and water their relative water wettability correlated very well with their imbibition behavior. This relation is shown in Fig. 3. It is seen that as the numerical value of the relative water wettability increases, so does the degree of water imbibition.

On the other hand the imbibition test on Core 12 shows no agreement between the imbibition behavior and the relative water wettability. In this experiment no oil was present in the core during either the imbibition test or the dye adsorption test. Furthermore, its relative water wettability determined by the dye adsorption test showed that the core was on the water-wet side of the wettability spectrum, despite the fact that it had been made so strongly water repellent by the silicone treatment that it would not imbibe water. This illustrates one important factor that must be considered in the application of the dye test to cores, namely, that both water and oil must be present in the core during the determination of dye adsorption capacity.

SUMMARY

1. A new method of measuring the relative water wettability of cores has been devised, based on measurements of dye adsorption capacities of the cores.

2. Experiments on mixtures of water-wet and oil-wet sand have shown the ability of the dye test to determine their relative water wettability with a high degree of accuracy.

3. The test is simple to apply to consolidated cores. Field cores can be tested as received without extraction or other handling that could alter their natural wettability.

4. Water imbibition rates into Berea standstone cores of different wettabilities correlate qualitatively with the relative water wettabilities of the cores measured by the dye adsorption test.

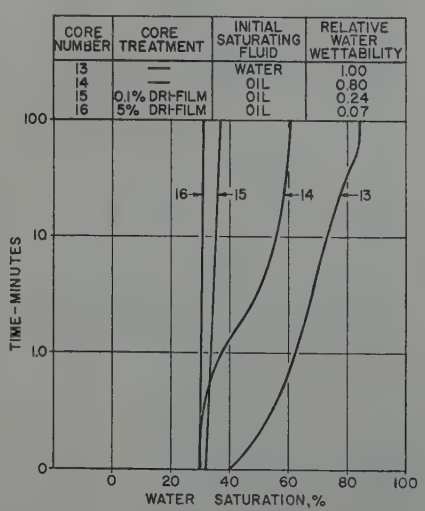

FIG. 3—IMBIBITION TEST ON BEREA CORES CONTAINING OIL AND IRREDUCIBLE WATER.

REFERENCES

1. Coley, F. H., Marsden, S. S. and Calhoun, J. C., Jr.: "A Study of the Effect of Wettability on the Behavior of Fluids in Synthetic Porous Media", *Prod. Monthly* (1956) **20,** 20.
2. Licastro, P. H. and Keller, G. V.: "Resistivity Measurements as a Criteria for Determining Fluid Distribution in the Bradford Sand," *Prod. Monthly* (1953) **17,** 17.
3. Richardson, J. G., Perkins, F. M. and Osoba, J. S.: "Differences in the Behavior of Fresh and Aged Cores", *Trans.* AIME (1955) **204,** 86.
4. Moore, T. F. and Slobod, R. L.: "Displacement of Oil by Water—Effect of Wettability, Rate and Viscosity on Recovery", Paper 502-G, presented at Petroleum Branch, AIME Fall Meeting in New Orleans (Oct. 2-5, 1955).
5. Kennedy, H. T., Burja, E. O. and Boghen, R. S.: "Investigation of the Effects of Wettability on the Recovery of Oil by Water Flooding", *Jour. Phys. Chem.* (1955) **59,** 867.
6. Benner, F. C., Dodd, C. G. and Bartell, F. E.: "Displacement Pressures for Petroleum Oil-Water Silica Systems", *Oil and Gas Jour.* (1942) **41,** No. 27, 199.
7. Killens, C. R., Nielsen, R. F. and Calhoun, J. C., Jr.: "Capillary Desaturation and Imbibition in Porous Rocks", *Prod. Monthly* (1953) **18,** 30.
8. Brown, R. J. S. and Fatt, I.: "Measurements of Fractional Wettability of Oilfield Rocks by the Nuclear Magnetic Relaxation Method", *Trans.* AIME (1956) **207,** 262.
9. Bartell, F. E.: *Alexander's Colloid Chemistry,* Chemical Catalog Co., N. Y. (1931), 41.
10. Jennings, H. Y., Jr.: "Surface Properties of Natural and Synthetic Porous Media", *Prod. Monthly* (1957) **21,** 20.
11. Shapiro, I. and Kolthoff, I. M.: "Studies on Ageing of Precipitates and Coprecipitates: XLIII Thermal Ageing of Precipitated Silica", *Jour.* ACS (1950) **72,** 776.
12. Geffen, T. M., Owens, W. W., Parish, D. R. and Morse, R. A.: "Experimental Investigation of Factors Affecting Laboratory Relative Permeability Measurements", *Trans.* AIME (1951) **192,** 99. ★★★

Mechanics of Differential Pressure Sticking of Drill Collars

H. D. OUTMANS
MEMBER AIME

UNION OIL CO. OF CALIFORNIA
BREA, CALIF.

ABSTRACT

Drilling progress is often delayed by sticking of the drill string. The development of preventive and remedial methods has been hampered by incomplete understanding of the sticking mechanism.

A recent laboratory investigation has indicated that one type of sticking may be attributed to the difference in pressure between the borehole and formation.

This paper shows, by means of soil mechanics, that the primary cause for differential pressure sticking is cessation of pipe movement, whereas differential pressure and standing time determine the severity of the sticking.

The analysis stresses the importance of using low-weight muds with low solids content and low water loss to alleviate differential pressure sticking and describes why packed hole drilling, long strings of drill collars, and a large deviation from the vertical are conducive to sticking.

Finally, preventive and remedial methods are evaluated, and a theory is presented on the release of stuck pipe by spotting oil.

INTRODUCTION

Since drilling with long strings of oversize drill collars has become standard practice in many areas, the incidence and severity of the stuck pipe problem has increased. It has been noticed that in the majority of these cases the sticking could not possibly be attributed to key seating or caving of shales. It appeared that, due to the differential pressure between the mud column and the formation fluid, the collars were pressed into the wall and so became "wall stuck". Points to note about differential pressure sticking are: (1) sticking is restricted to the drill collars, (2) the collars become stuck opposite a permeable formation, (3) the sticking occurs after an interruption of pipe movement, (4) circulation, if interrupted, can be restarted after the sticking is noticed, and (5) no large amounts of cuttings are circulated out after restarting circulation.

Helmick and Longley[1] investigated pipe sticking by differential pressure in the laboratory and found an empirical relationship between the differential pressure, the sticking time and the required pull-out force.

In this paper an explanation of the mechanism is given based on Terzaghi's theory of clay consolidation. A qualitative description is given in the following paragraphs while the derivation of formulas is given in Appendices.

This paper is a first attempt to explain pressure differential sticking and many points will require additional theoretical and practical investigation before the problem can be fully understood.

PRESSURE DIFFERENTIAL STICKING AS A CONSOLIDATION PROBLEM

In any borehole, where the mud pressure is higher than that exerted by the formation fluids, a mud cake is formed opposite the permeable sections of the hole and a continuous flow of filtrate takes place from the mud, through the cake and into the formation. This radial flow pattern requires a certain distribution of the hydraulic and the effective (grain-to-grain) stresses inside the mud cake. Any quantitative or qualitative change in the external pressure conditions will produce a change in the flow pattern and, consequently, also in the internal stress distribution inside the cake. In view of the low permeability and the high compressibility of a clay mud cake, the adjustment of the internal stress distribution is slow and is accompanied by a change in volume. Time dependent stresses are thus created which gradually diminish as the new state of equilibrium between internal and external pressures is approached.

Some 30 years ago, Terzaghi[2,6,7] developed his "Theory of Consolidation" to account for the time-dependent stresses and settling of clay formations under the influence of external loads. He derived a differential equation by which the time-dependent hydraulic stress and the consolidation can be computed for any point inside the layer during the consolidation process. His theory is based on the assumption that the change in stress is solely due to a change in water content and it may only be applied to one-dimensional consolidation phenomena. Other investigators[8,10] have expanded his theory to include processes of more than one dimension.

The difference between the external pressures on the mud cake before and after sticking is a qualitative one (isolation of part of the cake by the static contact with the drill collars after pipe movement has been stopped), and the time-dependent stresses thus created may be investigated by means of Terzaghi's theory. By this analysis the changes in the nature of the contact surface between the drill collars and the mud cake during the sticking can be explained; and the friction force between the two may be computed as a function of the sticking time, the borehole dimensions and the mud cake characteristics.

Original manuscript received in Society of Petroleum Engineers office Sept. 15, 1957. Revised manuscript received Aug. 11, 1958. Paper presented at Annual Fall Meeting of Southern California Petroleum Section in Los Angeles, Calif., Oct. 17-18, 1957.

[1]References given at end of paper.

THE STRESS DISTRIBUTION IN THE MUD CAKE

During Drilling

As a result of the difference between the pressure in the borehole and the fluid pressure of the formation, water from the mud flows into permeable formations through a filter cake. If the formation and the cake are homogeneous, Darcy's law, $v = (k/\mu) \cdot (dp/dr)$, may be applied to the radial flow.

If, in addition, the permeability of the cake is low compared to that of the formation, and the thickness of the cake is small compared to the radius of the borehole, then Darcy's law can be written as $v = (k/\mu) \cdot (p/h)$ (see Appendix 1).

The variables in this formula are different at each depth but independent of time and, consequently, a steady state of flow exists at all levels.

The ratio, p/h, in the formula is the differential hydraulic pressure gradient inside the mud cake. The differential hydraulic pressure, w, decreases linearly from p, at the transition between the mud and the cake to zero at the contact face between cake and formation. The differential hydraulic pressure is therefore, $w = (p/h)z$ (see Fig. 1). As the total differential pressure is equal to p and only part of this pressure is transmitted by w, the remaining stress, which is equal to $p - w$, must be transferred from one clay particle to the next by direct contact. This "solid", or rather "effective" stress, $s = p - w = (p/h) \cdot (h - z)$. Hence, the differential effective stress increases from zero at the mud cake interface to p at the formation.

As differential pressure sticking is always confined to the drill collar string, the tool joints apparently acting as stabilizers for the drill pipe, the position of the drill collars during drilling is an important factor in the wall sticking mechanism. In this connection mention should be made of the work by Lubinski and Woods on the buckling of drill collars[9]. Their investigations have indicated that during drilling, even when the deviation of the borehole is relatively small, the drill collars rest against the low side of the borehole. During rotation the bearing surface between the collars and the cake is thus, supposedly, lubricated by a film of liquid mud in the contact area. The pressure in this mud film is equal to the mud pressure plus the pressure exerted by the component of the weight of the drill collars normal to the hole.

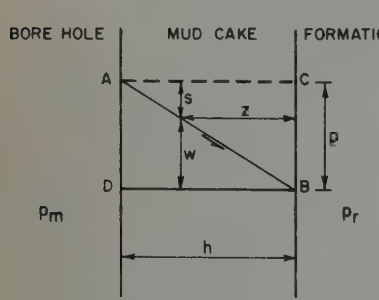

Fig. 1 — Vertical Section Through Borehole Showing the Differential Hydraulic Stress, w, and the Effective Stress, s, in the Mud Cake During Drilling.

If it is assumed that the mechanical erosion of the mud cake by the rotating collars in the contact area is about equal to the erosion by the annular mud stream outside the contact area, then the only force which determines the difference in cake thickness in these two areas is this excess mud pressure. (Actually, this assumption is only valid for low rotary speeds. For higher speeds the erosion in the contact zone will be more severe than outside of it.) As a result of this higher pressure, the mud cake in the bearing zone will be more compressed than outside this zone and the penetration of the drill collars into the cake and the angle of their dynamic contact may be computed (Appendices 2 and 3). It should be noted that the pressure component of the drill collars in the contact area remains extremely small, so that it can be considered to be zero with respect to the stress distribution within the cake. In other words, Fig. 1 also holds for the cake between the drill collars and the formation if both the mud pressure and the drill collar pressure are considered.

When Drilling is Interrupted

Stopping circulation and pipe movement both distinctly influence the stress distribution in the mud cake.

By stopping circulation the differential pressure is reduced to its static value. The magnitude of this reduction depends on a number of factors, such as depth of the hole, mud weight and clearance, and may easily be 25 per cent of the differential pressure during circulation. The effect of the pressure reduction will be examined in one of the following sections.

By stopping the pipe movement the previously existing dynamic contact between drill collars and mud cake becomes static, the bearing surface between the two is no longer lubricated, and after the water in the lubricating film has seeped into the cake radial filtration into the contact area ceases completely. The differential pressure on the mud cake remains unaltered as long as circulation is continued, but is now exerted by the drill collars instead of the mud. Filtrate will therefore continue to flow into the formation, but as no filtrate enters the cake its water content decreases and with it the hydraulic stresses throughout the cake until they have become equal to the formation fluid pressure.

This process is shown in Fig. 2. The differential pressure during circulation is indicated by $p = w + s$.

Curves 2, 3, etc., represent the hydraulic differential stress, w, in the mud cake at successive times after pipe movement has been stopped. The balance, $s = p - w$, is the effective stress in the mud cake which increases, simultaneously and by the same increments, as w decreases. The horizontal trend of the pressure curves at AD indicates that no filtrate enters the cake from the borehole.

The gradual change over from hydraulic to effective stress at the surface of the cake causes the friction between the drill collars and the cake and constitutes the essence of the wall-sticking mechanism.

Fig. 2 also shows that the effective stresses are at all times smaller at the isolated surface (AD) than inside the mud cake. As the internal coefficient of friction of clay will often be higher than that between steel and clay, shearing by the pull-out force will usually take place along the surface of contact and not in the interior of the cake.

The decrease in water content in the isolated part of the mud cake, as mentioned earlier, is accompanied by a reduction in porosity and hence in volume. The cake between the

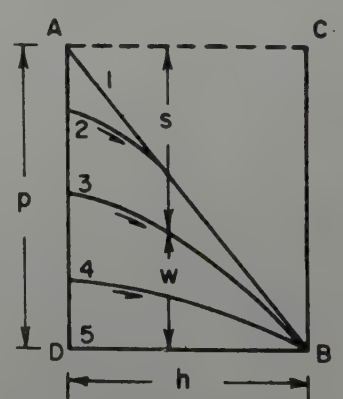

Fig. 2—Vertical Section Showing Successive Stages (1 to 5) of the Stresses, s and w, in the Mud Cake During Sticking.

collars and the formation shrinks. During the shrinking the area of static contact expands, new parts of the cake are isolated and in each additional point of contact the effective stresses also begin to increase; thus, contributing to the sticking force.

THE BASIC EQUATION FOR FRICTION BETWEEN DRILL COLLARS AND MUD CAKE

From the previous discussion it will be clear that the friction force between the collars and the mud cake may be expressed by the formula, $F = A_c \cdot p \cdot f_c$, in which A_c is the total contact area, p the differential pressure and f_c the friction factor between mud cake and pipe.

This formula may also be written, $F = A_c\ (wf_w + sf)$, where f_w and f are the friction factors between steel and water and between steel and clay, respectively. During drilling, $sf = 0$, and $F = A_c(p + p_p)f_w$, where p_p is pressure exerted by the drill collars normal to the wall. When pipe movement is stopped, the influx of water into the cake in the contact area ceases and s starts to increase. Eventually s becomes equal to p. Neglecting f_w which is small compared to f, and substituting $A_c = l \cdot d \cdot \alpha_c$, we have, $F = f \cdot l \cdot d \cdot s_1 \cdot \alpha_i + f \cdot l \cdot d \cdot s_2 \cdot (\alpha_c - \alpha_i) = F' + F''$, in which s_1 and s_2 are the solid stresses in the initial and in the shrinkage areas, F' and F'' the corresponding friction forces, and α_i and α_c are the initial and final angles of contact, respectively.

The drill collars are stuck if at any time the friction force, F, plus the buoyant weight of the drill string is larger than the maximum pull-out force, as determined by the strength of the string.

ANALYSIS OF THE FRICTION FORCE

In Appendix 5 the friction force, F', has been computed as a function of the sticking time for various mud and borehole characteristics. The concept "half value time" is introduced as a yardstick for the sticking time required to let F' increase to 50 per cent of its maximum value, i.e., when the effective stress at the surface of the mud cake has increased to 0.5 p (Line 3 in Fig. 2). The half value time, $t = (\mu\beta h^2)/6k$.

As the ratio, β/k, is fairly constant for any mud cake the half value time depends on the viscosity of the filtrate and the thickness of the cake in the contact zone. For example, if the viscosity is 0.5 cp (55°C) and the cake thickness is 1 cm, then assuming $\beta/k = 10^5$ sec/cm² · cp, the half value time is 8,300 sec. For a cake of 0.3 cm this would be 830 sec.

The half value of the friction force, F', is given by the formula, $F'_1 = 0.5\ flp$.

$$\sqrt[3]{\frac{3\pi\gamma\beta d \cdot h(d^2 - d_i^2)(D - 2h)\sin\delta}{4\ (D - d - 2h)}},$$

which shows that F'_1 increases with the coefficient of friction, the length of the stuck collars, the differential pressure, the compressibility, the thickness of the mud cake, the deviation of the borehole and the diameter of the collars. It decreases for larger diameters of the borehole.

For the two mud cakes in the stated examples and, assuming $D = 9\frac{5}{8}$ in., $d = 7$ in., $d_i = 3$ in., $p = 20$ kg/cm², $\delta = 5°$, and $f = 0.5$, the force F'_1 is 190 lb/ft stuck collar after 8,300 sec in the cake of 1 cm and 120 lb/ft after 830 sec in the cake of 0.3 cm. As F'_1 is 0.5 F' it follows that for a thick filter cake the friction force, F', is initially smaller than for a thin cake. Eventually, however, the thinner cake gives rise to the smaller value of F'.

The force F'' (see Appendices 6 and 7) is smaller than F' for large deviations and short sticking times. In straight holes, however, F''_1 may may be several times larger than F'_1.

The analysis of the friction force also shows that drilling with long strings of oversize drill collars is conducive to wall sticking by the following.

1. The axial extent of the contact zone is large.
2. The high annular velocity favors formation of thin mud cakes in the contact zone which leads to the rapid increase of the solid stresses to the "half value", and what may be more serious, to cake build-up and correspondingly fast increase in contact angle when circulation is stopped.
3. The small clearance tends to increase the initial contact area.

In order to offset these disadvantages of "packed hole drilling", which will be even more serious in deviated holes, the following measures, some of which have already been accepted in the drilling industry, are suggested.

1. The axial and circumferential area of contact may be reduced by using stabilizers or by welding "buttons" onto the collars. Another approach would be the use of twisted non-circular drill collars.
2. Using muds of excellent plastering properties which reduce the rate of cake build-up when circulation is stopped.
3. Keeping the interruptions of pipe movement as short as possible.
4. Developing efficient methods of reducing the friction factor, e.g., by drill collar coating.
5. Avoiding long strings of oversize drill collars in deviated holes.

EFFECT OF STOPPING CIRCULATION ON DIFFERENTIAL PRESSURE STICKING

In the previous sections it was assumed that circulation was continued after pipe movements were stopped. In reality stopping of circulation and pipe movement will usually coincide.

When only circulation is stopped, then the pressure at the bit will be reduced to its static value, the pressure differential across the mud cake becomes smaller and, with time, a new equilibrium is reached.

The pressure lines are given in Fig. 3. Initially, just after circulation is stopped the effective stress remains unchanged and the change in differential pressure is fully taken up by the hydraulic stress so that its distribution is given by Line EF (Curve 1). In view of the difference in pressure between B in the formation and F in the mud cake, water will flow into the mud cake (Curves 2 and 3) from the formation. This flow ceases when the gradient becomes horizontal at B (between Curves 3 and 4) and from then on the filtration is again exclusively from the mud through the cake into the formation (Curve 4) and eventually the equilibrium gradient is approached (Curve 5).

At the surface (ED) of the mud cake the influence of this stress ad-

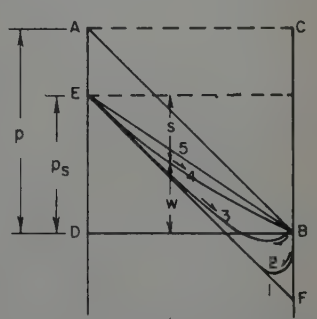

FIG. 3—SUCCESSIVE STATES OF STRESS IN THE MUD CAKE IF CIRCULATION IS INTERRUPTED (DRILL STRING KEPT MOVING).

justment is twofold. First, the gradient changes from EF to EB and, second, as the cake is no longer eroded by the ascending mud stream, it will increase in thickness. The first effect will be the same inside and outside the areas of (dynamic) contact between collars and cake but the second will be only noticeable outside the contact area. Consequently, the angle of contact between collars and cake increases (Appendix 4). When circulation is restarted, after pressure Curve EB has been reached, then a reverse process takes place and the curves are as in Fig. 4. Outside the contact area restarting of circulation will not only bring about a change in gradient but it will also erode the newly formed cake until its thickness, and thereby the contact angle, are reduced to their original values. This erosion, however, may be difficult to accomplish[5].

Combinations of Figs. 2 and 3 show the influence of stopping pipe movement and circulation on the solid stresses at the surface of the cake.

Figs. 5, 6 and 7 show that due to the then prevailing high differential pressure, interruption of pipe movement before circulation is stopped with lead to rapid development of the solid stresses at the surface of the cake. On the other hand, stopping circulation first tends to increase the contact angle.

When the drilling mud has good plastering properties and the diameter of the drill collars is "normal", then the increase in contact angle is small and stopping circulation well ahead of pipe movement would appear to be the best practice.

Once the collars have become stuck, restarting circulation will only be beneficial when the sticking is due to relatively low effective stresses in a large area of contact which may be reduced by erosion (oversize collars, poor quality mud). When the collars are stuck in a good mud cake and the erosion caused by restarting circulation is small, then the circulation will only lead to a more rapid increase of solid stresses and, hence, also of friction forces.

EFFECT OF PRESSURE REDUCTION, SPOTTING AND FRACTURING ON THE STUCK COLLARS

Pressure Reduction

The effect of circulating water instead of mud in the borehole after

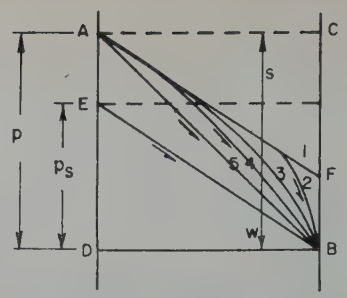

Fig. 4—Successive States of Stress in the Mud Cake if Circulation is Resumed (Drill String Kept Moving).

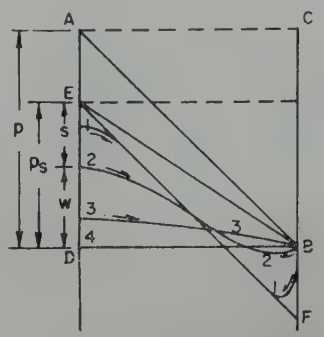

Fig. 5—Successive States of Stress in the Mud Cake Behind the Sticking Collars if Circulation and Pipe Movement are Stopped Simultaneously.

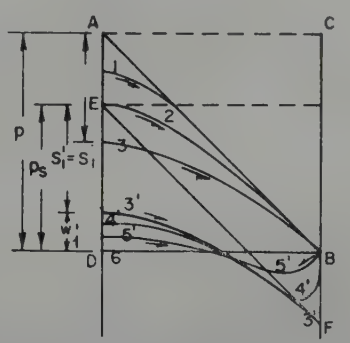

Fig. 6—Successive States of Stress if Pipe Movement is Stopped First and Circulation when $S_1 = 0.5\ p$.

the collars have become stuck may be described as follows.

Suppose that the mud pressure is p_m and that the reservoir pressure is p_f. Before the pipe stuck the hydraulic stress at the outside surface of the mud cake, $w_h = p_m$ and the solid stress there $s_h = 0$. At the contact face between mud cake and formation $w_o = p_f$ and $s_o = p_m - p_f$ (Fig. 8). During the sticking w_h decreases gradually to p_f and s_h increases to $p_m - p_f$ (Fig. 9). If the pressure is now reduced to p_m' by circulating fresh water ($p_m' < p_f$), then, initially, no change will be observed in the solid stresses and $s_h = s_o = p_m - p_f$. The hydraulic stress, however, will drop to $p_m' - (p_m - p_f)$, the pressure required for equilibrium with the reduced pressure in

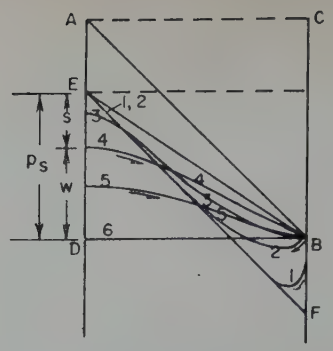

Fig. 7—Successive States of Stress if Circulation is Stopped First and Pipe Movement when Curve 2 is Reached.

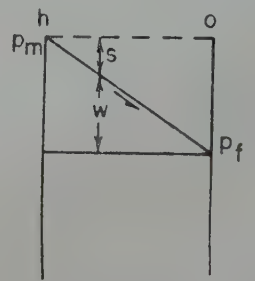

Fig. 8—Initial Stress State in Mud Cake.

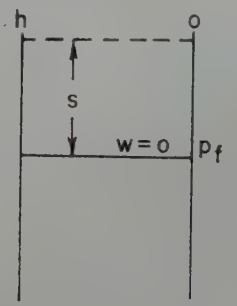

Fig. 9—Final Stress State in Mud Cake after Sticking.

the borehole. In the formation the reservoir pressure is of course unaltered and equal to p_f. At the cake formation interface the pressure drop is equal to $p_m - p_m'$, the formation starts to produce, the solid stress becomes negative and the mud cake is forced into the borehole (Fig. 10). The time required for the mud cake to detach itself from the wall depends on the difference between p_f and p_m' and on how strongly the cake is "anchored" to the wall. Consequently, if the collars can now be pulled then the plane of sliding will not be between the collars and the cake but between the cake and the formation.

As this phenomenon of cake collapse will not be limited to the stuck zone but extend to the entire permeable section of the hole, reducing the pressure to below the reservoir pressure will result in the gradual collapse of large sections of the mud cake, and the collars, although no

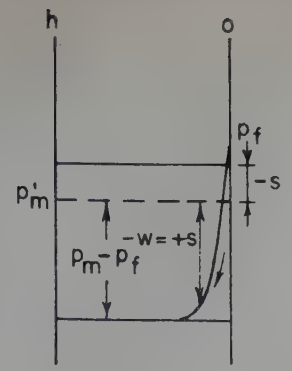

FIG. 10—A STRESS STATE IN MUD CAKE AFTER CIRCULATION TO WATER.

longer wall stuck, may now stick in this loose cake. It would, therefore, appear that this method of freeing wall-stuck pipe is only suitable if the permeable section of the hole is short if no difficulty has been experienced with unstable shales and if no abnormal pressure zones have been drilled through. The circulation with water will have to be continued for a considerable length of time if the formation pressure is low and if, due to poor plastering properties of the mud, the skin effect is pronounced.

The disadvantage of a pressure reduction in the entire borehole, as just described, may be avoided by screwing a formation tester onto the stuck drill collars after the drill pipe has been backed off. Reduction of the borehole pressure under the packer to atmospheric may then result in an immediate collapse of the mud cake and freeing the stuck collars. This method has met with some success[1].

The intermediate solution would be to reduce the pressure in the borehole to a value slightly above the reservoir pressure by circulating to a light mud. This would lead eventually to solid stresses in the mud cake equal to the difference between the reservoir pressure and the reduced borehole pressure. It seems doubtful, however, that solid stresses of this magnitude would permit pulling of the pipe.

SPOTTING[1]

The following theory is advanced for the mechanism effecting the release of stuck drill collars by "oil spotting". It is based on the well-known fact that clay-mud cakes are virtually impermeable to oil. Therefore, if the mud in the stuck zone is replaced by oil, filtration into the mud cake ceases. As, however, the pressure differential is unaltered by the spotting, filtration from the mud cake into the formation continues. This process is similar to the one producing the shrinkage of the cake in the contact zone. The effect of the spotted oil is thus to offset the increase in contact angle as caused by the shrinkage of the cake inside the contact zone by an equal shrinkage of the cake outside this zone. This residual pull-out force is thus only dependent on the differential pressure acting in the initial contact area (Appendix 8). It would, therefore, appear that the reduction in pull-out force by spotting is most pronounced in those cases where the initial angle of contact is small, i.e., in straight holes drilled with normal sized collars (Appendix 3).

FRACTURING

Instead of equalizing the pressure in the borehole and in the formation by reducing the former, this might be accomplished by forcing an increase in the latter. To this end the cake and the formation may be fractured by squeezing oil, thus permitting a relatively unobstructed flow of fluid into the formation behind the stuck collars. Once fracturing has taken place the pressure should then be released, allowing additional oil to flow by differential pressure into the formation through the fissures in the cake. The success of this method seems, however, dubious because: (1) the fractures would have to develop in the stuck zone, and (2) the differential pressure is initially increased thus accelerating the development of high solid stresses in the mud cake.

THEORETICAL CONCLUSIONS

1. When pipe movement is interrupted the static contact between the drill collars and the mud cake stops the flow of filtrate from the mud into the area thus isolated.

2. The influence of this shut-off on the stresses in the mud cake is twofold: (a) the stresses between the solid particles of the mud cake at its surface, as well as inside, start to increase with time while simultaneously the hydraulic stresses in the cake start to decrease at the same rate; and (b) as the pressure on the isolated area of the cake is unaltered, water will be squeezed out of it into the formation. As no water can enter the cake, the water content decreases and the cake shrinks.

3. As a result of the process outlined under 2a, the pressure on the contact surfaces between the drill collar and the mud cake changes gradually from hydraulic to solid pressure. Since the friction factor between steel and water is negligible compared to that between steel and clay, the force required to overcome the friction also increases with time.

4. In view of 2b the area of contact between the collars and the cake increases. In each new point of contact, the filtrate flow into the mud cake also ceases and additional friction forces are created.

5. The pull-out force required to overcome the friction must be equal to the sum of the friction forces described under 3 and 4.

6. The area of contact will also increase by additional deposition of mud particles at the edges of the contact zone if circulation is stopped. This increase may be eliminated by restarting circulation. The advantage of stopping circulation at an early stage is a reduced pressure differential.

7. Conditions conducive to wall sticking are: (a) oversize drill collars; (b) long strings of drill collars; (c) high deviation of the borehole; (d) high weight, high water loss, and high solids content of the mud; and (e) any interruption of pipe movement and long interruptions of circulation when mud quality is poor and annular velocity high.

8. Preventive measures against wall sticking are: (a) reducing the contact surface between collar and cake (stabilizers, buttons, twisted non-circular collars); (b) reducing the friction factor between steel and clay (coating, oil emulsion or oil-base mud); and (c) avoiding the conditions mentioned under 7.

9. It is suggested that the results obtained by spotting are due to shrinkage of the mud cake outside the contact area and the subsequent reduction in the angle of contact between collars and mud cake.

10. The method of freeing stuck drill collars by spotting is probably more effective if the friction force due to shrinkage of the cake is large compared to that developing in the initial area of contact, i.e., in straight holes drilled with normal size drill collars.

11. The great volume of loose mud cake in the borehole after circulating to water is caused by collapse of the cake under the influence of the reversed differential pressure.

12. Remedial measures against wall sticking are: (a) immediate breaking of circulation and application of the maximum allowable tension to the string as soon as the

sticking has been recognized to be caused by the differential pressure; (b) if conditions are suitable, reduction of the differential pressure by prolonged circulation of water or preferably of oil; (c) spotting and prolonged intermittent circulation of oil in batches; and, (d) reducing the pressure in the hole to atmospheric by connecting a formation tester to the collars after backing off the drill pipe. This method should prove more successful, if first, oil-base mud is spotted around the collars.

NOMENCLATURE

(Small metric static system, g = gram force)

α = angle of contact between drill collar and mud cake, measured between the points of maximum and of minimum deformation of the cake

β = coefficient of consolidation, $\frac{\Delta e}{\Delta p}$, cm^2/g

C = coefficient of contact angle, $\frac{\alpha}{\sqrt{\varepsilon}}$, $cm^{-\frac{1}{2}}$

c_d = coefficient of clay deposition (−)

D = diameter of the borehole, cm

d = OD of drill collars, cm (subscript i indicates ID)

δ = angle of deviation of the section of the hole where drill collars have stuck

e = volume of pores/total volume = porosity (−)

ε = deformation of the mud cake at the midpoint of contact, cm

F = friction force between mud cake and drill collars, g

f = coefficient of friction between clay and steel, (−)

γ = specific gravity, g/cm^3

h = thickness of mud cake, cm

k = permeability of mud cake [$(cm^4/g\ sec)$ cp] = 1,000 darcies

l = length of stuck drill collars, cm

μ = viscosity of filtrate, cp

p = difference between pressure in borehole and formation fluid, g/cm^2

r = distance between a point in mud cake or formation and center of borehole, cm

s = pressure between solid particle in mud cake (g/cm^2), the "effective" or "solid" stress

τ = reduced time, $\frac{k}{\mu\beta}\cdot\frac{t}{h^2}\cdot\frac{\pi 2}{4}$ (−)

v = velocity of filtrate inside mud cake before sticking, cm/sec

w = pressure of filtrate at a point in the mud cake in excess of reservoir pressure, g/cm^2

z = distance between a point inside the mud cake and the formation, cm

ACKNOWLEDGMENT

This paper was prepared during the author's association with the N. V. De Bataafsche Petroleum Maatschappij. He is indebted to members of this company for their advice and assistance during this investigation.

The author also wishes to express his appreciation to the management of the N. V. De Bataafsche Petroleum Maatschappij for permission to publish the paper.

REFERENCES

1. Helmick, W. E., and Longley, A.: *Drill and Prod. Prac.*, API (1957) 55.
2. Terzaghi, K.: *Theoretical Soil Mechanics*, New York (1957).
3. Keverling Buisman, A. S.: *Grondmechanica*, Delft (1940).
4. Faulk, J. H.: *Trans.* AIME (1956) **207**, 80.
5. Prokop, C. L.: *Trans.* AIME (1952) **195**, 5.
6. Terzaghi, K. and Peck, R. B.: *Soil Mechanics in Engineering Practice*, New York (1948).
7. Terzaghi, K. and Frölich, O. L.: *Theorie der Setzung von Tonschichten*, Vienna (1936).
8. Tan Tjon Kie: "Onderzoekingen over de Rheologische Eigenschappen van Klei", Thesis, Delft Technical U. with English summary (1954).
9. Lubinski, A. and Woods, H. B.: *Drill. and Prod. Prac.*, API (1953) 222.
10. Biot, M. A.: *Jour. Appl. Physics* (1941) **12**, 155.
11. Ferguson, C. K. and Klotz, Y. A.: *Trans.* AIME (1954) **201**, 29.

APPENDIX 1

PRESSURE GRADIENT IN MUD CAKE DURING DRILLING

In a cylindrical hole the pressure, p, of the filtrate in the mud cake and in the reservoir may be calculated from the following formulas (Fig. 11).

$$\text{mud cake, } p = p_o - \frac{p_o - p_x}{\lg r_o/(r_o - h)} \lg r/(r_o - h)$$
$$(r_o - h \leqslant r \leqslant r_o)$$

$$\text{formation, } p = p_x - \frac{p_x - p_e}{\lg r_e/r_o} \lg r/r_o$$
$$(r_o \leqslant r \leqslant r_e)\ .$$

At the boundary, between the mud cake and formation, the velocity of water which filters out of the mud cake is the same as flows into the formation. Hence, according to Darcy,

$$\frac{k_1}{\mu}\left(\frac{dp}{dr}\right)_{\substack{r=r_o \\ \text{(cake)}}} = \frac{k_2}{\mu}\left(\frac{dp}{dr}\right)_{\substack{r=r_o \\ \text{(formation)}}} \quad \ldots\ldots\ (1)$$

The pressure gradient for the mud cake is

$$-\frac{dp}{dr} = \frac{p_o - p_x}{r \lg r_o/(r_o - h)} \quad \ldots\ldots\ (2)$$

Eq. 1 may be written,

$$\frac{k_1}{\mu}\cdot\frac{p_o - p_x}{r_o \lg r_o/(r_o - h)} = \frac{k_2}{\mu}\cdot\frac{p_x - p_e}{r_o \lg r_e/r_o}\ ,$$

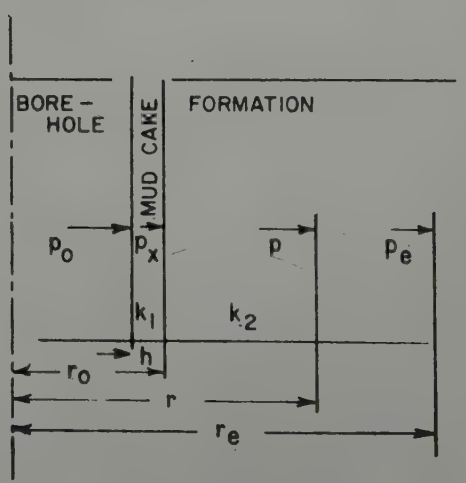

FIG. 11—VERTICAL SECTION THROUGH BOREHOLE SHOWING DIFFERENTIAL PRESSURES (p_o, p, p_e) AT DISTANCES r_o, r, r_e, FROM CENTER AND PERMEABILITIES (k_1, k_2) OF MUD CAKE AND FORMATION.

or

$$p_x = \frac{mp_o \cdot lg\, r_e + (p_o - mp_o) \cdot lg\, r_o - p_e \cdot lg\,(r_o - h)}{m \cdot lg\, r_e + (1 - m) \cdot lg\, r_o - lg\,(r_o - h)} \quad . \quad . \quad . \quad . \quad . \quad . \quad . \quad . \quad . \quad . \quad . \quad (3)$$

in which $m = k_1/k_2$.

By substituting p_x from Eq. 3 in Eq. 2,

$$-\frac{dp}{dr} = \frac{p_o - p_e}{r\,[m\, lg\, r_e + (1 - m)\, lg\, r_o - lg\,(r_o - h)]} \quad . \quad . \quad . \quad . \quad . \quad . \quad . \quad . \quad . \quad . \quad . \quad (4)$$

As the permeability of the formation is usually high compared to that of the mud cake, the permeability ratio m will be close to zero and Eq. 4 becomes,

$$-\frac{dp}{dr} = \frac{p_o - p_e}{r\, lg\, r_o/(r_o - h)} \quad . \quad . \quad . \quad . \quad . \quad . \quad . \quad (5)$$

In that case the reservoir pressure p_e will be reached at the boundary between the cake and the formation (Eq. 3). If the thickness of the mud cake is small compared to the radius of the borehole the term $lg\, r_o/(r_o - h)$ will be equal to h/r_o and as this ratio is small, the ratio r/r_o, which must satisfy the inequality, $1 - h/r_o < r/r_o < 1$, will be close to 1. Eq. 5 then becomes,

$$-\frac{dp}{dr} = \frac{p_o - p_e}{h} = \frac{p}{h} \quad . \quad . \quad . \quad . \quad . \quad . \quad . \quad (6)$$

This formula is not affected qualitatively by the presence of a low permeability invasion zone in the formation. Application of Eq. 3 then shows that the pressure gradient may be written,

$$-\frac{dp}{dr} = \frac{p}{h(1 + mn)} \quad . \quad . \quad . \quad . \quad . \quad . \quad . \quad . \quad (7)$$

where m is the permeability ratio of the mud cake and the invaded zone and n is the ratio of the thickness of the invaded zone and the mud cake. It is assumed that the invaded zone is not much thicker than the cake and that the permeabilities of the cake and the invaded zone are low compared to that of the uninvaded formation.

Eq. 7 shows that formation plugging reduces the pressure gradient in the cake.

APPENDIX 2

RELATION BETWEEN ANGLE OF CONTRACT AND DEFORMATION OF THE CAKE

The angle of contact, α, is related to the consolidation, ε, at the mid-point of contact by the geometric formulas,

$$\cos \alpha = \frac{\frac{1}{2} Ad - A \cdot \varepsilon - \varepsilon^2}{(\frac{1}{2}A + \varepsilon)d}, \text{ or } \sin \alpha = \frac{\varepsilon(A + \varepsilon)(A + d + \varepsilon)(d - \varepsilon)}{(\frac{1}{2}A + \varepsilon)d}, \quad . \quad . \quad . \quad (8)$$

in which $A = D - d - 2h$ equals the diametral clearance between the centric pipe and the mud cake (Fig. 12).

As ε is small relative to A and d, Eq. 8 may be approximated by $\alpha = C\sqrt{\varepsilon}$, in which $C = 2\,(1/A + 1/d)^{\frac{1}{2}}$.

This means that for all hole sizes, pipe diameters and thicknesses of mud cake, α is (approximately) proportional to the square root of the penetration at the mud point of the contact area, if this penetration is small relative to the clearance between the centered drill collar and the mud cake.

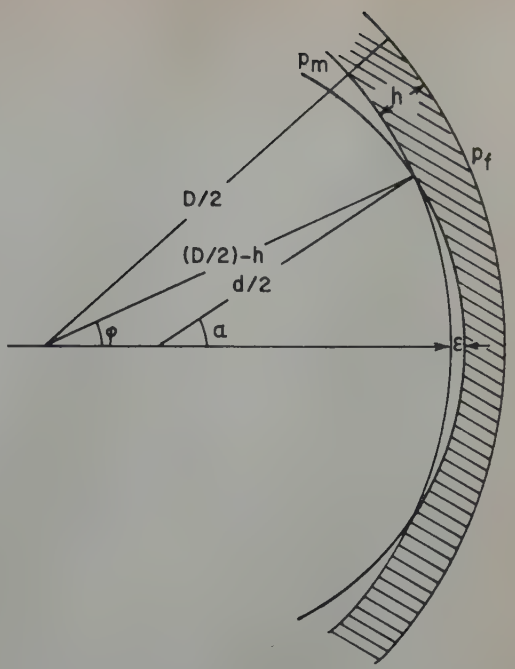

FIG. 12—CROSS SECTION OF BOREHOLE SHOWING CONTACT BETWEEN DRILL COLLAR AND MUD CAKE.

APPENDIX 3

THE ANGLE OF DYNAMIC CONTACT

If, in the section of the hole where the drill collars are resting against the lubricating film of mud, the deviation of the borehole from the vertical is δ degrees and if the angle of dynamic contact between the two surfaces (which is equal to the initial angle of static contact) is α_i, then the liquid pressure on the mud cake, as exerted per unit axial length by the component of the weight normal to the direction of the hole, is equal to $W_n = \frac{\pi\gamma}{4}(d^2 - d_i^2) \sin \delta$, in which γ is specific weight of drill collar material (7.85 gm/cm^3); d_i is ID of the collars, cm; and d is OD of the collars, cm.

The consolidation of the mud cake under the influence of a mud pressure, Δp_ψ, in excess of the differential pressure, p, is equal to $\frac{1}{2}\beta\, \Delta\, p_\psi h = \varepsilon_\psi$ or $\Delta p_\psi = 2\varepsilon_\psi/\beta h$. (It is supposed that the hydrodynamic pressure build-up in the lubricated zone may be neglected.) The situation is shown in Fig. 13; α_i is the angle of dynamic contact and ε_i the depth of penetration at the mid-point of the contact area. At an angle, ψ, the depth of penetration, $\varepsilon_\psi = \varepsilon_i - \varepsilon_o$.

For small values of α_i and ψ, according to Appendix 2, $\varepsilon_i = \alpha_i^2/C^2$ and $\varepsilon_o = \psi^2/C^2$, whence $\Delta p_\psi = 2(\alpha_i^2 - \psi^2)/\beta h C^2$.

The total force, per unit axial length and normal to the contact surface, is therefore equal to

$$\int_o^{\alpha_i} \Delta p_\psi d \cos \psi\, d\psi = (2d/hC^2\beta) \int_o^{\alpha_i} (\alpha_i^2 - \psi^2) \cos \psi\, d\psi.$$

For small values of α_i the force is equal to $(4d\,\alpha_i^2)/(3hC^2\beta)$ and for equilibrium $(4d\alpha_i^2)/(3hC^2\beta) = \frac{\pi\gamma}{4}(d^2 - d_i^2) \sin \delta$, or

$$\alpha_i = \sqrt{\frac{3\,\pi\,\gamma\,\beta\,h\,(d^2 - d_i^2)\,(D - 2h)\sin\delta}{4d^2\,(D - d - 2h)}}.$$

In order to evaluate α_i the following three examples are given.

1. $D = 9\frac{5}{8}$ in., $d = 7$ in., $d_i = 3$ in., $p = 20 \times 10^3$ g/cm², $\beta = 0.5 \times 10^{-2}$ cm²/kg, $h = 1$ cm, and $\delta = 5°$. Substituting these values in the formula gives $\alpha_i = 1°48'$.

2. $D = 9\frac{5}{8}$ in., $d = 7$ in., $d_i = 3$ in., $p = 70 \times 10^3$ g/cm², $\beta = 0.2 \times 10^{-2}$ cm²/kg, $h = 1.5$ cm, $\delta = 15°$, $\alpha_i = 2°28'$.

3. $D = 3$ in., $d = 2\frac{3}{8}$ in., $d_i = 1.815$ in., $p = 7 \times 10^3$ g/cm², $\beta = 6 \times 10^{-2}$ cm²/kg, $h = \frac{1}{8}$ in., $\delta = 90°$, $\alpha_i = 17°$, ($h = 5/32$ in., $\alpha_i = 18°25'$) (see Ref. 1)*.

The formula shows that α_i increases with the deviation of the borehole, the thickness of the mud cake, the compressibility and the OD of the drill collar. Furthermore, α_i decreases with the diameter of the borehole.

The compressibility, β, has been determined from Terzaghi's plot of the void ratio vs pressure for soft Detroit clay[6]. The compressibility decreases as the differential pressure increases.

APPENDIX 4

INCREASE IN CONTACT ANGLE DUE TO CAKE BUILD-UP

As sections of the mud cake are isolated and circulation is interrupted the remaining "free" cake starts to increase by additional deposition of mud particles, and also α_i increases.

If the initial angle of contact is equal to α_i then, according to Appendix 2, $\alpha_i = C_i\sqrt{\varepsilon_i}$.

After a time, t, the thickness of the mud cake will be equal to $\sqrt{(h_i^2 + 2c_d\,kpt)} = h$. The initial penetration, ε_i, will then have increased by the same amount as the free cake and is equal to $\varepsilon = \varepsilon_i + (h_i^2 + 2c_d\,kpt)^{\frac{1}{2}} - h_i$. The new angle of contact is $\alpha = C\sqrt{\varepsilon}$ and therefore,

$$\frac{\alpha^2}{C^2} = \frac{\alpha_i^2}{C_i^2} + (h_i^2 + 2c_d\,kpt)^{\frac{1}{2}} - h_i, \quad . \quad . \quad . \quad (9)$$

in which $C^2 = 4\dfrac{D - 2h}{(D - d - 2h)d}$,

and $C_i^2 = \dfrac{D - 2h_i}{(D - d - 2h_i)d}$.

*Tube filled with mercury.

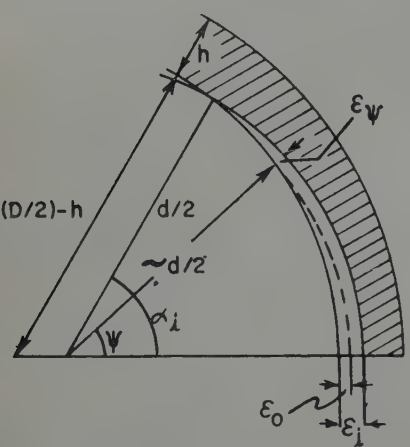

FIG. 13—CROSS SECTION OF BOREHOLE SHOWING INITIAL ANGLE OF CONTACT, α_i.

Substituting C^2 and C_i^2 in Eq. 9 gives

$$\alpha = \sqrt{\frac{D - 2h}{D - 2h_i}\cdot\left[\alpha_i^2 + \frac{(D - 2h_i)(h - h_i)}{d(D - d - 2h)}\right]},$$

in which $h = \sqrt{(h_i^2 + 2c_d\,kpt)}$. By restarting circulation, $h \to h_i$ and $\alpha \to \alpha_i$.

APPENDIX 5

SOLID STRESSES AT THE FACE OF THE MUD CAKE

Although the flow of filtrate through the mud cake is radial, the problem may be treated as one-dimensional in view of the relative thinness of the cake and relatively high permeability of the formation (Appendix 1).**

These one-dimensional problems are common in the theory of soil mechanics and were investigated by Terzaghi[7], who derived the formula, $c(\partial^2 w/\partial z^2) = (\partial w/\partial t)$, in which $c = k/(\mu\beta)$.

The boundary conditions for this equation in the case of wall sticking are: (1) the excess hydraulic stress at the formation is equal to zero at all times, or $w(o,t) = 0$; (2) the initial excess hydraulic stress distribution in the mud cake is linear, or $w(z,o) = (pz)/h$; and (3) no water can enter the cake during sticking, or $\partial\, w(h,t)/\partial z = 0$.

Although the mechanical analogy is not so obvious, the boundary value problem as defined by Terzaghi's equation and the boundary conditions 1 to 3 has an equivalent in hydraulic structure (the placing of a hydraulic fill on an impermeable base) which was solved by Terzaghi and this solution is therefore applicable also to the wall-sticking problem. (The same boundary value problem arises if in a slab of homogeneous material the temperature increases linearly from zero at one side to a given temperature at the other side which is then insulated, while the temperature at the first side is kept constant at zero.) Rigorous solution of the problem gives the following formula for the excess hydraulic stress.

$$w(z,\tau) = (8/\pi^2)\,p\sum_{n=1}^{\infty}\left[[(-1)^{n+1}/(2n-1)^2]\exp\left[-(2n-1)^2\tau\right]\right]\sin\left[(2n-1)\pi z/2h\right],$$

in which $\tau = (k\pi^2 t)/(4\mu\beta h^2)$.

The solid stress at the contact face between pipe and cake is then equal to

$$s(h,\tau) = p - w(h,\tau) = p\left[1 - (8/\pi^2)\sum_{n=1}^{\infty}\frac{\exp\left[-(2n-1)^2\tau\right]}{(2n-1)^2}\right].$$

As these formulas for w and s are not very suitable for engineering purposes, Terzaghi introduced an approximate solution assuming that the lines, $w(z,\tau)$, are parabolic for small values of τ (see Fig. 2).

Applying this method to the problem under consideration, the following formulas may be derived.

$$w(z,\tau) = p\left[1 - (\sqrt{6}/\pi)\sqrt{\tau}\left\{1 - \pi^2(1 - z/h)^2/24\tau\right\}\right].$$

This formula is valid for $0 \leqslant \tau \leqslant (\pi^2/24)$ and $1 - (2\sqrt{6}/\pi)\sqrt{\tau} \leqslant z/h \leqslant 1$.

Substituting $z = h$, the solid stress at the contact face,

**The small tangential flow along the line of contact between the drill collar and the mud cake is also neglected. This is permissible if the angle of contact is not too small and the mud cake is thin.

$$s(h,\tau) = p(\sqrt{6}/\pi)\sqrt{\tau}$$

for $0 \leqslant \tau \leqslant (\tau^2/24)$ (first period). For larger values of τ, the second period, the solid stress may be approximated by

$$s(h,\tau) = p\left[1 - \tfrac{1}{2}\exp - \left\{(12\tau/\pi^2) - \tfrac{1}{2}\right\}\right]$$

$(\pi^2/24) \leqslant \tau \leqslant \infty$ (second period).

In order to apply these formulas for numerical calculations the constants in the reduced time, $\tau = (k\pi^2 t)/(4\mu\beta h^2)$, have to be determined.

Terzaghi[6] found that for different clays the value of k/β varies from 10^{-3} to 10^{-4} cm^2 · cp/sec (depending on the liquid limit of the sample) if p is in the pressure range 1 to 4 kg/cm^2. As k and β both decrease rapidly for higher values of p, the ratio k/β will be fairly constant. Nevertheless, under actual borehole conditions, where p is often in the order of 50 atm, a value of 10^{-4} would probably be too low and although no accurate data are available it is suggested that the ratio may then approach 10^{-5} cm^2 · cp/sec.

If the borehole temperature in the stuck section is 55°C then $\mu = 0.5$ cp and for a cake of 1-cm thickness the length of the first period would be $1/6 \times l^2 \times 0.5 \times 10^5 = 8{,}300$ sec or 2 hours 18 min. For a cake of 0.3 cm the length of the first period would be 830 sec or 14 min.

During the first period the effective stress increases from zero to ½p (the half value).

In order to compare the solid stresses computed from the rigorous solution of the problem with those given by the approximation, reference is made to Fig. 14 and Table 1.

The approximation shows values of the solid stresses which are from 5 to 8 per cent too high, a margin small enough to justify use of this approximation in further calculations.

The friction force, $F' = s_1 \cdot f \cdot l \cdot d \cdot \alpha_i$ (see previous section "Analysis of Friction Force"). Substituting for s_1 the formula, $s\ (h,t)$, and for α_i the formula of Appendix 3, the following formula may de derived for F'.

$$F' = flp\sqrt[3]{\frac{3\pi\gamma\beta d(d^2 - d_i^2)(D - 2h)\ \sin\delta}{4h^2(D - d - 2h)}} \cdot \sqrt{\frac{3kt}{2}}$$

for $t \leqslant \dfrac{\mu\beta h^2}{6k}$,

and at the end of the first period,

$$F'_1 = \tfrac{1}{2}\ flp\sqrt[3]{\frac{3\pi\gamma\beta d \cdot h(d^2 - d_i^2)(D - 2h)\ \sin\delta}{4(D - d - 2h)}}.$$

The final value of F' is equal to $F'_\infty = 2F'_1$. Substituting the values of α_i, as computed in Appendix 3, in the formula for F'_1 and assuming $f = 0.5$, we have,

(1) $\alpha_i = 1°\ 48'$ $F'_1 = 2.7$ kg/cm of collar stuck
(2) $\alpha_i = 2°\ 28'$ $F'_1 = 12.5$ kg/cm of collar stuck
(3) $\alpha_i = 17°$ $F'_1 = 3.2$ kg/cm of collar stuck

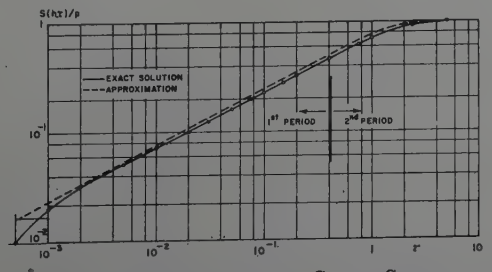

FIG. 14—RELATION BETWEEN SOLID STRESS AT SURFACE OF MUD CAKE AND STICKING TIME.

TABLE 1

$$s(h,\tau)/p = \begin{cases} 1 - (8/\pi^2)\sum_{n=1}^{\infty}\dfrac{\exp - (2n-1)^2\tau}{(2n-1)^2} & 0 \leq \tau \leq \infty \quad \text{(A)} \\ (\sqrt{6}/\pi)\sqrt{\tau} & 0 \leq \tau \leq (\pi^2/24) \quad \text{(B)} \\ 1 - \tfrac{1}{2}\exp - [(12\tau/\pi^2) - \tfrac{1}{2}] & (\pi^2/24) \leq \tau \leq \infty \quad \text{(C)} \end{cases}$$

τ	Formula A	Formula B	Formula C
0.0005	0.01 +	0.017	
0.0010	0.02 +	0.025	
0.0015	0.03	0.030	
0.0025	0.037	0.039	
0.0050	0.051	0.055	
0.0100	0.072	0.078	
0.0200	0.102	0.109	
0.0300	0.124	0.134	
0.0500	0.161	0.174	
0.0750	0.197	0.213	
0.1000	0.227	0.246	
0.1500	0.278	0.302	
0.2000	0.321	0.348	
0.4000	0.454	0.493	
0.7500	0.617		0.669
1.0000	0.702		0.756
2.5000	0.933		0.961
5.000	0.995		0.998

(4) $\alpha_i = 18°\ 25'$ $F'_1 = 3.5$ kg/cm of collar stuck

APPENDIX 6

SHRINKAGE OF MUD CAKE DURING STICKING

The specific shrinkage of a clay layer, due to changes in the external load is expressed by the formula[7], $(\partial\varepsilon/\partial z) = -\beta w(z,t)$. Therefore,

$$\varepsilon = E_o - \beta\int_o^h w(z,t)\,dz, \text{ in which } E_o = \beta\int_o^h w(z,o)\,dz.$$

For the wall sticking problem, $E_o = \tfrac{1}{2}\beta ph$ and with $w(z,t)$ from Appendix 5,

$$\varepsilon = \tfrac{1}{2}\beta ph\left[1 - (32/\pi^3)\sum_{n=1}^{\infty}\frac{(-1)^{n+1}\exp[-(2n-1)^2\tau]}{(2n-1)^3}\right],$$

for $0 \leqslant \tau \leqslant \infty$.

Again supposing that the curves for $w(z,\tau)$ are parabolic (see Appendix 5,) an approximate value for ε may be computed from the formulas, $\varepsilon = (4\beta ph\tau)/\pi^2$, for $0 \leqslant \tau \leqslant (\pi^2/24)$ (first period), and

$$\varepsilon - \tfrac{1}{2}\beta ph\left[1 - 2/3\exp - \{(12/\pi^2) - \tfrac{1}{2}\}\right],$$

for $(\pi^2/24) \leqslant \tau \leqslant \infty$ (second period).

These formulas show that initially the shrinkage is directly proportional to the sticking time.

Fig. 15 and Table 2 have been prepared to demonstrate the extremely small difference between the exact and approximating formulas.

The degree of shrinkage, $\varepsilon/(\tfrac{1}{2}\beta ph) = (8\tau)/\pi^2$, for $0 \leqslant \tau \leqslant (\pi^2/24)$, and at the end of the first period, $\varepsilon/(\tfrac{1}{2}\beta ph) = 1/3$. At the end of the second period, $w(z,t) = 0$ and $\varepsilon = \tfrac{1}{2}\beta ph$.

APPENDIX 7

EFFECT OF SHRINKAGE ON THE PULL-OUT FORCE

According to Appendices 5 and 6 the solid stress at the contact face during the period when $\tau < (\pi^2/24)$ is $s(h,\tau) = (p\sqrt{6}/\pi)\sqrt{\tau}$ and $\varepsilon_\tau = (4\beta ph\tau)/\pi^2$.

If for $\tau = 0$ the initial angle of contact is α_i and, by maintaining circulation no additional mud cake is deposited, then the initial penetration into the mud cake is ε_i and according to Appendix 2, $\varepsilon_i = \alpha_i^2/C^2$. When at time τ, the contact angle has increased to α_c, then the consolidation at the mid-point of contact is equal to $\varepsilon_c - \varepsilon_i = (\alpha_c^2 - \alpha_i^2)/C^2 = (4\beta\, ph\,\tau)/\pi^2$. The reduced time, τ, required for this consolidation is, therefore,

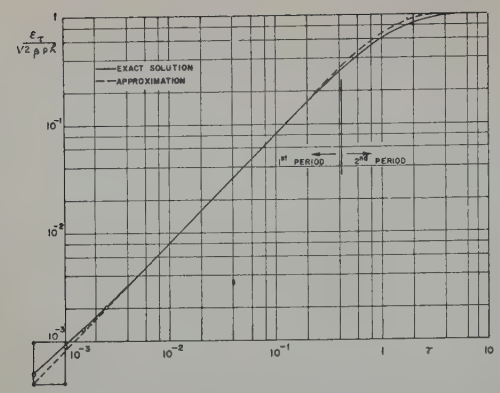

FIG. 15—RELATION BETWEEN SHRINKAGE OF MUD CAKE AND STICKING TIME.

$\tau_a = (\alpha_c^2 - \alpha_i^2)\pi^2/4\beta phC^2$. A point at the surface with contact angle, ψ $(\alpha_i < \psi < \alpha_c)$, comes into contact with the pipe after a time, $\tau_\psi = (\psi^2 - \alpha_i^2)\pi^2/4\beta phC^2$. As the consolidation proceeds and the angle of contact reaches α, the solid stresses at point ψ increase. The time during which the process takes place is $\tau_a - \tau_\psi = (\alpha_c^2 - \psi^2)\pi^2/4\beta phC^2$. The solid stresses at point ψ have then increased from zero to $s(\psi) = (p\sqrt{6}/\pi)\sqrt{\tau_a - \tau_\psi} = (1/C)\sqrt{p(\alpha_c^2 - \psi^2)/2\beta h}$.

The total radial force exerted on the pipe by particles of the mud cake in the range, $\alpha_i < \psi < \alpha_c$, is equal to

$$ld\int_{\alpha_i}^{\alpha_c} s(\psi)\,d\psi = (ld/C)\int_{\alpha_i}^{\alpha_c}\sqrt{3p(\alpha_c^2 - \psi^2)/2\beta h}\,d\psi$$

$= (ld/c)\sqrt{3p/2\beta h}\cdot \tfrac{1}{2}\alpha_c^2\,[\mathrm{Sin}^{-1}$

$\sqrt{1 - (\alpha_i/\alpha_c)^2} - (\alpha_i/\alpha_c)\sqrt{1 - (\alpha_i/\alpha_c)^2}] = F''$, where F'' is the additional pull-out force due to the increase in contact area during shrinkage of the mud cake.

As during the first period, $s = (p\sqrt{6}/\pi)\sqrt{\tau}$, and $\tau = (\alpha_c^2 - \alpha_i^2)\pi^2/4\beta phC^2$, the pull-out force $F' = sfld\alpha_i = lfd/C\sqrt{3p/2\beta h}\cdot\alpha_c^2\cdot(\alpha_i/\alpha_c)\sqrt{1 - (\alpha_i/\alpha_c)^2}$. By writing

$lft/C\sqrt{3p/2\beta h} = a$ and $\dfrac{2C}{\alpha_i\pi}\sqrt{\beta ph}\cdot\sqrt{\tau} =$

$\sqrt{(\alpha_c/\alpha_i)^2 - 1} = \tan\eta$, $F' = a\alpha_i^2\tan\eta$ and $F'' = \tfrac{1}{2}\,a\alpha_i^2$

$\left(\dfrac{\eta}{\cos^2\eta} - \tan\eta\right)$, or $F = F' + F'' = \tfrac{1}{2}a\alpha_i^2\left(\dfrac{\eta}{\cos^2\eta}\right.$

$\left. + \tan\eta\right) = \tfrac{1}{2}a\,\alpha^2\left[(1 + b^2\tau)\tan^{-1}b\sqrt{\tau} + b\sqrt{\tau}\right]$

$= a\alpha_i^2 b\sqrt{\tau}(1 + 1/3b^2\tau - \dfrac{1}{3.5}b^4\tau^2 + \dfrac{1}{5.7}b^6\tau^3 - \cdots) =$

$ab\alpha_i^2\sqrt{\tau}\left[1 + \sum_{n=1}^{\infty}\dfrac{-1)^{n-1}\cdot(b\tau)^n}{4n^2 - 1}\right]$, where $b = \dfrac{2C}{\alpha_i\pi}$

$\sqrt{\beta ph}$, $b^2\tau < 1$ and $\tau < \pi^2/24$.

This formula shows that a first approximation of F is given by $F = fld p\alpha_i\,(\sqrt{6}/\pi)\sqrt{\tau}$, which is the same as given in Appendix 5 if the correct values for α_i and τ are substituted.

The formula shows that the pull-out force is proportional to the square root of the sticking time and is directly proportional to the differential pressure. These conclusions are confirmed by laboratory experiment.[1]

The extent to which the pull-out force deviates from the square-root law depends on the relative magnitude of the increase in contact angle with time. To evaluate the ratio F''/F', the following two examples are given.

TABLE 2

$$\varepsilon_\tau/(\tfrac{1}{2}\beta ph) = \begin{cases} 1 - (32/\pi^3)\sum_{n=1}^{\infty}\dfrac{(-1)^{n+1}\exp[-(2n-1)^2\tau]}{(2n-1)^3} & 0 \le \tau \le \infty \quad (A) \\ (8\tau)/\pi^2 & 0 \le \tau \le (\pi^2/24) \quad (B) \\ 1 - 2/3\exp-[(12\tau/\pi^2) - \tfrac{1}{2}] & (\pi^2/24) \le \tau \le \infty \quad (C) \end{cases}$$

τ	Formula A	Formula B	Formula C
0.0005	0.0005	0.0004	
0.0010	0.0009	0.0008	
0.0015	0.0013	0.0012	
0.0025	0.0021	0.0020	
0.0050	0.0041	0.0041	
0.0100	0.0082	0.0081	
0.0200	0.0162	0.0162	
0.0300	0.0244	0.0243	
0.0500	0.0406	0.0406	
0.0750	0.0608	0.0608	
0.1000	0.0811	0.0811	
0.1500	0.1214	0.1217	
0.2000	0.1613	0.1622	
0.4000	0.3093	0.3244	
0.7500	0.5152		0.5585
1.0000	0.6203		0.6742
2.5000	0.9153		0.9669
5.0000	0.9930		0.9975

Example 1: $D = 9\frac{5}{8}$ in., $d = 7$ in., $h = 1$ cm, $d_i = 3$ in., $\beta = 0.5 \times 10^{-2}$ cm²/kg and $p = 20$ kg/cm² (Appendix 3). The initial angle of contact, $\alpha_i = 1°\ 48'$, and the angle of contact at the end of the first period, the length of which is $1/6\ h^2\mu\beta/k = 1/6 \times l^2 \times \frac{1}{2} \times 10^5 = 8{,}300$ sec, is equal to

$$\alpha_c = \sqrt{(\alpha_i^2 + 1/6\,\beta phC^2)} =$$

$\sqrt{(0.0313^2 + 1/6 \times 0.5 \times 10^{-2} \times 20 \times 1 \times 1.04^2} = 0.139$ or $\alpha_c = 8°$. $F_1''/F_1' = (1.571 - 0.226 - 0.219)/(2 \times 0.219) \sim 2{,}5$. As $F_1' = 2.7$ kg/cm of stuck collar (Appendix 5), it follows that $F_1 = F_1' + F_1'' = 3.5 \times 2.7 = 9.45$ kg/cm.

Example 2: $D = 3$ in. $d = 2\frac{3}{8}$ in., $d_i = 1{,}815$ in., $p = 7 \times 10^3$ g/cm². For $h = 5/32$ in., the initial angle of contact is $18°\ 25'$, assuming that $k = 0.6$ md, $\beta = 6 \times 10^{-2}$ cm²/kg and $\mu = 1$ cp, the length of the first period is in the order of $1/6 \times 0.397^2 \times 10^5 = 2{,}500$ sec $= 40$ min. The angle of contact at the end of the period is

$$\alpha_c = \sqrt{(0.3189^2 + 1/6 \times 6 \times 10^{-2} \times 7 \times 0.397 \times 5.70)} = 0.511 \qquad \alpha_c = 30°\ 45'.$$

$F_1''/F_1' = (1.571 - 0.673 - 0.487)/(2 \times 0.487) = 0.41$. The force, F_1'' is now less than the force F_1', and $F_1 = 1.41 \times 3.5 = 5$ kg/cm.

If the sticking continues beyond the first period, α_c increases until eventually, $\alpha_c = \sqrt{(\alpha_i^2 + \frac{1}{2}\beta\, phC^2)}$. Then the maximum required pull-out force, $F = pfld\sqrt{\alpha_i^2 + \frac{1}{2}\beta\, phC^2}$.

APPENDIX 8

THE FINAL PULL-OUT FORCE AFTER SPOTTING

It was shown in Appendix 7 that the final angle of contact between the mud cake and the embedded collar is equal to $\alpha_c = \sqrt{\alpha_i^2 + \frac{1}{2}\beta hpC^2}$. When oil is spotted the mud cake outside the contact area will, with time, be compressed to $h - \frac{1}{2}\beta hp$. The residual penetration of the collar into the mud cake is then equal to $\varepsilon_r = \varepsilon_c - \frac{1}{2}\beta hp$ or $\varepsilon_r = \varepsilon_i$ from which follows, $\alpha_r = \dfrac{C_r}{C_i}\,\alpha_i$, or

$$\alpha_r = \alpha_i\sqrt{\frac{D - 2h(1 - \frac{1}{2}\beta p)/(D - d - 2h)}{(D - 2h)/[D - d - 2h(1 - \frac{1}{2}\beta p)]}}.$$

As the factor under the root sign is very nearly equal to one, the residual angle of contact is equal to the initial angle and the final pull-out force $F_r = F'_\infty$. ★★★

Application of Decline Curves to Gravity-Drainage Reservoirs in the Stripper Stage

H. C. LEFKOVITS
C. S. MATTHEWS
MEMBER AIME

SHELL DEVELOPMENT CO.
SHELL OIL CO.
HOUSTON, TEX.

ABSTRACT

In a recent publication[1] it was shown that wells with a free surface in a homogeneous gravity-drainage reservoir have a hyperbolic decline with index $n = 2$, $q/q_i = 1/(1 + \gamma t)^2$. This paper reports efforts to extend this theory to practical field cases.

As a first step in making the extension, a large number of lease production curves from gravity-drainage fields in the stripper stage were fitted with the general hyperbolic decline equation, $q/q_i = 1/(1 + \gamma t)^n$, γ and n in each case being determined by statistical methods. It was found that this equation is reliable for decline curve extrapolation for periods up to at least 25 years.

The results obtained were disturbing in the sense that values for the index, n, were often smaller than one, which fact leads to the prediction that a well would produce an infinite amount of oil in infinite time. A theoretical investigation based on the results of the previous paper provides a suitable explanation for these low values of n. It suggests that these are obtained if production occurs from two or more layers of different permeability and thickness or two layers having different skin effects. It is predicted that as the more permeable layers are exhausted, the index of decline, n, will rise from a value smaller than 2, to $n = 2$.

A practical method is given for fitting the general hyperbolic decline Eq. 6 to production decline data. When this method is used, the index of decline observed in gravity-drainage reservoirs in the stripper stage when using only data over early years of decline usually agrees quite closely with that determined using data over 25 years or more. This indicates that the hyperbolic decline equation is reliable for predicting behavior of such reservoirs. A method is also suggested for taking into account any changes in the value of the index of decline, n, which may be expected during the life of a well or lease.

Manuscript received in Society of Petroleum Engineers office Sept. 15, 1957. Paper presented at Fall Meeting of Southern California Petroleum Section in Los Angeles, Oct. 17-18, 1957.

[1]References given at end of paper.

Discussion of this and all following technical papers is invited. Discussion in writing (three copies) may be sent to the office of the *Journal of Petroleum Technology*. Any discussion offered after Dec. 31, 1958, should be in the form of a new paper.

INTRODUCTION

As a result of both experimental work with models and theoretical deductions, it was recently concluded[1] that wells having a free surface in a homogeneous reservoir producing by pure gravity drainage should have a hyperbolic decline with $n = 2$.

$$\frac{q}{q_i} = \frac{1}{(1 + \gamma t)^2} \quad \ldots\ldots\ldots \quad (1)$$

The present report details efforts to extend this work on ideal homogeneous reservoirs to actual field cases. It should be remembered that both the previous work and the present extension are based on the assumption that the reservoir is at very low pressure, and hence, nearly all the potential available for driving fluid to the well is the gravity head. Attempts to apply conclusions of this study to reservoirs which have considerable pressures supplementing the gravity drive may lead to difficulty.

WELLS WITH NO FREE SURFACE

In a dipping gravity-drainage reservoir such as that shown in Fig. 1, some of the down-dip wells have no free surface. The previous study[1] showed that the up-dip wells, which have a free surface, should follow Eq. 1. The following approximate analysis, of a type which was justified experimentally for up-dip wells in the work just mentioned, leads to results for the down-dip wells.

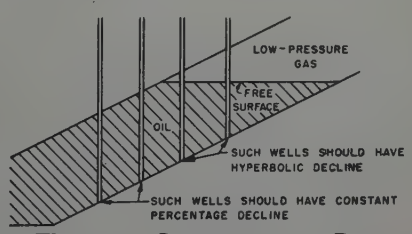

FIG. 1—WELLS IN A GRAVITY-DRAINAGE RESERVOIR.

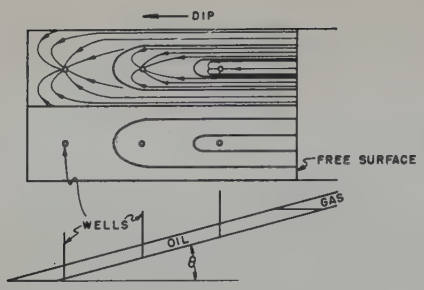

FIG. 2—DRAINAGE AREAS OF DOWN-DIP WELLS.

First, note that the drainage areas of these down-dip wells must, for an incompressible fluid, look something like those shown in Fig. 2. If no free surface is to form, fluid must flow into an area around each well to replace that which flows out. The flow in any drainage area may be approximated as a linear down-dip flow plus a radial flow, as shown in Fig. 3. In many cases the drop in flow potential in the linear section will be only a small fraction of the drop in the radial-flow section. Neglecting the linear drop, we can write after Muskat[2] the following equation for production rate at the well.

$$q = \frac{\pi k_o \Delta\rho g\,[2hH\cos\theta - (H\cos\theta)^2 - h_w^2]}{\mu_o \ln\dfrac{r_e}{r_w}} \quad . \quad . \quad . \quad . \quad . \quad . \quad . \quad . \quad . \quad . \quad . \quad . \quad . \quad (2)$$

This rate must be equal to the rate of change in drainage volume with time:

$$q = -\frac{d}{dt}(\text{drainage volume}) = -D\frac{dh}{dt}, \quad . \quad . \quad (3)$$

where D is a constant. Eq. 3 follows from the fact that the radial part of the drainage volume is constant, but the volume of the linear part is proportional to the height of the free surface, h.

Equating Eqs. 2 and 3, integrating, and resubstituting in Eq. 2 gives

$$\frac{q}{q_i} = e^{-at} \quad , \quad . \quad . \quad . \quad . \quad . \quad . \quad . \quad . \quad . \quad . \quad . \quad . \quad (4)$$

where q_i is the production rate at time $t = 0$, when $h = h_i$.

The quantity a is given by

$$a = \frac{2\pi k_o \Delta\rho g \sin\theta}{\mu_o w \phi (S_o - S_{or}) \ln\dfrac{r_e}{r_w}},$$

where w is the width of the linear part of the flow path.

Although this analysis is only approximate, it does indicate that in a limiting case certain wells in a gravity-drainage reservoir might experience an exponential decline according to Eq. 4. Such behavior gives a straight line when the rate, q, is plotted vs the time, t, on semi-log paper. This behavior has been called constant-percentage decline.

LAYERED RESERVOIRS

Layers With Free Surface

Suppose that at a particular well in our gravity-drainage reservoir the formation consists of different layers of porous medium separated by shale. Then, if the well is pumped off, each layer in which there is a free surface around the wellbore will have a decline

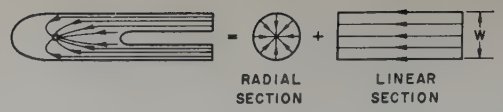

FIG. 3—APPROXIMATION OF DRAINAGE AREAS.

of the type given by Eq. 1. The combined behavior of the two layers is given by

$$\frac{q}{q_{i1}+q_{i2}} = \frac{q_{i1}}{q_{i1}+q_{i2}}\cdot\frac{1}{(1+\beta_1 t)^2} + \frac{q_{i2}}{q_{i1}+q_{i2}}\cdot\frac{1}{(1+\beta_2 t)^2} \quad , \quad . \quad (5)$$

where q_{i1} is initial rate in Layer 1, q_{i2} is initial rate in Layer 2, and β_1 and β_2 are constants. It can be shown analytically* that the combined behavior of the layers formally follows a hyperbolic equation for small times.

$$\frac{q}{q_i} = \frac{1}{(1+\gamma t)^n} \quad . \quad . \quad . \quad . \quad . \quad . \quad . \quad . \quad . \quad . \quad . \quad (6)$$

Although this behavior is formally true only for small times, it has been discovered empirically that it is a good approximation over a large fraction of the decline. The value of the constant, n, depends on the characteristics of the two layers; for the cases where an oil-gas free surface intersects the wellbore in each layer, $n \leq 2$. As an example, Fig. 4 shows the true behavior of a two-layer gravity-drainage reservoir with the following characteristics: $k_1/k_2 = 100$, and $h_{i1}/h_{i2} = 0.1$, where k *is* the permeability and h_i is the oil-zone thickness at time, $t = 0$, in any layer.

Also shown in Fig. 4, as circles and a dashed line, are the values obtained by fitting Eq. 6 to the true behavior at an early time. The value of n obtained in this case was 0.665. It may be seen that the values calculated for $n = 0.665$ agree quite well with the true behavior until the rate drops to about 15 per cent of initial rate. The reason for the disagreement after that time is that the most permeable layer is almost exhausted of fluid. Nearly all the production is coming from the thicker, less permeable layer, causing the decline to become like that of a homogeneous reservoir, $n = 2$.

The two-layer systems equivalent at early times (Fig. 4) to Eq. 6 are shown in Fig. 5.** Here the ratio of

*The analysis is made by using the binomial theorem to expand Eq. 5, collecting terms, and equating the leading coefficients to a similarly expanded Eq. 6.

**These curves are drawn for the case of no skin effect. For a permeability ratio less than 100, a skin in the more permeable layer usually causes n to approach 2, since it makes the reservoir appear to be more homogeneous. A skin in the less permeable layer causes the value of n to decrease, the reservoir behaving as if it had a greater permeability contrast than it actually does have.

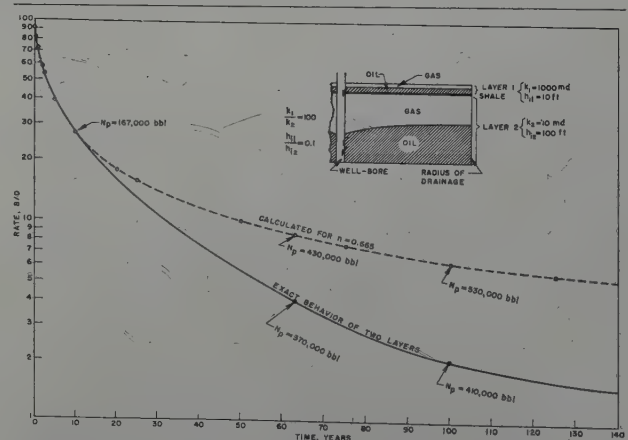

FIG. 4—PRODUCTION BY GRAVITY DRAINAGE FROM A TWO-LAYER RESERVOIR.

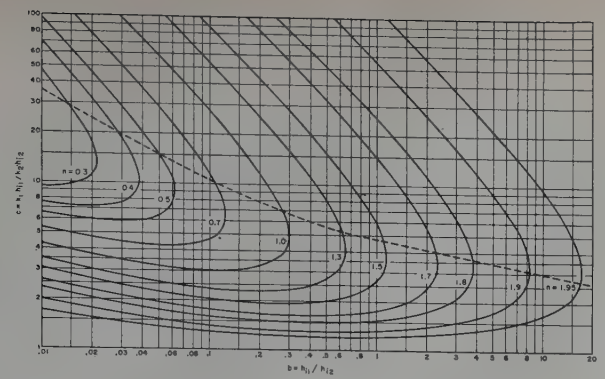

FIG. 5.—VALUES OF n FOR TWO-LAYER SYSTEMS.

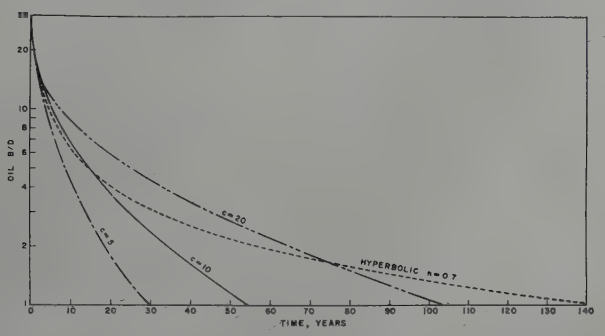

FIG. 6—THREE TWO-LAYER SYSTEMS HAVING HYPERBOLIC DECLINE ($n = 0.7$) AT EARLY TIME.

products of permeability and initial oil-layer thickness ($k_1h_{i1}/k_2h_{i2} = c$) is plotted vs the ratio of initial oil-layer thickness ($h_{i1}/h_{i2} = b$). It may be seen that there are innumerable layer systems which will give the same value of n at early times.

A comparison of the true behavior of three different two-layer systems, all of which may be fitted at early times by Eq. 6 with $n = 0.7$, is shown in Fig. 6. It may be seen that for low values of c the true behavior quickly falls below the calculated behavior for $n = 0.7$. For high values of c the true behavior matches $n = 0.7$ behavior at early times, rises above $n = 0.7$ behavior then falls below at very long times. The behavior of the $c = 10$ case is most like the behavior of Eq. 6 with $n = 0.7$.

By making additional comparisons of the type shown in Fig. 6, it was possible to find the two-layer system which best followed each curve of Eq. 6 for $n =$ constant. The intersection of the dotted line is Fig. 5 with each curve of $n =$ constant gives the best fitting curve for that value of n. For example, the best fitting curve for $n = 0.7$ is the two-layer system, $c = 10.5$ and $b = 0.108$.

It is believed that these "best fitting" two-layer cases may be quite useful in extrapolating decline curves for $n \leq 1$ to very long times. Thus, suppose that we had fitted some observed field data by means of Eq. 6 and had found that n was 0.7. We know that such a decline could not last indefinitely because it would mean that eventually our well would produce an infinite amount of oil.* An extrapolation to very long times might similarly be unreliable. Let us determine whether the behavior of a two-layer reservoir could be used to guide such extrapolations.

*For any value of $n \leq 1$, the ultimate recovery is infinite at infinite time.

TABLE 1—VALUES OF b, c AND d TO USE IN EXTRAPOLATIONS

These values of b, c and d when substituted in Eq. 7 give a curve which follows Eq. 6 the best, for the following values of n.

n	b	c	d
0.3	0.015	27.8	59.2
0.35	0.0215	23.5	48.8
0.4	0.0285	20	39.5
0.45	0.038	17.3	33.2
0.5	0.050	15	28.0
0.55	0.062	13.5	24.4
0.6	0.074	12.5	21.7
0.65	0.088	11.5	19.32
0.7	0.108	10.5	17.28
0.75	0.130	9.7	15.60
0.8	0.152	9.0	14.05
0.85	0.178	8.4	12.78
0.9	0.210	7.8	11.60
0.95	0.245	7.3	10.61
1.0	0.280	7.0	9.94
1.1	0.370	6.3	8.56
1.2	0.475	5.78	7.51
1.3	0.62	5.35	6.68
1.4	0.82	4.97	5.98
1.5	1.10	4.65	5.41
1.6	1.53	4.40	4.95
1.7	2.25	4.05	4.41
1.8	3.78	3.65	3.86
1.9	8.30	3.15	3.23
1.95	17.00	2.75	2.78

For a two-layer reservoir of subsurface properties, such that $c = 5$, the production rate decline would be given by the lower curve in Fig. 6, and if the properties were such that $c = 20$, the decline would be given by the upper curve. Thus, the best fitting curve, $c = 10$, gives a kind of average behavior of all two-layer curves for $n = 0.7$.

In the absence of better information, an extrapolation to long time based on this best fitting or average curve would seem to be the wisest. Similarly, extrapolation to long times for other values of n can be carried out with the best fitting curves indicated in Fig. 5 and tabulated in Table 1. The procedure for doing this will be indicated in a later section.

ONE LAYER WITH FREE SURFACE, ONE WITHOUT

In a manner similar to that indicated in the previous section, it may be shown that a well which penetrates two layers in a gravity-drainage reservoir, one of which has a free surface at the wellbore and one of which does not, will also have a hyperbolic decline for early times as given by Eq. 6. Values of n for such a combination range from zero to infinity.

An example of such a combination is shown in Fig. 7. For this particular combination of layers the behavior at early times may be fitted by the case $n = 1.05$. After a certain time the layer without a free surface produces at only a very low rate, and the decline approaches the $n = 2$ case. When the free surface reaches the wellbore in both layers, the exponent of decline may change again.

COMBINED BEHAVIOR OF TWO WELLS HAVING DIFFERENT SKIN EFFECTS

In actual analysis of gravity-drainage behavior we are usually concerned with lease decline curves in which the behavior of two or more wells is combined. If the wells are identical the combined behavior will be the same (relatively) as that of a single well. However, if the wells are identical except for skin effect it may be shown that the combined behavior will be different from that of a single well. To show this for the case where both wells follow Eq. 1, one need only add the rates for each well as calculated from that equation, noting, because of the difference in skin effect, that $\ln (r_e/r_w)_1 \neq \ln (r_e/r_w)_2$. If we set

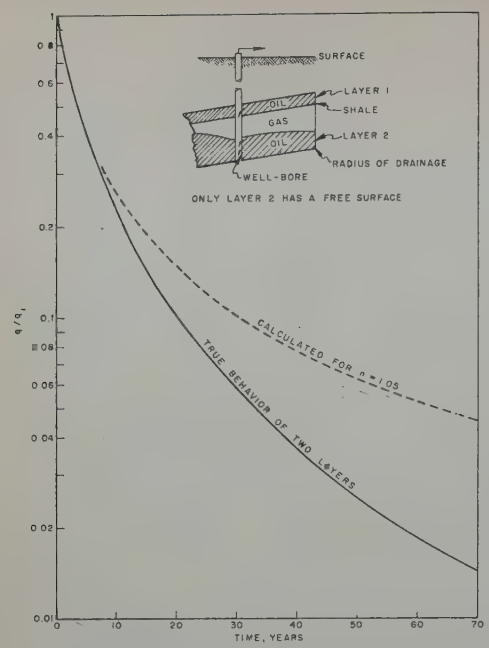

FIG. 7—PRODUCTION WHERE ONE LAYER HAS A FREE SURFACE (ONE DOES NOT).

$$\frac{\left[\ln\frac{r_e}{r_w}-\frac{1}{2}\right]_1}{\left[\ln\frac{r_e}{r_w}-\frac{1}{2}\right]_2}=A,$$

it is found after application of the binomial expansion to $(q_1+q_2)/(q_{i1}+q_{i2})$ that the decline at early times is of the type given by Eq. 6.

$$\frac{q}{q_i}=\frac{1}{(1+\gamma t)^n},$$

where

$$n=\frac{1}{\frac{3}{2}\,\frac{(1+A^2)(1+A)}{(1+A^2)^2}-1}.$$

For $A=1$ (both skin effects equal) the above expression gives $n=2$. Similarly, for $A=0$ and $A=\infty$, we have $n=2$. Minimum values of n occur for $A=0.25$ and $A=4$, where $n=1.45$. Thus, if we tried to fit Eq. 6 to the behavior of a lease containing two wells identical except for skin effect in a homogeneous reservoir with free surface, we might find apparent values of n varying between 1.45 and 2.0; this variation could occur even though each well, if fitted separately to Eq. 6, would give $n=2$.

From all the discussion thus far it would appear that we should not expect many lease decline curves to have an n value exactly equal to two. Deviations below this value could occur if two or more free-surface layers were connected to the well. Deviations above could be caused by presence of non-free-surface layers. Deviations could also be caused by combining the behavior of two or more wells and fitting Eq. 6 to lease behavior.

In view of all this possible complexity, it might be asked whether one could ever hope to extrapolate field data accurately. However, it will be shown in the next section that apparently this can be done in gravity-drainage-type reservoirs for periods of the order of 25 years and possibly more.

APPLICATION TO ACTUAL RESERVOIRS

METHOD

We have analyzed a number of actual field results to determine the observed range in values of n for gravity-drainage reservoirs. The method of analysis we used is a modification of a method proposed by H. M. Baud of the Shell Oil Co. The method consists of the following steps.

1. Calculate q_i by plotting for the early points either log q vs t or 1/q vs t, drawing the best line through these points and taking q_i from the value of the line at $t=0$. The plot of log q vs t will give the better value for q_i if the value of n is large (say greater than 2), while the $1/q$ plot will be better if n is low (say 2 or less).
2. Calculate $(q_i/q)^{1/n}$ for various values of n.
3. For each value of n find the value of γ that gives the best least squares fit to $(q_i/q)^{1/n}=1+\gamma t$.
4. Compute deviations between observed values of q and calculated values of q for each value of n. The value of n which gives the lowest standard deviation is selected as the best value of n for this particular value of q_i.
5. Choose slightly different values for q_i, repeating the above procedure until the q_i which gives the minimum standard deviation is found. The best value of n will be that corresponding to this value of q_i. The value of q_i chosen in Step 1 will very often be quite close to the "best" value of q_i.

This type of fitting can be done very rapidly on such computing machines as the IBM 650.

RESULTS

Three examples of field data fitted by this method are shown in Fig. 8. Since two curves are from different leases in the same field, we note that the value of n is not necessarily the same throughout one field. This is probably due to the fact that different layers or zones are open to production in the different leases in this field. A tabulation of values of n observed in several gravity-drainage fields is given in Table 2.

RELIABILITY OF EXTRAPOLATION

SHORT-TERM EXTRAPOLATION

The heading of this section is somewhat misleading since "short-term" may be 25 years or more. The point we wish to make is that, although an extrapolation based on a value of $n \leq 1$ may be adequate for many years, it cannot last forever. Before we consider this point in detail, let us first see how good the short-term extrapolation is.

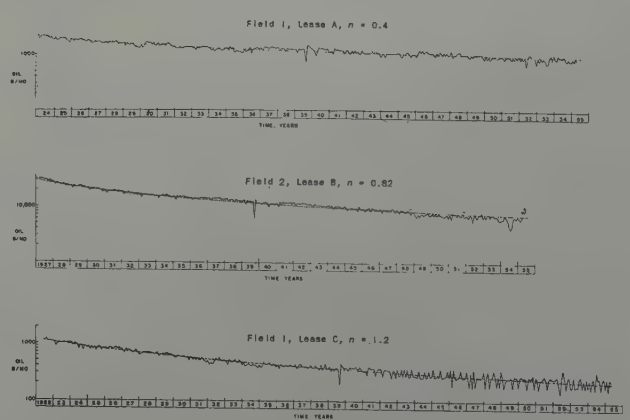

FIG. 8—FIELD DATA.

TABLE 2—VALUES OBTAINED FOR n IN GRAVITY-DRAINAGE FIELDS

Field No.	Lease	n	γ Years^{-1}
1	A	0.4	0.32568
2	A	0.54	0.28380
3	A	0.55	0.12796
4	A	0.65	0.60515
1	B	0.78	0.29264
2	B	0.82	0.18958
5	A	1.0	0.17708
1	C	1.2	0.09606
2	C	1.5	0.09400
2	D	1.6	0.05762
1	D	2.0	0.06404
1	E	3.1	0.04542
1	F	4.0	0.02168
3	B	8.0	0.00728
5	B	over 10	
3	C	over 10	

TABLE 3—RELIABILITY OF EXTRAPOLATION

Field No.	Lease	Production history used to determine n and γ, years	Best value of n
9	A	25	1.5
		18	1.4
		12	1.4
		6	0.4
10	A	27	1.5
		19	1.1
		13	1.5
		7	1.5
10	B	27	0.6
		19	0.6
		13	0.6
		7	0.7
11	A	31	0.4
		23	0.4
		16	0.4
		8	0.4
11	B	16	1.0
		12	1.1
		8	1.5
		4	1.5

The Tulsa area of Shell Oil Co. was the first to investigate the accuracy of short-term extrapolations. In their study, values of n and γ were determined for each of five leases using all the available production history, which ranged from 16 to 31 years. Next, n and γ were redetermined by using only the first 0.75 of past life, then 0.5 and 0.25 of the past life. Results are given in Table 3.

Except in one case, approximately the same value of n was obtained after analysis of seven years of life as after 25 or more. The exception was Field 9, where a six-year life history was used. Average yearly production figures were used in fitting these curves so that in this case, only six points were available. In all cases except that of Field 9, six-year life, the predicted ultimate recovery at economic limit, was in fairly good agreement whether based on long or short life.*

At Shell Development we studied the reliability of extrapolation somewhat less completely than did Tulsa. We omitted the last 10 years of life for a number of cases, and then recomputed the best values for n. Results are shown in Table 4. Since the values of n obtained were about the same in every case, it would appear that a reasonably accurate extrapolation can be made after five to seven years of life for periods of up to 27 years.

Long-term Extrapolation

Particularly when the value of n is low, the years of life to the economic limit may be well over 50. An extrapolation based on low values of n for such long periods may be unreliable, as discussed previously. A safer extrapolation method is to use the best fitting two-layer curves given in Table 1.

The procedure to use is as follows: (1) analyze the field data by the method discussed under "Application to Actual Reservoirs," determining best values of q_i, γ and n; (2) using Table 1, pick the values of b, c and d which give the best fitting two-layer curve for this value of n; and (3) substitute these values of q_i, b, c, d and γ into Eq. 7 and calculate q at any desired time. Eq. 7 may be obtained from Eq. 5 by taking $\beta_2 = \gamma/d$, $\beta_1 = c\gamma/d$, and noting that $q_{i1}/q_{i2} = bc$. The ultimate production from $t = 0$ to the time of economic limit, t_e, may be obtained from Eq. 8. It is necessary to obtain the time of economic limit by trial-and-error solution of Eq. 7 for t, at q = economic limit rate.

$$\frac{q}{q_i} = \frac{1}{1+bc}\left[\frac{1}{\left(1+\frac{\gamma t}{d}\right)^2} + \frac{bc}{\left(1+\frac{c\gamma t}{d}\right)^2}\right] \quad . \quad . \quad . \quad . \quad . \quad . \quad . \quad . \quad . \quad . \quad . \quad . \quad . \quad . \quad . \quad (7)$$

$$\frac{N_p}{q_i t} = \frac{1}{1+bc}\left(\frac{1}{1+\frac{\gamma t}{d}} + \frac{bc}{1+\frac{c\gamma t}{d}}\right) \quad . \quad . \quad (8)$$

Any consistent set of units may be used in these equations as well as in Eq. 6. The quantities, b, c and d, are dimensionless; γ must have units reciprocal to t; in Eq. 7, q_i may be in any units; in Eq. 8, q_i must have the same time unit as t. A consistent set is t = years, γ = years^{-1}, q_i = bbl/yr. If it is desired to use q_i in bbl/day, multiply q_i by 365 before substituting in Eq. 8.

TABLE 4—RELIABILITY OF EXTRAPOLATION

Field No.	Lease	Production history used, years		Best value of n	
		Case A	Case B	Case A	Case B
6	A	27	17	1.6	1.1
6	B	18	8	0.55	0.50
6	C	27	17	0.6	0.55
6	D	27	17	0.8	0.75
7	B	29	19	0.35	0.45
7	A	31	21	0.4	0.35
7	D	33	23	1.3	1.35
8	A	16	6	0.40	0.50
8	B	10	5	0.80	1.45
8	C	26	16	>38	16 to 17
8	D	16	6	0.8	1.05

EXAMPLE

For brevity, we will not go through the five steps given under "Method", but will take the answer obtained from such a procedure and show how it may be used in an extrapolation. Let us choose an example case where we found q_i = 2,900 bbl/mo, n = 0.5, and γ = 0.2701 yr^{-1}. Having determined the best values for q_i, n and γ, we may extrapolate into the future. Assuming that the n = 0.5 decline will last until the economic limit, we may calculate the time of economic limit from Eq. 6. For an economic limit rate of 500 bbl/mo we get

$$t_e = \frac{(2{,}900/500)^2 - 1}{0.2701} = 121 \text{ years.}$$

If this decline were to hold, the cumulative production from $t = 0$ to $t = t_e$ would be

$$N_p = \frac{(12\,q_i)}{\gamma(1-n)}[(1+\gamma t_e)^{1-n} - 1],$$

$$= 1{,}237{,}000 \text{ bbl}.$$

(The factor 12 converts q_i from bbl/mo to bbl/yr. Since γ has units of years^{-1}, N_p then is in bbl.)

It is questionable, however, if the n = 0.5 decline would continue for 121 years. To obtain a more realistic estimate of future production we can use the two-layer curve Eq. 7, taking values of b, c and d from Table 1. From this table we note that for n = 0.5, we have

*The difference between ultimate recoveries predicted by n = 1.5 and n = 1.0 is not nearly so great as that between n = 1.0 and n = 0.5.

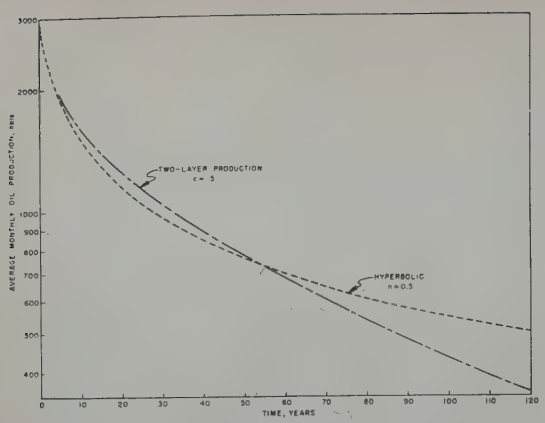

FIG. 9—COMPARISON OF HYPERBOLIC DECLINE ($n = 0.5$) WITH TWO-LAYER DECLINE.

$c = 15$, $b = 0.05$, and $d = 28$. Substituting in Eq. 7 we have

$$\frac{q}{q_i} = \frac{0.5714}{(1 + 0.00965t)^2} + \frac{0.4286}{(1 + 0.1447t)^2} \quad . \quad (9)$$

Values of q calculated from Eq. 9 for $q_i = 2{,}900$ bbl/mo are shown in Fig. 9. Shown for comparison are values calculated from the ordinary hyperbolic equation,

$$\frac{q}{q_i} = \frac{1}{(1 + 0.2701t)^{0.5}}.$$

This particular two-layer production curve rises above the $n = 0.5$ curve, then falls below at large time. The cumulative production from $t = 0$ to $t = t_e$ is given for the two-layer case by

$$N_p = \frac{(12\,q_i)t_e}{1 + bc}\left(\frac{1}{1 + \frac{\gamma t_e}{d}} + \frac{bc}{1 + \frac{c\gamma t_e}{d}}\right),$$

where the factor 12 converts q_i from bbl/mo to bbl/yr. Since t_e is in years, N_p is in barrels. For $t_e = 86.7$ years as obtained by trial-and-error solution of Eq. 9 at $q = 500$ bbl/mo, we get for the two-layer case, $N_p = 1{,}035{,}000$ bbl. This differs by 20 per cent from the estimate obtained by using the hyperbolic decline curve, $n = 0.5$.

CONCLUSIONS

The hyperbolic decline Eq. 6 has been found to be very useful and accurate in extrapolating decline curves for gravity-drainage-type reservoirs for periods of at least 25 years. Agreement of model and theoretical results and predictions with observed declines help to place methods of decline-curve extrapolation on a firm basis. This work has also indicated a reasonable method for extrapolating these curves to very long times—times at which the hyperbolic decline curve Eq. 6 may tend to predict an optimistic estimate of recovery.

NOMENCLATURE

$$a = \frac{2\pi k_o \Delta\rho g \sin\theta}{\mu_o \phi (S_o - S_{or}) w \ln (r_e/r_w)}$$

$b = h_{i1}/h_{i2}$

$c = k_2 h_{i1}/k_2 h_{i2}$

$$d = \frac{2(1 + bc^2)}{n(1 + bc)}$$

g = acceleration constant due to gravity

h = height of free surface of oil above bottom of formation or above a datum level

h_i = initial oil-gas interface level in an open hole at the radius of drainage, measured from bottom of formation; h_{i1} refers to Layer 1, and h_{i2} to Layer 2

h_w = oil-gas interface level in wellbore r_w measured from bottom of formation

H = formation thickness

k = absolute permeability; k_1 refers to Layer 1 and k_2 to Layer 2

k_o = permeability to oil

n = exponent in Eq. 6

p = pressure

q = rate of oil production

q_i = rate of oil production at time $t = 0$

N_p = cumulative oil production from time $t = 0$ to $t = t$

r = radial distance

r_e = radius of drainage

r_w = radius of wellbore

S = saturation, fraction of pore space

S_o = oil saturation in oil-filled part of reservoir (below free surface)

S_{or} = residual oil saturation (above free surface)

t = time

t_e = time at which economic limit rate is reached

w = width of linear part of flow path in Fig. 3

$$\alpha = \tfrac{1}{2}\left[1 + \sqrt{1 - \frac{1}{2\ln (r_e/r_w) - 1}}\right]$$

$$\beta_1 = \frac{k_{o1}\Delta\rho g h_{i1}}{\mu_o \phi (S_o - S_{or})(r_e^2 - r_w^2)\,\alpha\,[\ln (r_e/r_w) - \tfrac{1}{2}]}$$

$$\beta_2 = \frac{k_{o2}\Delta\rho g h_{i2}}{\mu_o \phi (S_o - S_{or})(r_e^2 - r_w^2)\,\alpha\,[\ln (r_e/r_w) - \tfrac{1}{2}]}$$

ϕ = porosity, fraction

γ = a constant in Eq. 6

θ = angle of dip

μ_o = oil viscosity

$\Delta\rho$ = difference between oil and gas density

ACKNOWLEDGMENT

The authors wish to acknowledge the able assistance of Betty Allen and Joy Cushman who performed all machine computations. Valuable suggestions and field data were furnished by R. A. Flohr, S. E. Rodriguez of the Pacific Coast area, E. H. Timmerman, H. B. Bridges, and M. P. Chrysler of the Tulsa area, and J. W. Walker of the Houston area.

REFERENCES

1. Matthews, C. S. and Lefkovits, H. C.: "Gravity-Drainage Performance of Depletion-Type Reservoirs", *Trans.* AIME (1956) **207**, 265.
2. Muskat, M.: *Flow of Homogeneous Fluids*, McGraw-Hill Book Co., N. Y. (1937) 375. ★★★

Improving Miscible Displacement by Gas-Water Injection

B. H. CAUDLE
A. B. DYES
MEMBERS AIME

THE ATLANTIC REFINING CO.
DALLAS, TEX.

ABSTRACT

Miscible displacement recovers all oil in the area contacted by the injected fluid, whereas water or immiscible gas drives usually leave substantial amounts of oil as residual. However, the poor mobility ratios associated with a gas-driven miscible displacement cause the sweep pattern efficiency to be much lower than that obtained with water flooding. One way in which the sweep efficiency in a miscible displacement process can be increased is by decreasing the mobility behind the flooding front. This can be achieved by injecting water along with the gas which drives the miscible slug. This water reduces the relative permeability to gas in this area and thus lowers the total mobility. The main operating conditions for the simultaneous injection process are that a zone of gas exists between the miscible slug and the leading edge of the water and that a sufficient amount of gas be injected with the water to form the gas volume which is being left in the water zone. Laboratory model studies have shown that the ultimate sweep pattern efficiency can be as high as 90 per cent for a five-spot flooding system. If gas alone is used as the driving medium an ultimate sweep-out efficiency of about 60 per cent would be obtained in the same system.

INTRODUCTION

The miscible displacement processes are a step towards total oil recovery. Conventional gas or water drives usually leave 25 to 50 per cent of the oil as residual in the swept portion of the reservoir. This residual can be eliminated if the oil is driven by a fluid with which it is miscible. At some reservoir conditions natural gas will become miscible with the oil. This is the "high pressure gas process".[1] More often, the oil does not contain enough light hydrocarbons to cause the gas to become miscible with the oil at reasonable pressures. In these cases a small band of fluid which is miscible both with the oil and gas must be kept between them[2]. Less than 2 per cent of the reservoir volume of the slug material is needed to keep the displacement miscible.

Both processes work in the same manner, recovering all of the oil in the portion of the reservoir contacted by the injected fluids. The only difference is the manner in which the miscibility between the oil and the injected gas is obtained. Previous publications have contained detailed descriptions of these processes.[1,2,3,4]

However, total displacement of the oil in the swept region does not guarantee an efficient recovery process. The amount of oil to be recovered is also determined by the fraction of the reservoir contacted by the flood. This fraction is largely determined by the mobilities of the fluids. (The fluid mobility is the permeability of the rock to that fluid divided by the fluid's viscosity, k/μ). This dependence of the fraction swept on the mobility ratio has been shown in previous studies.[5,6,7] Fig. 1 shows the ultimate fraction swept in a five-spot system as a function of the mobility ratio. The small drawings show the location of the areas left unswept for two different mobility ratios. The ultimate fraction of the reservoir swept is here considered to be attained when the producing stream contains less than 5 per cent oil at reservoir conditions.

THE GAS-DRIVEN MISCIBLE DISPLACEMENT

Since there is no oil left in the swept region after miscible displacement the mobility in this region is very high. It is often 50 times the mobility in the unswept regions. This means that the fraction of the reservoir contacted by the injected fluid will be less for a gas-driven miscible displacement than for a conventional water or gas drive. For a five-spot injection system, water would contact the entire reservoir volume, and the low pressure gas would contact about 90 per cent of this volume, while a gas-driven miscible displacement would only contact about 65 per cent of the reservoir. This poor sweep efficiency often offsets the benefits obtained through miscible displacement. Fig. 2 shows what the recovery curves for the three processes might look like for a five-spot system. The curves show the fraction of the in-place oil recovered as a function of reser-

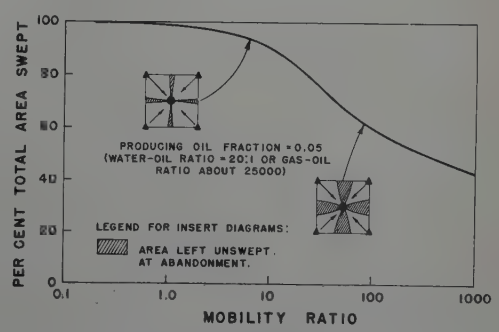

FIG. 1—EFFECT OF MOBILITY RATIO ON THE ULTIMATE AREA CONTACTED IN A FIVE-SPOT INJECTION SYSTEM.

Original manuscript received in Society of Petroleum Engineers office July 16, 1957. Revised manuscript received Sept. 17, 1958. Paper presented at 32nd Annual Fall Meeting of Society of Petroleum Engineers in Dallas, Tex., Oct. 6-9, 1957.

[1]References given at end of paper.

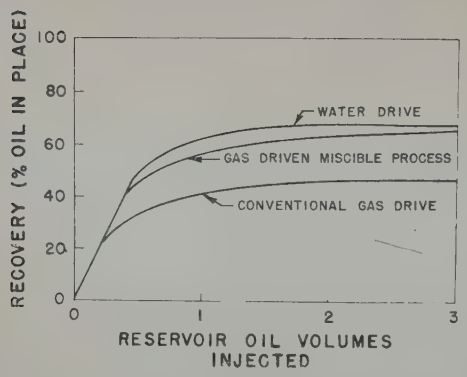

FIG. 2—COMPARISON OF THE GAS-DRIVEN MISCIBLE PROCESS WITH CONVENTIONAL INJECTION PROGRAMS.

voir volumes of fluids injected. For these data we have assumed that the water recovered 67 per cent of the oil in the area swept and that the low pressure gas recovered 50 per cent of this oil. Here, if only the recoveries are considered, the gas-driven miscible displacement is much better than a conventional gas drive; but it is not quite as good as a water flood. (Other factors, however, such as well injectivities or fluid availability will help determine which process is chosen.)

SIMULTANEOUS INJECTION OF GAS AND WATER BEHIND THE MISCIBLE DISPLACEMENT

The miscible displacement must invade a larger portion of the reservoir if it is to represent a generally improved process. Reducing the mobility in the swept region is one way in which the sweep efficiency may be increased. The fluid mobility in a porous medium may be reduced by (1) reducing the permeability of the matrix to that fluid, and (2) increasing the viscosities of the fluids in the region. The reduction of the permeability in the gas region is easily accomplished by injecting water along with the gas. This reduction in relative permeability during multi-phase flow is a well-defined characteristic of porous media which greatly reduces the fluid mobility. The mobility is further reduced because the water is more viscous than the gas which it replaces. In this manner the high mobility in the swept region can be greatly reduced and so increase the sweep efficiency of the process. The effect of different gas and water saturations on the mobility in the swept region is illustrated in Fig. 3. This simultaneous injection of gas and water behind the miscible displacement will make the miscible processes much more attractive.

To ensure miscible displacement, a zone of gas should be kept between the miscible slug and the region of water flow. If water flows into the miscible zone ahead of the gas, a reduction of the displacement efficiency occurs. On the other hand, if the gas zone were allowed to become large the operation would approach the poor sweep-out pattern performance of the gas-driven miscible process. If too high a ratio of gas-to-water is injected the gas will flow faster than the water and enlarge the gas zone. If the ratio is too low the water will flow faster than the gas and invade the miscible zone. The proper injection ratio will keep the gas zone at a constant volume as the flood progresses. This ratio can be determined from the relative permeability relationships, the water and gas viscosities and the saturations established in the region of simultaneous flow. A calculation of this ratio will be illus-

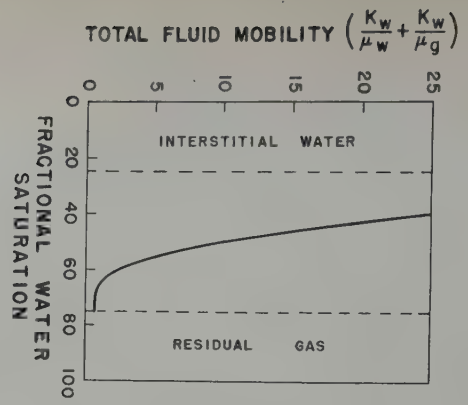

FIG. 3—TOTAL FLUID MOBILITY IN THE WATER-GAS ZONE AT VARIOUS WATER SATURATIONS.

trated in the discussion of the behavior of the sample five-spot reservoir.

EXPERIMENTAL

The effect of mobility ratio on the flood pattern has been described in the literature.[5] These results, however, are for systems in which the mobilities in only two regions were concerned. In the simultaneous gas-water injection process there are three regions of mobility which will influence the sweep pattern. These are: (1) the relatively low mobility oil region, (2) the high mobility gas zone, and (3) the lower mobility region in which both gas and water are flowing. The relatively narrow zone of miscible displacement which lies between the gas and the oil will not significantly affect the sweep efficiency for the process, no matter which miscible process is used. No one mobility ratio can be ascribed to the process. The relative mobilities of all three regions must be considered.

If we confine ourselves to the effect of the mobilities on the sweep efficiency, simple laboratory models with three zones of miscible fluids can show the benefits to be obtained by the simultaneous injection process. The models used represented elements from a large five-spot injection system. They were 0.25-in. thick and the distance between wells was about 10 in. Miscible oils were used to represent the three mobility regions. The X-ray shadowgraph technique[5] was used to determine the sweep-out pattern efficiencies. The mobilities in the oil region and in the water-swept region were equal. The mobility in the gas zone was 17 times higher, instead of 50 times higher as in the field. This number for the

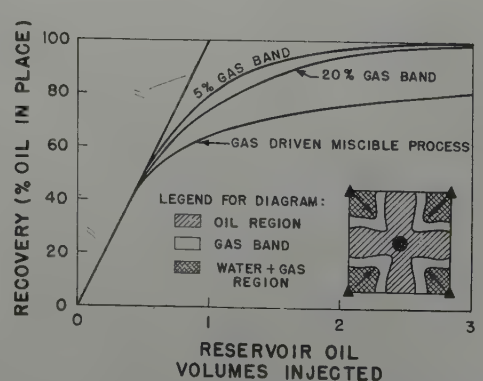

FIG. 4—EFFECT OF GAS BAND SIZE ON RECOVERY IN THE SIMULTANEOUS WATER-GAS INJECTION MISCIBLE PROCESS.

mobility in the gas zone was as high as could be obtained conveniently in the laboratory. The difference in the recovery histories between mobility ratios of 17 and 50 should not be significant in this study since both result in similarly poor sweep efficiencies.

Fig. 4 shows the results of this study. The per cent of the in-place oil produced (which for miscible processes is the same as the per cent of the reservoir area contacted) is shown as a function of the number of reservoir volumes injected. The result of two model studies is shown. In one study the gas zone occupied 20 per cent of the reservoir volume and in the other only 5 per cent. These results show that the simultaneous gas-water injection process will approach the high areal sweep efficiencies obtained with a conventional water drive. There is a noticeable difference between the curves for the 5 per cent and 20 per cent gas zones. This, however, is not nearly so striking as is the improvement over the gas-driven miscible displacement.

It should be remembered that these results apply directly only to uniform formations in which the effects of gravity are negligible. In cases where these factors are significant, the presence of the relatively low mobility water zone behind the advancing front will tend to offset their detrimental effects on the sweep efficiency.

APPLICATION OF THE SIMULTANEOUS INJECTION PROCESS

To illustrate better the mechanics of the simultaneous injection process and its benefits, a hypothetical case will be discussed. We will consider a five-spot injection pattern with: (1) a specific permeability of 1 darcy; (2) an oil viscosity of 1 cp; (3) a gas viscosity of 0.02 cp; (4) a water viscosity of 0.5 cp; (5) an interstitial (non-flowable) water saturation of 25 per cent; and (6) the relative permeability curves shown in Fig. 5. For this discussion it makes no difference whether the miscible displacement is obtained by the high pressure gas process or the miscible slug process.

First, the gas to water injection ratio must be calculated. As discussed earlier, the desired ratio is that at which the gas and the water flow at the same velocity. This ratio can be determined from the relative permeability curves and the fluid viscosity. In line with Darcy's law, the volumetric flow rate of a single fluid in a two-flowing-phase system is proportional to the mobility of the fluids (effective permeability/fluid viscosity). Therefore, the linear velocity of a fluid is proportional to its mobility divided by the fraction of the porosity which it must fill. Thus, for gas the relative velocity would be (effective permeability to gas) ÷ (gas viscosity) (fractional gas saturation); and for water (effective permeability to water) ÷ (water viscosity) (fractional water saturations over and above the interstitial water). From the proper relative permeability curves (Fig. 5) the relative velocities for gas and water as a function of gas saturation can be obtained. These values are then plotted as shown in Fig. 6. Here we see that the gas and water velocities will be the same at a fractional gas saturation of 0.31. The permeability ratio curve (k_w/k_g shown in Fig. 5) and Darcy's law show that a gas to water injection ratio of 0.7 (in terms of reservoir bbl) is necessary to maintain a fractional gas saturation value of 0.31. This is the desired injection ratio. In practice, a slightly higher gas-to-water injection ratio might be used to ensure the presence of a gas zone behind the miscible front. A similar type calculation can be made whenever the gas and water are considered to be segregated.

In the example five-spot segment a miscible displacement zone between the oil and gas is set up by either the high pressure gas or the miscible slug process. A quantity of gas equal to 5 per cent of the reservoir volume at reservoir conditions is injected to form the gas buffer zone. Then gas and water are injected in a ratio of 0.7 volumes of gas (at reservoir conditions) to one volume of water (at reservoir conditions). Then the recovery would be as shown in Fig. 7. Here the percentage of in-place oil recovered is shown as a function of total fluid injected (gas plus water). The solid curve shows the recovery to be obtained by the simultaneous gas-water injection process. In this case, 53 per cent of the in-place oil is recovered at breakthrough and 98 per cent is obtained when two reservoir volumes of fluid have been injected. The performance of the gas-driven miscible process for the same reservoir conditions is shown by the dashed line. Here, 42 per cent of the oil is recovered at breakthrough and 62 per cent is obtained when two reservoir volumes of gas have been injected.

As pointed out earlier, the gas-driven miscible slug process is generally competitive with water flooding. Therefore, the simultaneous injection process will probably result in greater recovery than will water flooding. The simultaneous injection process, however, has one limitation in common with water flooding. The injection wells must be able to take the more viscous water in sufficient amounts. If they can not, then the gas-driven miscible process should be considered.

CONCLUSIONS

The miscible displacement processes, as originally

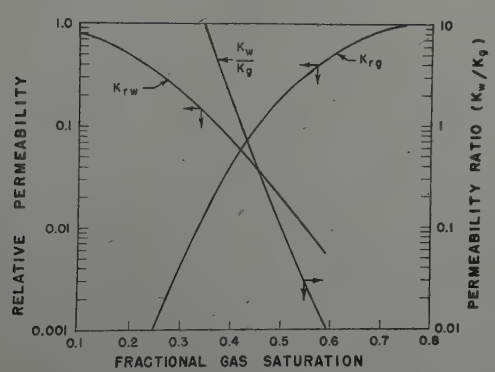

FIG. 5—GAS-WATER RELATIVE PERMEABILITY CURVES.

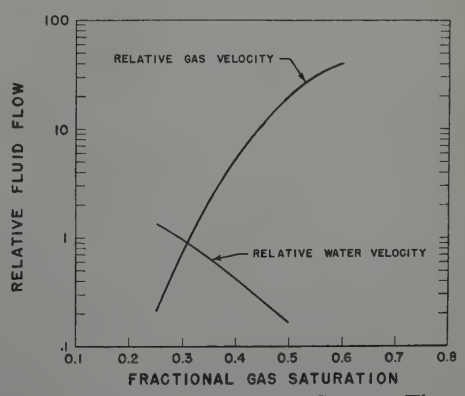

FIG. 6 — RELATIVE VELOCITIES OF GAS AND WATER AT VARIOUS GAS SATURATIONS.

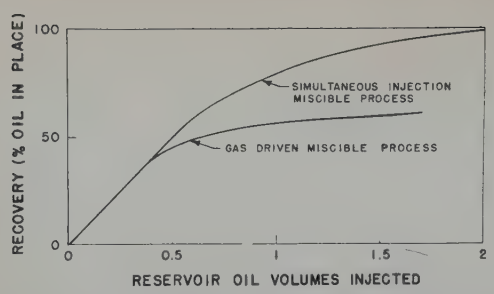

FIG. 7—PRODUCTION HISTORY FOR THE GAS DRIVEN AND THE GAS-WATER INJECTION MISCIBLE PROCESSES.

presented, consist of injecting gas to sweep the oil miscibly toward the producing wells. Because of the low viscosity of gas and the high displacement efficiency of the processes, the sweep-out pattern efficiency is usually poor—about 60 per cent of the reservoir area in a five-spot system at abandonment. Laboratory model studies have shown that the sweep-out pattern efficiency can be greatly increased by injecting a fluid of low mobility to follow the miscible displacement front. A simultaneous injection of water and gas in the proper ratio will create the desired low mobility zone and increase the sweep-out pattern efficiency while maintaining a miscible displacement of the oil. This improvement in recovery can be obtained at little risk, even though the gas-to-water injection ratio cannot be determined exactly. This is because (1) if too much gas is injected the process can only approach the mechanism of the gas-driven miscible displacement, and (2) if too little gas is injected the worst that can happen is that the reservoir will be subjected to a water drive. In any case the recovery of oil will be good.

We have not tried to cover all reservoir engineering possibilities in this paper. Each reservoir must be considered separately from an engineering point of view. Instead, we have tried to establish guide posts leading to a greater and more economical recovery of oil through miscible displacement.

REFERENCES

1. Slobod, R. L. and Koch, H. A., Jr.: "High Pressure Gas Injection — Mechanism of Recovery Increase", *Oil and Gas Jour.* (1953) **51,** 84.
2. Koch, H. A., Jr. and Slobod, R. L.: "Miscible Slug Process", *Trans.*, AIME (1957) **210,** 40.
3. Hall, H. N. and Geffen, T. M.: "A Laboratory Study of Solvent Flooding", *Trans.*, AIME (1957) **210,** 48.
4. Jenks, L. H., Campbell, J. B. and Binder, G. G., Jr.: "A Field Test of the Gas-Driven Liquid Propane Method of Oil Recovery", *Trans.*, AIME (1957) **210,** 34.
5. Dyes, A. B., Caudle, B. H., and Erickson, R. A.: "Oil Production After Breakthrough — As Influenced by Mobility Ratio", *Trans.*, AIME (1954) **201,** 81.
6. Craig, F. F., Jr., Geffen, T. M. and Morse, R. A.: "Oil Recovery of Pattern Gas or Water Injection Operations from Model Tests", *Trans.*, AIME (1955) **204,** 7.
7. Aronofsky, J. S. and Ramey, H. J., Jr.: "Mobility Ratio — Its Influence on Injection or Production Histories in Five-Spot Water Flood", *Trans.* AIME (1956) **207,** 205. ★★★

Extensions of the Muskat Depletion Performance Equation

R. D. WEST
MEMBER AIME

MENE GRANDE OIL CO.
MARACAIBO, VENEZUELA

ABSTRACT

Muskat's depletion performance equation is here derived considering the expansion behavior of the reservoir hydrocarbon system and a simple fractional-flow equation. This method of derivation leads logically to the two extensions that follow. The first of these is concerned with gravity segregation in a depletion-drive reservoir. The second is concerned with including an empirically determined term for water influx in the performance equation. The more general equation for gravity segregation when there is a primary gas cap and empirically-determined water influx is stated for completeness. These equations have been found useful in reservoir performance calculations in Eastern Venezuela.

A discussion on the methods of solving these equations follows, and considers firstly the effect of taking finite intervals in the numerical integration, and secondly, methods of incorporating the time functions involved in segregation in with the expansion behavior. The paper concludes with a brief general discussion on further extensions to the depletion performance equation.

INTRODUCTION

The two fundamental sources of energy by which oil is produced from a reservoir result from pressure depletion inside the boundaries of the reservoir and fluid encroachment across the boundaries of the reservoir. The wells in either case form low pressure outlets through which oil and gas may be produced by the expansive force of the reservoir fluids and associated encroaching fluids.

When the reservoir pressure is higher than the bubble-point pressure of the oil, so that there is no free gas in the reservoir, these expansive forces are the only ones available for the production of oil. However, when the reservoir pressure is less than the bubble-point pressure of the oil, free gas is vaporized as the pressure falls. With both oil and free-gas phases present, the additional forces of gravity and capillarity may operate on the gas-oil system, as they have previously operated on the oil-interstitial water system. Gravity tends to segregate the free gas from the oil due to their density difference. Capillarity opposes and eventually balances gravity as the more extreme free gas and oil saturations are reached, preventing the independent movement of free gas until it is above a certain saturation, and the independent movement of oil when it is below a certain saturation.

The type of depletion performance equation chosen for predicting the future performance of a reservoir depends on the amount of past history available. When the reservoir is somewhere past the halfway mark in depletion, some form of decline curve is often used. With less past history, material balance equations which incorporate empirical factors based on the past performance are often used. When, however, the amount of past history is small, the Muskat depletion performance equation will usually be used. The distinguishing feature of this type of equation is that empirical factors based on the over-all or macroscopic reservoir behavior are almost or entirely absent. Each parameter affecting the reservoir performance is ascribed an independent set of values based on measurements made on laboratory samples; that is, incorporating microscopic empirical factors.

In establishing Muskat-type depletion performance equations, it is necessary to consider the reservoir as consisting of a number of associated blocks, in each of which the saturations and pressures may be considered uniform, and in each of which all substances have uniform pressure-volume characteristics. Thus, a primary gas cap can usually be considered as one block and an aquifer as another. Gravity segregation may be negligible for practical purposes when the rock and oil properties are adverse and/or the dip or thickness of the reservoir is too small. In this case the whole oil leg may be considered as one block, except in very large reservoirs.

In very large reservoirs the fluid and rock properties may vary enough, particularly in the dip direction, for it to be necessary to divide the oil leg into a number of blocks, in each of which the relevant quantities may be considered uniform. When gravity segregation of the oil and free gas is not negligible, it is necessary to consider the space occupied by the initial oil leg as divided into two blocks, a secondary gas cap and an effective oil leg, in each of which saturations may be considered to be uniform. The total volume of these two blocks is thus constant, but the secondary gas cap grows continuously at the expense of the oil leg.

Muskat[1] derived depletion performance equations for the basic case of an oil reservoir with closed boundaries and without segregation, and for the case of an oil

Original manuscript received in Society of Petroleum Engineers office July 2, 1957. Revised manuscript received Oct. 15, 1958. Paper presented at 32nd Annual Fall Meeting of Society of Petroleum Engineers in Dallas, Tex., Oct. 6-9, 1957.

[1]References given at end of paper.

reservoir with a boundary open to a primary gas cap. These two cases are rederived in this paper using a different approach, because this serves as an introduction to the method used to develop equations for the extensions that follow. This approach also enables those meeting these equations for the first time to see the exact relationship between this differential form of the material balance equation and the other forms in use. The mathematical treatment is simple but it is felt that it gains more, in that physical significance of the terms is readily obtained, than it loses by being non-rigorous.

EXPANSION BEHAVIOR OF THE RESERVOIR SUBSTANCES

The expansibility of a reservoir fluid or solid is here defined as the rate of increase in volume of the substance with pressure decrease. If the standard volume of the substance (that is, its volume in any units whatever corrected to standard temperature and pressure) is V_s, and its volume factor at the reservoir temperature is B_s, the reservoir volume is $V_s \cdot B_s$. If the pressure falls by a small interval, Δp, and the volume factor increases to $(B_s + \Delta B_s)$, the rate of increase in volume of the substance with pressure decrease is

$$\frac{V_s\,(B_s + \Delta B_s) - V_s \cdot B_s}{\Delta p}$$

or $V_s \cdot \Delta B_s/\Delta p$. In the limit, as $\Delta p \to 0$, this expansibility is equal to $V_s \cdot dB_s/dp$. The expansibility of a reservoir substance is therefore equal to the standard volume of the substance multiplied by the rate of change of its volume factor with pressure.

The standard volume of the free gas in any block of the reservoir is equal to $\frac{V_p \cdot S_g}{B_g}$. The free gas expands as the pressure decreases and its expansibility is therefore $\frac{V_p \cdot S_g}{B_g} \cdot \frac{dB_g}{dp}$.

The standard volume of the oil in any block of the reservoir is equal to $\frac{V_p \cdot S_o}{B_o}$. As the pressure on the oil is decreased the oil itself shrinks, but gas is vaporized, and this gas causes an increase in total volume. The expansibility due to the oil shrinkage is $-\frac{V_p \cdot S_o}{B_o} \cdot \frac{dB_o}{dp}$ and that due to the liberation of solution gas is $\frac{V_p \cdot S_o}{B_o} \cdot B_g \cdot \frac{dR_s}{dp}$. The former expression may be referred to as the expansibility of the oil, and the latter as that of the solution gas.

The over-all expansibility of the hydrocarbon system in any block of the reservoir is therefore the sum of these three components,

$$V_p\left[S_g \cdot \frac{1}{B_g} \cdot \frac{dB_g}{dp} + S_o \cdot \frac{B_g}{B_o} \cdot \frac{dR_s}{dp} - S_o \cdot \frac{1}{B_o} \cdot \frac{dB_o}{dp}\right].$$

In addition to the hydrocarbon system, the reservoir system contains interstitial water and rock. The standard volume of the interstitial water is $\frac{V_p \cdot S_{wi}}{B_w}$, and its expansibility is therefore, $\frac{V_p \cdot S_{wi}}{B_w} \cdot \frac{dB_w}{dp}$. As the rock volume factor has been defined in terms of pore space and not in terms of the rock itself, the standard volume of the rock is therefore in effect, V_p, and the expansibility of the rock is $V_p \cdot \frac{dB_r}{dp}$.

The over-all expansibility of the fluids and solid in any block is therefore equal to

$$V_p\left[S_g \cdot \frac{1}{B_g} \cdot \frac{dB_g}{dp} + S_o \cdot \frac{B_g}{B_o} \cdot \frac{dR_s}{dp} - S_o \cdot \frac{1}{B_o} \cdot \frac{dB_o}{dp} + S_w \cdot \frac{1}{B_w} \cdot \frac{dB_w}{dp} + \frac{dB_r}{dp}\right]$$

However, below bubble-point pressure, the interstitial water and rock terms will usually be negligible, except in an aquifer.

PERFORMANCE OF ONE-BLOCK OIL RESERVOIR

In the simple one-block oil reservoir with closed boundaries, all of the fluid represented by the expansion for any pressure interval must be produced through the wells. By definition, the pressure and saturations are assumed to be uniform throughout the block, and segregation is therefore implicitly excluded. It is therefore possible to obtain a theoretical performance below bubble-point pressure in terms of oil desaturation as follows.

The rate at which the oil in the reservoir shrinks is $V_{p \cdot oil} \cdot \frac{S_o}{B_o} \cdot \frac{dB_o}{dp}$, as previously shown. The rate at which oil is produced from the wells is equal to the expansibility of the hydrocarbon system (thus, neglecting interstitial water and rock terms) multiplied by the fraction of oil in the total hydrocarbon flow. Since the absence of segregation implies the ignoring of gravity effects, the fraction of oil in the mixed oil and gas flow is given by

$$f_o = \frac{1}{1 + \frac{\mu_o}{\mu_g} \cdot \frac{k_{rg}}{k_{ro}}}.$$

The rate at which oil is produced from the wells is therefore,

$$V_{p \cdot oil} \cdot \frac{1}{1 + \frac{\mu_o}{\mu_g} \cdot \frac{k_{rg}}{k_{ro}}}\left[S_g \cdot \frac{1}{B_g} \cdot \frac{dB_g}{dp} + S_o \cdot \frac{B_g}{B_o} \cdot \frac{dR_s}{dp} - S_o \cdot \frac{1}{B_o} \cdot \frac{dB_o}{dp}\right].$$

This equation ignores any special effects due to radial-flow distribution around wells, unless the relative permeability ratio is adjusted to allow for them.

The rate of oil desaturation with pressure decrease, $V_{p \cdot oil} \cdot \frac{dS_o}{dp}$, is therefore equal to the sum of these two quantities, i.e.,

$$V_{p \cdot oil} \cdot \frac{dS_o}{dp} = V_{p \cdot oil} \frac{1}{1 + \frac{\mu_o}{\mu_g} \cdot \frac{k_{rg}}{k_{ro}}}\left[S_g \cdot \frac{1}{B_g} \cdot \frac{dB_g}{dp} + S_o \frac{B_g}{B_o} \cdot \frac{dR_s}{dp} - S_o \cdot \frac{1}{B_o} \cdot \frac{dB_o}{dp}\right] + V_{p \cdot oil}\, S_o \cdot \frac{1}{B_o} \cdot \frac{dB_o}{dp}.$$

Thus,

$$\frac{dS_o}{dp} = \frac{1}{1 + \frac{\mu_o}{\mu_g} \cdot \frac{k_{rg}}{k_{ro}}}\left[S_g \cdot \frac{1}{B_g} \frac{dB_g}{dp} + S_o \cdot \frac{B_g}{B_o} \cdot \frac{dR_s}{dp}\right.$$

$$- S_o \cdot \frac{1}{B_o} \cdot \frac{dB_o}{dp} + S_o \cdot \frac{1}{B_o} \cdot \frac{dB_o}{dp} + S_o \cdot \frac{\mu_o}{\mu_g} \frac{k_{rg}}{k_{ro}} \frac{1}{B_o} \frac{dB_o}{dp} \Bigg],$$

or

$$\frac{dS_o}{dp} = \frac{1}{1 + \frac{\mu_o}{\mu_g} \cdot \frac{k_{rg}}{k_{ro}}} \Bigg[S_g \cdot \frac{1}{B_g} \frac{dB_g}{dp} + S_o \cdot \frac{B_g}{B_o} \cdot \frac{dR_s}{dp} + S_o \cdot \frac{\mu_o}{\mu_g} \cdot \frac{k_{rg}}{k_{ro}} \cdot \frac{1}{B_o} \cdot \frac{dB_o}{dp} \Bigg].$$

This is, of course, the same as the equation developed by Muskat[1], except that he has $B_g \cdot \frac{d\frac{1}{B_g}}{dp}$ instead of $\frac{1}{B_g} \cdot \frac{dB_g}{dp}$. Numerically, these two terms are equal, but they are opposite in sign. The difference arises because of the non-rigorous development of the above equation.

PERFORMANCE OF TWO-BLOCK OIL RESERVOIR WITH PRIMARY GAS CAP

When a reservoir has a primary gas cap it must be considered as consisting of two blocks, the primary gas cap and the oil leg, in each of which the saturations are assumed to be uniform. Furthermore, it must be assumed that none of the fluids in the gas-cap block are produced through wells. In this case, all fluid represented by the expansion of the gas cap in any pressure interval is transferred into the oil-leg block.

The expansibility of the gas cap is,

$$V_{p \cdot ol} \cdot m_p \cdot \Bigg[S_{gp} \cdot \frac{1}{B_g} \cdot \frac{dB_g}{dp} + S_{op} \cdot \frac{B_g}{B_o} \cdot \frac{dR_s}{dp} - S_{op} \cdot \frac{1}{B_o} \cdot \frac{dB_o}{dp} \Bigg].$$

Adding this expansibility to that of the oil leg, and using the procedure just cited, the rate of oil desaturation for this type of reservoir mechanism is given by

$$\frac{dS_o}{dp} = \frac{1}{1 + \frac{\mu_o}{\mu_g} \cdot \frac{k_{rg}}{k_{ro}}} \Bigg[\Bigg[S_g \cdot \frac{1}{B_g} \cdot \frac{dB_g}{dp} + S_o \cdot \frac{B_g}{B_o} \cdot \frac{dR_s}{dp} + S_o \cdot \frac{\mu_o}{\mu_g} \cdot \frac{k_{rg}}{k_{ro}} \cdot \frac{1}{B_o} \cdot \frac{dB_o}{dp} \Bigg] + m_p \Bigg[S_{gp} \cdot \frac{1}{B_g} \cdot \frac{dB_g}{dp} + S_{op} \cdot \frac{B_g}{B_o} \cdot \frac{dR_s}{dp} - S_{op} \cdot \frac{1}{B_o} \cdot \frac{dB_o}{dp} \Bigg] \Bigg]$$

This equation is also the same as the one developed by Muskat[1], but with the same qualification mentioned earlier regarding the free gas term. One further assumption in this equation is that the expansibility of the gas cap is freely available to the oil leg; that is, it is not restricted by permeability or any other factor to any definite transference rate. This assumption is considered not unreasonable because of the low viscosity of gas and the fact that gas caps are often not bigger than the same order of magnitude as the oil leg.

SEGREGATION

Before considering the depletion performance equation for a reservoir with segregation, it is convenient to review the basic principles of segregation.

The forces of gravity and capillarity control the segregation of free gas and oil in the reservoir. Gravity is the force which initiates and maintains the segregation by virtue of the difference in density of the two fluids concerned. Capillarity opposes this segregation, and eventually balances it, at extreme free gas and oil saturations.

Since the reservoir oil is heavier than the free gas, it always tends to flow down-dip relative to the gas under the action of gravity. However, an equal reservoir volume of gas must flow up-dip relative to the oil, and the rate of segregation is therefore determined by whichever has the low mobility. Assuming that the reservoir is thin in relation to its length in the dip direction, the effective direction of segregation may be assumed to be along the dip direction. The gravitational force causing segregation in this direction is $(\rho_o - \rho_g) \cdot g \cdot \sin D$, and the segregation rate is therefore,

$$q_m = \left[\text{lower of } \frac{k_o}{\mu_o} \text{ and } \frac{k_g}{\mu_g} \right] \cdot A \cdot (\rho_o - \rho_g) \cdot g \cdot \sin D$$

In view of the assumption that the reservoir is thin in relation to its length in the dip direction, and that the effective direction of segregation is therefore along the dip direction, the cross-sectional area, A, through which segregation takes place is the slant height area of the reservoir. It is further assumed that in thin reservoirs the mobilities based on uniform saturations throughout the sand thickness will decide the segregation rates of the oil and gas phases. These assumptions are not true for thick reservoirs as described by Martin[2]. Since during depletion the reservoir pressure falls throughout the oil leg, solution gas is vaporized throughout the oil leg and is all involved in segregation. The effective area through which segregation takes place is therefore considered to be the average slant height area between the gas-oil contact at any time and the bottom of the oil leg.

While capillarity is at all times modifying the segregation of gas and oil, it can be shown that capillary pressures and their gradients are usually negligible in field-sized systems. However, there are circumstances in which the capillary pressure is not negligible, and other circumstances in which the capillary pressure gradient is not negligible, and the practical effects of capillarity may be considered under these two heads.

In a field-sized system, the capillary pressures are important in determining the threshold values of mobility at extreme saturations. Due to the capillary pressure, gas has no mobility independent of the oil below a certain gas saturation, and this saturation thus identifies the point at which segregation can begin. At the other extreme oil has no mobility below a certain oil saturation, and this saturation thus identifies the point at which segregation ceases. However, here a time element is involved, because as this oil saturation is approached the oil mobility becomes very small, although greater than zero. Thus, in practice, it has been found convenient to identify the oil saturation at which segregation ceases by that corresponding to a small but arbitrary value of oil flow measured as a fraction of the total flow. A limiting value of $f_o = 0.001$ has been found suitable. Using such a value to identify the point at which segregation ceases, a residual oil saturation in the secondary gas cap of 25 to 35 per cent commonly results, as opposed to the value of 5 to 15 per cent commonly quoted for primary gas caps. This latter range of values may be taken as an indication of possible ultimate residual oil values.

It can be shown that the capillary pressure gradients are important only when the gas and oil saturations change rapidly in a short distance. In a depletion-drive reservoir with gravity segregation, this is at the interface between the secondary gas cap and the oil leg. Terwilliger, *et al*[3], working on an air-brine system, have shown that while there is no sharp interface between the two fluids in a gravity-drained sand column, the greater part of the saturation change occurs in a stabilized zone in which all saturations maintain a constant relative position to one another. Work by Stahl, *et al*[4], on an air-Wilcox crude system also shows the formation of a stabilized zone (see Fig. 3 of their paper). This stabilized zone appears to be the product of capillary pressure gradients. The important point about it for field-sized systems is its length in relation to the production rate from the oil leg.

Both Terwilliger, *et al*[3], and Stahl, *et al*[4], showed that stabilized zones from 1- to 3-ft thick were formed as long as the drainage rate did not exceed the so-called "maximum rate of gravity drainage". This latter quantity is defined as the rate of segregation obtained from the equation given above when $S_o = 100$ per cent. These investigators used systems with liquid mobilities in the range of 2 to 3 darcy/cp. The length of the stabilized zone for higher production rates has not been adequately examined, nor has the problem of when a stabilized zone is no longer formed. However, in practice, the production rate from the oil leg will often not exceed the maximum rate of gravity drainage, and in these cases a relatively short stabilized zone may be expected to form, the thickness of which may be considered negligible in a field-sized system.

To summarize on segregation, the mobility and area through which it operates may be designated, and a sharp interface between the secondary gas cap may be assumed unless the oil production rate is very high.

PERFORMANCE OF TWO-BLOCK OIL RESERVOIR WITH SEGREGATION

The simplest case of an oil reservoir with segregation involves two blocks; a secondary gas cap and an oil leg. For the purpose of this paper it is assumed that the production rate is such that a sharp interface between the two blocks may be considered to exist, and that all production is from the oil leg. The secondary gas cap expands continuously at the expense of the oil leg, although the two blocks taken together have a fixed total size. The basic principle involved in establishing the depletion performance equation for this type of reservoir is that the whole system is considered to obey the expansion behavior previously given, with the sizes of the blocks changing in accordance with the segregation behavior previously given.

The expansibility of the secondary gas cap is

$$V_{p\cdot ol}\, m_s \cdot \left[S_{gs} \cdot \frac{1}{B_g} \cdot \frac{dB_g}{dp} + S_{os} \cdot \frac{B_g}{B_o} \cdot \frac{dR_s}{dp} - S_{os} \cdot \frac{1}{B_o} \cdot \frac{dB_o}{dp} \right],$$

and since it is assumed that there is no production from this block, this is the rate of fluid transfer into the oil-leg block. Proceeding as before, the equation relating the oil desaturation rate with pressure decline is

$$\frac{dS_o}{dp} = \frac{1}{1 + \frac{\mu_o}{\mu_g} \cdot \frac{k_{rg}}{k_{ro}}} \left[\left[S_g \cdot \frac{1}{B_g} \cdot \frac{dB_g}{dp} + S_o \cdot \frac{B_g}{B_o} \cdot \frac{dR_s}{dp} + S_o \cdot \frac{\mu_o}{\mu_g} \cdot \frac{k_{rg}}{k_{ro}} \cdot \frac{1}{B_o} \cdot \frac{dB_o}{dp} \right] + m_s \left[S_{gs} \cdot \frac{1}{B_g} \cdot \frac{dB_g}{dp} + S_{os} \cdot \frac{B_g}{B_o} \cdot \frac{dR_s}{dp} - S_{os} \cdot \frac{1}{B_o} \cdot \frac{dB_o}{dp} \right] \right]$$

It will be noticed that this equation is similar to the equation for an oil reservoir without segregation, but with a primary gas cap, except that a varying term, m_s, is used to relate the size of the secondary gas cap to that of the oil leg. The subordinate equations used to calculate the change in m_s from the segregation behavior are given later.

WATER INFLUX IN A COMBINATION-DRIVE RESERVOIR

When a reservoir has an aquifer associated with it, it must again be considered in two blocks — the oil leg and the aquifer — in each of which saturations are assumed to be uniform. If none of the aquifer water is produced from the aquifer block, the fluid represented by the expansion of the aquifer for any interval is transferred into the oil-leg block. Using the same procedure as cited the expansibility of the aquifer is

$$V_{p\cdot ol} \cdot m_a \cdot \left[\frac{1}{B_w} \cdot \frac{dB_w}{dp} + \frac{dB_r}{dp} \right],$$

and a depletion performance equation could be established as

$$\frac{dS_o}{dp} = \frac{1}{1 + \frac{\mu_o}{\mu_g} \cdot \frac{k_{rg}}{k_{ro}}} \cdot \left[\left[S_g \cdot \frac{1}{B_g} \cdot \frac{dB_g}{dp} + S_o \cdot \frac{B_g}{B_o} \cdot \frac{dR_s}{dp} + S_o \cdot \frac{\mu_o}{\mu_g} \cdot \frac{k_{rg}}{k_{ro}} \cdot \frac{1}{B_o} \cdot \frac{dB_o}{dp} \right] + m_a \left[\frac{1}{B_w} \cdot \frac{dB_w}{dp} + \frac{dB_r}{dp} \right] \right].$$

However, as with the gas cap, this equation includes the assumption that the expansion capacity is freely available to the oil leg. But whereas the assumption is often considered reasonable in the gas-cap case, it is not considered reasonable with an aquifer since the aquifer is usually much larger than the oil leg and the water viscosity is considerably higher than gas viscosity. One approach might be to consider incorporating a pressure lag factor in the term including the expansibility of the aquifer. Here it is intended to discuss one way of another approach, an empirical one, that has been found useful. In this method the water influx is determined empirically using the material balance equation and volumetric determinations of the oil leg. The influx rate against pressure decline, dE/dp, is then determined, and this influx rate is then plotted against pressure. If this plot of dE/dp against pressure is a straight line, dE/dp may be assumed to be constant. If not, the relationship between dE/dp and pressure may be found by standard regression techniques. In either case values of dE/dp may now be predicted for future performance, providing the oil off-take rate is not changed rapidly.

This quantity, dE/dp, is used by noting that it is the *effective* expansibility of the aquifer, and is therefore equal to

$$V_{p\cdot ol} \cdot m_a \cdot \left[\frac{1}{B_w} \cdot \frac{dB_w}{dp} + \frac{dB_r}{dp} \right]$$

times its lag correction factor. The depletion performance equation therefore becomes

$$\frac{dS_o}{dp} = \frac{1}{1 + \frac{\mu_o}{\mu_g} \cdot \frac{k_{rg}}{k_{ro}}} \cdot \left[S_g \cdot \frac{1}{B_g} \cdot \frac{dB_g}{dp} + S_o \cdot \frac{B_g}{B_o} \cdot \frac{dR_s}{dp} + S_o \cdot \frac{\mu_o}{\mu_g} \cdot \frac{k_{rg}}{k_{ro}} \cdot \frac{1}{B_o} \cdot \frac{dB_o}{dp} + \frac{1}{V_{p \cdot oi}} \cdot \frac{dE}{dp} \right].$$

There are two ways of using the equation when it is obtained. When the influx rate is small in relation to the production rate, and/or for relatively short prediction periods, the cumulative water influx may be converted to a water saturation averaged over the reservoir, and the gas saturation and hence the relative permeability ratio changed accordingly. With larger influx rates and/or longer prediction periods, a third block, an invaded oil-leg block, must be considered which grows continuously at the expense of the oil-leg block. An average oil saturation can be ascribed to this block from fractional-flow curve considerations, and a sharp interface between this and the oil leg itself can be assumed. The variation of the ratio of the pore volume of this invaded block to that of the oil leg can therefore be calculated and incorporated in the performance equation.

GRAVITY SEGREGATION IN A COMBINATION-DRIVE RESERVOIR

Putting together the results of the last two sections, the depletion performance equation for a combination-drive reservoir considered in four blocks (primary gas cap, secondary gas cap, oil leg and aquifer) may be stated as follows.

$$\frac{dS_o}{dp} = \frac{1}{1 + \frac{\mu_o}{\mu_g} \cdot \frac{k_{rg}}{k_{ro}}} \left[\left[S_g \cdot \frac{1}{B_g} \cdot \frac{dB_g}{dp} + S_o \cdot \frac{B_g}{B_o} \cdot \frac{dR_s}{dp} + S_o \cdot \frac{\mu_o}{\mu_g} \cdot \frac{k_{rg}}{k_{ro}} \cdot \frac{1}{B_o} \cdot \frac{dB_o}{dp} + \frac{1}{V_{p \cdot oi}} \cdot \frac{dE}{dp} \right] + m_p \left[S_{gp} \cdot \frac{1}{B_g} \cdot \frac{dB_g}{dp} + S_{op} \cdot \frac{B_g}{B_o} \cdot \frac{dR_s}{dp} - S_{op} \cdot \frac{1}{B_o} \cdot \frac{dB_o}{dp} \right] + m_s \left[S_{gs} \cdot \frac{1}{B_g} \cdot \frac{dB_g}{dp} + S_{os} \cdot \frac{B_g}{B_o} \cdot \frac{dR_s}{dp} - S_{os} \cdot \frac{1}{B_o} \cdot \frac{dB_o}{dp} \right] \right]$$

The same segregation equation as before is used to obtain the variations in m_s.

NUMERICAL SOLUTION OF DEPLETION PERFORMANCE EQUATIONS

These depletion performance equations cannot be integrated formally, and it is therefore necessary to integrate them numerically. In this numerical integration a sequence of relatively small but nonetheless finite pressure decrements is considered; 100 psi being a suitable interval in many cases. These numerical integration procedures are well known, and it is intended to mention only those points special to the equations developed here. It is convenient to consider these points under the two heads of solving for the expansibilities and solving for the segregation variables.

SOLVING FOR THE EXPANSIBILITIES

The expansibility applied to a finite pressure interval becomes a finite expansion, and it is necessary to convert the expansibilities in the depletion performance equation to forms applicable to finite intervals.

Each pressure decrement involves a fall from an initial pressure to a final pressure. The amount of material involved in the expansion is identified by the standard volumes present at the beginning of the interval. Since the expansion is the difference between the initial and final volume, corresponding to the initial and final pressures, the solution gas vaporized during the interval and the oil and gas produced during the interval are involved as their volumes at the final pressure. The viscosity ratio, and the rates of change of the volume factors with pressure, are involved as the average values for the interval (because, for instance, $\Delta B_o = [dB_o/dp]_{av} \cdot \Delta p$). Similarly, the relative permeability ratio should be that corresponding to the average saturations during the interval (*not* the average ratio itself).

The basic depletion performance equation therefore becomes, for a finite pressure decrement,

$$\Delta S_o = \frac{1}{1 + \left(\frac{\mu_o}{\mu_g}\right)_{av} \left(\frac{k_{rg}}{k_{ro}}\right)_{\overline{S_g}}} \left[S_{gi} \cdot \frac{1}{B_{gi}} \cdot \left(\frac{dB_g}{dp}\right)_{av} + S_{oi} \cdot \frac{B_g f}{B_{oi}} \cdot \left(\frac{dR_s}{dp}\right)_{av} + S_{oi} \cdot \left(\frac{\mu_o}{\mu_g}\right)_{av} \cdot \left(\frac{k_{rg}}{k_{ro}}\right)_{\overline{S_g}} \frac{1}{B_{oi}} \cdot \left(\frac{dB_o}{dp}\right)_{av} \right] \Delta p .$$

The other equations are modified in a similar way.

In the equation just cited, all values except the average gas saturation, on which the relative permeability ratio is based, are determined directly. It is possible to consider each term in the equation as consisting of a pressure function multiplied by a saturation function. Values may be assigned to the pressure functions in advance, but the saturation functions must be calculated for each decrement in turn. The average gas saturation, which is not determined directly, may be predicted as follows. The values of ΔS_o, for equal pressure decrements, increase smoothly until at some point beyond where the equilibrium gas saturation is reached. At this point the term,

$$S_{oi} \cdot \left(\frac{\mu_o}{\mu_g}\right)_{av} \cdot \left(\frac{k_{rg}}{k_{ro}}\right)_{\overline{S_g}} \cdot \frac{1}{B_{oi}} \cdot \left(\frac{dB_o}{dp}\right)_{av}$$

increases less than

$$1 + \left(\frac{\mu_o}{\mu_g}\right)_{av} \cdot \left(\frac{k_{rg}}{k_{ro}}\right)_{\overline{S_g}},$$

and the values of ΔS_o pass through a maximum near this point and thereafter start decreasing smoothly. A plot of ΔS_o against pressure enables a prediction of the average gas saturation for the next interval to be made, and with experience the prediction can be done very close. In any case, if the predicted value is too much in error a more accurate average saturation may be determined using the final value calculated using the predicted average, and the line of calculation repeated.

Using the values as identified, and not all initial or final values as has often been done, no more complex method of numerical integration is required. This point has been confirmed using machine computations with pressure decrements as small as 10 psi.

SOLVING FOR THE SEGREGATION VARIABLES

Segregation cannot begin until the equilibrium gas saturation is reached, since this is the saturation at which the gas has a mobility independent of the oil.

This is not necessarily the point at which k_{rg}/k_{ro} becomes greater than zero, since it may be argued that some gas is carried along entrained in the oil at lower saturations. Segregation requires the gas to have an independent mobility. The equilibrium gas saturation will not be known with any great accuracy, and unnecessary calculation may often be saved by making it coincide with the gas saturation at the end of a convenient pressure interval. The calculation to this point is the same with or without segregation. The procedure for the next pressure decrement is as follows.

1. Calculate ΔS_o for the next interval as if there were no segregation, and knowing the off-take rate, obtain the time, Δt, taken to produce this pressure decrement.

2. Calculate k_o/μ_o and k_g/μ_g corresponding to the average gas and oil saturation for the interval, and find out which is the lesser; the lesser is used.

3. Plot the slant height cross-sectional area of the reservoir at different structural positions in the reservoir as a curve against position. Whence obtain a plot of the average cross-sectional area between any structural position and the bottom of the reservoir against the position of the upper limit.

4. Compute q_m and Q_m according to the following.

$$q_m = \left[\text{lesser of } \frac{k_o}{\mu_o} \text{ and } \frac{k_g}{\mu_g}\right] \cdot A \cdot (\rho_o - \rho_g) \cdot g \cdot \sin D \cdot \frac{1}{B_o}, \text{ and } Q_m = q_m \cdot \Delta t ,$$

where the appropriate value for A is used from the plot obtained in Step 3.

5. Compute m_s and the increase in oil saturation in the oil leg, ΔS_{om}, from the following sequence of equations.

$$\Delta V_{ps} = \frac{Q_m \cdot B_o f}{S_o f - S_{os}}$$

$$V_{ps} = \Sigma \Delta V_{ps}$$

$$V_{p \cdot ol} = \text{initial } V_{p \cdot ol} - V_{ps}$$

$$m_s = \frac{V_{ps}}{V_{p \cdot ol} \text{ final}}$$

$$\Delta S_{om} = \frac{Q_m B_o f}{V_{p \cdot ol} \text{ final}}$$

6. Return to the table in which the gas-cap term is calculated and insert the values of m_s corresponding to the average of the one previously used (zero in this first line) and the one just determined. Calculate a revised secondary gas-cap term.

7. Return to the table in which ΔS_o is calculated and add ΔS_{om} to the value of S_o for the end of the interval. Using this value of $(S_o + \Delta S_{om})$ and the value of S_o for the beginning of the interval, determine a revised value of K_{rg}/K_{ro} corresponding to the revised average gas saturation during the interval.

8. Using the new value of S_o without ΔS_{om} being added for the interval, recalculate the time taken for the interval.

9. Using the new value of S_o with ΔS_{om} being added for the interval, recalculate k_g/μ_g, k_o/μ_o, thence the revised segregation rate q_m, and thence revised values to $V_{p \cdot ol}$, m_s and S_{om}. These revised values are now inserted and used in starting the calculation for the next interval.

The calculations for the intervals from now on follow the same general pattern but are greatly facilitated by keeping running plots of ΔS_o, ΔS_{om}, V_{ps}, m_s and the other variables against pressure. After the first interval, predicted values may be used from these plots, and the derivation of the second approximation as just described is made considerably more accurate, if not unnecessary in some cases.

OTHER EXTENSIONS TO THE MUSKAT EQUATION

It will be noted that the basic depletion performance equation consists of a simple expansibility multiplied by a simple fractional-flow equation. The extensions just given use the same fractional-flow equation but include extensions to the expansibility. It might be deduced from this that the most general depletion performance equation should be in the nature of the most general expansibility multiplied by the most general fractional-flow equation, and that in general specific extensions should involve the extension of either the one or the other part. This appears to be true providing production is only from one block. For instance, the given segregation case was derived by considering an extension to the expansibility and using subsidiary equations to identify the change in saturation due to the segregation itself. In general, it appears that extending the expansibility terms offers the more useful approach to extending the basic depletion performance equation.

It was mentioned earlier that with more than one block the treatment given includes two important assumptions. One is that the expansibility of a block outside the oil leg is freely available to the oil leg. The second is that none of the fluid from a block outside the oil leg is produced. The first assumption may be eliminated if the equation is modified in having a lag factor associated with the expansibility of any block outside the oil leg.

To eliminate the assumption that no outside block fluid should be produced, the fractional-flow equation must be changed to a form which will allow for the production of these fluids when they are produced through wells in the oil-leg block. Thus, with water produced from the oil-leg block the fractional-flow equation would have to be extended to include a term which would allow for this water production. However, if the case is to be considered where there is production outside the oil leg itself, these differential forms of the depletion performance equation cannot be used unless it is possible by some other means to express the relationship between the production from any one block to any other block. This is because the effective expansibility of any block would be the total expansibility less the production rate from the block itself. Equations of the nature developed by McCord[5] for gravity segregation in Western Venezuela are necessary to allow for multi-block production when no simple ratio of producing rates between blocks can be obtained.

CONCLUSIONS

1. Muskat's depletion performance equation may be derived by considering the expansion behavior of the reservoir hydrocarbon system together with a simple fractional-flow equation.

2. Using a more extended expansion behavior for a two-block system (secondary gas cap and oil leg), a depletion performance equation may be derived for gravity segregation in a depletion-drive reservoir.

3. This method of extending the expansion behavior

term leads to a simple way of including empirically determined influx rates into the basic equation.

4. In general, depletion performance equations may be tailor-made for reservoirs by dividing the reservoir into blocks in each of which saturations may be assumed uniform, considering the expansion behavior of each block and the related flow equations, and producing an equation of the nature of a set of expansibilities multiplied by a fractional-flow equation.

NOMENCLATURE*

B_r = rock volume factor referred to initial pore volume
m_p = ratio of pore volume of primary gas cap to that of oil leg
m_s = ratio of pore volume of secondary gas cap to that of oil leg at any time
m_a = ratio of pore volume of aquifer to that of oil leg
V_p = pore volume of any block
$V_{p\cdot ol}$ = pore volume of oil leg at any time
V_{ps} = pore volume of secondary gas cap at any time

*See AIME Symbols List in *Trans.* AIME (1957) **207**, 363, for other symbol definitions.

SUBSCRIPTS

m = refers to segregation variable
p = refers to primary gas cap
s = refers to secondary gas cap

ACKNOWLEDGMENT

The author wishes to thank the Mene Grande Oil Co. for permission to publish this paper, and to express appreciation to his colleagues who helped in its preparation.

REFERENCES

1. Muskat, M.: *Physical Principles of Oil Production*, McGraw-Hill Book Co., N. Y. (1949) 408.
2. Martin, J. C.: "Reservoir Analysis Based on Gravity Segregation for Pressure Maintenance Operations", *Trans.* AIME (1958) **213**, 220.
3. Terwilliger, P. L., *et al*: "An Experimental and Theoretical Investigation of Gravity Drainage Performance", *Trans.* AIME (1951) **192**, 285.
4. Stahl, O. C., *et al*: "Gravity Drainage of Liquids from Unconsolidated Wilcox Sand", *Pet. Engr.* (Jan., 1943).
5. McCord, D. R.: "Performance Predictions Incorporating Gravity Drainage and Gas-Cap Pressure Maintenance—LL-370 Area, Bolivar Coastal Field", *Trans.* AIME (1953) **198**, 231.

★★★

The Simplification of the Material Balance Formulas by the Laplace Transformation

WILLIAM HURST
MEMBER AIME

PETROLEUM CONSULTANT
HOUSTON, TEX.

ABSTRACT

For many years the author has been cognizant of the difficulty encountered by some in treating with the water influx formulas for unsteady-state fluid flow as pertain to the material balance equation. This has particularly applied in establishing reservoir performance and identifying reservoir pressure, which to the practicing engineer has entailed a trial-and-error procedure, and for others has necessitated resorting to computing devices and reiteration processes.

In retrospect this difficulty stems from the fact that reservoir pressure in the material balance formulas, as well as associated with the water influx equations, is an inexplicit term, and the work reported in the past is irrefutable. However, what will be presented in this paper is another approach to the problem, whereby the entire material balance equation will be treated by the Laplace transformation, and reservoir pressure which hereto has been inexplicit, can now be isolated by mathematical procedure to relate that parameter with all the factors contributing to its change.

This is the simplification entailed, that treats first with an undersaturated oil reservoir as an integrated effect from the inception of production. The second phase pertains to saturated oil reservoirs that encompass a survey traverse. Although both methods of approach are necessarily different in aspect, the most interesting fact is that the mathematics so deduced are identical. Both the linear and radial water-drive systems are incorporated, for which an illustrated factual example is offered for the latter, treating with a saturated oil reservoir.

INTRODUCTION

What is performed in this work is the simplification of an involved computation by advanced analysis. Although such may be construed as a contradiction when one treats with higher mathematics; nevertheless, when direction is given to such an undertaking the results can be most revealing.

Likewise, it is to be mentioned that the bases for these mathematics have been developed on the expediency of the occasion. This is not to be inferred as a qualification of this work, but rather the demands frequently placed upon the author in his private practice in meeting a time limit. A situation, instead of being fraught with hazards, often has given emphasis to creative thought.

What will be entailed in this work is the simplification of the material balance formulas by the Laplace Transformation. Although this reveals entirely new horizons that will be given expression in a forthcoming tract, it suffices in the present instance to limit our attention to this phase of the development that treats both with an undersaturated and saturated oil reservoir.

To orient the reader's thoughts as to what is involved in this simplification is the recognition that reservoir pressure, as such, is an inexplicit term in the material balance equation. This is the independent parameter that defines the total history of performance in the author's[1] unsteady-state water influx formulas, as well as the basis for the physical dependency of fluid behavior within the formation as prescribed in the Schilthuis[2] material balance equation. Therefore, to isolate reservoir pressure, which is the most essential factor in any reservoir study, is rather a cumbersome procedure entailing either a trial-and-error calculation for the engineer; or as some prefer, a reiteration process performed on a computing device.

However, once such an equation can be transcribed as a Laplace transformation, this inexplicitness so expressed can be alleviated to identify reservoir pressure as an explicit function of all the factors contributing to its change. This is the simplification encompassed, that will treat first with an undersaturated oil reservoir as an integrated effect from the inception of production, and secondly, with a saturated oil reservoir as a survey traverse. Although the two approaches are necessarily different because of the physics involved, it is an interesting commentary that the mathematics are identical, showing the interdependency of the two methods.

In order to acquaint the reader with this development, the simplest case will be treated first; namely, an undersaturated oil reservoir subject to a linear water drive. However, what may be construed for this example as an idealistic case is actually a most practical application in certain parts of the world, where the size of the fields are so large that radial water-drive approaches the configuration of a linear drive.

Further, to avoid the repetition of much symbolism, frequent references will be made to the work of the author and an associate on Laplace Transformations[3],

Original manuscript received in Society of Petroleum Engineers office Feb. 5, 1958. Revised manuscript received July 1, 1958. Paper presented at Production and Reservoir Engineering Conference in Tulsa, Okla., March 20-21, 1958.

[1]References given at end of paper.

which probably has served as the most practical application for this analytical tool to reservoir performance.

However, to offer the reader continuity with the work contained in that paper,[3] and the requirements for symbol standardization now mandatory for publication in the AIME, the previous identification for the Laplace transformation as expressed for cumulative pressure drop,

$$\overline{\Delta P} = \int_0^\infty e^{-pt}\Delta P(t)\,dt$$

must be recognized as

$$\overline{\Delta p} = \int_0^\infty e^{-pt_D}\Delta p(t_D)\,dt_D \quad . \quad . \quad . \quad . \quad . \quad . \quad . \quad (1)$$

This likewise applies to the radial water influx relationship,

$$Z = 2\pi fcHR_b^2 \int_0^t \frac{d\Delta P}{dt'} Q(t - t')\,dt'$$

that now conforms to

$$W_e = 2\pi\phi c_w hr_b^2 \int_0^{t_D} \frac{d\Delta p}{dt'_D} Q(t_D - t'_D)\,dt'_D \quad . \quad . \quad (2)$$

UNDERSATURATED OIL RESERVOIR

For an undersaturated oil reservoir, the material balance is expressed as

$$N(B_o - B_{oi}) = N_p B_o - W_e \quad . \quad . \quad . \quad . \quad . \quad . \quad (3)$$

where B_o, the formation factor, is the conversion of the oil volume from stock tank to reservoir conditions, and W_e represents the cumulative water influx from an adjoining aquifer. The subscript i refers to initial reservoir conditions.

Since the change in volume of the fluid with the lowering of formation pressure is the expansion of the oil body, then

$$B_o = B_{oi}\,[1 + c_o(p_i - p)] \quad . \quad . \quad . \quad . \quad . \quad . \quad (4)$$

and

$$(B_o - B_{oi}) = B_{oi}c_o(p_i - p) \quad . \quad . \quad . \quad . \quad . \quad . \quad (5)$$

This relation introduced in Eq. 3 yields

$$W_e = N_p B_{oi} - (N - N_p)B_{oi}c_o(p_i - p) \quad . \quad (6)$$

Further, if it is assumed that the expansion for the oil voided is small in comparison with the expansion of the reserve initially in place, then Eq. 6 becomes

$$W_e = N_p B_{oi} - NB_{oi}c_o(p_i - p) \quad . \quad . \quad . \quad . \quad (7)$$

However, it is now necessary to relate the water influx from the adjoining aquifer, or

$$W_e = A\phi c_w \int_0^{t_D} \frac{d\Delta p}{dt'_D} Q(t_D - t'_D)\,dt'_D \quad . \quad . \quad . \quad (8)$$

where

$$Q(t_D) = \frac{2t_D^{1/2}}{\sqrt{\pi}}; \text{ and } t_D = \frac{kt}{\phi\mu_w c_w} \quad . \quad . \quad . \quad . \quad (9)$$

This is the application of the superposition theorem for the constant pressure terminal case[1,3] that determines the linear water influx across the lateral surface, A, of the reservoir proper, induced by the varying cumulative pressure drop, $\Delta p = (p_i - p)$, incurred by the voidage.

If the water-drive formula is introduced in Eq. 7 with the stipulation that the rate of oil production or voidage, q_o, is constant, then

$$N_p = q_o t \quad . \quad . \quad . \quad . \quad . \quad . \quad . \quad . \quad . \quad . \quad (10)$$

and

$$A\phi c_w \int_0^{t_D} \frac{d\Delta p}{dt'_D} Q(t_D - t'_D)\,dt'_D = B_{oi}q_o t - NB_{oi}c_o(p_i - p)$$

$$= \frac{\phi\mu_w c_w B_{oi} q_o t_D}{k} - NB_{oi}c_o\Delta p \quad . \quad . \quad . \quad . \quad . \quad . \quad . \quad (11)$$

where the designation for cumulative pressure drop as Δp, will henceforth remain intact as not to cause conflict with p, the operator for the Laplace transformation, as perforce must appear in these equations.

However, what is portrayed in Eq. 11 is the inexplicitness for cumulative pressure drop, as previously mentioned, with that term appearing both under the integration sign and the functional relationship identifying that equality, and to all apparent purposes an impasse in proceeding with any further analytical deduction. Such would be the case except for the recognition that the integral for the water influx term, Eq. 8, is in conformance with a theorem, although previously enunciated in the Laplace Transformation[3] and given only limited treatment in that work, will now be exploited to the fullest in the development of the simplification of the material balance equations. Namely, if $\overline{P_1}(p)$ is the transform of $P_1(t_D)$, and $\overline{P_2}(p)$ is the transform of $P_2(t_D)$, then the product of these two transforms, or $\overline{P_3}(p)$, is in turn equal to the transform of the integral containing both $P_1(t_D)$, and $P_2(t_D)$, or

$$P_3(t_D) = \int_0^{t_D} P_1(t'_D)P_2(t - t'_D)\,dt'_D \quad . \quad . \quad . \quad . \quad (12)$$

Unfortunately, neither time nor space permits the analytical deduction of this theorem, nor can it be promised that a comprehensive development will be found in most texts treating with the Laplace Transformations. It is for this reason that the detailed analyses as so entailed will be deferred to the forthcoming tract, as such has a significant bearing on other work dealing with reservoir performance.

Therefore, what might have been an impasse, the utilization of this theorem with respect to the water influx term, and transcribing the entirety of Eq. 11 as Laplace transforms, gives

$$A\phi c_w p\overline{\Delta p}\overline{Q} = \frac{\phi\mu_w c_w B_{oi} q_o}{kp^2} - NB_{oi}\overline{\Delta p} \quad . \quad (13)$$

Further, since the transform for $Q(t_D)$ is $1/p^{3/2}$ for a linear system, as shown in the Laplace Transformation[3], then Eq. 13 becomes

$$A\phi c_w \frac{\overline{\Delta p}}{p^{\frac{1}{2}}} = \frac{\phi\mu_w c_w B_{oi} q_o}{kp^2} - NB_{oi}c_o\overline{\Delta p} \quad . \quad . \quad (14)$$

Thus, where Δp heretofore has been an intractable term, it can now be solved explicitly algebraically to give

$$\overline{\Delta p} = \frac{\phi\mu_w c_w q_o}{kNc_o} \frac{1}{p^{3/2}(\lambda + p^{\frac{1}{2}})} \quad . \quad . \quad . \quad . \quad (15)$$

with

$$\lambda = \frac{A\phi c_w}{NB_{oi}c_o} \quad . \quad . \quad . \quad . \quad . \quad . \quad . \quad . \quad . \quad (16)$$

a constant containing the reserves initially in place, as

well as those physical parameters associated with the oil reservoir and the aquifer.

The inversion for Eq. 15 follows from a suitable Fourier integral table such as C and F[4], Eq. 552.9 to give

$$\Delta p = \frac{\phi\mu_w c_w q_o}{kNc_o\lambda^2}\left[e^{\lambda^2 t_D} erfc(\lambda t_D^{\frac{1}{2}}) - 1 + \frac{2\lambda t_D^{\frac{1}{2}}}{\pi^{\frac{1}{2}}}\right] \quad . \quad . \quad . \quad . \quad . \quad . \quad . \quad . \quad . \quad . \quad . \quad (17)$$

where

$$erfc(\lambda t_D^{\frac{1}{2}}) = \frac{2}{\sqrt{\pi}}\int_{\lambda t_D^{\frac{1}{2}}}^{\infty} e^{-z^2} dz = 1 - \frac{2}{\sqrt{\pi}}\int_0^{\lambda t_D^{\frac{1}{2}}} e^{-z^2} dz \quad . \quad . \quad . \quad . \quad . \quad . \quad . \quad . \quad . \quad . \quad . \quad (18)$$

which is the probability integral.

The deduction as so ascribed to Eq. 17 for an undersaturated oil reservoir, offers the clue for solutions of the more involved cases for the material balance equations; such as saturated oil reservoirs that will shortly engage our attention, although not exactly in this same format.

However, what this equation expresses is that at time zero the pressure drop is zero, and at small times the pressure change is by virtue of the voidage and the expansion of the oil in the reservoir. For time large the lowering in pressure is essentially the water-drive encountered in the field for the rate of fluid voided, which are all known conditions applicable to this type reservoir. Nevertheless, what is most important, pressure change is now independent of any reference to past pressure history, which indicates the simplification obtained.

There are associated problems connected with this study, such as the variation of oil production over the known life of the field. This again is the use of the superposition theorem, although applied in a somewhat different fashion. Thus, the reference to Eq. 11, with the condition that

$$N_p = \frac{\phi\mu_w c_w}{k}\int_0^{t_D} q_o dt_D \quad . \quad . \quad . \quad . \quad . \quad . \quad . \quad . \quad (19)$$

yields

$$A\phi c_w \int_0^{t_D} \frac{d\Delta p}{dt_D'} Q(t_D - t_D')\, dt_D' =$$

$$\frac{\phi\mu_w c_w B_{oi}}{k}\int_0^{t_D} q_o dt_D - NB_{oi}c_o\Delta p \quad . \quad . \quad . \quad . \quad (20)$$

This relationship expressed in Laplace transformations shows that

$$A\phi c_w p\bar{\Delta p}\bar{Q} = \frac{\phi\mu_w c_w B_{oi}}{k}\frac{\bar{q}_o}{p} - NB_{oi}c_o\bar{\Delta p} \quad . \quad (21)$$

where $\bar{q}_o$ is the transform for the variable rate of production. The substitution of all factors pertaining to this formula gives

$$\bar{\Delta p} = \frac{\phi\mu_w c_w}{kNc_o}\frac{\bar{q}_o}{p^{\frac{1}{2}}(\lambda + p^{\frac{1}{2}})} \quad . \quad . \quad . \quad . \quad . \quad . \quad (22)$$

for which the inversion by Eq. 12 reveals that

$$\Delta p = \frac{\phi\mu_w c_w}{kNc_o}\int_0^{t_D} q_o(t_D')M'[\lambda^2(t_D - t_D')]dt_D' \quad . \quad (23)$$

with

$$M(\lambda^2 t_D) = \frac{1}{\lambda^2}\left[e^{\lambda^2 t_D} erfc\,(\lambda t_D^{1/2}) - 1 + \frac{2\lambda t_D^{1/2}}{\pi^{\frac{1}{2}}}\right] \quad . \quad . \quad . \quad . \quad . \quad . \quad . \quad . \quad . \quad . \quad . \quad (24)$$

as previously established, and

$$M'(\lambda^2 t_D) = e^{\lambda^2 t_D} erfc\,(\lambda t_D^{1/2}) \quad . \quad . \quad . \quad . \quad (25)$$

the differentiation for Eq. 24 with respect to t_D.

Where such variations in rates of production may be subject to a regulatory body's ruling for the employment of an allocation formula, or more so by the increased production from the normal process of exploitation and development of a field, to give the equivalent of a step-wide change in production rates such as $q_o = q_{oi}$, $0 \leqslant t_D' \leqslant t_{D1}$; $q_o = q_{o1}$, $t_{D1} \leqslant t_D' \leqslant t_{D2}$; $q_o = q_{o2}$, $t_{D2} \leqslant t_D \leqslant t_{D3}$, etc., then the integration for Eq. 23 immediately becomes

$$\Delta p = \frac{\phi\mu_w c_w}{kNc_o}\Big[q_{oi}M(\lambda^2 t_D) + (q_{o1} - q_{oi})M[\lambda^2(t_D - t_{D1})] + \cdots + (q_{on} - q_{on-1})M[\lambda^2(t_D - t_{Dn})]\Big] \quad . \quad . \quad . \quad . \quad . \quad . \quad . \quad . \quad . \quad . \quad . \quad (26)$$

A formula which the reader will recognize is compatible with the variable rate problem for a flowing oil well such as given in the Laplace Transformation[3], except that what is now subscribed are those physical parameters associated with the reservoir and aquifer that necessarily must enter for the solution so portrayed.

One other point of significance. In the treatment of Eq. 6 to obtain Eq. 11, it was assumed that the expansion of the reserves in place were uneffected by that voided. Although such an assumption is valid in the early stages of production, where the yield of several thousand barrels would not change the order of magnitude for millions of barrels of oil initially in place, the question still remains whether this assumption would apply for intermediate times. For large time this is of little consequence, as Eq. 17 reflects the balance between production rate and water drive observed for undersaturated oil reservoirs. However, it is to investigate intermediate times that the treatment for the more rigorous solution is invoked.

To avoid the complexities that such an investigation can entail, this problem is again referred to the constant rate case. Thus, the substitution of all factors pertaining to Eq. 6 yields the relationship,

$$A\phi c_w \int_0^{t_D} \frac{d\Delta p}{dt_D'} Q(t_D - t_D')\, dt_D' =$$

$$\frac{\phi\mu_w c_w B_{oi} q_o t_D}{k} - NB_{oi}c_o\Delta p + \frac{\phi\mu_w c_w B_{oi} c_o q_o t_D \Delta p}{k} \quad . \quad . \quad . \quad . \quad . \quad . \quad . \quad . \quad . \quad . \quad . \quad (27)$$

However, in introducing the Laplace transformations the last term on the right-hand side, $t_D\Delta p$, offers complications since we are dealing with two variables, time and cumulative pressure drop as a product, which must be related as a transform.

The answer lies in the recognition that the operator p can likewise be treated as a variable, an observation noticeable by its absence from the mathematical literature, but given impetus here in the solution of a practical engineering problem. Thus, the reference to Eq. 1 for the Laplace transformation,

$$\bar{\Delta p} = \int_0^{\infty} e^{-pt_D}\Delta p(t_D)\, dt_D \quad . \quad . \quad . \quad . \quad . \quad . \quad (28)$$

shows that its differentiation with respect to p gives

$$\frac{d\bar{\Delta}p}{dp} = -\int_0^\infty e^{-pt_D} t_D \Delta p(t_D)\, dt_D \quad . \quad . \quad . \quad . \quad (29)$$

which is the transform for the product, $t_D\Delta p$.

Therefore, the more rigorous solution for Eq. 6, defined as Laplace transformations, is a first-order linear differential equation for which the operator p serves as the independent variable, or

$$\frac{d\bar{\Delta}p}{dp} + B\left(\frac{\lambda}{\sqrt{p}} + 1\right)\bar{\Delta}p - \frac{1}{c_o p^2} = 0 \quad . \quad (30)$$

where λ, given by Eq. 16, and

$$B = \frac{kN}{\phi\mu_w c_w q_o} \quad . \quad . \quad . \quad . \quad . \quad . \quad . \quad . \quad . \quad (31)$$

are both constants.

Eq. 30 can be solved by orthodox means, but for the purpose at hand the solution will be resolved by series expansions.

In the development of the series Eq. 30 can be further simplified by letting $v = \sqrt{p}$, or

$$\frac{d\bar{\Delta}p}{dv} + 2B(\lambda + v)\bar{\Delta}p - \frac{2}{c_o v^3} = 0 \quad . \quad . \quad . \quad (32)$$

Further, if we consider the early stages of production and recognize that for time small, p must be large, then the series expansion that can yield rapid convergence for large values of v is expressed as

$$\bar{\Delta}p = \frac{A_o}{v^s} + \frac{A_1}{v^{s+1}} + \ldots + \frac{A_j}{v^{s+j}} \quad . \quad . \quad . \quad . \quad (33)$$

where s and the coefficient A_j are unknown.

Thus, a term-by-term differentiation in Eq. 32 and collecting those constants associated with the variable v, raised to a power, establishes that $s = 4$, for which $A_o = 1/c_oB$, $A_1 = -\lambda/c_oB$, and

$$A_j = \frac{(2+j)A_{j-2} - 2B\lambda A_{j-1}}{2B} \quad . \quad . \quad . \quad . \quad (34)$$

However, since B is large, as it represents the equivalent time factor for producing all the reserves initially in place, Eq. 31, then Eq. 34 can be further simplified to give

$$Af = -\lambda A_{j-1} \quad . \quad . \quad . \quad . \quad . \quad . \quad . \quad . \quad . \quad (35)$$

Thus, the series expansion for Eq. 33 can be written,

$$\bar{\Delta}p = \frac{1}{c_oB\lambda^2}\sum_{j=0,1,2} \frac{(-1)^j \lambda^{j+2}}{p^{2+j/2}} \quad . \quad . \quad . \quad . \quad (36)$$

Its inversion is given as

$$\Delta p = \frac{\phi\mu_w c_w q_o}{kNc_o\lambda^2}\left[\frac{(\lambda^2 t_D)}{1!} - \frac{(\lambda^2 t_D)^{3/2}}{(3/2)!} + \frac{(\lambda^2 t_D)^2}{2!} - \frac{(\lambda^2 t_D)^{5/2}}{(5/2)!} + \ldots + \frac{(-1)^j(\lambda^2 t_D)^{1+j/2}}{(1+j/2)!}\right] \quad . \quad . \quad (37)$$

which is the identity for Eq. 17, and applies for $|\lambda^2 t_D| < 1$.

For time large, or p small, the series expansion that can give rapid convergence is expressed as

$$\bar{\Delta}p = \frac{A_o}{v^s} + \frac{A_1}{v^{s-1}} + \ldots + \frac{A_j}{v^{s-j}} \quad . \quad . \quad . \quad . \quad (38)$$

This relationship employed in Eq. 32, in the identical manner as the previous example, shows that $s = 3$, with $A_o = 1/c_oB\lambda$; and

$$A_j = \frac{[(4-j) - 2B]A_{j-1}}{2B\lambda} \quad . \quad . \quad . \quad . \quad . \quad . \quad (39)$$

If it is recognized as before that B is large as well as its association with λ, since the latter is finite, then

$$A_j = -\frac{A_{j-1}}{\lambda} \quad . \quad . \quad . \quad . \quad . \quad . \quad . \quad . \quad . \quad (40)$$

for which

$$\bar{\Delta}p = \frac{1}{c_oB\lambda^2}\sum_{j=0,1,2} \frac{(-1)^j}{\lambda^{j-1}p^{(3-j)/2}} \quad . \quad . \quad . \quad . \quad . \quad (41)$$

This inversion gives

$$\Delta p = \frac{\phi\mu_w c_w q_o}{kNc_o\lambda^2}\left\{\frac{2(\lambda t_D)^{1/2}}{\sqrt{\pi}}\left[1 + \frac{1}{2(\lambda^2 t_D)} - \frac{1}{4(\lambda^2 t_D)^2} + \frac{3}{8(\lambda^2 t_D)^3} - \frac{1\cdot 3\cdot 5}{16(\lambda^2 t_D)^4} + \ldots\right] - 1\right\} \quad . \quad (42)$$

which is the expansion for Eq. 17 when time is large.

It is well to recapitulate and review what has been accomplished. By subscribing the most rigorous solution for Eq. 6 and recognizing from factual field data that B can be large, we obtain the solutions identified with Eq. 17 that apply both for small and large times. This is no singular set of circumstances, as the explanation is contained in the meaning of the basic differential formula, Eq. 30, describing this rigorous case. Thus, if B is large, the differential in that formula assigned to the expansion of the fluid voided is nullified, and Eq. 30 reduces to Eq. 15. If such conditions can prevail for both small and large time, the fact that this nullification can be so invoked from the most rigorous interpretation of the problem shows that Eq. 17 is equally applicable for intermediate times.

MATERIAL BALANCE EQUATION WITH RADIAL WATER DRIVE

As previously mentioned, the choice for the presentation of the linear case has only served to demonstrate the basic principles involved because of the simplicity of the mathematics. Thus, where the linear case may have practical application would be of unusual circumstances in the U. S., where our problems are more concerned with radial water drive. It is this case that will now be offered in the treatment of the undersaturated oil reservoir.

For a radial system subject to water drive, the cumulative water influx term applicable to material balance studies is expressed by Eq. 2, a relationship originally developed by the author[1] from the interpretation of mathematical physics to fluid flow. The same format as for linear water drive prevails; namely, the dependency upon past performance history, as necessarily must apply. Therefore, what is now involved is to remove this interdependency on past pressure history in the application of the material balance equation.

Thus, the introduction of that relationship in Eq. 7 in the exact connotation as defined for water influx gives

$$2\pi\phi c_w h r_b^2 \int_0^{t_D} \frac{d\Delta p}{dt'_D} Q(t_D - t'_D)\, dt'_D = N_p B_{oi} - NB_{oi}c_o\Delta p = \frac{\phi\mu_w c_w r_b^2 B_{oi} q_o t_D}{k} - NB_{oi}c_o\Delta p \quad . \quad (43)$$

which pertains to a constant rate, and dimensionless time, t_D, is identified by

$$t_D = \frac{kt}{\phi\mu_w c_w r_b^2} \quad . \quad . \quad . \quad . \quad . \quad . \quad . \quad . \quad . \quad (44)$$

for a radial system. By reason of the enunciation of the principle defined by Eq. 12, the above relationship

can be immediately expressed by Laplace transforms to give

$$2\pi c_w h r_b^2 p\bar{\Delta}p\bar{Q} = \frac{\phi\mu_w c_w r_b^2 B_{oi} q_o}{kp^2} - NB_{oi}c_o\bar{\Delta}p \quad . \quad . \quad . \quad . \quad . \quad . \quad . \quad . \quad . \quad . \quad . \quad (45)$$

Further, it is shown in the earlier paper[3] that the radial transform for $Q(t_D)$ is given by Eq. VI-27 in that publication, or

$$\bar{Q} = \frac{K_1(p^{1/2})}{p^{3/2}K_o(p^{1/2})} \quad . \quad . \quad . \quad . \quad . \quad . \quad . \quad . \quad . \quad . \quad (46)$$

where K_o and K_1 are the modified Bessel functions of the second kind, corresponding to zero and the first order, respectively, and p, as before, is the operator for dimensionless time, t_D.

Eq. 46, substituted in Eq. 45 and absorbing all physical parameters as constants in the undertaking of the explicit algebraic solution for $\bar{\Delta}p$, gives

$$\bar{\Delta}p = \frac{\phi\mu_w c_w r_b^2 q_o}{kNc_o} \frac{K_o(p^{1/2})}{p^{3/2}[\sigma K_1(p^{1/2}) + p^{1/2}K_o(p^{1/2})]} \quad . \quad . \quad . \quad . \quad . \quad . \quad . \quad . \quad . \quad . \quad . \quad (47)$$

where

$$\sigma = \frac{2\pi\phi c_w h r_b^2}{NB_{oi}c_o} \quad . \quad . \quad . \quad . \quad . \quad . \quad . \quad . \quad . \quad . \quad (48)$$

is fixed. It now only remains to perform the inversion for Eq. 47 to define the cumulative pressure drop, Δp, as a function of all the factors that contribute to its change, which evidences the simplification entailed for the radial case.

This follows from Mellin's inversion formula expressed by

$$P(t_D) = \frac{1}{2\pi i}\int_{\gamma-i\infty}^{\gamma+i\infty} e^{\lambda t_D}\bar{P}(\lambda)d\lambda \quad . \quad . \quad . \quad . \quad . \quad (49)$$

The integration as implied in Eq. 49 is in the complex plane $\lambda = x + iy$, where the integration as performed is along a straight line parallel to the imaginary axis, and γ distance removed on the positive axis, extending from minus to positive infinity, such that all poles contained in the Laplace transformation, $\bar{P}(\lambda)$, are to the left of this straight line.

However, by virtue of Cauchy's theorem, the path so prescribed for $\bar{P}(\lambda)$, or $\bar{\Delta}p$ of Eq. 47, can be replaced by a path of integration along the semi-circle of infinite radius, with a "cut" along the negative real axis, using the origin as a branch point as illustrated in Fig. 1. The value for this integrand along the infinite circle is zero in the second and third quadrant, leaving the integration along each side of the cut on the negative real axis. Since these Bessel relationships are single valued in the direction of their traverse, as established from their transcendental function, Eq. VI-18 of the Laplace Transformation[3], they constitute the integration for Eq. 49.

Further, since the branch point or origin herein referred to represents an irreducible pole of infinite order, the classical procedure of containing the path around that pole would be of little avail. The expediency in a case such as this is to incorporate the time limits in the integral of Eq. 49 for which one such limit represents a known boundary condition, such as Δp is zero at time zero. Thus, by invoking a difference formula by reason of these time limits, this irreducible pole is explicitly cancelled out.

As this method of integration is illustrated in the Laplace Transformation[3], this procedure will be foregone

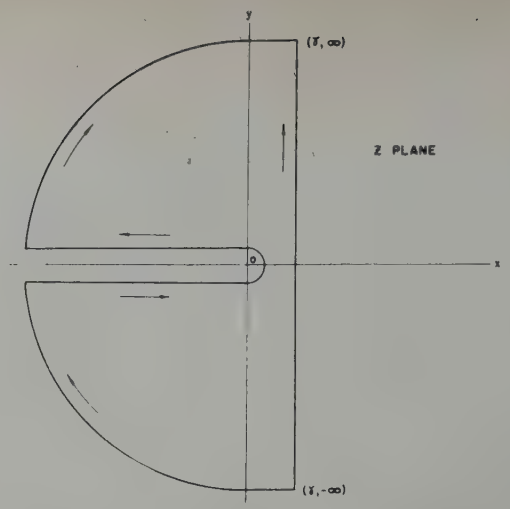

FIG. 1—CONTOUR INTEGRATION IN THE COMPLEX PLANE.

and the inversion for Eq. 47 can be immediately expressed as

$$\Delta p = \frac{\phi\mu_w c_w r_b^2 q_o}{kNc_o} N(\sigma,t_D) \quad . \quad . \quad . \quad . \quad . \quad . \quad (50)$$

with

$$N(\sigma,t_D) = \frac{4\sigma}{\pi^2}\int_0^\infty \frac{(1 - e^{-u^2 t_D})du}{u^3\{[\sigma J_1(u) - uJ_o(u)]^2 + [\sigma Y_1(u) - uY_o(u)]^2\}} \quad . \quad . \quad . \quad . \quad . \quad . \quad . \quad . \quad (51)$$

This is the simplification of the material balance equation for an undersaturated oil reservoir, subject to radial water drive, where $J_o(u)$ and $J_1(u)$ are the Bessel functions of the first kind of zero and unit orders. $Y_o(u)$ and $Y_1(u)$ are the Bessel functions of the second kind of the respective orders, for which comprehensive tables can be found in WBF[5].

At this point it is well to make a comparison between the analytical functions deduced for the material balance equations. In the linear case it is fortuitous that $M(\lambda^2 t_D)$, Eq. 24, has its regular parameter, λ^2, associated with time as a product such that one set of work curves is all that is required to undertake the linear calculation. However, with respect to the radial case the relationship, $N(\sigma,t_D)$, shows that this function is dependent on both σ and t_D as separate variables, such that a different set of work curves are necessary for every reservoir parameter, σ, which is considered. This does not present any complications, nor what may be at first appearance the formidable nature for Eq. 51, as that relationship lends itself very aptly to the computations of the necessary work curves. These curves, once performed, have continuous usage and form the repertoire of the practicing engineer. Such a set of work curves are shown in Fig. 2, prepared especially for the undertaking of the illustrative problem treated in the Appendix.

Finally, as in the previous case, where a conservation body may invoke nominations that change the production rate in a field, the step function can be introduced to give the relationship,

$$\Delta p = \frac{\phi\mu_w c_w r_b^2}{kNc_o}[q_{o_i}N(\sigma,t_D) + (q_{o_1} - q_{o_i})N(\sigma,t_D - t_{D_1}) + \ldots + (q_{o_n} - q_{o_{n-1}})N(\sigma,t_D - t_{D_n})] \quad . \quad . \quad . \quad . \quad . \quad . \quad . \quad . \quad . \quad . \quad . \quad (52)$$

In these developments it will be observed that no account has been taken for water produced with the oil, an intentional oversight to keep the mathematics simple. However, in reservoir mechanics the procedures for improvising have always been the strong forte of the engineer, and in this connection the water produced can be converted to a pseudo volume of oil voided by the application of their initial formation volume factors, which permits for the occurrence of even this phenomenon.

Though the methods now deduced may be considered as one phase of the simplified material balance equation, applicable only to the conditions that prevail for an undersaturated oil reservoir, they have already received extensive application by the author. However, in the following section dealing with the "Saturated Oil Reservoir", the reader will observe that the context of the material balance equation is retained in its entirety to reveal even a much simpler relationship than that established here. In this respect the presentation that follows represents a more rigorous interpretation for the material balance equation that applies for any condition encountered in reservoir performance, and possibly constitutes the most significant aspect of this entire presentation.

SATURATED OIL RESERVOIR

In treating with the many variances for a saturated oil reservoir that are dependent upon laboratory and factual field observations, the unique equation of state that previously identified an undersaturated oil, and permitted the solution for that problem along classical lines, no longer applies. Primarily, as what is involved for a saturated oil reservoir, is an accounting of the gas liberated from solution with the lowering of formation pressure and the manner of its voidage that form an integral part of the material balance relationship. It is the recognition of these physical variants that the solution for this problem must proceed into unexplored fields, which is in the realm of creative mathematics. The obtainment of this objective will be evidenced to the reader in the proof and factual example which are offered in this text.

In principle what is entailed in this development constitutes a survey traverse in which the production data and the physical parameters for fluid behavior, established for a previous survey, explicitly define the subsequent reservoir pressure. Such is independent of the pressure history that is mandatory in the earlier work[1] for the determination of the water influx term, for which this simplification nullifies the reiteration of such calculations for every survey encompassed. This is the cause

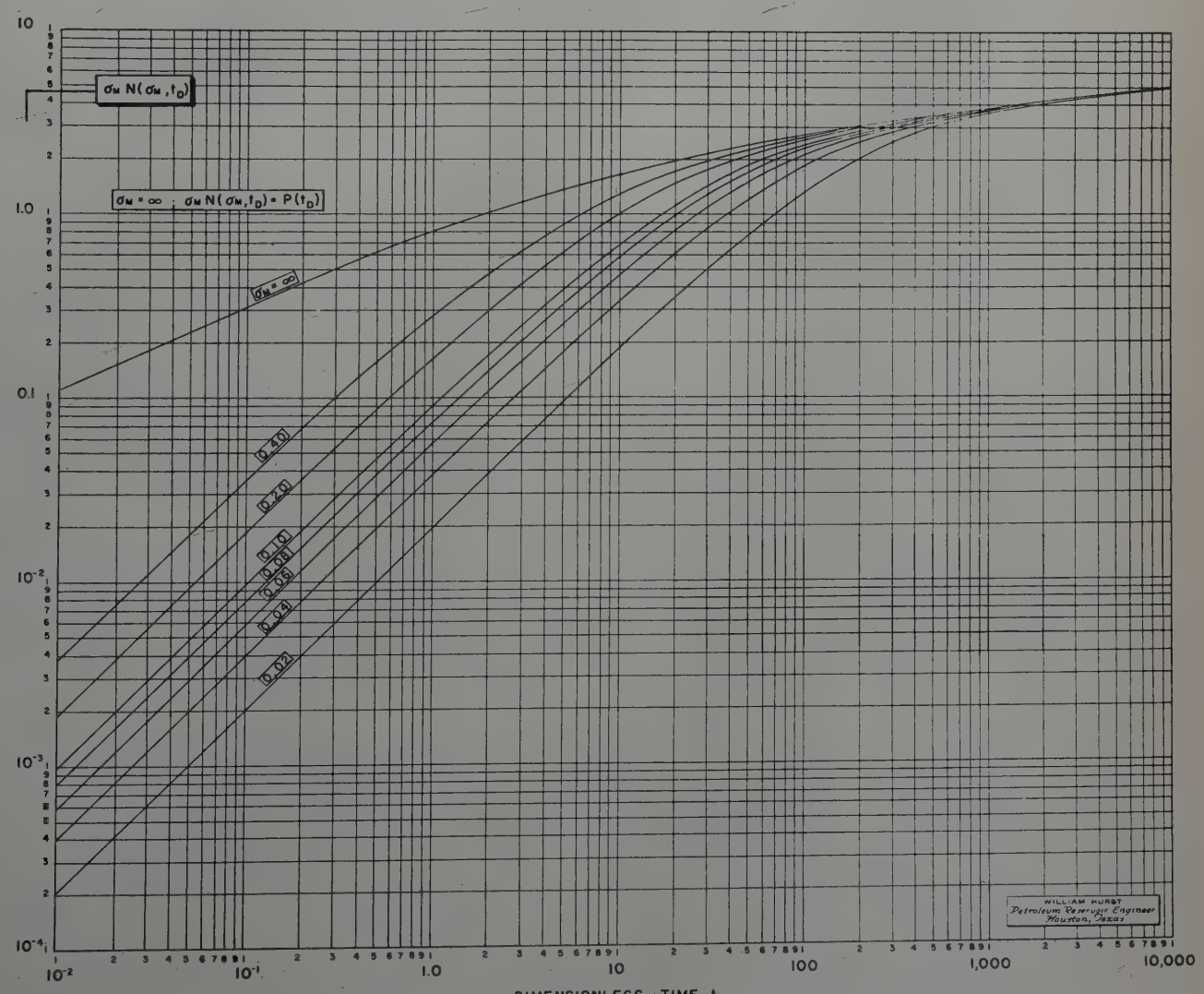

FIG. 2—CURVES OF MATERIAL BALANCE FORMULAS: $\sigma_M N(\sigma_M, t_D)$ VS σ_M AND t_D.

celebre that has given impetus to the use of computing devices whereby the role now changes and the engineer is again recognized as the principal.

To envision this development, a saturated oil reservoir can be described as one in which gas is at equilibrium in solution with the oil such that any drop in reservoir pressure gives rise to the evolvement of free gas. This free gas can segregate to the highest structural points in the formation, although some will be entrapped by the lithological nature of the sand in the oil column, and much of it will be produced with the oil. The derivation of the material balance equation for a saturated oil reservoir is referred to the original work[2], for which the essential formula is now reproduced in the AIME symbols,

$$N(B_t - B_{ti}) = N_p(B_t + (R_p - R_{si})B_g) + W_p - W_e \quad . \quad (53)$$

The terms so incorporated are identical with Eq. 3, except for the following differences. The relationship, B_t, identified with the flash liberation, has reference to that volume of oil and all the gas liberated from solution at reservoir conditions, to its corresponding volume of oil at stock-tank conditions. The term, $R_p - R_{si}$, is the cumulative free gas-oil ratio produced in excess of its initial solution gas-oil ratio, and this in turn is converted to reservoir volume by the gas laws as expressed by the specific volume factor, B_g. Finally, W_p is the cumulative water produced with the oil.

In the application of Eq. 53, all conditions pertaining to the reservoir performance to a previous survey corresponding to t_M, are known, and we wish to determine the cumulative pressure drop to a subsequent survey in time, t. Then, if the increment increase for this period is represented in the material balance equation, the relationship takes the form

$$\begin{aligned} &N\delta B_t + N(B_{tM} - B_{ti}) = \\ &N_{pM}(B_{tM} + (R_{pM} - R_{si})B_{gM}) + N_{pM}\delta(B_t + (R_p - R_{si})B_g) + \delta N_p(B_{tM} + (R_{pM} - R_{si})B_{gM}) \\ &+ \delta N_p\delta(B_t + (R_p - R_{si})B_g) + W_{pM} + \delta W_p - W_{eM} - \delta W_e \quad . \quad (54) \end{aligned}$$

where δ reflects the change for this increased time, and the affixing of the subscript M refers to the reference survey.

If this increment is now excessive, the term defined by $\delta N_p\delta(B_t + (R_p - R_{si})B_g)$, constitutes a second-order effect, comparable to a second-order differential, which is negligible. Further, if it is considered within this time interval that the basic data can be extrapolated linearly with respect to the essential reservoir parameters that contribute to this change, the method reveals the simplified relationship for the cumulative pressure drop for the later time, independently of the pressure history that has transpired during the course of the field's performance.

Such recognizable factors that effect this change are as follows.

$$\delta B_t = a_1(p_M - p_t) \quad . \quad (55)$$

where a_1 is the slope of the flash liberation curve for the time period specified, established for B_t plotted vs pressure, with p_t, less than p_M, that gives rise to this increment.

Further,

$$\delta(B_t + (R_p - R_{si})B_g) = a_2(p_M - p_t) \quad . \quad (56)$$

is postulated on the factual data at hand, as the variance incurred in gas-oil ratio, corrected to reservoir condition, will be related to the total oil produced and the change in formation pressure. Possibly other forms can be invoked for Eq. 56, or this expression even deleted from Eq. 54, depending upon the interpretations of the particular reservoir under consideration, and would constitute refinements, but does not distract from the generalization of the method as herein deduced.

Finally,

$$\delta W_p = a_3\delta N_p \quad . \quad (57)$$

where a_3 is the water-oil ratio for the period considered. This value is often determined from the empirical relationship of oil produced vs water produced, established from the known production data. In brief what is subscribed for a_1, a_2 and a_3 are instantaneous ratios, although variants through the entire reservoir performance are only remained affixed during this increment of time change as designated by the reference survey.

By differentiation of the material balance equation with respect to time, and recognizing those terms in Eq. 54 that are variables, Eq. 53 takes the form,

$$\begin{aligned} N\frac{dB_t}{dp}\frac{dp}{dt} &= N_{pM}\frac{d(B_t + (R_p - R_{si})B_g)}{dp}\frac{dp}{dt} \\ &+ q_o(B_{tM} + (R_{pM} - R_{si})B_{gM}) + \frac{dW_p}{dt} - \frac{dW_e}{dt} \quad . \quad (58) \end{aligned}$$

where q_o is the constant rate of oil production for the time increment specified. Further, if we introduce the conditions expressed by Eqs. 55, 56 and 57, and interchange the instantaneous pressure change for the cumulative pressure drop, Eq. 58 becomes

$$\begin{aligned} Na_1\frac{d\Delta p}{dt} &= N_{pM}a_2\frac{d\Delta p}{dt} + q_o(B_{tM} + (R_{pM} - R_{si}) \\ &B_{gM} + a_3) - \frac{dW_e}{dt} \quad . \quad (59) \end{aligned}$$

The first case considered is that for linear water drive. The instantaneous rate of water influx so defined in Eq. 59 is established from the cumulative water influx, Eq. 8, in differentiating the latter with respect to $t_D = Kt/\phi\mu_w c_w$, or

$$\frac{dW_e}{dt_D} = A\phi c_w\int_0^{t_D}\frac{d\Delta p}{dt'_D}Q'(t_D - t'_D)dt'_D \quad . \quad (60)$$

where $Q'(t_D)$ is the differentiation of $Q(t_D)$, for which $Q(t_D)$ is zero for time zero, Eq. 9. It is essentially this characteristic, as well as the fact that Δp is zero at time zero, that permits the interpretation of a differentiation by the Laplace transformation, which is exactly the form Eq. 59 now takes to give

$$Na_1p\bar{\Delta}p = N_{pM}a_2p\bar{\Delta}p + \frac{\phi\mu_w c_w q_o}{kp}(B_{tM} + (R_{pM} - R_{si})B_{gM} + a_3) - A\phi c_w p^2\bar{\Delta}p\bar{Q} \quad . \quad (61)$$

As in the previous treatment, $\bar{\Delta}p$ can now be explicitly solved algebraically, to yield

$$\bar{\Delta}p = \frac{q_o\mu_w(B_{tM} + (R_{pM} - R_{si})B_{gM} + a_3)}{kA}\frac{\lambda_M}{p^{3/2}(\lambda_M + p^{1/2})} \quad . \quad (62)$$

with

$$\lambda_M = \frac{A\phi c_w}{(Na_1 - N_{pM}a_2)} \quad . \quad (63)$$

The Laplace transform deduced in Eq. 62, the reader will recognize, is identical with the corresponding transform established for the undersaturated oil reservoir, Eq. 15, which shows the similarity between both methods and permits the inversion to be immediately written as

$$\Delta p = \frac{q_o\mu_w(B_{tM} + (R_{pM} - R_{si})B_{gM} + a_3)}{kA} \lambda_M M(\lambda_M^2 t_D) \quad . . . . (64)$$

Likewise, for a radial water drive the comparable form to Eq. 62 can be expressed in Laplace transforms to give

$$\overline{\Delta p} = \frac{q_o\mu_w(B_{tM} + (R_{pM} - R_{si})B_{gM} + a_3)}{2\pi kh} \frac{\sigma_M K_o(\sqrt{p})}{p^{3/2}[\sigma_M K_1(\sqrt{p}) + p^{1/2}K_o(\sqrt{p})]} \quad . . . (65)$$

where

$$\sigma_M = \frac{2\pi\phi c_w h r_b^2}{(Na_1 - N_{pM}a_2)} \quad . . . . (66)$$

Therefore, the cumulative pressure drop incurred in a saturated oil reservoir can be explicitly defined as

$$\Delta p = \frac{q_o\mu_w(B_{tM} + (R_{pM} - R_{si})B_{gM} + a_3)}{2\pi kh} \sigma_M N(\sigma_M, t_D) \quad . . . . (67)$$

which follows from Eqs. 47 and 50.

For a reservoir with a gas cap, and underlain by an oil column, the method still applies. This would necessitate the introduction of the expansion of the gas cap as an additional algebraic term, comparable to the relationships expressed by Eqs. 55, 56 and 57. However, to illustrate this method would only be a repetition of the results now accomplished, therefore its presentation is omitted.

Further, what has been deduced here for an infinite aquifer would equally apply to a limited water drive. Since a limited aquifer entails a series expansion, as shown in the earlier work[3], Eq. 65 would likewise conform to a series expansion, obtained by algebraic division, for which the inversion must be performed. This holds little interest for the author, except to define the resolution of that problem for others, as his primary purpose here is to encompass the broad scope revealed by these simplified material balance equations.

Essentially, what has been deduced in Eqs. 64 and 67 is a survey traverse, where each individual survey furnishes the data for determining the ensuing pressure drop. In this respect the parameters λ_M and σ_M are re-established for every succeeding survey. The time factor, t_D, merely denotes the total time elapsed from the inception of production to the subsequent time for which such pressure changes are computed. In the true meaning of these equations the results are dependent upon past reservoir performance, but the need for invoking the pressure history for every resulting survey has been eliminated by the simplification developed.

It is only after the completion of this entire work, and before the submittal of this publication, that time has been made available to prepare the necessary work curves to investigate a factual field performance that is illustrated in the Appendix. In this connection the reader's attention is directed to Fig. 3 which shows the comparison between this simplified method and the actual observed reservoir pressures. It suffices to say that the author has employed only the briefest of calculations to show the checks thus obtained. Of further interest, the points as illustrated are established from the previous quarterly survey which evidences the facility for this method to investigate any portion of the production history independently of what has transpired. Probably of most significance, it may now be evident to the reader that this method offers a simplified means for predicting reservoir performance.

In addition to this derivation, a more rigorous interpretation has been invoked. This takes into account the total voidage incurred in time, t_M, which will be illustrated for the radial water-drive phenomenon.

Thus, the integration for Eq. 59 in the time interim, t_M, to t, yields

$$Na_1\Delta p - Na_1\Delta p_M = N_{pM}a_2\Delta p - N_{pM}a_2\Delta p_M + q_o(B_{tM} + (R_{pM} - R_{si})B_{gM} + a_3)t - q_o(B_{tM} + (R_{pM} - R_{si}) B_{gM} + a_3)t_M - W_e + W_{eM} \quad . . . . (68)$$

Recognizing, therefore, that what is implied for W_{eM} is the total water influx, or what corresponds to its replacement of the total fluids voided as expressed by the material balance formula, Eq. 53, then Eq. 68 becomes

$$Na_1\Delta p = N_{pM}a_2\Delta p + q_o(B_{tM} + (R_{pM} - R_{si})B_{gM} + a_3)\, t + C_m - W_e \quad . . . . (69)$$

with

$$C_M = (Na_1 - N_{pM}a_2)\,\Delta p_M + N_{pM}(B_{tM} + (R_{pM} - R_{si})\,B_{gM}) + W_{pM} - N(B_{tM} - B_{ti}) - q_o(B_{tM} + (R_{pM} - R_{si})B_{gM} + a_3)t_M \quad . . . . (70)$$

a constant, ascribing all those terms fixed that are entirely dependent upon the previous survey.

In brief, what is prescribed by Eq. 69 are these variables involved such as cumulative pressure drop, time and the pressure history as reflected by the water influx term, W_e, Eq. 2, all referred back to the original time for the inception of production. It is this concept essentially, and the identification of those variables for the total domain of their variation that now extends beyond the reference survey, which permits the substitution for Eq. 69 by the Laplace transformations,

$$Na_1\overline{\Delta p} = N_{pM}a_2\overline{\Delta p} + \frac{\phi\mu_w c_w r_b^2}{k} \frac{q_o(B_{tM} + (R_{pM} - R_{si})B_{gM} + a_3)}{p^2} + \frac{C_M}{p} - 2\pi\phi C_w h r_b^2 p\overline{\Delta p}\overline{Q} \quad . . . . (71)$$

or,

$$\overline{\Delta p} = \frac{q_o\mu_w(B_{tM} + (R_{pM} - R_{si})B_{gM} + a_3)}{2\pi kh} \frac{\sigma_M}{p^2(1 + \sigma_M p\overline{Q})} + \frac{C_M}{2\pi\phi c_w h r_b^2} \frac{\sigma_M}{p(1 + \sigma_M p\overline{Q})} \quad . . . . (72)$$

with σ_M a constant as previously identified by Eq. 66.

In this connection it can be mentioned that the subscribing of the water influx to the total perimeter of the field is in the nature of a mathematical notation that does not necessarily apply in practice. The actual designation for this coefficient associated with the water influx term can only be established from factual field

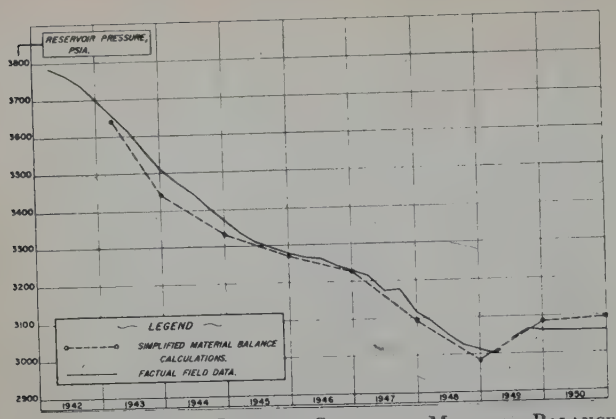

FIG. 3—COMPARISON BETWEEN SIMPLIFIED MATERIAL BALANCE CALCULATIONS AND OBSERVED RESERVOIR PRESSURE.

data that necessarily must appear in σ_M, as well as in those parameters dependent upon this factor as represented in Eqs. 67 and 72.

To continue, the extension for Eq. 72, expressed in Bessel functions, gives the relation,

$$\bar{\Delta p} = \frac{q_o\mu_w(B_{tM} + (R_{pM} - R_{si})B_{gM} + a_3)}{2\pi kh} \frac{\sigma_M K_o(\sqrt{p})}{p^{3/2}[\sigma_M K_1(\sqrt{p}) + p^{1/2}K_o(\sqrt{p})]} + \frac{C_M}{2\pi\phi c_w h r_b^2} \frac{\sigma_M K_o(\sqrt{p})}{p^{1/2}[\sigma_M K_1(\sqrt{p}) + p^{1/2}K_o(\sqrt{p})]} \quad . \quad . \quad . \quad . \quad (73)$$

for which the inversion is the formula,

$$\Delta p = \frac{q_o\mu_w(B_{tM} + (R_{pM} - R_{si})B_{gM} + a_3)}{2\pi kh} \sigma_M N(\sigma_M, t_D) + \frac{C_M}{2\pi\phi c_w h r_b^2}\sigma_M N'(\sigma_M, t_D) \quad . \quad (74)$$

where $N'(\sigma_M,t_D)$ is the differentiation of $N(\sigma_M,t_D)$ with respect to t_D, or

$$N'(\sigma_M, t_D) = \frac{4\sigma_M}{\pi^2}\int_0^\infty \frac{e^{-u^2 t_D}du}{u\{[\sigma_M J_1(u) - uJ_o(u)]^2 + [\sigma_M Y_1(u) - uY_o(u)]^2\}} \quad . \quad . \quad . \quad . \quad . \quad . \quad . \quad . \quad (75)$$

which follows from Eq. 51. With reference to Eq. 74, the reader will observe that this relation is identical with Eq. 67, except for the addition of a second term.

It is well to compare the two methods deduced by the relationship of Eq. 72 which incorporates both applications. If the water drive is zero, as reflected by the Q transform in that formula, then its inversion reveals the explicit relationship for solution drive that would prevail for the conditions specified, as identified by the material balance equation. In its implication this illustrates that the mechanics so formulated can give the integrated effects for every survey traversed. However, what is more important, this shows that the variables involved are uneffected by the assignment of a constant rate, q_o, over the time increment designated, but moreso for a fixed C_M, for which these same variables would equally apply for the designation of the pressure history by the appropriate transforms as now introduced in that formula.

It is the recognition of the rigorosity for this second method that permits the investigation of the first. Primarily, as a critical examination of Eq. 72 shows that for time small, with p large, the second term in that formula is most predominant; and conversely, for time large, with p small, the first term becomes predominant. These same results are evidenced from the formulations for $N(\sigma_M,t_D)$ and $N'(\sigma_M,t_D)$, given by Eqs. 51 and 75. In essence, the application for the first method becomes more effective with increased time.

We shall pursue this thought in examining the extent that this second term, and second method, may have an effect in early times. This has particular reference to the meaning for C_M and Eq. 70. Thus, for time zero, C_M is zero, but more important, what is entailed in that formula is an approximation for the integration by parts for the terms $N(B_{tM} - B_{ti})$ and $N_{pM}(B_{tM} + (R_{pM} - R_{si})B_{gM})$. Since these are present as nullifying effects, C_M at early times and conceivably at more extended times, can either be zero or insignificant. This, joined with any appreciable value for $2\pi\phi c_w h r_b^2$, can render this second term even more inconsequential.

Since this is the time period for the predominance for the second method and the contributions forthcoming from C_M, these second-order effects so evidenced lend greater weight to the significance of the first method and the simplification it entails. To the extent that the second method can only be deduced as a refinement for the first, but even so substantiates the validity for the latter, which is the purpose for this presentation.

Finally, this chapter would not be complete without drawing certain analogies between these simplified material balance formulas and the constant rate case for producing wells, discussed at length in the Laplace Transformation[3] that has reference to an earlier work. Thus, if time is large, with p small, the relationship expressed for a saturated oil reservoir subject to radial water drive, Eq. 65, takes the form

$$\bar{\Delta p} = \frac{q_o\mu_w(B_{tM} + (R_{pM} - R_{si})B_{gM} + a_3)}{2\pi kh} \frac{K_o(p^{1/2})}{p} \quad . \quad . \quad . \quad . \quad . \quad . \quad . \quad . \quad . \quad . \quad . \quad (76)$$

for which the Laplace transform is identified with the constant rate case for a producing well (see Eq. VIII-B of Ref. 3). Thus, Eq. 76 can be immediately expressed as

$$\Delta p = \frac{q_o\mu_w(B_{tM} + (R_{pM} - R_{si})B_{gM} + a_3)}{2\pi kh} P(t_D) \quad . \quad . \quad . \quad . \quad . \quad . \quad . \quad . \quad . \quad . \quad . \quad (77)$$

where the coefficient associated with $P(t_D)$ is the unit rate of production for the composite of oil and gas produced from the reservoir.

The significances of Eq. 77 are several fold. First of all the reader will recall that the basis for this formula is a survey traverse, in which the variable rates have been accounted for as a cumulative production. If it develops for large time that this pressure drop is independent of this cumulative production, but only dependent upon the final rate of production and the total time involved, then what is stated by Eq. 77 is that the applicability for the superposition theorem, or Duhamel's principle, is superfluous in the treatment of the variable rate problem for dimensionless t_D large. Since this is essentially the situation that prevails for producing wells, such variable rate studies can be expressed by the final rate of production to yield the cumulative pressure drop. In this connection the reader has only to apply this con-

cept, associated with the superposition theorem, to realize the close numerical checks obtained.

What has been evinced here finds its counterpart in a critical examination of the mathematics for the superposition theorem to show that this is a most apt approximation.

The second point is one of deduction, but nevertheless, of importance in the consideration of two-phase fluid flow for a producing well. Where the friction drop incurred in the sand proper for oil is the largest of the two factors for composite fluid flow into the wellbore, the unit rate of production given in Eq. 77 can account for the gas produced with the oil. In this respect the gas-oil ratio must be related to the amount of free gas that can be contained within the lithological entrapments of the oil column. Nor can this be prescribed by relative permeability, particularly as gas segregation has been evidenced in formations of lowest structural relief.

Probably of most interest in the development of Eq. 77 is the identification of the material balance equation with the flow formula for a producing well. Since in the former static or shut-in pressure obtained in pressure surveys constitutes the essential parameter employed in material balance studies to define the reserves in place and the influx of fluid from an external source, implies by virtue of this identification that static pressure has the same interpretations for well performance as pertains to reservoir behavior.

The credibility for this assertion is evidenced by factual field data. Thus, in any static bottom-hole pressure survey, the plotting of an isobaric map can reveal isolated pressure sinks, or lowered pressure areas that reflect the character of individual well performances that have occurred in the past. The fact that we statistically weigh bottom-hole pressure data for employment in material balance calculations is to encompass the reservoir study for the field as a whole. Further, the rapidity of a pressure drawdown and build-up for a producing well can largely be influenced by the skin effect, for which our present known technology still applies; as this could well be a superimposed effect upon a slowly changing pressure gradient in the formation proper. If this situation prevails, then we have in Eq. 77 the basis for calculating permeability in situ, or formation capacity, postulated on the over-all static pressure drop for a producing well.

Finally, as the reader may surmise from this work, if pressure as such can be explicitly identified in a material balance equation it can be transcribed through a common aquifer to indicate the pressure lowering in an adjoining field. Such effects are retroactive from one reservoir to the other to indicate the interference pattern between fields. This study has now been developed from the mathematics herein deduced and will receive publication. What is established is the incorporation of the actual physical data, such as PVT analyses relating to the oil and gas voidage for each individual field and their areal extents with respect to the common aquifer. As would be expected, the mathematics for such an undertaking have proved complex, but the final results evidence their adaptability by the engineer.

NOMENCLATURE

r_b = radius of field, L
B_o = oil formation volume factor, dimensionless
N = initial oil in place, corrected to stock-tank conditions, L^3
N_p = cumulative oil produced, L^3
W_e = cumulative water influx, L^3
c_o = oil compressibility, volume per volume per unit pressure change
p_i = initial reservoir pressure, m/Lt^2
p = reservoir pressure, m/Lt^2
$\Delta p = p_i - p$, cumulative pressure drop, m/Lt^2
h = net pay thickness, L
t_D = dimensionless time
t = absolute time
k = absolute permeability, L^2
ϕ = porosity, expressed as a fraction
μ_w = viscosity of water, m/Lt
c_w = water compressibility, volume per volume per unit pressure drop
A = lateral surface exposed to water influx, L^2
q_o = rate of oil production, L^3/t
B_t = volume of reservoir oil and its liberated solution gas per unit volume of stock-tank oil, dimensionless
R_p = cumulative gas-oil ratio
R_{si} = initial solution gas-oil ratio
B_g = gas formation volume factor, or specific volume, expressed as volume of gas at reservoir condition per unit volume at standard condition
W_p = cumulative water production, L^3
a_1, a_2, a_3 = instantaneous slopes of physical parameters at reference survey, t_M

REFERENCES

1. Hurst, William: "Water Influx Into a Reservoir and Its Application to the Equation of Volumetric Balance", *Trans.* AIME (1943) **151,** 263.
2. Schilthuis, R. J.: "Active Oil and Reservoir Energy", *Trans.* AIME (1936) **118,** 31.
3. van Everdingen, A. F. and Hurst, William: "The Application of the Laplace Transformation to Flow Problems in Reservoirs", *Trans.* AIME (1949) **186,** 305.
4. Campbell, George A. and Foster, Ronald M.: "Fourier Integrals For Practical Application", Amer. Tel. and Tel. Co. (1942).
5. Watson, G. N.: *A Treatise on the Theory of Bessel Functions.* Cambridge Univ. Press (1944).
6. van Everdingen, A. F., Timmerman, E. H. and McMahan, J. J.: "Application of the Material Balance Equation to a Partial Water-Drive Reservoir", *Trans.* AIME (1953) **198,** 51.

APPENDIX

The factual example employed for this illustrative calculation relates to a paper titled, "Application Of The Material Balance Equation To A Partial Water-Drive Reservoir", by Van Everdingen, *et al*[6]. This publication was chosen only because of the detail with which the production data was compiled. Therefore, the authors should not infer that there is any purpose served here to change the status quo of their over-all conclusions, as the primary objective is to present the simplified material balance calculations.

To incorporate this portion of the work the reader must be prepared to treat with the change of symbols, as that publication[6] employs its own distinctive nomenclature. Furthermore, the AIME has now adopted its set of symbols, and unfortunately this investigator still thinks in the traditional symbolism of Schilthuis' formula, and the employment of millions of barrels of oil as a unit. This is augmented by the fact that we must deal with dimensionless time, and the equivalent cgs units for permeability. However, we will attempt to clarify these many aspects.

In converting the essential constants of the cited paper to the basic precepts of Eq. 67, the factor,

$$B = 181.89 \quad . \quad . \quad . \quad . \quad . \quad . \quad . \quad . \quad . \quad . \quad (78)$$

associated with the water influx term in that work and could be defined as barrels of cumulative water influx per psi pressure drop, is identified in the corresponding legend as cc/atm when expressed as

$$2\pi\phi c_w h r_b^2 = (181.89)(14.7)(.159)(10)^6$$
$$= 425.13150(10)^6 \text{ cc/atm} \quad . \quad . \quad . \quad . \quad . \quad (79)$$

where 1 atm = 14.7 psi, and 1 bbl = 159,000 cc.

The ΔT, as reported in Table 1 of the reference paper[6] for each quarterly survey, or

$$\Delta T = \frac{k(30.4)(3)(86{,}400)}{\phi\mu_w c_w r_b^2} = 15 \quad . \quad . \quad . \quad (80)$$

gives the equivalent dimensionless time for 1 sec, and

$$\frac{k}{\phi\mu_w c_w r_b^2} = 1.90363(10)^{-6} \quad . \quad . \quad . \quad . \quad . \quad (81)$$

where 86,400 sec constitutes a day for a 30.4-day month.

Thus, the product for Eqs. 79 and 81 immediately yields the constant,

$$\frac{2\pi kh}{\mu_w} = 809.29308 \quad . \quad . \quad . \quad . \quad . \quad . \quad . \quad (82)$$

invoked in Eq. 67.

The determination for a_1 and a_2, Eqs. 55 and 56, follows from the transcendental functions already subscribed in that publication[6] where the flash differential is given by

$$B_t = \frac{1}{0.650}\left[\frac{p_b - p}{1.73117p + 0.00042536p^2} + 1\right]$$
$$. \quad . \quad . \quad . \quad . \quad . \quad . \quad . \quad . \quad . \quad . \quad . \quad (83)$$

where 0.650 is the shrinkage factor for this slightly undersaturated crude that prevails at the bubble-point pressure, p_b = 3,690 psia, although the initial reservoir pressure, p_i = 3,793 psia.

Therefore, by the ordinary process of differentiating Eq. 83, and setting the limit for a previous pressure survey, p_M, a_1 can be expressed as

$$a_1 = \left|\frac{dB_t}{dp}\right|_{p=p_M} \quad . \quad . \quad . \quad . \quad . \quad . \quad . \quad . \quad . \quad (84)$$

where in this context the basic unit is the reciprocal of pressure in psi. The affixing of the absolute value for Eq. 84 is in conformance with Eq. 55 as we are differentiating with respect to Δp and not pressure per se, for which the latter would necessarily be negative in slope.

Correspondingly, the relationship for the specific volume factor for gas is given in that paper[6] and can be expressed in these symbols as

$$B_g = \frac{1}{5.615E} =$$
$$\frac{1}{(-158.107 + 0.455244p - 0.000025854p^2)}$$
$$. \quad . \quad . \quad . \quad . \quad . \quad . \quad . \quad . \quad . \quad . \quad . \quad (85)$$

Since this is associated with the gas-oil ratio in cubic feet per barrel, the authors[6] have already subscribed the necessary conversion factor.

Again, by the process of differentiation, this equation of state can be expressed as

$$\left(\frac{dB_g}{\Delta p}\right)_{\Delta p_M} = \left|\frac{dB_g}{dp}\right|_{p_M} \quad . \quad . \quad . \quad . \quad . \quad . \quad . \quad (86)$$

with the limit set at the previous survey and the units being the reciprocal for pressure in psi.

Therefore, recognizing what is implied for Eq. 56, then

$$a_2 = \left|\frac{dB_t}{dp}\right|_{p_M} + (R_{pM} - R_{si})\left|\frac{dB_g}{dp}\right|_{p_M}$$
$$+ \left(\frac{dR_p}{d\Delta p}\right)_{\Delta p_M} B_{gM} \quad . \quad . \quad . \quad . \quad . \quad . \quad . \quad . \quad (87)$$

If the cumulative gas-oil ratio remains fairly constant this last term is eliminated.

Thus, taking account of the units ascribed to Eqs. 78, 84 and 86, then

$$\sigma_M = \frac{B}{(Na_1 - N_{pM}a_2)} \quad . \quad . \quad . \quad . \quad . \quad . \quad . \quad (88)$$

where N, the reserves initially in place, is 26,146,000 bbl of oil, corrected to stock-tank conditions.

The actual illustrative calculation can only be shown in part, as space does not permit each detailed step. What will be portrayed is the employment of the data for the third survey of 1945, to calculate the pressure for the fourth survey of 1945, or what would correspond to the first of 1946. The reference is Table 1 of Ref. 6.

For the third survey of 1945 the average reservoir pressure is 3,293 psia, after 2,970,088 bbl of oil have been produced. Therefore, from the equations of state, the essential parameters can be immediately established, to give

$$B_{tM} = 1.59768; \; a_1 = \left|\frac{dB_t}{dp}\right|_{p_M} = 0.00017520$$
$$. \quad . \quad . \quad . \quad . \quad . \quad . \quad . \quad . \quad . \quad . \quad . \quad (89)$$

and

$$B_{gM} = 0.00094283; \left|\frac{dB_g}{dp}\right|_{p_M} = 0.25332(10)^{-6} \quad .$$

Thus, in conformance with Eq. 87,

$$a_2 = 0.00017520 + (1{,}006 - 900)(0.25332)(10)^{-6}$$
$$+ \frac{(1{,}006 - 987)(0.00094283)}{(3{,}309 - 3{,}293)} = 0.0013217 \quad . \quad (90)$$

A word of explanation with respect to the latter: the solution gas-oil ratio in this field is 900 cu ft/bbl. Further, the rate of change of the gas-oil ratio as so ascribed is postulated on the increasing ratio as reflected from the second to the third survey with the lowering of their respective reservoir pressures. Although such in itself serves as an approximation, the writer has found that if the previously increasing gas-oil ratios to the reference survey are plotted vs cumulative pressure drop, an index prism mounting on a protractor offers a fairly excellent means for establishing this slope at the reference point, once a smooth curve is drawn through all points.

Thus, in subscribing the values as pertain to Eq. 88,

$$\sigma_M = \frac{181.89}{[(26{,}146{,}000)(0.00017520) - (2{,}970{,}088)(0.0013217)]}$$
$$= 0.27760 \quad . \quad . \quad . \quad . \quad . \quad (91)$$

Now we have to project our thoughts that will encompass the rate of oil production from the third survey to the end of the fourth survey, which is the survey under consideration in the calculation of this pressure drop. For this three-month period (as referred to in Table 1 of Ref. 6) 2,257.24 B/D of oil are produced, or

$$q_o = (2{,}257.24)(1.84) = 4{,}153.32 \text{ cc/sec} \quad . \quad (92)$$

where 1 B/D = 1.840 cc/sec.

Further, the water-oil ratio, Eq. 57, determined graphically for the reference survey in 1945, gives

$$a_3 = 0.50344 \text{ bbl/bbl} \quad . \quad . \quad . \quad . \quad . \quad . \quad . \quad . \quad (93)$$

Therefore, to recapitulate the steps herein subscribed, for $\sigma_M = 0.27760$; and $t_D = 240$, the dimensionless time for the survey in question, given in Table 1 of the cited paper[6],

$$\sigma_M N(\sigma_M, t_D) = 3.15 \quad . \quad . \quad . \quad . \quad . \quad . \quad . \quad . \quad (94)$$

which is established from Fig. 2 of the present work. Thus, the substitution of all values in Eq. 67 developed in the text, or

$$\Delta p = \frac{q_o \mu_w (B_{tM} + (R_{pM} - R_{si}) B_{gM} + a_3)}{2\pi kh} \sigma_M N(\sigma_M, t_D)$$

gives

$$\Delta p = \frac{4{,}153.32 \left[\begin{matrix} 1.59768 + (1{,}006 - 900).00094283 \\ + .50344 \end{matrix} \right]}{809.29308} \times (3.15)$$

$$= 35.58213 \text{ atm; or } 523.06 \text{ psi} \quad . \quad . \quad . \quad . \quad . \quad . \quad . \quad (95)$$

Since the initial pressure for the field is 3,793 psia, then

$$p = 3{,}793 - 523.06 = 3{,}270 \text{ psia} \quad . \quad . \quad . \quad (96)$$

as against 3,277 psia, observed.

The consistency of the trend by what is computed by these simplified material balance calculations, and the actually observed field data is shown in Fig. 3 to indicate the close conformity so established. However, what will now be evident to the reader is that the dependency upon past pressure history performance is non-existent, which is the objective that this investigator has set out to accomplish. ★★★

Reverse-Wetting Logging

JOHN W. GRAHAM
JUNIOR MEMBER AIME

HUMBLE OIL & REFINING CO.
HOUSTON, TEX.

INTRODUCTION

The most common method of identifying hydrocarbon-bearing strata in a well that penetrates many different formations involves measurement and interpretation of the electrical properties of the formations as determined by electrical logs. Even though this method is used extensively, and even though in a great many instances it is capable of indicating presence of oil or gas, situations arise for which it is extremely difficult, if not impossible, to deduce the presence of hydrocarbons. These situations may involve the following.

1. A thin formation, bounded by highly resistive formations, in which it is impossible to obtain the actual resistivity of the uninvaded zone with existing logging devices.
2. A formation in which invasion has been so extensive that a value for the uninvaded zone resistivity cannot be obtained.
3. A very shaly formation in which the resistivity index, *I*, is lower than that usually associated with productive formations.
4. Laminated formations comprised of thin productive sands separated by thin shale streaks in which the individual sand and shale streaks are too thin to permit measurement of uninvaded-zone resistivity with existing logging devices.
5. Productive formations in which the water saturation is high.

To extend the utility of electric log interpretation to identification of hydrocarbons in all types of formations, there is strong incentive to find a method not subject to these limitations.

Some time ago, in connection with research on the wettability of reservoir rock, an investigation was conducted in which the resistivities of cores were measured shortly after they were removed from a core barrel, and again after they had been extracted and restored to their original oil and brine saturation.[1] The resistivities after extraction were generally lower. Other tests made on the cores indicated that they were more nearly water wet after they were extracted; thus, it was assumed that the observed changes in resistivities were due to a change in wettability of the cores. Other experiments[2,3] have shown that resistivities of rock samples are sharply dependent on wettability. These experiments have shown that oil-wet samples are more resistive than water-wet samples.

To obtain an understanding of how the wetting properties of the surfaces of core material affect electrical resistivity, a series of experiments was conducted. Two groups of core samples were prepared for testing. One group contained brine, but no residual oil. The other group was saturated with brine, flooded with oil to a low water saturation, then flooded with brine to a final residual oil saturation. Resistivity measurements were made on each group. Both groups were then flooded with the original brine to which a chemical had been added that renders sand and clay surfaces preferentially oil wet, a so-called reverse-wetting agent. Very little change in resistivity was observed in cores containing only water. The group containing residual oil, however, showed resistivity increases of 100 to 200 per cent.

These experiments showed that the resistivity of a core containing oil could be altered by changing wettability of the core. Moreover, the possibility was introduced that reverse-wetting agents might be employed as the basis for a logging method for identification of oil-bearing strata. Since behavior of a porous rock containing gas and water might be expected to be similar to that of a rock containing oil and water, such a method should also be applicable to identification of gas-bearing zones. In principle the wettability of the invaded zone could be reversed without altering conductivity of the interstitial water or the hydrocarbon saturation therein. Those strata showing significantly increased invaded-zone resistivities would, therefore, contain hydrocarbons; those with no significant change would be filled only with water.

Addition of a reverse-wetting agent to a hydrocarbon-bearing zone which is, by nature, already preferentially oil wet would not result in an enhancement of its resistivity. It is generally believed, however, that most hydrocarbon-bearing strata are preferentially water wet.

Manuscript received in Society of Petroleum Engineers office July 14, 1958. Paper presented at 33rd Annual Fall Meeting of Society of Petroleum Engineers in Houston, Tex., Oct. 5-8, 1958.
[1]References given at end of paper.
Discussion of this and all following technical papers is invited. Discussion in writing (three copies) may be sent to the office of the *Journal of Petroleum Technology*. Any discussion offered after Dec. 31, 1958, should be in the form of a new paper.

(The possibility exists, of course, that some reservoirs may be preferentially oil wet. In either the oil-wet or water-wet case, the reverse-wetting technique may be useful in determining in situ wettability.) More important, those strata difficult to identify from the electric log by virtue of their high water saturations and correspondingly low resistivity are almost certainly preferentially water wet. Consequently, the reverse-wetting technique should be a useful logging method for detecting the presence of hydrocarbon-bearing zones containing even small amounts of oil or gas.

With the objective of developing a useful logging technique, a laboratory investigation was initiated for development of a more complete understanding of the reverse-wetting phenomenon, and tests of the technique as a hydrocarbon-locating method were then made in the field.

LABORATORY INVESTIGATION

A number of points pertinent to use of the reverse-wetting technique in locating hydrocarbon-bearing strata were explored in laboratory investigation. These points include type of reservoir rock amenable to the treatment, nature and amount of the agent required, rate of attainment of increased resistivity and its persistence, effect of characteristics of oil in the rock on the resistivity increase, and influence of temperature on the enhancement of resistivity. Experiments designed to elucidate these points are described in following sections.

Types of Reservoir Rock Amenable to Treatment

To investigate the type of reservoir rock in which resistivity could be increased by addition of a reverse-wetting agent, a number of samples of sandstone, shaly sand, limestone and artificially prepared quartz cores were prepared to contain residual oil and brine. Another group of similar samples was saturated with brine only. Resistivities of corresponding samples in the two groups were measured. Wetting characteristics of the samples were then changed from predominantly water wet to predominantly oil wet by flooding the samples with a dilute solution of a reverse-wetting agent dissolved in brine of the same resistivity as that used in saturating the cores originally. Resistivity of each sample was again measured.

Results of these experiments are shown in Tables 1 and 2. Table 1 contains results obtained with samples completely saturated with brine. It can be seen that only an insignificant change resulted from contact with the agent. Table 2 shows the results obtained with cores containing brine and residual oil. In all cases the resistivity was increased significantly.

From these experiments it can be expected that the resistivity of reservoir rock containing brine and residual oil is increased by addition of reverse-wetting agent regardless of the type of reservoir rock.

Nature and Amount of Agent Required

As illustrated in Table 2 all reverse-wetting agents tested resulted in an increase in resistivity of the cores containing brine and residual oil. From this it appears that the pertinent characteristic of the agent is its ability to render the rock surface preferentially wet to the hydrocarbon. An auxiliary experiment demonstrated that the action of the reverse-wetting agent in increasing resistivity is not due to a reduction in interfacial tension *per se*. A core containing residual oil was treated with a non-ionic surfactant, and it was observed that the core was not made oil wet. Resistivity of the core after treatment with this agent was slightly lower than its original resistivity.

In the experiments, tabulated in Tables 1 and 2, concentration of reverse-wetting agent utilized was in each case in the range of 2 to 5 per cent. Although no extensive investigation was conducted to determine permissible limits of concentration, it was concluded on the basis of laboratory experiments that about 2 per cent concentration of the reverse-wetting agent is probably adequate.

Rate of Attainment of Increased Resistivity

To study rate of attainment of the resistivity increase brought about by alteration of wettability, a Berea core containing residual oil and brine was placed in a conventional waterflooding apparatus so that the core re-

TABLE 1—BRINE-SATURATED CORES

Core material	Brine resistivity, (ohm-m)	Wetting agent used*	Core resistivity before contact with reverse-wetting agent (ohm-m)	Core resistivity after contact with reverse-wetting agent (ohm-m)	Resistivity increase (per cent)
Berea sandstone	1.01	A	14.1	16.4	16
Berea sandstone	1.01	A	13.7	16.4	20
Berea sandstone	1.01	A	14.7	16.5	12
Berea sandstone	1.01	A	14.5	16.4	13
Fused quartz	1.01	A	4.4	4.8	10
Fused quartz	1.01	A	4.6	5.0	10
Shaly sand (Borregas field)	1.01	A	9.2	12.4	35
Leuders lime (quarry)	1.00	G	8.3	7.7	−7
Leuders lime (quarry)	1.00	G	9.3	8.5	−9
Berea sandstone	1.00	G	17.0	17.3	2
Berea sandstone	1.00	G	13.2	13.4	2

*See Table 2

TABLE 2—CORES CONTAINING RESIDUAL OIL

Core material	Brine resistivity, (ohm-m)	Wetting agent used*	Core resistivity before contact with reverse-wetting agent (ohm-m)	Core resistivity after contact with reverse-wetting agent (ohm-m)	Resistivity increase (per cent)
Berea sandstone (outcrop)	0.0435	A	1.24	2.15	73
Berea sandstone (outcrop)	0.0435	A	1.23	2.18	77
Berea sandstone (outcrop)	0.0435	A	1.20	3.14	162
Fused quartz	0.0435	A	0.28	0.73	160
Fused quartz	0.0435	A	0.28	0.65	130
Fused quartz	0.0435	A	0.29	0.93	220
Shaly sand (Seeligson field)	0.0435	A	0.94	1.72	80
Shaly sand (Borregas field)	0.0435	A	1.13	2.14	89
Berea sandstone	0.987	B	31.6	48.3	56
Berea sandstone	0.987	C	31.3	80.3	156
Berea sandstone	0.987	D	30.5	57.1	87
Berea sandstone	0.987	E	32.2	61.2	90
Berea sandstone	0.987	F	30.2	42.2	40
Limestone (Picton field)	1.00	G	28.4	55.5	96
Limestone (Picton field)	1.00	G	39.4	86.4	119
Leuders lime (quarry)	1.00	G	21.2	42.5	100
Leuders lime (quarry)	1.00	G	20.6	30.6	49
Berea sandstone	1.00	G	28.4	111	292
Berea sandstone	1.00	G	30.4	82.5	171

*A—Octadecyl amine acetate
B—Cetyl dimethyl amine acetate
C—Tetrosan (a cationic surface active agent sold by Onyx Oil & Chemical Co., Jersey City, N. J.)
D—Primene JM-T acetate (prepared from a tertiary octylamine sold by Rohm & Haas)
E—Arquad 2-C (dicoco dimethyl ammonium chloride; sold by Armour Chemical Div., Chicago, Ill.)
F—Amine acetate prepared from Primene 81-R (an amine sold by Rohm & Haas containing a 12-carbon and 15-carbon chain)
G—Armac CD-50 (a mixture of acetic acid salts of fatty amines; sold by Armour Chemical Div., Chicago, Ill.)

sistivity could be measured while flooding was in progress. Brine containing reverse-wetting agent was then flooded through the core at a rate of one pore volume every 140 seconds. Resistivity measurements were made periodically.

Results of this test are shown graphically in Fig. 1. There appeared to be no appreciable time lag between time of contact with the agent and the subsequent resistivity increase.

Shown in Fig. 1 are transient effects during periods of no flow. Resistivity under static conditions increased appreciably; it was 43 per cent higher than resistivity during flow. To elucidate this unexpected transient behavior, another experiment was conducted with a water-wet Berea core containing residual kerosene in which the static and dynamic resistivities were determined when brine containing no reverse-wetting agent was passed through the core. For the latter case it was observed that the static value was only 13 per cent higher than the dynamic value. Hence, it was concluded that alteration of wettability leads to a considerable magnification of this transient effect.

As a result of this investigation it was concluded that, for all practical purposes, the resistivity increase associated with reversal of wettability is attained almost instantaneously after introduction of the agent.

Persistence of Induced Resistivity Increase

To determine length of time that the resistivity increase brought about by a reverse-wetting agent persists, use was made of a Berea sandstone core containing brine and residual kerosene. Resistivity of this core was measured. The core was then flooded with a few pore volumes of a solution of 2 per cent coco amine acetate in brine, after which core resistivity was measured periodically for several days.

Results of this experiment are shown in Fig. 2, where core resistivity is plotted as a function of elapsed time. The resistivity increase in Berea sandstone associated with reverse wetting persisted for at least 79 days.

Another factor affecting persistence was studied, namely the influence of prolonged flushing with brine containing no additive on the resistivity increase induced by introduction of a reverse-wetting agent into an oil-bearing rock. A Berea core containing 1-ohm-m brine and residual kerosene was treated with reverse-wetting agent and then flushed with a copious volume of brine containing no agent. Core resistivity was measured periodically. Results of resistivity measurements are shown in Fig. 3 as a function of the amount of brine flushed through the core. After 74 pore volumes of brine had been flowed through the core resistivity was reduced from a high of 99 to 64 ohm-m, which was still twice the resistivity before wettability of the core was altered.

These observations indicate that increased resistivity resulting from introduction of a reverse-wetting agent persists over long periods of time, and that the effect persists even after extended flushing of treated rock with an agent-free solution.

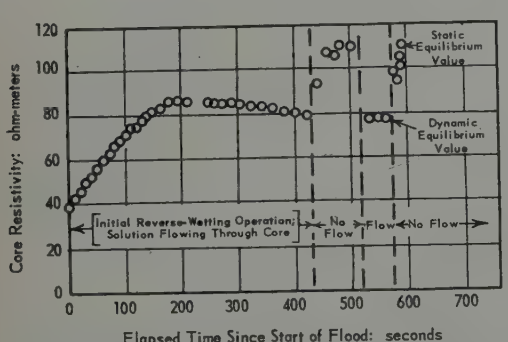

Fig. 1—Resistivity of Berea Core Containing Residual Oil (A) While Flowing Reverse-wetting Solution Through Core, and (B) During Periods of No Flow.

Effect of Type of Hydrocarbon on Resistivity Increase

As a matter of convenience, all experiments discussed previously employed kerosene as the residual hydrocarbon phase. To determine whether the same results could be obtained with crude oil as the residual hydrocarbon, an experiment was performed using crude oil from the Conroe field, Montgomery County, Tex., in a Berea sandstone core. Treatment of the core, which contained brine and Conroe crude at residual oil saturation, with a reverse-wetting agent resulted in a threefold resistivity increase; this demonstrated that results obtained with kerosene should be applicable to reservoir rocks which contain crude oil.

No experiments comparable to those described in preceding sections were performed in which gas was substituted for oil as the residual hydrocarbon phase. In auxiliary experiments, however, visual observation was made of the wettability behavior of glass surfaces treated by reverse-wetting agents and it was evident that reverse-wetting agents in aqueous solution produce preferential gas wettability. It is thus likely that treatment of a reservoir rock containing brine and gas at residual saturation would result in increased resistivity.

Effect of High Temperature on Resistivity Increase

All experiments discussed previously were conducted at room temperature, approximately 70°F. To examine effect of increased temperature on resistivity increase, a Berea core containing brine and residual kerosene was flushed with several pore volumes of a 1 per cent solution of coco amine acetate in brine. Resistivity of the core was measured. The core was then placed in a container filled with reverse-wetting solution and heated to approximately 150°F for five days. Resistivity at the end of this period was essentially the same as that before heating, indicating that no deleterious effects on the resistivity increase were introduced by higher temperature.

THEORY

Through laboratory experience we may postulate a mechanism which accounts for the increase in resistivity of an oil-containing porous rock on addition of a reverse-wetting agent.

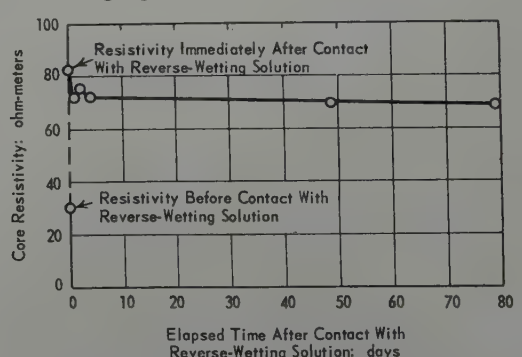

Fig. 2—Persistence of Reverse-wetting Resistivity Increase.

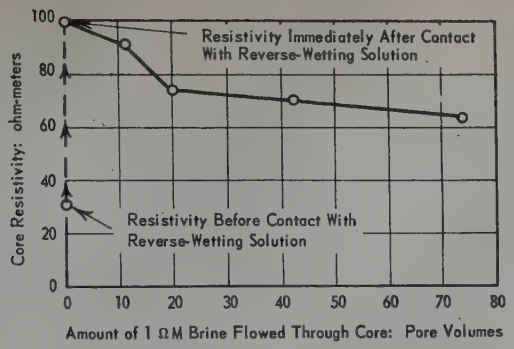

FIG. 3—EFFECT OF BRINE FLOODING ON INDUCED RESISTIVITY.

The increase in resistivity is caused by a redistribution of the liquids within the pores brought about by a change in the wetting of the surfaces (see Fig. 4).

Fig. 4a shows a cluster of sand grains containing brine and a residual oil globule. Since brine is the wetting phase and oil the non-wetting phase, a thin film of water separates the oil globule from the nearest sand grains. When a potential gradient is applied across this assemblage, current flows in the maze of capillaries containing brine.

After passage of the reverse-wetting solution, the capillaries originally filled with brine are coated with a layer of adsorbed ions which render sand surfaces oil wet. The oil globule is now able to grasp, so to speak, the sand grains, and moves into a new equilibrium configuration consistent with the new wettability condition. Such a configuration is shown in Fig. 4b. Now the oil can more sharply restrict the flow of current in the capillaries than it could when the matrix was completely water wet. Thus, electric resistivity is increased.

In a shaly sample the adsorption of a cationic agent upon the shale surfaces may sharply reduce the effect of double-layer conductivity. This may increase the resistivity of the sample slightly. However, laboratory work has shown that the change caused by this phenomenon is small when compared to the change caused by reverse wetting in a similar sample containing an oil saturation.

FIELD TESTS

Since the laboratory investigation demonstrated that the resistivity of porous rock containing brine and oil at residual saturation could be increased several-fold by addition of a reverse-wetting agent, plans were made for field testing the technique of locating hydrocarbon-bearing strata by use of a reverse-wetting agent.

Two ways in which the reverse-wetting agent might be used were considered. One procedure consisted of (1) drilling through a suspected hydrocarbon-bearing zone with ordinary mud, (2) running an appropriate log, (3) displacing the original mud with a new mud or liquid containing a reverse-wetting agent, (4) disturbing the filter cake on the wall of the hole so that the agent might penetrate porous strata, and (5) running a second log. Strata containing hydrocarbons were expected to exhibit an appreciably higher resistivity after introduction of the agent.

Another method of employing the reverse-wetting technique consisted of adding the agent to the fluid used during drilling into a zone which might contain hydrocarbons. In this case there is not available for comparison a log made without the use of the reverse-wetting agent, but on the other hand, the high resistivity in-

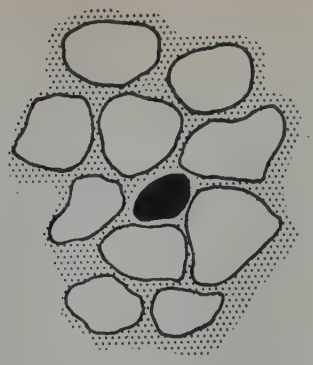

(a) Residual Oil Globule in Water-Wet Sand

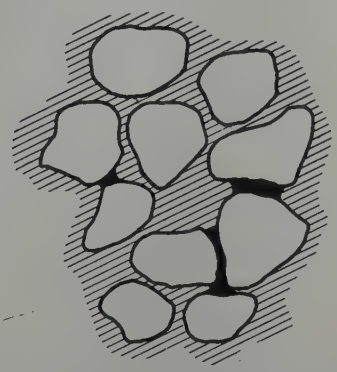

(b) New Equilibrium Configuration of Residual Oil After Influx of Reverse-Wetting Solution

FIG. 4—MECHANISM OF REVERSE-WETTING RESISTIVITY INCREASE.

duced by the agent in the invaded zone should produce characteristic features on short-spacing logs.

Use was made of both of the foregoing methods in testing reverse-wetting logging in the field.

A test conducted in California followed the procedure employing before and after logging. In this test the well was drilled to total depth with natural mud; then the zone of interest was reamed with a reverse-wetting mud. Logs were run both before and after using the special mud.

A test was conducted in North Texas with the "single-stage" procedure. In this procedure the reverse-wetting agent was added to the mud used in drilling the zone of interest. These two tests are described in the following sections.

CALIFORNIA FIELD TEST

The California well chosen for a field test was to be completed in an interval that had produced in the area for a number of years. In previous wells drilled in this field, great difficulty was experienced in delineating the zones which would produce oil in commercial quantities and those which would produce only water. The electric logs were of limited use in this delineation because throughout the zone the water saturations calculated from data obtained with the induction and Micro-Log ranged from 75 to 100 per cent. It was hoped that completely oil-free sands could be detected by use of the reverse-wetting logging technique.

PROCEDURE

The test well was a field development well scheduled for a total depth of 7,450 ft. The well was drilled to 6,600 ft with an 8¾-in. bit. At 6,600 ft hole size was reduced to 7⅝ in., and the well was drilled to the total

depth of 7,450 ft. At this point electric logs were run in the natural water-base mud used to drill the well.

Following logging of the well, the natural mud was displaced with a starch-stabilized mud which was weighted with calcium carbonate. This mud would accommodate the reverse-wetting agent. The mud filtrate was designed to have approximately the same resistivity properties as filtrate from the original mud. To effect complete invasion of the reverse-wetting mud filtrate into the formation of interest, the 7⅝-in. hole was reamed with an 8¾-in. bit. (Auxiliary tests in other wells indicated uniform invasion could not be obtained by disturbing the original mud cake with cementing scratchers in the presence of the reverse-wetting mud.) Following the reaming operation electric logs were run again. Since the reverse-wetting mud was designed to have nearly the same resistivity properties as the natural mud used to drill the hole, the before and after logs could be compared directly.

RESULTS

The MicroLog obtained after reaming with reverse-wetting mud was radically different from that obtained before reaming. Portions of both MicroLogs are shown in Fig. 5. Whereas the before log was normal with positive separation, i.e., lower resistivity on the 1 × 1 in. micro-inverse curve than on the 2-in. micro-normal curve, the after log revealed large increases in resistivity and negative separation in every permeable zone. (The negative separation, i.e., higher resistivity on the 1 × 1 in. micro-inverse curve, suggests the adsorption of the reverse-wetting agent in the form of a thin annulus immediately adjacent to the wellbore.) In addition, the resistivities shown on both the 1- and 2-in. electrode-spacing curves were substantially larger after reaming with the reverse-wetting mud. Resistivity increases indicated by the 2-in. curves ranged from 80 to 250 per cent. Since a substantial increase in invaded-zone resistivity indicates presence of residual oil in the invaded zone, it was concluded that every zone within the reamed section of the hole contained some oil. This conclusion was confirmed by examination of all sidewall cores from the reamed interval.

Fig. 6 shows a comparison of the MicroLaterologs obtained before and after reaming with the reverse-wetting mud. As was the case with the MicroLog, the after MicroLaterolog indicated increased invaded-zone resistivity in every permeable stratum within the reamed section of hole.

An unexpected result was observed when the before and after potential curves, also shown in Fig. 6, were compared. It was observed that the SP curve was developed in a normal manner when the before logs were run in the original mud. The SP curve obtained on the after logs, however, showed no development. The curve started at the shale base line and remained essentially at that value throughout the interval which was reamed with reverse-wetting mud. Upon entering the hole above the reamed section, the SP curve resumed a normal appearance. The reason for this behavior is not clear; however, auxiliary experiments suggest the depressed potential may result, in part, from a change in sign of the streaming potential when the filtrate flows through the cake of the special mud. Since the chemical used was a cationic surface-active agent, adsorption on the clay surfaces could produce this effect.

North Texas Field Test

In the North Texas field chosen for investigation of the single-stage procedure, the productive sand is extremely difficult to delineate by use of electric logs. The potential is usually not well developed, and the resistivity of the producing sand is virtually the same as that of overlying and underlying shales. Also, water saturations of above 60 per cent are calculated from induction and MicroLogs run in wells in the area. The oil sand is thus not one which would normally be recognized as a productive member from examination of the usual electric logs alone.

Because the productive zone is usually not recognizable from normal electric log data, this field presented an ideal opportunity for testing reverse-wetting logging. The decision was made to incorporate the agent in the mud used in coring the pay and to evaluate results by comparing logs made in the test well with logs of nearby wells drilled with ordinary mud.

PROCEDURE

The test well was drilled with a conventional water-

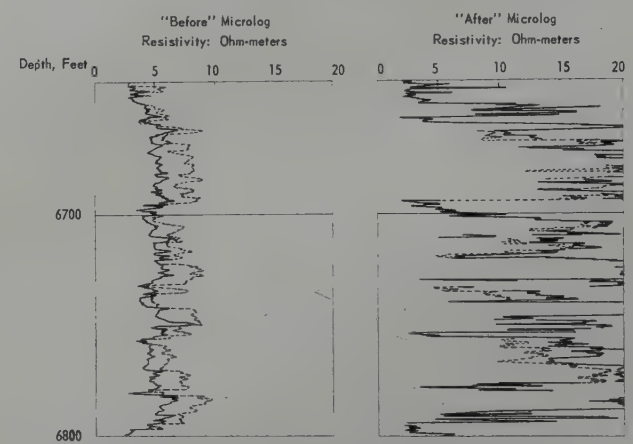

Fig. 5—Comparison of Before and After MicroLogs, California Field Trial.

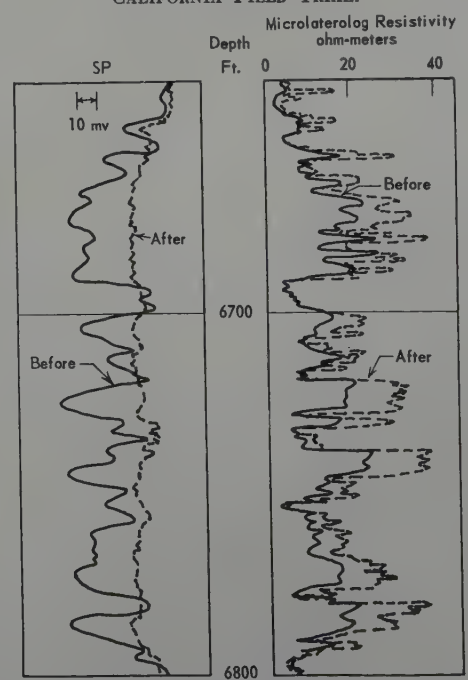

Fig. 6—Comparison of Logs Obtained Before and After Reaming with Reverse-wetting Mud, California Field Trial.

base mud. Just above the producing horizon a special mud containing the reverse-wetting agent was placed in the hole. The mud was composed of ground oyster shells, starch and guar flour in fresh water; the reverse-wetting agent was coco amine acetate added in sufficient amount to yield a concentration of about 4 per cent. (This particular wetting agent, though effective, produced a severe foaming problem.) Care was taken to ensure that this mud had very nearly the same resistivity as muds used in drilling other wells in the field. The pay section was cored with this mud in the hole, using a diamond core barrel. Finally, an induction-electric log, a MicroLog, and MicroLaterolog were run in the well.

RESULTS

Fig. 7 presents a comparison of the micro-inverse curves from the test well and the two offset wells. The micro-inverse curves were used because they demonstrate most clearly resistivity in the zone very close to the wellbore. As shown in Fig. 7, the micro-inverse curve shows a marked increase in resistivity opposite the productive zone of the test well. In comparison, the micro-inverse curves of offset wells do not indicate a high resistivity.

Fig. 8 shows a comparison of the MicroLaterolog run in the test well and resistivity values obtained from treated and untreated cores from the producing interval of the test well. To obtain measurements on the cores, it was first necessary to restore the water-wet condition which existed before drilling with the special mud. A solution was injected into the cores to restore water wetness. They were then flushed with kerosene and flooded to residual oil with brine. Once residual oil-brine saturation was established, resistivities were measured. The cores were rendered oil wet with the brine solution containing reverse-wetting agent, and the resistivity measurements repeated. The brine solution used was adjusted to have a resistivity close to the resistivity of the filtrate from the field mud at bottom-hole temperature. As shown in Fig. 8 the MicroLaterolog resistivity curve falls between the before and after resistivity values obtained with cores from the test well. This position of the curve is expected because the reverse-wetting agent is adsorbed on the surfaces of sand nearest the wellbore, and the region farther in the formation will approach normal invaded-zone resistivity. Therefore, the MicroLaterolog records a resistivity somewhere between the two extremes.

In view of results obtained with the MicroLog, the

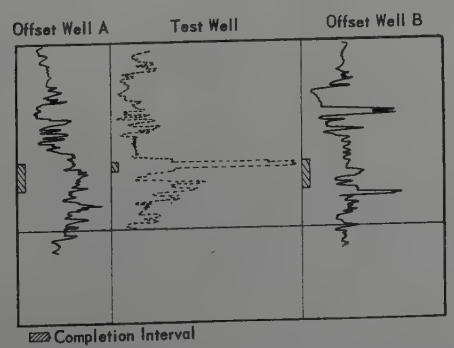

FIG. 7—NORTH TEXAS FIELD TEST, 1 × 1 IN. MICRO-INVERSE CURVES.

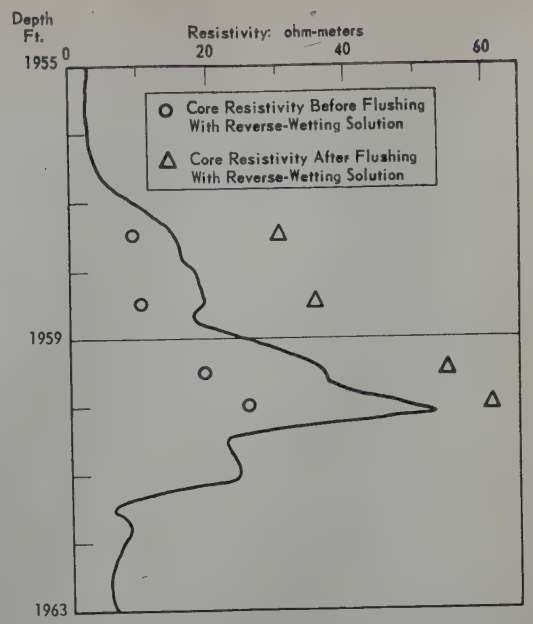

FIG. 8—COMPARISON OF MICROLATEROLOG WITH BEFORE AND AFTER RESISTIVITY VALUES OBTAINED WITH CORES FROM TEST WELL, NORTH TEXAS FIELD TRIAL.

MicroLaterolog and cores from the test well, it is concluded that the high resistivity observed in the pay of the test well was attributable to use of the reverse-wetting agent.

CONCLUSIONS

1. It has been demonstrated in the laboratory that addition of a reverse-wetting agent to a water-wet porous rock containing brine and oil at residual saturation results in a marked increase in resistivity of the rock.

2. Field tests have demonstrated that resistivity of oil sands, as measured by short-spacing logs, can be increased materially by introduction of a reverse-wetting agent.

3. The reverse-wetting logging technique may be particularly valuable in identifying hydrocarbons in thin beds, in highly invaded formations, in shaly formations and in formations containing high water saturations.

4. This logging technique may be useful in determining the in situ wettability of earth formations.

ACKNOWLEDGMENT

Significant contributions were made by a number of people who assisted in many phases of the development work and in the successful conduct of the field experimentation. Among these were J. S. Osoba, F. M. Perkins, Jr., C. L. Prokop and R. A. Salathiel.

REFERENCES

1. Richardson, J. G., Perkins, F. M., Jr., and Osoba, J. S.: "Differences in Behavior of Fresh and Aged East Texas Woodbine Cores", *Trans.* AIME (1955) **204**, 86.
2. Keller, G. V.: "Effect of Wettability on the Electrical Resistivity of Sand", *Oil and Gas Jour.* (Jan. 5, 1953) **51**, 62.
3. Licastro, P. H. and Keller, G. V.: "Resistivity Measurements as a Criterion For Determining Fluid Distribution in the Bradford Sand", *Prod. Monthly* (May, 1953) **17**, 17.

★★★

A Laboratory Study of Oil Recovery by Solution Gas Drive

L. L. HANDY
MEMBER AIME

CALIFORNIA RESEARCH CORP.
LA HABRA, CALIF.

INTRODUCTION

Many differences can be imagined between gas-oil flow in which the gas is supplied at the face of the core and gas-oil flow in which the flowing gas was originally dissolved in the oil. If capillary pressure characteristics and flow requirements control gas saturation distribution, the gas would be expected to be located at preferred sites within the porous medium as determined by pore sizes. On the other hand, during solution gas drive the gas first appears as bubbles through a nucleation process. Nothing in self-nucleation theory specifies at which sites the first bubbles should be formed. In all probability they will be randomly distributed throughout the porous medium. Furthermore, it is not at all certain that even at low rates of production the gas will redistribute itself after nucleation to the channels normally occupied by gas in simple gas flow.

Stewart, *et al*[1], have shown that at least for some limestone samples, oil recoveries could not be predicted for all rates of production using any one set of relative gas and oil permeabilities. An important factor in controlling recoveries during solution gas drive was the rate of bubble formation, higher rates giving higher recoveries. Stewart, *et al*[1], attributed the increase in recovery to a better distribution of the gas phase in heterogeneous limestone samples than is obtained by simple external gas drive. Differences in recovery from these causes were not reported for sandstone cores.

In the experiments to be reported here, oil recovery, pressure and producing GOR history were measured during solution gas drive for a 5-ft sandstone core. The results were compared with predictions from the Muskat method for computing solution gas-drive behavior using external gas-drive relative permeability. The effects of changing the rate of production and oil viscosity were studied.

At high laboratory rates of average pressure decline, two observations were made which would not have been predicted by Muskat's depletion theory: (1) oil recovery increased with increasing rate of production for a given viscosity oil, and (2) oil recovery increased with increasing oil viscosity for a given high rate of production. Both of these observations are explained as consequences of diffusion control of gas saturations superimposed on the normal gas-oil flow requirements. Furthermore, discontinuous gas phase flow appears to be significant during solution gas drive.

The laboratory tests were performed at rates of average pressure decline many times greater than the maximum possible rate of average pressure decline in an actual oil field. It is, therefore, not possible to draw any direct conclusions regarding the effect of rate on recovery for the solution gas-drive mechanism under actual field conditions. However, at the lower laboratory rates, recoveries were nearly independent of rate and could be predicted by the Muskat method, using external gas-drive relative permeability data. These results suggest that at normal oilfield rates the effect of rate on recovery for the solution gas-drive mechanism is negligible.

EXPERIMENTAL PROCEDURES

The core material for the pressure depletion studies was Bandera sandstone from an outcrop in the Mid-Continent. This sandstone was selected because of its low permeability (about 10 md), which would permit the development of substantial pressure gradients in the core at moderate flow rates. The core was 5-ft long and 2-in. in diameter. Its properties are listed in Table 1. Relative gas-to-oil permeability ratios were measured by an external gas-drive method[2]. The results are shown for a short 2-in. core and for the 5-ft core in Fig. 8.

Oils used in the pressure depletion experiments were kerosene and a highly refined white oil (standard white oil No. 3) with gas-free viscosities of 1.8 and 25 cp, respectively. The gas was a naturally occurring methane from Gough field, Inglewood, Calif. The oil viscosities, gas solubilities and formation volume factors are plotted as functions of pressure at 75°F in Figs. 1 and 2. Methane viscosities and compressibilities were obtained from the literature[3,4].

A core mounting was required which could withstand up to 2,500 psi internal pressure. This was obtained by first encasing the core completely in a plastic resin (Scotch Cast, manufactured by Minnesota Mining & Manufacturing Co.) The plastic covered core was then inserted into a steel pipe equipped with screw caps so that the plastic coating could be pressured from

TABLE 1—PROPERTIES OF BANDERA SANDSTONE CORE

Oil permeability	7.41 md
Porosity	16.0 per cent
Pore volume	440 cc
Length	152 cm
Cross-sectional area	18.1 cm^2
Water saturation	0

Original manuscript received in Society of Petroleum Engineers office Jan. 16, 1957. Revised manuscript received June 26, 1958.
[1]References given at end of paper.

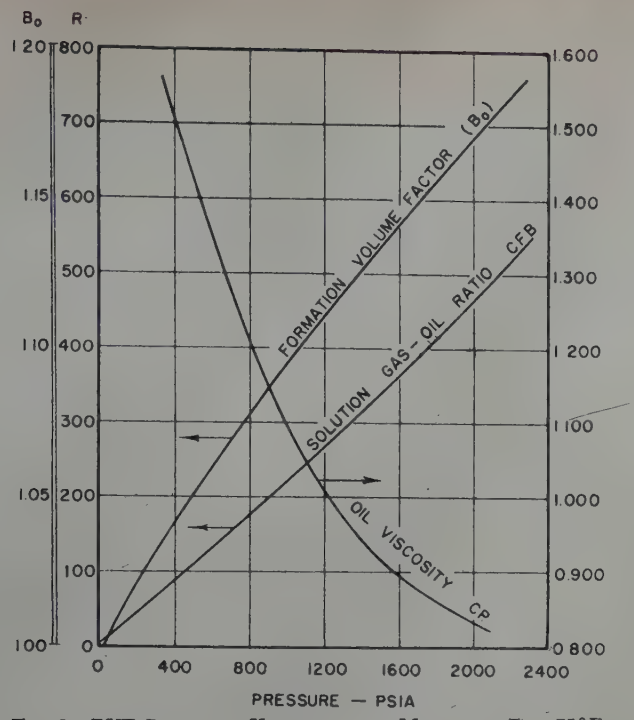

FIG. 1—PVT DATA FOR KEROSENE AND METHANE, $T = 75°F$.

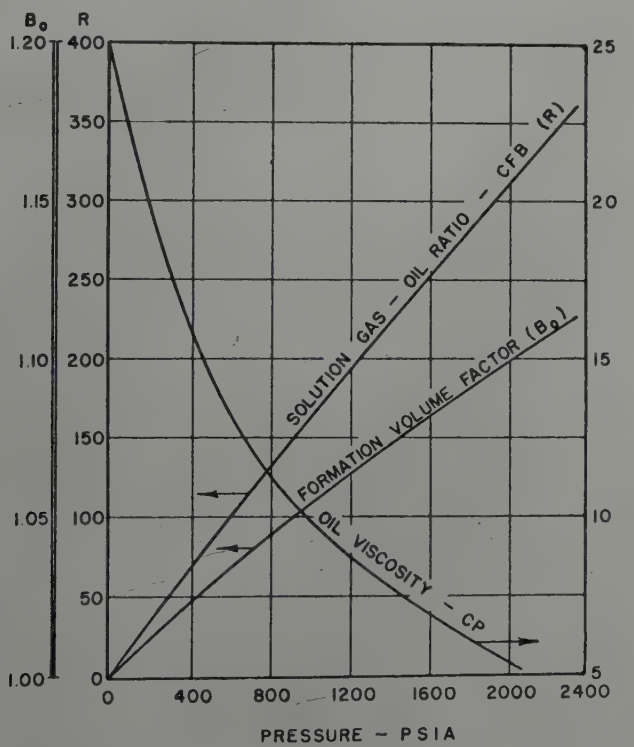

FIG. 2—PVT DATA FOR NO. 3 WHITE OIL AND METHANE, $T = 75°F$.

the outside. The annular space between the plastic mounted core and the pipe was filled with oil which could be pressured at 3,000 psig. Inlet and outlet connections and 11 pressure taps were made through the pipe using high pressure fittings. O-rings were used for pressure seals where required.

The core was saturated with oil by evacuating and then flushing with methane. The methane was displaced by flooding with oil until a residual methane saturation was obtained. At that time the oil pressure was increased to 2,000 psig to dissolve the residual methane. A Grove back-pressure regulator at the downstream end of the core was set to maintain 2,000-psig pressure in the core and flooding with dead oil continued. When the core was completely saturated with oil, gas-saturated oil was flowed through the core at pressures greater than the bubble point until all of the dead oil was displaced, as determined by the producing GOR. The core was ready then for the pressure depletion experiments.

Two methods of producing oil were used; either the oil was produced at a constant volumetric rate, or the downstream pressure was reduced at a constant rate. For most of the experiments downstream pressure was held constant after it reached approximately one-tenth of the original bubble-point pressure. Measurements made during the depletion experiments were of cumulative gas and oil production and of pressures at the 11 pressure taps, all as functions of time.

EXPERIMENTAL RESULTS

The results of the pressure depletion experiments are summarized in graphs of average pressure vs cumulative produced oil and producing GOR vs cumulative oil. In each case a comparison is shown for observed solution gas-drive behavior with that calculated using the Muskat method for computing solution gas-drive performance[5]. External gas-drive k_g/k_o data for the long core were used in the calculations.

Average pressure, as a function of oil recovery in per cent of original stock-tank oil in place, is shown in Fig. 3 for 1.8-cp oil. At the highest rate, 19.6 per cent of the original stock-tank oil was recovered. At the two lower rates, recovery was about 15.2 per cent of the original stock-tank oil. For the same terminal pressure the recovery predicted by the Muskat method, using external gas drive k_g/k_o data, was 15.2 per cent. The calculated pressures were, however, as much as 300 psi greater than the observed pressures during early

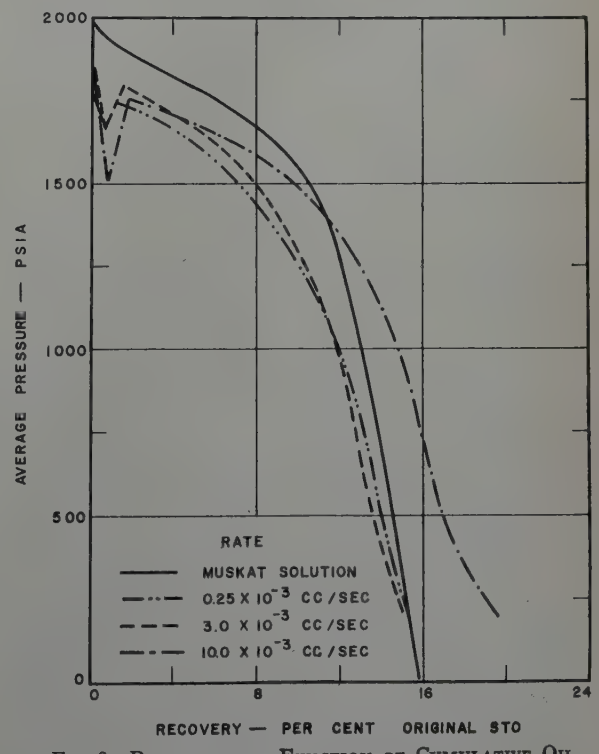

FIG. 3—PRESSURE AS A FUNCTION OF CUMULATIVE OIL RECOVERY, 1.8-CP OIL.

phases of production. The difference is partially explained by PVT non-equilibrium, which was known to exist during the experiments. Material balance calculations showed that the amount of gas actually released from solution in the oil was substantially less than equilibrium PVT data indicated it should be for the existing average core pressure.

The instantaneous GOR's as functions of cumulative produced oil in per cent original stock-tank oil are shown in Fig. 4 for 1.8-cp oil. Until 4 per cent of the original stock-tank oil was recovered, the producing GOR decreased for all runs. At high depletion rates, the producing GOR did not exceed the original GOR (the ratio at zero recovery) until 11 per cent of the original stock-tank oil was recovered. The producing GOR reached a maximum and decreased toward the end of depletion for all runs with kerosene.

A greater variation in oil recovery as a function of producing rate was observed for white oil than for kerosene. Average pressure vs cumulative produced oil is plotted in Fig. 5. Two methods for controlling rates were used in the white oil experiments. In one the oil production rate was held constant; in the other, the rate of pressure decline at the downstream end of the core was maintained constant. (For comparison, the initial producing rate was about 1.0×10^{-2} cc/sec when the pressure was reduced at a rate of 2.0 psi/sec.) At constant rate of pressure decline the oil production rate is highest during the early part of the run and decreases as the run progresses. A maximum recovery of 22.8 per cent was obtained at the highest producing rate. At the lowest producing rate the recovery was 9.7 per cent of the original stock-tank oil. Observed depletion behavior at the lowest rate was in close agreement with predicted behavior calculated by the Muskat method.

Instantaneous GOR's, plotted against cumulative produced oil, are shown in Fig. 6. The curve for a production rate of 3.0×10^{-3} cc/sec illustrates a phenomenon observed in several of the depletion runs. The instantaneous gas-oil ratio reached a maximum at the same time that the downstream pressure reached its minimum. When the downstream pressure was no longer being reduced, the GOR declined abruptly and then continued its rise to a new maximum. A maximum early in the run was also observed for the highest rate in which the reduction of the downstream pressure was at a rate of 2.0 psi/sec. The maximum occurred much earlier in the run at the high rate but coincided with reaching the minimum in the downstream pressure.

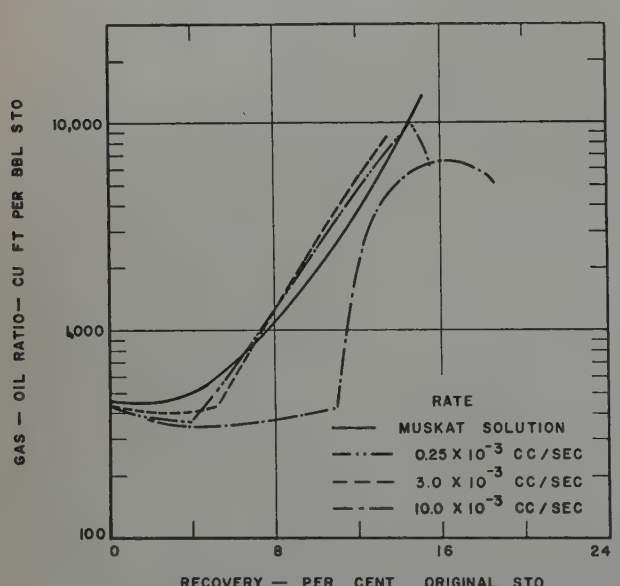

FIG. 4—INSTANTANEOUS GOR AS A FUNCTION OF CUMULATIVE OIL RECOVERY, 1.8-CP OIL.

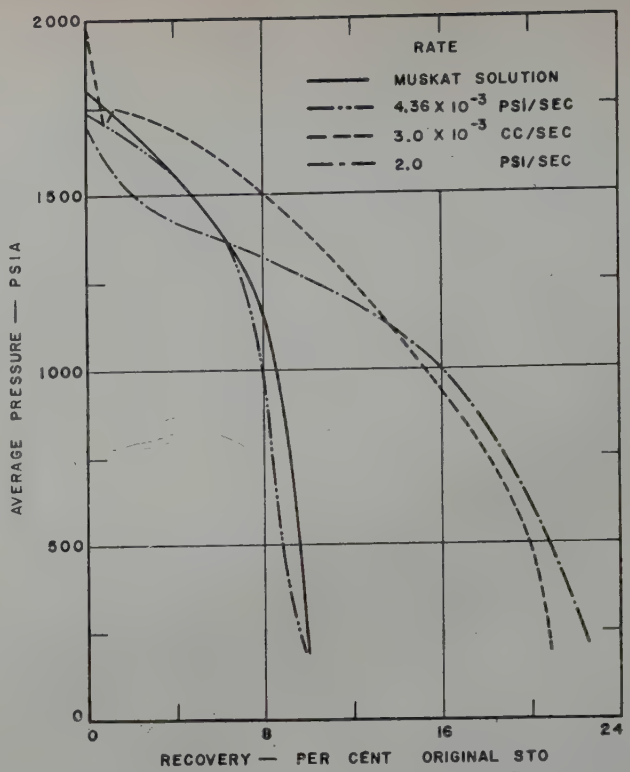

FIG. 5—AVERAGE PRESSURE AS A FUNCTION OF CUMULATIVE OIL RECOVERY, 25-CP OIL.

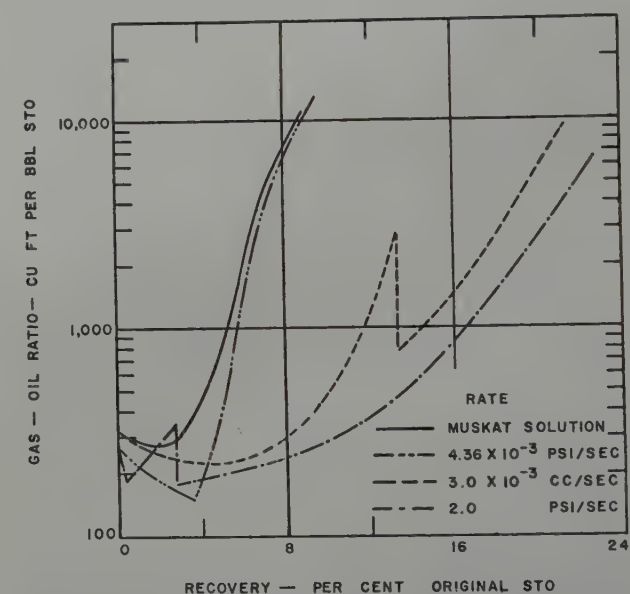

FIG. 6—INSTANTANEOUS GOR AS A FUNCTION OF CUMULATIVE OIL RECOVERY, 25-CP OIL.

The effect of rate and oil viscosity on cumulative oil recovery is illustrated in Fig. 7. Total produced oil in per cent original stock-tank oil is plotted vs initial producing rate in per cent original stock-tank oil per day. For both kerosene and white oil, recovery increased with rate at the higher rates, but showed evidence of becoming rate-independent at low rates. All rates of pressure decline were greater than field rates of average pressure decline.

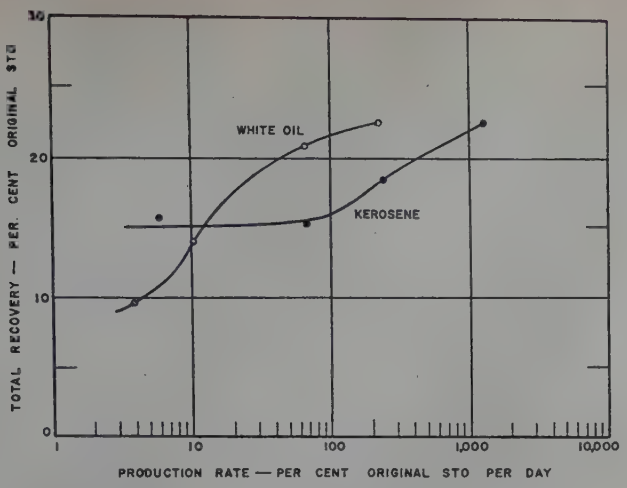

FIG. 7—EFFECT OF PRODUCTION RATE ON TOTAL RECOVERY.

Another method for comparing observed with predicted depletion behavior is to compare k_g/k_o curves for the core, computed from production and pressure data, with k_g/k_o curves measured by other methods. The permeability ratios were calculated using the same assumptions that are used in calculating field k_g/k_o curves, namely, that no saturation gradients or pressure gradients were present in the core. In Fig. 8 the field-type k_g/k_o's are compared with external gas-drive permeability ratios measured on the long core and on small cores of the same core material. The agreement was very good for the slow rate experiments, but at higher rates considerable divergence was observed.

Some qualitative evidence of the effect of gas saturation, rate of pressure decline and diffusion coefficients on PVT non-equilibrium was obtained for the Bandera core. At any time during the depletion process a material balance calculation could be made. The amount of gas actually released from solution then could be compared with that which would have been released at the existing core pressure if equilibrium had existed.

In Fig. 9, supersaturation (psi) is plotted against average gas saturation for three depletion runs; kerosene at initial production rates of 1.0×10^{-2} and 3.0×10^{-3} cc/sec, and No. 3 white oil at an initial production rate of 3.0×10^{-3} cc/sec. Supersaturation is defined here as the difference between the equilibrium pressure corresponding to the observed solution GOR computed by material balance and the observed average pressure. If appreciable pressure gradients were present in the core, supersaturation might have differed appreciably from one end of the core to the other, but no measure of this variation was possible. Supersaturation reached a maximum after nucleation at about 15 per cent average gas saturation in the kerosene runs. This maximum corresponded to the maximum rate of pressure decline required to maintain the initial flow rate. No such maximum was observed for the No. 3 white oil because the downstream pressure reached its minimum early in the depletion process.

A PROPOSED SOLUTION GAS-DRIVE MECHANISM

Deviations from pressure depletion theory which a postulated mechanism of solution gas-drive should explain are as follows: (1) higher oil recoveries at high producing rates, (2) increasing oil recovery with increasing oil viscosity at a given high initial producing

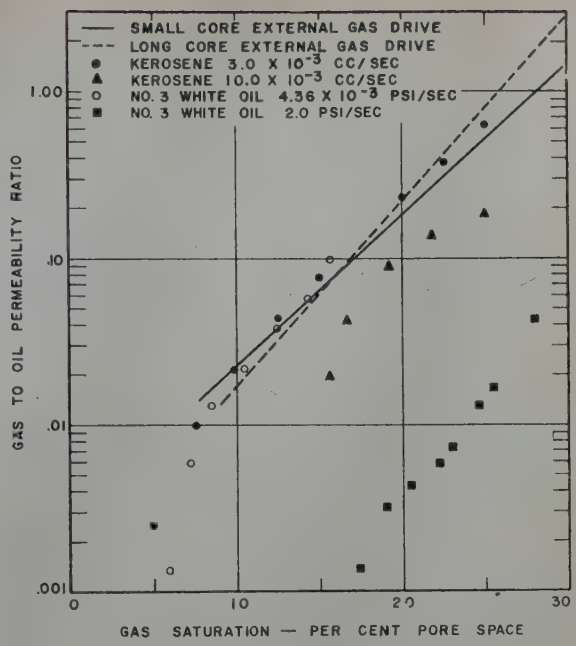
SMALL CORE EXTERNAL GAS DRIVE
LONG CORE EXTERNAL GAS DRIVE
KEROSENE 3.0 X 10⁻³ CC/SEC
KEROSENE 10.0 X 10⁻³ CC/SEC
NO. 3 WHITE OIL 4.36 X 10⁻³ PSI/SEC
NO. 3 WHITE OIL 2.0 PSI/SEC
GAS TO OIL PERMEABILITY RATIO
GAS SATURATION — PER CENT PORE SPACE

FIG. 8—COMPARISON OF FIELD-TYPE GAS-OIL PERMEABILITY RATIOS WITH EXTERNAL GAS-DRIVE RATIOS.

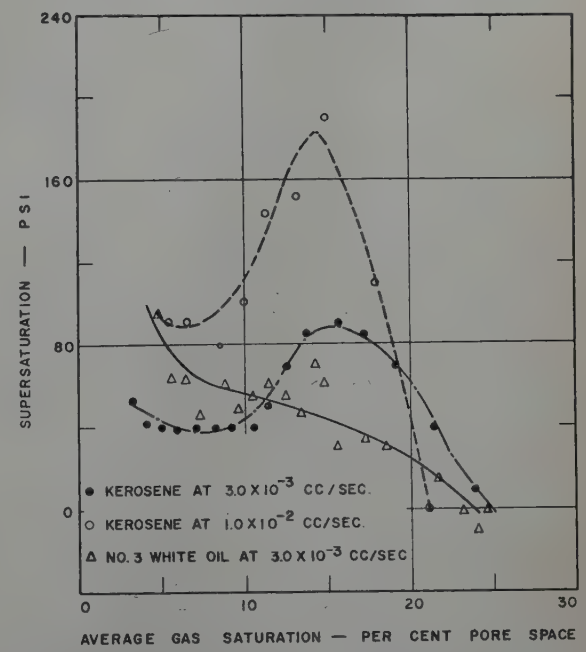
SUPERSATURATION — PSI
KEROSENE AT 3.0 X 10⁻³ CC/SEC.
KEROSENE AT 1.0 X 10⁻² CC/SEC.
NO. 3 WHITE OIL AT 3.0 X 10⁻³ CC/SEC
AVERAGE GAS SATURATION — PER CENT PORE SPACE

FIG. 9—SUPERSATURATION AS A FUNCTION OF GAS SATURATION DURING PRESSURE DEPLETION.

rate, and (3) abrupt changes in producing GOR when the pressure is stabilized at the downstream end of the core after a period of declining pressures.

A mechanism can be proposed which will explain qualitatively the experimental observations. The data show that nucleation and diffusion effects considerably increase the complexity of solution gas drive compared to external gas drive. In external gas drive the fluid distribution within the porous medium must adjust only to satisfy the requirements of flow capacity and capillary pressure equilibrium. Solution gas drive requires in addition that the gas phase be distributed sufficiently to provide for an adequate rate of diffusion of dissolved gas through the oil to a gas-oil interface. A gas saturation sufficient for the existing gas-oil flow rate may not be sufficient for diffusion of dissolved gas.

PVT Non-equilibrium and Gas Saturations

If a porous medium completely saturated with live oil is considered, nucleation theory predicts that the pressure must be reduced appreciably below the bubble point before any gas bubbles appear. The extent of supersaturation before a free gas phase is formed depends primarily on the presence or absence of nucleating agents in the oil or on the rock surfaces. In the absence of foreign nuclei the theory of self-nucleation indicates that the rate of bubble formation is a function of interfacial tension, contact angle and the degree of supersaturation. A review of self-nucleation theory has been presented by La Mer[6] and its application to reservoir fluids discussed by Hunt and Berry[7].

As soon as a gas bubble appears within the porous medium, diffusion effects become operative. Diffusion tends to reduce supersaturation and to decrease the probability of forming new bubbles. Eventually a condition is reached in which gas is well distributed throughout the porous medium and at no site is the degree of supersaturation great enough to permit significant nucleation. The gas saturation required to eliminate nucleation depends primarily on three factors: (1) rate of pressure decline, (2) the diffusion coefficient of the gas dissolved in the oil, and (3) the degree of supersaturation required for significant nucleation.

Gas Flow During Solution Gas Drive

Although Hunt and Berry developed equations to predict the number of bubbles formed and the average supersaturation during pressure depletion, they did not relate the result to gas-oil flow. In a simple multiphase-flow theory gas saturations are determined only by gas-oil flowing ratios and the capillary-pressure relationships. In the nucleation theory the gas saturation is generated by an entirely different mechanism. The saturation determined by nucleation and diffusion processes may, as a matter of fact, be quite different from that required for gas flow. If equations of the type proposed by Hunt and Berry are included with the usual equations for transient gas-oil flow, it becomes apparent that not all of these equations can be satisfied simultaneously when there is a high degree of supersaturation. Experimental results indicate that at high rates of pressure decline the gas flow equation is the equation that requires modification.

If nucleation and diffusion path length are the primary factors controlling the gas saturations, the apparent relative gas permeability will not be uniquely related to the observed saturations. The physical condition that could give rise to this situation is that at least part of the gas phase is not connected in continuous gas channels. Many observations, including microscopic examination of multiphase flow in sandstone thin sections, indicate considerable discontinuous gas phase flow in solution gas systems.

A possible mechanism for discontinuous gas phase flow is illustrated in Fig. 10. After nucleation occurs the new gas bubble grows by diffusion and expansion to a size too large to permit flow in the oil stream as illustrated in Panels 1 and 2 of Fig. 10. However, as the gas continues to accumulate the pressure in the gas phase increases over that in the oil until the gas breaks through the larger pore openings, as shown in Panel 3 of Fig. 10. Once an escape channel has been established the gas flows out more rapidly than it accumulates from diffusion and expansion. The pressure declines in the gas phase and oil imbibes into the

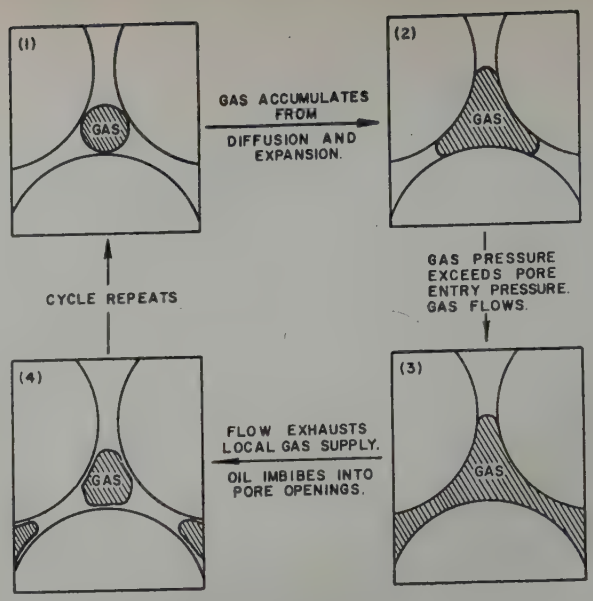

Fig. 10—Diagram of Intermittent Gas Flow in Solution Gas Drive.

pore openings interrupting the gas flow (Panel 4, Fig. 10). The residual gas again accumulates more gas and the cycle is repeated. The gas flow rate in a mechanism such as this would be related to the accumulation and discharge frequency of the isolated gas "islands" and not directly related to the gas saturation. With no change in gas saturation, apparent relative gas permeability may vary several-fold depending on the accumulation and discharge rate. Although the illustration is for a single pore, any single gas island may encompass several pores.

If the discontinuous gas-flow mechanism is correct, an explanation should be possible for the anomalous experimental observations. First, at high rates of pressure decline the development of a gas saturation would be diffusion controlled rather than flow controlled. Consequently, a higher gas saturation develops than that required to satisfy the flowing GOR. Increased gas saturations without increased flowing GOR's result in higher oil recoveries. High rates might be expected, therefore, to improve recovery. Second, the effect of oil viscosity must result, at least partly, from the lower diffusion coefficients for dissolved gas in higher viscosity oils. A decrease in the diffusion coefficients has an effect similar to that for an increase in the rate of pressure decline. Shorter diffusion path lengths are required for gas to evolve at the same rate. Again, higher gas saturations are required for a given flowing GOR, giving higher oil recoveries. For discontinuous gas phase flow, oil viscosity itself may have direct effects which have not been considered.

Finally, the abrupt decreases in the instantaneous GOR's with abrupt changes in production practice result from the accompanying changes in the rate of gas generation at the downstream end of the core. A free gas phase is generated both from gas expansion and from gas evolution from the oil. According to the discontinuous gas phase postulate, a decrease in the GOR can result from a sudden decrease in the accumulation and discharge rate for gas in the gas islands without any appreciable change in the gas saturation.

If the mechanism postulated here is correct, the theoretical calculation of pressure depletion behavior becomes extremely complex, particularly at the rates in-

volved in these experiments. A number of factors are required which are not easily determined. The relation between nucleation rate and the degree of supersaturation must be known. The diffusion coefficients must be determined. A parameter relating diffusion path length to gas saturation must be established. An exact solution of the problem is unlikely, but under certain producing conditions approximate solutions may be obtained which agree with experiments.

One of the conditions for which satisfactory solutions can be obtained is that of low producing rates. Fortunately, the low rates are the rates of interest in reservoir engineering. If the production rate is low, flow requirements control gas saturations for most of the producing history. At low rates, therefore, satisfactory agreement may be obtained between conventional theory and experiment.

CONCLUSIONS

In laboratory solution gas-drive experiments, high rates of oil production were found to increase oil recovery. The higher the oil viscosity the lower the production rate for which increased recovery was observed. All rates were much greater than average rates of pressure decline in oil reservoirs.

For the lower laboratory rates, still much greater than field rates, recovery was predicted satisfactorily using external gas-drive relative permeability data. These results indicate that for reservoir calculations external gas-drive data can be used to predict solution gas-drive behavior. The use of external gas-drive data has been recommended previously by Stewart, *et al.*

A mechanism is postulated for gas saturation development and for gas flow in solution gas systems. The basic premise of this hypothesis is that the gas phase is not continuous during much of the depletion process. But, although discontinuous, gas movement does occur. The additional complexity of solution gas drive is a result of original bubble formation in oil-filled pore spaces and diffusion of dissolved gas from the oil to the gas-oil interfaces after they are formed. The rate effects on recovery are explained as a result of diffusion control vs flow control of gas saturations.

REFERENCES

1. Stewart, C. R., Hunt, C. B., Jr., Schneider, F. N., Geffen, T. M. and Berry, V. J., Jr.: "The Role of Bubble Formation in Oil Recovery by Solution Gas Drives in Limestones", *Trans.* AIME (1954) **201,** 294.
2. Welge, H. J.: "A Simplified Method for Computing Oil Recovery by Gas or Water Drive", *Trans.* AIME (1952) **195,** 91.
3. Carr, N. L., Kobayashi, R. and Burrows, D. B.: "Viscosity of Hydrocarbon Gases under Pressure", *Trans.* AIME (1954) **201,** 264.
4. Olds, R. H., Reamer, H. H., Sage, B. H. and Lacey, W. N.: "Volumetric Behavior of Methane", *Ind. and Engr. Chem.* (1943) **35,** 922.
5. Muskat, M.: *Physical Principles of Oil Production,* McGraw-Hill Book Co., N. Y. (1949).
6. LaMer, V. K.: "Nucleation in Phase Transitions", *Ind. and Engr. Chem.* (1952) **44,** 1270.
7. Hunt, E. B., Jr. and Berry, V. J., Jr.: "Evolution of Gas from Liquids Flowing through Porous Media", *AIChE Jour.* (Dec. 1956) **2,** 560. ★★★

A Practical Utilization of the Theory of Bingham Plastic Flow in Stationary Pipes and Annuli

J. C. MELROSE
J. G. SAVINS
W. R. FOSTER
E. R. PARISH

MAGNOLIA PETROLEUM CO.
DALLAS, TEX.

INTRODUCTION

The practical analysis of the hydrodynamics of the wellbore has long been a subject of interest to engineers. This paper presents a simplified solution to the problem of computing the pressure drop for the flow of drilling mud in the annulus of the wellbore. This solution is, however, an exact and rigorous solution under the assumptions which have been imposed. These assumptions are that the drilling fluid is a Bingham plastic fluid* and that the annulus is formed by two concentric, stationary, cylindrical pipes. It is further assumed that the fluid is incompressible and that its motion is isothermal and in a steady state.

This problem under the same assumptions has been attacked by previous authors. Beck, Nuss and Dunn[3] proposed that the equation for the flow of a Bingham plastic fluid in a cylindrical pipe could be applied to an annulus if the pipe radius were replaced in the equation by the hydraulic radius. This equation, known as the Buckingham-Reiner equation[4] (see Appendix 1), was also used in an approximate form. Van Olphen[5] pointed out that even for a simple or Newtonian fluid the pipe equation (Poiseuille's law) could not be converted to the Lamb equation[6] descriptive of flow in an annulus (see Appendix 1) by using the hydraulic radius. Van Olphen further attempted to give a solution for the annular flow of a Bingham plastic fluid by introducing approximations similar to those which have been used in the case of the Buckingham-Reiner equation. Other attempts to provide approximate or exact solutions have been made by Grodde[7] and by Mori and Ototake[8].

The present authors some years ago in unpublished work derived the correct expressions relating the pressure drop and flow rate for this problem. It was found that the solution consisted of two simultaneous equations, one of which contained a logarithmic term. Thus, obtaining numerical results for any particular case of interest involves very tedious trial-and-error computations. Very recently Laird[9] presented the correct derivation of the two equations which are given in full detail in Appendix 1.

In order to reduce the amount of calculation time which would be involved in providing a complete tabular or graphical solution to the problem, a high-speed electronic digital computer has been utilized. For this purpose the two simultaneous equations were transformed into more compact expressions by introducing reduced variables. These expressions are given in the following theoretical section.

A similar procedure in this problem has been developed by Fredrickson and Bird[10]. Their tabular results, however, are very incomplete in the range of practical interest for problems of wellbore hydrodynamics. We have furthermore been able to express our graphical results in terms of convenient and familiar dimensionless groups.

THEORETICAL DEVELOPMENT

Use of Reduced Variables

In terms of reduced variables the two simultaneous equations just discussed take the following form,

$$qx = g(x, z, \alpha) \quad . \quad . \quad . \quad . \quad . \quad . \quad . \quad . \quad . \quad (1)$$

$$h(x, z, \alpha) = 0 \quad . \quad . \quad . \quad . \quad . \quad . \quad . \quad . \quad . \quad (2)$$

The reduced variables q, x, α and z are defined in terms of the various measured quantities, where Q is volumetric flow rate, $\Delta P/L$ is pressure gradient, D_1 is OD of inner pipe, D_2 is ID of outer pipe, μ is plastic viscosity, and ϕ is yield point. Thus, we have a dimensionless volume flux,

$$q = \frac{32\mu Q}{\pi\phi D_2^3} \quad , \quad . \quad . \quad . \quad . \quad . \quad . \quad . \quad . \quad . \quad (3a)$$

a dimensionless reciprocal pressure gradient,

$$x = \frac{4\phi L}{D_2(1-\alpha)\Delta P} \quad , \quad . \quad . \quad . \quad . \quad . \quad . \quad . \quad . \quad (3b)$$

and the ratio of the pipe diameters

$$\alpha = D_1/D_2 \quad . \quad . \quad . \quad . \quad . \quad . \quad . \quad . \quad . \quad . \quad (3c)$$

Before introducing the fourth reduced variable, z, it is of interest to consider the physical significance of the parameter x. As may be seen from the velocity profile of Fig. 1 the Bingham plastic fluid has the interesting property that a portion of the stream flows at a uniform velocity without shearing action. This section of the stream is situated approximately in the center of the conduit and is known as the "plug flow" region. Its existence is due to the fact that the shearing stresses within the region do not exceed the yield point, which is one of the two flow properties characterizing the fluid. The parameter x then turns out to be the ratio of the

Original manuscript received in Society of Petroleum Engineers office July 15, 1957. Revised manuscript received Nov. 3, 1958. Paper presented at 32nd Annual Fall Meeting of Society of Petroleum Engineers in Dallas, Tex., Oct. 6-9, 1957.

*On the basis of this model the interpretation of rheological data obtained with a rotational viscometer has been previously discussed.[1,2]

[3]References given at end of paper.

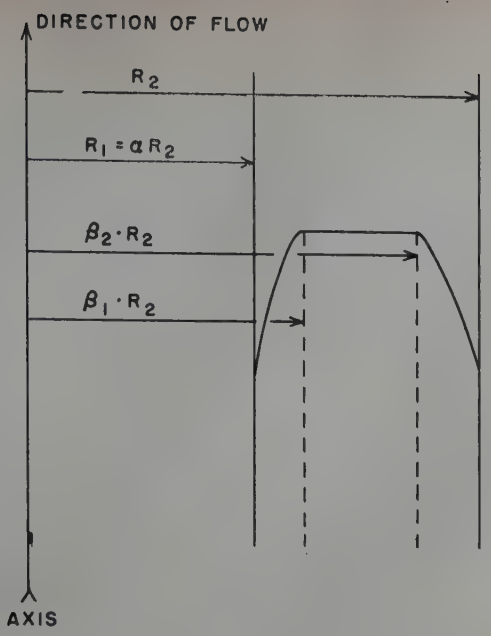

FIG. 1—VELOCITY DISTRIBUTION IN ANNULUS.

radial distance across the plug to the radial distance across the annulus. That is, x is actually a measure of the relative size of the plug flow region. Accordingly, in terms of the reduced plug boundaries defined in Fig. 1, we have

$$x = \frac{\beta_2 - \beta_1}{1 - \alpha} \quad . \quad . \quad . \quad . \quad . \quad . \quad . \quad . \quad . \quad . \quad . \quad (4a)$$

The reduced variable z can now be identified as twice the arithmetic average of the reduced plug boundaries,

$$z = \beta_1 + \beta_2 \quad . \quad . \quad . \quad . \quad . \quad . \quad . \quad . \quad . \quad . \quad . \quad (4b)$$

Thus, z is a parameter defining the position of the plug in the annulus. In contrast to the variables, q, x and α it is noted that z is defined in terms of quantities which are usually unobserved. It should be pointed out, however, that in the limiting case of a Newtonian fluid, β_1 and β_2 are identical and equal to the radius corresponding to maximum velocity (zero stress) in the annulus. (For the Bingham plastic the radius of zero stress, β_o, is equal to $\sqrt{\beta_1\beta_2}$). Thus, $x = 0$, and from the limiting case of Eq. 2 (see Eq. 6) it is found that

$$z_o^2 = 4\beta_0^2 = \frac{2(1 - \alpha^2)}{\log_e (1/\alpha)} \quad . \quad . \quad . \quad . \quad . \quad . \quad . \quad . \quad (4c)$$

METHOD OF SOLUTION AND RESULTS

The fundamental equations establishing the flow rate-pressure drop relationship, Eqs. 1 and 2, can now be given explicit formulation as follows.

$$qx = g(x,z,\alpha) = (1 + \alpha)(1 + \alpha^2) - 4/3(1 + \alpha^3)x - \tfrac{1}{2}(1 + \alpha)\{z^2 - (1 - \alpha)^2x^2\} + 1/3\,xz^3 \quad . \quad . \quad . \quad (5)$$

$$h(x,z,\alpha) = (1 - \alpha^2)(1 - 2x) + (1 - \alpha)\,xz + \tfrac{1}{2}\{z^2 - (1 - \alpha)^2x^2\}\left\{\log_e(\alpha) + \log_e\frac{z + (1 - \alpha)x}{z - (1 - \alpha)x}\right\} = 0$$

$$. \quad . \quad . \quad . \quad . \quad . \quad . \quad . \quad . \quad . \quad . \quad . \quad . \quad . \quad . \quad . \quad (6)$$

The procedure used with these equations was first to solve Eq. 6 for selected values of x and α. The values of z so obtained were then used, with the assumed values of x and α, to solve Eq. 5 for the parameter $g(x,z,\alpha)$. The Newton-Raphson iterative procedure[11] was adopted in using the high-speed computer for these operations.

In view of the form of Eq. 1 and the nature of the reduced variables q and x, the parameter $g\ (x,z,\alpha)$ can be regarded as a reduced hydrodynamic conductance for the present problem. It is to be noted that solutions for the cases of $x = 0$ and $\alpha = 0$ were included in the results obtained from the computer operations. Thus, values of $g(x,z,\alpha)$ corresponding to solutions of the Poiseuille, Lamb, and Buckingham-Reiner equations have also been tabulated. Explicit forms for the function $g(x,z,\alpha)$ for these and other special cases are presented in a later section.

In Table 1 are given the values of $g(x,z,\alpha)$ for the range in α from 0.0 to 1.0 in increments of 0.1. For each value of α the corresponding range in x is from 0.0 to 1.0 in increments of 0.02. Thus, sufficient entries of the independent variable x are given to permit the construction of accurate graphs relating flow rate and pressure drop. In Fig. 2 an example of such a graph is given in terms of the reduced variables q and x. It is to be noted that the curve for $\alpha = 0$ corresponds to the exact form of the Buckingham-Reiner equation. For practical problems the range of α used in Table 1 and Fig. 2 is entirely adequate.

Although the parameter z is not involved when Table 1 or Fig. 2 is used to obtain the relationship between flow rate and pressure gradient, numerical values of

TABLE 1—REDUCED HYDRODYNAMIC CONDUCTANCE, $g(x, z, \alpha)$

α / x	.000000	.100000	.200000	.300000	.400000
.00	1.000000	.638053	.532222	.434419	.340564
.02	.973333	.619643	.516601	.421556	.330424
.04	.946668	.601252	.500991	.408703	.320298
.06	.920004	.582885	.485406	.395869	.310186
.08	.893347	.564557	.469856	.383066	.300097
.10	.866700	.546280	.454352	.370301	.290040
.12	.840069	.528066	.438905	.357586	.280022
.14	.813461	.509927	.423528	.344930	.270051
.16	.786885	.491876	.408230	.332341	.260135
.18	.760350	.473924	.393025	.319832	.250282
.20	.733867	.456085	.377922	.307410	.240501
.22	.707448	.438370	.362933	.295086	.230797
.24	.681106	.420792	.348070	.282899	.221181
.26	.654857	.403364	.333345	.270770	.211658
.28	.628716	.386096	.318767	.258797	.202238
.30	.602700	.369003	.304350	.246962	.192928
.32	.576829	.352097	.290103	.235272	.183736
.34	.551121	.335390	.276040	.223740	.174670
.36	.525599	.318896	.262172	.212373	.165737
.38	.500284	.302627	.248510	.201183	.156946
.40	.475200	.286599	.235067	.190179	.148305
.42	.450372	.270823	.221854	.179371	.139822
.44	.425827	.255314	.208884	.168770	.131504
.46	.401592	.240086	.196169	.158385	.123361
.48	.377695	.225155	.183721	.148227	.115399
.50	.354167	.210534	.171552	.138307	.107627
.52	.331039	.196239	.159677	.128634	.100053
.54	.308344	.182296	.148107	.119220	.092686
.56	.286115	.168703	.136856	.110074	.085534
.58	.264388	.155485	.125938	.101208	.078605
.60	.243200	.142658	.115365	.092632	.071907
.62	.222588	.130241	.105152	.084357	.065449
.64	.202591	.118251	.095312	.076395	.059239
.66	.183249	.106708	.085869	.068756	.053286
.68	.164605	.095630	.076822	.061453	.047598
.70	.146700	.085037	.068192	.054496	.042185
.72	.129580	.074950	.059995	.047896	.037054
.74	.113289	.065390	.052246	.041667	.032215
.76	.097874	.056378	.044962	.035819	.027677
.78	.083384	.047938	.038158	.030371	.023448
.80	.069867	.040092	.031850	.025324	.019537
.82	.057374	.032864	.026057	.020695	.015954
.84	.045957	.026279	.020794	.016497	.012708
.86	.035669	.020363	.016080	.012742	.009811
.88	.026565	.015142	.011932	.009444	.007267
.90	.018700	.010643	.008369	.006617	.005087
.92	.012131	.006894	.005410	.004272	.003282
.94	.006916	.003924	.003074	.002424	.001861
.96	.003116	.001766	.001379	.001087	.000833
.98	.000789	.000446	.000348	.000274	.000209
1.00	.000000	.000000	.000000	.000000	.000000

α / x	.500000	.600000	.700000	.800000	.900000	1.000000
.00	.251968	.171402	.102215	.048039	.012668	.000000
.02	.244444	.166274	.099152	.046593	.012292	.000000
.04	.236926	.161149	.096092	.045159	.011912	.000000
.06	.229420	.156033	.093037	.043722	.011534	.000000
.08	.221932	.150929	.089990	.042289	.011155	.000000
.10	.214467	.145841	.086952	.040861	.010778	.000000
.12	.207033	.140773	.083926	.039437	.010403	.000000
.14	.199641	.135730	.080915	.038021	.010030	.000000
.16	.192295	.130716	.077921	.036613	.009660	.000000
.18	.184965	.125734	.074947	.035214	.009292	.000000
.20	.177707	.120788	.071994	.033825	.008921	.000000
.22	.170509	.115883	.069066	.032448	.008559	.000000
.24	.163376	.111023	.066163	.031084	.008196	.000000
.26	.156322	.106214	.063285	.029734	.007839	.000000
.28	.149328	.101452	.060452	.028398	.007491	.000000
.30	.142425	.096750	.057646	.027080	.007150	.000000
.32	.135612	.092110	.054877	.025777	.006799	.000000
.34	.128892	.087534	.052145	.024492	.006459	.000000
.36	.122273	.083027	.049457	.023223	.006127	.000000
.38	.115765	.078594	.046812	.021984	.005799	.000000
.40	.109361	.074237	.044212	.020762	.005475	.000000
.42	.103080	.069962	.041662	.019563	.005161	.000000
.44	.096923	.065773	.039163	.018383	.004853	.000000
.46	.090897	.061673	.036719	.017240	.004546	.000000
.48	.085007	.057668	.034329	.016118	.004252	.000000
.50	.079255	.053758	.031999	.015021	.003962	.000000
.52	.073660	.049951	.029729	.013956	.003680	.000000
.54	.068216	.046250	.027523	.012919	.003408	.000000
.56	.062932	.042660	.025383	.011914	.003145	.000000
.58	.057815	.039183	.023311	.010940	.002886	.000000
.60	.052872	.035825	.021311	.010000	.002641	.000000
.62	.048107	.032590	.019384	.009090	.002401	.000000
.64	.043527	.029480	.017532	.008226	.002172	.000000
.66	.039140	.026503	.015759	.007393	.001949	.000000
.68	.034949	.023660	.014066	.006599	.001741	.000000
.70	.030963	.020956	.012457	.005842	.001543	.000000
.72	.027187	.018396	.010933	.005128	.001349	.000000
.74	.023623	.015983	.009493	.004454	.001178	.000000
.76	.020290	.013723	.008153	.003824	.0010011	.000000
.78	.017183	.011616	.006901	.003236	.0008456	.000000
.80	.014314	.009674	.005743	.002693	.0007015	.000000
.82	.011682	.007895	.004688	.002196	.0005681	.000000
.84	.009301	.006284	.003731	.001748	.0004463	.000000
.86	.007175	.004847	.002876	.001349	.0003358	.000000
.88	.005312	.003587	.002128	.000997	.0002368	.000000
.90	.003716	.002509	.001488	.000697	.0001587	.000000
.92	.002397	.001637	.000959	.000448	.0001023	.000000
.94	.001358	.000916	.000543	.000255	.0000570	.000000
.96	.000608	.000410	.000242	.000113	.0000253	.000000
.98	.000153	.000103	.000060	.000028	.0000011	.000000
1.00	.000000	.000000	.000000	.000000	.000000	.000000

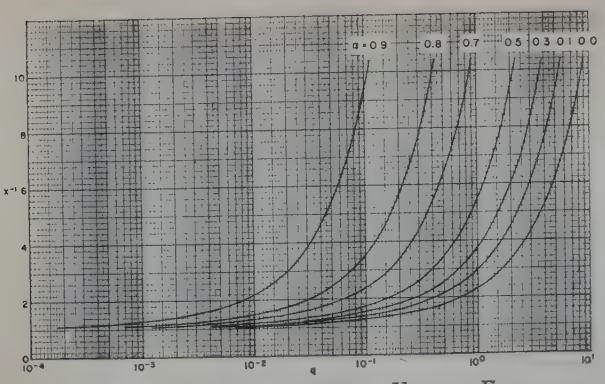

FIG. 2—PRESSURE GRADIENT VS VOLUME FLUX (REDUCED FORM).

this quantity should find application in certain fundamental studies of Bingham plastic flow. For example, it is recalled that, taken together, z and x define the position and size of the plug flow region. For this reason, in Table 2 are given values of z for the same ranges of x and α as are used in Table 1.

In some studies it may be of interest to determine the shear rates and shearing stresses at the walls of the inner and outer pipe. The expressions for these quantities can be conveniently written in terms of a dimensionless correlation parameter, $F(x,z,\alpha)$, as follows,

$$\dot{e} \text{ (rate of shear)} = \frac{\phi}{\mu} F \quad . \quad . \quad . \quad . \quad . \quad (7a)$$

$$p \text{ (shear stress)} = \phi(F + 1) \quad . \quad . \quad . \quad . \quad (7b)$$

For the outer and inner walls we have, respectively,

$$F_2(x,z,\alpha) = \frac{1}{4(1-\alpha)x}\{(1-\alpha)^2x^2 - z^2 + 4[1-(1-\alpha)x]\} \quad . \quad . \quad . \quad . \quad . \quad . \quad . \quad . \quad . \quad (8a)$$

$$F_1(x,z,\alpha) = \frac{1}{\alpha x}\{1+\alpha-x(1+\alpha+F_2)\} \quad . \quad (8b)$$

Table 3 gives values of $F_2(x,z,\alpha)$ for the same ranges as are used in Tables 1 and 2. In order to simplify the practical determination of F_2 from experimental data the relationship between q and x (Table 1 and Fig. 2) may be utilized. This permits the construction of a graph giving the relationship between q and F_2 as is shown in Figs. 3 and 4.

SIGNIFICANCE OF THE CONDUCTANCE FUNCTION

The reduced hydrodynamic conductance function, $g(x,z,\alpha)$, provides an extremely valuable way of indicating the nature of the mathematical expressions relating flow rate and pressure gradient for various special cases. For example, flow of a Newtonian fluid in a pipe can be summarized by the conditions,

$$\alpha = 0, x = 0 \quad . \quad . \quad . \quad . \quad . \quad . \quad . \quad . \quad . \quad . \quad (9a)$$

whence it follows from Eqs. 5 and 6,

$$z = 0 \quad . \quad . \quad . \quad . \quad . \quad . \quad . \quad . \quad . \quad . \quad . \quad (9b)$$

and

$$g(x,z,\alpha) = g(0,0,0) = 1 \quad . \quad . \quad . \quad . \quad . \quad . \quad (9c)$$

Again, for Newtonian flow in an annulus,

$$x = 0 \quad . \quad . \quad . \quad . \quad . \quad . \quad . \quad . \quad . \quad . \quad . \quad (10a)$$

whence

$$z = z_o = \sqrt{\frac{2(1-\alpha^2)}{\log_e(1/\alpha)}} \quad . \quad . \quad . \quad . \quad . \quad . \quad (10b)$$

and

$$g(x,z,\alpha) = g(0,z_o,\alpha) = (1+\alpha)\left\{1+\alpha^2 - \frac{(1-\alpha^2)}{\log_e(1/\alpha)}\right\} \quad . \quad . \quad . \quad . \quad . \quad . \quad . \quad . \quad (10c)$$

The case of a Bingham plastic fluid flowing in a pipe gives

$$\alpha = 0, \quad . \quad . \quad . \quad . \quad . \quad . \quad . \quad . \quad . \quad . \quad . \quad (11a)$$

whence

$$z = x \quad . \quad . \quad . \quad . \quad . \quad . \quad . \quad . \quad . \quad . \quad . \quad (11b)$$

and

$$g(x,z,\alpha) = g(x,x,0) = 1 - 4/3\,x \times 1/3\,x^4 \quad (11c)$$

Yet another limiting case exists for which the flow rate-pressure gradient relationship is known in explicit form. This case is that of plane rectilinear flow between fixed parallel plates, i.e., slit flow (see Appendix 1). The flow in an annulus, of course, is approached by this case with increasing accuracy as the annular clearance is decreased. For a Newtonian fluid this case can be represented by

TABLE 2—PLUG POSITION FUNCTION, z

α/x	.000000	.100000	.200000	.300000	.400000	.500000	.600000	.700000	.800000	.900000	1.000000
.00	.000000	.927309	1.092228	1.229496	1.354060	1.471068	1.582955	1.691078	1.795280	1.899121	2.000000
.02	.020000	.924523	1.090346	1.228216	1.353209	1.470523	1.582631	1.690908	1.795210	1.899104	2.000000
.04	.040000	.921877	1.088626	1.227045	1.352426	1.470024	1.582334	1.690752	1.796143	1.899088	2.000000
.06	.060000	.919679	1.087066	1.225981	1.351716	1.469571	1.582064	1.690610	1.796084	1.899074	2.000000
.08	.080000	.917830	1.085668	1.225026	1.351078	1.469163	1.581822	1.690482	1.796030	1.899062	2.000000
.10	.100000	.915833	1.084433	1.224181	1.350512	1.468801	1.581606	1.690368	1.795983	1.899050	2.000000
.12	.120000	.914890	1.083362	1.223444	1.350018	1.468484	1.581418	1.690269	1.795941	1.899041	2.000000
.14	.140000	.913004	1.082456	1.222817	1.349597	1.468214	1.581256	1.690184	1.795906	1.899032	2.000000
.16	.160000	.911175	1.081715	1.222300	1.349248	1.467989	1.581122	1.690113	1.795876	1.899024	2.000000
.18	.180000	.911406	1.081140	1.221893	1.348971	1.467810	1.581015	1.690057	1.795852	1.899019	2.000000
.20	.200000	.910599	1.080732	1.221597	1.348767	1.467677	1.580936	1.690014	1.795835	1.899015	2.000000
.22	.220000	.910453	1.080491	1.221411	1.348636	1.467590	1.580883	1.689987	1.795823	1.899012	2.000000
.24	.240000	.910471	1.080417	1.221336	1.348577	1.467550	1.580857	1.689973	1.795817	1.899012	2.000000
.26	.260000	.910754	1.080512	1.221373	1.348591	1.467550	1.580857	1.689973	1.795817	1.899012	2.000000
.28	.280000	.911302	1.080774	1.221520	1.348678	1.467606	1.580888	1.689988	1.795823	1.899012	2.000000
.30	.300000	.912115	1.081205	1.221778	1.348837	1.467703	1.580944	1.690017	1.795834	1.899012	2.000000
.32	.320000	.913195	1.081805	1.222148	1.349070	1.467846	1.581027	1.690060	1.795853	1.899019	2.000000
.34	.340000	.914541	1.082574	1.222629	1.349375	1.468036	1.581137	1.690117	1.795877	1.899025	2.000000
.36	.360000	.916154	1.083511	1.223221	1.349754	1.468271	1.581275	1.690189	1.795906	1.899032	2.000000
.38	.380000	.918032	1.084618	1.223925	1.350205	1.468553	1.581440	1.690275	1.795942	1.899040	2.000000
.40	.400000	.920177	1.085893	1.224741	1.350730	1.468880	1.581632	1.690375	1.795984	1.899050	2.000000
.42	.420000	.922586	1.087337	1.225667	1.351327	1.469254	1.581851	1.690489	1.796032	1.899061	2.000000
.44	.440000	.925260	1.088949	1.226705	1.351997	1.469674	1.582097	1.690618	1.796085	1.899073	2.000000
.46	.460000	.928198	1.090730	1.227855	1.352740	1.470140	1.582371	1.690761	1.796145	1.899088	2.000000
.48	.480000	.931398	1.092679	1.229115	1.353556	1.470652	1.582672	1.690918	1.796210	1.899103	2.000000
.50	.500000	.934859	1.094795	1.230486	1.354445	1.471210	1.583000	1.691090	1.796282	1.899120	2.000000
.52	.520000	.938581	1.097079	1.231969	1.355407	1.471814	1.583355	1.691276	1.796359	1.899139	2.000000
.54	.540000	.942542	1.099530	1.233562	1.356441	1.472464	1.583738	1.691476	1.796443	1.899158	2.000000
.56	.560000	.946775	1.102146	1.235265	1.357548	1.473159	1.584147	1.691690	1.796532	1.899179	2.000000
.58	.580000	.951262	1.104928	1.237079	1.358727	1.473901	1.584584	1.691919	1.796627	1.899201	2.000000
.60	.600000	.956002	1.107876	1.239003	1.359979	1.474689	1.585043	1.692161	1.796729	1.899223	2.000000
.62	.620000	.960992	1.110987	1.241036	1.361303	1.475523	1.585539	1.692418	1.796836	1.899249	2.000000
.64	.640000	.966230	1.114263	1.243179	1.362700	1.476402	1.586057	1.692689	1.796948	1.899275	2.000000
.66	.660000	.971714	1.117685	1.245432	1.364169	1.477327	1.586602	1.692975	1.797068	1.899306	2.000000
.68	.680000	.977442	1.121282	1.247792	1.365710	1.478299	1.587175	1.693275	1.797192	1.899334	2.000000
.70	.700000	.983411	1.125041	1.250262	1.367322	1.479315	1.587774	1.693589	1.797324	1.899364	2.000000
.72	.720000	.989618	1.128959	1.252840	1.369006	1.480377	1.588401	1.693917	1.797460	1.899398	2.000000
.74	.740000	.996060	1.133036	1.255526	1.370762	1.481486	1.589054	1.694259	1.797604	1.899428	2.000000
.76	.760000	1.002736	1.137272	1.258320	1.372589	1.482639	1.589735	1.694616	1.797751	1.899463	2.000000
.78	.780000	1.009642	1.141664	1.261205	1.374488	1.483837	1.590442	1.694987	1.797907	1.899501	2.000000
.80	.800000	1.016776	1.146212	1.264210	1.376458	1.485082	1.591177	1.695371	1.798068	1.899535	2.000000
.82	.820000	1.024134	1.150914	1.267320	1.378499	1.486372	1.591938	1.695770	1.798236	1.899578	2.000000
.84	.840000	1.031714	1.155770	1.270536	1.380611	1.487708	1.592727	1.696183	1.798407	1.899618	2.000000
.86	.860000	1.039514	1.160779	1.273858	1.382781	1.489088	1.593541	1.696612	1.798584	1.899658	2.000000
.88	.880000	1.047530	1.165938	1.277283	1.385033	1.490514	1.594384	1.697054	1.798771	1.899695	2.000000
.90	.900000	1.055759	1.171248	1.280812	1.387353	1.491986	1.595253	1.697511	1.798962	1.899745	2.000000
.92	.920000	1.064201	1.176706	1.284445	1.389745	1.493494	1.596151	1.697980	1.799160	1.899783	2.000000
.94	.940000	1.072859	1.182312	1.288180	1.392206	1.495053	1.597072	1.698463	1.799356	1.899831	2.000000
.96	.960000	1.081695	1.188068	1.292018	1.394734	1.496659	1.598014	1.698967	1.799573	1.899869	2.000000
.98	.980000	1.090749	1.193960	1.295960	1.397339	1.498304	1.598985	1.699477	1.799783	1.899887	2.000000
1.00	1.000000	1.100000	1.200000	1.300000	1.400000	1.500000	1.600000	1.700000	1.800000	1.900000	2.000000

TABLE 3—CORRELATION PARAMETER, $F_2(x, z, \alpha)$

α/x	.000000	.100000	.200000	.300000	.400000
.02	49.000000	42.688472	42.928125	43.494107	44.186666
.04	24.000000	20.883680	20.999296	21.278035	21.619895
.06	15.666666	13.616203	13.690572	13.873392	14.098363
.08	11.500000	9.983090	10.036796	10.171607	10.337968
.10	9.000000	7.803722	7.845000	7.951000	8.082125
.12	7.333333	6.351226	6.384218	6.470922	6.578576
.14	6.142857	5.314067	5.341138	5.414081	5.504880
.16	5.250000	4.536510	4.559121	4.621696	4.699843
.18	4.555555	3.932006	3.951163	4.005654	4.073912
.20	4.000000	3.448638	3.465015	3.513017	3.573375
.22	3.545454	3.053371	3.067485	3.110162	3.164015
.24	3.166666	2.724178	2.736406	2.774462	2.822038
.26	2.846153	2.445811	2.456430	2.490892	2.534663
.28	2.571428	2.207371	2.216629	2.247831	2.287633
.30	2.333333	2.000870	2.008947	2.037321	2.073652
.32	2.125000	1.820321	1.827373	1.853258	1.886549
.34	1.941176	1.661143	1.667288	1.690997	1.721568
.36	1.777777	1.519776	1.525121	1.546855	1.575011
.38	1.631578	1.393399	1.398034	1.418007	1.443991
.40	1.500000	1.279770	1.283773	1.302142	1.326166
.42	1.380952	1.177056	1.180498	1.197423	1.219652
.44	1.272727	1.083775	1.086711	1.102313	1.122907
.46	1.173913	.998695	1.001175	1.015566	1.034655
.48	1.083333	.920787	.922851	.936138	.953836
.50	1.000000	.849183	.850887	.863142	.879558
.52	.923076	.783162	.784537	.795837	.811065
.54	.851851	.722124	.723177	.733597	.747716
.56	.785714	.665491	.666277	.675880	.688950
.58	.724137	.613825	.613372	.622210	.634310
.60	.666666	.563726	.564067	.572184	.583368
.62	.612903	.517853	.518004	.525449	.535772
.64	.562500	.474900	.474882	.481696	.491810
.66	.515151	.434595	.434450	.440660	.449400
.68	.470588	.396711	.396443	.402090	.410110
.70	.428571	.361031	.360660	.365785	.373107
.72	.388888	.327376	.326916	.331547	.338217
.74	.351351	.295574	.295054	.299213	.305259
.76	.315789	.265486	.264913	.268632	.274084
.78	.282051	.236972	.236366	.239684	.244551
.80	.250000	.209916	.209292	.212218	.216541
.82	.219512	.184210	.183586	.186136	.189939
.84	.190476	.159755	.159140	.161343	.164642
.86	.162790	.136459	.135875	.137740	.140586
.88	.136363	.114248	.113707	.115259	.117642
.90	.111111	.093046	.092559	.093813	.095763
.92	.086956	.072780	.072367	.073342	.074868
.94	.063829	.053392	.053071	.053780	.054898
.96	.041666	.034846	.034606	.035070	.035802
.98	.020408	.017057	.016935	.017157	.017508
1.00	.000000	.000000	.000000	.000000	.000000

α/x	.500000	.600000	.700000	.800000	.900000
.02	44.941250	45.729375	46.535833	47.352500	48.175000
.04	21.992750	22.382343	22.781250	23.185312	23.591875
.06	14.343833	14.600416	14.863333	15.129583	15.397916
.08	10.519687	10.709843	10.904583	11.101875	11.300625
.10	8.225600	8.375750	8.529583	8.685500	8.842500
.12	6.696458	6.819895	6.946388	7.074583	7.203750
.14	5.604428	5.708750	5.815654	5.924107	6.033392
.16	4.785625	4.875546	4.967760	5.061328	5.155625
.18	4.148972	4.227673	4.308425	4.390277	4.472916
.20	3.639900	3.709500	3.781000	3.853562	3.926625
.22	3.223340	3.285653	3.349583	3.414488	3.479886
.24	2.876437	2.932552	2.990173	3.048645	3.107500
.26	2.583057	2.633894	2.686121	2.739134	2.792500
.28	2.331660	2.377968	2.425565	2.473883	2.522589
.30	2.113950	2.156270	2.199833	2.244111	2.288750
.32	1.923468	1.962363	2.002369	2.042968	2.083906
.34	1.755529	1.791341	1.828186	1.865588	1.903308
.36	1.606347	1.639409	1.673425	1.707986	1.742847
.38	1.472960	1.503536	1.535000	1.565973	1.597276
.40	1.352975	1.381296	1.410479	1.440093	1.470000
.42	1.244511	1.270773	1.297837	1.325357	1.353154
.44	1.145965	1.170369	1.195511	1.221051	1.246875
.46	1.056065	1.078736	1.102101	1.125869	1.149836
.48	.973729	.994804	1.016527	1.038645	1.060789
.50	.898040	.917625	.937850	.958400	.979200
.52	.828230	.846442	.865240	.884375	.903701
.54	.763648	.780578	.798070	.815856	.833842
.56	.703750	.719475	.735714	.752254	.768973
.58	.648025	.662618	.677701	.693060	.708577
.60	.596075	.609604	.623597	.637833	.652250
.62	.547524	.560040	.572997	.586189	.599556
.64	.502054	.513623	.525598	.537792	.550156
.66	.459393	.470056	.481098	.492348	.503750
.68	.419286	.429090	.439252	.449613	.461110
.70	.381514	.390508	.399821	.409321	.418964
.72	.345888	.354097	.362615	.371302	.380069
.74	.312222	.319695	.327432	.335337	.343378
.76	.280381	.287129	.294144	.301299	.308585
.78	.250205	.256274	.262574	.269006	.275544
.80	.221575	.226992	.232614	.238343	.244250
.82	.194384	.199169	.204136	.209207	.214390
.84	.168523	.172700	.177043	.181473	.186011
.86	.143901	.147520	.151220	.155043	.158982
.88	.120431	.123465	.126609	.129815	.133238
.90	.098038	.100527	.103101	.105736	.108500
.92	.076668	.078614	.080643	.082703	.085000
.94	.056228	.057666	.059166	.060704	.062420
.96	.036671	.037620	.038585	.039583	.040911
.98	.017948	.018437	.018886	.019375	.020484
1.00	.000000	.000000	.000000	.000000	.000000

$$\lim_{\alpha \to 1} z = 2 \quad . \quad . \quad . \quad . \quad . \quad . \quad . \quad . \quad . \quad . \quad (12a)$$

and

$$\lim_{\alpha \to 1} g(x,z,\alpha) = g(0,2,1) = 2/3\ (1+\alpha)(1-\alpha)^2 \quad . \quad . \quad . \quad . \quad . \quad . \quad . \quad . \quad . \quad . \quad (12b)$$

For a Bingham plastic fluid the same geometry gives

$$\lim_{\alpha \to 1} z = 2 \quad . \quad . \quad . \quad . \quad . \quad . \quad . \quad . \quad . \quad . \quad (13a)$$

and

$$\lim_{\alpha \to 1} g(x,z,\alpha) = g(x,2,1) = 2/3(1+\alpha)\ (1-\alpha)^2(1-3/2\ x\ +\ \tfrac{1}{2}\ x^3) \quad . \quad (13b)$$

The latter case has been discussed by Prager[12].

It is an extremely important fact for the subsequent development of practical procedures that for Newtonian flow in an annulus the conductance function $g(0,z_o,\alpha)$ approaches that of a narrow annulus to a high degree of approximation, even at a value of α as low as 0.5. This fact has been noted in the literature by many authors, for example Becker[13], Winkel[14] and Carpenter, *et al*[15]. In Fig. 5, the conductance functions defined by Eqs. 10c and 12b are plotted so as to indicate the high accuracy which the narrow annulus approximation provides in this case.

Normalization of the Conductance Function

The close agreement between the curves of Fig. 5 suggests that it will be convenient, except for the case of $\alpha = 0$, to normalize the general conductance function,

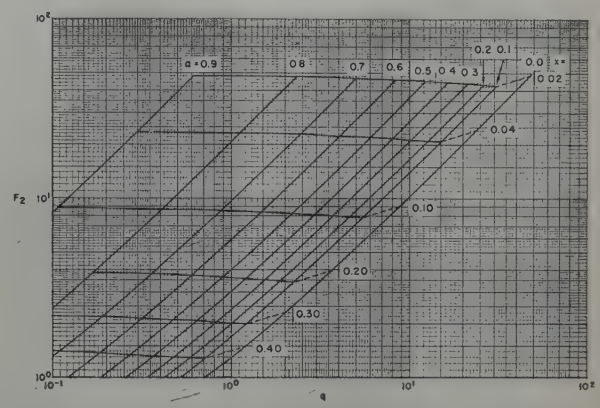

FIG. 3—CORRELATION PARAMETER VS REDUCED VOLUME FLUX.

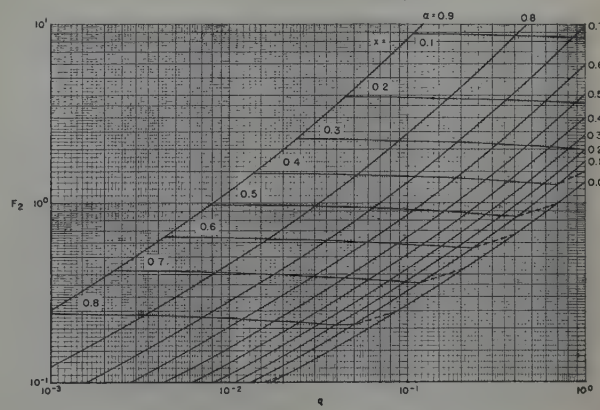

FIG. 4—CORRELATION PARAMETER VS REDUCED VOLUME FLUX.

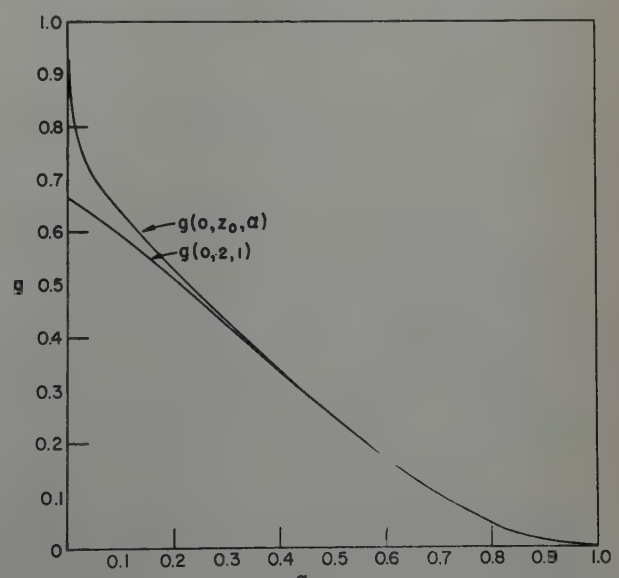

FIG. 5—REDUCED HYDRODYNAMIC CONDUCTANCE FUNCTIONS FROM LAMB AND NARROW ANNULUS EQUATIONS.

$g(x,z,\alpha)$, on the basis of the conductance for a Newtonian fluid in a narrow annulus, $g(0,2,1)$. Carrying out this procedure we define the normalized conductance as

$$\gamma = \frac{g(x,z,\alpha)}{g(0,2,1)} = \frac{3g(x,z,\alpha)}{2(1+\alpha)(1-\alpha)^2} \quad . \quad . \quad (14)$$

Similarly, for the flow of a Bingham plastic fluid in a pipe, if we normalize on the basis of the flow of a Newtonian fluid, a form which is actually unchanged results,

$$\gamma_0 = \frac{g(x,x,0)}{g(0,0,0)} = 1 - 4/3\, x + 1/3\, x^4 \quad . \quad . \quad (15)$$

Finally, it is of interest to obtain the normalized conductance for the case of the narrow annulus,

$$\gamma_1 = \frac{g(x,2,1)}{g(0,2,1)} = 1 - 3/2\, x + 1/2\, x^3 \quad . \quad . \quad (16)$$

In order to show that the success of the narrow annulus approximation for Newtonian fluids also extends to the case of Bingham plastic fluids, Fig. 6 shows plots of the normalized conductance functions defined in Eqs. 14, 15 and 16 vs the reduced variable x. For the general function, γ, a value of $\alpha = 0.1$ is assumed. It is of interest that previous proposals[3,5,7,9] of approximate and exact solutions for the present problem can be compactly represented in terms of the function γ. These forms are given in Appendix 2.

USE OF DIMENSIONLESS GROUPS

For many years engineers engaged in fluid flow problems involving Newtonian fluids have found it convenient to express their flow equations in terms of certain well-known dimensionless groups. These groups have been chosen primarily on the basis of their utility in correlating data on turbulent flow and on the transition from laminar to turbulent flow. However, the flow equations applicable to laminar flow are also conveniently simplified by the use of these groups, which are, for isothermal flow,

$$R_e = \frac{4mV\rho}{\mu} \quad \text{(Reynolds number)} \quad . \quad . \quad (17)$$

and

$$f = \frac{2m\Delta P}{V^2\rho L} \quad \text{(friction factor)}, \quad . \quad . \quad . \quad (18)$$

where ρ is fluid density,

$$m = \frac{D_2}{4}(1-\alpha) = \text{hydraulic radius}, \quad . \quad (19a)$$

and

$$V = \frac{4Q}{\pi D_2^2(1-\alpha^2)} = \text{mean fluid velocity} \quad (19b)$$

As yet no reliable information is available on turbulent flow, or the transition to turbulence, for the case of Bingham fluids. Hence, the choice of the dimensionless groups has not yet been standardized through usage. One choice, used by several authors since 1947, is based on the following dimensional group which may be termed the characteristic velocity,

$$V_c = \frac{4m\tau_0}{\mu} \quad . \quad . \quad . \quad . \quad . \quad . \quad . \quad . \quad . \quad (20)$$

A dimensionless group, the Bingham number, is then defined as

$$Bi = \frac{V_c}{V} \quad . \quad . \quad . \quad . \quad . \quad . \quad . \quad . \quad . \quad . \quad (21)$$

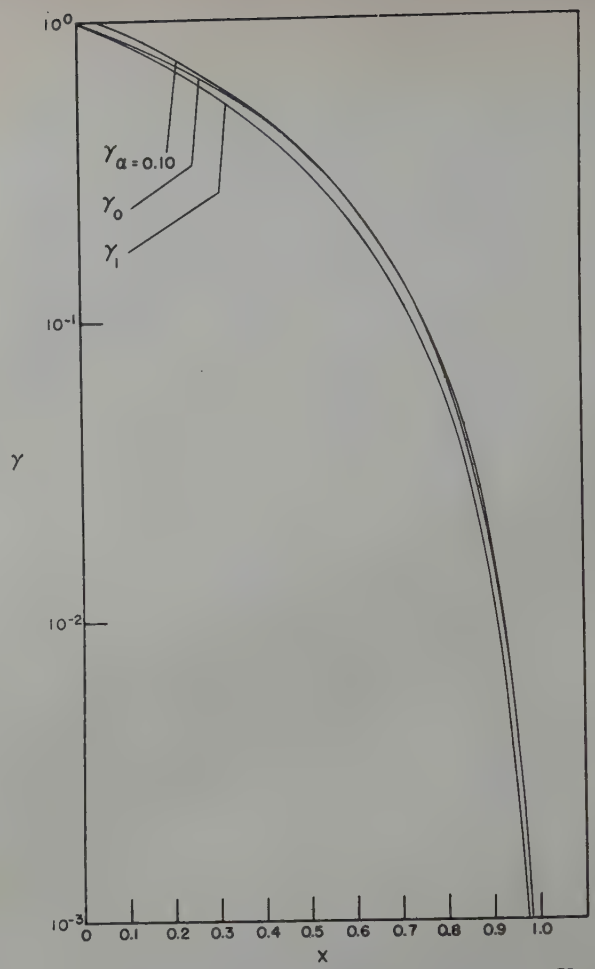

FIG. 6—NORMALIZED HYDRODYNAMIC CONDUCTANCE VALUES FROM EXACT, NARROW ANNULUS AND PIPE SOLUTIONS.

It is of interest that the dimensionless group introduced by Hedstrom[16] is equal to the product of the Bingham and Reynolds numbers. For the sake of emphasis we may note that to obtain a numerical value of the Bingham number for any particular case, the required data include only the hydraulic radius, the mean fluid velocity and the rheological properties of the fluid. In wellbore applications the range of values of *Bi* which will be encountered can be estimated to be 0 to 100.

Using Eqs. 19 and 20 the expression for the Bingham number can easily be transformed to

$$Bi = \frac{\pi D_2^3(1+\alpha)(1-\alpha)^2\phi}{4\mu Q}, \quad . \quad . \quad . \quad . \quad (22)$$

which, with Eqs. 3a and 1, gives

$$Bi = \frac{8(1+\alpha)(1-\alpha)^2 x}{g(x,z,\alpha)} \quad . \quad . \quad . \quad . \quad . \quad (23)$$

It is clear that the Bingham number is equally applicable to flow in pipes and in annuli. In the latter case Eq. 23 can be simplified by introducing the normalized conductance function, γ, which was defined in Eq. 14. This gives

$$Bi = \frac{12x}{\gamma}, \quad . \quad . \quad . \quad . \quad . \quad . \quad . \quad . \quad . \quad . \quad (24)$$

while for the special case of a narrow annulus,

$$Bi = \frac{12x}{\gamma_1} \quad . \quad . \quad . \quad . \quad . \quad . \quad . \quad . \quad . \quad . \quad (25)$$

In the case of pipe flow Eq. 15 defines the normalized conductance, whence it is found that

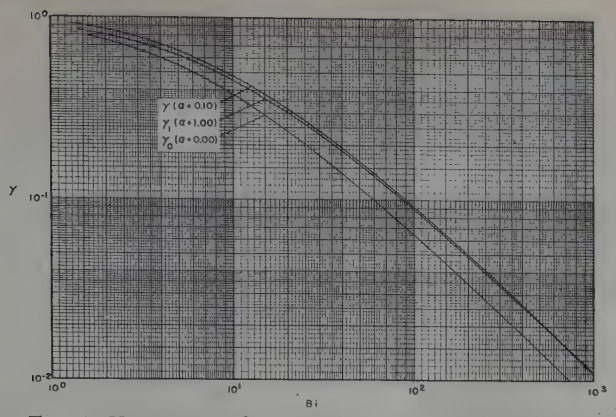

FIG. 7—NORMALIZED CONDUCTANCE VS BINGHAM NUMBER.

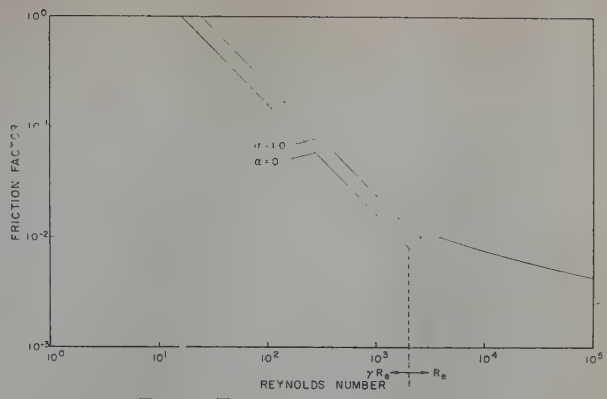

FIG. 8—FRICTION FACTOR DIAGRAM.

$$Bi = \frac{8x}{\gamma_o} \quad . \quad . \quad . \quad . \quad . \quad . \quad . \quad . \quad . \quad . \quad . \quad (26)$$

It is now possible to exhibit a rather remarkable property of the normalized conductance function, γ. When this parameter is plotted against the Bingham number, *Bi*, curves are obtained for various values of α which lie very close to each other, as shown in Fig. 7. That is, the *Bi* vs γ plot is extremely insensitive to the value of α. The usefulness of this result is readily apparent in that a very accurate estimate for γ, at a given value of *Bi*, is given by γ_1, the normalized conductance for the narrow annulus. This statement, of course, is restricted to values of α greater than 0.1.

A practical method of obtaining friction factors, and hence of pressure drops, can now be easily developed. By multiplying Eqs. 17 and 18 together another expression for *Bi* results,

$$Bi = \frac{2\phi L}{D_2(1-\alpha)\Delta P}(fR_e) \quad . \quad . \quad . \quad . \quad . \quad (27)$$

which, by virtue of Eq. 3b, can be written as

$$Bi = \frac{x}{2}(fR_e) \quad . \quad . \quad . \quad . \quad . \quad . \quad . \quad . \quad . \quad . \quad (28)$$

Equating the expression for the Bingham number given by this result with that of Eq. 24, it is found that

$$f = \frac{24}{\gamma R_e} \quad . \quad . \quad . \quad . \quad . \quad . \quad . \quad . \quad . \quad . \quad (29)$$

while for the special cases, Eqs. 25 and 26 yield

$$f = \frac{16}{\gamma_o R_e} \text{ (pipe)} \quad . \quad . \quad . \quad . \quad . \quad . \quad . \quad . \quad (30a)$$

and

$$f = \frac{24}{\gamma_1 R_e} \text{(narrow annulus)} \quad . \quad . \quad . \quad . \quad (30b)$$

It should be noted that Eqs. 29 and 30 are alternatively obtainable directly from the definitions of f, R_e, γ, γ_o, and γ_1.

In Fig. 8 are given plots of Eqs. 30a and 30b for the range of values of $\gamma_o R_e$ or $\gamma_1 R_e$ up to 2,000. Beyond this point the Stanton-Pannell type of plot for turbulent flow is shown. In view of the excellent estimate for γ which is provided by the γ_1 vs *Bi* plot of Fig. 7, the γ_1 curve of Fig. 8 will of course give very nearly correct values for the friction factor. The procedure which is recommended for using Figs. 7 and 8 is discussed in a later section and in Appendix 3.

INITIATION OF FLOW

When certain drilling fluids remain in a quiescent state a gel structure develops. The strength of this structure is important since it must be broken before the system will flow freely. The pressure gradient required to rupture this structure and initiate flow in annuli and pipes can be estimated from Eq. 3b, taking the value of the parameter x to be unity. For a condition of no flow the yield point, ϕ, is replaced with the gel strength, S_t, developed during the quiescent period. For an annulus we obtain

$$\frac{\Delta P}{L} = \frac{4S_t}{D_2(1-\alpha)} \quad . \quad . \quad . \quad . \quad . \quad . \quad . \quad . \quad (31a)$$

and for a pipe,

$$\frac{\Delta P}{L} = \frac{4S_t}{D} \quad . \quad . \quad . \quad . \quad . \quad . \quad . \quad . \quad . \quad . \quad (31b)$$

where D is ID of inner pipe. Neglecting the difference between D and D_1, i.e., the thickness of the inner pipe, we can write for the total pressure gradient required to rupture gel contained in both a pipe and annular section,

$$\frac{\Delta P}{L} = \frac{4S_t}{D_2\alpha(1-\alpha)} \quad . \quad . \quad . \quad . \quad . \quad . \quad . \quad . \quad (32)$$

PRACTICAL APPLICATION

It seems desirable to summarize briefly the pertinent points which form the basis of the practical procedures given in detail in Appendix 3. The first point is that the narrow annulus equation is used for calculating Bingham plastic and Newtonian friction losses where the conduit is an annular space. Both Figs. 6 and 7 showed that the case of $\alpha = 0.10$ deviated only slightly from that for the case of $\alpha = 1.0$. Accordingly, Fig. 8 shows only the two limiting cases of $\alpha = 0$ and $\alpha = 1.0$. The second point is the use of γ_o and γ_1 to relate the friction factor to the Reynolds number for viscous flow in pipes and annuli, respectively. Fig. 7 shows that these functions are fractional coefficients, each having a maximum limiting value of 1.0, i.e., the Newtonian case. From this it is easy to see that $\gamma_o R_e$ (Eq. 30a) or $\gamma_1 R_e$, (Eq. 30b) is a modified Reynolds number when the flowing material is a Bingham plastic and the conventional Reynolds number when the material is a Newtonian liquid. An obvious advantage here of the normalized hydrodynamic conductance is that the familiar concept of the friction factor-Reynolds number diagram for viscous flow is preserved. The third point concerns the handling of the turbulent region. Since there are appreciable uncertainties and inconsistencies surrounding the turbulent behavior of Newtonian liquids in annuli[17–20] and little fundamental information about the behavior of the Bingham plastic in turbulent flow, an assumption must be introduced. For want of better information we assume, as in the case of flow in a

pipe, that turbulent flow predominates in the case of Newtonian flow in an annulus when $R_e > 2{,}000$; for the turbulent region we further assume that the Stanton-Pannell correlation for turbulent flow within smooth commercial pipes provides satisfactory approximate values for annular friction losses in turbulence. In the case of the Bingham plastic we assume that turbulence occurs in an annulus or pipe when the modified Reynolds numbers, $\gamma_1 R_e$ and $\gamma_o R_e$, exceed 2,000, and that in fully developed turbulent flow the Stanton-Pannell correlation provides satisfactory approximate values for Bingham plastic friction losses. Furthermore, in fully developed turbulent flow the Reynolds number for the Bingham plastic is calculated using the plastic viscosity, following the suggestion of Hedstrom[16].

The uncertainties just discussed and the possible effects of factors such as pipe rotation and eccentricity, and downhole changes in rheological properties must be kept in mind when comparing friction losses calculated according to the following procedures with those observed in actual field practice. Although the results must be viewed with unavoidable reservations the procedures will provide reasonably reliable estimates of tubing and annulus friction losses.

The groups described in the preceding sections are based on a consistent set of force and dimensional units. However, it is often impractical to adhere strictly to any particular scheme since working data are often gathered from a variety of sources and terminology is governed by the dictates of local customs. The suggested system of units described in Table 4 was developed with these limitations in mind.

Sample Calculations

The following examples illustrate the methods outlined in Appendix 3 for estimating dynamic and static friction losses in tubing and annuli for Bingham plastics. Note that the system of units described in Table 4 is used exclusively in these samples.

Over-all Friction Losses (Drilling Mud)

Dimensions of pipe and hole and circulating rate are as follows.

Hole diameter	(D_2)	= 6.5 in.
OD of drill pipe	(D_1)	= 3.5 in.
ID of drill pipe	(D)	= 2.875 in.
Depth	(L)	= 5000 ft
Circulation rate	(Q)	= 4.5 bbl/min

Mud properties are as follows:

Plastic viscosity	(μ)	= 38 cp
Yield point	(ϕ)	= 17 lb/100 ft²
Density	(ρ)	= 10.6 lb/gal

Friction Loss in the Drill Pipe

$$V = \frac{(17.16)\ (4.5)}{(2.875)^2} = 9.34 \text{ ft/sec}$$

$$Bi = \frac{(39.9)\ (2.875)\ (17)}{(38)\ \ (9.34)} = 5.49$$

$\gamma_o = 0.535$ (from Fig. 7 and $\alpha = 0$)

$$\gamma_o R_e = (0.535)\left[\frac{(927.7)\ (2.875)\ (9.34)\ (10.6)}{(38)}\right]$$

$$= 3{,}718$$

$\gamma_o R_e > 2{,}000$

$R_e = 6{,}950$

$f = 0.0083$ (from Fig. 8 and Stanton-Pannell curve)

$$\frac{\Delta P}{L} = \frac{(0.0083)\ (9.34)^2\ (10.6)}{(25.81)\ \ (2.865)} = 0.1033 \text{ psi/ft}$$

Friction Loss in the Annulus Between Drill Pipe and Hole

$\alpha = 3.5/6.5 = 0.5385$

$$V = \frac{(17.16)\ (4.5)}{(6.5)^2\ [1 - (0.5385)^2]} = 2.57 \text{ ft/sec}$$

$$Bi = \frac{(39.9)\,(6.51)\,(1 - 0.5385)\,(17)}{(38)\ \ (2.57)} = 20.83$$

$\gamma_1 = 0.295$ (from Fig. 7 and $\alpha = 1.0$)

$$\gamma_1 R_e = \frac{(927.7)\,(6.5)\,(1 - 0.5385)\,(2.57)\,(10.6)\,(0.295)}{(38)} = 588$$

$\gamma_1 R_e < 2{,}000$

$f = 0.0410$ (from Fig. 8 and $\alpha = 1.0$)

$$\frac{\Delta P}{L} = \frac{(0.0410)\ (2.57)^2\ (10.6)}{(25.81)\,(6.5)\,(1-0.5385)} = 0.0371 \text{ psi/ft}$$

Over-all Friction Loss in Pipe and Annulus

$$5{,}000\ (0.1033 + 0.0371) = 702 \text{ psi}$$

Friction Loss in Annulus (Cement)

Dimensions of pipe and hole and circulating rate are as follows:

Hole diameter	(D_2)	= 9 in.
OD of casing	(D_1)	= 7 in.
Depth	(L)	= 1,300 ft
Circulation rate	(Q)	= 2 bbl/min

Cement properties are as follows:

Portland (type 1) cement		
Plastic viscosity	(μ)	= 370 cp
Yield point	(ϕ)	= 110 lb/100 ft²
Density	(ρ)	= 14 lb/gal

Friction Loss Due to Flow

$\alpha = 7/9 = 0.7777$

$$V = \frac{(17.16)\ (20)}{(9)^2\,[1 - (0.7777)^2]} = 1.07 \text{ ft/sec}$$

$$Bi = \frac{(39.9)\,(9)\,(1-0.7777)\,(110)}{(370)\ \ (0.107)} = 22.18$$

$\gamma_1 = 0.285$ (from Fig. 7 and $\alpha = 1.0$)

$$\gamma_1 R_e = \frac{(927.7)\,(9)\,(1-0.7777)\ (1.07)\,(14)\,(0.285)}{370} = 21.4$$

$\gamma_1 R_e < 2{,}000$

$f = 1.15$ (from Fig. 8 and $\alpha = 1.0$)

$$\frac{\Delta P}{L} = \frac{(1.15)\ (1.07)^2\,(14)}{(25.81)\,(9)\,(1-0.7777)} = 0.3569 \text{ psi/ft}$$

$\Delta P = 464$ psi

Total Pressure Required to Initiate Flow

Circulation has been stopped for a period of one hour.

TABLE 4—SUGGESTED SCHEME OF ENGINEERING UNITS

Quantity	Notation	Units
Viscosity	μ	
Plastic viscosity	μ	cp
Yield point	ϕ	lb/100 ft²
Gel strength at time t	S_t	lb/100 ft²
Density	ρ	lb/gal
Friction loss	$\Delta P/L$	psi/ft
Flow rate	Q	bbl/min
OD of inner pipe	D_1	in.
ID of outer pipe	D_2	in.
D_1/D_2	α	dimensionless
Fluid velocity	$V = \frac{(17.16)\ Q}{D_2^2(1-\alpha^2)}$	ft/sec
Reynolds number	$R_e = \frac{(927.7)\ D_2(1-\alpha)\ V\rho}{\mu}$	dimensionless
Friction factor	$f = \frac{(25.81)\ D_2\ (1-\alpha)\triangle P}{V^2\rho L}$	dimensionless
Bingham number	$Bi = \frac{(39.9)\ D_2\ (1-\alpha)\ \phi}{\mu V}$	dimensionless

A pilot test on a portion of the drilling fluid shows that a gel strength of 50 lb/100 ft^2 develops during this time interval.

Dimensions of pipe and hole are as follows: hole diameter (D_2) = 9.875 in.; OD of drill pipe (D_1) = 4.5 in.; $\alpha = 4.5/9.875 = 0.4557$; and

$$\frac{\Delta P}{L} = \frac{(3.33 \times 10^{-3})\ (50)}{(9.875)\ (0.4557)\ (1 - 0.4557)} = 0.0680 \text{ psi/ft}$$

ACKNOWLEDGMENT

The authors wish to acknowledge the contributions of W. C. Schwemer and J. S. McNiel, Jr. to the approach developed in this paper. We also wish to express our appreciation to the Magnolia Petroleum Co. (a Socony Mobil affiliate) for permission to publish this paper.

REFERENCES

1. Melrose, J. C. and Lilienthal, W. B.: *Trans.* AIME (1951) **192,** 159.
2. Savins, J. G. and Roper, W. F.: *Drill. and Prod. Prac.*, API, 1954 (1955) 7.
3. Beck, R. W., Nuss, W. F. and Dunn, T. H.: *Drill. and Prod. Prac.*, API (1947) 9.
4. Reiner, M.: *Deformation and Flow* (1949) 39.
5. Van Olphen, H.: *Jour. Inst. Pet.* (1950) **36,** 223.
6. Lamb, H.: *Hydrodynamics* (1924) 5th ed., 555.
7. Grodde, K. H.: *Erd. u. Kohle* (1953) **6,** 380.
8. Mori, Y. and Ototake, N.: *Chem. Engr.* (Japan) (1953) **17,** 224.
9. Laird, W. M.: *Ind. Engr. Chem.* (1957) **49,** 138.
10. Frederickson, A. G. and Bird, R. B.: *Ind. Engr. Chem.* (1958) **50,** 347.
11. Scarborough, J. B.: *Numerical Mathematical Analysis* (1955) 3rd ed., 192, 203.
12. Prager, W.: *Rheology* (1956) edited by F. R. Eirich, **1,** 93.
13. Becker, E.: *Zeit. ver deut. Ing.* (1907) **51,** 1133.
14. Winkel, R.: *Zeit. angew. Math. Mech.* (1923) **3,** 251.
15. Carpenter, F. G., Colburn, A. P. and Schoenborn, E. M.: *Trans.* AIChE (1946) **42,** 165.
16. Hedstrom, B. O. A.: *Ind. Engr. Chem.* (1952) **44,** 651; see also Weltmann, R. N.: *Ind. Engr. Chem.* (1956) **48,** 386.
17. Monrad, C. C. and Pelton, J. F.: *Trans.* AIChE (1942) **38,** 593.
18. Rothfus, R. R., Monrad, C. C. and Senecal, V. E.: *Ind. Engr. Chem.* (1950) **42,** 2511.
19. Nootbaar, R. F. and Kintner, R. C.: *Bull,* Ohio State U. Engr. Exp. Sta. (1952) No. 149.
20. Prengle, R. S. and Rothfus, R. R.: *Ind. Engr. Chem.* (1955) **47,** 379.

APPENDIX 1

SUMMARY OF FUNDAMENTAL FLOW EQUATIONS

NEWTONIAN FLUIDS

Pipe (Poiseuille equation):

$$Q = \frac{\pi D^4 \Delta P}{128 \mu L}.$$

Slit:

$$Q = \frac{W D_s^3 \Delta P}{12 \mu L},$$

where W is length of slit and D_s is width of slit.

Annulus (Lamb equation):

$$Q = \frac{\pi D_2^4 \Delta P}{128 \mu L}(1 - \alpha^2)\left[1 + \alpha^2 - \frac{(1 - \alpha^2)}{\log_e (1/\alpha)}\right].$$

Narrow Annulus (same as slit case):

$$W = \frac{\pi}{2} D_2 (1 + \alpha)$$

$$D_s = \frac{1}{2} D_2 (1 - \alpha).$$

BINGHAM PLASTIC FLUIDS

Pipe (Buckingham-Reiner equation):

$$Q = \frac{\pi D^4 \Delta P}{128 \mu L}\left[1 - \frac{4}{3}\left(\frac{4\phi L}{D \Delta P}\right) + \frac{1}{3}\left(\frac{4\phi L}{D \Delta P}\right)^4\right].$$

Slit:

$$Q = \frac{W D_2^3 \Delta P}{12 \mu L}\left[1 - \frac{3}{2}\left(\frac{2\phi L}{D_s \Delta P}\right) + \frac{1}{2}\left(\frac{2\phi L}{D_s \Delta P}\right)^3\right].$$

Annulus (see Fig. 1 for definition of β_1 and β_2):

$$Q = \frac{\pi D_2^4 \Delta P}{128 \mu L}\left[(1 - \alpha^2)(1 + \alpha^2 - 2\beta_1\beta_2) - \frac{4}{3}\left(\frac{4\phi L}{D_2 \Delta P}\right)\left\{1 + \alpha^3 - \frac{1}{4}\left[\left(\frac{4\phi L}{D_2 \Delta P}\right)^2 + 4\beta_1\beta_2\right]^{3/2}\right\}\right],$$

with the subsidiary condition that

$$0 = 1 - \alpha^2 - 2\left(\frac{4\phi L}{D_2 \Delta P}\right)\left\{1 + \alpha^2 - \frac{1}{2}\left[\left(\frac{4\phi L}{D_2 \Delta P}\right)^2 + 4\beta_1\beta_2\right]^{1/2}\right\} + 2\beta_1\beta_2 \left\{\log_e(\alpha) + \log_e \frac{\left[\left(\frac{4\phi L}{D_2 \Delta P}\right)^2 \beta_1\beta_2\right]^{1/2} + \left(\frac{4\phi L}{D_2 \Delta P}\right)}{\left[\left(\frac{4\phi L}{D_2 \Delta P}\right)^2 + 4\beta_1\beta_2\right]^{1/2} - \left(\frac{4\phi L}{D_2 \Delta P}\right)}\right\}.$$

APPENDIX 2

RESULTS OF OTHER INVESTIGATORS

Beck, Nuss and Dunn[3]:

$$\gamma = \frac{3}{2} - 2x.$$

Van Olphen[5]:

$$\gamma = \gamma_N\left[1 - 4x\left(\frac{1 - \alpha}{1 + \alpha}\right)\right] + 6x\,(1 + \alpha)^{-1}(1 - \alpha)^{-2}\left[(1 - \alpha)(1 + \alpha^2) - \frac{1}{3}(1 - \alpha^3)\right],$$

where

$$\gamma_N = \frac{3}{2}\,(1 - \alpha)^{-2}\left\{1 + \alpha^2 - \frac{(1 - \alpha^2)}{\log_e (1/\alpha)}\right\}.$$

Grodde[7]:

$$\gamma = 1 - x^3$$

Laird (approximate solution)[9]:

$$\gamma = \gamma_N(1 - 2x) + 3x(1 + \alpha)^{-1}(1 - \alpha)^{-2}\left[(1 + \alpha)(1 + \alpha^2) - \frac{2}{3}(1 + \alpha^3) - \frac{2\sqrt{2}}{3}\left\{1 + \alpha^2 - \frac{2}{3}(1 - \alpha)^2\gamma_N\right\}^{3/2}\right].$$

APPENDIX 3

STEPS IN CALCULATION OF FRICTION LOSSES

FRICTION LOSSES IN PIPE (BINGHAM PLASTIC)

$$D_2 = D;\ \alpha = 0$$

Step (a)

Calculate,

$$V = (17.16)\frac{Q}{D^2}$$

$$Bi = (39.9)\frac{D\phi}{\mu V}$$

Step (b)

Refer to Fig. 7, find γ_o corresponding to Bi on the curve labeled $\alpha = 0$.

Step (c)

Calculate,

$$\gamma_o R_e = (927.7)\gamma_o\left(\frac{DV\rho}{\mu}\right)$$

Skip Step (d) and go on to Step (e) if $\gamma_o R_e > 2{,}000$ since this means the material is in turbulent flow.

Step (d) $\gamma_o R_e < 2{,}000$

Refer to Fig. 8, find f corresponding to $\gamma_o R_e$ on the curve labeled $\alpha = 0$.

Step (e) $\gamma_o R_e > 2{,}000$

Refer to Fig. 8, find f corresponding to R_e on the Stanton-Pannell line.

Step (f)

Calculate,

$$\frac{\Delta P}{L} = \frac{fV^2\rho}{(25.81)D}$$

Friction Losses in Annuli (Bingham Plastic)

Step (a)

Calculate,

$$\alpha = D_1/D_2$$

$$V = \frac{(17.16)Q}{D_2^2(1-\alpha^2)}$$

$$Bi = \frac{(39.9)D_2(1-\alpha)\phi}{\mu V}$$

Step (b)

Refer to Fig. 7, find γ_1 corresponding to Bi on the curve labeled $\alpha = 1.0$.

Step (c)

Calculate,

$$\gamma_1 R_e = (927.7)\gamma_1\left[\frac{D_2\ (1-\alpha)V\rho}{\mu}\right]$$

Skip Step (d) and go on to Step (e) if $\gamma_1 R_e > 2{,}000$ since this means the material is in turbulent flow.

Step (d) $\gamma_1 R_e < 2{,}000$

Refer to Fig. 8, find f corresponding to $\gamma_1 R_e$ on the curve labeled $\alpha = 1.0$.

Step (e) $\gamma_1 R_e > 2{,}000$

Refer to Fig. 8, find f corresponding to R_e on the Stanton-Pannell line.

Step (f)

Calculate,

$$\frac{\Delta P}{L} = \frac{fV^2\rho}{(25.81)D_2(1-\alpha)}$$

Pressure Required to Initiate Flow

drill pipe

$$D_2 = D;\ \alpha = 0$$

Calculate,

$$\frac{\Delta P}{L} = (3.333 \times 10^{-3})\frac{S_t}{D}$$

annulus

Calculate,

$$\alpha = D_1/D_2$$

$$\frac{\Delta P}{L} = \frac{(3.333 \times 10^{-3})S_t}{D_2(1-\alpha)}$$

total (pipe plus annulus)

Calculate,

$$\alpha = D_1/D_2$$

$$\frac{\Delta P}{L} = \frac{(3.333 \times 10^{-3})S_t}{D_2\alpha(1-\alpha)}$$

★★★

Generalized Newtonian (Pseudoplastic) Flow in Stationary Pipes and Annuli

J. G. SAVINS | MAGNOLIA PETROLEUM CO. DALLAS, TEX.

INTRODUCTION

The first paper in this series[1] outlined practical methods for applying the theory of steady-state flow of an ideal Bingham plastic liquid through a circular pipe and axially through a stationary concentric annulus to the engineering analysis of friction loss problems.

In the present paper the properties of another useful rheological model, the pseudoplastic generalized Newtonian liquid, are considered. The terminology applied to the rheological models is derived from the following classification of rheological models. The term "generalized Newtonian" is a class designation applied to models which do not have yield points but which exhibit a dependence on shear rate. The term "pseudoplastic" applies to a sub-group of models within this class which exhibit a decrease in "viscosity" with increasing shear rate. The term "power model" refers to a mathematical model proposed for describing the behavior of the pseudoplastic liquid. This model is of interest since certain of the salt saturated, oil emulsion, and "low solids" drilling fluids, inverted emulsion- and oil-base drilling fluids, aqueous gels, gelled crudes and blocking agents employed in hydraulic fracturing operations are of this type.

The present treatment considers the equations describing steady-state Poiseuille flow through a circular pipe and a stationary concentric annulus, and Couette flow between concentric rotating cylinders for a particular pseudoplastic model. As in the previous paper[1] it is demonstrated how these equations can be applied to engineering calculations of friction losses. Graphical procedures for recovering the various flow curves and example calculations are included. A method for simplifying turbulent-flow correlations is also proposed.

PROPERTIES OF PSEUDOPLASTIC GENERALIZED NEWTONIAN LIQUID

In contrast to the Bingham plastic the generalized Newtonian liquid is yield point-free. However, in the flow region the relation between stress and rate of shear is not linear as it is with ordinary Newtonian fluids. If the stress increases with shear rate at a less than linear rate the system is called pseudoplastic. While there is no yield point in this system, the Bingham advocates[2] coined the term pseudoplastic to distinguish this kind of behavior from Bingham plastic behavior. For the pseudoplastic a plot of flow rate vs friction loss or rpm vs torque, from pipe flow or rotational viscometer measurements, respectively, generally has three qualities: (1) it can be clearly extrapolated toward the origin; (2) there is very little slope at the origin. This accounts for the high apparent viscosities at low mixing and pumping rates; and (3) the flow curve possesses a continuous curvature which gradually diminishes as the shear increases.

Rheological measurements on a pseudoplastic liquid can be easily misinterpreted as indicating Bingham plastic behavior. A typical case in point is illustrated in Fig. 1. These data were obtained from measurements on an oil-emulsion mud using a commercially available rotational-type viscometer (Model 35 Fann V-G meter). Applying the "two-point"* method[3] gives a plastic viscosity of 17 cp and a yield point of 24 lb/100 ft^2; at the same time weighting material settles very easily in this system. This illustrates that it is not possible to distinguish between the pseudoplastic and the Bingham plastic from only two data points.

It is possible to determine qualitatively which model is more appropriate by a combination of dynamic and static measurements. Experience indicates that the simplest criterion for the Bingham plastic liquid is that the calculated dynamic yield point should be of the same magnitude as the measured gel strengths. For the oil-emulsion drilling fluid illustrated in Fig. 1, a value of 4 lb/100 ft^2 was obtained for gel strengths measured

*In the two-point method the plastic viscosity is proportional to the reciprocal of the differential slope, while the yield point is read directly from the intercept on the dial reading axis corresponding to zero rpm.

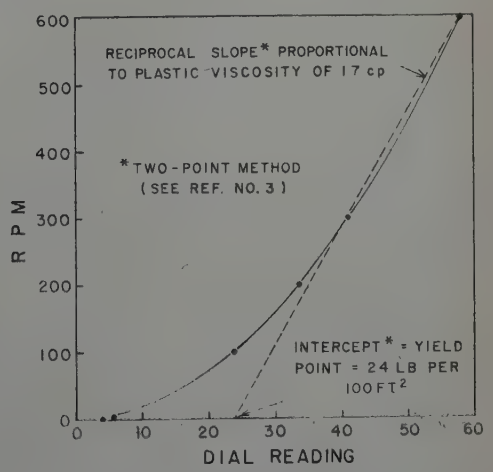

FIG. 1—TYPICAL FLOW CURVE, OIL EMULSION DRILLING FLUID.

Original manuscript received in Society of Petroleum Engineers office May 27, 1958. Revised manuscript received Nov. 3, 1958.
[1]References given at end of paper.

after 0 and 10-minute rest times. Thus, if the calculated yield point is significantly larger than the static gel strengths, the system may be pseudoplastic. If the gels measured at the longer rest times are quite low and there is little evidence of thixotropy, as is often the case in well stabilized drilling fluids, the system is definitely pseudoplastic. Another useful criterion which can be applied where more than two data points are available, e.g., from use of the Model 35 V-G meter, is that on a logarithmic plot most pseudoplastic flow curves are straight lines while the Bingham plastic flow curve is continuously curved concave to the dial reading axis.

Fortunately, there will be many cases where a friction loss calculated using the Bingham model and one calculated using the pseudoplastic model will differ only by an amount well within the limits of accuracy with which the independent variables can be measured. However, the practice of predicting the "suspending power" of a mud for weighting material or of a fracturing fluid for sand from a calculated yield point can give rise to serious error if the material is actually pseudoplastic.

POWER MODEL LIQUID

There have been various mathematical models proposed for the pseudoplastic fluids. One that has found widespread use is called the "power model", defined as a body for which the rate of shear is proportional to some power of the shearing stress.

$$\dot{e} = k\tau^N , \quad . \quad . \quad . \quad . \quad . \quad . \quad . \quad . \quad . \quad . \quad . \quad (1)$$

where $\dot{e}$ is shear rate in two dimensional flow, τ is shearing stress, and k,N are rheological parameters ($N>1$). Its flow curve is a straight line on a logarithmic plot. Reiner[2] discusses the shortcomings of this model in considerable detail. It is clear that it does not correctly portray the behavior of real fluids as $\tau \to 0$ and again as $\tau \to \infty$. However, these limitations appear to be unimportant for many practical problems and the model has been applied with surprising accuracy to the design of piping systems involving the manufacture, handling and application of a significant number of pseudoplastic materials.

BASIC FLOW EQUATIONS

The Pipe Case

The equation[4] for slip-free flow of a power model liquid in a cylindrical pipe is as follows.

$$(2N + 6)\frac{V}{D} = k\left(\frac{D\Delta p}{4L}\right)^N, \quad . \quad . \quad . \quad . \quad . \quad . \quad (2)$$

where V is bulk average velocity, D is pipe ID, and $\frac{\Delta P}{L}$ is pressure gradient.

It is convenient to write Eq. 2 in the form

$$D_p = \gamma_p k \tau_p^N , \quad . \quad . \quad . \quad . \quad . \quad . \quad . \quad . \quad . \quad . \quad (3a)$$

where

$$\gamma_p = \frac{8}{2N+6} \quad . \quad . \quad . \quad . \quad . \quad . \quad . \quad . \quad . \quad . \quad (3b)$$

$$\tau_p = \frac{D\Delta p}{4L} \quad . \quad . \quad . \quad . \quad . \quad . \quad . \quad . \quad . \quad . \quad (3c)$$

$$D_p = \frac{8V}{D} \quad . \quad . \quad . \quad . \quad . \quad . \quad . \quad . \quad . \quad . \quad (3d)$$

When plotted on logarithmic paper as D_p vs τ_p a straight line is produced. It is seen that N is the slope whereas the intercept of the line on the τ_p or $\frac{D\Delta p}{4L}$ axis where D_p is unity, is related to $\gamma_p k$,

$$\left(\frac{D\Delta p}{4L}\right)_{int.} = K'_p, \quad . \quad . \quad . \quad . \quad . \quad . \quad . \quad . \quad . \quad (4a)$$

where

$$K'_p = (\gamma_p k)^{-n'} \quad . \quad . \quad . \quad . \quad . \quad . \quad . \quad . \quad . \quad . \quad (4b)$$

$$n' = N^{-1} \quad . \quad . \quad . \quad . \quad . \quad . \quad . \quad . \quad . \quad . \quad . \quad (4c)$$

It is of interest to note that Farrow, *et al*[5], Fischer[6], Krieger and Maron[7] and Weltmann[8], among others, and more recently Metzner and Reed[9], have pointed out the feasibility of characterizing the degree of non-Newtonian behavior of various materials through the parameter N or its reciprocal.

With this method of plotting flow data for a pseudoplastic liquid the following precautions need to be observed. From the hydrodynamics of flow in a cylindrical tube the term $\frac{D\Delta p}{4L}$ is always the wall shearing stress, but the term D_p is the wall shear rate only for the simple Newtonian liquid. In the case of the model presented here the wall shear rate is D_p/γ_p. Neglect of the term has led several investigators into serious errors in correlating flow data on a given liquid from measurements in different geometries. It should also be noted that the intercept from this logarithmic plot is a dual function of both the rheological properties and conduit geometry. This means that in the K'_p form the intercept is applicable only to problems involving flow in cylindrical tubing.

The Concentric Annulus Case

An analytical expression for the flow of a power model liquid in a concentric annulus of circular section has been derived by Fredrickson and Bird[10],

$$Q = \frac{\pi D_2^3 k}{8}\left(\frac{D_2\Delta p}{4L}\right)^N \Omega_p , \quad . \quad . \quad . \quad . \quad . \quad . \quad . \quad (5a)$$

where

$$\Omega_p = \left[\sum_{\substack{i=0 \\ i=\frac{N+3}{2}}}^{N+1} \Xi_{N_i}\lambda^{2i} + \Xi_N\lambda^{N+3}\right], \quad . \quad . \quad . \quad (5b)$$

in which

$$\Xi_{Ni} = \binom{N+1}{i}\frac{(-1)^i}{N-2i+3}\left[1-(-1)^{N+1}\alpha^{N-2i+3}\right] \quad . \quad . \quad . \quad . \quad . \quad . \quad (5c)$$

$$\Xi_N = \binom{N+1}{\frac{N-1}{2}}(-1)^{\frac{N-1}{2}}\ln(1/\alpha) \quad (N \text{ odd}) \quad . \quad . \quad . \quad . \quad . \quad . \quad . \quad . \quad . \quad . \quad (5d)$$

$$\Xi_N = 2\sum_{i=0}^{N+1}\frac{\binom{N+1}{i}(-1)^i}{2i-N+1} \quad (N \text{ even}), \quad . \quad . \quad . \quad . \quad . \quad . \quad . \quad . \quad . \quad . \quad (5e)$$

$$\binom{N+1}{\frac{N-1}{2}} = \frac{(N+1)!}{\left(\frac{N-1}{2}\right)!\left(\frac{N+1}{2}\right)!},$$

$$\binom{N+1}{i} = \frac{(N+1)!}{i!(N+1-i)!},$$

λ = values of r/R for which $\tau = 0$,
D_2 = inside diameter of outer tube, and
αD_2 = outside diameter of inner tube.

Eq. 5b may also be expressed as

$$\Omega_p = \frac{(1-\alpha)^{N+2}}{(N+2)}\ \Upsilon \quad \ldots\ldots\ldots \quad (5f)$$

Fredrickson and Bird[10] hav tabulated values of Υ for selected values of N and α. However, it is difficult to apply their method to the practical engineering problems of relating flow rate to friction losses since it is first necessary to find Υ by interpolation, solve Eq. 5f for Ω_p, and finally express Eq. 5a in terms of these parameters.

From the very satisfactory manner in which the flow of a Bingham plastic liquid in a concentric annulus can be considered as plane rectilinear flow between fixed parallel plates[1], it seems desirable to examine the analogous equation for the slip-free flow of a power model liquid in a narrow annulus. Now the expression describing the flow of a power model liquid between fixed parallel plates[11] is

$$Q = \frac{WD_s^2 k}{(2N+4)}\left(\frac{D_s \Delta p}{2L}\right)^N, \quad \ldots\ldots \quad (6a)$$

where D_s is width of the rectangular section and W is length of the section ($W >> D_s$). Making the substitutions,

$$W = \frac{\pi D_2}{2}(1+\alpha) \quad \ldots\ldots\ldots \quad (6b)$$

$$D_s = \frac{D_2}{2}(1-\alpha), \quad \ldots\ldots\ldots \quad (6c)$$

we obtain the following equation describing slip-free flow of a power model liquid in a narrow concentric annulus.

$$Q = \frac{\pi D_2^3 k}{8}\left(\frac{D_2 \Delta p}{4L}\right)^N \Theta, \quad \ldots\ldots \quad (6d)$$

where

$$\Theta = \frac{(1-\alpha)^{N+2}}{(N+2)}\left(\frac{1+\alpha}{2}\right). \quad \ldots\ldots \quad (6e)$$

It is seen that the complicated term Υ appearing in Eqs. 5a and 5f is replaced in Eq. 6d by the group, $\left(\frac{1+\alpha}{2}\right)$.

In Table 1 are presented ratios of $\Upsilon \Big/ \frac{1+\alpha}{2}$ for selected values of N and α. For a fixed value of N the maximum error occurs at the lowest value of α; for example, at $N = 2$ the error is 13.99 per cent at $\alpha = 0.1$, but only 0.04 per cent at $\alpha = 0.9$. For a fixed value of α the error increases with increasing deviation from simple Newtonian behavior; for example at $\alpha = .3$ the error is 2.28 per cent at $N = 1$, 5.87 per cent at $N = 3$ and 11.1 per cent at $N = 10$. However, a majority of the pseudoplastic drilling and fracturing fluids, gels, etc., will probably have $N < 3$, α usually occuring between 0.3 and 0.9.

On the basis of the cited ranges in N and α and a probable maximum error of about 5 per cent, it appears that the simpler narrow annulus expression, Eq. 6d, will relate flow rate and friction loss with an accuracy well within the acceptable limits of practical engineering applications.

Rewriting Eq. 6d in the form of Eq. 2 gives

$$\frac{(4N+8)V}{D_2(1-\alpha)} = k\left[\frac{D_2(1-\alpha)\Delta p}{4L}\right]^N \quad \ldots \quad (7)$$

Eq. 7 reduces to the equation for plane rectilinear flow of a Newtonian liquid between fixed parallel plates when $N = 1$. It is convenient to rewrite Eq. 7 in the form

$$D_A = \gamma_A k \tau_A^N, \quad \ldots\ldots\ldots \quad (8a)$$

$$\gamma_A = \left(\frac{12}{4N+8}\right) \quad \ldots\ldots\ldots \quad (8b)$$

$$\tau_A = \frac{D_2(1-\alpha)\Delta p}{4L} \quad \ldots\ldots\ldots \quad (8c)$$

$$D_A = \frac{12V}{D_2(1-\alpha)} \quad \ldots\ldots\ldots \quad (8d)$$

When plotted on logarithmic paper as D_A vs τ_A a straight line is produced. Again, N is the slope while the intercept on the τ_A or $D_2\frac{(1-\alpha)\Delta p}{4L}$ axis where D_A is unity, is related to $\gamma_A k$,

$$\left[\frac{D_2(1-\alpha)\Delta p}{4L}\right]_{int.} = K'_A, \quad \ldots\ldots \quad (9a)$$

where

$$K'_A = (\gamma_A k)^{-n'} \quad \ldots\ldots\ldots \quad (9b)$$

Here the shear rate is D_A/γ_A.

The Rotational Viscometer Case

The equation which describes the behavior of a power model liquid in the rotational viscometer, in the absence of slip, is[5]

$$D_v = \frac{2\beta^2\omega}{\beta^2-1} = k\gamma_v \tau_v^N, \quad \ldots\ldots \quad (10)$$

where

$\beta = R_2/R_1$
$\tau_v = T/2\pi R_1^2 L$
R_2 = outer cylinder radius
R_1 = inner cylinder radius
ω = angular velocity
T = torque
L = inner cylinder effective length

$$\gamma_v = \left(\frac{\beta^2}{N\beta^{2N}}\right)\left(\frac{\beta^{2N}-1}{\beta^2-1}\right)$$

When plotted on logarithmic paper as $\frac{2\beta^2\omega}{\beta^2-1}$ vs $\frac{T}{2\pi R_1^2 L}$ a straight line is produced. By way of contrast, when a Bingham plastic liquid is plotted in this manner the plot will be continuously curved in a direction concave to the τ_v or $T/2\pi R_1^2 L$ axis throughout most of the range, followed toward the lower end of the range

TABLE 1—COMPARISON BETWEEN EXACT AND NARROW ANNULUS SOLUTIONS FOR POWER MODEL LIQUID IN CONCENTRIC ANNULUS

Ratio = $\Upsilon \Big/ \frac{1+\alpha}{2}$

α/N	1	2	3	4	5	6	7	8	9	10
0.1	1.0741	1.1399	1.1903	1.2281	1.2588	1.2810	1.2999	1.3153	1.3283	1.3393
0.2	1.0394	1.0741	1.1019	1.1226	1.1396	1.1531	1.1644	1.1736	1.1814	1.1882
0.3	1.0228	1.0431	1.0587	1.0716	1.0814	1.0898	1.0965	1.1021	1.1068	1.1110
0.4	1.0133	1.0255	1.0350	1.0423	1.0488	1.0530	1.0572	1.0596	1.0636	1.0659
0.5	1.0079	1.0147	1.0201	1.0246	1.0281	1.0309	1.0334	1.0346	1.0359	1.0370
0.6	1.0042	1.0080	1.0101	1.0133	1.0160	1.0180	1.0200	1.0210	1.0220	1.0230
0.7	1.00199	1.0038	1.0054	1.00599	1.00799	1.00905	1.00999	1.01105	1.01199	1.0130
0.8	1.00087	1.00165	1.00243	1.00298	1.00354	1.00398	1.00454	1.00498	1.00554	1.00598
0.9	1.000209	1.000419	1.00063	1.00084	1.00105	1.001156	1.001366	1.00157	1.00178	1.00199

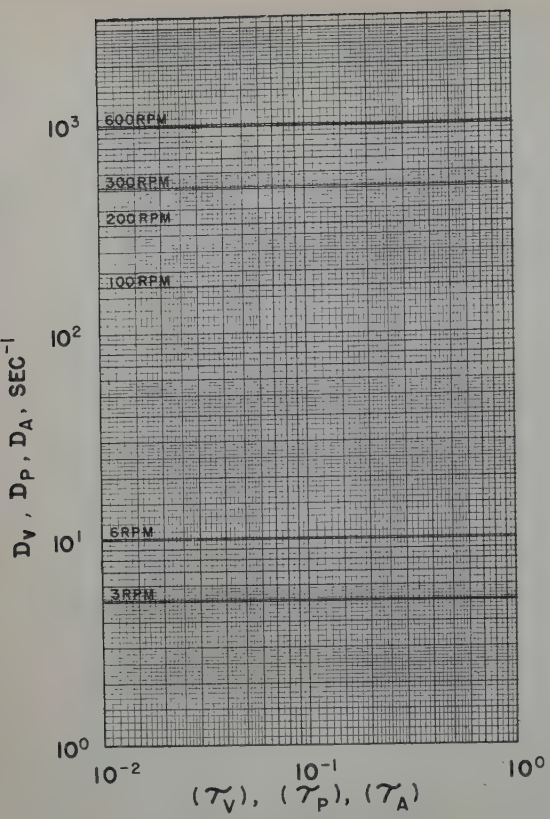

FIG. 2—PLOTTING SHEET.

by a region which will appear to be linear. These differences provide a ready means of distinguishing between the power model and the Bingham plastic. Returning to the logarithmic plot of the power model, N is the slope of the line; however, the intercept of the line on the τ_v or $T/2\pi R_1^2 L$ axis where $\frac{2\beta^2\omega}{\beta^2-1}$ is unity, is related to $\gamma_v k$,

$$\left(\frac{T}{2\pi R_1^2 L}\right)_{int.} = K'_v, \quad . \quad . \quad . \quad . \quad . \quad . \quad . \quad . \quad (11a)$$

where

$$K'_v = (\gamma_v k)^{n'} \quad . \quad . \quad . \quad . \quad . \quad . \quad . \quad . \quad . \quad . \quad (11b)$$

The term $T/2\pi R_1^2 L$ is always the shearing stress at the surface of the inner cylinder, but the term $\frac{2\beta^2\omega}{\beta^2-1}$ is the shear rate at the surface of the inner cylinder only for the simple Newtonian liquid. For the power model liquid the shear rate is $\frac{2\beta^2\omega}{\gamma_v(\beta^2-1)}$. In the case of the intercept from the logarithmic plot it should be noted from the stated definition of K'_p, K'_A and K'_v that flow data on a given power model liquid obtained in tubing or annular sections of varying sizes will form a composite plot, i.e., a single straight line, for either pipe or annular section data, whereas the flow data on the same liquid obtained in the rotational viscometer with inner and outer cylinders of varying sizes will form a family of parallel straight lines.

CORRELATIONS BETWEEN ROTATIONAL VISCOMETER, PIPE AND ANNULAR SECTION

It is evident from Eqs. 3, 8 and 10 that in logarithmic plots these expressions give rise to curves with identical slope but with different intercept values. The relationship expressed by Eqs. 4, 9 and 11 also indicates that the latter values can be readily expressed in terms of one another. This feature is the basis for correlating rotational viscometer, pipe and annular section flow curves.

ROTATIONAL VISCOMETER — PIPE CORRELATION

It follows from Eqs. 4b and 11b that

$$K'_p = K'_v \Big/ \left(\frac{\gamma_v}{\gamma_p}\right)^{-n'} \quad . \quad . \quad . \quad . \quad . \quad . \quad . \quad . \quad (12)$$

This expression conveniently relates the rotational viscometer and pipe flow curves in terms of β, the rotor bob radii ratio, and N or n', the slope of a logarithmic plot of Eq. 10. Since γ_v/γ_p is a function solely of β and N or n', a table or graph of K'_v/K'_p may be readily prepared for a given value of β and any range in N or n'. Table 2 gives values of $\frac{K'_v}{K'_p}$ for a 1 to 10 range in N and also includes corresponding values of γ_p and γ_v. For purposes of illustration the latter term is based on $\beta = 1.0678$, the radii ratio used in the commercially available viscometer referred to earlier. A graphical solution of Eq. 12 is described in Appendix A and illustrated in Fig. 3.

ROTATIONAL VISCOMETER — ANNULUS SECTION CORRELATION

Following the same plan as was used for the pipe case we can write from Eqs. 9b and 11b,

$$K'_A = K'_v \Big/ \left(\frac{\gamma_v}{\gamma_A}\right)^{-n'} \quad . \quad . \quad . \quad . \quad . \quad . \quad . \quad . \quad (13)$$

Again, $\frac{\gamma_v}{\gamma_A}$ is a function solely of β and N. Table 3

TABLE 2—ROTATIONAL VISCOMETER* — PIPE CORRELATION FUNCTIONS

N	n'	γ_p	γ_v	K'_v/K'_p
1.0000	1.00	1.00000	1.00000	1.0000
1.1111	0.90	0.97297	0.99318	0.9817
1.2500	0.80	0.94117	0.98437	0.9647
1.4285	0.70	0.90324	0.97229	0.9493
1.6666	0.60	0.85715	0.95844	0.9352
2.0000	0.50	0.80000	0.93853	0.9232
2.5000	0.40	0.72727	0.90959	0.9144
3.3333	0.30	0.63158	0.86421	0.9102
5.0000	0.20	0.50000	0.78239	0.9143
10.0000	0.10	0.30769	0.59411	0.9363

*Using $\beta = 1.0678$

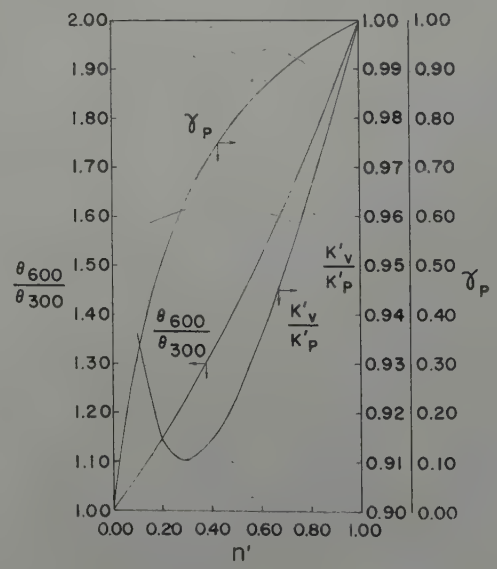

FIG. 3—PIPE CORRELATION DIAGRAM.

summarizes values of $\frac{K'_v}{K'_A}$ for a 1 to 10 range in N and also includes corresponding values of γ_A and γ_v. A graphical solution of Eq. 13 is described in Appendix A and illustrated in Fig. 4.

PRACTICAL APPLICATION

Predicting Pipe and Annulus Flow Curves from Rotational Viscometer Data

It was convenient, in view of extensive correlations already tabulated, to base the procedures described in Appendix B for constructing the pipe and annulus flow curves from rotational viscometer data on the design features of a specific design of rotational viscometer, the Model 35 Fann V-G meter. However, the procedures can be regarded as guides, useful with any rotational viscometer design from which the stress at the inner cylinder, τ_v, and the radii ratio, β, can be determined.

With regard to the mentioned instrument, there are six fixed values of $\frac{2\beta^2\omega}{\beta^2 - 1}$ corresponding to the six speed settings as shown in Table 4. The relationship between n' and the ratio of the 600-rpm dial reading θ_{600} to the 300-rpm dial reading θ_{300} is

$$n' = 3.32 \log \frac{\theta_{600}}{\theta_{300}} \quad . \quad . \quad . \quad . \quad . \quad . \quad . \quad . \quad . \quad (14)$$

Table 5 summarizes some values of $\frac{\theta_{600}}{\theta_{300}}$ for the range from 1.00 to 0.10 in n'. The relationship between τ_v in lb/ft^2 and any dial reading θ when the instrument is equipped with the standard torsion spring unit is

$$\tau_v = (0.01066)\theta \quad , \quad . \quad . \quad . \quad . \quad . \quad . \quad . \quad . \quad (15a)$$

and when range extension springs are available,

$$\tau_v = (RF)(0.01066)\theta \quad . \quad . \quad . \quad . \quad . \quad . \quad . \quad (15b)$$

where RF is range extension factor for the spring, i.e., 1/5, 1, 3, 5, etc.

The Criterion for Turbulence

It is desirable from an engineering viewpoint to preserve the concept of the friction factor-Reynolds number diagram when developing a method which defines a criterion for turbulence for any given rheological model. Metzner and Reed[9] correlated laminar and turbulent pipe flow data from the literature on the conventional friction factor plot. However, their development contains a cumbersome Reynolds number expression, the calculation of which can be simplified for the power model liquid. Furthermore, for this model, laminar friction loss calculations can become less involved compared to the method they employ. Weltmann[8] also retains the basic form of the friction factor plot, modeling her method for the generalized Newtonian after Hedstrom's[12] treatment for Bingham plastic flow in pipes. A disadvantage of Weltmann's method is the necessity for interpolating between curves of constant N which are superimposed on the friction factor plot.

TABLE 3—ROTATIONAL VISCOMETER* ANNULUS SECTION CORRELATION FUNCTIONS

N	n'	γ_A	γ_v	K'_v/K'_A
1.0000	1.00	1.00000	1.00000	1.0000
1.1111	0.90	0.96428	0.99318	0.9737
1.2500	0.80	0.92307	0.98437	0.9498
1.4285	0.70	0.97501	0.97299	0.9284
1.6666	0.60	0.81819	0.95844	0.9094
2.0000	0.50	0.75000	0.93853	0.8939
2.5000	0.40	0.66666	0.90959	0.8831
3.3333	0.30	0.56250	0.86421	0.8791
5.0000	0.20	0.42857	0.78239	0.8866
10.000	0.10	2.25000	0.59411	0.9170

*Using $\beta = 1.0678$

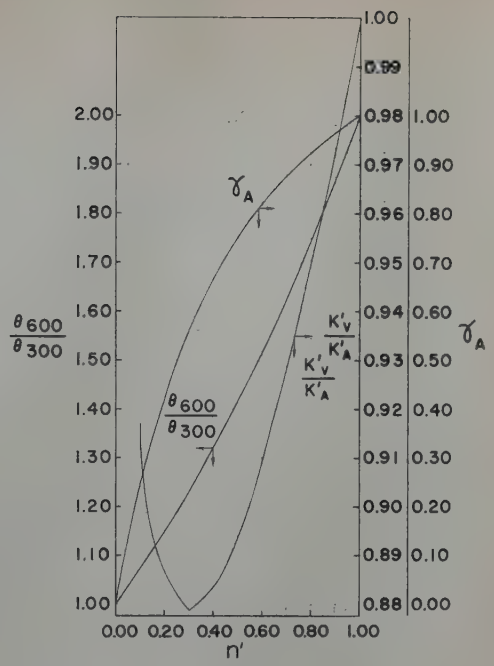

FIG. 4—ANNULAR SECTION CORRELATION DIAGRAM.

The method developed here likewise preserves the concept of the friction factor-Reynolds number relationship but does so in a simpler manner for the power model liquid. It is assumed that the transition between laminar and turbulent flow in both pipe and annular section occurs when a modified Reynolds number exceeds 2,000 and that in turbulent flow, friction factors for both pipe and annular section correlate on the Stanton-Pannell-type curve. The limitations involved are discussed in a following section.

The modified Reynolds number is developed as follows from the relationship,

$$f = \tau\left(\frac{2}{V^2\rho}\right), \quad . \quad . \quad . \quad . \quad . \quad . \quad . \quad . \quad . \quad (16a)$$

where

$$\tau = \left(\frac{\text{cross section}}{\text{wetted perimeter}}\right)\frac{\Delta p}{L} \quad . \quad . \quad . \quad . \quad (16b)$$

Now the usual friction factor-Reynolds number rela-

TABLE 4—THE NEWTONIAN SHEAR RATE AT THE INNER CYLINDER AS A FUNCTION OF RPM SETTING*

rpm	$\frac{2\beta^2\omega}{\beta^2 - 1}$ (sec^{-1})
600	1,022
300	511
200	340
100	170
6	10.2
3	5.1

*Standard rotor-bob combination and speed settings (Model 35 Fann V-G meter)

TABLE 5—VALUES OF N AND n' AS A FUNCTION OF $\frac{\theta_{600}}{\theta_{300}}$

N	n'	$\frac{\theta_{600}}{\theta_{300}}$
1.000	1.00	2.000
1.111	0.90	1.867
1.250	0.80	1.741
1.428	0.70	1.625
1.666	0.60	1.516
2.000	0.50	1.414
2.500	0.40	1.320
3.333	0.30	1.231
5.000	0.20	1.149
10.00	0.10	1.072

tionships in viscous flow for the pipe and narrow annulus are as follows.

Pipe $f = 16/R_e$ . . . . . (17a)

Annular section ($\alpha \rightarrow 1$) $f = 24/R_e$ . . . . . (17b)

Combining Eqs. 16 and 17, we can write the following Reynolds number groups for the simple Newtonian liquid.

Pipe $R_e = 8V^2\rho/\tau_p$ . . . . . (18a)

Annular section ($\alpha \rightarrow 1$) $R_e = 12V^2\rho/\tau_A$ . . . . . (18b)

By analogy for the power model liquid we can write,

Pipe $\gamma_p R_e = 8V^2\rho/\tau_p$ . . . . . (19a)

Annular section ($\alpha \rightarrow 1$) $\gamma_A R_e = 12V^2\rho/\tau_A$, ... (19b)

where the products $\gamma_p R_e$ and $\gamma_A R_e$ are the modified Reynolds number, reducing to Eqs. 18a and 18b when $N = 1$. The group $\gamma_p R_e$ is identical with the modified Reynolds number $\left(\frac{D^{1/N}V^{2-1/N}\rho}{K'_p\ 8^{1/N-1}}\right)$ described by Metzner and Reed[9].

Limitations

The procedures just described for handling the turbulent flow region for the power model liquid are based on assumptions similar in principal to those suggested elsewhere for non-Newtonian liquids[1,8,9,12]. These assumptions are: (1) the onset of turbulence can be expressed in terms of an arbitrarily chosen value of the modified Reynolds number and (2) in turbulent flow, friction factor data for both pipe and annular section can be correlated on a Stanton-Pannell-type curve.

These are tentative proposals still lacking experimental verification over a wide range of non-Newtonian behavior for the power model liquid. It is unlikely that they will yield much more than a qualitative idea about turbulent region friction losses for highly pseudoplastic power model liquids. For example, it certainly appears logical to expect that for flow in tubes the more pronounced viscosity gradient between wall and axis accompanying increased non-Newtonian behavior might effectively retard the onset of turbulence through a damping-like action on eddy sites and other points of disturbance. The net result would then be expected to be the appearance of a spectrum of critical modified Reynolds numbers and turbulent friction loss correlations for varying degrees of non-Newtonian behavior unless the modified Reynolds number can be redefined to include a damping term.

Calculation of Friction Losses

Appendix B describes procedures for predicting pipe and annulus flow curves from rotational viscometer data. Once these flow curves are constructed it is an easy matter to determine if a point of interest lies in laminar or turbulent flow using the procedures outlined in Appendix B. Briefly, the group D_p or D_A is calculated according to Eqs. 3d or 8d and located on the appropriate flow curve. Then τ_p or τ_A (Eqs. 3c or 8c) is found by inspection and the modified Reynolds number calculated from Eqs. 19a or 19b.

If the flow is laminar, i.e., $\gamma_p R_e$ or $\gamma_A R_e < 2{,}000$, the friction loss $\Delta p/L$ is simply

Pipe $\Delta p/L = 4\tau_p/D$ . . . . . (20a)

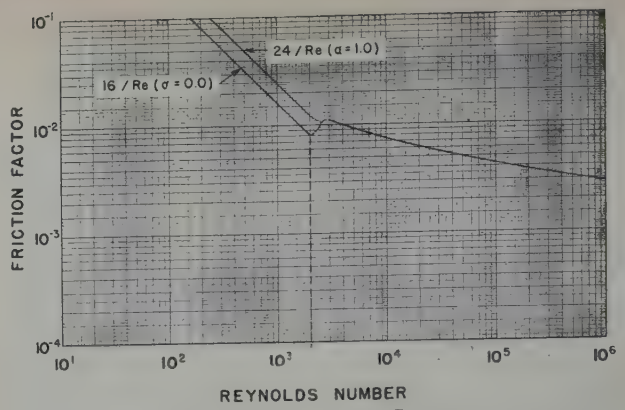

Fig. 5—Friction Factor Diagram.

Annular section ($\alpha \rightarrow 1$) $\Delta p/L = 4\tau_A/D_2(1 - \alpha)$. (20b)

If the flow is turbulent the friction factor (f) corresponding to $\gamma_p R_e$ or $\gamma_A R_e$ is found from a Stanton-Pannell-type correlation, Fig. 5. The friction loss $\Delta p/L$ is then simply

Pipe $\Delta p/L = \dfrac{2fV^2\rho}{D}$ . . . . . (21a)

Annular section ($\alpha \rightarrow 1$) $\Delta p/L = \dfrac{2fV^2\rho}{D_2(1 - \alpha)}$ . . (21b)

Sample Calculations

The following examples illustrate the methods outlined in Appendices A and B for predicting friction losses in tubing and annuli for power-model-type systems. Note that the system of units described in Table 6 is used exclusively in these examples.

The following data were recorded for a fracturing fluid using the standard Model 35 V-G meter (range factor = 1.0).

rpm	θ	τ_v*
600	58.0	0.618
300	41.0	0.437
200	33.5	0.357
100	23.7	0.253
6	5.8	0.0618
3	4.1	0.0437

*$\tau_v = (1)\ (0.01066)\theta$

These τ_v values are plotted in Fig. 6 as Curve V. By inspection, $K'_v = 0.0193$ and $\theta_{600}/\theta_{300} = 1.415$.

From Fig. 3, $n' = 0.50$, $K'_v/K'_p = 0.9233$, and $\therefore\ K'_p = 0.02090$. Using $K'_p = 0.02090$ as the base point, Curve P, the pipe flow curve, is plotted in Fig. 6.

Dimensions of tubing, circulation rate, and fluid density are as follows.

EXAMPLE NO. 1

ID of tubing $(D) = 2$ in.
Circulation rate $(Q) = 1.63$ bbl/min
Density $(\rho) = 7.508$ lb/gal

$$V = \frac{[17.16]\quad (1.63)}{(2)^2} = 7 \text{ ft/sec}$$

$$D_p = \frac{[96](7)}{(2)} = 336 \text{ sec}^{-1}$$

$\tau_p = 0.385$ lb/ft² (from Curve P, the abscissa value corresponding to $D_p = 336$ sec^{-1})

$$\gamma_p R_e = \frac{[1.858]\quad (7)^2\quad (7.508)}{(0.385)} = 1{,}775$$

$\gamma_p R_e < 2{,}000$

TABLE 6—TERMS AND SYSTEM OF UNITS USED IN FRICTION LOSS CALCULATIONS

Quantity	Notation	Units
Bulk average velocity	V	ft/sec
Correlation variable (annulus)	D_A	sec^{-1}
Correlation variable (pipe)	D_p	sec^{-1}
Correlation variable (rot. visc.)	D_v	sec^{-1}
Density	ρ	lb/gal
Dial reading	θ	degrees
Diameter ratio (annular section)	α	dimensionless
Diameter ratio (rotational visc.)	β	dimensionless
Flow curve intercept (annulus)	K'_A	lb (force)-$sec^{n'}/ft^2$
Flow curve intercept (pipe)	K'_p	lb (force)-$sec^{n'}/ft^2$
Flow curve intercept (rot. visc.)	K'_v	lb (force)-$sec^{n'}/ft^2$
Flow rate	Q	bbl/min
Friction factor	f	dimensionless
Friction loss	$\Delta p/L$	psi/ft
ID of outer pipe	D_2	in.
Modified Reynolds No. (annulus)	$\gamma_A R_e$	dimensionless
Modified Reynolds No. (pipe)	$\gamma_p R_e$	dimensionless
OD of inner pipe	D_1	in.
Reciprocal structure No.	n'	dimensionless
Shear rate factor (rot. visc.)	γ_v	dimensionless
Shear rate factor (annulus)	γ_A	dimensionless
Shear rate factor (pipe)	γ_p	dimensionless
Shear stress (annulus)	τ_A	lb/ft^2
Shear stress (pipe)	τ_p	lb/ft^2
Shear stress (rotational viscometer)	τ_v	lb/ft^2

$$\frac{\Delta p}{L} = \frac{(0.385)}{[3]\ (2)} = 0.06416 \text{ psi/ft}$$

EXAMPLE NO. 2

D, ρ = unchanged

$Q = 4.66$ bbl/min

$$V = \frac{[17.16]\ (4.66)}{(2)^2} = 20 \text{ ft/sec}$$

$$D_p = \frac{[96]\ (20)}{(2)} = 960^{-1}$$

$\tau_p = 0.652$ lb/ft² (from Curve P, the abscissa value corresponding to $D_p = 960$ sec^{-1})

$$\gamma_p R_e = \frac{[1.858]\ (20)^2\ (7.508)}{(0.652)} = 8{,}558$$

$\gamma_p R_e > 2{,}000$

$f = 0.0079$ (from Fig. 5, Stanton-Pannell curve, where $\gamma_p R_e = 8{,}558$)

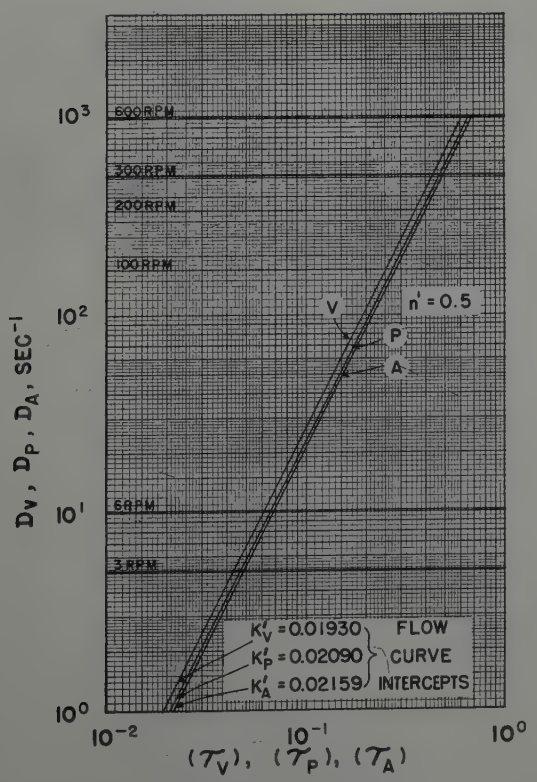

FIG. 6—EXAMPLE PLOT OF VG METER DATA AND RESULTING PIPE AND ANNULAR SECTION FLOW CURVES.

$$\Delta p/L = \frac{[0.03872]\ (0.0079)\ (20)^2\ (7.508)}{(2)}$$

$$= 0.4592 \text{ psi/ft}$$

Similar procedures were followed in constructing the annular section flow curve ($\alpha = 0.50$) plotted as Curve A in Fig. 6.

REFERENCES

1. Melrose, J. C., Savins, J. G., Foster, W. R. and Parish, E. R.: "A Practical Utilization of the Theory of Bingham Plastic Flow in Stationary Pipes and Annuli", *Trans.* AIME (1958) **213**, 324.
2. Reiner, M.: *Deformation and Flow*, H. K. Lewis and Co., Ltd., London (1949).
3. Savins, J. G. and Roper, W. F.: "A Direct-Indicating Viscometer for Drilling Fluids", *Drill. and Prod. Prac.*, API (1954) 7.
4. Porter, A. W. and Rao, P. A. M.: "The Law of Capillary Flow in the Case of Colloids", *Trans.* Faraday Soc. (1927) **23**, 311.
5. Farrow, F. D., Lowe, G. M. and Neale, S. M.: "The Flow of Starch Pastes—Flow at High and Low Rates of Shear", *Jour. Text. Inst.* (1928) **19**, T18.
6. Fischer, E. K.: *Colloidal Dispersions*, John Wiley and Sons, Inc., N. Y. (1950).
7. Krieger, I. M. and Maron, S. H.: "Rheology of Synthetic Latex. I. Test of Some Flow Equations", *Jour. Coll. Sci.* (1951) **6**, 528.
8. Weltmann, R. N.: "Friction Factors for Flow of Non-Newtonian Materials in Pipelines", *Ind. Eng. Chem.* (1956) **48**, 386.
9. Metzner, A. B. and Reed, J. C.: "Flow of Non-Newtonian Fluids—Correlation of the Laminar, Transition and Turbulent-Flow Regions", *AIChE Jour.* (1955) **1**, 434.
10. Fredrickson, A. G. and Bird, R. B.: "Non-Newtonian Flow in Annuli", *Ind. Eng. Chem.* (1958) **50**, 347.
11. Mooney, M. and Black, S. A.: "A Generalized Fluidity Power Law and Laws of Extrusion", *Jour. Coll. Sci.* (1952) **7**, 204.
12. Hedstrom, B. O. A.: "Flow of Plastic Materials in Pipes", *Ind. Eng. Chem.* (1952) **44**, 651.

APPENDIX A

DESCRIPTION OF GRAPHICAL AIDS

Plotting Sheet

A sample plotting sheet is presented in Fig. 2. The ordinate scale is labeled D_v, D_p and D_A, sec^{-1}. The scale is indexed as 10°, 10, etc. Horizontal lines are drawn across the plotting sheet from the following ordinate points: 1,022, 511, 340, 170, 10.2 and 5.1, and labeled 600, 300, 200, 100, 6 and 3 rpm, respectively. (These are the values, see Table 4, of the Newtonian shear rate at the wall of the inner cylinder of the Model 35 V-G meter when the standard rotor-bob combination is used.)

The abscissa scale is labeled (τ_v), (τ_p) and (τ_A), lb/ft^2. It is indexed as 10^{-2}, 10^{-1}, 10^0, etc.

Pipe Correlation Diagram

A sample correlation diagram is presented in Fig. 3. The curves are graphical solutions of Eqs. 3b, 12 and 14, and have been provided to facilitate accurate interpolation.

The ordinate scale, left margin, is labeled $\theta_{600}/\theta_{300}$ and is indexed as 1:00; 1.10; 1.20; 1.30; 1.40; 1.50; 1.60; 1.70; 1.80; 1.90 and 2.00. The right margin consists of a double scale. The inner scale is labeled. K'_v/K'_p and is indexed as 0.90; 0.91; 0.92; 0.93; 0.94; 0.95; 0.96; 0.97; 0.98; 0.99 and 1.00. The outer scale is labeled γ_p and is indexed as 0; 0.10; 0.20; 0.30; 0.40; 0.50; 0.60; 0.70; 0.80; 0.90 and 1.00.

The abscissa scale is labeled n' and is indexed as 0.00; 0.10; 0.20; 0.30; 0.40; 0.50; 0.60; 0.70; 0.80; 0.90 and 1.00.

Annular Section Correlation Diagram

A sample correlation diagram is presented in Fig. 4. The curves are graphical solutions of Eqs. 8b, 13 and 14.

The ordinate scale, left margin, is labeled $\theta_{600}/\theta_{300}$ and is indexed as 1.00; 1.10; 1.20; 1.30; 1.40; 1.50; 1.60; 1.70; 1.80; 1.90 and 2.00. The right margin consists of a double scale. The inner scale is labeled K'_v/K'_A and is indexed as 0.88; 0.89; 0.90; 0.91; 0.92; 0.93; 0.94; 0.95; 0.96; 0.97; 0.98; 0.99 and 1.00. The outer scale is labeled γ_A and is indexed as 0; 0.10; 0.20; 0.30; 0.40; 0.50; 0.60; 0.70; 0.80; 0.90 and 1.00.

The abscissa scale is labeled n' and is indexed as 0.00; 0.10; 0.20; 0.30; 0.40; 0.50; 0.60; 0.70; 0.80; 0.90 and 1.00.

APPENDIX B

PROCEDURES FOR CONSTRUCTING FLOW CURVES

The V-G Meter Curve

Multiply the dial reading θ at each speed setting by (RF) (0.01066), where RF is the range extension factor, to obtain τ_v values. (Note: $RF = 1.0$ for the standard version of the Model 35 V-G meter.) Record on the plotting sheet, Fig. 2, τ_{600} on the 600-rpm line, τ_{300} on the 300-rpm line, etc., and construct the best line through the points. If the line is significantly concave to the τ_v axis, the method outlined in the first paper[3] for computing pressure drop due to Bingham plastic flow should be used.

The Pipe Flow Curve

On the plotting sheet read the intercept K'_v from the V-G meter curve on the scale where D_p is unity. Next, determine $\theta_{600}/\theta_{300}$. On the pipe correlation diagram, Fig. 3, read n' corresponding to $\theta_{600}/\theta_{300}$. Next, read K'_v/K'_p corresponding to n'. From K'_v/K'_p and K'_v find K'_p. With K'_p as the base point draw a straight line parallel to the V-G meter curve; this displaced line is the pipe flow curve.

The Annular Section Flow Curve

On the plotting sheet read the intercept K'_v from the V-G meter curve on the scale where D_A is unity. Next, determine $\theta_{600}/\theta_{300}$. On the annular section correlation diagram, Fig. 4, read n' corresponding to $\theta_{600}/\theta_{300}$. Next, read K'_v/K'_A corresponding to n'. From K'_v/K'_A and K'_v find K'_A. With K'_A as the base point draw a straight line parallel to the V-G meter curve; this displaced line is the annular section flow curve.

Friction Loss in Pipe

Step (a)
Calculate

$$V = (17.16)\frac{Q}{D^2}$$

$$D_p = (96)\frac{V}{D}.$$

Step (b)
Find τ_p, lb/ft², corresponding to D_p by inspection from the pipe flow curve

Step (c)
Calculate

$$\gamma_p R_e = (1.858)\frac{V^2\rho}{\tau_p}.$$

Step (d) $\gamma_p R_e < 2{,}000$

$$\frac{\Delta p}{L} = \frac{\tau_p}{(3)\ D}.$$

Step (e) $\gamma_p R_e > 2{,}000$
Refer to Fig. 5; find f corresponding to $\gamma_p R_e$ on the Stanton-Pannell line.

Step (f)
Calculate

$$\frac{\Delta p}{L} = (0.03872)\frac{fV^2\rho}{D}$$

Friction Loss in Annular Section

Step (a)
Calculate

$$\alpha = D_1/D_2$$

$$V = (17.16)\frac{Q}{D_2^2(1-\alpha^2)}$$

$$D_A = (144)\frac{V}{D_2(1-\alpha)}.$$

Step (b)
Find τ_A, lb/ft², corresponding to D_A by inspection from the annular section flow curve.

Step (c)
Calculate

$$\gamma_A R_e = (2.787)\frac{V^2\rho}{\tau_A}.$$

Step (d)
$\gamma_A R_e < 2{,}000$

$$\frac{\Delta p}{L} = \frac{\tau_A}{(3)\ D_2(1-\alpha)}.$$

Step (e) $\gamma_A R_e > 2{,}000$
Refer to Fig. 5; find f corresponding to $\gamma_A R_e$ on the Stanton-Pannell line.

Step (f)
Calculate

$$\frac{\Delta p}{L} = (0.03872)\frac{fV^2\rho}{D_2(1-\alpha)}.$$

★★★

A Correlation of the Electrical Properties of Drilling Fluids with Solids Content

HAROLD L. OVERTON
JUNIOR MEMBER AIME
LEONARD B. LIPSON
MEMBER AIME

UNIVERSITY OF HOUSTON
HOUSTON, TEX.

ABSTRACT

An approach to the study of the electrical properties of drilling muds, their cakes and their filtrates was made by treating the drilling fluid as a porous medium. During this study it was found that the weight parameter was omitted from previous investigations on electrical properties. Patnode in 1949 made a similar approach to this investigation. His work showed that there was a variation of resistivity relationships with per cent fluid present in a given suspension. This present study extends Patnode's investigation to one in terms of the solids fraction of the drilling fluids. Previous investigations were made on low weight muds where the effect of the solids fraction was obscured. The following equations were fitted to data taken from 94 field muds and 47 laboratory muds (see Tables 1 and 2).

$$R_{mf} = C\,(R_m)^{1.07} \quad . \quad . \quad . \quad . \quad . \quad . \quad . \quad . \quad . \quad (1)$$

The parameter, C, is a complex function of the solids content, or mud weight, of a drilling fluid. It was also found that

$$\frac{R_{mc}}{R_{mf}} \leq 0.69 \left(\frac{R_m}{R_{mf}}\right)^{2.65} \quad . \quad . \quad . \quad . \quad . \quad . \quad . \quad . \quad . \quad (2)$$

for all drilling muds examined. A nomograph is presented combining Eqs. 1 and 2.

INTRODUCTION

It is generally recognized that the materials present in drilling muds affect the relationship between mud filtrate and mud resistivities. However, most electric log interpretations proceed with the assumption that the mud resistivity and temperature are the only important parameters needed to obtain a filtrate resistivity or a mud cake resistivity.

Lamont[1] suggests that only average relationships exist between mud cake, mud filtrate and mud resistivities. He indicates that there is limited accuracy when these intercorrelated factors are used since no other measureable variable is apparent. A previous paper by Patnode[2] indicates that drilling fluids may be considered to be a system of fluids in solid particles which may be correlated electrically in a manner similar to rock solids. The equation for the resistivity factor.

$$F = (\text{per cent fluid})^m = \frac{R_{\text{suspension}}}{R_{\text{water}}}, \quad . \quad . \quad (3)$$

is satisfied for a given clay type in water, but the value of m varies as different materials are used in the water. The resistivity factor is not constant for a given amount of clay. As is suspected it varies as the solids fraction conducts electrical current.

Since both weighting material and clay solids are present in commonly used drilling fluids, it is expected that both materials contribute to the variation of the m factor in Eq. 3. An extension of Patnode's work is presented in this paper to show some of the interrelations which exist between the resistivities of mud cake, mud filtrate and mud. Use of these data enable a more accurate calculation of mud filtrate and mud cake resistivities if only the mud resistivity and weight are measured.

EXPERIMENTAL

The measurements of mud weight, fluid and solids resistivity, alkalinity, and chloride content of mud samples were made in this research. Mud samples representing drilling fluids from 94 Louisiana and Texas wells (Table 1) and 47 laboratory-constructed systems (Table 2) were used in the experimentation. The measurements of the mud properties were made both in the field and in the laboratory.

The tests on the properties of weight, alkalinity and chloride ion were standard tests as described by API specifications. The resistivity measuring devices were constructed in the laboratory for this study. For details on the resistivity equipment see Fig. 1. The fluid cell

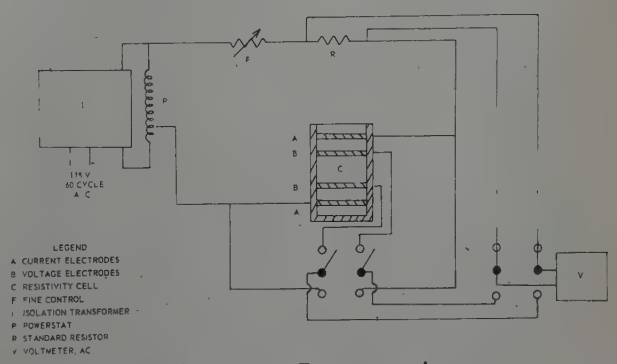

FIG. 1—DIAGRAM OF RESISTIVITY APPARATUS.

Original manuscript received in Society of Petroleum Engineers Office July 28, 1958. Revised manuscript received Nov. 7, 1958.
[1]References given at end of paper.

. 1 was calibrated against KCl solutions in easure the cell constant. This cell and its onstant were used at a standard reference of 75°F. The vacuum tube Voltmeter used ıl measurements was calibrated against a .boratory standard. The mud cake resistivity was measured with a similar four-electrode cell which was placed in the mud cup during an API standard filtration test. This cell was open on either end for the formation of cake around the electrodes and on top of the API filter paper. A differential pressure of 100 psi was exerted during the filtration and the temperature was held at 75°F. The mud cake was aged in the cell for a minimum time of 16 hours. The actual resistivity measurement was made after the cell had been removed from the filter cup, the excess mud and cake scraped free of the cell, and the cell wiped clean. This cell was also calibrated against KCl reference solutions periodically. It was found that the mud cake resistivity could be duplicated within 5 per cent error between independent filtrations.

TABLE 1—FIELD MUDS TESTED

Mud and description	R_{mf} (ohm-m)	R_{mc} (ohm-m)	R_m (ohm-m)	Mud wt. lb/gal
1. High lime	.365	3.22	.863	17.1
2. High lime	.278	2.35	.748	16.0
3. Native mud	.619	1.48	.747	9.7
4. Phosphate	1.81	1.80	1.97	10.5
5. High lime	.203	1.72	.46	14.5
6. Phosphate	2.05	2.47	2.75	10.6
7. High lime	.124	.70	.264	13.5
8. Red mud	1.66	2.00	2.03	10.0
9. High lime	.715	3.27	1.62	13.4
10. Surfactant	.416	2.61	1.18	16.7
11. T-6	.695	5.43	1.78	16.0
12. T-8	.54	4.16	1.39	15.5
13. Phosphate	1.84	1.97	2.68	9.7
14. Phosphate	2.16	3.25	2.74	9.8
15. T-8	.76	3.03	1.20	12.8
16. Sat. salt	.041	.316	.0834	14.3
17. Phosphate	4.12	3.16	5.08	9.7
18. Phosphate	1.60	2.61	2.14	9.0
19. Native mud	4.25	2.95	4.45	9.5
20. Phosphate	3.70	2.92	4.22	9.7
21. Native mud	12.30	3.95	13.60	10.2
22. Native mud	15.60	4.24	13.90	10.0
23. High lime	.252	2.31	.68	16.4
24. Red mud	2.93	2.41	2.97	10.1
25. Red mud	1.79	1.71	2.21	10.0
26. Red mud	1.64	1.75	1.92	10.1
27. Phosphate	3.14	2.52	3.27	9.9
28. Red mud	3.63	2.50	3.79	10.0
29. Red mud	2.49	1.83	2.41	9.8
30. Red mud	5.94	3.81	6.32	10.0
31. Shale ban	.655	2.57	1.24	10.5
32. T-8	.60	3.61	1.46	14.0
33. Low lime, 10% oil	1.36	2.13	1.40	12.8
34. Low lime, 11% oil	.60	2.21	1.05	11.8
35. T-8 12% oil	.547	2.83	1.33	14.0
36. Red mud	2.29	2.21	2.82	10.3
37. High lime	.317	1.18	.574	13.3
38. T-8, 10% oil	.777	3.27	1.46	10.8
39. Red mud, 20% oil	.670	4.59	1.76	18.7
40. Red mud	1.37	7.80	2.83	18.6
41. Red mud	1.41	3.13	1.80	11.0
42. T-8, 16% oil	.80	2.63	1.13	11.2
43. Shale ban, 6% oil	.56	2.26	1.02	12.4
44. Gypsum	.48	2.31	1.03	15.4
45. T-8	.552	3.27	1.31	13.8
46. High lime, oil emul.	.365	3.23	.863	17.1
47. High lime, oil emul.	.278	2.25	.748	16.0
48. Native mud, w/gel	.619	1.57	.747	9.7
49. Phosphate mud	1.81	1.80	1.97	10.5
50. Lime & oil	.203	1.74	.46	14.5
51. Phosphate & oil	2.05	2.43	2.75	10.6
52. Unknown	.124	.704	.264	13.5
53. Unknown	1.66	1.68	2.03	10.0
54. High lime, oil emul.	.164	1.58	1.30	17.0
55. T-8	.715	2.72	1.62	13.4
56. Calcium surfactant	.416	2.61	1.18	16.7
57. T-8	.695	5.67	1.78	15.9
58. T-8 Kombreak all clay	.54	4.17	1.39	15.5
59. Low pH phosphate gel	1.84	1.98	2.68	9.7
60. Low pH phosphate gel	2.16	2.56	2.74	9.8
61. T-8, no oil	.76	3.03	1.20	12.8
62. Sat. salt, low pH, oil emul.	.041	.316	.0834	14.3
63. Low pH, phosphate, oil emul.	4.12	3.16	5.08	9.7
64. Low pH, oil emul.	1.60	2.61	2.14	9.0
65. Native mud	4.25	2.95	4.45	9.5
66. Low pH, phosphate	3.70	2.92	4.22	9.7
67. High lime & oil	.214	2.28	.618	16.8
68. Native mud	12.3	3.95	13.60	10.2
69. Native mud	15.6	4.24	13.90	
70. High lime, oil emul.	.252	2.31	.68	16.4
71. Red mud	3.76		3.60	9.5
72. Sapp	2.93	2.41	2.97	10.1
73. Caustic phosphate	1.79	1.71	2.21	10.0
74. Red & phosphate	1.64	1.75	1.92	10.1
75. Emulsite phosphate	3.14	2.52	3.27	9.9
76. Red-phosphate	3.63	2.50	3.79	10.0
77. Red-phosphate	2.49	1.83	2.41	9.8
78. Red-phosphate	5.94	3.81	6.32	10.0
79. Shale ban, oil, red mud	.655	2.57	1.24	10.5
80. T-8 & red mud	.60	3.61	1.46	14.0
81. Lime & oil	1.36			12.8
82. Lime & oil	.60	2.21	1.05	11.8
83. T-8 & oil	.547	2.83	1.33	14.0
84. Red mud	2.29	2.21	2.82	10.3
85. Lime & CMC	.317	1.18	.574	13.3
86. T-8, oil, & red mud	.777	3.27	1.46	10.8
87. Oil & high pH red	.670	4.59	1.76	18.7
88. Phosphate & CMC	1.37	7.80	2.83	18.6
89. Red mud & phosphate	1.41	3.13	1.80	11.0
90. Saltwater mud			.137	
91. T-8, oil, & lime	.80	2.63	1.13	11.2
92. Shale ban, oil, lime	.56	2.26	1.02	12.4
93. Gypsum red mud	.48	2.31	1.03	15.4
94. T-8	.552	3.27	1.31	13.8

EFFECT OF WEIGHTING MATERIAL ON RESISTIVITY

Since the amount of solids present in any medium affects its over-all resistivity, this seemed to be the important factor. The solids portion of drilling suspensions mostly consists of clay colloids and weighting material, usually barium sulfate. The effects of each of these two materials are vastly different since the latter is not of colloidal size as used in drilling fluids.

Barium sulfate is a poor conductor of electrical current as compared to clay in suspension or to salt water. Therefore, it is easily seen that the resistivity of a clay water suspension increases as resistive weighting material is added. Hence, mud weight is an entering parameter necessary to calculate the resistivity of a mud sample if the mud water resistivity is known. For practical calculation only the mud resistivity is known; the mud filtrate resistivity is determined for a given weight by the following general equation.

TABLE 2—LAB MUDS TESTED

Mud and description	R_{mf} (ohm-m)	R_m (ohm-m)	Mud wt. lb/gal
1. Red mud	6.81	6.99	8.89
2. " "	.978		
3. " "	.503	.631	
4. " "	4.75	4.05	8.81
5. " "	.945	1.03	
6. " "	.55	.612	
7. " "	3.37	3.35	9.86
8. " "	.331	.67	9.86
9. " "	3.93	3.35	9.02
10. " "	.823	.958	9.02
11. " "	.462	.627	9.02
12. Lime mud	.419	1.47	8.90
13. " "	.317	.346	8.90
14. " "	.270	.317	8.90
15. " "	.338	.392	8.90
16. " "	.286	.325	8.90
17. " "	.237	.263	8.90
18. " "	.396	.428	8.90
19. " "	.311	.299	8.90
20. " "	.260	.292	8.90
21. " "	.320	.369	8.93
22. " "	.269		8.93
23. " "	.232	.272	8.93
24. " "	.348	.383	8.91
25. " "	.289	.339	8.91
26. " "	.244	.278	8.91
27. " "	.347	.427	9.00
28. " "	.287	.350	9.00
29. " "	.239	.287	9.00
30. " "	.238	.263	9.00
31. " "	.199	.221	9.00
32. " "	.173	.203	9.00
33. " "	.330	.402	9.50
34. " "	.307	.410	9.50
35. " "	.370	.431	9.50
36. " "	.390	.494	9.50
37. " "	.307	.393	9.50
38. " "	.251	.268	9.50
39. " "	.189	.247	9.50
40. " "	.169	.226	9.50
41. " "	.152	.200	9.50
42. " "	.390	.477	9.50
43. " "	.299	.374	9.50
44. " "	.241	.331	9.50
45. " "	.430	.618	10.00
46. " "	.322	.441	10.00
47. " "	.558	.580	10.00

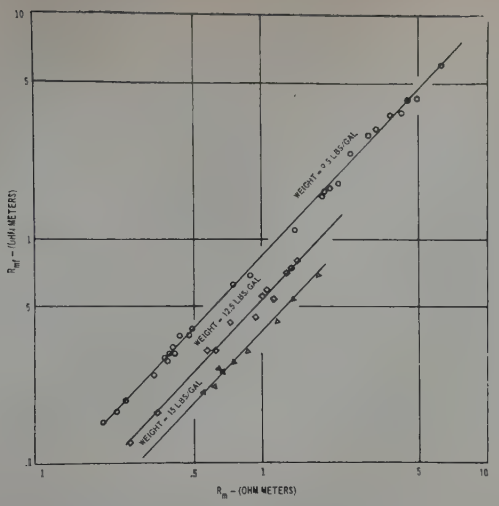

FIG. 2—MUD RESISTIVITY VARIATION AS MUD WEIGHT IS CHANGED FOR 61 FIELD AND LABORATORY MUDS.

$$R_{mf} = C\ (R_m)^m \quad . \quad . \quad . \quad . \quad . \quad . \quad . \quad . \quad . \quad . \quad (4)$$

Fig. 2 shows the relationship between R_{mf} and R_m for three weight ranges. The individual weights represent averages of the weight range. For example, 9.5 lb/gal represents weights from 9.0 to 10.0 lb/gal mud weight. Note that a fairly consistent slope on this graph is maintained for the three weight ranges. For the normal range of useage ($R_m < 5$ ohm-m) these graphs are represented by

$$R_{mf} = C(R_m)^{1.07} \quad . \quad . \quad . \quad . \quad . \quad . \quad . \quad . \quad . \quad . \quad (1)$$

This relation is not strictly correct at high resistivities since the clay in suspension conducts current somewhat and the value of C is not constant.

For the influence of weight material alone it is interesting to note the change of the constant, C, for the different mud weights. Fig. 3 shows this relationship. This graph presents a qualitative check on the previous work because of the nature of the resistivity factor. At 8.3 lb/gal the C factor should be approximately unity, as R_{mf} is equal to R_m for muds of approximately 1-ohm-m resistivity. For practical purposes the C factor varies inversely with weight up to weights of about 14 lb/gal. This condition holds notwithstanding the fact that muds with weights below 10 lb/gal consist mostly of clay and water. Muds not in this weight category contain increasing barium sulfate. Note in Fig. 3 that the C factor is asymptotic with the fraction, 0.35. The reason for this is not clear but it is possible that the minimum effective porosity is reached at weights of about 15 lb/gal. The minimum effective porosity indicates the minimum fluid (as viewed electrically) which a unit amount of the mud contains regardless of the solids present. Since the conductivity of the filtrate from a unit amount of mud mainly determines the mud conductivity, the weight material present in a drilling mud does not further affect the mud conductivity after the minimum porosity is reached. Further investigation is being made on this phenomenon.

EFFECT OF CLAY ON MUD RESISTIVITY

Fig. 2 indicates that the slope, m, of the graph of R_{mf} vs R_m is constant. This suggests that R_m is a function only of R_{mf} for a given mud weight. This is true for practical consideration but not in theory. Actually the clay component contributes its own conductive properties. The resistivity factor, F, of any porous system allows inspection of the contribution to conductivity by clay. It is known that F is not constant in porous rock for several reasons: the liquid in the porous system is not the only conductor and the electrolyte itself affects the conductivity of the solids portion of the system.

Fig. 4 shows that the mud resistivity factor, F_m, is also not a constant for a given amount of solids. Note that the resistivity factor becomes smaller when the mud resistivity exceeds 1 ohm-m. For practical electric logging work and for conditions where the mud resistivity does not exceed 10 ohm-m the mud resistivity factor remains approximately constant. However, some native muds which have mud resistivities less than filtrate resistivities are exceptions to this generality. In these cases the clay material definitely conducts electrical current. A well-dispersed clay and water suspension maintains its own conductivity which is not entirely dependent upon added electrolytes.

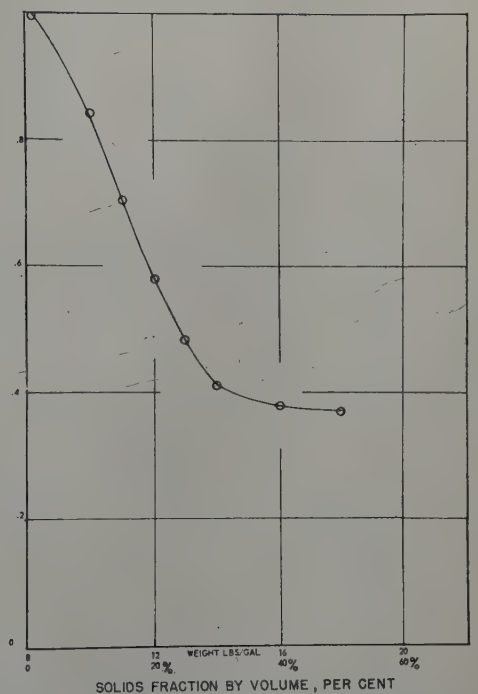

FIG. 3—VARIATION OF C IN THE EQUATION, $R_{mf} = C(R_m)^{1.07}$, AS MUD WEIGHT IS VARIED.

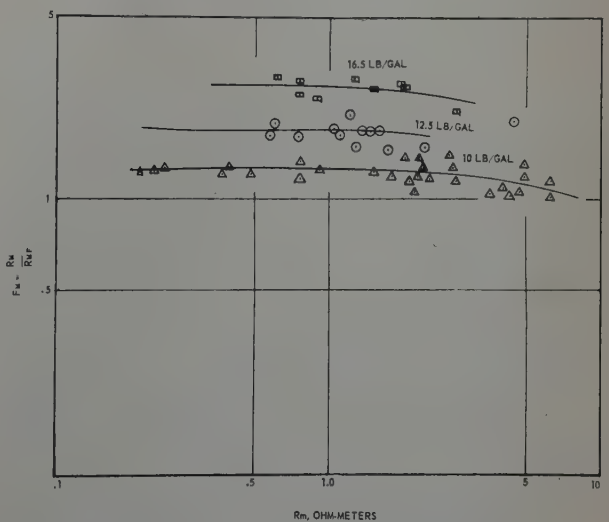

FIG. 4—VARIATION OF THE MUD RESISTIVITY FACTOR WITH MUD RESISTIVITY FOR 55 FIELD MUDS OF VARYING WEIGHTS.

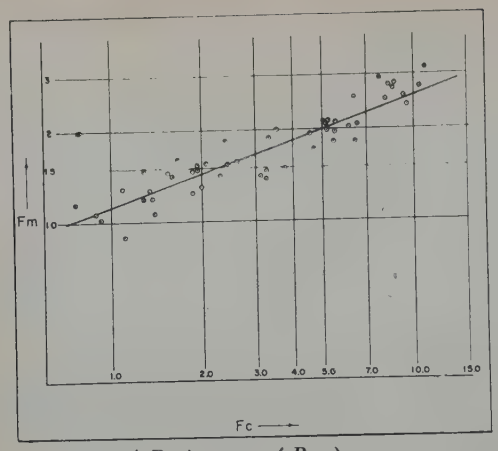

FIG. 5—$F_m \left(\frac{R_m}{R_{mf}}\right) \times F_c \left(\frac{R_{mc}}{R_{mf}}\right)$ FOR 51 FIELD MUDS.

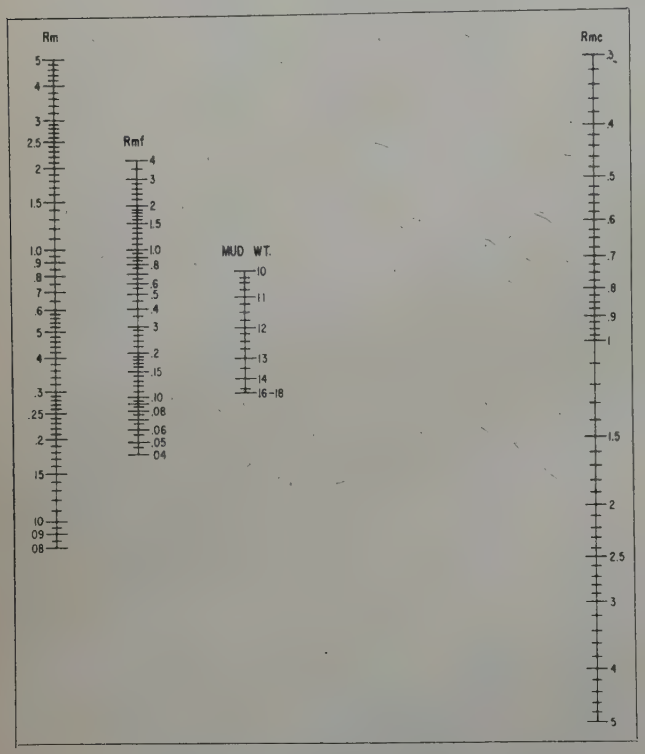

FIG. 6—CHART FOR DETERMINING R_{mc} AND R_{mf} FROM R_m AND MUD WEIGHT.

THE RELATION OF R_m TO R_{mc}

For the practical range of resistivities already mentioned, the R_{mc} is very nearly a function of R_m. When the cake resistivity factor, F_c, is plotted against the mud resistivity factor, F_m, the following relation exists.

$$F_c = C' \ (F_m)^k \quad . \quad . \quad . \quad . \quad . \quad . \quad . \quad . \quad . \quad . \quad (5)$$

This function is not affected by solids as is the function,

$$R_{mf} = C \ (R_m)^m \ ,$$

since both porous systems contain the same weighting material and clay. Obviously, the weight material affects the resistivities of both mud and mud cake similarly. The average of all experimental data from Fig. 5 yields

$$F_c = 0.69 \ (F_m)^{2.65} \quad . \quad . \quad . \quad . \quad . \quad . \quad . \quad . \quad . \quad (6)$$

Hence, the compacted mud cake behaves electrically somewhat as its parent suspension. It should be noted that Eq. 6 represents data measured at constant temperature and pressure differential. It is suspected that larger differentials across the mud cake affect the porosity and the resistivity factor of the cake. These possibilities are also being investigated.

Since R_{mf} is determined by Eq. 1 when R_m and mud weight are known, it is possible to construct a nomograph which solves for R_{mf} directly. Use of Eq. 5 allows solution of R_{mc} simultaneously. Fig. 6 shows the nomograph representative of the resistivity relations as API filtration conditions. This nomograph is most accurate for drilling muds which have weights less than 14 lb/gal and resistivities more than 0.15 ohm-m.

CONCLUSIONS

For the range of drilling mud resistivities from 0.1 to 10 ohm-m, the mud and filtrate resistivities are related as follows.

$$R_{mf} = C \ (R_m)^{1.07}$$

The numerical value of C depends primarily upon the mud weight. The actual numbers are associated in the following manner.

Mud Weight (lb/gal)	C
10	.847
11	.708
12	.584
13	.488
14	.412
16	.380

The resistivity factors of mud and mud cake are related by

$$F_c = \frac{R_{mc}}{R_{mf}} = 0.69 \ (F_m)^{2.65}$$

for the range of mud resistivities just listed.

Fig. 6 is presented for rapid calculation of R_{mc} and R_{mf} when the mud weights and resistivities are known. The nomograph uses the preceding equations and the constants noted in Fig. 3. This method presents a more accurate calculation of cake and filtrate resistivity data than is presently made when the effect of the weight fraction is not considered.

ACKNOWLEDGMENTS

Acknowledgment is made of the financial support of the Schlumberger Well Surveying Corp. and the U. of Houston. The laboratory assistance of Jack E. Kimmons and James E. Cornett is appreciated.

REFERENCES

1. Lamont, Norman: "Relationships Between the Mud Resistivity, Mud Filtrate Resistivity, and the Mud Cake Resistivity of Oil Emulsion Mud Systems", *Trans.* AIME (1957) **210**, 387.
2. Panode, H. W.: "Relationship of Drilling Mud Resistivity to Mud Filtrate Resistivity", *Trans.* AIME (1949) **186**, 14.

★★★

Profitability of Capital Expenditures for Development Drilling and Producing Property Appraisal

J. J. ARPS
MEMBER AIME

THE BRITISH-AMERICAN OIL PRODUCING CO.
DALLAS, TEX.

ABSTRACT

The appraisal of producing properties and profitability analysis of a proposed capital expenditure are based on the same principles. In both problems a projection of future cash income is compared to one or more capital expenditures. Several different methods have been in use either to compute a price to obtain a given earning power on the investment or to compute the earning power which will result from a given capital expenditure. One of these, the "Average Annual Rate of Return" method, computes in a simple manner the ratio of the present value of the future earnings after amortization to the present value of the undepreciated balances of the investment over the life of a project. This method, not well known generally, appears to have some rather unique advantages in reducing the computation work required, eliminating trial-and-error solutions, and providing a more accurate answer when applied to oil industry investments subject to the unit-of-production basis of amortization. Its derivation is given and its versatility demonstrated in the solution of certain everyday investment problems. A number of charts, useful in applying this method to profitability analysis and appraisal work, are provided. The current trend in the market values of producing properties is shown.

INTRODUCTION

Making sound capital expenditure decisions requires an objective means of measuring the productivity of individual investment proposals. Since the best measure of the economic worth of such proposals is their ability to produce profits, it is common practice to grade proposed capital expenditures according to their annual earning power as a percentage of the outstanding capital. The same principles which govern the determination of the rate of return of proposed capital expenditures also apply generally to the problem of determining the appraisal value or purchase price of income-producing oil and gas properties.

Both problems are of prime importance in the producing phase of the oil business, where management is faced daily with decisions to drill or not to drill certain development wells, or with the determination of the appraisal value of producing properties.

The common feature in both problems is that a projection of future cash income is compared with a known or estimated capital investment to determine its earning power or annual rate of return. In the case of development drilling, the cost of the proposed well can usually be estimated with a fair degree of accuracy and the problem consists of finding the rate of return on the invested capital. In the case of appraising producing properties, on the other hand, the desired rate of return is usually known in advance and the problem consists of determining the purchase price which, for the given income projection, results in the required rate of return.

Certain accounting procedures common to the oil and gas producing business make these two problems and their solutions somewhat different from corresponding problems in other industries, and, in certain ways, simpler. The main difference is in the amortization policy which, for oil and gas production, is frequently on a unit-of-production basis, compared to the amortization on a time basis used in many other industries. The purpose of this paper is to discuss briefly the various methods currently in use for the measurement of productivity of invested capital in producing properties and, in more detail, the derivation and application of what will be called the "Average Annual Rate of Return Method". This rather interesting and not too well known method has some very definite advantages in the solution of many problems common to the oil industry. For the sake of simplicity, federal income tax considerations have been disregarded in the examples used, since they do not affect the principles involved. The use of the production payment route in the sale or purchase of producing properties, which has been amply covered in many other publications, has also not been included in this analysis.

METHODS FOR MEASURING THE EARNING POWER OF INVESTED CAPITAL

Of the many different methods used to measure the earning power of invested capital, four are applicable to oil or gas production ventures. Depending on whether these four methods utilize one or two interest rates, and whether a fixed amortization pattern is used, they may be classified as follows.

Original manuscript received in Society of Petroleum Engineers office July 19, 1957. Revised manuscript received May 26, 1958. Paper presented at 32nd Annual Fall Meeting of Society of Petroleum Engineers in Dallas, Tex., Oct. 6-9, 1957.

	I. One interest rate	II. Two interest rates
A. No fixed amortization pattern	Discounted Cash Flow Method	Hoskold's Method
B. Fixed amortization pattern	Accounting Method	Average Annual Rate of Return Method

The so-called "Pay-out Time Method" has not been included in this discussion since it does not provide a measure of the over-all earning power of a project[1].

IA Discounted Cash Flow Method

This method, which is sometimes also referred to as the "Investor's Method"[2] or "Internal Rate of Return Method", has been extensively reviewed in recent literature[1,3,4,5], and is quite popular with many major oil companies. It is based on the principle that in making an investment outlay one is actually buying a series of future annual incomes. The rate of return of a proposed venture is then the maximum interest rate which one could pay on the capital tied up over the life of the investment and still break even. The time pattern of the future earnings is given proper weight.

Since no amortization pattern needs to be adopted, this method is particularly suited to property evaluation, since it involves only the discounting of the projected cash flow to present value by means of the desired rate of interest.

Profitability analysis with this method is somewhat laborious, since it consists of finding by trial-and-error the interest rate which will discount future earnings of a project down to a present value equal to the required investment.

The computed earning power is not necessarily the same as the average rate of return later shown on a company's books, since the investment, if made, is often amortized on a unit-of-production basis. However, no provision for this amortization pattern is made in the Discounted Cash Flow Method.

In the example given in Table 1 and Fig. 1, the earning power computed by the Discounted Cash Flow Method would have been 11.918 per cent per year as compared to 11.753 per cent with the Average Annual Rate of Return Method.

IB Accounting Method

This method, which is sometimes referred to as the "Average Book Method"[2], is closely related to many of the concepts used in conventional accounting procedure and computes the rate of return of a proposed venture as the ratio of the average of the net annual profits over the life of the proposition (after amortization) to the average book investment over its life. It takes into account the actual amortization pattern.

If the amortization is on a unit-of-production basis, the method may be illustrated with the diagram of Fig. 1, which for a typical example shows annual net earnings e and amortization a above the time axis, while the diminishing yearly investment balances, B, are shown below the time axis. A more detailed discussion of this chart will be given under the Average Annual Rate of Return Method, II B. Basically, the rate of return with this accounting method is represented by the ratio of the total of the net profits, $\Sigma e - \Sigma a = E - C$, to the total of the undepreciated balances, ΣB. Compared to the other methods the accounting method does not give proper weight to the time pattern of earnings. Declining and growing earning patterns, for instance, are treated alike.

In the example given in Table 1 and Fig. 1 the earning power computed by the Accounting Method would have shown 11.730 per cent per year as compared to 11.753 per cent with the average Annual Rate of Return Method.

IIA Hoskold's Method[6,7]

This method, which is still quite popular in mine evaluations, is particularly suited to ventures which have a limited profitable life (such as mines) and where the original capital must be returned at the expiration of the venture. It presupposes a uniform return at a speculative interest rate, r'', on the original capital and provides for redemption of capital at abandonment time by annual reinvestment of the balance of the yearly earnings at a safe rate of interest, r. No fixed depreciation pattern is assumed, but proper weight is given to the specific time pattern of future earnings. *Profitability analysis* is a straightforward calculation by the formula,

$$r'' = \frac{r}{\left(1 + \frac{r}{100}\right)^{t} - 1} \times \left(\frac{P}{C} - 1\right), \quad . \quad . \quad . \quad (1)$$

where P is the value of projected net earnings (before depreciation) including compound interest at r per cent per year computed at abandonment time, C is initial capital investment, and t is the total project life in years.

This profitability formula applied to the example given in Table 1 and Fig. 1 shows a constant speculative return of 6.815 per cent per year on the initial capital investment, when a safe interest rate of 5 per cent is used, as compared to 11.753 per cent on the declining balance as computed for the Average Annual Rate of Return Method. *Property evaluation* is also a straightforward calculation by the formula

[1]References given at end of paper.

TABLE 1—AVERAGE ANNUAL RATE OF RETURN COMPUTATION

	1	2	3	4	5	6	7	8	9	10	Total
1. Year (t)											
2. Production rate bbl/yr	27,194	20,168	14,962	11,101	8,236	6,110	4,523	3,362	2,494	1,850	100,000 bbl
3. Earnings after royalty, local taxes, and lifting costs @ $2 per bbl	$ 54,388	$40,366	$29,924	$22,202	$16,472	$12,220	$ 9,046	$ 6,724	$ 4,988	$ 3,700	$200,000
4. Mid-year 5 per cent discount factor*	.97561	.92915	.88491	.84277	.80263	.76442	.72802	.69335	.66033	.62889	Avg. :.87580
5. Present value future earnings; (4) × (3)	$ 53,061	$37,478	$26,480	$18,711	$13,221	$ 9,341	$ 6,586	$ 4,662	$ 3,294	$ 2,327	$175,161

$$\text{Average annual rate of return on \$150,000 investment} = \frac{(5)(.8758)(200{,}000 - 150{,}000)}{(1 - .8758)(150{,}000)} = 11.753 \text{ per cent}$$

Proof of Average Annual Rate of Return Formula

6. Amortization; (2) × $1.50	$ 40,791	$30,252	$22,443	$16,652	$12,354	$ 9,165	$ 6,784	$ 5,043	$ 3,741	$ 2,775	$150,000
7. Investment at year's end	$109,209	$78,957	$56,514	$39,862	$27,508	$18,343	$11,559	$ 6,516	$ 2,775	0	—
8. Average investment during year	$129,604	$94,083	$67,736	$48,188	$33,685	$22,926	$14,951	$ 9,038	$ 4,646	$ 1,388	$426,245
9. 11.753 per cent return on average investment	$ 15,223	$11,058	$ 7,961	$ 5,664	$ 3,959	$ 2,695	$ 1,757	$ 1,062	$ 546	$ 163	$ 50,098
10. 5 per cent discount factor**	.95604	.91059	.86732	.82617	.78703	.74984	.71461	.68141	.65101	.62889	(Avg.: .87408)
11. Present value of 11.753 per cent return on average investment; (10) × (9)	$ 14,563	$10,069	$ 6,905	$ 4,679	$ 3,116	$ 2,021	$ 1,256	$ 724	$ 355	$ 102	$ 43,790
12. Present value of net profits after amortization; (4) × [(3) − (6)]	$ 13,265	$ 9,370	$ 6,620	$ 4,678	$ 3,305	$ 2,335	$ 1,646	$ 1,165	$ 824	$ 582	$ 43,790

*$(1.025)^{-t} \times (1.05)^{1-t}$

**$\dfrac{(7) \times 1.05^{-t} + \frac{1}{2} \times (6) \times 1.025^{-1} \times 1.05^{1-t}}{(7) + \frac{1}{2} \times (6)}$

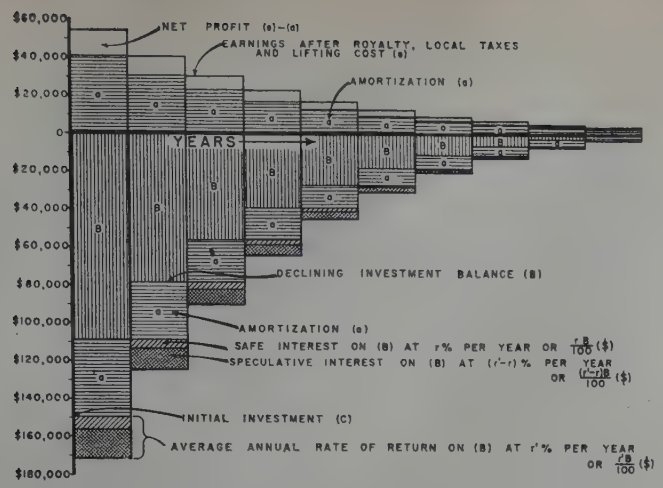

FIG. 1—DIAGRAM ILLUSTRATING THE DERIVATION OF THE AVERAGE ANNUAL RATE OF RETURN FACTOR.

$$C = \frac{P}{1 + \frac{r''}{r}\left[\left(1 + \frac{r}{100}\right)^{t} - 1\right]} \quad . \quad . \quad . \quad . \quad . \quad (2)$$

The interesting feature of this method is its concept of a safe or bank interest rate, r, which is utilized to build up the amortization account to full return of the invested capital at the end of the project's life, while at the same time a constant speculative interest rate, r'', is earned on the original capital investment throughout the same period.

IIB AVERAGE ANNUAL RATE OF RETURN METHOD

The average rate of return computed by this method is essentially the ratio of the present value of the future earnings after amortization to the present value of the undepreciated balance of the investment over the life of the property. The method is particularly suitable for investments in oil and gas producing properties, where amortization of the invested capital is on a unit-of-production basis, and offers the following advantages over the methods previously discussed under IA, IB, and IIA.

1. It yields an average annual rate of return which corresponds more closely to the one later shown by the company's books, since the same amortization pattern is used. This is not necessarily the case with Methods IA and IIA.

2. The time pattern of the earnings is properly weighted. This is not the case with Method IB.

3. Profitability analysis is a straightforward computation; no trial-and-error procedure is involved as in Method IA.

4. Property evaluation is a straightforward computation; no trial-and-error procedure is involved as in Method IB.

The average Annual Rate of Return Method has the following disadvantages.

1. The method loses its simplicity when the amortization of the investment is not proportional to the production, since the average deferment factor on production will then not be the same as the average deferment factor on the amortization payments. It is therefore not applicable when amortization is strictly on a time basis, unless the production is at a constant rate.

2. The method cannot be used to calculate the profitability of an incremental investment. In such a case the differences are usually computed between the income projection as a result of the added investment and the projection without this investment, and the results compared with the incremental investment. For this type of work the Discounted Cash Flow Method (IA) is better suited.[1]

The Average Annual Rate of Return Method and its derivation will be discussed with the aid of the diagram of Fig. 1, which represents a more-or-less typical example of a producing well which is expected to make 100,000 gross bbl of oil over a period of 10 years. Production from this well is declining at a constant percentage of 25.84 per cent per year. The crude price is $3.20/bbl, while the net income per gross bbl after one-eighth royalty (40 cents), local taxes (5 per cent of $2.80, or 14 cents), and average operating expenses (66 cents) is assumed to be constant at $2.00/bbl. It is assumed further that the well can be drilled and completed for $150,000. The vertical columns in the top portion of the diagram of Fig. 1 represent the declining earnings, e, from this well over its 10-year life. Time is shown on the horizontal axis. The amortization of the $150,000 drilling investment, C, which is proportional to the number of barrels produced and to the production revenue, is shown as the horizontally hachured portion, a, of these columns. The remaining portion of the operating revenue, represented by the blank top portions of the columns, is the net profit $e - a$.

The columns in the bottom portion of this graph below the time axis represent the declining balances, B, of the $150,000 drilling investment (vertical hachuring), the amortization, a, applied during each year (horizontal hachuring) and the interest, $\frac{rB}{100}$, at the rate of r per cent per year on the outstanding balances (diagonal hachuring).

DERIVATION OF THE GENERAL FORMULA

The weighted average deferment factor (defined as the ratio of the discounted value of the future production increments to the undiscounted total future production) for r per cent interest per year on the production and, therefore, also on the total operating net revenue ($E = \Sigma e$) will be designated as D. Since the amortization is on a unit-of-production basis, the same average deferment factor, D, applies to the total of these amortization payments ($C = \Sigma a$).

If the drilling investment, C, had been borrowed from a bank it would be obvious that this indebtedness could be discharged by returning each year the annual amortization payments, a, to the bank plus an annual interest payment of $\frac{rB}{100}$ at the bank's rate of r per cent on the remaining balances, B.

The present value of the combined amortization payments, $D\Sigma a$, plus the present value of the interest payments, $\frac{rD'}{100}\Sigma B$, is therefore equal to the total original investment, C, regardless of the amortization pattern used[8].

$$C = D\Sigma a + \frac{rD'}{100}\Sigma B, \quad . \quad . \quad . \quad . \quad . \quad . \quad . \quad . \quad (3)$$

in which D is the weighted average deferment factor on the production of the well, the total earnings and the combined amortization payments, while D' is the weighted average deferment factor on the undepreciated balances, B, of the investment. Both deferment factors are computed at the same safe interest rate, r, which in this example is assumed to be 5 per cent per year, compounded annually. Since $\Sigma a = C$, it follows that

$$C(1 - D) = \frac{rD'}{100}\Sigma B, \quad . \quad . \quad . \quad . \quad . \quad . \quad . \quad . \quad (4)$$

and the present value of 1 per cent interest on the undepreciated balances is

$$\frac{D' \Sigma B}{100} = \frac{C(1-D)}{r} \quad \ldots \ldots \ldots \quad (5)$$

Some 20 years ago the engineering staff of the Shell Oil Co. first combined this expression with the present value of net profits after amortization,

$$D(\Sigma e - \Sigma a) = D(E - C), \quad \ldots \ldots \quad (6)$$

and demonstrated that if the present value of 1 per cent interest on the undepreciated balances of the investment equals $\frac{C(1-D)}{r}$, then the present value of the net profits after amortization, $D(E-C)$, must be equivalent to an earning power or average annual rate of return r', expressed in per cent of the undepreciated balances of the investment of:

$$r' = \frac{r D (E - C)}{(1 - D) C} \text{ per cent per year.} \quad \ldots \quad (7)$$

This very useful and logical relationship represents the equivalent annual rate of return on the undepreciated balances of the investment, provided the investment is amortized on a unit-of-production basis.

The data portrayed on the graph of Fig. 1 are shown in tabular form in Table 1. The top portion of this table shows the computations normally required to arrive at the average annual rate of return from a given investment, if the income projection is irregular. If the rate of production or income is constant with time, or if it follows constant percentage or harmonic decline,[14] the necessary average deferment factor or multiplier may be more readily obtained from appropriate tables or charts, such as Figs. 2, 3 and 4.

The bottom portion of Table 1 is not necessary for the computation, but is provided to show proof that the present value of the net earnings after amortization of $43,790 is equal to the present value of the computed average annual rate of return of 11.753 per cent on the undepreciated balances of the investment.

It may be noted that no trial-and-error calculation is necessary, as is the case with the Discounted Cash Flow Method.

FORMULA FOR MULTIPLE INVESTMENT

When more than one capital investment is to be made during the life of a well or a property, the total present value of the combined investments is equal to $D_c C$, in which D_c is the average deferment factor used in discounting the various capital investments back to the initial investment date. In that case Eq. 3 takes the following form.

$$D_c C = D \Sigma a + \frac{r D'}{100} \Sigma B, \quad \ldots \ldots \quad (8)$$

and

$$C(D_c - D) = \frac{r D'}{100} \Sigma B. \quad \ldots \ldots \quad (9)$$

so that

$$r' = \frac{r D (E - C)}{(D_c - D) C} \text{ per cent per year.} \quad \ldots \quad (10)$$

FORMULA FOR SPECULATIVE RATE OF RETURN

Since the average annual rate of return, r', represents the total equivalent return on the undepreciated balances, it is sometimes customary, particularly when capital for the venture is borrowed at the safe interest rate, r, to separate this bank interest from the total earning power and show only the speculative portion of the return, $r' - r$, thus modifying Eq. 7 to

$$r' - r = \frac{r D (E - C)}{(1 - D) C} - r = \frac{r (DE - C)}{(1 - D) C} \text{ per cent per year,} \quad \ldots \quad (11)$$

and Eq. 10 to

$$r' - r = \frac{r (DE - C)}{(D_c - D) C} \text{ per cent per year.} \quad \ldots \quad (12)$$

This speculative interest portion is shown cross-hachured in Fig. 1.

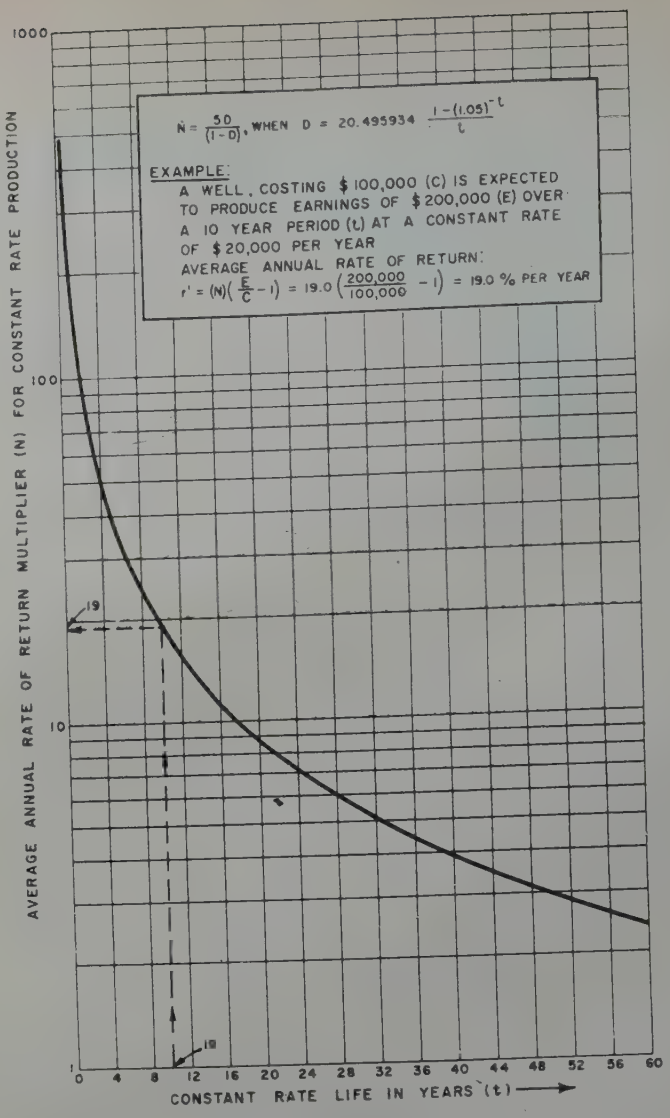
AVERAGE ANNUAL RATE OF RETURN MULTIPLIER (N) FOR CONSTANT RATE PRODUCTION
1000
100
10
1
N = 50/(1-D), WHEN D = 20.495934 (1-(1.05)^-t)/t
EXAMPLE:
A WELL, COSTING $100,000 (C) IS EXPECTED TO PRODUCE EARNINGS OF $200,000 (E) OVER A 10 YEAR PERIOD (t) AT A CONSTANT RATE OF $20,000 PER YEAR
AVERAGE ANNUAL RATE OF RETURN:
r' = (N)(E/C - 1) = 19.0 (200,000/100,000 - 1) = 19.0 % PER YEAR
19
19
0 4 8 12 16 20 24 28 32 36 40 44 48 52 56 60
CONSTANT RATE LIFE IN YEARS (t)

FIG. 2—AVERAGE ANNUAL RATE OF RETURN MULTIPLIER (N) FOR CONSTANT RATE PRODUCTION ($r = 5$ PER CENT PER YEAR).

GENERAL APPRAISAL FORMULA

The usefulness of the general expression of Eq. 7 may be further demonstrated by converting it to an appraisal formula for determining the price, C, to be paid for a given well or property when a certain total rate of return of r' per cent per year is desired on the outstanding balances of the capital during the life of the well.

$$C = \frac{DE}{\frac{r'}{r} - D\left(\frac{r'}{r} - 1\right)}. \quad \ldots \ldots \quad (13)$$

If, for instance, a purchase of a well or a producing prop-

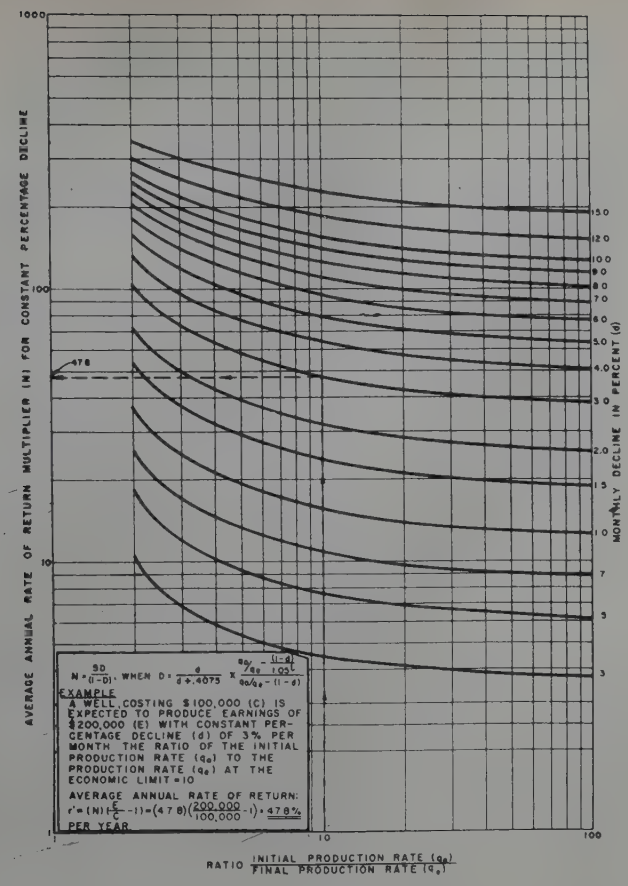
AVERAGE ANNUAL RATE OF RETURN MULTIPLIER (N) FOR CONSTANT PERCENTAGE DECLINE
MONTHLY DECLINE IN PERCENT (d)
RATIO INITIAL PRODUCTION RATE (qo) / FINAL PRODUCTION RATE (qe)
EXAMPLE
A WELL COSTING $100,000 (C) IS EXPECTED TO PRODUCE EARNINGS OF $200,000 (E) WITH CONSTANT PERCENTAGE DECLINE (d) OF 3% PER MONTH. THE RATIO OF THE INITIAL PRODUCTION RATE (qo) TO THE PRODUCTION RATE (qe) AT THE ECONOMIC LIMIT = 10
AVERAGE ANNUAL RATE OF RETURN:
PER YEAR.

Fig. 3—Average Annual Rate of Return Multiplier (N) for Constant Percentage Decline (r = 5 Per Cent Per Year).

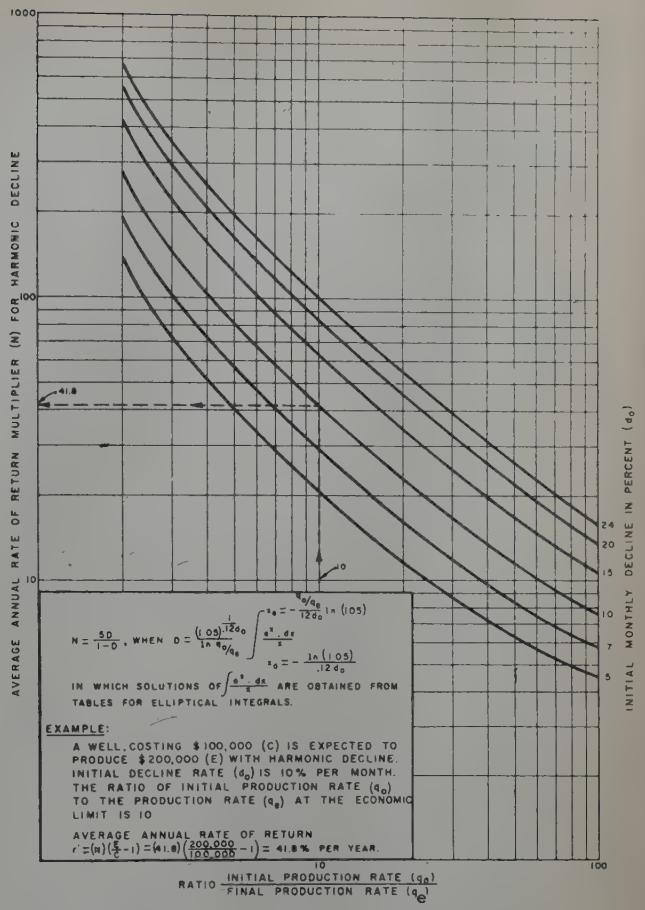
AVERAGE ANNUAL RATE OF RETURN MULTIPLIER (N) FOR HARMONIC DECLINE
INITIAL MONTHLY DECLINE IN PERCENT (do)
RATIO INITIAL PRODUCTION RATE (qo) / FINAL PRODUCTION RATE (qe)
IN WHICH SOLUTIONS OF ∫ e^s/s ds ARE OBTAINED FROM TABLES FOR ELLIPTICAL INTEGRALS.
EXAMPLE:
A WELL, COSTING $100,000 (C) IS EXPECTED TO PRODUCE $200,000 (E) WITH HARMONIC DECLINE. INITIAL DECLINE RATE (do) IS 10% PER MONTH. THE RATIO OF INITIAL PRODUCTION RATE (qo) TO THE PRODUCTION RATE (qe) AT THE ECONOMIC LIMIT IS 10
AVERAGE ANNUAL RATE OF RETURN
PER YEAR.

Fig. 4—Average Annual Rate of Return Multiplier (N) for Harmonic Decline (r = 5 Per Cent Per Year).

erty like the one in the example of Fig. 1 and Table 1 is contemplated, and if it is desired to make an average annual rate of return, r', of 15 per cent per year on this purchase, one could afford to pay, according to Eq. 13,

$$C = \frac{(.8758)\ (200{,}000)}{3 - (.8758)\ (3 - 1)} = \$140{,}300.$$

APPRAISAL FORMULA FOR OIL LAND REQUIRING ADDITIONAL INVESTMENT

When the property to be purchased requires the making of an additional investment, C', such as would be the case at a land sale involving proved undeveloped acreage, the price to be offered for the land would be

$$C = \frac{DE}{\frac{r'}{r} - D\left(\frac{r'}{r} - 1\right)} - C' \quad \ldots \ldots \quad (14)$$

For instance, if a tract of land were up for bidding from which production earnings could be expected, as shown in Table 1, and where it could be estimated that development costs of $50,000 would be necessary, the maximum bid for an average annual rate of return, r', of 20 per cent per year, according to Eq. 14, would be

$$C = \frac{(.8758)\ (200{,}000)}{4 - (.8758)\ (4 - 1)} - 50{,}000 = \$77{,}600.$$

EQUIVALENT WORKING AND OVER-RIDING ROYALTY INTERESTS

Another frequently encountered problem which can be readily solved with the foregoing formulas may be illustrated by the following example.

An operator is preparing to drill a well, which may be expected to produce earnings as shown in Table 1 and which will cost $100,000. He has a partner who owns one-half of the working interest and who does not have the cash available to pay for his one-half of the $100,000 well cost. This partner therefore wants to exchange his one-half working interest for an over-riding royalty. Future net earnings to the one-half working interest are estimated at (.5) ($200,000 − $100,000), or $50,000, while a 1 per cent over-ride will return, after local taxes of 5 per cent (.01) (100,000) (3.20 − .16), or $3,040. The partner may therefore ask for an over-riding royalty of 50,000 ÷ 3,040 or 16.55 per cent. This computation is not correct, however, since the over-riding royalty owner does not put up any of the investment and does not share the risk of drilling and operating. A more equitable solution is for the operator to first evaluate, by means of Eq. 14, the value of the one-half working interest on the basis of a reasonable rate of return including a consideration of the risks involved, of, say, 15 per cent per year. Thus,

$$\frac{(.5)\ (.8758)\ (100{,}000 \times \$2)}{3 - (.8758)\ (3 - 1)} = \$50{,}000 = \$20{,}150.$$

The appraisal value of a 1 per cent over-riding royalty is then determined on the same basis as follows,

$$\frac{(.01)\ (.8758)\ (100{,}000)\ (3.20 - .16)}{3 - (.8758)\ (3 - 1)} = \$2{,}133.$$

The proper equivalent over-riding royalty on this basis is, therefore, $20,150 ÷ $2,133 = 9.45 per cent.

CHARTS FOR AVERAGE ANNUAL RATE OF RETURN MULTIPLIER (N)

Since the Rate-of-Return formula of Eq. 7 involves the multiplier function, $N = \frac{rD}{1 - D}$, it has been found convenient to prepare special charts showing the value of this function, N, for a base interest rate, r, of 5 per cent per year for the following cases: (1) production at constant rate for a given number of years, t (Fig. 2); (2) production with constant percentage decline[14] (percentage drop in production rate per unit of time constant) for a given ratio between initial and final rates, q_o/q_e, and given monthly decline, d (Fig. 3); and (3) production with harmonic decline[14] (percentage drop in production rate per unit of time proportional to the production rate) for a given ratio between initial and final rates, q_o/q_e, and a given initial monthly decline, d_o (Fig. 4).

For each of these cases the formula for computation of the multiplier values, N, is given on the chart. Finding the average annual rate of return, r', by means of these charts for a given set of conditions consists simply of multiplying the ratio of future earnings and investment minus one ($E/C - 1$) with the multiplier value, N, from the chart. The use of each chart is illustrated with a numerical example.

CHARTS FOR APPRAISAL VALUE MULTIPLIER (M)

Since the appraisal formulas of Eqs. 13 and 14 involve the multiplier function, $M = \frac{D}{\frac{r'}{r} - D\left(\frac{r'}{r} - 1\right)}$ it has been found convenient to prepare special charts showing the value of this function, M, for a base interest rate r of 5 per cent per year, and for the desired rate of return, r', which naturally varies between companies and also depends on the degree of risk involved. Multiplier charts for the following cases are shown in this paper; similar ones may be easily prepared for different rates of return, r'.

1. Production at constant rate for a given number of years, t; separate curves are provided for a rate of return, r', of 5, 10, 15, 20 and 25 per cent (Fig. 5).
2. Production with constant percentage decline for a given ratio between initial and final rates, q_o/q_e, a given monthly decline, d, and a desired rate of return, r', of 20 per cent per year (Fig. 6).
3. Production with harmonic decline for a given ratio between initial and final rates, q_o/q_e, a given initial monthly decline, d_o, and a desired rate of return, r', of 20 per cent per year (Fig. 7).

For each of these cases the formula for computation of the multiplier values, M, is given on the chart. Finding the appraisal value, C, by means of these charts for a given set of conditions consists of simply multiplying the expected total future earnings, E, with the multiplier value, M, from the proper chart. The use of each chart is illustrated with a numerical example.

CURRENT TRENDS IN MARKET VALUE OF PRODUCING PROPERTIES

Fig. 8 shows on the lower horizontal axis the average 5 per cent deferment factor, D, for a given income projection, while the vertical axis represents the values of the corresponding appraisal value multipliers, M. This multiplier represents the fraction of undeferred future net earnings which can be paid to realize a predetermined average annual rate of return, r', on the invested capital. Curves are shown, based on the relationship:

$$M = \frac{D}{\frac{r'}{5} - D\left(\frac{r'}{5} - 1\right)}$$

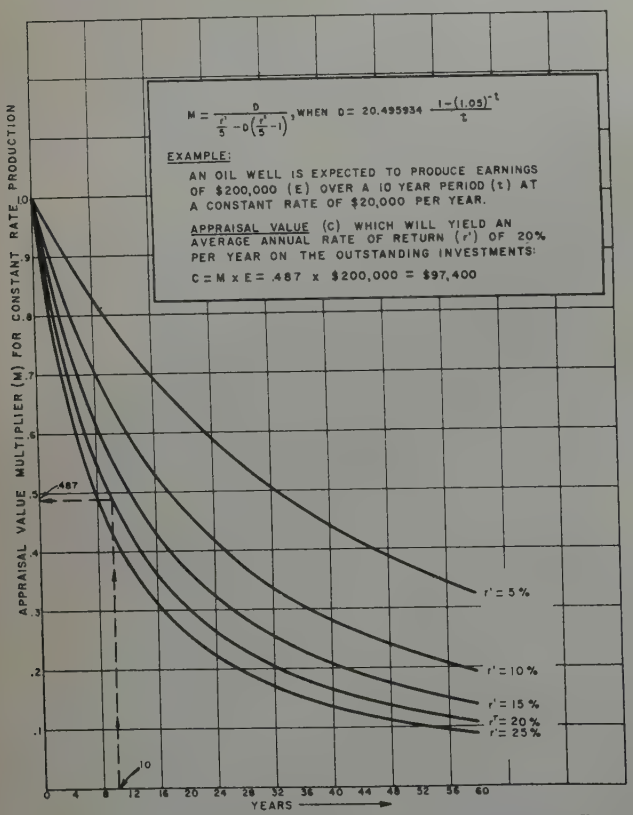
M = D / (r'/5 − D(r'/5 − 1)), WHEN D = 20.495934 (1 − (1.05)^−t)/t
EXAMPLE:
AN OIL WELL IS EXPECTED TO PRODUCE EARNINGS OF $200,000 (E) OVER A 10 YEAR PERIOD (t) AT A CONSTANT RATE OF $20,000 PER YEAR.
APPRAISAL VALUE (C) WHICH WILL YIELD AN AVERAGE ANNUAL RATE OF RETURN (r') OF 20% PER YEAR ON THE OUTSTANDING INVESTMENTS:
C = M x E = .487 x $200,000 = $97,400
APPRAISAL VALUE MULTIPLIER (M) FOR CONSTANT RATE PRODUCTION
YEARS
r' = 5%
r' = 10%
r' = 15%
r' = 20%
r' = 25%
.487
10

FIG. 5—APPRAISAL VALUE MULTIPLIER (M) FOR CONSTANT RATE PRODUCTION ($r = 5$ PER CENT PER YEAR).

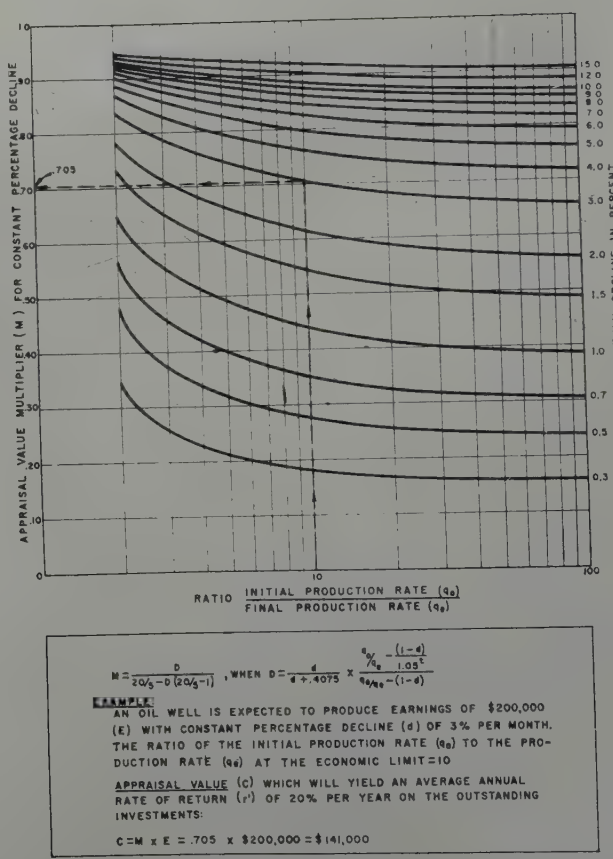
APPRAISAL VALUE MULTIPLIER (M) FOR CONSTANT PERCENTAGE DECLINE
MONTHLY DECLINE IN PERCENT
.705
RATIO INITIAL PRODUCTION RATE (q_o) / FINAL PRODUCTION RATE (q_e)
M = D / (20/3 − D(20/3 − 1)), WHEN D = d/(d + .4075) × (q_o/q_e − (1 − d)/1.05^t) / (q_o/q_e − (1 − d))
EXAMPLE:
AN OIL WELL IS EXPECTED TO PRODUCE EARNINGS OF $200,000 (E) WITH CONSTANT PERCENTAGE DECLINE (d) OF 3% PER MONTH. THE RATIO OF THE INITIAL PRODUCTION RATE (q_o) TO THE PRODUCTION RATE (q_e) AT THE ECONOMIC LIMIT = 10
APPRAISAL VALUE (C) WHICH WILL YIELD AN AVERAGE ANNUAL RATE OF RETURN (r') OF 20% PER YEAR ON THE OUTSTANDING INVESTMENTS:
C = M x E = .705 x $200,000 = $141,000

FIG. 6—APPRAISAL VALUE MULTIPLIER (M) FOR CONSTANT PERCENTAGE DECLINE ($r = 5$ PER CENT PER YEAR; $r' = 20$ PER CENT PER YEAR).

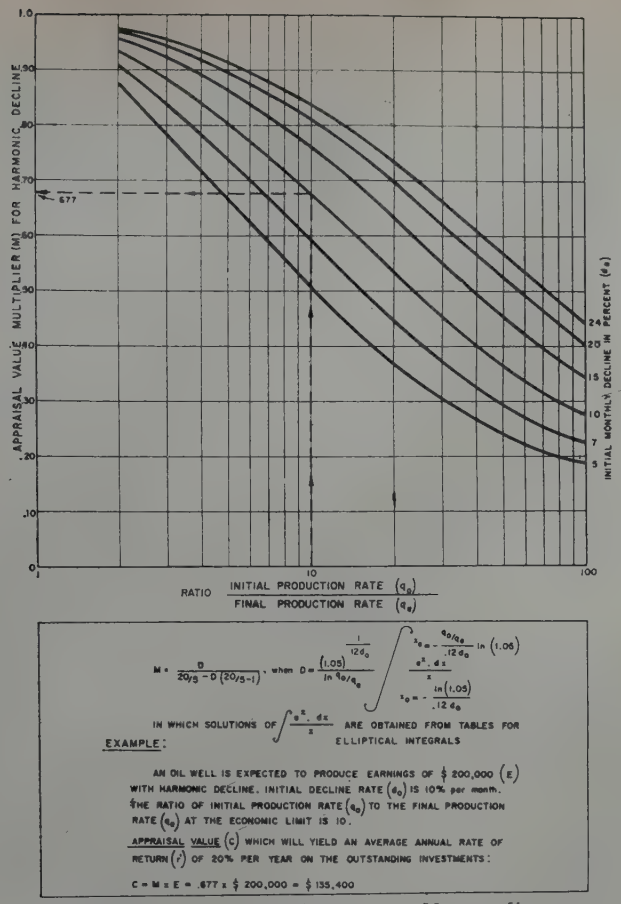
APPRAISAL VALUE MULTIPLIER (M) FOR HARMONIC DECLINE
INITIAL MONTHLY DECLINE IN PERCENT (d_0)
.677
RATIO INITIAL PRODUCTION RATE (q_0) / FINAL PRODUCTION RATE (q_f)
$M = \frac{D}{20/3 - D(20/3 - 1)}$, when $D = \frac{(1.05)^{\frac{1}{12 d_0}}}{\ln q_0/q_f} \int_{x_0 = -\frac{q_0/q_f}{12 d_0} \ln (1.05)}^{x_0 = -\frac{\ln (1.05)}{12 d_0}} \frac{e^x \cdot dx}{x}$
IN WHICH SOLUTIONS OF $\int \frac{e^x \cdot dx}{x}$ ARE OBTAINED FROM TABLES FOR ELLIPTICAL INTEGRALS
EXAMPLE:
AN OIL WELL IS EXPECTED TO PRODUCE EARNINGS OF $ 200,000 (E) WITH HARMONIC DECLINE. INITIAL DECLINE RATE (d_0) IS 10% per month. THE RATIO OF INITIAL PRODUCTION RATE (q_0) TO THE FINAL PRODUCTION RATE (q_f) AT THE ECONOMIC LIMIT IS 10.
APPRAISAL VALUE (C) WHICH WILL YIELD AN AVERAGE ANNUAL RATE OF RETURN (r') OF 20% PER YEAR ON THE OUTSTANDING INVESTMENTS:
C = M x E = .677 x $ 200,000 = $ 135,400

FIG. 7—APPRAISAL VALUE MULTIPLIER (M) FOR HARMONIC DECLINE (r = 5 PER CENT PER YEAR; r' = 20 PER CENT PER YEAR).

for different rates of return, r'. On the upper horizontal axis the equivalent number of years of constant rate production is plotted for comparison, which would have the same average 5 per cent deferment factors shown on the lower horizontal scale.

On this network of curves, each of which corresponds to a given average annual rate of return, r', are plotted some 34 points representing actual property transactions during recent years, and for which the multiplier, M, and the 5 per cent deferment factor were known.

Also shown on this chart in graphical form are some of the formulas for the value of producing properties which have been proposed or mentioned in the postwar literature.

1. The formula proposed by the 1951 subcommittee of the Committee on Valuation of Securities of the NAIC[9]: "The value of the oil, gas and condensate in the ground securing the loan, as determined by the said independent licensed petroleum engineer, shall be one-half of the present worth of future net revenues (before depreciation and federal taxes), which have been discounted to the present worth at the yield of the loan, based on cost price compounded at least annually over the expected period of realization from the reserves . . .

". . . The allowable value for statement purposes of the total unpaid oil and gas production loan, shall not in any event exceed in amount the resulting value arrived at in the preceding paragraph."

This definition apparently refers to the maximum allowable loan value rather than market or appraisal value. Curve 2, showing this relationship in Fig. 8, is based on an assumed loan yield of 5 per cent per year.

2. DeGolyer Formula A[10]: "I am familiar with cases in which the seller and buyer have arrived at a trading figure which was approximately one-half of the future net revenue (before depreciation and federal taxes), discounted at 4 per cent."

3. Terry-Hill formula[11]: "Annual net cash revenues (after federal taxes) are discounted, in this case at 8 per cent, compounded annually, to arrive at the total present worth of future net receipts, here considered to approximate the value of the property . . . . There is nothing sacred about the 8 per cent factor used in this case as the rate of discount, but it appears to the authors to result in a reasonable estimate of the fair market value for this type of property as indicated by sales of similar properties."

Curve 3 is based on an assumed federal income tax rate of 30 per cent of net revenue, based on the example given in the paper.

4. Gruy's Formula[12]: "Two-thirds of future net cash earnings, before depreciation and federal taxes, discounted at 5 per cent."

Although this formula was probably in use before Gruy's talk in 1952, no earlier published reference is known to the author.

5. DeGolyer Formula B[10]: "It is rather surprising more often than not the latter method (i.e. one-half of a 4 per cent discounted value; see Formula A) is very close to the future net revenue (before depreciation and federal taxes) discounted at 10½ per cent per year."

6. Fagin's "Fair Market Value Yardstick"[13]: "Which empirically relates the fair market value as a percentage of undeferred future net income (before depreciation and federal taxes) to the average discount factor at 5 per cent interest, shown by the projection in the engineer's report."

7. BA-CANGOC formula: "Three-fourths of the future net cash earnings before depreciation and federal taxes, discounted at 6 per cent."

This formula was used in 1956 by the Evaluation Committee in appraising U. S. producing properties for the purpose of evaluating relative assets of The British-American Oil Co., Ltd., and the former Canadian Gulf Oil Corp. as a preliminary to the merger of the latter company with the first. The ¾ ratio was based on an assumed average federal income tax rate of 25 per cent.

The purpose of showing data on actual transactions and various appraisal formulas in use is not to recommend any single formula as the only valid one but merely to show the general pattern in such values and the trends in current thinking.

It should further be stressed that the basis of the projection of future earnings is a reliable estimate of underground reserves and such an estimate should therefore always be made by a well qualified professional petroleum engineer, who has had long-time experience with the area involved.

An interesting point is that very few property transactions have taken place when the remaining life was short and the corresponding deferment factor high (above .85). One reason might be that possible prices for such properties are approaching the future undiscounted revenue and the prospective buyer would lose most of his "cushion" which protects him against uncertainties in the reserve estimates and projections. Another reason is that the owner of such properties is quite close to realizing the income himself, and, except for tax reasons, is therefore under less pressure to sell.

Due to the "leverage" afforded by the production payment route of purchasing properties the actual rate of return on the equity capital is usually substantially higher than indicated for the deal as a whole.

The data of Fig. 8 demonstrate that in the range where most properties are traded, and considering the entire transaction, an average annual rate of return before federal taxes, of somewhere between 7 and 20 per cent per year is not out of line. Also, among the various formulas discussed

those illustrated by Curves 4, 5, 6 and 7 seem to be the most realistic.

In judging the relative positions of the data in Fig. 8 it should be pointed out that most of the long-life deals on the left side are in the East Texas field, where the risk of errors in reserve estimating is relatively small and where the greatest benefits will be obtained from any long-term inflationary trends. This probably explains why the indicated average annual rate of return for such deals is under 7 per cent per year.

CONCLUSION

The average annual rate of return method discussed in this paper provides an accurate and versatile tool in profitability analysis and appraisal work.

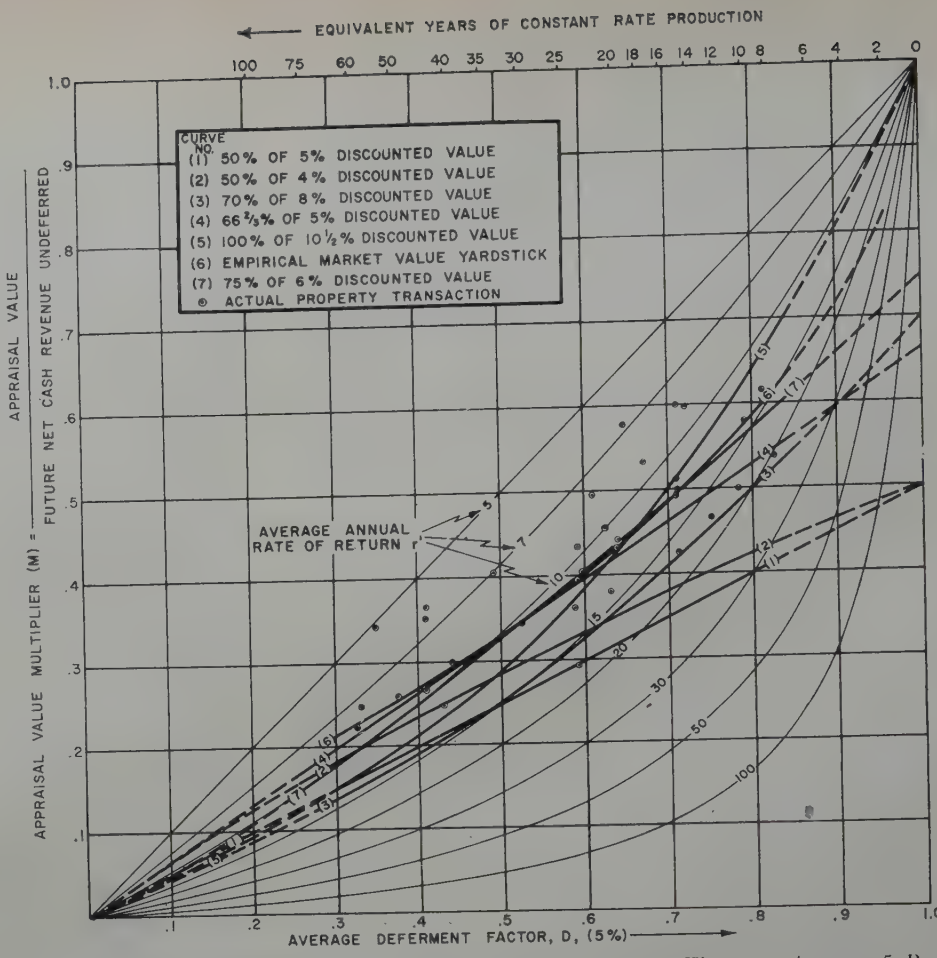
EQUIVALENT YEARS OF CONSTANT RATE PRODUCTION
100 75 60 50 40 35 30 25 20 18 16 14 12 10 8 6 4 2 0
APPRAISAL VALUE MULTIPLIER (M) = APPRAISAL VALUE / FUTURE NET CASH REVENUE UNDEFERRED
CURVE NO.
(1) 50% OF 5% DISCOUNTED VALUE
(2) 50% OF 4% DISCOUNTED VALUE
(3) 70% OF 8% DISCOUNTED VALUE
(4) 66⅔% OF 5% DISCOUNTED VALUE
(5) 100% OF 10½% DISCOUNTED VALUE
(6) EMPIRICAL MARKET VALUE YARDSTICK
(7) 75% OF 6% DISCOUNTED VALUE
⊛ ACTUAL PROPERTY TRANSACTION
AVERAGE ANNUAL RATE OF RETURN r'
AVERAGE DEFERMENT FACTOR, D, (5%)

FIG. 8—APPRAISAL VALUE MULTIPLIER (M) AS A FUNCTION OF THE WEIGHTED AVERAGE 5 PER CENT DEFERMENT FACTOR (D) FOR DIFFERENT VALUES OF AVERAGE ANNUAL RATE OF RETURN (r') AND ITS RELATIONSHIP TO ACTUAL PROPERTY TRANSACTIONS AND APPRAISAL FORMULAS.

NOMENCLATURE

a = amortization of the investment C on a unit-of-production basis, dollars per year.
B = undepreciated balance of the investment at a given time, dollars
C = original investment or appraisal value, dollars
C' = additional capital investment after purchase, dollars
d = production decline, per cent per month
d_o = initial production decline, per cent per month (for harmonic decline)
D = weighted average deferment factor on production and earnings at interest rate r
D' = weighted average deferment factor on the undepreciated balances of the investment at interest rate r
D_c = weighted average deferment factor on the capital investments, at interest rate r
e = net earnings from production after royalty, local taxes and operating expenses, dollars per year
E = combined net earnings from production after royalty, local taxes and operating expenses over the life of a well or property, undeferred, dollars
M = multiplier for determining appraisal value ($C = ME$).
N = average annual rate of return multiplier for determining $r' = N(E/C - 1)$ per cent per year
P = value of the projected net earnings from production at abandonment time (before depreciation), including compound interest at r per cent per year, in the case of the Hoskold method
r = safe rate of interest, per cent per year
r' = average annual rate of return, per cent per year
r'' = speculative rate of interest in the case of the Hoskold method, per cent per year
q_o = initial production rate, bbl/month
q_e = final production rate at economic limit, bbl/month
t = total project life in years in the case of the Hoskold method; in other applications number of years
X = "dummy fraction" for evaluation of elliptical integral
X_o, X_e = limits of same

REFERENCES

1. Glanville, J. W.: *Jour. Pet. Tech.* (June, 1957) **IX,** No. 6, 12.
2. Hill, H. G.: "A New Method of Computing Rate of Return on Capital Expenditures", Report to Philadelphia Chapter of Natl. Soc. for Business Budgeting (Aug., 1953).
3. Reistle, C. E.: *Jour. Pet. Tech.* (June, 1956) **VIII,** No. 6, 11.
4. Dean, J.: *Harvard Business Review* (Feb., 1955) 120.
5. Dean, J.: *Capital Budgeting,* Columbia Univ. Press (1951).
6. Hoskold, H. D.: *The Engineer's Valuing Assistant,* Longman's Green & Co. (1877).
7. Parks, R. D.: *Examination and Valuation of Mineral Property,* Addison-Wesley Press, Inc. (1949) Chap. 12, 13.
8. Thuesen, H. G.: *Engineering Economy,* Prentice-Hall (1950).
9. Report and Proposals with Respect to the Principles of Valuation of the Committee on Valuation of Securities of the National Association of Insurance Commissioners (Oil and Gas Production Loans) (June 15, 1951) 30.
10. DeGolyer, E. L.: "Evaluation", presentation to the Oil and Gas Institute, Southwestern Legal Foundation, Dallas (March 26, 1949).
11. Terry, L. F., and Hill, K. E.: *Jour. Pet. Tech.* (July, 1953) **V,** No. 7, 23.
12. Gruy, H. J.: Talk before Petroleum Engineers Club of Dallas (Oct. 17, 1952).
13. Fagin, K. M.: Talk before Study Group, Dallas Section, AIME (Nov. 1, 1956).
14. Arps, J. J.: *Trans.* AIME (1945) **60,** 228. ★★★

Further Discussion of Paper Published in
***Transactions* Volume 213, (1958)**

Producing Wells on Casing Flow — An Analysis of Flowing Pressure Gradients

P. B. BAXENDELL
MEMBER AIME

COMPAÑÍA SHELL DE VENEZUELA, LTD.
MARACAIBO, VENEZUELA

(Published as T.P. 8027, Page 202)

DISCUSSION

FRED H. POETTMANN
MEMBER AIME

THE OHIO OIL CO.
LITTLETON, COLO.

P. B. Baxendell is to be complimented for an excellent piece of work. To our knowledge there has been no previous publication of field data on the flow of oil and gas through the annulus of a well. It is certainly gratifying to see this work on annular flow confirm the previous published correlation procedure on tubing flow. It extends considerably the range under which reliable gas-lift calculations can be made.

Baxendell discussed this work with us about a year ago and was kind enough to send a large scale plot of his correlation. We had been designing gas-lift installations on flow through the annulus, assuming that the original correlation of the f factor based on tubing flow[1] was valid as long as we stayed within the same mass velocity range on which the correlation was based. Doing this work necessitated the use of an equivalent diameter for the annular flow. The equivalent diameter is defined as

$$4\left(\frac{\text{area of stream cross section}}{\text{wetted perimeter}}\right)$$

and for the case of an annulus is $D_1 - D_2$. Substituting this in the basic equation correlating energy loss along with the area to flow required to convert the velocity, v, to volumetric flow rate, D^5 (Baxendell's Eq. 7) becomes $(D_1 - D_2)^3 \times (D_1 + D_2)^2$. This is equivalent to Baxendell's expression, $(D_1^2 - D_2^2)^2 \times D_e$, where D_e is $(D_1 - D_2)$. Similarly, the D in 1.4737×10^{-5} (MQ/D) becomes $(D_1 + D_2)$ for annular flow.

On receipt of Baxendell's data, we, of course, recalculated it to put it into the form we were using, and to see how well it agreed with the correlation based on tubing flow. Fig. 1 shows the results, which were certainly gratifying. For low values of $(D_1 - D_2)$ ρv, the data coincide with the data on flow through tubing, whereas at high values the data on flow through the annuli appear to be leveling off to a constant value. For very high rates of flow where the turbulence is very high, one might expect the value f to level out and become constant.

A bulletin published in 1914 by the U. of Wisconsin presented results of a large number of laboratory tests in air lifting water through short lengths of 1.25-in. tubing[2]. It was possible to correlate a random sampling of

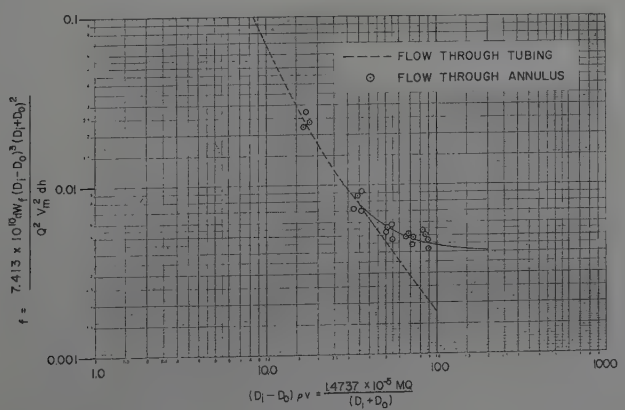

FIG. 1—CORRELATION OF DATA ON FLOW THROUGH ANNULI.

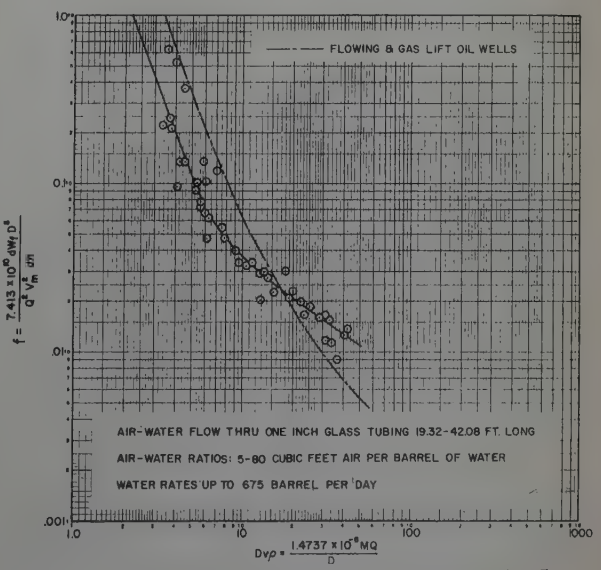
FLOWING & GAS LIFT OIL WELLS
AIR-WATER FLOW THRU ONE INCH GLASS TUBING 19.32-42.08 FT. LONG
AIR-WATER RATIOS: 5-80 CUBIC FEET AIR PER BARREL OF WATER
WATER RATES UP TO 675 BARREL PER DAY
1.0
0.01
.001
1.0
10
100
1000
$f = \frac{7.413 \times 10^{10} gW_f D^5}{Q^2 V_m^2 dh}$
$Dv\rho = \frac{1.4737 \times 10^{-5} MQ}{D}$

FIG. 2—CORRELATION OF U. OF WISCONSIN DATA ON AIR LIFT.

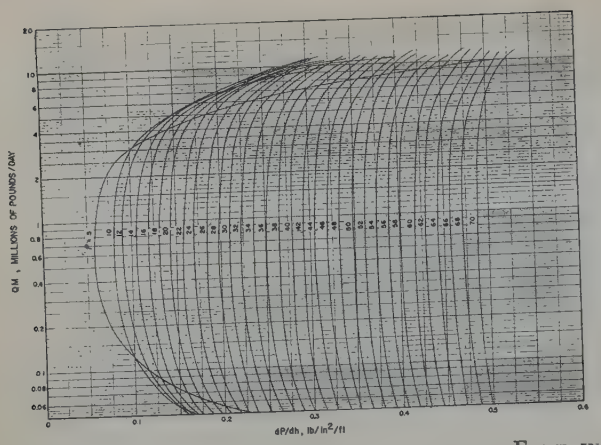

FIG. 3—CALCULATION OF PRESSURE TRAVERSES FOR FLOW IN ANNULUS. TUBING SIZE 2.5-IN. NOMINAL (6.5 LB/FT, 2.441-IN. ID, 2.875-IN. OD); CASING SIZE 7.0-IN. NOMINAL (26 LB/FT, 6.276-IN. ID).

the data using the same correlating procedure, Fig. 2. For low values of $Dv\rho$, the f factor curve lay to the left of the curve for flowing oil and gas-lift wells. At high values it crosses over and appears to want to level out as was the case from Baxendell's data.

The correlation technique certainly is subject to additional improvement so that all the data, such as the multiphase annular flow, air-water flow, etc., all fall on the same correlating curve. It is our belief that the f factor has been properly defined and that the improvement will come by defining properly the abscissa of the f factor plot. We are aware of work now under way which gives evidence of doing this.

Using Baxendell's data, pressure gradient charts of the type shown in Fig. 3 were prepared. These charts are used in the design of the gas-lift installations when the flow is through the annulus.

REFERENCES

1. Poettmann, F. H. and Carpenter, P. G.: "The Multiphase Flow of Gas, Oil, and Water Through Vertical Flow Strings", *Drill. and Prod. Prac.*, API (1952) 257.
2. Davis, G. J. and Weidner, C. E.: *Bull.*, U. of Wisconsin, No. 667. ★★★

Development and Field Testing of a Core Barrel for Recovering Unconsolidated Oil Sands

A. B. HILDEBRANDT
H. C. BRIDWELL
JUNIOR MEMBER AIME
J. M. KELLNER

THE CARTER OIL CO.
TULSA, OKLA.

ABSTRACT

The rubber-sleeve core barrel was developed to improve core recovery from unconsolidated sands, where it is most difficult to obtain cores with conventional barrels. The use of a rubber-sleeve core retainer, together with other departures from usual design, has required a considerable amount of testing to prove its operability. Tests run in shallow experimental holes and in drilling wells in the U. S. and Venezuela have, to a large extent, proved the operation of the barrel. Internal mechanism troubles, such as sandbinding of the sleeve, have been largely overcome. Cores have been recovered from completely unconsolidated sands where conventional coring has almost been abandoned because of poor recovery. In addition to retaining the core until brought to the surface, the barrel gives a "packaged-as-cut" core, which is convenient for handling and transportation. In the initial work, drag blade cutters, roller cutters, and tungsten carbide insert cutters were used for cutting unconsolidated sands.

Further bit head development is presently being conducted using diamond heads in unconsolidated sands where shales, hard sands, and limestones are encountered in adjacent formations. This work should render the barrel capable of cutting and recovering most types of formations, possibly including broken and fractured formations. This development is being carried on in cooperation with a diamond bit manufacturer.

Original manuscript received in Society of Petroleum Engineers office on July 18, 1957. Revised manuscript received Nov. 20, 1957. Paper presented at 32nd Annual Fall Meeting of Society of Petroleum Engineers in Dallas, Tex., Oct. 6-9, 1957.

INTRODUCTION

For many years the oil industry has needed greater recovery of cores from unconsolidated formations. Conventional equipment has been used to core unconsolidated sands with little success. Specifically, a core barrel was needed which would recover unconsolidated sands in a condition that would give useful reservoir information.

DEVELOPMENT OF THE RUBBER-SLEEVE CORE BARREL

Basic Requirements of Unconsolidated Sand Coring

The basic need was defined as a core barrel that would obtain a continuous unconsolidated core with sand grains in place as deposited in the formation. A preliminary survey of coring equipment and search of the literature pointed out the weaknesses of conventional core barrels. Laboratory tests using unconsolidated sand in a metal tube simulated actual sand movement into the core barrel during conventional coring. In conventional barrels the core sometimes crumbles and bridges, or fails under compressive column action, becomes oversize, and wedges against the walls of the inner barrel.

The core barrel requirements established by the surveys and preliminary tests are as follows.

1. The core should be held together as it is cut so it cannot crumble and bridge against the walls of the coring tool, care being taken not to permit damage from fluid circulation.
2. The core should be continuously supported as it is cut so it will not have to support itself in compression.
3. The core should be packaged in the barrel to retain an undisturbed condition during the trip out of the well.

The packaging should be such that the core can be removed from the barrel and shipped to the core analysis laboratory without physical disturbance or alteration of fluid content by exposure to the atmosphere.

Operation of the Rubber-Sleeve Core Barrel

The rubber-sleeve core barrel (Fig. 1) meets the basic requirements for the recovery of unconsolidated sands.

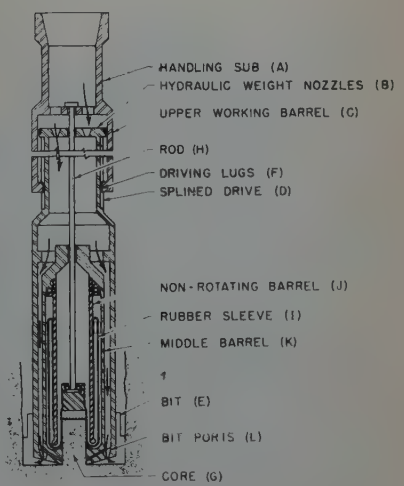

FIG. 1—SCHEMATIC DRAWING OF RUBBER-SLEEVE CORE BARREL.

The principal working parts of the rubber-sleeve core barrel are shown by the schematic drawing in Fig. 1. The barrel, which operates on the bottom of a conventional drill string the same as conventional drilling equipment, is attached to the drill string by the handling sub (A). The hydraulic nozzles (B) are the source of weight for cutting the core. The pressure drop across the nozzles is controlled by the flow rate of the mud pumps at the surface. The drill string and upper working barrel (C) do not advance during the coring operation. The spline drive (D) and lower half of the core barrel advance into the borehole as the core is cut by the bit (E). The upper barrel rotates the lower barrel through the driving lugs (F) in a spline drive.

As the bit advances into the formation, cutting the core (G), the rod (H), which is attached to the upper barrel, remains stationary, supporting the upper end of the rubber sleeve. Advance of the lower end of the non-rotating barrel (J) forces the rubber sleeve to shrink over the walls of the core. The rubber sleeve is smaller in diameter than the core and therefore forms a tightly stretched skin to hold the contents of the core in place. Longitudinal fabric cords in the rubber sleeve keep it from stretching lengthwise. The rubber sleeve is preloaded on the non-rotating barrel (J) at the well surface and is pulled off the inner barrel as the core enters. Since the rubber sleeve is positively displaced into the non-rotating barrel as coring progresses, the core that is being cut is never in compression from the core above it. This prevents compressive column failure of the core. The squeeze of the rubber sleeve on the core precludes the use of mechanical spring core catchers and offers a smooth entrance to the core. The non-rotating barrel and the rod are swiveled to eliminate torque on the core. The middle barrel (K) protects the rubber sleeve and the core from the drilling mud as the mud passes to the bit head ports (L). A suitable J-slot release mechanism unlocks the spline drive when hole bottom is reached and the drill pipe is rotated. A change in weight indicator reading signals full advance of the barrel.

DEVELOPMENT TESTING

Five and Ten-Foot Core Barrels

Progressive testing of early designs for development purposes was conducted with a 5-ft rubber-sleeve core barrel in shallow Arkansas River sands at depths between 20 and 80 ft, near Sand Springs, Okla. This coring in completely unconsolidated sands using air, water and bentonite mud as drilling fluids, was to determine the operating characteristics of the functional parts of the barrel. The operation of the barrel proved to be independent of the type of fluid used if there was sufficient fluid to remove the cuttings. This phase of testing was continued until the barrel functioned satisfactorily in recovering full-length cores of the unconsolidated formation. It was apparent after this testing that the coring program should be extended to deep wells to properly test the rubber sleeve and bit head. Determination of performance in unconsolidated sands at greater overburden pressures and under deep-well hydraulic conditions was considered essential to proper evaluation.

The barrel was tested in California, Alabama, and Louisiana in fields where unconsolidated sands are encountered. This deep-well testing revealed problems of sanding of the spline drive, bearings, packing and rubber-sleeve packaging system. After continued testing in these areas, revisions to the barrel eliminated these problems. Bit head design problems also became apparent during this phase of testing. The bit head cutting face contour and nozzle arrangement must be such that the circulation fluid cleans the bit but does not wash away the unconsolidated sand. Also, the bit must be capable of penetrating any hard formations and gummy shales that are adjacent to the unconsolidated formations. Progressive changes in tungsten-carbide-tipped cutter heads were made until a final field test in a 3,200-ft well in Alabama resulted in an average of 95 per cent recovery from six cores cut in unconsolidated sand and shale.

The need for recovery improvements in certain poorly consolidated oil sands in Venezuelan producing zones prompted the building of two barrels capable of cutting 10-ft cores. These barrels incorporated improvements based on experience gained with the 5-ft barrel. A check run of one of these barrels resulted in an average recovery of 63 per cent at depths from 1,500 to 4,200 ft in a Southern Louisiana well. The formation varied from unconsolidated sand to shales. Drag blade, roller, and tungsten-carbide-tipped cutters were tried. Following this, two barrels were shipped to Venezuela and tests were conducted in which 89 per cent of the formation penetrated (unconsolidated oil sand and shale) was recovered for analysis. However, this testing and a later test pointed

Fig. 2—Diamond Bit Heads Used in Coring Tests. From Left to Right are Bits 1, 2, and 3.

out the desirability of having a bit head that will penetrate hard or gummy formations intermingled with soft sands. Such formations presented particular difficulty in penetration and retention of cores because of their tendency to ball-up and clog bit face water courses. This impeded circulation and retarded advance of the core head.

Diamond Bit Development

Work is presently being conducted on further bit head development. Several diamond heads have been fabricated and tested to determine their operability. Some of these are illustrated in Fig. 2. After preliminary near-surface testing at Sand Springs, Okla., these bits were run in a deep-well test in Bayou Choctaw, La. Unconsolidated oil sands, shales, lignites, and hard sands were encountered in this well. Further coring is planned to compare the performance of the rubber-sleeve barrel with conventional practice in these formations. The results of these tests are tabulated in Table 1. It is apparent from test results that the bits illustrated in Fig. 2 are operable designs. Further improvements in bit design now in progress are expected to result in a bit head whose recovery performance in unconsolidated oil sands, hard rock, and friable or gummy shale formations should be even more acceptable. Additional coring experiments are being conducted, and it is contemplated that the barrel will soon be available to industry.

TABLE 1—FIELD TESTS OF THE 10-FOOT CORE BARREL, BAYOU CHOCTAW, LA.

Test No.	Bit Weight (lb)	Type Formation	Depth*	Formation Penetration (ft)	Core Recovery (ft-in.)	Core Recovery (Per cent)	Diamond Head of Fig. 2
1	4,000	Unconsolidated Sand	1,580	10	9-2	90	1
2	5,000-7,000	Unconsolidated Sand and Shale	1,590	10	4	40	Not shown
3	5,000-7,000	Unconsolidated Sand	3,245	10	0	0	Not shown
4	5,000-7,000	Unconsolidated Sand	3,255	10	0	0	2
5	7,000-5,000	Unconsolidated Sand and Shale	3,685	10	9-8	97	1
6	7,000-5,000	Unconsolidated and Consolidated Sand	3,695	10	3	30	Not shown
7	4,000	Unconsolidated Sand	3,705	10	9-9	98	2
8	4,000	Unconsolidated Sand and Shale	3,715	10	9-6	95	1
9	4,000	Unconsolidated Sand	3,725	10	10	100	2
10	3,000-5,000	Unconsolidated Sand and Lignite	3,735	10	9-7	96	3
11	3,000-5,000	Hard Oil Sand and Lime	4,027	4**	4	100	3
12	6,000-7,000	Hard Oil Sand and Lime	4,035	6	4	66	1

Circulation Fluid—Bentonite Mud; Circulation Rates 150 to 225 gpm
Bit Rotation 50-70 rpm
*Top of Core
**Coring was stopped at 4-ft penetration because of a tool joint washout in the drill pipe above the core barrel

OTHER POSSIBLE APPLICATIONS

Reduced core contamination is a prospect for this barrel, inasmuch as the rubber sleeve encases a core shortly after it passes the bit head.

Also promising is the utility of the barrel in recovering broken formations that tend to bridge in conventional barrels.

CONCLUSIONS

The following conclusions can be drawn from the results of the experimental work.

1. The rubber-sleeve core barrel is sound in principle and applicable in practice for the recovery of unconsolidated oil sands.

2. Present bit head development should render the barrel capable of cutting and recovering unconsolidated oil sands in areas where gummy shales and hard sands are encountered adjacent to the unconsolidated sands.

3. Some potential for adapting the operating principle of this barrel to other than unconsolidated sand coring may exist.

ACKNOWLEDGMENT

Appreciation is hereby expressed by the authors of the management of The Carter Oil Co. for permission to publish this paper. The authors also wish to acknowledge the efforts of the many people, in both the Research and Production Depts. of The Carter Oil Co., whose work in this project have made this paper possible. The authors are grateful for assistance rendered by the staff of the Christensen Diamond Products Co. ★★★

T. N. 467

A Copper Ion Displacement Test for Screening Corrosion Inhibitors

WILLIAM B. HUGHES | TRETOLITE CO., DIV. PETROLITE CORP. ST. LOUIS, MO.

ABSTRACT

A method for the selection of the most suitable corrosion inhibitor for a particular system is given. The method involves the evaluation of surface passivity by means of copper ion displacement after the metal surface has been subjected to the corrosive atmosphere. The application of the method to the selection of suitable inhibitors for use in producing wells is described.

Correlation with recognized laboratory tests has been found to be good within the limitations of the test.

The use of the test to evaluate inhibitor persistence is described.

INTRODUCTION

Corrosion as it is associated with the industry shows wide variations in its qualitative as well as its quantitative aspects. This complicates the work of the corrosion engineer.

In the past few years the efforts of the corrosion engineer have been further taxed by the large numbers of products being marketed as corrosion inhibitors by various manufacturers. These products are submitted to him together with a limited amount of data to support their use as inhibitors. The data are usually authentic and reliable yet all too often when these products are applied to an actual corrosive system the results are disappointing due to the ineffectiveness of the inhibitor and the corrosive system.

The corrosion engineer must select a comparatively limited number of inhibitors for field trial from the large number available. The selection is usually made on the basis of a standardized laboratory test such as that adopted by the National Association of Corrosion Engineers or by field experience in an area; however, testing of this type is discouraging on large numbers of compounds, particularly in view of the specificity of environment.

It has been an object of this work to devise a method which will allow the corrosion engineer to select the best inhibitor for a specific environment under field conditions. The test would of necessity be rapid and inexpensive. It would preferably eliminate the need for expensive and delicate instruments.

STATEMENT OF THEORY

The test as developed makes use of the fact that metal ions will be displaced from solution by metals having a more positive electrode potential. Thus, if an active iron surface is exposed to a solution of a copper salt, free copper will plate spontaneously on the iron surface as it is displaced from the salt solution by iron ions.

If the iron surface is passified, as by coating with an insulating-type organic corrosion inhibitor, it is no longer capable of displacing the copper ions due to its own limited ionization. The result will be a change in the amount of copper plated upon exposure to a neutral copper salt solution.

In practice it has been found possible to measure the magnitude of the alteration of the cell potential by determining the copper deposited on a standard iron surface under controlled conditions. This means that, as the film builds up, the resulting shift in the electrode potential tends to cause the iron surface to act more like a noble metal, resulting in a reduction in the cell potential to a point that copper will no longer plate spontaneously.

Obviously, the salts of other metals such as silver, gold or platinum might be used for this operation; however, copper was selected because of the color difference of the plate, the comparatively low cost of copper salts and the ease of evaluation of the plated copper. Furthermore, its high cell potential provides a substantial driving energy.

The determination of the copper is readily done colorimetrically by dissolving it in 5 per cent ammonium hydroxide solution containing 2 per cent potassium persulfate. The blue color of the copper ammonic complex ion so developed may be compared with standards prepared by dissolving known quantities of copper powder in the same reagent.

In routine screening it is seldom desirable to determine the amount of copper plated. It is usually more important to determine the concentration of inhibitor required to prevent the plating of copper.

Original manuscript received in Society of Petroleum Engineers office on July 15, 1957. Revised manuscript received Nov. 22, 1957. Paper presented at 32nd Annual Fall Meeting of Society of Petroleum Engineers in Dallas, Tex., Oct. 6-9, 1957.

DESCRIPTION OF THE TEST

The test is run by immersing 1-in. square, sand-blasted coupons prepared from 0.006-in. thick shim stock in brine from the corrosive source for five minutes. The coupons are then transferred without drying to a solution of a known concentration of the inhibitor in the oil from the corrosive source, where they are allowed to remain for an additional five minutes. The coupons are then transferred to a 10 per cent solution of copper sulfate where they are allowed to remain for 30 seconds. Blank determinations are made in the same manner but omitting the inhibitor. The lowest concentration of inhibitor required to prevent the plating of copper is taken as the criterion for a pass.

In application, the fluids from a naturally occurring corrosive source are used, together with a group of known corrosion inhibitors, since this method is designed to select only from known inhibitors. It is not intended to replace other evaluation tests. The method presupposes that a film forming corrosion inhibitor is available. No consideration is given to a chemical having a limited film life such as a primary amine. These materials will look good under some circumstances in this test, but they will show short film life so they will actually be poor inhibitors. Conversely, a compound which acts strictly by cationic activity (such as quaternary ammonium salts) rather than through an adsorption mechanism will show a poor result on the test, although in practice such materials may be good inhibitors.

It is evident that the method is designed as a qualitative evaluation. Any quantitative aspects must be considered on an empirical basis. Several factors such as time and temperature will need to be considered in such a study.

The test as it is run will preclude the necessity for wetting studies on the spot. By treating the water-wet metal the factor of oil wetting is adequately considered. It may be desirable to study wetting along with this method. This may be done by drying the coupon after exposure to the brine and prior to treatment by the inhibited oil.

EVALUATION OF THE METHOD

In an evaluation of the test method on producing wells, several of these were selected where field experience with recognized corrosion inhibitors was available. The test was applied to the freshly produced fluids at the wellhead. Table 1 shows the effectiveness of the inhibitors as rated by the test method and in relation to extended field experience.

In practice the quantitative aspects of this method are questionable since the inhibitor has a much longer contact time in the field, and, thus, a longer time to reach the equilibrium state.

These tests showed a correlation between field results on a group of known corrosion inhibitors. The next step was to select a chemical which was less obvious as an inhibitor and which had not been tried in an actual producing well and which did not conform to the popular conception of a corrosion inhibiting structure.

The well selected for this study was near Greggton, Tex. Samples of the fluids from this well were shipped to the laboratory for evaluation. A new type of corrosion inhibitor was selected for this application. It was found to give no copper plating at 100 ppm, while the commercial inhibitor being used in this well required 300 ppm to pass. A field trial showed the selected compound to be somewhat better than the commercial inhibitor with iron content of the produced fluids being reduced from an average of 124.2 to 97.9 ppm. The significance of this work lies primarily in the fact that a small amount of well fluid was shipped to the laboratory and a chemical was selected on the basis of this sample. The chemical structure used in this test was significantly different from that of the commercial corrosion inhibitors used in this area.

The application of this method to fluids shipped to the laboratory is to be recommended only with some reservation. It may lead to errors in selection due to the changes which occur in well fluids with time. These changes are not fully understood, but they have been long recognized in connection with other work on well fluids.

A more extensive test was run in a well at Cotton Valley, La. Again the inhibitor was selected on the basis of samples of fluid shipped to the laboratory. In this case a well known commercial inhibitor was being used with success in this well. An experimental formulation, differing considerably in structure from the commercial inhibitor, was selected for comparison with the commercial compound. Both passed the copper test at 200 ppm, indicating that they should be comparable in field use. A sample of this experimental compound was then tried in the well. Table 2 shows the results of this in terms of coupon losses and iron analyses.

Although the test is of short duration, little change in the protection afforded the system is indicated, showing the validity of the evaluation by the copper ion test.

Application of the test has also been made to determine the corrosive potential of a waterflood well. In this case the produced water was being mixed with fresh water before injection. The optimum ratio of produced to fresh water was determined. Using an inhibitor and water from a Louisiana waterflood injection well it was determined that a 50-50 mixture of fresh water to produced water was more corrosive than a 70-30 ratio. The first mixture required 600 ppm of an inhibitor to pass while at the 70-30 ratio only 350

TABLE 1

Pool or Field	Inhibitor	Min. Pass Conc. ppm
Rhodessa	A	600+
	B	600+
	C	350+
	D	200
Field Data: Inhibitor D proved the best of these inhibitors. C failed		
Greenwood	E	300
	C	600+
	B	400+
Field Data: Inhibitor E is the best of these in this location.		
Haynesville	D	300
	F	600+
Field Data: A competitive test run here shows D superior to F.		
Jacksonboro	J	1,600+
	F	1,000
Field Data: Inhibitor F has been found superior to J in this location.		

TABLE 2

Date	Compound	Amt. (gal) per test period	MPY	Iron (ppm)
11/29 to 12/13	Commercial	35	0.97	24
12/13 to 12/27	Commercial	35	0.59	64
12/27 to 1/10	Commercial	31.5	0.30	94
Average		33.8	0.45	60.7
1/10 to 1/24	Experimental	35	1.39	27
1/24 to 2/27	Experimental	24.5	0.46	25
2/7 to 2/21	Experimental	35	0.93	38
2/21 to 3/7	Experimental	35	1.10	9
3/7 to 3/21	Experimental	28	0.62	24
3/21 to 4/4	Experimental	35	1.05	8
Average		32.9	0.82	21.8

ppm of this compound was required for a pass. Iron analysis at the injection well confirmed that the 50-50 mixture was indeed more corrosive. Further, the use of the inhibitor in the 70-30 mixture reduced the penetration from 3.44 to 0.72 MPY in three weeks.

CORRELATION WITH STATIC WEIGHT LOSS TESTS

Of considerable interest is the application of this test to laboratory procedures. It has been found to correlate quite closely with static weight-loss tests and with such standard tests as the ASTM Steam Turbine Oil (spindle) test. It has been found to be adaptable to a more critical evaluation of the factors contributing to the process of corrosion and to the inhibitor function.

Several static weight-loss tests have been correlated with the copper ion displacement test. Among the commonly used tests is the one which has been adopted by the National Association of Corrosion Engineers[1] as a standard screening test. The results in Table 3 show a correlation of the copper ion displacement test with this test.

The test has been found also to correlate quite well with the ASTM Spindle test.[2] Table 4 shows the results of this correlation in which several compounds have been compared directly. Again, the criterion for passing the copper ion test is the concentration in parts per million required to completely inhibit the plating of copper.

Still another rather close correlation has been found in evaluating inhibitors for tanker corrosion. This test has been described by Malcolmson, et al.[3] It involves subjecting the coupon to a sea water-hydrocarbon system for one week followed by a sea water-air system for an additional week. Table 5 shows the results of a typical test series. Again the amount of inhibitor required to inhibit copper is reported in parts per million.

Although the above tests show correlation in a general way, the most valuable use of the test in the laboratory lies in defining the response of inhibitors to certain variables in the corrosion process. For example, such things as pH response, salinity effects or temperature response can be rapidly determined. The results will need to be confirmed by weight-loss tests, but fewer compounds will need to be handled in such tests.

The test is also useful in the determination of the influence of various factors over the persistence of a corrosion inhibitor. This technique is slightly different

TABLE 3

Inhibitor	Copper Ion Test-ppm required to inhibit copper	Per cent Protection NACE test
A	100	87
B	100	92
C	200	78
D	400	64
E	600	48
F	1,000	16
G	1,500	8

TABLE 4

Inhibitor	Copper Ion test ppm to pass	ASTM Spindle test observed rust rating
A	50	R1
B	100	R3
C	200	R4
D	200	R5
E	1,600	R7

TABLE 5

Inhibitor	Copper ion test ppm to pass	Cycle test Per cent protection
A	100	91.0
B	100	86.1
C	200	52.2
D	500	33.6
E	500	35.7
F	800	29.8

in that a film of inhibitor must first be placed on the coupon by evaporation of a solvent from a known concentration of inhibitor. This evaporated film is then studied by the copper ion displacement test to determine the persistence of its insulating properties under pre-determined conditions. A typical experiment would involve the evaporation of an alcoholic solution of inhibitor on the surface of a group of coupons. The coupons would then be subjected to brine from a corrosive source at a mild agitation rate. Coupons would be removed and placed in copper salt solution at intervals to determine the time at which complete protection is no longer possible and the time at which no protection is found. Such measurements can be made under a variety of conditions to study the influence of various factors on persistence.

CONCLUSION

From the data presented it is concluded that the copper ion displacement test is a useful tool for screening inhibitors for both laboratory and field.

REFERENCES

1. Reported at the Ninth Annual NACE Conference, Chicago, March, 1953.
2. ATSM D-665-54.
3. Reported at the Annual Meeting of the Society of Naval Architects and Marine Engineers, New York, Nov., 1952.

★★★

T. N. 2001

A Report on the Displacement Log

R. H. WINN* | HALLIBURTON OIL WELL CEMENTING CO. HOUSTON, TEX.

INTRODUCTION AND HISTORY

Campbell and Martin[1] described a new exploratory logging tool which was developed as the result of a new concept of the phenomenon that takes place when a porous formation containing mobile hydrocarbons and irreducible interstitial water is invaded by mud filtrate. They postulate that invasion will create a bank of interstitial water between the flushed zone and the undisturbed formation. This postulate was confirmed by Wyllie.[1]

Thus, if R_{mf} is greater than R_w and mobile hydrocarbons are present, the resistivity profile with increasing radii from the borehole is high:low:high, as shown in Fig. 1. If mobile hydrocarbons are absent, the bank of interstitial water is indistinguishable from the undisturbed formation and the resistivity profile, when R_{mf} is greater than R_w, is high:low, as shown in Fig. 2. The zone containing the bank of interstitial water and residual oil was named the "low zone".

Campbell and Martin conducted extensive electrolytic wedge and resistivity analog model studies to select a logging system that would reflect the presence or absence of the low zone. The system they selected was that of a family of lateral curves. The model studies indicated that the presence of a low zone could be detected in approximately 60 to 70 per cent of the producing sand reservoirs with a family of lateral curves provided that the sonde effectively occupies 90 per cent of the diameter of the hole. These studies were conducted with $D_i = 5d$. The presence or absence of the low zone is best determined by a plot of the apparent resistivity vs spacing as shown in Figs. 3 and 4. A dip or inflection in the profile that repeats at successive depth intervals is considered diagnostic. To reduce the shunting effect of the hole and mud, a sonde of insulating material that is surrounded by a series of flexible rubber bumpers was designed. The bumper efficiency is considered to be the ratio of the bumper diameter to the hole diameter. Field tests conducted by Campbell and Martin on 10 wells with a tool that provided for station readings indicated that dips or inflections could be detected in 19 out of 25 known producing zones.

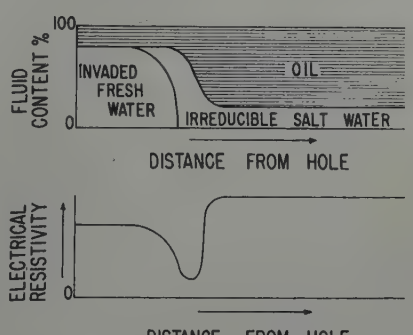

FIG. 1—OIL ZONE AFTER INVASION.

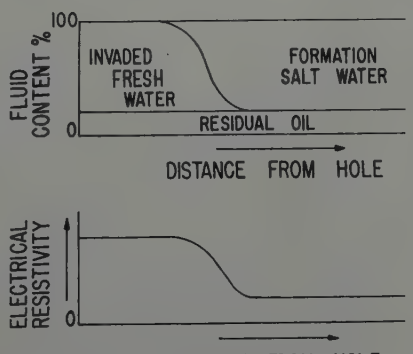

FIG. 2—WATER ZONE AFTER INVASION.

INSTRUMENT DEVELOPMENT

Halliburton developed a logging system to simultaneously and continuously record eight lateral curves. The instrumentation is described in the literature.[1] The original logs made

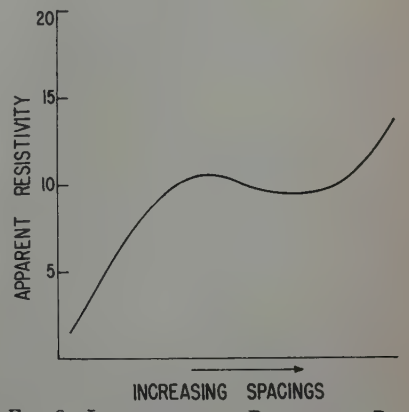

FIG. 3—ILLUSTRATING A DIP IN THE RESISTIVITY PROFILE.

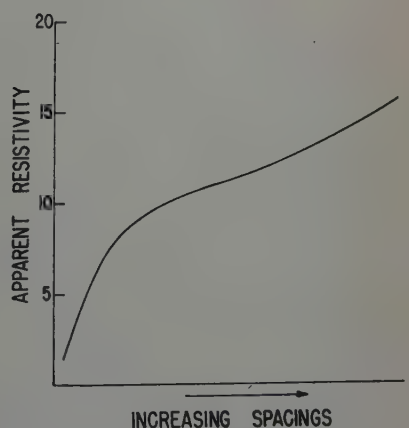

FIG. 4—ILLUSTRATING AN INFLECTION IN THE RESISTIVITY PROFILE.

Manuscript received in Society of Petroleum Engineers office on July 15, 1957. Paper presented at 32nd Annual Fall Meeting of Society of Petroleum Engineers in Dallas, Tex., Oct. 6-9, 1957.

*Presently associated with Welex, Inc., as president of Welex de Venezuela, C. A.

[1]Reference given at end of paper.

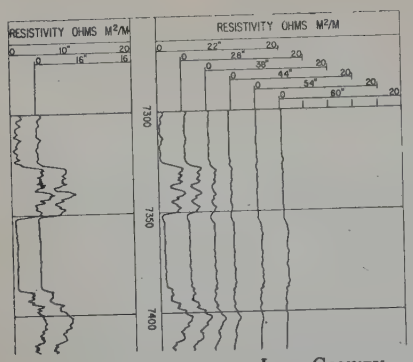

FIG. 5—DISPLACEMENT LOG, CONVENTIONAL DEPTH SCALE.

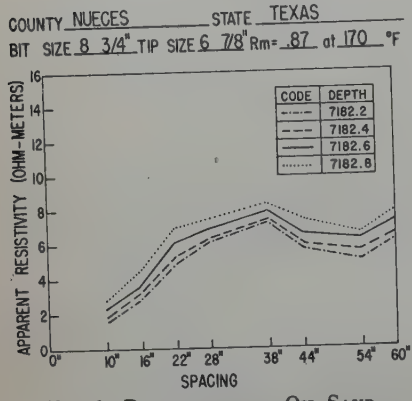

FIG. 6—PROFILES OF AN OIL SAND.

with this instrument used spacings of 10, 16, 22, 28, 36, 44, 54, and 60 in. A typical record made on conventional depth scales is shown in Fig. 5. Typical profiles in an oil sand are shown in Fig. 6. Notice that only the longer spacing shows the presence of the high resistivity presumably associated with the virgin formation. Several such logs indicated the need for a longer spacing and a better distribution of spacing. The bumper section was redesigned to provide spacings of 16, 24, 32, 40, 48, 56, 64, and 72 in., and the bumper section extended to 30 in. beyond the electrodes associated with the longest spacing.

INTERPRETATION TECHNIQUE

It is necessary to resolve the log into profile form to determine the presence or absence of a dip or inflection. In effect, this is plotting the departure curve at each point. A mechanical reader was developed for this purpose. This expedites the operation but it is still time consuming and laborious. Conventional log scales are too compressed for this operation so a scale of 1 in. of log equals 4 ft of hole was used in most of the records. Fig. 7 shows a typical log and the profiles plotted from that log. Profiles were normally plotted at each foot of the porous sections as indicated by the self potential or a contact log.

An experienced log analyst can become very proficient in the use and understanding of the profile log except when interbedding of contrasting lithology occurs. When such interbedding occurs over a short depth interval the profiles are difficult to rationalize. The profile log, however, does not replace either the conventional log or the contact log, and a contact-caliper log is almost essential to an understanding of the profiles.

FIELD TESTS

The latest tool design has been used to survey 18 wells in Oklahoma and Texas. In 11 of these wells there are 21 known productive zones. The profiles indicate the presence of the low zone in 13 of these zones for a success ratio of 62 per cent. The indications have been graded as six "good dips", one "fair dip", four "poor dips", and two "inflections". A good dip is illustrated in the logs and profiles shown in Figs. 8 and 9.

This zone was tested as a direct result of the profile log and produced 62 bbl of oil with no water in a 24-hour test. The displacement log can be considered uniquely diagnostic in this well since the true resistivity is of the order of 1 ohm-m and conventional log interpretation is far from definitive in these low resistivity zones. The dip is approximately 14 per cent in magnitude. One other low resistivity oil producing zone gave a similar deflection. It is also pertinent to observe that the presence of the low zone is indicated in only 7 ft out of a total of 24 productive ft. Since these 7 ft are at the top of the bed and there is little change in the apparent resistivities in the lower 17 ft, it might be suspected that the low zone was originally created throughout the 24 ft and has disappeared in the lower section with time.

In those zones where the profiles are considered diagnostic, the ratio of the diagnostic profile footage to the total productive footage is 25 per cent. These statistics, however, are heavily weighted by one Gulf Coast well. If this well is excluded, the zone success ratio is 71 per cent and the ratio of diagnostic footage to productive footage is 32 per cent.

In one zone in one well a good dip was obtained on several profiles that led to a test through perforations that produced 100 per cent salt water. No explanation has been forthcoming.

A review of all data indicates that the success ratio might be improved

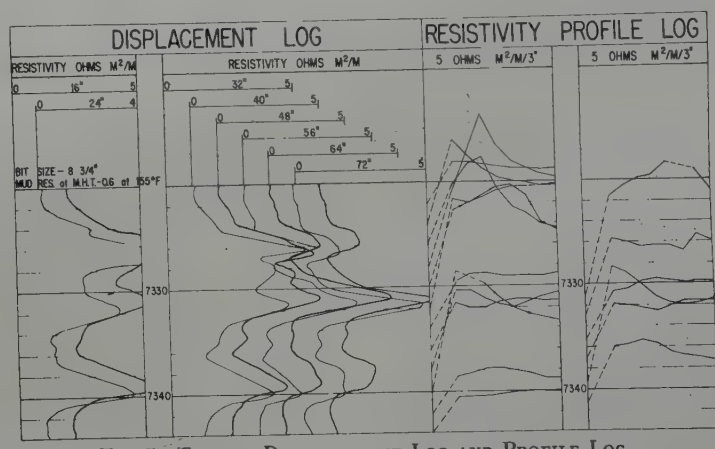

FIG. 7—TYPICAL DISPLACEMENT LOG AND PROFILE LOG.

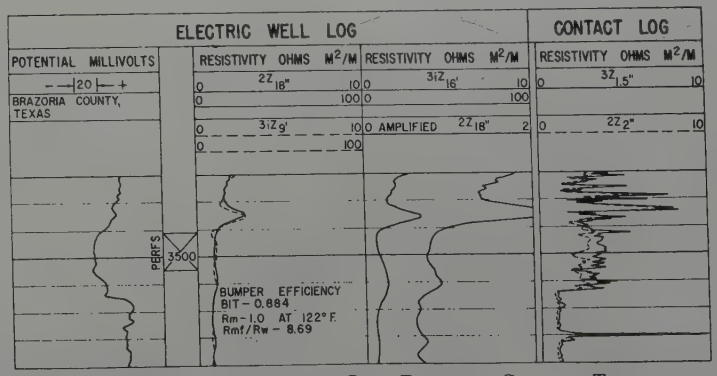

FIG. 8—LOG AND CONTACT LOG, BRAZORIA COUNTY, TEX.

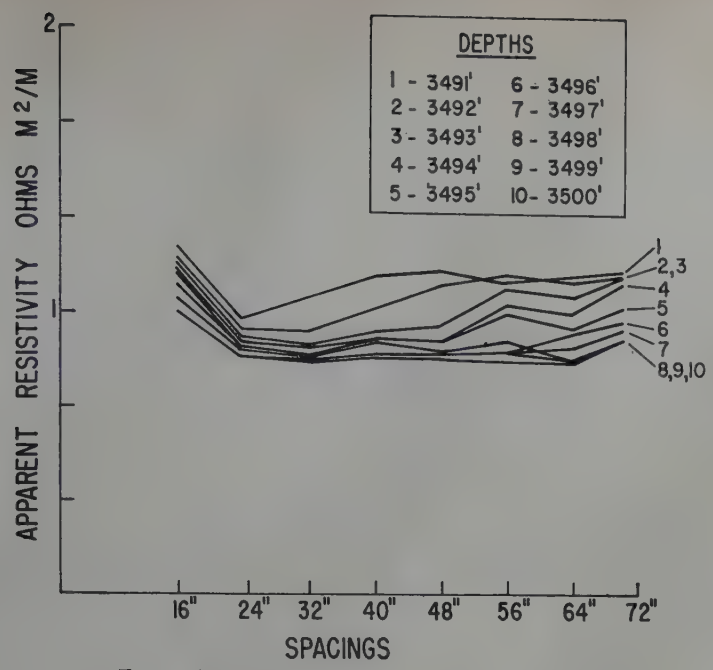

FIG. 9—RESISTIVITY PROFILES OF SAND IN FIG. 8.

by an increased density of spacings and more efficient bumpers. If only the zones where the bumpers occupy 86 per cent or more of the diameter of the hole are considered, the zone success ratio becomes 67 per cent and the anomaly footage becomes 36 per cent. An automatic recording of the profiles would be highly desirable. To achieve more efficient bumpers appears difficult. Bumpers were used on 37 wells in Oklahoma and Texas. On 12 wells, or 32 per cent, it proved impossible to reach bottom. The average bumper efficiency to bit size in these wells was 85 per cent.

CONCLUSIONS

1. There is definite evidence that the low zone is often present and log interpretation data need be supplied to account for the effect on all resistivity logging tools.

2. The ability to detect the low zone may be uniquely diagnostic in low resistivity producing reservoirs.

3. In some formations the low zone may be dynamic and dissipate with time.

4. The system of detection used is able to clearly delineate the presence of the low zone in a disappointing percentage of the total productive feet.

5. The bumpers, which are essential to the system, present serious operational problems in their present form. Mechanically controlled variable diameter bumpers might solve this problem.

The information obtained in these surveys indicates that the basic concept of the low zone should be utilized in logging techniques. Ideally, the influence of the hole should be electrically removed. The possibilities of three or more properly focused resistivity curves is obvious and undoubtedly will be pursued. However, these systems involve formidable problems and mechanically controlled variable diameter bumpers together with a greater density of curves might yield acceptable results.

REFERENCE

1. Campbell, W. M., and Martin, J. L.: "Displacement Logging — A New Exploratory Tool," *Trans.* AIME (1955) **204**, 233.

★★★

T. N. 2002

Application of a Resistance Network for Studying Mobility Ratio Effects

M. A. NOBLES* MEMBER AIME
HAROLD B. JANZEN JUNIOR MEMBER AIME

OKLAHOMA STATE UNIVERSITY
STILLWATER, OKLA.
CONTINENTAL OIL CO.
PONCA CITY, OKLA.

INTRODUCTION

Since 1950, several papers have been published which have described various methods for studying mobility ratio effects. The methods which have been described for studying mobility ratio effects include X-ray shadowgraph techniques, stepwise potentiometric model procedures, stepwise numerical procedures, gelatin model studies and fluid mapper model studies.[1,2,4,6,7,8,9,10,11] The purpose of this paper is to describe a procedure for using a resistance network for studying mobility effects.

DESCRIPTION OF APPARATUS

The basic unit of the experimental model consisted of a network of 840 resistors fastened to a sheet of black Lucite which was mounted on a wooden frame, Fig. 1. The dimensions of the Lucite sheet were 36 × 36 in. The resistors were fastened to the Lucite sheet at mesh points by means of snaps. The mesh points were arranged in a square pattern, 30 × 30 in., spaced at intervals of 1½ in.

The snap fasteners permitted several resistors to be "stacked" in parallel. By adding additional resistors to the basic unit, the specific resistance on each side of the flood front could be varied.

The square network of resistors represented one of four symmetrical elements of a five-spot well pattern. The current input was analogous to an injection well and the current output was analogous to a production well.[3]

The power supply was essentially a full wave transformer-rectifier system for converting alternating-current into direct-current. The DC voltage could be varied from 41.43 to 290 v in steps of 41.43 v by selecting the proper outlet jacks. The major components of the power supply were: a Triro power transformer, R 11-A; a dual 5Y3 vacuum tube; two gas filled OD-3 tubes; and a Triplett voltmeter, model 227-1, range 0 to 500 DC v.

The voltages at the mesh points were determined with a Keithley electrometer, model 210, No. 185, manufactured by Keithley Instruments, Cleveland, Ohio.

A Heathkit vacuum tube volt-

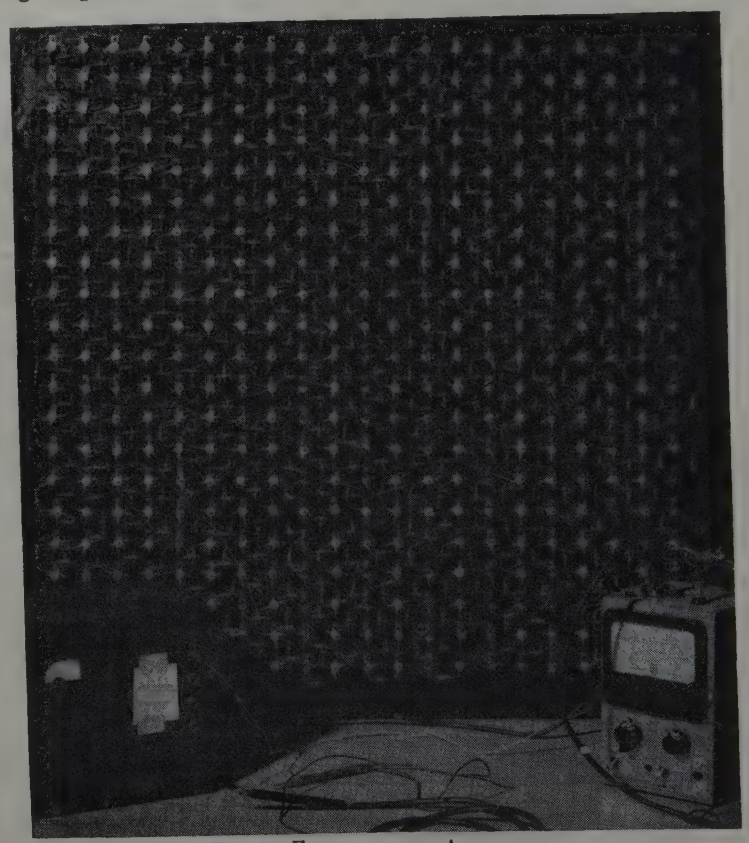

FIG. 1—EXPERIMENTAL APPARATUS.

Original manuscript received in Society of Petroleum Engineers office on Aug. 1, 1957.
*Now a faculty member in the Dept. of Petroleum Engineering of Louisiana Polytechnic Institute, Ruston, La.
[1]References given at end of paper.

meter, model V-6, manufactured by the Heath Co., Benton Harbor, Mich., was used to measure the total resistance of the network.

EXPERIMENTAL PROCEDURE

The effect of mobility ratio on a five-spot steady-state, fluid injection operation was determined by advancing the "flood front" on the electrical resistance network from an initially assumed position and shape, to "breakthrough" in five or six increments. For this study mobility ratio, M, was assumed to be the ratio of the conductivity behind the flood front to the conductivity ahead of the flood front. The flood front was advanced in increments by the following approximate method.[1,5]

1. An initial radial flood front was assumed and the potential distribution was determined by measuring the voltage drop between the current input and each mesh point in the resistance network with a vacuum tube voltmeter.

2. The equipotential lines were drawn and streamlines were plotted orthogonally to the equipotential lines. The direction of a streamline at a mesh point can also be determined by measuring the voltage drops across any two perpendicular resistors from the point and taking the vector sum of the two voltage drops. After much experimenting, it was believed that drawing of orthogonal lines to the equipotential lines was sufficiently accurate for the mobility ratio study.

3. The potential distribution was assumed to remain constant while the flood front was advanced to a new position corresponding to some increment of time, $\triangle t$, by the use of the relationship,[5]

$$\triangle t = \frac{(\triangle S)^2}{\triangle P},$$

where $\triangle S$ is the distance between two equipressure lines measured along a streamline, $\triangle P$ is the potential difference between two equipotential lines, and $\triangle t$ is relative time.

4. After the flood front had been advanced, the resistances in the network were changed to correspond to the new flood front and the potential distribution was again determined.

5. The entire stepwise process was repeated until breakthrough.

The area swept-out by the flood was determined by planimetering. The total resistance of the network was determined either by direct measurements with an ohmmeter or by measurements of voltage drops across the network and across a known resistance in series with the network.

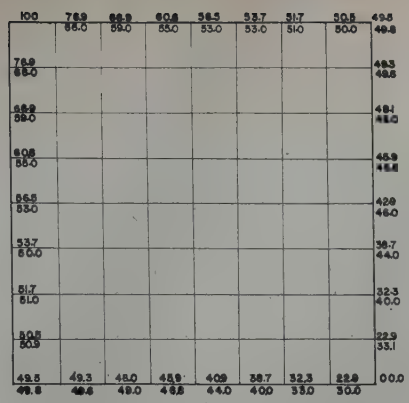

FIG. 2—BOUNDARY VALUES FOR A FIVE-SPOT FLOOD PATTERN. THE UPPER VALUES WERE DETERMINED WITH THE RESISTANCE NETWORK AND THE LOWER VALUES WERE TAKEN FROM CALHOUN.[5]

The resistance networks were assembled with one and two megohm resistors. Mobility ratios of 1/6, ¼, ½, 1, 2, 4, and 6 were studied.

RESULTS AND DISCUSSION

The upper values in Fig. 2 are the boundary values for a five-spot flood pattern which were determined with the resistance network. The lower values in Fig. 2 are the results of potentiometric studies.[5,13] The differences between the two sets of values become increasingly larger as the mesh points approach the wells. Potentials vary logarithmically with distance for short distances from wellbores (sinks or sources) accounts for the variations between potential values measured with the resistance network and those obtained with an electrolytic model. Finer meshes in the resistance network near the wells would have given more accurate values of potentials.

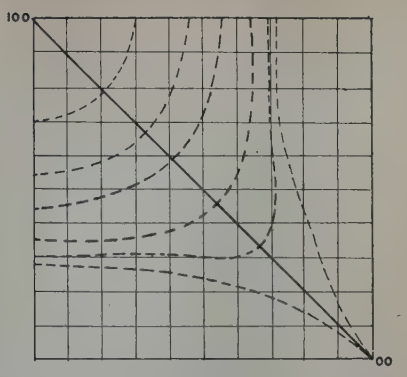

FIG. 3—INTERFACE POSITIONS FOR $M = 6$.

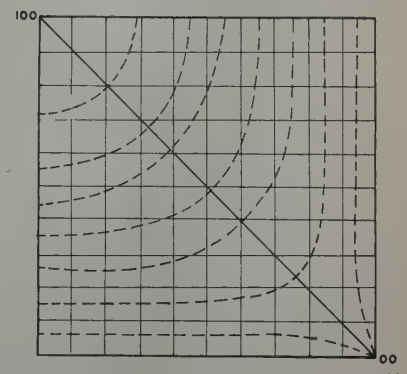

FIG. 4—INTERFACE POSITIONS FOR $M = 1/6$.

The interface positions of flood fronts for mobility ratios of 1/6 and 6 are given respectively in Figs. 3 and 4. The figures indicate that the areal sweep efficiencies increase as the mobility ratio decreases.

The areal sweep efficiency at breakthrough is plotted against mobility ratio in Fig. 5. The solid line represents the results of this study; the dashed line was taken from Craig, et. al.[8], and is the result of X-ray shadowgraph studies; the dashed line with dots was taken from Aronofsky, et. al.[2], and is the result of potentiometric studies. The value of 71 per cent for the mobility ratio of one compares favorably with the value obtained analytically by Mus-

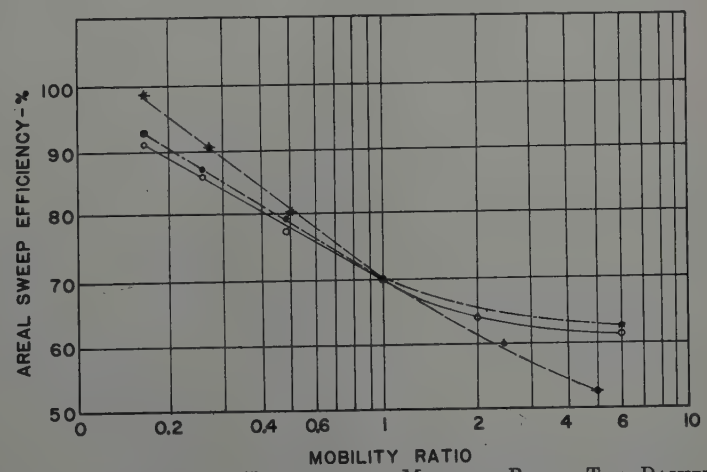

FIG. 5—AREAL SWEEP EFFICIENCY VS MOBILITY RATIO. THE DASHED LINE IS THE RESULT OF X-RAY SHADOWGRAPHS.[8] THE IRREGULARLY BROKEN LINE IS THE RESULT OF POTENTIOMETRIC STUDIES.[2]

kat.[11] At the lower end of the curve the values for areal sweep efficiency as determined with the resistance network were higher than those determined by X-ray shadowgraph studies and at the upper end of the curve the results were just the opposite. Between mobility ratios of 1/6 and 6 the areal sweep efficiencies determined by this method differ by 1 or 2 per cent from those obtained by potentiometric methods.

The flow equation for both electrical and fluid flow can be written in the form,

$$\text{Rate} = \frac{\text{Driving Force}}{\text{Resistance}} \quad . \quad . \quad (1)$$

or

$$Q = K\frac{P}{R} \quad , \quad . \quad . \quad . \quad . \quad . \quad (2)$$

where Q is the flow rate, P is the driving force or pressure, R is the resistance, and K is a proportionality constant. If the equation for the initial condition is divided into Eq. 2 the following results are obtained.

$$\frac{Q}{Q_i} = \frac{PR_i}{P_iR} \quad , \quad . \quad . \quad . \quad . \quad (3)$$

where the subscript i indicates initial conditions.

If the injection pressure during a flood remains constant, Eq. 3 becomes,

$$\frac{Q}{Q_i} = \frac{R_i}{R} \quad . \quad . \quad . \quad . \quad . \quad (4)$$

Eq. 4 indicates that the ratio of the flow rate at any time to the initial flow rate is equal to the initial resistance of the flood network to the resistance at any time.

Fig. 6 is a plot of R_i/R vs nose advance* for several mobility ratios.

*Nose advance in this paper has the same meaning as used by Aronofsky, et al.[2]

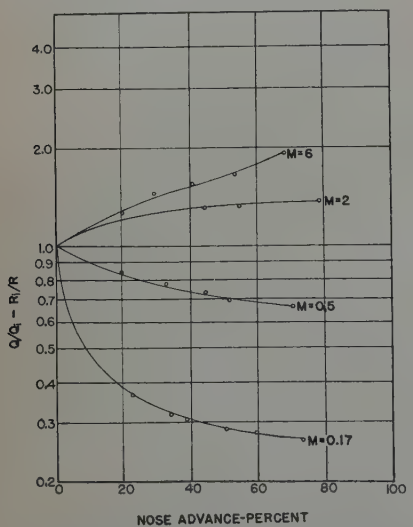

FIG. 6—CHANGE IN INJECTION RATE AT CONSTANT PRESSURE VS NOSE ADVANCE FOR VARIOUS MOBILITY RATIOS.

The curves indicate that the injection rate at constant pressure for mobility ratios less than one decreases with the advance of the flood front and increases for mobility ratios greater than one.

Plots of swept area vs nose advance for various mobility ratios are given in Fig. 7. The shapes of the curves were very similar to those obtained by potentiometric studies. In fact, the values obtained by the resistance network study differed little from those obtained by potentiometric studies.[2]

The relative time of breakthrough for various mobility ratios is given in Fig. 8. The curve designated with x is the result of potentiometric studies. The two curves are similar in shape; however, the potentiometric study obtained values which were lower at large mobility ratios and were greater at small mobility ratios. The differences in values for the two curves range from 0 to 15 per cent.

As the flood front advanced there was a general shift of the equipotential lines. The 50 per cent equipotential line shifted toward the producing well as the flood front advanced. A plot of the location of the 50 per cent equipotential line on the diagonal streamline vs nose advance for

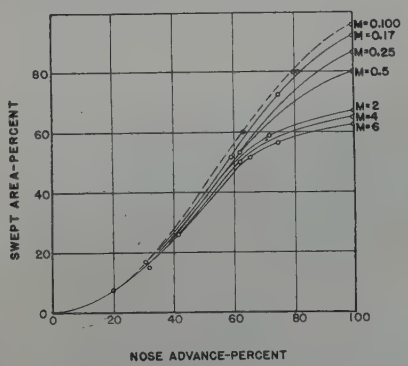

FIG. 7—SWEPT AREA VS NOSE ADVANCE FOR VARIOUS MOBILITY RATIOS. THE DASHED LINES ARE THE RESULTS OF POTENTIOMETRIC STUDIES.

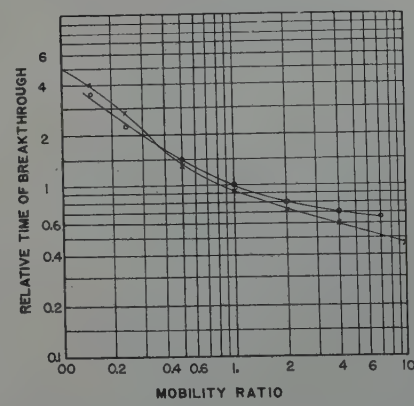

FIG. 8—RELATIVE BREAKTHROUGH TIME. THE CURVE x GIVES THE RESULTS OF POTENTIOMETRIC STUDIES.[2]

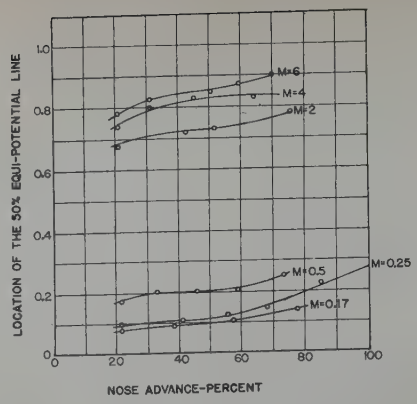

FIG. 9—LOCATION OF THE 50 PER CENT EQUIPOTENTIAL LINE AS A FUNCTION OF NOSE ADVANCE ALONG THE DIAGONAL STREAMLINE.

various mobility ratios is given in Fig. 9. The location refers to the fraction of the diagonal line taken from the injection well.

CONCLUSION

Although on the resistance network the flood front is wavy, results of mobility studies with the resistance network compare very favorably with the potentiometric studies. Slight deviations from the potentiometric results tend to increase as the mobility ratio differs increasingly from one.

ACKNOWLEDGMENT

The authors wish to thank Phillips Petroleum Co. for permission to publish this paper.

REFERENCES

1. Aronofsky, J. S.: *Trans.* AIME (1952) **195**, 15.
2. Aronofsky, J. S., and Ramey, H. J., Jr.: *Trans.* AIME (1956) **207**, 205.
3. Bruce, W. A.: *Trans.* AIME (1943) **151**, 112.
4. Burton, Melvin B., Jr., and Crawford, Paul B.: *Trans.* AIME (1956) **207**, 333.
5. Calhoun, John C., Jr.: *Fundamentals of Reservoir Engineering*, University of Oklahoma Press, Norman, Okla. (1953) 336.
6. Caudle, B. H., Erickson, R. A., and Slobod, R. L.: *Trans.* AIME (1955) **204**, 79.
7. Cheek, Rex E., and Menzie, Donald E.: *Trans.* AIME (1955) **204**, 278.
8. Craig, F. F., Jr., Geffen, T. M., and Morse, R. A.: *Trans.* AIME (1955) **204**, 7.
9. Dyes, A. B., Caudle, B. H., and Erickson, R. A.: *Trans.* AIME (1954) **201**, 81.
10. Fay, C. H., and Prats, M.: *Proc.*, Third World Petroleum Congress, Section II (1951) 555.
11. Muskat, M.: *Physical Principles of Oil Production*, McGraw-Hill Book Co., Inc., N. Y. (1949) 660.
12. Slobod, R. L., and Caudle, B. H.: *Trans.* AIME (1952) **195**, 265.
13. Wyckoff, R. D., Botset, H. G., and Muskat, M.: *Trans.* AIME (1933), **103**, 219. ★★★

Evidence of Chromatographic Effect During Flow of Gases Through Oilfield Cores

W. A. ROPER* — THE RICE INSTITUTE, HOUSTON, TEX.
TODD DOSCHER, MEMBER AIME — SHELL DEVELOPMENT CO., HOUSTON, TEX.
RIKI KOBAYASHI, JUNIOR MEMBER AIME — THE RICE INSTITUTE, HOUSTON, TEX.

INTRODUCTION

The chromatographic effect refers to the separation of constituents in a moving fluid phase which occurs when the phase is passed over a stationary phase, either solid or liquid, or large areal extent. In performing chemical analyses, the large surface contact area is provided in the case of gas-solid chromatography by-passing the gas over a porous solid and for gas-liquid chromatography by-passing the gas over a porous solid which has been coated with a nonvolatile liquid. The porous medium is usually placed in a cylindrical tube, although it may be a relatively flat sheet as in paper chromatography.

According to one theory,[1] the separation results from the difference in time spent by various components in the stationary phase. A gaseous component which is completely insoluble in the stationary phase, or is not adsorbed on the solid, proceeds unimpeded through the column.

The versatility and power of the various types of chromatography for the analysis of complex mixtures are evident from their widespread use in performing chemical analyses and from the large number of symposia, books, and papers devoted to the subject in recent years.[1,2,4,5,6,8,12] Associated developments are the application of chromatography to the determination of heats of solution, heats of adsorption, solubilities or K-values, etc.[1,3,10,11]

Gas-liquid chromatography analyses may be characterized by the manner in which the samples are introduced and displaced from the column[1]. The three techniques used are known as (1) frontal analysis, (2) displacement analysis, and (3) elution analysis. The frontal analysis is performed by displacing an inert gas from the column by a continuous stream of the sample. As indicated in Fig. 1(A), all but the first fraction leaving the column represent mixtures rather than pure components. The displacement analysis is conducted by filling the column with a sample, then displacing it with a more strongly adsorbed or absorbed vapor. The resulting chromatogram is illustrated by Fig. 1(B). Finally, in the elution analysis a small sample of the mixture to be analyzed is introduced as a "plug" into a flowing stream of carrier gas to give an elution-type chromatogram, Fig. 1(C). The three techniques may be used to provide models to which flow patterns in other physical situations may be compared.

PURPOSE OF THIS INVESTIGATION

The purpose of this investigation was to determine whether natural reservoir rocks, when coated with crude oil, provided sufficient surface areas to give rise to a chromatographic separation of light hydrocarbon constituents. The tests were conducted with the light hydrocarbons in the gaseous state.

SANDS TESTED

Two sands of widely different permeabilities have been studied: (1) Ventura core (16 md), and (2) Torpedo sandstone core (578 md). Table 1 gives a description of the cores that were tested. With the exception of one frontal-type flow arrangement which was performed on Core 3, the tests were of the elution-type in which a methane-propane mixture was eluted through the core by means of helium.

The Ventura core, when impregnated with a weathered crude from the same field, became so impermeable to gas flow that it was necessary to conduct the tests on the granulated cores (Cores 2 and 3).

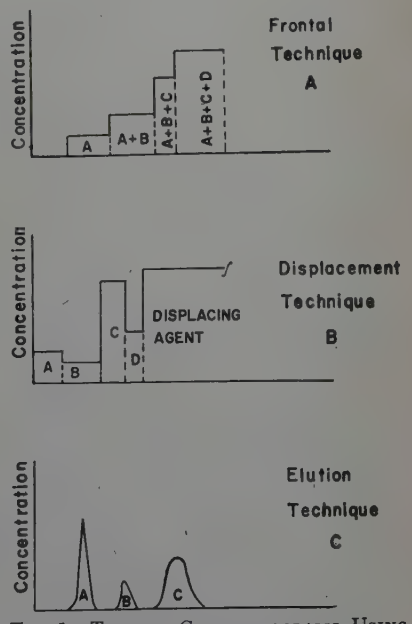

FIG. 1—TYPICAL CHROMATOGRAMS USING DIFFERENT FLOW TECHNIQUES.

Original manuscript received in Society of Petroleum Engineers office on July 22, 1957. Revised manuscript received Dec. 23, 1957.
*Presently with The Texas Co., Bellaire, Tex.
[1]References given at end of paper.

TABLE 1

Core No.	Core Description	Cross Section	Length	Porosity (per cent)	Permeability (md)
1	Ventura core as Received	0.75 in. dia.	6.62 in.	23.9	16
2	Crushed Ventura core with 4-wt per cent Ventura crude	0.305 in. I.D. copper tubing	3.41 ft		
3	Crushed Ventura core with 4-wt per cent Ventura crude	0.305 in I.D. copper tubing	8.93 ft		
4	Extracted Torpedo sandstone core	Square core, ½ in. on each side	11.75 in.	19.6	578
5	Torpedo Sandstone with 8.86 per cent Saturation with Ventura crude	Square core, ½ in. on each side	11.75 in.	17.8*	531*

*With oil in place

Cores 4 and 5 represent the same sandstone cores with and without the Ventura crude. A square core was chosen to permit ease of fabrication. The cores were painted with Epon plastic and mounted in Lucite.

REFERENCE TO EQUIPMENT

The equipment used in the test was essentially that used by Rangel to study K-values of methane and propane in *n*-decane.[11] Some modifications were made to decrease the "dead volume" between the end of the core and the thermal conductivity detector cell to reduce remixing of the gases during flow from the core to the cell. The various cores were substituted in place of the chromatographic column in the original apparatus. A differential pressure gauge placed across the cores and a flowmeter permitted the calculation of gas permeabilities. The tests were conducted at a room temperature of 26° C and at pressures ranging from 17 to 27.2 lb/sq in. abs.

PRESENTATION OF RESULTS

A qualitative idea of the degree of separation obtained is indicated by Figs. 2 through 5, corresponding to the cores indicated. Little or no resolution of the methane and propane peaks were obtained by eluting the mixture through Core 4, the dry Torpedo sandstone. It should be emphasized that the chromatograms correspond to cores of different length and that Cores 2 and 3 were obtained by crushing the consolidated Ventura core.

Fig. 2 shows the very slight separation of methane and propane by elution of the mixture through the weathered Ventura core. The location of the elution curves for pure methane and pure propane are shown on the same scale as a means of identifying the location of methane and propane in the lowest chromatogram shown in Fig. 2, the chromatogram for the mixture. To circumvent the extremely low permeability to gas of the Ventura core impregnated with Ventura crude, the core was crushed prior to impregnation with the crude. The resulting chromatograms for the crushed core placed in copper tubes are shown in Figs. 3 and 4. Cores 2 and 3 are identical except for their lengths. A virtually complete separation of the methane-propane mixture occurred on the longer core. The Ventura core represents a "dirty sand," probably having a high specific surface area.

The Torpedo sandstone, a "clean sand," was tested with and without crude oil on its grain surfaces. The extracted sandstone showed no apparent separation. However, with 8.86 volume per cent of the void space occupied by the Ventura crude on the sandstone, the chromatogram shown in Fig. 5 was obtained. Thus, the separation is attributed to the liquid phase which acquires a large surface area on the solid surface. For the liquid saturations used, the peaks obtained in the chromatogram were quite asymmetric, indicating the existence of condensation sites of varying activities. The vapor molecules compete with one another for these positions in the fixed phase.[1,5]

Fig. 6 gives a frontal chromatogram of Core 3 with a mixture of methane and propane. The leading edge of the front consists of pure methane and helium, i.e., the methane forges ahead of the propane. Since a mixture of methane and propane was used to displace the helium from the core, the methane-helium front is followed by the methane-propane mixture. The mercury capillary pressure curves, Fig. 7, for the Ventura and Torpedo cores indicates the wide differences in the pore structure of the two cores tested.

QUANTITATIVE CALCULATIONS

Interpretations of the data may be made from a study of the parameters frequently calculated for analytical columns. The following calculations were made on the cores studied: (1)

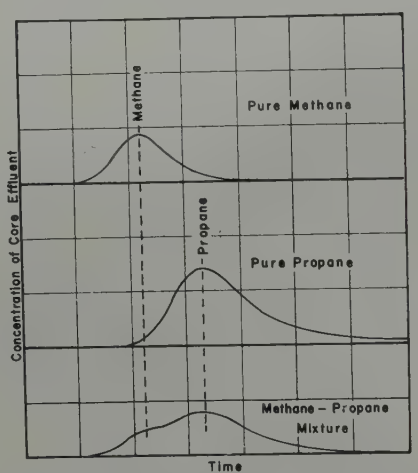

FIG. 2—ELUTION CURVE FOR WEATHERED VENTURA CORE (CORE 1).

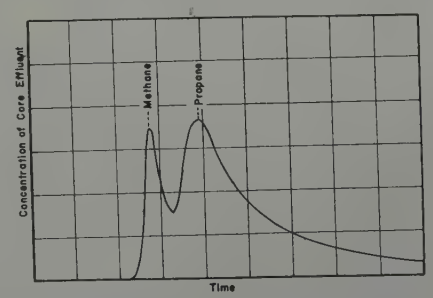

FIG. 3—ELUTION CURVE FOR GROUND VENTURA CORE WITH 4 WEIGHT PER CENT VENTURA CRUDE (CORE 2).

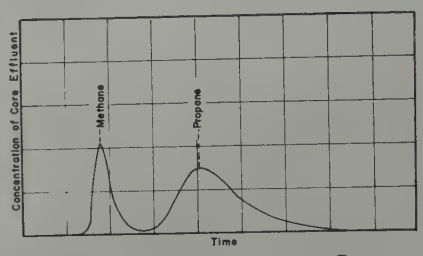

FIG. 4—ELUTION CURVE FOR GROUND VENTURA WITH 4 WEIGHT PER CENT VENTURA CRUDE (CORE 3).

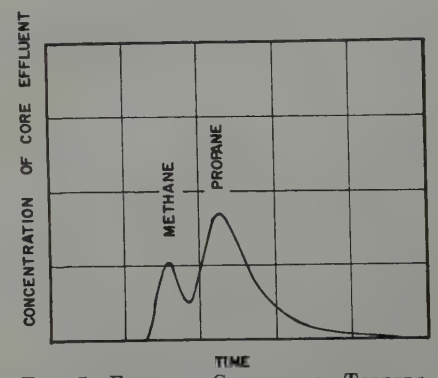

FIG. 5—ELUTION CURVE FOR TORPEDO SANDSTONE WITH 8.86 PER CENT VENTURA CRUDE (CORE 5).

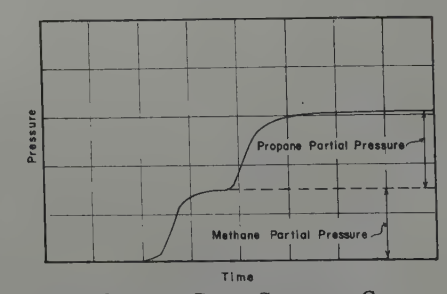

FIG. 6—FRONTAL DRIVE CURVE FOR GROUND VENTURA CORE WITH 4 WEIGHT PER CENT VENTURA CRUDE (CORE 3).

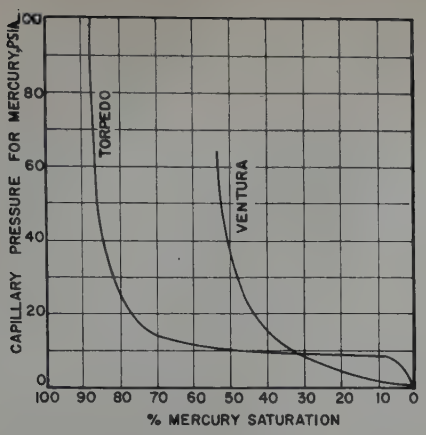

FIG. 7—MERCURY CAPILLARY PRESSURE CURVES FOR CORES TESTED.

corrected retention time, (2) ratio of corrected retention volume to pore volume, (3) relative velocity of components, and (4) theoretical plates per foot of core.

The definitions of the quantities used in the above calculations are as follows.

1. Corrected retention time (minutes) is equal to the time that a component in question is retained in the core or column by virtue of adsorption or absorption and is equal to the difference in time required for a nonadsorbed or nonabsorbed component and the component in question to flow through the column.

2. Corrected retention volume (cc) is the volume of carrier gas required to elute the component in question through the core or column minus one pore volume of gas. The retention volume is equal to the retention time times the flow rate (cc/min) at the weighted average core pressure.

3. Pore volume (cc) is equal to the void volume (cc) of the core under test conditions.

4. Relative velocity of a component is equal to the ratio of the velocities of two components. Thus, the relative velocity of helium to methane is given by:

$$\frac{He}{CH_4} = \frac{\dfrac{\text{Corrected } CH_4 \text{ retention time (minutes)}}{} + \dfrac{\text{Pore volume (cc)}}{\text{He flow rate (cc/min)}}}{\dfrac{\text{Pore volume (cc)}}{\text{He flow rate (cc/min)}}}$$

5. Theoretical plates are defined such that the height equivalent to a theoretical plate (HETP) is the length of core or packing required in order that the gas leaving it may be considered to be in equilibrium with the average stationary liquid concentration in the same section. In accordance with the theory of James and Martin,[4] the number of theoretical plates, n, is given by:

$$n = \frac{2\pi h^2 l^2}{A^2},$$

TABLE 2—RESULT OF COMPUTATIONS

A. Corrected Retention Time and Retention Volume

Core No.	Retention time (min) Methane	Retention time (min) Propane	Retention volume (cc) Methane	Retention volume (cc) Propane	Flow Rate (cc/min)
1	0.24	1.36	3.24	18.4	13.5
2	1.29	2.38	54.5	103	43.2
3	1.88	4.18	82.6	184	44.0
5	0.18	0.85	9.85	46.5	54.8

B. Ratio of Corrected Retention Volume to Pore Volume of Column

Core No.	Ratio Methane	Ratio Propane
1	0.339	1.93
2	4.46	8.45
3	2.58	5.74
5	0.287	1.35

C. Relative Velocities

Core No.	Helium / Methane	Helium / Propane	Methane / Propane
1	1.3	2.9	2.2
2	5.6	9.4	1.7
3	2.6	6.7	1.9
5	1.4	2.7	1.8

where h is peak height (cm), l is retention distance (cm) corrected for the distance the chart travels while helium flows from the sample inlet to the detector cell, and A is the peak area (cm^2).

The corrected retention times and volumes for the flow of methane and propane through various cores are listed in Table 2-A. The retention time for propane is observed to be from 2 to 5 times that of methane (Table 2-A). Using polyglycols as a stationary liquid phase, Adlard[9] showed that for pentane through *n*-decane, the increase in the number of $-CH_2-$ groups plotted vs the log of the corrected retention volume gives a linear relationship. The retention times of homologs in a given column using a given stationary phase may be estimated in this manner.

The ratios of the corrected retention volume to the pore volume of the column gives the retention volume per unit volume of void space (Table 2-B). The values indicated that the volume of elution gas required to displace a plug of propane through the core may be considerably greater than the void volume. That is, the displacement with crude oil on the core is not pistonwise.

The relative velocity of methane to propane was 2.2 for Core 1 (Ventura) and 1.8 for Core 5 (Torpedo), Fig. 2(C). The relative velocities of methane to higher molecular weight constituents may be expected to be considerably higher.

The number of theoretical plates per foot of core for the Torpedo sandstone with 8.86 volume per cent oil saturation was 1.6 for methane and 5.9 for propane.

CONCLUSIONS

The surface areas of many oilfield cores, when partially saturated with oil, are sufficiently large enough to produce gas-liquid chromatographic effects when longitudinal diffusion is substantially absent. This effect results in a different rate of flow for each component when a mixture of components is eluted with a substantially pure substance. These effects may be significant in certain production operations and in the characterization of oilfield cores.

ACKNOWLEDGMENT

The authors wish to acknowledge the contributions of the Shell Development Co. in the preparation of the cores and in supplying the crude oil sample.

REFERENCES

1. Phillips, C.: *Gas Chromatography*, Academic Press, Inc., N. Y. (1956).
2. Desty, D. H.: *Vapor Phase Chromatography*, Butterworth Scientific Publications, London (1957).
3. Greene, S. A., and Pust, H.: "Determination of Heats of Adsorption by Gas Adsorption Chromatography," paper presented at ACS meeting, Miami, Fla. (April 7-12, 1957).
4. James, A. T., and Martin, A. J. P.: *Biochem. Jour.* (1952) **50,** 679.
5. Keulemans, A. I. M.: *Gas Chromatography*, Reinhold Publishing Corp., N. Y. (1957).
6. Lederer, E., and Lederer, M.: *Chromatography, a Review of Principles and Applications*, Elsevier Pub. Co., Houston (1954).
7. Littlewood, A. B., Phillips, C. S. G., and Price, D. T.: *Jour.*, ACS (1955) 1480.
8. Miner, Roy W. (Editor): New York Academy of Sciences, conference on Chromatography held by Section of Physics and Chemistry (1948) **49,** 141.
9. Adlard, E. R.: *Vapor Phase Chromatography*, Butterworth Scientific Publications, London (1957).
10. Porter, P. E., Deal, C. H., and Stross, F. H.: *Jour.*, ACS (1956) **78,** 2999.
11. Rangel, Enrique T.: MS Thesis, The Rice Institute (1956).
12. Strain, H. H.: *Chromatographic Adsorption Analysis*, N. Y. Interscience Publishers, Inc., N. Y. (1942). ★★★

T. N. 2004

Pore Volume Compressibilities of Sandstone Reservoir Rocks

I. FATT*
MEMBER AIME

CALIFORNIA RESEARCH CORP.
LA HABRA, CALIF.

ABSTRACT

Pore volume compressibilities measured in the laboratory on core samples are reported for typical reservoir sandstones at reservoir pressures. These compressibilities are different for each reservoir sample and cannot be correlated to porosity. The compressibilities are also functions of pressure.

INTRODUCTION

In recent years several authors have pointed out the importance of including pore volume compressibility of the reservoir rock in certain reservoir engineering calculations. Hall[1] showed that in calculating the hydrocarbon volume of an undersaturated reservoir from the production per unit change in reservoir pressure, the neglect of rock compressibility could, in the extreme case of low porosity rock, lead to results in error by a factor of two. Hawkins[2] and Hobson and Mrosovsky[3] showed that both rock and interstitial water compressibilities must be included to achieve satisfactory accuracy in this calculation.

Although rock compressibility is an important reservoir property in these calculations, very few data are available. Hall[1] made compressibility measurements on a few samples in a small pressure range. No other direct pore volume compressibility measurements have been reported. Geertsma[4] discussed the elasticity of reservoir rock but did not present any new data. In this paper, rock compressibilities suitable for reservoir calculations are reported for a variety of sandstones typical of U. S. reservoirs. The measurements were made through a range of pressures which is also typical of reservoirs.

EXPERIMENTAL PROCEDURE

Plugs 1 in. in diameter and 2- to 3-in. long were diamond drilled, 14 from cores from seven oil-bearing or potentially oil-bearing sandstone, one from a quarried sandstone, and another from a shallow, oil-free, pure orthoquartzite. The plugs were extracted in toluene, vacuum dried, and then weighed. The plugs were then saturated with kerosene and reweighed. This gave pore volume. They were then again extracted in toluene, vacuum dried, and jacketed in 0.004-in. thick copper foil. A short length of ¼-in high pressure tubing led from the jacket. The jacketed sample was then saturated with kerosene and placed in the hydraulic pressure cell as shown in Fig. 1. Movement of the mercury slug showed the change in pore volume of the sample under a given pressure change. Temperature was about 72° F for all measurements.

Before taking any measurements, the external pressure on the sample was raised to 10,000 psig and kept there for several hours. This formed the thin copper jacket around the plug. The pressure was then removed and the sample left at least overnight, during which time it recovered its original pore volume.

An external pressure of 12,000 psig was then applied and held constant. The change in pore volume was noted as the internal pressure was raised in 1,000 psig increments to 10,000 psig. The internal pressure was then reduced to zero, again noting pore volume changes,

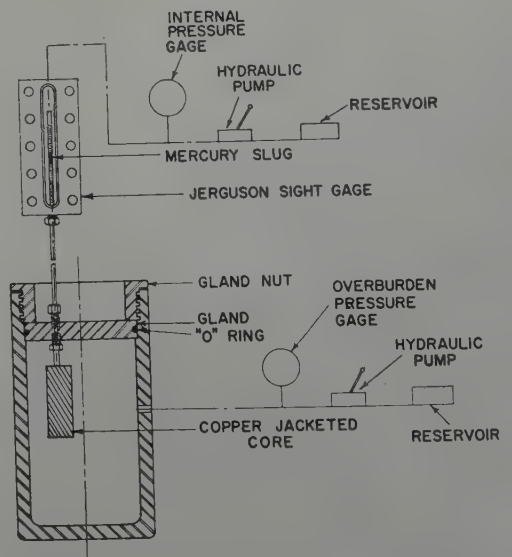

FIG. 1—EXPERIMENTAL EQUIPMENT FOR MEASURING PORE VOLUME COMPACTION AND COMPRESSIBILITY.

Original manuscript received in Society of Petroleum Engineers office on Sept. 3, 1957. Revised manuscript received Jan. 6, 1958.
*Presently associate professor of petroleum engineering at University of California, Berkeley.
[1]References given at end of paper.

and the external pressure was reduced to 6,000 psig. After allowing several hours or overnight for the sample to recover, the pore volume change was noted as the internal pressure was raised to 6,000 psig and then reduced to zero.

To obtain the change in pore volume of the sample when the internal pressure was raised, it was necessary to subtract the change in volume of the kerosene in the sample, connecting line, and sight gauge from the total observed volume change as indicated by movement of the mercury slug. The change in volume of the kerosene was calculated from the compressibility of kerosene given in the International Critical Tables[5].

Pore volume compressibility was calculated by graphically differentiating a plot of pore volume vs pressure. Samples were discarded if there was a hysteresis loop in this curve. This partially accounts for the absence of data on sandstones with porosities higher than about 20 per cent. Hysteresis was usually present for the soft, high porosity sandstones.

Compressibilities were also obtained for a pack of 28 to 35 mesh "flint shot" unconsolidated sand. The sand was tamped into a 1-in. diameter by a 3-in. long cylinder of 0.004-in. copper foil. The cylinder was soldered closed and a tubing lead attached. The sand pack, after saturating with kerosene, was placed in the cell of Fig. 1 and 2,000 psig external pressure applied for several minutes. The pressure was removed and then reapplied every 10 minutes until there was a constant amount of kerosene produced from the pack upon application of 2,000 psig external pressure. About 15 pressure cycles were required before the pore volume vs external pressure curve was free of hysteresis. To avoid crushing the grains, pressures above 2,000 psig were never applied to the sand pack. (Brandt[6] has given an equation from which it can be shown that for spherical quartz grains in contact, the external pressure should be less than 3,000 psig to keep compressive stresses at the grain contacts below the compressive strength of quartz.) Changes in pore volume of the sand pack were noted when the external pressure was maintained constant at 2,000 psig and internal pressure was varied from 0 to 2,000 psig.

RESULTS

The pore volume compressibilities as a function of net overburden pressure for eight representative consolidated samples and the sand pack are shown in Figs. 2 and 3. Note that the compressibility scales are different in the two plots. The pore volume compressibility is defined as the change in pore volume per unit pore volume per psi change in pressure of the fluid in the pore spaces while the external pressure is kept constant. In a reservoir the external pressure is the pressure of the overburden. The net overburden pressure is defined as the external pressure minus 85 per cent of the internal pressure. Brandt[6] introduced the 85 per cent factor to take into account the fact that the internal fluid pressure does not wholly react against the external pressure. The factor is structure dependent and therefore not the same for all rocks. It is also pressure dependent. For the rocks and pressure range used in this study the factor probably varies from 75 to 100 per cent with an average of 85 per cent.

The low pressure part of each curve, below 6,000 psig, was obtained at 6,000 psig external pressure; the high pressure part was obtained at 12,000 psig external pressure. There was enough overlap in the net overburden pressure to indicate that the pore volume compressibility was a continuous, smooth, function of net overburden pressure.

The pore volume compressibilities (Figs. 2 and 3 plus 10 other samples) could not be correlated with porosity.

DISCUSSION OF DATA

The data of Figs. 2 and 3 are probably accurate to $\pm$ 15 per cent. The reproducibility of the pore volume data is $\pm$ 5 per cent. However, the graphical differentiation of the pore volume-pressure curve required for the calculation of compressibility introduces additional uncertainty. Another factor reducing the accuracy of the compressibility data is the correction for compressibility of the kerosene in the sample and connecting lines. Any uncertainty in the kerosene compressibility is doubled in the calculated pore volume compressibility.

Although the data in Figs. 2 and 3 are accurate only to $\pm$ 15 per cent, they show clearly that, at a given

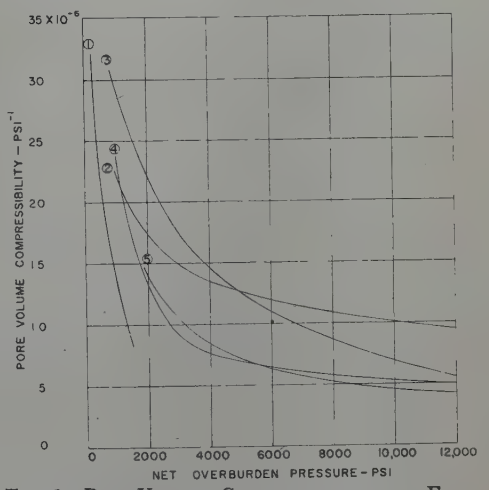

FIG. 2—PORE VOLUME COMPRESSIBILITY AS A FUNCTION OF NET OVERBURDEN PRESSURE ($P_e - 0.85\,P_i$).

Curve 1: Unconsolidated sand, 28 to 35 mesh flint shot, porosity—36 per cent.
Curve 2: Basal Tuscaloosa sandstone, Mississippi, porosity—13 per cent.
Curve 3: Sandstone from wildcat, Santa Rosa County, Fla., porosity—15 per cent.
Curve 4: Sandstone from Ventura Basin field, Calif., porosity—10 per cent.
Curve 5. Sandstone from West Montalvo area field, Calif., porosity—12 per cent.

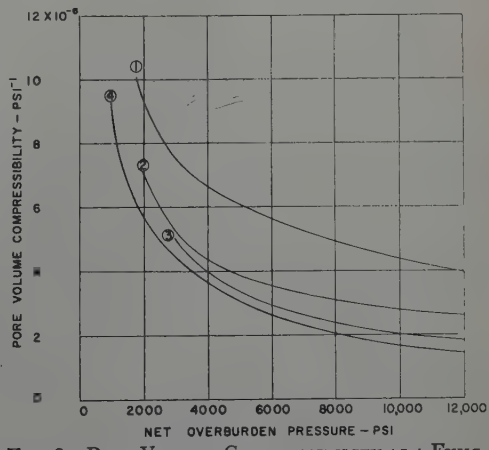

FIG. 3—PORE VOLUME COMPRESSIBILITY AS A FUNCTION OF NET OVERBURDEN PRESSURE ($P_e - 0.85\,P_i$).

Curve 1: Weber sandstone, Rangely field, Colo., porosity—12 per cent.
Curve 2: Sandstone from Nevada wildcat, porosity—13 per cent.
Curve 3: Strawn sandstone, Sherman field, Tex., porosity—13 per cent.
Curve 4: Bradford sandstone, Pennsylvania, porosity—15 per cent.

pressure, there may be a fourfold difference in pore volume compressibility from one sandstone to another. Furthermore, the compressibilities for each sample are functions of pressure.

The compressibilities reported in Fig. 2, except for the unconsolidated sand, are for sandstones containing poorly sorted grains and from 20 to 45 per cent cement and intergranular detrital material*. These compressibilities are higher than those given in Fig. 3 which are for sandstones containing well-sorted grains and only 10 to 30 per cent cement and intergranular detrital material. These observations point to a possible relation between compressibility and composition of sandstones. There are, as yet, too few data to allow a definite conclusion.

The absence of a correlation between compressibility and porosity data reported in this paper is contrary to the conclusion reached by Hall.[1] However, Hall had only four sandstone samples so that his correlation, for sandstones at least, may be fortuitous. Also, Hall used only a single external pressure, 3,000 psig, and a small range of internal pressures, 0 to 1,500 psig. Within this limited pressure range and for a few samples a compressibility-porosity correlation may exist but the data collected during the course of this study did not show it. On the other hand, the data of this study are concentrated in the porosity range of 10 to 15 per cent with only one sample near 20 per cent. The absence of a correlation may be the result of this small porosity range.

Although some of the curves in Figs. 2 and 3 cross, still they all seem to have the same characteristic shape. This suggests that a single analytical expression with separate constants for each sample would fit all the data. In the range from 2,000 to 10,000 psig, these data can be expressed approximately by $C = A - B \log P$, where A and B are constants for each sample. This logarithmic relation is useful in interpolating between measured data points or for a short extrapolation beyond the measured pressure range.

These results suggest that laboratory measured compressibilities be used in reservoir calculations if more than just an approximate calculation is being made.

A word of caution is appropriate here in connection with the use of laboratory measured compressibilities in reservoir calculations. Geertsma[4] has pointed out correctly that the laboratory measured compressibilities may be greater than those in the reservoir by a factor of two. This is because laboratory measurements are made on samples which are at simulated hydrostatic overburden pressure whereas the stresses in a reservoir may not be hydrostatic. If the reservoir is surrounded by an immovable boundary, then the weight of the overburden may not apply a hydrostatic stress. A virgin reservoir in which the fluid pressure is equal to the pressure of a column of water to the surface may be under hydrostatic stress. But as the reservoir is depleted, the vertical stress may become greater than the horizontal stresses. The ratio of laboratory compressibilities to those existing in the reservoir would be unity in the unproduced reservoir and gradually approach two as the reservoir pressure is depleted. Stress conditions in petroleum reservoirs are not yet known with any degree of certainty. Further study of this problem is needed.

*These properties were estimated by conventional petrographic thin-section analysis.

REFERENCES

1. Hall, H. N.: "Compressibility of Reservoir Rocks," *Trans.* AIME (1953) **198,** 309.
2. Hawkins, M. F., Jr.: "Material Balances in Expansion Type Reservoirs above Bubble Point", *Trans.* AIME (1955) **204,** 267.
3. Hobson, G. D., and Mrosovsky, I.: "Material Balance above the Bubble Point", *Trans.* AIME (1956) **207,** 347.
4. Geertsma, J.: "The Effect of Fluid Pressure Decline on Volume Changes of Porous Rocks", *Trans.* AIME (1957) **210,** 331.
5. *International Critical Tables*, McGraw-Hill Book Co., N. Y., 1st Ed. (1927) 146.
6. Brandt, H.: "A Study of the Speed of Sound in Porous Granular Media", *Trans.* ASME (1955) **77,** 479. ★★★

T. N. 2005

The Application of the Buckley-Leverett Frontal Advance Theory to Petroleum Recovery

STEPHEN G. DARDAGANIAN*
JUNIOR MEMBER AIME

A & M COLLEGE OF TEXAS
COLLEGE STATION, TEX.

INTRODUCTION

Basically, the Buckley-Leverett theory involves two systems which are similar in nature but are differentiated by time. These systems may be described by the fractional flow and frontal advance equations which essentially characterize the mechanics of oil movement while being expelled from the reservoir.

The fractional flow equation originally developed by Leverett[1] may be expressed in the more usable form

$$f_d = \frac{Q_d}{Q_t} = \frac{1 + .001127 \frac{k_o}{\mu_o} \frac{A}{Q_t} \left[\left|\frac{\partial P_c}{\partial s}\right| - .433\, \Delta\gamma \sin\theta\right]}{1 + \frac{k_o}{\mu_o} \frac{\mu_d}{k_d}} \quad . \quad . \quad . \quad . \quad . \quad . \quad . \quad . \quad . \quad (1)$$

The development of this equation[2] is based on Darcy's law describing fluid flow through porous media and applies to the flow at only one point (it is a point function). For simplification, the fractional flow equation is written in the above form because the capillary forces always increase the fractional flow of the displacing phase regardless of the direction of flow or the displacing phase.

If, for simplicity, the effects due to gravity and capillary pressure differences are neglected, the fraction of the displacing fluid, f_d, at any point in the flowing stream is related to the properties of the system by

$$f_d = \frac{1}{1 + \frac{k_o}{\mu_o} \frac{\mu_d}{k_d}} \quad . \quad . \quad . \quad (2)$$

Thus, it is seen that in the absence of capillary and gravitational effects, f_d for a given sand and fluids varies only with saturation and pressure. The magnitude of the viscosity ratio, $\frac{\mu_d}{\mu_o}$, has an effective range (range of about 30) in the system where gas is displacing oil and a much smaller range for water displacing oil.

In order to make the fractional flow equation more versatile, it is necessary to connect the fractional flow at a given point and saturation with time. This problem was approached by Buckley and Leverett[3] who developed the frontal advance equation,

$$\frac{\Delta x}{\Delta T} = \frac{Q'_t}{Af} \left(\frac{\Delta f_d}{\Delta S_d}\right)_{S_d} \quad . \quad . \quad (3)$$

Eq. 3 states that the rate of advance of a plane that has a fixed saturation, S_d, is proportional to the change in composition of the flow stream caused by a small change in the saturation of the displacing fluid. It is, essentially, a transformation of a material balance equation representing the net rate of accumulation of the displacing phase within a homogeneous sand block. This accumulation is proportional to the difference between the rate at which the displacing fluid enters the sand and that at which it leaves.

Eq. 3 describes the velocity with which a plane of constant displacing phase saturation advances through a porous system. Buckley and Leverett,[3] Babson,[4] Kern,[5] Welge,[6] and others have adequately discussed the basic mechanism and application of the fractional flow and frontal advance equations.

APPLICATIONS OF THE FRONTAL ADVANCE THEORY TO PETROLEUM RECOVERY

Two general applications of the Buckley-Leverett frontal advance theory involve the system in which the oil is being displaced by an expanding gas cap overlying the oil zone and that in which the oil is being displaced by water.

Displacement by Gas in the Presence of an Immobile Water Saturation

A system in which gas is the displacing phase may be thought of as having two forces effecting the displacement process. These forces are the gravitational force and that force exerted by the displacing gas. The gravitational effects control the displacing efficiency of the gas. The gravitational effect will be less at higher rates of flow, thereby reducing the effectiveness of the displacement of the oil by the gas. The more efficient displacements occur at flow rates which are less than the gravity free fall rate. Capillary forces can be neglected without materially changing the magnitude of the gas saturation.

The Mile Six pool is used herein to illustrate the calculating procedures in evaluating gas drive-gravity drainage field performance. These calculations represent the determination of the gas-oil contact when the distribution of the hydrocarbon pore volume is considered. Two methods

Original manuscript received in Society of Petroleum Engineers office on March 11, 1957. Revised manuscript received Feb. 26, 1958. Paper presented at Joint University of Texas-A & M College of Texas Student Chapters of AIME Regional Meeting in Austin, Tex., Feb. 14-15, 1957.

*Presently completing The Atlantic Refining Co. training program, Dallas, Tex.

[1]References given at end of paper.

are available for making such calculations: a linear block method and a volumetric invasion method.

The linear block method involves the treatment of the reservoir as a uniform block. The displacement of oil by the advancing gas cap is evaluated by

$$f_g = \frac{1 + .001127\frac{k_o}{\mu_o}\frac{A}{Q_t}(-.433\,\Delta\gamma\,\sin\theta)}{1 + \frac{k_o}{\mu_o}\cdot\frac{\mu_d}{k_d}}, \quad . . . . . (4)$$

which is the same as Eq. 1 except that the capillary forces are neglected. It should be noted that the cross-sectional area normal to flow must be determined before the fractional flow can be evaluated. There are two methods presented by Amyx, Bass, and Whiting which can be used for the determination of this area. A reservoir voidage rate of 9,177 B/D and other properties reported by Welge and Anders[7] were used in the calculations shown in Fig. 1.

In order to determine the position of the gas-oil contact at any time, it is necessary to solve the following equations for various values of time or gas-oil contact position

$$L = \frac{Q_t\,T}{5.61\,fA}\left(\frac{df_g}{dS_g}\right)_f,$$

or

$$T = \frac{5.61\,LAf}{Q_t\left(\frac{df_g}{dS_g}\right)_f} \quad . . . (5)$$

These are essentially forms of Eq. 3. Eq. 5 may be restated in terms of hydrocarbon pore space provided the fractional flow equation is expressed with gas saturation as a fraction of hydrocarbon pore volume (as shown in Fig. 1). The following is noted:

$$f' = f(1 - S_w),$$

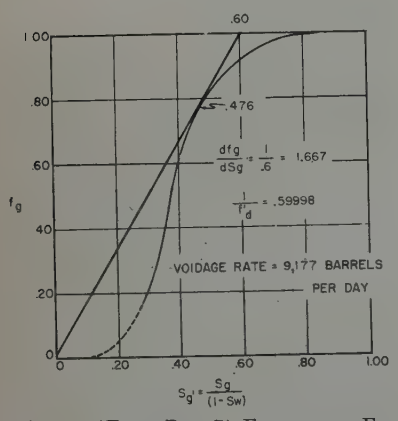

FIG. 1—(FROM REF. 7) FRACTIONAL FLOW OF A GAS AS A FUNCTION OF GAS SATURATION EXPRESSED AS A FRACTION OF HYDROCARBON OCCUPIED PORE SPACE.

$$S'_g = \frac{S_g}{(1 - S_w)},$$

and

$$\frac{df_g}{dS_g} = \frac{1}{(1 - S_w)}\,\frac{df_g}{dS'_g}.$$

Using the above definitions, Eq. 5 may be rewritten as

$$L = \frac{Q_t}{5.61}\,\frac{T}{f'\,A}\left(\frac{df_g}{dS'_g}\right)_f$$

or

$$Q_tT = \frac{5.61\,L\,Af'}{\left(\frac{df_g}{dS'_g}\right)_f} \quad . . . (6)$$

where Q_tT is the cumulative reservoir voidage.

The volumetric invasion method involves the use of the hydrocarbon pore distribution. The invaded hydrocarbon pore volume appears in Eq. 6 as: hydrocarbon pore volume $= L\,A\,f\,(1 - S_w)$, cu ft such that its value can be read directly from Fig. 2 which shows the distribution of the hydrocarbon pore volume of the oil zone with depth in the Mile Six pool. The distance along the bedding planes (L) is converted to vertical heights by $h = L\,\sin\,\theta$. This conversion is performed because the vertical displacement of the gas-oil contact is of basic importance in reservoir study.

Using the modified form of Eq. 6 such that

$$\Delta h = \frac{Q_tT\,\sin\,\theta}{5.61\,A\,f'\,(1 - S_w)}\left(\frac{df_g}{dS'_g}\right), \quad . . . . . (7)$$

the saturation distribution with height may be calculated. As the position of the front is specified in each case, the cumulative reservoir voidage term may be replaced by Eq. 6 such that Eq. 7 becomes

$$\Delta h = L\,\sin\,\theta\left[\frac{df_g}{dS'_g}\Big/\left(\frac{df_g}{dS'_g}\right)_f\right] \quad . . . . . (8)$$

Thus, for any given position of the gas-oil contact denoted by L, the saturation distribution can be determined.

Sample calculations for the determination of the gas-oil contact when the distribution of the hydrocarbon pore volume is taken into consideration are presented in Table 1. The data calculated in Table 1 are plotted in Fig. 3, which shows a comparison of the computed position of the gas-oil contact to that observed from field data. Only small deviations are noticed at low values of cumulative production with the deviation increasing with increased production.

The time and cumulative production are readily obtained as it was assumed that the rate of reservoir voidage was a constant and that no production occurred behind the front. Thus, $Q_tT = N_pB_o$, where Q_t and B_o are known, and Q_tT is expressed and calculated as a function of the gas-oil contact position by Eq. 6.

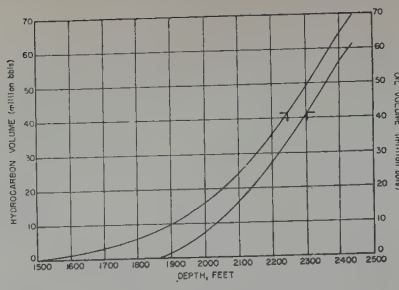

FIG. 2—(FROM REF. 7) DISTRIBUTION OF HYDROCARBON PORE VOLUME IN THE OIL ZONE WITH DEPTH, MILE SIX POOL.

DISPLACEMENT BY WATER

The fractional flow and frontal advance calculations for a system in which water is the displacing phase are basically the same as the calculations for a system in which gas is the displacing phase. However, the latter generally occurs in a system in which a third immobile phase (water) is usually present, whereas, in a water-drive system, the third phase (gas) may or may not be present and may exist either in a mobile or immobile state.

Pressure is the controlling factor which defines the state of the third phase (gas) in a water-drive system. If the reservoir exists at a pressure above the bubble-point pressure of the oil, no free gas phase will exist, and the system may be evaluated as a two-phase system. Assuming the reservoir exists at a pressure slightly below the bubble-point pressure of the oil, the gas that has been evolved from the oil may be thought of as being immobile. This system may be evaluated as a three-phase system with an immobile third phase. If, however, the reservoir exists at a pressure sufficiently below the bubble point such that the evolved gas has mobility, the problem will then become one involving three mobile phases. The treatment of such a problem will now be discussed.

Consider a reservoir in which a gas phase has been created by production and pressure depletion. The saturation distribution is such that three mobile phases exist. The fractional flow-frontal advance theory breaks down when applied to this system as a whole. However, this problem may be simplified remembering that an oil bank develops ahead of a waterflood front when flooding in the presence of a mobile

TABLE 1—CALCULATION OF GAS-CAP POSITION AS A FUNCTION OF CUMULATIVE PRODUCTION
(Voidage Rate—9,177 B/D, $B_o = 1.196$)

L	Δh	h	$\frac{LAf(1-Sw)+}{5.61}$ (MM)	Q_tT*	T (Days)	N_p** (MM)
100	30.07	1,905	1.6	0.96	98	0.803
300	90.21	1,965	5.05	3.03	310	2.53
1,000	300.71	2,175	24.0	14.40	1,474	12.04
1,500	451.0	2,326	44.6	26.76	2,739	22.37

* $Q_t T = \frac{LAf(1-S_{wc})}{5.61}(S_{ga})_f$

** $Np = \frac{TQ_t}{B_o}$

+ From Fig. 2

gas saturation. This complex system of three mobile phases may now be thought of as two separate systems in which only two mobile phases exist. One system is that in which the oil bank displaces the gas to an immobile saturation. In the second system, the advancing water bank displaces the oil from the porous rock in the presence of an immobile gas phase. By combining the evaluations of these systems, it is then possible to arrive at an evaluation of the system as a whole. The methods for such evaluations are developed in the following paragraphs.

The residual gas saturation developed during a flood is a function of the rock and fluid properties and can be determined from flow tests on the rock. During a water flood, the oil bank that builds ahead of the water front tends to displace any free gas from the system. Since the viscosity of the displacing oil is considerably greater than that of the displaced gas, the oil bank essentially displaces the gas with a piston-like effect. The gas is reduced to a "trapped" saturation assuming the pressure is such that it does not go into solution. Fig. 4 presents data adapted from flow tests performed by Kruger[9] on the amount of gas trapped by water flooding a gas-saturated core. This shows that the magnitude of the residual gas saturation obtained is a function of the amount of gas initially present.

The frontal advance theory may be used to evaluate the displacement of oil by water in the presence of the immobile gas. It is concluded that the residual oil saturation by water displacement will be a function of the residual gas within the oil bank. The effect of the residual gas saturation on the residual oil may be computed by the fractional flow-frontal advance theory if appropriate relative permeability data are available. From such data and frontal advance concepts the residual oil saturation at breakthrough of water may be calculated as a function of the viscosity ratio, μ_w/μ_o. For a given reservoir, the viscosity of water at reservoir conditions is essentially independent of the pressure. Therefore, the only variable effecting the residual oil saturation that varies with pressure is the oil viscosity. Using the oil and water viscosity data applying to a particular reservoir, the variation of the viscosity ratio with pressure may be calculated. Fig. 5 illustrates a family of curves defining the residual oil saturation as a function of the pressure and gas saturation.

The initial free gas saturation may be determined from material balance calculations, and by utilizing data such as that shown in Fig. 4, the residual gas saturation existing in the oil bank may be estimated. The residual oil saturation then may be determined from the residual gas saturation and the reservoir pressure by the utilization of such data as presented in Fig. 5.

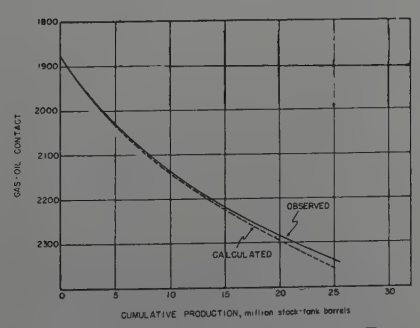

FIG. 3—(FROM REF. 2) COMPUTED POSITION OF GAS-OIL CONTACT COMPARED TO THAT OBSERVED FROM FIELD DATA.

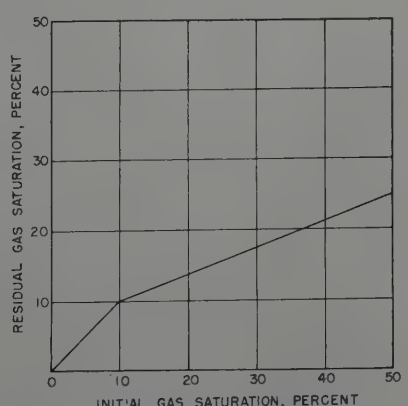

FIG. 4—(FROM REF. 9) ESTIMATED GAS ENTRAPMENT AFTER OIL FLOOD.

In the development of this evaluating process, the residual gas saturation developed by the advancing oil bank is considered to be the same as the residual gas saturation behind the waterflood front such that the water flood has no effect on the gas saturation. In addition, the residual oil saturation is thought of as essentially being equal to the average oil saturation behind the front. Thus, the residual oil may be defined by $(1 - S_{gr} - S_{wa})$. The second phase of recovery (displacement of oil after breakthrough of the flood front) is not considered since the economic value of such recovery is sometimes relatively low.

Optimum Pressure for Initiating a Water Flood

By evaluating the performance of solution gas-drive reservoirs, the free gas saturation and recovery as a function of pressure decline may be calculated. The effect of initiating and maintaining a water flood at a given pressure may be determined as shown in Table 2. The results of applying this procedure to other systems are shown in Fig. 6. Curves A, B, C, and D are based on the calculated performance of a solution gas-drive given by Muskat[10]. The waterflood recoveries were estimated from the data in Fig. 4 and curves corresponding to Fig. 5 prepared for each API oil. The curves in Fig. 6 consider 100 per cent pattern efficiency. Note that Curves A and B show maximums in total oil recovery at pressures below the bubble-point pressure (3,000 psi for all of the oils).

The maximums in total oil recovery are attributed to the effect of the free gas saturation in reducing the residual oil following a water flood. Maximums do not occur in Curves C and D. This is attributed to the effect of the greater shrinkage of the higher gravity oils. Curve E illustrates the effect of pattern efficiency on the optimum flooding pressure.

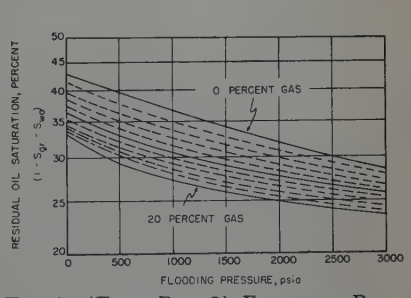

FIG. 5—(FROM REF. 8) EFFECT OF PRESSURE ON RESIDUAL OIL SATURATION BY WATER FLOODING FOR A 30° API CRUDE OIL.

TABLE 2—EXAMPLE OF EVALUATION OF OPTIMUM PRESSURE AT WHICH TO INITIATE A WATER FLOOD IN A SOLUTION GAS-DRIVE RESERVOIR
(For a 30° API Stock-Tank Oil)

(1)	(2)	(3) Cumulative* Recovery Fraction of Pore Space	(4)	(5)	(6)	(7)	(8)	(9)	(10)	(11)
Pressure (psia)	B_o*	S_o''	.555-S_o''	S_o	S_g	S_{gr}**	S_{or}**	$S_{or}-B_o$	Total Recovery Fraction of Pore Space	Total Recovery Per cent of Initial Oil
3,000	1.352	0	.555	.750	0	0	.285	.2108	.3442	62.02
2,800	1.339	.014	.541	.724	.026	.026	.283	.2114	.3436	61.91
2,600	1.328	.031	.524	.696	.054	.054	.276	.2078	.3472	62.56
2,400	1.316	.052	.503	.662	.088	.088	.272	.2067	.3483	62.76
2,200	1.303	.073	.482	.628	.122	.110	.269	.2064	.3486	62.81
2,000	1.290	.086	.469	.605	.145	.117	.270	.2093	.3457	62.29
1,800	1.278	.097	.458	.585	.165	.123	.273	.2136	.3414	61.51
1,600	1.263	.105	.450	.568	.182	.130	.276	.2185	.3365	60.63
1,400	1.249	.113	.442	.552	.198	.136	.281	.2250	.3300	59.46
1,000	1.217	.125	.430	.523	.227	.147	.288	.2366	.3184	57.37
100	1.085	.145	.410	.445	.305	.177	.330	.3041	.2509	45.21

*Data from Muskat[10]

$$S_o'' = \frac{S_{oi}}{B_{oi}} - \frac{S_o}{B_o} \qquad (S_w = 25 \text{ per cent})$$

**Determined from laboratory tests

Note that the maximum in recovery is accentuated and shifted to a lower pressure by lowering the sweep efficiency. It should be emphasized that the recovery data of Fig. 6 is total recovery as per cent of oil in place and, therefore, includes both primary and secondary recovery. The procedure outlined, together with appropriate flow tests on core samples, may be used to estimate the optimum pressure at which to initiate a water flood.

CONCLUSIONS

The methods of performance evaluation basically developed from the Buckley-Leverett frontal advance theory are not restricted to any one particular system but may be generally applied to a variety of systems in which the production mechanisms vary. In order to effectively employ the outlined evaluation procedures, it is required that a certain amount of laboratory and field data be available. The following information is needed for such evaluations.

1. Sufficient information to construct relative permeability or permeability ratio curves.
2. Appropriate fluid viscosity data to construct viscosity ratio curves.
3. Complete field data describing the structural parameters of the reservoir (areal extent, dip angle, thickness).
4. Laboratory data characterizing the reservoir rock (effective porosity and absolute permeability).
5. Field data giving a complete history of pressure, cumulative production, producing gas-oil ratio, and fluid injection associated with secondary recovery operations.
6. Densities of the reservoir fluids.
7. Data characterizing the rock-fluid interaction (capillary pressure data).
8. Analysis of the reservoir oil indicating the apparent bubble-point pressure and gas in solution.

With the proper modifications, this method of performance evaluation may be applied with reasonable success to systems other than those indicated; however, the restrictions imposed by the assumptions made in the development of this theory should be noted.

An important application of the fractional flow-frontal advance theory is its use in the determination of the optimum pressure at which to initiate a water flood in a combination drive reservoir. This theory makes it possible to utilize laboratory data obtained at low pressures to evaluate reservoir performance. Heretofore, this type of evaluation has been considered to require laboratory data obtained at high pressures, thus, involving considerable expense.

NOMENCLATURE*

f' = hydrocarbon porosity
f_d = fraction of the displacing fluid in the flowing stream
Δh = vertical distance traveled by the gas-oil contact, ft
P = pressure, psia
P_c = capillary pressure defined as the difference between the pressure in the oil phase minus the pressure in the displacing phase ($P_o - P_d$), psi
Q = flow in reservoir, B/D
Q'_t = total flow at any time in reservoir, cu ft/day
s = distance along the flow path, ft
S' = fluid saturation expressed as a fraction of the hydrocarbon pore space
T = time, days
$\left(\frac{df_o}{dS_g}\right)_f$ = derivations of the fractional flow equation evaluated at the gas saturation which exists at the front
$\Delta\gamma$ = specific gravity difference between oil and displacing phase ($\gamma_o - \gamma_d$)
θ = dip angle from the horizontal, it is to be considered positive when the direction of flow is downward and negative when the direction of flow is upward
ρ = fluid density (specific gravity of water is one)

SUBSCRIPTS

a = average behind the front
d = displacing phase

*See AIME Symbols List in *Trans.* AIME (1957) **207**, 363, for other symbol definitions.

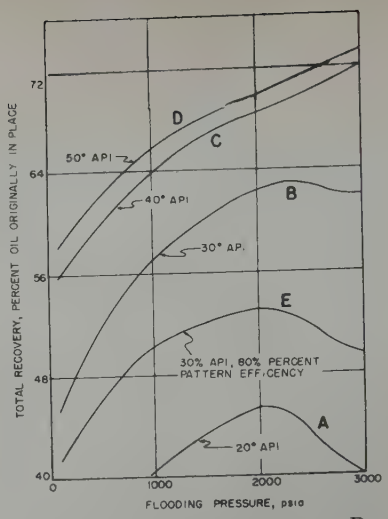

FIG. 6—(FROM REF. 8) EFFECT OF PRESSURE AND FLUID PROPERTIES ON TOTAL OIL RECOVERY BY SOLUTION GAS DRIVE FOLLOWED BY WATER FLOOD AT CONSTANT PRESSURE.

REFERENCES

1. Leverett, M. C.: *Trans.* AIME (1941) **142,** 152.
2. Amyx, J. W., Bass, D. M., and Whiting, R. L.: Unpublished text for Industry Summer School in Petroleum Reservoir Engineering, Texas A & M, 1956.
3. Buckley, S. E., and Leverett, M. C.: *Trans.* AIME (1942) **146,** 107.
4. Babson, E. C.: *Trans.* AIME (1944) **155,** 120.
5. Kern, L. R.: *Trans.* AIME (1952) **195,** 39.
6. Welge, H. J.: *Trans.* AIME (1952) **195,** 91.
7. Anders, E. L., Jr.: *Trans.* AIME (1953) **198,** 279.
8. Amyx, J. W.: "The Effect of Free Gas Saturation on Oil Recovery by Partial Water Drive and Water Flooding," report, Texas A & M (May, 1956).
9. Kruger, W. D.: "The Effect of Saturation History on the Residual Gas Content of Core after Waterflooding," MS thesis, Texas A & M, 1953.
10. Muskat, M.: *Physical Principles of Oil Production,* McGraw-Hill Book Co., N. Y. (1949) 421, 502. ★★★

A Method for Determining Optimum Second Stage Pressure in Three Stage Separation

KENNETH F. WHINERY
JUNIOR MEMBER AIME
JOHN M. CAMPBELL
MEMBER AIME

PHILLIPS PETROLEUM CO.
SHIDLER, OKLA.
UNIVERSITY OF OKLAHOMA
NORMAN, OKLA.

INTRODUCTION

This investigation was prompted by the absence of a simple, accurate method to predict optimum second stage separation pressure in three stage separation operations. Three stage separation as used here includes two separators plus the stock tank. The first stage pressure is usually fixed by gas sales conditions and the third stage is at atmospheric pressure. Thus, the second stage pressure is the only one that may be varied indiscriminantly during production operations. No variations in temperature were considered in this study, even though it will vary among systems, for a change in temperature has little effect on the optimum pressure.

Optimum pressures may be determined from flash calculations, but these are tedious unless a computer is available. An early attempt to develop a simpler method[1] yielded an equation which gave the optimum pressure only as a function of initial and final pressure. Experience, however, confirms theoretical relationships which show that composition as well as pressure and temperature must be a factor. This indicates that the basic relationship should be an equation of the form,

$$P_2 = A\ (P_1)^n \quad . \quad . \quad . \quad . \quad . \quad . \quad . \quad . \quad . \quad . \quad (1)$$

where P_2 is second stage pressure, P_1 is first stage pressure, A is a function of P_s (stock-tank pressure) and the system composition, and n is a function of the number of stages and the system composition.

Fig. 1 shows the basic variation of P_2 with P for a fixed system composition. A series of such figures clearly showed the effect of composition. The peak of each curve reflects that second stage pressure at which the stock-tank recovery (gal/MMcf) residue gas is a maximum value.

DEVELOPMENT OF NEW CORRELATION

Wellstreams having 17 different analyses, ranging from low gravity crude to condensate, were used to determine the effect of composition. Each wellstream was flashed through three stages to determine the optimum second stage pressure for each first stage pressure. Equilibrium vaporization ratios proposed by Latham and Campbell were used throughout. The heptane plus fraction, for simplicity, was assumed to have the properties of octane.

The results were subjected to an empirical analysis in an attempt to develop a correlation that would be (1) simple, (2) accurate, and (3) eliminate the need for any flash vaporization calculations. This analysis yielded two equations, one for wellstreams having a specific gravity greater than one (air = 1.0) and one for those less than one. For crude streams (specific gravity > 1.0),

$$P_2 = A(P_1)^{0.636} + C \quad . \quad . \quad . \quad . \quad . \quad . \quad . \quad . \quad (2)$$

$$C = \frac{A + 0.057}{0.0233} \quad . \quad . \quad . \quad . \quad . \quad . \quad . \quad . \quad (2A)$$

For condensate (specific gravity < 1.0),

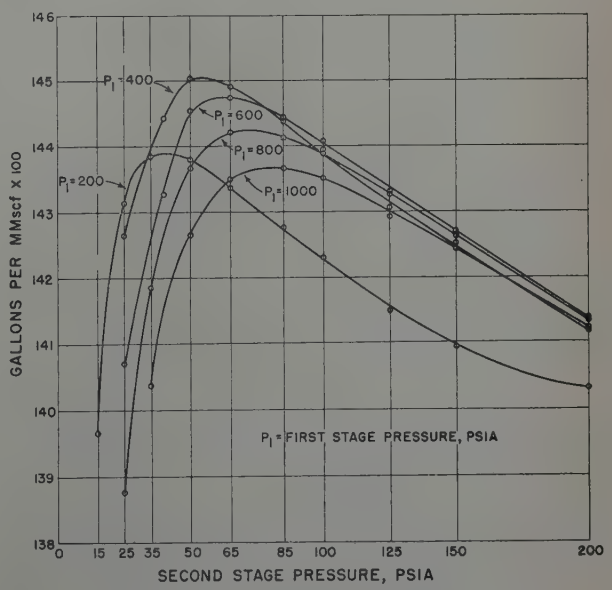

FIG. 1—QUANTITY OF STOCK-TANK LIQUID (ANALYSIS 6) TEMPERATURE 80°F.

Original manuscript received in Society of Petroleum Engineers office July 18, 1957. Revised manuscript received Feb. 26, 1958. Paper presented at 32nd Annual Fall Meeting of Society of Petroleum Engineers in Dallas, Tex., Oct. 6-9, 1957.
[1]References given at end of paper.

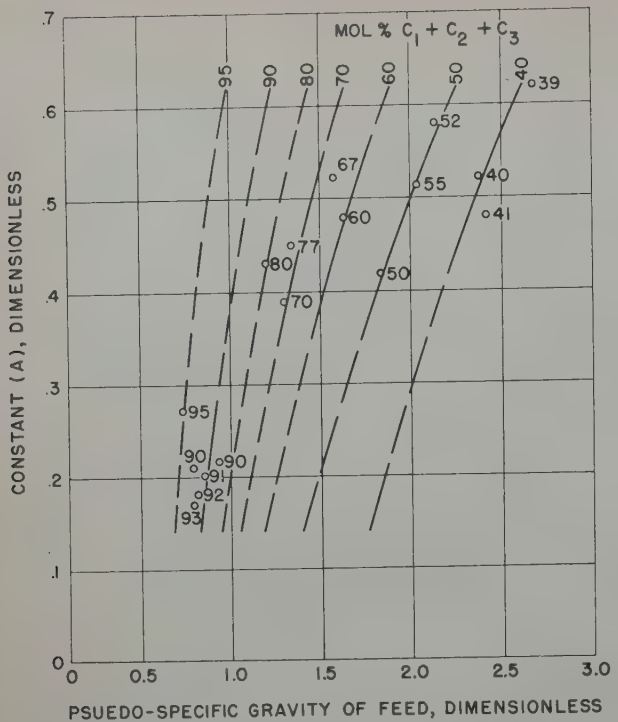

FIG. 2—CONSTANT (A) VS PSEUDO-SPECIFIC GRAVITY OF FEED, TEMPERATURE 80°F.

$$P_2 = A(P_1)^{0.765} + C_2 \quad . \quad . \quad . \quad . \quad . \quad . \quad . \quad . \quad . \quad (3)$$

$$C_2 = \frac{A + 0.028}{0.012} \quad . \quad . \quad . \quad . \quad . \quad . \quad . \quad . \quad (3A)$$

As might be expected from Eq. 1 the constants A and C are functions of composition. It was found that composition could be expressed in terms of the wellstream specific gravity and the percentages of methane, ethane and propane. This is shown in Fig. 2. Fig. 3 shows the basis for Eqs. 2A and 3A.

One may therefore determine optimum pressure knowing only the specific gravity of the wellstream, the percentage of methane, ethane and propane, and the first stage pressure. This may be illustrated with an example.

EXAMPLE

Determine the optimum second stage pressure, for a three stage separation, for a wellstream having the following composition, if $P_1 = 500$ psia.

(1) Component	(2) Mol Fraction	(3) Mol Weight	(4) 2 × 3
C_1	.40	16.01	6.40
C_2	.20	30.07	6.01
C_3	.10	44.09	4.41
C_4	.10	58.12	5.81
C_5	.10	72.15	7.22
C_6	.05	86.17	4.31
C_7 + (C_8)	.05	115.22	5.76
	1.00		39.92

$$\text{Specific gravity} = \frac{39.92}{28.96} = 1.38$$

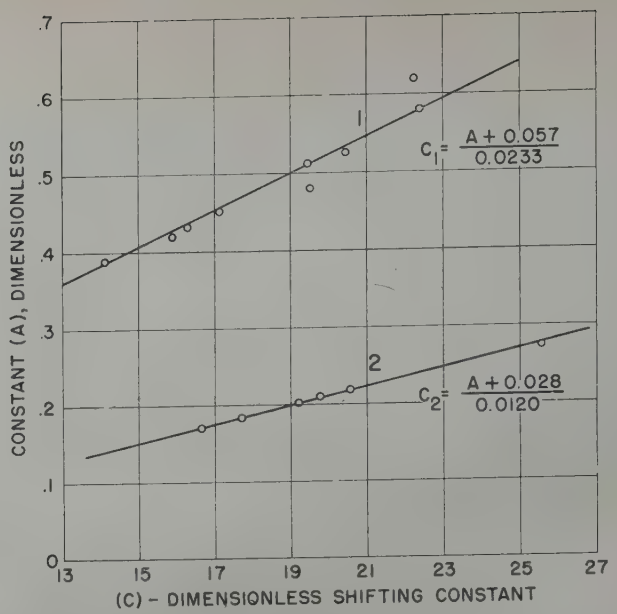

FIG. 3—DIMENSIONLESS SHIFTING CONSTANT VS CONSTANT (A).

$C_1 + C_2 + C_3 = 70$ per cent

From Fig. 2, $A = 0.421$; consequently, from Eq. 2A,

$$C = \frac{0.421 + 0.057}{0.0233} = 20.5.$$

If all values are substituted into Eq. 2,

$$P_2 = 0.421\ (500)^{0.686} + 20.5 = 50.5 \text{ psia}$$

This correlation is not the absolute solution to all three stage separation problems, nor is it intended to be so. It should, further, not be misconstrued as a replacement for a digital computer where such is available to perform flash calculations. Instead, it is a tool for the field engineer where time and expediency are of prime importance. It is the opinion of the authors, confirmed by field results, that this correlation is flexible and will yield results with a mean error of ± 5 per cent.

ACKNOWLEDGMENT

The authors wish to thank the Continental Oil Co. and the Sohio Petroleum Co. for making the use of their computers available to the School of Petroleum Engineering

REFERENCES

1. Whiteley, Burton: "Optimum Conditions for Condensate Recovery," MPE Thesis, The University of Tulsa, Tulsa, Okla. (1947) 21, 43.
2. Campbell, J. M., and Latham, J. A.: "Composite Equilibrium Ratios for Separation Calculations," Paper 900-G, presented at 32nd Annual Fall Meeting of Society of Petroleum Engineers, Dallas, Tex. (Oct. 6-9, 1957).
3. Whinery, K. F.: MS Thesis, University of Oklahoma, Norman, Okla. (1957). ★★★

Evaluation of Porosity Derivation from Neutron Logs

R. H. WIDMYER
JUNIOR MEMBER AIME
G. M. WOOD

THE TEXAS CO.
BELLAIRE, TEX.

ABSTRACT

In order to evaluate the quantitative determination of porosity by various neutron logging systems, four test wells were constructed to simulate some of the possible variables found in field logging conditions.

All of the test holes contain sections of limestone with one section of sandstone included in one well. Each well has a representative section of high, medium, and low porosity. Three borehole sizes are represented by three of the test wells, all containing fresh water. One test well contains saturated brine.

Statistical and time constant checks are made for each system evaluated. Runs and repeat runs are made with the sonde centered and eccentric.

Factors evaluated are the effect of borehole size, sonde position, salinity, chemical composition of rock, and statistical variation. A semi-quantitative method of evaluation of these effects is used giving the average maximum per cent error possible for each. Drift and calibration procedures are also discussed.

The effect of the various factors appears to be largely a function of the phenomena detected as well as the means of detection. Graphic illustrations of some of these effects are presented.

It is concluded, that for accurate log interpretation, the hole size and sonde position should be known.

INTRODUCTION

The use of neutron logs for the derivation of porosity has become an accepted practice in many areas. In recent years, many different neutron logging systems have been offered to the industry. The neutron sources presently available are of the radium-beryllium or polonium-beryllium type. Detector types used are ionization chambers, Geiger-Mueller-type counters, proportional counters, or scintillation detectors used to detect or measure gamma rays, thermal neutrons, epithermal neutrons, fast neutrons or combinations of these. It is well-known that all systems do not respond alike in all environments. As a result, testing facilities and an evaluation method were developed for use in evaluating the porosity discriminating ability of neutron logging systems using conditions simulating those normally encountered in the field. With such an evaluation, the suitability of a logging system can be determined for selected field conditions.

Revised manuscript received in Society of Petroleum Engineers office March 13, 1958. Paper presented at Fall Meeting of Southern California Petroleum Section in Los Angeles, Oct. 17-18, 1957.

TEST FACILITIES

The testing facilities consist of wells containing rocks of various porosities, constructed to include as many parameters as practicable. Three pits were drilled to a depth of 20 ft and the fourth to a depth of 9 ft, all having 48-in. diameters. Rat holes were dug to a depth of 6 ft in the center of each pit and fitted with sections of pipe having appropriate diameters. The top of this pipe was located approximately 8 in. above the pit bottom. A 6-in. layer of cement was then poured on the bottom and while still wet, 42-in. OD corrugated, galvanized culvert pipe was set on bottom and centered in place. This pipe extends approximately 1 ft above the surface of the ground. The annulus around the culvert pipe was then filled with cement to the top. A 1- or 2-in. layer of sand was placed on the cement bottom to provide an adjustable bed on which to place the series of rocks set in each hole. A cross section of a typical test well containing the porous rocks is shown in Fig. 1.

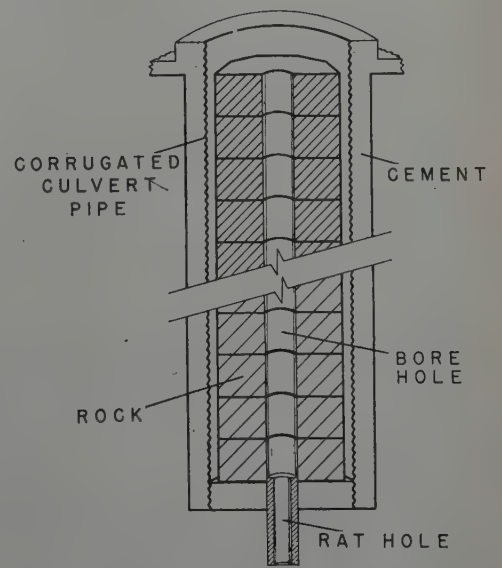

FIG. 1—CROSS SECTION OF TYPICAL TEST WELL.

The rocks selected were clean limestones or sandstones in three representative porosities; one below 2 per cent, one over 25 per cent and one intermediate porosity. The original quarried pieces were cut into 3 × 3 × 1-ft blocks. The four corners from each block were then removed leaving the block in an octagonal shape. The top and bottom surfaces of the blocks were machined smooth and parallel so that, when stacked, there would be negligible space or artificial porosity at the contact between the blocks. Each block then had a hole bored through the center to one of three diameters, 6, 7½, or 9 in. Average porosities for each block were obtained from analyses of cores from the removed corners.

The individual blocks of each major porosity and hole size were arranged so there would be a minimum difference in porosity between adjacent blocks. In this order, they were evacuated in a tank structurally designed to withstand collapse at the vacuum necessary for proper evacuation. A schematic illustration of the evacuation tank is shown in Fig. 2. With the arrangement shown, the blocks were handled readily with a sling through the center hole, and the size of the tank opening could be kept to a minimum to reduce the possibility of the gasket leaking.

The tank was evacuated to a pressure of 1 or 2 mm of mercury with suitable moisture traps in the system. The period of evacuation lasted from two to six hours, depending upon the porosity involved. Based upon several preliminary evacuation periods of two or three days, these times were considered adequate to obtain a satisfactory water saturation. After this period the tank, with the vacuum maintained, was filled with water until the block was completely covered. The pressure was then allowed to return to normal with a period of time allowed for the water to saturate the block.

The first blocks were each weighed before and after saturation and the porosity measured in this manner was checked against the previously measured porosity until it was established, by the close agreement of the two porosities, that a very effective saturation of the blocks was being accomplished.

As each block was saturated, it was lowered into its pit, leveled, aligned with the lower blocks, and covered with fresh water. The blocks for the 9-ft pit were saturated with brine and the pit was filled with brine. A friction cone device, adapted for each of the hole sizes, was used to lower the blocks into position in the pit. Guides on the device, extending below the block being handled, enabled alignment with the underlying block.

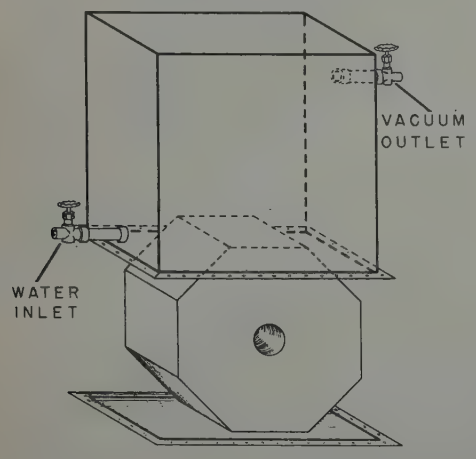

FIG. 2—EVACUATION TANK FOR ROCK SATURATION.

The completed test well set-up consists of three 18-ft fresh water wells and one 7-ft saturated brine well. Each of the fresh water wells has limestone rocks of the three representative porosities. Three different borehole sizes (6, 7½, and 9 in.) are represented by these three wells, each containing 18 ft of rock. The 5 or 6 ft of each porosity section are found to be satisfactory from a bed thickness standpoint in consideration of the very low logging speed used during evaluation runs. The 7½-in. bore fresh water well contains a 3-ft section of medium porosity sandstone. The 7½-in. bore brine well has limestone sections of only the medium and highest porosities.

Within the limits of the parameters available in these test wells, it is possible to evaluate the effect of variation in the borehole size, sonde position, salinity of the borehole fluid and/or formation fluid, and rock composition (clean limestone to sandstone) as well as the effect of a wide range of porosity on the neutron log response.

TEST PROCEDURE AND EVALUATION METHOD

A standard procedure has been established for obtaining neutron logs for evaluation. Calibration, instrument zero, statistical and time constant checks are made before and after survey operations. Logs are obtained with the sonde centered and then in contact with the wall of the borehole. Each run is repeated to obtain a quality control.

When quantitative interpretations are attempted using a neutron log, it is desirable to know the accuracy of the measurements or the possible errors involved. Consequently, a method has been devised whereby a semi-quantitative determination of the average maximum per cent error possible could be established for each of the factors evaluated. This value will be referred to as "error" for the purposes of this discussion.

Using this method, the relative effects or significance of each of the factors are evaluated in the same units and can be compared on a common basis. The errors are expressed in percentages and are identified as follows.

E_{st} is error due to statistical variation, E_d is error due to borehole diameter variation (6 in. and 9 in.), E_p is error due to sonde position variation, E_c is error due to change in the rock composition from limestone to sandstone, and E_{si} is error due to variation in the salinity of the borehole and/or formation fluid.

With these values obtained for the various conditions available in the test wells, it is thus possible to determine the relative suitability of neutron systems for specific field conditions by consideration of the applicable errors. Although generally additive the relative importance of each error must be considered and the final analysis weighted accordingly.

Fig. 3 is a schematic presentation of the test runs of a hypothetical neutron logging system plotted in the conventional manner, i.e., the logarithmic plot of porosity vs the instrument response. The instrument response is expressed in terms of response units (RU) so that all systems can be normalized to a common basis for comparison and evaluation. The intercept of the decentralized instrument response in the 6-in. borehole with the 1 per cent ϕ line has been selected as the point of normalization and this response assigned a value of 70 response units.

The details of the method used to evaluate the various

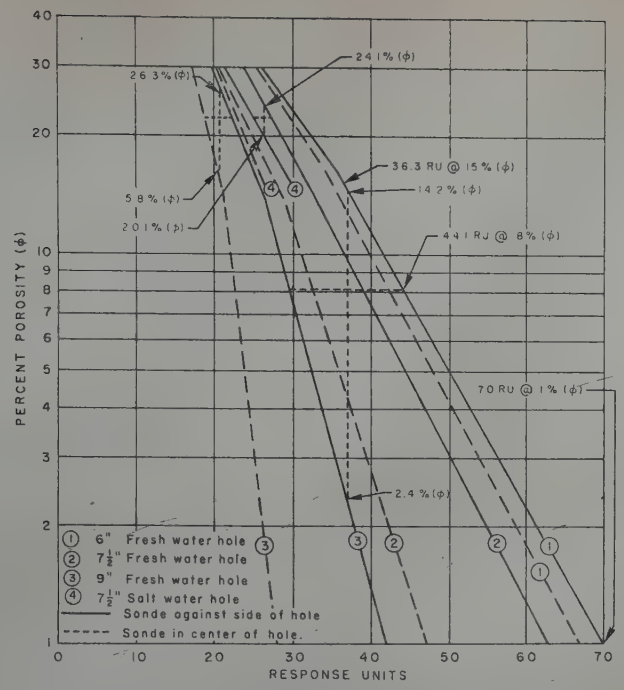

FIG. 3—POROSITY VS INSTRUMENT RESPONSE FOR HYPOTHETICAL NEUTRON SYSTEM.

error components are most readily explained by making calculations using the data of Fig. 3.

In order to reduce the information to a reasonable amount of numerical data, the porosity ranges of 1 to 15 per cent and 15 to 29 per cent are considered separately, and the maximum possible error at the midpoint of each of these porosity ranges (8 per cent ϕ for the low range and 22 per cent ϕ for the high range) is used to determine the error for the porosity range under consideration.

For the determination of E_{st}, the number of response units within which the statistical variation will occur 90 per cent of the time (statistical error) is found for the instrument response at the midpoint of the porosity zone under consideration. This can be obtained using the statistical runs made at various counting rates without knowing the actual counting rates involved. However, caution should be exercised to normalize all the runs to one sensitivity.

Referring to Fig. 3, a sample derivation of the E_{st} will be given for the curve of the 6-in. hole, solid Line 1, in the low porosity range (1 to 15 per cent porosity). For purposes of this example, it will be assumed that the statistical error is ± 5 per cent. Multiplying this value by the instrument response at the average porosity for the range (44.1 RU at 8 per cent porosity) gives the average statistical error for the range of ±2.2 RU. From the signal of 70 RU at 1 per cent porosity and 36.3 RU at 15 per cent porosity, we see that a 1 per cent change gives an average signal change of 2.4 RU per porosity unit over this porosity range, where porosity units are introduced to eliminate confusion between per cent porosity and other percentages. The statistical error corresponds to a ϕ unit error of ±0.92 ϕ units. This value is divided by the average porosity for the range (8 per cent porosity) to give an E_{st} of ±11.5 per cent. While this figure has been labelled E_{st} it should be remembered that the statistical fluctuations will be even larger than this 10 per cent of the time.

Generally, the slopes of the plots of instrument response vs porosity are not parallel for various hole sizes or sonde positions, and the subsequent calculations of the other errors were developed for such conditions.

An example of the determination of the error due to borehole diameter variation between 6 and 9 in., E_d, is shown for the low porosity portion (1 to 15 per cent) of the decentralized 6 and 9-in. curves of Fig. 3 (solid Lines 1 and 3). The average of the responses of these decentralized curves at 8 per cent porosity is determined and the porosity spread between the curves at this midpoint is measured to be 11.8 ϕ units. The deviation from the mean is ±5.9 ϕ units. This ± porosity spread divided by the average porosity (8 per cent) of the range being considered gives the E_d of ±74 per cent. The same technique can be applied to the determination of the E_d for the high porosity range (15 to 29 per cent).

The error due to sonde position variation, E_p, is determined by a method similar to that used for borehole size variation. Referring to the 9-in. borehole centralized (dashed Line 3) and decentralized (solid Line 3) curves in the high porosity range (15 to 29 per cent) of the example shown in Fig. 3, the maximum porosity spread between the centralized and decentralized curves at the 22 per cent midpoint is determined to be 10.5 ϕ units. This value divided by the average porosity (22 per cent) of the range being considered gives an E_p of 48 per cent.

The error due to variation of the salinity of the borehole and/or formation fluid, E_{sl}, is determined by the same general method as for variation in sonde position and hole size. Referring to Fig. 3, the maximum porosity spread at the midpoint of the 22 per cent porosity line drawn between the decentralized 7½-in. borehole fresh (solid Line 2) and salt water (solid Line 4) curves is found to be 4.0 ϕ units. This value divided by the average porosity (22 per cent) of the range gives an E_{sl} of 18 per cent.

The effect of change in rock composition from limestone to sandstone, E_c is evaluated by a comparison of the known porosity of a sand section with the porosity of a limestone giving the same instrument response in the same diameter borehole and sonde position.

DISCUSSION

A number of different systems have been run in the

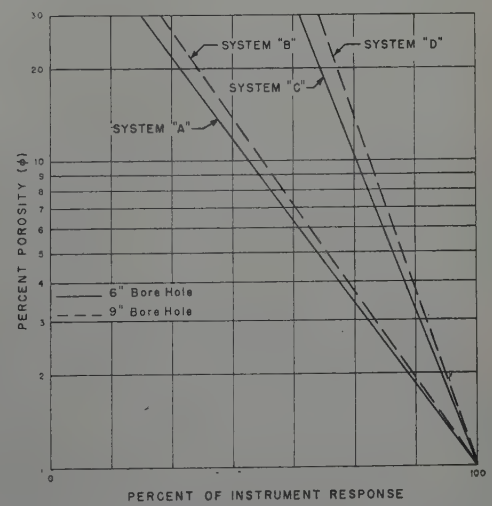

FIG. 4—RANGE OF SIGNALS WITH SONDES DECENTRALIZED. ALL CURVES NORMALIZED TO COMMON POINT AT 1 PER CENT ϕ.

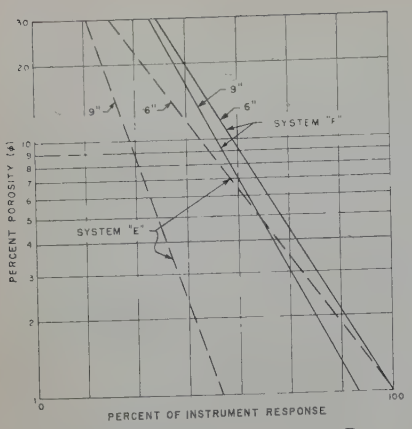

FIG. 5—EFFECT OF THE BOREHOLE DIAMETER FOR TWO SYSTEMS.

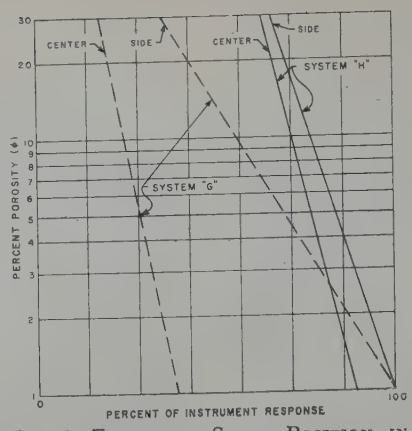

FIG. 6—EFFECT OF SONDE POSITION IN 9-IN. BOREHOLE.

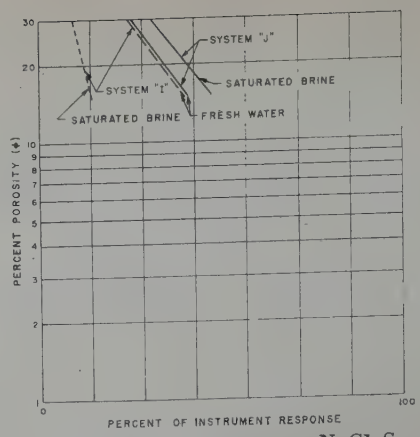

FIG. 7—EFFECTS OF SATURATED NaCl SOLUTIONS ON SYSTEMS USING DECENTRALIZED SONDES IN 7½-IN. BOREHOLE.

test wells. The factors evaluated affected the instrument response of various systems to different degrees. The range of effects that has been observed for the individual factors can give some indication of the error for each factor. The error inherent in most of the factors evaluated is also partly a function of the slope of the curve.

The total signal for any instrument is the result of a combination of the effects of the instrument design, borehole environment and the environment of the formation.[1] The effect of these two environments will vary for different systems. This variation alters the instrument response to porosity. Fig. 4 illustrates the difference in response for several systems when decentralized in the 6- and 9-in. test wells. For comparison, these curves have been normalized to a common point at 1 per cent porosity.

Variations in borehole diameter have a significant effect.[2] Generally, with an increase in diameter the response is lowered and the instrument is apt to be less sensitive to changes in porosity. Fig. 5 illustrates the difference in magnitude of the effect of borehole diameter variation on two different systems.

Another factor which has a pronounced effect is the position of the sonde in the borehole. The effect of change of position of the sonde from against the wall to a centralized position in the bore is similar to that of an increase in borehole size. Fig. 6 illustrates the range of this effect on two systems in the 9-in. test well. The sensitivity can be expected to be smaller with a decrease in borehole diameter. (The instrument responses of the decentralized sondes at the 1 per cent porosity intercept have been normalized.)

The presence of NaCl in the formation and/or borehole may have an effect on some neutron systems.[3] Fig. 7 illustrates how this factor affects the response of two different systems in 7½-in. test wells using a decentralized sonde. It is to be expected that any decrease in the NaCl concentration would reduce the magnitude of this effect.

The difference in composition between a limestone and a clean sand has very little effect on the response of most systems so that the porosity correlation established in limestone sections may generally be considered applicable to clean quartz sands.

No quantitative determination of the error involved with instrument drift has been established for these evaluations. However, it is assumed that if any drift is observed during a test under ideal laboratory conditions at ambient temperature, there is a distinct possibility of instability under field conditions.

To investigate the effects of cemented casing upon instrument response, a joint of 7-in. OD casing, sheathed with a uniform layer of typical oilfield cement, has been used in the 9-in. bore limestone well. There was negligible space between the cement and rock surface. The relative effect of the factors evaluated generally remained comparable to non-cased conditions. Further tests, using decentralized casing, were not made because under field conditions there is no way to establish the position of the casing and sonde with respect to the hole, and even though the effects were accurately known, the application of this knowledge would not be possible.

A good calibration method should calibrate the entire system from source to a recorder, so that the failure or partial breakdown of any component part will be readily detected.

CONCLUSIONS

Instrument response curves obtained from laboratory test facilities of this nature should not be used for direct porosity determinations from field logs until such time as their applicability in a given location has been demonstrated. If they are not directly applicable, calibration curves should be developed for each area based upon reliable logging and core data.[1,2]

It is realized that there are many possible alternative test facilities and evaluation methods.[3] However, those presented here will cover adequately and equitably some of the important factors affecting neutron log responses.

It is concluded, from evaluations using this method, that the factors which might have the greatest effect on the reliability of neutron derived porosities are variations in the borehole diameter and in the position of the sonde in the hole.

REFERENCES

1. Bush, R. E., and Mardock, E. S.: "Some Preliminary Investigations of Quantitative Interpretations of Radioactivity Logs", *Trans.* AIME (1950) **189,** 19.
2. Scotty, C. B., and Egan, E. F.: "Neutron Derived Porosity Influence of Bore Hole Diameter", *Trans.* AIME (1952) **195,** 203.
3. Dewan, J. T.: "Neutron Log Correction Charts for Borehole Conditions and Bed Thickness", *Trans.* AIME (1956) **207,** 50.

★★★

Some Thermal Characteristics of Porous Rocks

WILBUR H. SOMERTON
MEMBER AIME

UNIVERSITY OF CALIFORNIA
BERKELEY, CALIF.

ABSTRACT

Results of experimental measurements of heat capacities and thermal conductivities of some typical porous rocks are presented. Measured heat capacities agree closely with values calculated from known chemical compositions of the rocks. On the basis of this agreement, heat capacities of fluid-saturated rocks were calculated. Thermal conductivities of the rock samples were measured under various conditions of fluid saturation. From these data thermal diffusivities were calculated. A significant variation of thermal diffusivity with temperature is indicated.

INTRODUCTION

Knowledge of the thermal characteristics of fluid-bearing porous rocks has become increasingly important with the development of thermal oil-recovery processes. Reliable thermal data for petroleum reservoir rocks are not available and approximate values are generally assumed for reservoir calculations. The effects of temperature, pressure and fluid saturation on thermal properties of porous rocks have not been carefully studied.

The purpose of the present work was to measure and report the thermal characteristics of some typical porous rocks. A group of eight sedimentary rock samples, including limestone, shale, sandstone and siltstone, was selected for the study. Properties reported include heat capacities, thermal conductivities and thermal diffusivities. The effect of fluid saturation on these properties was also considered.

Determinations of thermal properties require precise measurements which are time consuming and difficult to reduce to a routine basis. Methods have not been developed for measurement of thermal properties under conditions of pressure, temperature, and fluid saturation, which may be encountered in thermal recovery processes. As one approach to these problems, some preliminary work on methods of estimating thermal properties from other more readily measurable characteristics of the rock-fluid system is reported.

SAMPLE PREPARATION AND PRELIMINARY ANALYSES

The samples selected for the studies were oilfield cores from within, or closely associated with oil-productive zones. Descriptions of individual samples are given in Table 1. Clay minerals present in the samples were determined by differential thermal analysis (DTA). Quartz content was estimated from DTA cooling curves.

For all but the thermal conductivity tests, a representative 200-gm sample of each core was disaggregated, thoroughly extracted in dioxane and oven dried at 100°C. The cleaned and dried sample was carefully split into appropriate portions for the several tests.

Chemical analyses of the samples were obtained to permit calculations of heat capacities by methods which are outlined later. Results of chemical analyses are given in Table 2.

MEASURED HEAT CAPACITIES

Heat contents of the test samples were measured by a Bunsen-type calorimeter. The heat content of the unknown sample is measured relative to the known heat content of platinum. The apparatus is referred to as a relative error type because of the comparative measurements, and has the advantage of canceling systematic errors. Experimental results are reproducible within ±0.5 per cent.

A temperature base of 298.16° K is taken for heat content measurements. Measurements were made at five temperatures (260, 440, 620, 800 and 980°F). It was necessary to preheat the sample above the maximum experimental temperature to eliminate volatile constituents. Assuming the weight loss on pre-heating was mostly water, a correction to the observed heat content was made to account for the water originally present in the sample. This latter procedure was followed in the determination of calculated heat contents as will be described later. The apparatus and the method of measure-

TABLE 1—DESCRIPTION OF TEST SAMPLES

Sample	Description	Porosity	Principal Minerals: Quartz (per cent)	Principal Minerals: Clay Mineral	Principal Minerals: Other
1—Sandstone	Well-cons., med.-coarse grain	0.196	80	Tr. Kaolin.	Tr. Pyrite
2—Sandstone	Poor-cons., med.-fine grain	0.273	40	Illite (?)	Feldspars
3—Silty Sand	Poor-cons., poorly sorted	0.207	20	Kaolin. type	Feldspars
4—Silty Sand	Medium hard, poorly sorted	0.225	20	Kaolin. type	Feldspars
5—Siltstone	Medium hard, broken	0.296	20	Kaolin. type	Feldspars
6—Siltstone	Hard	0.199	25	Illite	Feldspars
7—Shale	Hard, laminated	0.071	40	Illite-Kaolin.	----------
8—Limestone	Granular, uniform texture	0.186	....	----------	Ca. Carb.
9—Sand	Unconsolidated, fine-grained	0.38	100	----------	----------
10—Sand	Unconsolidated, coarse-grained	0.34	100	----------	----------

Revised manuscript received in office of Society of Petroleum Engineers March 3, 1958. Paper presented at Fall Meeting of Southern California Petroleum Section in Los Angeles, Oct. 17-18, 1957.

TABLE 2—CHEMICAL ANALYSES OF TEST SAMPLES

Sample	SiO_2	Al_2O_3	Fe_2O_3	MgO	CaO	Na_2O	K_2O	TiO_2	CO_2	H_2O
1—Sandstone	89.78	6.74	0.78	0.08	0.03	0.22	0.78	0.01	0.23	1.35
2—Sandstone	67.67	17.29*	3.78	1.55	1.96	1.84	1.02**	----*	2.05**	2.84
3—Silty Sand	66.02	17.66*	4.01	1.44	2.49	1.85	1.03**	----*	2.05**	3.45
4—Silty Sand	67.50	17.66*	3.24	1.70	2.08	1.84	1.02**	----*	2.05**	2.91
5—Siltstone	66.04	18.10*	4.39	1.39	1.38	1.86	1.03**	----*	2.07**	3.74
6—Siltstone	66.42	17.01	4.13	1.66	3.02	1.88	0.54	0.17	1.89	3.28
7—Shale	66.98	15.42	6.15	1.96	2.22	0.97	----	----	3.52	2.78
8—Limestone	0.30	0.07	0.03	0.45	55.19	----	----	----	43.77	0.19

*Reported Al_2O_3 includes TiO_2
**Estimated

ment employed did not permit heat content determination of fluid-saturated samples.

Heat capacity is by definition the first derivative of heat content with respect to temperature. This is represented by the slope of the heat content vs temperature curve at a given temperature. Variations of experimentally determined heat capacities with temperature are shown graphically in Figs. 1 and 2. The maximum deviation of the heat capacities between any of the samples at a given temperature is less than 10 per cent. The heavy smooth curves of Fig. 2 are calculated from heat content values from the literature[1] for pure quartz and pure calcite. It will be observed that the limestone curve follows closely the calcite curve. The quartz-rich sandstone curve closely approaches the pure quartz curve except at the two highest temperaures. This deviation may be due to experimental errors, for at these temperatures fairly significant differences between calculated and experimental values of heat content were observed. For the remaining samples the heat capacity appears to be a function of the silica-alumina ratio. In general, the lower this ratio the higher is the heat capacity. This is not true for the shale sample; the high iron content in this case appears to have a depressing effect on the heat capacity.

CALCULATED HEAT CAPACITIES

According to Kopp's law the heat content of a compound is equal to the sum of the heat contents of its constituent elements. Extension of this law for complex mineral assemblages such as sandstones, shales, and limestones was tested in the present study.

Heat content values for the constituent oxides of the rock samples were obtained from a compilation by Kelley[1]. Applying these values to the chemical analyses of the test samples, heat contents were calculated at each of the experimental temperatures. The heat contents for combined water were obtained by subtracting the heat contents for MgO from those for $Mg(OH)_2$. Heat contents for CO_2 were likewise obtained by subtracting the heat contents of CaO from $CaCO_3$. Fig. 3 shows a plot of calculated vs measured heat content values. The broken line is the diagonal representing perfect agreement between calculated and measured values. The maximum deviation is less than 2 per cent.

[1]References given at end of paper.

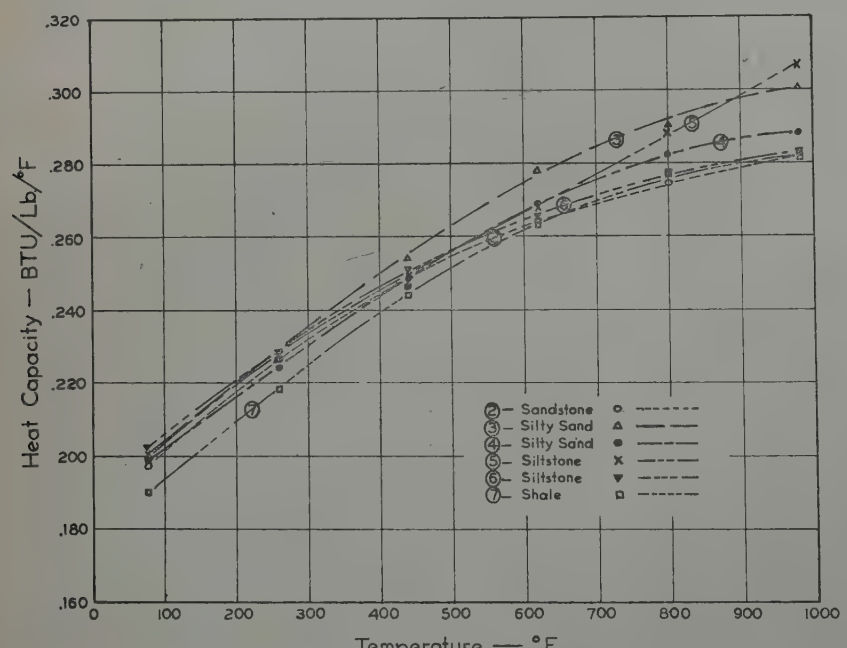

FIG. 1—EXPERIMENTAL HEAT CAPACITIES.

HEAT CAPACITY OF FLUID-SATURATED POROUS ROCKS

Based on the agreement between calculated and measured heat content of mineral aggregates, it was assumed that the heat content of fluid-saturated porous rocks may also be calculated by a summation of the heat content of the rock and fluid constituents, on a weight per cent basis. No accounting was made for heats of evaporation of fluid constituents. In reservoir calculations these additional heat requirements must be considered, but it is suggested that separate calculations be made based on prevailing temperature and pressure conditions.

Heat capacities per cubic foot of porous rock are reported in Table 3. The total volumes of saturating fluids per cubic foot of porous rock were calculated from the known porosities of the rock samples. The two fluids considered were water and methane. Heat capacities and specific weights for water were obtained from Keenan and Keyes[2]. Heat capacities for methane at atmospheric pressure and experimental temperatures were obtained by interpolation of API-U. S. Bureau of Standards data. Values of the heat capacities of methane at elevated pressures were calculated by methods outlined by Edmister.[3]

The effects of methane and water saturations on the heat capacity of the several rock samples at one temperature (620°F) are shown in Table 3. It will be observed that vapor or gas saturation has negligible effect on heat capacities of rocks. This is due primarily to the relatively small mass of gas or vapor which can occupy the pore space of rocks. The presence of liquids may, on the other hand, significantly alter the heat capacities of the rocks. The effect of liquid- and vapor-phase water saturation on the heat capacity of sandstone Sample 2 is shown in Fig. 4. The presence of liquid water may increase the heat capacity by 35 per cent or more, depending upon the prevailing pressures and temperatures.

Heat capacity data for crude oils at elevated pressures and temperatures are generally unavailable. From reported values at atmospheric pres-

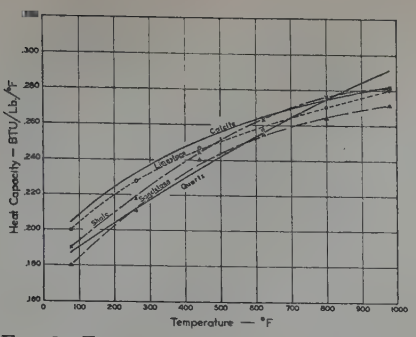

FIG. 2—EXPERIMENTAL HEAT CAPACITIES.

sure and temperature, it may be deduced that crude oil saturation will increase heat capacity of rocks by about one-half the amount of the increase by water saturation.

THERMAL CONDUCTIVITY

Thermal conductivities of the several rock samples were measured by a comparative-type apparatus similar to that described by Zierfuss and van der Vliet[4]. To determine thermal conductivity, the steady-state heat flow characteristics of the test samples are compared to those of a crown glass standard. The average operating temperature at which the present measurements were made was 90°F.

Samples 1, 6, 7 and 8 were sufficiently well consolidated to permit preparation of the necessary test specimens. Samples 2 through 5 were either too poorly consolidated or too broken to provide satisfactory specimens. As a consequence, it was necessary to disaggregate these samples to pass a 35-mesh screen and pack the loose material into the test chamber. The original porosities of these samples could not be restored by this method without causing damage to the test chamber. To examine effects of repacking on thermal conductivity, duplicate tests at constant porosity were run on Samples 9 and 10. No significant difference was noted for Sample 10 and the difference for Sample 9 was within the observed limits of reproducibility (±5 per cent).

Results of thermal conductivity measurements are shown in Table 4. The important influence of liquid saturation on the thermal conductivity of porous rocks is apparent. The increase in conductivity is related to the conductivity of the saturating fluid. An approximate correlation between rock and fluid properties and thermal conductivity has been developed by Asaad.[5] This correlation may be expressed as follows.

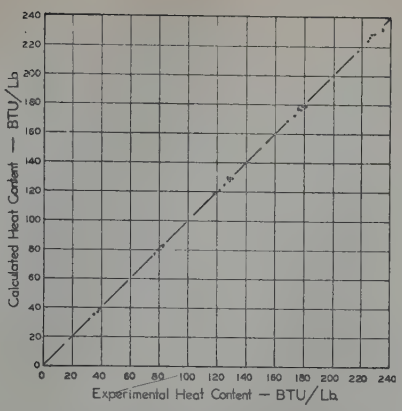

FIG. 3—COMPARISON OF CALCULATED AND MEASURED HEAT CONTENTS.

$$\frac{K}{k_1} = \left(\frac{k_2}{k_1}\right)^m,$$

where K is thermal conductivity of fluid-saturated rock, k_1 is thermal conductivity of rock solids, k_2 is thermal conductivity of the saturating fluid, m is an empirical exponent = $c \times \phi$, ϕ is fractional porosity, and c is a correlation factor $\cong$ 1.0.

The quantity k_1 is difficult to evaluate. Randomly oriented quartz crystals in good thermal contact have a thermal conductivity of approximately 5.0 Btu/hr sq ft ° F/ft[1]. The thermal conductivity of feldspar is considerably lower, approximately 1.2 Btu/hr sq ft°F/ft. Asaad proposed the extrapolation of a logarithmic plot of K vs k_2 data, for the same core saturated with fluids of different conductivities, until $K = k_2$. The value obtained is assumed to be the thermal conductivity of the rock solids. This procedure was followed for several of the test samples, where there were sufficient data, and the resulting k_1 values are shown in Table 5. It will be observed that the quartz-rich samples show values of k_1 close to that of pure quartz crystals. The feldspar-rich samples give values closer to that of feldspar.

The exponent m and the factor c have also been evaluated and are reported in Table 5. A value of c close to unity applies generally to the unconsolidated samples, but a marked deviation from unity is observed for the consolidated samples. This deviation cannot be explained entirely on the basis of differences in mineral composition as was proposed by Asaad. It would appear likely that a factor related to the structural characteristics of the rock matrix would improve the correlation.

Assuming a value of c equal to unity, conductivity values for the disaggregated samples at original porosities were estimated. These values are shown in parentheses in Table 6.

The present apparatus did not permit thermal conductivity measurements at elevated pressures or temperatures. Early work by Birch and Clark[6] indicated that the thermal conductivity of most minerals and rocks decreases markedly with increased temperature. Results reported for a quartzitic sandstone and a limestone have been reproduced in Fig. 5. Increased overburden pressure should improve grain contact and increase thermal conductivity.

THERMAL DIFFUSIVITY

In nonsteady-state conduction of heat in a body, the temperature and temperature distribution are controlled by the thermal conductivity and the thermal storage capacity of

TABLE 3—CALCULATED HEAT CAPACITIES OF FLUID-SATURATED ROCKS
(Heat Capacity at 620°F and Pressure Indicated—Btu/cu ft/°F)

	14.7 Psia			500 Psia		1,500 Psia		3,000 Psia	
Sample	Dry	Methane	Water	Methane	Water	Methane	Water	Methane	Water
1—Sandstone	34.0	34.0	34.0	34.1	34.1	34.3	34.9	34.6	45.9
2—Sandstone	32.9	32.9	32.9	33.0	33.0	33.3	34.0	33.7	47.6
3—Silty Sand	35.6	35.6	35.6	35.7	35.7	36.0	36.5	36.3	49.1
4—Silty Sand	33.5	33.5	33.5	33.5	33.6	33.9	34.5	34.3	48.3
5—Siltstone	32.0	32.0	32.0	32.1	32.1	32.5	33.2	32.9	48.7
6—Siltstone	33.6	33.6	33.6	33.7	33.7	34.0	34.6	34.3	47.7
7—Shale	39.6	39.6	39.6	39.6	39.6	39.7	40.0	39.9	40.1
8—Limestone	35.4	35.4	35.4	35.5	35.5	35.7	36.2	36.0	46.8

TABLE 4—MEASURED THERMAL CONDUCTIVITIES AT 90°F
(Thermal Conductivity—Btu/Hr sq ft °F/Ft)

Sample	Porosity	Air	Oil[1]	Water[2]	Oil and Water[3]
1—Sandstone	0.196	0.507	0.787	1.592	1.425
2—Sandstone[4]	0.40	0.285	0.577	1.050	.....
3—Silty Sand[4]	0.40	0.285	.....	.....	.....
4—Silty Sand[4]	0.43	0.261	0.625	1.110	.....
5—Siltstone[4]	0.36	0.338	0.553	1.036	.....
6—Siltstone	0.199	0.396		Core Damaged	
7—Shale	0.071	0.603	.....	0.975	.....
8—Limestone	0.186	0.983	1.245	2.050	1.690
9—Sand (Fine)	0.38	0.362	(0.80)	1.590	.....
Run 2	0.38	0.345	.....	.....	.....
10—Sand (Coarse)	0.34	0.322	0.950	1.775	.....
Run 2	0.34	0.323	.....	.....	.....

[1]Light lubricating oil, $k_2 = 0.077$
[2]Distilled water, $k_2 = 0.353$
[3]Approximately 35 per cent water—65 per cent oil
[4]Disaggregated samples

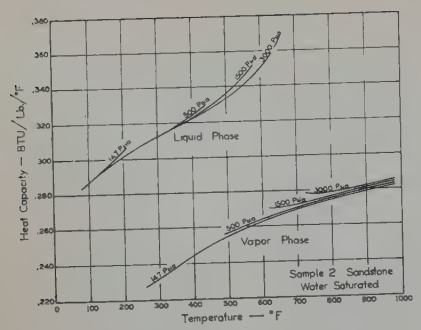

FIG. 4—INFLUENCE OF PRESSURE AND TEMPERATURE ON HEAT CAPACITY OF A WATER-SATURATED ROCK.

the body. Thermal diffusivity, an expression of the latter quantities, is defined as the ratio of thermal conductivity to the product of weight density and heat capacity. In many engineering applications, this quantity is considered to be a constant for a given material[7].

Thermal diffusivities for the rock samples tested have been calculated and are shown in Table 6. Values were calculated for the cores fully saturated with air and with water at atmospheric pressure and temperature of 90°F. Since heat capacity increases with temperature and thermal conductivity for rocks may be assumed to decrease with increased temperature, the effect of temperature on diffusivity may be large. The present data did not permit evaluation of this variation because of the lack of thermal conductivity data at elevated temperatures. However, calculations were made for a dry quartzitic sandstone based on thermal conductivity data from Birch and Clark[6] and heat capacity data from Kelley[1]. Results of the calculations are shown graphically in Fig. 6.

CONCLUSIONS

1. Heat capacities of rocks may be calculated from chemical analyses with considerable accuracy. Reasonable estimates of heat capacity can be made from a knowledge of the mineral content. In general, quartz-rich rocks display lower heat capacities than do rocks with high feldspar and clay content.

2. Calculated heat capacities of fluid-saturated rocks show that gas or vapor saturation has minor effect on heat capacity. Liquid water saturation may increase the heat capacity by more than 35 per cent, depending on the prevailing temperature and pressure and the porosity of the rock. Crude oil saturation may be expected to increase heat capacity by about one-half of this amount.

3. Considerably more work is needed to correlate thermal conductivity of fluid-saturated rocks with other characteristics of the rock and the saturating fluid. High quartz content rocks with good grain contact display higher thermal conductivities than do rocks with high feldspar and clay mineral content and poorer grain contact. Liquid saturation increases thermal conductivity markedly; the amount of increase is dependent upon the thermal conductivity of the saturating fluid. The influence of elevated pressures and temperatures on thermal conductivity was not investigated but earlier work[6] indicated that these effects could be large. In general, the thermal conductivity of rocks decreases with increased temperature.

4. Calculations show that thermal diffusivity is very sensitive to temperature changes, decreasing with increased temperature. Additional work is needed to evaluate the influence of elevated temperatures and pressures on the thermal diffusivity of fluid-saturated rocks.

TABLE 5—CALCULATED CORRELATION VALUES

Sample	k_1	m	ϕ	c
1—Sandstone	5.7	0.460	0.196	2.3
2—Sandstone	2.2	0.395	0.40	1.0
4—Silty Sand	2.3	0.385	0.43	0.9
5—Siltstone	2.2	0.410	0.36	1.1
8—Limestone	4.8	0.325	0.186	1.7
9—Sand (Fine)	5.4	0.445	0.38	1.2
10—Sand (Coarse)	5.4	0.410	0.34	1.2

TABLE 6—CALCULATED THERMAL DIFFUSIVITIES

Sample	Bulk Density (lb/cu ft) Air	Bulk Density (lb/cu ft) Water	Heat Capacity (Btu/lb/°F) Air	Heat Capacity (Btu/lb/°F) Water	Thermal Conductivity (Btu/hr sq ft °F/ft) Air	Thermal Conductivity (Btu/hr sq ft °F/ft) Water	Thermal Diffusivity (sq ft/hr) Air	Thermal Diffusivity (sq ft/hr) Water
1—Sandstone	130	142	0.183	0.252	0.507	1.592	0.0213	0.0445
2—Sandstone (Original)	90	115	0.200	0.374	0.285	1.050	0.0158	0.0244
3—Silty Sand (Original)	109	126	0.200	0.308	(0.34)*	(1.32)	(0.0156)	(0.0340)
4—Silty Sand (Original)	90	115	0.202	0.376	0.285	(1.05)	0.0157	(0.0242)
5—Siltstone (Original)	119	132	0.202	0.288	(0.40)	(1.50)	(0.0167)	(0.0394)
6—Siltstone	85	112	0.200	0.393	0.261	1.110	0.0153	0.0249
7—Shale	116	130	0.200	0.286	(0.47)	(1.51)	(0.0202)	(0.0406)
8—Limestone	96	118	0.202	0.351	0.338	1.036	0.0174	0.0250
9—Sand (Fine)	105	123	0.202	0.318	(0.44)	(1.29)	(0.0207)	(0.0329)
10—Sand (Coarse)	120	132	0.204	0.276	0.396	(1.51)	0.0162	(0.0414)
	145	149	0.192	0.213	0.603	0.975	0.0216	0.0307
	137	149	0.202	0.266	0.983	2.050	0.0355	0.0517
	102	126	0.183	0.339	0.362	1.590	0.0194	0.0372
	109	130	0.183	0.315	0.322	1.775	0.0161	0.0433

*Values in parentheses estimated

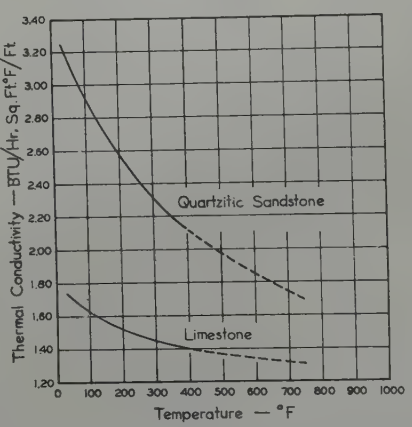

FIG. 5—VARIATION OF THERMAL CONDUCTIVITY WITH TEMPERATURE (BIRCH AND CLARK[2]).

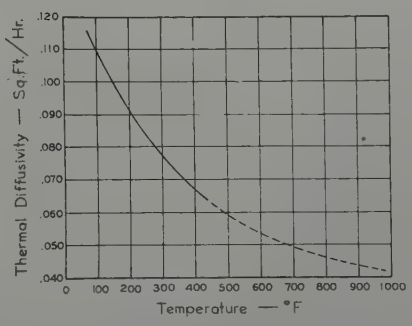

FIG. 6—ESTIMATED THERMAL DIFFUSIVITY OF QUARTZITIC SANDSTONE (KELLEY[1] AND BIRCH AND CLARK[2]).

ACKNOWLEDGMENTS

The author wishes to acknowledge the assistance of the following: Richfield Oil Corp. for partial financial support; Richard Thornton, graduate student in petroleum engineering, who did much of the experimental work; and K. K. Kelley, supervising engineer, Thermodynamics Station, USBM, for his many helpful suggestions.

REFERENCES

1. Kelley, K. K.: "Contributions to the Data on Theoretical Metallurgy", *Bull.*, USBM (1949) 476.
2. Keenan, J. H., and Keyes, F. G.: *Thermodynamic Properties of Steam*, John Wiley & Sons, Inc., N. Y., 1936.
3. Edmister, U. C.: "Applications of Thermodynamics to Petroleum Processing: Part XIII—Heat Capacities", *Petroleum Refiner* (1948) **27**, No. 11, 609.
4. Zierfuss, H., and van der Vliet, G.: "Laboratory Measurements of Heat Conductivity of Sedimentary Rocks", *Bull.*, AAPG (1956) **40**, No. 10, 2475.
5. Asaad, Yousri: "A Study of the Thermal Conductivity of Fluid Bearing Porous Rocks" PhD thesis, U. of Calif., (June, 1955).
6. Birch, F., and Clark, H.: "The Thermal Conductivity of Rocks and Its Dependence upon Temperature and Composition", *American Journal of Science*, (1940) **238**, Part I, No. 8, 529; also Part II, No. 9, 613.
7. Giedt, W. H.: *Principles of Engineering Heat Transfer*, D. Van Nostrand, Princeton, N. J. (1957). ★★★

Bubble Point Pressure Correlation

J. A. LASATER | MAGNOLIA PETROLEUM CO.
DALLAS, TEX.

ABSTRACT

A correlation of the bubble point pressure for black oil systems is developed using the standard physical-chemical equations of solutions. The correlation is based on 158 experimentally measured bubble point pressures of 137 independent systems and is expressed in terms of the usually measured field parameters—flash separation gas-oil ratio, tank oil gravity, total gas gravity, and reservoir temperature.

The data were obtained on systems produced in Canada, Western and Mid-Continental United States, and South America. The average error (algebraic) in the representation is 3.8 per cent, and the maximum error encountered is 14.7 per cent.

INTRODUCTION

In the absence of experimentally measured properties of reservoir fluids, it is often necessary for the field engineer to make estimates regarding the fluid properties based on the usually measured producing parameters. To aid in these estimations, various correlations have appeared in the literature in recent years. Among the pertinent properties of interest is the bubble point pressure. A correlation for this parameter has been reported by Standing[1]. However, this correlation was based essentially on California produced crudes and this limitation was pointed out with its presentation. The correlation presented in this paper utilized data on crude oil systems from Canada, Western and Mid-Continental United States, and South America.

Original manuscript received in Society of Petroleum Engineers office Sept. 15, 1957. Revised manuscript received April 3, 1958. Paper presented at Fall Meeting of Southern California Petroleum Section in Los Angeles, Oct. 17-18, 1957.

[1]References given at end of paper.

CORRELATION DEVELOPMENT

The basic assumption used in this development is the same as employed by Standing[1],

$$p_b = f(R, \gamma_g, t, \Gamma). \quad . \quad . \quad . \quad (1)$$

There is a wide variety of ways to combine these parameters; however, in this instance the combination was made on the basis of Henry's law[2]. Accordingly, the relationship proposed is

$$p_b = y_g H'. \quad . \quad . \quad . \quad . \quad . \quad . \quad (2)$$

Although Eq. 2 defines an individual system, it is of limited value since H' is a function of gas-phase composition and the system temperature.

It was observed that for the systems where the bubble point was measured at several temperatures that the ratio of the bubble point pressures and the ratio of the corresponding absolute temperatures (°R) were practically identical. Thus, for correlation purposes the bubble point pressure may be taken as a direct function of the absolute temperature. This relation is valid only for those systems that are not near the critical point. Accordingly, this correlation will be inadequate for systems in the region of the critical point.

The solubility of the various hydrocarbons found in the gas phase increases with the molecular weight. Thus, the saturation pressure should be inversely related to the gas gravity.

Applying these principles to Eq. 2 and rearranging terms gives:

$$\frac{(p_b)(\gamma_g)}{T} = y_g H \quad . \quad . \quad (3)$$

The variables on the left side of Eq. 3 were designated as the "bubble point pressure factor".

$$p_f = \frac{n_g}{n_g + n_o} H \quad . \quad . \quad . \quad (4)$$

The number of mols of tank oil per barrel is a function of the "molecular weight" of the tank oil. Although the tank oil is a complex mixture, it was assumed for the purposes of this correlation that a unique molecular weight could be assigned to a given oil. This was designated as the "effective molecular weight", and was related to the oil gravity,

$$M_o = f(\Gamma). \quad . \quad . \quad . \quad . \quad . \quad (5)$$

This empirical relationship was developed simultaneously with the correlation by assuming values of M_o and working to obtain a smooth curve for both the correlation and the effective molecular weight. The relationship between the oil gravity and the effective molecular weight used in this correlation is shown in Fig. 1.

The effective molecular weight is somewhat higher than the molecular weight of the C_{7+} fraction. The difference between these values is largest for the low-gravity systems. It is noted that this effective molecular

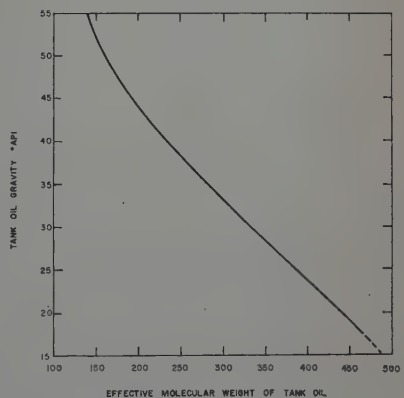

FIG. 1—EFFECTIVE MOLECULAR WEIGHT RELATED TO TANK OIL GRAVITY.

weight relationship corresponds closely to that given for crude oil systems with a UOP characterization factor[3] of 11.8.

The relationship between the bubble point pressure factors calculated from the experimental data and the gas mol fraction is shown graphically in Fig. 2. Representative values of the curve are given in Table 1. Since the representation of Fig. 2 is not a linear function of the variables, H is not a constant. Thus, a simple analytical expression was not obtained, and it is necessary to rely on the graphical representation of Fig. 2 to obtain p_f from y_g.

The bubble point pressure for a given gas-oil system may be obtained from the correlation by the utilization of Figs. 1 and 2. The effective molecular weight is established from the crude oil gravity, Fig. 1, and the gas mol fraction is obtained from the following equation.

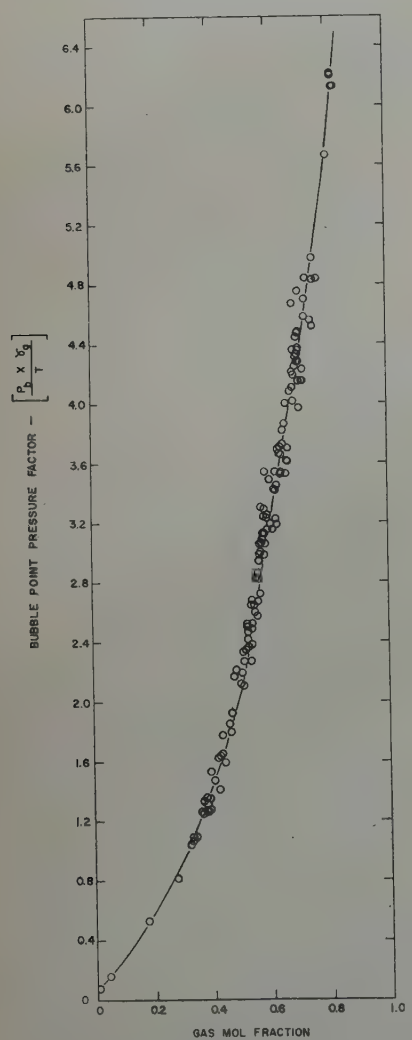

FIG. 2—CORRELATION OF BUBBLE POINT PRESSURE FACTOR.

TABLE 1—SMOOTHED BUBBLE POINT FACTOR FUNCTION

Gas Mol Fraction	Bubble Point Pressure Factor
0.05	0.17
0.100	0.30
0.150	0.43
0.200	0.58
0.250	0.75
0.300	0.94
0.350	1.19
0.400	1.47
0.450	1.74
0.500	2.10
0.550	2.70
0.600	3.29
0.650	3.80
0.700	4.30
0.750	4.90
0.800	5.70
0.850	6.70

$$y_g = \frac{R/379.3}{R/379.3 + \frac{350\,\gamma_o}{M_o}}. \quad . \quad (6)$$

The value of the gas mol fraction is applied in Fig. 2 to obtain the bubble point pressure factor. The bubble point pressure is calculated by use of the following equation

$$p_b = \frac{(p_f)(t + 459.6)}{\gamma_g}. \quad . \quad (7)$$

The 158 experimentally determined bubble point pressures of the 137 independent crude oil systems were compared with the values predicted by the correlation. This comparison showed an algebraic deviation of 3.8 per cent. Approximately 21 per cent of the data points show a deviation of 0.5 per cent, and 80 per cent have a deviation of less than 6.5 per cent. The maximum error encountered was 14.7 per cent.

The ranges of the field measured parameters covered in this correlation were as follows.

Bubble point pressures	48-5780 psia
Flash gas-oil ratios	3-2905 cu ft/bbl
Tank oil gravities	17.9-51.1° API
Total Gas gravities (air = 1.0)	0.574-1.223
Reservoir temperatures	82-272°F
Separator stages (stock tank = 1)	1-3
Separator temperatures	34-106°F
Separator pressures	15-605 psia

This correlation was based on systems essentially free of non-hydrocarbon material. The presence of large amounts of nitrogen, carbon dioxide, hydrogen sulfide, etc., will result in the predicted bubble point being low. The following is given as a guide to the effect of the presence of non-hydrocarbon materials.

Component	Per Cent of Gas	Error in Predicted p_b (Per Cent low)
Carbon dioxide	9.1	5.0
Hydrogen sulfide Carbon dioxide	3.1 3.1	1.1
Nitrogen Carbon dioxide	2.5 0.3	2.7

A calculation chart has been prepared based on this correlation that permits rapid graphical evaluation of the predicted bubble point. This calculation chart is shown in Fig. 3. The error distribution using the calculation chart is essentially the same as found for the correlation.

CONCLUSION

The correlation is generally applicable to a large number of producing areas and provides a rapid method of estimating the bubble point pressure of crude systems with a reasonable degree of accuracy.

NOMENCLATURE

f = function
γ_g = total gas gravity (air = 1.0)
γ_o = tank oil specific gravity
H' = general Henry's law constant
H = specific Henry's law constant (independent of gas composition and temperature)
M_o = effective molecular weight of tank oil
n_g = mols of gas
n_o = mols of tank oil
y_g = mol fraction of gas
p_b = bubble point pressure, psia
p_f = bubble point pressure, factor
R = total flash separation gas-oil ratio, cu ft/bbl (measured at 60°F)
Γ = tank oil gravity, °API (corrected to 60°F)
t = temperature, °F
T = absolute temperature, °R

ACKNOWLEDGMENT

The author is indebted to C. A. Connally and L. G. Sharp for their many helpful suggestions pertaining to the phase behavior of fluids, and to the Magnolia Petroleum Co. for permission to publish this work.

REFERENCES

1. Standing, M. B.: *Drill. and Prod. Prac.*, API (1947) 275.
2. Hougen, O. A., and Watson, K. M.: *Chemical Process Principles*, John Wiley & Sons, Inc., N. Y. (1943) **1**, 146.
3. Watson, K. M., and Murphy, G. F.: *Ind. Engr. Chem.* (1935) **27**, 1460.

★★★

FIG. 3—CHART FOR CALCULATION OF BUBBLE POINT PRESSURE.

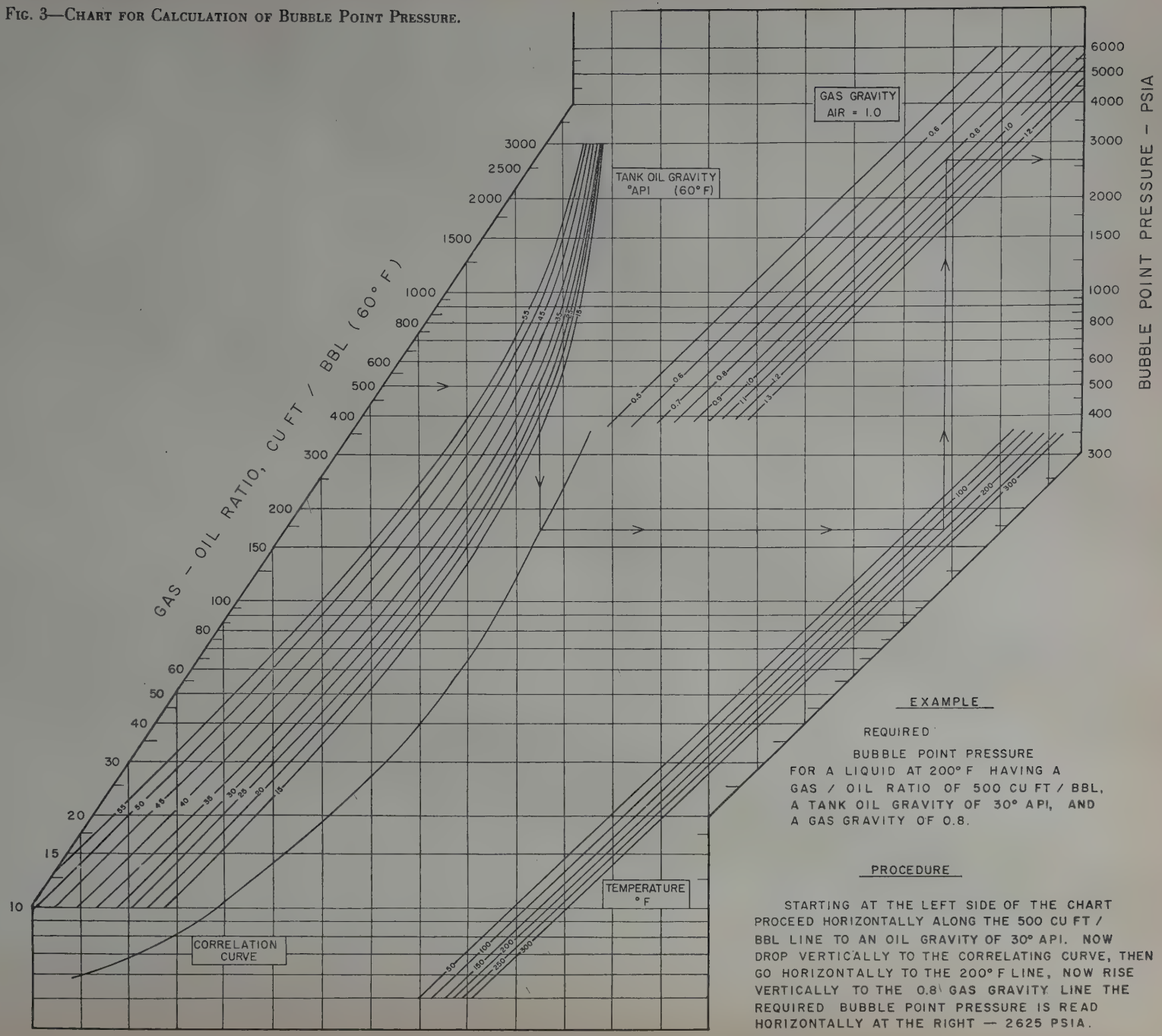
GAS - OIL RATIO, CU FT / BBL (60° F)
BUBBLE POINT PRESSURE - PSIA
GAS GRAVITY AIR = 1.0
TANK OIL GRAVITY °API (60° F)
TEMPERATURE °F
CORRELATION CURVE
EXAMPLE
REQUIRED
BUBBLE POINT PRESSURE FOR A LIQUID AT 200° F HAVING A GAS / OIL RATIO OF 500 CU FT / BBL, A TANK OIL GRAVITY OF 30° API, AND A GAS GRAVITY OF 0.8.
PROCEDURE
STARTING AT THE LEFT SIDE OF THE CHART PROCEED HORIZONTALLY ALONG THE 500 CU FT / BBL LINE TO AN OIL GRAVITY OF 30° API. NOW DROP VERTICALLY TO THE CORRELATING CURVE, THEN GO HORIZONTALLY TO THE 200° F LINE, NOW RISE VERTICALLY TO THE 0.8 GAS GRAVITY LINE THE REQUIRED BUBBLE POINT PRESSURE IS READ HORIZONTALLY AT THE RIGHT — 2625 PSIA.

T. N. 2010

Laboratory Evaluation of Prospective Enriched Gas-Drive Projects

D. M. KEHN
MEMBER AIME
G. T. PYNDUS
ASSOCIATE MEMBER AIME
M. H. GASKELL
JUNIOR MEMBER AIME

HUMBLE OIL & REFINING CO.
HOUSTON, TEX.

INTRODUCTION

Much attention has been given in the past few years to methods of increasing the recovery of oil from proven reserves. Numerous laboratories have made investigations to evaluate the possibilities of increased oil recovery by high-pressure injection of dry gas, injection of a propane slug followed by dry gas, solvent flooding, and by the injection at relatively low pressures of gases enriched with ethane and propane. Several years ago, Whorton and Kieschnick[1] published the results of laboratory studies on high-pressure gas injection which showed that, in the case of light oils, recoveries could be considerably increased by sweeping the reservoir with dry gas at pressures in excess of 3,000 psig. The increase was attributed by those authors to the vaporization of oil at the invading gas front and viscosity and solubility effects produced at the front by the invading gas.

Later, Stone and Crump[2] presented the results of a series of displacement experiments in which a light undersaturated crude oil was displaced from sand-packed columns with unusually high recoveries when the displacing gas was a rich condensate or a dry gas enriched with ethane or propane. They also conducted similar experiments at higher pressure on heavy undersaturated crude oil, although in this case the increase in recovery was not as great as in the case of the light oils. In both cases, viscosity reduction and swelling of the by-passed oil behind the invading gas front were believed to be responsible for the more favorable recovery of the original oil in place.

Within the past year, other investigators[3,4] have presented the results of laboratory studies of miscible slug and solvent flooding recovery processes. This paper describes the laboratory methods developed for evaluating benefits to be obtained by enriched gas drive in specific reservoirs, and presents the results of several displacements of crude oils which possess a wide range of physical properties. The displacements were conducted at reservoir conditions of temperature and pressure.

DESCRIPTION OF THE APPARATUS AND PROCEDURE

The apparatus used in the following experiments consisted of a sand-packed tube which served as the model reservoir, a cylinder of injection fluid, and a mercury pump. The stainless steel tube, 8 ft long and 0.53 in. ID, was packed with a graded quartz sand. The high-pressure pump discharged mercury into the bottom of the injection fluid cylinder at a constant rate as low as 1 cc/hr. The average porosity and permeability of the sand column were 34.6 per cent and 3.25 darcies, respectively. In each case the tube was charged by the displacement of salt water by the reservoir oil under consideration.

EVALUATION OF OIL RECOVERY FROM FOUR FIELDS

Recently a project was initiated to evaluate oil recovery by enriched gas drive from three oil reservoirs. Samples from a fourth reservoir (in this case high-viscosity oil) were studied with a view to obtaining recovery information of general applicability to low-grade, high-viscosity crudes. The oils from these four reservoirs exhibited a wide range of physical properties, and the reservoir conditions of pressure and temperature simulated in the laboratory represented several typical field conditions under which enriched gas drive might be employed.

INTERMEDIATE-GRAVITY CRUDE

One of the reservoirs selected for laboratory displacement experiments produced an intermediate-gravity crude (29.6° API) by solution gas drive and a weak water drive. A low recovery in the range of 10 to 20 per cent was anticipated. Four displacement experiments were made to determine the effect of injection gas composition and initial gas saturation upon recovery of oil from the laboratory model.

Two types of reservoir oil were used in these experiments. In the first run, a desaturated crude with a bubble point of 395 psi was charged to the tube. In the three subsequent runs, a simulated original reservoir oil was charged at 2,000 psi and produced by solution gas drive to 300 psi before beginning gas injec-

Original manuscript received in Society of Petroleum Engineers office July 19, 1957. Revised manuscript received April 14, 1958. Paper presented at 32nd Annual Fall Meeting of Society of Petroleum Engineers in Dallas, Tex., Oct. 6-9, 1957.
[1]References given at end of paper.

tion. The properties of this oil are shown in Table 1 as Oil A.

Three different gases were used for this series of displacements. The first two runs were made using a mixture of propane and a low-pressure separator gas containing 9.3 per cent propane and heavier. The third run was made with the low-pressure separator gas alone. The fourth run utilized a slug of enriched gas driven by a dry plant residue gas containing 0.5 per cent propane plus.

There was little difference in recovery between the first two runs. In Run 1, a gas saturation did not exist in the tube at the start of gas injection, but in Run 2, a gas saturation was present. These results are shown in Table 2. They indicate that in both cases the invading enriched gas was sufficiently miscible with the oil to produce conditions necessary for high recovery. The results of Runs 3 and 4 are also shown in Table 2. In Run 3, oil was displaced with separator gas alone to serve as a basis for comparison with the enriched gas displacements. In Run 4, in which the enriched injection gas was introduced as a slug followed by plant residue gas, a high recovery was achieved at one pore volume gas injected. This was attributed to the lower injection rate used in this run; the low rate permitted more nearly complete equilibrium to be established between the invading gas and the resident fluid.

TABLE 1—PROPERTIES OF CRUDE OILS

Component	A Mol Per cent	B Mol Per cent	C Mol Per cent	D Mol Per cent	E Mol Per cent
Methane	29.26	39.37	43.81	7.18	2.40
Ethane	4.22	4.71	4.72	0.63	0.28
Propane	4.99	2.98	2.86	0.84	0.88
Iso-Butane	1.29	0.97	0.91	0.79	0.83
n-Butane	3.32	0.90	0.85	0.85	1.69
Iso-Pentane	2.29	0.87	0.80	0.52	1.96
n-Pentane	1.72	0.83	0.76	0.96	2.00
Heavier Fraction	52.91	49.37	45.29	88.23	89.94
Total	100.00	100.00	100.00	100.00	100.00
GOR, cu ft/bbl	359	600	747	38	11
Saturation pressure, psig	1,650 (150° F)	2,520 (190° F)	3,190 (190° F)	300 (151° F)	90 (147° F)
Viscosity at saturation pressure, cp	2.15	0.320	0.260	19.0	26.8
Gravity, °API	29.6	39.3	39.0	21.5	21.9

TABLE 2—RESULTS OF DISPLACEMENTS USING INTERMEDIATE-GRAVITY CRUDE (30° API)

Run No.	Saturation pressure (psi at 150° F)	Injection gas*	Displacement pressure (psi)	At One Pore Volume Gas Injected		Final Conditions		
				Recovery (Per cent)	GOR (cu ft/bbl)	Recovery (Per cent)	GOR (cu ft/bbl)	Pore volumes gas injected
1	395	Separator gas + 41 per cent propane	2,000	60.7	2,200	86.3	65,900	2.95
2	1,650	Separator gas + 41 per cent propane	2,000	59.8**	1,600	93.3	31,910	2.60
3	1,650	Separator gas	2,000	40.4**	4,700	51.9	20,560	2.35
4	1,650	0.46 pore volume of 49 per cent C_1 — 20 per cent C_2 — 31 per cent C_3 — followed by plant residue gas	2,000	73.7**	300	88.2	27,300	1.39

*All gas analyses are given on mol per cent basis.
**Includes oil recovery by dissolved gas drive from 2,000 to 300 psi.

TABLE 3—RESULTS OF DISPLACEMENT USING HIGH-GRAVITY CRUDE (39° API)

Run No.	Saturation pressure (psi at 190° F)	Injection fluid	Displacement pressure (psi)	At One Pore Volume gas injected		Final Conditions		
				Recovery (Per cent)	GOR (cu ft/bbl)	Recovery (Per cent)	GOR (cu ft/bbl)	Pore volumes gas injected
5	2,520	Separator gas	2,550	25.5	9,750	30.9	39,400	1.80
6	2,520	Separator gas	3,500	43.6	10,000	47.1	88,300	1.49
7	2,520	60 per cent separator gas — 30 per cent C_2 — 10 per cent C_3	3,000	87.0	2,700	90.2	10,200	1.20
8	3,190	80 per cent separator gas — 20 per cent C_2	3,000	47.3*	6,800	50.2	11,300	1.23
9	3,190	59.1 per cent separator gas — 40.9 per cent C_2	3,000	75.5*	3,200	81.2	28,000	1.38
10	3,190	63.9 per cent separator gas — 36.1 per cent C_3	2,000	79.5*	1,170	91.7	40,900	1.71
11	3,190	1.13 P-V water followed by 48.5 per cent separator gas — 51.5 per cent C_3	2,000	87.2**	800	97.9	10,600	1.37
12	3,190	0.52 P-V slug of 50 per cent separator gas — 17.5 per cent C_2 — 32.5 per cent C_3 followed by separator gas	2,000	84.5*	830	99.8	15,540	1.50
13	3,190	0.10 P-V slug of 50 per cent separator gas — 17.5 percent C_2 — 32.5 per cent C_3 followed by separator gas	2,000	81.0*	2,850	84.0	15,930	1.18

*Includes oil recovery by dissolved gas drive from 3,190 to 2,000 psi.
**Includes oil recovery by dissolved gas and water drive, 68.7 per cent.

HIGH-GRAVITY CRUDE

A series of 16 displacements were made from the sand-packed model reservoir by using a high-gravity, low-viscosity crude oil from a reservoir partially pressure depleted by a combination of water and dissolved gas drive. These displacement experiments investigated the effect of pressure, gas composition, slug injection, water flooding prior to gas injection, and injection rate in the laboratory model upon recovery of oil. The results of nine of the more interesting of these runs are reported here.

Properties of the reservoir oil samples used in these experiments are given in Table 1 as Oils B and C. The first of these two samples represented the oil existing in the reservoir at the present time. The second sample represented a simulated original reservoir fluid.

Displacement with No Initial Gas Saturation

In the first three displacements, the sand-packed tube was charged with the oil sample having a bubble point of 2,520 psi. The first displacement was made with a field separator gas at 30 psi above the bubble point of the oil, and the second displacement was made at nearly 1,000 psi above the bubble point. The field separator gas contained 2.5 per cent propane and heavier. From the results of these displacements (Runs 5 and 6) shown in Table 3, it can be seen that increased recovery was obtained at the higher pressure. These recovery figures provided a basis for evaluating the effectiveness of the enriched gas-drive experiments which followed.

A third gas drive in which the displacing gas was a combination of separator gas, ethane, and propane was made on the 2,520-psi bubble point oil. This mixture was injected at 3,000 psi and at a rate calculated to advance the gas front about 4 ft/day. The results shown in Fig. 1 indicate that at 3,000 psi this mixture is fairly effective in displacing the oil from the sand-packed tube.

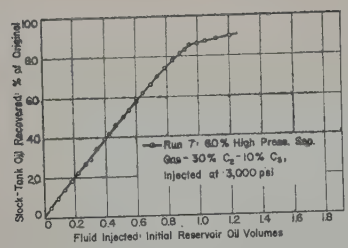
Stock-Tank Oil Recovered: % of Original
Run 7: 60% High Press. Sep. Gas - 30% C2 - 10% C3, Injected at 3,000 psi
Fluid Injected: Initial Reservoir Oil Volumes

FIG. 1—PER CENT RECOVERY VS VOLUME OF FLUID INJECTED—HIGH-GRAVITY CRUDE.

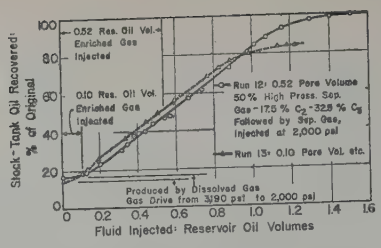
0.52 Res. Oil Vol. Enriched Gas Injected
0.10 Res. Oil Vol. Enriched Gas Injected
Run 12: 0.52 Pore Volume 50% High Press. Sep. Gas - 17.5 % C2 - 32.5 % C3 Followed by Sep. Gas, injected at 2,000 psi
Run 13: 0.10 Pore Vol. etc.
Produced by Dissolved Gas Gas Drive from 3,190 psi to 2,000 psi
Stock-Tank Oil Recovered: % of Original
Fluid Injected: Reservoir Oil Volumes

FIG. 2—PER CENT RECOVERY VS VOLUME OF FLUID INJECTED—HIGH-GRAVITY CRUDE. EFFECT OF SLUG SIZE.

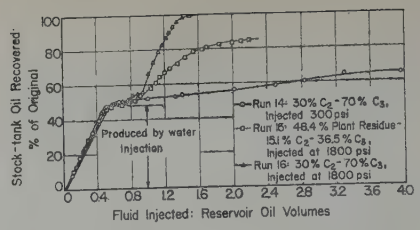
Run 14: 30% C2 - 70% C3, Injected 300 psi
Run 15: 48.4 % Plant Residue - 15.1 % C2 - 36.5 % C3, Injected at 1800 psi
Run 16: 30% C2 - 70% C3, Injected at 1800 psi
Produced by water injection
Stock-tank Oil Recovered: % of Original
Fluid Injected: Reservoir Oil Volumes

FIG. 3—PER CENT RECOVERY VS VOLUME OF FLUID INJECTED—LOW-GRAVITY CRUDE.

DISPLACEMENT WITH INITIAL GAS SATURATION

In the remainder of the runs using high-gravity crude, a 3,190-psi bubble point oil (Oil C) was charged to the tube and then was produced by dissolved gas drive until the pressure had declined to 2,000 psi. At this point, displacement experiments were conducted with the enriched gases.

Two runs (Runs 8 and 9) were conducted with ethane as the enriching agent added to field separator gas. The effect of the ethane content of the gas can be seen in Table 3.

In order to obtain some idea of the relative effectiveness of propane as an enriching component compared to ethane, a run was conducted using propane with separator gas. The results of the experiment (Run 10), which was made at 2,000 psi, are shown in the table. At this pressure, 36.1 per cent propane was more effective than 40 per cent ethane at 3,000 psi.

It was of interest to know what effect water flooding a sand prior to enriched gas injection would have on recovery. Accordingly, Run 11 was conducted by flooding the sand-packed tube with formation water after production of 19.5 per cent of the oil by solution gas drive. Water was injected continuously at 2,000 psi until no further oil was found in the effluent. A mixture of propane and separator gas was then injected at 2,000 psi. Although a considerable volume of water was produced after gas injection started, final oil recovery was high. These results indicate that high recoveries are possible by enriched gas drive even though sands have been previously invaded by water.

Runs 12 and 13 involved injecting enriched gas slugs at 2,000 psi and driving these slugs with separator gas. From Fig. 2, where per cent recovery is plotted vs pore volumes gas injected, it can be seen that the smaller slug gave a significantly lower recovery in the model reservoir.

LOW-GRAVITY CRUDE

The third reservoir studied produced a low-gravity (22° API), high-viscosity crude oil and was in an advanced stage of depletion by a combination dissolved gas and water drive. A series of three displacements were made to investigate under simulated reservoir conditions the effect of displacement pressure and gas composition on recovery from the sand-packed tube. For each of the three runs (Runs 14, 15, and 16), the sand-packed tube was charged with a simulated reservoir oil. The properties of this oil are given in Table 1 as Oil D.

Two injection gas mixtures were used in the three displacements. One displacement was made at the depleted pressure of the reservoir, and two displacements were made at the original reservoir pressure. For the first and third displacements, a mixture containing ethane and propane was used. In the second displacement, a mixture was injected which consisted of a dry plant residue gas, ethane, and propane.

The results of these displacements are tabulated in Table 4 and are presented in Fig. 3 where the per cent recovery is plotted vs the pore volumes of fluid injected. Inasmuch as the water percentage in the produced fluid from this reservoir is 25 per cent, water was injected prior to gas in the model until the fluid produced was approximately 25 per cent water.

In the first run, the model reservoir was charged and the displacement made at 300 psi. Total recovery obtained by both water flooding and gas drive amounted to 65 per cent. The second run was made with the methane-ethane-propane mixture at 1,800 psi. Although the gas used contained less of the enriching components, a higher recovery was obtained apparently because of the increased solubility of the gas in the oil.

The third run was made at 1,800 psi with the same ethane-propane mixture used for the first run. At the pressure and temperature of the run, the ethane-propane mixture was in the liquid state, and the displacement process could be termed a solvent flood. As anticipated under these conditions, complete recovery of the oil was obtained.

HIGH-VISCOSITY, UNDERSATURATED CRUDE

In order to determine what effect, if any, undersaturation had on the recovery of low-gravity, asphaltic crude oil, two displacements were made with this type of oil saturated at different pressures. The properties of the wellhead sample saturated at 90 psi are given in Table 1 as Oil E.

For the first run (Run 17), the saturation pressure of the wellhead sample was increased to 1,500 psi by the addition of methane. This sample had a GOR of 189 cu ft/bbl of 22.2° API gravity oil, and its vis-

TABLE 4—RESULTS OF DISPLACEMENTS USING LOW-GRAVITY CRUDE (22° API)

Run No.	Saturation pressure (psi at 151° F)	Injection fluid	Displacement pressure (psi)	At end water injection recovery (per cent)	At One Pore Volume Gas Injected		Final Conditions		
					Recovery (Per cent)	GOR (cu ft/bbl)	Recovery (Per cent)	GOR (cu ft/bbl)	Pore volumes gas injected
14	300	0.51 P-V water followed by 30 per cent C_2 — 70 per cent C_3	300	48.0	54.2	580	65.2	10,300	3.45
15	300	0.51 P-V water followed by 48.4 per cent residue gas — 15.1 per cent C_2 — 36.5 per cent C_3	1,800	46.8	77.9	3,200	85.3	69,143	1.59
16	300	0.46 P-V water followed by 30 per cent C_2 — 70 per cent C_3	1,800	45.4	99.8	10,000	100.0	28,040	1.12

cosity at the displacement conditions of 1,700 psi and 147°F was 12.4 cp. The gas used in this displacement was a methane-propane mixture.

In the second run (Run 18), the wellhead sample saturated at 90 psi was charged to the tube. This sample had a GOR of 20 cu ft/bbl of 22.4° API gravity oil, and its viscosity at the displacement conditions of 1,500 psi and 147°F was 34.5 cp.

The results of these two displacements are presented in Table 5. The agreement in recovery between these two runs indicated—in the case of viscous, low-gravity crudes — that saturated oils were as susceptible to efficient displacement by enriched gas drive as were undersaturated oils.

TABLE 5—RESULTS OF DISPLACEMENTS USING HIGH-VISCOSITY CRUDE

Run No.	Saturation pressure (psi at 147°F)	Viscosity (cp)	Injection fluid	Displacement Pressure (psi)	At One Pore Volume Gas Injected		Final Conditions		
					Recovery (per cent)	GOR (cu ft/bbl)	Recovery (per cent)	GOR (cu ft/bbl)	Pore volumes gas injected
17	1,500	12.4	59 per cent C_1 — 41 per cent C_3	1,700	58.5	310	91.0	67,000	2.25
18	90	34.5	59 per cent C_1 — 41 per cent C_3	1,500	59.5	400	92.2	29,000	1.79

LIMITATIONS OF TECHNIQUE

It should be recognized that the methods described in this report for estimating oil recovery by enriched gas drive are subject to certain limitations and that precautions should be taken in translating laboratory data to field performance. In cases where complete miscibility is established between invading fluid and resident oil, the effect of the porous medium in homogeneous systems appears to be of limited importance. When two-phase flow occurs in the sand or reservoir rock, factors such as capillary pressure and relative permeability characteristics must be considered. Under these circumstances, the recoveries from the sand-packed tube are at best *relative* to recoveries obtained by conventional recovery methods on the same model reservoir.

A second limitation in the application of the recovery results obtained from the sand-packed tube is the difference between the area swept in the model and that swept in the field reservoir rock by the particular driving fluid under consideration. Channeling, gravity segregation, and reservoir heterogeneities may in some cases be factors that significantly affect recovery from an actual reservoir. They must be taken into consideration in application of laboratory data obtained on homogeneous sand in small-diameter columns.

CONCLUSIONS

Based on the experimental work described in this report, the following conclusions were drawn.

1. Recovery of oil by injection of gases enriched with ethane, propane, or heavier components can be simulated in the laboratory by displacing the crude oil from a sand-packed tube at reservoir conditions of temperature and pressure with gases of interest. However, channeling, gravity segregation, reservoir heterogeneities, and other factors should be considered when applying the laboratory recoveries to field operations.

2. Concentrations of enriching components of the order of 40 to 50 mol per cent in the injection gas are required for these systems in order to effect recoveries above 80 per cent of the oil originally in place.

3. High water saturation does not prevent the effective displacement of the remaining oil when a sufficiently enriched gas is used as the driving fluid.

4. The presence of an initial gas saturation in the sand-packed tube does not prevent the attainment of high recoveries of intermediate-gravity oils by repressuring with enriched gas.

5. With high-gravity oils, substantial recoveries can be effected in the presence of a free gas saturation with repressuring.

6. High recoveries can be obtained by enriched gas drive whether the oil is originally saturated or undersaturated with gas at the displacement pressure.

REFERENCES

1. Whorton, L. P., and Kieschnick, W. L., Jr.: "Oil Recovery by High-Pressure Gas Injection," *Oil and Gas Jour.* (April 6, 1950) **48,** 78.
2. Stone, H. L., and Crump, J. S.: "The Effect of Gas Composition Upon Oil Recovery by Gas Drive," *Trans.* AIME (1956) **207,** 105.
3. Koch, H. A., Jr., and Slobod, R. L.: "Miscible Slug Process," *Trans.* AIME (1957) **210,** 40.
4. Hall, H. N., and Geffen, T. M.: "Laboratory Study of Solvent Flooding," *Trans.* AIME (1957) **210,** 48. ★★★

T. N. 2011

The Effective Compressibility of Reservoir Rock and Its Effects on Permeability

A. S. McLATCHIE
R. A. HEMSTOCK
J. W. YOUNG
MEMBER AIME

IMPERIAL OIL LTD.
CALGARY, ALTA.

ABSTRACT

Results and experimental procedures are presented covering a preliminary laboratory investigation of the compaction of reservoir rocks and its effect on porosity and permeability.

"Effective" compressibility was measured by subjecting core material to an overburden load and reducing pore pressure. Preliminary results showed relatively high effective compressibilities which varied from 1.8×10^{-6} *pore volume/pore volume/lb/in.*^{2} *for limestones to* 7.7×10^{-6} *pore volume/pore volume/lb/in.*^{2} *and even higher for sandstone reservoirs containing large amounts of fine clay material. It appeared from the initial results that the effective compressibility of the material could not be correlated directly with porosity and that other factors, such as the amount of clay material present might have to be taken into account. The work to date has indicated that effective compressibility factors will have to be measured for the particular reservoirs being studied.*

Oil permeability of core material was measured under various effective overburden loads from 0 to 8,000 psi. It has been found that reduction of permeability in clean sands was relatively small and the results agreed with published data. For sandstones containing large amounts of clay, preliminary tests indicated very large reductions in permeability with increasing effective overburden pressures. It is planned to continue laboratory work on this phase because of its importance in low-permeability reservoirs.

INTRODUCTION

During the past few years increasing interest has been shown in the differences obtained between conventional laboratory measurements on cores at atmospheric pressure and those when reservoir conditions are simulated. Since these data are used as the basis for calculations and the prediction of reservoir behavior, their evaluation under reservoir conditions is most important.

The effect of the compressibility of the rock upon the reservoir behavior, as fluid pressure declines, is an important subject which has been insufficiently studied. The total pressure on any plane through a reservoir is the result of the grain-to-grain rock pressure due to the overburden and the pressure of the interstitial fluid on the plane. As reservoir fluid pressure declines, the net load on the rock phase must increase, and the result is the compaction of the rock structure which produces a decrease in pore volume. Simultaneously, the rock grains expand into the pore space as the fluid pressure declines. The result of these two effects is defined as the effective compressibility of the rock and is expressed in units of pore volume/original pore volume/psi.

Work was started by Imperial in 1954 on the effects of pressure on the porosity of reservoir rock. These studies established effective compressibility factors for some limestones and dolomites. Since that time effective compressibilities have been obtained for other Canadian and some U. S. reservoir rocks. In conjunction with the study of porosity, an investigation has also been initiated to determine the effects of pressure on permeability. One outcrop and several reservoir sandstone cores have been tested to date.

ROCK COMPRESSIBILITY

Apparatus and Procedure

A diagram of the apparatus used in these studies is shown in Fig. 1. The equipment was constructed so that a uniform pressure, equivalent to the reservoir overburden, could be applied by the oil pump and transmitted on all sides of the core through the Lucite sheath. The sample was completely saturated by circulating brine through the mounted core. Pressure in

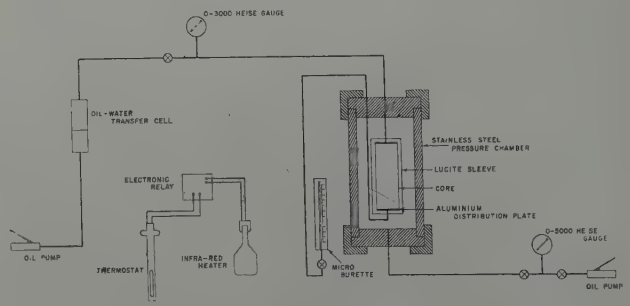

FIG. 1—ROCK COMPRESSIBILITY APPARATUS.

Original manuscript received in Society of Petroleum Engineers office July 15, 1957. Revised manuscript received April 3, 1958. Paper presented at 32nd Annual Fall Meeting of Society of Petroleum Engineers in Dallas, Tex., Oct. 6-9, 1957.

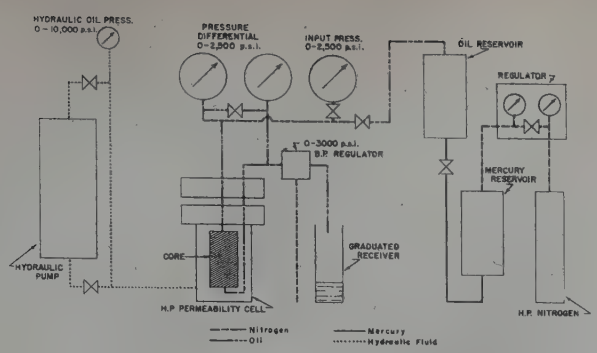

FIG. 2—SCHEMATIC DIAGRAM OF HIGH PRESSURE PERMEABILITY APPARATUS.

this liquid phase was then raised to that in the reservoir. Reservoir drawdown was simulated by reducing the pore liquid pressure and the expelled fluid was accurately measured. By correcting for fluid compressibility, a value for the effective compressibility of the core was calculated. Since accurate temperature control was required for satisfactory results, the whole apparatus was enclosed in an air bath.

TYPICAL RESULTS

While there was considerable difficulty in initially assembling and calibrating the apparatus, a leak-proof arrangement has been developed which is simple to operate, and has given reproducible results for several limestone and sandstone reservoirs in Western Canada. Limestone with small vugs from a depth of 3,200 ft exhibited an average compressibility of 2.2×10^{-6} pv/pv/psi while fine, intergranular limestone cores at 5,400 ft had an average compressibility of 5.1×10^{-6} pv/pv/psi. A sandstone core at 5,300 ft had a compressibility of 7.7×10^{-6} pv/pv/psi.

HIGH PRESSURE PERMEABILITY

APPARATUS AND PROCEDURE

The equipment used to determine oil permeabilities under reservoir pressure and temperature conditions is shown schematically in Fig. 2. The plastic sheathed core was suspended in a high pressure, insulated steel cell. Pressure was exerted on the external surface of the plastic by means of a hydraulic oil pump, capable of operating to 10,000 psi. Flowing oil pressure was obtained by applying 2,500 psi gas pressure on a mercury reservoir, the mercury in turn pressurizing the oil. This method was employed in order to minimize the solution of gas in the flowing oil. Heise gauges were used for pressure measurements and have proved satisfactory for pressure differentials in excess of 100 psi. A Wianko pressure transducer was added to improve the accuracy of the lower differential pressure measurements. Volumes of flowing oil were collected and measured at atmospheric pressure. Two types of receivers were used: one, a standard calibrated glass cylinder, and the other a set of fractional pipettes permitting measurement to 1/100 cc. The entire apparatus was enclosed in a thermostatically controlled air bath.

The equipment has been tested to 10,000 psi and is working consistently at 7,000-psi external oil pressure and 2,000-psi flowing oil pressure.

The viscosities of the flowing oil at elevated temperatures and pressures were obtained by means of a high pressure, rolling-ball viscosimeter. The compressibility of the oil was also determined and the volumes collected during a test were corrected for pressure changes.

Oil permeabilities obtained at zero effective overburden pressure were used as the reference permeability. The effective overburden pressure exerted on the core was taken to be the pressure difference between the external hydraulic oil and the average of the inlet and outlet flowing oil pressures. Measurements of the oil permeabilities were made for each 1,000-psi increment of external pressure until 5,000-psi effective overburden pressure had been exerted. Permeabilities were also measured as the effective overburden was decreased. The oil permeability at each effective overburden pressure was then calculated as a percentage of the original "reference" permeability and plotted against the effective overburden pressure. It should be noted that the mean flowing pressure was kept approximately constant as the effective overburden pressure was increased during the test.

TYPICAL RESULTS

The results of tests on unextracted, oil-cut sandstone cores and selected extracted cores from Western Canada are presented in Table 1 and are shown in plotted form in Fig. 3. This group of cores varied greatly in clay content. This preliminary data obtained on shaly cores indicates that the lower the reference permeability, the greater the percentage reduction in permeability will be at a given effective overburden pressure.

TABLE 1—HIGH PRESSURE PERMEABILITY RESULTS

Core No.	Oil Perm. (md)	Mean flow oil pressure (psi)	Per cent reduction at effective overburden pressure, psig					Core Type
			1,000	2,000	3,000	4,000	5,000	
86A-1	3.7	22	5.3	10.8	14.5	17.0	20.4	Dirty shaly-sand unextracted
86A-1	3.0	16	—	10.9	—	14.7	—	Core remounted 6.8 per cent residual brine
14	15.0	15	3.5	6.5	8.5	10.4	12.0	Clean sand unextracted
11	0.23	240	31.0	52.0	62.0	67.5	70.0	Dirty shaly sand unextracted
86A-2	3.8	30	11.0	16.8	20.8	24.0		Dirty shaly sand unextracted
6	0.007	450	51.5	78.8	89.4	96.4		Very dirty shaly sand unextracted
6	0.005	450	—	92.6	—	approx. 100		Core remounted
Outcrop	102	7	4.0	7.6	10.7	13.0	14.0	Clean unextracted sand
Sandstone	102	2,000	7.0	9.2	11.3	12.2	15.7	Clean unextracted sand
10B	0.07	1,850	8.0	12.8	15.3	16.4	16.4	Clean sand—37.1 per cent residual water
10B	0.47	1,850	8.0	10.3	11.5	12.3	12.8	Core remounted—7.2 per cent residual brine
14C	3.5	2,000	2.5	4.3	5.6	6.4	7.0	Clean sand—38.2 per cent residual water
14C	6.9	1,950	7.3	9.1	11.2	15.4	17.2	Residual brine 6.9 per cent
6B	3.1	50	5.4	8.4	9.8	10.2	10.4	Clean sand—17.5 per cent residual water
24B	0.6	60	8.2	12.9	16.2	18.5	19.5	Clean sand—38.0 per cent residual water
23B	28.7	10	2.0	6.1	8.1	9.9	10.6	Residual brine 7.0 per cent
14B	8.8	2,025	4.4	8.4	11.6	14.0	14.9	Clean sand—zero residual water
7B	50.5	1,950	10.2	13.9	16.2	17.6	18.0	Clean sand—zero residual water
7B	44.0	1,850	6.4	8.8	13.4	14.6	17.1	Core remounted—zero residual water
3C	3.8	1,900	3.2	6.4	9.2	11.7	13.8	Clean sand—zero residual water

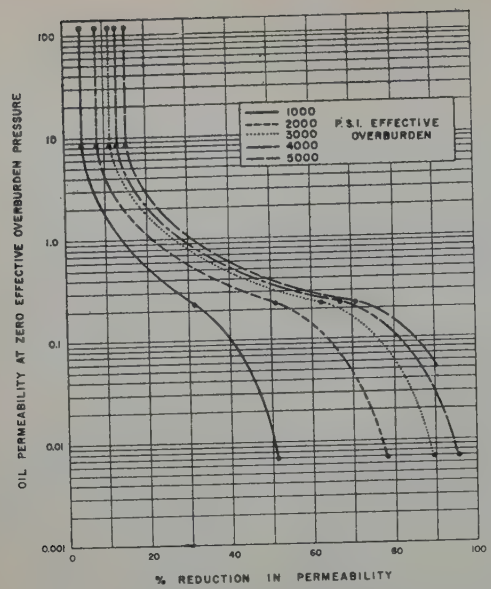

FIG. 3—REDUCTION IN PERMEABILITY VS EFFECTIVE OVERBURDEN PRESSURE.

The results of other investigators[1,2,3,4] show that the percentage reduction in permeability generally increases as the initial permeability increases. The apparent discrepancy may be due to the fact that most previous work was limited to clean sandstone and limestone cores.

Several cores were subjected to various effective overburden pressures, but returned to zero pressure before each increase in external pressure. Results obtained for one of these cores is shown in Fig. 4. For cores of higher permeability, such as that illustrated, the total percentage reduction in permeability at zero effective overburden for numerous pressure cycles was about 4 per cent, but in the shaly cores of low permeability the reduction was as high as 60 per cent. Although this suggests that some irreversible deformation of structure had occurred, some of these cores had essentially regained their initial permeability after a year. However, since irreversible behavior was also noted by Carpenter and Spencer[5], further study is required.

CONCLUSIONS

The apparatus and procedures given here have proven satisfactory for measuring both effective compressibility and variations in permeability with overburden pressure, provided one assumes equal stresses in all directions in the reservoir. A cell of another design is required if differential stresses are desired.

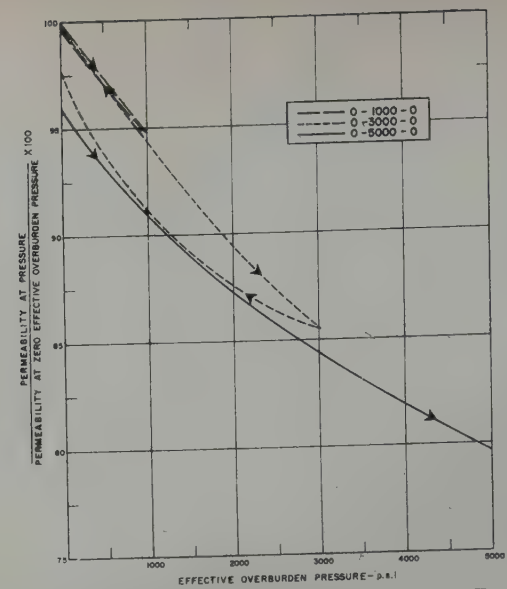

FIG. 4—REDUCTION IN PERMEABILITY VS EFFECTIVE OVERBURDEN PRESSURE (THREE PRESSURE CYCLES).

Lucite has proven satisfactory for mounting extracted cores. However, a technique for handling fresh cores, obtained using crude or oil-base mud, requires some development. Initial tests with polyethylene indicate that this material may withstand the action of some of the extraction solvents, but since the mounting temperature is similar to that required for Lucite, its use on unextracted, oil-cut cores will not be possible.

Studies are being continued on the compressibility of various rocks and the effect of pressure on permeability.

ACKNOWLEDGMENT

The authors wish to thank W. H. White and A. E. Scheidegger for their advice and also the management of Imperial Oil Ltd., Producing Dept., Western Regional offices, for permission to publish this paper.

REFERENCES

1. Hall, H. N.: "Compressibility of Reservoir Rocks", *Trans.* AIME (1953) **198,** 309.
2. Fatt, I.: "The Effect of Overburden Pressure on Relative Permeability", *Trans.* AIME (1953) **198,** 325.
3. Fatt, I., and Davis, D. H.: "Reduction in Permeability with Overburden Pressure", *Trans.* AIME (1952) **195,** 329.
4. Botset, H. G., and Reed, D. W.: "Experiment on Compressibility of Sand," *Bull.* AAPG (July, 1935) **19,** No. 7, 1053.
5. Carpenter, C. B., and Spencer, G. B.: "Measurements and Compressibility of Consolidated Oil Bearing Sandstones", RI 3540, USBM (Oct., 1940). ★★★

A Linear Programming Model for Scheduling Crude Oil Production

A. S. LEE
J. S. ARONOFSKY
MEMBER AIME

MAGNOLIA PETROLEUM CO.
DALLAS, TEX.

INTRODUCTION

In recent years considerable progress has been made in the development and application of mathematical techniques for the solution of certain problems involving economic "strategies". Such a problem might involve, for example, the scheduling of shipments of a commodity from a number of sources to a number of destinations. The object would be to schedule the shipments in a manner so as to satisfy the destination requirements and at the same time minimize the transportation costs. The solution to such a problem is not necessarily intuitively obvious. The "obvious" solution is frequently far from optimum. If the shipments are to be made from, for example, only two sources to four destinations, the optimum schedule is readily found. However, if shipments are to be made from, say, 10 sources to several hundred destinations, even a competent and experienced scheduler may spend considerable time in finding a reasonable answer. Even then he is not sure that he has the optimum solution. Furthermore, he has no way of knowing how far from optimum the answer is. Consequently, he does not know whether he should accept this solution or seek a better one.

Prior to the advent of large high-speed digital computers, little more could be done with such problems because of their great size and multiplicity of possible solutions. A problem involving 20 sources and 50 destinations would require choosing, from a very large number of possible combinations, the optimum combination of 1,000 variables. The best one could do was to utilize intuition, extrapolation from past experience, and other non-exact approaches. With a high-speed computer, however, such problems can be solved providing a reasonable computational procedure (or algorithm) can be utilized. The purpose of this paper is to describe such a procedure (linear programming) and to apply this procedure to a production scheduling problem.

THE RESERVOIR PROBLEM

A simple reservoir model is used throughout this analysis to illustrate the use of linear programming. Even the simplest reservoir behavior problem is nonlinear in both space and time, but if the geometry is fixed for a particular study and the time variable is quantized, the resultant system may be described by linear constraints on the variable production rates.

Crude oil is available from five separate sources and is delivered to a pipeline. Sources 1, 2, 3 and 4 are ideal reservoirs and therefore are subjected to reservoir flow restrictions. Source 5 is labeled "Outside Source" and crude oil from this source is assumed to be available in unlimited quantities without considering reservoir conditions. The general problem is to determine the schedule of crude oil production from five sources which, over an eight-year period and subject to certain restrictions, will result in maximum profit.

"Profit" is defined to encompass all economic factors and expenses involved in producing and selling crude oil to a pipeline facility. Such economic factors are lumped to the extent that the term represents the dollars profit from one barrel of crude oil from any of the five sources entering the pipeline system. Table 1 presents the assumed profit per barrel for oil from any of the five sources over each of the four time periods. In this chart the eight years is broken into four equal intervals of two years. The selection of four time periods of two years each and the values representing the potential profit are completely arbitrary selections for the purpose of illustrating this idealized reservoir problem. In any practical application of this work a careful economic study would have to be made in order to estimate potential unit profits for time periods as far in the future as eight years. In this particular study it is assumed that all of the potential unit profits (C_{ij}) are known and fixed before the production schedule is attempted.

For each reservoir arbitrary values are assigned for

TABLE 1—POTENTIAL PROFIT CHART—SINGLE WELL SYSTEM
(C_{ij} = potential profit, $/bbl)

Reservoir					Outside source
Time	1	2	3	4	5
1	0.10	0.13	0.20	0.40	0.05
2	0.17	0.18	0.23	0.46	0.09
3	0.20	0.22	0.30	0.49	0.16
4	0.23	0.28	0.36	0.52	0.20

Original manuscript received in Society of Petroleum Engineers office May 10, 1957. Revised manuscript received May 5, 1958. Paper presented at 32nd Annual Fall Meeting of Society of Petroleum Engineers in Dallas, Tex., Oct. 6-9, 1957.

permeability, viscosity, outer radius, initial pressure, etc. It is assumed that all of the reservoir parameters remain constant throughout the eight-year period of study. It is further assumed that each reservoir contains a single ideal liquid in a homogeneous porous medium under the influence of an infinite water drive. An additional assumption is that the radial flow formulas for infinite water drive are applicable.[1,2] For such an infinite water-drive system, the following equation represents the relation between well pressure and production rate.

$$P_w(\tau) = P_o - \frac{\mu}{2\pi hk} QP(\tau) , \quad . \ . \ . \ . \ . \quad (1)$$

where τ represents dimensionless time, P_w is well pressure, P_o the initial pressure of the reservoir, and $P(\tau)$ is the function developed and described by Van Everdingen and Hurst[2]. Time is a continuous variable and Eq. 1 determines the well pressure at any instant of time provided the production rate, Q, the initial pressure, P_o, and the other physical parameters are known for this reservoir.

Now the pressure in the j^{th} reservoir at the end of the i^{th} time period may be written,

$$P_{wj}(\tau_{ij}) = P_{oj} - \frac{\mu_j}{2\pi h_j k_j} \sum_{k=1}^{i} (Q_{kj} - Q_{k-1,j}) P(\tau_{ij} - \tau_{k-1,j}) , \ . \ . \ . \ . \ . \ . \ . \ . \quad (2)$$

where Q_{ij} is the average production rate of the j^{th} reservoir during the i^{th} time period, P_{oj} is initial pressure of the j^{th} reservoir, τ_{ij} is dimensionless time and $P(\tau_{ij}) = \frac{1}{2}(\ln \tau_i + .80907)$, $\tau_i \geq 1{,}000$.

The well pressures (in all four reservoirs) are not allowed to go below some arbitrary value, such as 1 atm. Thus, there are 16 linear constraints on the production rates, Q_{ij} (one for each reservoir for each of the four time periods). The set of 16 inequalities is represented by

$$P_{wj}(\tau_{ij}) \geq 1 \qquad i,j = 1(1)\,4. \ . \ . \ . \ . \ . \quad (3)$$

The next set of constraints considered is represented by

$$\sum_{i=1}^{4} Q_{ij}\,\Delta t \leq F_j \quad j = 1(1)\,4 , \ . \ . \ . \ . \quad (4)$$

where F_j represents the original volume of oil in place in the j^{th} reservoir.

An additional set of four constraints is represented by Ineq. 5, which states that the production rate in any time period may not exceed the pipeline capacity, R.

$$\sum_{j=1}^{5} Q_{ij}\,\Delta t \leq R \qquad i = 1(1)\,4 , \ . \ . \ . \quad (5)$$

where Q_{ij} is the volume rate of oil purchased from the outside source in the i^{th} time period.

The set Ineq. 3 contributes 16 inequalities which constrain the individual reservoir production rates. Ineq. 4 contributes four inequalities which constrain the cumulative production from each reservoir. Ineq. 5 contributes four inequalities which represent the pipeline limitations. In total there are 24 linear inequalities expressed in terms of the unknown, Q_{ij}. The problem then is to find values of Q_{ij} that will satisfy Ineqs. 3, 4 and 5 with the additional requirement that the chosen Q_{ij} shall result in maximum profit. That is,

$$\sum_{j=1}^{5} \sum_{i=1}^{4} Q_{ij}\,\Delta t\, C_{ij} = \text{Maximum} . \ . \ . \quad (6)$$

C_{ij} represents the potential unit profit in the i^{th} time period for the oil produced from the j^{th} reservoir as given in Table 1.

The problem has been described, therefore, in terms of the maximization of a linear functional whose variables are subject to linear constraints.

RESULTS FOR SINGLE WELL SYSTEM

Tables 2 through 5 show the results of four different studies of this model. Table 2 presents the optimum schedule of production rates for each time period and for all five sources. The profit of $\$27.6 \times 10^6$ is the maximum profit that can be realized for this case. Also listed in Table 2 is the cumulative oil produced, the initial oil in place, and the recovery from each of the

TABLE 2—CASE 1
(Production Rates, cm³/sec)

	Source				
Time	1	2	3	4	5
1					102,606
2	1,008	4,834		51,303	45,461
3					102,606
4			11,414		91,192
Cumulative production (cm³) × 63.12 × 10⁶	1,008	4,834	11,414	51,303	341,865
Oil in place (cm³) × 63.12 × 10⁶	1,008	4,834	11,414	51,303	
Per cent recovery	100	100	100	100	

Profit = $\$27.6 \times 10^6$
R = 102,606 cm³/sec
Each time period is two years

TABLE 3—CASE 2
(Production Rates cm³/sec)

	Source				
Time	1	2	3	4	5
1	1,015	63	11,403	51,062	39,063
2	985	4,842	156	49,707	46,917
3	16	0	0	1,837	100,752
4	0	4,763	11,269	0	86,574
Cumulative production (cm³) × 63.12 × 10⁶	2,016	9,668	22,828	102,606	273,306
Oil in place (cm³) × 63.12 × 10⁶	2,016	9,668	22,828	102,606	
Per cent recovery	100	100	100	100	

Profit = $\$35.1 \times 10^6$
R = 102,606 cm³/sec

TABLE 4—CASE 3
(Production Rates cm³/sec)

	Source				
Time	1	2	3	4	5
1	1,015	4,844	11,403	51,062	34,282
2	985	4,707	11,087	49,707	36,120
3	968	4,631	10,911	48,950	37,146
4	957	4,578	10,790	48,429	37,852
Cumulative production (cm³) × 63.12 × 10⁶	3,925	18,760	44,191	198,148	145,400
Oil in place (cm³) × 63.12 × 10⁶	4,032	19,336	45,656	205,212	
Per cent recovery	97	97	97	97	

Profit = $\$41.3 \times 10^6$
R = 102,606 cm³/sec

TABLE 5—CASE 4
(Production Rates cm³/sec)

	Source				
Time	1	2	3	4	5
1	1,015	4,844	11,403	51,062	34,282
2	985	4,707	11,087	49,707	36,120
3	968	4,631	10,911	48,950	37,146
4	957	4,578	10,790	48,429	37,852
Cumulative production (cm³) × 63.12 × 10⁶	3,925	18,760	44,191	198,148	145,400
Oil in place (cm³) × 63.12 × 10⁶	4,032	38,672	136,968	205,212	
Per cent recovery	97	49	32	97	

Profit = $\$41.3 \times 10^6$
R = 102,606 cm³/sec

[1]References given at end of paper.

four reservoirs. Recovery here is defined to be the fraction of the initial oil in place that has been produced. In the first case the pressure constraints represented by Ineq. 3 played no role because it was not possible to withdraw at such a high rate that the well pressure would be reduced to 1 atm. Since the constraints of Ineq. 3 play no role in Case 1, these pressure constraints could be completely eliminated from this particular case. As there are only eight remaining constraints, there can be only eight non-zero values of the 20 Q_{ij}.

In Case 2, the F_j's are doubled. In certain instances some of the constraints of Ineq. 3 are tight, i.e., equalities. For example, in Reservoir 1 the well pressure at the end of the first time period has dropped to 1 atm.

In Case 3 we again double the F_j's. The recovery is 97 per cent from all four reservoirs; however, production is scheduled for all four time periods from the five sources. In addition, the well pressure has been reduced to 1 atm in every reservoir at the end of all four time periods. The pressure distribution for Reservoir 1, Case 3, is plotted in Fig. 1. The well pressure drops from the initial reservoir pressure to 1 atm at the conclusion of the first time period. The well pressure then rises as the rate is reduced and falls to 1 atm at the conclusion of the second time period. This pattern is repeated for the third and fourth time periods.

In the next case (Case 4), F_2 is again doubled, and F_3 is tripled. The results for this case are given in Table 5. For Reservoirs 2 and 3, the recovery is now 49 and 32 per cent, respectively. This analysis is valid for a single well in each reservoir. The next section presents a method for treating multi-well systems.

MULTI-WELL SYSTEM

Prior to designing a linear programming model for a multi-well system it is necessary to examine the set of constraints in Ineq. 3. These constraints were originally developed by considering the relation between well pressure and production rates for a single well system. In a multi-well system with interference, it is necessary to have equations that relate the well pressure to production rates when more than one well is being produced. Reservoir 3 now has two wells, designated as Well *a* and Well *b*, separated by distance, *d*. r_{ab} represents the distance, *d*, divided by the well radius. It is assumed that the compressibility and viscosity of the water are the same as that of the oil, so it is permissible to use a superposition principle to relate well pressures and rates (infinite system). Such an analysis has been described in detail and solutions are available.[3]

The pressure in Well *a* at the end of the i^{th} time period is

$$P_{w,3a}(\tau_i) = \left[P_{o,3a} - A_3 \left\{\sum_{k=1}^{i}\left(Q_{k,3a}[P(1,\tau_i - \tau_{k-1}) - P(1,\tau_i - \tau_k)] + Q_{k,3b}[P(r_{ab},\tau_i - \tau_{k-1}) - P(r_{ab},\tau_i - \tau_k)]\right)\right\}\right] \geq 1, \; i = 1(1)\; 4\,, \quad . \quad . \quad . \quad . \quad . \quad . \quad (7)$$

where P_{0a} is initial pressure, A_3 is $\mu_3/2\pi h_3 k_3$, Q_{i3a} is production rate during i^{th} time period from Well 3_a, Q_{i3b} is production rate during i^{th} time period from Well 3_b, τ is dimensionless time, and r_{ab} is well spacing ratio $= \dfrac{\text{distance between the two well centers}}{\text{well radius}}$.

$$P(r_{ab},\tau) = \tfrac{1}{2}\left[\ln\frac{4\tau}{r_{ab}^2} - 0.57722\right], \; \frac{4\tau}{r_{ab}^2} \geq 2{,}000\,. \quad . \quad . \quad . \quad . \quad . \quad . \quad . \quad . \quad . \quad . \quad . \quad . \quad . \quad (8)$$

There are multi-well reservoir systems where it would not be possible to express the function, $P(r_{ab},\tau)$, as an analytical expression. In such cases one can approximate the *P* function either by numerical computations on a digital computer or analog solutions on an electric analyzer.

Similar constraints may be written for Well 3_b. The constraints on Reservoirs 1, 2 and 4 will remain as before. The potential unit profits are assumed to be the same for both 3_a and 3_b, and equal to the value assumed for Reservoir 3 in the one-well system. The potential unit profits for Sources 1, 2, 4 and 5 remain the same as in the single well case. It would be a simple matter to modify the potential unit profit values for Reservoir 3 to take into consideration the additional cost required to drill more wells, but such factors have not been considered in this study.

The results for Case 5 are given in Table 6. The well spacing ratio, r_{ab}, and the F_j's and *R* are the same as those for Case 4.

In Case 5 the additional well increased the cumulative production for Reservoir 3 by 9 per cent to total cumulative recovery of 41 per cent.

CONCLUSIONS

It is worthwhile to examine the limitations of the present model. One very obvious shortcoming is that only four time periods were considered. It would be much more realistic if there were 20 or more time periods rather than four. Then the well pressure could

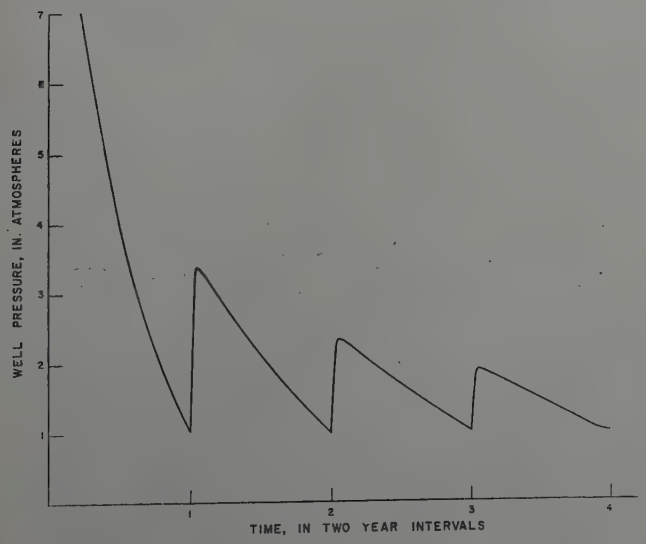

FIG. 1—RESERVOIR 1, CASE 3.

TABLE 6—CASE 5
(Production Rates cm³/sec)

Time	Source 1	2	3a	3b	4	5
1	1,015	4,844	7,316	7,316	51,062	31,053
2	985	4,707	7,056	7,056	49,707	33,095
3	968	4,631	6,913	6,913	48,950	34,231
4	957	4,578	6,815	6,815	48,429	35,012
Cumulative production (cm³) × 63.12 × 10⁶	3,925	18,760	56,200		198,148	133,391
Oil in place (cm³) × 63.12 × 10⁶	4,032	38,672	136,968		205,212	
Per cent recovery	97	49	41		97	

Profit = \$49.0 × 10⁶
R = 102,606 cm³/sec
r_{ab} = 250

decrease to 1 atm at 20 points instead of only four points. In Fig. 1, the well pressure was reduced to 1 atm at only four points, whereas in a real reservoir system the well pressure could remain at 1 atm for the entire time period of eight years. Use of a larger number of time periods would not make the analysis more difficult, but it would increase the computing time. If, for instance, we consider 20 time periods, then we would have a system of 124 linear constraints on 120 variables. Another limitation is the fact that we considered only a single well and then a two-well system. However, methods are indicated for the introduction of two, three, or any number of wells following this procedure. The inclusion of additional wells merely increases the size of the linear programming model.

No attempt is made in this paper to evaluate all of the important reservoir considerations. In most cases it would be extremely difficult to present a linear relation between well pressure and rates. Even in the case where linear relations can be deduced it is doubtful whether analytical solutions would be available relating well pressure, rate, and time. However, such relations between well pressure, rate and time can be approximated either by analog devices or independent and separate computations on digital computers. Economic factors, which would play an important role in any practical situation, are not emphasized in this study.

REFERENCES

1. Muskat, M.: *Physical Principles of Oil Production*, McGraw-Hill Book Co., Inc., N. Y. (1949).
2. Van Everdingen, A. F. and Hurst, W.: "The Application of the Laplace Transformation to Flow Problems in Reservoirs", *Trans.* AIME (1949) **186**, 305.
3. Mortada, M.: "A Practical Method for Treating Oilfield Interference in Water-Drive Reservoirs", *Trans.* AIME (1955) **204**, 217.
4. Charnes, A., Cooper, W. and Henderson, A.: *An Introduction to Linear Programming*, John Wiley & Sons, N. Y. (1953).
5. Koopmans, T. (editor): *Activity Analysis of Production and Allocation*, John Wiley & Sons, N. Y. (1951).
6. Tucker, A.: *Game Theory and Programming*, Oklahoma State Univ., Stillwater, Okla. (1955).
7. Vajda, S.: *The Theory of Games and Linear Programming*, Methuen & Co., Wiley, N. Y. (1956).
8. Kuhn, H. and Tucker, A. (editors): *Linear Inequalities and Related Systems*, Princeton Univ. Press, Princeton, N. J. (1956).
9. Morgenstern, O. (editor): *Economic Activity Analysis*, John Wiley & Sons, N. Y. (1954).
10. Antosiewicz, H. (editor): *Proc.*, Second Symposium on Linear Programming, Washington (1955) **I, II.** ★★★

Effect of Low Frequency Percussion in Drilling Hard Rock

E. TOPANELIAN, JR. | GULF RESEARCH & DEVELOPMENT CO. PITTSBURGH, PA.

INTRODUCTION

In the development of a fluid-operated hammer drill[1] for accelerated penetration of hard rock formations in oil wells, a research investigation was conducted to evaluate the percussion effects obtained with different design characteristics and to determine the possibilities of percussion in the low frequency range. Tests were conducted on granite blocks and comparable impact forces were measured with a load cell under selected test conditions. These full-scale laboratory tests provided an evaluation of the effectiveness of percussion which was further supported by actual downhole field performance.

While much pertinent data have been presented by other investigators[2,3,4,5], the method of evaluation described in this article resulted in good correlation between laboratory and field performance and may be applicable in other low frequency percussion developments.

EXPERIMENTAL METHOD

For these tests the bit was held stationary and the test block was rotated and forced upward against the bit by a hydraulically-lifted rotary table. "Weight on bit" was calculated from pressure readings on the fluid system of the lifting cylinders—corrected for tare and friction. Percussion was obtained with several tubular hammers of different weights up to 320 lb. These were lifted mechanically and allowed to drop by gravity from various heights onto a slidably-mounted bit sub or "floating anvil" for calibration of the load cell response with known kinetic energy of the hammers. During evaluation of percussion effects, the hammers were hydraulically operated to provide a range of percussion frequencies up to 1,020 blows per minute delivered to the anvil.

To obtain comparable test readings, the load cell of the strain gauge type, was attached to the bottom of the anvil or bit sub in place of the bit. The load cell rested on a typical granite test block mounted on the drilling table. The latter was hydraulically supported as in the actual drilling operation. The effect of support resistance was the same for all tools when calibrating. Impact forces so determined were thus directly comparable with one another for the purposes of this investigation.

When a roller bit was substituted for the load cell for actual drilling, the impact force would probably be reduced due to the resiliency of the bit body, legs, cones and teeth and the penetration of the teeth into the rock. However, since the bits and rock specimens were uniform in these tests, an evaluation of actual tool performance, in terms of parameters previously determined with the load cell at the selected standard conditions of calibration, proved satisfactory.

Throughout these tests, 8¾-in. standard tricone, hard rock toothed roller bits and carbide-insert roller bits were used. Rotary speeds were 50 and 100 rpm; static weight on bit was applied up to 40,000 lb, and percussion frequencies up to 1,020 blows per minute were available. During this investigation it was found that toothed bits on which the teeth had developed flat ends about 3/16 in. wide did not change appreciably for the duration of a test. Hence, all toothed bits used in this study were in this condition. Conventional reference curves obtained in these tests show that increasing weight on bit by 2:1 yielded an increased penetration rate of approximately 2.7:1, while an increase in rotary speed of 2:1 netted an increased penetration rate of roughly 1.7:1. Results are thus of the same order as those reported for hard rock drilling by other investigators.[6]

CALIBRATION

Under the selected standard test conditions previously described, with the lifting table hydraulically supported, and the anvil interposed between hammer and load cell, the hammers were dropped from known heights. Thus, with the kinetic energy of the hammer known, the corresponding maximum impact force shown by the cell was determined. (It may be of passing interest to note here that special drop tests with the hammers showed that no appreciable reduction in impact force resulted from introduction of the anvil or bit sub.)

From these calibrations, it was possible to determine the theoretical kinetic energy available in the hammer from the maximum impact force shown by the load cell while operat-

Original manuscript received in Society of Petroleum Engineers office July 15, 1957. Revised manuscript received May 5, 1958. Paper presented at 32nd Annual Fall Meeting of Society of Petroleum Engineers in Dallas, Tex., Oct. 6-9, 1957.

[1]References given at end of paper.

ing a percussion tool with the table hydraulically supported and cell mounted in the same manner as stated. The maximum impact forces and hammer energies so determined are pertinent to the later discussion of Figs. 3, 4 and 5.

These impact forces are the same as would be available and *delivered to the bit* if the resistance of the latter, while actually drilling, was the same as that of the load cell mounted as described.

For purposes of this study, the term "impact force available at the bit" denotes the impact force shown by the load cell as determined with all pertinent test rig conditions exactly as for drilling except that the load cell was mounted in place of the bit.

TEST RESULTS

The laboratory investigation yielded some data applicable to the subsitution of percussion for the static weight on bit as well as the effect of percussion superimposed on the conventional static weight on bit. Fig. 1 shows some results obtained at rotary table speeds of 50 and 100 rpm. It will be noted that the effect of percussion was fairly uniform when superimposed on static weights of 10,000 to 40,000 lb on bit at either speed. It may also be seen by comparing the curves for 100 rpm that percussion (of the order of 420 blows per minute and impact force of 240,000 lb available at bit as determined under the standard test conditions) achieved the same penetration rate with 10,000 lb static weight carried on the bit as conventional drilling did with 40,000 lb of static weight on the bit. At 50 rpm the net effect of the percussion was greater, or equivalent to that of about 55,000 lb of static weight. In other words, percussion effects of this order could be substituted for the static weight equivalent to that of fifteen 7¼-in. drill collars without loss of penetration rate.

By the addition of percussion of this order to conventional drilling, approximately the same incremental increase in penetration rate was obtained at both rotary speeds of 50 and 100 rpm. However, the ratio between the conventional and percussion penetration rates obtained at the two speeds changed. For example, when carrying 30,000 lb static weight on bit and rotating at 50 rpm, the penetration rate with percussion was three times the conventional rate, whereas when rotating at 100 rpm the penetration rate with percussion was twice the conventional rate. With 10,000 lb on the bit, however, the ratio was approximately the same for the two speeds, since conventional drilling ceased to be effective at about 7,000 lb weight on bit in the test granite used. The penetration rate with percussion and 10,000 lb static weight on bit was over 20 times that for conventional drilling alone with the same weight on bit.

A comparison of the effect of percussion with two different types of hard rock bits is graphically presented in Fig. 2. Percussion was just as effective with the carbide-insert bit as it was with the toothed bit. The carbide-insert bit showed some advantage at the heavier static loadings due to a higher conventional base rate for that bit, but the increments due to percussion were substantially the same for both bits.

A very convenient element in this study of percussion tools was the $I \times F$ factor; that is, the product of impact force in pounds and frequency in blows per minute, available at the bit at the standard test condition. Fig. 3 shows the effects of various $I \times F$ factors from 60×10^6 to 127×10^6. While the lower curves are for toothed bits and the upper curves for carbide-insert bits, it has been shown (Fig. 2) that they are approximately interchangeable with respect to percussion increment. Conventional base curves are shown for both.

Fig. 4 shows the approximate penetration increments obtained by percussion corresponding to various $I \times F$ factors available at the bit. These increments were obtained from Fig. 3. The arbitrary straight line drawn in Fig. 4 indicated that for practical design purposes percussion effect could be closely predicted by $I \times F$ factor available at the bit. This factor was used in further design and development work with percussion tools in the low frequency range.

An application of this in tool development is shown in Fig. 5, where $I \times F$ factor was held at approximately 100×10^6 and the same hammer weight was used for both curves. The higher frequency and lighter impact force were selected as providing the more favorable conditions for extended life of the bit bearings.

The actual penetration rates shown in all tests apply only to the test granite or its equivalent in atmosphere. In field tests with hard formations downhole under hydrostatic pressure, reduced penetration rates for both conventional and percussion drilling were recorded. However, the *ratio* of improvement by percussion was of the same order as that found in these tests. Thus, appraisal of percussion tools in the investigation

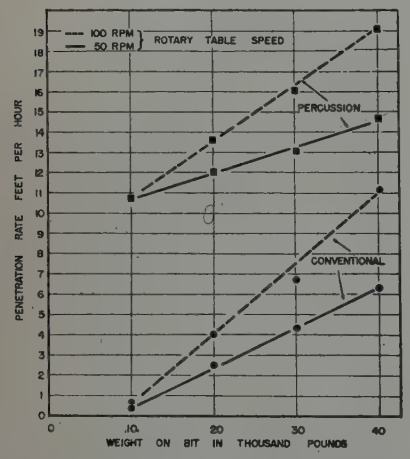

FIG. 1—EFFECT OF PERCUSSION ON DRILLING RATE AT TWO SPEEDS WITH TOOTHED BIT IN GRANITE.

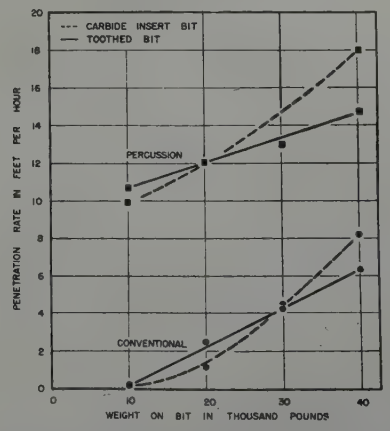

FIG. 2—EFFECT OF PERCUSSION WITH TWO TYPES OF HARD ROCK BITS IN GRANITE, ROTARY SPEED 50 RPM.

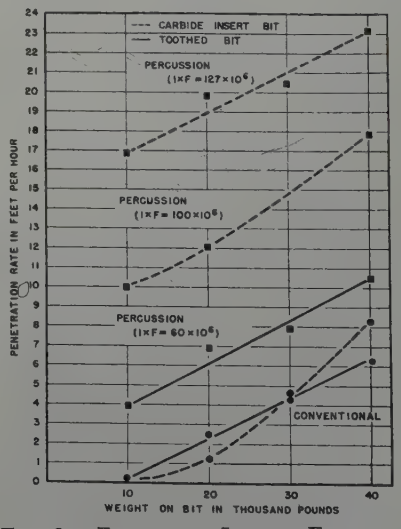

FIG. 3—EFFECT OF IMPACT FORCE × FREQUENCY FACTOR ON DRILLING RATE, ROTARY SPEED 50 RPM.

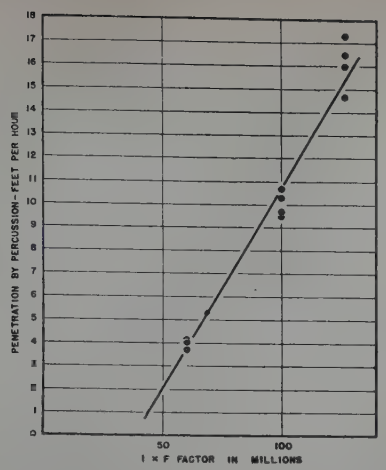

FIG. 4—PENETRATION DUE TO PERCUSSION VS $I \times F$ FACTOR.

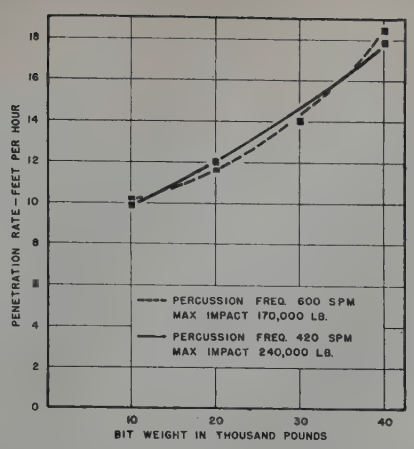
PENETRATION RATE-FEET PER HOUR
PERCUSSION FREQ. 600 SPM
MAX IMPACT 170,000 LB.
PERCUSSION FREQ. 420 SPM
MAX IMPACT 240,000 LB.
BIT WEIGHT IN THOUSAND POUNDS

FIG. 5—EFFECT OF MAINTAINING $I \times F$ FACTOR CONSTANT.

described was found to be indicative of their relative field performance where drillability of the rock in laboratory and field was of the same order of magnitude.

It may be of interest to note that in these tests no consistent relationship was found between performance and hammer energy or horsepower available at the bit.

Horsepower was determined from the kinetic energy of the hammer blow, as indicated by the calibrated load cell at the standard test condition, multiplied by the frequency of percussion.

Referring to Fig. 5, the percussion horsepower available at the bit is compared as follows, with the $I \times F$ factor available at the same point and condition:

1. Solid Curve; hp = 21; $I \times F = 100{,}800{,}000$
2. Dotted Curve; hp = 15; $I \times F = 102{,}000{,}000$

(Horsepower being put into the bit conventionally with bit weight of 30,000 lb was approximately 12 hp in both cases.)

In Fig. 3, top curve, the percussion horsepower available at the bit was 14 and the $I \times F = 125{,}000{,}000$.

FIELD RESULTS

A comparison of the laboratory evaluation of the percussion tool performance with the actual percussion tool performance in the field was made where weight on bit, drilling fluid, rotary speed and hardness of formation were approximately equivalent for both conventional drilling and conventional drilling with percussion superimposed. Tool A with $I \times F = 60 \times 10^6$ was operated in the field on West Texas "chert section" at a depth of 8,900 ft. Tool B with $I \times F = 100 \times 10^6$ was operated on Appalachian "Salt Sand" at depths of 700 and 5,700 ft.

Performance of these tools on granite in the laboratory is taken from Fig. 3 and sample comparisons with field performance are shown in Tables 1 and 2.

CONCLUSIONS

In this particular investigation of the effect of percussion frequencies in the order of 320 to 1,020 blows per minute, the following was observed.

1. The $I \times F$ factor provided a practical parameter for evaluating the performance of these hammer-type percussion tools in this frequency range.

2. Percussion of this order superimposed on conventional drilling more than doubled the penetration rate produced by static weight normally carried on bit.

3. Percussion effects of this order might be employed to produce the same penetration rate as the drill collars commonly used for conventional drilling.

4. Evaluation on the basis of the ratio,

$$\frac{\text{Penetration rate with percussion drilling}}{\text{Penetration rate with conventional drilling}}$$

provided a satisfactory correlation between laboratory and field results, under the conditions described.

TABLE 1—DRILLING PERFORMANCE—TOOL A
(Tests approximately at 50 rpm and 20,000 lb weight on bit)

Test No.	Drilling Method	Rate (ft/hr)	Average (ft/hr)	Ratio*
Field				
1	Percussion	6.7	6.7	2.2
2	Conventional	3.0	3.0	
Lab				
1	Percussion	6.0	6.0	2.4
2	Conventional	2.5	2.5	

*Ratio: Penetration rate with percussion drilling / Penetration rate with conventional drilling

TABLE 2—DRILLING PERFORMANCE—TOOL B
All tests at 50 rpm with 38,000 lb weight on bit

Test No.	Drilling method	Rate (ft/hr)	Average (ft/hr)	Ratio*
Field				
1	Percussion	8.29	8.29	2.3
2	Conventional	3.75	3.59	
3	Conventional	3.43		
4	Percussion	7.15	7.67	
5	Percussion	8.20		2.8
6	Conventional	2.73	2.73	
Lab				
1	Percussion	17.4	17.4	2.2
2	Conventional	7.8	7.8	

*Ratio: Penetration rate with percussion drilling / Penetration rate with conventional drilling

ACKNOWLEDGMENT

The author greatly appreciates the assistance of G. S. Peterson and other personnel at the Gulf Research Center participating in this project. Also the production divisions of Gulf Oil Corp. and United Fuel Gas Co. were most helpful in field testing.

REFERENCES

1. "New Percussion Drill Shows Great Promise", *Pet. Engr.* (July, 1957) **29**, B33.
2. Cline, W. H., Jr.: "Progress Report on a Fluid Actuated Rotary Percussion Engine", paper presented at Pet. Mech. Engr. Conf., Pet. Div. ASME, Houston, Tex. (Sept. 28-30, 1953).
3. Tagiev, E. I., *et al.*: "The Influence of Vibration on the Rate of Rotary Drilling of Hard Rocks with a Three Cutter Chisel", *Neft. Khoz.* (1955) **33**, 9, 20.
4. Simon, R.: "Theory of Rock Drilling", paper presented at 6th Annual Drilling and Blasting Symposium, U. of Minnesota, Minneapolis, Minn. (Oct. 11-13, 1956).
5. Wanamaker, J. A.: "Rotary Percussion Drilling in West Texas", *World Oil* (Sept., 1951) **133**, 182.
6. Bobo, R. A., Hoch, R. S. and Ormsby, G. S.: "Keys to Successful Competitive Drilling", *World Oil* (March, 1955) **140**, 113. ★★★

T. N. 2014

Note on Buckling of Tubing in Pumping Wells

T. SELDENRATH
JUNIOR MEMBER AIME
A. W. WRIGHT*

COMPAÑIA SHELL de VENEZUELA
MARACAIBO, VENEZUELA

ABSTRACT

This paper is written as a discussion of the paper, "Buckling of Tubing in Pumping Wells, Its Effects and Means for Controlling It" by Arthur Lubinski and K. A. Blenkarn, which was published in the March, 1957, issue of JOURNAL OF PETROLEUM TECHNOLOGY. *An analogy is drawn between the buckling of tubing in pumping wells and a tube, fitted with frictionless pistons, linked by an inelastic rod, and which is subject to an internal pressure. A simple derivation shows that the critical internal pressure exerts a hydrostatic force on the piston which is close to the Euler load for compression buckling of the same tube. While the results agree with those of Ref. 1, the basis of calculations has been changed and clarified.*

The presence of internal upsets at the pistons is discussed.

INTRODUCTION

In the Appendix[1], Lubinski and Blenkarn state that a tube with ends closed by frictionless pistons connected by an inelastic rod (Fig. 1) will behave as a column loaded with a force equal to the tension force in the rod. They note that, while the fluid may not resist a shear force, the moment in every cross section is piston force multiplied by the elastic line deflection (c.f., the loaded column). Since the equations of the elastic lines are similar in the two cases, the solution is carried over from the loaded column.

On the contrary it is suggested that while the method of solution remains unchanged from the column case, the actual stress distribution is different, a fact which is taken into account in this note.

A simple method of approximating the buckling pressure is given, and their reasoning in our mathematical language is continued.

GENERAL EQUATIONS

The equation of an elastic line, initially straight in the x direction (Fig. 2), is given by

$$\frac{d^2y}{dx^2} = -\frac{M_x}{EI}.$$

In the case of a loaded column, this may be written: $d^2y/dx^2 = -P/EI\ (y + \varepsilon)$. For the pressurized tube it was shown, by analogy with the loaded column, that $d^2y/dx^2 = -P_k/EI\ (y + \varepsilon)$, where $P_k = A.p$. This equation has a solution that, for $P_k = \pi^2 EI/l^2$, any deflection is stable (a criterion for buckling). An attempt will be made to describe more precisely, the forces acting on the tube, and to analyze the buckling conditions.

DISCUSSION

If the tube assumed a deflected position, the volume between the pistons would increase so that in deflecting, the energy of the fluid would decrease. When the increase in elastic energy of the tube (due to bending) is equal to the decrease of fluid pressure energy, buckling conditions exist.

Analyzing the forces on the tube (Fig. 3), two transverse forces, T_1, T_2, exerted by the pistons, are balanced by a resultant of the pressure elements which are linearly dependent on the local curvature of the elastic line (Fig. 4).

$$\bar{T}_1 + \bar{T}_2 = \bar{R}_1$$

$$\bar{R}_1 + \bar{R}_2 = 0$$

Unlike most buckling cases, the forces depend on the shape of the elastic line, a condition that makes a rigorous mathematical treatment difficult. Several approximations may be used to clarify the problem.

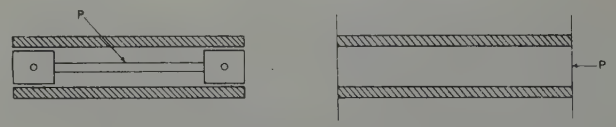

FIG. 1—SCHEMATIC DIAGRAM OF TUBE.

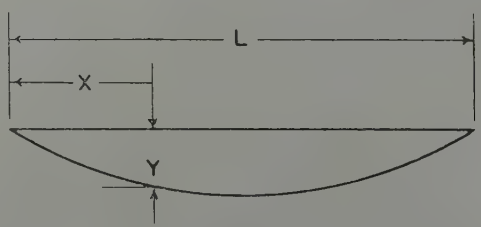

FIG. 2—SCHEMATIC DIAGRAM.

Original manuscript received in Society of Petroleum Engineers office Feb. 24, 1958. Revised manuscript received April 30, 1958.
*Deceased, Dec., 1957.
[1]References given at end of paper.

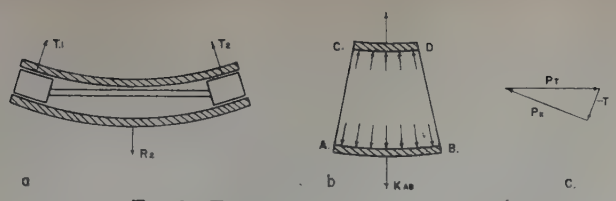

FIG. 3—FORCES ACTING ON THE TUBE.

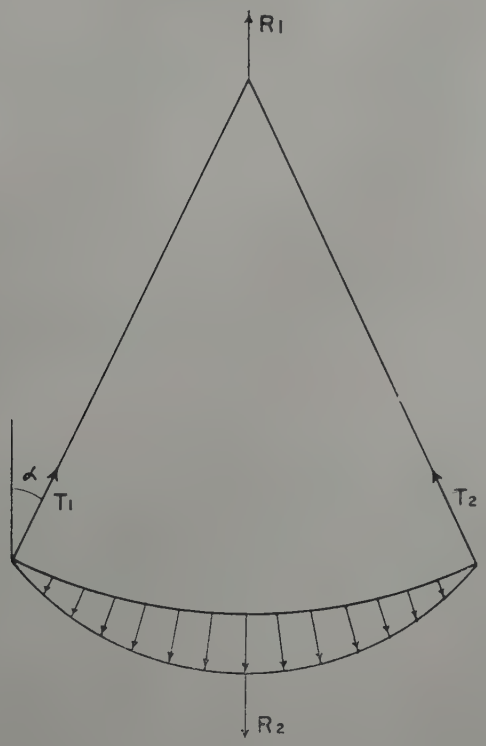

FIG. 4—FORCES EXERTED BY PISTONS AND FLUID ON THE TUBE.

Since α is small, the axial components of both the pressure elements acting on the tube, and T_1, T_2 are of second order. To simplify calculations, the force distribution (due to the fluid pressure) is approximated by two separate cases: (1) a uniformly loaded beam, having a lower moment in every cross section (Fig. 5a), and (2) a beam with a point load at mid-span, having a higher moment in every cross section (Fig. 5b).

CASE 1

$$T = P_k \text{ Tan } \alpha \text{ (Fig. 3c)}, \quad . \quad . \quad . \quad . \quad . \quad . \quad . \quad (1)$$

$$e = \frac{10\,T}{EI}\,\frac{l^3}{384} \text{(Fig. 5a)}, \quad . \quad . \quad . \quad . \quad . \quad . \quad . \quad (2)$$

and

$$\alpha = \text{Tan } \alpha \approx 3.2\, e/l \text{ (Ref. 2)} \quad . \quad . \quad . \quad . \quad . \quad (3)$$

From Eqs. 1 and 3, $T \approx 3.2\, P_k\, e/l$ . . . . . (4)

When the system buckles, deflection e may take any value. Thus, eliminating e from Eqs. 2 and 4,

$$P_k = \frac{12EI}{l^2} \quad . \quad . \quad . \quad . \quad . \quad . \quad . \quad . \quad . \quad . \quad . \quad (5)$$

CASE 2

$$e = \frac{2Tl^3}{48EI} \text{ (Fig. 5b)}, \quad . \quad . \quad . \quad . \quad . \quad . \quad . \quad . \quad (6)$$

$$\alpha = \text{Tan } \alpha \approx \frac{3e}{l} \quad . \quad . \quad . \quad . \quad . \quad . \quad . \quad . \quad . \quad (7)$$

Thus,

$$T \approx 3P_k\, e/l \quad . \quad . \quad . \quad . \quad . \quad . \quad . \quad . \quad . \quad . \quad . \quad (8)$$

Eliminating e from Eqs. 6 and 8,

$$P_k \approx \frac{8EI}{l^2} \quad . \quad . \quad . \quad . \quad . \quad . \quad . \quad . \quad . \quad . \quad . \quad (9)$$

According to Euler theory, buckling occurs in a column when P (an end load) $= \pi^2 \frac{EI}{l^2}$ (Ref. 2), which is indeed between the two cases.

In the loaded column case, the compression forces are axial and do not vary due to the buckling, while the moment at any section depends linearly on the deflection. On the contrary, in the pressurized tube case, the forces act normally to the elastic line, and vary linearly with the deflection. In the latter case, the moment arm of every force is almost independent of the deflection.

If the ends of the tube are internally upset (Fig. 6), a new condition prevails. The force on a shoulder due to the fluid pressure has a small tranverse component (dependent on the end slope of the elastic line) and a large axial component, almost independent of the end slope, but whose moment varies linearly with the deflection (Fig. 7).

$$A = A_1 + A_2$$
$$P_k = p.A_1$$
$$P_s = p.A_2 = P_k A_2/A_1$$
$$P_{st} = P_k \cdot A_2/A_1 \text{ Tan } x$$
$$P_{sa} \approx P_s \approx P_2 A_2/A_1 .$$

Resultant tranverse component of shoulder and piston forces, $P_k A_2/A_1$ Tan α + P_k Tan α = P_k A/A_1 Tan α.

Resultant axial component of shoulder force, P_k A_2/A_1 Cos $\alpha \approx P_k A_2/A_1$.

It is noted that the resultant tranverse component is

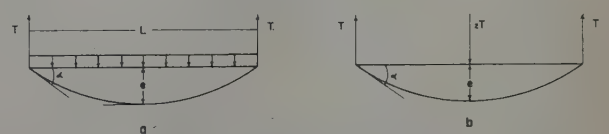

FIG. 5—DISTRIBUTION OF FORCES ACTING ON A BEAM.

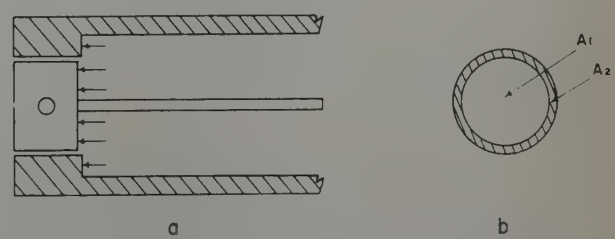

FIG. 6—TUBE WITH INTERNAL UPSET ENDS.

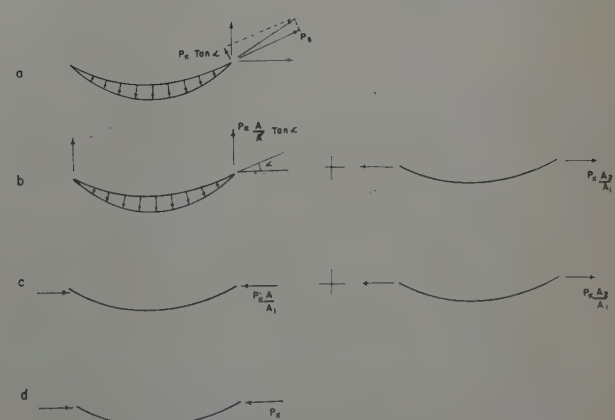

FIG. 7—DIAGRAM OF FORCES ON A TUBE WITH INTERNAL UPSET ENDS.

independent of the ratio in which the area A is divided between piston and shoulder.

Fig. 7 demonstrated that the equivalent end load is equal in magnitude to the hydrostatic force on the piston only.

Buckling involves a shortening of the distance between the ends of the tube, but no net axial stresses are introduced by internal pressure. However, the presence of shoulders causes an axial tension which delays buckling.

It is also interesting to note that tube dilation causes an increase in the moment of inertia, which in turn delays buckling. This last effect is paramount in the Bourdon tube.

CONCLUSIONS

1. Buckling may occur in a pressurized tube with ends closed by two frictionless pistons connected by an inelastic rod.

2. The critical hydrostatic force on the pistons approximates or equals the buckling end load: $12EI/l^2 > P_k > 8EI/l^2$.

3. If the tube ends are internally upset, the critical internal pressure is increased, and a net axial stress is introduced into the tube.

4. Many more practical applications than mentioned in Ref. 1 can be found, especially if similar cases, involving different pressures inside and outside a tube are included. Using the Lubinski theory as discussed in this note, interesting observations can be made in the following cases: (a) free hanging strings at greater depths, (b) lubricated rod pumping, and (c) sandfracing and producing of PTWC wells with two fixed tubing points, e.g., Baker Model D production packer and Otis-SOB packer.

5. Temperature effects and reduced collapse resistance might make it less attractive to use tension anchors in deep wells.

NOMENCLATURE

l = length of undeflected tube
x = distance from origin along undeflected elastic line
y = deflection of elastic line
E = Young's modulus for tube material
I = moment of inertia of tube section
M_x = moment of tube section at x
P = axial load on a column
ε = infinitely small initial deflection of the elastic line
P_k = force on pistons due to fluid pressure
P_t = tension in rod
p = fluid pressure
A = cross-sectional area of tube hole
A_1 = piston area when internal upsets are introduced
A_2 = shoulder area
T = transverse force exerted by piston on tube
B = resultant of forces exerted by pistons on tube
B_2 = resultant of hydrostatic force elements on the tube
α = end slope of the elastic line
e = deflection at mid-span
P_s = hydrostatic force on shoulder
P_{st} = component of P_s transverse to undeflected elastic line (y direction)
P_{sa} = component of P_s parallel to undeflected elastic line (x direction)

REFERENCES

1. Lubinski, A. and Blenkarn, K. A.: "Buckling of Tubing in Pumping Wells, Its Effect and Means for Controlling It", *Trans.* AIME (1957) **210**, 73.
2. *Theoretische Grundlagen*: Hütte. W. Ernst und Sohn, Berlin, Germany. ★★★

Application of Statistics to the Analysis of Production Decline Data

A. T. CHATAS
W. W. YANKIE, JR.
MEMBERS AIME

RESERVOIR ANALYSTS
DALLAS, TEX.

INTRODUCTION

The appraisal of an oil lease may often be made through production decline analysis, which requires description of the functional relationship between the oil production rate and either cumulative production or time. Heretofore, attempts to define the function appropriate to a given set of production data have depended to some extent on subjective procedures. The purpose here is to introduce an objective solution, obtained by combining the principle of least squares with the theory of equations.

MATHEMATICAL ANALYSIS

The fundamental differential equation appropriate to a general class of decline curves may be written,

$$n = -\frac{d}{dt}\left(\frac{q_o}{dq_o/dt}\right) = -\frac{d}{dt}(1/D) \quad . \quad . \quad (1)$$

Solution of Eq. 1 for general boundary conditions may be written in terms of either the cumulative oil production or time:

$$q_o^{1-n} = [(n-1)D_i(q_o)_i^{-n}]N_p + (q_o)_i^{1-n}, \quad . \quad (2)$$

and

$$q_o^{-n} = [nD_i(q_o)_i^{-n}]t + (q_o)_i^{-n}. \quad . \quad . \quad . \quad . \quad (3)$$

These equations constitute the mathematical expression of the so-called hyperbolic decline. Their complete description for a given set of production data requires the numerical evaluation of the three parameters[1,2], n, D_i and $(q_o)_i$.

For the special case of $n = 0$, Eq. 2 becomes

$$q_o = (q_o)_i - D_iN_p, \quad . \quad . \quad . \quad . \quad . \quad . \quad . \quad (4)$$

with the corresponding expression in terms of time being

$$q_o = (q_o)_i e^{-D_i t} \quad . \quad . \quad . \quad . \quad . \quad . \quad . \quad . \quad . \quad . \quad (5)$$

Similarly, for the special case of $n = 1$, Eq. 3 becomes

$$q_o = \frac{(q_o)_i}{1 + D_it} \quad , \quad . \quad . \quad . \quad . \quad . \quad . \quad . \quad . \quad . \quad (6)$$

with the corresponding expression in terms of cumulative oil production being

$$q_o = (q_o)_i e^{-(D/q_o)_i N_p} \quad . \quad . \quad . \quad . \quad . \quad . \quad . \quad . \quad . \quad (7)$$

Eqs. 4 and 5 constitute the mathematical description of the so-called exponential decline; Eqs. 6 and 7 are the mathematical description of the harmonic decline.[1,2]

Returning to the hyperbolic expressions, Eqs. 2 and 3 may also be written,

$$q_o^a = sN_p + b \quad . \quad . \quad . \quad . \quad . \quad . \quad . \quad . \quad . \quad . \quad (8)$$

and

$$q_o^{a'} = s't + b' \quad , \quad . \quad . \quad . \quad . \quad . \quad . \quad . \quad . \quad . \quad (9)$$

where $a = 1 - n$; $s = (n-1)D_i(q_o)_i^{-n}$; $b = (q_o)_i^{1-n}$;

$$a' = -n; \; s' = nD_i(q_o)_i^{-n}; \text{ and } b' = (q_o)_i^{-n}.$$

Note that both Eqs. 8 and 9 are linear in either time or cumulative production with respect to an exponential function of the production rate. In other words, a straight line relationship results for both variables when associated with the appropriate power of q_o. This fact is of prime importance in the application of statistical analysis.

STATISTICAL ANALYSIS

For a given oil lease, the time, production rate and cumulative production are recorded records. To establish predictive formulas from Eqs. 2 and 3, it remains to determine numerical values for the three parameters [n, D_i and $(q_o)_i$] through an investigation of the past history.

Upon interpreting a, s and b as parameters, Eq. 8 may be expressed for every time interval of interest, j, over the past history as follows.

$$(q_o)_j^a = s(N_p)_j + b \quad . \quad . \quad . \quad . \quad . \quad . \quad . \quad . \quad . \quad (10)$$

In general, Eq. 10 will not be satisfied exactly, because of the assumptions in the expression of Eq. 1, and the errors and anomalies universally associated with production data. It will instead define the residual,

$$s(N_p)_j + b - (q_o)_j^a = d_j. \quad . \quad . \quad . \quad . \quad . \quad (11)$$

Squaring both sides and summing over all the data points, m, under consideration yields

$$\sum_{j=1}^{m}\left[s(N_p)_j + b - (q_o)_j^a\right]^2 = \sum_{j=1}^{m} d_j^2 = E \quad . \quad . \quad (12)$$

Original manuscript received in Society of Petroleum Engineers office Feb. 18, 1957. Revised manuscript received May 6, 1958. Paper presented at Joint University of Texas-Texas A&M Student Chapter Regional Meeting in Austin, Tex., Feb. 14-15, 1957

[1]References given at end of paper.

The theory of least squares requires that the sum of the weighted squares of the residuals be a minimum. On the basis of a unit weighting factor, the required minima are given by

$$\sum_{j=1}^{m}(N_p)_j^2 + b\sum_{j=1}^{m}(N_p)_j = \sum_{j=1}^{m}(N_p)_j(q_o)_j^a \quad . \quad . \quad (13)$$

$$s\sum_{j=1}^{m}(N_p)_j + bm = \sum_{j=1}^{m}(q_o)_j^a \quad . \quad . \quad . \quad . \quad . \quad . \quad (14)$$

and

$$s\sum_{j=1}^{m}(N_p)_j(q_o)_j^a \log (q_o)_j + b\sum_{j=1}^{m}(q_o)_j^a \log (q_o)_j = \sum_{j=1}^{m}(q_o)_j^{2a} \log (q_o)_j, \quad . \quad . \quad . \quad . \quad . \quad . \quad . \quad . \quad (15)$$

which are the normal equations. Their simultaneous solution expresses the most probable values of a, s and b, in accordance with the theory of least squares.[3]

Here, then, are three independent equations in three unknowns, a, s and b. It is noted at once that the occurrence of a as a nonlinear element precludes an explicit solution. Nevertheless, a numerical solution can be obtained in the following manner.

For the moment disregard a as an unknown. Then the foregoing system of equations would reduce to three linear equations in two unknowns, s and b. If the matrix of the coefficients of s and b is of rank 2, the equations are consistent provided the rank of the augmented matrix, containing all the summed elements, is also of rank 2. Physical considerations guarantee the existence of the slope and intercept, s and b, and the consistency of the equations. Therefore, to reverse the argument, it follows that the determinant formed from the augmented matrix must vanish. Consequently,

$$\begin{vmatrix} \sum_{j=1}^{m}(N_p)_j^2 & \sum_{j=1}^{m}(N_p)_j & \sum_{j=1}^{m}(N_p)_j(q_o)_j^a \\ \sum_{j=1}^{m}(N_p)_j & m & \sum_{j=1}^{m}(q_o)_j^a \\ \sum_{j=1}^{m}(N_p)_j(q_o)_j^a \log (q_o)_j & \sum_{j=1}^{m}(q_o)_j^a \log (q_o)_j & \sum_{j=1}^{m}(q_o)_j^{2a} \log (q_o)_j \end{vmatrix} = 0 \quad . \quad . \quad . \quad . \quad . \quad . \quad (16)$$

This determinant provides an equation involving a as the only unknown, and the value of a that forces the determinant to vanish constitutes the desired solution.[4,5]

Once a has been evaluated, Eqs. 13 and 14 may be solved simultaneously to yield values for s and b. Thus,

$$\Delta = m\sum_{j=1}^{m}(N_p)_j^2 - \left[\sum_{j=1}^{m}(N_p)_j\right]^2, \quad . \quad . \quad (17)$$

$$s\Delta = m\sum_{j=1}^{m}(N_p)_j(q_o)_j^a - \sum_{j=1}^{m}(N_p)_j\sum_{j=1}^{m}(q_o)_j^a, \quad (18)$$

and

$$b\Delta = \sum_{j=1}^{m}(N_p)_j^2\sum_{j=1}^{m}(q_o)_j^a - \sum_{j=1}^{m}(N_p)_j\sum_{j=1}^{m}(N_p)_j(q_o)_j^a \quad . \quad . \quad . \quad . \quad . \quad . \quad . \quad . \quad . \quad . \quad (19)$$

Then, by virtue of Eqs. 2 and 8, $n = 1 - a$; $(q_o)_i = (b)^{1/a}$; and $D_i = -\dfrac{s(q_o)_i^n}{a}$, which establishes the parameters originally sought.[3,6]

Precisely the same rationale may be employed with Eq. 9 to yield the alternative set of equations, related to time instead of cumulative production, for the solution of the problem. They are as follows.[3,4,5]

$$\Delta' = m\sum_{j=1}^{m}t_j^2 - \left[\sum_{j=1}^{m}t_j\right]^2, \quad . \quad . \quad . \quad . \quad (21)$$

$$s'\Delta' = m\sum_{j=1}^{m}t_j(q_o)_j^{a'} - \sum_{j=1}^{m}t_j\sum_{j=1}^{m}(q_o)_j^{a'}, \quad . \quad . \quad (22)$$

and

$$b'\Delta' = \sum_{j=1}^{m}t_j^2\sum_{j=1}^{m}(q_o)_j - \sum_{j=1}^{m}t_j\sum_{j=1}^{m}t_j(q_o)_j^{a'} \quad . \quad (23)$$

And by virtue of Eqs. 3 and 9, $n = -a'$; $(q_o)_i = (b')^{-1/n}$; $D_i = -\dfrac{s'}{b'a'}$.

Finally, for the special case of the exponential decline, where $n = o$, evaluation of the remaining parameters, $(q_o)_i$ and D_i, may be obtained as follows:[3,6]

$$D_i\Delta = m\sum_{j=1}^{m}(N_p)_j(q_o)_j - \sum_{j=1}^{m}(N_p)_j\sum_{j=1}^{m}(q_o)_j, \quad . \quad . \quad . \quad . \quad . \quad . \quad . \quad . \quad . \quad . \quad . \quad (24)$$

and

$$(q_o)_i\Delta = \sum_{j=1}^{m}(N_p)_j^2\sum_{j=1}^{m}(q_o)_j - \sum_{j=1}^{m}(N_p)_j\sum_{j=1}^{m}(N_p)_j(q_o)_j, \quad . \quad . \quad . \quad . \quad . \quad . \quad . \quad . \quad . \quad . \quad . \quad (25)$$

or in terms of time,

$$D_i\Delta' = -\ln 10\left[m\sum_{j=1}^{m}t_j \log (q_o)_j - \sum_{j=1}^{m}t_j\sum_{j=1}^{m}\log (q_o)_j\right], \quad . \quad . \quad . \quad . \quad . \quad . \quad . \quad . \quad . \quad . \quad . \quad . \quad (26)$$

and

$$\Delta' \log (q_o)_i = \sum_{j=1}^{m}t_j^2\sum_{j=1}^{m}\log (q_o)_j - \sum_{j=1}^{m}t_j\sum_{j=1}^{m}t_j \log (q_o)_j \quad . \quad . \quad . \quad . \quad . \quad . \quad . \quad . \quad . \quad . \quad . \quad . \quad (27)$$

And for the special case of the harmonic decline, where $n = 1$, these same parameters may be obtained as follows:

$$\Delta \log (q_o)_i = \sum_{j=1}^{m}(N_p)_j^2\sum_{j=1}^{m}\log (q_o)_j - \sum_{j=1}^{m}(N_p)_j\sum_{j=1}^{m}(N_p)_j \log (q_o)_j, \quad . \quad . \quad . \quad . \quad . \quad (28)$$

and

$$D_i\Delta = -(q_o)_i \ln 10\left[m\sum_{j=1}^{m}(N_p)_j \log (q_o)_j - \sum_{j=1}^{m}(N_p)_j\sum_{j=1}^{m}\log (q_o)_j\right] \quad . \quad . \quad . \quad . \quad . \quad . \quad . \quad (29)$$

In terms of time,

$$\Delta'/(q_o)_i = \sum_{j=1}^{m}t_j^2\sum_{j=1}^{m}1/(q_o)_j - \sum_{j=1}^{m}t_j\sum_{j=1}^{m}t_j/(q_o)_j, \quad . \quad . \quad . \quad . \quad . \quad . \quad . \quad . \quad . \quad . \quad . \quad . \quad (30)$$

and

$$D_i\Delta' = (q_o)_i\left[m\sum_{j=1}^{m}t_j/(q_o)_j - \sum_{j=1}^{m}t_j\sum_{j=1}^{m}1/(q_o)_j\right] \quad (31)$$

$$\begin{vmatrix} \sum_{j=1}^{m}t_j^2 & \sum_{j=1}^{m}t_j & \sum_{j=1}^{m}t_j(q_o)_j^{a'} \\ \sum_{j=1}^{m}t_j & m & \sum_{j=1}^{m}(q_o)_j^{a'} \\ \sum_{j=1}^{m}t_j(q_o)_j^{a'} \log (q_o)_j & \sum_{j=1}^{m}(q_o)_j^{a'} \log (q_o)_j & \sum_{j=1}^{m}(q_o)_j^{2a'} \log (q_o)_j \end{vmatrix} = 0 \quad . \quad . \quad . \quad . \quad . \quad . \quad . \quad . \quad . \quad . \quad (20)$$

Except for the augmented determinants, Eqs. 16 and 20, all the relations following Eq. 16 lend themselves to explicit solution. The two determinants may be solved by iterative procedures for their zero value by either desk calculator or digital machine computation. The Remington-Rand Univac and the Royal McBee LGP-30 have been successfully programmed for this purpose.

In conclusion, it bears mention that the mathematical and statistical principles employed in this analysis of production decline data have been extended to solve other problems; for example, the linearization of certain classes of curves in semilog and log-log coordinates through the least square evaluation of additive constants. Evidently, this use of the augmented determinant provides a general means of numerically solving a consistent system of equations which includes a nonlinear term.

NOMENCLATURE

a, a' = positive constant or parameter
b, b' = intercept of least square line
d = residual
i = subscript: initial decline conditions
j = subscript: index symbol; an element of the set $1, 2 \ldots, m$
m = upper limit of the set of j's
n = production decline parameter
q_o = rate of oil production
s, s' = slope of least square line
t = time
D = production decline ratio
E = error function
N_p = cumulative oil production
Δ, Δ' = determinant of coefficients

ACKNOWLEDGMENTS

Grateful acknowledgment is made to W. C. Skinner of the Magnolia Petroleum Co.'s Field Research Laboratories, who checked the accuracy of the mathematical procedures and called attention to an error in an earlier manuscript; and to Jan J. Arps of The British-American Oil Producing Co., who reviewed the manuscript and made some valuable criticisms and suggestions.

REFERENCES

1. Arps, J. J.: "Analysis of Decline Curves", *Trans.* AIME (1945) **160**, 228.
2. Arps, J. J.: "Estimation of Primary Oil Reserves", *Trans.* AIME (1956) **207**, 182.
3. Deming, W. E: *Statistical Adjustment of Data,* John Wiley & Sons, Inc., N. Y. (1943).
4. Sokolnikoff, Ivan S. and Elizabeth S.: *Higher Mathematics for Engineers and Physicists,* McGraw-Hill Book Co., Inc., N. Y., 2nd Ed. (1941).
5. Burrington, Richard S. and Torrance, Charles C.: *Higher Mathematics With Applications To Science And Engineering,* McGraw-Hill Book Co., Inc., N. Y. (1939).
6. Larkey, C. S.: "Mathematical Determination of Production Decline Curves", *Trans.* AIME (1925) **71**, 1322. ★★★

Identification of Mixtures of Waters from Chemical Water Analyses

J. C. McKINNELL
MEMBER AIME

STANDARD OIL CO. OF CALIFORNIA
TAFT, CALIF.

ABSTRACT

Identification of complex mixtures of waters presents many problems that can be solved by graphical methods described in this paper. Examples are presented to show the application of these methods to the correlation of oilfield waters and the determination of the percentage of each water in mixtures of two and three waters.

INTRODUCTION

Correlation of waters and identification of mixtures of two and three waters is important in secondary recovery evaluation studies and studies involving underground movement of waters. The importance of such studies suggests the need for a method to correlate a great number of water analyses to accurately identify and improve the understanding of mixtures of waters.

Geochemical analyses of waters furnish a quantitative measure of each of the ions present in a water. Table 1 shows a portion of the data on many oilfield water analysis report forms in use today. Under "parts per million" are listed the quantitative amounts of each ion in milligrams per liter. Following the work of Stabler[1] and Palmer[2], some laboratories have reported additional data to indicate the reaction capacity, or reacting value of each ion. Table 1 lists data under two subheads for the "reacting value". Under the first subhead, the reacting value is reported in gram equivalents per million, hereinafter called equivalents per million. This value is determined by multiplying milligrams per liter of the ion by a factor equal to the reciprocal of the equivalent weight of the ion. Under the second subhead (per cent) is listed the percentage of each ion based on the total equivalents per million.

Sodium is not usually an analyzed value in routine analyses, but is determined by the difference between total negative equivalent per million values and the sum of all of positive ion values for which analyses were made. This difference is reported as sodium, hereafter labelled "sodium". On this basis, the subtotals of the equivalent per million and per cent reacting values of the positive and negative ions are equal.

Original manuscript received in Society of Petroleum Engineers office July 15, 1957. Revised manuscript received May 13, 1958. Paper presented at 32nd Annual Fall Meeting of Society of Petroleum Engineers in Dallas, Tex., Oct. 6-9, 1957.

[1]References given at end of paper.

CORRELATION OF WATER ANALYSES DATA

Previously reported methods for correlating oilfield waters have used part of the data in Table 1, and can be classified into two categories.

Correlation by Chemical Character

Correlation methods using the chemical character of waters, as represented by the per cent reacting values of the ionic constituents, have been used by Palmer[2] and Tickell[3]. These methods have the limitation of neglecting the ionic concentration of the waters. This limitation can be serious in areas where waters have the same chemical character, but differ in concentration.

Correlation by Concentration of the Ionic Constituents

The Reistle[4] and the Stiff[5] methods use the ionic concentration in parts per million and equivalents per million. These methods are effective in differentiating waters of similar chemical character and varying concentration, as in the highly saline waters of the Mid-Continent area.

These methods have the disadvantage that they correlate waters by comparing many graphs of individual water analyses to determine the similarity to, or the variance from "type" waters.

PROPOSED METHOD OF CORRELATING WATER ANALYSES DATA

Correlation graphs presented in Fig. 1 represent water analyses data as points to facilitate the correlation of waters. The graph on the left of Fig. 1 is a plot of per cent reacting value of magnesium vs calcium. The right

TABLE 1—GEOCHEMICAL ANALYSIS OF WATER
(Sample No. 152)

Ions		Parts per Million		Reacting Value	
Positive		Milligrams per Liter		Equivalents per Million	Per cent
Sodium	Na^+	9,185.9		399.44	24.99
Calcium	Ca^{++}	7,693.4		383.90	24.02
Magnesium	Mg^{++}	191.1		15.72	0.99
Barium	Ba^{++}	0		0	0
Strontium	Sr^{++}	0		0	0
			Subtotal	799.06	Subtotal 50.00
Negative					
Sulfate	$SO_4^=$	209.9		4.37	0.27
Chloride	Cl^-	27,862.1		785.79	49.17
Carbonate	$CO_3^=$	0		0	0
Bicarbonate	HCO_3^-	543.1		8.90	0.56
Hydroxide	OH^-	0		0	0
Iodide	I^-	0		0	0
			Subtotal	799.06	Subtotal 50.00
Total		45,585.5		1,598.12	100.00

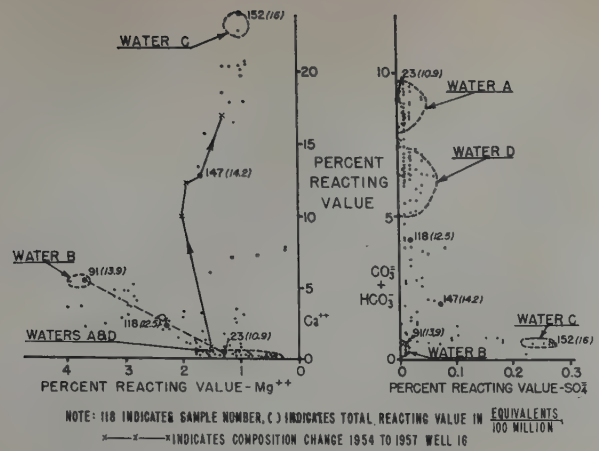

FIG. 1—CORRELATION OF WATERS.

graph is a plot of per cent reacting value of sulfate vs the sum of carbonate and bicarbonate.

Table 2 contains data for the labelled samples in Fig. 1. Total reacting values in equivalents per million divided by 100 are shown in parentheses after the sample number. The ionic concentrations can be compared by multiplying the plotted percentage values by the total reacting value.

Many oilfield water analyses report only the presence of the three positive ions, sodium, calcium and magnesium. Plotting of calcium and magnesium percentages in effect indicates the sodium per cent reacting value. Similarly, plotting the negative sulfate ion vs the sum of the negative carbonate and bicarbonate ion percentages will usually indicate the per cent reacting value of chloride by difference.

Fig. 1 shows 167 water analyses plotted as points on both graphs. Many of the points fall in definite groups. Points representing waters of equal total reacting value and lying in proximity to each other may represent a type water. They also can be similar mixtures of type waters. All available data should be used to determine that they represent waters from a common source. The outline of points representing waters from a common source is considered to be the approximate limits of a type water. As a large amount of data are plotted, the type waters may be represented as an average value which can be verified by intersecting trends of known water mixtures. The approximate limits of four type waters are indicated and labelled as waters A, B, C and D. Points falling between type waters are mixtures. A water, represented by a point lying near a straight line between two type waters and with an intermediate total reacting value, may be a mixture of the two waters. The mixture can be more accurately identified as explained in the section "Mixture of Two Waters". Similarly, a point lying between three type waters may be a mixture of the three and can also be identified as explained in the section "Mixture of Three Waters".

Changes in composition can be followed by connecting plotted points of samples of interest. The solid line through Samples 23 and 147 on the positive ion graph shows the trend of six samples from the same well.

Equivalent per million values can be plotted in a manner similar to Fig. 1 to provide an alternate correlating method. This method is not illustrated, but is used in the same manner as the per cent reacting value plots. Choice of methods will depend on the particular problem. Per cent reacting values can be used to advantage when correlating waters of different chemical character, but similar ionic concentrations. Equivalent per million values can be used when correlating similar waters with varying ionic concentrations.

TABLE 2—WATER ANALYSIS DATA USED IN FIG. 1; PER CENT REACTING VALUE

No. Sample	Date	Na+	Ca++	Mg++	$SO_4^=$	Cl-	HCO_3^- & $CO_3^=$	Total Equiv. Per Million
23	2-2-54	48.39	0.32	1.27	0.00	40.94	9.06	1,090
91	1-19-51	40.85	5.45	3.70	0.01	49.41	0.57	1,392
118	12-1-54	45.36	2.33	2.28	0.02	45.77	4.18	1,247
147	2-4-56	35.51	12.76	1.71	0.07	48.00	1.93	1,422
152	2-16-56	24.99	24.02	0.99	0.27	49.17	0.56	1,598

IDENTIFICATION OF A MIXTURE OF TWO WATERS

When waters mix without loss or gain of ions, the resulting mixture should contain an amount of each ion in proportion to the percentage of each water in the mixture. Such a mixture will hereinafter be referred to as an ideal mixture. Precipitation, base exchange, or other reactions may occur to result in mixtures that are not ideal. Therefore, it is advisable to compare all ions when studying mixtures of water.

Sample 118, which lies near the dashed line in Fig. 1, appears to be a mixture of Water A (Sample 23) and Water B (Sample 91) and will be used as an example. Table 3 gives the data for these waters that have been used to construct the simple proportion chart, Fig. 2.

All values of Sample 118 do not fall on a vertical straight line which would represent an ideal mixture of Waters A and B. The best vertical line representing the points is drawn at 51 per cent Water B and 49 per cent Water A. The magnesium, bicarbonate, chloride and the total reacting values for the mixture fall on the vertical line indicating precipitation has not occurred. Calcium appears to be 16 equivalents per million too low and sodium appears to be 16 equivalents too high for an ideal mixture. A possible explanation of these variances from an ideal mixture of Waters A and B is that base exchange has occurred as the water mixture passed through sands containing clay. The sulfate ion is considered of no significance in this sample because of its very low concentration in the three waters.

TABLE 3—WATER ANALYSIS DATA USED IN FIGURES 1, 2, AND 5; EQUIVALENTS PER MILLION

Ions	Water A	Water B	Water C	Sample 118	Sample 147
Na^+	527	569	399	566	505
Ca^{++}	14	76	384	29	182
Mg^{++}	4	51	16	29	24
$SO_4^=$	0.05	0.2	4	0.3	1
Cl^-	446	688	786	571	683
$CO_3^=$	0	0	0	0	0
HCO_3^-	99	8	9	52	27
Total	1,090	1,392	1,598	1,247	1,422

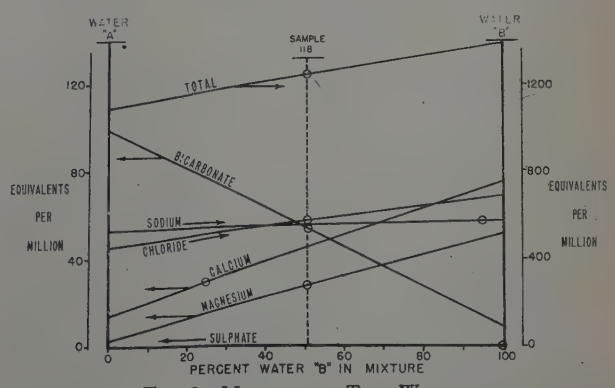

FIG. 2—MIXTURE OF TWO WATERS.

IDENTIFICATION OF A MIXTURE OF THREE WATERS

A method which can be used to identify a mixture of three waters is based on the use of an equilateral triangular prism. An isometric view of such a prism is shown in Fig. 3. Planes drawn within the prism are used to represent each ion. For simplicity, only the calcium and magnesium planes are shown. The calcium plane will be discussed to illustrate the principles of the method and the construction of proportion charts.

The position of the calcium plane in the prism is determined by placing the equivalents per million values of calcium for each of Waters I, II and III on the three vertical axes of the prism. The value of calcium in a particular mixture of the three waters will be a point on the calcium plane. A horizontal line through this point can be drawn to intersect two of the three edges of the calcium plane. Fig. 4 illustrates the method of determining where such horizontal lines intersect the edges of the planes. On the left of Fig. 4 is a view of the three sides of the prism opened to a plane. The solid lines connecting the vertical axes are the edges of the calcium and magnesium planes shown in Fig. 3. A horizontal dashed line is drawn as shown from the calcium value on the mixture column to intersect the edges of the calcium plane at X and Y. Vertical dashed lines from X and Y intersect the edges of the prism base at X′ and Y′. Points X′ and Y′ on the trilinear chart will form a line which is a projection of the horizontal line in the calcium plane. The magnesium line Z′W′ on the trilinear chart is drawn in a similar manner.

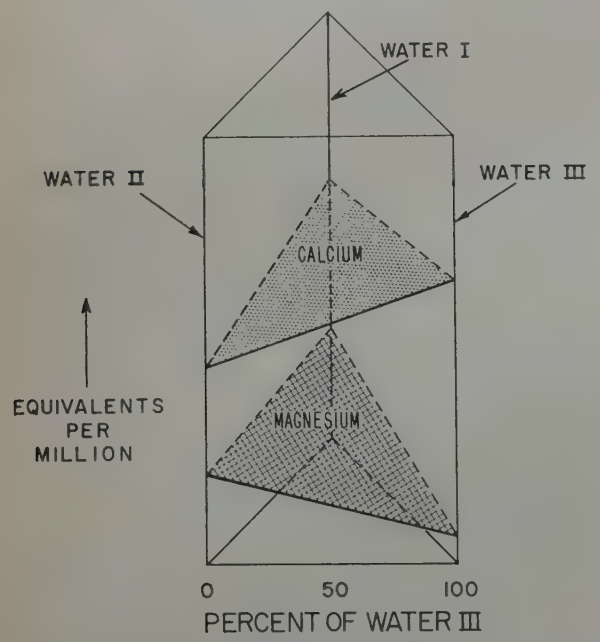

FIG. 3—TRIANGULAR PRISM REPRESENTING MIXTURES OF THREE WATERS.

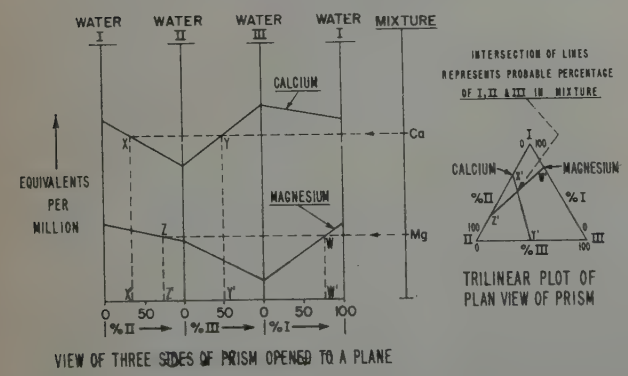

FIG. 4—CONSTRUCTION CHART—MIXTURE OF THREE WATERS.

If no loss or gain of any ion occurs as a result of mixing, the projected lines for all the ions in the mixture should intersect at a point on the trilinear chart to represent an ideal mixture. The point of intersection represents a vertical line in the prism which is determined by points on each of the ion planes at the concentration of each ion in the mixture.

Sample 147 of Fig. 1 is used as an example. Table 3 contains the data for Waters A, B, C and Sample 147 which are used on the proportion chart, Fig. 5. The total reacting value lines in Fig. 5 are used to explain the procedure. The plotted points of 1,090 on the left vertical Column A, 1,392 on Column B, 1,598 on Column C and 1,090 on the right Column A are connected as shown. A point is placed at 1,422 on the Sample 147 column to represent the total reacting value of the mixture. A horizontal dashed line is drawn from this point to intersect the total reacting value lines BC and CA. Vertical dashed lines from these intersection points intersect the abscissa at 15 per cent C and 35 per cent A. A straight line is drawn to connect 15 per cent C and 35 per cent A on the edges of the trilinear chart in Fig. 6. The other six lines on the trilinear chart, each of which represent an ion, are constructed in a similar manner.

It will be noted that all seven lines do not intersect at a point. The point best representing the intersections of all lines is found at the 21 per cent A, 32 per cent B and 47 per cent C. This mixture of Waters A, B and C would result in approximately the same chemical composition as Sample 147. Lines not passing through this intersection point indicate a difference in ionic concentration from an ideal mixture of the three waters. The mixture is identified by the point that has the least amount of variance of all ions from an ideal mixture. The variance of all of the ions in the mixture has been calculated and is listed in the last column of Table 4. The indicated equality of the sodium gain and the calcium loss lends support to the conclusion that calcium is base exchanging with sodium as the water mixture passes through sands containing clay.

The variance from an ideal mixture can also be graphically determined by parallel shifting of lines as shown by the dashed lines for sodium and calcium in Fig. 6. The equivalents per million values of the ideal mixture represented by the shifted lines can be determined by reversing the procedure and reading values in Fig. 5.

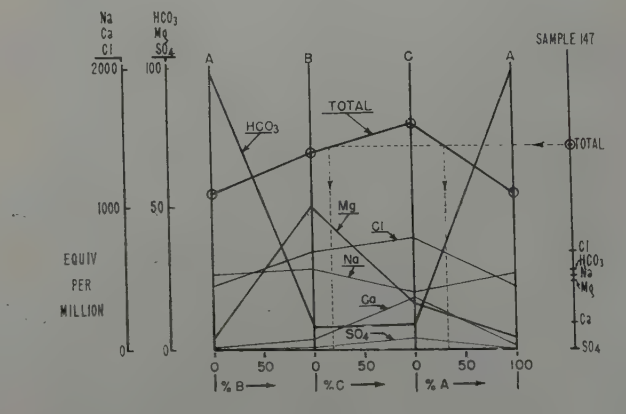

FIG. 5—PROPORTION CHART—MIXTURE OF THREE WATERS.

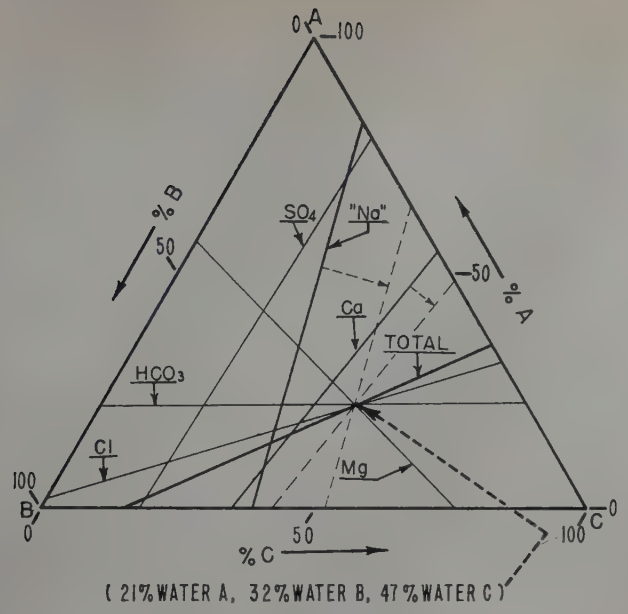

FIG. 6—TRILINEAR CHART—MIXTURE OF THREE WATERS.

CONCLUSIONS

The graphs presented in this paper offer the following advantages for correlating waters.

1. Numerous water analyses data can be plotted as points for rapid and easy correlation.

2. Type waters can be readily distinguished from mixtures of waters by comparing their placement as points on the correlation graphs and their ionic concentration.

3. Trends of changes in composition of waters can be followed.

4. The correlation graphs make available all previously plotted data for immediate comparison. Possible errors of interpretation should be reduced to a minimum.

Proportion charts to identify two and three water mixtures supplement the correlating graphs and confirm the conclusion that waters can be correlated and mixtures can be identified by the proposed methods.

TABLE 4—CALCULATED VS ACTUAL ANALYSIS, A MIXTURE OF THREE WATERS—SAMPLE 147
(Equivalents per Million)

	Water A	Water B	Water C	Calculated: 21 per cent A	32 per cent B	47 per cent C	Total (1)	Sample 147 (2)	Column (2) − (1)
Na^+	527	569	399	111	182	187	480	505	+25
Ca^{++}	14	76	384	3	24	180	207	182	−25
Mg^{++}	4	51	16	1	16	7	24	24	0
$SO_4^=$	0.05	0.2	4	0	0	2	2	1	− 1
Cl^-	446	688	786	93	220	370	683	683	0
HCO_3^-	99	8	9	21	2	4	27	27	0
Total	1,090	1,392	1,598	229	444	750	1,423	1,422	− 1

ACKNOWLEDGMENT

The author wishes to thank the Standard Oil Co. of California for permission to publish this paper and to acknowledge the encouragement and suggestions of D. E. Silcox in developing these methods.

REFERENCES

1. Stabler, Herman: "The Industrial Application of Water Analysis", Water Supply Paper 274, USGS (1911).
2. Palmer, Chase: "The Geochemical Interpretation of Water Analyses", *Bull.*, USGS (1911) 479.
3. Tickell, F. G.: "A Method for the Graphical Interpretation of Water Analysis", Report, California State Oil and Gas Supervisor (1921) **6**, (9) 5.
4. Reistle, C. E.: "Identification of Oil Field Waters by Chemical Analysis", TP 404, USBM (1927).
5. Stiff, Henry A.: "The Interpretation of Chemical Water Analysis by Means of Patterns", *Trans.* AIME (1951) **192**, 376. ★★★

T. N. 2017

The Thermal Recovery Process – An Analysis of Laboratory Combustion Data

A. L. BENHAM
JUNIOR MEMBER AIME
FRED H. POETTMANN
MEMBER AIME

THE OHIO OIL CO.
LITTLETON, COLO.

ABSTRACT

By considering the stoichiometry of the underground combustion process, an equation was derived relating the point velocity of the combustion front as a function of the air flux, fuel content, efficiency of oxygen utilization, hydrogen:carbon ratio, and ratio of carbon dioxide to carbon monoxide produced. In addition, an equation for calculating the amount of injected air necessary to produce the oil from 1 cu ft of reservoir space was derived. This equation has a direct bearing on evaluating compression costs for the process. Values calculated from these equations are in good agreement with experimentally observed values obtained from laboratory tube runs reported in the literature. The equations are also useful for analyzing experimental data for inconsistencies.

INTRODUCTION

The injection of energy in the form of heat into an oil-bearing formation as a means of increasing the recovery of oil has been the subject of much discussion and experimentation as far back as 1920. The ideas have ranged from the injection of steam to the direct use of electricity as a means of getting thermal energy into a formation.

However, most laboratory and field studies have been confined to the process whereby a portion of the crude in the reservoir is burned to generate the necessary heat to increase the mobility of the oil by reducing its viscosity. A recent paper by W. L. Martin, *et al.*[1], described the results of a number of laboratory experiments in which the combustion process was studied in a sandpack. Studies such as this indicate that with the temperatures involved, the oil is partially coked in this process and it is this coke which provides the fuel for combustion. The combustion of this residual coke can be analyzed theoretically by applying simple stoichiometric principles to the combustion process.

It is the purpose of this paper to compare the results reported in these experiments with those obtained from theoretical considerations. The variables studied by Martin, *et al*, among others, include combustion front velocity, air flux, oxygen utilization, fuel concentration, ratio of carbon dioxide and carbon monoxide in combustion gases, and the hydrogen:carbon ratio of the residual fuel. All these variables come into consideration when the stoichiometry of the combustion process is studied. The experimental conditions and results are tabulated in Tables 3 and 4 of Ref. 1. For purposes of comparison with calculated results, it was necessary to change the units of a number of the variables.

UNDERGROUND COMBUSTION STOICHIOMETRY

The combustion or oxidation of the carbonaceous residue or "coke" on the sand can be described in terms of the equation:

$$CH_n + \left[\frac{2m+1}{2m+2} + \frac{n}{4}\right] O_2 \rightarrow \left[\frac{m}{m+1}\right] CO_2 + \left[\frac{1}{1+m}\right] CO + \frac{n}{2} H_2O, \quad \ldots \quad (1)$$

where n is atomic ratio of hydrogen to carbon, m is ratio of moles of CO_2 to CO produced, and CH_n is taken as the unit molecular weight, realizing that actually the coke has a large range of high molecular weights.

Assuming that all the fuel laid down in the sand is burned, the ratio of moles of oxygen consumed to moles of coke can be written as follows.

$$\frac{\text{Moles } O_2}{\text{Moles coke}} = \left[\frac{2m+1}{2m+2} + \frac{n}{4}\right] \quad \ldots \quad (2)$$

In terms of moles O_2 per pound of coke,

$$\frac{\text{Moles } O_2}{\text{Lb coke}} = \left[\frac{2m+1}{2m+2} + \frac{n}{4}\right]\left[\frac{1}{12+n}\right], \quad \ldots \quad (3)$$

where $12 + n$ is the molecular weight in pounds per mole.

If the O_2 consumed is measured in standard cubic feet (60°F and 1 atm) and the coke in pounds per cubic foot of formation, Z, then:

Original manuscript received in Society of Petroleum Engineers office Jan. 13, 1958. Revised manuscript received June 6, 1958.
[1]Reference at end of paper.

$$\frac{\text{scf } O_2}{\text{cu ft reservoir}} = 379\left[\frac{2m+1}{2m+2}+\frac{n}{4}\right]\left[\frac{1}{12+n}\right]Z \quad . \quad . \quad . \quad . \quad . \quad . \quad . \quad . \quad . \quad . \quad . \quad . \quad . \quad . \quad . \quad . \quad (4)$$

or in standard cubic feet of air (where Y is the fraction of oxygen consumed),

$$\frac{\text{scf air}}{\text{cu ft reservoir}} = \frac{379}{0.21Y}\left[\frac{2m+1}{2m+2}+\frac{n}{4}\right]\left[\frac{1}{12+n}\right]Z \quad . \quad . \quad . \quad . \quad . \quad . \quad . \quad . \quad . \quad . \quad . \quad . \quad . \quad . \quad . \quad . \quad (5)$$

379 is the standard cubic feet of gas at 60°F and 1 atm occupied by 1-lb mole of the gas.

In general, combustion takes place in a relatively narrow zone which moves in the direction of air movement. The combustion front may be defined as an integrated average position within this zone determined by the degree of consumption of the coked residue in the zone. If V_F is defined as the velocity of a point in the combustion front (ft/hr) and A the cross-sectional area of the reservoir at a point in the front (sq ft), then V_FA is the volume of reservoir burned in one hour. Multiplying both sides of Eq. 5 by V_FA results in

$$\frac{(\text{scf air})\ (V_FA)}{\text{cu ft reservoir}} = \frac{379}{0.21Y}\left[\frac{2m+1}{2m+2}+\frac{n}{4}\right]\left[\frac{1}{12+n}\right] ZV_FA \quad . \quad . \quad . \quad . \quad . \quad . \quad . \quad . \quad . \quad . \quad . \quad . \quad . \quad . \quad . \quad . \quad (6)$$

Simplifying and rearranging:

$$\frac{\text{scf air}}{\text{hr } A} = \frac{379}{0.21Y}\left[\frac{2m+1}{2m+2}+\frac{n}{4}\right]\left[\frac{1}{12+n}\right] ZV_F \quad . \quad . \quad . \quad . \quad . \quad . \quad . \quad . \quad . \quad . \quad . \quad . \quad . \quad . \quad . \quad . \quad (7)$$

Defining $\frac{(\text{scf air})}{\text{hr } A}$ as Φ_F, the air flux at the point in the combustion front, and writing Eq. 7 in terms of V_F, the point velocity of front movement,

$$V_F = \frac{1.109 \times 10^{-3}(12+n)}{\left[\frac{2m+1}{m+1}+\frac{n}{2}\right]Z} Y\Phi_F \quad . \quad . \quad . \quad (8)$$

The constant 1.109×10^{-3} has the units of pound moles of oxygen per standard cubic foot of air at 60°F and 1 atm pressure.

One of the important factors in determining the economics of an in situ combustion process is the amount of air required to produce the oil in 1 cu ft of reservoir space. The limiting value of this variable can be obtained by calculating the amount of air required to move the combustion front through 1 cu ft of reservoir space. Eq. 8 can be rearranged as follows,

$$\frac{\Phi_F}{V_F} = \frac{\left[\frac{2m+1}{m+1}+\frac{n}{2}\right]Z}{1.109 \times 10^{-3}(12+n)Y} \quad . \quad . \quad . \quad (9)$$

The ratio of Φ_F/V_F is equal to the volume of air necessary to sweep the oil out of 1 cu ft of reservoir volume behind the front.

COMPARISON WITH EXPERIMENTAL TUBE RUN DATA

Of the six variables appearing in Eq. 8, one can assume any five as independent variables and the sixth as the dependent variable. Using the experimental data appearing in Tables 3 and 4 of Ref. 1, after reduction to the proper units, the experimental values were substituted into Eq. 8 and the calculated dependent variable compared with the experimentally observed value. In the case of the air required per cubic foot of formation, Eq. 9 was used. The results of this comparison are tabulated in Table 1. The agreement is good, particularly in Runs 13 through 17. Run 18 was interrupted and there is some question as to the accuracy of the experimentally measured results. In Runs 13 through 17, the discrepancy between calculated and experimental values of frontal velocity and fuel concentration varied from − 3.7 to − 8.8 per cent. In the case of the air flux, oxygen utilization and air required, this discrepancy ranged from + 3.5 to + 8.0 per cent. For any given variable, the deviations are all in the same direction.

It is helpful to understand the method of measuring combustion front velocity used by Martin, *et al*,[1] before comparing their results with those predicted by stoichiometry. They defined the rate of advance of the combustion front under steady-state operation as the rate of advance of a certain temperature level thought to be representative of combustion conditions. The correspondence between the velocity of movement of a given temperature level and the velocity of the actual combustion front will depend upon the existence or non-existence of transients in the tube runs. It is interesting to note that an error of 1 to 6 in. in defining the position of the front as a function of time in the authors' tube runs would account for the deviations given in Table 1.

In analyzing the experimental data, there appear to be two inconsistencies in the observed measurements. The first is oxygen utilization. From observations in the literature and our own experience, one would expect that oxygen utilization would approach 100 per cent. The experimental values of oxygen utilization reported appear to be quite low. This could have been due to channeling of air along the walls of the tube. Assuming this to be the case and since the air flux reported is the gross value, this discrepancy would not show any effect when substituted into Eq. 8, since the product of oxygen utilization, Y, times air flux, Φ_F, would be equal to the effective values sustaining the combustion. However, in determining the minimum fluxes necessary to sustain combustion at the ignition temperature, any channeling resulting in inefficient oxygen utilization would certainly result in a larger experimentally measured value of flux than was actually the case.

TABLE 1—COMPARISON OF CALCULATED VS EXPERIMENTALLY MEASURED VARIABLES.

Run No.	n	m	V_F		Φ_F		Z**		Y		Air required Φ_F/V_F	
			exp.	calc.	exp.	calc.	exp.	calc.	exp.	calc.	exp.	calc.
13	1.33	3.38	0.121	0.128	29.5	27.9	1.19	1.26	0.849	0.802	245	230
14	1.33	2.61	0.136	0.147	29.7	27.4	1.12	1.22	0.901	0.830	219	202
15	1.405	3.21	0.127	0.132	31.8	30.6	1.33	1.38	0.914	0.880	251	242
16	1.24	3.00	0.215	0.223	63.5	61.2	1.45	1.50	0.823	0.793	295	285
17	0.975	3.85	0.350	0.374	125.0	117.0	1.27	1.36	0.603	0.564	358	335
18*	1.33 (assumed)	3.68	0.036	0.042	10.7	9.2	1.47	1.71	0.956	0.818	301	258

*Run 18 was interrupted and therefore the experimental results from a steady-state standpoint are in question.
**Experimental values of Z were obtained by converting pounds of carbon burned per 100 lb of sand from Table 4 of Ref. 1, using the experimentally measured values of C:H ratio and 36 per cent porosity. A value of 2.65 was assumed for the specific gravity of the sand particles.

TABLE 2—COMPARISON OF CALCULATED VS EXPERIMENTALLY MEASURED VARIABLES ASSUMING $n = 1.6$

Run No.	n	m	V_F exp.	V_F calc.	Φ_F exp.	Φ_F calc.	Z** exp.	Z** calc.	Y exp.	Y calc.	Air required Φ_F/V_F exp.	Air required Φ_F/V_F calc.
13	1.6	3.38	0.121	0.122	29.5	29.3	1.20	1.21	0.849	0.844	245	244
14	1.6	2.61	0.136	0.141	29.7	28.7	1.14	1.18	0.901	0.870	219	212
15	1.6	3.21	0.127	0.127	31.8	31.8	1.35	1.35	0.914	0.914	251	251
16	1.6	3.00	0.215	0.207	63.5	65.8	1.49	1.44	0.823	0.853	295	306
17	1.6	3.85	0.350	0.356	125.0	123.0	1.34	1.36	0.603	0.594	358	353
18*	1.6	3.68	0.036	0.040	10.7	9.7	1.50	1.65	0.956	0.870	301	274

*Run 18 was interrupted and therefore the experimental results from a steady-state standpoint are in question.
**Experimental values of Z were obtained by converting pounds of carbon burned per 100 lb of sand from Table 4 of Ref. 1, using 1.6 as the H:C atomic ratio, 36 per cent porosity of the sand pack as reported, and 2.65 as the specific gravity of the sand particles.

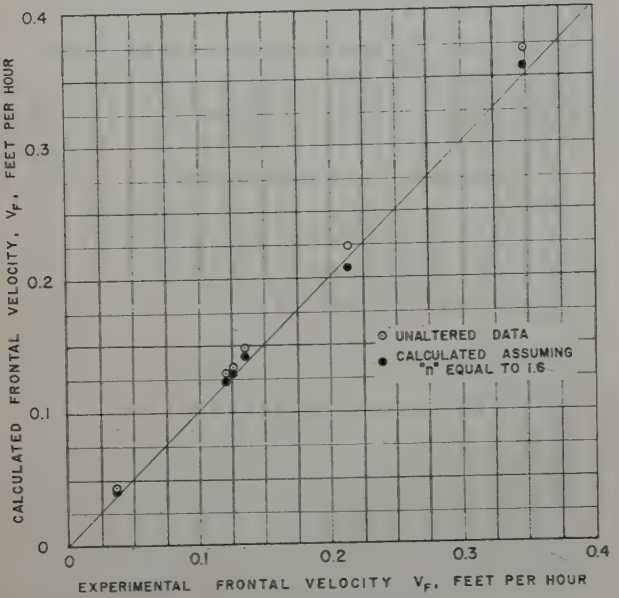

FIG. 1—COMPARISON OF CALCULATED VS EXPERIMENTAL FRONTAL VELOCITY.

The second inconsistency was in the observed hydrogen:carbon atomic ratio. For a given crude oil and reservoir rock, one would expect the hydrogen:carbon ratio to remain relatively constant. The validity of this supposition can be evaluated by using Eq. 8. Assuming the hydrogen:carbon ratio to be constant and equal to 1.6 and correcting the observed carbon consumption to residual fuel concentration, using the value of 1.6, values of the variables were again calculated and compared to the experimentally observed values (see Table 2). The agreement this time is much better, varying from -3.5 to $+3.5$ per cent for frontal velocity and residual fuel concentration, and from -3.6 to $+3.4$ per cent for flux, oxygen utilization and air required for Runs 13 through 17. Again, Run 18, although the agreement improved, was not included in this comparison because of the question regarding the accuracy of the experimental data. A plot of the calculated vs the experimental frontal velocity is shown in Fig. 1 for both calculated cases.

The contention that n is a relatively constant value would seem to be borne out by these calculations. However, it is also shown that a large variation in the value of n, as much as 50 to 70 per cent, has only a minor effect on the value of the frontal velocity, air flux, fuel concentration and combustion efficiency.

CONCLUSIONS

From a consideration of the stoichiometry of the combustion reaction of the underground combustion process, an equation can be derived relating frontal velocity at a point, air flux, oxygen utilization, residual fuel concentration, hydrogen:carbon ratio and the ratio of carbon dioxide to carbon monoxide in the combustion gases. Values calculated from this equation are in good agreement with experimentally observed values obtained from tube runs reported in the literature.[1] The equation is also useful in analyzing experimental data for apparent inconsistencies.

REFERENCE

1. Martin, William L., Alexander, John D. and Dew, John N.: "Process Variables of In Situ Combustion," *Trans.* AIME (1958) **213**, 28.

★★★

On the Streaming Potential Problem in Well Logging

M. R. J. WYLLIE
MEMBER AIME
A. J. de WITTE
J. E. WARREN
JUNIOR MEMBER AIME

GULF RESEARCH & DEVELOPMENT CO.
PITTSBURGH, PA.

ABSTRACT

It has been suggested that streaming potentials are not normally logged because the streaming potentials known to be generated across mud filter cakes are substantially cancelled by streaming potentials generated in contiguous shale beds. Laboratory measurements of streaming potentials across hand specimens of shale have been adduced as evidence to support the suggestion. The experiments show that streaming potential depends on the resistivity of the equilibrating solution and on pressure drop. Measurements were made perpendicular to the bedding planes of the shales.

The mechanism of streaming potential generation in shale which the suggested cancellation theory implies has been critically examined. Conclusions reached are tested by comparing self potentials logged before and immediately after changing the resistivity (but not the weight) of mud in a borehole. The resultant SP change is found to equal the theoretical electrochemical potential change, i.e., cancellation of streaming potential is independent of mud resistivity. Since streaming potentials generated across mud filter cakes depend critically upon mud resistivity, shale streaming potential in situ must be equally sensitive.

Using plausible values for the permeability, porosity and compressibility of shale, the van Everdingen-Hurst approach shows that the pressure drop between borehole pressure and formation pressure in a radially homogeneous shale is unlikely to coincide with the zone of filtrate invasion. If, perchance, this coincidence occurs with one mud a change to a second must result in non-coincidence, i.e., a SP logged in the second mud should show a streaming potential. The dilemma may be overcome by postulating: (1) permeabilities of shales parallel to their bedding planes greatly exceed their cross-bedding permeabilities; (2) a resistivity-sensitive mud cake of low permeability forms either on the face of, or probably in the laminations of, many shales.

These postulates are examined with reference to the pressure and SP histories of the McClosky and Aux Vases zones in the Illinois Basin and some support for them found.

It is concluded that a definitive solution to the streaming potential problem does not exist.

Original manuscript received in Society of Petroleum Engineers office Feb. 4, 1958. Revised manuscript received April 28, 1958.

INTRODUCTION

Recently Gondouin and Scala[1] published a contribution to the streaming potential problem which is notable particularly for the elegance of its experimental techniques. The conclusions drawn by Gondouin and Scala from their studies amplified those previously suggested by Schenck[2]. In essence they suggested that the streaming potentials known to develop across mud filter cakes[3] are not normally observed on SP logs because they are largely cancelled by streaming potentials generated in adjacent shales.

This suggestion appears so reasonable that many workers in the logging field will be prone to accept it. We incline strongly to the view that the suggestion is basically correct. Nevertheless, it is important to realize that the cancellation hypothesis in the form put forward by Gondouin and Scala does not appear to meet all the known experimental facts. It is the principal intention of this note to call attention to what appears to be a flaw in the relevancy of the experimental evidence adduced by Gondouin and Scala and to suggest an alternative hypothesis to remove it. The consequences of the new hypothesis are compared with field data which, we believe, are unique. A second but not less important purpose of this note is to emphasize that even the new hypothesis does not fully explain all field observations. Hence we conclude that further study of the streaming potential problem is required before it can be said that a definitive solution to it has been attained.

The bare experimental bones of laboratory data on streaming potentials appear to be as follows.

1. A streaming potential is developed across a mud filter cake. This streaming potential is virtually independent of cake thickness but depends on the mud resistivity. The relationship is of the form, $E_{kmc} = k_1 p^Y$, where $k_1 = f_1(R_m)$.

2. A streaming potential is developed across a shale. This potential is independent of shale thickness but depends on the resistivity of the permeating solution if the shale has been first equilibrated in this solution. The relationship is of the form, $E_{ks} = k_2 p$, where $k_2 = f_2(R_{mf})$.

The relationship in (1) was determined first by Wyllie[3], confirmed by Gondouin and Scala and qualita-

[1]References given at end of paper.

tively checked also by Sen Gupta and Banerjee[4]. The relationship in (2) was established by Schenck[2]; it forms the subject of Gondouin and Scala's paper. We note that for reasons of experimental practicability, all streaming potential measurements on shales have been made with the pressure difference causing flow directed perpendicular to the bedding planes of the shale.

Conclusions concerning streaming potentials which are based on field observations are less definite. The principal ones which might be acceptable to a majority of logging specialists are: (1) in regions where subsurface pressures are normal the streaming potential component of the SP curve is small or zero, (2) in regions where subsurface pressures are abnormally low streaming potentials are sometimes evident, and, (3) if the hydrostatic pressure in a borehole is suddenly altered the magnitude of the SP opposite sands is altered.

THEORETICAL DISCUSSION

The SP as measured and defined is the difference between the borehole potential opposite sands and shales. Thus, only the algebraic difference between streaming potentials generated in sands and shales can be recorded. The streaming potential in a sand is, in most cases, the streaming potential across the mud filter cake which sheaths the sand face[3]. This streaming potential is a function of mud resistivity. If the resistivity but not the density of a drilling mud is changed, not only does the electrochemical component of the SP change but so also does the filter-cake streaming potential. What happens under similar circumstances to the streaming potential generated in a shale? We have a reasonable amount of field evidence, for example that shown in Fig. 1, which suggests that the shale streaming potential changes by virtually the same amount as the filter-cake

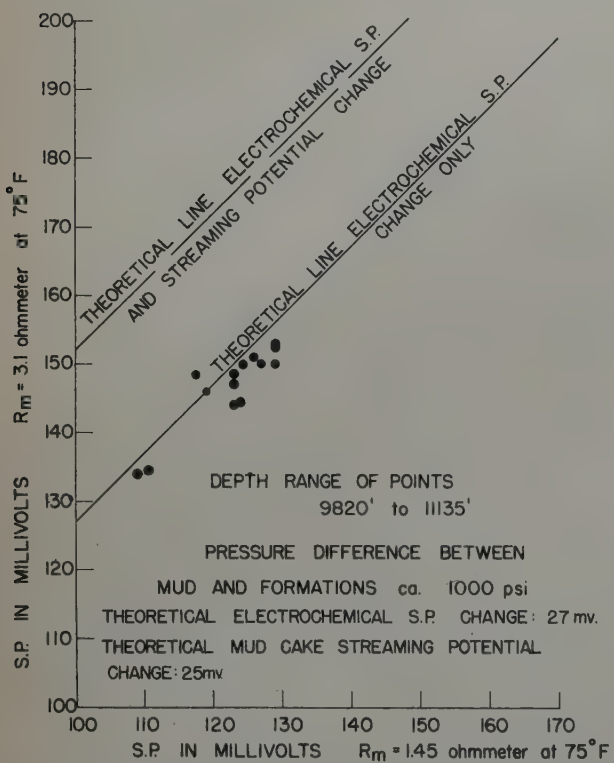
THEORETICAL LINE ELECTROCHEMICAL S.P. AND STREAMING POTENTIAL CHANGE
THEORETICAL LINE ELECTROCHEMICAL S.P. CHANGE ONLY
DEPTH RANGE OF POINTS 9820' to 11135'
PRESSURE DIFFERENCE BETWEEN MUD AND FORMATIONS ca. 1000 psi
THEORETICAL ELECTROCHEMICAL S.P. CHANGE: 27 mv.
THEORETICAL MUD CAKE STREAMING POTENTIAL CHANGE: 25mv
S.P. IN MILLIVOLTS Rm = 3.1 ohmmeter at 75°F
S.P. IN MILLIVOLTS Rm = 1.45 ohmmeter at 75°F
200
190
180
170
160
150
140
130
120
110
100
100 110 120 130 140 150 160 170

FIG. 1—CHANGE OF SP RESULTING FROM CHANGE IN MUD COMPARED WITH THEORETICAL ELECTROCHEMICAL CHANGE AND CHANGE EXPECTED IF STREAMING POTENTIAL IN SHALE IS INDEPENDENT OF MUD RESISTIVITY.

streaming potential. That is, the field data indicate that the change in SP resulting from a deliberate change in mud resistivity closely approximates the theoretical change in electrochemical SP. These data, we believe, are incompatible not only with the experimental results of Gondouin and Scala but also with the transient pressure distributions that exist in sands and shales penetrated by a borehole containing weighted mud.

Gondouin and Scala show experimentally that the streaming potential across a shale depends both on the resistivity of the fluid that saturates the shale and the pressure drop across it; they show also that the permeabilities of shales in a direction perpendicular to their bedding planes are in the range of 10^{-4} to 10^{-6} md. It seems possible that the permeabilities of many shales are much larger in a direction parallel to their bedding planes; indeed, data obtained when investigating lost returns indicate that horizontal permeabilities may depend upon the difference between mud and formation pressures.

Fig. 2 shows, as a function of time, what percentage of the difference between the borehole mud pressure

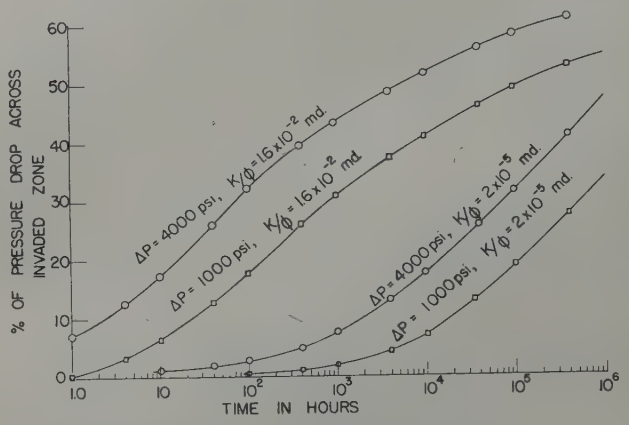
% OF PRESSURE DROP ACROSS INVADED ZONE
TIME IN HOURS
ΔP = 4000 psi, K/φ = 15x10⁻² md.
ΔP = 1000 psi, K/φ = 15x10⁻² md.
ΔP = 4000 psi, K/φ = 2x10⁻⁵ md.
ΔP = 1000 psi, K/φ = 2x10⁻⁵ md.
60
50
40
30
20
10
0
1.0 10 10² 10³ 10⁴ 10⁵ 10⁶

FIG. 2—PERCENTAGE OF THE PRESSURE DIFFERENCE BETWEEN MUD PRESSURE AND FORMATION PRESSURE WHICH OCCURS ACROSS THE FILTRATE INVADED ZONE OF A SHALE SHOWN AS A FUNCTION OF THE TIME AFTER THE SHALE HAS BEEN DRILLED.

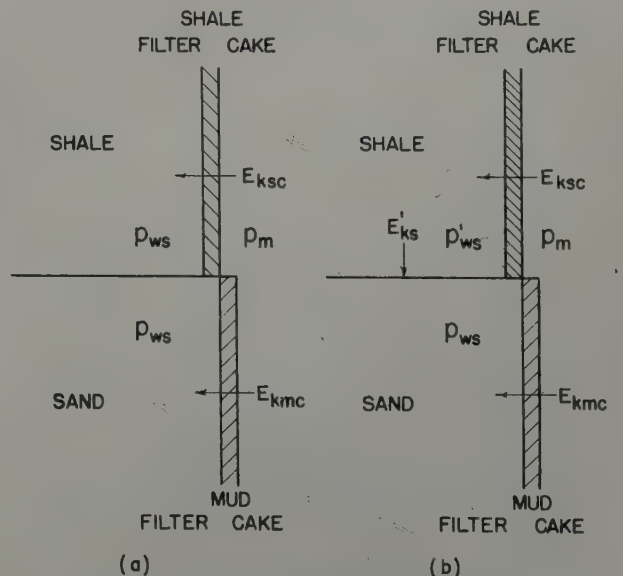

FIG. 3—PRESSURE AND STREAMING POTENTIAL DISTRIBUTION WHERE (A) PRESSURES IN SAND AND SHALE ARE EQUAL; AND (B) PRESSURE IN SHALE EXCEEDS THAT IN SAND.

and the formation pressure of a shale, at the same level, occurs across the zone of mud filtrate invasion into the shale. The method of calculation uses numerical results from van Everdingen and Hurst[5], and from Jaeger[6]. Details of the assumptions made are given in the Appendix. It will suffice here to note the following. Even when horizontal shale permeabilities between 10^{-6} and 10^{-3} md are assumed, only a small percentage of the total pressure drop occurs across the invaded zone in the normal time interval between drilling a shale and logging it, i.e., from 2 to 200 hours approximately. The pressure drop is largely concentrated in that part of the shale which is uninvaded. Thus, the streaming potential into the shale consists of two potentials in series. One is in the uninvaded zone and one in the invaded. Since streaming potential is proportional to pressure drop, the sum of the two potentials is likely to be dominated by the streaming potential in the virgin shale. *And this will be constant and independent of mud resistivity.*

This conclusion can be tested experimentally. When a mud of high resistivity is used and no potential in excess of an electrochemical potential is observed, the shale and filter-cake streaming potentials presumably cancel. A change to a mud of lower resistivity, by decreasing the streaming potential across the filter cake, should result in a SP smaller than that anticipated from electrochemical considerations only. That is, the SP recorded in the mud of lower resistivity should be less than the original SP by the sum of the eletrochemical potential change and the change in the streaming potential across the filter cake on the sand. Fig. 1 is typical of field data which, we believe, show this conclusion to be unfounded. The expected streaming potential change is based on the curves given in Fig. 4.

The case cited is that in which the formation pressures of sands and adjacent shales are the same.

If data of the kind shown in Fig. 1 are to be explicable, it appears to us that streaming potentials generated by both the shale and filter cake must be functions of the mud resistivity. In order to rationalize this belief it is necessary to postulate that a filter cake is built up either between the foliations of a shale or directly on its borehole face. This filter cake must have properties very similar to those of a filter cake formed on a sand; in particular, the permeability of shale filter cakes must be smaller by several orders of magnitude than the permeability of shales *measured parallel to their bedding planes.*

On this view the major portion of the pressure drop between the mud column and the shale occurs across

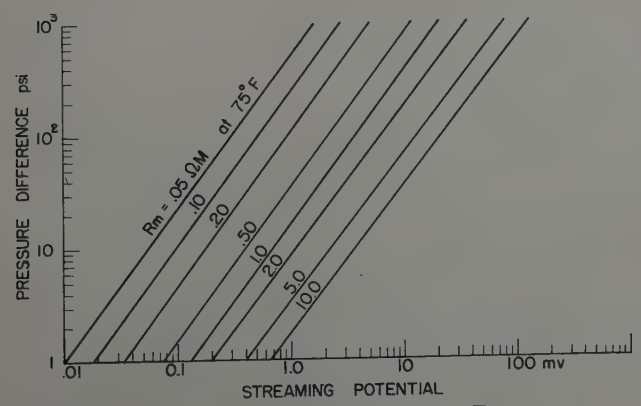

FIG. 4—AVERAGE STREAMING POTENTIAL THROUGH MUD CAKE VS PRESSURE DIFFERENCE FOR VARIOUS R_m (REF. 3).

the shale filter cake. The streaming potential generated in the shale is thus located immediately adjacent to the borehole; like that across a sand filter cake it will strongly depend on mud resistivity. The approximate pressure and streaming potential distributions to be expected when the formation and shale pressures are respectively equal and unequal are shown in Fig. 3.

PHYSICAL MODELS

When the pressures in sand and shale are equal the net streaming potential logged will be $|E_{kmc} - E_{ksc}|$; any observable streaming potential component of the SP will result from differences in the electrochemical nature of the shale and sand filter cakes and/or differences in the pressure drops across the two cakes. The latter factor depends on the respective thicknesses of the cakes and the ratios between their permeabilities and those of the media on which they form. This is the case shown in Fig. 3a. In general the quantity $|E_{kmc} - E_{ksc}|$ would be expected to be small. The very large volume of practical SP interpretations, successfully carried out in the industry on the assumption that no streaming potentials exist, seems to confirm this expectation.

If for some reason the hydrostatic pressure in a shale differs from that in a contiguous sand, the condition shown in Fig. 3b arises. This condition may be caused, for example, if the sand is lenticular, contains undersaturated oil and is rapidly depleted. Owing to the *low vertical permeabilities* of shales the pressure in the shale lags behind that in the sand; to a first approximation, the shale pressure may be considered to remain at the original pressure of the virgin sand. There are now three streaming potentials. As before two of these occur across the filter cakes. The third is caused by water expressed from the compacting shale into the contiguous low pressure sand. The streaming potential logged is now $|E_{kmc} - E_{ksc} - E'_{ks}|$. We shall call this Case 1.

If the depth of filtrate invasion into a shale is small and the formation of a filter cake on the shale is not postulated, a second approach may be made to the calculation of the streaming potential arising under the conditions shown in Fig. 3b. It indicates that the streaming potential logged should merely be the difference between the streaming potentials generated across the filter cake on the sand and across the uninvaded (virgin) shale. As already noted this approach does not appear to conform to data of the kind shown in Fig. 1.* We shall call this Case 2.

CASE 1

$$E_{kmc} = f_1(R_m)\ (p_m - p_{ws})^Y$$
$$E_{ksc} = f_1(R_m)\ (p_m - p'_{ws})^Y$$
$$E'_{ks} = k_2(p'_{ws} - p_{ws})$$

If R_m is known, approximate values for E_{kmc} and E_{ksc} may be calculated from the correlation of experimental data presented by Wyllie[3] and shown here as Fig. 4.

The value of E'_{ks} is the streaming potential generated in a material containing cation-exchange material. Much evidence suggests that the cation transference number of a shale in situ approaches unity, i.e., that shale behaves in situ as an almost perfect cation-permeable membrane.[7] For such membranes the proportionality constant, k_2, always seems to be close to mv/100 psi[8]. Such a figure is not incompatible with the experimental data of Gondouin and Scala. Thus,

*But this mechanism may be important in the case of shales which are not bedded and on (or in) which a filter cake does not readily form.

CASE 2

$$E'_{ks} = \frac{1.0}{100}(p'_{ws} - p_{ws}) \text{ mv for pressures in psi.}$$

$$E_{kmc} = f_1(R_m)\ (p_m - p_{ws})^Y$$

$$E_{ks} = \frac{1.0}{100}(p_m - p_{ws})$$

In Case 2, E_{ks} is the streaming potential across a virgin shale bed. It is assumed that the proportionality constant is 1 mv/100 psi for both horizontal and vertical flow of fluid in the shale.

ANALYSIS OF FIELD DATA

The McClosky producing zone and the Aux Vases sand in the Illinois Basin are locally notorious for the abnormal size of the SP they develop. An example is shown in Fig. 5. The waters in these pays have been analyzed frequently; the analyses are consistent. Typical figures for the McClosky zone are $Na^+ = 39{,}832$; $Ca^{++} = 6{,}088$; $Mg^{++} = 1{,}892$; $Cl^- = 76{,}170$; $SO_4^{--} = 2{,}020$; $HCO_3^- = 69$; and total = 126,091 (all figures are in mg/liter). A water of such analysis and high salinity, it is pertinent to note, will not give rise to a significant bi-ionic potential[9]. The Aux Vases sand contains water very similar to the McClosky zone and lies just above it.

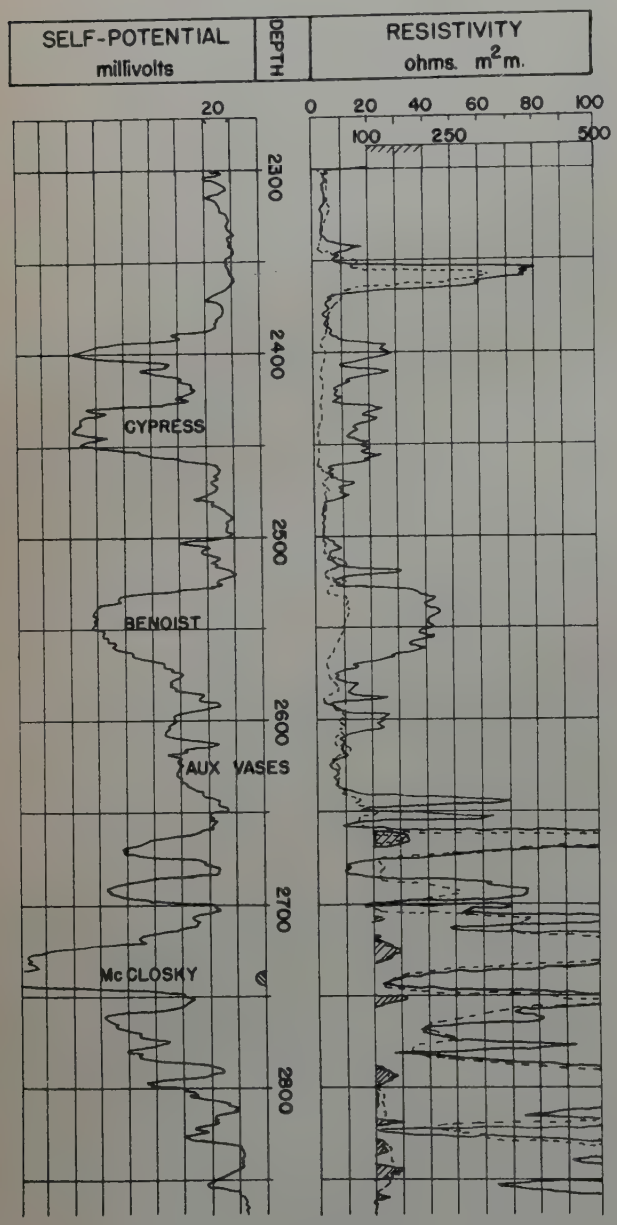

FIG. 5—ABNORMAL DEVELOPMENT OF SP OF McCLOSKY ZONE (BHP—320 PSI) BY COMPARISON WITH SP OPPOSITE OTHER FORMATIONS WITH SIMILAR CONNATE WATER (BHP—1,300 PSI CA).

The following data were garnered concerning logs run in wells penetrating the McClosky zone and/or the Aux Vases sand: (1) field in which log was run, (2) date on which log was run, (3) resistivity and weight of mud used, (4) SP opposite McClosky zone and/or Aux Vases sand, (5) subsurface depth of McClosky zone and/or Aux Vases sand, (6) temperature of McClosky zone and/or Aux Vases sand, and (7) bottom-hole pressures measured in the McClosky zone and/or Aux Vases sand in various fields and the dates of these measurements.

The bottom-hole pressure data were then plotted as a function of time in the manner shown in Figs. 6 and 7. Fig. 6 represents the best suite of data obtained. Fig. 7 is typical of those whose quality was less satisfactory and which had to be smoothed to produce a consistent decline curve. From these curves (data for eight fields were available) the approximate formation pressure at the time a log was run was obtained.

By using $R_m - R_{mf}$ correlation charts[10] the filtrate resistivity of each mud was determined; the filtrate resistivity was converted to an activity using the charts given in Ref. 3. The salinity of the McClosky and Aux

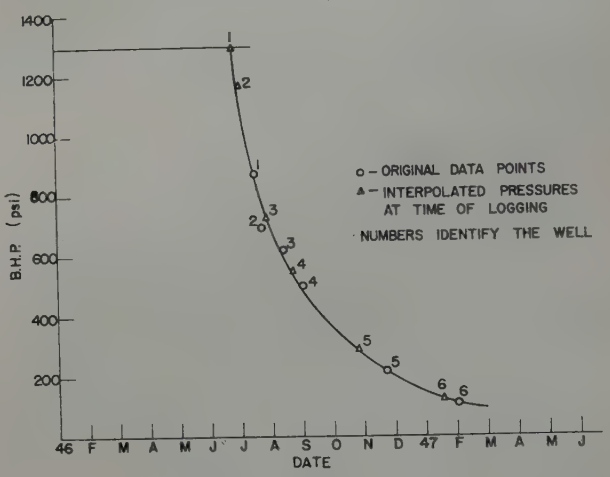

FIG. 6—PRESSURE DECLINE CURVE, AUX VASES SAND, SOUTH STANFORD FIELD, CLAY COUNTY, ILL.

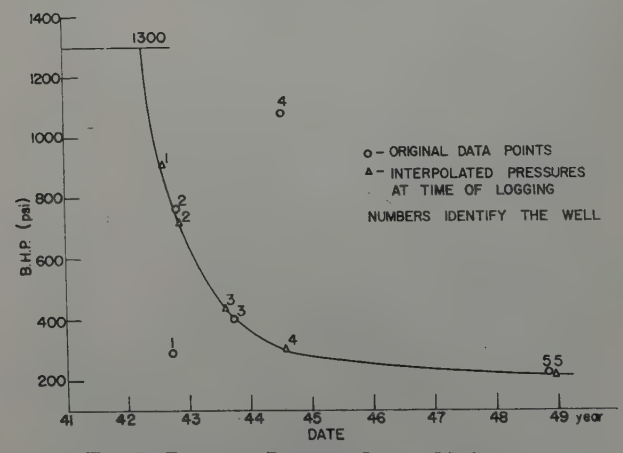

FIG. 7—PRESSURE DECLINE CURVE, McCLOSKY ZONE, EAST DUNDAS FIELD, RICHLAND COUNTY, ILL.

Vases waters was similarly expressed as activities. The electrochemical component, E_c, of each SP was then computed for the formation temperatures applicable and the streaming potential component from the difference between the observed total SP and the computed electrochemical SP; i.e., $E - E_c$.

As a first approximation the hydrostatic pressure in the shale, p'_{ws}, was assumed to be the pressure in the McClosky zone or Aux Vases sand in each field at the time of discovery. The appropriate pressure at the time of logging, p_{ws}, was obtained, as already noted, by interpolation from the smoothed pressure decline curves. The mud pressure, p_m, opposite each zone was computed from the density of the mud used and the subsurface depth of the zone. Thus, the quantities, $(p_m - p_{ws})$, $(p - p'_{ws})$ and $(p'_{ws} - p_{ws})$, were found. By using Fig. 4, E_{kmc} and E_{ksc} could be estimated since the resistivities of the muds employed were also known. Figs. 8 and 9 show plots of $E - E_c$ vs $E_{kmc} - E_{ksc} - E'_{ks}$ (Case 1) and $E_{kmc} - E_{ks}$ (Case 2).

The most characteristic feature of both Figs. 8 and 9 is the scatter of points. Clearly it would be unwise to base any dogmatic conclusions upon such data. Nevertheless their significance must be judged against a background made up of the following facts.

1. No attempt was made to adjust E for the effects of bed thickness.

2. The calculated value of E_{kmc} and E_{ksc} were based on averages taken from Ref. 3 which shows that variations of individual muds from the average may be quite large.

3. The calculation of E_c was based on average values of R_{mf} obtained from the Schlumberger correlation; here again significant divergences of particular muds from the average are not uncommon.

4. The pressure data used were not impeccable although the best available. In all cases it was assumed that p'_{ws} was the original discovery pressure; this is necessarily an oversimplification since p'_{ws} must tend to p_{ws} with time after discovery.

5. The assumption that for all virgin shales in situ the streaming potential is 1.0 mv/100 psi needs confirmation. It is pertinent to note the absence of any systematic shale baseline shift across formations suffering rapid pressure decline. This indicates that the streaming potential generated in two adjoining shales must be very similar (although not necessarily 1.0 mv/100 psi)*.

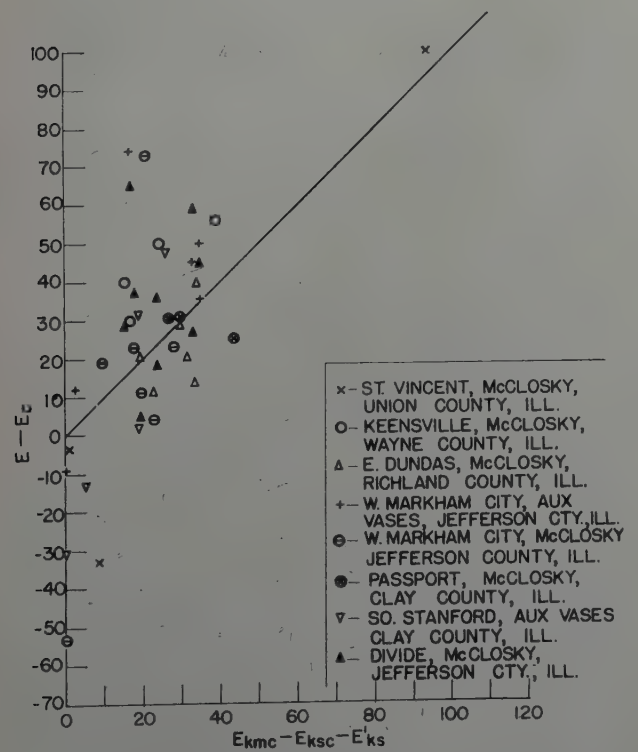
E − Ec
Ekmc − Eksc − E'ks
× – ST. VINCENT, McCLOSKY, UNION COUNTY, ILL.
O – KEENSVILLE, McCLOSKY, WAYNE COUNTY, ILL.
Δ – E. DUNDAS, McCLOSKY, RICHLAND COUNTY, ILL.
+ – W. MARKHAM CITY, AUX VASES, JEFFERSON CTY., ILL.
⊖ – W. MARKHAM CITY, McCLOSKY JEFFERSON COUNTY, ILL.
⊗ – PASSPORT, McCLOSKY, CLAY COUNTY, ILL.
▽ – SO. STANFORD, AUX VASES CLAY COUNTY, ILL.
▲ – DIVIDE, McCLOSKY, JEFFERSON CTY., ILL.

FIG. 8—PLOT OF EXCESS SP $(E - E_c)$ VS CALCULATED STREAMING POTENTIAL $(E_{kmc} - E_{ksc} - E'_{ks})$ BASED ON THE ASSUMPTION OF A SHALE FILTER CAKE (CASE 1).

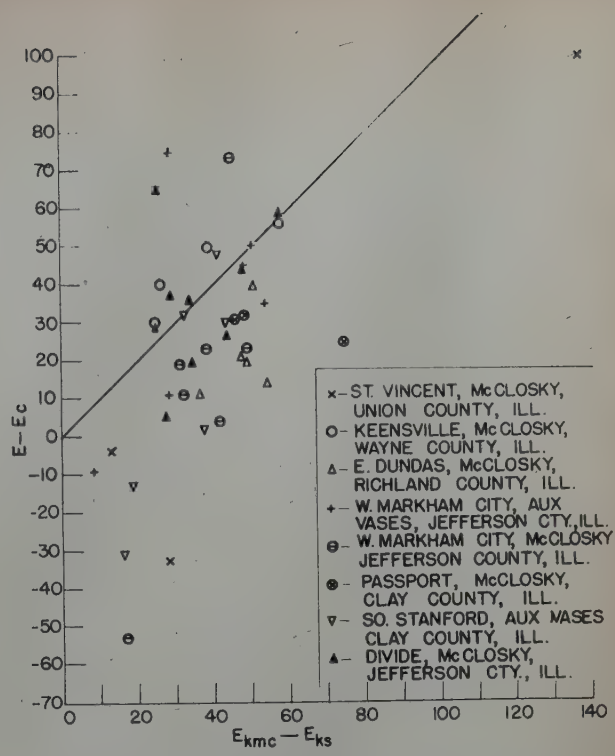
E − Ec
Ekmc − Eks
× – ST. VINCENT, McCLOSKY, UNION COUNTY, ILL.
O – KEENSVILLE, McCLOSKY, WAYNE COUNTY, ILL.
Δ – E. DUNDAS, McCLOSKY, RICHLAND COUNTY, ILL.
+ – W. MARKHAM CITY, AUX VASES, JEFFERSON CTY., ILL.
⊖ – W. MARKHAM CITY, McCLOSKY JEFFERSON COUNTY, ILL.
⊗ – PASSPORT, McCLOSKY, CLAY COUNTY, ILL.
▽ – SO. STANFORD, AUX VASES CLAY COUNTY, ILL.
▲ – DIVIDE, McCLOSKY, JEFFERSON CTY., ILL.

FIG. 9—PLOT OF EXCESS SP $(E - E_c)$ VS CALCULATED STREAMING POTENTIAL $(E_{kmc} - E_{ks})$ BASED ON THE ASSUMPTION OF NO SHALE FILTER CAKE (CASE 2).

DISCUSSION OF RESULTS

If viewed in their most favorable light the data shown in Fig. 8 may be held to indicate reasonable over-all agreement, both qualitative and quantitative, between excess potentials deduced from the SP log and streaming potentials calculated on the assumptions of Case 1.

The points shown in Fig. 9 are even more scattered than those of Fig. 8. Nevertheless, to use this observation as a significant factor with which to buttress the merits of the Case 1 assumption against that of Case 2 seems unwise. The data of Fig. 9 are more decisively influenced than those of Fig. 8 by the assumption made concerning the magnitude of streaming potentials generated in virgin shale. A different assumed value for the constant relating potential to pressure could reduce the scatter and make the points fall closer to the 45° line. In particular the horizontal component of the streaming potential probably exceeds 1 mv/100 psi. We feel our

*The general absence of shale baseline shifts on logs implies a homogeneity in the electrokinetic character of shales which is belied by the laboratory data of Gondouin and Scala. This paradox resembles that which characterizes the electrochemical properties of shales (see Ref. 7). It is resolved if our assumption is accepted; i.e., the significant electrokinetic effects of shales are generated in filter cakes near their borehole surfaces and, thus, are related more to the properties of the mud than to the shale itself.

preference for the Case 1 assumptions over those of Case 2 is sustained by data such as those shown in Fig. 1.

If viewed more unfavorably it could be argued that the data shown in Figs. 8 and 9 are too scattered even to justify the view that the excess potentials of the Illinois Basin have an electrokinetic origin. The fact that two methods of calculating streaming potential as different as those of Cases 1 and 2 both lead to rather similar results is an additional argument against attributing much significance to the data.

We take an intermediate view. The data plotted are probably as good as any that can be obtained without engaging upon an expensive and very lengthy system of field observations. The fact that, in Fig. 8 particularly, most of the points are in the range of 20 to 40 mv may be undesirable experimentally but is inevitable practically, i.e., having regard to the fact that mud resistivities and bottom-hole and mud pressures are inevitably similar in most wells of a field. Nevertheless, when a mud of exceptionally high resistivity was used and the excess potential was estimated to be 100 mv, the streaming potential calculated was 94 mv (Case 1) and 137 mv (Case 2). The fact that no form of electrochemical potential will explain the SP abnormalities of the Illinois Basin is also an argument in favor of their electrokinetic origin. We base this statement on the results of both theoretical and experimental investigations we have made. Using samples of McClosky reservoir rock, we endeavored to generate bi-ionic potentials and potentials resulting from the differential oxidation of electronically conducting minerals; all our efforts led to negative results.

SUMMARY AND CONCLUSIONS

In summary we suggest that electrokinetic potentials may be observed in cases where shales are not in hydrostatic balance with adjacent sands. In cases where hydrostatic equilibrium exists, net streaming potentials are likely to be negligible. Mechanistically, we feel these two beliefs can be rationalized if it is assumed that there exist on shales filter cakes whose properties strongly resemble those of filter cake formed on sands. In particular, their electrokinetic properties must be a strong function of mud resistivity.

We conclude by drawing attention to observations which we do not feel can be unequivocally explained by any present streaming potential hypothesis. We refer to the well substantiated fact (see, for example, Fig. 11 of Gondouin and Scala[1]) that a change in mud pressure will change the magnitude of the recorded SP. It can be argued, as was done by Gondouin and Scala, that this increase is merely a measure of the difference in the electrokinetic properties of a shale and the filter cake of an adjacent sand. We can argue similarly that the SP change represents differences between the properties of filter cakes formed on shales and sands. This seems unduly glib. In ordinary logging the pressure difference between mud column and formations is largely arbitrary and controlled by the mud weight carried. It seems generally true that no streaming potential is observed. Yet if this pressure difference is changed the SP changes. It is not likely that such behavior is due to chance alone.

We have endeavored to explain the sensitivity of the SP to changes in mud pressure by a consideration of the transient pressure behavior in the shale and sand filter cakes. No logical explanation is evident. A possible starting point for a fuller investigation is a detailed analysis of the pressure and potential distributions that exist in a permeable sand bed sheathed by a filter cake and contained between much less permeable shales. The distribution we show in Fig. 4 is grossly oversimplified. Until this has been done we cannot feel that a convincing explanation has been afforded of all effects of pressure on the SP log.

REFERENCES

1. Gondouin, M. and Scala, C.: "Streaming Potential and the SP Log", *Trans.*, AIME (1958) **213,** 170.
2. Schenck, K. D.: "Investigation of the Streaming Potential Developed in Formations of Low Permeability", MS Thesis, U. of Oklahoma (1955).
3. Wyllie, M. R. J.: "An Investigation of the Electrokinetic Component of the SP Curve", *Trans.*, AIME (1951) **192,** 1.
4. Sen Gupta, N. C. and Banerjee, C. G.: "A Laboratory Method of Evaluating Streaming Potentials Across Mud Sheaths", *Jour. Inst. Pet.* (1955) **41,** 207.
5. Van Everdingen, A. F. and Hurst, W.: "The Application of the Laplace Transformation to Flow Problems in Reservoirs", *Trans.*, AIME (1949) **186,** 305.
6. Jaeger, J. C.: "Numerical Values for the Temperature in Radial Heat Flow", *Jour. of Math. & Physics* (1956) **34,** 316.
7. Wyllie, M. R. J.: "Role of Clay in Well Log Interpretation", *Bull.*, Div. of Mines, California (1955) No. 169, 282.
8. McKelvey, J. G., Spiegler, K. S. and Wyllie, M. R. J.: "Ultrafiltration of Salt Solutions Through Ion-Exchange Membranes", presented to AIChE meeting, Baltimore, Md. (Sept. 1957) in press.
9. Gondouin, M., Tixier, M. P. and Simard, G. L.: "An Experimental Study on the Influence of the Chemical Composition of Electrolytes on the SP Curve", *Trans.*, AIME (1957) **210,** 58.
10. Log Interpretation Charts, Schlumberger Well Surveying Corp. (1954).

APPENDIX

Let us make the following assumptions about the physical system.

1. The shale bed is a homogeneous porous medium of a constant thickness that is completely saturated with water initially.

2. The flow is two-dimensional and obeys Darcy's law.

3. The liquid density is approximately a linear function of pressure; i.e., $\rho = \rho_i [1 + c(p - p_i)]$.

4. No filter cake is formed on the shale.

5. The filtrate has the same compressibility, density and viscosity as the formation water.

6. The filtrate completely displaces the formation water in a piston-like manner.

If these conditions are met, the governing equation for the system is the radial diffusivity equation,

$$\frac{1}{r}\frac{\partial}{\partial r}\left(r\frac{\partial p}{\partial r}\right) = \frac{\phi u c}{k}\frac{\partial p}{\partial t} \quad \ldots\ldots\ldots \quad (1)$$

Assuming that the formation is infinite in radial extent, that the pressure at the wellbore, due to the mud column, is constant and that the formation had a uniform initial pressure, the initial and boundary conditions are the following.

$$\left.\begin{aligned} p(r,o) &= p_i \\ p(\infty,t) &= p_i \\ p(r_w,t) &= p_w \end{aligned}\right\} \quad \ldots\ldots\ldots \quad (2)$$

Eqs. 1 and 2 may be re-written in simpler form by introducing new variables.

$$\frac{1}{R}\frac{\partial}{\partial R}\left(R\frac{\partial P}{\partial R}\right)=\frac{\partial P}{\partial \tau} \quad . \quad . \quad . \quad . \quad . \quad . \quad . \quad . \quad (3)$$

$$\left.\begin{aligned} P(R,0) &= 0 \\ P(\infty,\tau) &= 0 \\ P(1,\tau) &= 1 \end{aligned}\right\} \quad , \quad . \quad . \quad . \quad . \quad . \quad . \quad . \quad . \quad (4)$$

where $R = r/r_w$, $\tau = Kt/\phi u c r_w^2$ and $P = (p - p_i)/(p_w - p_i)$.

The solution of Eq. 3 subject to Eq. 4 will give the pressure distribution in the shale. Numerical values for this solution were tabulated by Jaeger[6].

The cumulative flow into the shale bed is given by

$$Q = \int_o^t q\,dt = \frac{2\pi Kh(p_w - p_i)}{\mu}\int_o^t \left|\left(\frac{\partial P}{\partial R}\right)_{R=1}\right| dt\,,$$

and

$$Q = 2\pi\phi h(p_w - p_i)cr_w^2\int_o^\tau \left|\left(\frac{\partial P}{\partial R}\right)_{R=1}\right| d\tau \quad (5)$$

The integral in Eq. 5 was evaluated by Van Everdingen and Hurst[5] for the physical system defined by Eqs. 3 and 4. The integral was defined as $\overline{Q}$ and given as a function of τ. Therefore,

$$Q = 2\pi\phi h(p_w - p_i)\ cr_w^2\overline{Q}(\tau) \quad . \quad . \quad . \quad . \quad (6)$$

Since the filtrate completely displaces the formation water, Q may also be expressed in terms of the radius of invasion, r_f.

$$Q = \pi\phi h(r_f^2 - r_w^2) \quad . \quad . \quad . \quad . \quad . \quad . \quad . \quad . \quad (7)$$

Equating Eqs. 6 and 7 and using the previously defined variable, R,

$$R_f = \sqrt{1 + 2c(p_w - p_i)\overline{Q}(\tau)} \quad . \quad . \quad . \quad . \quad (8)$$

Eq. 8 defines R_f in terms of τ; since the solution to Eqs. 3 and 4 gives P as a function of R and τ, the pressure at the filtrate-formation water interface, P_f, is determinate. The fraction of the total pressure drop occurring across the invaded zone is then

$$\frac{(\Delta p)\text{ invaded}}{(\Delta p)\text{ total}} = 1 - P_f \quad . \quad . \quad . \quad . \quad . \quad (9)$$

Since p and P are related linearly the same expression holds for the fraction of the actual pressure drop, $p_w - p_i$.

In Eq. 7 it was implicitly assumed that the density of the water was constant; however, if the pressure drop across the invaded zone is large, this assumption will introduce a small error. To compensate for this, Eqs. 7 and 8 may be re-written as follows.

$$Q = \pi\phi h\alpha(r_f^2 - r_w^2) \quad , \quad . \quad . \quad . \quad . \quad . \quad . \quad . \quad (10)$$

$$R_f = \sqrt{1 + 2\alpha c(p_w - p_i)\overline{Q}(\tau)} = \frac{1 + c[(p_w - p_i)P_{ave}]}{1 + c(p_w - p_i)} \quad . \quad . \quad . \quad (11)$$

where P_{ave} = average pressure in the invaded zone.

These equations are solved with α equal to unity. The average pressure is then determined and a corrected value for α is found. The equations are then solved again. This iterative process is continued until there is no appreciable change in R_f.

Numerical Example

The fraction of the pressure drop occurring across the invaded zone was determined for the following.

Case 1:

$(p_w - p_i) = 1{,}000$ psi
(a) $K = 4 \times 10^{-3}$ md, $\phi = .25$
(b) $K = 10^{-6}$ md, $\phi = .05$

Case 2:

$(p_w - p_i) = 2{,}000$ psi
(a) $K = 4 \times 10^{-3}$ md, $\phi = .25$
(b) $K = 10^{-6}$ md, $\phi = .05$

In all cases, $\mu = 1$ cp, $c = 3 \times 10^{-6}$ psi^{-1} and $r_w = .25$ ft.

The results are presented graphically in Fig. 2. ★★★

DISCUSSION

M. GONDOUIN
JUNIOR MEMBER AIME

SCHLUMBERGER WELL SURVEYING CORP.
RIDGEFIELD, CONN.

In order to explain the field observation that a "streaming potential" correction to the SP is often unnecessary, Wyllie and co-authors propose the interesting hypothesis that a mud cake is formed on the shales as well as on the permeable formations and that the streaming potentials from each mutually cancel. While this possibility should certainly not be rejected "a priori", more factual evidence would be needed before the existence of a "shale filter cake" is accepted.

Laboratory measurements of shale streaming potentials using mud, such as those of Schenck[1] or of Hill and Anderson[2], show essentially the same values of potential as when a clear solution of the same resistivity is used, so that the postulate of a shale mud filter cake responsible for the shale streaming potential is not indispensable. On the contrary, the evidence presented by Hill, *et al*, indicates that mud cakes built on low permeability filter beds do not contribute very much to the over-all streaming potential since most of the pressure drop occurs into the formation proper.

In arguing for the need of assuming a mud cake on the shales, Wyllie, *et al*, place great emphasis on a calculation of the location of the pressure front with respect to the invasion front in shale. It may be noted however that their calculation neglects entirely the shale matrix compressibility and ionic diffusion[4]. Due to matrix compressibility the "effective" water compressibility in a porous rock may often be several times larger than the numerical value of $C = 3 \times 10^{-6}$ psi^{-1} taken in this calculation. Extensive alteration of shale in the vicinity of the borehole, as shown from sonic logs[3], may be taken as an indication that mud filtrate penetration into the shale formation is quite deep, which would be difficult to explain if diffusion effects were negligible, as implied in the present paper. When these factors are taken into account, the assumption that the pressure drop $(p_m - p_{ws})$ occurs entirely in the virgin shale does not appear justified.

The seemingly better grouping of points in Fig. 8, compared to that of Fig. 9, may be interpreted simply

as an indication that the streaming potential across the mud/shale interface must include the mud resistivity as a variable. Such would be the case for shale streaming potential as well as for the hypothetical shale mud filter cake streaming potential if one removed the unjustified assumption that shale streaming potentials are constant regardless of the filtering fluid resistivity. In fact, laboratory results[2,4] show that the shale streaming potentials differ widely at solution resistivities corresponding respectively to the McClosky formation water ($\sim .06\ \Omega m$ @75°F) and to the mud filtrate resistivities (~ 1 to $3\Omega\ m$). In view of the very restrictive character of the assumptions on which the calculation of $E_{kmc} - E_{ks}$ is based, it seems difficult to derive from the plot of Fig. 9 any definite conclusion regarding the existence of the shale filter cake.

Finally, it may be relevant to suggest that field experimental results such as those presented in Fig. 1 be taken with great caution. The SP change observed when the mud resistivity is changed while the mud weight is kept constant is not a simple phenomenon. When a new mud is introduced in the hole, the mud cake resulting from the previous mud effectively separates two fluids of different resistivities (or activities), and due to its cation-exchange properties an additional chemical or membrane potential is set up, namely,

R_{mf_2} in mud No. 2 / Mud cake from mud No. 1 / R_{mf_1} trapped in invaded zone

for which,

$$E_{mc} = K \log \frac{R_{mf_1}}{R_{mf_2}},$$

with $K \leqslant 59$ @ 75°F.

It is only when the filtration of R_{mf_2} through the mud cake has brought the resistivity of the fluid in the back of the mud cake, No. 1 from R_{mf_1} to R_{mf_2}, that the mud cake membrance potential disappears. The existence of such potentials in wells where mud cake separates two fluids of different resistivities has been shown in a recent paper[5], and field experimental results on streaming potential to be published shortly indicate that it may take several days after a mud resistivity change before the SP reaches an equilibrium value. For this reason it is difficult to derive any quantitative information from SP logs run immediately after a mud changeover.

REFERENCES

1. Schenck, K. D.: MS thesis, U. of Oklahoma, 1955.
2. Hill, H. J. and Anderson, A. E.: "Streaming-Potential Phenomena in SP Log Interpretation", Paper 1119-G, presented at 33rd Annual Fall Meeting of Society of Petroleum Engineers in Houston, Tex. (Oct. 5-8, 1958).
3. Hicks, W. G.: Paper 32, SEG Meeting, San Antonio, Tex. (Oct., 1958).
4. Gondouin, M. and Scala, C.: "Streaming Potential and the SP Log", *Trans.* AIME (1958) **213**, 170.
5. Segesman, F. and Tixier, M. P.: "Some Effects of Invasion on the SP Curve", Paper 1120-G, presented at 33rd Annual Fall Meeting of Society of Petroleum Engineers in Houston, Tex. (Oct. 5-8, 1958).

AUTHORS' REPLY TO M. GONDOUIN

Gondouin's discussion reveals that his views on the present status of the streaming potential problem differ from ours. This is admirable because it is from a consideration of such expressed differences that further knowledge will come. However, it is apparent from certain of Gondouin's comments that in our effort to compress our material within the compass of a Technical Note we have tended to obscure our arguments. We can only apologize for this and do our best here to clarify some of the key points which we tried to include in the Note.

Gondouin observes correctly that if a shale is highly impermeable the fraction of the pressure drop that will occur across any filter cake formed on its face will be small. We do not dispute this. It is our explicit hypothesis that the permeability of shale filter cakes must be smaller by several orders of magnitude than the permeability of shales *measured parallel to their bedding planes*. It is the requirement that measurements be made parallel to the bedding planes that we conceive to be critical. All permeability and other measurements by Schenk and Hill and Anderson were made perpendicular to bedding planes. We would like to amplify this concept.

Gondouin notes that the acoustic velocity of a shale near a borehole differs from that of the same shale located further from the borehole. We have observed the same phenomenon. Gondouin attributes the velocity difference (actually a decrease in velocity) to relatively deep contamination of the shale by mud filtrate. It has been shown[1] that the principal factors affecting the velocity of a porous body are its porosity and the differential compacting pressure to which it is subjected, i.e., the difference between the geostatic pressure on the solid matrix and hydrostatic pressure on the pore fluids. The time-average formula shows the velocity difference resulting from a change in the salinity of the interstitial water in a low-porosity material like shale to be a second-order effect when compared with pressure effects. We suggest that the stress relief in the vicinity of the borehole (which actually results from the presence of the borehole) radically reduces (20 per cent differences are common) acoustic velocity adjacent to the borehole wall by reducing the effective differential compacting pressure on the shale laminae in this region. A local increase in horizontal permeability (flow between the laminae) is also very probable. The blocking of this permeable zone by mud debris may well be our hypothetical filter cake.

Opinions may differ concerning the value of the effective water compressibility to be taken in calculating the rate of radial movement of a pressure front. We shall merely note that the permeability and porosity to be assumed are of equal importance; we have covered a wide range of these variables and have not simplified our calculations by assuming a linear system[2]. It is important to note that whether one does or does not believe in higher values of effective compressibility or the importance of molecular diffusion, the results of changing mud resistivity (exemplified by Fig. 1 of our Note) remain crucial. It is in evaluating such experiments that there seems to be a difference of opinion between Gondouin and ourselves.

We have rather consistently found that a change

in mud resistivity results in a new and stable SP by the time we rerun our log. For example, in the first paper published on the quantitative evaluation of the SP[3], there are shown three SP logs run in the same well within 48 hours (Fig. 2 of Ref. 3). The mud resistivity was twice radically changed within this period by addition of sodium chloride. The SP differences are almost precisely those expected from the electrochemical theory of the SP. That this and similar observations are coincidental seems unlikely. We shall nevertheless look forward to reviewing Gondouin's work in this connection.

We are indeed aware of certain phenomena which accompany the change of mud in a borehole. At Gulf we call "the potential paradox" the fact that on initially changing mud resistivity little if any SP change should occur. The paradox results, of course, because a mud filter cake on a sand may act as a virtually perfect anion impermeable membrane. Assuming perfect membrane performance for simplicity, we see that on first changing the mud we have

$$R_{mf_2} \Big/ \text{mud cake membrane} \Big/ R_{mf_1} \Big/ R_w \Big/ \text{shale membrane} \Big/ R_{mf_2},$$

with potential given approximately by

$$E_c = 59 \log \frac{R_{mf_2}}{R_{mf_1}} + 11 \log \frac{R_w}{R_{mf_1}} + 59 \log \frac{R_w}{R_{mf_2}}$$

$$= 70 \log \frac{R_w}{R_{mf_1}} \quad . \quad . \quad . \quad . \quad . \quad . \quad . \quad . \quad . \quad . \quad . \quad (1)$$

After filtrate from Mud No. 2 has fully penetrated the filter cake we have

$$R_{mf_2} \Big/ \text{mud cake membrane} \Big/ R_{mf_2} \Big/ R_{mf_1} \Big/ R_w \Big/ \text{shale membrane} \Big/ R_{mf_2}$$

$$E_c = 59 \log \frac{R_{mf_2}}{R_{mf_2}} + 11 \log \frac{R_{mf_1}}{R_{mf_2}} + 11 \log \frac{R_w}{R_{mf_1}}$$

$$+ 59 \log \frac{R_w}{R_{mf_2}} = 70 \log \frac{R_w}{R_{mf_2}} \quad . \quad . \quad . \quad . \quad . \quad . \quad . \quad . \quad (2)$$

During percolation of Filtrate No. 2 through the filter cake formed by Mud No. 1 the electrochemical potential will tend to change from that given by Eq. 1 just cited to that given by Eq. 2. Simultaneously the streaming potential will vary. The prime factors controlling this period of potential instability will be the pressure difference across the cake and the cake thickness and permeability. It is our experience that the period of potential instability is less than 24 hours. If this is not true then correspondences between theory and observation (see Fig. 1 of our Note and Fig. 2 of Ref. 3) represent singular lacunae in the laws of probability. We believe, therefore, that the arguments given in our Note concerning the importance of these potential changes have not been effectively gainsaid.

Finally we should like to stress once more a well-known fact. Many logs possess shale-baselines of truly remarkable constancy. A consideration of this phenomenon shows that for constancy to be evident not only must the electrochemical properties of all shales be identical but their electrokinetic properties must be equally similar. According to the laboratory experiments specifically quoted by Gondouin all shales are not electrokinetically identical. Our hypothesis of a shale filter cake would remove the necessity for identity. We do not adduce this fact as one of vital significance because we believe that in situ it is possible for all shales to be electrokinetically identical for the same reasons that they are apparently electrochemically ideal and identical. And just as the electrochemical ideality of shales cannot be demonstrated in the laboratory[4], so we believe that the true electrokinetic properties of shales in situ may not be subject to laboratory verification.* Thus, it is possible that all present laboratory data on shale streaming potentials are unreliable. We emphasize again that the last word on the streaming potential problem has yet to be written.

REFERENCES

1. Wyllie, M. R. J., Gregory, A. R. and Gardner, G. H. F.: *Geophysics* (1958) **23,** 459.
2. Gondouin, M. and Scala, C.: "Streaming Potential and the SP Log", *Trans.* AIME (1958) **213,** 170.
3. Wyllie, M. R. J.: "A Quantative Analysis of the Electro-Chemical Component of the S. P. Curve", *Trans.* AIME (1949) **186,** 17.
4. Gondouin, M., Tixier, M. P. and Simard, G. L.: "An Experimental Study on the Influence of the Chemical Composition of Electrolytes on the SP Curve", *Trans.* AIME (1957) **210,** 58. ★★★

*It is worth noting that a *perfect* shale membrane would produce streaming potentials utterly independent of the salinity of muds in the borehole, i.e., all salt would be excluded from entering with the permeating solution.

T. N. 2019

Pressure Interference Correction to the Material Balance Equation for Water-Drive Reservoirs Using a Digital Computer

MICHAEL P. ROBINSON
JUNIOR MEMBER AIME

TEXAS EXPLORATION CO.
CALGARY, ALTA.

Abstract

The material balance equation for partial or complete water-drive reservoirs has been re-arranged to include a pressure interference term. This pressure interference term was obtained from the theory established by Mortada. A successful program was devised to solve the resulting equation in a few hours on a medium sized, digital computer. No prior knowledge of the properties of the aquifer is required in the solution. Trial calculations are made using various assumed combinations of aquifer properties. The optimum value of the constant expressing the aquifer properties corresponds to the best fit obtained between observed and calculated field history. Details of the method of calculation are illustrated by an example.

INTRODUCTION

A method of calculating the material balance equation for a partial water-drive reservoir completed in an aquifer has been described in the literature.[1,2] Pressure interference from other pools located in the same aquifer is not taken into account in this solution. When present, the pressure interference effect must be included in order to make a complete performance analysis. A correction for this effect has been developed using the theory established by Mortada.[3]

Manual calculation of the material balance for water-drive reservoirs is a formidable task. Such manual calculation when interference effects are included would be impossible to complete in any reasonable time period. However, a medium-sized stored program, digital computer can be used satisfactorily. The method is described in the following sections.

THEORETICAL CONSIDERATIONS

The material balance equation for a reservoir producing by partial or total water drive, as proposed by Van Everdingen, *et al*,[1,2] is

$$Y = Na + Z\Sigma\Delta p'Q(t_D), \quad . \quad (1)$$

This relationship is linear for Z/a vs $[\Sigma\Delta p'Q(t_D)]/a$, from which the slope, Z, and the intercept, N, can be obtained by the least-squares method from the data points. It is not necessary to know the aquifer properties to obtain optimum values for Z and N. Various assumptions are made for Δt_D:

$$\Delta t_D = \frac{k\Delta t}{\phi\mu c_w r_b^2}, \quad . \quad . \quad . \quad (2)$$

where Δt is production time, seconds (oilfield units-days) between the equal successive time intervals into which the history is divided. t_D is Δt_D times the number of equal time periods from t_o, i.e., the total dimensionless time interval from t_o. It is noted that the dimensionless time interval, Δt_D, involves all the relevant aquifer properties. Accordingly, any assumption of Δt_D is an assumption of the combined aquifer properties which pertain to the solution of the equation.

Deviations of the data points from a straight line are calculated for each assumption of Δt_D, and the value of Δt_D corresponding to the minimum deviation is chosen as the optimum solution. This method is described in Ref. 1 and 2.

The material balance solution is usually made with an initial assumption that the reservoir being studied is located in an infinite aquifer from which there are no other withdrawals. Deviation of the points by amounts greater than can be attributed to inaccuracies in field data may be the result of: (1) boundary effects of a limited aquifer, (2) pressure interference from other pools completed in the same aquifer, and (3) a combination of these effects. Differentiation of these effects can be made only on the basis of geologic data.

Pressure interference from other fields will result in a pressure drop at the original oil-water boundary having an interference component, $\Delta p'_{in}$. The measured instantaneous pressure drops at the oil-water

Original manuscript received in Society of Petroleum Engineers office Jan. 22, 1958. Revised manuscript received Aug. 22, 1958. Paper presented at Fourth Annual Joint Meeting of Rocky Mountain Petroleum Sections in Denver, Colo., March 3-4, 1958.
[1]References given at end of paper.

boundary, $\Delta p'$, will then be too large by $\Delta p'_{in}$. Computed values of water influx $[Z\Sigma\Delta p'Q(t_D)]/a$, will be too high by $[Z\Sigma\Delta p'_{in}Q(t_D)]/a$.

Correction for pressure interference from other reservoirs completed in the same "infinite" aquifer can be made as described by Mortada. The pressure drop in the aquifer at a distance r_e from a reservoir j after n production periods is given by:

$$(\Delta p_{in})'_j = \left(\frac{\mu}{\theta kh}\right) \sum_{j\,1}^{n} \left[\Delta We' P(r_D t_D)\right]_j \quad . \quad . \quad . \quad . \quad . \quad . \quad . \quad . \quad (3)$$

If a series of fields are all completed in the same infinite aquifer, and influx to each is radial, the conversion factor will be equal to $\mu/2\pi kh$ (absolute units) $= 884.7$, $\mu/2\pi kh$ (oilfield units). This factor can be assumed constant, provided that the aquifer has reasonably constant properties, at least within the area in which the fields are located. In practice, this assumption can be checked by solving Eq. 3 for $r_D = 1.0$ and, hence, determining the value of the constant, $\mu/2\pi\ kh$, for each field.

As described by Mortada,[3] the superposition theorem indicates that the pressure effects from the interfering fields will be additive at the field of interest. That is, the total interference pressure drop at the field of interest by k interfering fields will be:

$$\sum_{1}^{j=k} (\Delta p_{in})_j = \frac{\mu}{2\pi\ kh} \sum_{1}^{j=k} \sum_{1}^{n} \left[\Delta We' P(r_D t_D)\right]_j \quad . \quad . \quad . \quad . \quad . \quad (4)$$

For simplification, the double summation will be replaced by:

$$\Delta I = \sum_{1}^{j=k} \sum_{1}^{n} \left[\Delta We' P(r_D t_D)\right]_j \quad . \quad . \quad . \quad . \quad . \quad . \quad . \quad . \quad (4a)$$

The original material balance, Eq. 1 corrected for interference pressure effects described by Eq. 4a then becomes

$$Y = Na + Z \sum_{1}^{n} \Delta p' Q(t_D) - \frac{Z\mu}{2\pi\ kh} \sum_{1}^{n} \Delta I' Q(t_D) \quad , \quad . \quad . \quad . \quad . \quad (5)$$

where the prime notation again refers to the instantaneous pressure drop occurring at the beginning of each time period.

When the aquifer has constant properties and all fields produce radially, $Z = 2\pi\ \phi hc_w r_b^2$ and the value of $\Delta t/\Delta t_D$ obtained from Eq. 2 can be substituted in Eq. 5 to give:

$$\frac{Y}{a} + \frac{\Delta t}{a\Delta t_D} \sum_{1}^{n} \Delta I' Q(t_D) = N + \left[Z \sum_{1}^{n} \Delta p' Q(t_D)\right] / a \quad . \quad . \quad . \quad . \quad . \quad (6)$$

Eq. 6 is the material balance equation corrected for pressure interference from any number of other fields completed in the same aquifer. This equation can be solved in the same manner as Eq. 1, because the term, $\Delta t[\Sigma\Delta I' Q(t_D)]/a\Delta t_D$, will increase the values of Y/a so that they fall on a straight line, as shown in Fig. 2. The selected actual time interval, Δt, is known. Assumptions can be made for the aquifer properties in the time conversion factor, Δt_D. The optimum value of Δt_D corresponds to the best straight-line fit as determined by least-squares methods on the calculated points.

APPLICATION

Preliminary Considerations

The equation described applies only to an infinite aquifer of moderately constant properties. One linear boundary can be accounted for, using image fields as described by Mortada,[3] without any change in procedure. To include the effects of linear flow, a limited aquifer, changing aquifer properties or a single strongly curved boundary requires extensive modification to the material balance presented in Eq. 6. These complications have not been considered in this paper. Therefore, to apply the method described, the geology and geometry of the aquifer should be studied to ensure that the assumptions are valid.

Data Required

Two factors are required in addition to those normally used in a material balance solution. These are the effective radius of the original

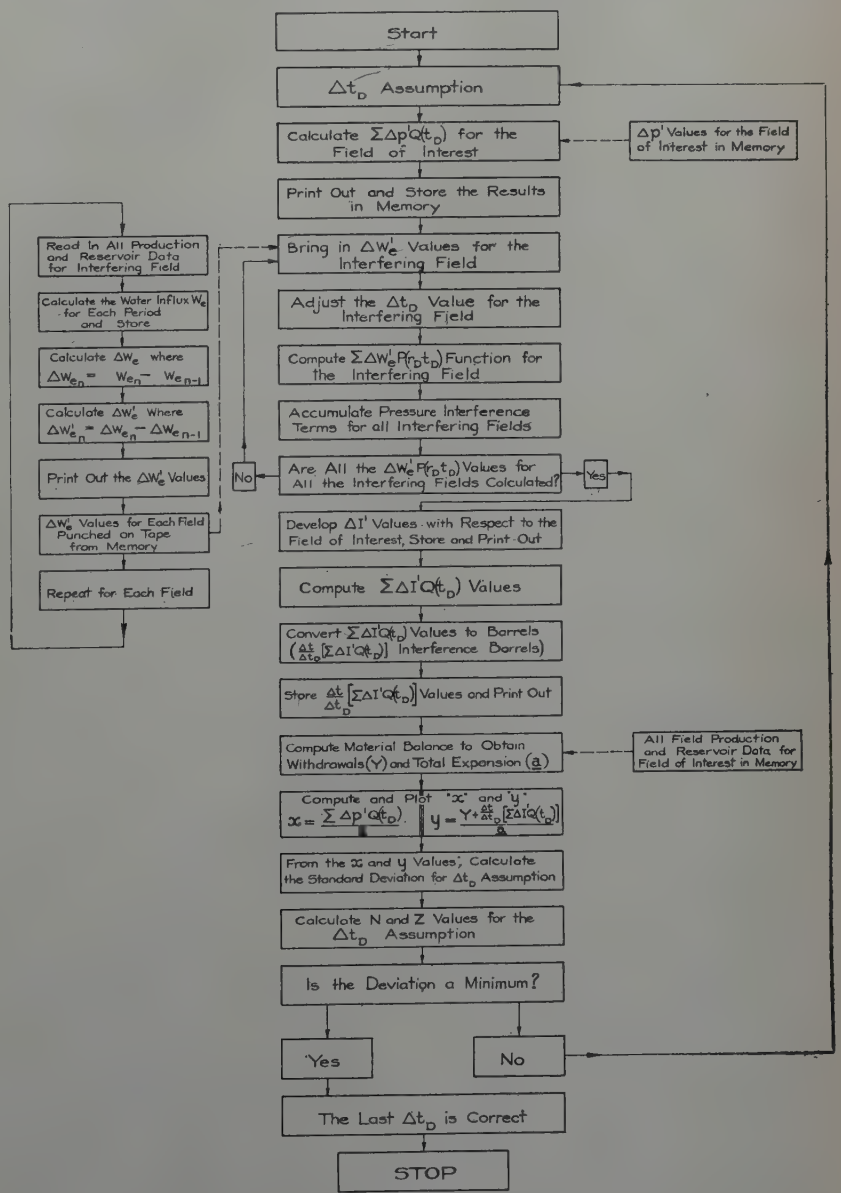
Start
Δt_D Assumption
Calculate ΣΔp'Q(t_D) for the Field of Interest
Δp' Values for the Field of Interest in Memory
Print Out and Store the Results in Memory
Read In All Production and Reservoir Data for Interfering Field
Bring in ΔW'_e Values for the Interfering Field
Calculate the Water Influx W_e for Each Period and Store
Adjust the Δt_D Value for the Interfering Field
Calculate ΔW_e where ΔW_en = W_en − W_e(n-1)
Compute ΣΔW'_e P(r_D t_D) Function for the Interfering Field
Calculate ΔW'_e where ΔW'_en = ΔW_en − ΔW_e(n-1)
Accumulate Pressure Interference Terms for all Interfering Fields
Print Out the ΔW'_e Values
No
Are All the ΔW'_e P(r_D t_D) Values for All the Interfering Fields Calculated?
Yes
ΔW'_e Values for Each Field Punched on Tape from Memory
Develop ΔI' Values with Respect to the Field of Interest, Store and Print Out
Repeat for Each Field
Compute ΣΔI'Q(t_D) Values
Convert ΣΔI'Q(t_D) Values to Barrels (Δt/Δt_D [ΣΔI'Q(t_D)] Interference Barrels)
Store Δt/Δt_D [ΣΔI'Q(t_D)] Values and Print Out
Compute Material Balance to Obtain Withdrawals (Y) and Total Expansion (a)
All Field Production and Reservoir Data for Field of Interest in Memory
Compute and Plot "x" and "y"
x = Σ Δp'Q(t_D) / Δ
y = Y + Δt/Δt_D [ΣΔI'Q(t_D)] / Δ
From the x and y Values, Calculate the Standard Deviation for Δt_D Assumption
Calculate N and Z Values for the Δt_D Assumption
Is the Deviation a Minimum?
Yes
No
The Last Δt_D is Correct
STOP

FIG. 1—FLOW DIAGRAM, MATERIAL BALANCE PROGRAM.

oil-water boundary, r_b, and the distance between the center of each interfering field and the center of the field of interest, r_e.

Programing

A simplified flow diagram for the program designed for medium sized computer is presented in Fig. 1. The step-by-step calculation procedure is described in Appendix 1 by using an example.

A feature of this program is the space and time saving obtained by fitting curves to the unit functions, $Q(t_D)$ and $P(r_D t_D)$. Values for these functions were required between dimensionless time, $t_D = 1$ and $t_D = 16{,}000$. The entire memory was too small to store a sufficient number of $Q(t_D)$ values to obtain accurate intermediate results using an interpolation routine. Tape storage was too slow. Finally, the range of values required was divided into five segments and curves were fitted to each segment. The constants for these curves were stored and provided accurate values for $Q(t_D)$ throughout the entire range of t_D. A similar technique was applied to the $P(r_D t_D)$ functions. The method used to obtain these curves is described in Appendix 2.

Calculation

Initially, an assumption for the aquifer properties, Δt_D, is made at about the mid-point of the range of values. The calculation routine can then be carried out and standard deviation of the obtained points determined by the method of least squares. Various other values of Δt_D are used and the deviation of each set of points determined. A plot of deviation vs the Δt_D values can be used to obtain the optimum Δt_D corresponding to the minimum deviation. This value of Δt_D, which represents the aquifer, is used to obtain a final solution of the material balance equation. From this solution the best values of the original oil in place, N, and the water influx index, Z, are calculated.

The actual field case considered had a 10 year history and 19 interfering fields. Computing time for each assumption for Δt_D was two hours. During this time the machine performed an estimated 800,000 arithmetic and logical operations.

The computing time could have been shortened by leaving out the volumetric balance calculations. However, it is convenient to leave these in to allow adaptation of the program to predictions.

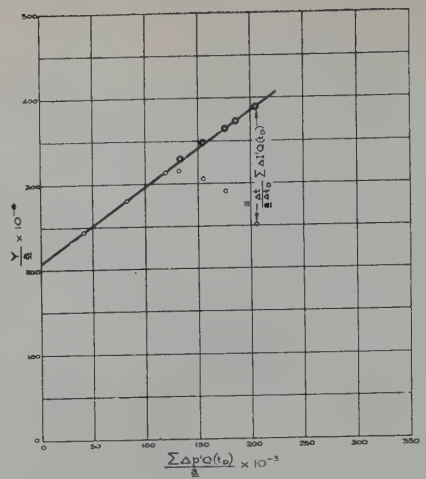

Fig. 2 — Material Balance Equation Plot for Field of Interest-(A), $\Delta t_{D_{(A)}} = 20$.

CONCLUSIONS

From the system of fields studied in our work, we concluded that:

1. The additional term added to the material balance equation for water-drive reservoirs satisfactorily describes the pressure interference effects.

2. The form of this correction term is such that the aquifer properties do not have to be known, but can be determined in the solution to the equation.

3. A medium sized digital computer can be used to solve the corrected equation conveniently and quickly.

NOMENCLATURE*

Y = cumulative volume of fluid withdrawals (oil, gas and water) in reservoir volumes to the end of the production period considered, cc (oilfield units, bbl)

Na = total expansion of oil, free gas, connate water and rock, cc (oilfield units, bbl)

n = original stock tank oil in place cc (oilfield units, bbl)

a = total expansion factor, vol/vol

$Z\Sigma\Delta p'Q(t_D)$ = cumulative water influx to the end of the production period considered, cc (oilfield units, bbl)

Z = proportionality constant required to convert reduced units to cubic centimeters (oilfiield units, bbl)
$= \theta\phi hc_w r_b^2$ absolute units $= 0.178\,\theta\phi hc_w r_b^2$ (oilfield units)

θ = angle in radians of sector equivalent to the oilfield

r_b = radius of original oil-water boundary, cm (oilfield units, ft)

$\Delta p'$ = instantaneous pressure drop at the original oil-water boundary, measured at the start of each time interval for which the analysis is to be made, atm (oilfield units, psi)

$Q(t_D)$ = unit function, acting for dimensionless time, t_D, and relating cumulative water influx to unit pressure drop at the original oil-water boundary

t_D = dimensionless time
$= \dfrac{kt}{\phi\mu c_w r_b^2}$ absolute units $= 0.00634\,\dfrac{kt}{\phi\mu c_w r_b^2}$ (oilfield units)

$\left(\dfrac{\mu}{\theta kh}\right)_j$ = factor to convert reduced units into actual units of pressure

$(\Delta We')_j$ = instantaneous change in rate of water influx into reservoir, j, that occurs at the beginning of each equal time interval for which the analysis is made, cc/sec (oilfield units, B/D)

$P(r_D t_D)_j$ = unit function relating cumulative pressure drop at a dimensionless ra-

*See AIME Symbols List in *Trans.* AIME (1956) 207, 363, for other symbol definitions.

dius, r_D, to unit water influx at the original oil-water boundary acting for a total dimensionless time, t_D

$r_D = \frac{r_e}{r_b}$

r_e = radial distance from the center of the interfering field to center of field of interest

r_b = radius of oil-water boundary of the interfering field (expressed in the same units as r_e)

n = number of equal time periods

$()_j$ = refers to field, j (Note—"field of interest" is the field for which the material balance equation is to be solved)

ACKNOWLEDGMENTS

We wish to thank the management of both The Texas Co. and Texaco Exploration Co. for their permission to publish this paper. Credit for the development of the method and much of the programming is due J. G. Debanné of The Texas Co. in Houston. The remainder of the study is the result of the combined efforts of the reservoir engineering section of Texaco Exploration Co.

REFERENCES

1. Van Everdingen, A. F.: Lecture notes from "CPE 383 Performance Prediction of Several Reservoir Mechanisms", U. of Texas (Aug. 26-Sept. 27, 1955).
2. Van Everdingen, A. F., Timmerman, E. H. and McMahon, J. J.: "Application of the Material Balance Equation to a Partial Water-Drive Reservoir", *Trans.* AIME (1953) **198,** 51.
3. Mortada, M.: "A Practical Method for Treating Interference in Water-Drive Reservoirs", *Trans.* AIME (1955) **204,** 217.
4. Van Everdingen, A. F. and Hurst, W.: "The Application of the Laplace Transformation to Flow Problems in Reservoirs", *Trans.* AIME (1949) **186,** 305.
5. Chatas, A.: "A Practical Treatment of Nonsteady-State Flow Problems in Reservoir Systems", *Pet. Engr.* (1953) **25,** No. 6, B-38.
6. Milne, W. E.: *Numerical Calculus,* Princeton University Press (1949), 219.

TABLE 1—BASIC FIELD DATA.

Time period	Data for Field of Interest: Field A — Withdrawals res. vol—Y (bbl)	Pressure at orig. OWC p(psig)	Pressure drop Δp(psi)	Expansion factors (a)	Interfering Fields: Field B — Cum. water influx, We (bbl)	Field C — Cum. water influx, We (bbl)
0		2,400				
1	3,600,000	2,300	100	0.0147		
2	7,300,000	2,220	180	0.0261		
3	10,950,000	2,160	240	0.0352	Field discovered	Field discovered
4	15,750,000	2,100	300	0.0503	2,730,000	1,281,000
5	18,300,000	2,050	350	0.0601	6,760,000	3,340,000
6	20,300,000	2,000	400	0.0704	11,403,000	5,832,000
7	23,400,000	1,950	450	0.0850	16,266,000	8,494,000
8	24,800,000	1,900	500	0.0952	26,609,000	13,840,800

	Field A	Field B	Field C
Area of oil-water contact (acres)	1,130	8,030	4,520
Equivalent radius of oil-water contact (miles)	0.75	2.0	1.5
Distance from interfering field to field of interest (miles)		4	3

Note: (1) Y corrected to reservoir barrels by material balance
(2) We is obtained from material balance on interfering fields

TABLE 2—CALCULATED WATER INFLUX FOR THE FIELD OF INTEREST NOT CORRECTED FOR INTERFERENCE
$\Delta t_D = 20$(assumed)

Time period	Pressure drop Δp(psi)	$\Delta p'$ Change in pressure drop (psi)	t_D dimensionless time	Qt_D	$\Delta p'Q(t_D)$	$\frac{\Delta p'Q(t_D)}{a}$ Water influx (not oilfield units)
0						
1	100	50	20	12.32	613	41,700
2	180	90	40	20.89	2,155	82,600
3	240	70	60	28.69	4,177	119,500
4	300	60	80	36.06	6,580	131,500
5	350	55	100	43.13	9,343	155,600
6	400	50	120	49.97	12,368	176,500
7	450	50	140	56.62	15,823	186,000
8	500	50	160	63.13	19,498	205,000

APPENDIX 1

DESCRIPTION OF THE METHOD OF CALCULATION

An actual material balance calculation has been made satisfactorily, correcting for interference from 19 fields. This system is too complex to present briefly. A hypothetical example has been given where Fields B and C have caused pressure interference on Field A, the field of interest. These fields are completed in an infinite, homogeneous aquifer.

The field histories and physical data required to make the computation are shown in Table 1. It will be noted that the expansion factors, a for Field A, and the cumulative water influx into Fields B and C are given, rather than the basic expansion pressure and volumetric data. These factors and the water influxes were obtained by volumetric balance.

The method of calculation is illustrated by reference to Tables 2, 3 and 4. This arrangement is not necessarily the order in which the machine performed these operations.

Most of the tabulated calculations, made for a Δt_D assumption of 20 for Field A, are self-explanatory. The following require some comment.

1. The instantaneous change in rate of water influx $\Delta We'$ for Field B (Table 3, Col. 3): these values of $\Delta We'$ are the second differences of the cumulative water influx to the end of each period, given in Col. 2, i.e., $\Delta We_n = We_n - We_{n-1}$ and $\Delta We'_n = \Delta We_n - \Delta We_{n-1}$.

The figures obtained are expressed as changes in rate measured in barrels per half year. To keep the units consistent they should be divided by Δt, the number of days in a half year. This step is unnecessary since the factor $1/\Delta t$ can be maintained as a constant outside the summation signs until the last step in the water interference term calculation. At this stage the $1/\Delta t$ cancels, i.e., water influx term $= (\Delta t/a\Delta t_D)[(1/\Delta t)\ \Sigma\Delta I'Q(t_D)]$ where $\Delta I'$ values are for a half year.

2. Values of dimensionless time, t_D, for Field B (Table 3, Col. 4): for Field A it was assumed that $\Delta t_D = 20 = k\Delta t/\phi\mu c_w r_b^2$, where $r_b = 0.75$ for Field A. Then for Field B, where $r_b = 2.0$, $\Delta t_D = 20 + (0.75)^2/2^2 \approx 3$. This value was used to determine t_D for Field B.

RESULTS

The results of these computations, assuming a $\Delta t_D = 20$ for Field A, are summarized in Table 4. Fig. 2 shows the plot that results by neglecting the water interference term, $(\Delta t/a\Delta t_D)\ \Sigma\Delta I'Q(t_D)$, and the correction that results by adding this term. The value, $\Delta t_D = 20$, was selected because it gives the least deviation between calculated and field data.

TABLE 3—INTERFERENCE EFFECTS FROM FIELDS B AND C

Time Period	We Bbl × 10^3	FIELD B: $\Delta We'$ bbl/½yr² × 10^3 (Δt_D = 20 for field of interest; Equivalent Δt_D = 3 for Field B)	$t_D(B)$	$P(r_D t_D)$	$\Sigma \Delta We' P(r_D t_D)$ × 10^3	We bbl × 10^3	FIELD C: $\Delta We'$bbl/½yr × 10^3 (Δt_D = 20 for field of interest; Equivalent Δt_D = 5 for Field C)	$t_D(C)$	$P(r_D t_D)$	$\Sigma \Delta We' P(r_D t_D)$ × 10^3	$\Sigma\Sigma \Delta We' P(r_D t_D)$ × 10^3	$\Delta l'$ × 10^3
0												
1												
2								0				
3			0					5	0.71	909	2,373	1,136
4	2,730	2,730	3	0.500	1,364	1,281	1,281	10	0.98	1,808	4,528	2,264
5	6,760	1,300	6	0.760	2,720	3,340	778	15	1.15	2,543	6,347	2,037
6	11,403	613	9	0.920	3,804	5,832	443	20	1.29	3,092	7,734	1,603
7	16,266	220	12	1.050	4,642	8,494	170	25	1.38	5,341	13,315	3,484
8	26,609	5,480	16	1.150	7,974	13,840	2,683					

r_D = 2 for Field B to Field A
r_D = 2 for Field C to Field A
We = cumulative water influx
$\Delta We'$ = change in rate of water influx
$t_D(B)$ = dimensionless time (total)
$\Sigma \Delta We' P(r_D t_D)$ = pressure drop—not oilfield units
$\Sigma\Sigma \Delta We' P(r_D t_D)$ = total pressure drop—not oilfield units
$\Delta l'$ = change in pressure drop by interference

APPENDIX 2

DETERMINATION OF $Q(t_D)$ and $P(r_D t_D)$ FUNCTIONS

Van Everdingen and Hurst[4] give Eq. V1-28 for the function, $Q(t_D)$, and V1-21 for the function, $P(r_D t_D)$. Values for these functions can be found in the original paper and the papers for Chatas[5] and Mortada[4], respectively.

Solution of Eq. V1-28 for $Q(t_D)$ takes one hour of machine time per value of t_D. This is completely unsatisfactory for use in the calculation. Therefore, curves were fitted over the range required using the method of reciprocal differences as described by Milne[6].

The following lists are values of $Q(t_D)$ given by Chatas[5] as compared to those computed from the fitted curves.

TABLE 4—MATERIAL BALANCE EQUATION FOR FIELD OF INTEREST, A, CORRECTED FOR PRESSURE INTERFERENCE. (Δt_D assumed 20)

Time Period	$\Delta l'$* × 10^3	$\Sigma \Delta l' Q(t_D)$** × 10^3	$\frac{\Delta t}{a\Delta t_D(A)} \Sigma \Delta l' Q(t_D)$ Interference correction (bbl) × 10^3	Y/a Fluid withdrawals (bbl) × 10^3	$Y/a + \frac{\Delta t}{a\Delta t_D(A)} \Sigma \Delta l' Q(t_D)$ × 10^3	$\frac{\Delta p' Q(t_D)}{a}$†
0	0	0	0			
1	0	0	0	245,000	245,000	41,700
2	0	0	0	280,000	280,000	82,600
3	0	0	0	313,000	313,000	119,500
4	1,136	14,000	14,000	315,000	329,000	131,500
5	2,264	51,640	43,000	305,000	348,000	155,600
6	2,037	105,000	75,000	290,000	365,000	176,500
7	1,603	168,320	99,100	275,000	374,100	186,000
8	3,484	265,900	140,000	250,000	390,000	205,000

*From Table 3
**t_D and Qt_D from Table 2, Col. 4 and 5
†From Table 2

t_D	$Q(t_D)$ Chatas	$Q(t_D)$ Computer	Deviation	Per cent deviation
0.5	1.020	1.020	0.000	0.000
1.0	1.569	1.569	0.000	0.000
5.0	4.539	4.542	0.003	0.066
25.0	14.573	14.573	0.000	0.000
50.0	24.855	24.861	0.006	0.024
250.0	91.084	91.077	0.007	0.008
500.0	162.698	162.691	0.007	0.004
1,000.0	293.514	293.513	0.001	0.000
2,000.0	534.145	534.138	0.007	0.001
5,000.0	1,192.198	1,192.174	0.024	0.002
8,000.0	1,807.278	1,806.859	0.419	0.023
Average				0.0012

The accuracy indicated by the percentage deviation is very satisfactory. Each value was found by the computer in four seconds.

$P(r_D t_D)$ functions involve two independent variables, r_D and t_D, for $r_D^2/4t_D < 0.05$; the function was approximated by:

$$P(r_D t_D) \approx \tfrac{1}{2} \ln t_D + 0.40454. \quad (7)$$

For values of $r_D^2/4t_D > 0.05$, curves were fitted by the reciprocal difference method to values of $P(r_D t_D)$ from Mortada[3]. Suitable accuracy was obtained. ★★★

T. N. 2020

Linear Waterflood Behavior and End Effects in Water-Wet Porous Media

J. R. KYTE
L. A. RAPOPORT
MEMBER AIME

JERSEY PRODUCTION RESEARCH CO.
TULSA, OKLA.

INTRODUCTION

Theory indicates that linear waterfloods should exhibit scaling and stabilization properties in both oil-wet and water-wet porous media[1]. Experimental verification of these properties in oil-wet media was obtained some time ago[1], and more recently, Perkins[2], employing a high permeability unconsolidated sand and a low oil-to-water viscosity ratio, has obtained flooding data in a water-wet medium which follow the pattern of scaling and stabilization. Also, Root and Calhoun[3] have found similar trends in the displacement of gas by liquids from unconsolidated sands. In general, however, the experimental evidence appears still somewhat conflicting since scaling and stabilization of water floods in water-wet media has not been observed in most of the studies to date[4,5,6].

The purpose of this paper is to provide a more comprehensive picture of waterflood behavior in water-wet media and to corroborate the validity of the scaling and stabilization concepts. The need for differentiating between the intrinsic nature of water-oil displacements *inside* a porous medium and perturbating secondary end effects is discussed, pertinent experimental procedures are outlined and the results of flooding tests conducted at low and at high oil-to-water viscosity ratios on consolidated, water-wet Alundum cores are analyzed.

Original manuscript received in Society of Petroleum Engineers office July 15, 1957. Revised manuscript received June 12, 1958. Paper presented at 32nd Annual Fall Meeting of Society of Petroleum Engineers in Dallas, Tex., Oct. 6-9, 1957.
[1]References given at end of paper.

END EFFECTS IN WATER-WET MEDIA

Outlet End Effects

The peculiar feature of the outlet end effect in water-wet cores is that it not only results in an excessive wetting phase saturation at the outflow face,[1,7] but that it also *retards* the moment of water breakthrough; i.e., causes an undue delay in the appearance of water in the produced effluent. Conditions existing in a water-wet core when water first arrives at the outflow face are schematically shown in Fig. 1. At this flooding stage the saturation distribution, Fig. 1a, has not yet been distorted by the outlet end effect. A water-invaded pore at the outlet core face, opening into the oil-filled void space between the end of the core and the end plate of the flooding cell, is illustrated in Fig. 1b. The curvature of the water-oil interface is concave toward the outlet, and the pressure on the water side of the interface is lower than on the oil side by an amount equal to a certain capillary pressure (Fig. 1c). Before the water (of this particular pore) can be produced from the core, it is apparent that the pressure in the water phase must exceed that in the oil outside the core. Accordingly, when water first reaches the outlet face, it will not leave the core but will accumulate inside, and only oil will be produced. Eventually, as the water injection is continued, sufficient pressure is built up in the water to reverse the curvature of the interfaces in the outlet pores, and only then will water be produced from the core. This stage, illustrated in Fig. 2, corresponds to the conventional "water breakthrough" observed in flooding experiments.

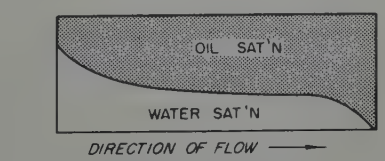

(a) FLUID SATURATION DISTRIBUTIONS

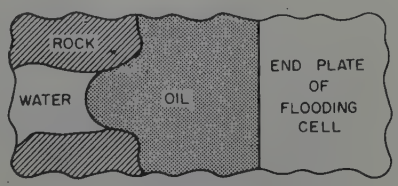

(b) WATER INVADED PORE AT THE OUTLET FACE

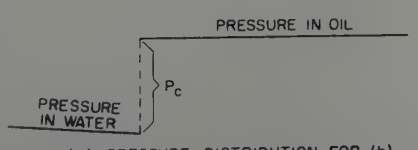

(c) PRESSURE DISTRIBUTION FOR (b)

FIG. 1—CONDITIONS EXISTING IN A WATER-WET CORE WHEN WATER FIRST ARRIVES AT THE OUTLET FACE.

For purposes of discussion, it is convenient to distinguish between the flooding stage at which water first arrives at the outlet face of a core (Fig. 1) and the stage at which water is first produced from the core (Fig. 2). The former will be referred to as "water arrival" and the latter water breakthrough. In oil-wet media

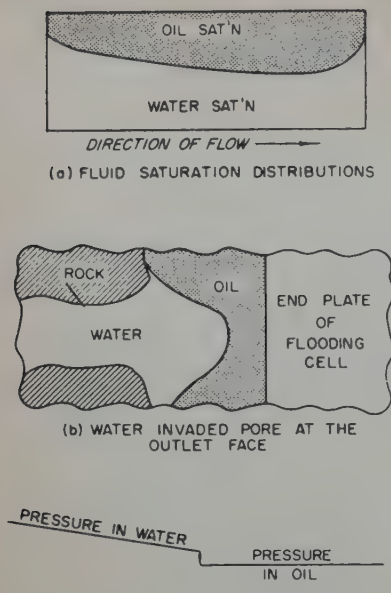

FIG. 2 — CONDITIONS EXISTING IN A WATER-WET CORE WHEN WATER PRODUCTION STARTS.

these two flooding stages occur simultaneously, whereas in water-wet media, water breakthrough will occur at some time after water arrival.

On the basis of theoretical considerations it can be inferred that the relative importance of the outlet end effect, which is localized, will decrease as the length of the flooded system, the rate of injection, or the fluid viscosities are increased. Accordingly, it may be anticipated that the outlet end effect in water-wet media will not alter the trend toward stabilization of linear floods.

INLET END EFFECTS

The inlet end-effect, detected by Jones-Parra, *et al*[4] in some of their experiments, develops in water-wet media as a result of spontaneous, localized imbibition. Water injected into the flooding cell first contacts the inlet face of the core only in a localized area. As soon as the water touches the core, it will spontaneously imbibe into the core at the point of contact. At the same time, there will be a counterflow of oil from the core to replace the water which has imbibed. As the flood progresses, water tends to continue entering the core only in a localized area. Such conditions, in turn, contribute to the establishment of a region of non-linear flow within the core.*

*Observation of the inlet core face during water floods of a viscous oil has supplied direct evidence supporting these considerations regarding the inlet end effect. During the entire flood, the injection water was seen to cover only a small portion (about 10 per cent) of the core face near the injection port.

While a quantitative evaluation of the inlet end effect in water-wet systems has not been undertaken, this inlet end effect would be *more pronounced* under the following conditions.

1. *For short systems,* in which end effects are always relatively more significant.

2. *For high water injection rates;* although water may enter a water-wet core only over a portion of the inlet face, capillary forces within the core tend to distribute this water over the entire cross-sectional area. At low rates these capillary forces are of relatively great importance in the over-all pressure distribution and can efficiently counteract appreciable distortion from linear behavior. At high flooding rates, however, the influence of the capillary forces within the core is comparatively small, and non-linear flow behavior will be more pronounced.

3. *For high oil-to-water viscosity ratios;* in this case the comparatively low resistance to fluid flow in the water-invaded region will tend to cause further growth of this region in the direction of the pressure gradient. Thus, the distortion from linear behavior occurring as a result of localized water injection at the inlet face is magnified. Conversely, in the displacement of low-viscosity oil, the flow resistance in the water-invaded region is high compared to that of the oil-saturated spaces. Such conditions tend to counteract the water "fingering" originated by the end effect, so that linear flooding behavior is achieved more readily.

EXPERIMENTAL PROCEDURE

Three Alundum cores which had been checked to insure uniformity were used in the experiments. Properties of these cores are presented in Table 1.

The cores showed a pronounced preferential water wettability as evidenced by spontaneous, very rapid imbibition of 65 per cent of pore volume of water upon immersion of oil-saturated cores in water. This wettability was maintained throughout the tests by heating the cores for several hours at 500°C between runs.

The liquids used in the experiments were purified Soltrol-C or refined white oils as the oil phase, and water or mixtures of water and glycerin as the aqueous phase. Waterflood tests were performed on oil-saturated cores at three different oil-to-water viscosity ratios: 1.61:1, 9.1:1, and 102:1.

TABLE 1—SUMMARY OF CORE PROPERTIES

Alundum core no.	Length (cm)	Diameter (cm)	Air permeability (md)	Porosity
1	8.41	3.99	508	.237
2	9.27	3.94	532	.236
3	32.80	4.04	574	.240

As previously indicated, flooding results obtained after water reaches the outflow face of a core sample can be influenced by outlet end effects. However, at the very moment of water arrival at the outflow face, these phenomena are not yet in existence. A special procedure was developed, therefore, to determine precisely this moment of "water-arrival". A phenolphthalein indicator is applied in water solution to the outlet face of the clean, muffled core. The core is then dried, saturated with oil, and flooded with a water phase containing a small amount of ammonia. When the ammonia solution first arrives at the outflow face, a sharp coloration appears which is clearly visible through a Lucite end plate.

RESULTS AND DISCUSSION

WATERFLOOD BEHAVIOR AT LOW OIL-TO-WATER VISCOSITY RATIOS

Results of the floods conducted at an oil-to-water viscosity ratio of 1.61:1 are presented in Fig. 3. Shown are oil recoveries at water breakthrough and at water arrival as functions of the scaling coefficient, $LV\mu_w$. The influence of the outlet end effect on flooding behavior in water-wet media is clearly demonstrated by the differences observed in oil recovery at water arrival and at water breakthrough. These differences are seen to be as much as 35 per cent of pore volume at low values of the scaling coefficient but are only about 2 per cent of pore volume at the higher values of $LV\mu_w$. Thus, as predicted by theoretical considerations, it is seen that for water-wet cores: (1) at low $LV\mu_w$ values the outlet end effect delays water production, resulting in an abnormal ac-

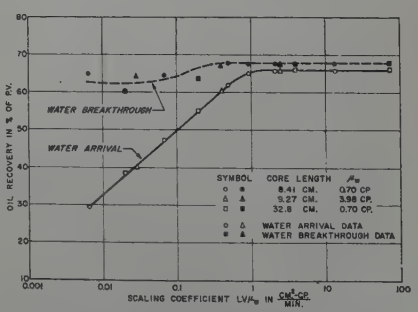

FIG. 3 — CORRELATION OF WATERFLOOD TEST DATA. STRONGLY WATER-WET ALUNDUM CORES; OIL-WATER VISCOSITY RATIO, 1.61.

cumulation of water in the core and excessive oil production at water breakthrough; and (2) the influence of the end effect becomes less pronounced as $LV\mu_w$ is increased.

The relationship between oil recovery at water arrival and the scaling coefficient, shown in Fig. 3, is similar to those obtained at water breakthrough for oil-wet media[1]. This relationship exhibits both the scaling and stabilization properties. Oil recoveries correlate well with the scaling coefficient and are seen to increase with increasing values of $LV\mu_w$ until the flooding behavior becomes stabilized, i.e., oil recovery is unchanged with increasing values of $LV\mu_w$. Moreover, the excellent correlation of water arrival data for the 1.61 oil-to-water viscosity ratio also confirms that the inlet end effect has generally little influence on flooding behavior at low viscosity ratios. Altogether, then, the experimental results presented in Fig. 3 are in complete agreement with the linear waterflood theory.

Waterflood Behavior at High Oil-To-Water Viscosity Ratios

Water arrival and water breakthrough data for flooding tests at a 102:1 oil-to-water viscosity ratio are presented in Fig. 4. As in the case of the low viscosity ratio there is considerable spread between the water arrival and the water breakthrough data at low values of the scaling coefficient. Moreover, the water breakthrough data are again seen to be considerably more scattered than the water arrival data.

As regards the data of water arrival, excellent correlation is observed at low values of $LV\mu_w$. In this region, the oil recoveries for both the long and short cores do not deviate from the correlation curve by more than 1.5 per cent of pore volume. At high values of the scaling coefficient, however, the water arrival data for the long core differ from those for the short core. Also

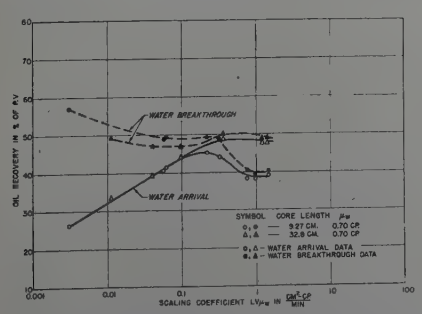

Fig. 4 — Correlation of Waterflood Test Data. Strongly Water-wet Cores; Oil-water Viscosity Ratio, 102.

in apparent conflict with theory is the decrease in oil recovery at water arrival for the short core as $LV\mu_w$ increases. This anomalous behavior can be interpreted in the light of theoretical considerations regarding the inlet end effect.

Since the inlet end effect should be less pronounced at low flow rates, this accounts for the satisfactory scaling observed in tests with the viscous oils at low $LV\mu_w$ values. At higher flow rates (e.g., higher values of $LV\mu_w$) it was pointed out that the inlet end effect should cause greater deviation from linear flow. This in turn would tend to yield lower oil recoveries at water arrival. Thus, with increasing flooding rates, one would expect the oil recovery at water arrival to increase on one hand because of the stabilization process but to decrease on the other because of the establishment of non-linear flow as a result of the inlet end effect. Such coexisting phenomena readily explains the increase and subsequent decrease in the oil recovery at water arrival with increasing values of $LV\mu_w$ as observed for the short core in Fig. 4. As the inlet end effect is relatively more pronounced in short cores, it is also not surprising that at high flow rates the oil recoveries at water arrival are less for the short core than for the long core.

The somewhat inconsistent results obtained at high viscosity ratios and high injection rates can be more fully evaluated by consideration of the waterflood oil recovery curves in Fig. 5. Oil recoveries, as a function of the cumulative water injected, are shown for the 102:1 viscosity ratio for both the long and short cores. In both cases the curves represent flooding tests for which water injection rates were sufficiently great to insure stabilized flooding behavior and to render outlet end effects unimportant.

From inspection of the flooding curves shown in Fig. 5 it is apparent that although rather large differences in oil recoveries may occur at the very moment of water breakthrough, the curves rapidly converge and become almost identical soon after breakthrough. For instance the greatest discrepancy in oil recoveries occurs after injection of 0.5 pore volume of water and amounts to only 3 per cent of pore volume. Thus, while the inlet end effect may cause premature water breakthrough in short cores, it does not significantly distort the over-all relationship be-

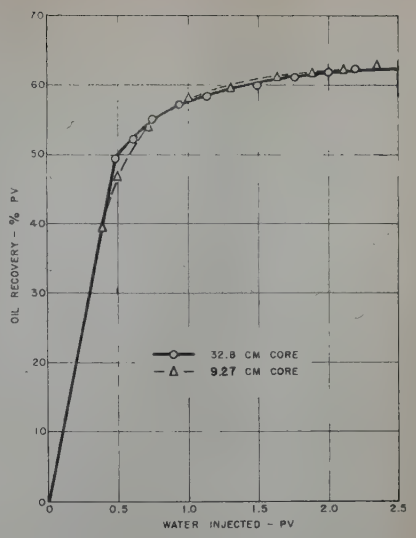

Fig. 5—Comparison of Flooding Curves Strongly Water-wet Alundum; Oil-water Viscosity Ratio, 102.

tween oil recovery and cumulative injection.

Although the data are not shown, results obtained for the 9.1:1 viscosity ratio are similar to those for the 102:1 ratio, except as would be expected, the influence of the inlet end effect is considerably less pronounced.

Practical Considerations

The present data corroborate the important conclusion reached in previous studies[1] that field water floods are usually stabilized. This, in turn, means that evaluations of field behavior should be generally based on laboratory tests conducted in such a manner as to insure stabilized flooding conditions. It has been demonstrated that under such conditions the over-all flooding behavior is not significantly influenced by either inlet or outlet end effects. However, the manner in which stabilized flooding can be actually attained and/or observed in the case of water-wet core samples merits some discussion.

In conventional flooding tests on water-wet cores where usually the moment of water breakthrough but not that of water arrival can be observed, the outlet end effects complicate the determination of conditions (i.e., of the rate) at which stabilized flooding behavior is attained. In oil-wet media the outlet end effect does not cause any "undue" accumulation of water within the core prior to breakthrough; therefore, the oil recovery at water breakthrough or at any given subsequent flooding stage will always be found to increase as the scaling coefficient is increased until stabilized flooding

conditions have been attained. Such a simple trend cannot be relied upon in the case of water-wet cores since the oil recovery at a given flooding stage (water breakthrough, in particular) may increase, decrease, or remain fairly constant as the flood rate is increased (see Figs. 3 and 4).

In attempting to describe the conditions necessary for stabilized flooding behavior in water-wet media, a physical concept of such flooding behavior is helpful. A water flood is stabilized if the capillary pressure gradient in the direction of flow is small compared to the imposed pressure gradient. Thus, stabilized flooding behavior is in effect achieved by imposing a sufficiently high pressure drop across the system. Theory, as well as experience, suggests that the magnitude of the capillary pressure gradients in water-wet systems are of the same order as in oil-wet systems. In stabilization tests on a variety of oil-wet reservoir cores, the maximum total pressure drop across the core necessary to achieve stabilization was found to be of the order of 50 psi, regardless of the core length. Thus, waterflood tests performed at this total pressure drop or greater should in most cases also insure stabilization in water-wet systems.

In view of the particular features of the outlet end effect in water-wet media, revealed by the present studies, it is logical to inquire if stabilized flooding tests are actually necessary to simulate field recovery behavior. For instance, in unstabilized tests at the 1.61 oil-to-water viscosity ratio (Fig. 3), the water may arrive very early at the outlet core face, but it is not produced until the oil recovery from the core approaches that obtained at water breakthrough in stabilized tests. Thus, because of the "compensating" influence of the outlet end effect in water-wet media, oil recovery behavior for unstabilized flooding tests may sometimes be quite similar to that obtained under stabilized conditions. However, it will be noted that at the 102 oil-to-water viscosity ratio (Fig. 4) the oil recovery at water breakthrough in an unstabilized flood can be significantly greater than under stabilized conditions. Furthermore, this discrepancy will persist at flooding stages considerably past breakthrough. Thus, it is preferable to insure stabilized flooding conditions in laboratory tests, rather than to rely upon the compensating influence of end effects.

CONCLUSIONS

1. In the absence of end effects, linear waterflood behavior in water-wet media is subject to the same general principles of scaling and stabilization which had previously been found applicable to oil-wet media.

2. At low values of the scaling coefficient, $LV\mu_w$, the outlet end effect can appreciably distort flooding behavior in water-wet media. This end effect delays water production, resulting in excessive oil recovery prior to the moment of water breakthrough. However, at values of the scaling coefficient sufficiently great to insure stabilized flooding conditions, the influence of the outlet end effect becomes less pronounced and does not appreciably distort the flooding behavior.

3. At high rates and high oil-to-water viscosity ratios an inlet end effect causes deviation from linear flow in water-wet cores, resulting in early water breakthrough. Although this end effect may sometimes cause a significant reduction in oil recovery at water breakthrough, it does not appreciably distort the over-all flooding behavior (relationship between oil recovery and cumulative water injection).

4. From Conclusions 2 and 3 it follows that stabilized water floods in water-wet cores are not appreciably distorted by end effects. As most field water floods are stabilized, this means that laboratory flooding tests performed under stabilized conditions on representative reservoir core samples may be employed to predict waterflood oil recovery from water-wet reservoirs. Stabilized flooding conditions can usually be achieved by performing the flooding tests under an imposed total pressure drop of 50 psi or greater, regardless of the core length.

NOMENCLATURE

L = total length of flooded system (cm)
V = total flow rate per unit cross-sectional area (cm/min)
μ_w = water viscosity (cp)
μ_o = oil viscosity (cp)

ACKNOWLEDGMENT

The authors are indebted to R. L. Dalton for his assistance in obtaining much of the experimental data. They wish to thank The Jersey Production Research Co. for permission to publish this paper.

REFERENCES

1. Rapoport, L. A. and Leas, W. J.: "Properties of Linear Water Floods", *Trans.* AIME (1953) **198,** 139.
2. Perkins, F. M., Jr.: "An Investigation of the Role of Capillary Forces in Laboratory Waterfloods", *Trans.* AIME (1957) **210,** 409.
3. Root, P. J. and Calhoun, J. C., Jr.: "Displacement of Gas by Water from Unconsolidated Sands", *Prod. Monthly* (Aug., 1954) **18,** 18.
4. Jones-Parra, J., Stahl, C. D. and Calhoun J. C., Jr.: "A Theoretical and Experimental Study of Constant Rate Displacements in Water-Wet Systems", *Prod. Monthly* (Jan., 1954) **18,** 18.
5. Engelberts, W. F. and Klinkenberg, L. J.: "Laboratory Experiments on the Displacement of Oil by Water from Packs of Granular Material", *Proc.*, Third World Pet. Congress, The Hague (1951) Sec. 2, 544.
6. Moore, T. F. and Slobod, R. L.: "Displacement of Oil by Water—Effect of Wettability, Rate, and Viscosity on Recovery", Paper 502-G, presented at Petroleum Branch AIME Fall Meeting in New Orleans (1955).
7. Douglas, Jim, Jr., Blair, P. M. and Wagner, R. J.: "Calculation of Linear Waterflood Behavior Including The Effects of Capillary Pressure", *Trans.* AIME (1958) **213,** 96. ★★★

Limitations on Pressure Predictions for Water-Drive Reservoirs

L. H. SIMONS
H. H. SPAIN
MEMBER AIME

HUMBLE OIL & REFINING CO.
HOUSTON, TEX.

ABSTRACT

Five water-drive fields, for which pressure predictions had been made within a few years after discovery, were re-studied when four to five years of additional pressure and production data became available. It was found that forecasts of the pressure in water-drive reservoirs may be subject to considerable uncertainty. Predictions can be erroneous when there is insufficient pressure history to define the characteristics of the aquifer, and when there are errors in the pressure, production or geologic data.

INTRODUCTION

The efficient operation of an oil or gas reservoir requires that the important characteristics of the reservoir be determined soon after its discovery. It is especially desirable to evaluate the pressure-production relationship quickly, for this relationship provides a basis for deducing the type of production mechanism that is operative, and for making pressure predictions. The pressure predictions, in turn, provide a basis for calculating efficient rates of production, determining whether water or gas should be injected, etc.

The importance of pressure prediction is such that forecasts should be made as accurate as possible, and the limits of error well defined. Historically, pressure forecasts for some fields have proved very accurate, while for others the forecasts were so erroneous that they resulted in the adoption of wrong, or at best, unnecessary production practices.

Pressure predictions made for water-drive fields are especially subject to error. Accurate forecasting for these fields requires that much be known not only about the reservoir proper but about the adjacent water-filled rock as well. The water-containing rock, or aquifer, may extend for many miles, and often there is only meager data regarding its thickness, permeability and porosity. Much of the information must be inferred from the previous pressure behavior of the reservoir. A brief pressure history may provide little information about the characteristics of the aquifer. Hence, pressure predictions made early in the life of water-drive fields can be incorrect.

The work described in this paper was done to determine the degree of reliability which can be expected of pressure predictions made within a few years after water-drive fields are discovered. Five fields, for which the original pressure predictions had been based on less than seven years' history, were re-examined with the aid of four to five years of additional pressure data. Where the predictions were inaccurate, the reasons for failure were ascertained. The studies were accomplished by use of the electric reservoir analyzer.[1]

The analyzer was first adjusted to repeat the original pressure-production match using the same values for the various parameters as were used in the original study. Then, the actual production rates experienced during the time elapsed since the initial study were set into the analyzer, and the pressure behavior indicated by the machine for this period was compared with that which actually occurred. Where the pressure profile traced out by the analyzer deviated from the observed field behavior, the analyzer was readjusted to obtain a better over-all match. The old and the new solutions were compared to determine the reasons for any differences.

COMPARISON OF PREDICTED RESERVOIR PRESSURE BEHAVIOR WITH ACTUAL PERFORMANCE

FIELD A

The original pressure-production match is entirely adequate as evidenced by the pressure match of the field's history subsequent to Jan., 1952 (see Fig. 1).

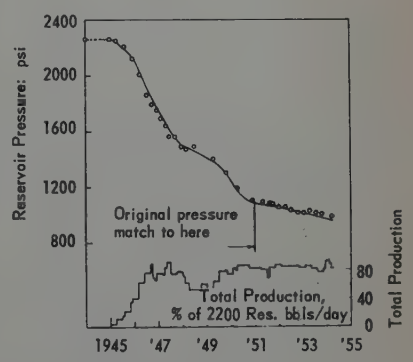

FIG. 1—FIELD A.

Original manuscript received in Society of Petroleum Engineers office July 15, 1957. Revised manuscript received June 23, 1958. Paper presented at 32nd Annual Fall Meeting of Society of Petroleum Engineers in Dallas, Tex., Oct. 6-9, 1957.

[1]References given at end of paper.

FIELD B

The original pressure-production match of Oct., 1950, showed a pressure decline of 150 psi under the observed field pressure by Nov., 1954 (see Fig. 2).

ALTERATIONS NECESSARY TO MATCH ENTIRE PRESSURE HISTORY

A new match was achieved by assigning permeabilities of 130 md to the outer water-drive zones in contrast to permeabilities in the range of 48 to 78 md assumed for the original match, and by lowering permeabilities from 19 to 10 md in the first water zone and from 48 to 33 md in the second water zone. These changes were sufficient to yield a satisfactory pressure match.

FIELD C

The original pressure-production match of April, 1951 showed a pressure decline to March, 1955 of 165 psi below that which was actually observed (see Fig. 3).

ALTERATIONS NECESSARY TO MATCH ENTIRE PRESSURE HISTORY

The original match was based on an assumed aquifer of 6.3-mile radius, divided into seven zones. The permeabilities of the first two zones were assumed to be 23 md and those of the remaining zones to be 190 md. The new match was achieved by assuming that the aquifer was greater in extent and by increasing the permeability of the second water zone. Three additional water zones were added to extend the aquifer radius to 10.9 miles. The permeability of the second water zone was increased from 23 to 63 md, while the permeabilities of the three new water zones (8, 9 and 10) were assumed to be 18, 7 and 5 md, respectively. A more satisfactory pressure match for the earlier part of the field pressure history was obtained when the initial reservoir pressure was lowered to 2,680 psi from the former estimated value, 2,725 psi.

FIELD D

The original pressure match of Oct., 1950 predicted a pressure for Sept., 1954, which was 295 psi above the observed Sept., 1954, reservoir pressure (Fig. 4).

ALTERATIONS NECESSARY TO MATCH ENTIRE PRESSURE HISTORY

Two possible causes for the discrepancy between the predicted and the observed pressure behavior were investigated.

The first possibility considered was that the aquifer available to Field D is smaller than was assumed when the original analyzer study was made. However, it was found that a smaller aquifer would not provide an acceptable pressure match.

The possibility that interfield communication was occurring was investigated next, as a small field had been discovered near Field D in Feb., 1951, and produces from the same formation. By withdrawing from Zone 1 (the reservoir zone) the sum of the productions from Field D and the small, nearby field, a satisfactory pressure match of Field D was obtained. It appears, therefore, that Field D is not an isolated field but that the smaller field could for practical purposes be considered an extension of the original field.

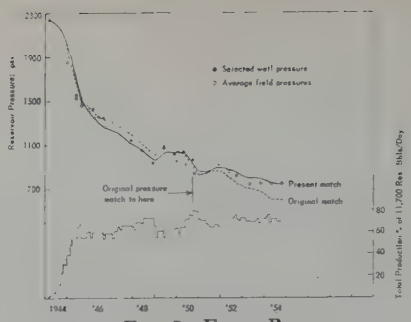

FIG. 2—FIELD B.

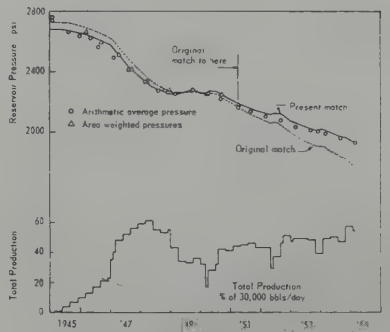

FIG. 3—FIELD C.

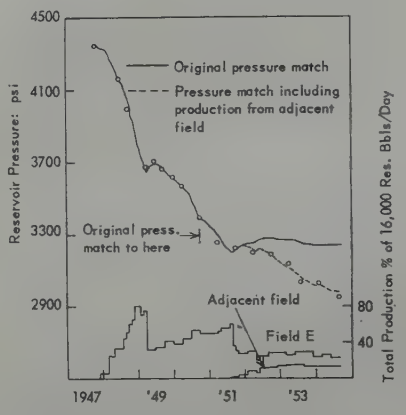

FIG. 4—FIELD D.

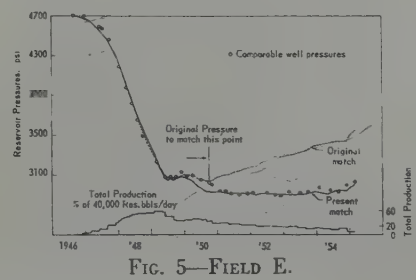

FIG. 5—FIELD E.

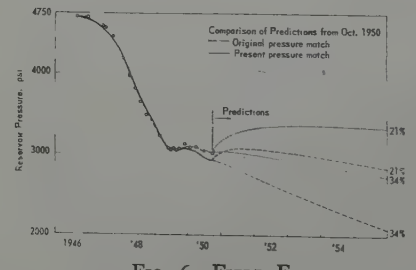

FIG. 6—FIELD E.

FIELD E

The predicted pressure for March, 1955 made from the original match of Oct., 1950 was 540 psi above the reservoir pressure in March, 1955 as shown in Fig. 5. The pressure history shown is that of a selected group of wells in which the pressures were measured during each survey. If the pressures measured in all of the wells are averaged, a very erratic pressure history results, probably because of the large pressure gradients that exist in this reservoir.

ALTERATIONS NECESSARY TO MATCH ENTIRE PRESSURE HISTORY

The large discrepancy between analyzer and field pressures was the result of assuming an aquifer of infinite extent in the original study. An extremely large aquifer was necessary in the original match to cause the analyzer pressure trace to duplicate satisfactorily the five pressure surveys immediately prior to Oct., 1950. It was found in the new study that a finite aquifer of some 19 miles in radius yielded a satisfactory pressure match of the entire field history except for the period from Nov., 1949 to Oct., 1950. Therefore, it must be assumed that the pressures selected for the field from the five pressure surveys made during that period were not representative of the field behavior.

REASONS FOR INACCURACY OF PREDICTIONS

In each case the cause of the deviation of the predicted pressure from

actual performance was either inaccurate data or insufficient pressure-production history to reveal the characteristics of the aquifer.

Inaccurate Data

The result of obtaining a match to a set of data in which some of the values were erroneous was demonstrated by the studies of Fields C and E. The original pressure prediction for Field E was based upon a perfectly acceptable match of the existing pressure history, yet the additional information gained from the six months immediately following the prediction indicated a very different size for the aquifer. In retrospect it appears that the pressures obtained from the five pressure surveys made immediately prior to the initial reservoir study were too high.

In the case of Field C it now appears that the original pressure reported for the field was erroneously high. This is indicated by the fact that for several years subsequent to the initial pressure point the analyzer curve paralleled but was displaced upward from the observed pressures. Resolving inconsistencies such as this requires the exercise of careful judgment. The relationship between analyzer results and observed data cited here as indicative of an erroneous initial pressure could be the correct relationship for some fields — fields where the initial pressures were correctly measured, but subsequent surveys made before the fields were fully developed reflected local pressure drawdowns rather than the average pressures for the entire reservoirs.

Insufficient Pressure-Production History

Failure to obtain an accurate prediction of pressure for Fields D and B resulted from insufficient pressure history to permit description of the aquifer.

The problem of having insufficient data on a reservoir at the time a pressure-production match is attempted cannot be circumvented, but the results obtained can still be used provided it is recognized that more information is required to define the reservoir and its associated aquifer. Patterson, Dutton and Ellis[2] have shown that the reliability of reservoir predictions is largely a function of the characteristics of the aquifer and, if sufficient time has not elapsed for the pressure drawdown in the oil pool to have affected the pressure in the outer part of the aquifer, then the characteristics and areal extent of the aquifer cannot be determined by a pressure match. They described a procedure to determine the minimum size aquifer associated with a reservoir. To accomplish this the reservoir analyzer is arranged to represent as large an aquifer as may exist and is adjusted to match the pressure history of the reservoir. Then, the resistors representing the outer part of the aquifer are varied. If variation of the resistance in a zone does not affect the pressure in the field, then obviously no information can be obtained on the characteristics of that zone. The outermost zone in which variations of the resistance will affect the analyzer match represents the minimum extent of the aquifer; i.e., the aquifer must be at least that large. Where geologic data indicate that the aquifer is actually larger than this minimum, it is suggested that predicted results be reported on the basis of the minimum aquifer that will satisfy the pressure-production behavior of the reservoir, and also on the basis of the larger aquifer indicated from geologic data which will satisfy the same pressure-production data. In this way the range of pressure values reported will very likely encompass the actual reservoir behavior.

COMPARISON OF PREDICTIONS OF FIELD E BASED ON ORIGINAL AND PRESENT MATCHES

Predictions for Field E based on the two reservoir matches, shown in Fig. 5, serve to show that even approximate analyzer matches yield useful information about the future reservoir performance. In Fig. 6 the predictions for the original match beginning in Oct., 1950 reveal a pressure difference of 655 psi by Jan., 1956 between production rates of 21 and 34 per cent of 40,000 reservoir B/D. Predictions based on the more accurate pressure match for the same period show a pressure difference of 760 psi between the 21 and 34 per cent production rates. Hence, the relative difference in the predicted behavior of the reservoir is only 105 psi during this five-year interval for these widely divergent analyzer matches.

CONCLUSIONS

This re-examination of the predictions of pressure behavior of five water-drive fields has demonstrated that predictions based upon a few years' pressure history are subject to considerable uncertainty.

Errors in pressure, production, or geologic data can cause inaccurate predictions to be made. Such errors often can be detected by careful analysis of the data.

A short-period pressure performance provides information only about that part of the aquifer near the field. The number of years for which reliable pressure predictions can be made is limited by the amount of information available from other sources on the characteristics of the more remote portions of the aquifer. It appears advisable to indicate the expected uncertainty in pressure forecasts by providing alternative predictions, one based upon the smallest aquifer which will adequately reproduce past performance, and another based upon the largest aquifer considered possible.

The determination of the relative pressure behavior for different production rates from a reservoir is not subject to the same degree of uncertainty which characterizes a forecast of the absolute pressures in a reservoir. Early studies of a reservoir can provide useful information regarding the merits of various production rates.

The periodic re-study of a reservoir results in increasingly accurate forecasts of pressure behavior and provides additional information regarding the characteristics of the reservoir and its associated aquifer.

REFERENCES

1. Bruce, W. A.: "An Electrical Device for Analyzing Oil-Reservoir Behavior", *Trans.* AIME (1943) **151**, 112.
2. Patterson, O. L., Dutton, G., and Ellis, H. E.: "The Determination of the Water Injection Program for the Delhi Field by Means of the Automatic Multi-Pool Analyzer", *Trans.* AIME (1956) **207**, 73. ★★★

Effect of Applied Pressure on the Conductivity, Porosity and Permeability of Sandstones

D. O. WYBLE | MICHIGAN COLLEGE OF MINING AND TECHNOLOGY
HOUGHTON, MICH.

ABSTRACT

A pressurizing system was designed and built to apply a radial pressure of 5,000 psi to rock samples. Samples of the Bradford, Weir and Kirkwood sandstones were subjected to radial pressures parallel and perpendicular to the bedding in the system and the changes in conductivity, porosity and permeability were determined.

Asymptotic decreases in conductivity, porosity and Klinkenberg permeability were observed over the 0- to 3,500-psi range. From these data, the increase of formation factor over the same range was calculated. The cementation exponent expressed in the Archie equation was found to increase with pressure.

The rate of change varied from formation to formation. Only small differences were observed for samples taken parallel to the bedding as compared to those taken perpendicular to it except for the Bradford sand.

Above 3,500 psi the data are not good enough to tell if the properties continue to fall-off asymptotically or in a different manner. A possible explanation for the probable limit of the asymptotic rate around 3,500 to 4,500 psi is that this represents the maximum pressure which the formations have undergone during their geological life as a result of burial.

INTRODUCTION

For many years measurements have been made in the laboratory of the properties of oil-bearing sandstones with little consideration being given to whether these properties had been changed when the samples were moved from their original position in the ground to the laboratory.

Relatively little has been reported in the literature on the effect of pressure on the properties of sandstones. The changes in permeability for eight typical consolidated oil-bearing sandstone samples with overburden pressure (0- to 15,000-psi range) was presented by Fatt[2] and Davis[1] in graphical form. In 1953 Fatt[2] also reported the relationship between porosity and overburden pressure for four typical consolidated oil-bearing sandstone samples (0- to 5,000-psi range). Fatt[3] later described the changes of formation factor and porosity of 20 typical oil-bearing sandstone samples with overburden pressure changes (0- to 5,000-psi range) giving the values of the coefficients and exponents in the Archie[4] equation,

$$F = \phi^{-m} \quad . \quad . \quad . \quad . \quad . \quad . \quad . \quad . \quad . \quad . \quad . \quad (1)$$

and the more general Winsauer equation[5],

$$F = C\phi^{-k} \quad . \quad . \quad . \quad . \quad . \quad . \quad . \quad . \quad . \quad . \quad . \quad (2)$$

where C, k and m are empirical constants, F is the formation factor, and ϕ is the porosity.

During the experiments of this investigation the core was contained in a neoprene rubber sleeve as shown in Fig. 1. It was held between two steel end members which were mounted in a steel cylinder. The unassembled pressure cylinder with its component parts is shown in Fig. 2. The core was insulated from the two steel end members by a Teflon sleeve with a small hole in the

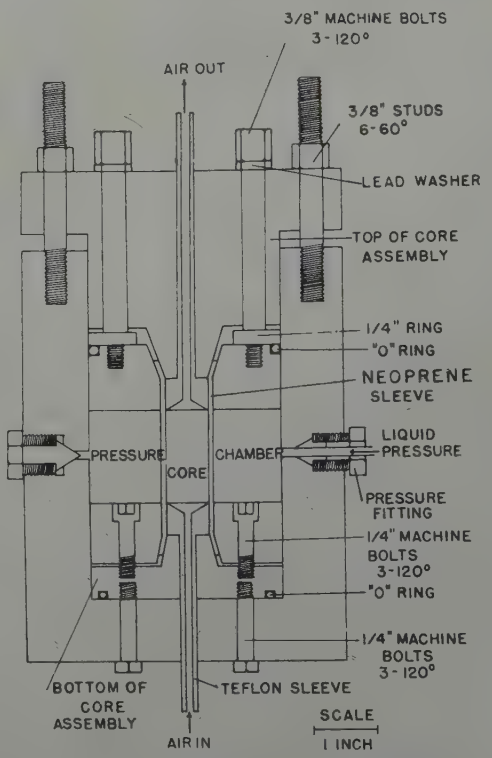

FIG. 1—PRESSURE CHAMBER — ELECTRODES REMOVED FOR PERMEABILITY MEASUREMENTS.

Original manuscript received in Society of Petroleum Engineers office March 24, 1958. Revised manuscript received July 28, 1958. This paper is a condensation of a PhD thesis in geophysics by the author on file in the Pennsylvania State U. Library.
[1]References given at end of paper.

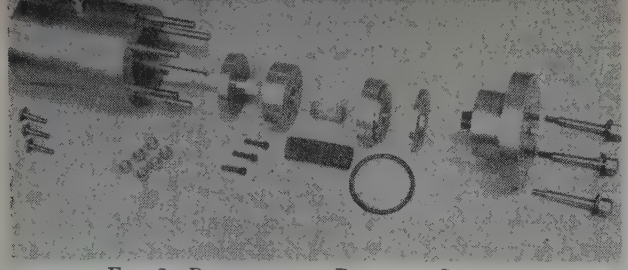

FIG. 2—DISASSEMBLED PRESSURE CHAMBER.

center. In operation, the space between the Teflon sleeve and the walls of the pressure chamber was filled with kerosene under pressure. When pressure was applied to the kerosene a radial pressure of 0- to 5,000 psi could be applied to the cylindrical cores while the axial stresses were at atmospheric. It is not known whether the effects of radial pressure on the properties of the samples would be identical with the effect of overburden pressure. It should be noted here that this stress system is different from the more conventional hydrostatic stress system used by Fatt.

Sixteen cylindrical samples 0.75 in. in diameter and 1.5 in. long were cut from sandstone cores using a diamond drill. These samples were cut parallel and perpendicular to the bedding plane of the Weir, Kirkwood and Bradford sandstone formation samples. The Bradford and Weir sands are low-rank greywackes and the Kirkwood is a fairly clean orthoquartzite according to the Krynine[6] classification. Details of the apparatus, experimental procedure, core preparation and accuracy of the measurements are discussed by Wyble[7] in a thesis on which this paper is based.

OBSERVED DATA

The values of conductivity, porosity, permeability and formation factor at room temperature and atmospheric pressure are presented in Table 1. The average changes of these properties with pressure for each formation are shown in Figs. 3, 4 and 5. The term "horizontal" applies to samples taken parallel to the bedding plane and the term "vertical" to samples taken perpendicular to the bedding plane. Using Table 1 and Figs. 3, 4 and 5 one can construct a similar figure for formation factor as a function of pressure.

Resistivities and conductivities were calculated from measured resistance values and core dimensions. The ratio between the conductivity at a given pressure and the conductivity at zero pressure were computed for each core over the 0- to 5,000-psi range. These ratios were converted into percentages and averaged for the samples parallel to the bedding plane and for the samples perpendicular to the bedding plane of each formation and plotted as a function of pressure (Figs. 3, 4

TABLE 1—SAMPLE CHARACTERISTICS AT ATMOSPHERIC PRESSURE

(Cores were cut parallel to bedding except for cores marked V, which were cut with their axis at right angles to the bedding.)

Weir Cores	W20B	W20BV	W31B	W31BV	W39B	W39BV
Brine porosity	16.6	16.0	14.3	14.0	12.9	13.0
Conductivity (mho/cm) $(10)^{-8}$	2.17	2.33	1.75	1.53	1.33	1.39
Permeability, md	3.19	4.63	1.42	1.68	1.08	1.83
Formation factor	35.4	33.1	43.8	51.2	58.8	57.2
Kirkwood Cores	**K65**	**K65V**	**K67**	**K67V**	**K67V1**	
Brine porosity	18.7	18.6	12.6	13.1	12.9	
Conductivity (mho/cm) $(10)^{-8}$	2.94	2.53	1.56	1.50	1.68	
Permeability, md	34.8	22.2	2.38	.74	1.25	
Formation factor	26.2	30.4	49.2	51.2	45.9	
Bradford Cores	**B20**	**B23**	**B26**	**B29V**	**B29V1**	
Brine porosity	9.0	10.6	11.6	11.0	11.1	
Conductivity, (mho/cm) $(10)^{-3}$	.640	.625	1.35	.939	.952	
Permeability, md	.476	1.42	10.3	2.48	2.48	
Formation factor	127.5	123.0	57.7	81.9	80.9	

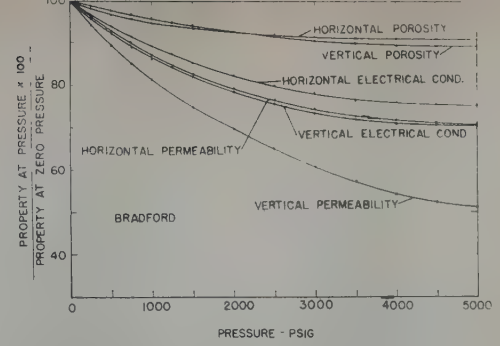

FIG. 3—BRADFORD SAND — AVERAGE CHANGE OF PROPERTIES WITH PRESSURE.

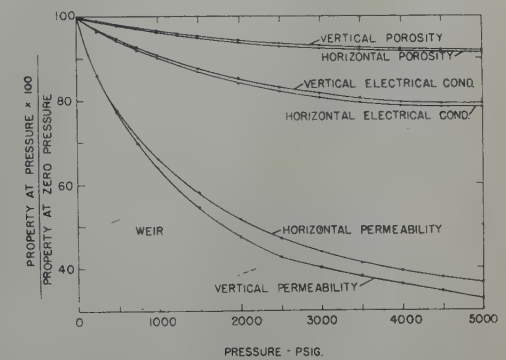

FIG. 4—WEIR SAND — AVERAGE CHANGE OF PROPERTIES WITH PRESSURE.

and 5). The maximum deviation for any individual sample of its group (Bradford, Weir or Kirkwood) was 6.6 per cent while for most samples it was less than 3.0 per cent. No correction was applied for the effect of clay conductivity on these data.

Porosity data are presented similarly. The maximum deviation of the ratio for any sample at 5,000 psi from the average value of its group was 1.2 per cent. Klinkenberg permeabilities[8] are presented in the same way. The maximum deviation of the ratio for any individual sample at 5,000 psi from the averaged value of its group was 11.45 per cent, while for most of the samples it was less than 10 per cent. The greater variation of individual permeability values as compared to porosity and conductivity is to be expected, considering the lesser accuracy of permeability measurements and the greater range of its decrease with increasing pressure.

RELATIONSHIP BETWEEN PROPERTIES AND PRESSURE

The general shape of Figs. 3, 4 and 5 is an exponential decrease approaching a fixed value of the ratio of the given property under pressure to the same property at zero pressure. In Fig. 6 observed values of conductivity less this asymptotic limit are plotted against pressure on semi-logarithmic paper. This can also be done for the other properties. The following equation describes a straight line on such a plot.

$$100\,\frac{(W_P)}{W_0} - B = (100 - B)\ 10^{-\alpha P}, \quad . \quad (3)$$

where W_P is the value of the property under consideration at pressure P; W_0 is the value of the property at zero pressure; B is the per cent to which the curve is asymptotic; and α is the coefficient of exponential decrease (determined from the slope of the semi-logarithmic plot).

Values of B and α are given in Table 2 for all properties measured. The plot of Fig. 6 approximated a

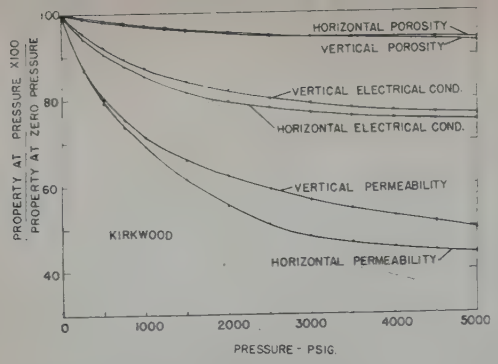

FIG. 5—KIRKWOOD SAND — AVERAGE CHANGE OF PROPERTIES WITH PRESSURE.

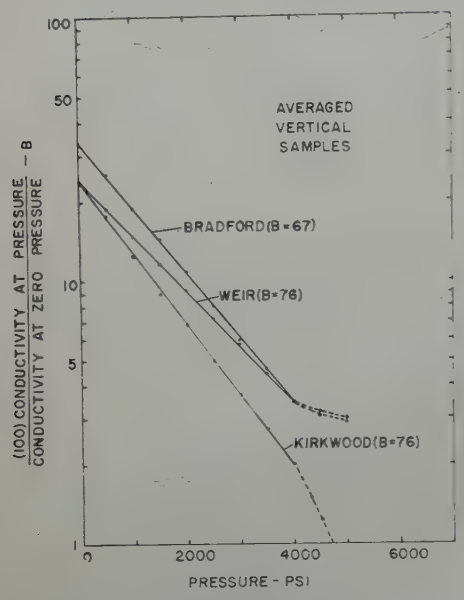

FIG. 6—CONDUCTIVITY VS PRESSURE PLOT FOR EQ. 3.

straight line only in the range of 0 to 3,500 psi. At higher pressures, the shape of the curve is very sensitive to the value of B chosen, and small inaccuracies in the data can cause large scatter of the points. The right-hand column of Table 2 shows the maximum deviations of the observed values of conductivity, porosity and permeability from the average values.

The constants and exponents of the Archie[4] and Winsauer[5] equations using the data from Figs. 3, 4 and 5 at certain pressures are shown in Table 3. These data were processed by the least-squares method of adjustment in a manner similar to that by Fatt[3]. In this method of adjustment two values of the constants should be determined for the Archie[4] and Winsauer[5] equations depending on the coordinate minimized. The values of the cementation exponent in the Archie equation were the same for both. A third value could also be determined but this did not seem feasible. As previously pointed out, the properties show a decided change beyond 3,500 psi which is in agreement with the constants in Table 3.

For pressures greater than 3,500 psi it was impossible to find a good fit to an asymptotic curve representing the dependence of the rock properties studied on pressure. The sudden change of the constants in the Winsauer equation indicate this. From purely physical considerations it would be expected that some further decrease in porosity, permeability and conductivity beyond the asymptotic value, B, of Eq. 3 would continue to occur as pressure was increased.

A possible explanation is that B represents a limiting

TABLE 2—VALUES OF B AND α FOR EQ. 3

	B_ϕ	Porosity $10^4\alpha$	Max. dev. of each observation from averaged curves (per cent)
Weir horizontal	90.5	2.75	0.4
Weir vertical	90.5	1.94	0.8
Kirkwood horizontal	93.5	2.11	0.9
Kirkwood vertical	92.5	1.82	1.2
Bradford horizontal	90.5	3.11	0.3
Bradford vertical	86.0	1.60	0.1

	B_σ	Conductivity $10^4\alpha$	Max. dev. of each observation from averaged curves (per cent)
Weir horizontal	76.0	2.33	3.6
Weir vertical	76.0	2.12	2.4
Kirkwood horizontal	74.0	3.44	6.6
Kirkwood vertical	76.0	2.66	6.6
Bradford horizontal	73.0	2.40	1.3
Bradford vertical	67.0	2.48	1.0

	B_K	Permeability $10^4\alpha$	Max. dev. of each observation from averaged curves (per cent)
Weir horizontal	34.0	2.77	10.2
Weir vertical	33.0	3.22	11.4
Kirkwood horizontal	43.0	3.44	7.5
Kirkwood vertical	52.0	3.60	11.2
Bradford horizontal	68.5	2.27	1.6
Bradford vertical	44.0	1.78	1.7

TABLE 3—CONSTANTS

Pressure (psi)	Archie equation (F)	Winsauer equation: F minimized (F)	Winsauer equation: ϕ minimized (F)
0	$\phi^{-1.97}$	$.72\ \phi^{-2.10}$	$.45\ \phi^{-2.26}$
1,000	$\phi^{-2.00}$	$.84\ \phi^{-2.09}$	$.55\ \phi^{-2.29}$
2,000	$\phi^{-2.02}$	$.92\ \phi^{-2.13}$	$.52\ \phi^{-2.33}$
3,000	$\phi^{-2.04}$	$.79\ \phi^{-2.11}$	$.42\ \phi^{-2.44}$
4,000	$\phi^{-2.06}$	$.42\ \phi^{-2.45}$	$.05\ \phi^{-3.50}$
5,000	$\phi^{-2.04}$	$.23\ \phi^{-2.73}$	$.002\ \phi^{-5.12}$

value of elastic deformation of the matrix, beyond which a different, much slower type of deformation occurs. At low pressures deformation may occur by the closing of small cracks without appreciable deformation of individual sand grains or reorientation of grains in the matrix. Further change would be much slower, too slow to be noted in the pressure range studied, and would involve distortion of individual grains.

Even though a different pressurizing system was used in this work, the results obtained here are consistent with observations by Fatt[2,3]. The general shape of Fatt's plots are similar to those presented here.

ACKNOWLEDGMENTS

Sincere appreciation is expressed to B. F. Howell, Jr., for his helpful guidance and criticism throughout this work. Special thanks are due E. James Moore, Pasquale H. Licastro, Robert J. Watson and Krishna Kamath for their time spent in discussions and the valuable suggestions arising out of these discussions. The courtesy of I. Fatt in sending the writer a copy of his paper[3] before publication is gratefully acknowledged.

Thanks are also due to the Mineral Industries Instrument Shop for the excellent workmanship in making the components of the pressurizing system. The assistance of the Magnolia Petroleum Co. in supplying funds for supplies and equipment used in this research is gratefully acknowledged.

REFERENCES

1. Fatt, I. and Davis, D. H.: *Trans.*, AIME (1952) **195**, 329.
2. Fatt, I: *Trans.*, AIME (1953) **198**, 325.
3. Fatt, I.: *Bull.*, AAPG (Nov., 1957) 2456.
4. Archie, G. E.: *Trans.*, AIME (1942) **146**, 54.
5. Winsauer, W. O., Shearin, H. M., Jr., Masson, P. H. and Williams, M.: *Bull.*, AAPG (1952) **36**, 235.
6. Krynine, P. D.: *Jour. Geol.* (1948) **56**, 130.
7. Wyble, D. O.: "Effect of Pressure on the Conductivity, Porosity and Permeability of Oil-Bearing Sandstones", PhD thesis, The Pennsylvania State U.
8. Klinkenberg, L. J.: *Drill. and Prod. Prac.*, API (1941) 200.

★★★

The Importance of Reliable Data in Gas-Condensate Recovery Calculations

R. F. HINDS
MEMBER AIME

CORE LABORATORIES, INC.
DALLAS, TEX.

INTRODUCTION

With the continued deep drilling of today, increasing numbers of high pressure and high temperature gas-condensate reservoirs are being discovered. Correspondingly, the ranges of properties of gas-condensate reservoir fluids are also being increased. The literature[1,2,3] contains several excellent reviews of the property ranges in presently known condensate reservoirs. When one examines these property ranges, it becomes apparent that the need for reliable data is great if the engineer is to evaluate properly or appraise a gas-condensate reservoir.

It is the purpose of this paper to present phase-behavior data that will point out some of the important variables that influence recovery from gas-condensate reservoirs produced by pressure depletion. All these variables may be resolved into two major categories: the hydrocarbon composition of the reservoir fluid and the physical properties of the reservoir. But the variables which we will consider are those which are usually determined from well tests shortly after discovery and are, consequently, readily available to the engineer. They are as follows: (1) the producing separator gas-stock-tank liquid ratio, (2) stock-tank liquid gravity, and (3) reservoir temperature.

Laboratory depletion studies have been performed on several reservoir fluids to illustrate the effect of changes in the considered variables upon ultimate recoveries. The deviation factors, Z, of a series of reservoir fluids were determined experimentally to illustrate their order of magnitude and their effect upon the calculation of in-place reserves existing at high pressures and temperatures. The procedures followed in conjunction with the performance of these studies and their associated calculations are illustrated in Fig. 1. For the purpose of this paper, the depletion recoveries are expressed only in terms of per cent of initial stock-tank liquid, with the abandonment pressure assumed to be 500 psig.

VARIATION OF RECOVERY WITH INITIAL PRODUCING SEPARATOR GAS-STOCK-TANK LIQUID RATIO

The producing separator gas-stock-tank liquid ratio has long been one of the principal criteria in assumptions and generalized correlations[4] used for the estimation of ultimate recovery from gas-condensate reservoirs. Fig. 2 presents a plot of the cumulative recovery of stock-tank liquid at abandonment as a function of the initial producing separator gas-stock-tank liquid ratio. The graphical illustration represents the results of 44 laboratory depletion studies performed on actual gas-condensate fluids. These data are presented not only to illustrate the general trend of ultimate recovery increase with initial producing ratio increase but to emphasize the considerable variation in possible recovery at any given producing ratio.

Table 1 presents the properties of two actual reservoir fluids chosen to illustrate the approximate extremities of producing ratios for gas-condensate systems. The fluids designated as A and B exhibited initial producing ratios of 3,400 and 114,000 scf/bbl, respectively. Fig. 3 presents a graphical comparison of the cumulative stock-tank liquid recoveries, calculated from the well-stream compositions and produced volumes for each fluid during depletion. It is to be noted that Fluid A exhibited a recovery of only 16.5 per cent when produced to an assumed abandonment pressure of 500 psig while the corresponding recovery for Fluid B was calculated to be 62.2 per cent. This difference in recovery, which exemplifies the general trend of recovery increase with initial producing ratio increase, is readily explained by consid-

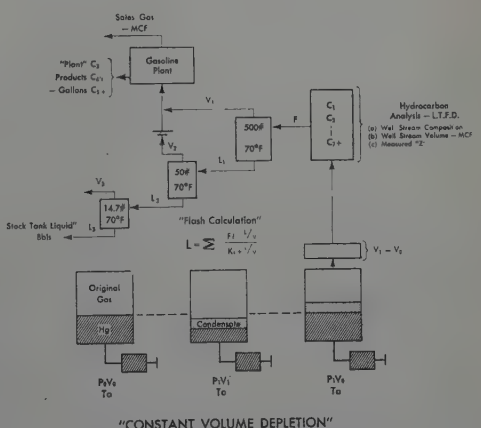

FIG. 1—LABORATORY AND CALCULATION PROCEDURES USED IN OBTAINING DEPLETION RECOVERIES.

Original manuscript received in Society of Petroleum Engineers office March 10, 1958. Revised manuscript received Oct. 22, 1958. Paper presented at Gas Technology Symposium in Shreveport, La., April 17-18, 1958.

[1]References given at end of paper.

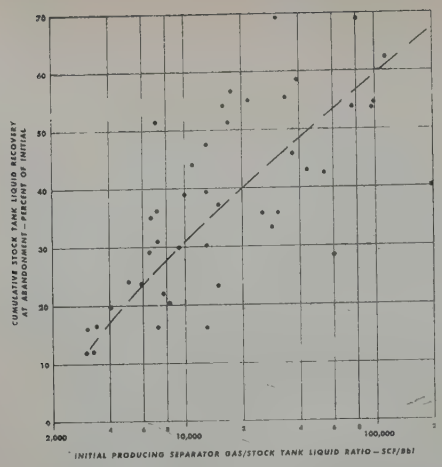
CUMULATIVE STOCK TANK LIQUID RECOVERY AT ABANDONMENT—PERCENT OF INITIAL
INITIAL PRODUCING SEPARATOR GAS/STOCK TANK LIQUID RATIO—SCF/BBL

FIG. 2—VARIATION OF CUMULATIVE RECOVERY AT ABANDONMENT WITH INITIAL PRODUCING GAS-LIQUID RATIO.

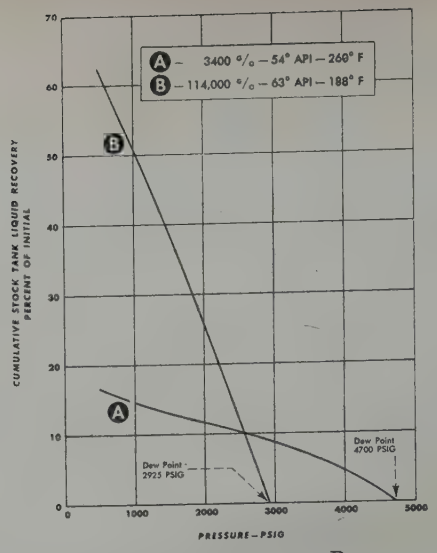
A — 3400 °/₀ — 54° API — 260° F
B — 114,000 °/₀ — 63° API — 188° F
CUMULATIVE STOCK TANK LIQUID RECOVERY PERCENT OF INITIAL
Dew Point 2925 PSIG
Dew Point 4700 PSIG
PRESSURE—PSIG

FIG. 3—CUMULATIVE DEPLETION RECOVERY FOR TWO EXTREMES OF INITIAL PRODUCING GAS-LIQUID RATIOS.

eration of the composition of the hydrocarbon systems.

As the initial producing ratio increases the ratio of the light hydrocarbons (C_1, C_2 . . . . C_4's) to the heavier components (C_5 +) increases in the well stream. During depletion, the higher this ratio the greater is the volatility imposed upon the heavy components. This results in less retrograde condensation and, consequently, greater recovery.

VARIATION OF RECOVERY WITH INITIAL STOCK-TANK LIQUID GRAVITY

Referring again to Fig. 2, it is to be pointed out that quite obviously in many cases there is a considerable variation in ultimate recovery for a specific initial producing ratio. Hydrocarbon composition again is the major cause. One of the most important variables influencing these recovery differences is the properties of the heptanes and heavier which for our purpose are reflected in the stock-tank liquid gravity.

Table 2 presents the properties of two actual reservoir fluids chosen to illustrate the effect of initial stock-tank liquid gravity upon recovery. The two fluids, designated as C and D were chosen with similar producing ratios of 13,000 scf/bbl each, but with a wide variation in stock-tank liquid gravities of 47° and 68° API, respectively. The wide variation in stock-tank gravities corresponds to the heptanes and heavier gravities of 42.1° and 58.7° API, respectively. The laboratory depletion studies were performed at similar reservoir temperatures to provide further emphasis to the effect of initial gravities. The comparison of the cumulative stock-tank liquid recoveries resulting from the depletions is illustrated in Fig. 4. The recovery for Fluid C at 500 psig was calculated to be 30.3 per cent while the corresponding recovery for Fluid D was found to be 47.5 per cent.

These data indicate that for similar producing ratios and similar reservoir temperatures, the reservoir fluid with the more volatile heptanes and heavier, or higher stock-tank-API gravity, would yield the greater recovery during depletion.

VARIATION OF RECOVERY WITH RESERVOIR TEMPERATURE

The effects of temperatures upon dew-point pressure and retrograde condensation for specific reservoir fluids have long been recognized and have been presented in the literature[5,6] in the form of phase diagrams. However, there has been very little data presented to illustrate the effect of temperature upon depletion recoveries. With reference to Fig. 2 again, the variation in ultimate recovery for a specific initial producing ratio can be attributed in part to the effect of reservoir temperature. The extent of the effect of temperature, of course, will depend upon the hydrocarbon composition of the reservoir fluid.

Table 3 presents the properties of a specific reservoir fluid chosen to illustrate the effect of reservoir temperature, alone, upon depletion recoveries. The fluid designated as E yields an initial producing ratio of 7,100 scf/bbl with an associated stock-tank liquid gravity of 53° API. The molecular weight and gravity of the

TABLE 1—PROPERTIES OF RESERVOIR FLUIDS CHOSEN TO ILLUSTRATE THE APPROXIMATE EXTREMITIES OF PRODUCING SEPARATOR GAS-STOCK-TANK LIQUID RATIOS FOR GAS-CONDENSATE FLUIDS

	Reservoir Fluid (A)	Reservoir Fluid (B)
Separator gas-stock-tank liquid ratio, scf/bbl	3,400	114,000
Stock-tank liquid gravity, °API	54	63
Hydrocarbon composition		
Component	Mol per cent	Mol per cent
Methane	65.5	93.4
Ethane	9.2	3.8
Propane	4.5	1.0
Butanes	4.0	0.6
Pentanes	2.6	0.3
Hexanes	2.2	0.2
Heptanes plus	12.0	0.7
Totals	100.0	100.0
Properties of heptanes plus		
API gravity @ 60°F	45.6	54.2
Specific gravity @ 60/60°F	0.799	0.762
Molecular weight	184	145

TABLE 2—PROPERTIES OF RESERVOIR FLUIDS CHOSEN TO ILLUSTRATE THE VARIATION OF RECOVERY WITH STOCK-TANK LIQUID GRAVITY

	Reservoir Fluid (C)	Reservoir Fluid (D)
Separator gas-stock-tank liquid ratio, scf/bbl	13,000	13,000
Stock-tank liquid gravity, °API	47	68
Hydrocarbon composition		
Component	Mol per cent	Mol per cent
Methane	84.0	80.1
Ethane	6.3	6.5
Propane	2.6	2.9
Butanes	1.5	3.0
Pentanes	0.7	2.1
Hexanes	0.6	1.6
Heptanes plus	4.2	3.8
Totals	100.0	100.0
Properties of heptanes plus		
API gravity @ 60°F	42.1	58.7
Specific gravity @ 60/60°F	0.815	0.744
Molecular weight	180	130

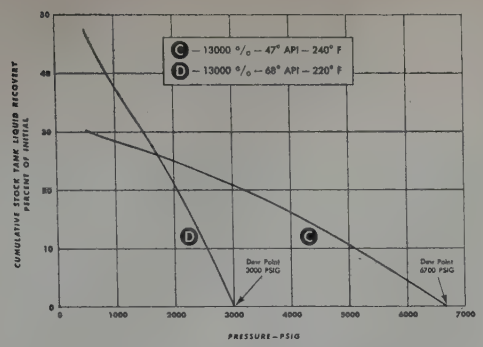
C – 13000 °/₀ – 47° API – 240° F
D – 13000 °/₀ – 68° API – 220° F
CUMULATIVE STOCK TANK LIQUID RECOVERY PERCENT OF INITIAL
Dew Point 3000 PSIG
Dew Point 6700 PSIG
PRESSURE – PSIG

FIG. 4 — VARIATION OF CUMULATIVE DEPLETION RECOVERY WITH INITIAL STOCK-TANK LIQUID GRAVITY.

heptanes and heavier are 160 and 46.2° API, respectively.

Laboratory depletion studies were performed on Fluid E at temperatures of 120°, 240°, and 300°F. It was felt that this temperature range would encompass the majority of gas-condensate reservoirs of practical significance. The cumulative recovery curves for the three temperatures are presented as a function of pressure decline in Fig. 5. Abandonment recoveries at 500 psig were found to be 16.1 per cent at 120°F, 36.2 per cent at 240°F, and 51.5 per cent at 300°F. These values represent a spread of 35.4 per cent over the temperature range of 120° to 300°F.

The increase in recovery due to temperature increase for a specific reservoir fluid is due primarily to the fact that the heptanes and heavier, which constitute the greater portion of stock-tank liquid, increase in volatility with temperature increase. This results again in less retrograde condensation and, consequently, greater recovery. For a given initial producing ratio, the reservoir temperature appears to have a more pronounced effect upon ultimate recovery by pressure depletion than does the initial stock-tank liquid gravity, when each is considered as an independent variable.

IMPORTANCE OF A DEVIATION FACTOR (Z) IN CALCULATING "IN-PLACE" RESERVES

Discovery of the very high pressure and high temperature gas-condensate reservoirs in recent years has necessitated the use of accurate deviation factors in the calculation of in-place reserves.

Table 4 presents a list of eight measured deviation factors tabulated as a function of initial producing gas-liquid ratio and reservoir pressure-temperature. The table is presented to demonstrate the tremendous magnitude of these values, which range from 1.275 at 244°F and 7,700 psig to 2.038 at 205°F and 11,000 psig. An extreme case is used as an example to illustrate its effect upon in-place reserve estimates. The example fluid exhibited an initial producing ratio of 6,200 scf/bbl and existed as a single vapor phase at reservoir conditions of 9,000 psig and 238°F. The measured deviation factor for these conditions was 1.517. This value, when used in volumetric calculations, shows 51.7 per cent less actual reserves than would be calculated if the deviation factor is neglected.

TABLE 3—PROPERTIES OF A RESERVOIR FLUID CHOSEN TO ILLUSTRATE THE VARIATION OF RECOVERY WITH RESERVOIR TEMPERATURE

	Reservoir Fluid (E)
Separator gas-stock-tank liquid ratio, scf/bbl	7,100
Stock-tank liquid gravity, °API	53
Hydrocarbon composition	
Component	Mol per cent
Methane	78.1
Ethane	6.4
Propane	3.8
Butanes	2.1
Pentanes	1.5
Hexanes	1.3
Heptanes plus	6.8
Total	100.0
Properties of heptanes plus	
API gravity @ 60°F	46.3
Specific gravity @ 60/60°F	0.796
Molecular weight	160

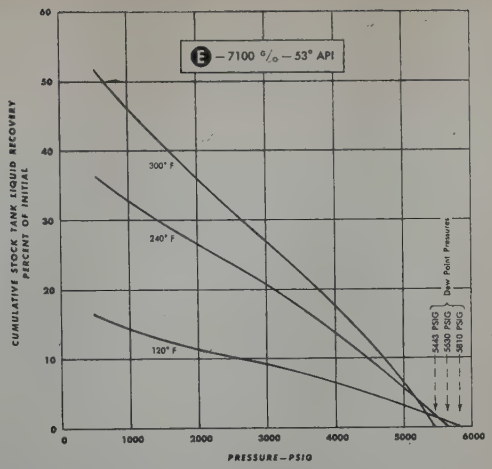

FIG. 5 — VARIATION OF CUMULATIVE DEPLETION RECOVERY WITH RESERVOIR TEMPERATURE.

TABLE 4—THE MAGNITUDE OF DEVIATION FACTORS (Z) MEASURED AT HIGH PRESSURES AND TEMPERATURES FOR LOW-RATIO GAS-CONDENSATE FLUIDS

Producing separator gas-stock-tank liquid ratio (scf/bbl)	Reservoir pressure (psig)	Reservoir temperature (°F)	Measured deviation factor (Z)
15,000	9,500	239	1.440
13,000	7,700	244	1.275
13,000	8,200	213	1.326
6,600	8,400	267	1.420
6,200	9,000	238	1.517*
5,100	7,400	278	1.335
4,000	8,000	240	1.449
3,000 (critical)	11,000	205	2.038

*The use of this Z factor in a volumetric calculation would show 51.7 per cent less actual reserves than would be calculated if Z is neglected.

CONCLUSIONS

Ultimate recoveries from gas-condensate reservoirs produced by pressure depletion will vary considerably, depending upon their initial hydrocarbon composition and reservoir physical properties. The wide variation in these recoveries then emphasizes the importance and need for having reliable data for each specific reservoir and gas-condensate system studied.

ACKNOWLEDGMENT

The author wishes to acknowledge the helpful discussions and suggestions of E. H. Koepf and F. O. Reudelhuber of the Core Laboratories, Inc. in the preparation of this paper.

REFERENCES

1. Thornton, O. F.: "Gas-Condensate Reservoirs—A Review", *Pet. Engr. Ref. Annual* (1947) 124.
2. Sloan, J. Paul: "Phase Behavior of Natural Gas and Condensate Systems", *Pet. Engr.* (1950) **2**, B-54.
3. Allen, J. C.: "Factors Affecting the Classification of Oil and Gas Wells", API Spring Meeting, Shreveport, La. (1952).
4. Brinkley, T. W. and Curtis, R. C.: "Calculation of Natural Condensate Recovery", *World Oil* (1951) **132**, 7, 178.
5. Katz, D. L. and Kurata, F.: "Retrograde Condensation", *I & EC* (1940) **32**, 817.
6. Eilerts, C. K.: *Phase Relations of Gas-Condensate Fluids—Test Results, Apparatus and Techniques*, Monograph 10, USBM, American Gas Assn. (1957) **1**, 271. ★★★

A Comparison of Calculated k_{rg}/k_{ro} Ratios with a Correlation of Field Data

MICHAEL A. TORCASO
M. R. J. WYLLIE
MEMBER AIME

GULF RESEARCH & DEVELOPMENT CO.
PITTSBURGH, PA.

ABSTRACT

It is shown that k_{rg}/k_{ro} ratios computed on the assumption that the average sandstone reservoir has a pore-size distribution characterized by a linear $1/P_c^2$ saturation plot are in good agreement with corresponding k_{rg}/k_{ro} ratios obtained by Wahl, Mullins and Elfrink by the correlation of field measurements.

EQUATION FOR CALCULATING k_{rg}/k_{ro} RATIOS

Methods of calculating relative permeability data have recently been reviewed and extended.[1] It was shown that for sandstone reservoirs where $1/P_c^2$ is approximately a linear function of effective saturation (as suggested first by Corey[2]) it is possible to express relative permeabilities in very simple terms. For systems wetted by connate water and producing oil and gas (gas saturation growing at the expense of oil) the expression for the k_{rg}/k_{ro} ratio is

$$k_{rg}/k_{ro} = \frac{(1 - S^*)^2 [1 - (S^*)^2]}{(S^*)^4}, \quad \ldots\ldots\ldots\ldots (1)$$

where S^* = effective saturation = $\frac{S_o}{1 - S_{wi}}$.

The accuracy of Eq. 1 has been frequently confirmed in our laboratories; because of its simplicity we make routine use of it in the analytical solution of problems in reservoir engineering. Nevertheless, comparisons of the k_{rg}/k_{ro} ratios yielded by Eq. 1 with appropriate reservoir data have been few. The publication by Wahl, Mullins and Elfrink[3] of an empirical equation for k_{rg}/k_{ro} ratios is thus of interest since this equation is specifically stated to be based on the correlation of field measurements made on sandstone reservoirs. Not surprisingly these authors found that it was necessary to

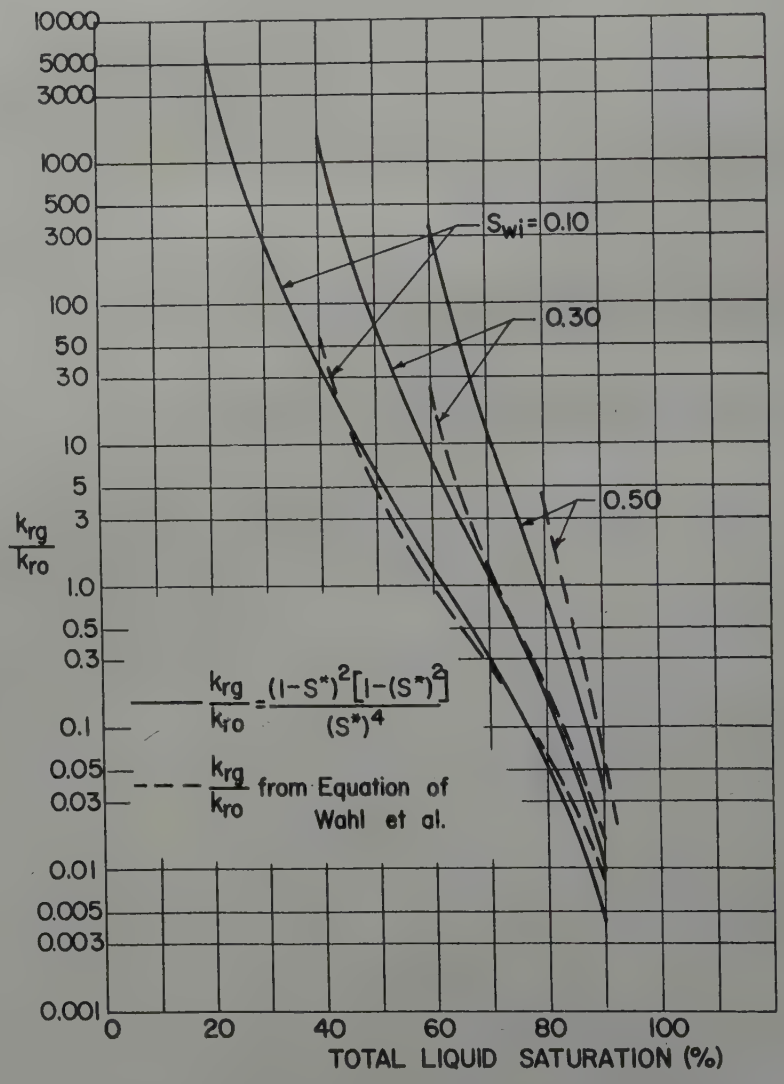

FIG. 1—COMPARISON BETWEEN k_{rg}/k_{ro} CALCULATED FOR TYPICAL SANDSTONE PORE-SIZE DISTRIBUTIONS AND k_{rg}/k_{ro} BASED ON THE CORRELATED PERFORMANCE DATA OF SANDSTONE RESERVOIRS.

Original manuscript received in Society of Petroleum Engineers office Aug. 15, 1958. Revised manuscript received Oct. 29, 1958.
[1]References given at end of paper.

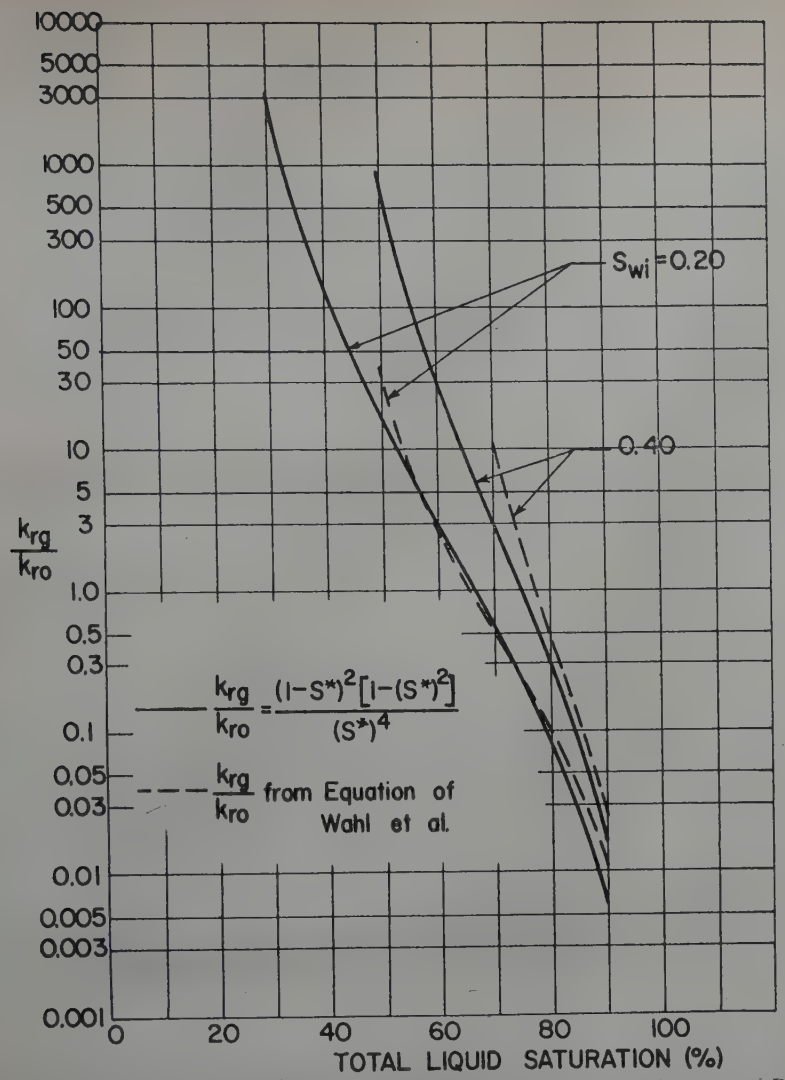

FIG. 2—COMPARISON BETWEEN k_{rg}/k_{ro} CALCULATED FOR TYPICAL SANDSTONE PORE-SIZE DISTRIBUTIONS AND k_{rg}/k_{ro} BASED ON THE CORRELATED PERFORMANCE DATA OF SANDSTONE RESERVOIRS.

treat the interstitial water saturation as a parameter. This parameter we treat as S_{wi} in Eq. 1 for effective saturation.

Figs. 1 and 2 give a comparison between k_{rg}/k_{ro} calculated from the Wahl, *et al*, empirical equation and calculated from Eq. 1. S_{wi} values of 0.10, 0.20, 0.30, 0.40 and 0.50 were chosen. When the fact is considered that the Wahl, *et al*, empirical equation causes k_{rg}/k_{ro} to go to infinity at a total liquid saturation of $S_{wi}+0.25$, the agreement between the two sets of curves is excellent. The divergence at $S_{wi} = 0.40$ and 0.50 can possibly be attributed to the scarcity and atypical nature of reservoirs producing oil and gas at such high water saturations.

CONCLUSION

We conclude that Eq. 1 is a simple and useful expression for calculating k_{rg}/k_{ro} ratios in sandstone reservoirs for which an average water saturation has been obtained either by electric log or core analysis. It is an expression particularly useful in the analytical formulation of problems in reservoir engineering.

REFERENCES

1. Wyllie, M. R. J. and Gardner, G. H. F.: "The Generalized Kozeny-Carman Equation", *World Oil* (March and April, 1958) **146,** No. 4, 121; and **146,** No. 5, 210.
2. Corey, A. T.: "The Interrelation between Gas and Oil Relative Permeabilities", *Prod. Monthly* (1954) **19,** No. 1, 38.
3. Wahl, W. L., Mullins, L. D. and Elfrink, E. B.: "Estimation of Ultimate Recovery from Solution Gas-Drive Reservoirs", *Trans.* AIME (1958) **213,** 132. ★★★

The Effect of Temperature on the Flow Properties of Clay-Water Drilling Muds

S. SRINI-VASAN*
JUNIOR MEMBER AIME
CARL GATLIN**
MEMBER AIME

UNIVERSITY OF TULSA
TULSA, OKLA.

INTRODUCTION

In the past few years the hydraulic aspects of rotary drilling have received considerable attention. It is generally recognized that accurate prediction of circulating pressures is desirable, particularly in those areas where a delicate pressure balance is necessary to prevent both blowouts and lost circulation. For calculation purposes the standard hydraulic equations for the pipeline flow of Newtonian fluids have been altered to facilitate similar calculations for non-Newtonian or plastic fluids.[1,2] This latter classification includes most colloidal types of drilling muds.

Two properties: plastic viscosity, μ_p, and Bingham yield value, Y_B, are commonly used to define the flow characteristics of a plastic fluid. These are commonly obtained with multispeed viscosimeters such as the Fann V-G meter.[3] Normally these measurements are obtained at some surface temperature, and are not corrected to circulating temperatures for calculation purposes. This may result in considerable error, particularly in the laminar flow calculations which commonly apply to the drill pipe-borehole annulus. The purpose of this study was to investigate the effect of temperature on the flow properties of some water-base muds.

EXPERIMENTAL PROCEDURE

A laboratory model Fann V-G meter was used for measurement of viscosities, yield values and gel strengths. An aluminum water jacket with O-ring seals was machined to fit around the mud cup of the Fann meter.

All mud samples were prepared by thorough mixing in a Hobart mixer. Viscosity and gel strength measurements were made with the Fann meter using standard procedures. Flow properties of muds were studied at 80, 120, 160 and 180°F.

The compositions of the test samples are given in Table 1.

Original manuscript received in Society of Petroleum Engineers office Sept. 27, 1957. Revised manuscript received Nov. 6, 1958.
*Recently returned to India.
**Currently studying for PhD as a graduate fellow at Pennsylvania State U., State College, Pa.
[1]References given at end of paper.

RESULTS

Effect of Temperature on Flow Properties

The typical effect of temperature on the flow properties of these drilling muds is illustrated by Fig. 1. It was found that plastic viscosity and apparent viscosity decreased with an increase of temperature. However, the curves were not linear, and did not appear to follow any definite trends or patterns. Yield point data showed much more scattering.[4]

Since a usable method for predicting drilling mud flow behavior with temperature was desired, an attempt was made to find a simple relationship between these variables. The basic approach used by Havenaar[5] for predicting the same effect on turbulent viscosity resulted in Fig. 2, which shows that

TABLE 1—COMPOSITION OF MUD SAMPLES TESTED

Sample No.	Composition
32	8 per cent bentonite mud
34	3 per cent bentonite mud
35	4 per cent bentonite mud
36	8 per cent bentonite mud
39	10 lb/gal, 4 per cent bentonite, barite mud
42	15 lb/gal, 4 per cent bentonite, barite mud
43	10 lb/gal, 10 per cent (by volume) diesel oil, 4 per cent bentonite, barite emulsion mud
45	15 lb/gal, 10 per cent (by volume) diesel oil, 4 per cent bentonite, barite emulsion mud
47	10 lb/gal, 4 per cent bentonite, barite, surfactant (DMS) mud
48	15 lb/gal, 4 per cent bentonite, barite, surfactant (DMS) mud
49	10 lb/gal, low lime treated (1 lb/bbl), 4 per cent bentonite, barite mud
50	15 lb/gal, low lime treated (1 lb/bbl), 4 per cent bentonite, barite mud
51	8 per cent bentonite mud

Note: All mud samples referred to are water-base muds; per cents are by weight unless otherwise specified.

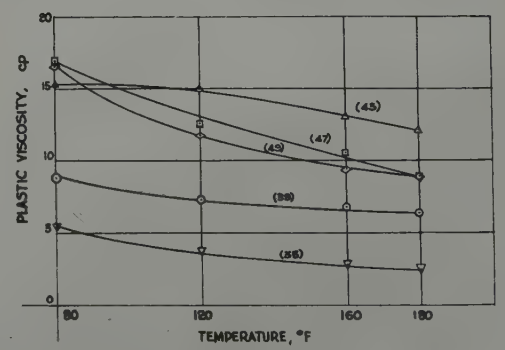

Fig. 1—Plastic Viscosity vs Temperature.

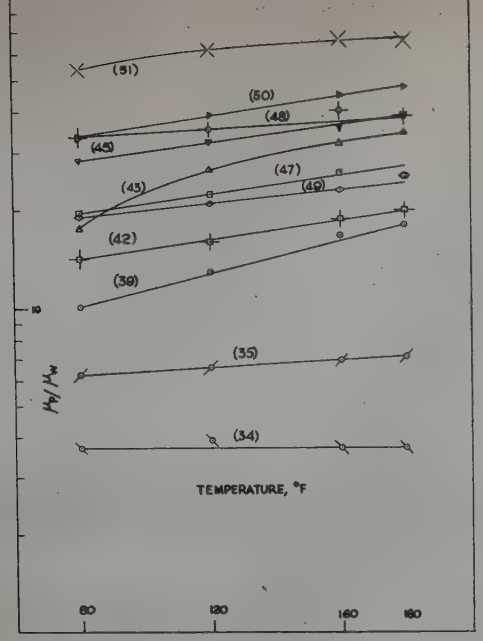

FIG. 2—μ_p/μ_w VS TEMPERATURE.

$$\log\frac{\mu_p}{\mu_w} = a + bT \quad . \quad . \quad . \quad . \quad . \quad . \quad . \quad . \quad (1)$$

where μ_p is plastic viscosity of mud at temperature, T; μ_w is water viscosity at same temperature, T; a,b are intercept and slope of line, respectively; and T is temperature, °F.

All muds tested fit this relationship closely except the emulsion mud (No. 43). Its deviation was probably due to changes in emulsion quality which would not have occurred in a completely stabilized system. A similar plot of apparent (600 rpm) viscosity is shown in Fig. 3.

These observations make it possible to predict the flow properties (μ_p and Y_B) of these or similar muds at common borehole temperatures; if they are known at two lower temperatures. Data from this study indicate that this relationship is valid to at least 200°F. Yield values may be calculated from plastic and apparent viscosity values using the following relationship.

$$Y_B = 2\,(\mu_a - \mu_p) \quad . \quad . \quad . \quad . \quad . \quad . \quad . \quad . \quad . \quad (2)$$

where Y_B is Bingham yield value, lb/100 ft^2; and μ_a, μ_p are apparent and plastic viscosities of the mud in question at the desired temperature, cp.

Knowledge of flow property behavior to 200°F will cover pressure drop predictions in wells as deep as 15,000 ft in the Gulf Coast area. This assumes that the average flow temperature in the annulus is approximated by the arithmetic average of bottom-hole circulating and discharge temperatures. Data on down-hole circulating temperatures are available in API RP-10B, or from a convenient curve prepared by Smith.[6]

EFFECT OF TEMPERATURE ON GEL STRENGTH

Gel strength behavior is shown in Fig. 4. As expected, each mud had its own characteristic behavior and no correlation was attempted.

CONCLUSION

Flow property variation with temperature to 200°F of clay-water muds may be predicted by the method presented in this paper. This of course does not apply to other systems which might undergo appreciable chemical alteration at the temperatures in question.

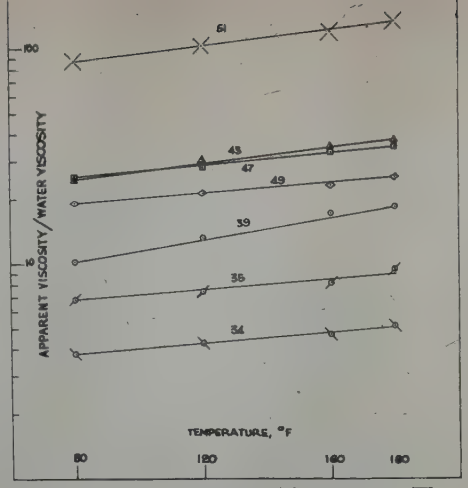

FIG. 3—APPARENT VISCOSITY/VISCOSITY OF WATER VS TEMPERATURE.

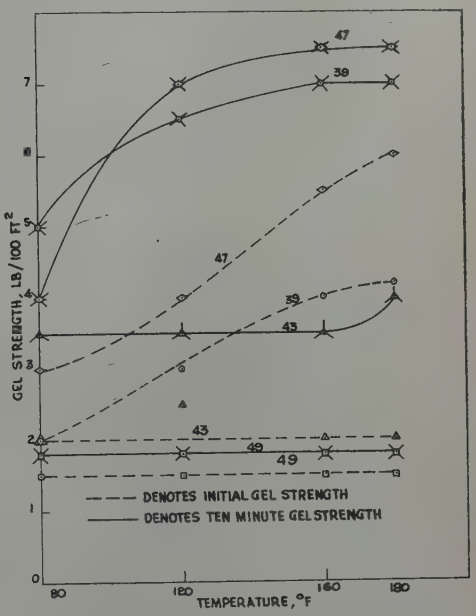

FIG. 4—GEL STRENGTH VS TEMPERATURE FOR DIFFERENT MUDS.

ACKNOWLEDGMENTS

The generosity of the Magnet Cove Barium Corp., Houston, Tex., in providing the Fann V-G meter and the necessary mud materials for this project is gratefully acknowledged. The authors also wish to express their thanks to the U. of Tulsa where this work was performed. Special thanks are due James Lummus of the Pan American Petroleum Corp. for his suggestion and help.

REFERENCES

1. Beck, R. W., Nuss, W. F. and Dunn, T. H.: "The Flow Properties of Drilling Muds", *Drill. and Prod. Prac.*, API (1947) 9.
2. Ormsby, G. S.: "Calculation and Control of Mud Pressures in Drilling and Completion Operations", *Drill. and Prod. Prac.*, API (1954) 44.
3. *Training Course for Mud Engineers*, Magnet Cove Barium Corp., Houston, Tex. (1955).
4. Srini-Vasan, S.: "A Study of the Effect of Temperature on Flow Properties of Non-Newtonian Drilling Fluids", MS thesis, U. of Tulsa (May, 1957).
5. Havenaar, I.: "The Pumpability of Clay-Water Drilling Fluids", *Trans.* AIME (1954) **201**, 287.
6. Smith, D. K.: "Cementing Procedures and Materials", *Pet. Engr.* (April, 1955). ★★★

INDEX

Petroleum Transactions, Volume 213

A

ALEXANDER, J. D., et al.: *Process Variables of In Situ Combustion,* 28 (Feb. JPT)

APPRAISAL: *See also* Profitability
oil lease: mathematical analysis of production decline data (Tech. Note) Aug. JPT, 399

ARONOFSKY, J. S., and LEE, A. S.: *Linear Programming Model for Scheduling Crude Oil Production,* (Tech. Note) July JPT, 389

ARONOFSKY, J. S., et al.: *Model for Mechanism of Oil Recovery from Porous Matrix Due to Water Invasion in Fractured Reservoirs,* 17 (Jan. JPT)

ARPS, J. J.: *Profitability of Capital Expenditures for Development Drilling and Producing Property Appraisal,* 337 (July JPT)

B

BARFIELD, E. C., and MCCARTY, D. G.: *Use of High-Speed Computers for Predicting Flood-Out Patterns,* 139 (Summary July JPT, 60A)

BAXENDELL, P. B.: *Producing Wells on Casing Flow — Analysis of Flowing Pressure Gradients,* 202 (Summary Aug. JPT, 59); discussion, 345

BENHAM, A. L. and POETTMANN, F. H.: *Thermal Recovery Process — An Analysis of Laboratory Combustion Data,* (Tech. Note) Sept. JPT, 406

BENTONITE: proper use in cement, 26 (Feb. JPT)

BERNARD, G. G., and HOLBROOK, O. C.: *Determination of Wettability by Dye Adsorption,* 261 (Summary Oct. JPT, 244A)

BERRY, V. J. JR., and JACOBY, R. H.: *Method for Predicting Pressure Maintenance Performance for Reservoirs Producing Volatile Crude Oil,* 59 (March JPT)

BINDER, G. G. JR., et al.: *Miscible Fluid Displacement in Porous Media,* 76 (Apr. JPT)

BINGHAM PLASTIC: flow in stationary pipes and annuli, practical use of theory, 316 (Summary Dec. JPT, 76)

BINKLEY, G. W., et al.: *Factors Affecting Rate of Deposition of Cement in Unfractured Perforations During Squeeze-Cementing Operations,* 51 (March JPT)

BLACK OIL SYSTEMS: bubble point pressure, (Tech. Note) May JPT, 379

BLAIR, P. M. et al.: *Calculation of Linear Waterflood Behavior Including Effects of Capillary Pressure,* 96 (Summary June JPT, 131A)

BLENKARN, K. A., and LUBINSKI, A.: *Buckling of Tubing in Pumping Wells, Its Effects and Means for Controlling It, (Trans.* (1957) 210, 73); discussion, Aug. JPT, 396

BOBEK, J. E., et al.: *Reservoir Rock Wettability — Its Significance and Evaluation,* 155 (July JPT)

BOTTOM-HOLE PRESSURE: recording desirable for wells showing anomalous build-up, 44 (Feb. JPT)
recording on same chart with wellhead pressure during formation fracturing, 65 (March JPT)

BRIDWELL, H. C., et al.: *Development and Field Testing of a Core Barrel for Recovering Unconsolidated Oil Sands,* (Tech. Note) Jan. JPT, 347

BUBBLE point pressure for black oil systems, (Tech. Note) May JPT, 379

BUCKLEY-LEVERETT frontal advance theory applied to petroleum recovery, (Tech Note) Apr. JPT, 365

C

CALCULATING MACHINE: punch-card type: annular pressure gradients in gas-lift casing flow, 202 (Summary Aug. JPT, 59)

CALIFORNIA: thermal recovery of oil at South Belridge, 236 (Oct. JPT)

CAMPBELL, J. M., and WHINERY, K. F.: *Method for Determining Optimum Second Stage Pressure in Three Stage Separation,* (Tech. Note) Apr. JPT, 369

CAPITAL EXPENDITURE FOR DEVELOPMENT DRILLING: profitability analysis by method of average annual rate of return computation, 337 (July JPT)

CARPENTER, C. W. JR., et al.: *Laboratory Studies of Five-Spot Waterflood Performance,* 113 (Summary June JPT, 131A)

CARTER, GREG, and SMITH, D. K.: *Properties of Cementing Compositions at Elevated Temperatures and Pressure,* 20 (Feb. JPT); discussion, 26 (Feb. JPT)

CAUDLE, B. H., and DYES, A. B.: *Improving Miscible Displacement by Gas-Water Injection,* 281 (Nov. JPT)

CAUDLE, B. H., et al.: *Effect of Fractures on Sweep-Out Pattern,* 245 (Oct. JPT)

CEMENT: bentonite content, proper use, 26 (Feb. JPT)
strength loss: X-ray study of causes, 20 (Feb. JPT)

CEMENTING: squeeze: *See* Squeeze

CEMENT SLURRIES: deposition properties needed to restrict formation of nodes inside casing, 51 (March JPT)

CHARTS: identification of complex mixtures of oilfield waters, (Tech. Note) Sept. JPT, 402

CHATAS, A. T., and YANKIE, W. W. JR.: *Application of Statistics to Analysis of Production Decline Data,* (Tech. Note) Aug. JPT, 399

CHEMICALS: maintaining clear water for drilling, 70 (Apr. JPT)

CHROMATOGRAPHY: gas-liquid: definitions and three techniques for studying oilfield cores, (Tech. Note) March JPT, 359

COLLINS, R. E., et al.: *Factors Affecting Rate of Deposition of Cement in Unfractured Perforations During Squeeze-Cementing Operations,* 51 (March JPT)

COMBUSTION method of oil recovery (*see also* Thermal Recovery):
equations for calculating amount of injected air and analyzing experimental data, (Tech. Note) Sept. JPT, 406
fluid dynamics during process, 146 (Summary July JPT, 60A)
zones ahead of combustion zone, calculation of production histories, 146 (Summary July JPT, 60A)

COMPUTERS: digital: calculation of linear waterflood behavior, including capillary pressure, 96 (Summary June JPT, 131A)
high-speed: analysis of reservoir performance in two and three space dimensions, 139 (Summary July JPT, 60A)
pressure interference correction to material balance equation for water-drive reservoirs, 418 (Summary Sept. JPT, 95)
Guyod analog, 11 (Jan. JPT)

CONDUCTIVITY: effect of applied pressure, samples of Bradford, Weir, and Kirkwood sandstones, (Tech. Note) Nov. JPT, 430

CONLEY, F. R., et al.: *Deterioration of Miscible Zones in Porous Media,* 228 (Summary Sept. JPT, 90A)

COPPER ion displacement test for selection of suitable corrosion inhibitors, (Tech. Note) Jan. JPT, 350

CORE BARRELS, RUBBER SLEEVE: bit head for use in many types of formations, (Tech. Note) Jan. JPT, 347
development and field testing in unconsolidated sands, (Tech. Note) Jan. JPT, 347

CORES, OILFIELD: flow of gases: evidence of chromatographic effect, (Tech. Note) March JPT, 359
pore volume compressibilities of sandstone reservoir rock (Tech. Note) March JPT, 362

CORROSION INHIBITORS: selection for particular systems by copper ion displacement test, (Tech. Note) Jan. JPT, 350

CRAZE, R. C.: *Spacing of Natural Gas Wells,* 213 (Sept. JPT)

D

DARDAGANIAN, S. G.: *Application of the Buckley-Leverett Frontal Advance Theory to Petroleum Recovery,* (Tech. Note) Apr. JPT, 365

DECLINE CURVE ANALYSIS: application to gravity-drainage reservoirs in stripper stage, 275 (Nov. JPT)

DENEKAS, M. O., et al.: *Reservoir Rock Wettability — Its Significance and Evaluation,* 155 (July JPT)

DEPLETION: Muskat equation: derivation considering expansion behavior of reservoir hydrocarbon system and simple fractional flow equation, 285 (Summary Nov. JPT, 67)

DETERGENT SLUGS: *See* Water Flooding

DEW, J. N., et al.: *Deterioration of Miscible Zones in Porous Media,* 228 (Summary Sept. JPT, 90A)

DEW, J. N., et al.: *Process Variables of In Situ Combustion,* 28 (Feb. JPT)

DE WITTE, A. J., et al.: *Streaming Potential Problem in Well Logging,* 409 (Summary Sept. JPT, 90A; discussion, 415

DIAMOND BIT HEADS: development for use with rubber-sleeve core barrel, (Tech. Note) Jan. JPT, 347

DISPLACEMENT LOGGING: low zone concept should be utilized and other controls are needed, (Tech. Note) Feb. JPT, 353

DOUGLAS, JIM, JR.: *Application of Numerical Methods to Predict Recovery from Thin Oil Columns,* 193 (Summary Aug. JPT, 59)

DOUGLAS, JIM JR., et al.: *Calculation of Linear Waterflood Behavior Including the Effects of Capillary Pressure,* 96 (Summary June JPT, 131A)

DOSCHER, TODD, et al: *Evidence of Chromatographic Effect During Flow of Gases Through Oilfield Cores,* (Tech. Note) March JPT, 359

DRAINAGE: field evidence, 214 (Sept. JPT)

DRAPER, A. L. et al.: *Miscible Fluid Displacement in Porous Media,* 76 (Apr. JPT)

DRILL BITS: for use with rubber-sleeve core barrel, (Tech. Note) Jan. JPT, 347

DRILLING: differential pressure sticking of collars, theoretical analysis, including formulas for pull-out force, 265 (Summary Oct. JPT, 244A)
drag coefficients, or friction factors, or rock cuttings, 180 (Aug. JPT)
effect of pressure on rock drillability: laboratory tests using water and air as fluids, 1 (Jan. JPT)

hard rock: low-frequency percussion: correlation between laboratory and field performance, (Tech. Note) July JPT, 393

hole cleaning: recommendations for air and gas drilling, 180 (Aug. JPT)

DRILLING FLUIDS: chemicals for maintaining clear water, 70 (Apr. JPT)

electrical properties: correlation with solids content, 333 (Summary Dec. JPT, 76

DRILLING MUD: clay-water: effect of temperature on flow properties, (Tech. Note) Dec. JPT, 438

DUMBAULD, G. K., et al.: *Factors Affecting Rate of Deposition of Cement in Unfractured Perforations During Squeeze-Cementing Operations,* 51 (March JPT)

DYE ADSORPTION TEST: for determining relative water wettability of porous media, 261 (Summary Oct. JPT, 244A)

DYES, A. B., and CAUDLE, B. H.: *Improving Miscible Displacement by Gas-Water Injection,* 281 (Nov. JPT)

DYES, A. B., et al.: *Effect of Fractures on Sweep-Out Pattern,* 245 (Oct. JPT)

DYKE, P. M., et al: *Application of Numerical Methods to Predict Recovery from Thin Oil Columns,* 193 (Summary Aug. JPT, 59)

E

ECKEL, J. R.: *Effect of Pressure on Rock Drillability,* 1 (Jan. JPT)

ELECTRICAL LOGGING: water saturation verified by porosity balance check, 161 (July JPT)

ELFRINK, E. B., et al.: *Estimation of Ultimate Recovery from Solution Gas-Drive Reservoirs,* 132 (June JPT)

F

FATT, I.: *Pore Volume Compressibilities of Sandstone Reservoir Rocks,* (Tech. Note) March JPT, 362

FLOW (*see also* Fluid Flow): Bingham plastic in stationary pipes and annuli: practical utilization of the theory, 316 (Summary Dec. JPT, 76)

casing: calculation of annular pressure gradients in form suitable for punch-card machines, 202 (Summary Aug. JPT, 59)

generalized Newtonian (pseudoplastic) in stationary pipes and annuli, 325 (Summary Dec. JPT, 76)

laminar and turbulent in heterogeneous porosity limestones, laboratory study, 121 (Summary June JPT, 131A)

FLUE GAS: substitute for hydrocarbon gas for injection in miscible slug process, 7 (Jan. JPT)

FLUID FLOW: effect of rate and viscosity on laboratory determination of oil-water relative permeabilities, 36 (Feb. JPT)

laminar and turbulent flow in heterogeneous porosity limestones, laboratory study, 121 (Summary June JPT, 131A)

FORMATION FRACTURES: created by stimulation treatments: effect on sweep-out efficiency in water flooding, 245 (Oct. JPT)

FORMATION FRACTURING: surface recording of bottomhole and wellhead pressures on same chart, 65 (March JPT)

FOSTER, W. R., et al.: *Practical Utilization of the Theory of Bingham Plastic Flow in Stationary Pipes and Annuli,* 316 (Summary Dec. JPT, 76)

FOX, J. E. JR., et al.: *Use of Chemicals to Maintain Clear Water for Drilling,* 70 (Apr. JPT)

G

GALLUS, J. P., et al.: *Use of Chemicals to Maintain Clear Water for Drilling,* 70 (Apr. JPT)

GAS-CONDENSATE RESERVOIR: estimate of recovery: variables that influence, 60 (Nov. JPT)

production history compared with laboratory and calculated behavior prediction, 127 (June JPT)

GAS DRIVE: (*see also* Solution): Buckley-Leverett frontal advance theory, (Tech. Note) Apr. JPT, 365

enriched: laboratory evaluation of prospective projects, (Tech. Note) June JPT, 382

flue gas in new miscible slug process, 7 (Jan. JPT)

gas-water an improvement in miscible displacement, 281 (Nov. JPT)

GAS INJECTION INTO VOLATILE OIL RESERVOIRS: conventional frontal drive methods inadequate to predict oil recovery, 59 (March JPT)

efficiency of oil recovery, 59 (March JPT)

prediction of vaporization of oil by multi-component flash calculations, 59 (March JPT)

GASKELL, M. H., et al.: *Laboratory Evaluation of Prospective Enriched Gas-Drive Projects,* (Tech. Note) June JPT, 382

GAS LIFT: casing flow: calculation of annular pressure gradients, 202 (Summary Aug. JPT, 59)

GAS-WATER INJECTION: benefits, 281 (Nov. JPT)

GAS WELLS: spacing: sound programs, 213 (Sept. JPT)

GATES, C. F. and RAMEY, H. J. JR.: *Field Results of South Belridge Thermal Recovery Experiment,* 236 (Oct. JPT)

GATLIN, CARL, and SRINI-VASAN, S.: *Effect of Temperature on Flow Properties of Clay-Water Drilling Muds,* (Tech. Note) Dec. JPT, 438

GERGINS, R. L., et al.: *Fluid Dynamics During an Underground Combustion Process,* 146 (Summary July JPT, 60A)

GODBEY, J. K., and HODGES, H. D.: *Pressure Measurements During Formation Fracturing Operations,* 65 (March JPT)

GONDOUIN, M.: *Discussion On the Streaming Potential Problem in Well Logging*, 415

GONDOUIN, M., and SCALA, C.: *Streaming Potential and the SP Log*, 170 (Aug. JPT)

GOURNAY, L. S., et al.: *Effect of Fluid-Flow Rate and Viscosity on Laboratory Determinations of Oil-Water Relative Permeabilities*, 36 (Feb. JPT)

GRAHAM, J. W.: *Reverse-Wetting Logging*, 304 (Dec. JPT)

GRAVITY DRAINAGE: *See* Reservoirs

GRAY, K. E.: *Cutting Carrying Capacity of Air at Pressures Above Atmospheric*, 180 (Aug. JPT)

GUYOD ANALOG COMPUTER, 11 (Jan. JPT)

H

HANDY, L. L.: *Laboratory Study of Oil Recovery by Solution Gas Drive*, 310 (Dec. JPT)

HARRISON, N. H., et al.: *Comparison Between the Predicted and Actual Production History of a Condensate Reservoir*, 127 (June JPT)

HAZEBROEK, P., et al.: *Pressure Fall-Off in Water Injection Wells*, 250 (Summary Oct. JPT, 244A)

HEMSTOCK, R. A., et al.: *Effective Compressibility of Reservoir Rock and Its Effects on Permeability*, (Tech. Note) June JPT, 386

HENDERSON, J. H., et al.: *Fluid Dynamics During an Underground Combustion Process*, 146 (Summary July JPT, 60A)

HILDEBRANDT, A. B., et al.: *Development and Field Testing of a Core Barrel for Recovering Unconsolidated Oil Sands*, (Tech. Note) Jan. JPT, 347

HINDS, R. F.: *Importance of Reliable Data in Gas-Condensate Recovery Calculations*, (Tech. Note) Nov. JPT, 433

HODGES, H. D., and GODBEY, J. K.: *Pressure Measurements During Formation Fracturing Operations*, 65 (March JPT)

HOLBROOK, O. C., and BERNARD, G. G.: *Determination of Wettability by Dye Adsorption*, 261 (Summary Oct. JPT, 244A)

HOWELL, J. N., and JESSEN, F. W.: *Effect of Flow Rate on Paraffin Accumulation in Plastic, Steel, and Coated Pipe*, 80 (Apr. JPT)

HUGHES, W. B.: *Copper Ion Displacement Test for Screening Corrosion Inhibitors*, (Tech. Note) Jan. JPT, 350

HUMP BUILD-UPS: study of causes, 44 (Feb. JPT)

HURST, WILLIAM: *Simplification of the Material Balance Formulas by the Laplace Transformation*, 292 (Summary Nov. JPT, 67)

HUTCHINSON, C. A. JR., and KOCH, H. A. JR.: *Miscible Displacements of Reservoir Oil Using Flue Gas*, 7 (Jan. JPT)

HYDRAULIC FRACTURING EQUIPMENT: flow capacity of fractures: effect on well productivity, 91 (May JPT)

HYDROCARBON-BEARING STRATA: discovery by reverse-wetting logging, 304 (Dec. JPT)

J

JACOBY, R. H., and BERRY, V. J. JR.: *Method for Predicting Pressure Maintenance Performance for Reservoirs Producing Volatile Crude Oil*, 59 (March JPT)

JANZEN, H. B., and NOBLES, M. A.: *Application of a Resistance Network for Studying Mobility Ratio Effects*, (Tech. Note) Feb. JPT, 356

JESSEN, F. W., and HOWELL, J. N.: *Effect of Flow Rate on Paraffin Accumulation in Plastic, Steel, and Coated Pipe*, 80 (Apr. JPT)

K

KEHN, D. M., et al.: *Laboratory Evaluation of Prospective Enriched Gas-Drive Projects*, (Tech. Note) June JPT, 382

KELLNER, J. M., et al.: *Development and Field Testing of a Core Barrel for Recovering Unconsolidated Oil Sands*, (Tech. Note) Jan. JPT, 347

KEMP, C. E., et al.: *Effect of Fractures on Sweep-Out Pattern*, 245 (Oct. JPT)

KOBAYASHI, RIKI, et al.: *Evidence of Chromatographic Effect During Flow of Gases Through Oilfield Cores*, (Tech. Note) March JPT, 359

KOCH, H. A. JR., and HUTCHINSON, C. A. JR.: *Miscible Displacements of Reservoir Oil Using Flue Gas*, 7 (Jan. JPT)

KYTE, J. R., and RAPOPORT, L. A.: *Linear Waterflood Behavior and End Effects in Water-Wet Porous Media* (Tech. Note) Oct. JPT, 423

L

LACEY, J. W., et al.: *Miscible Fluid Displacement in Porous Media*, 76 (Apr. JPT)

LASATER, J. A.: *Bubble Point Pressure Correlation*, (Tech. Note) May JPT, 379

LEAS, W. J., et al.: *Laboratory Studies of Five-Spot Waterflood Performance*, 113 (Summary June JPT, 131A)

LEE, A. S., and ARONOFSKY, J. S.: *Linear Programming Model for Scheduling Crude Oil Production*, (Tech. Note) July JPT, 389

LEFKOVITS, H. C., and MATTHEWS, C. S.: *Application of Decline Curves to Gravity-Drainage Reservoirs in the Stripper Stage*, 275 (Nov. JPT)

LINEAR PROGRAMING MODEL FOR SCHEDULING CRUDE OIL PRODUCTION, (Tech. Note) July JPT, 389

LIPSON, L. B., and OVERTON, H. L.: *Correlation of Electrical Properties of Drilling Fluids With Solids Content*, 333 (Summary Dec. JPT, 76)

LOG INTERPRETATION: methods using porosity balance check for water saturation, 161 (July JPT)

porosity balance check for water saturation, 161 (July JPT)

LUBINSKI, A., and BLENKARN, K. A.: *Buckling of Tubing in Pumping Wells, Its Effects and Means for Controlling It.* (*Trans.*, 1957 210, 73); discussion, Aug. JPT, 396

LUMMUS, J. L., et al.: *Use of Chemicals to Maintain Clear Water for Drilling,* 70 (Apr. JPT)

M

MARTIN, J. C.: *Reservoir Analysis for Pressure Maintenance Operations Based on Complete Segregation of Mobile Fluids,* 220 (Summary Sept. JPT, 90A)

MARTIN, W. L., et al.: *Process Variables of In Situ Combustion,* 28 (Feb. JPT)

MASSE, L., et al.: *Model for Mechanism of Oil Recovery from Porous Matrix Due to Water Invasion in Fractured Reservoirs,* 17 (Jan. JPT)

MATERIAL BALANCE EQUATION: simplification by Laplace transformation, 292 (Summary Nov. JPT, 67)

MATTHEWS, C. S., et al.: *Pressure Fall-Off in Water Injection Wells,* 250 (Summary Oct. JPT, 244A)

MATTHEWS, C. S., and LEFKOVITS, H. C.: *Application of Decline Curves to Gravity-Drainage Reservoirs in the Stripper Stage,* 275 (Nov. JPT)

MATTHEWS, C. S., and STEGEMEIER, G. L.: *Study of Anomalous Pressure Build-Up Behavior,* 44 (Feb. JPT)

MATTAX, C. C., et al.: *Reservoir Rock Wettability—Its Significance and Evaluation,* 155 (July JPT)

MCCARTY, D. G., and BARFIELD, E. C.: *Use of High-Speed Computers for Predicting Flood-Out Patterns,* 139 (Summary July JPT, 60A)

MCKINNELL, J. C.: *Identification of Mixtures of Waters from Chemical Water Analyses,* (Tech. Note) Sept. JPT, 402

MCLATCHIE, A. S., et al.: *Effective Compressibility of Reservoir Rock and Its Effects on Permeability,* (Tech. Note) June JPT, 386

MELDAU, R. F., and WORTHINGTON, A. E.: *Departure Curves for the Self-Potential Log,* 11 (Jan. JPT)

MELROSE, J. C., et al.: *Practical Utilization of the Theory of Bingham Plastic Flow in Stationary Pipes and Annuli,* 316 (Summary Dec. JPT, 76)

MOBILITY RATIO: *See* Water Flooding

MODELS: abstract: mechanism of oil recovery from porous matrix due to water invasion in fractured reservoirs, 17 (Jan. JPT)

flow experiments of five-spot water floods, 113 (Summary June JPT, 131A)

fractures in five-spot flood, effect on sweep-out pattern, 245 (Oct. JPT)

Guyod analog computer, 11 (Jan. JPT)

linear programing for scheduling crude oil production, (Tech. Note) July JPT, 389

numerical: high-speed digital computer prediction of flood-out patterns, 139 (Summary July JPT, 60A)

transparent: study of viscous fingering, 103 (Summary July JPT, 60A)

MORGAN, B. E.: *Discussion on Properties of Cementing Compositions at Elevated Temperatures and Pressure,* 26 (Feb. JPT)

MULLINS, L. D., et al.: *Estimation of Ultimate Recovery from Solution Gas-Drive Reservoirs,* 132 (June JPT)

MUSKAT DEPLETION PERFORMANCE EQUATION: derivation considering expansion behavior of reservoir hydrocarbon system and a simple fractional flow equation, 285 (Summary Nov. JPT, 67)

N

NATANSON, S. G., et al.: *Model for Mechanism of Oil Recovery from Porous Matrix Due to Water Invasion in Fractured Reservoirs,* 17 (Jan. JPT)

NEUTRON LOGS: porosity derivation: evaluation of effect of borehole size, sonde position, salinity, chemical composition of rock, and statistical variation, (Tech. Note) May JPT, 371

NISLE, R. G.: *Effect of Partial Penetration on Pressure Build-Up in Oil Wells,* 85 (May JPT)

NOBLES, M. A., and JANZEN, H. B.: *Application of a Resistance Network for Studying Mobility Ratio Effects,* (Tech. Note) Feb. JPT, 356

O

OIL BANK: definition, 146 (Summary July JPT, 60A)

OIL RECOVERY: Buckley-Leverett frontal advance theory. (Tech. Note) Apr. JPT, 365

gas-condensate reservoirs: variables that influence estimate (Tech. Note) Nov. JPT, 433

gas injection into volatile oil reservoirs, efficiency, 59 (March JPT)

gravity-drainage reservoirs: miscible fluid displacement, 76 (Apr. JPT)

miscible zones: laboratory study of deterioration, 228 (Summary Sept. JPT, 90A)

solution gas drive: estimation, 132 (June JPT)

OIL SANDS: water saturation: log interpretation of methods using porosity balance, 161 (July JPT)

OIL WELLS: partially penetrating: pressure build-up, 85 (May JPT)

pressure build-up: humps studied for causes, 44 (Feb. JPT)

OUTMANS, H. D.: *Mechanics of Differential Pressure Sticking of Drill Collars,* 265 (Summary Oct. JPT, 244A)

OVERTON, H. L., and LIPSON, L. B.: *Correlation of Electrical Properties of Drilling Fluids With Solids Content,* 333 (Summary Dec. JPT, 76)

OWENS, W. W., and STEWART, C. R.: *Laboratory Study of Laminar and Turbulent Flow in Heterogeneous Porosity Limestones,* 121 (Summary June JPT, 131A)

P

PARAFFIN DEPOSITION IN FLOW LINES: composition of deposits, 80 (Apr. JPT)
control by use of plastic materials, 80 (Apr. JPT)
effect of flow rate, 80 (Apr. JPT)

PARISH, E. R., et al.: *Practical Utilization of the Theory of Bingham Plastic Flow in Stationary Pipes and Annuli,* 316 (Summary Dec. JPT, 76)

PERMEABILITY: effect of applied pressure, samples of Bradford, Weir, and Kirkwood sandstones, (Tech. Note) Nov. JPT, 430
relative: *See* Relative
reservoir rock: effect of effective compressibility, (Tech. Note) June JPT, 386

POETTMANN, F. H., and BENHAM, A. L.: *Thermal Recovery Process—An Analysis of Laboratory Combustion Data,* (Tech. Note) Sept. JPT, 406

POETTMANN, F. H.: *Discussion on Producing Wells on Casing Flow—An Analysis of Flowing Pressure Gradients,* 345

POROSITY: balance, check of water saturation in log interpretation, 161 (July JPT)
derivation from neutron logs: evaluation of effect of borehole size, sonde position, salinity, chemical composition of rock, and statistical variation, (Tech. Note) May JPT, 371
effect of applied pressure, samples of Bradford, Weir, and Kirkwood sandstones, (Tech. Note) Nov. JPT, 430
limestone, heterogeneous type: laminar and turbulent flow, laboratory study, 121 (Summary June JPT, 131A)
reservoir rock: effect of effective compressibility, (Tech. Note) June JPT, 386

POROUS MEDIA: dye adsorption test for determining relative water wettability, 261 (Summary Oct. JPT, 244A)
miscible fluid displacement, 76 (Apr. JPT)
miscible zones: laboratory study of deterioration, 228 (Summary Sept. JPT, 90A)

PRESSURE BUILD-UP IN OIL WELLS: effect of partial penetration, 85 (May JPT)
study of humps as causes, 44 (Feb. JPT)

PRESSURE MAINTENANCE: predicting performance for reservoirs producing volatile crude oil, 59 (March JPT)
reservoir analysis based on complete segregation of mobile fluids, 220 (Summary Sept. JPT, 90A)

PRODUCTION DECLINE DATA: analysis by principle of least squares combined with theory of equations, (Tech. Note) Aug. JPT, 399

PRODUCTION OF OIL FROM RESERVOIRS: in situ combustion, process variables, 28 (Feb. JPT)

PROFITABILITY: analysis of proposed capital expenditure: average annual rate of return computing method, 337 (July JPT)

PYNDUS, G. T., et al.: *Laboratory Evaluation of Prospective Enriched Gas-Drive Projects,* (Tech. Note) June JPT, 382

R

RACHFORD, H. H. JR., et al.: *Application of Numerical Methods to Predict Recovery from Thin Oil Columns,* 193 (Summary Aug. JPT, 59)

RAINBOW, H., et al.: *Pressure Fall-Off in Water Injection Wells,* 250 (Summary Oct. JPT, 244A)

RAMEY, H. J. JR., and GATES, C. F.: *Field Results of South Belridge Thermal Recovery Experiment,* 236 (Oct. JPT)

RAPOPORT, L. A., et al.: *Laboratory Studies of Five-Spot Waterflood Performance,* 113 (Summary June JPT, 131A)

RAPOPORT, L. A., and KYTE, J. R.: *Linear Waterflood Behavior and End Effects in Water-Wet Porous Media,* (Tech. Note) Oct. JPT, 423

REED, D. W., et al.: *Fluid Dynamics During an Underground Combustion Process,* 146 (Summary July JPT, 60A)

REGIER, S., et al.: *Comparison Between the Predicted and Actual Production History of a Condensate Reservoir,* 127 (June JPT)

RELATIVE PERMEABILITY: k_{rg}/k_{ro} ratio for sandstone: calculated compared with field data, (Tech. Note) Dec. JPT, 436
oil-water: effect of fluid flow rate and viscosity on laboratory determinations, 36 (Feb. JPT)

RESERVOIR OIL: miscible displacements using flue gas instead of hydrocarbon gas, 7 (Jan. JPT)

RESERVOIR PERFORMANCE: (*see also* Water Flooding): simplification of material balance equation by Laplace transformation, 292 (Summary Nov. JPT, 67)

RESERVOIR ROCK: compressibility, effective, effect on porosity and permeability, (Tech Note) June JPT, 386
drillability: effect of pressure, laboratory tests, 1 (Jan. JPT)
heat capacities and thermal conductivities, measured and calculated, (Tech. Note) May JPT, 375
sandstone: pore volume compressibilities measured on core samples, (Tech. Note) March JPT, 362
thermal diffusivity, variation with temperature, (Tech. Note) May JPT, 375

RESERVOIRS: fractured: oil recovery due to water invasion computed by abstract reasoning, 17 (Jan. JPT)
gravity drainage: decline curve analysis in stripper stage, 275 (Nov. JPT)
oil recovery by miscible fluid displacement, 76 (Apr. JPT)
water saturation: log interpretation using porosity balance check, 161 (July JPT)

REVERSE-WETTING LOGGING: location of oil-bearing formations and identification of their in situ wettability, 304 (Dec. JPT)
technique, 304 (Dec. JPT)

ROBINSON, M. P.: *Pressure Interference Correction to the Material Balance Equation for Water-Drive Reservoirs Using a Digital Computer*, 418 (Summary Sept. JPT, 95)

RODGERS, J. K., et al.: *Comparison Between the Predicted and Actual Production History of a Condensate Reservoir*, 127 (June JPT)

ROPER, W. A., et al.: *Evidence of Chromatographic Effect During Flow of Gases Through Oilfield Cores*, (Tech. Note) March JPT, 359

S

SANDBERG, C. R., et al.: *Effect of Fluid-Flow Rate and Viscosity on Laboratory Determinations of Oil-Water Relative Permeabilities*, 36 (Feb. JPT)

SANDSTONES: Bradford, Weir, and Kirkwood: maximum pressure, geological life, (Tech. Note) Nov. JPT, 430
conductivity, porosity, and permeability: effect of applied pressure, (Tech. Note) Nov. JPT, 430
k_{rg}/k_{ro} ratios: calculated compared with field data, (Tech. Note) Dec. JPT, 436

SAUNDERS, C. D., et al.: *Hydraulic Fracturing—Fracture Flow Capacity vs Well Productivity*, 91 (May JPT)

SAVINS, J. G.: *Generalized Newtonian (Pseudoplastic) Flow in Stationary Pipes and Annuli*, 325 (Summary Dec. JPT, 76)

SAVINS, J. G., et al.: *Practical Utilization of the Theory of Bingham Plastic Flow in Stationary Pipes and Annuli*, 316 (Summary Dec. JPT, 76)

SCALA, C., and GONDOUIN, M.: *Streaming Potential and the SP Log*, 170 (Aug. JPT)

SCHEDULING CRUDE OIL PRODUCTION: linear programming, (Tech. Note) July JPT, 389

SELDENRATH, T., and WRIGHT, A. W.: *Buckling of Tubing in Pumping Wells*, (Tech. Note) Aug. JPT, 396

SELF-POTENTIAL LOG: departure curves: analog computer study, 11 (Jan. JPT)

SEPARATION: three-stage: predicting optimum second stage pressure, (Tech. Note) Apr. JPT, 369

SHALY SANDS: log interpretation for water saturation, 161 (July JPT)

SIEVERT, J. A., et al.: *Deterioration of Miscible Zones in Porous Media*, 228 (Summary Sept. JPT, 90A)

SIMONS, L. H., and SPAIN, H. H.: *Limitations on Pressure Predictions for Water-Drive Reservoirs*, (Tech. Note) Oct. JPT, 427

SIPPEL, R. F., et al.: *Effect of Fluid-Flow Rate and Viscosity on Laboratory Determinations of Oil-Water Relative Permeabilities*, 36 (Feb. JPT)

SMITH, D. K., and CARTER, GREG: *Properties of Cementing Compositions at Elevated Temperatures and Pressure*, 20 (Feb. JPT); discussion, 26 (Feb. JPT)

SOLUTION GAS DRIVE: mechanism of oil recovery, laboratory study, 310 (Dec. JPT)
ultimate recovery, estimation, 132 (June JPT)

SOMERTON, W. H.: *Some Thermal Characteristics of Porous Rocks*, (Tech. Note) May JPT, 375

SOUTH BELRIDGE FIELD: *See* California

SP LOG: streaming potentials: contribution to, 170 (Aug. JPT)
problems, 409 (Summary Sept. JPT, 90A)

SPAIN, H. H., and SIMONS, L. H.: *Limitations on Pressure Predictions for Water-Drive Reservoirs*, (Tech. Note) Oct. JPT, 427

SQUEEZE CEMENTING: deposition properties needed in cement slurries to restrict formation of nodes inside casing, 51 (March JPT)
factors affecting deposition of cement in unfractured perforations, 51 (March JPT)
filtration time required to control amount of deposition of cement in and about unfractured perforations, 51 (March JPT)
prediction of rate of deposition of cement in and about unfractured perforations, 51 (March JPT)

SRINI-VASAN, S., and GATLIN, CARL: *Effect of Temperature on Flow Properties of Clay-Water Drilling Muds*, (Tech. Note) Dec. JPT, 438

STEGEMEIER, G. L., and MATTHEWS, C. S.: *Study of Anomalous Pressure Build-Up Behavior*, 44 (Feb. JPT)

STEWART, C. R., and OWENS, W. W.: *Laboratory Study of Laminar and Turbulent Flow in Heterogeneous Porosity Limestones*, 121 (Summary June JPT, 131A)

STREAMING POTENTIALS: problem in well logging, 409 (Summary Sept. JPT, 90A)
shales and mud cakes: contribution to SP log, 170 (Aug. JPT)

STRIPLING, A. A.: *Velocity Log Characteristics*, 207 (Sept. JPT)

T

TABER, J. J.: *Injection of Detergent Slugs in Water Floods*, 186 (Summary Aug. JPT, 59)

TAYLOR, R. D., et al.: *Application of Numerical Methods to Predict Recovery from Thin Oil Columns*, 193 (Summary Aug. JPT, 59)

THERMAL CHARACTERISTICS OF TYPICAL POROUS ROCKS, (Tech. Note) May JPT, 375

THERMAL RECOVERY OF OIL (*see also* Combustion Method): effect on equipment, 236 (Oct. JPT)
field test, South Belridge, California, 236 (Oct. JPT)

TINSLEY, J. M., et al.: *Hydraulic Fracturing—Fracture Flow Capacity vs Well Productivity*, 91 (May JPT)

TIXIER, M. P.: *Porosity Balance Verifies Water Saturation Determined from Logs*, 161 (July JPT)

TOPANELIAN, E. JR.: *Effect of Low Frequency Percussion in Drilling Hard Rock*, (Tech. Note) July JPT, 393

TORCASO, MICHAEL, A. and WYLLIE, M. R. J.: *Comparison of Calculated k_{rg}/k_{ro} Ratios With a Correlation of Field Data,* (Tech. Note) Dec. JPT, 436

TUBING: in pumping wells: buckling, analogy with tube fitted with frictionless pistons, (Tech. Note) Aug. JPT, 396

U

UNCONSOLIDATED OIL SANDS: rubber-sleeve core barrel: development and field testing, (Tech. Note) Jan. JPT, 347

V

VAN DER POEL, C., and VAN MEURS, P.: *Theoretical Description of Water-Drive Processes Involving Viscous Fingering,* 103 (Summary July JPT, 60A)

VAN MEURS, P., and VAN DER POEL, C.: *Theoretical Description of Water-Drive Processes Involving Viscous Fingering,* 103 (Summary July JPT, 60A)

VAN POOLLEN, H. K., et al.: *Hydraulic Fracturing—Fracture Flow Capacity vs Well Productivity,* 91 (May JPT)

VELOCITY LOGGING: advantages and limitations, 207 (Sept. JPT)

systems: (1) one transmitter and one receiver, (2) one transmitter and two receivers, 207 (Sept. JPT)

VENEZUELA: gradient curves, casing flow, Mara/Maracaibo conditions, 202 (Summary Aug. JPT, 59)

reservoir performance of highly permeable Bolivar coastal fields showing fluid segregation, 220 (Summary Sept. JPT, 90A)

VISCOUS FINGERING: *See* Water Drive

W

WAGNER, R. J., et al.: *Calculation of Linear Waterflood Behavior Including the Effects of Capillary Pressure,* 96 (Summary June JPT, 131A)

WAHL, W. L., et al.: *Estimation of Ultimate Recovery from Solution Gas-Drive Reservoirs,* 132 (June JPT)

WARREN, J. E., et al.: *Streaming Potential Problem in Well Logging,* 409 (Summary Sept. JPT, 90A); discussion, 415

WATER BANK: definition, 146 (Summary July JPT, 60A)

WATER DRIVE: (*see also* Water Flooding): gas-cap reservoir: numerical methods for predicting recovery from thin oil columns, 193 (Summary Aug. JPT, 59)

material balance equation, pressure interference correction by digital computer, 416 (Summary Sept. JPT, 95)

pressure predictions: restudy showing uncertainty, (Tech. Note) Oct. JPT, 427

viscous fingering: effect on production performance, 103 (Summary July JPT, 60A)

study in transparent models compared with scaled laboratory study of sand-filled tubes, 103 (Summary July JPT, 60A)

theory predicting performance with regularly spaced wells, 103 (Summary July JPT, 60A)

WATER FLOODING: (*see also* Water Drive): Buckley-Leverett frontal advance theory, (Tech. Note) Apr. JPT, 365

detergent slugs: effectiveness and rate of advance, 186 (Summary Aug. JPT, 59)

experiments with Alundum powder and Berea sandstone, 186 (Summary Aug. JPT, 59)

five-spot: performance, laboratory study, 113 (Summary June JPT, 131A)

sweep-out pattern in relation to fractures created by stimulation treatments, 245 (Oct. JPT)

flood behavior in water-wet media: corroboration of validity of scaling and stabilization concepts, (Tech. Note) Oct. JPT, 423

gas-water injection an improvement in miscible displacement, 281 (Nov. JPT)

linear flood: calculation by electronic digital computer, including capillary pressure, 96 (Summary June JPT, 131A)

miscible zones: laboratory study of deterioration, 228 (Summary Sept. JPT, 90A)

mobility ratio: effects: resistance network study, (Tech. Note) Feb. JPT, 356

Pressure fall-off: new method for determining behavior of pattern wells when closed in, 250 (Summary Oct. JPT, 244A)

two-dimensional analyses by high-speed digital computer for predicting flood-out patterns, 139 (Summary July JPT, 60A)

wettability of reservoir rock: effect on oil recovery, 155 (July JPT)

WATERS: oilfield: identification of complex mixtures by graphical methods, (Tech. Note) Sept. JPT, 402

WATER SATURATION: log interpretation, porosity balance check, 161 (July JPT)

WELL PRODUCTIVITY: effect of fracture flow capacity in hydraulic fracturing, 91 (May JPT)

WELL SPACING: drainage: field evidence, 214 (Sept. JPT)

natural gas: sound program, 213 (Sept. JPT)

WEST, R. D.: *Extensions of the Muskat Depletion Performance Equation,* 285 (Summary Nov. JPT, 67)

WETTABILITY: earth formations: determination by reverse-wetting logging, 304 (Dec. JPT)

porous media: dye adsorption test, 261 (Summary Oct. JPT, 244A)

reservoir rock: conditions controlling, 155 (July JPT)

evaluation and significance, 155 (July JPT)

WHINERY, K. F., and CAMPBELL, J. M.: *Method for Determining Optimum Second Stage Pressure in Three Stage Separation,* (Tech. Note) Apr. JPT, 369

WIDMYER, R. H., and WOOD, G. M.: *Evaluation of Porosity Derivation from Neutron Logs*, (Tech. Note) May JPT, 371

WILSON, L. A., et al.: *Fluid Dynamics During an Underground Combustion Process*, 146 (Summary July JPT, 60A)

WINN, R. H.: *Report on the Displacement Log* (Tech. Note) Feb. JPT, 353

WOOD, G. M., and WIDMYER, R. H.: *Evaluation of Porosity Derivation from Neutron Logs*, (Tech. Note) May JPT, 371

WORTHINGTON, A. E., and MELDAU, R. F.: *Departure Curves for the Self-Potential Log*, 11 (Jan. JPT)

WRIGHT, A. W., and SELDENRATH, T.: *Buckling of Tubing in Pumping Wells*, (Tech. Note) Aug. JPT, 396

WYBLE, D. O.: *Effect of Applied Pressure on Conductivity, Porosity, and Permeability of Sandstones*, (Tech. Note) Nov. JPT, 430

WYGAL, R. J., et al.: *Fluid Dynamics During an Underground Combustion Process*, 146 (Summary July JPT, 60A)

WYLLIE, M. R. J., and TORCASO, MICHAEL A.: *Comparison of Calculated k_{rg}/k_{ro} Ratios with a Correlation of Field Data*, (Tech. Note) Dec. JPT, 436

WYLLIE, M. R. J., et al.: *On the Streaming Potential Problem in Well Logging*, 409 (Summary Sept. JPT, 90A); discussion, 415

Y

YANKIE, W. W. JR., and CHATAS, A. T.: *Application of Statistics to Analysis of Production Decline Data*, (Tech. Note) Aug. JPT, 399

YOUNG, J. W., et al.: *Effective Compressibility of Reservoir Rock and Its Effects on Permeability*, (Tech. Note) June JPT, 386